Vol. 19, No. 1, March, 2020
ISSN (Print): 0972-6268; ISSN (Online) : 2395-3454

Nature Environment & Pollution Technology

A Multidisciplinary, International Journal on Diverse Aspects of Environment

Technoscience Publications
website: www.neptjournal.com

Technoscience Publications
A-504, Bliss Avenue, Balewadi,
Opp. SKP Campus, Pune-411 045
Maharashtra, India

www.neptjournal.com

Nature Environment and Pollution Technology

(An International Quarterly Scientific Research Journal)

Published by : Mrs. T. P. Goel, B-34, Dev Nagar, Tonk Road, Jaipur-302 018 Rajasthan, India

Managing Office : Technoscience Publications, A-504, Bliss Avenue, Balewadi, Pune-411 045, Maharashtra, India

E-mail : contact@neptjournal.com; journalnept@gmail.com

INSTRUCTIONS TO AUTHORS

Scope of the Journal

The Journal publishes original research/review papers covering almost all aspects of environment like monitoring, control and management of air, water, soil and noise pollution; solid waste management; industrial hygiene and occupational health hazards; biomedical aspects of pollution; conservation and management of resources; environmental laws and legal aspects of pollution; toxicology; radiation and recycling etc. Reports of important events, environmental news, environmental highlights and book reviews are also published in the journal.

Format of Manuscript

- The manuscript (*mss*) should be typed in double space leaving wide margins on both the sides.
- First page of mss should contain only the title of the paper, name(s) of author(s) and name and address of Organization(s) where the work has been carried out along with the affiliation of the authors.

Continued on back inner cover...

Nature Environment and Pollution Technology

Vol. 19, No. (1), March, 2020

CONTENTS

The Journal is Currently Abstracted and Indexed in:

- International Scientific Indexing (UAE) with Impact Factor 2.236 (2018)
- NAAS Rating of the Journal (2019) = 3.85
- Scopus®, SJR (0.146) 2018
- Index Copernicus (2016) = 109.45
- EI Compendex of Elsevier
- Indian Science Abstracts, New Delhi, India
- Chemical Abstracts, U.S.A.
- Elsevier Bibliographic Databases
- Pollution Abstracts, U.S.A.
- Paryavaran Abstract, New Delhi, India
- Zoological Records
- Indian Citation Index (ICI)
- Electronic Social and Science Citation Index (ESSCI)
- EBSCO: Environment Index™
- Zetoc
- Google Scholar
- ProQuest, U.K.
- J-Gate
- Environment Abstract, U.S.A.
- British Library
- Centre for Research Libraries
- WorldCat (OCLC)
- JournalSeek
- Connect Journals (India)
- CSA: Environmental Sciences and Pollution Management
- Research Bible (Japan)
- Indian Science
- Geobase
- Elektronische Zeitschriftenbibliothek (EZB)
- SHERPA/RoMEO
- Directory of Science
- CNKI Scholar (China National Knowledge Infrastructure)
- Access to Global Online Research in Agriculture (AGORA)
- AGRIS (UN-FAO)
- Full papers are available on the Journal's Website: www.neptjournal.com

UDL-EDGE (Malaysia) Products like *i*-Journals, *i*-Focus and *i*-Future

The journal is also included in the UGC CARE (A Group) list of journals in India

www.neptjournal.com

Nature Environment and Pollution Technology

Nature Environment and Pollution Technology
An International Quarterly Scientific Journal

p-ISSN: 0972-6268
e-ISSN: 2395-3454

Vol. 19 | No. 1 | pp. 1-15 | 2020

Original Research Paper | Open Access

Study on Removal of Thallium from Wastewater by Chitosan/Fly Ash Composite Adsorbent

Li Hai-hua*†, Chen Jie*, Hua Yong-peng, Yan Shao-feng**, E. Zheng-yang* and Su Hang***

*Faculty of Environmental and Municipal Engineering, North China University of Water Resources and Electric Power, Zhengzhou 450011, China

**Henan Academy of Environmental Protection Sciences, Zhengzhou 450011, China

†Corresponding author: Li Hai-hua

Nat. Env. & Poll. Tech.
Website: www.neptjournal.com

Received: 11-06-2019
Accepted: 24-07-2019

Key Words:
Thallium
Chitosan
Fly ash
Wastewater

ABSTRACT

Thallium (TI) is a kind of emerging contaminant with strong toxicity. In this study, a low-cost, renewable, biologically low-toxic and environmentally friendly fly ash/chitosan (FACS) composite adsorption material was synthesized by combining the characteristics of chitosan and fly ash to remove thallium from wastewater. SEM, FTIR and XRD analyses showed that the adsorbent mainly contained silicate compounds, and the surface of the particles contained a large number of micro porous structures. The adsorption process was rapid, reaching the adsorption equilibrium after 60min. When the pH value was 8, FACS had the best adsorption effect on TI, which was not conducive to the adsorption of TI in either strong acid or strong base environment. The co-existence of Fe3+ and Mn2+ could facilitate the adsorption of TI by FACS. The adsorption isotherm data were better fitted for the Freundlich model, while the Second-order kinetic model was more suitable for describing the kinetic data. Since the main chemical bond composition and chemical groups of FACS would not change after the adsorption of TI, the removal rate of TI was still high when it was reused after desorption. Because of its simple operation, low cost and reusability, FACS is considered to have certain potential in the removal of TI from wastewater.

INTRODUCTION

Thallium (TI) is a rare heavy metal element in the third main group, but it is widely found in nature (Liu et al. 2017, Xiao et al. 2012). In the past few decades, very low concentrations of thallium were contained in uncontaminated natural freshwater (Del-valls et al. 1999, Cheam et al. 1995) . However, due to the human activities such as mining, smelting and coal burning, the content of thallium in natural water is rising in recent years (Zhang et al. 2018). Once, as it was an unconventional test indicator in water, soil and solid waste, the problem of thallium pollution has been ignored. In fact, thallium, a highly toxic heavy metal contaminant, is one of the most toxic metals that poison mammals, and it is even more toxic than many of the highly regarded heavy metals such as mercury, cadmium, lead and zinc (Zhang et al. 2018, Wick et al. 2018, Xiao et al. 2018). Considering the toxicity and environmental pollution, TI has been listed as a priority pollutant by many official agencies (Liu et al. 2017). Therefore, the removal of thallium from wastewater seems to be particularly important.

So far, several technologies for removing thallium from water or wastewater have been reported, such as chemical precipitation (Liu et al. 2017), ion exchange (Li et al. 2017), solvent extraction (Rajesh & Subramanian 2006), adsorption (Birungi & Chirwa 2015, Huangfu et al. 2017) and biological methods (Saljooghi et al. 2011, Zolgharnein et al. 2011). Among these methods, adsorption is highly regarded by the researchers because of its high removal efficiency and simple operation. Varieties of materials such as titanium peroxide (Zhang et al. 2018), manganese dioxide (Huangfu et al. 2017), multiwalled carbon nanotubes (Pu et al. 2013), modified anion exchange resins (Li et al. 2017), Sawdust (Memon et al. 2008), fungi (Chen et al. 2018), and algae (Birungi & Chirwa 2015) have been used as adsorbents to remove TI from wastewater. Unfortunately, among these adsorbents, some are expensive, some cannot be reused, and others are hardly to obtain. As a result, it is urgent to develop a highly efficient adsorbent that is not only inexpensive but also easy to prepare and regenerate to remove TI from wastewater.

Fly ash (FA), is a kind of industrial waste formed by high-temperature calcination of pulverized coal. Due to its high porosity, large specific surface area and high adsorption activity, more and more people use it to make adsorption for environmental pollutant treatment (Ge et al. 2018). Chitosan (CS) is a product of the deacetylation of

chitin, and it is widely found in nature. Due to its biodegradability, biocompatibility and renewability, chitosan has been recognized as one of the most promising materials for adsorbents (Fan et al. 2012, Kuroiwa et al. 2017). So far, there have been some researches on fly ash/chitosan composite adsorbents. For example, Wen et al. (2011) used chitosan to coat fly ash to prepare a composite biosorbent and then studied the structural characteristics of the adsorbent and the adsorption effect on Cr(VI) in aqueous solution. Pan et al. (2011) prepared chitosan/fly-ash-cenospheres/γ-Fe_2O_3 magnetic composites by using microemulsion process and explored the removal of bisphenol A and 2,4,6-trichlorobenzene from aqueous solution. Yang et al. (2018) synthesized a new macromolecular xanthogen chitosan heavy metal chelation flocculant to treat wastewater containing Cu^{2+}. Rathinam et al. (2018) used synthetic chitosan-lysozyme biocomposites to effectively remove dyes and heavy metals from aqueous solutions. However, there is no research on the use of fly ash/chitosan (FACS) composite adsorbents to remove TI from polluted water. So, the purpose of this research was to synthesize fly ash/chitosan (FACS) composite adsorbent and analyse its characteristics by FIRT, SEM and XRD. The effects of the adsorbent on TI were investigated by changing some influencing factors, such as pH of the solution, reaction time, the amount of adsorbent, coexisting ions and rotational speed. The data of adsorption kinetics was explored. Meanwhile, we used two isotherm models to evaluate this adsorbent. Finally, we tested it for its reproducibility.

MATERIALS AND METHODS

Materials

The chitosan used in this study was purchased from Beijing Solarbio Science & Technology Co. Ltd. Fly ash was purchased from Lanke Water Purification Materials Co., Ltd. All the chemicals used in the study were of analytical grade. TI single element standard solution, which is an international standard substance, was purchased from Steel Research Institute of Iron and Steel Testing Technology Co., Ltd.

PHS-3C pH meter manufactured by Shanghai Yidian Scientific Instrument Co., Ltd. was used to measure the pH of the solution. The atomic absorption spectrum of the sample was measured by using a PinAAcle 900Z atomic absorption spectrometer manufactured by Perkin Elmer. The sample was oscillated with zh-d type all-temperature oscillator produced by Jintan Jingda Instrument Manufacturing Co., Ltd. Scanning electron microscopy analysis of the samples, Fourier infrared spectroscopy and X-ray diffraction analysis were performed by qualified units.

Preparation of Composite Adsorbent

The chitosan/fly ash (FACS) was thoroughly mixed at a mass ratio of 1:12.5, and then glacial acetic acid was added at a concentration of 4%, wherein the mass ratio of glacial acetic acid to the mixture was 3:5. All the materials were mixed and stirred thoroughly, and then prepared into small particles with a particle size of 1~3mm. After this, small particles were dried to obtain the FACS composite adsorbent. It should be noted that the co-existing ions were not added during the experiment, and the composite adsorbent adsorbing the aqueous solution only containing TI (I) was represented by TFACS. Similarly, the composite adsorbent, which adsorbed the solution containing only the coexisting ion Fe^{3+}, was represented by Fe-FACS, the composite adsorbent adsorbing the solution in which Mn^{2+} ions were added was represented by Mn-FACS, and the composite adsorbent adsorbing the solution in which the Fe^{3+}/Mn^{2+} mixed ion was added was represented by FM-FACS.

Characterization of Adsorbents

The FACS of unabsorbed heavy metal and the composite materials TFACS, Fe-FACS, Mn-FACS and FM-FACS adsorbed with heavy metals were scanned by scanning electron microscope to observe the structural characteristics. The infrared spectra of the composite TFACS, Fe-FACS, Mn-FACS and FM-FACS were tested by FTIR spectroscopy and the changes of covalent bonds and corresponding groups were observed. The XRD patterns of the FACS composite adsorbent were obtained by X-ray diffraction in the range of 2θ =10~80°, and the diffraction peaks in the spectrum were observed to analyse the crystallinity of FACS.

Experimental Design

The experimental parameters such as pH, contact time, the amount of adsorbent, presence of coexisting ions and rotational speed on the removal of TI were studied in a batch mode of operations. 80mL of TI-containing wastewater with an initial concentration of 0.01mg/L was added into a 250 mL volumetric flask, and the experimental conditions were changed to carry out a batch adsorption experiment. All the experiments were carried out under constant temperature conditions. After the desired time, the supernatant was taken to determine the content of thallium in the wastewater.

Adsorption Kinetics

The adsorption rate is a crucial indicator to evaluate the applicability of the given adsorbent for practical application because of its decisive role on the initial investment. The kinetics of adsorption that describes the solute uptake

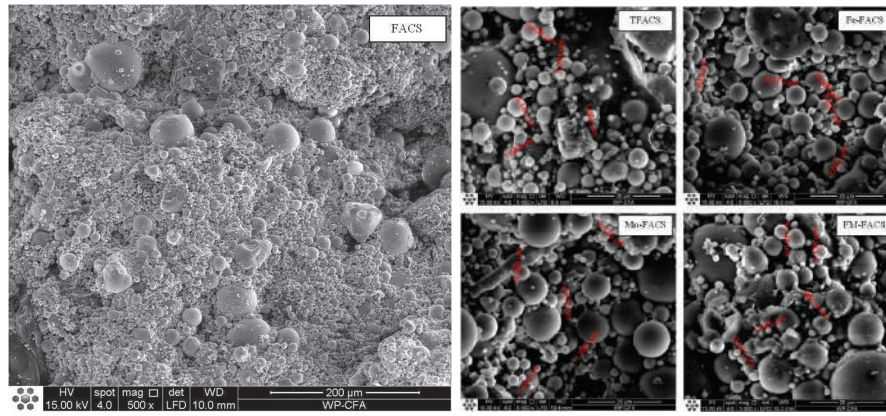

Fig. 1: The SEM pictures of various FACS.

rate is one of the most important characteristics that define the efficiency of adsorption (Wan et al. 2014, Xiong et al. 2013). The First-order kinetics model is expressed as the follow equation (Keskinkan et al. 2004):

$$\ln(q_e - q_t) = \ln q_e - k_1 t$$

The Second-order kinetics model is expressed as the following equation (Xiong et al. 2013):

$$\frac{t}{q_t} = \frac{1}{k_2 q_e^2} + \frac{t}{q_e}$$

Where, q_e and q_t are the amounts of Tl(I) adsorbed at equilibrium and at time t, respectively.

Adsorption Isotherms

The adsorption isotherm describes the relationship between the adsorption capacity of adsorbent and the equilibrium concentration of adsorbent, and it plays an important role in understanding the adsorption process (Zhang et al. 2008, Li et al. 2018, Tran et al. 2017). Langmuir and Freundlich are two different isothermal adsorption models. The Langmuir model was established based on the assumption that the adsorbent surface was uniform, and the equation was expressed as (Rahmani et al. 2010, Saad et al. 2018):

$$\frac{C_e}{q_e} = \frac{C_e}{q_0} + \frac{1}{bq_0} \quad \ldots(3)$$

Where, C_e is the equilibrium concentration of the solution (mg/L), q_e is the amount of heavy metal adsorbed per unit weight of adsorbent at a specified equilibrium (mg/g), q_0 is the saturated adsorption capacity of monomolecular coverage (mg/g), and b is the adsorption rate constant (L/mg).

The Freundlich equation is an empirical equation for describing the surface heterogeneity of adsorbent (Rahmani et al. 2010, Saad et al. 2018) and given as:

$$\ln q_e = \ln k + \frac{1}{n} \ln C_e \quad \ldots(4)$$

Where, C_e is the mass concentration of solute at adsorption equilibrium (mg/L), q_e is the equilibrium adsorption quantity (mg/g), k is the Freundlich constant representing the adsorption capacity (mg/g), and n is a constant representing the adsorption intensity.

RESULTS AND DISCUSSION

Characterization of Adsorbents

In order to observe the morphological changes before and after adsorption of FACS composite adsorption materials, the original FACS and the TFACS, Fe-FACS, Mn-FACS and FM-FACS after adsorption were analysed by scanning electron microscopy, and the results are presented in Fig. 1. It can be seen from Fig. 1 that the surface of the FACS particles contained a large number of microporous structures, and there was more particulate matter in the outer layer. The foremost reason is that the FACS consists of a large amount of fly ash particles, and the particles are connected to each other. It indicates that the colloidal solution formed by the dissolution of chitosan was solidified by fly ash to make both of them fully mixed together to form FACS particles. The SEM scan showed that the FACS particles were filled with micropores after the adsorption. Minimum particle sizes of TFACS, Fe-FACS, Mn-FACS and FM-FACS particles were 1.600µm, 1.840µm, 1.294µm and 0.866µm, respectively. It is not hard to find that, compared with Fe-FACS, Mn-FACS and FM-FACS, TFACS with only TI adsorption had

more pore structures, indicating that the surface porosity of adsorbent particles had a small change when only TI was adsorbed. The main reason for the above phenomenon is that in the presence of co-existing ions Fe^{3+}, Mn^{2+} and Fe^{3+}/Mn^{2+}, FACS also adsorbed Fe^{3+} and Mn^{2+} to some extent in the process of adsorbing TI, so the surface porosity of Fe-FACS, Mn-FACS and FM-FACS particles decreased significantly compared to FACS.

Fourier infrared spectroscopy was used to detect and analyse FACS, TFACS, Fe-FACS, Mn-FACS and FM-FACS respectively, in order to understand the molecular structure and group changes in FACS composite adsorbents before and after adsorption. The Fourier infrared spectrum is shown in Fig. 2.

As can be seen from Fig. 2a, in the FACS spectrum, the chemical absorption peak of the O-H bond was at 3424.69 cm^{-1}, the characteristic absorption peak of C-H bond was at 1611.81 cm^{-1}~1449.81 cm^{-1}, and the characteristic infrared absorption peak of Si-O bond was at 1074.70 cm^{-1}. In combination with the FTIR diagram to which silicate

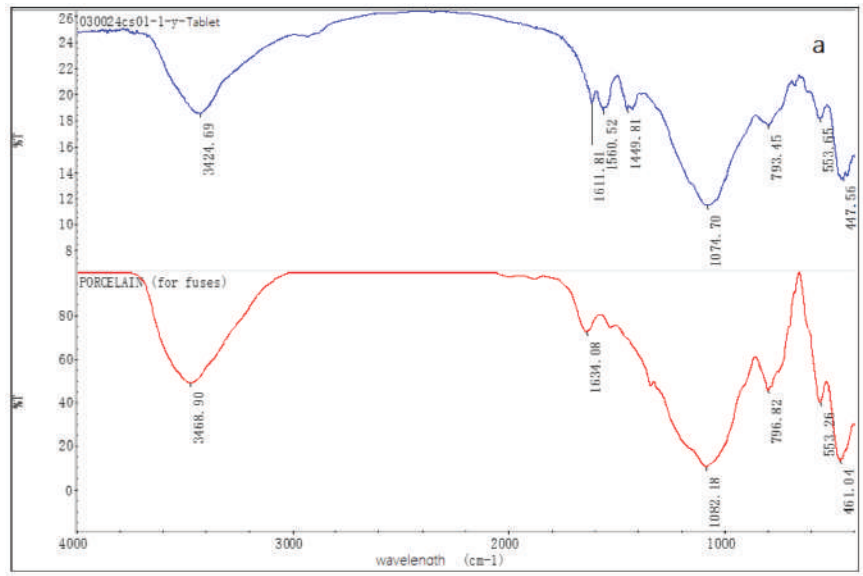

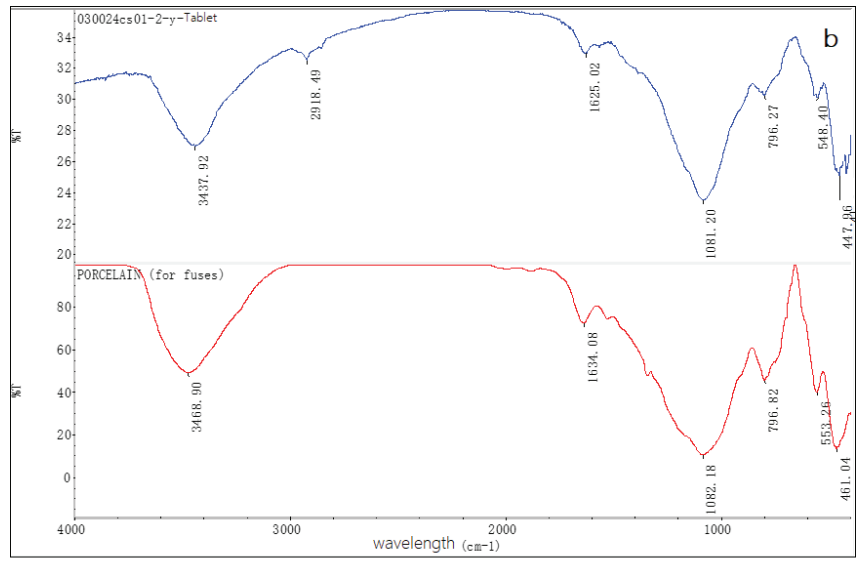

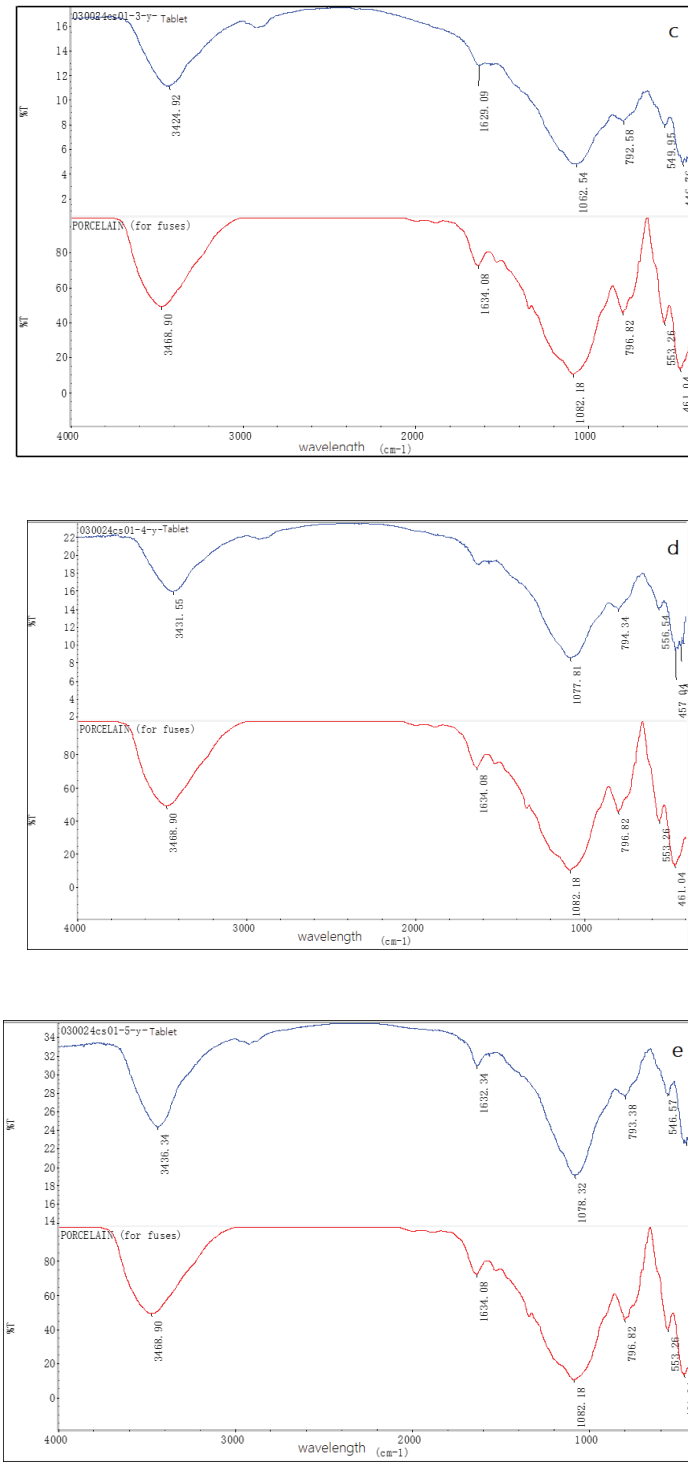

Fig. 2: The FTIR pictures of FACS.

compounds were matched, it can be seen that the FACS mainly consisted of silicon-containing compound.

It can be found from Fig. 2b that in the TFACS spectrum, the stretching vibration peak of the O-H bond was at 3437.92 cm^{-1}, C-H key characteristic absorption peak was at 1625.02 cm^{-1}, and Si-O key characteristic in absorption peak was at 1081.20 cm^{-1}. At the same time, in combination with the FTIR diagram to which silicate compounds were matched, it can be seen that TFACS mainly consisted of silicon-containing compounds, and a special vibration peak was generated at 2918.49 cm^{-1} after the adsorption of thallium.

As shown in Fig. 2c, in the Fe-FACS spectrum, the characteristic chemical absorption peak of the O-H bond was at 3424.92 cm^{-1}, the characteristic absorption peak of the C-H bond was at 1629.09 cm^{-1}, and the characteristic infrared absorption peak of Si-O bond was at 1062.54 cm^{-1}. Matching the FTIR map, it can be seen that the Fe-FACS mainly consisted of silicon-containing compounds.

As described in Fig. 2d, in the Mn-FACS spectrum, the characteristic chemical absorption peak of the O-H bond was at 3431.55 cm^{-1}, the characteristic absorption peak of the C-H bond was at 1634.08 cm^{-1}, and the characteristic infrared absorption peak of Si-O bond was at 1077.81 cm^{-1}. Then based on the matching of silicate compounds with FTIR diagram, it can be considered that the Mn-FACS mainly consisted of silicon-containing compounds.

According to Fig. 2e, in the FM-FACS spectrum, the stretching vibration peak of the O-H bond was at 3463.34 cm^{-1}, the characteristic absorption peak of C-H bond was at 1632.34 cm^{-1}, and the Si-O bond characteristic infrared absorption peak was at 1078.32 cm^{-1}. Compared to silicate compounds matching FTIR diagram, it can be considered that in FM-FACS there were mainly silicon-containing compounds.

In summary, FACS adsorption materials mainly contain silicate compounds, which are related to the main chemical composition of fly ash. After adsorption of TI-containing wastewater in different systems, the principal chemical bond composition and chemical groups of the adsorption materials do not change.

Chitosan has a strong hydrogen bond within and between molecules, which makes the molecular chain of CS rigid to a certain extent, and then forms a certain crystal shape, which shows an adsorption peak in XRD pattern 2θ in the Angle scanning mode. However, mixing fly ash with CS to make FACS adsorption material would do harm to the crystal shape of CS. The XRD pattern of FACS is illustrated

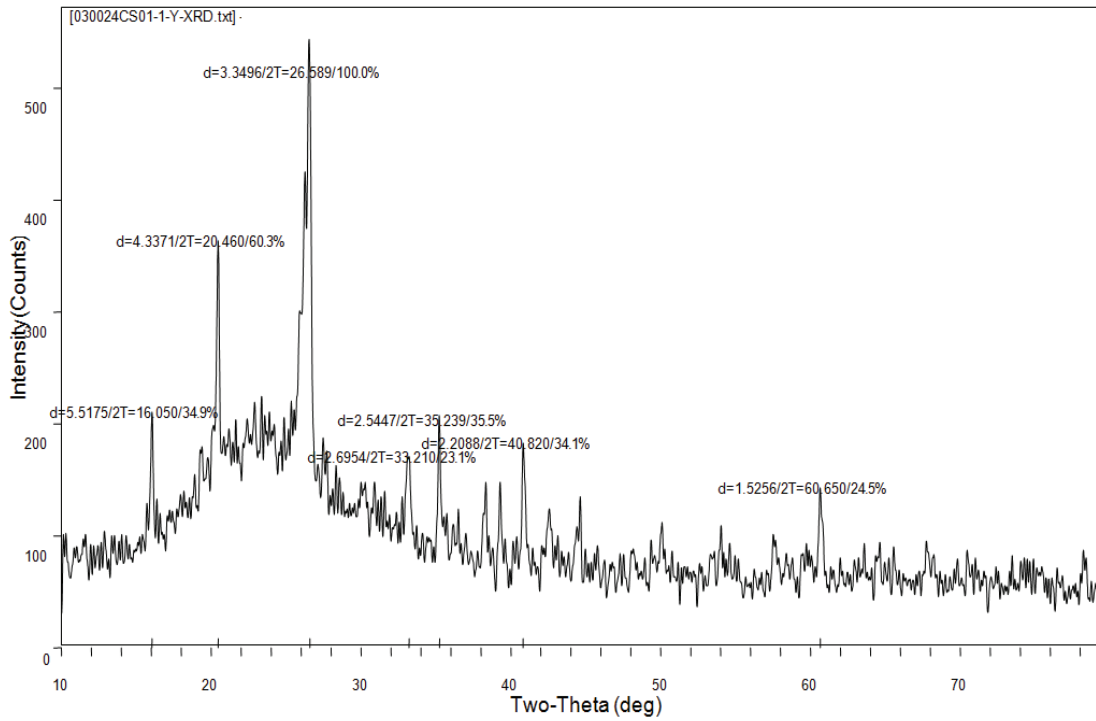

Fig. 3: The XRD picture of FACS.

in Fig. 3, and the diffraction matching pattern is shown in Fig. 4. As can be seen from Fig. 3, FACS exhibited two major diffraction peaks at 2θ = 20.460° and 2θ = 26.589°. Compared with the XRD pattern of sillimanite, it is easy to see in Fig. 4 that there were also two distinct diffraction peaks in the XRD pattern of sillimanite at 2θ=20.456° and 2θ=26.610°. The matching between the two was extremely high, indicating that the XRD pattern of FACS was a sillimanite map. In the above diffraction pattern, there was no diffraction peak of CS, which indicates that CS would undergo oxidation and substitution reaction with the addition of glacial acetic acid. In addition, after mixing with fly ash, the molecular structure of CS was changed and the crystal form of CS was destroyed. Therefore, only the crystal diffraction peaks of silicon-containing compounds whose crystal forms were not destroyed in the FACS diffraction pattern could be found, which further indicates that the main components of FACS were silicon-containing compounds.

Effect of Solution pH Value on Adsorption

Since the pH value of the solution determines the surface charge of the adsorbent and the degree and shape of the adsorbent, it has a significant impact on the adsorption of heavy metal (Salam et al. 2011). 80mL thallium-containing wastewater with an initial concentration of 0.010mg/L was loaded into a 250mL conical flask, and 3g adsorbent was added. The same operations were carried in 7 conical flasks, and the pH value of the solution in the flasks was adjusted to 4, 5, 6, 7, 8, 9, 10 with HCl or NaOH, respectively. After shaking at a constant temperature for 2 minutes, the adsorbent was thoroughly mixed with the liquid and permitted to stand for 2 hours, after which the supernatant was taken to determine the TI content. According to the results, the adsorption effect of the adsorbent on TI under different pH conditions was plotted, as shown in Fig. 5.

It is clear that when the pH was 8, the FACS was best for the adsorption of thallium, and the maximum amount of adsorption was 0.173 of μg/g. When pH rose from 4 to 6, thallium concentration in the supernatant fluid increased with the increase of pH value, while adsorption capacity decreased gradually, which indicates that in this process, the adsorption effect showed a gradual decline with the increase of pH value. On the contrary, with the pH increasing from 6 to 8, the TI concentration gradually decreased, while the adsorption amount of FACS increased gradually, indicating that the adsorption effect also gradually increased with the increase of pH value. In addition, when the pH was equal to 9 or 10, the concentration of thallium in the solution was consistent with that when the pH was 4

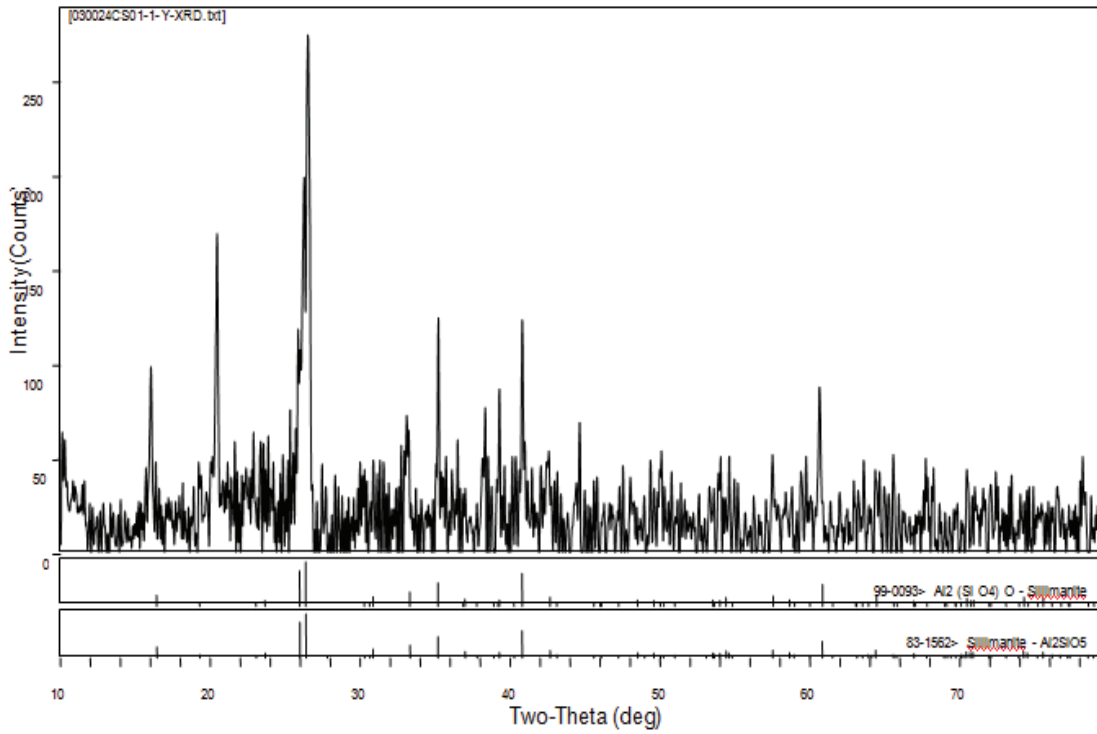

Fig. 4: The matched XRD picture of FACS.

and the concentration was high, and the FACS adsorption amount was small, which means that in an acidic or basic environment, the FACS composite adsorption material was not ideal for the absorption of thallium. At low pH, it could be attributed to the competition between the excessive proton H^+ and the ion metal on the surface of the adsorbent that made the adsorption of TI by adsorbent difficult (Hamadi & Nabih 2018). On the other hand, when the pH value was too high, the adsorption effect of the adsorbent on TI also unsatisfactory, which may be due to more OH^- damaged Si-O bonds of the adsorbent.

Effect of Reaction Time on Adsorption

80mL thallium-containing wastewater with an initial concentration of 0.010mg/L was loaded into a 250mL conical flask, and 3g adsorbent was added respectively, and the same solution pH value was kept. The mixture was shaken at a constant temperature for 2 minutes in order to thoroughly mix the adsorbent with the liquid, and then the solution was allowed to stand. After 15, 30, 60, 90, 120 and 150 min, the supernatant was taken to determine the content of thallium. The effect of reaction time on adsorption is shown in Fig. 6.

It shows that at the beginning of the adsorption, thallium concentration in the solution decreased with the increase of adsorption time, while the FACS adsorption capacity increased gradually. When the adsorption was carried out for 60 min, the concentration of thallium in the solution reached the minimum, while the adsorption amount reached the maximum, which was 0.182μg/g. After the adsorption was conducted for 60 min, the concentration of thallium in the solution gradually increased with the increase of adsorption time, this is because the adsorption has reached saturation. With the increase of adsorption time, the parsing phenomenon began to appear in the solution. It was found that concentration of thallium in

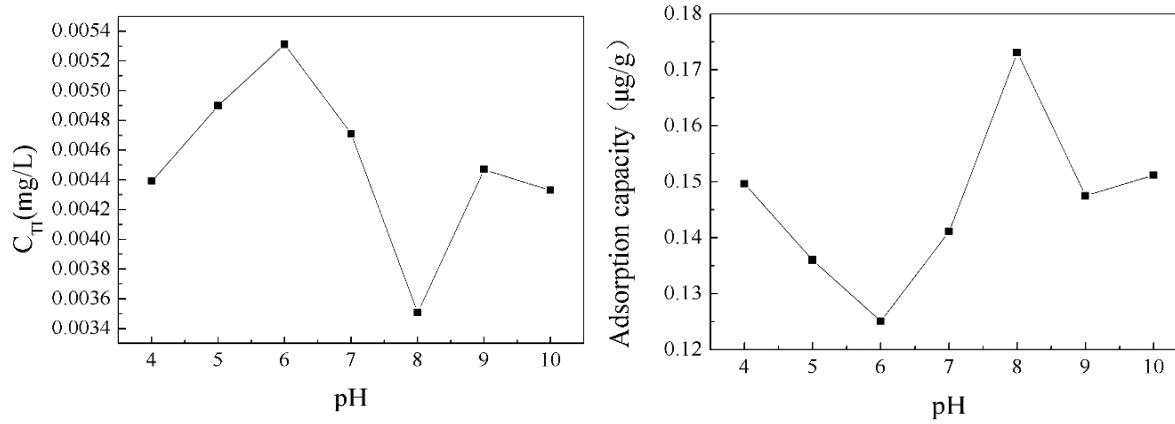

Fig. 5: The effect of solution pH on adsorption.

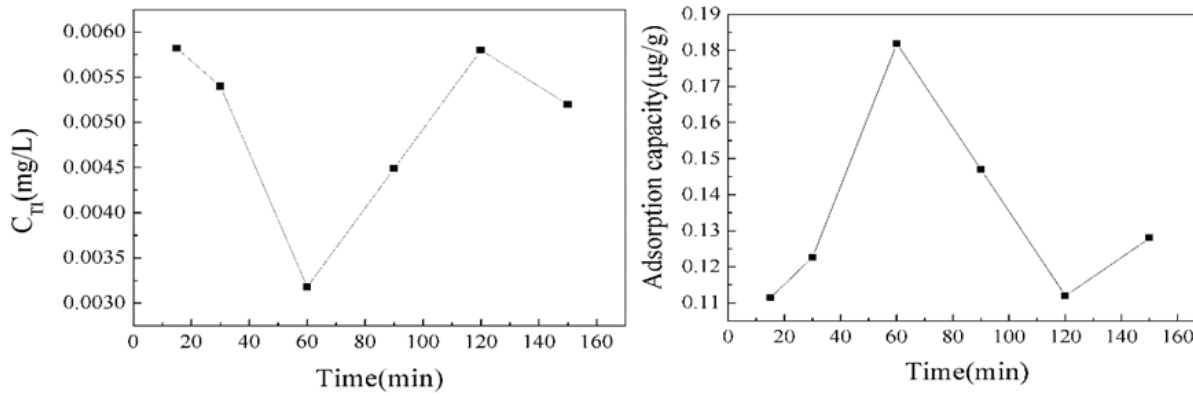

Fig. 6: The effect of reaction time on adsorption.

the solution was reduced again after 120 min, at which point the FACS composite adsorption material resorbed after desorption. Therefore, the reaction of the FACS on the thallium in the wastewater is a kind of adsorption - the alternate process of the absorption cycle. When the reaction time was at 60 min, FACS compound adsorption material reached saturated adsorption, and adsorption effect was best.

Effect of the Amount of Adsorbent on the Adsorption Effect

80mL wastewater containing thallium with an initial concentration of 0.010mg/L was loaded into six 250mL conical flasks, and adsorbents of 1g, 2g, 3g, 4g, 5g and 6g were added, respectively. The pH of the solution was kept same in all the conical flasks, and the solution was shaken at a

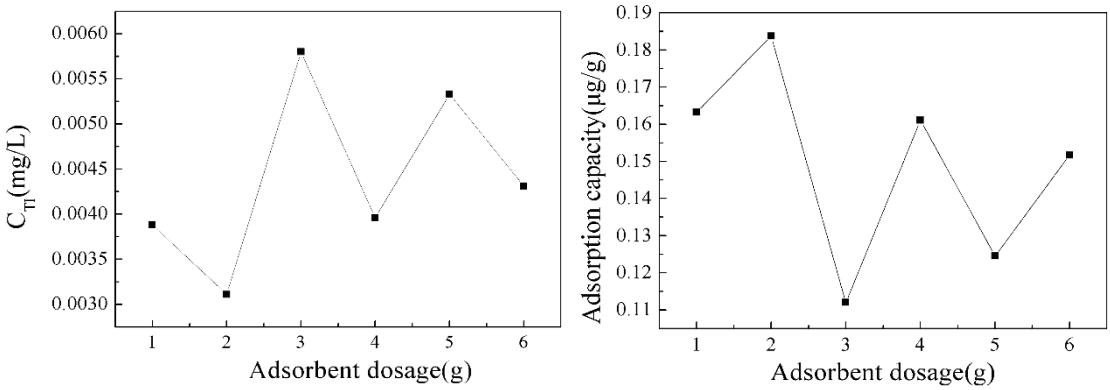

Fig. 7: The effect of adsorbent dose on adsorption.

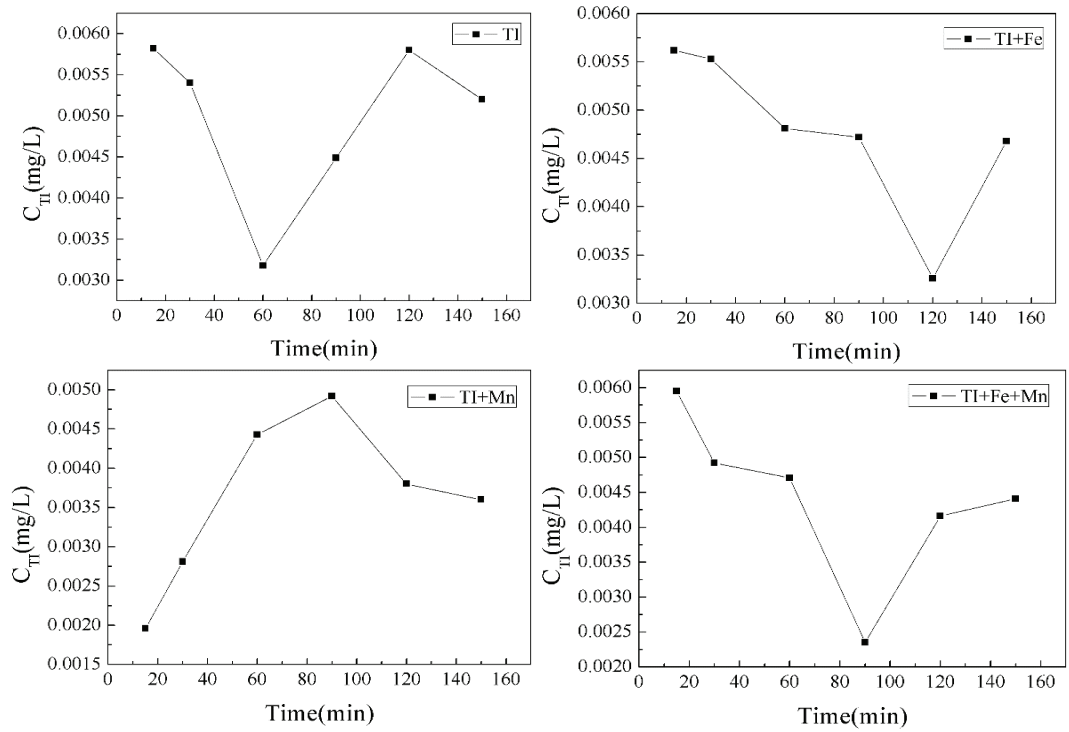

Fig. 8: Variations in the concentration of thallium with time in solutions of different systems in the presence of coexisting ions.

constant temperature for 2 minutes to allow the adsorbent to mix well with the liquid and let it stand. Two hours later, the supernatant was taken to determine the content of thallium, and the results are presented in Fig. 7.

It can be seen directly from the Fig. 7 that by adding the 2g adsorbent, the adsorption quantity of thallium was largest, and adsorbent adsorption effect was best. However, when the amount of adsorbent was more than 2g, the adsorption capacity of thallium by FACS was significantly less than that of the solution with 2g of adsorbent. The reason for this phenomenon may be that when the amount of adsorbent is too much, there would be an adsorption bridge between adsorbent particles, which would affect the adsorption of thallium. On the other hand, the adsorption of thallium may be affected by the intermolecular interaction between ions on the surface of the adsorbent due to the high adsorption dose. In addition, when the amount of adsorbent was less than 2g, the adsorption amount of thallium was also less. Obviously, when the amount of adsorbent was not enough, the heavy metal thallium in water cannot be fully removed.

Effect of Coexisting Ions on Adsorption

In this study, the effects of Fe^{3+}, Mn^{2+} and Fe^{3+}/Mn^{2+} on the removal of TI by FACS were studied respectively. 80mL thallium-containing wastewater with an initial concentration of 0.010mg/L was added into the 250mL conical flask, and 5mL $FeCl_3$ solution, $MnCl_3$ solution and $FeCl_3/MnCl_3$ mixed solution with a concentration of 0.05mg/L were added, respectively. 3g FACS was added to each conical flask with the same pH value. The conical flasks were shaken so that the solution was fully mixed with the adsorbent. After 15, 30, 60, 90, 120 and 150min, the supernatant was successively taken to determine the content of thallium for analysis. The variations in the concentration of thallium with time in solutions of different systems are illustrated in Fig. 8 and the adsorption amounts of thallium by adsorbent are shown in Fig. 9.

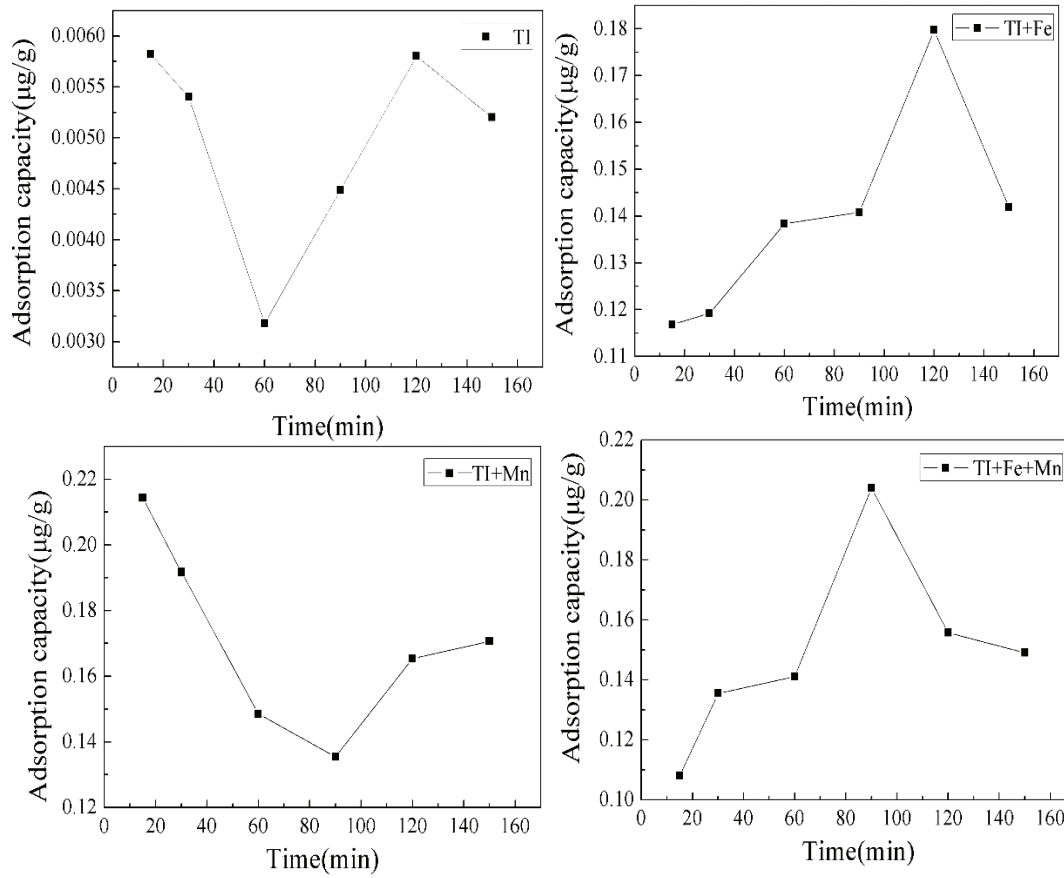

Fig. 9: The variations in the amount of adsorption with time in the presence of coexisting ions.

As can be observed in the figures, when there were no coexisting ions in the solution, the adsorption capacity of FACS on TI increased rapidly between 15 to 60min, and the concentration of TI in the solution decreased significantly. The adsorption saturation was achieved at 60min, and then the concentration of thallium in the solution increased again. When the coexisting ion Fe^{3+} was present, the concentration of thallium in the solution slowly decreases in the first 90min. From 90 to 120min, the adsorption amount increased sharply and the cesium concentration decreased rapidly. At 120min, the amount of adsorption reached its maximum and reached adsorption saturation. Probably due to the presence of the coexisting ion Fe^{3+}, there was competitive adsorption between Fe^{3+} and the TI in the solution for the first 90min of the reaction. When Mn^{2+} was present in the solution, the concentration of strontium in the solution tended to increase continuously between 15 to 90min of the reaction. However, between 90 to 150min, the thallium concentration in the solution showed a trend of gradual decrease. Perhaps Mn^{2+} has a sufficiently strong preferential adsorption capacity over TI, so that the presence of Mn^{2+} seriously disturbed the adsorption behaviour of the adsorbent on TI during the first 90 minutes of the reaction. When TI, Fe^{3+} and Mn^{2+} were present in the solution, the TI concentration in the solution decreased significantly during the first 30 min of the reaction. Between 30 to 60min, the content of TI was still decreasing, but at a slower speed than before. Between 60 to 90min, the content of TI in the solution presented a sharp decline trend again, during which time the adsorption amount of TI by the adsorbent increased significantly. Then, at 90min, the concentration of TI reached the minimum, and the adsorption capacity of the adsorbent on TI was greater than that in the absence of coexisting ions. This is because the fact that Fe^{3+} and Mn^{2+} are hydrolysed to hydroxide. Except for sediment, they can be used as a new adsorbent to increase the adsorption of TI (Li et al. 2016). After 90 min, the concentration of TI increased in the solution because the FACS reached saturation and desorption occurred.

Effect of Rotation Speed on Adsorption Effect

80mL thallium-containing wastewater with an initial concentration of 0.010mg/L was added into seven 250mL conical flasks. Then 3g adsorbent was added into each flask. Under the same pH, the adsorbent and solution were mixed evenly by shaking. The rotational speed of the thermostatic oscillator was set to 100, 125, 150, 175, 200, 225, and 250r/min, respectively. After the constant temperature oscillation for 120min, the solution was settled and the supernatant was taken to determine the content of thallium in the solution. According to the measurement results, the influence of different oscillation speeds on the adsorption effect of TI was plotted (Fig. 10).

As can be seen, when the rotation speed was 225r/min, the concentration of thallium in the solution was the lowest, and the adsorption amount of the FACS composite adsorbent to TI was the largest. When the rotation speed was between 100 and 175r/min, there was fluctuation in the TI concentration in the solution, but the thallium content in the solution was always higher than that when the rotation speed was 225 r/min, and the thallium content in the solution reached a peak at 175r/min. It may be that the adsorption of TI by FACS adsorbent in the solution is a kind of "adsorption-desorption-re-absorption" alternating complex phenomenon due to the low rotation speed. The adsorption effect of FACS to TI in the second stage was not ideal. At the rotational speed of 175-225r/min, the adsorption amount of TI by FACS increased gradually, while the concentration of TI in the

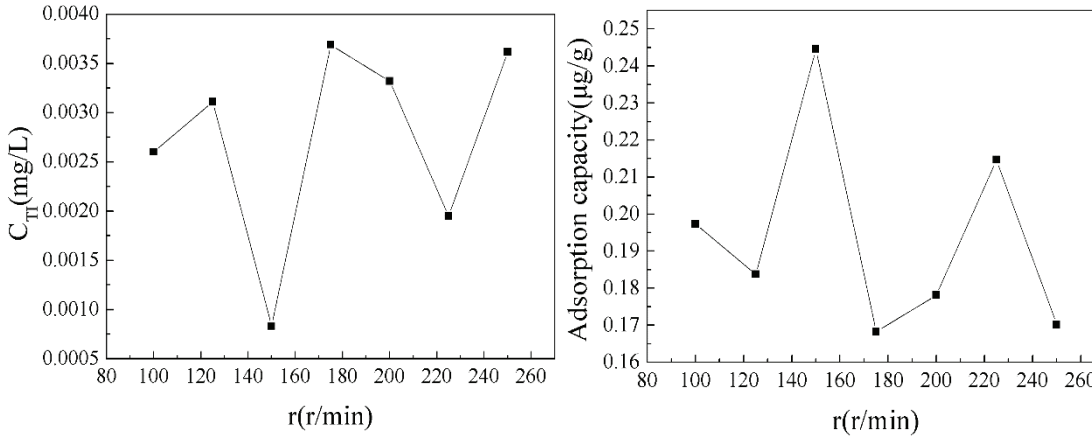

Fig. 10: Influence of different oscillation speeds on thallium adsorption.

solution decreased gradually. However, the thallium concentration in the solution increased sharply as the rotation speed continued to increase. It can be seen that when the speed was too high, severe turbulence was not good for the adsorption of TI in the solution by FACS composite adsorbent.

Adsorption kinetics

In the present study, kinetic sorption data were treated with two simplified kinetic models including First-order kinetics model and Second-order kinetics model. First-order kinetics fitting results are shown in Table 1 and Fig. 11, and the results of Second-order kinetics fitting in Table 2 and Fig. 12.

It is obvious that the second order model fitted better than the first order model, which means chemical adsorption is the main speed limit step.

Adsorption Isotherms

Both Langmuir and Freundlich models were used to fit the adsorption isotherms in this study. The higher regression coefficient (Table 3) indicates that the Freundlich model has better fitting effect on isotherm than the Langmuir model (Fig. 13), which proves that the adsorption of TI (I) by FACS belongs to multi-molecular layer adsorption on heterogeneous phase surface.

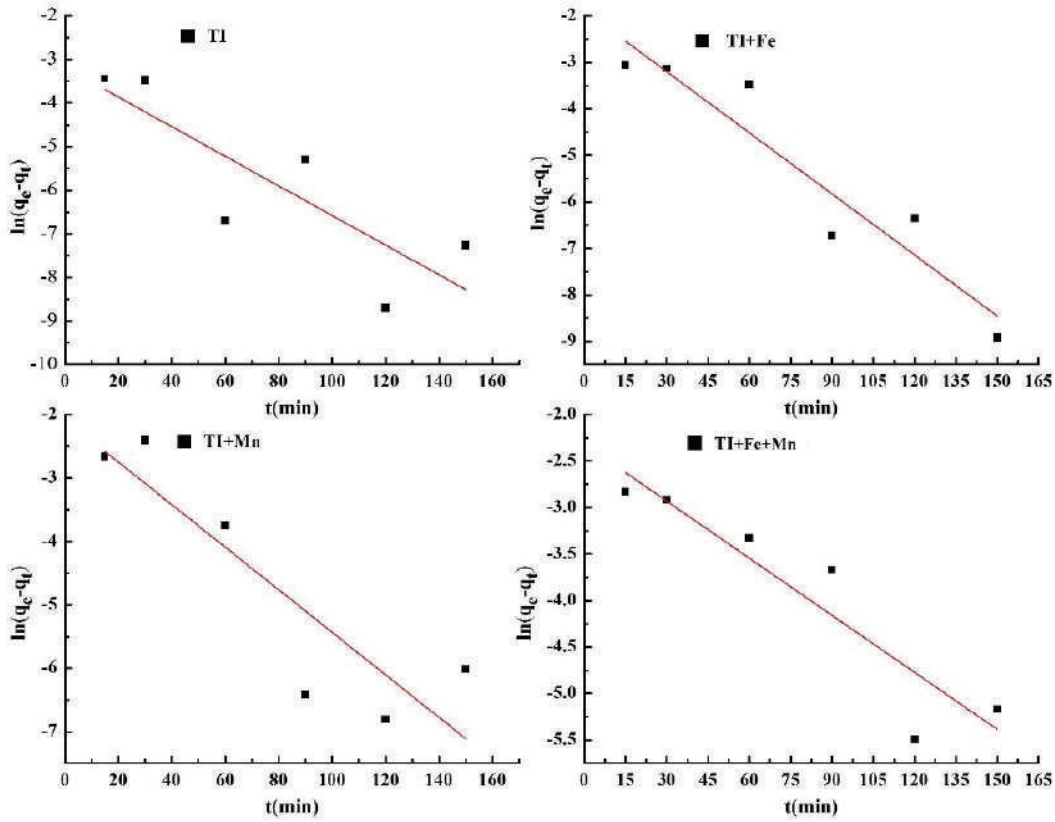

Fig. 11: The First-order kinetic fitting curve.

Table 1: The First-order kinetics fitting parameters.

Reaction system	q_e	q_e^*	k_1	R^2
TI	0.04147	0.17830	0.03397	0.6260
TI+Fe	0.15138	0.20920	0.04379	0.8724
TI+Mn	0.12504	0.22350	0.03355	0.7416
TI+Fe+Mn	0.09855	0.20970	0.02046	0.8302

Table 2: The Second-order kinetics fitting parameters.

Reaction system	q_e	q_e^*	k_2	R^2
TI	0.21589	0.17830	0.65565	0.99903
TI+Fe	0.20648	0.20920	1.05966	0.99238
TI+Mn	0.21206	0.22350	0.45198	0.99222
TI+Fe+Mn	0.21589	0.20970	0.43697	0.99069

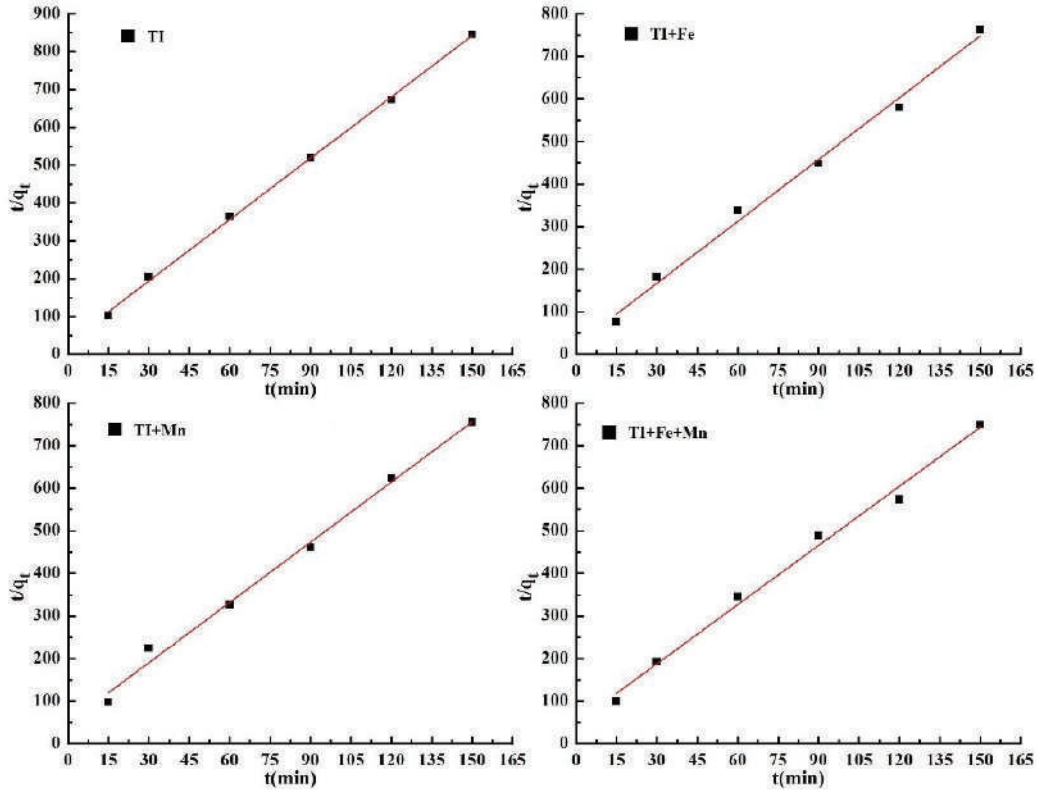

Fig. 12: The Second-order kinetics fitting curve.

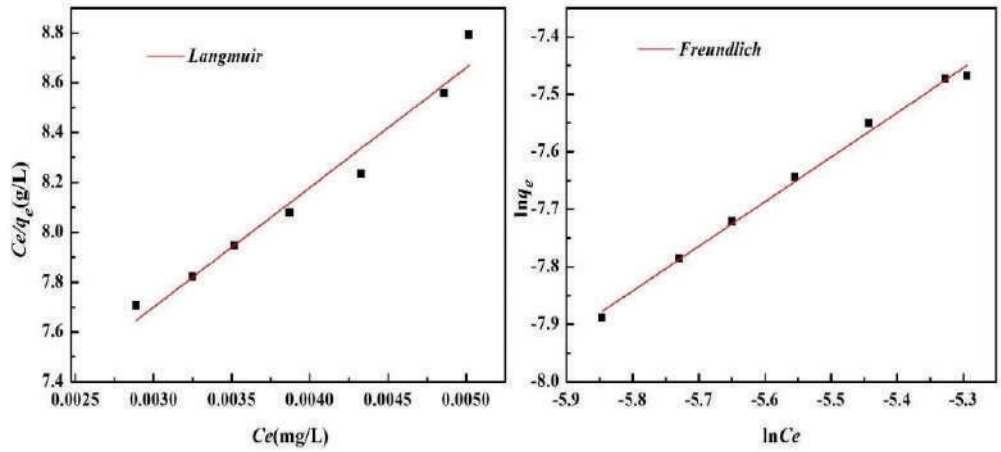

Fig. 13: Isothermal fitting curves of Langmuir and Freundlich.

Reuse of Complex Adsorbent

Because the economy of the adsorption process depends on the regeneration of the adsorbent, the study of desorption is of great importance. The saturated FACS composite adsorbent was repeatedly rinsed with deionized water and then dried. Then, the composite adsorbent was immersed in a sodium chloride solution with a concentration of 1 mol/L for desorption. During the desorption process, the solution was stirred for 1 minute every 2 hours. TI (I) solution was adsorbed by dried FACS for 15, 30, 45, 60, 90, 120 and 150min, respectively. The supernatant was taken in order to measure the concentration of TI (I) in the solution, and the adsorption was calculated. The results are shown in Fig. 14.

Fig. 14 shows that the adsorption step took 60 min to achieve equilibrium and the adsorption capacity was about 0.114 μg/g. The removal rate of TI (I) by FACS composite adsorption material reused after desorption was still about 43%, which proves that FACS composite adsorption material still had high activity after regeneration and could be reused in the treatment of TI polluted wastewater. FACS belongs to the adsorption of environmentally friendly materials.

CONCLUSIONS

The prepared FACS composite adsorbent is a low-cost, renewable, low toxic, environmentally friendly adsorbent material. The surface of FACS particles contains lots of microporous structures and has a large porosity, which is conducive to its adsorption of TI in wastewater. It is mainly of silicate structure. After adsorption of TI-containing wastewater in different systems, the main chemical bond composition and chemical groups of the adsorption material would not change. The experiments of different influencing factors showed that with a pH value of 8, FACS had the best adsorption effect on TI in water. Whether the pH was too high or too low, it had a negative effect on the adsorption. The "adsorption-desorption" period of FACS occurred at 120min, and the adsorption effect was best when the reaction was carried out to 60min, and the adsorption saturation was achieved. When 2g adsorbent was added into 80mL thallium-containing wastewater with an initial concentration of 0.01mg/L, the removal effect was best. When coexisting ions Fe^{3+} and Mn^{2+} were separately present in the solution with TI, both of them had an adverse effect on the removal of TI. However, when Fe^{3+}, Mn^{2+} and TI were simultaneously present in the solution, they had a positive effect on the adsorption. The adsorption effect was optimal when the rotation speed was 225r/min, because the turbulence in the adsorption process is not conducive to the adsorption of TI in the solution by FACS composite adsorbent. The adsorption of TI by FACS was multi-molecular layer adsorption on the surface of heterogeneous reaction. The

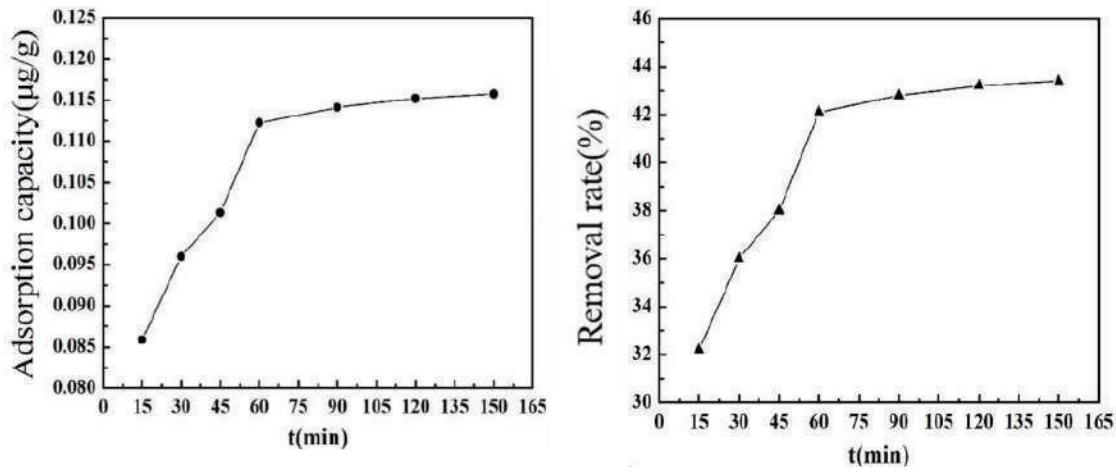

Fig. 14: The change in adsorption capacity and removal rate with time.

Table 3: Langmuir and Freundlich isothermal fitting parameters.

Langmuir isothermal fitting			Freundlich isothermal fitting		
q_0(mg/g)	b(L/mg)	R^2	n	k	R^2
0.00054	76.60795	0.95820	1.29096	0.03512	0.99438

driving force of the process was the covalent force formed by ion exchange or covalent electron pair between adsorbent and adsorbate. After being analysed and reused, FACS still had superior adsorption efficiency. We believe that FACS composite adsorbent is a kind of economical material with simple operation, low price and recyclability, and has potential application in removing TI from wastewater.

REFERENCES

Birungi, Z.S. and Chirwa, E.M.N. 2015. The adsorption potential and recovery of thallium using green micro-algae from eutrophic water sources. J. Hazard. Mater., 299: 67-77.

Cheam, V., Lechner, J., Desrosiers, R., Sekerka, I., Lawson, G. and Mudroch, A. 1995. Dissolved and total thallium in Great Lakes waters. Journal of Great Lakes Research, 21: 384-394.

Chen, K.N., Li, H.S., Kong, L.J., Peng, Y., Chen, D.Y., Xia, J.R. and Long, J.Y. 2018. Biosorption of thallium (I) and cadmium (II) with the dried biomass of *Pestalotiopsis* sp. FW-JCCW: Isotherm, kinetic, thermodynamic and mechanism. J. Desalination and Water Treatment, 111: 297-309.

Del-valls, T.A., Saenz, V., Arias, A.M. and Blasco, J. 1999. Thallium in the marine environment: First ecotoxicological assessments in the Guadalquivir estuary and its potential adverse effect on the Donana European natural reserve after the Aznalcollar mining spill. J. Ciencias Marinas, 25: 161-175.

Fan, L.L., Luo, C.N., Li, X.J., Lu, F.G., Qiu, H.M. and Sun, M. 2012. Fabrication of novel magnetic chitosan grafted with graphene oxide to enhance adsorption properties for methyl blue. Journal of Hazardous Materials, 215-216: 272-279.

Ge, J.C., Yoon, S.K. and Choi, N.J. 2018. Application of fly ash as an adsorbent for removal of air and water pollutants. J. Applied Sciences, 8(7):1-24.

Hamadi, A. and Nabih, K. 2018. Synthesis of zeolites materials using fly ash and oil shale ash and their applications in removing heavy metals from aqueous solutions. Journal of Chemistry, 2018: 1-12.

Huangfu, X.L., Ma, C.X., Ma, J., He, Q., Yang, C., Zhou, J., Jiang, J. and Wang, Y.A. 2017. Effective removal of trace thallium from surface water by nanosized manganese dioxide enhanced quartz sand filtration. Chemosphere, 189: 1-9.

Keskinkan, O., Goksu, M.Z.L., Basibuyuk, M. and Forster, C.F. 2004. Heavy metal adsorption properties of a submerged aquatic plant (*Ceratophyllum demersum*). J. Bioresource Technology, 92(2): 197-200.

Kuroiwa, T., Takada, H., Shogen, A., Saito, K., Kobayashi, I., Uemura, K. and Kanazawa, A. 2017. Cross-linkable chitosan-based hydrogel microbeads with pH-responsive adsorption properties for organic dyes prepared using size-tunable microchannel emulsification technique. J. Colloids and Surfaces A: Physicochemical and Engineering Aspects, 514: 69-78.

Li, H.H., Yan, W.F., Meng, R.J. and Liang, Q. 2016. Influence of coexistent ions Fe^{3+} and Mn^{2+} on arsenic (iii) adsorption behaviour onto river sediment. Nature Environment & Pollution Technology, 15: 305-310.

Li, H.S., Chen, Y.H., Long, J.Y., Jiang, D.Q., Liu, J., Li, S.J., Qi, J.Y., Zhang, P., Wang, J., Gong, J., Wu, Q.H. and Chen, D.Y. 2017. Simultaneous removal of thallium and chloride from a highly saline industrial wastewater using modified anion exchange resins. Journal of Hazardous Materials, 333: 179-185.

Li, H.S., Li, X.W., Xiao, T.F., Chen, Y.H., Long, J.Y., Zhang, G.S., Zhang, P., Li, C.l., Zhuang, L.Z. and Li, K.K. 2018. Efficient removal of thallium(I) from wastewater using flower-like manganese dioxide coated magnetic pyrite cinder. J. Chemical Engineering Journal, 353: 867-877.

Liu, Y.L., Wang, L., Wang, X.S., Huang, Z.S., Xu, C.B., Yang, T., Zhao, X.D., Qi, J.Y. and Ma, J. 2017. Highly efficient removal of trace thallium from contaminated source waters with ferrate: Role of *in situ* formed ferric nanoparticle. J. Water Research, 124: 149-157.

Memon, S.Q., Memon, N., Solangi, A.R. and Memon, J.U.R. 2008. Sawdust: A green and economical sorbent for thallium removal. J. Chemical Engineering Journal, 140: 235-240.

Pan, J.M., Yao, H., Li, X.X., Wang, B., Huo, P.W., Xu, W.Z., Ou, H.X. and Yan, Y.S. 2011. Synthesis of chitosan/γ-Fe2O3/fly-ash-cenospheres composites for the fast removal of bisphenol A and 2, 4, 6-trichlorophenol from aqueous solutions. Journal of Hazardous Materials, 190: 276-284.

Pu, Y.B., Yang, X.F., Zheng, H., Wang, D.S., Su, Y. and He, J. 2013. Adsorption and desorption of thallium(I) on multiwalled carbon nanotubes. J. Chemical Engineering Journal, 219: 403-410.

Rahmani, A., Mousavi, H.Z. and Fazli, M. 2010. Effect of nanostructure alumina on adsorption of heavy metals. J. Desalination, 253(1-3):94-100.

Rajesh, N. and Subramanian, M.S. 2006. A study of the extraction behavior of thallium with tribenzylamine as the extractant. J. Hazard. Mater., 135: 74-77.

Rathinam, K., Singh, S.P., Arnusch, C.J. and Kasher, R. 2018. An environmentally-friendly chitosan-lysozyme biocomposite for the effective removal of dyes and heavy metals from aqueous solutions. J. Carbohydrate Polymers, 199: 506-515.

Saad, A.H.A., Azzam, A.M., El-Wakeel, S.T., Mostafa, B.B. and El-latif, M.B.A. 2018. Removal of toxic metal ions from wastewater using ZnO@ Chitosan coreshell nanocomposite. J. Environmental Nanotechnology, Monitoring & Management, 9: 67-75.

Salam, O.E. A., Reiad, N.A. and EIShafei, M.M. 2011. A study of the removal characteristics of heavy metals from wastewater by low-cost adsorbents. Journal of Advanced Research, 2(4): 297-303.

Saljooghi, A.S. and Fatemi, S.J. 2011. Removal of thallium by deferasirox in rats as biological model. Journal of Applied Toxicology, 31: 139-143.

Tran, H.N., You, S.J., Hosseini-Bandegharaei, A. and Chao, H.P. 2017. Mistakes and inconsistencies regarding adsorption of contaminants from aqueous solutions: A critical review. J. Water Research, 120: 88-116.

Wan, S.L., Ma, M.H., Lv, L., Qian, L.P., Xu, S.Y., Xue, Y. and Ma, Z.Z. 2014. Selective capture of thallium(I) ion from aqueous solutions by amorphous hydrous manganese dioxide. Chemical Engineering Journal, 239: 200-206.

Wen, Y., Tang, Z.R., Chen, Y. and Gu, Y.X. 2011. Adsorption of Cr(VI) from aqueous solutions using chitosan-coated fly ash composite as biosorbent . Chemical Engineering Journal, 175: 110-116.

Wick, S., Baeyens, B. and Fernandes, M.M. 2018. Thallium adsorption onto illite. J. Environmental Science & Technology, 52: 571-580.

Xiao, T.F., Yang, F., Li, S.H., Zheng, B.S. and Ning, Z.P. 2012. Thallium pollution in China: A geoenvironmental perspective. J. Science of the Total Environment, 421-422: 51-58.

Xiong, C.H., Pi, L.L., Chen, X.Y., Yang, L.Q., Ma, C.N. and Zheng, X.M. 2013. Adsorption behavior of Hg^{2+} in aqueous solutions on a novel chelating cross-linked chitosan microsphere. J. Carbohydrate Polymers, 98(1): 1222-1228.

Yang, K., Wang, G., Chen, X.M., Wang, X. and Liu, F.L. 2018. Treatment of wastewater containing Cu^{2+} using a novel macromolecular heavy metal chelating flocculant xanthated chitosan. J. Colloids and Surfaces A: Physicochemical and Engineering Aspects, 558: 384-391.

Zhang, G.S., Fan, F., Li, X.P., Qi, J.Y. and Chen, Y.H. 2018. Superior adsorption of thallium(I) on titanium peroxide: Performance and mechanism. Chemical Engineering Journal, 331:471-479.

Zhang, L., Huang, T., Zhang, M., Guo, X.J. and Yuan, Z. 2008. Studies on the capability and behavior of adsorption of thallium on nano-Al_2O_3. J. Journal of Hazardous Materials, 157: 352-357.

Zolgharnein, J., Asanjarani, N. and Shariatmanesh, T. 2011. Removal of thallium(I) from aqueous solution using modified sugar beet pulp. J. Toxicological and Environmental Chemistry, 93: 207-214.

Nature Environment and Pollution Technology
An International Quarterly Scientific Journal

p-ISSN: 0972-6268
e-ISSN: 2395-3454

Vol. 19 | No. 1 | pp. 17-28 | 2020

Original Research Paper | Open Access

Assessment of Seasonal and Spatial Variation of Groundwater Quality in the Coastal Sahel of Doukkala, Morocco

Imane EL Adnani†, Abdelkader Younsi, Khalid Ibno Namr, Abderrahim El Achheb and El Mehdi Irzan
Laboratory of Geosciences and Environment Techniques, Chouaib Doukkali University, Faculty of Sciences, Ben Maachou Road, B.P. 20 Avenue des Facultés, El Jadida, Morocco
†Corresponding author: Imane EL Adnani

Nat. Env. & Poll. Tech.
Website: www.neptjournal.com

Received: 09-04-2019
Accepted: 02-07-2019

Key Words:
Groundwater quality
Variability
Sahel of Doukkala

ABSTRACT

The current research is set in the context of the impact of climate change at the regional level, particularly focused on seasonal variations and their influence on the physico-chemical characteristics of groundwater in the rural and urban areas of coastal Sahel of Doukkala. The main objective of this study was to evaluate the quality to explain the phenomena at the origin of the mineralization of groundwater. Two measurement campaigns of sampling were carried out on 30 wells, in 2016 and 2018 (dry and wet season). The water points were piezometrically surveyed. In situ, the same water points were measured for temperature, pH, and electrical conductivity, using a multiparameter conductivity meter and a pH meter. The chemical analysis was carried out at the Laboratory of Geosciences and Environmental Technics using volumetry (Ca^{2+}, Mg^{2+}, Cl^- and HCO_3^-) and spectrophotometry methods (SO_4^{2-}, Na^+ and K^+); total dissolved solids (TDS) were computed by multiplying the EC by a factor (0.55 to 0.75), depending on relative concentrations of ions. Total hardness (TH) was calculated by taking the differential value between Mg^{2+} and Ca^{2+}. For the reliability of the results obtained, we proceeded to the application of the ionic balance. The obtained water quality data was subjected to multivariate statistical techniques to evaluate homogeneity and heterogeneity between sampling water and to differentiate water quality variables for temporal variations.The elements are all significantly different among seasons. The dry season was positively associated with EC, TDS, Cl^-, Na^+, SO_4^{2-} and K^+ and negatively associated with temperature, and pH. The wet season was in contrast associated with high values of NO_3^- and pH. These results show that the majority of well water in the study area represents strong mineralization that far exceeds standards, especially during the dry period, with an average EC of 416.04 µS/cm, while the wet season is lower at 382.6 µS/cm. The hydrochemical classification of water from the Piper diagram revealed only one hydro facies, which is the chlorinated sodium facies. In conclusion, the variability of groundwater quality could be explained by the fact that in the dry season, there is concentration and in the wet season, there is ionic dilution and may also reflect the effect of anthropogenic activity.

INTRODUCTION

The challenge in the coming years is undoubtedly to ensure the sustainable management of water resources without hindering economic and social development. Globally, groundwater is one of the most precious sources of natural resources. Groundwater contributes to 80% of rural domestic water needs and 50% of urban water needs. According to World Health Organization (2011), 80% of diseases in human beings are caused by water. Problems associated with groundwater exploitation include the following: declining water tables, wells running dry (seasonality) increasing pumping costs, competitive deepening of wells, groundwater subsidence, loss of wetlands and flowing springs and rivers, salt water intrusion, groundwater degradation from natural toxins (fluoride and arsenic, spreading or leaking of anthropogenically used substances from point and non-point sources (FAO 2003, Richardson et al. 2004).

In fact, this vital resource no longer seems to meet today's growing population demand and development needs. This water deficit is caused in particular by the growth in water needs and its irrational use, as well as climate change (UNESCO 1987). In addition, these climatic variabilities have led to a disruption in the frequencies and intensities of precipitation and periods of drought (Berdai 1997). The succession of extremely loss-making and/or extremely surplus years (high and rapid rises) favours soil erosion and subsequently accelerates the transfer of surface pollution to watercourses and then to underground aquifers, which in turn deteriorates water quality. This water problem is therefore aggravated by the almost regular decrease in rainfall over the past fifty years,

seasonal irregularities, the rapid increase in desertification and the progressive degradation of environmental factors (Ahoussi et al. 2012). In fact, estimates made by UNESCO in 2003 indicate that globally groundwater provides about 50% of current potable water supplies,40% of the demand of self-supplied industry and 20% of water use in irrigated agriculture. Groundwater is the most realistic water supply option in much of Africa to meet dispersed rural demand (Foster et al. 2000).

In a country with limited water resources, such as Morocco, where the hydrological context is marked by spatial and temporal variability, the water problem is becoming increasingly worrying (Agoussine & Bouchaou 2004). In addition, groundwater is a very slow-running reservoir and its use for drinking water supply and irrigation purposes may lead to its depletion.

At the regional level, a number of studies on groundwater with respect to drinking and irrigation purposes have been carried out in the different parts of the region (Ambroggi & Thuille 1952, Gigout 1952,1955, Ferre 1969, Ferre et al. 1975, Chtaini 1987, Fakir 1991, Fakir et al. 2003, DRPE 1992, DRHT 1994, Souhel et al. 2000, El Achheb 2002, El Achheb 2003, Chofqi 2004, Hilali 2002, El Hasnaoui et al. 2006, Kaid Rasou 2009, Oulaaross 2009, El Hasnaoui et al. 2011, Fadili et al. 2012), but little work on the effect of seasonal changes on the qualitative aspect of groundwater has so far been done in the rural and urban area of coastal Sahel of Doukkala.

Human activities in our study area are constantly increasing, increasing water consumption and consequently hindering polluting discharges. In agricultural areas, the need to increase production in order to meet food needs requires the intensification of irrigation and the use of agricultural products (fertilizers and pesticides...). This promotes the leaching of excess products from the products used and their transfer to groundwater (El Achheb 2002). The multiplication of industrial activities, for its part, generates multiple pollutants of very varied nature and severity (toxic substances, heavy metals, etc.), thus threatening the sustainability of environmental systems as a whole (El Hasnaoui et al. 2006), especially since the region is considered for the coming years to be Morocco's second largest industrial centre. The industrial image of this region is characterized by the weight of the chemical (Jorf Lasfer OCP complex), agri-food (e. g. sugar factories, dairy and pharmaceutical units) industries (Souhel et al. 2000).

A more complete diagnosis of the current situation of the contamination and a rigorous follow-up of its evolution, are of great necessity for the safeguarding of this resource. It is with this in mind that our work aims to assess the seasonal quality of well water in the Doukkala coastal Sahel, in order to explain the phenomena that cause the mineralization of these waters.

The goal of this study is to assess the spatiotemporal variation of physico-chemical water quality parameters within the aquifer of the Sahel coastal of Doukkala, especially since in this area the population is mainly rural, increasingly turning to well water (most of which is damaged or abandoned) and using it for domestic needs, ignoring the quality of these resources.

According to this study we hypothesized that during the dry season when the input of water is low, most water quality chemical parameters would have higher concentrations (as compared to the wet season) due to resuspension, absence of dilution, and increased evaporation. We also hypothesized that water quality would vary spatially throughout the aquifer, with the highest concentrations of terrestrially derived pollutants (like nitrate, sulphate...) are found near the agricultural areas, the controlled landfill and both the industrial area which are the main sources. So, these spatiotemporal variations are essentially caused by the intensification of agricultural, climate variability, industrial and domestic activities.

It is essential to have a good knowledge of the nature and the chemistry of groundwater variations that can occur as a result of physical processes and anthropogenic activities. It is expected that this type of study will guide proponent's groundwater development projects, especially in the developing countries, point the need for intensified efforts to cope with the different types of imbalances.

MATERIALS AND METHODS

Study Area Description

The study area is part of the coastal Sahel basin of Doukkala which belongs to the Western Moroccan Meseta. It lies between latitudes 33°2.451' and 33°15.798' N and longitudes 8°29.150' and 8°39.082' W. The area is bordered southwest by the municipality of Sidi Abed, south east by the municipality of Sebt des Oulad Aissa and on the northwest by the Atlantic Ocean. This region covers an area of 195 km^2, includes an urban area (the city of El Jadida) and an industrial complex (Jorf Laasfar) (Fig. 1).

Climatic Setting

Climate is semi-arid with minimum temperature of 18°C in winter and maximum temperature of 23°C in summer. The average rainfall is 380.08 mm.

According to unpublished data of the regional direc-

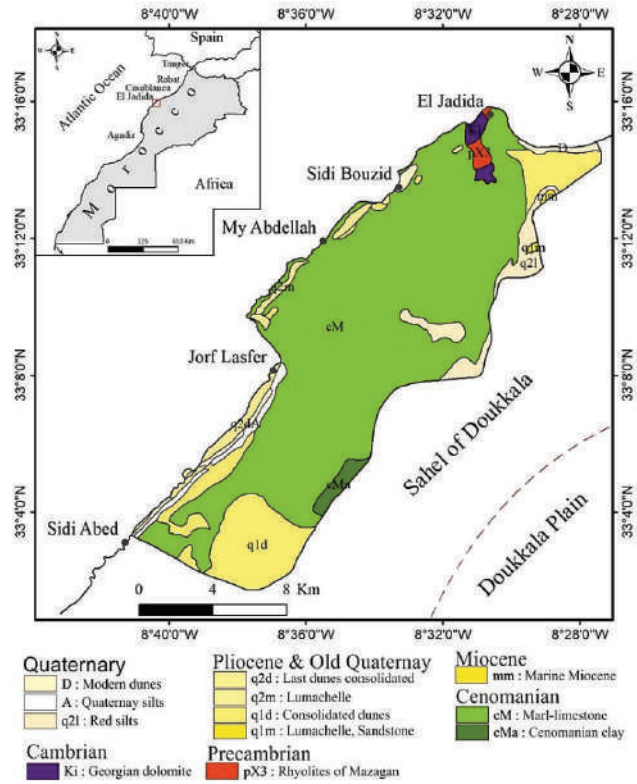

Fig. 1: Location and geology simplified map of the study area (Ferré & Ruhard 1975, Oulaarous 2009).

torate of agriculture, from the year 2016-2018, the average annual rainfall in El Jadida station was 400 mm with a minimum of 0 mm recorded in June, July and August respectively in 2016 and 2017. The maximum monthly rainfall (139 mm) was occurred during March. In terms of the regional rainfall variability, 2018 is a rainy year compared to 2016. Seasonal fluctuations in water levels during 2016-2018 correspond to rainfall (DRH 2016-2018) (Fig. 2).

Geological and Hydrogeological Setting

The study area consists of highly varied geological formations such as of limestone and marl formations of Cenomanian (Cretaceous) age (Fig. 3), resting in angular discordance on the basal Palaeozoic monoclinal dolomites (El Achheb 2002).

Rainfall is the main recharge source for groundwater in the area. The Cenomanian formations represent the most extensive aquifer at the study area (Ferré & Ruhard 1975). The calcareous layers form a fractured and karstic aquifer which is up to 100 m thick.

Test pumping in the vicinity of El Jadida revealed permeability values in the range of 5×10^{-6} to 10^{-5} m/s for the studied aquifer (Souhel & El Achheb 2000).

Experimental Setup and Methods

Groundwater samples collected from 30 dug wells in June during a period of two years 2016 and 2018, covering both wet and dry periods (Fig. 4), these water points are located in urban and rural areas characterized by different activities (agricultural, industrial...). The water samples were taken according to Rodier's techniques (1984), collected in prewashed (with detergent, diluted HNO_3 and double de-ionized distilled water, respectively). Prior to sampling, all the sampling containers were rinsed thoroughly with the groundwater, filled with refusal (to avoid the formation of air bubbles) and kept at low temperature (2-4°C).

Field samples were analysed immediately for hydrogen ion concentration (pH), temperature and electrical conductivity (EC), using a HACH multiparameter conductivity meter, model 44 600 and a WTW pH meter, pH 522 with combined electrode.

Other parameters were later analysed in Laboratory of Geosciences and Environmental Techniques of Chouaïb Doukkali University. These parameters include important

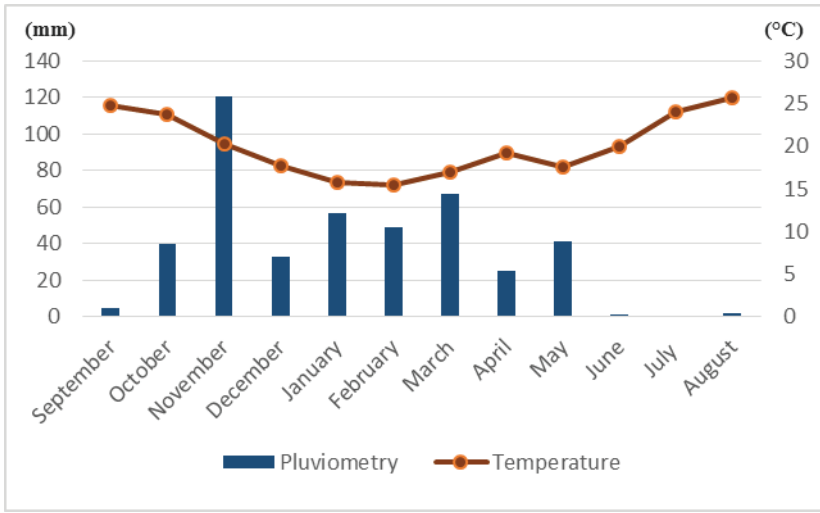

Fig. 2: Monthly variation of pluviometry and temperatures at El Jadida station between 2015 and 2018 (C.P.M).

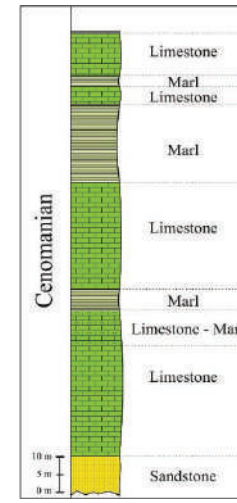

Fig. 3: Portion of the synthetic stratigraphic log of the Cenomanian of the study area (D.R.H 1990).

cations such as calcium (Ca^{2+}), magnesium (Mg^{2+}), sodium (Na^{+}), potassium (K^{+}) as well as anions such as bicarbonates (HCO_3^{-}), chlorides (Cl^{-}) and sulphates (SO_4^{2-}). Total dissolved solids (TDS) were computed by multiplying the EC by a factor (0.55 to 0.75), depending on relative concentrations of ions (Sudhakar et al. 2013). Total hardness (TH) was calculated by taking the differential value between Mg^{2+} and Ca^{2+} (ISO 1984), these two elements were analysed titrimetrically, using standard EDTA. Sodium (Na^{+}) and potassium (K^{+}) were measured, using a flame photometer. Bicarbonate (HCO_3^{-}) were estimated by titrating with H_2SO_4. Chloride (Cl^{-}) was determined titrimetrically by standard $AgNO_3$ titration. Sulphate (H_2SO_4) and nitrate (NO_3^{-}) were analysed, using spectrophotometer. All parameters are expressed in milligrams per litre (mg/L) and milliequivalents per litre (meq/L), except pH (units) and EC. The EC is expressed in microsiemens per centimetre (µS/cm) at 25°C.

For the reliability of the results obtained, we proceeded to the application of the ionic balance (taking the relationship between the total cations and the total anions) and an error of 10% was accepted (Domenico & Schwartz 1998, Rodier 2009).

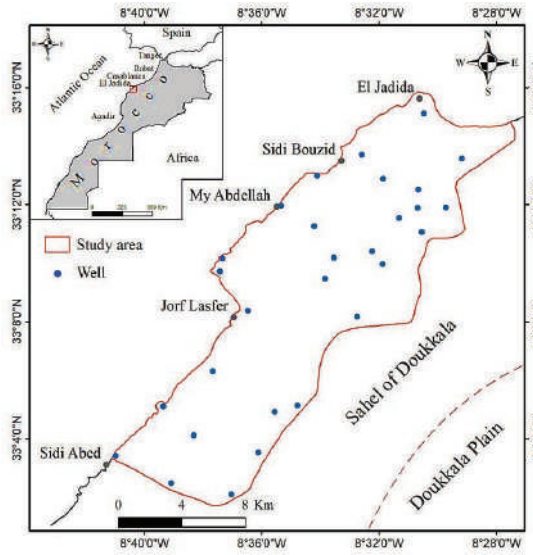

Fig. 4: Location of sampling points in the study area

The processing of the collected physico-chemical data was carried out using multivariate hydrochemical and statistical methods. The hydrochemical method required the use of the Piper diagram for hydrochemical classification. The statistical approach that has been used to study the phenomena underlying water mineralization, water aggregation and identify the factors responsible for these aggregations is based on multivariate statistical techniques. The statistical analysis was carried out on 30 descriptors and all parameters (13 variables) in wet and dry periods. Concentration differences for each water quality variable between the wet and dry season were examined using the Mann-Whitney U test, and differences among seasons were examined using one-way ANOVA, both at a significance level of $p < 0.05$.

The box plot analysis was used to assess temporal variability in water quality parameter concentrations based on the median, minimum, maximum, and 25th and 75th percentile values (Dou et al. 2016). The reservoir water quality variables were also subjected to multivariate statistical techniques using principal component analysis (PCA), which is one of the most commonly used multivariate statistical techniques. Its purpose is therefore to establish a relationship between the various physico-chemical parameters and to better assess the effect of anthropogenic activities on the quality of the groundwater sampled (Quinn & Keough 2002). The statistical analysis was performed using Statgraphics 16.1 software and IBM SPSS statistics 20.

The application of all these different methods made it possible to assess seasonal quality in order to explain the phenomena responsible for variations in groundwater mineralization in our study area.

RESULTS

From Table 1, the results of the physico-chemical analyses of water samples are shown and the WHO prescribed guideline used in the description of groundwater quality characteristics in the study area.

Spatial descriptive statistics result of the analysed parameters showed that there are parameters that express significant changes during the study period, indicating spatial variability of chemical composition among sampling sites (Table 1) for wet and dry seasons, respectively.

83.33% of the water analyses carried out in two seasons have an ionic balance of less than 5%, so these analyses are satisfactory. However, 16.67% of the analyses carried out on groundwater have an ionic balance of between 5 and 10%, so these analyses are of acceptable quality.

WHO- World Health Organization, SD- Standard deviation, CV- Coefficient of variation, WT- Water temperature TH- Total hardness, EC- Electrical conductivity, TDS- Total dissolved solids

The pH values of groundwater varied from 7.2 to 8.65 during dry season and 7.1 to 8.3 during wet season. EC values ranged from 101.9 to 955 μS/cm during dry season whereas during wet season it was 82-86.1 μS/cm. Respective minimum and maximum TDS values observed were

Table 1: Descriptive characteristics of physico-chemical parameters of groundwater quality for wet and dry seasons in the study area.

	WHO standards	Dry season					Wet season				
Parameters		Min	Max	Mean	SD	CV	Min	Max	Mean	SD	CV
pH	6.5 - 9.5	7.2	8.65	7.77	0.33	4.31	7.1	8.3	7.69	0.34	4.42
WT (*°C*)	< 25	21.4	24.8	22.7	0.92	4.04	19.4	24.1	21.87	1.33	6.08
TH (mg/L)		2.5	129.14	37.06	25.5	68.81	10.5	114.25	35.68	23.67	66.33
EC (*µS/cm*)	> 400	101.9	955	416.04	215.46	5178.7	82.8	86.1	382.6	196.96	5147.77
TDS (mg/L)		50.95	477.5	208.02	107.73	2589.4	41.4	429.95	191.30	98.47	5147.77
Ca^{2+} (mg/L)	< 100	16	372	128.57	83.21	64.72	28	420	165	99.51	60.31
Mg^{2+} (mg/L)	< 50	1.2	460	100.77	99.06	98.31	3.6	296.4	76.96	72.85	94.67
Na^{+} (mg/L)	< 150	220	3066	695.17	623.47	89.68	81	1500	541.84	335.28	61.88
K^{+} (mg/L)	< 12	3.8	31.5	12.47	6.66	53.38	5.1	75	18.9	14.25	75.44
HCO_3^{-} (mg/L)		158.6	890.6	443.43	163.01	36.76	183	671	370.88	115.81	31.22
Cl^{-} (mg/L)	< 200	221.9	2644.75	1061.45	689.47	64.95	272.75	2502.8	994.58	616.02	61.93
SO_4^{2-} (mg/L)	< 250	25.64	454.59	112.42	91.89	81.73	41.61	714.54	264.19	190.23	72
NO_3^{-} (mg/L)	< 50	6.76	165.93	52.02	37.04	71.2	9.6	383.62	69.97	76	108.62

41.4 and 477.5 mg/L during wet season and 50.95-429.95 mg/L during dry season. The total hardness ranged from 2.5 to 129.14 mg/L during the dry season and 10.5 to 114.25 mg/L during wet season. During both seasons, concentrations of major elements exceed the permitted limits (WHO). For nitrate, the highest value was 383.62 mg/L during the dry season and 165.93 mg/L during the wet season. The results of analyses show that the highest concentration of Cl^- was recorded at dry season with a value of 2644.75 mg/L and with a minimum of 221.9, but in the wet season, concentrations fluctuate between 272.75 and 2502.8 mg/L. In the case of sulphates, the variations in concentrations are in the order of 25.64 to 454.59 during the dry season, and 41.6 to 714.54 mg/L during the wet season.

Groundwater has highly variable sodium concentrations during two seasons. In wet season, they range from 81 mg/L to 1500 mg/L with an average concentration of 541.84 mg/L, but in dry season, it varies between 220 and 3066 mg/L with an average of 695.17 mg/L.

The distributions of pH, EC, TDS, TH, the major elements in both seasons are presented as a projection graph resulting from the analysis of the principal component (Figs. 5 and 6).

Analyses of the Principal Component

During the wet season, the principal component analysis extracted 80.24% of the variance of that season's data (Fig. 5a). Of this, the first factor (PC1) extracted 57% of the variance and was correlated positively with all variables (CE, TDS, Cl^-, TH, Mg^{2+}, Na^+) with a lesser degree of NO_3^- and K^+. In its negative part, PC1 is controlled by the variable WT, HCO_3^- and pH. The group of variables Ca^{2+}, Mg^{2+} reflects the calcium and magnesium mineralization acquired as a result of water-rock interactions. On the other hand, the group of variables K^+ and NO_3^- seems to characterize a change that would occur near the soil surface. These variables have a superficial origin and reflect anthropogenic pollution. The grouping of these variables in the positive part of the PC1 factor means that these chemical variables are acquired after a slow residence time. This grouping expresses mineralization related to agricultural activities. The factor PC1 is determined by the variable SO_4^{2-} in its positive part to which the pH is opposed and to a lesser degree the temperature (T°C). The PC1 factor is considered as a mineralization axis of both natural (water-rock contact) and anthropogenic origin.

The second factor (PC2) explained 22% of the variance (Fig. 5a), positively correlated with HCO_3^-, Mg^{2+}, NO_3^-, K^+ and pH. The most correlated variables are NO_3^- and K^+ which represent the surface parameters that are found at depth due to infiltration. Indeed, these parameters would come mainly from fertilizers used in agricultural activities.

However, factor PC2 provides information on the spatial origin of ions through direct infiltration of surface water and both anthropogenic degradation from agricultural sources, then the PC2 is an indicator of surface inputs.

The projection of individuals in the factorial plane PC1-PC2 (Fig. 5b) shows 3 classes. Class 1 takes into account all highly mineralized waters in the study area. Class 2 includes all waters with low mineral content and high pH content. Class 3 contains waters rich in bicarbonates and sulphates.

During the dry season, the representation of the data

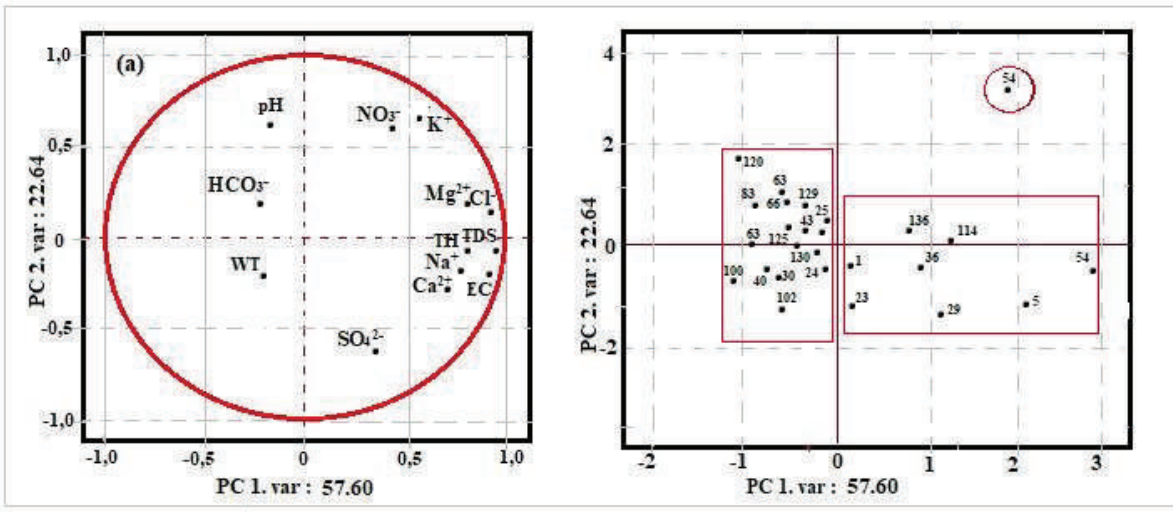

Fig. 5 (a): Wet season PCA analysis and (b) a graph of statistical units in the PC1-PC2 factorial design of study area.

in the factorial plane PC1-PC2 expresses 81.01% of the total variance of the point cloud including 53.79% for the factor PC1 (Fig. 6a). The physico-chemical parameters: CE, TDS, Mg^{2+}, TH, Cl^- and K^+ are well correlated with each other and have a significant weight in the prevalence of the phenomenon represented by PC1. The CE and TDS elements are characteristic of the natural mineralization of water in its host (Murdey & Blavoux 1986), while Cl^- and Mg^{2+} reflect induced mineralization. In this case, this axis expresses the residence time of the elements; it is an indicator of mineralization (Hani et al. 1997).

PC2 explained 27% and was determined by NO_3^- but also by HCO_3^- and Na^+. These parameters are inversely correlated to Ca^{2+} and SO_4^{2-}. The factor PC2 reflects the environmental conditions and their influence on the chemical variations of the water and represents the surface inputs. It is also an indicator of natural (HCO_3^-) and induced (NO_3^-) mineralization (Fig. 6a).

The projection of individuals in the factor plane PC1-PC2 (Fig. 6b), shows three classes. Class (1) is composed of a single water point rich in nitrates and characterized by a low sulphate content. Class (2) consists of highly miner-

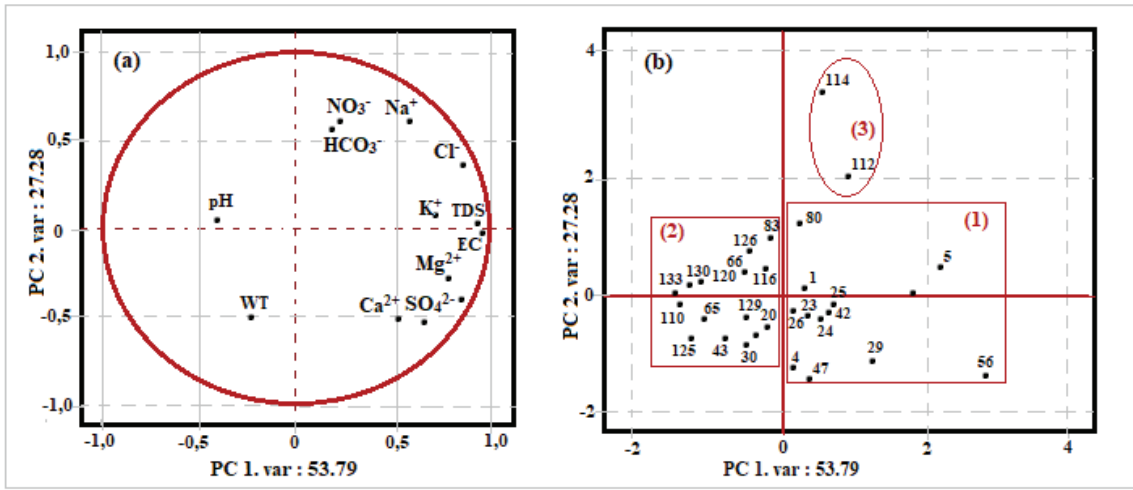

Fig. 6 (a): Dry season PCA analysis and (b) a graph of statistical units in the PC1-PC2 factorial design of study area.

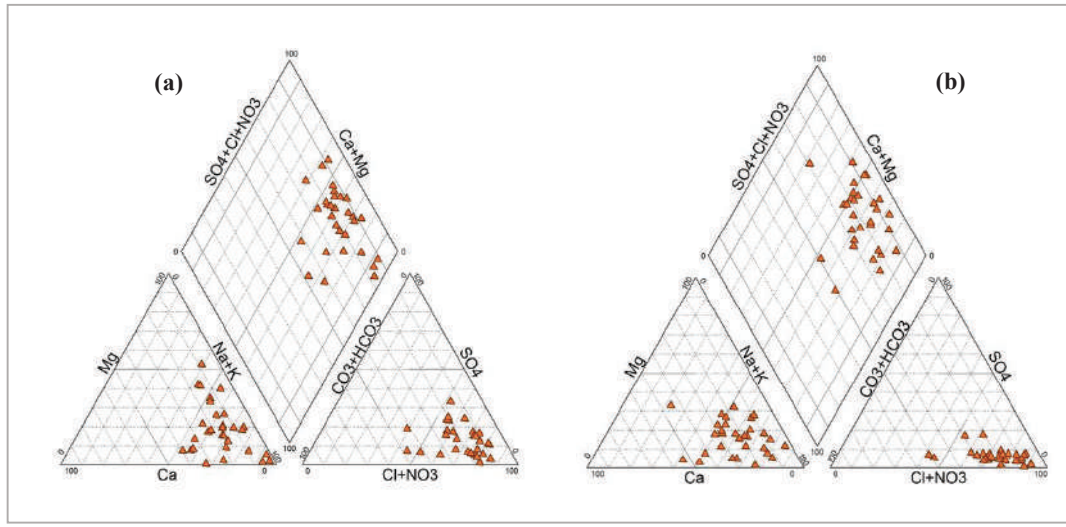

Fig. 7: Classification of well water using the Piper diagram in the dry (a) and wet (2) season.

alized waters whose ionic acquisition is under the control of mineralization-residence time. Class (3) is located in the negative part of factor 1 and includes waters with low mineral content.

Hydrochemical Classification

In order to determine the chemical facies of the waters of the studied aquifer, we used a Piper diagram (Eblin 2014) which indicated that hydrochemical classification of the groundwater sampled (Figs. 7a and 7b) shows only one facies: the chlorinated sodium facies.

DISCUSSION

We found that there was a distinct seasonal pattern in water quality of the study area. The most parameters were higher during the dry season in contrast to the wet season.

Water temperature: The variations in water temperature show that in the wet season the temperature of groundwater is lower than in the dry season (Fig. 8a). This observed increase in the dry season is most likely associated with an elevation in surface water temperature due to the higher air temperature.

Temperature variations are strongly influenced by environmental conditions related to the geographical location of the locality, the geology of the terrain crossed, the hydrology of the ecosystem and especially the climate (Rodier 1984). In both, the dry and wet seasons, the lowest temperature values were obtained either early or late in the day. Indeed, previous studies by Reggam et al. (2015) in Algeria and Makhoukh et al. (2011) in Morocco have shown high temperature values during the dry season and the lowest during the wet season.

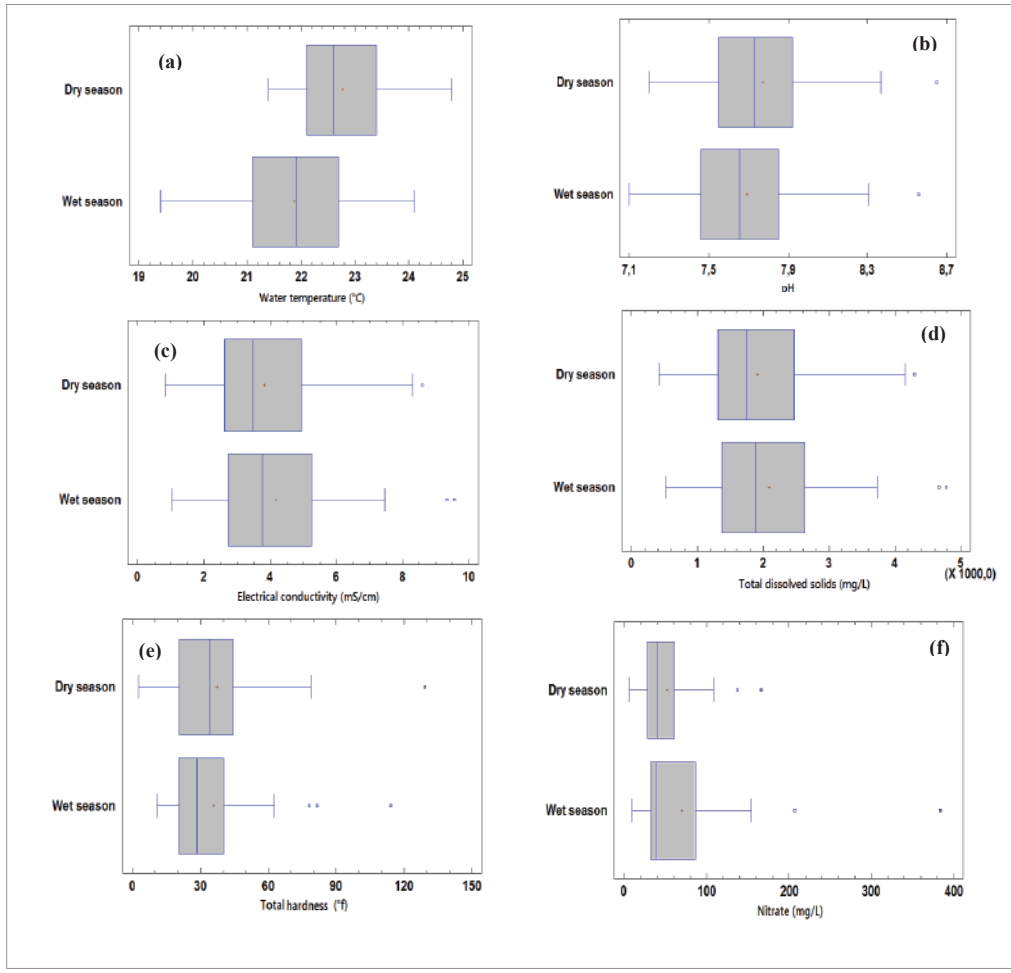

Fig. 8: Box and whisker plot of seasonal variation of water quality parameters. Water temperature (a), pH (b), Electrical conductivity (c), Total dissolved solids (d), Total hardness (e), Nitrate (f), Small red squares represent the median values, boxes represent the interquartile range, plus signs represent the extremes, small blue dots represent the outliers, and range bars show the maximum and minimum values.

Therefore, the water temperature must be determined because it is used as a good measure of contamination because it has a marked effect on bacteria and chemical reaction rates in the water (Mink 1964, Dixey 1972, Hutton 1983).

pH: The measurement of pH is one of the most frequently used tests in water chemistry (Hem 1985). The results of analyses of water samples show pH of groundwater is all within the WHO allowable limit of 7-9.2.

The high pH value during the dry season (Fig. 8b) could be due to the low water level during the dry season causing a concentration of base cations, or an excess of primary productivity over respiration during that season, consuming CO_2 and reducing H^+. Further, the study area also encompasses extensive agricultural fields. Another reason for the observed low pH values could be thus related to the use of acid producing fertilizers like ammonium sulphate and super phosphate of lime as manure for agriculture use (Raghunath et al. 2001), especially that the study area also includes extensive agricultural fields is particularly important (El Adnani et al. 2018).

Electrical conductivity (EC): The EC mean values were observed to be statistically highest in dry season, in contrast to the wet season. The distribution of EC values is presented in Fig. 8c.

The occurrence of high EC values in the study area might also be due to addition of some salts through the prevailing agricultural activities (El Achheb 2002). Comparatively zones with low EC values (<100µS/cm) are due to dilution of soluble salts by rainfall (Raghunath et al. 2001).

The EC of most of the groundwater samples showed decreasing trend in wet season (Fig. 8c) and magnitude of decrease might have been influenced by rainfall characteristics, geology, soil and land use activities, topography of the area and its drainability (Laluraj et al. 2006).

Total dissolved solids (TDS): The concentration of total dissolved solids in groundwater are noted to be higher in wet season than in dry season (Fig. 8d). This is consistent with the findings of Bowell et al (1996) and Efe et al. (2005).

During the dry season, the increased concentration of TDS may be associated with evaporation and the absence of a dilution effect, while the lower values during the wet season are hypothesized to be due to dilution from the tributaries.

The low mineralization of groundwater during the rainy season is due to dilution by rainwater input as the majority of wells are not constructed and receive runoff directly (Laluraj et al. 2006), or it could be due to the hydrogeological properties of rocks (a strong influence on the extent of water/rock reaction). Zones with high groundwater-flow velocities usually will have relatively low dissolved solids because of the shorter groundwater- rock contact time and high water/rock ratios, and vice-versa (Langmuir 1997).

EC and TDS were common for both wet and dry (Figs. 8c and 8d). There was a highly significant positive correlation of TDS with EC both in the wet and the dry season ($r = 0.99$ at $p < 0.01$).

Total hardness (TH): The seasonal variation shows that hardness is lower during wet season (Fig. 8e), probably due to strong dilution, which can be explained by the solvent action of rainwater coming in contact with soil and especially with the rocks characterizing our study area such as limestone and marl limestone formations (Fig. 3) (Souhel et al. 2000) rocks is capable of dissolving calcium and magnesium that promote water hardness.

Although, water harness has no harmful on human health except that it can react with ordinary soap to form scum, plume solvent, scale formation in boilers and in hot water systems (Maxwell et al. 2012).

Nitrate: It is evident that concentration of nitrate was quite variable from season to season. The high values of NO_3^- during the wet season (Fig. 8f) returns to the high rate of precipitation that facilitate infiltration of the amount of fertilizer applied.

The spatial variation in nitrate content in groundwater might be due to different degrees of evaporation/recharge, amount of fertilizer applied, anthropogenic activities, microbial reactions, nature of vegetation cover and adsorption/desorption processes in the soil system (Datta et al. 1996, 1997, Martin et al. 2006).

Chloride: The seasonal variations of chloride show an increase during the dry season compared to the wet season (Fig. 9a) which can be attributed to the local environment of the wells or the chemical composition of the groundwater is strongly affected by excess fertilizer spread over the last 20 years, in particular, chloride (from potassium fertilizers) (El Adnani et al. 2018).

The weakness of chlorides in the wet season is mainly related to the extent and intensity of precipitation during that season. Chloride levels in open pit and borehole waters indicate that seawater in the region has a significant influence on the salt content of groundwater resources, particularly the leaching of salt crystals from aerosols and sea spray (Younsi et al. 2001). The chloride content of water is an indication of the intrusion of seawater. The levels of chloride in open-well and borehole waters indicates that

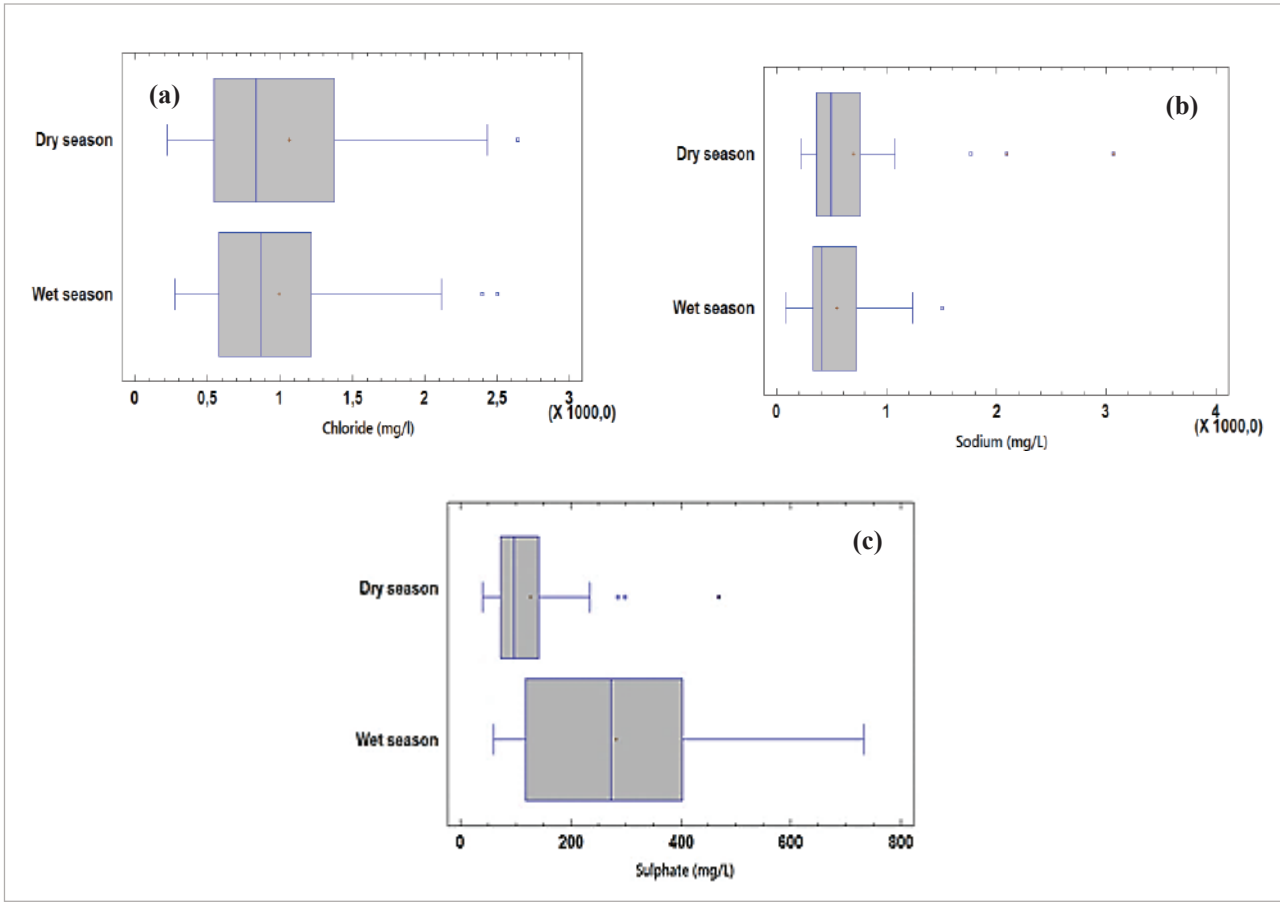

Fig. 9: Box and whisker plot of seasonal variation of water quality parameters. Chloride (a), Sodium (b) and Sulphate (c).

sea water within the area has a great influence on the salt content of the underground water resources (Efe et al. 2005, Maxwell et al. 2012).

Sodium: The reduction in the current study of the concentration of sodium during the wet season (Fig. 9b) may be associated with dilution by rainwater.

As noted above, the potential source of the Na+ in water may be related to leaks of leachate from CET to studied water (El Adnani et al. 2018), or other sources can be cited, such as leaching of NaCl crystals from sea spray with over-concentration by the possible effect of evaporation, recirculation of saline drainage waters in agricultural sectors (Younsi et al. 2001).

Sulphate: The results of analyses show that the highest concentration of SO_4^{2-} was recorded at the wet season (Fig. 9c). A significant difference in sulphate concentrations was observed for both seasons which can be explained by the fact that rainwater seems to contain more sulphates than water from wells and boreholes. This may result from high level combustion of sulphur-containing hydrocarbon emissions in the study area, specifically in the vicinity of the industrial area (El Hasnaoui et al. 2006, 2011). Oxidation of sulphur containing compounds after rainwater water has been charged to ground water resources may increase the acidity and toxicity of open-well and borehole water resources.

The study of the mechanism for acquiring water chemistry in the study area using multivariate statistical analysis methods made it possible to observe, in a first approach, three main mechanisms responsible for the evolution of groundwater mineralization in the study area. The three main mechanisms are: mineralization, residence time and spatial origin of ions.

The acquisition of ions is essentially through rock-water interactions, which is the important phenomenon in water mineralization. The limestones and marls of the formations dominate the geology of the region and characterize the

Cenomanian aquifer, which explains the dominant Ca^{2+} contents for cations in groundwater.

The acidity of the waters and the abundance of precipitation cause a very intense and complete alteration of the primary minerals of the parent rock by hydrolysis (Eblin et al. 2014). This hydrolysis is, therefore, important in both the rainy and dry seasons. Indeed, in both the rainy and dry seasons, the mineralization of the waters studied is of both natural (water-rock contact) and anthropogenic origin.

In view of the findings revealed by this study, it is recommended that there is necessary to place two meteorological stations in the area for local measurement of precipitation, temperature and evapotranspiration. The risk of contamination by seawater must be controlled, it would therefore be necessary to set up a network of monitoring piezometers (with continuous recording), in order to control the fluctuation of the piezometric surface and to regularly monitor the quality of the groundwater to preserve these resources; to conclude, authorities must be required to authorize the use of low-flow pumps and the generalization of economic irrigation methods such as drip irrigation. Propose changes in agricultural practices and especially monitor effluent treatment at landfills and industrial areas.

CONCLUSION

In this study, the measured parameters showed a seasonal fluctuation, with concentrations mainly higher during the dry season than during the wet season. This assessment provided information on the characteristics of groundwater in the coastal zone of the Sahel of Doukkala. Physico-chemical analyses show that the water is highly mineralized with an average electrical conductivity of 382,6 µS/cm in the wet season and 416,04 µS/cm in the dry season. Multivariate statistical analysis methods indicate that the different processes responsible for the acquisition of groundwater chemistry studied are: the residence time of the water in contact with the rock, the infiltration of substances related to anthropogenic activities (agricultural fertilizers, household and industrial waste...) and the intensity of rainfall.

REFERENCES

Agoussine, M. and Bouchaou, L. 2004. The major problems of water management in Morocco. Science and Planetary Changes/Drought, 15(2): 187-194.

Ahoussi, K. E., Koffi, Y. B., Kouassi, A. M., Soro, G., Soro, N. and Biemi, J. 2012. Physico-chemical and bacteriological characterization of the water resources of localities located near the Ébrié Lagoon in the commune of Marcory (District of Abidjan, Ivory Coast): case of the village of Abia Koumassi. European Journal of Scientific Research, 89(3): 359-383.

Ambroggi, R. and Thuille, G. 1952. Abada-Doukhala. In: Hydrogéologie du Maroc. Notes et Mémoires. Services Géologique Maroc, N° 97.

Berdai, H. 1997. Synthesis of work carried out in Morocco on nitric pollution of groundwater. Studies Division, Testing Experiments and Standardization Service, Rabat.

Bowell, R.J., McEdonney, S., Warren, A. and Bwankuzo, M. 1996. Biogeochemical factors affecting groundwater quality in central Tanzania. Geological Society, London, Special Publications, 113(1): 107-130.

Chofqi, A. 2004. Highlighting the mechanisms of contamination of groundwater by leachate from an uncontrolled landfill (El Jadida-Maroc). Geology, hydrogeology, geoelectric, geochemistry and epidemiology, pp. 184.

Chtaini, A. 1987. Hydrogeological Study of the Doukkala Sahel (Morocco). Doctoral Dissertation, Joseph Fourier University (Grenoble), pp. 157.

D.R.H . 1990. Projet de réalisation des sondages à l'air sur la région des Doukkala, Rabat, Maroc.

Datta, P.S. and Tyagi, S.K. 1996. Major ion chemistry of groundwater in Delhi area: Chemical weathering processes and groundwater flow regime. J. Geolog. Soc. India, 47(2): 179-188.

Datta, P.S., Deb, D.L. and Tyagi, S.K. 1997. Assessment of groundwater contamination from fertilizers in the Delhi area based on 18O, NO_3^- and K^+ composition. Journal of Contaminant Hydrology, 27(3-4): 249-262.

Dixey, F.A. 1972. A Practical Handbook on Water Supply. 2nd edition, Thomas Murby & Co, London.

Domenico, P. A. and Schwartz, F.W. 1998. Physical and Chemical Hydrogeology. Vol. 1, Wiley, pp. 506.

Dou, M., Zhang, Y. and Li, G. 2016. Temporal and spatial characteristics of the water pollutant concentration in Huaihe River Basin from 2003 to 2012, China. Environmental Monitoring and Assessment, 9: 188-522.

DRHT 1994. Elaboration d'un schéma d'exploitation des eaux souterraines du Sahel (Maroc). Rapp. Projet : DRPE-FAO. TCP/MOR/2251.

DRPE 1992. Etude par prospection électrique : Région des Abda et des Doukkala, (21 Mars 1990-10 Juillet 1990, 08 octobre 1992-15 novembre 1992). GEOATLAS. Tome 1: texte et planches.

Eblin, S.G., Soro, G.M., Sombo, A.P., Aka, N., Kambiré, O. and Soro, N. 2014. Hydrochimie des eaux souterraines de la région d'Adiaké (Sud-Est côtier de la Côte d'Ivoire). Larhyss Journal, 17: 193-214.

Efe, S.I., Ogban, F.E., Horsfall, M. and Akporhonor, E.E. 2005. Seasonal variation of physico-chemical characteristics in water resources quality in western Niger Delta region, Nigeria. Journal of Applied Science and Environmental Management, 9(1): 191-195.

El Achheb, A. 2002. Contribution à l'étude de la minéralisation et identification des sources de contaminations des eaux souterraines, application au système aquifère du Bassin Sahel Doukkala (Maroc). Thèse d'état, Univ Chouaïb Doukkali, El Jadida, pp. 206.

El Achheb, A., Mania, J. and Mudry, J. 2003. Mécanismes d'acquisition de la minéralisation des eaux souterraines dans le bassin Sahel des Doukkala (Maroc Occidental). Approche par des traceurs hydrogéochimiques. IGME. Madrid, pp. 113-123.

El Adnani, I., Younsi, A., Ibno Namr, K., El Achheb, A. and Irzan, E.M. 2018. The influence of anthropogenic activities on groundwater quality of southwest region of El Jadida city (Sahel of Doukkala, Morocco), European Journal of Scientific Research, 151: 96-111.

El Hasnaoui, B., Garmes, H., Younsi, A., Mountadar, M. and Mouhab, I. 2006. Problèmes de contamination fluorurée en zone industrielle (Cas du Jorf Lasfar, Maroc). Approche pluridisciplinaire dans le Colloque Internationale, Mines: Exploration, Exploitation et Impact environnementale (M3E), Bouznika, 20-21 Avril, pp. 53.

El Hasnaoui, B., Younsi, A., Mountadar, M., Garmes, H. and Mouhab, I. 2011. Impacts négatifs d'une zone industrielle sur les eaux souterraines et sur le cheptel (Cas du Jorf Lasfar, Maroc): Approches pluridisciplinaires. Déchets sciences techniques, N°59, 2945.

Fadili, A. 2014. Etude hydrogéologique et géophysique de l'extension de l'intrusion marine dans le sahel de l'Oualidia (Maroc): Analyse

statistique, hydrochimie et prospection électrique. Thèse Doct, Univ. Chouaib Doukkali, El Jadida, Maroc., pp. 289.

Fakir, Y. 2001. Caractérisation hydrogéologique et hydrochimique des aquifères côtiers du Sahel de Safi à Oualidia (Méséta côtière- Maroc). Thèse 3éme cycle. Univ. Cadi Ayyad, Marrakech, pp. 143.

Fakir, Y. and Razack, M. 2003. Hydrodynamic characterization of a Sahelian coastal aquifer using the ocean tide effect (Dridrate Aquifer, Morocco). Hydrological Sciences-Journal-des Sciences Hydrologiques, 48(3).

FAO (Food and Agriculture Organization) 1997. Seawater Intrusion in Coastal Aquifers: Guidelines for Study, Monitoring and Control. FAO Water Reports 11. Rome Italy: FAO; 163 p.

Ferre, M. 1969. Hydrologie et hydrogéologie des Abda- Doukkala. Thèse du Docteur Ingénieur- Nancy.

Ferre, M. and Ruhard, J.P. 1975. Les bassins des Abda-Doukkala et du Sahel de Azemmour à Safi. In: Ressources en eau du Maroc. Notes mém. *S*erv. Géol Maroc, 2(231): 261-298.

Foster, S., Chilton, J., Moench, M., Cardy, F. and Schiffler, M. 2000. Groundwater in rural development: Facing the challenges of supply and resource sustainability. World Bank Technical, Washington. Paper No 464.

Gigout, M. 1952. Les ressources en eau souterraine des Doukkala et Abda (Maroc occidental). Rapp. Inéd. Seconde thèse.

Gigout, M. 1955. Enseignement de trois forages sur la stratigraphie du Crétacé des Doukkala. Notes mém. Serv. géol. Maroc, t. 11(123): 44-55.

Hani A, Djarbri L, Mania J. 1997. Etude des caractéristiques physico-chimiques du massif cristallophyllien de Séraïdi (nordest Algérien). Hard Rock Hydrosystems (Proceedings of Rabat Symposium S2 1997). IAHS Publ., N°.241: 41-59.

Hem, J.D. 1985. Study and Interpretation of The Chemical Characteristics of Natural Water. 3rd edition, US Geological Survey water-supply, paper 2254.

Hilali, M. 2002. Hydrogéologie et modélisation de l'intrusion marine dans les aquifères côtiers de Martil et du Sahel-Maroc. Thèse de Doctorat. Ecole Mohammadia d'Ingénieurs Rabat.

Hutton, L.G. 1983. Field testing of water in developing countries. Water Resources Center, Unwin Brothers Limited, Britain. 125 pp.

ISO 1984. Total Hardness of Water by Photocolorimetry, Standard Methods 2340C Hardness. Hach Company/ Hach Lange GmbH, 2015. Edition 1, 1-13.

Kaid Rassou, K. 2009. Etudes des interactions entre les eaux souterraines et les eaux de surface dans le bassin côteir d'Oualidia, These doctorat es science Univ. Marrakech, pp. 193.

Laluraj. C. M. and Gopinath Girish 2001. Assessment on seasonal variation of groundwater quality of phreatic aquifers-a river basin system. Environmental Monitoring and Assessment, 117: 45-57.

Langmuir, D. 1997. Aqueous Environmental Chemistry, Prentice-Hall, Inc., New Jersey, pp. 600.

Makhoukh, M., Sbaa, M., Berrahou, A. and Clooster, V.M. 2011. Contribution à l'étude physico-chimique des eaux superficielles de l'oued Moulouya (Maroc oriental). Larhyss Journal, 9: 149-169.

Martin, C., Molénat, J., Gascuel-Odoux, C., Vouillamoz, J.M., Robain, H., Ruiz, L., Faucheux, M. and Aquilina, L. 2006. Modelling the effect of physical and chemical characteristics of shallow aquifers on water and nitrate transport in small agricultural catchments. Journal of Hydrology, 326: 25-42.

Maxwell, I.O. and Ahola, O. 2012. Seasonal variation in physico-chemical characteristics of rural groundwater of Benue State, Nigeria. Journal of Asian Scientific Research, 2(10): 574-586.

Mink, J.F. 1964. Groundwater temperatures in tropical island environment. Journal of Geophysical Research, 66: 5230-5250.

Murdey, J. and Blavoux, B.1986. Utilisation de l'analyse en composantes principales (sur variables centrées réduites) pour l'étude du fonctionnement hydrocinématique de trois aquifères karstiques du Sud-Est de la France. Hydrogéologie, n° 1: 53-59.

Oulaaross, Z. 2009. Etude climatologique, hydrogéologique et géophysique du Sahel Côtier des Doukkala (Maroc). Apport de l'analyse statistique et de l'inversion des données géoélectriques à l'étude du biseau salé de la lagune de Sidi Moussa Thèse Doct, Univ. Chouaib Doukkali, El Jadida, Maroc. pp. 279.

Quinn, G.P. and Keough, M.J. 2002. Experimental Design and Data Analysis for Biologists. United States of America by Cambridge University Press, New York, pp. 553.

Raghunath, R. Sreedhara, Murthy, T. R. and Raghavan, B. R. 2001. Spatial distribution of pH, EC and total dissolved solids of Nethravathi river basin, Karnataka state, India, Pollution Research, 20(3): 413-418.

Reggam, A., Bouchelaghem, H. and Houhamdi, M. 2015. Qualité physico-chimique des eaux de l'Oued Seybouse (Nord-Est de l'Algérie): caractérisation et analyse en composantes principales. J. Mater. Environ. Sci., 6(5): 1417-1425.

Richardson, S., Evans, R., Middlemis, H., Ross, J., Howe, P., Hiller, J. and Dyson, P. 2004. Guiding Principles for Sustainable Groundwater Management. IAH Background Paper, MDBC (Murray- Darling Basin Commission), REM (Resource & Environmental Management Pty Ltd.), Australia.

Rodier, J. 1984. L'analyse de l'eau : eaux naturelles, eaux résiduaires, et eau de mer. 7ème édition, Dunod Technique, 1136 pp.

Rodier, J. 2009. L'analyse de l'eau. 9ème édition. DUNOD, Paris, France.

Souhel, A. and El Achheb, A. 2000. Cadre géologique des principaux aquifères de la plaine des Doukkala. Actes de la 2ème session de L'université de printemps des Doukkala-Abda. Université. Chouaïb Doukkali, El Jadida, (Maroc), 3: 71-73.

Sudhakar, A. and Narsimha, A. 2013. Suitability and assessment of groundwater for irrigation purpose: A case study of Kushaiguda area, Ranga Reddy district, Andhra Pradesh, India. Pelagia Research Library, Advances in Applied Science Research, 4(6): 75-81.

UNESCO 1987. Groundwater Problems in Coastal Areas. United Nations Educational, Scientific and Cultural Organization, pp. 582.

UNESCO 2003. Water for People: Water for Life. 1st edition. The United Nations' world water development report, Berghahn Books, 543 pp.

WHO 2011. World Health Statistics. WHO Department of Health Statistics and Informatics of the Innovation, Information, Evidence and Research Cluster, France, pp. 162.

Younsi, A., Mania, J., Lhadi, E.K. and Mudry, J. 2001. Incidences de pluies exceptionnelles sur un aquifère libre côtier en zone semi-aride (Chaouia, Maroc). Revue des sciences de l'eau, 14(2): 115-130.

Nature Environment and Pollution Technology
An International Quarterly Scientific Journal

p-ISSN: 0972-6268
e-ISSN: 2395-3454

Vol. 19 | No. 1 | pp. 29-40 | 2020

Original Research Paper | Open Access

Adsorption of Methylene Blue Using Chemically Enhanced *Platanus orientalis* Leaf Powder: Kinetics and Mechanisms

Baba Imoro Musah†, Lai Peng and Yifeng Xu

Department of Environmental Science and Engineering, School of Resources and Environmental Engineering, Wuhan University of Technology, Luoshi Road No. 122, Hongshan, Wuhan, Hubei, 430070, PR China

†Corresponding author: Baba Imoro Musah

Nat. Env. & Poll. Tech.
Website: www.neptjournal.com

Received: 30-04-2019
Accepted: 02-07-2019

Key Words:
Adsorption
Methylene blue
Chemical impregnation
Platanus orientalis
Leaf powder

ABSTRACT

The adsorption of methylene blue in an aqueous medium using two activated carbons AC1 and AC1 + H_3PO_4 was studied. The AC1+ H_3PO_4 adsorbent, which was inoculated with phosphoric acid, had better methylene blue removal capacity compared with AC1 adsorbent which had only thermal treatment. The optimum activation temperature for both adsorbents was 500°C while the suitable activation time was 180 min. The best pH in this investigation was 6. With AC1 + H_3PO_4 adsorbent, 100% removal of methylene blue was recorded for concentrations 20 to 100 mg.L^{-1} and the suitable adsorbent dosage was 3 g.L^{-1}. The effect of temperature showed insignificant effect on the adsorption of methylene blue ions. The SEM results for AC1 + H_3PO_4 adsorbent showed better pores compared with AC1, an indication that, the injection of phosphoric acid into it before the activation played a significant role in enhancing the porosity of the adsorbent surface.

INTRODUCTION

Textile, paper, painting and coating industries are major sources of dye pollutants. Large amount of dye wastewater are emptied into freshwater bodies which have negative consequences on the environment and human health (Oliveira et al. 2008). When exposed to light and water, methylene blue is difficult to fade and hard to be treated in wastewater by simple techniques such as biological treatment and chemical precipitation (Oliveira et al. 2008). In the production chain, it is reported that between the range of 1 to 15% the dye is lost and it is discharged as wastewater (Galindo et al. 2001, El-Sharkawy et al. 2007). Dye wastewater that ends up in fresh water bodies cause havoc to aquatic species by increasing toxicity chemical oxygen demand (COD). It also affects the photosynthetic activities of aquatic plants through the reduction of light penetration (Oliveira et al. 2008). It has been reported that, high COD, biological oxygen demand (BOD5) values, particulate matter (PM) and sediments, grease and oil in effluents lead to the depletion of dissolved oxygen creating serious consequences on aquatic species (Wang et al. 2011).

Methylene blue (MB) wastewater can be treated by photocatalytic degradation (El-Sharkawy et al. 2007). Generally, MB has poor biodegradability or resistance to environmental conditions (Tsai et al. 2001). Research indicates that, there are over 100,000 available commercial dyes and more than 7 × 10^5 t dye-materials are produced yearly (Lee et al. 2006). Methylene blue is used in many industries e.g. dyeing of silks, paper, plastic, leather, but it has wider usage in the synthetic textile fibre industries as the most suitable substrate (Oliveira et al. 2008). There are various classification of dyes such as anionic- direct, acid and reactive dyes; cationic - basic dyes; and non-ionic- disperse dyes (Fu & Viraraghavan 2001). The textile industry emission or discharge standards vary for many countries for different indicators e.g. China is COD 100 mg.L^1, BOD_5 25 mg.L^{-1} and pH 6-9; in Germany, COD 160 mg.L^{-1} and BOD_5 25 mg.L^{-1}; in Jordan COD 160 mg.L^{-1}, BOD_5 60 mg.L^{-1} and pH 6-9; Oman COD 150 mg.L^{-1} and BOD_5; Tunisia COD 90 mg.L^{-1}, BOD_5 30 mg.L^{-1} and pH 6.5-8.5 (Wang et al. 2011, WHO 2006, Sawal 1986).

Wastewater from dye-stuff and textile industries have dye concentrations below 1 g/dm^3, high alkalinity, biochemical oxygen demand, chemical oxygen demand and total oxygen dissolved solids (Kaushik & Malik 2009). Methylene blue is a cationic dye widely used in silk, cotton and wool processing as dyes (El-Sharkawy et al. 2007).

There are different treatment techniques that can be employed in the removal of environmental pollutants such as dyes. They include membrane filtration (Abid et al. 2012), electrochemical (Babu et al. 2011), reduction (Wali 2015), oxidation (Murthy et al. 2011), adsorption (Weng & Pan

Fig. 1: (a) leaf, (b) leaf powder inoculated with H_3PO_4 and (c) activated carbon.

2007), electrocoagulation (Akyol 2012), photocatalytic degradation (Sleiman et al. 2007). However, in the case of methylene blue $C_{16}H_{18}ClN_3S.3H_2O$, it is resilient to fading when exposed to water and light making it difficult to be removed from wastewaters through commonly used techniques like biological and chemical precipitation (Franca et al. 2009).

Adsorption as a technique for removing different kinds of pollutants such as heavy metals, dye among others in wastewater is reported to be an efficient method (El-Sharkawy et al. 2007). In this research adsorption technique is employed due the following reasons: environmentally friendly, ease of operation, wide range adsorbent sources among others are reported by some past studies (Saengbutr et al. 2014, Tong et al. 2010, Rashed 2013 and Lupascu & Povar 2016). With regards to industrial wastewater handling, adsorption processes serve as very interesting Alternative, especially when organic substances removal or recovering important chemicals are involved (Worch 2012).

The use of activated carbon as adsorbents are effective given that they have highly developed pore and large surface area with high degree of surface reactivity (Dias et al. 2007).

In recent times, there's rising interest in new techniques regarding the production of cost effective, efficient and eco-friendly adsorbents for large scale utilization. In view of this, agricultural by-products or plant waste materials are of interest to research for utilization as adsorbents; wheat brand (Çiçek et al. 2007), green pea peels (Dod et al. 2012), mango leaves (Kamsonlian et al. 2012), yellow passion fruit waste (Pavan et al. 2008), rice hull ash (Wang & Lin 2008), neem leaves (Saengbutr et al. 2014), hevea brasilliensis seed coat (Hameed & Daud 2008). It is reported that plant leaves contain certain constituents, e.g. polyphenols, lignin, pigments and protein making it suitable to provide active sites for binding dyes (Abadian et al. 2015). This study considers *platanus orientalis* leaf powder as a potential adsorbent for the removal of methylene blue in an aqueous solution.

MATERIALS AND METHODS

Materials and Chemicals

The adsorbent material for this investigation was obtained in December 2015, from Wuhan University of Technology campus, China. It went through systematic processing stages until the final product (AC) was obtained. Sample activated carbons were subsequently stored in a desiccator at room temperature (25°C) to keep it free from moisture contact. Fig. 1a is the leaf sample, 1b is leaf powder inoculated with H_3PO_4 and 1c is activated carbon.

The following chemicals were used in the investigation e.g. methylene blue trihydrate, phosphoric acid (H_3PO_4), sodium hydroxide (NaOH) and hydrochloric acid (HCl). The rest of the chemicals used in the study were: sodium chloride (NaCl), potassium bromide (KBr), ethanol (CH_3CH_2OH), all by China Sinopharm Chemical Reagents Co. Ltd. A 1000 mg/L stock solution methylene blue was prepared using deionized water obtained from Milli-Q Direct 16 distillation machine with Vent Filter MPK01. Different concentrations of methylene blue such as 20, 40, 60, 80, 100, 120 and 140 $mg.L^{-1}$ were subsequently prepared from the stock solution for use in the investigation. All chemicals and reagents used in the investigation were of analytical grade.

Sample Activation

A total of 40 g of dried fallen *platanus orientalis* leaf powder (FPOLP) was used for two sets of activations in this investigation involving methylene blue. First, 20 g of FPOLP was thermally treated (pyrolyzed) in an electric furnace for 180 min at temperature 500°C. After that, the activated sample labelled AC1 and it was allowed to cool and the black activated sample obtained was reweighed. It emerged that after subjecting the FPOLP to the above temperature and duration, 63.4% of the sample got lost through the application of heat leaving only 36.6% representing 7.32 g in the process.

Another sample constituting 20 g of FPOLP was impregnated with 30 wt % of H_3PO_4 solution with a ratio of 1:1 (Demiral & Güngör 2015scanning electron microscopy (SEM, Prahas et al. 2008). The sample was thoroughly mixed to ensure uniformity and kept for 12 h, afterward the mixed sample was heated at 80°C to ensure that excess water is evaporated for 4 h in an oven 101-1AB, manufactured by Tianjin Taisite Instrument Co. Ltd. The mixed sample was put into a crucible and then pyrolyze at 500°C for 180 min. Once heating was over, the sample was allowed to cool down. Finally, it was washed repeatedly with deionized water till the pH of the mixture became neutral (7.0). The particulates were separated using Ø12.5 cm filter paper made in Hangzhou (GB/T1914-2007). It was oven dried at 80°C for 12 h, it was reweighed as 10.16 g which represented 50.8% of adsorbent retained after chemical and thermal treatment. It was then labelled AC1 + H_3PO_4 preserved in capped petri dish and stored in desiccator for subsequent use.

Batch Adsorption

The removal efficiency and equilibrium adsorption capacities were determined from batch experiments conducted using isothermal shaker. Different adsorbent dosages were investigated e.g. 1, 2, 3 and 4 $g.L^{-1}$. At the end of the investigations into the adsorbent dosage, 3 $g.L^{-1}$ was found to be the optimum dosage and it was used for further investigations. To each conical flask, 3 $g.L^{-1}$ adsorbents (AC1 and AC1+ H_3PO_4) were applied to 25 mL of methylene blue solution. The shaking frequencies were maintained for 120 min with agitation speed of 150 rpm.

At the end of the quaking process, Whatman filter papers were used to separate the adsorbent. Fourier transform infrared (FT-IR) thermo-scientific NICOLET (iS10) Spectrometer was employed to identify the functional groups on the surface of the adsorbent. About 0.05 g of potassium bromide (KBr) were mixed with 0.01 g of the adsorbent, compressed into a light tablet shape. The FT-IR spectrometer were allowed to calibrate 32 times to set the background and the spectra were recorded in the band range of 4000 nm to 500 nm for subsequent analysis. The amount of MB absorbed at equilibrium (mg/g) was obtained using Eq. 1

$$q_e = \frac{(C_o - C_e)}{m} V \quad \ldots(1)$$

Where, C_0 is the initial dye concentration (mg/L), C_t is the concentration of solution at time t, V is the volume of the solution (L) and m is the mass of the adsorbent (g).

The methylene blue removal efficiency (R in %) was calculated using Eq. 2

$$R = \frac{(C_e - C_t)}{C_o} \times 100\% \quad \ldots(2)$$

Sample Characterization

The effect of dye solution pH was investigated. The initial pH range of methylene blue solutions were varied from 2 to 10. The pH was controlled by adding 0.1 M dilute HCl and 0.1 M NaOH solutions using Cyberscan pH 2100-meter Eutech instruments. The pH of point zero charge (pH_{pzc}) of the adsorbent was equally investigated because there is a correlation between the surface behaviour of the adsorbent and adsorbate. The uptake of dye can be explained based on the pH_{pzc} of the adsorbent (Cardenas-Peña et al. 2012). The investigation was done by the solid addition method (Ponnusami et al. 2008).

An amount of 2 $g.L^{-1}$ of AC1+H_3PO_4 adsorbent was added to 50 mL of 0.1M NaCl solution into six 250 mL conical flasks. The pHs were regulated in the range of 2 to 12 using 0.1 M NaOH and 0.1 M HCl solutions respectively. A number of batch absorptions were conducted with the electrolyte solution; the mixtures were allowed to agitate in a shaker for 12 h. The initial pHs were labelled (pH_i) and the final pH labelled (pH_f). The change in pH (ΔpH) determined by this relationship as follows; ($\Delta pH = pH_i - pH_f$), the ΔpH is plotted against the pH_i. The pH_{pzc} of the adsorbent is the point on the graph where it is equal to zero (0) (Cardenas-Peña et al. 2012).

Several 250 mL conical flasks each containing 25 mL of methylene blue solution of 100 $mg.L^{-1}$ concentration were prepared. Varied amounts of adsorbent in the range of 1 to 4 $g.L^{-1}$ applied under 25°C temperature condition at pH 6 to each flask containing the methylene blue solution. These flasks were vigorously agitated in shaker at a speed of 150 rpm for 120 min. The mixtures were then filtered after the desired time had elapsed using filter papers. The adsorbate was then used for analysis by employing spectrophotometer calibrated or standardized at 665 nm. The amount of methylene blue absorbed is calculated in each case using origin 8 application software. SEM analysis was done using analytical JSM-IT300, a product by JEOL Ltd. Japan.

RESULTS AND DISCUSSION

Effect of Adsorbent Surface Modification

Inquiries were carried out with AC1 and AC1+H_3PO_4 adsorbents respectively, with constant dosage of 3 $g.L^{-1}$ in 25 mL methylene blue solution. The concentrations of methylene blue were varied in the following order 20, 40, 60, 80, 100, 120 and 140 $mg.L^{-1}$. Fig. 2 illustrates the results from this investigation, it is evident that AC1 adsorbent has less efficiency in the removal of methylene blue after the concentration increased from 20 $mg.L^{-1}$. For AC1 + H_3PO_4 adsorbent on the other hand showed high removal efficiency

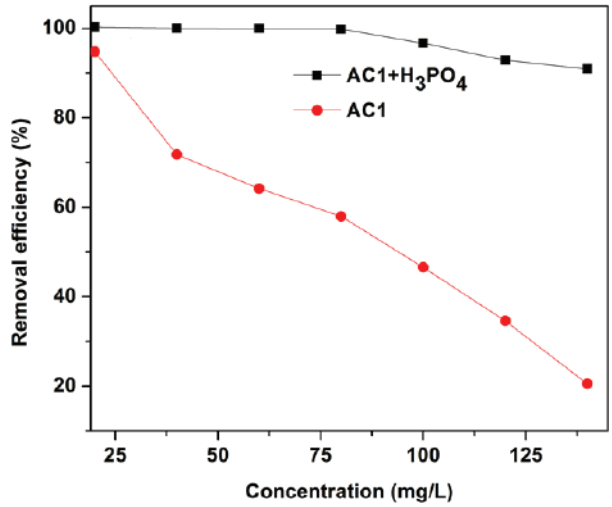

Fig. 2: Effect of adsorbents surface modification. Removal efficiency using AC1 and AC1+H_3PO_4, with adsorbents dosage of 3 g.L^{-1} at temperature 25°C, time 2 h and neutral pH with agitation speed at 150 rpm.

for all initial methylene blue concentrations studied.

Decolourization of aqueous methylene blue solution was 100% for AC1 + H_3PO_4 at 20, 40, 60 mg.L^{-1}. It declined to 99.8, 96.7, 92.9 and 90.9% at 80, 100,120 and 140 mg.L^{-1} respectively.

When AC1 adsorbent, removal efficiency stood at 94.7, 71.7 and 64.2% with concentration 20, 40 and 60 mg.L^{-1} respectively.

The removal efficiency still reduced significantly to 58.0% with a concentration of 80 mg.L^{-1} and 46.5% with 100 mg.L^{-1}, consequently, an increase in methylene blue concentration to 120 mg.L^{-1} showed a downward trend of 34.5% removal of methylene blue and eventually reduced to 20.5% with a concentration of 140 mg.L^{-1}.

The trends observed could be explained by the fact that, the adsorbent surface becomes saturated with the increase in methylene blue concentration as similarly reported (Xiong et al. 2010).

Effect of pH

The effect of pH on methylene blue adsorption was examined using AC1 and AC1+H_3PO_4 adsorbents respectively in 100 mg.L^{-1} initial methylene blue concentration with adsorbent dosage 3 g.L^{-1} at temperature 25°C. Initial pH of methylene blue solution was adjusted between 2 to 10 in Fig. 3a. The pH of point zero charge (pHpzc) of the adsorbent was studied in the range of 0 to 12 as shown in Fig. 3b.

When the initial pH was first increased from 2 to 4 in Fig. 3a, the removal efficiency of dye increased from 98.6% to 99.2%. Removal efficiency further increased to 100% when initial pH was augmented to 6, but both pH 8 and 10 recorded same slight decline in methylene blue removal efficiencies at 99.4% as in Fig. 3a.

In the case of using AC1 adsorbent, when the pH was adjusted from pH 2 to 4, the removal efficiency increased from 49.8 to 70.5%. Additional increase in pH to 6 resulted in a rise in the methylene blue removal percentage to 82.9% in Fig. 3a. Further increase in initial methylene blue pH between 8 and 10, resulted in a minimal reduction in removal efficiency to 81.8 and 79.6% respectively as represented in Fig. 3a.

In Fig. 3b shows the results of pH at point of zero charge (pHP_{zc}) of the adsorbent surface. The pHP_{zc} was recorded at pH 1.8 in (Fig. 3b) lower than pH 6 at which maximum adsorption of the dye took place. There is some correlation between solution pH and pHp_{zc}. It is reported that if the optimum pH of a solution is great than the pHPzc, the electrostatic force of attraction between positively charge dyes and negatively charged AC1+H_3PO_4 adsorbent is greatly enhanced and vice versa (El Qada et al. 2008). Since this study revealed pH 6 as optimum, it is clear that, pH had some influence on the adsorption of methylene blue as explained. Similar corroborative report suggests that, hydrogen reduces between pH 6 and 7, this gives rise to enhanced adsorption (Nethaji et al. 2013).

Effect of Adsorbent Dosage

The effect of adsorbent dosage was studied using AC1 and AC1+H_3PO_4 respectively in Fig. 4.

In order to determine the suitable quantity of the adsor-

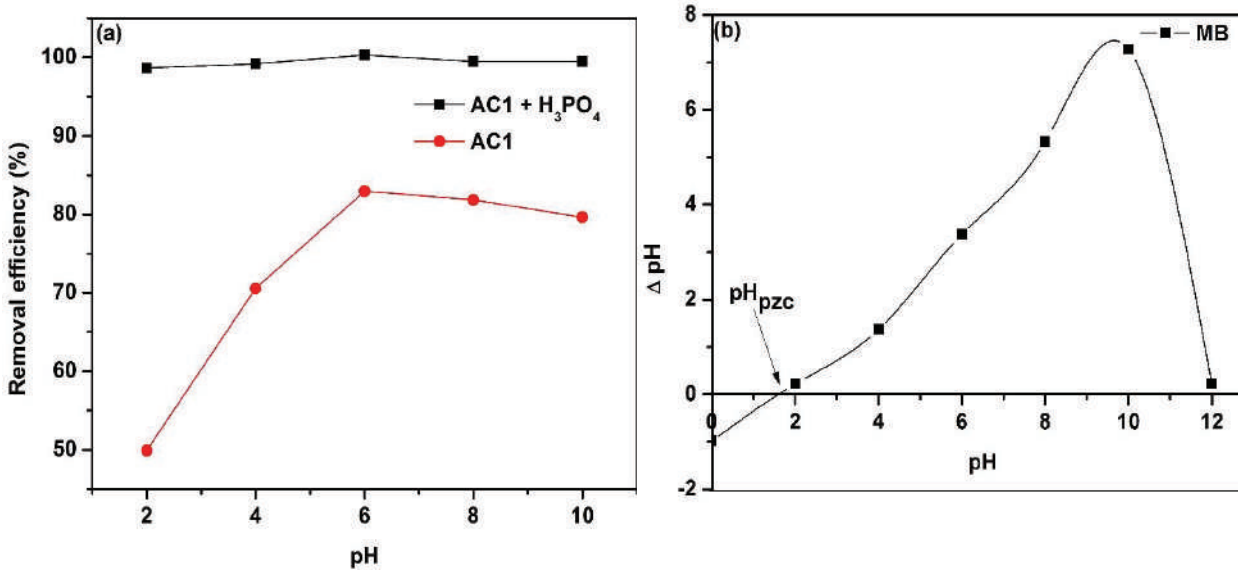

Fig. 3: Effect of pH (a) removal efficiency and (b) pH_{pzc} at temperature 25°C.

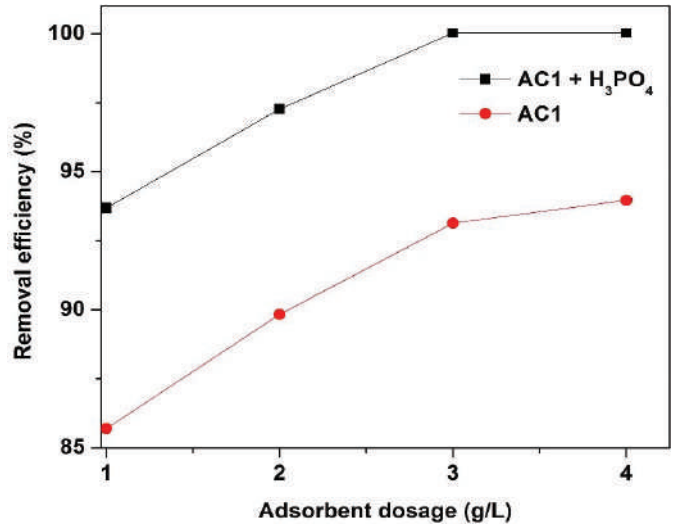

Fig. 4: Effect of adsorbent dosage on methylene blue adsorption, 100 $mg.L^{-1}$, temperature 25°C, at pH 6 with agitation speed of 150 rpm and time 2 h.

bent to achieve enough removal of dyes, varied dosages in the order 1, 2, 3 and 4 $g.L^{-1}$ per 25 mL solution of methylene blue were applied in each 250 mL conical flask. All other parameters e.g. initial concentration 100 $mg.L^{-1}$, temperature 25°C, pH 6, shaking speed 150 rpm and contact time with absorbent 2 h were kept constant while varying the adsorbent dosage. The results obtained are presented in Fig. 4. It is clear that, when AC1 adsorbent was increased from 1 $g.L^{-1}$ to 3 $g.L^{-1}$, the removal efficiency moved from 85.7 to 93.1%. When the adsorbent dosage was further increased to 4 $g.L^{-1}$, the depletion of dyes slightly changed to 93.9%. Likewise, with the application of AC1+H_3PO_4 adsorbent, it was also noticed that, increasing adsorbent dosage resulted in increase in dyes depletion. When the adsorbent dosage was varied from 1 $g.L^{-1}$ to 3 $g.L^{-1}$, removal of dyes increased from 93.6% to 100%. No further variation in the adsorbent dosage was deemed necessary given the outcome recorded.

Effect of Initial Methylene Blue Concentration

Investigation was carried out to evaluate the effect of initial

methylene blue concentration on adsorption. The results of the findings are shown in Fig. 5 using AC1 and AC1+H_3PO_4 adsorbents respectively.

The evaluation was done using constant adsorbent dosage of 3 g.L^{-1} in 25 mL solution of methylene blue at temperature 25°C. The initial concentrations were varied in this order 20, 40, 60, 80,100, 120 and 140 mg.L^{-1} at pH 6 for 2 h. For AC1 adsorbent, 100% of the dye was removed at initial concentration of 20 mg.L^{-1} but reduced to 84.6% at initial concentration 140 mg.L^{-1}.

The unit adsorption capacity increased from 6.6 to 39.5 mg.g-1 using AC1 adsorbent when initial concentration was varied from 20 mg.L-1 to 140 mg.L-1. This pattern as observed in this investigation has some similarity with other studies involving methylene blue (Elizalde-González et al. 2007, Demirbas et al. 2008).

It was observed that, 100% of the methylene blue was using AC1+ H_3PO_4 adsorbent for initial concentrations from 20 to 100 mg.L^{-1}. However, the removal efficiency steadily declined upon further increase in initial methylene blue concentration between 120 and 140 mg.L^{-1} with corresponding removals at 96.3 and 91.9% respectively.

The adsorption capacity for AC1+ H_3PO_4 adsorbent increased from 6.6 to 42.9 mg.g^{-1} when initial concentration was augmented from 20 mg.L^{-1} to 140 mg.L^{-1}. It is obvious from the above finding that, increasing concentration negatively affected the amount of dyes removed for adsorbents. This finding is attributed to the saturation of empty sites within the adsorbent (Garg et al. 2004, Hameed et al. 2008).

Effect of Contact Time

This was studied in order to evaluate its impact on methylene blue uptake. This investigation was done using varied intervals of time as indicated in Fig. 6, as a result the equilibrium time was also determined.

Every other parameter in essentially was kept constant while time was adjusted within the intervals 5, 10, 20, 30, 40, 80 and 120 minutes since it was the only factor under evaluation in this case as indicated in Fig. 6. The results showed that, 80 min contact time was enough for the system to reach equilibrium with the given initial concentration. In Fig. 6 above, the adsorption process was a little bit rapid during the initial stages (from 0 to 40 min) with corresponding adsorption capacity from 28.7 to 32.8 mg.g^{-1}. This slow incremental trend continued until the system reached equilibrium with a maximum adsorption capacity of 33.34 mg.g^{-1}. The rapid uptake phenomenon may have occurred due to high presence of unoccupied or relatively vacant sites in the adsorbent at the initial stages. As the vacant sites were being occupied in the process of the adsorption, dye uptake slowed down due to a reduction in active vacant sites on the surface of AC1+H_3PO_4 adsorbent. There is a corroborative finding to what was recorded (Hameed et al. 2008)low-cost, locally available sorbent, pomelo (Citrus grandis).

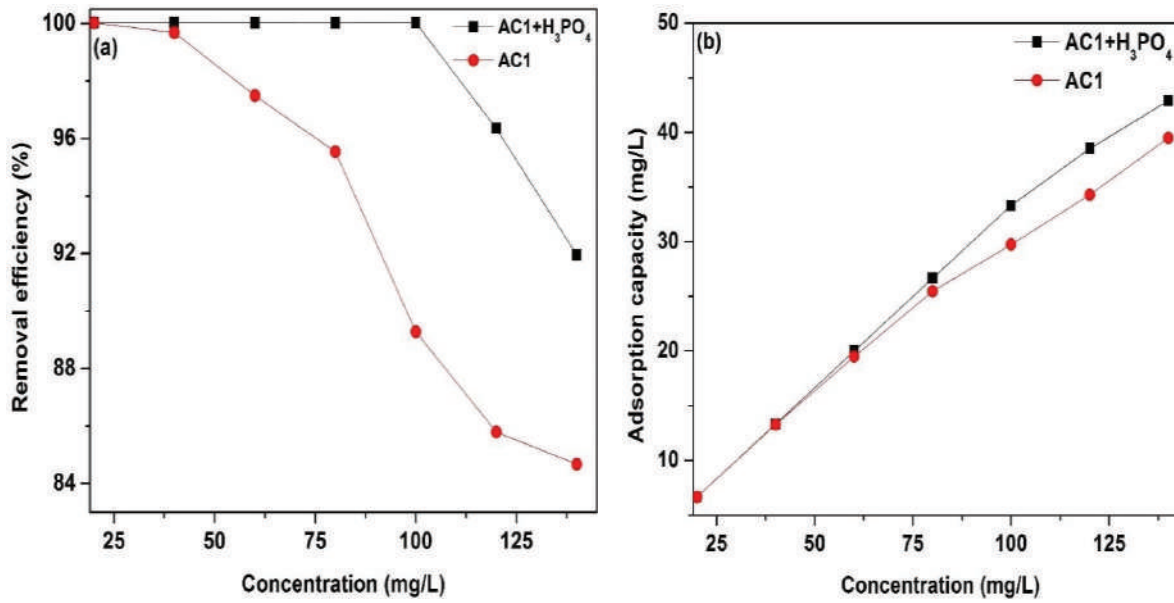

Fig. 5: Effect of initial methylene blue concentration (a) removal efficiency and (b) adsorption capacity, with adsorbent dosage 3 g.L^{-1}, at pH 6, time 2 h at temperature 25°C and agitation speed of 150 rpm.

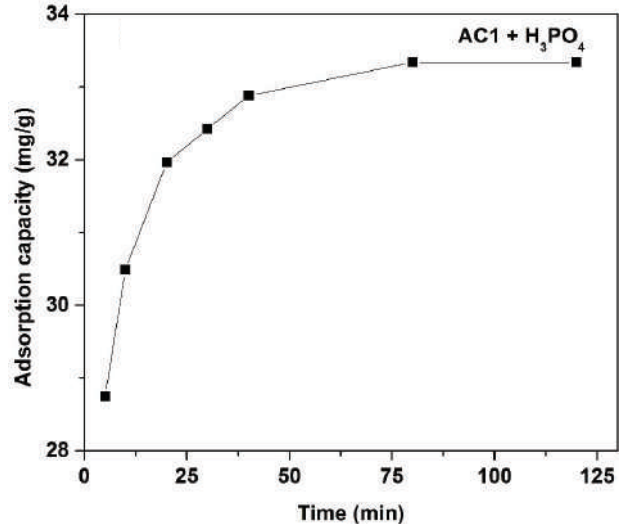

Fig. 6: Effect of contact time on methylene blue adsorption using AC1+H_3PO_4 adsorbent; initial concentration 100 mg.L^{-1}, pH 6, at temperature 25°C, agitation speed 150 rpm and adsorbent dosage 3 g.L^{-1}.

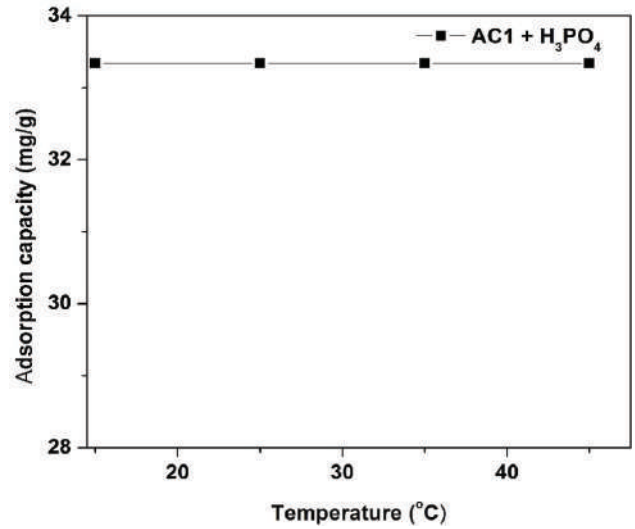

Fig. 7: Effect of temperature on methylene blue adsorption with initial concentration 100 mg.L^{-1}, time 2 h, adsorbent dosage 3 g.L^{-1} (AC1+H_3PO_4), agitation speed 150 rpm at pH 6.

Effect of Temperature

The effect of temperature on methylene blue uptake was investigate studied with different temperatures ranging from 15 to 45°C. Since the evaluation here was relating to heat variation, the other parameters such as initial methylene blue concentration 100 mg.L^{-1}, adsorbent dosage 3 g.L^{-1} (AC1+H_3PO_4), pH 6, contact time 2 h and agitation speed at 150 rpm were maintained. Fig. 7, showed that, temperature variation had little or no effect on the removal percentage of methylene blue when temperature was increased from 15°C to 45°C. This outcome means temperature changes did not influence the adsorption process. The adsorption capacity recorded 33.34 mg.g^{-1}.

Adsorption Kinetics

Kinetics relates directly to thermodynamic equilibrium rate pertaining to a system that is not in an equilibrium state, thus the process of adsorption would linger on until equilibrium is established. However, in the case of desorption, the process is the reverse till the attainment of equilibrium.

The adsorption rates can effectively be evaluated using Lagergren (Ho 2004) pseudo-first-order model for kinetics

together with Ho & McKay modified formula (Ho & McKay 1999). The equation (Eq. 3) is modelled as:

$$\frac{d_{qt}}{d_t} = k_1 (q_e - q_t) \quad \ldots(3)$$

Where q_e and q_t are the amount of dye absorbed ($mg.g^{-1}$) at equilibrium and at time, t (min) respectively and k_1 is the equilibrium rate constant of pseudo-first-order adsorption (min^{-1}).

The variables in equation (Eq. 3) are defined as: q_e is the adsorbed quantity of ions or molecules at equilibrium point ($mg.g^{-1}$), q_t is the quantum of molecules uptaken at a given period in the adsorption process while k_1 represents the rate constant for pseudo-first-order kinetic model (1/h). But, in order to determine the rate constant, equation (Eq. 3) was standardized into a linear form to allow a plotting of $\ln(q_e-q_t)$ against period. The intercept and slope of the plot were determined from the relationship. Equation 4 can be rearranged in this order taking into account the boundary conditions (Ho & Mckay 1998), t = 0 to t and $q_t = 0$ to q_t as:

$$\log (q_e - q_t) = \log (q_e) - \frac{d_{qt}}{dt} \quad \ldots(4)$$

The plot of log (q_e - q_t) versus *t* was made and the slope and intercept from this relationship was used to determine the first-order rate constant, k_1 in Fig 8a.

For the evaluation of adsorption kinetics data, essentially not every data may fit well in pseudo-first-order equation, thus to overcome this limitation, pseudo-first-order model was additionally employed due to its general flexibility for the data analysis (Ho & McKay 1999). The new equation was reorganized into equation (Eq.5) as follows:

$$\frac{d_{qt}}{dt} = k_2 (q_e - q_t)^2 \quad \ldots(5)$$

Where, k_2 represents the equilibrium rate constant of pseudo-second-order adsorption (g/mg min).

In equation (Eq. 5), k_2 is defined as pseudo-second-order kinetic rate constant (g/mg min). But for determination of the dynamics relating to rate and other variables, pseudo-second-order equation (Eq. 5) was rearranged. The suitability of this model is verified after getting linear graph from the plot of $\frac{t}{q}$ against t. The value of k_2 was determined from the intercept and the slope respectively. The rearranged equation (Eq. 10) is below and $k_2 q_e^2$ is equal to initial rate of adsorption h (mg/g.min). Equation (5) taking into consideration the boundary condition (Ho 2004) t = 0 to t and $q_t = 0$ to q_t gives rise to the following:

$$\frac{1}{q_e - q_t} = \frac{1}{q_e} k_2 t \quad \ldots(6)$$

The above equation (6) is the integrated rate law for pseudo-second-order interaction and it can be rearranged in a linearized form as:

$$\frac{t}{q_t} = \frac{1}{k_{2q^2e}} + \frac{1}{q_e} t \quad \ldots(7)$$

The second-order rate constant, k_2 was determined from

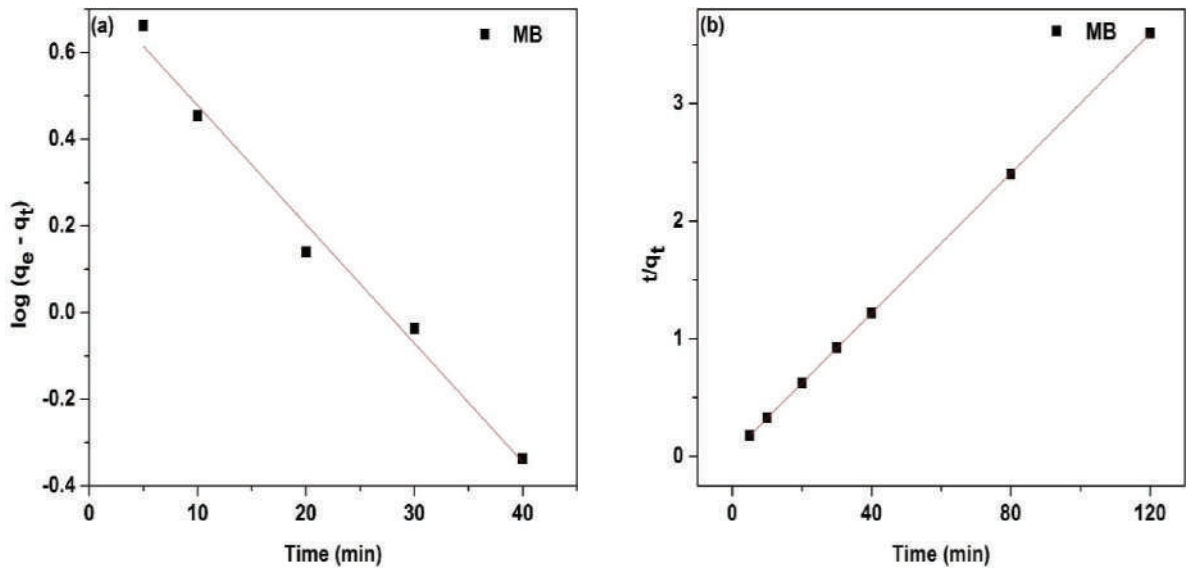

Fig. 8: (a) Pseudo-first-order kinetic and (b) Pseudo-second-order kinetic; on methylene, blue adsorption with initial concentration 100 $mg.L^{-1}$, adsorbent dosage 3 $g.L^{-1}$ (AC1+H_3PO_4), agitation speed 150 rpm at pH 6.

Table 1: Pseudo-first and second-order adsorption rate constants for 100 mg L initial methylene blue concentration.

Experiment	Pseudo-first-order			Pseudo-second-order		
Exq_e (mg g^{-1})	k_1 (min^{-1})	cal q_e, ($mg.g^{-1}$)	R^2	k_2 ($g.mg^{-1}$ min^{-1})	cal q_e ($mg.g^{-1}$)	R^2
42.90	0.083	27.44	0.982	0.029	38.40	0.999

a calculation using the slope and intercept of the plot $\frac{t}{q_t}$ versus t.

The Pseudo-first and second-order adsorption rate constants for 100 mg L initial methylene blue concentration are given in Table 1.

Adsorption Mechanisms

The surface morphology, and pores of an adsorbent is dependent on the adsorbent type. In this study, two different methods (Nowicki et al. 2010); physical and chemical activation were employed in the preparation of the adsorbent for the adsorption. Physical activation involves the subjection of a raw material or waste to higher degree of heating either in an oxygen, steam or carbon monoxide condition in a temperature regime such as 300-1200°C (Nowicki & Pietrzak 2010). While in the chemical activation process, the dried leaf powder was largely inoculated with 1:1 phosphoric acid (H_3PO_3) solution (Yakout & Sharaf El-Deen 2016), air-dried and subsequently subjected to thermal treated at 500°C for 3 h. The adsorbents (FPOLP, AC1 and AC1 + H_3PO_4) were spectrally (FTIR) examined with the aid of a spectrometer as shown in Fig. 9. The thermal treatments of AC1 and AC1 + H_3PO_4 adsorbents respectively, could be responsible for the shift of peaks for AC1 graph labelled (B) and for AC1 + H_3PO_4 graph labelled (A) all in Fig. 9. Again, the subsequent chemical injection (H_3PO_4) on AC1 + H_3PO_4 adsorbent effectively changed its morphology, making it more porous as observed in the SEM in Fig. 10b. Apart from acids, other chemicals such as salts, e.g. $ZnCl_2$ (Hu et al. 2009) or base, e.g. KOH (Evbuomwan et al. 2012) could have been used to enhance the porosity of surface area of the adsorbent. The main objective of the activation is essentially to optimize the surface area (micro and mesoporous) availability on the FPOLP for efficient adsorption. From the results, firmed by the SEM analysis, the chemical activation had proven to be more effective compared to the physical activation alone. Similar study has been sighted by Mohammad & Rahbar-kelishami (2014) has been sighted, however, it is important to stress that, the explanation given about the adsorbent preparation is quite ambiguous.

FTIR Spectra Analysis

The spectra analysis of three different samples (a) AC1 + H_3PO_4, (b) AC1 and (c) FPOLP are presented in Fig. 9. In Fig. 9a, the peak 1081 cm^{-1} may be assigned to strong C-O stretching, this functional group is associated with primary alcohol (Pradhan 2011).

Peak 1161 cm^{-1} is generated due to robust C-O stretching and it may be the effect of aliphatic ether. The peak at 1384 cm^{-1} is intermediate bending due to O-H and its functionality could most likely be phenol. However, the strong C=C stretching effect likely generated the peak at 1613 cm^{-1} (Kundu et al. 2008).

The peaks between 3400 and 3550 cm^{-1} on spectra Fig. 9c (FPOLP) could be allotted to great dominance O-H functional group, thus representing free hydroxyl fundamentals located in the FPOLP. The peaks at 2850 and 2925 cm^{-1} may be assigned to aromatic elements, however after being subjected to higher temperature (500°C) in an oxidized environment for 180 min, led to the disappearance of the two peaks in Fig. 9a and 9b.

The peaks between 1626 and 1629 cm^{-1} have the characteristics of carbonyl functionality due to the effect of -COOH (Jokar et al. 2016). However, band 1318 cm^{-1} and 1400 cm^{-1} could be associated with aromatic nitriles which play a significant role in obtaining amines in hydrogenation process (Thusnavis et al. 2011, Wu et al. 2008). After subjection to different modifications in an oxidized condition, peak 1318 and 1048 cm^{-1} in Fig. 9c varnished in Fig. 9a and Fig. 9b, which are attributable to primary alcohol which could easily be oxidized to aldehydes or carboxylic acid depending on the reaction condition. Peak shift occurred at 1081 cm^{-1} (Fig. 9a) compared to the peak at 1048 cm^{-1} in Fig. 9c, this could possibly be the result of the modification effect. From the investigation conducted, the multiple modification had significant reflection in the adsorption attributes on adsorbent AC1 + H_3PO_4. It is reported that, the activation of carbon materials with oxidizing agents help generate oxygen-related functionalities that enhances the adsorption capabilities of the adsorbent during adsorption (Li et al. 2002, Do 1998).

SEM Analysis

Investigations were conducted on samples AC1 and AC1+ H_3PO_4 adsorbents respectively, employing scanning electron microscopic techniques. The results revealed very porous morphological features after it was treated with phosphoric acid (1:1) for 4 h prior to thermal treatment for 3 h for AC1 + H_3PO_4 adsorbent. Fig. 10a (AC1) adsorbent showed cell-

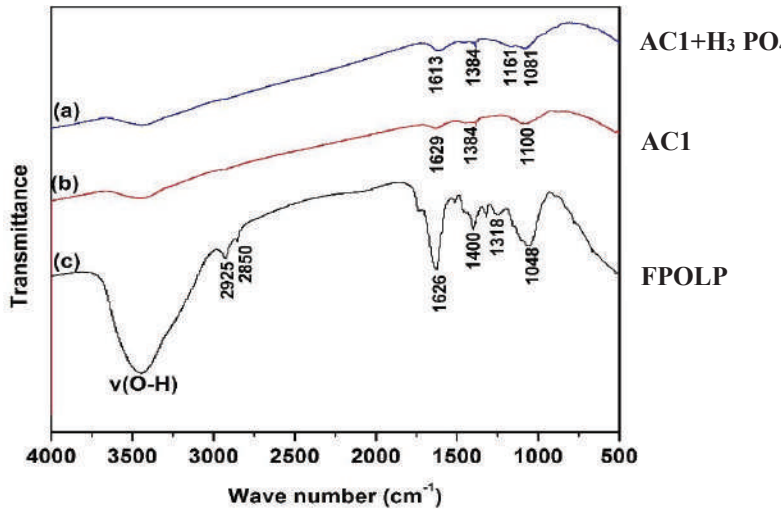

Fig. 9: FTIR Spectra graph (a) AC1 + H_3PO_4 (b) AC1 and (c) FPOLP adsorbents respectively.

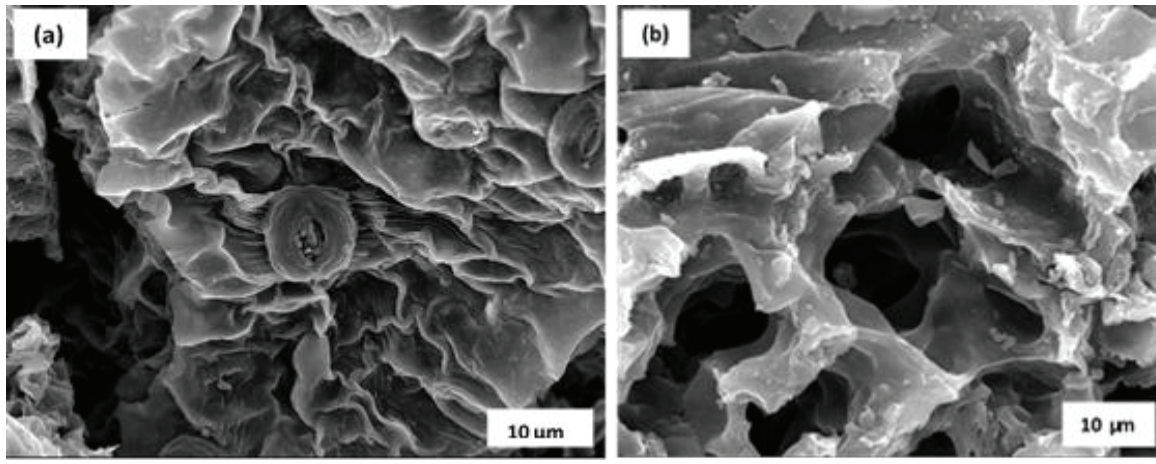

Fig. 10: SEM results (a) AC1 and (b) AC1+H_3PO_4 adsorbents respectively.

like pores on the surface of the adsorbent while Fig. 10b (AC1 + H_3PO_4) adsorbent revealed the inner pores present in the adsorbent.

The presence of both surface and inner pores on the adsorbent may have contributed significantly to the overwhelming adsorption of the dye molecules. The injection of oxygenated compounds into carbonaceous materials may have increased the level of porosity on the adsorbent which effectively enhance the adsorption capabilities as the adsorption investigation showed a remarkable removal, in some cases as earlier reported (Yakout & Sharaf 2016, Prahas et al. 2008, Altenor et al. 2009, Dias et al. 2007). The effectiveness of an adsorbent may be influenced by varied parameters such as the porosity and high surface area. In addition, the solubility as well as the affinity that exist between the particulates and the adsorbent could result in a hydrophobic and hydrophilic interaction.

CONCLUSION

This study involved the investigation of Methylene blue using two different absorbents prepared from fallen P. *orientalis* leaves powder. For AC1 adsorbent, it was thermally treated at 500°C for 2 h, while AC1+H_3PO_4 adsorbent was injected with phosphoric acid 1:1 solution followed by thermal treatment at same temperature and time as AC1. The removal efficiency reduced from 100% to 84.6% when MB concentration was

varied from 20 to 140 mg.L^{-1} for AC1 adsorbent, whereas for AC1+H_3PO_4, removal efficiency decreased from 100% to 91.6% when MB concentration increased from 20 to 140 mg.L^{-1}. The effect of solution pH revealed pH 6 as the optimum condition for maximum adsorption, from the range of 2 to10. The optimum adsorbent dosage was 3 g.L^{-1} at equilibrium time of 80 min and maximum adsorption was 42.9 mg.g^{-1}. The surface morphology of AC1+H_3PO_4 after an SEM examination confirms earlier reports which suggest that phosphoric acid injection could enhance the surface characteristics of adsorbents, hence a fulfilment of one of the objectives of this study which was to ascertain the veracity of potential of phosphoric acid as activation agent for adsorbents. FPOLP has proven to be a cheap source of activated carbon with good potential for adsorbing methylene blue.

ACKNOWLEDGEMENT

This research could not have been successfully executed without the financial backing of Wuhan University of Technology (WUT:2016IVA046), Natural Science Foundation of China (Ref. 5104205) and Hubei Provincial Science Foundation (Ref. 2016CFB268), are graciously appreciated and acknowledged.

REFERENCES

Abadian, S., Rahbar-Kelishami, A., Norouzbeigi, R. and Peydayesh, M. 2015. Cu(II) adsorption onto *Platanus orientalis* leaf powder: Kinetic, isotherm, and thermodynamic studies. Res. Chem. Intermed., 41: 7669-7681.

Abid, M.F., Zablouk, M.A. and Abid-Alameer, A.M. 2012. Experimental study of dye removal from industrial wastewater by membrane technologies of reverse osmosis and nanofiltration. Iranian J. Environ. Health Sci. Eng., 9: 17.

Akyol, A. 2012. Treatment of paint manufacturing wastewater by electrocoagulation. Desalination, 285: 91-99.

Altenor, S., Carene, B., Emmanuel, E., Lambert, J., Ehrhardt, J.J. and Gaspard, S. 2009. Adsorption studies of methylene blue and phenol onto vetiver roots activated carbon prepared by chemical activation. J. Hazard. Mater., 165: 1029-1039.

Babu, B.R., Parande, A.K. and Kumar, S.A. 2011. Treatment of dye effluent by electrochemical and biological processes. Open J. Saf. Sci. Technol., 1: 12-18.

Cardenas-Peña, A.M., Ibanez, J.G. and Vasquez-Medrano, R. 2012. Determination of the point of zero charge for electrocoagulation precipitates from an iron anode. Int. J. Electrochem. Sci., 7: 6142-6153.

Çiçek, F., Özer, D., Özer, A. and Özer, A. 2007. Low cost removal of reactive dyes using wheat brand. J. Hazard. Mater., 146: 408-416.

Demiral, H. and Güngör, C. 2015. Adsorption of copper (II) from aqueous solutions on activated carbon prepared from grape bagasse. J. Clean. Prod., 124: 103-113.

Demirbas, E., Kobya, M. and Sulak, M.T. 2008. Adsorption kinetics of a basic dye from aqueous solutions onto apricot stone activated carbon. Bioresour. Technol., 99: 5368-5373.

Dias, J.M., Alvim-Ferraz, M.C.M., Almeida, M.F., Rivera-Utrilla, J. and Sánchez-Polo, M. 2007. Waste materials for activated carbon preparation and its use in aqueous-phase treatment: A review. J. Environ. Manage., 85: 833-846.

Do, D.D. 1998. Adsorption Analysis: Equilibria and Kinetics. Vol. 2, Imperial College Press, London.

Dod, R., Banerjee, G. and Saini, S. 2012. Adsorption of methylene blue using green pea peels (Pisum sativum): a cost-effective option for dye-based wastewater treatment. Biotechnol. Bioprocess Eng., 17: 862-874.

El Qada, E.N., Allen, S.J. and Walker, G.M. 2008. Adsorption of basic dyes from aqueous solution onto activated carbons. Chem. Eng. J., 135: 174-184.

Elizalde-González, M.P., Mattusch, J., Peláez-Cid, A.A. and Wennrich, R. 2007. Characterization of adsorbent materials prepared from avocado kernel seeds: Natural, activated and carbonized forms. J. Anal. Appl. Pyrolysis, 78: 185-193.

El-Sharkawy, E.A., Soliman, A.Y. and Al-Amer, K.M. 2007. Comparative study for the removal of methylene blue via adsorption and photocatalytic degradation. J. Colloid Interface Sci., 310: 498-508.

Evbuomwan, B.O., Abutu, A.S and Ezeh, C.P. 2012. The effects of carbonization temperature on some physicochemical properties of bamboo based activated carbon by potassium hydroxide (KOH) activation. Greener J. Phys. Sci., 3: 187-191.

Franca, A.S., Oliveira, L.S. and Ferreira, M.E. 2009. Kinetics and equilibrium studies of methylene blue adsorption by spent coffee grounds. Desalination 249: 267-272.

Fu, Y. and Viraraghavan, T. 2001. Fungal decolorization of dye wastewaters: A review. Bioresour. Technol., 79: 251-262.

Galindo, C., Jacques, P. and Kalt, A. 2001. Photooxidation of the phenylazonaphthol AO20 on TIO2: Kinetic and mechanistic investigations. Chemosphere, 45: 997-1005.

Garg, V.K, Amita, M., Kumar, R. and Gupta, R. 2004. Basic dye (methylene blue) removal from simulated wastewater by adsorption using Indian rosewood sawdust: a timber industry waste. Dye Pigment, 63: 243-250.

Hameed, B.H. and Daud, F.B.M. 2008. Adsorption studies of basic dye on activated carbon derived from agricultural waste: *Hevea brasiliensis* seed coat. Chem. Eng. J., 139: 48-55.

Hameed, B.H., Mahmoud, D.K and Ahmad, Al. 2008. Sorption of basic dye from aqueous solution by pomelo (*Citrus grandis*) peel in a batch system. Colloids Surfaces A: Physicochem. Eng. Asp., 316: 78-84.

Ho, Y.S. 2004. Citation review of Lagergren kinetic rate equation on adsorption reactions. Scientometrics 59: 171-177.

Ho, Y.S. and Mckay, G. 1999. Pseudo-second order model for sorption processes. Process Biochem., 34: 451-465.

Ho, Y.S. and Mckay, G. 1998. Sorption of dyes from aqueous solution by peat. Chem. Eng. J., 70: 115-124.

Hu, C., Zhou, J., He, S., Luo, Z. and Cen, K. 2009. Effect of chemical activation of an activated carbon using zinc chloride on elemental mercury adsorption. Fuel Process. Technol., 90: 812-817.

Jokar, M., Farahani, T.S. and Ramezanzadeh, B. 2016. Electrochemical and surface characterizations of *Morus alba* pendula leaves extract (MAPLE) as a green corrosion inhibitor for steel in 1M HCl. J. Taiwan Inst. Chem. Eng., 63: 436-452.

Kamsonlian, S., Suresh, S., Ramanaiah, V., Majumder, C.B., Chand, S. and Kumar, A. 2012. Biosorptive behaviour of mango leaf powder and rice husk for arsenic(III) from aqueous solutions. Int. J. Environ. Sci. Technol., 9: 565-578.

Kaushik, P. and Malik, A. 2009. Fungal dye decolourization: recent advances and future potential. Environ. Int., 35: 127-141.

Kundu, S., Wang, Y., Xia, W. and Muhler, M. 2008. Thermal stability and reducibility of oxygen-containing functional groups on multiwalled carbon nanotube surfaces: A quantitative high-resolution XPS and TPD/TPR study. J. Phys. Chem. C., 112: 16869-16878.

Lee, J.W. and Choi, S.P., Thiruvenkatachari, R., Shim, W.G. and Moon, H. 2006. Evaluation of the performance of adsorption and coagulation processes for the maximum removal of reactive dyes. Dye Pigment, 69: 196-203.

Li, L., Quinlivan, P.A. and Knappe, D.R.U. 2002. Effects of activated car-

bon surface chemistry and pore structure on the adsorption of organic contaminants from aqueous solution. Carbon N. Y., 40: 2085-2100.

Lupascu, T. and Povar, I. 2016. Analysis of adsorption technologies of water and wastewater treatment used in the republic of Moldova. American Journal of Chemical Engineering, 4(6): 147-153.

Murthy, U.N., Rekha, H.B. and Bhavya, J.G. 2011. Performance of electrochemical oxidation in treating textile dye wastewater by stainless steel anode. International Journal of Environmental Science and Development, 2(6): 483.

Nethaji, S., Sivasamy, A. and Mandal, A.B. 2013. Adsorption isotherms, kinetics and mechanism for the adsorption of cationic and anionic dyes onto carbonaceous particles prepared from *Juglans regia* shell biomass. Int. J. Environ. Sci. Technol., 10: 231-242.

Nowicki, P. and Pietrzak, R. 2010. Carbonaceous adsorbents prepared by physical activation of pine sawdust and their application for removal of NO_2 in dry and wet conditions. Bioresour. Technol., 101: 5802-5807

Nowicki, P., Skrzypczak, M. and Pietrzak, R. 2010. Effect of activation method on the physicochemical properties and NO_2 removal abilities of sorbents obtained from plum stones (*Prunus domestica*). Chem. Eng. J., 162: 723-729.

Oliveira, L.S., Franca, A.S., Alves, T.M. and Rocha, S.D.F. 2008. Evaluation of untreated coffee husks as potential biosorbents for treatment of dye contaminated waters. J. Hazard. Mater., 155: 507-512.

Pavan, F.A., Lima, E.C., Dias, S.L.P. and Mazzocato, A.C. 2008. Methylene blue biosorption from aqueous solutions by yellow passion fruit waste. J. Hazard. Mater., 150: 703-712.

Ponnusami, V., Vikram, S. and Srivastava, S.N. 2008. Guava (*Psidium guajava*) leaf powder: Novel adsorbent for removal of methylene blue from aqueous solutions. J. Hazard. Mater., 152: 276-286.

Pradhan, S. 2011. Production and characterization of activated carbon produced from a suitable Industrial sludge. Doctoral Thesis.

Prahas, D., Kartika, Y., Indraswati, N. and Ismadji, S. 2008. Activated carbon from jackfruit peel waste by H_3PO_4 chemical activation: Pore structure and surface chemistry characterization. Chem. Eng. J., 140: 32-42.

Rashed, M.N. 2013. Adsorption technique for the removal of organic pollutants from water and wastewater. In: Organic Pollutants-Monitoring, Risk and Treatment. Intech Open.

Saengbutr, K., Wangphon, N. and Wanchanthuek, R. 2014. The investigation of experimental condition and kinetic study of methylene blue adsorption onto neem (*Azadirachta indica*) leaf powder. International Journal of Scientific and Research Publications, 4(10): 2250-3153.

Sawal, M. 1986. General standards for discharge of environmental pollutants. Environ. Rules., 2: 545-560.

Sleiman, M., Vildozo, D., Ferronato, C. and Chovelon, J.M. 2007. Photocatalytic degradation of azo dye Metanil yellow: Optimization and kinetic modeling using a chemometric approach. Appl. Catal. B Environ., 77: 1-11.

Thusnavis, K.P., Vinod Kumar, M. and Sankara Narayana Pillai, G.R. 2011. Seed extract of *Psidium guajava* as ecofriendly corrosion inhibitor for carbon steel in hydrochloric acid medium. J. Mater. Sci. Technol., 27: 1143-1149.

Tong, D.S., Hui, C., Zhou, C., Lu, Y., Yu, H., Zhang, G.F. and Yu, W.H. 2010. Applied clay science adsorption of acid red G dye on octadecyl trimethylammonium montmorillonite. Appl. Clay Sci., 50: 427-431.

Tsai, W.T., Chang, C.Y., Lin, M.C., Chien, S.F., Sun, H.F. and Hsieh, M.F. 2001. Adsorption of acid dye onto activated carbons prepared from agricultural waste bagasse by $ZnCl_2$ activation. Chemosphere, 45: 51-58.

Wali, K.M.F. 2015. Color removal and cod reduction of dyeing bath wastewater by Fenton reaction. Int. J. Waste Resour., 5: 1-6.

Wang, L.H. and Lin, C.I. 2008. Adsorption of lead(II) ion from aqueous solution using rice hull ash. Ind. Eng. Chem. Res., 47: 4891-4897.

Wang, Z., Xue, M., Huang, K. and Liu, Z., 2011. Textile dyeing wastewater treatment. Advances in treating textile effluent, 5: 91-116.

Weng, C.H. and Pan, Y.F. 2007. Adsorption of a cationic dye (methylene blue) onto spent activated clay. J. Hazard. Mater., 144: 355-362.

Worch, Eckhard 2012. Adsorption Technology in Water Treatment: Fundamentals, Processes, and Modeling. Walter de Gruyter.

World Health Organization 2006. A Compendium of Standards for Wastewater Reuse in The Eastern Mediterranean Region. WHO-EM/CEH/142/E. 19.

Wu, B., Zhang, J., Yang, M., Yue, Y., Ma, L.J. and Yu, X.Q. 2008. Raney Ni/KBH4: An efficient and mild system for the reduction of nitriles to amines. Arkivoc., 95-102.

Xiong, L., Yang, Y., Mai, J., Sun, W., Zhang, C., Wei, D., Chen, Q. and Ni, J. 2010. Adsorption behavior of methylene blue onto titanate nanotubes. Chem. Eng. J., 156: 313-320.

Yakout, S.M. and Sharaf EL-Deen, G. 2016. Characterization of activated carbon prepared by phosphoric acid activation of olive stones. Arab. J. Chem., 9: S1155-S1162.

Nature Environment and Pollution Technology
An International Quarterly Scientific Journal

p-ISSN: 0972-6268
e-ISSN: 2395-3454

Vol. 19 | No. 1 | pp. 41-56 | 2020

Original Research Paper | Open Access

Comparative *In Vitro* Assessment of Hydrocarbon Degradation Potential of *Pleurotus ostreatus* MP 5 and *Pleurotus ostreatus* MTCC 1804

Madhavi Tiwari*†, Ashish Saraf and Meghna Shrivastava***
*MATS School of Sciences, MATS University, Raipur-494001, C.G., India
**Faculty of Sciences, MATS University, Raipur-494001, C.G., India
†Corresponding author: Madhavi Tiwari

Nat. Env. & Poll. Tech.
Website: www.neptjournal.com

Received: 30-06-2019
Accepted: 29-08-2019

Key Words:
Pleurotus ostreatus
Mycoremediation
Hydrocarbon degradation
PAHs
Bioremediation
White rot fungus

ABSTRACT

Mycoremediation, involving the use of fungus for bioremediation, is one of the promising cost-effective methods for cleaning up the carcinogenic and mutagenic polycyclic aromatic hydrocarbons present in the environment. The present study deals with the isolation of white rot fungus from Chhattisgarh forest, India followed by identification based on ITS sequencing. Identification revealed MP 5 closely related to *Pleurotus ostreatus* isolate 6689 with 99% sequence similarity. Comparative primary screening assay of both the wild isolate and reference strain of *Pleurotus ostreatus* MTCC 1804 was performed by measuring the growth diameter of mycelia on minimal salt media enriched with 2% used engine oil (v/v). The fungal isolate MP 5 showed highest average growth rate. Confirmatory test was conducted via orbital shaking method and spectroscopic study was carried out at 600 nm which displayed degradation within 7 days and percentage of degradation was calculated. Level of degradation was 69.7 ± 0.351% and 64.7 ± 1.153% respectively for *Pleurotus ostreatus* MP 5 and *Pleurotus ostreatus* MTCC 1804. Degradation potential of both the isolates were evaluated in terms of chemical characterization via Fourier transform infrared spectroscopy (FTIR) which revealed bands formation based on the presence of different functional groups indicating oxidative degradation of hydrocarbons.

INTRODUCTION

Engine oil or motor oil is always on high demand globally and is used all over around the world in vehicles and other power generating engines. Improperly and illegitimately discharging of spent engine oil by automobile industries and other power generating stations into water bodies, farming lands and other arable lands is quite frequent. This disposed and spilled oil left unattended for several years further give rise to pollution of soil, water and air causing lethal environmental hazards. Oil contains more than 30 parent polyaromatic hydrocarbons (PAHs) which again constitutes hundreds of different hydrocarbon compounds such as paraffins, naphthene, aromatics as well as organic sulphur compounds, organic nitrogen compounds and oxygen containing hydrocarbons (Jawhari & Ihsan 2014). Increased use and demand of engines which in turn uses engine oil is the first and foremost reason for soil pollution. Leaving the spent oil unattended for several years reduces the fertility of the soil and converts it into a barren land. Both the used and unused engine oil are similar except that the used one comprises some additional chemicals which may have built up when engine runs by reacting with carcinogenic and mutagenic metals found in used motor oil that comes from engine parts as they wear down (Adongbede & Sanni 2014). According to various researchers it's a known fact that used motor oil contains metals and heavy polycyclic aromatic hydrocarbons which contribute to chronic hazards including mutagenicity and carcinogenicity (Boonchan et al. 2000, Hagwell et al. 1992, Keith & Telliard 1979). Undesirable presence of petroleum hydrocarbons in the environment is toxic, mutagenic and carcinogenic (Clemente et al. 2001). Therefore, the most ominous problems that the world is grappling today is the environmental pollution by petroleum hydrocarbons and its hazardous effects on ecosystem.

The objective of solving environmental pollution problems with the application of biotechnological processes involving microorganism is rapidly growing in recent decades. Among such application of biotechnological processes, mycoremediation is one which can be defined as the use of fungal systems to catalyse the destruction or transformation of various hazardous chemicals to less harmful forms (Thomas et al. 1998). As it is simple to maintain, applicable over large areas, cost effective and leads to complete destruction of the contaminant, it has been proved out to be one of the fascinating approaches for cleaning up of the petroleum hydrocarbons (Huesemann 1994). The term mycoremediation was coined by Paul Stamets which specifically refers

to the use of fungal mycelia in bioremediation. One of the primary roles of fungi in the ecosystem is decomposition, which is performed by the mycelium. It has been reported by Barr et al. (1994), that fungi secrete nonspecific extracellular enzymes such as laccase, lignin peroxidase and manganese peroxidase, that give these fungi the ability to degrade lignin and also used to degrade a wide range of hydrocarbon pollutants that resemble the lignin structure such as total petroleum hydrocarbons (TPHs), dichlorodiphenyltrichloroethane (DDT), trinitrotoluene (TNT), polychlorinated biphenyl (PCB) and polycyclic aromatic hydrocarbons (PAHs). Mycelial enzymes can decompose many resistant materials made by humans or nature, because many of the bonds that hold plant material together are like the bonds found in petroleum products including diesel and oil (Stamets 2005).

Application of higher fungi like mushrooms has been known in the remediation of polluted soil for some years now. The application of white-rot fungi in bioremediation is now considered to be economical because the fungi can be cultured on varieties of inexpensive agricultural or forest wastes such as rice straw, corn cobs and sawdust. According to the recent studies, *P. ostreatus* can degrade a variety of polycyclic aromatic hydrocarbons (PAH) (Sack & Gunther 1993). Emuh (2010) proclaimed that the mushroom hypha and mycelia possess the capability to break down and absorb the crude oil and heavy metals present in polluted soil through the secretion of enzymes into environmentally safe levels. Zebulun et al. (2011) reported his work on decontamination of anthracene-polluted soil through a white rot fungus (*P. ostreatus*) which induced biodegradation. Further he divulged that lignolytic enzymes such as lignin peroxidase, laccase and manganese peroxidase by *P. ostreatus* catalysed the degradation of anthracene. Similarly, Okparanma et al. (2011) broadcasted that spent white-rot fungi (*P. ostreatus*) substrate can be utilized to remediate Nigerian oil-based drill cuttings constituting PAHs. The oyster mushroom*, P. ostreatus*, can degrade 80-95% of all PAHs present in soil (Steffen et al. 2007).

The utility of mushroom for biodegradation has beguiling probability because of their potentiality to degrade lignin and other resembling compounds like PAHs. According to the previous explorations involving white rot fungi and their capability to degrade petroleum hydrocarbons, several auspicious results have been reported. Hence the present investigation purposes to isolate white rot fungi and to perform comparative evaluation of hydrocarbon degradation potential of both wild isolate and reference strain of *Pleurotus ostreatus* MTCC 1804 which may prove to be a promising isolate for mycoremediation studies.

MATERIALS AND METHODS

Chemicals and Reagents

All the media used during the experiment were purchased from Himedia Laboratories Pvt. Limited (Mumbai, India). All the fine chemicals used were procured from SRL Chemicals, India with highest purity and analytical grade. Used engine oil of Castrol Company was procured from automobile workshop.

Source of Fungal Cultures

Fruiting bodies of the Basidiomycete samples were collected from Geedam forest spread across Dantewada district, Chhattisgarh, India. The samples were apparently brought to the laboratory in sterilized bags and were refrigerated at 4°C in refrigerator until they were processed. The materials were used for experimental procedures within 24 hours. *Pleurotus ostreatus* MTCC 1804 as reference strain was procured from Microbial Type Culture Collection (MTCC), Chandigarh, India. The fungus was propagated on Potato Dextrose Agar (PDA Himedia) at 25ºC for 7 days, maintained in agar slants and sub cultured after every 15 days.

Isolation of White Rot Fungus

The tissues of the wild isolate were inoculated into PDA (Himedia) prepared following the manufacturer's instructions. The pure culture of the test organism was incubated at room temperature for 7 days in biological oxygen demand (BOD) incubator. Culture was maintained in agar slants and subcultured after every 15 days.

Molecular Identification

Molecular characterization of the wild fungal isolate was achieved through ITS sequencing. Identification process was completed by comparing the ITS regions of the fungal isolate with NCBI data available and the closest neighbour with 99% similarity index was assigned. The identification was done by NCMR, Pune, Maharashtra, India.

Comparative Primary Screening

For primary screening, a selective carbon free media known as Mineral Salts Medium (MSM) [v/v] of Mills et al. (1978) as modified by Okpokwasili & Okorie (1988) was prepared which was later supplemented with 50 mg/mL ampicillin and 2% of filtered sterile used engine oil (Vanishree et al. 2014). 1 cm^2 mycelial plug of pure fungal isolate was aseptically inoculated in MSM with the help of cork borer, and incubated at 25°C for 7 days and the growth rates were recorded daily by measuring the diameter of the radial extension of fungal mycelium (Thenmozhi et al. 2013). Pure fungal isolates

were also inoculated on MSM without oil which served as control. All the inoculations were performed in triplicates. The growth rates of both the wild isolate and reference strain were recorded daily by measuring the diameter of the radial extension of the mycelium. Measurements were done by measuring at least two diameters per plate and average of diameters were used as the colony diameter at that time of measurement (cm/day) (dos Santos et al. 2008). According to dos Santos et al. (2008) colony growth rates were further evaluated by regressing the colony diameter against the days after inoculation. Fungal isolates which showed heavy sporulation, more abundant aerial mycelium and greater colony diameter were considered as organisms utilizing hydrocarbons as their carbon source which were later confirmed through confirmatory screening (Thenmozhi et al. 2013).

Confirmatory Screening *(Orbital Shaking Method)*

To confirm the hydrocarbon degrading capability of the both the wild isolate and reference strain a modified technique based on the redox indicator 2, 6- dichlorophenol indophenol (DCPIP) was performed and purposely Bacto Bushnell- Hass (BH) broth medium was prepared (Hanson et al. 1993). A control flask without inoculum was also prepared. Three agar plugs from 7 days old culture of pure fungal isolates were picked from the surface of the Petri dish with the help of cork borer and aseptically inoculated into 50 mL of sterilized BH broth medium using 150 mL Erlenmeyer flask and later, also incorporated with 0.2 % (v/v) Tween 80, 2% (v/v) crude oil and redox reagent (2% 2, 6- dichlorophenol indophenols). All the flasks were incubated in orbital shaking incubator at 25°C with constant shaking at 180 rpm for 7 days. The aliquots inside the flask were supervised daily for colour change from deep blue to colourless. After 7 days of incubation period, filtration of the broth of all the flasks was accomplished with the help of filter paper for the separation of fungal biomass, proximately followed by centrifugation at 8000 rpm for 15 minutes. Supernatants obtained after centrifugation were assayed spectrophotometrically at 600 nm with the help of UV-VIS spectrophotometer (Systronics Double Beam Spectrophotometer 2203) and the percentage of biodegradation was evaluated via the following equation (Hanson et al. 1993, Tiwari et al. 2017)

Percentage (%) of Degradation = [1- Absorbance of treated sample/ Absorbance of control] x 100

Biodegradation Assay of Hydrocarbon by Fungal Cultures

Three agar discs of fresh pure cultures of duo fungal isolates were inoculated into 50 ml of BH broth in Erlenmeyer flask (150 mL) comprising 0.2 % (v/v) Tween 80 and 2% (v/v) crude oil. Meanwhile control flask was also prepared accordingly but with no inoculum. Later all the flasks were incubated in orbital shaking incubator at temperature 25°C with constant shaking at 180 rpm for 7 days. Again after 7 days of incubation, broths were filtered with the help of filter paper to separate the biomass which was weighed for the dry weight of fungal biomass by constant weighing (Hanson et al. 1993).

FTIR Analysis

Two-three mycelial plugs of the fungal isolates were inoculated in Czapeck dox broth with 2 % v/v used motor oil in a 250 mL Erlenmeyer flask. Control experiment containing same medium contents but without inoculum was performed. The flasks were agitated at 200 rpm at 25ºC for a period of 30 days and the content of each test including the control were harvested and subjected to FT-IR analysis (Thenmozhi et al. 2013). After harvesting all the samples including the control, were dried at 70ºC overnight before analysis to convert them into powdered form. KBr pellet was used as a background reference (Velioğlu et al. 2015). Approximately 1 mg of each of the samples were mixed with approximately 100 mg of dried KBr separately and then pressed to form a pellet for measurement. The FTIR spectra were broadcasted on the Perkin Elmer Inc. – Spectrum BX FTIR spectrometer, in the 4000-400 cm^{-1} spectral region.

Statistical Analysis

An analysis of variance (ANOVA) was performed to establish if there were any significant differences between the growth rates of the strains and their control plates at 95% confidence level ($P £ 0.05$). T test was also performed to statistically compare the means of colony diameter (cm/day) of both the isolates, percentage of degradation (%) and biodegradation assay of hydrocarbon in terms of fungal biomass (g/50 mL) at 95% confidence level ($P \leq 0.05$).

RESULTS

Isolation of White Rot Fungus and Cultivation of *Ostreatus* MTCC 1804

Tissue culture of wild isolate MP 5 on PDA followed by 7 days of incubation gave pure culture of cottony white coloured mycelium with glossy surface (Fig. 1). Likewise procured culture, *Pleurotus ostreatus* MTCC 1804 also gave the mycelium with same appearance (Fig. 2).

Molecular Identification

The isolated white rot fungus was identified based on ITS sequencing and sequence of the identified isolate was

generated using NCBI data base, and the confidence in identification was limited by both the availability and the extent of homology shown by the ~550 bp sequence of the sample with its closest neighbour in the database. Molecular characterization of the wild isolate which exhibited high sequence similarity (~99%) to that of *Pleurotus ostreatus* isolate 6689 (accession No. AY450345.1). Fig. 3 shows the nucleotide sequence in FASTA format which was resulted out based on ITS sequencing. After identification process, MP 5 isolate was also got deposited in NCMR Pune, in general deposition repository under accession No. MCC 1815.

Colony Growth Evaluation

Colony growth rate evaluation was done to investigate the primary screening of hydrocarbon degradation potential of both the isolates based on colony diameter. As the colony growth rates (cm/day) were calculated by regressing the colony diameter against the days after inoculation it was resulted out that the growth curves of the isolates, based on colony diameters as a function of time, were typical of fungal growth. The correlation coefficients (r^2) were greater than 0.95 (r^2 for MP 5 = 0.99, r^2 for MP 5 control = 1 and r^2 for *Pleurotus ostreatus* MTCC 1804 = 0.99, r^2 for *Pleurotus ostreatus* MTCC 1804 = 0.97), which indicated that the linear regression satisfactorily explained the variation of the colony diameter as a function of time.

The mean values and standard deviations for the growth rates of MP 5 and *Pleurotus ostreatus* MTCC 1804 strain including control are represented in Table 1. According to Table 1, it was resulted out that both the strains showed highest average colony growth each day (cm/day) in terms of diameter (mean ± sd) on MSM plates supplemented with 2 % oil as compared to their control MSM plates which was not supplemented with oil also explained graphically in Fig. 4 (for MP 5) and Fig. 5 (for *P.ostreatus* MTCC 1804). All these differences between the strains and their control plates was found to be significant at $p \leq 0.05$ at 95% confidence level as calculated by ANOVA.

On comparison it was also evaluated out that the wild strain MP 5 showed highest average colony growth rate (cm/day) with mean ± sd 3.2 ± 0.057 more than *Pleurotus ostreatus* MTCC 1804 which exhibited mean ± sd 1.2 ± 0.115 as depicted graphically in Fig. 6. This comparison was also significant at $p \leq 0.05$ at %95 confidence level as calculated by t-test.

Fig. 1: *P. ostreatus* MP 5.

Fig. 2: *P. ostreatus* MTCC 1804.

GGAAGtTTGTTGCTGGCCTCTAGGGGCATGTGCACGCTTCACTAGTCTTTCAACCACCTGTGAACTTT
TGATAGATCTGTGAAGTCGTCTCTCAAGTCGTCAGACTTGGTTGCTGGGATTTAAACGTCTCGGTGTGACTAC
GCAGTCTATTTACTTACACACCCCAAATGTATGTCTACGAATGTCATTTAATGGGCCTTGTGCCTTTAAACCATAA
TACAACTTTCAACAACGGATCTCTTGGCTCTCGCATCGATGAAGAACGCAGCGAAATGCGATAAGTAATG
TGAATTGCAGAATTCAGTGAATCATCGAATCTTTGAACGCACCTTGCGCCCCTTGGTATTCCGAGGGGCATGCC
TGTTTGAGTGTCATTAAATTCTCAAACTCACTTTGGTTTCTTTCCAATTGTGATGTTTGGATTGTTGGGGGCTGC
TGGCCTTcGACAGGTCGGCTCCTCTTAAATGCATTAGCAGGACTTCTCATTGCCTCTGCGCATGATGTGATAA
TTATCACTCATCAATAGCACGCATGAATAGAGTCCAGCTCTCTAATCGTCCGCAAGGACAATTTGACAATTTGACC
TCAAATCAGGTAGGACTACCCGCTGAACTTAAGCATATCAATAAGCGGAGGAAGAT

Fig. 3: The~550 bp nucleotide sequence of fungal isolate MP 5.

Table 1: Average colony growth rates± standard deviations (cm/day) (n = 3) and statistical analysis of data of MP 5 and *Pleurotus ostreatus* MTCC 1804 on MSM + 2% oil and their control plates after 7 days:

No. of days	*Pleurotus ostreatus* MP 5		*Pleurotus ostreatus* MTCC 1804	
	MSM + oil plate	Control plate	MSM + oil plate	Control plate
	Mean ± SD	Mean ± SD	Mean ± SD	Mean ± SD
Day 1	0.2 ± 0.057	0 ± 0	0.1 ± 0.057	0 ± 0
Day 2	0.8 ± 0.1	0.2 ± 0.057	0.3 ± 0.1	0 ± 0
Day 3	1.4 ± 0.057	0.4 ± 0.1	0.5 ± 0.1	0.1 ± 0.057
Day 4	1.8±0	0.6 ± 0.057	0.7 ± 0.057	0.2 ± 0.1
Day 5	2.2 ± 0.152	0.8 ± 0.152	0.9 ± 0.057	0.3 ± 0.1
Day 6	2.8 ± 0.208	1.0 ± 0.1	1.0 ± 0.057	0.4 ± 0.152
Day 7	3.2 ± 0.057	1.2 ± 0.057	1.2 ± 0.115	0.5 ± 0.152

Growth rates between the fungal isolates MP 5 and *Pleurotus ostreatus* MTCC 1804 and their respective control plates are significantly different from each other at the 95% confidence level and significant at $p \leq 0.05$, p value was calculated by one-way ANOVA. Comparison of the average colony growth rates (cm/day) between MP 5 and *Pleurotus ostreatus* MTCC 1804 in terms of diameter is also significant at $p \leq 0.05$ level which was calculated by t-test.

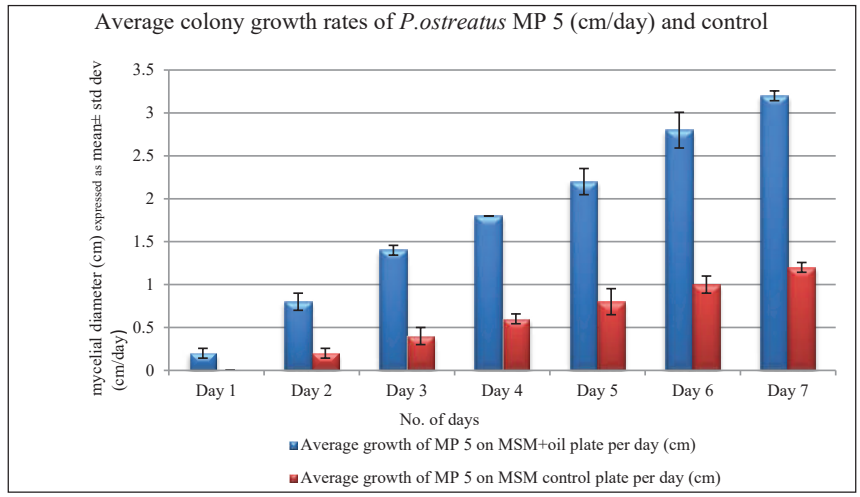

Fig. 4: Average colony growth rates (cm/day) of *Pleurotus ostreatus* MP 5 and control plates. Each bar represents Mean ± SD of two separate observations (n = 2). The results were statistically significant at $p \leq 0.05$.

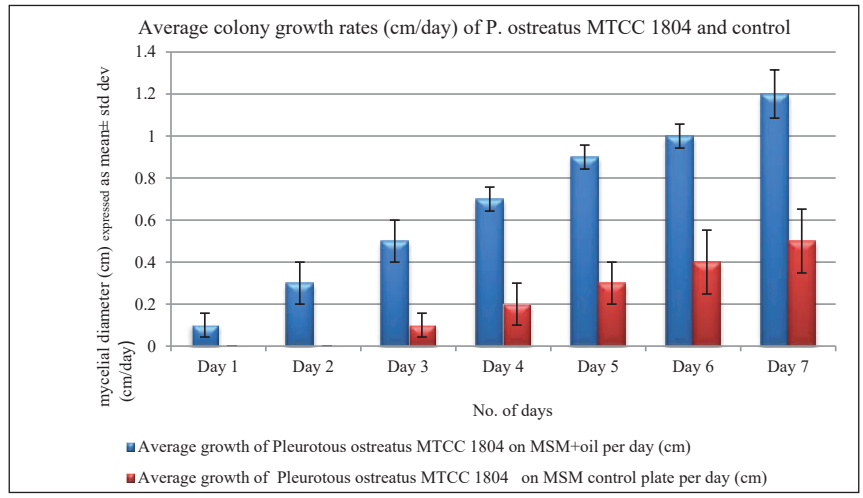

Fig. 5: Average colony growth rates (cm/day) of *Pleurotus ostreatus* MTCC 1804 and control plates. Each bar represents Mean ± SD of two separate observations (n = 2). The results were statistically significant at $p \leq 0.05$.

Confirmatory Screening (Orbital Shaking Method)

2, 6-dichlorophenol indophenols (2, 6-DCPIP) test or redox indicator test was performed to detect the potential of most efficient strain to degrade oil (hydrocarbon) revealed that BH broth inoculated with each fungal isolates changed colour from blue to colourless and gave 100 % response as tabulated in Table 2 which can be visualized in Figs. 7(a) and (b). Table 3 describes the measurement of total colour change as an absorbance value in terms of mean ± SD using spectrophotometer recorded as 0.459 ± 0.005 and 0.536 ± 0.017 for *Pleurotu sostreatus* MP 5 and *Pleurotus ostreatus* MTCC 1804 found to be significant at $p \leq 0.05$ calculated by T test which correlates to the potentiality of the isolate to utilize hydrocarbon.

Based on the absorbance values of filtrates obtained spectrophotometrically after centrifugation, percentage or level of hydrocarbon degradation of the duo fungal isolates were calculated which are expressed in Table 4. Higher percentage of degradation of oil was shown by the fungal isolate MP 5 which was recorded as 69.7±0.351 (mean±SD). Percent of degradation recorded for *Pleurotus ostreatus* MTCC 1804 was 64.7 ± 1.153 (mean ± SD) which was less as compared to MP 5, also elaborated graphically in Fig. 8. Differences in percentage of degradation of both the isolates was found to be significant at $p \leq 0.05$ calculated by t-test.

Biodegradation Assay of Hydrocarbon by Fungal Cultures

Biodegradation assay in terms of fungal biomass revealed

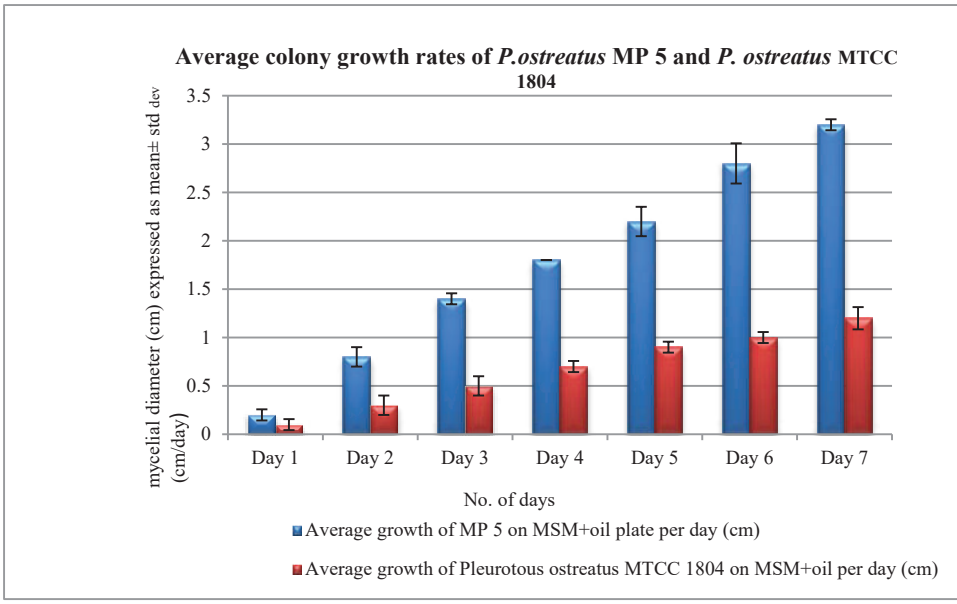

Fig. 6: Average colony growth rates (cm/day) of *Pleurotus ostreatus* MP 5 and *Pleurotus ostreatus* MTCC 1804. Each bar represents Mean ± SD of

Table 2: DCPIP test of fungal isolates for colour change with 2% DCPIP (BH broth + 0.2 % tween 80 +2 % crude oil + 2 % DCPIP).

S.No.	Fungal isolates	Colour change (blue to colourless)			Percentage of response (%)
		flask I	flask II	flask III	
1.	Control	-	-	-	0
2.	*Pleurotus ostreatus* MP 5	+	+	+	100
3.	*Pleurotus ostreatus* MTCC 1804	+	+	+	100

Table 3: Absorbance values of fungal isolates with 2 % DCPIP (50 ml BH broth + 0.2 % tween 80 + 2% crude oil + 2 % DCPIP) in terms of Mean±SD (n=3).

S.No.	Fungal isolates	Optical density (OD) (at 600 nm) Mean ± SD
1.	Negative Control	1.523 ± 0.001
2.	MP 5	0.459 ± 0.005
3.	*Pleurotus ostreatus* MTCC 1804	0.536 ± 0.017

Comparison of the absorbance (od) between MP 5 and *Pleurotus ostreatus* MTCC 1804 at 600 nm is also significant at $p \leq 0.05$ level which was calculated by t-test.

Table 4: Percentage of oil degradation of fungal isolates represented as Mean±SD (n = 3) of fungal isolates with 2% DCPIP (50 mL BH broth + 0.2% tween 80 + 2% crude oil + 2% DCPIP)**.**

S. No.	Fungal isolates	Percentage of degradation (Mean±SD)
1.	*Pleurotus ostreatus* MP 5	69.7 ± 0.351
2.	*Pleurotus ostreatus* MTCC 1804	64.7 ± 1.153

Comparison of percentage of degradation of both the isolates is found to be statistically significant at $p \leq 0.05$ level as calculated by t-test.

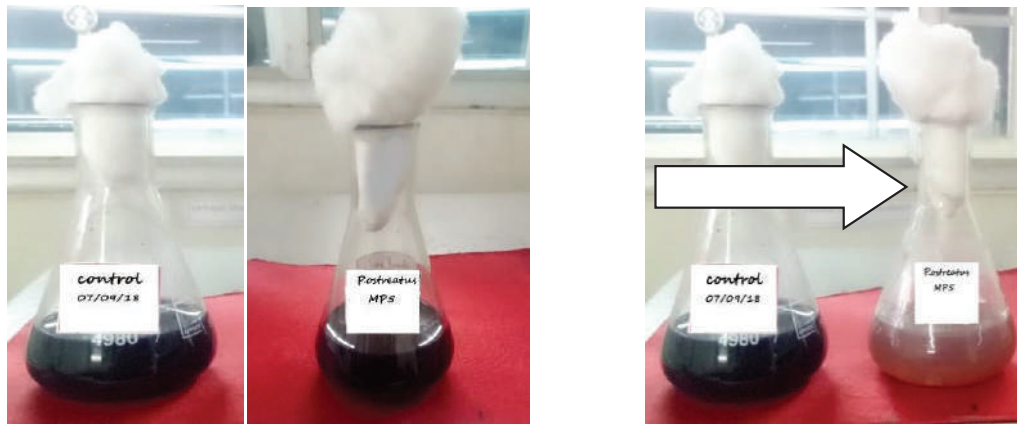

Fig. 7 (a): depicting DCPIP test, visualizing colour change from blue to colourless after biodegradation.

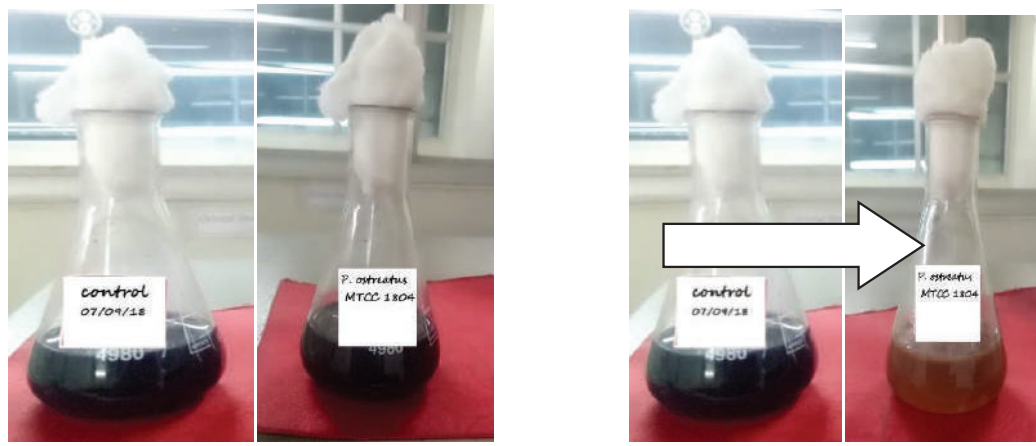

Fig. 7 (b): depicting DCPIP test, visualizing colour change from blue to colourless before after biodegradation.

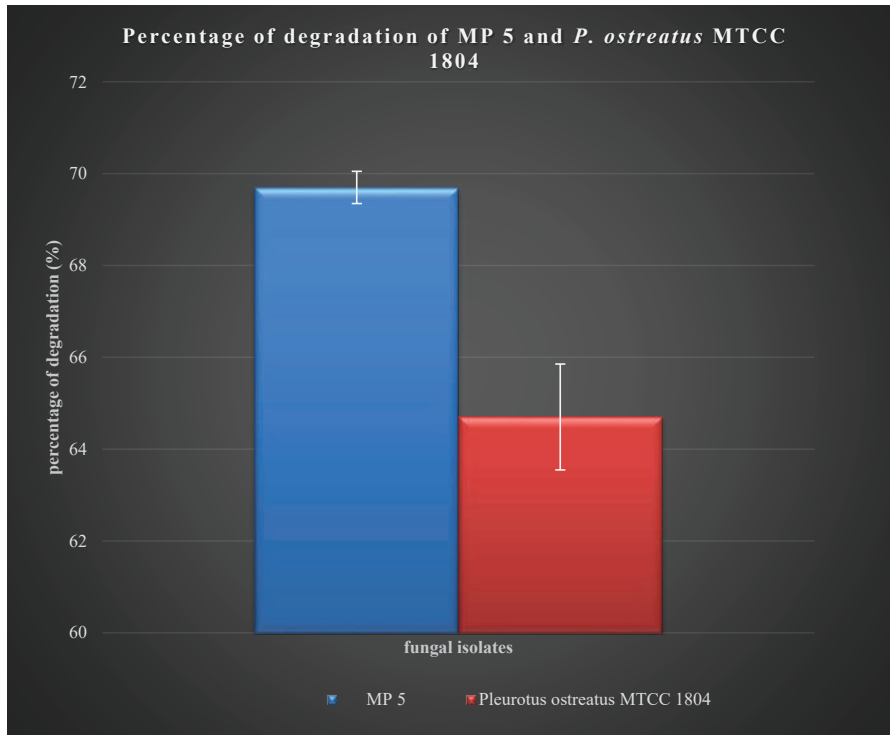

Fig. 8: Percentage degradation of MP 5 and *P. ostreatus* MTCC 1804. Each bar represents Mean ± SD of two separate observations (n = 2). The results were statistically significant at $p \leq 0.05$.

that at concentration of 2% (v/v) oil in BH broth, MP 5 gave better result than the reference strain on the basis of its bulk mass which was estimated out as 0.334 ± 0.009 g/50 mL as tabulated in Table 5 and graphically depicted in Fig. 9. Fungal biomass estimated out for reference strain was 0.308 ± 0.007 g/50 mL. This differences between dry weight of fungal biomass was found to be significant at $p \leq 0.05$ as calculated by T test.

FTIR Analysis

FTIR analysis of both the isolates including control described hydrocarbon degradation potential of MP 5 and *Pleurotus ostreatus* MTCC 1804 via the formation of various peaks indicating the presence of different functional groups formed during degradation (Figs. 10, 11 and 12).

DISCUSSION

The main aim of this investigation was to perform comparative study between the hydrocarbon degradation potential of two white rot fungal isolates for which primary screening, confirmatory screening, biodegradation assay, molecular identification and FTIR analysis were performed. Morphological and biochemical uniqueness of fungi are globally used for their identification, but divergence of close homologous cultures requires extensive molecular techniques (Shahriarinour et al. 2011). Promising techniques to identify a diversified range of fungi to the species level involves PCR amplification with universal primers targeted to conserved regions within the rRNA complex and subsequent DNA sequencing of the internal transcribed spacer (ITS) regions (Chen et al. 1999). According to White et al. (2001) PCR primer sets are routinely used for amplification of ITS regions. Therefore, the identification of the potential wild isolate was performed by NCMR, Pune, Maharashtra, India based on molecular technique involving ITS sequencing. To study the molecular identification of the selected wild isolate able to degrade benzo[a]pyrene based on ITS sequencing. Sourav et al. (2011) reported *Pleurotus ostreatus,* which is somewhat like the finding of the present investigation of molecular identification based on ITS sequencing.

dos Santos et al. (2008) confirmed the use of colony growth rate evaluation to investigate the growth rate of filamentous fungi in different hydrocarbons and oil derivatives and suggest this methodology as a tool to demonstrate the biodegradation potential of fungal strains. Present analysis demonstrated that the correlation coefficients (r^2) were greater than 0.95 which indicated that the linear regression

Table 5: Dry weight of fungal isolates represented in terms of Mean±SD (n = 3) (50 mL BH broth + 0.2 % tween 80 + 2% crude oil).

S. No.	Fungal isolates	Dry weight of fungal biomass (mean±sd) (g/50mL)
1.	*Pleurotus ostreatus* MP 5	0.334 ± 0.009
2.	*Pleurotus ostreatus* MTCC 1804	0.308 ± 0.007

Dry weight of both the fungal isolates shows statistically significant differences at $P \leq 0.05$ level as calculated by t-test.

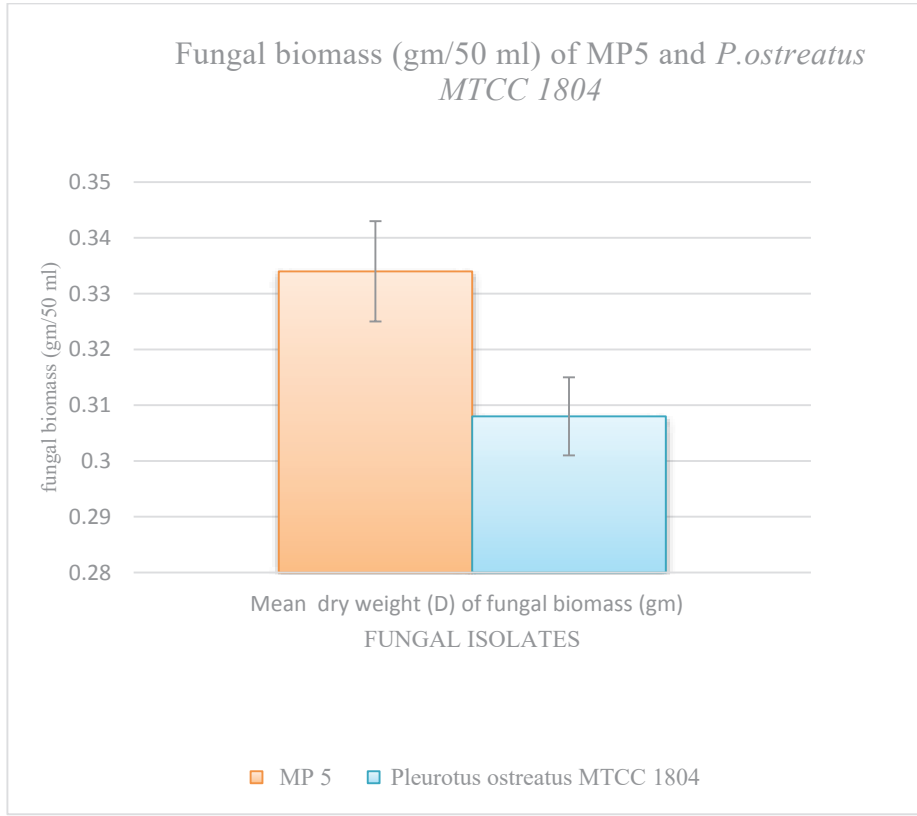

Fig. 9: Fungal biomass of MP 5 and *P. ostreatus* MTCC 1804. Each bar represents Mean±SD of two separate observations (n = 2). The results were statistically significant at $p \leq 0.05$.

satisfactorily explained the variation of the colony diameter as a function of time. dos Santos et al. (2008) supports the present analysis by reporting that during his experiments of colony growth evaluation of four fungal isolates on plates containing a specific hydrocarbon or petroleum derivative as the only carbon source, correlation coefficients (r^2) were greater than 0.95 (data not shown), indicating that the linear regression adequately explained the variation of the colony diameter as a function of time.

Experiments performed by Thenmozhi et al. (2013) revealed that that the fungal isolates JJF3 *Aspergillus niger* and JJF9 *Aspergillus luchiencis* with average colony diameter as 2.7 and 3.72 cm/day as compared to other fungal isolates exhibited bigger colony diameter, heavy sporulation, and abundant aerial mycelium on selective media (MSM) amended with 1% used engine oil. These evaluations foresighted those as hydrocarbon degraders which further elaborated their capability to utilize used engine oil as a carbon source for their growth. Likewise, in the present study, the highest average colony growth rate in terms of colony diameter (cm/day) observed for *Pleurotus ostreatus* MP 5 on MSM amended with 2 % oil was recorded as 3.2 ± 0.057 cm (mean±day) respectively which interpreted that mycelium of this fungal isolate proliferated rapidly forming heavy sporulation and dense hyphae than *Pleurotus ostreatus* MTCC 1804 (0.308 ± 0.007). Similarly, Popa et al. (2013) evaluated the ability of two isolates of *P. ostreatus* (P50, P421) and a sample of *P. ostreatus* collected from Chitila woods to use crude-oil

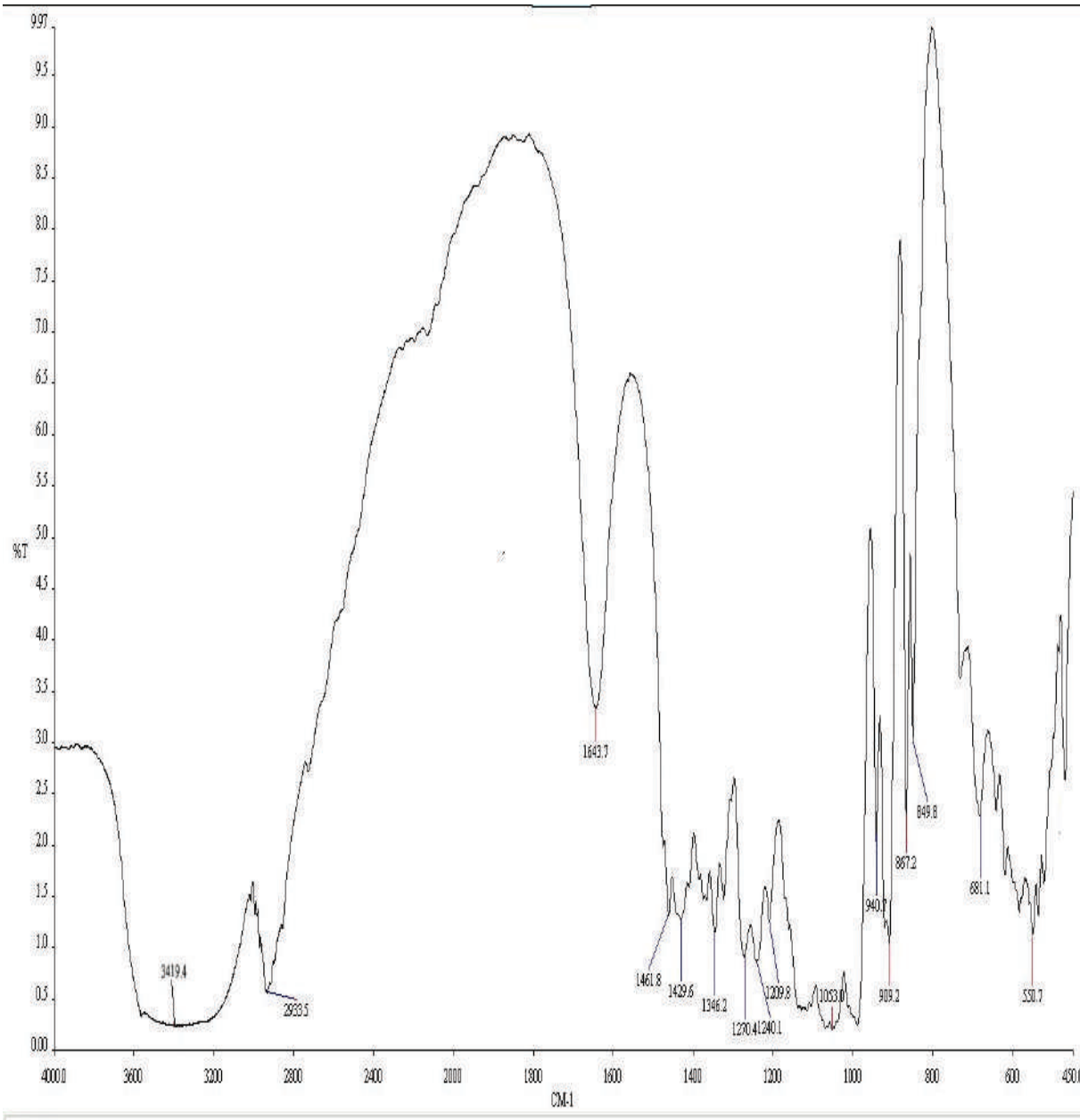

Fig. 10: FTIR spectrum of control sample.

as a carbon source for which he inoculated mycelia inoculum on MSM plates with crude oil (1 mL) spread on the entire carbon free mineral salt medium (MSM) surface and in plates with pieces of filter paper soaked in crude oil and placed around the inoculum. Evaluation done every day for 14 days, by measuring the radial growth of mycelia (in cm) and extrapolated as growing percentage to culture plate diameter (9 cm) revealed that both isolates of *P. ostreatus* as well as *P. ostreatus* originated from Chitila forest were able to utilize the crude oil as a source of carbon and energy in their metabolism.

Confirmatory screening also known as orbital shaking method also known as redox indicator test and DCPIP test in the present study is based on the principle of change in colour of BH broth from blue to colourless incorporated with fungal isolates, 0.2 % (v/v) Tween 80, 2% (v/v) crude oil and

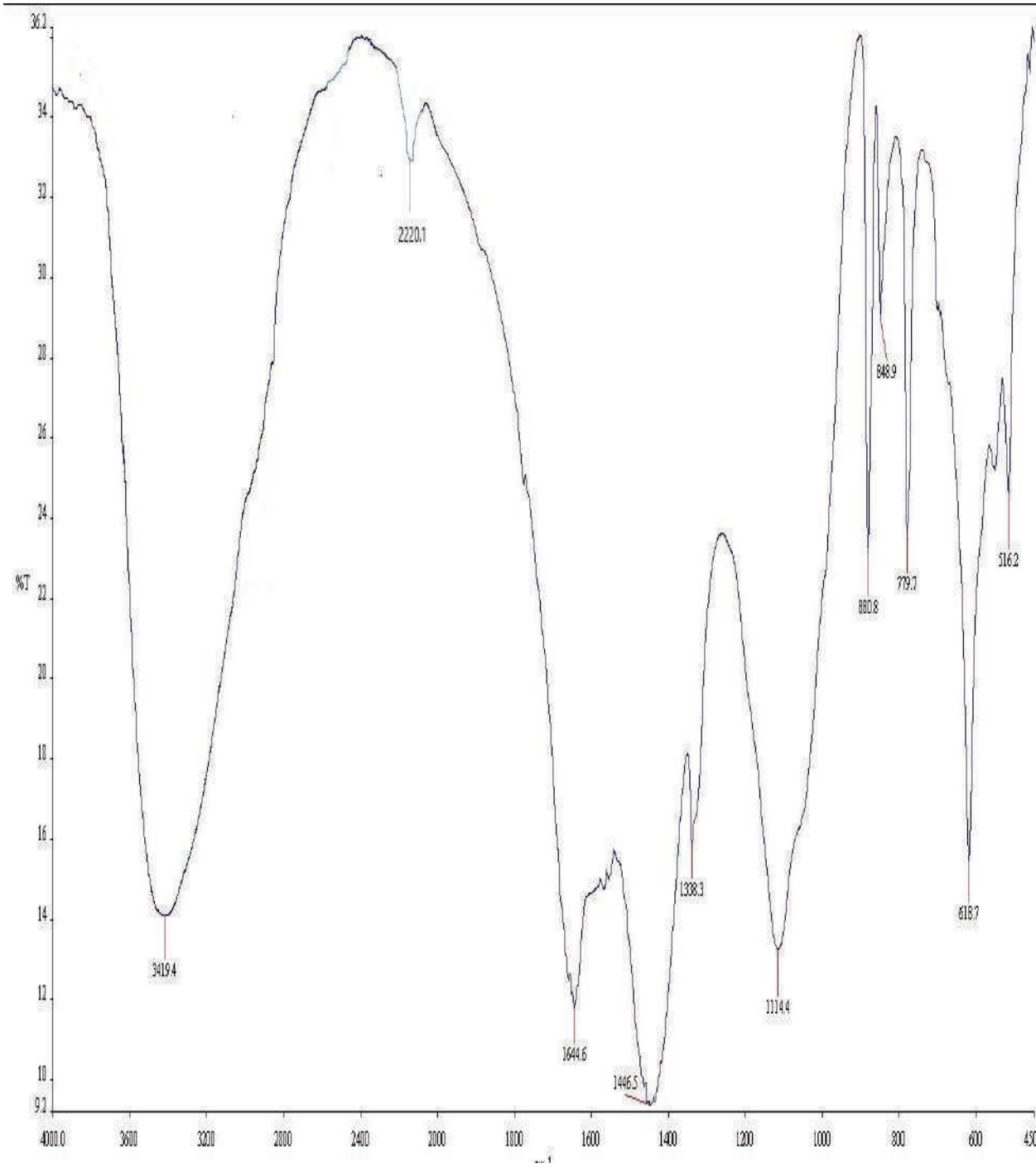

Fig. 11: FTIR spectrum of *P. ostreatus* MP 5.

redox reagent (2% 2, 6- dichlorophenol indophenols). This screening method is also known as redox indicator technique which is applied to assess the ability of fungal isolates to degrade crude oil in the presence of redox indicator 2, 6-DCPIP (Hanson et al. 1993). The main principle behind this degradation using redox reagent is that after incorporation of an electron acceptor such as DCPIP to the broth inoculated with fungi supplemented with oil and tween 80, it becomes possible to assess the ability of fungi to utilize the substrate by visualizing the colour change of DCPIP from blue (ox-

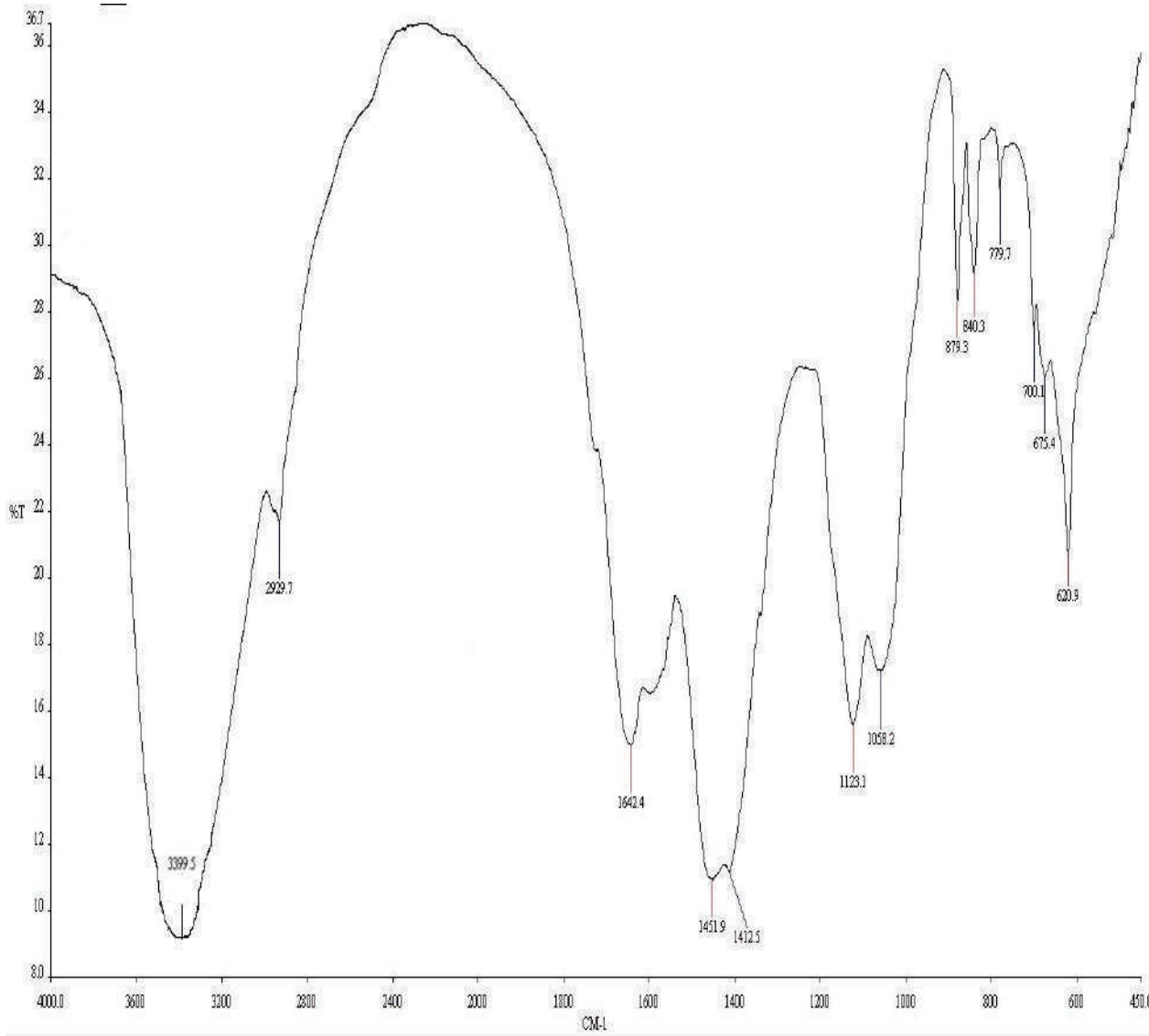

Fig. 12: FTIR spectrum of *P. ostreatus* MTCC 1804.

idized) to colourless (reduced) (Al-Nasrawi 2012). Tween 80 acts as an emulsifier which facilitates active contact between hydrocarbon and the isolate (Hanson et al. 1993). Three indication which verifies the ability of fungi involved in biodegradation process is firstly the change in colour of broth from dark blue to colourless, secondly the disappearance of crude oil from the broth and thirdly developing a mass of fungal biomass growth in the bottom of the broth (Hanson et al. 1993).

Colour transformation from blue to colourless during biodegradation process involving the specific isolates ramparts the fact that isolates are potential hydrocarbon oxidizers and the colour transformation can be measured as an absorbance value using spectrophotometer (George et al. 2009). The present investigation confirms the ability of *Pleurotus ostreatus* MP 5 and *Pleurotus ostreatus* MTCC 1804 to degrade used engine oil by displaying colour change from blue to colourless after seven days of incubation in shaking incubator.

As Yoshida et al. (2001) observed a peak in absorbance at 600 nm therefore; absorbance at a wavelength of 600 nm was recorded for fungal isolates. According to Undugoda et al. (2016) the higher hydrocarbon degrading fungi have low absorbance values after the incubation period as compared

to the control whereas lower hydrocarbon degrading fungi possess high absorbance values. The present comparative assessment reported that wild isolate *Pleurotus ostreatus* MP 5 (OD = 0.459 ± 0.005) has proved itself as a more potent hydrocarbon degrader than *Pleurotus ostreatus* MTCC 1804 (OD = 0.536 ± 0.017) by displaying the fastest onset colour disappearance (decrease in absorbance of broth medium) and hence, highest capability of biodegradation. Thus the present investigation is supported by the reports of Khan et al. (2015) who reported that Aspergillus sp., Penicillium sp. and Rhizopus sp. displayed the colour transformation from blue to colourless in the BH broth incorporated with the fungal isolates comprised with 0.1% (v/v) Tween 80 and 1% (v/v) petrol, kerosene and diesel and 0.008 mg/50 mL of redox indicator and hence showed the highest capability of biodegradation. The high rate of petroleum products (hydrocarbon) degradation by the wild isolate may be due to their enzyme production responses during their growth phases which could be supported by the reports and findings of Bogan & Lamar (1996) according to which during the growth phases of white rot fungi, extracellular ligninolytic enzymes are produced in response to their growth phases.

Percentage of degradation of each fungal isolate was calculated on the basis of absorbance value obtained after applying the formula, according to which *Pleurotus ostreatus* MP 5 gave higher percentage of degradation as compared to that of *Pleurotus ostreatus* MTCC 1804. Percentage of hydrocarbon degradation calculated for *Pleurotus ostreatus* MP 5 and *Pleurotus ostreatus* MTCC 1804 was 69.7 ± 0.351% and 64.7 ± 1.153%. Similarly, Ekundayo (2014) worked on comparative Studies on biodegradative abilities of *Pleurotus ostreatus* and *P. pulmonarius* in soils contaminated with crude and used engine Oils and investigated that *P. ostreatus* reduced the initial total hydrocarbon content (THC) to 8% and 9% in soils polluted with 20% of crude and used engine oils, respectively, which was lower than that of *P.pulmonarius.* Mineralization of various PAHs by white rot fungus *Pleurotus ostreatus* was reported by Bezalel et al. (1995) according to whom, *Pleurotus ostreatus* was able to mineralize to 7.0% of [14C]catechol, 3.0% of[14C] phenanthrene, 0.4% of [14C]pyrene, and 0.19% of [14C] benzo[*a*]pyrene followed by incubation of 11 days. Besides, the implication of the wild strain MP 5 as a more potent hydrocarbon degrader than that of the reference strain *Pleurotus ostreatus* MTCC 1804 from our result is similar to the findings of Sourav et al. (2013) while testing the potentiality of the isolate *P. ostreatus* PO-3 and *P.ostreatus* MTCC 142 to degrade 1 µg/mL of Benzo[*a*]pyrene BaP, a high molecular weight polycyclic aromatic hydrocarbon (HMW PAH) under liquid condition, reported that isolate *P. ostreatus* PO-3 has better degradation potential than *P. ostreatus* MTCC 142 and concluded that the level of degradation were 32% and 29% respectively for *Pleurotus ostreatus* isolate PO-3 and *Pleurotus ostreatus* MTCC 142.

Proliferation of a mass of fungal growth in the bottom of culture medium supplemented with oil is one of the indications of those fungi which are capable of degrading hydrocarbon (Al-Nasrawi 2012). Therefore, biodegradation assay of both the fungal strains in terms of fungal biomass was performed according to which it was found out that at concentration of 2% oil, *P. ostreatus* MP 5 gave better performance in terms of biomass as compared to that of the reference strain *Pleurotus ostreatus* MTCC 1804. The bulk mass weighed out for *P. ostreatus* MP 5 and *Pleurotus ostreatus* MTCC 1804 was estimated as 0.334±0.009 g/50 mL and 0.308±0.007 g/50 mL respectively. Experiments performed by Sourav et al. (2013) documented that in the proximity of PAH, the biomass proliferation by the PO-3 isolate was higher than that of *P. ostreatus* MTCC 142 which was calculated as about 51 and 43 mg/50 mL of media which reinforces our present findings in terms of biodegradation essay.

The capability of the fungus to degrade PAH is related to its ability to produce lac case and similar enzymes (Sourav et al. 2013). Therefore, it could be concluded that *P. ostreatus* MP 5 isolate could degrade PAH better than *P. ostreatus* MTCC 142 possibly due to its ability to synthesize higher titers of laccase and manganese peroxidase. Likewise, a native isolate of *P. ostreatus* HP-1 (Genbank Accession No. EU420068) was discovered to comprise an excellent laccase producing ability (Rubailo et al. 2008).

Since the trends of hydrocarbon degradation were assessed overtime and FTIR was utilized and applied to elucidate the degradation of oil spilled from vehicles in the contaminated soil therefore, FTIR spectroscopy has been prove to be a very useful tool in performing preliminary tests in order to predict remediation performance so as to select an appropriate approach for clean- up technologies (Bhat et al. 2011). The present study on comparison of the hydrocarbon degradation potential of the two fungal isolates was finally confirmed by spectral analysis using FTIR to assess biodegradation experiments. Identification and interpretation of peaks indicating various functional groups were done with the reference of available literatures (Bhat et al. 2011, Sohal et al. 2019, Srivastava & Saraf 2019).

The FTIR spectrum monitored for untreated sample, i.e. control as depicted in Fig. 10 indicated a broad peak at 3419.4 cm^{-1} corresponding to O-H stretching vibrations of alcohols. Absorption band around 2933.5 cm^{-1} is assigned to C-H stretching in alkanes (aliphatic compounds), at

1643.7 cm^{-1} indicating C=C stretching of alkenes (aliphatic compounds). Another prominent spectrum which appeared between 1346.2 cm^{-1} to 1461.8 cm^{-1} can be ascribed to the bending vibration of C-H in alkenes (aliphatic compounds). The presence of carboxylic acid functional group in the molecule was confirmed by medium intensity band in the region of 1270.4 cm^{-1} and 1240.1 cm^{-1} for C-O stretching of carboxylic acids. Another bands revealed at 1209.8 and 1053.0 cm^{-1} indicating C-O stretching of alcohols; at 940.7 cm^{-1} indicates S-O stretching in sulphonates; at 909.2 cm^{-1} indicating C-H bends in alkenes; at 867.2 cm^{-1} indicating S-O stretching in sulphonates; at 849.8 cm^{-1} corresponding to C-H bends in aromatics; at lower wave length of 681.1 cm^{-1} and 550.7 cm^{-1} indicating C-Cl stretching signifying the presence of alkyl halides.

The FT-IR spectrum of treated sample with *Pleurotus ostreatus* MTCC 1804 (Fig. 12) after 30 days of microbial incubation indicated the formation of new bands at 3399.5 cm^{-1} indicating O-H stretching vibrations of alcohols; at 2929.7 cm^{-1} corresponding to C-H stretching of alkanes; at 1642.4 cm^{-1} signifying N-H bend in amides. C=C stretching in aromatic compound ring was indicated at 1451.9 cm^{-1}. Spectrum at 1412.5 cm^{-1} can be ascribed to the bending vibration of O-H in carboxylic acids (-COOH). Absorption peaks at 1123.1 and 1058.2 cm^{-1} signified C-O stretching of alcohols (OH). Modification of functional groups at these absorption spectrum indicated the conversion of C-O stretching of carboxylic acids at 1270.4 cm^{-1} and 1240.1 cm^{-1} as depicted in control into C-O stretching of alcohols (OH) at 1123.1 cm^{-1} and 1058.2 may be due to the microbial oxidation of used oil which is supported with the findings of Bhat et al. (2011) who reported the same at 2363.2 cm^{-1}. Formation of new bands at 879.3 cm^{-1}, 840.3 cm^{-1} and 779.7 cm^{-1} indicated C-H bending in aromatics. The appearance of another prominent peak at 700.1 cm^{-1} confirmed C-H bending in alkenes. The absorption peak around 675.4 and 620.9 cm^{-1} was reported as C-Cl stretching in alkyl halides. Besides, it was observed that there is significant change in transmittance which increased in the sample treated with *P. ostreatus* MTCC 1804 as compared to that of control representing degradation of complex mixtures.

The FTIR spectrum obtained to assess the biodegradation capability of P. *ostreatus* MP 5 (Fig. 11) also showed the formation of new bands with different intensity of wavelength which at first indicated a broad spectrum at 3419.4 cm^{-1} corresponding to O-H stretching vibrations of alcohols. Another prominent spectrum which appeared at 2220.1 cm^{-1} can be ascribed to C-N stretching in nitriles. Here the conversion of -C-H stretching in aliphatic compounds as depicted in control or the untreated sample into nitrile groups may be due to the hydrocarbon degradation by wild isolate MP 5 which was in total accordance with the result of FTIR analysis performed by Bhat et al. (2011) for the mycoremediation of hydrocarbon contaminated soil who also concluded the conversion of aliphatic compounds into nitrile groups during hydrocarbon degradation. Another characteristic absorption band at 1644.6 cm^{-1} showed C=C stretching in alkenes. Absorption band around 1446.5 cm^{-1} is assigned to the bending vibration of asymmetric C=C stretching in aromatic. Another prominent absorption peak around 1338.3 cm^{-1} reported as C-H bending in alkenes. The presence of another absorption band at wavelength 1114.4 cm^{-1} indicated C-O stretching of alcohols may be due to the microbial oxidation of used oil. Another new band revealed at 880.8 cm^{-1} and 848.9 cm^{-1} indicated the presence of C-H bending (meta) and C-H bending (para) in aromatics which further indicated the conversion of alkenes as reported in control at 909.2 cm^{-1} into aromatic compounds. The absorption peak around 779.7 cm^{-1} was reported as C-Cl stretching in alkyl halides. At lower wave length of 618.7 and 516.2 cm^{-1} occurrence of C- Br stretching of alkyl halides was revealed out. Apart from all these modifications of functional groups which occurred during degradation process, the percent transmittance increased as compared to that of control and *P. ostreatus* MTCC 1804 which finally confirmed the higher degradation potential of wild isolate MP 5.

CONCLUSION

The present study reveals that the molecular identification technique like ITS sequencing was carried out for the potent isolate which revealed that the isolate MP 5 shares a 99% sequence similarity to that of *Pleurotus ostreatus* isolate 6689 (accession No. AY450345.1). Primary screening assay confirmed that the wild isolate *P. ostreatus* MP 5 showed highest average growth rate on MSM supplemented with 2% oil. Confirmatory test conducted for both the isolates through orbital shaking method for detection of biodegradation by spectrophotometric method at 600 nm displayed degradation within 7 days and level of hydrocarbon degradation figured out for *P. ostreatus* MP 5 and *Pleurotus ostreatus* MTCC 1804 was 69.7 ± 0.351% and 64.7 ± 1.153%. The FTIR spectrum of control and treated samples with fungal isolates showed different peaks based on the presence of different functional groups indicating oxidative degradation of hydrocarbons by microbes. Thus, it can be concluded from the present investigation that the wild isolate *P. ostreatus* MP 5 had better potential for degrading hydrocarbon in comparison to *P. ostreatus* MTCC 1804 which can be served as a better potential hydrocarbon degrader for mycoremediation studies.

ACKNOWLEDGEMENT

As the research was supported by MATS school of Biological and Chemical Sciences (MSBCS), Raipur, C.G so, we are very thankful to MSBCS for providing all the laboratory facilities required for the completion of this research paper. We are also immensely great full to one of the co-author Dr. Ashish Saraf, for sharing his pearls of wisdom with us during this research. We would also like to show our gratitude to Dr. Deepak Konar, Department of Chemistry, Bose institute, Calcutta for conducting the FTIR analysis and Dr. Rohit Sharma and Dr. Abhay Bajaj, NCMR Pune for the ITS sequencing.

REFERENCES

Adongbede, E.M. and Sanni, R.O. 2014. Biodegradation of engine oil by *Agaricus campestris* (a white rot fungus). J. Bioremed. Biodeg, 5(262): 2.

Al-Nasrawi, H. 2012. Biodegradation of crude oil by fungi isolated from Gulf of Mexico. Journal of Bioremediation and Biodegradation, 3(04): 1-6.

Boonchan, S., Britz, M.L. and Stanley, G.A. 2000. Degradation and mineralization of high-molecular-weight polycyclic aromatic hydrocarbons by defined fungal-bacterial cocultures. Appl. Environ. Microbiol., 66(3): 1007-1019.

Barr, D.P. and Aust, S.D. 1994. Mechanisms white rot fungi use to degrade pollutants. Environmental Science & Technology, 28(2): 78A-87A.

Bogan, B.W. and Lamar, R.T. 1996. Polycyclic aromatic hydrocarbon-degrading capabilities of *Phanerochaete laevis* HHB-1625 and its extracellular ligninolytic enzymes. Appl. Environ. Microbiol., 62(5): 1597-1603.

Bezalel, L. Hadar, Y. and Cerniglia, C.E. 1996. Mineralization of polycyclic aromatic hydrocarbons by the white rot fungus *Pleurotus ostreatus*. Appl. Environ. Microbiol., 62(1): 292-295.

Bhat, M.M. Kumar, D. Narain, K. Shukla, R.N. and Yunus, M. 2011. Mycoremediation of hydrocarbon contaminated soil-FTIR based analysis. World Appl. Sci. J., 15: 1547-1552.

Clemente, A. Anazawa, T.A. and Durrant, L.R. 2001. Biodegradation of polycyclic aromatic hydrocarbons by soil fungi. Brazilian Journal of Microbiology, 32(4): 255-261.

Chen, D.H. and Ronald, P.C.1999. A rapid DNA minipreparation method suitable for AFLP and other PCR applications. Plant Molecular Biology Reporter, 17(1): 53-57.

dos Santos, E.O. da Rosa, C.C. dos Passos, C.T. Sanzo, A.V.L. Burkert, J.F.D.M. Kalil, S.J. and Burkert, C.A.V. 2008. Pre-screening of filamentous fungi isolated from a contaminated site in Southern Brazil for bioaugmentation purposes. African Journal of Biotechnology, 7(9): 1314-1317.

Emuh, F.N. 2010. Mushroom as a purifier of crude oil polluted soil. Inter. J. Sci. Nat.,1(2): 127-132.

Ekundayo, F.O. 2014. Comparative studies on biodegradative abilities of *Pleurotus ostreatus* and *P. Pulmonarius* in soils contaminated with crude and used engine oils. Advances in Microbiology, 4(12): 849.

George-Okafor, U. Tasie, F. and Muotoe-Okafor, F. 2009. Hydrocarbon degradation potentials of indigenous fungal isolates from petroleum contaminated soils. Journal of Physical and Natural Sciences, 3(1): 1-6.

Hagwell, I.S. Delfino, L.M. and Rao, J.J. 1992. Partitioning of polycyclic aromatic hydrocarbons in soil by microbial consortium. International Biodeterioration Biodegradation, 54: 61-67.

Huesemann, M.H. 1994. Guidelines for land□treating petroleum hydrocarbon□contaminated soils. Soil and Sediment Contamination, 3(3): 299-318.

Hanson, K.G., Desai, J.D. and Desai, A.J. 1993. A rapid and simple screening technique for potential crude oil degrading microorganisms. Biotechnology Techniques, 7(10): 745-748.

Jawhari, A.L. and Ihsan, F.H. 2014. Ability of some soil fungi in biodegradation of petroleum hydrocarbon. Journal of Applied & Environmental Microbiology, 2(2): 46-52.

Keith, L. and Telliard, W. 1979. ES &T special report: Priority pollutants: A perspective view. Environmental Science & Technology, 13(4): 416-423.

Khan, S.R., Ji, N.K., Kumar, R.N. and Patel, J.G. 2015. In vitro study on assessment of petrol, kerosene and diesel degrading potential of indigenous fungal isolates from different petroleum product effected soils. International Journal of Recent Research and Review, 8(1): 8-15.

Mills. A.L. Breuil, C. and Colwell, R.R. 1978. Enumeration of petroleum-degrading marine and estuarine microorganisms by the most-probable number. Canadian Journal Microbiology, 24: 552-557.

Okparanma, R.N., Ayotamuno, J.M., Davis, D.D. and Allagoa, M. 2011. Mycoremediation of polycyclic aromatic hydrocarbons (PAH)-contaminated oil-based drill-cuttings. African Journal of Biotechnology, 10(26): 5149-5156.

Okpokwasili, G.C. and Okorie, B.B. 1988. Biodeterioration potentials of microorganisms isolated from car engine lubricating oil. Tribology International, 21(4): 215-220.

Popa, G. Nicolcioiu, M.B. and Cornea, C.P. 2013. *In vitro* evaluation of crude oil degradation potential of some *Pleurotus ostreatus* isolates. Scientific Bulletin. Series F. Biotechnologies, 17: 143-146.

Rubailo, A.I. and Oberenko, A. V. 2008. Polycyclic aromatic hydrocarbons as priority pollutants. Journal of Siberian Federal University, 4(1): 344-354

Stamets, P. 2005. Mycelium Running: How Mushrooms Can Help Save The World. Random House Digital, Inc.

Sack, U. and Günther, T. 1993. Metabolism of PAH by fungi and correlation with extracellular enzymatic activities. Journal of Basic microbiology, 33(4): 269-277.

Steffen, K.T. Schubert, S. Tuomela, M. Hatakka, A. and Hofrichter, M. 2007. Enhancement of bioconversion of high-molecular mass polycyclic aromatic hydrocarbons in contaminated non-sterile soil by litter-decomposing fungi. Biodegradation, 18(3): 359-369.

Shahriarinour, M. Wahab, M.N.A. Ariff, A. and Mohamad, R. 2011. Screening, isolation and selection of cellulolytic fungi from oil palm empty fruit bunch fibre. Biotechnology, 10(1): 108-113.

Sourav, B. Arijit, D. Palaniswamy, M. and Angayarkanni, J. 2013. Molecular characterization of Pleurotus ostreatus PO-3 involved in mycoremediation of benzo[a]pyrene. International Research Journal of Biological Sciences, 2(8): 48-53.

Sohal, J.K. Saraf, A. Shukla, K. and Shrivastava, M. 2019. Determination of antioxidant potential of biochemically synthesized silver nanoparticles using aloe vera gel extract. Plant Science Today, 6(2): 208-217.

Srivastava, M. and Saraf, A. 2019. Antimicrobial activity of bioactive molecules isolated from filamentous fungi. Int. Res. J. Biological Sci., 8(3): 13-18.

Tiwari, M. and Saraf, A. 2017. Isolation, screening and identification of hydrocarbon degrading potential of indigenous fungus from oil contaminated soil of Modha Para automobile shop of Raipur, CG. International Journal of Advance Research in Science and Engineering, 6(10): 782-795.

Thomas, S. Becker, P. Pinza, M.R. and Word, J.Q. 1998. Mycoremediation of aged petroleum hydrocarbon contaminants in soil. Washington State Department of Transport. Publication No. WA-RD 464.1.

Thenmozhi, R. Arumugam, K. Nagasathya, A. Thajuddin, N and Paneerselvam, A. 2013. Studies on mycoremediation of used engine oil contaminated soil samples. Advances in Applied Science Research, 4(2): 1.

Undugoda, L.J.S. Kannangara, S. and Sirisena, D.M. 2016. Aromatic hydrocarbon degrading fungi inhabiting the phyllosphere of ornamental plants on roadsides of urban areas in Sri Lanka. J. Bioremed. Biodeg., 7(328): 2.

Vanishree, M. Thatheyus, A.J. and Ramya, D. 2014. Biodegradation of

petrol using *Aspergillus* sp. Annual Research & Review in Biology, 4(6): 914-923.

Velioğlu, Z. and Ürek, R.Ö. 2015. Biosurfactant production by Pleurotus ostreatus in submerged and solid-state fermentation systems. Turkish Journal of Biology, 39(1): 160-166.

White, N.A. Dehal, P.K. Duncan, J.M. Williams, N.A. Gartland, J.S. Palfreyman, J.W. and Cooke DEL. 2001. Molecular analysis of intraspecific variation between building and "wild" isolates of *Serpula lacrymans* and their relatedness to *S. himantioides*. Mycol. Res, 105(4): 447-452.

Yoshida, N. Hoashi, J. Morita, T. McNiven, S.J. Nakamura, H. and Karube, I. 2001. Improvement of a mediator-type biochemical oxygen demand sensor for on-site measurement. Journal of Biotechnology, 88(3): 269-275.

Zebulun, H.O. Isikhuemhen, O.S. and Inyang, H. 2011. Decontamination of anthracene-polluted soil through white rot fungus-induced biodegradation. The Environmentalist, 31(1): 11-19.

Nature Environment and Pollution Technology
An International Quarterly Scientific Journal

p-ISSN: 0972-6268
e-ISSN: 2395-3454

Vol. 19 | No. 1 | pp. 57-70 | 2020

Original Research Paper | Open Access

A Novel Approach to Utilize Used Disposable Paper Cups for the Development of Adsorbent and its Application for the Malachite Green and Rhodamine-B Dyes Removal from Aqueous Solutions

Kshipra Shukla, Alka Verma, Lata Verma, Shalu Rawat and Jiwan Singh†
Department of Environmental Science, Babasaheb Bhimrao Ambedkar University, Lucknow-226025, India
†Corresponding author: Jiwan Singh

Nat. Env. & Poll. Tech.
Website: www.neptjournal.com
Received: 12-06-2019
Accepted: 23-07-2019

Key Words:
Malachite Green
Rhodamine-B
Adsorption
AC@PC adsorbent

ABSTRACT

This study focuses on the removal of organic dyes, such as Malachite Green (MG) and Rhodamine-B (Rh-B) from an aqueous solution with the help of a novel adsorbent (activated carbon) with magnetic property prepared by used disposal paper cups (AC@PC) at 500°C. The synthesized AC@PC adsorbent was characterized by using Fourier transform infrared spectroscopy (FTIR), X-ray diffraction (XRD), scanning electron microscopy (SEM), Energy dispersive X-ray spectroscopy (EDS) and point of zero charge (pHZPC). Adsorption of MG and Rh-B onto the AC@PC adsorbent from aqueous solution was investigated systematically. Langmuir, Freundlich and Temkin isotherms were also studied, however, it has been observed that Langmuir isotherm model was best fitted for both the dyes, which describe the adsorption behaviour at equilibrium. Pseudo-first and pseudo-second order kinetic model describe the rate of adsorption. Kinetic study explained that the process of adsorption followed the pseudo-second order model. Thermodynamic parameters such as enthalpy (ΔH°), entropy (ΔS°) and Gibb's free energy (ΔG°) were also studied and revealed that the adsorption of MG was endothermic, whereas adsorption of Rh-B was exothermic onto the AC@PC. The prepared adsorbent shows potentially high adsorption properties for both the dyes.

INTRODUCTION

India is facing very serious problem of solid waste disposal. The waste contributes to landfills and are post-consumer products that means those substances which cannot be recycled or reused any longer (Arumugam et al. 2015). Paper cup waste disposal is a major issue in terms of environment as it is mainly composed of paper with high strength that can be easily recycled but the inner layer is lined with thin film of polyethylene and make paper cups recycling very complicated (Arumugam et al. 2018). These disposable cups are widely used all over the world for serving tea, coffee, soft-drinks and for many other purposes. Generation of municipal solid waste in India is approximately 1,88,550 tonnes per day of which 35% by weight constitutes post-consumer waste that causes serious problems to the society and environment (Arumugam et al. 2018). Post-consumer waste can be elaborated as the waste generated by the end consumer (Arena et al. 2016). In India solid waste management is a very big task for the generated waste. The paper waste can be very effective for removal of pollutants from water when it converted into an adsorbent. Utilization of paper cup waste for the adsorption purpose can reduce the problem of disposable of paper cup waste.

The discharge of water from the industries may hold pollutants such as dyes, heavy metals into the aqueous solution that disrupt the ecosystem of aquatic animals and plants and also causes various health problems in human beings. Several industries, for example, cosmetics, plastics, textile, processing, rubber etc. uses different classes of dyes (Kono 2015). Dyes are growing to be a very challenging class of pollutants to the environment causing many health hazards (Ngulube et al. 2017). Dyes are mainly the chemical compounds or complex organic molecules that imparts colour to the surface or fabric when comes in contact (Yagub et al. 2014).

Many industries discharge effluent into water bodies containing highly coloured species with large amount of toxic substances that not only cause health related problems but also degrade the aesthetic values of water bodies (Kant 2012). About 10,000 dyes produced yearly of which 7.105 metric tons are available in market. Around 15% of dye materials are misplaced in effluent discharged from various manufacturing and processing operations in industrial activities (Gupta et al. 2012). The dye effluent from industries contain certain chemicals that could be lethal, carcinogenic or mutagenic to living organisms (Noel & Rajan 2014). Synthetic dyes are highly soluble in water and are the common pollutants that

pollute water and normally found in industrial wastewater in trace amount (Crini 2006).

MG is usually used for the dyeing of the cotton, leather, paper, silk and also in different industries such as manufacturing of paints and printing inks. It is persistent in environment and acutely toxic to many aquatic and terrestrial animals (Gupta et al. 2016). While, Rh-B dye is used in textile, printing industries and photographic industries and it is a xanthene dye. Rh-B causes many health problems such as irritation of the eye, skin, and respiratory tract. This dye is carcinogenic, and also causes developmental and reproductive toxicity (Bhattacharya et al. 2014).

Numerous chemicals, physical and biological techniques, comprising biosorption, ozonation, adsorption, coagulation, advance oxidation, liquid-liquid extraction and membrane filtration have been extensively used for dyes treatment from the wastewater (Pathania et al. 2017). Among all the techniques used adsorption is very efficient, cheapest and eco-friendly method as it gives the best results when used for dyes removal from aqueous medium (Yagub et al. 2014).

The waste paper cups used for the preparation of AC@PC adsorbent is used for the first time as an adsorbent for the removal of MG and Rh-B. The main objective of this work is to synthesize the low-cost adsorbent with magnetic properties from waste disposable paper cups and its application for removal of MG and Rh-B dye from an aqueous solution. The present study is focusing on the management of waste disposable cups as well as for the treatment of water pollutants.

MATERIALS AND METHODS

Materials

Rh-B dye ($C_{21}H_{31}ClN_2O_3$) and MG dye ($C_{23}H_{25}N_2Cl$) were obtained from Thermo Fisher Scientific India Pvt. Ltd. These dyes were used directly without any purification. Double distilled water was used to prepare the solution of these dyes. PCs were collected from canteen of Babasaheb Bhimrao Ambedkar University, Lucknow, (U.P.), India.

Preparation of AC@PC Novel Adsorbents

Collected waste PCs were washed to eliminate filths present on the surface and then dried in hot air oven. After that, these paper cups were cut into small pieces and dipped into hot water (temperature 60-70°C) for 3-4 hours and then the thin lining made up of polyethylene was separated from the paper part. Wet paper clumps were removed from hot water and again dried in hot air oven at 105°C for 24h. The dried material was grinded and sieved with 0.25 mm sieve. Then 30 g of grounded material was added to the $FeCl_3$ solution (15g $FeCl_3$ + 150 mL distilled water). The mixture was kept on magnetic stirrer (model no. 1MLH, REMI, India) and stirred for four hours. The material was then filtered and kept overnight in an oven for drying. After drying, the material was kept in muffle furnace (IMPACT, 11C 106B) at 500°C for two hours then the material was crushed by mortar pestle to change it into powder form and was washed with deionized water for 2-3 times, oven dried for overnight and then it was used for the adsorption study (Lunge et al. 2014).

Characterization

Surface morphological structure of AC@PC sample was examined using SEM (JSM-6490 LV, JEOL, Japan). For SEM analysis the sample was coated on a tacky carbon tape and then mounted on a stub into a sample holder. EDS done for the determination of elemental composition of AC@PC.

An infrared spectrum was recorded using Infrared Spectrometer (Nicolet^{TM} 6700, Thermo Scientific, USA) for the functional group determinations present on the surface of AC@PC. The sample were prepared mixing spectroscopy grade KBr with oven dried (at 105°C) sample in an agate mortar.

XRD (Powder Diffractometer PW3040/60, PaNanalytical Neitherland) was used for the analysis of crystalline structure of AC@PC. Scanning of sample was done at the rate of 2° min^{-1} from 10°-80°.

Zeta nanosizer (Nano-ZS90), was used for analysing the particle size and zeta potential of AC@PC. Zeta potential of AC@PC was done at different pH (2, 4, 6, 8 and 10).

The pH_{ZPC} of synthesized material (AC@PC) was determined by using 0.1 M NaCl solution with different pH (2, 4, 6, 8 and 10). These pH values were adjusted by using solutions of 0.1 N HCl and 0.1 N NaOH. A 20 mL NaCl solution and 0.2 g adsorbent were taken and left for 48 hrs after that the pH of solution was measured by a pH meter. The pH_{zpc} value was attained by plotting the graph of initial pH against final pH (Singh et al. 2016).

Batch Adsorption Studies

Batch adsorption experiment was performed with AC@PC for MG and Rh-B removal from an aqueous medium. Initial concentrations were prepared in the range of 5-30 mg/L by diluting standard solution of 1000 mg/L of MG and Rh-B dyes separately. Adsorption studies were performed at different temperatures 25°C, 35°C and 45°C. Different doses in g/L (0.5, 1, 1.5, 2, 3, 3.5 and 4) were taken to optimize the dose at which the maximum adsorption of dye occurs. The dose study revealed that the maximum adsorption was obtained

with the dose of 3 g/L. A fixed dose of AC@PC (3 g/L) was taken for further study. All experiments were conducted in duplicate with 100 mL of dye solution in a 250 mL conical flask at 100 rpm for 300 min.

The conical flasks having samples were taken out from orbital shaker at different interval of time (5, 15, 30, 60, 120, 180, 240 and 300 min). All experiments were performed at normal temperature of 25°C except temperature study conducted at 35°C and 45°C. All experiments were conducted at neutral pH except pH study (pH 4, 5, 6, 7, 8, 9 and 10). The pH of working solution was maintained by 0.1 M NaOH or HCl, solution pH was then measured by using pH meter (water analyser, 372, Systronic India Limited). After that the solution was filtered and analysed to determine the remaining concentration using UV-Vis spectrophotometer (Model No. 117, Systronic India Ltd.).

The amount of dye (MG and Rh-B) q_t (mg/g) adsorbed on AC@PC, was evaluated by following equation:

$$\text{Removal } \% = \frac{C_0 - C_e}{C_0} \times 100 \quad \ldots(1)$$

Where, C_0 is the initial concentration (mg/L) and C_e is the equilibrium concentration (mg/L).

The adsorption capacity of adsorbent at equilibrium was calculated by following equation (Ibrahim et al. 2019):

$$q_e = \frac{C_0 - C_e}{m} \times V \quad \ldots(2)$$

Where,

V = volume of dye solution (L)

m = mass of adsorbent (g)

RESULT AND DISCUSSION

Adsorbent Characterization

SEM and EDS analysis: Fig. 1 (a) shows that the adsorbent has an irregular porous surface with cuboid/pyramid shaped crystal structures which may be responsible for the adsorption of MG and Rh-B. The EDS (Fig. 1b) analysis is mainly done to identify the elemental composition of material. The EDS analysis of AC@PC adsorbent shows the presence of various elements. AC@PC containing highest carbon content with 72.01%. Iron and aluminium content were present in the material and it was confirmed by SEM-EDS analysis. The lower point of zero charge value of AC@PC was due to the presence of Fe on the surface of adsorbent which caused acidic property (Karunanayake et al. 2018).

FTIR spectroscopy: The Fig. 1(c) shows FTIR spectrum of AC@PC before and after adsorption, that shows the presence of several functional groups on adsorbents surface. Peak at 3339.67 cm^{-1} signifies -OH stretching that denotes the presence of hydroxyl or phenol groups and the peak at 2926.7 cm^{-1} denote $-CH_3$ and $-CH_2-$ in aliphatic compound. C=O stretch was also represented by peaks at 1713.1 cm^{-1} beside these groups, peaks at 1587.5 cm^{-1} indicates the presence of $-NH_2$ stretch, peak at 1235.4 cm^{-1} represents C-N in aromatic amines, peak at 545.99 cm^{-1} represents COO- group in carboxylic acid (Magdalane et al. 2017).

Fig. 1(c) also describes the FTIR spectrum after adsorption of MG dye, peak at 2926.7 cm^{-1} represents $-CH_3$ and $-CH_2-$ in aliphatic compound and this peak also present in after adsorption in case of both the dyes. C=C stretching in vinyl ethers represented by peak at 1619.3 cm^{-1} and peak 1305.5 cm^{-1} shows N=N-O in azoxy salts compound, peak at 773.03 cm^{-1} also appeared that attribute to C-O bond bending vibration (Sartape et al. 2017). The Fig. 1(c) also shows the FTIR stretches present on adsorbents surface after adsorption of Rh-B dye.

Spectrum of FTIR analysis of AC@PC after adsorption of Rh-B showed the presence of stretches at 1462.4 cm^{-1} that correspond to $-CH_3$ in aliphatic compounds, peaks at 1368.7 cm^{-1} represents in aliphatic nitro compound, however peak at 1164.6 cm^{-1} represents -C-OH group of alcohol, and peak at 1031.9 cm^{-1} represents CH_2- O-H stretching of primary alcohols.

A peak at 545.99 cm^{-1} which represents C-C=O stretching in carboxylic acid present on adsorbent before adsorption but after adsorption it was observed as the reduced peaks height and new peaks were identified as follows -C=C- and N=N-O stretch in case of MG and CH_2-O-H in case of Rh-B. FTIR results show that after adsorption of MG and Rh-B shows a new peak having C-O and $-CH_3$ in aliphatic compound, respectively.

X-ray diffraction analysis: Fig. 1 (d) represents the XRD pattern of AC@PC which is almost similar to the magnetite. There are five characteristic peaks were obtained for Fe_3O_4 ($2\theta = 33.84°, 36.23°, 49.4°, 54.73°$ and $63.0°$), having indices (220, 311, 400, 422 and 440) (Lunge et al. 2014). Appearance of narrower and sharper peaks indicates the crystalline nature of AC@PC.

Particle size analysis (PSA): The particle size of AC@PC was determined by using Zeta nanosizer (Nano-ZS90), after blending it in uniform mixture in ethyl alcohol at room temperature. Obtained result has been plotted in Fig. 2(a) that shows broad peak in between the range of 150-350 nm that means the particle of AC@PC are in micrometre. Large size of the particles might be due to the clumping of particles with each other.

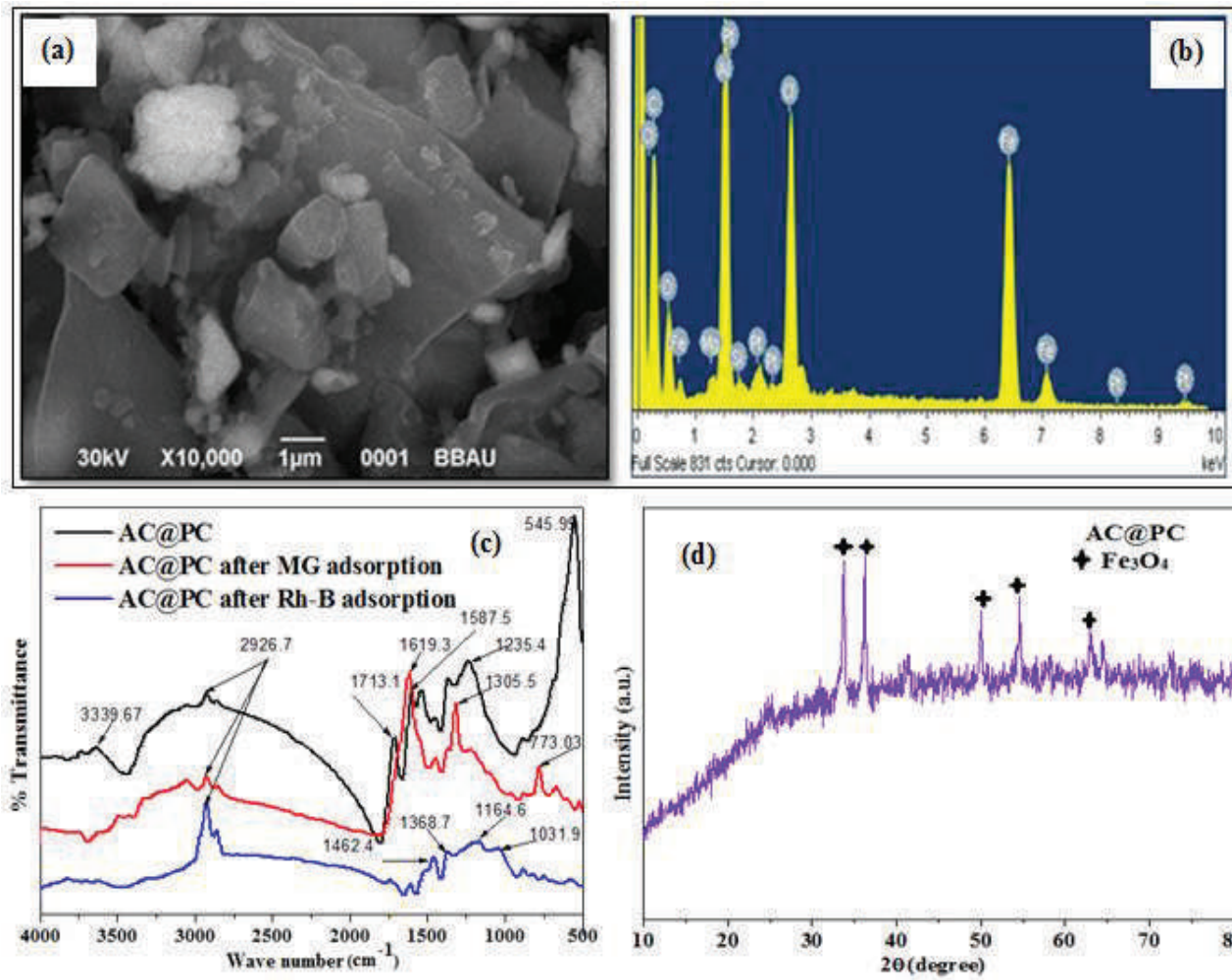

Fig. 1: Characterization (a) SEM and (b) EDS images of AC@PC, (c) FTIR spectrum of AC@PC before and after adsorption of dyes and (d) XRD image of AC@PC adsorbent.

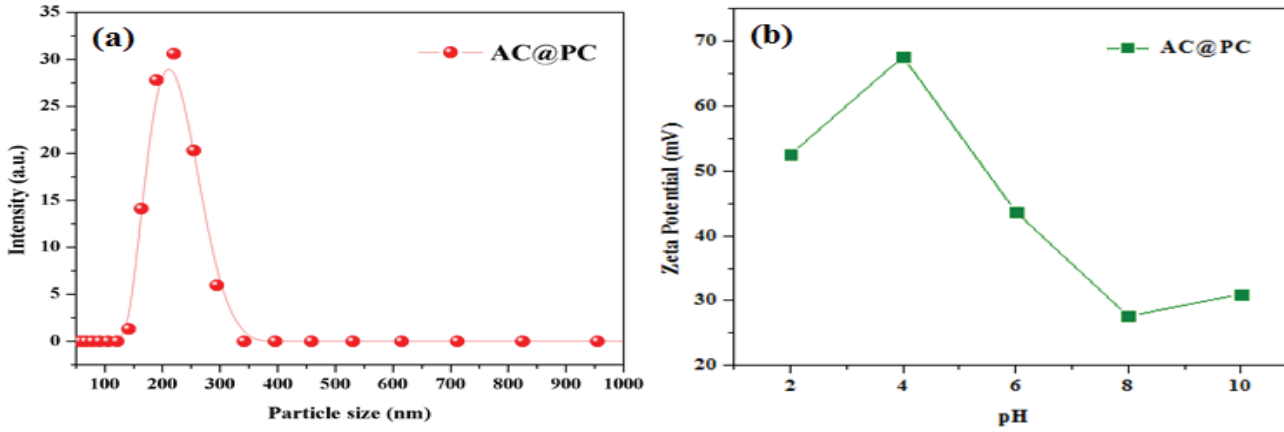

Fig. 2: (a) Particle size analysis and (b) Zeta potential of AC@PC.

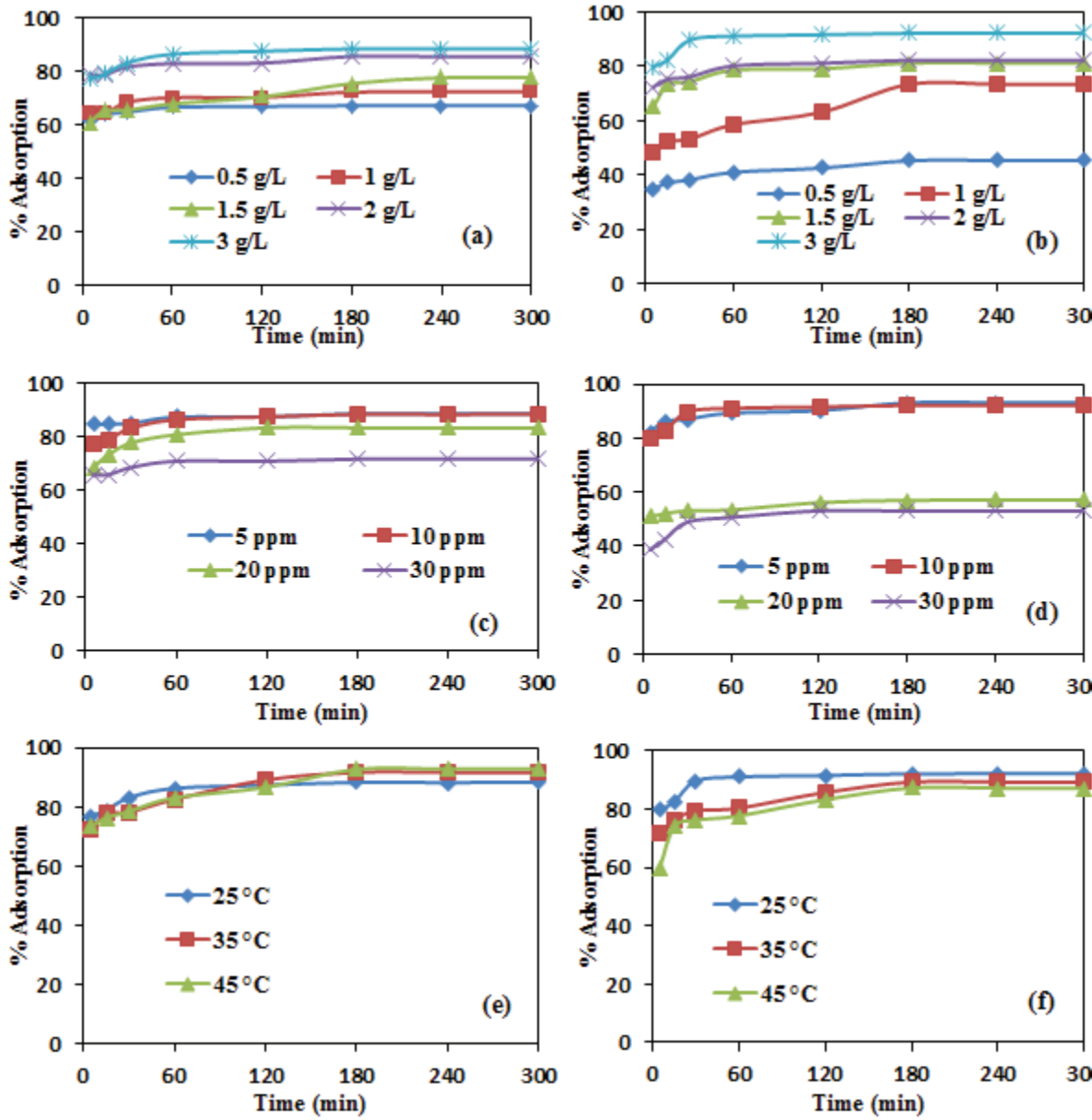

Fig. 3: Batch adsorption (a) and (b) Effect of dose, (c) and (d) effect of initial dye concentration, (e) and (f) effect of temperature for MG and Rh-B respectively.

Zeta potential: For the determination of zeta potential of synthesized AC@PC zeta nanosizer (Nano-ZS90), was used. The stability of adsorbent is identified by the magnitude of zeta potential in a dispersion medium. It works on the principle of electrostatic repulsion between the adsorbent and the dispersion medium (Gautam et al. 2018). The result obtained by zeta potential analysis at different pH is shown in Fig. 2(b). The adsorbent AC@PC was stable at acidic as well as at basic pH but highly stable at pH 2 (53.4 mV).

Point zero charge (pH_{ZPC}): Point zero charge determination of adsorbent is one of the very important characteristics to identify the pH value at which the adsorbent surface becomes neutral. The pHzpc of AC@PC was found to be 2.6. It means that the prepared material was acidic in nature and it may have ability to remove the cationic dyes. The high temperature (500°C) used in the AC@PC preparation process and $FeCl_3$ used to develop the magnetic properties in the material also imparts the acidic nature to the material.

Batch Adsorption Studies

Effect of dosage: Adsorbent dose is considered as a significant parameter of adsorption study, since it helps in determination of adsorbent capacity that how much amount of adsorbent could adsorb the maximum amount of initial concentration of dye, by varying amount of adsorbent while keeping other factors constant like, temperature, initial dye concentration, pH etc. Effect of adsorbent doses on the adsorption capacity was examined by taking different quantity of adsorbent dose in the range of (0.5, 1.0, 1.5, 2.0, 2.5 and 3.0 g/L) were added with an initial MG and Rh-B dyes initial concentration of 10 mg/L with contact time of 5-300 min at constant temperature of 25°C (298K) and neutral pH with shaking speed of 100 rpm. It was observed that on increasing dose from 0.5 g/L to 3 g/L, the removal percentages of both the dyes were increased. As shown in Fig. 3 (a) and (b), removal of MG and Rh-B was increased from 67.19 to 88.37% and 45.33 to 92.19%, respectively, when the amount of material increased from 0.5 to 3 g/L.

An increase in removal percentage of dyes on AC@PC happened due to the availability of adsorption sites on adsorbent surface, which provides more surface area for adsorption of dyes. Conversely, after a certain limit, increasing adsorbent concentration may cause agglomeration or overlapping of adsorbent sites, thus reducing the total surface area provided to dyes for adsorption (Gao et al. 2019).

Effect of concentration and contact time: In the adsorption study, initial dye concentration is very crucial parameter; removal percentage of dye is tremendously dependent on the amount of initial concentration of dye and also on the binding sites availability on the surface of adsorbent. The effect of initial concentration of dye (5 mg/L to 30 mg/L) and contact time was studied at 25°C (298K), the pH 7 with altering contact time (5-300 min). Fig. 3 (c) and (d) show that the removal percentages of MG and Rh-B were increased on increasing contact time from 5 to 300 min and decreases with increase in concentration of both the dyes. The removal percentage of MG was decreased from 88.43% to 71.64% while removal percentage of Rh-B was decreased from 93.08 % to 53.07 % on increasing initial dye concentration from 5 mg/L to 30 mg/L.

Usually the removal percentage of both dyes decreases as the initial concentration was increased which might be because of presence of limited adsorption sites and saturation of adsorbent (Salleh et al. 2011) and increase in initial dyes concentration, resulting an increase in adsorption capacity (Singh et al. 2015). The adsorbent having maximum adsorption capacity of 7.164 mg/g as shown in Fig. 4(c) for MG and 5.307 mg/g for Rh-B at 30 mg/L (Fig. 4e).

Effect of temperature on adsorption: The effect of temperature study was performed at various temperatures (25, 35 and 45°C) while retaining other experimental conditions constant such as dose of adsorbent (3 g/L), initial dyes concentration (10 mg/L) and pH 7 to check the effect of temperature on the rate of adsorption. Fig. 3(e) shows that the removal percentage was achieved about 88% at 25°C, however, when temperature increased up to 45°C, removal percentage was increased approximately 93% in case of MG and it shows the endothermic adsorption process, this might be due to the activation of some specific active sites on AC@PC surface and increasing mobility of dye molecules with increasing temperature (Yagub et al. 2014). On the other hand, Fig. 3(f) shows the exothermic adsorption of Rh-B i.e., removal percentage was decreased from 92.19% to 87.19% with an increase in temperature from 25 to 45°C. Exothermic process of adsorption might be because of adsorptive forces decreased between the active sites present on the surface of adsorbent and dye, while increasing temperature results in decrease in adsorption percentage (Salleh et al. 2011) or may be due to the dye molecules have a tendency to leave the solid phase and outflow to liquid phase at higher temperature (Nassar et al. 2016). In case of MG dye, it was observed that the adsorption was increased with increase in temperature and the maximum adsorption capacity was obtained as 3.093 mg/g at 45°C as shown in Fig. 4(d). Fig. 4(f) shows that the adsorption capacity of AC@PC was found to be the best at 25°C with 3.073 mg/g, while adsorption capacity of Rh-B was decreased from 3.070802 mg/g to 2.909148 mg/g with an increasing temperature from 25°C to 45°C.

Effect of pH value: A solution pH also affects the adsorption capacity of adsorbent, so it becomes necessary to study the effect of pH on the process of adsorption. Although varying the range of pH leads to the change of adsorptive molecules and surface assets of adsorbent. The effect of pH on the removal of MG and Rh-B through AC@PC adsorbent performed on different pH values in the range of 2-10 at 25°C temperature, initial dyes concentration 10 mg/L with a dose of adsorbent 3 g/L. To regulate the solution pH, 0.1 N HCl and 0.1 N NaOH was used. It was found that a slight difference in removal percentages were observed at different pH (4, 5, 6, 7, 8, 9 and 10), the highest removal percentage 88.37% (MG) and 92.74% (Rh-B) was observed at pH 7, as shown in Fig. 4(a) and (b). Minimum removal percentage of MG was achieved 86.33% at pH 10 as shown in Fig. 4(a). It was reported that the highest removal of MG dye was observed at 6 pH and minimum adsorption was occurred under acidic condition i.e., at pH 3 (Amiri et al. 2017). Whereas, in this study minimum adsorption percentage of Rh-B was found 89.36% at pH 4 and maximum adsorption takes place at pH 7 (92.7 %) (Fig. 4b). It has been reported in a research that

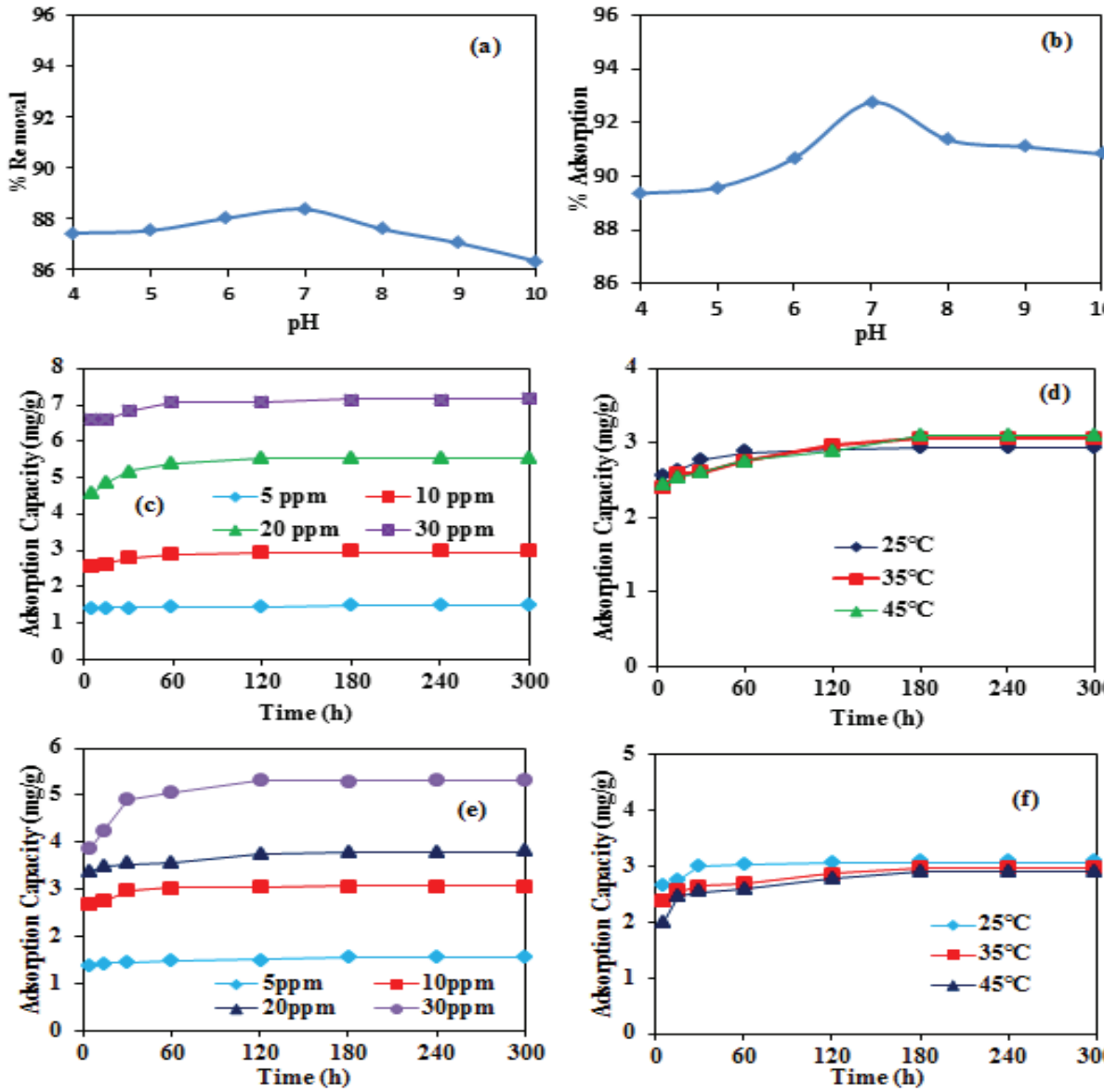

Fig. 4: Effect of pH on adsorption of (a) MG and (b) Rh-B and adsorption capacity of AC@PC for (c) (d) MG and (e) (f) Rh-B at different concentration and temperature respectively.

the maximum removal of Rh-B dye was found at pH 2.1, (Guo et al. 2005) this happen because of the neutralization of OH^- ions present on adsorbent's surface and an increase in the hydrogen ions concentration (Saini et al. 2017). In the present study, the AC@PC adsorbent is of acidic nature, that means hydrogen ions were present on surface of adsorbent whereas both these dyes are cationic dyes with positive charge. At lower pH the H^+ ions concentration on AC@PC was higher that causes the electrostatic repulsion between the adsorbate and adsorbent which is not favourable for dyes removal. At pH 6 and pH 7 the concentration of H^+ ions decreased that protrudes the adsorption through electrostatic attraction, resulting in the neutralization of mixture of adsorbent and adsorbate and shows the maximum removal at neutral pH (Zhang et al. 2016).

Adsorption Isotherms

For optimizing the adsorption design of adsorption system of MG and Rh-B after the effective application of the adsorption techniques it is essential to explain the various adsorption

Table 1: Isotherm parameters for removal of MG and Rh- B by synthesized AC@PC adsorbent.

		MG	Rh-B
Langmuir isotherm	Q_e (mg/g)	9.6246	5.2548
	B (L/mg)	0.3567	0.8855
	RL	0.0854	0.0362
	R^2	0.9929	0.9515
Freundlich Isotherm	K_F (mg/g(L/mg)$^{1/n}$)	2.3624	15.3789
	N	1.7247	1.2450
	R^2	0.9471	0.8602
Temkin Isotherm	B	2.1488	0.8032
	K_T (L/g)	2.21934	1.341635
	R^2	0.9952	0.8602

isotherm models because the adsorption isotherm models undoubtedly describe the correlation between the initial dyes concentration in a solution and amount of dye adsorbed by the adsorbent (Shu et al. 2015). In this work, most commonly known isotherms models were applied for analysing the data obtained through experiments; these models are given as follows: Langmuir, Freundlich and Temkin model of isotherms.

Langmuir isotherm: The Langmuir isotherm model explains that the adsorption happens on homogeneous surface of adsorbent without any interface between adsorbed molecules of dye i.e., monolayer adsorption. For the equilibrium study of MG and Rh-B adsorption, the experiments were performed at different temperatures (25, 35 and 45°**C**) with various initial concentrations of both the dyes (MG and Rh-B) in range of 5-30 mg/L.

The Langmuir isotherm linearly expressed by following equation (Singh et al. 2016):

$$\frac{C_e}{q_e} = \frac{1}{Q_0 \mathrm{b}} + \frac{C_e}{Q_0} \quad \ldots(3)$$

Where,

C_e = Dyes concentration at equilibrium point (mg/L)

q_e = Amount of adsorbate adsorbed at equilibrium (mg/g)

Q_0 = Langmuir constant, maximum capacity of monolayer adsorption (mg/g)

b = rate of adsorption (L/mg)

Linear slope ($1/Q_0$) was obtained after plotting graph of experimental data between C_e/q_e against C_e as shown in the Fig. 5 (a) and (b), the dimensionless separation factor R_L can be expressed by following equation:

$$R_L = \frac{1}{\left(1 + \mathrm{b}C_0\right)} \quad \ldots(4)$$

Where,

C_0 = initial solute concentration (mg/L)

R_L = degree of adsorption

The R_L, separation factor was calculated to check the favourability of adsorption process. The values of R_L, separation factor for the adsorption of MG (Fig. 5a) and Rh-B (Fig. 5b) on the surface of AC@PC adsorbent were occurred in the range of 0.0854-0.359 and 0.0362-0.1842, respectively. Since the R_L values are between 0 and 1, hence is favourable for the adsorption of both MG and Rh-B onto the AC@PC adsorbent surface (Table 1).

Freundlich isotherm: Freundlich isotherm describes the heterogeneous nature of adsorbent. Following equation is used to express the linear form of Freundlich's isotherm model for adsorption process (Hameed and Ahmad, 2009):

$$\ln q_e = \ln K_F + \left(\frac{1}{\mathrm{n}}\right) \ln C_e \quad \ldots(5)$$

Where,

q_e = amount of dyes adsorbed at equilibrium (mg/g)

C_e = concentration of MG and Rh-B at equilibrium point (mg/L)

K_F and n = Freundlich constant, denotes adsorption capacity of AC@PC adsorbent [(mg/g)(L/mg)$^{1/n}$]

The K_F and n values were obtained from the linear slope and intercept of $\ln C_e$ and $\ln q_e$. If the value of 1/n of the slope is between 0 and 1 then it confirms the heterogeneous nature of adsorbent surface and if the values are closer to 0 it shows that the adsorbent surface is highly heterogeneous (Singh et al. 2016). It was observed that the value of Freundlich constant i.e., n for MG and Rh-B dyes was 1.7247 and 1.2450 with R^2 values 0.9471 and 0.8602 respectively as shown in Table 1.

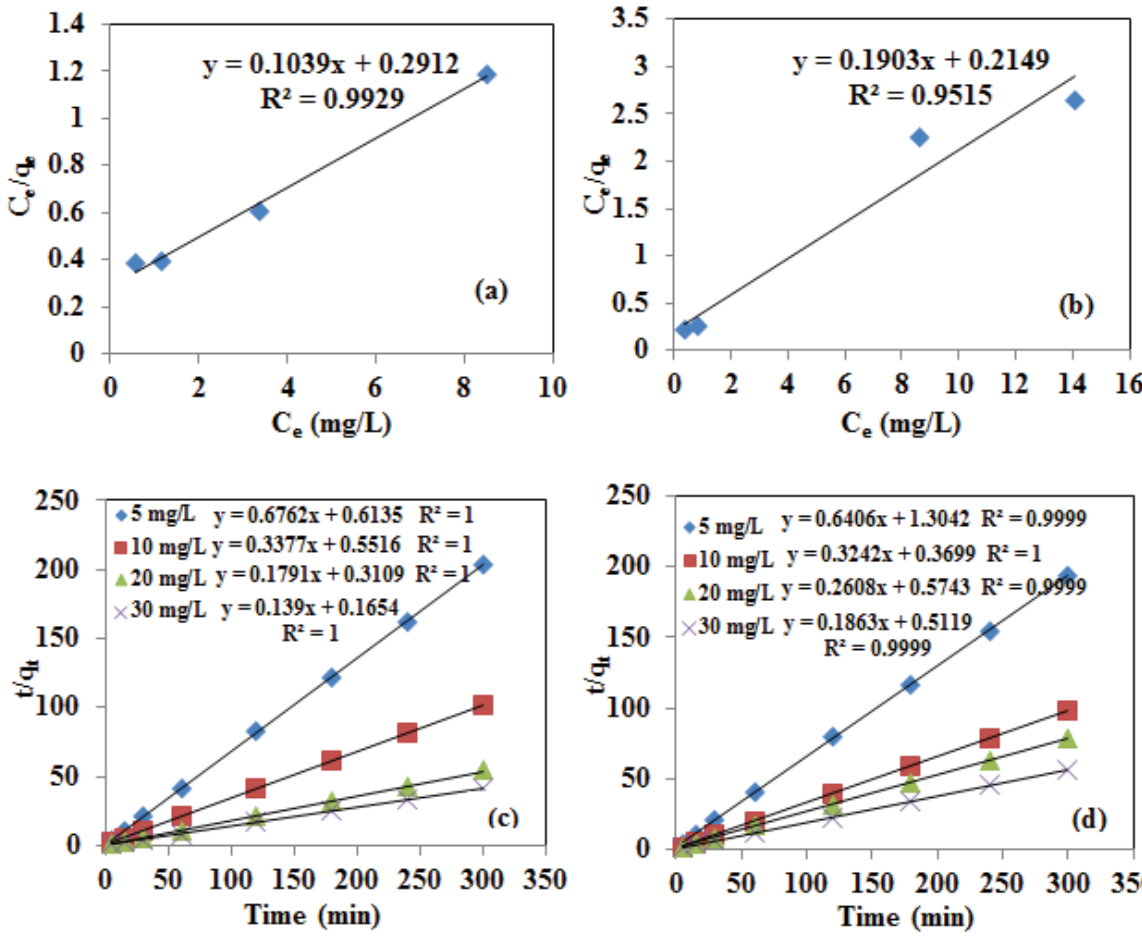

Fig. 5: (a) and (b) Langmuir isotherm plots and (c) and (d) pseudo-second order plots of MG and Rh-B, respectively.

After studying the Langmuir and Freundlich isotherms of adsorption process it was observed that the equilibrium data obtained for MG and Rh-B dyes were best fitted to Langmuir isotherm with R^2 values 0.9929 and 0.9515, respectively that was higher than the R^2 values obtained in Freundlich isotherm.

Temkin isotherm: The linearised graph of Temkin isotherm was obtained by plotting q_e against $\ln C_e$. The K_T value was resolute by slope and intercept of resulted curve. This model undertakes that the heat of absorption that relates with the dye molecules, a function of temperature in the layer would decrease linearly not logarithmically (Chun et al. 2005), as shown in the Eq. 6;

$$q_e = B \ln K_T + B \ln C_e \quad \ldots(6)$$

Where,

B = Temkin constant related to heat of adsorption

K_T = Temkin isotherm equilibrium binding constant

q_e = quantity of dyes adsorbed at equilibrium (mg/g)

C_e = concentration of MG and Rh-B at equilibrium (mg/L)

From the plot of Temkin isotherm the obtained values of $K_T = 2.21934$, $B = 2.1488$, $R^2 = 0.9952$ for MG dye and the values of $K_T = 1.341635$, $B = 0.8032$, $R^2 = 0.8602$ for Rh-B dye.

Kinetic Study

Pseudo-first-order kinetics: Kinetic study involves the analysis of data obtained by experiments using intraparticle diffusion model, pseudo-first-order and pseudo-second-order (Dastkhoon et al. 2017). The kinetics studies were done to comprehend the adsorption process characteristics.

The pseudo-first-order kinetics model is being broadly used to designate the adsorption rate constant in kinetic process (Ho & McKay 1999).

$$\log q_e - q_t = log q_e - \left(\frac{k_1}{2.303}\right) \quad \ldots(6)$$

Where, q_e and q_t denotes the quantity of dyes (MG and Rh-B) in terms of mg/g adsorbed on AC@PC adsorbent at

Table 2: Values of kinetic parameters pseudo first order and second order.

Kinetics			Pseudo first order kinetics			Pseudo second order		
		C_0 (mg/L)	q_e (mg/g)	k_1 (min^{-1})	R^2	q_e (mg/g)	k_2 (g/mg. min)	R^2
AC@PC	MG	5	0.0742	0.002649	0.9103	1.4788	0.7453	1
		10	0.3629	0.004082	0.9877	2.9612	0.2067	1
		20	0.7120	0.003474	0.8811	5.5834	0.1031	1
		30	0.7120	0.003561	0.7857	7.1942	0.1168	1
	Rh-B	5	0.2123	0.003865	0.9050	1.5610	0.3146	0.999
		10	0.3202	0.004993	0.8417	3.0845	0.2841	1
		20	0.4530	0.002996	0.9475	3.8343	0.1184	0.999
		30	1.0690	0.004386	0.9583	5.3676	0.0678	0.999

time t (min) at equilibrium point. K_1 (min^{-1}) represents rate constant for the MG and Rh-B adsorption. Values of k_1 and q_e were obtained by calculating $\log(q_e\text{-}q_t)$ against t plots with different dyes initial concentrations of MG and Rh-B. It was observed that adsorption data was not fitted with pseudo-first order with R^2 value = 0.785-0.910 for MG and R^2 value = 0.841-0.958 for Rh-B (Table 2).

Pseudo-second-order kinetics: The experimental records were examined by using pseudo-second-order kinetics (Li et al. 2013). The equation for pseudo-second-order kinetics is expressed below:

$$\frac{t}{qt} = \frac{1}{\left(k_2 q_e^2\right)} + \left(\frac{1}{q_e}\right)t \qquad \ldots(8)$$

Here, k_2 (g/(mg.min) is constant for pseudo second order kinetic. q_e denotes the adsorption capacity at equilibrium.

Values of pseudo second order kinetic parameters were calculated from the plot of t/q_t against t (Figs. 5c and d). The linear regression coefficient (R^2) values for both the kinetic models are given in Table 3. The pseudo second order model was best fitted with kinetic data with R^2 value =1 for MG (Fig. 5c) and R^2 value = 0.999 for Rh-B (Fig. 5d).

Intraparticle diffusion model: An experimental model for intraparticle diffusion mechanism, reported by Albadarin et al. (2017) was used. The solute transfer in process of solid-liquid sorption is commonly illustrated by intraparticle diffusion model. Intraparticle diffusion model is represented by following equation:

$$q_t = k_i t^{1/2} + c \qquad \ldots(9)$$

Here, k_i (mg/g.min$^{1/2}$) symbolizes the rate constant for intraparticle diffusion and constant C (mg/g) is associated with the boundary layer and was calculated through graph plotted between q_t and $t^{1/2}$. Intraparticle diffusion model is a rate limiting step. The intraparticle diffusion is consider as rate limiting step when a linear regression passage origin is found after plotting the graph between q_t and $t^{1/2}$. Fig. 6 shows that the plots did not passed through the origin in case of both the dyes (MG (Fig. 6a) and Rh-B (Fig. 6b)). This signifies that the intraparticle diffusion model was not only the rate controlling factor and other mechanisms are also involved (Saleh et al. 2016).

Thermodynamic Study

Thermodynamic study includes calculation of Gibb's free energy (ΔG°), change in entropy (ΔS) and enthalpy (ΔH) from the following equations for adsorption of MG and Rh-B dyes (Singh et al. 2016)

$$\text{Kc} = \frac{qe}{Ce} \qquad \ldots(10)$$

$$\ln \text{Kc} = \frac{\Delta S}{R} - \frac{\Delta \text{H}}{RT} \qquad \ldots(11)$$

$$\Delta G^\circ = -RT\,Ln\,Kc \qquad \ldots(12)$$

Where, C_e is the concentration of the dye (mg/L) in the solution and q_e is the amount of dye adsorbed at equilibrium (mg/g), T(K) is the absolute temperature and K_c is the thermodynamic equilibrium constant.

The standard Gibb's energy (ΔG°) was calculated by the value of K_c (L/g) obtained at different temperatures and R is the universal gas constant (8.314 J/mol K). The values of thermodynamic constants were calculated by graph of $\ln K_c$ plotted against 1/T. The thermodynamic data shows that the MG dye (Fig. 6c) adsorption by AC@PC adsorbent was endothermic that was proved by the positive value of ΔH° (22.51348 J/mol) (Table 3), whereas spontaneous nature of adsorption process which is favourable at all temperatures described by negative value of ΔG° (Mahmoodi et al. 2011). The standard entropy i.e., ΔS° (83.15663 J/mol K) for MG

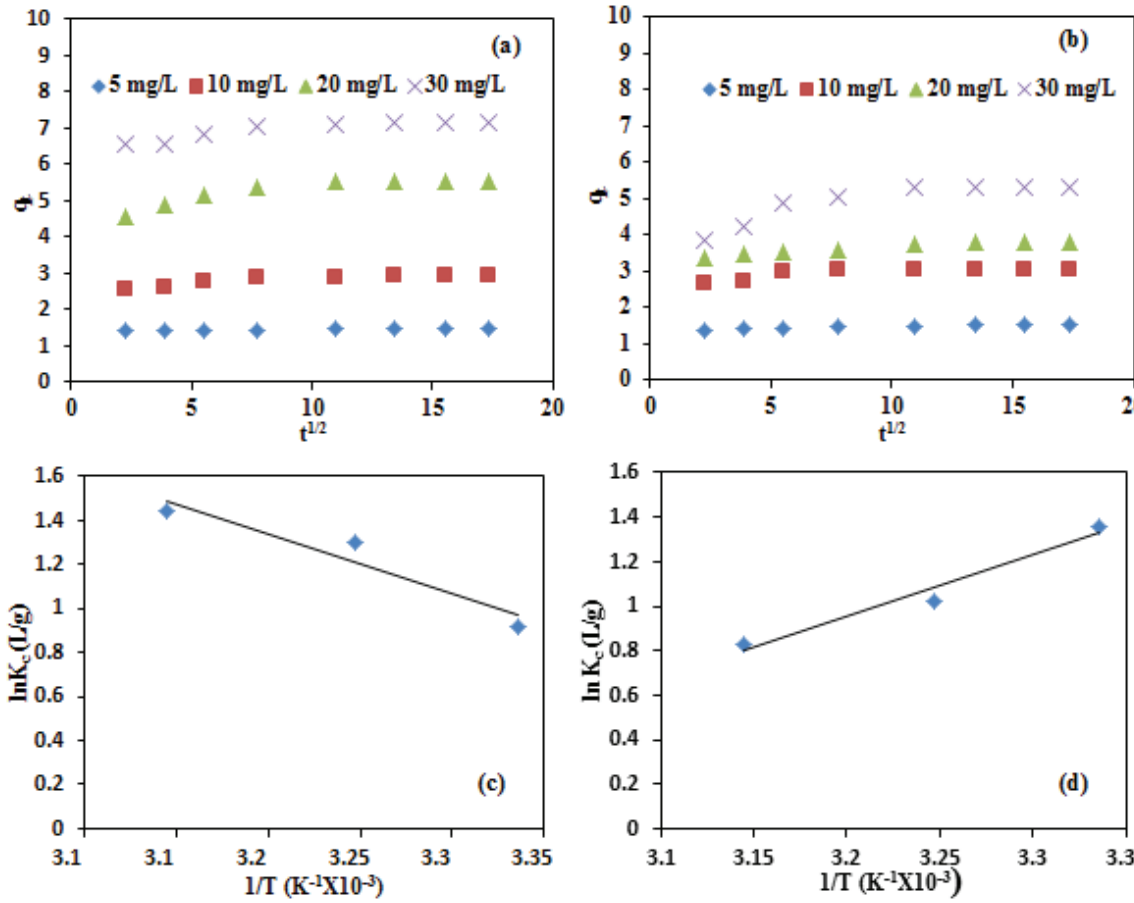

Fig. 6: (a) and (b) Intraparticle diffusion model and (c) and (d) thermodynamics plot of MG and Rh-B, respectively.

Table 3: Thermodynamic parameters of MG and Rh-B adsorption onto AC@PC adsorbent.

Parameters	Temperature (K)	AC@PC	
		MG	Rh-B
ΔG° (KJ/mol)	298	-24.7582	19.64981
	308	-25.5897	20.30998
	318	-26.4213	20.97014
ΔH° (J/mol)		22.51348	-23.10210
ΔS° (J/mol K)		83.15663	-66.01648

adsorption was positive, it represents that the degree of adsorbent-adsorbate interface randomness during adsorption process of dye. However, in case of Rh-B (Fig. 6d) value of ΔG° was positive. The negative values -23.10210 J/mol and -66.01648 J/mol K of ΔH° and ΔS°, respectively, (Table 3) confirmed that the thermodynamic process was exothermic, on increasing temperature the initial adsorption rate was decreased. It was examined that the value of ΔG° increases with increasing temperature which indicates greater adsorption at lower temperature. For Rh-B negative value of ΔS° revealed good affinity of AC@PC. Analogous result was also reported by Shu et al. (2015). This study explained that adsorption of Rh-B onto the adsorbate (rice husk and activated carbon) was exothermic in nature with negative values of ΔH° and ΔS°.

Mechanism

Mechanism of dyes adsorption can be described by various

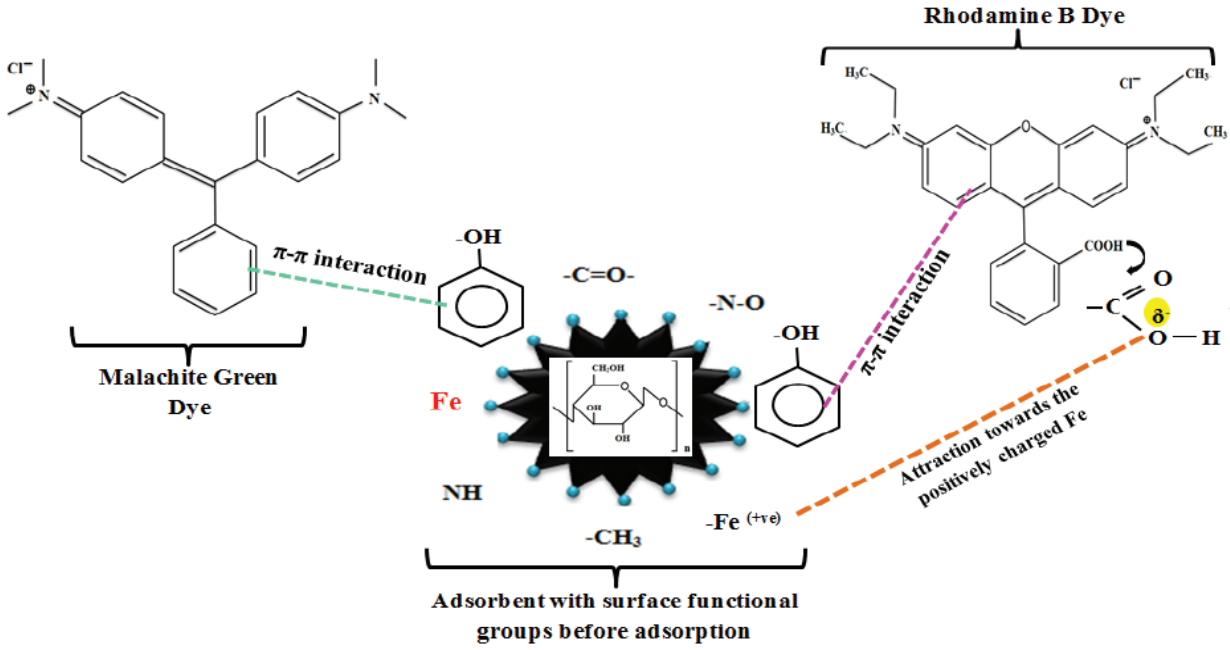

Fig. 7: Mechanism of dyes adsorption on AC@PC.

processes. In this study, Langmuir isotherm was best fitted. The Langmuir isotherm signifies the monolayer adsorption onto a determinate number of homogeneous sites. The homogeneous nature of adsorption phenomenon can also be explained by FTIR results that represent the functional groups are present on the surface of adsorbent that may be responsible for enhancing the removal percentage of adsorbent. As shown in Fig. 7, FTIR results revealed the presence of several functional groups like hydroxyl, phenol, carboxylic acid, benzene ring, amine, methyl, and nitro group on the surface of adsorbent before adsorption of dyes. But after adsorption of dyes, some changes were also observed in the functional group composition. In case of MG, -NH, -CH, and C=H groups are mainly responsible groups for adsorption of dye. Whereas, in case of Rh-B adsorbent, after adsorption shows that OH, -CH, -C=O, -C-O and N-C=O functional groups had key role in removal. FTIR result revealed the possibility of ion exchange of dyes on adsorbent surface and helps to increase the adsorption percentage and provide more active binding sites for adsorption of dyes. Elemental analysis was done by EDS that shows that higher carbon content was present in adsorbent that provides large surface area to the adsorbent; more the surface area more the adsorption of dyes.

The adsorption of organic dyes onto the surface of activated carbon in this study can be explained on the basis of mainly two major mechanisms i.e., electrostatic attraction and p-p interaction. The electrostatic attraction mechanism undertakes the attraction of partially negative species towards the positively charged species, as the surface functional group (Fe) on adsorbent acts as an electron acceptor while Rh-B dye has a partially negatively charged group that attracted towards the Fe present on the adsorbent surface with positive charge. On the other hand, p-p interaction, takes place in between the benzene ring present in adsorbate and on adsorbent surface. Adsorption of MG and Rh-B through AC@PC was occurred by p-p interaction a similar mechanism was also reported by Gao et al. 2019 (MG) and Cheng et al. 2017 (Rh-B).

CONCLUSIONS

A simple and cost-effective method to synthesize adsorbent from waste disposable cups at 500°C temperature in muffle furnace and then used for removal of MG and (Rh-B) dyes from an aqueous solution. AC@PC is low cost and easily available material. Prepared AC@PC adsorbent showed excellent removal ability for MG and Rh-B dyes. The adsorption behaviour of MG and Rh-B was analysed methodically and observed that pseudo-second-order kinetic with the $R^2 > 0.999$ was followed by both the dyes. The Langmuir model of isotherm was best fitted to the experimental data of equilibrium study. It can be concluded that disposable waste cups can be effectively used for the synthesis of adsorbent which is cost effective and the synthesized adsorbent AC@PC from waste paper cups could be used to remove effectively the basic dyes from dye contaminated water. An application of waste cups in water

treatment not only treats water but also minimize the waste generation.

ACKNOWLEDGMENT

The authors are very grateful to acknowledge the support of UGC-BSR research start-up-grant (Project No. F. 30-382/2017, BSR) and Science and Engineering Research Board (SERB), Department of Science and Technology (DST) (Reference no. ECR/2016/001924), Government of India.

REFERENCES

Albadarin, A.B., Collins, M.N., Naushad, M., Shirazian, S., Walker, G. and Mangwandi, C. 2017. Activated lignin-chitosan extruded blends for efficient adsorption of methylene blue. Chem. Eng. J., 307: 264-272.

Amiri, M., Niasari, M.S., Akbari, A. and Gholami, T. 2017. Removal of malachite green (a toxic dye) from water by cobalt ferrite silica magnetic nanocomposite: Herbal and green sol-gel autocombustion synthesis. Int. J. Hydrog. Energy., 42(39): 24846-24860.

Arena, U., Ardolino, F. and Gregorio F.D. 2016. Technological, environmental and social aspects of a recycling process of post-consumer absorbent hygiene products. J. Clean. Prod., 127: 289-301.

Arumugam, K., Ganesan, S., Muthunarayanan, V., Vivek, S., Sugumar, S. and Munusamy, V. 2015. Potentiality of *Eisenia fetida* to degrade disposable paper cups-an ecofriendly solution to solid waste pollution. Environ. Sci. Pollut. Res., 22(4): 2868-2876.

Arumugam, K., Renganathan, S., Babalola, O.O. and Muthunarayanan, V. 2018. Investigation on paper cup waste degradation by bacterial consortium and Eudrillus eugeinea through vermicomposting. Waste Manage., 74: 185-193.

Bhattacharya, K., Gupta, S. and Sharma, G. 2014. Interactions of the dye, rhodamine-B with kaolinite and montmorillonite in water. Appl. Clay. Sci., 99: 7-17.

Chun, J.H., Jeon, S.K., Kim, N.Y. and Chun, J.Y. 2005. The phase shift method for determining Langmuir and Temkin adsorption isotherms of over potentially deposited hydrogen for the cathodic H_2 evaluation reaction at the poly-Pt/H_2SO_4 aqueous electrolyte interface. Int. J. Hydrog. Energy., 30(13-14): 1423-1436.

Cheng, Z.L., Li, Y.X. and Liu, Z. 2017. Novel adsorption materials based on graphene oxide/Beta zeolite composite materials and their adsorption performance for rhodamine B. J. Alloys. Compd., 708: 255-263.

Crini, G. 2006. Non-conventional low-cost adsorbents for dye removal: A review. Bioresour. Technol., 97(9): 1061-1085.

Dastkhoon, M., Ghaedi, M., Asfaram, A., Azqhandi, M.H.A. and Purkait, M.K. 2017. Simultaneous removal of dyes onto nanowires adsorbent use of ultrasound assisted adsorption to clean waste water: Chemometrics for modeling and optimization, multicomponent adsorption and kinetic study. Chem. Eng. Res. Des., 124: 222-237.

Gao, M., Wang, Z., Yang, C., Ning, J., Zhou, Z and Li, G. 2019. Novel magnetic graphene oxide decorated with persimmon tannins for efficient adsorption of malachite green from aqueous solutions. Colloids Surf. A Physicochem. Eng. Asp., 566: 48-57.

Gautam, A., Rawat, S., Verma, L., Singh, J., Sikarwar, S., Yadav, B.C. and Kalamdhad, A.S. 2018. Green synthesis of iron nanoparticle from extract of waste tea: An application for phenol red removal from aqueous solution. Environ. Nanotechnol. Monit. Manage., 10: 377-387.

Guo, Y., Zhao, J., Zhang, H., Yang, S., Qi, J., Wang, Z. and Xu, H. 2005. Use of rice husk-based porous carbon for adsorption of Rhodamine B from aqueous solutions. Dyes Pigm., 66(2): 123-128.

Gupta, N., Kushwaha, A.K. and Chattopadhyaya, M.C. 2016. Application of potato (*Solanum tuberosum*) plant wastes for the removal of methylene blue and malachite green dye from aqueous solution. Arab. J. Chem., 9: 707-716.

Gupta, V.K., Pathania, D., Agarwal, S. and Singh, P. 2012. Adsorptional photocatalytic degradation of methylene blue onto pectin-CuS nanocomposite under solar light. J. Hazard. Mater., 243: 179-186.

Hameed, B.H. and Ahmad, A.A. 2009. Batch adsorption of methylene blue from aqueous solution by garlic peel, an agricultural waste biomass. J. Hazard. Mater., 164(2-3): 870-875.

Ho, Y.S. and McKay, G. 1999. Pseudo-second order model for sorption processes. Process Biochem., 34(5): 451-465.

Ibrahim, M., Siddiqe, A., Verma, L., Singh, J. and Koduru, J.R. 2019. Adsorptive removal of fluoride from aqueous solution by biogenic iron permeated activated carbon derived from sweet lime waste. Acta Chim. Slov., 66(1): 123-136.

Kant, R. 2012. Adsorption of dye eosin from an aqueous solution on two different samples of activated carbon by static batch method. J. Water Resource Prot., 4(02): 93-98.

Karunanayake, A., Todd, O.A., Crowely, M., Ricchetti, L., Pittman, Jr C.U., Anderson, R., Mohan, D. and Mlsna, T. 2018. Lead and cadmium remediation using magnetized and nonmagnetized biochar from Douglas fir. Chem. Eng. J., 331: 480-491.

Kono, H. 2015. Preparation and characterization of amphoteric cellulose hydrogels as adsorbents for the anionic dyes in aqueous solutions. Gels., 1(1): 94-116

Li, Y.H., Du, Q.J., Liu, T.H., Sun, J.K., Wang, Y.H., Wu, S.L., Wang, Z.H., Xia, Y.Z. and Xia, L.H. 2013. Methylene blue adsorption ongraphene oxide/calcium alginate composites. Carbohydr. Polym., 95(1): 501-507.

Lunge, S., Singh, S. and Sinha, A. 2014. Magnetic iron oxide (Fe_3O_4) nano- particles from tea waste for arsenic removal. J. Magn. Magn. Mater. 356: 21-31.

Magdalane, C.M., Kaviyarasu, K., Vijaya, J.J., Jayakumar, C., Maaza, M. and Jeyaraj, B. 2017. Photocatalytic degradation effect of malachite green and catalytic hydrogenation by UV illuminated CeO2/CdO multilayered nanoplatelet arrays: Investigation of antifungal and antimicrobial activities. J. Photochem. Photobiol. B., 169: 110-123.

Mahmoodi, N., Hayati, M.B., Arami, M. and Lan, C. 2011. Adsorption of textile dyes on pine cone from colored wastewater: kinetic, equilibrium and thermodynamic studies. Desalination, 268(1-3): 117-125.

Nassar, M.Y., Mohamed, T.Y., Ahmed, I.S. and Sami, I. 2017. MgO nanostructure via a sol-gel combustion synthesis method using different fuels: An efficient nano-adsorbent for the removal of some anionic textile dyes. J. Mol. Liq., 225: 730-740.

Ngulube, T., Gumbo, J.R., Masindi, V. and Maity, A. 2017. An update on synthetic dyes adsorption onto clay based minerals: A state-of-art review. J. Environ. Manage., 191: 35-57.

Noel, D.S. and Rajan, M.R. 2014. Impact of dyeing industry effluent on groundwater quality by water quality index and correlation analysis. J. Pollut. Eff. Control., 2: 1-4.

Pathania, D., Sharma, S. and Singh, P. 2017. Removal of methylene blue by adsorption onto activated carbon developed from Ficus carica bast. Arab. J. Chem., 10: 1445-1451.

Saini, J., Garg, V.K. and Kataria, N. 2017. Removal of Orange G and Rhodamine B dyes from aqueous system using hydrothermally synthesized zinc oxide loaded activated carbon (ZnO-AC). J. Environ. Chem. Eng., 5(1): 884-892.

Saleh, T.A., Siddiqui, M.N. and Al-Arfaj, A.A. 2016. Kinetic and intraparticle diffusion studies of carbon nanotubes-titania for desulfurization of fuels. Petrol. Sci. Technol., 34(16): 1468-1474.

Salleh, M.A.M., Mahmoud, D.K., Karim, W.A. and Idris, A. 2011. Cationic anionic dye adsorption by agricultural solid waste: a comprehensive review. Desalination, 280(1-3): 1-13.

Sartape, A.S., Mandhare, A.M., Jadhav, V.V., Raut, P.D., Anuse, M.A. and Kolekar, S.S. 2017. Removal of malachite green dye from aqueous solution with adsorption technique using *Limonia acidissima* (wood apple) shell as low cost adsorbent. Arab J. Chem., 10: 3229-3238.

Shu, J., Wang, Z., Huang, Y., Huang, N., Ren, C. and Zhang, W. 2015. Adsorption removal of Congo red from aqueous solution by polyhedral Cu2O nanoparticles: Kinetics, isotherms, thermodynamics and mechanism analysis. J. Alloys Compd., 633: 338-346.

Singh, J. and Lee, B.K. 2015. Hydrometallurgical recovery of heavy metals from low grade automobile shredder residue (ASR): an application of advance Fenton process (AFP). J. Environ. Manage., 161: 1-10.

Singh, J., Reddy, K.J., Chang, Y.Y., Kang, S.H. and Yang, J.K. 2016. A novel reutilization method for automobile shredder residue as an adsorbent for the removal of methylene blue: Mechanisms and heavy metal recovery using an ultrasonically assisted acid. Process Saf. Environ., 99: 88-97.

Yagub, M.T., Sen, T.K., Afroze, S. and Ang, H.M. 2014. Dye and its removal from aqueous solution by adsorption: A review. Adv. Colloid Interface Sci., 209: 172-184.

Zhang, F., Ma, B.L., Jiang, X.P. and Ji, Y.F. 2016. Dual function magnetic hydroxyapatite nano powder for removal of malachite green and Congo red from aqueous solution. Powder Technol., 302: 207-214.

Nature Environment and Pollution Technology
An International Quarterly Scientific Journal

p-ISSN: 0972-6268
e-ISSN: 2395-3454

Vol. 19 | No. 1 | pp. 71-82 | 2020

Original Research Paper | Open Access

Assessing Ecological Conditions of Microtopography for Vegetation Restoration on the Chinese Loess Plateau

Huan Ma *(***)†, Qingke Zhu, Xining Zhao* and Yuan Liu*****

*College of Water Resources and Architectural Engineering, Northwest Agricultural & Forestry University, Yangling 712100, P.R. China

**Forestry Ecological Engineering Research Center (Ministry of Education), Beijing Forestry University, Beijing 100083, P.R. China

***Powerchina Northwest Engineering Corporation, Xi'an 710065, P.R. China

†Corresponding author: Ma Huan

Nat. Env. & Poll. Tech.
Website: www.neptjournal.com

Received: 14-06-2019
Accepted: 24-07-2019

Key Words:
Loess plateau
Microtopographic heterogeneity
Plant diversity
Soil nutrients
Soil water

ABSTRACT

Microtopographies affect large portions of the Chinese Loess Plateau after years of water erosion. Vegetation restoration has proven to be an effective way to conserve water and soil, however, studies of the influence of microtopography on naturally recovered vegetation on the Chinese Loess Plateau have long been absent. The objective of this study was to determine the influence of microtopography on the vegetation structure and plant diversity of naturally restored vegetation and compare the soil physicochemical properties of different microtopographies with those of undisturbed slopes on the Loess Plateau. We identified five types of microtopographies that are mainly shaped by runoff in the study area, and examined vegetation structures, plant diversity, soil nutrients and soil water storage compared with undisturbed slopes. The results show that vegetation communities on loess slopes are still in an early successional stage after 14 years of natural recovery. Vegetation diversity was significantly different among microtopographies. Four types of microtopography have better soil conditions for vegetation restoration; scarps are the exception. Our results suggest that microtopographies can create some better condition plots for precision designed artificial restoration of vegetation, which is necessary to accelerate the succession process on the Loess Plateau.

INTRODUCTION

The Loess Plateau in China covers a large area totalling 624,000 km^2. The soil erosion on the Loess Plateau not only leads to the degradation of local land but also sends sediment to the lower reaches of the Yellow River, increasing the flooding risk (Mcvicar et al. 2007). Vegetation restoration on the Loess Plateau has been proven to be an effective way to improve soil texture (Li et al. 2006) and decrease the soil erosion ratio (Zheng 2006). To control soil erosion, the Chinese government has historically focused on a series of vegetation restoration projects on the Loess Plateau. To pursue an endpoint in which forests can rapidly develop a closed canopy with minimal labour investment, a vegetation restoration model on the Loess Plateau in which plants are planted with the same row spacing along contours based on the site conditions of slopes using fast growing trees and shrubs has often been adopted for restoration (Zhu et al. 2012). However, these projects have met with mixed success (Jiao et al. 2012). After years of water erosion on the Loess Plateau, there are numerous potholes and gullies distributing all over slopes. This type of topographic heterogeneity can lead to the redistribution of precipitation by affecting overland flow (Liu et al. 2004) and evaporation (Price et al. 1998). The unevenness of soil water moisture and inappropriate selection of species together result in forest degradation and the development of low productivity forests with small but old trees (Zhu et al. 2012). However, better soil water conditions can also be created by the uneven surface (Mott et al. 1974). Higher species diversity can appear in the sites where the micro-environment has greater heterogeneity in both the horizontal and vertical directions, and a complex community structure implies the use of multiple environmental resources (He et al. 1997).

Topographic heterogeneity on a fine scale has long been recognized as an important factor in vegetation restoration (Rossell et al. 2009). Early in the 1960s, studies found that small topographic differences can significantly affect species distributions and succession in herbaceous communities (Zedler et al. 1969). Subsequent studies have illustrated that a small amount of heterogeneity in topography can affect the microenvironment of the understory (Beatty 1984), soil texture (Martinez-Turanzas et al. 1997), and soil nutrients

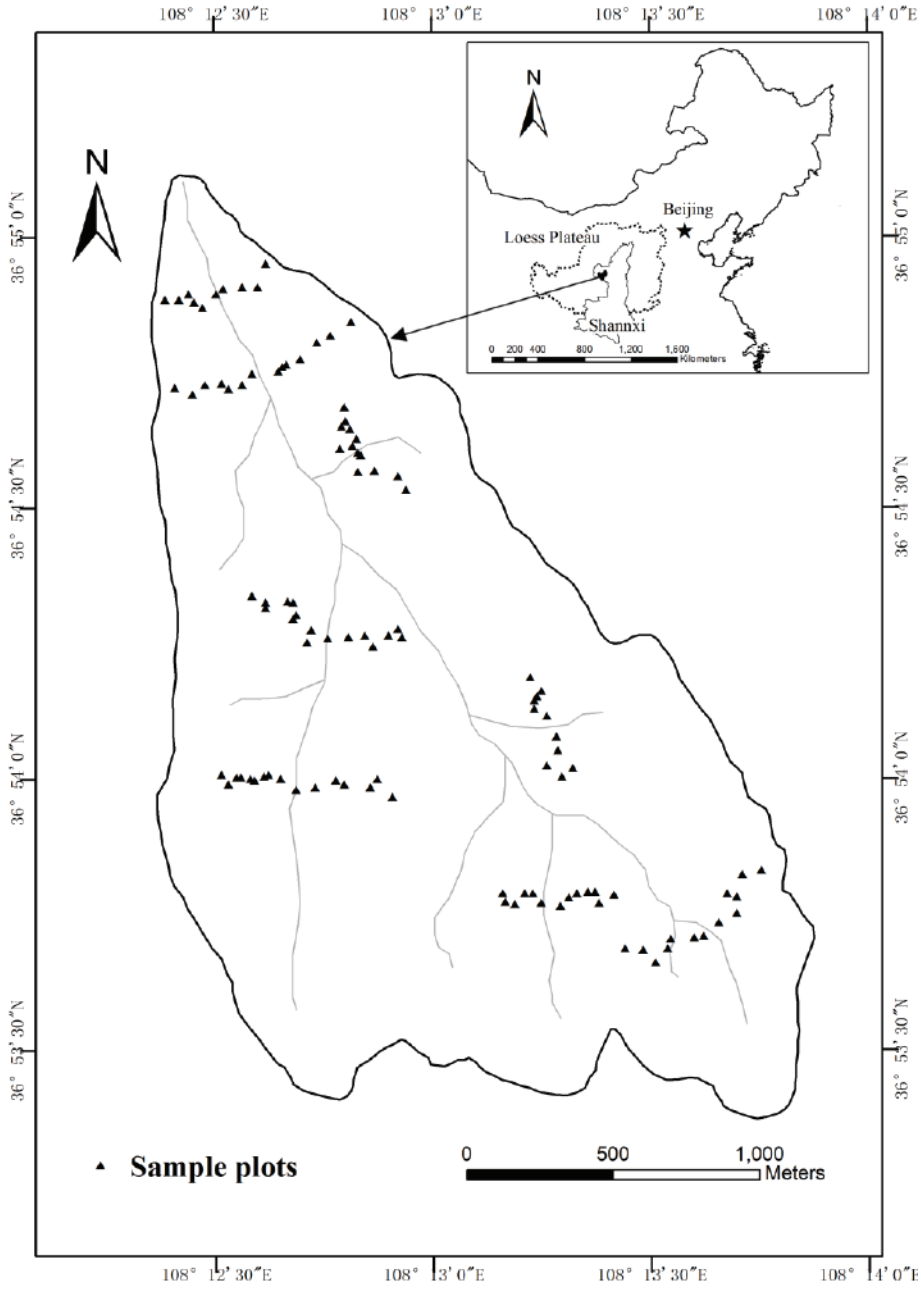

Fig.1: The distribution of sample plots in the Hegou watershed.

(Moser et al. 2009). This small topographic heterogeneity is often created by disturbances, such as tree fall (Moser et al. 2009), animal activities (Pavone et al. 1985), soil erosion (Zhu et al. 2012), sedimentation (Werner et al. 2002) and landslides (Sakai et al. 1993). These disturbances create bare soil with different characteristics that different pioneer plants can opportunistically invade, and the pioneer plants can establish communities different from those in surrounding forests (Guariguata 1990). A small amount of topographic heterogeneity can also affect the vegetation structure (Hara et al. 1996), composition (Milton et al. 1985), and succession (Gilland et al. 2014) of early successional plants and eventually the development of different late-successional communities.

Previous studies have primarily focused on microtopography in wetlands (Domínguez-Cadena et al. 2016), where the microtopography is often created by tree fall (Šamonil et al. 2016). These microtopographies, such as mounds, pools and pits, are usually on a scale of less than 5 m due to the specific hydrological and environmental conditions (Beatty 1984). Microtopographies that are created by landslides on a larger scale in hilly area were also reported (Nagamatsu et al. 1997). There are also lots of microtopographies exist in the Loess Plateau. These microtopographies were different from those mentioned in previous studies both in scale and the cause they emerged. Microtopography on the Loess Plateau was shaped by several types of soil erosion, among which water erosion is the main type (Fang et al. 2008), and on a spatial scale larger than 1 m^2. Studies have assessed the soil properties and vegetation structure responses after vegetation restoration projects on the Loess Plateau (Zeng et al. 2016), but none have addressed the effect of microtopography on edaphic or botanical factors. In addition, vegetation restoration on the Loess Plateau focuses on matching tree species with site in slope scale, whereas the small scale of topographic heterogeneity that under the slope scale may significantly impact the quality of vegetation restoration. No studies have assessed the influence of microtopography to natural recovered vegetation on the Chinese Loess Plateau. The objects of this study were to (1) analyse the impact of microtopography, relative to other topographical factors, on vegetation structure and species diversity, (2) determine the vegetation structures and species diversity among different microtopographies, and (3) compare soil physiochemical properties among different microtopographies in order to determine precisely suitable position using microtopography as an indicator for vegetation restoration on the Loess Plateau.

MATERIALS AND METHODS

Study Site

The study was conducted in the 4.25 km^2 Hegou (36°54'09" - 36°54'23" N, 108°12'50" - 108°13'01" E) watershed, located in Wuqi County, northern Shaanxi Province. The area is characterized by a temperate continental monsoon climate that is warm and dry, with an annual mean temperature of 7.8°C and mean annual precipitation of 466 mm (based on data spanning 1957-2009). The annual variation in precipitation is large, and there is an uneven distribution in different seasons, with most precipitation occurring from June to September. The soil type of this area is cultivated loessal soils. The land surface can easily be eroded and forms many types of microtopographies due to the specific character of precipitation and human activities. Fig. 1 shows the distribution of the sample plots in the Hegou watershed.

Classification of Microtopography

According to field observations, slopes in the Loess Plateau usually can be classified as undisturbed slope and disturbed slope due to the severe soil erosion. The disturbed slope part formed several kinds of microtopographies. The microtopographies on the Loess Plateau are usually larger in extent compared with those in wetlands. We defined 5 main forms of microtopography on the Loess Plateau, which are scarp, ephemeral gully, sinkhole, platform and gully (Fig. 2). Most of the slopes in the Loess Plateau are consisted of these microtopographies and the undisturbed slopes. The scarp is an area with a substantially steeper than the other parts of the slopes. The ephemeral gully is the primary stage of gully erosion development, and it is larger than a rill and smaller than a gully. The sinkhole is a crater on the ground shaped by running water. The platform is an area with a substantially gentle gradient than the other parts of the slopes. The gully is a landform created by running water, eroding sharply into soil and with a V-shaped cross section. Besides the five kinds of microtopographies mentioned above, we also took undisturbed slope, the rest of slope where no microtopography developed, into consideration as reference.

Data Collection

Vegetation data were collected in July 2012, and 8 transects were established across the watershed from the head to the outlet for four different slope aspects. Sample plots were placed in every microtopography on transects and undisturbed slopes nearby as reference. The sample size was 1 m × 1 m because shrubs and trees are rare. Along each transect, 14-17 plots were located. A total of 95 plots were recorded, within which there were 14 scarp samples, 15 ephemeral gully samples, 17 sinkhole samples, 14 platform samples, 15 gully samples and 15 undisturbed slope samples. The cover of each sample plot and species was estimated visually by two observers working together. Shrubs and trees were recorded when encountered. Slope gradient, aspect and position on slope were all recorded. We adopted the common classification of slope aspects (Zhu et al. 2012) on the Loess Plateau, which are sunny slope (157.5°-247.5° N), semi-sunny slope (112.5°-157.5° N and 247.5°-292.5° N), semi-shady slope (67.5°-112.5° N and 292.5°-337.5° N) and shady slope (0-67.5° N and 337.5°-360° N).

Soil sample plots were also taken in vegetation plots. Soil samples were taken from six points in an S-shaped pattern to a depth of 60 cm in each plot. Soil analysis was carried out according to the methods described by the Agricultural Chemistry Committee of the Chinese Soil Academy (1984): organic matter by the $K_2Cr_2O_7$ method; total N by the K_2SO_4 – $CuSO_4$ – Se distillation method; total P by the $HClO_4$ –

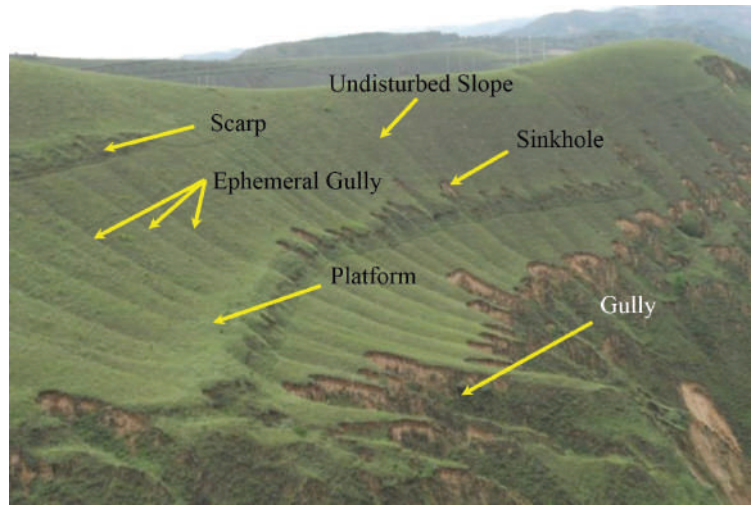

Fig. 2: Demonstration of undisturbed slope and five types of microtopographies: scarp, ephemeral gully, sinkhole, platform and gully.

H_2SO_4 colorimetric method; extractable ammonium-N by the diffusion method with 1N NaOH 10 mL, 2% H_3BO_3, and 0.005N HCl at a temperature of 40°C for 24 hours; extractable P by the 0.5 M $NaHCO_3$ extraction (1:20) colorimetric method; and extractable K with the atomic absorption spectrum method with 1 M NH_4OAC extraction (1:20, pH = 7).

For long-term observations, soil water content was monitored in fixed plots. Three PVC pipes with lengths of 2 m were pounded into the soil for each type of microtopography and undisturbed slopes. Plots that were analogous in slope gradient and aspect were arranged on the slopes to eliminate unnecessary disruption. A portable Time Domain Reflectometry (TDR) instrument was used to measure the soil water content twice per month from May 2011 to April 2012. The measurement was made from the ground surface downward to a depth of 200 cm at 20 cm intervals. For each depth interval, the soil moisture content was measured three times, and the means of the three measurements were taken as the soil moisture content of the depth interval.

Data Analysis

The measures of vegetation structure included vegetation cover, height and relative importance value (RIV). Margalef's (Clifford et al. 1976) index for species richness, the Alatalo index (Alatalo 1977) for evenness, and the Shannon-Wiener diversity index (Shannon et al. 1950) were used as the measures of plant diversity. Soil nutrient levels and soil water storage were used as measures to assess ecological conditions. The differences among microtopographies and undisturbed slopes were compared with analysis of variance (ANOVA) and a least significant difference (LSD) test using SPSS V20.0 (SPSS Inc., Chicago IL, USA). The equations used to calculate Margalef's index, the Alatalo index, the Shannon-Wiener index, RIV and soil water storage are as follows:

$$\text{Margalef's index: } M_a = (S-1)/\ln N \quad \ldots(1)$$

$$\text{Alatalo index: } E_a = (1/\Sigma_{i=1}^{s} P_i^2 - 1)(e^H - 1) \quad \ldots(2)$$

$$\text{Shannon-Wiener index: } H' = -\Sigma_{i=1}^{S}(P_i \ln P_i) \quad \ldots(3)$$

$$\text{Relative importance value: } RIV = (C_r + H_r)/200 \quad \ldots(4)$$

$$\text{Soil water storage: } D_w = 0.1\Sigma_1^n VSWC * H_s \quad \ldots(5)$$

Where, S is the number of species, P_i is the proportion of individuals or the abundance of the i^{th} species expressed as a proportion of the total number in the community, ln is the log base-e, N is the total number of all species. C_r is relative coverage and H_r is relative height. VSWC is the soil volumetric water content of each soil layer, *n* is the number of soil layers, and H_s is the depth of each soil layer.

A canonical correlation analysis was used to examine the relationship between plant community characteristics and topographical factors. A canonical correlation analysis (CCA) is a way of making sense of cross-covariance matrices. If there are two vectors $X = (X_1, ..., X_n)$ and $Y = (Y_1, ..., Y_m)$ of random variables, and there are correlations among the variables, then a canonical-correlation analysis will find linear combinations of X_i and Y_j that have the maximum correlation with each other (Härdle et al. 2007). The two vectors here represent plant community characteristics and topographical factors. The plant community characteristics vector includes vegetation cover (X_1), average height (X_2), biomass (X_3), and Shannon-Weiner index (X_4). The topographical factors

vectors include slope aspect (Y_1), slope gradient (Y_2), slope position (Y_3) and microtopography position (Y_4). The slope aspect, slope position and microtopography were all quantified as follows: sunny slope 1, semi-sunny slope 2, semi-shady slope 3, shady slope 4; top of slope 1, middle of slope 2, bottom of slope 3; and scarp 1, ephemeral gully 2, sinkhole 3, platform 4, gully 5.

RESULTS

Relationship between Topographical Factors and Plant Communities

The canonical correlation analysis shows that for topographical factors and plant communities, there are four canonical dimensions, of which only the first two are statistically significant at the 0.05 level (Table 1). Characteristic roots of the four canonical dimensions show that 70% of total information was explained by the first two dimensions. For the first canonical dimension, the linear combination of the topographical factors v_1, correlation coefficient of v_1 and raw data Y_1 indicate that slope aspect and microtopography position have an obvious positive correlation with v_1. Correspondingly, u_1, the linear combination of the plant community characteristics, has a positive correlation with the Shannon index. For the second canonical dimension, the linear combination of the topographical factors, v_2, was most relevant to microtopography position. Correspondingly, the Shannon-Weiner index has a negative correlation with the linear combination of the plant community characteristics u_2.

Vegetation Structure

A total of 64 species were found in the Hegou watershed, among which 55 species were present in the undisturbed slope plots and 64 species were present in the microtopography plots. Only 4 shrub species were found in scarps, sinkholes and gullies: *Prinsepia uniflora*, *Caragana korshinskii*, *Spiraea blumei* and *Armeniaca vulgaris.* Most (approximately 53.5%) of species belong to the Leguminoseae, Gramineae and Asteraceae (Fig. 3), which accounted for 25.5%, 16.4% and 12.7% of species, respectively. Asteraceae occupied a relatively small proportion in ephemeral gullies and undisturbed slopes, and grasses accounted for a relatively high percentage in sinkholes. A higher cover (73.33%) was recorded in gullies than in the other microtopographies ($p = 0.03$) (Table 3). The average cover in all microtopographies was greater than on undisturbed slopes, and the average height of herbs in sinkholes ($p = 0.03$) was 48.11 cm and in gullies ($p = 0.02$) was 42.00 cm, which were nearly double the heights of those in other microtopographies and slopes.

Table 2 gives the relative importance values (RIVs) greater or equal to 0.05 for species found in the Hegou watershed in microtopographies and undisturbed slopes. *Artemisia giraldii* and *Artemisia sacrorum* were the dominant species on undisturbed slopes and all microtopographies that had the maximum RIV. The accompanying species were primarily *Stipa capillata*, *Lespedeza bicolor* and *Poa annua* L. in all sites. However, scarps had *Prinsepia uniflora*, gullies had *Caragana korshinskii*, and platforms had *Phragmites*

Table 1: Canonical variables and their correlation coefficients with original variables. s, Standardized canonical coefficients for each variable; r, correlation coefficient between standardized canonical coefficients and variables; R, correlation coefficient of canonical variables Xi and Yi; **, significance level of 0.01; *, significance level of 0.05.

Canonical variable		Plant community characteristics vectors				Topographical factors vectors			
		X_1	X_2	X_3	X_4	Y_1	Y_2	Y_3	Y_4
I	s	0.079	0.238	0.368	0.804				
R = 0.644**						0.768	0.077	0.230	0.461
	r	0.633	0.503	0.557	0.287	0.833	-0.099	0.291	0.652
II	s	-0.499	-0.584	0.871	1.596				
R = 0.477*						-0.589	-0.404	-0.217	0.787
	r	-0.232	0.035	0.387	-0.721	-0.385	-0.545	0.039	0.713
III	s	-0.571	-0.009	0.842	1.403				
R = 0.366						-0.351	0.768	0.430	0.373
	r	-0.167	0.291	0.505	0.390	-0.377	0.706	0.554	0.233
IV	s	-0.600	-0.746	0.638	-3.281				
R = 0.112						0.008	0.555	-0.903	0.478
	r	0.110	-0.531	0.135	0.166	0.126	0.442	-0.779	0.106

australis as unique accompanying species. In addition, the RIV of *Artemisia giraldii* in the sinkholes was much greater than in the other microtopographies.

Plant Diversity

Table 3 presents the plant diversity indices of microtopographies in the Hegou watershed. Margalef's richness index values were in the following order: scarp > platform > gully > ephemeral gully > undisturbed slope. The scarp had the highest Margalef index value of 2.49, but the difference was not significant among the microtopographies. The Alatalo evenness index differed among the microtopographies. The maximum Alatalo index appeared in ephemeral gullies ($p = 0.02$) at 0.618. The minimum Alatalo index appeared in the platform (0.03) at 0.414. The Shannon-Wiener index in scarps was the highest but not significantly ($p = 0.354$). In general, compared with microtopographies, fewer species were distributed on undisturbed slopes in a relatively uniform pattern, implying an unstable community structure on undisturbed slopes. Among all microtopographies, scarps, gullies and ephemeral gullies had more species and more homogeneous plant distribution. Sinkholes were primarily

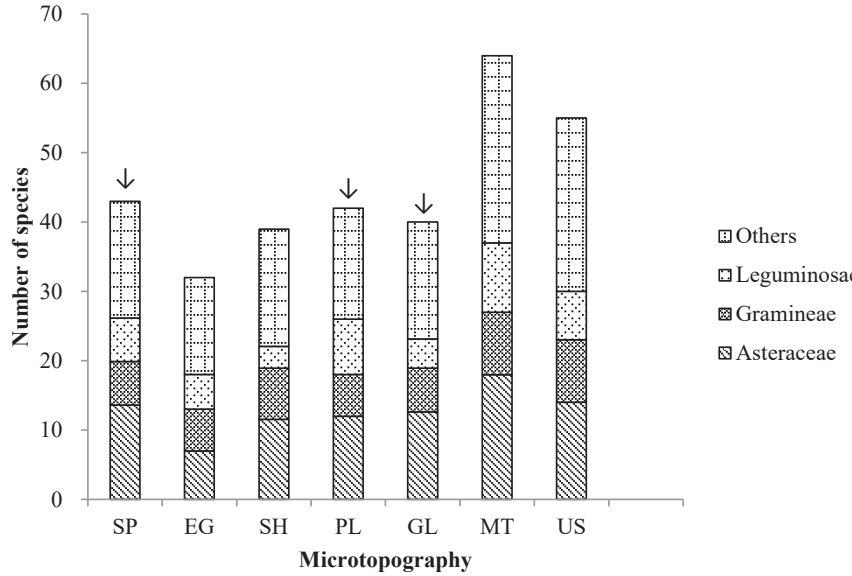

Fig. 3: Species compositions of different microtopographies in the Hegou watershed. Bars indicate the number of species in microtopographies and on undisturbed slopes. Arrows indicate plots in which shrubs appeared. SP: scarp; EG: ephemeral gully; SH: sinkhole; PL: platform; GL: gully; MT: take all the microtopographies above as a whole; US: undisturbed slope.

Table 2: Relative importance values (RIVs) for species found in the Hegou watershed across different microtopographies. SP: scarp; EG: ephemeral gully; SH: sinkhole; PL: platform; GL: gully; US: undisturbed slope.

Plant Species	Microtopography					
	SP	EG	SH	PL	GL	US
Artemisia giraldii Pamp.	0.155	1.173	0.269	0.110	0.198	0.169
Artemisia sacrorum Ledeb.	0.162	0.178	0.144	0.182	0.192	0.179
Stipa capillata Linn.	0.118	0.152		0.088	0.065	0.093
Lespedeza bicolor Turcz.	0.062	0.064		0.094		0.084
Poa annua L.			0.092	0.064	0.066	0.056
Potentilla acaulis L.	0.074					
Thymus mongolicus Ronn		0.054	0.054			
Prinsepia uniflora Batal.	0.062				0.059	
Phragmites australis				0.052		
Potentilla chinensis Ser.		0.052				
Caragana korshinskii Kom					0.050	

Table 3: Cover, average height, species richness and diversity values of microtopographies and undisturbed slopes in the Hegou watershed. SP: scarp; EG: ephemeral gully; SH: sinkhole; PL: platform; GL: gully; US: undisturbed slope. Average height was calculated excluding shrubs and tree seedlings. All values are means±SE. Letters indicate significant pairwise differences between means within a row at p = 0.05.

	Microtopography					
	SP	EG	SH	PF	GL	US
Cover (%)	68.07 ± 3.91^{b}	67.35 ± 3.87^{b}	66.39 ± 4.20^{b}	64.64 ± 3.97^{b}	74.33 ± 3.89^{a}	63.35 ± 2.29^{b}
Average height (cm)	28.00 ± 2.80^{ab}	24.57 ± 2.39^{a}	48.11 ± 4.53^{b}	23.79 ± 2.18^{a}	42.00 ± 5.56^{b}	26.30 ± 1.72^{a}
Margalef's index	2.491 ± 0.102	2.256 ± 0.093	1.984 ± 0.081	2.339 ± 0.122	2.346 ± 0.077	2.023 ± 0.082
Shannon-Wiener index	1.695 ± 0.082^{a}	1.62 ± 0.091^{ab}	1.375 ± 0.087^{b}	1.39 ± 0.120^{b}	1.58 ± 0.084^{ab}	1.36 ± 0.063^{b}
Alatalo index	0.56 ± 0.027^{bc}	0.618 ± 0.032^{c}	0.46 ± 0.029^{ab}	0.41 ± 0.037^{a}	0.52 ± 0.022^{abc}	0.517 ± 0.027^{abc}

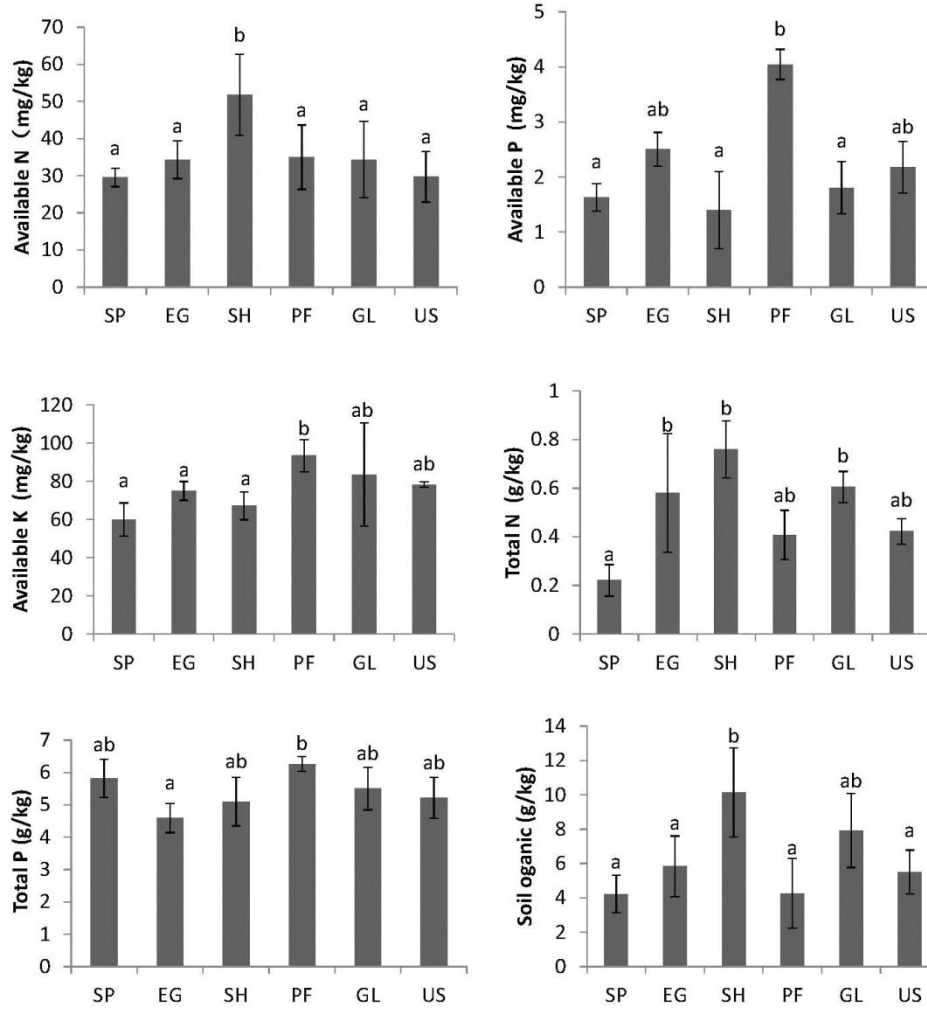

Fig. 4: The soil nutrient in the 0-60 cm layers of different microtopographies. SP: scarp; EG: ephemeral gully; SH: sinkhole; PL: platform; GL: gully; US: undisturbed slope. Bar heights indicate means, arrows indicate SE, and letters indicate significant differences at p = 0.05.

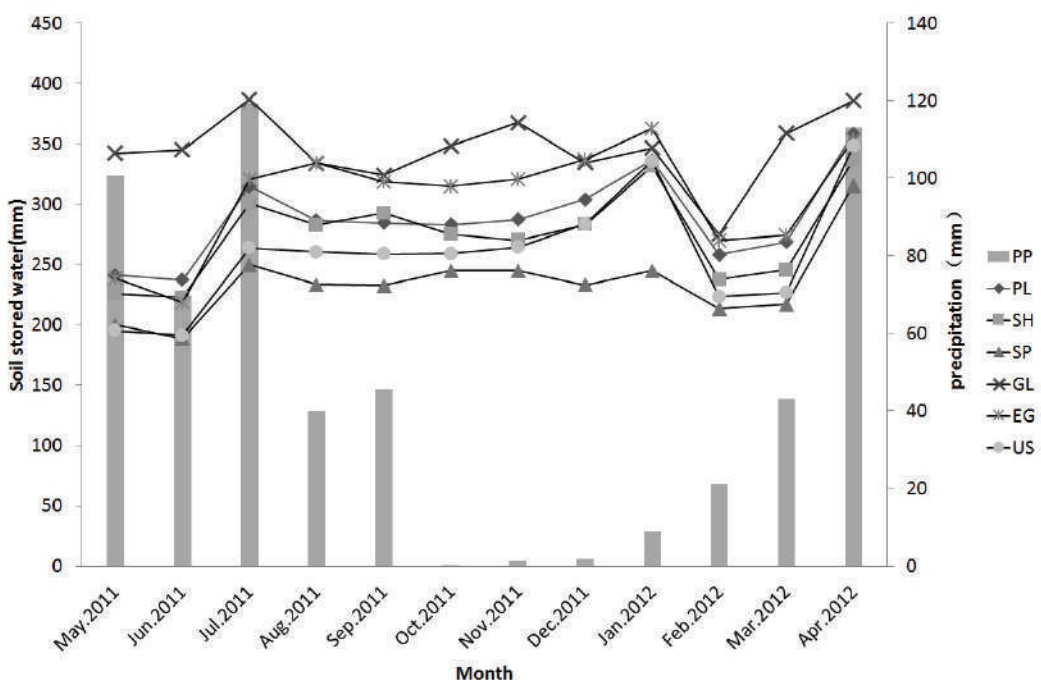

Fig. 5: Soil water storage in 180 cm of five microtopography types and an undisturbed slope from May 2011 to April 2012. SP: scarp; EG: ephemeral gully; SH: sinkhole; PL: platform; GL: gully; US: undisturbed slope; PP: precipitation.

monodominant communities, which were lower in species diversity and species evenness. Platforms showed similar characteristics with sinkhole, but the indices were slightly lower.

Soil Nutrients

Available N, total N and organic matter in sinkholes were higher than in the other microtopographies and undisturbed slopes, among which organic matter in sinkholes ($p = 0.02$) was significantly higher than the others. Available P, available K and total P in platforms were higher than the other microtopographies ($p = 0.084$) and undisturbed slopes ($p = 0.013$). The soil nutrients in ephemeral gullies were largely the same as undisturbed slopes, except the total P which was slightly lower. Scarps had the minimum content characteristics of soil nutrients compared with the other microtopography positions. Gullies were at an intermediate level of soil nutrients for all the six soil nutrients (Fig. 4)

Soil Water

Fig. 5 gives the precipitation characteristics of the Loess Plateau region in northern Shaanxi. The uneven annual rainfall makes it very dry in winter and rainy in summer. According to the soil water storage value, microtopographies and undisturbed slopes showed significant differences ($F = 11.916$, $df = 5$, $p < 0.001$), which, arranged in descending order, were gully > ephemeral gully > platform > sinkhole > undisturbed slope > scarp. Among all the microtopographies, gullies showed a remarkable ability to store water. Gullies maintained soil water at a high level and could also increase the soil water content rapidly even after a small rainfall event. The vertical distribution of the soil water content shows that water levels in the 60-180 cm depth range were significantly high (Fig. 6). Conversely, the soil water storage of the scarp ranged from 188.8 mm to 315.5 mm, with an average of 234.8 mm, which was the lowest of all the microtopographies. Scarps also have a poor holding water capacity, such that strong rainfall contributes little to increasing the soil water content (July, 2011). Generally, microtopographies more or less performed better than undisturbed slopes in storing water, except for the scarp.

DISCUSSION

Due to the influence of solar radiation, slope aspect can largely determine the soil moisture on the Loess Plateau. Therefore, slope aspect is the most important factor impacting plant growing. However, vegetation restoration practice was usually implemented under the slope scale, the plants influence factors that under slope scale should be considered. Alexander using elevation data from airborne

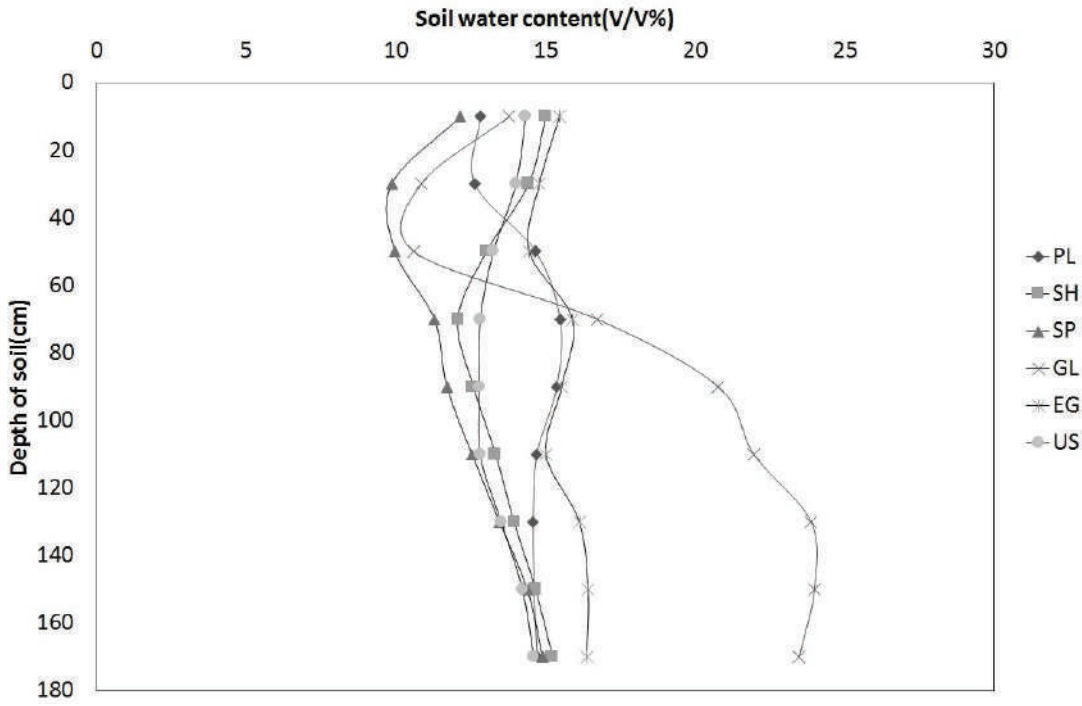

Fig. 6: Soil water content in the 0–180 cm layers of five types of microtopography and an undisturbed slope. SP: scarp; EG: ephemeral gully; SH: sinkhole; PL: platform; GL: gully; US: undisturbed slope.

laser scanner found microtopographies at a small spatial scale of a few decimetres could be an indicator of vegetation (Alexander et al. 2016). More severe disturbance to create microtopographies was also found to have potential benefits when introducing specialist species of calcareous grassland for restoration in Pegsdon Hills, Bedfordshire, UK (Wagner et al. 2016). These former studies have well illustrated that microtopographies have obvious impact to vegetation. Similarly, results of a canonical correlation analysis suggested that characteristics of microtopography were the main factors affecting the characteristics of vegetation, with the exception of slope aspect.

The vegetation species richness corresponds to habitat heterogeneity. In this study, we found that there were more species on the microtopography plots compare with undisturbed slope plots. Unlike vegetation in wetland, where excessive water in pools usually leads to lower plant cover (Sleeper et al. 2016), microtopographies on the Loess Plateau have opposite effect. Amongst all the microtopographies, plants in gullies have higher cover and plant height. Pioneer tree species with rapid growth can seize the habitat in gullies where they have an adequate water supply (Hu et al. 2007). Shrubs and pioneer tree species appeared firstly in gullies. Qin (2009) found that the dominant species and primary companion species are usually xerophytic because of the droughty soil water conditions on the Loess Plateau. However, in this study, we found hygrophytes on platforms, such as *Phragmites australis*, indicating that habitat heterogeneity come out of microtopographies. Sinkholes are a type of microtopography that can easily obtain water supply and accumulate fertile soil from runoff, which enables plants to reach greater heights. The microtopographies described above exhibited better growing environments for plants compared to undisturbed slope.

Soil nutrients can affect biomass production, species composition, and diversity (Critchley et al. 2002). Grazing exclusion was improved that had significant positive effects on improving soil nutrients (Li et al. 2016). Peng et al. (2005) showed that total N was gradually increased along with vegetation restoration years in An 'Sai on the Loess Plateau. In our study, soil nutrients content was increased in every site more or less compared with Peng's result and microtopographies performed more remarkably. Phosphorus is closely related to plant biomass (Jiao et al. 2008), and we found that it is significantly higher on platforms indicating that platforms have aggregation effect to some of the nutrient elements.

Soil water is one key factor limiting vegetation restoration (Chen et al. 2007). However, we found soil water among microtopographies that under the slope scale has significant

difference. The soil stored water in gullies was approximately 100mm more that undisturbed slopes every month in the year 2011-2012. Additionally, the disturbed slope soil water content in our study was similar compared to Wang et al. (2014) found on grass land in Suide, Shannxi Province. Microtopographies, especially gullies, ephemeral gullies and platforms indeed performed relatively wetter soil condition than undisturbed slopes.

Soil and water conservation is one of the main functions of ecological restoration on the Loess Plateau (Chen et al. 2008). One of the main reasons for revegetation is to achieve the recovery goal in a short time. Some researchers advocate natural recovery as more suitable for the ecosystem on the Loess Plateau (Jiao et al. 2012) due to the shortage of precipitation. Soil desiccation is common in current reforestation activities on the Loess Plateau (Cao et al. 2010) because too many tree seedlings are planted in small watersheds, where the incoming water cannot match the water outflow. Our study indicates that soil properties vary with the heterogeneity of topography on a fine scale. Small heterogeneity of topography can lead to fertile areas on slopes, especially with regard to the soil water content. Our study shows that soil water content is significantly different within the slope scale, implying that not every plot on slopes is necessarily inappropriate for planting. In addition, our study shows that pioneer species were still dominant in the study area after 14 years of natural recovery. Previous study suggests that successful revegetation should plant a mix of grass, shrubs and trees (Fu et al. 2000). Because actively sowing species on the Loess Plateau is likely to enhance species diversity and optimize species composition (Wang 2006), it is useful to develop an effective way to restore vegetation artificially. Creating topographic heterogeneity proved to be an active and effective approach to ecological restoration (Gilland et al. 2014). However, implementing similar measures is not easy on the Loess Plateau due to the poor local economic situation. In this case, artificially vegetation restoration using naturally formed microtopographies as indicator for species choosing may be an economic and effective way.

The soil water content and appearance of shrubs imply that platforms have a higher carrying capacity for plants compared to undisturbed slopes. Sinkholes can cluster soil nutrients and collect water, which is similar to what was found in a bottomland hardwood forest in Texas (Simmons et al. 2011) Relatively better soil water conditions suggest that sinkholes can be treated as natural tree planting locations. Ephemeral gullies are the initial stage of gully erosion, which will lead to greater soil erosion as they develop (Xu et al. 2016). However, plants grow in frequent soil erosion, and deposition environment requires a greater water supply and need to be resistant to rushing runoff. Gully erosion is the primary source of sediment loss on the Loess Plateau (Li et al. 2015). In this paper, we found that gullies have a remarkable water storage capacity and maintain a surplus of water after it is taken up by plants. The emergence of aquatic plants also indicates gullies have humid environment. Species that are resistant to flooding should be chosen for vegetation restoration in gullies, and higher densities are acceptable. Slope gradient largely influences soil erosion (Fox et al. 2000), which lowers the soil water storage and soil nutrients in scarps compared with other four microtopographies. To improve ecological restoration, we suggest maintaining the status of scarps and reducing human interference during artificial vegetation restoration.

CONCLUSION

Microtopography was the second main factor affecting the characteristics of vegetation besides slope aspect on the Loess Plateau. In the natural recovery site, vegetation structure, plant diversity, soil nutrients and soil water content were significantly different across microtopographic features. According to the soil water storage value, microtopographies and undisturbed slopes arranged in descending order were gully > ephemeral gully > platform > sinkhole > undisturbed slope > scarp. An effective vegetation configuration mode requires more accurate design. Vegetation configuration on slopes should be in accordance with the microtopography. Species that require more water can be planted in gullies, ephemeral gullies and platforms. A small number of seedlings could also be planted in sinkholes to prevent further soil erosion. In addition, species planted on undisturbed slopes should have a lower water requirement compared with those planted on the microtopographies described above. Scarps should maintain the status quo and recover naturally.

ACKNOWLEDGEMENTS

We would like to extend our sincere gratitude to Zong Kai Wu and Guang Liang Liu for their help in providing local support during the study. We are grateful to Yingying Zhang and Wenjuan Ma for valuable assistance. We would like to thank Matthew R. and Jennie L. for linguistic improvement of the manuscript.

REFERENCES

Alatalo, R. 1977. Components of diversity: Multivariate analysis with interaction. Ecology, 58(4): 900-906.

Alexander, C., Deák, B. and Heilmeier H. 2016. Micro-topography driven vegetation patterns in open mosaic landscapes. Ecological Indicators, 60: 906-920.

Beatty, S.W. 1984. Influence of microtopography and canopy species on spatial patterns of forest understory plants. Ecology, 65(5): 1406-1419.

Cao, S., Tian, T., Chen, L., Dong, X., Yu, X. and Wang, G. 2010. Damage caused to the environment by reforestation policies in arid and semi-arid areas of China. Annals of Biology, 39(4): 279-283.

Chen, H., Shao, M. and Li, Y. 2008. Soil desiccation in the Loess Plateau of China. Geoderma, 143(1): 91-100.

Chen, L., Huang, Z., Gong, J., Fu, B. and Huang, Y. 2007. The effect of land cover/vegetation on soil water dynamic in the hilly area of the loess plateau, China. Catena, 70: 200-208.

Clifford, H. T. and Stephenson, W. 1976. An Introduction to Numerical Classification. Academic Express, London.

Critchley, C.N.R., Chambers, B.J., Fowbert, J.A., Sanderson, R.A., Bhogal, A. and Rose, S.C. 2002. Association between lowland grassland plant communities and soil properties. Biological Conservation, 105: 199-215.

Domínguez-Cadena, R., Riosmena-Rodríguez, R., León-De, La Luz and J.L. 2016. Forest structure and species composition of mangroves in the eastern Baja California Peninsula: The role of microtopography. Wetlands, 36(3): 515-523.

Fang, H.Y., Cai, Q.G., Chen, H. and Li, Q.Y. 2008. Effect of rainfall regime and slope on runoff in a gullied loess region on the Loess Plateau in China. Environmental Management, 42(3): 402-411.

Fox, D. M. and Bryan, R. B. 2000. The relationship of soil loss by interrill erosion to slope gradient. Catena, 38(3): 211-222.

Fu, B. J. and Chen, L. D. 2000. Agricultural landscape spatial pattern analysis in the semi-arid hill area of the Loess Plateau, China. Journal of Arid Environments, 44(3): 291-303.

Gilland, K. E. and Mccarthy, B. C. 2014. Microtopography influences early successional plant communities on experimental coal surface mine land reclamation. Restoration Ecology, 22(2): 232-239.

Guariguata, M. R. 1990. Land slide disturbance and forest regeneration in the upper Luquillo mountains of Puerto Rico. The Journal of Ecology, 78: 814-832.

Hara, M., Hirata, K., Fujihara, M. and Oono, K. 1996. Vegetation structure in relation to micro-landform in an evergreen broad-leaved forest on Amami Ohshima Island, south-west Japan. Ecological Research, 11(3): 325-337.

Härdle, W. and Simar, L. 2007. Applied Multivariate Statistical Analysis. Springer Verlag, NewYork.

He, J. S. and Chen, W. L. 1997. A review of gradient changes in species diversity of land plant community. Acta Ecologica Sinica, 17(1); 93-101.

Hu, Z. W. and Shen, Z. H. 2007. Impacts of topography on the spatial pattern of the age of forest community. Chinese Journal of Plant Ecology, 31(4): 814-824.

Jiao, J., Tzanopoulos, J., Xofis, P. and Mitchley, J. 2008. Factors affecting distribution of vegetation types on abandoned cropland in the hilly-gullied Loess Plateau region of China. Pedosphere, 18(1): 24-33.

Jiao, J., Zhang, Z., Bai, W., Jia, Y. and Wang, N. 2012. Assessing the ecological success of restoration by afforestation on the Chinese Loess Plateau. Restoration Ecology, 20(2): 240-249.

Li, H., Zhang, F., Mao, S., Zhu, J., Yang, Y., He, H. and Li, Y. 2016. Effects of grazing exclusion on ssoil properties in Maqin Alpine Meadow, Tibetan Plateau, China. Polish Journal of Environmental Studies, 25(4): 1583-1587.

Li, Y. Y. and Shao, M. A. 2006. Change of soil physical properties under long-term natural vegetation restoration in the Loess Plateau of China. Journal of Arid Environments, 64(1): 77-96.

Li, Z., Zhang, Y., Zhu, Q., He, Y. and Yao, W. 2015. Assessment of bank gully development and vegetation coverage on the Chinese Loess Plateau. Geomorphology, 228: 462-469.

Liu, Q. Q. and Singh, V. P. 2004. Effect of microtopography, slope length and gradient, and vegetative cover on overland flow through simulation. Journal of Hydrologic Engineering, 9(5): 375-382.

Martinez-Turanzas, G.A., Coffin, D. P. and Burke, I. C. 1997. Development of microtopography in a semi-arid grassland: Effects of disturbance size and soil texture. Plant and Soil, 191(2): 163-171.

McVicar, T.R., Li, L., Van Niel, T.G., Zhang, L., Li, R., Yang, Q., Zhang, X., Mu, X., Wen, Z., Liu, W. and Zhao, Y.A. 2007. Developing a decision support tool for China's re-vegetation program: Simulating regional impacts of afforestation on average annual streamflow in the Loess Plateau. Forest Ecology and Management, 251(1): 65-81.

Milton, L., Lieberman, D., Hartshorn, G.S. and Peralta, R. 1985. Small-scale altitudinal variation in lowland wet tropical forest vegetation. Journal of Ecology, 73(2): 505-516.

Moser, K. F., Ahn, C. and Noe, G. B. 2009. The influence of microtopography on soil nutrients in created mitigation wetlands. Restoration Ecology, 17(5): 641-651.

Mott, J. J. and Mccomb, A. J. 1974. Patterns in annual vegetation and soil microrelief in an arid region of Western Australia. Journal of Ecology, 62(1): 115-126.

Nagamatsu, D. and Miura, O. 1997. Soil disturbance regime in relation to micro-scale landforms and its effects on vegetation structure in a hilly area in Japan. Plant Ecology, 133(2): 191-200.

Pavone, L. V. and Reader, R.J. 1985. Effect of microtopography on the survival and reproduction of *Medicago lupulina*. The Journal of Ecology, 73: 685-694.

Peng, W.Y., Zhang, K.L., Chen, Y. and Yang, Q.K. 2005. Research on soil quality change after returning farmland to forest on the loess sloping croplands. Journal of Natural Resources, 20(2): 272-278 (in Chinese).

Price, J., Rochefort, L. and Quinty, F. 1998. Energy and moisture considerations on cutover peatlands: Surface microtopography, mulch cover and sphagnum regeneration. Ecological Engineering, 10(4): 293-312.

Qin, W., Zhu, Q.K., Zhang, Y.Q. and Zhao, L.L. 2009. Dynamics of plant community species diversity in the process of ecological rehabilitation in north Shaanxi loess area. Chinese Journal of Applied Ecology, 20(2): 403-409 (in Chinese).

Rossell, I.M., Moorhead, K.K., Alvarado, H. and Warren, R.J. 2009. Succession of a southern Appalachian mountain wetland six years following hydrologic and microtopographic restoration. Restoration Ecology, 17(2): 205-214.

Sakai, A. and Ohsawa, M. 1993. Vegetation pattern and microtopography on a landslide scar of Mt Kiyosumi, central Japan. Ecological Research, 8(1): 47-56.

Šamonil, P., Valtera, M., Schaetzl, R.J., Adam, D., Vašíčková, I., Daněk, P., Janík, D. and Tejnecký, V. 2016. Impacts of old, comparatively stable, tree throw microtopography on soils and forest dynamics in the northern hardwoods of Michigan, USA. Catena, 140: 55-65.

Shannon, C. E., Weaver, W. and Wiener, N. 1950. The Mathematical Theory of Communication. University of Illinois Press, Urbana.

Simmons, M. E., Ben, Wu X. and Whisenant, S. G. 2011. Plant and soil responses to created microtopography and soil treatments in bottomland hardwood forest restoration. Restoration Ecology, 19(1): 136-146.

Sleeper, B. E. and Robert, L. F. 2016. Edaphic and vegetative responses to forested wetland restoration with created microtopography in Arkansas. Ecological Restoration, 34(2): 117-123.

Wagner, M., Bullock, J.M., Hulmes, L., Hulmes, S., Peyton, J., Amy, S.R., Savage, J., Tallowin, J.B., Heard, M.S. and Pywell, R.F.2016. Creation of micro-topographic features: A new tool for introducing specialist species of calcareous grassland to restored sites? Applied Vegetation Science, 19(1): 89-100.

Wang, G. 2006. Can the restoration of natural vegetation be accelerated on the Chinese Loess Plateau? A study of the response of the leaf carbon isotope ratio of dominant species to changing soil carbon and nitrogen levels. Ecological Research, 21(2): 188-196.

Wang, X., Zhang, W., Wang, Z., Liu, X. and Wang, S. 2014. Soil moisture status under deep-rooted and shallow-rooted vegetation in the semi-

arid area of Loess Plateau in China. Polish Journal of Environmental Studies, 23(2): 511-520.

Werner, K. J. and Zedler, J. B. 2002. How sedge meadow soils, microtopography, and vegetation respond to sedimentation. Wetlands, 22(3): 451-466.

Xu, M. X., Qiang, L. and Glenn, W. 2016. Degradation of soil physicochemical quality by ephemeral gully erosion on sloping cropland of the hilly Loess Plateau, China. Soil and Tillage Research, 155(1): 9-18.

Zedler, J. B. and Zedler, P. H. 1969. Association of species and their relationship to microtopography within old fields. Ecology, 50(3): 432-442.

Zeng, Q., Li, X., Dong, Y., An, S. and Darboux, F. 2016. Soil and plant components ecological stoichiometry in four steppe communities in the Loess Plateau of China. Catena, 147: 481-488.

Zheng, F. 2006. Effect of vegetation changes on soil erosion on the Loess Plateau. Pedosphere, 16(4): 420-427.

Zhu, Q. K., Zhang, Y. and Zhao, L. L. 2012. Vegetation Restoration and Simulated Natural Forestation in the Loess Plateau, Northern Shaanxi, China. Science Press, Beijing (in Chinese).

Nature Environment and Pollution Technology
An International Quarterly Scientific Journal

p-ISSN: 0972-6268
e-ISSN: 2395-3454

Vol. 19 | No. 1 | pp. 83-92 | 2020

Original Research Paper | Open Access

Analysis of Spatial Heterogeneity in Coupling Development of Industrialization and Resource Environmental Bearing Capacity

Ying Huang*, Zhi Zhou and Qin Qin*****
*College of Information Engineering, Wuhan University of Engineering Science, Wuhan, 430200, China
**College of Land and Resources, Agricultural University of Hebei, Baoding, 071001, China
***Department of Tourism, Sport and Society, Lincoln University, Christchurch, 7674, New Zealand
†Corresponding author: Zhi Zhou

Nat. Env. & Poll. Tech.
Website: www.neptjournal.com

Received: 14-12-2019
Accepted: 18-01-2020

Key Words:
Industrialization
Resource environmental bearing capacity
Coordination degree
Comprehensive evaluation
Spatial heterogeneity

ABSTRACT

The contradiction between supply and demand of resource environment has become increasingly severe because of population expansion and the rapid development of industrial economy. Spatial quantitative evaluation of coupling strength and mutual promotion between industrialization and resource environmental bearing capacity based on panel data can facilitate industrialization and promote sustainable and healthy development of regional economy objectively, scientifically, and rationally. This study proposed a three-level comprehensive evaluation matrix for clustering and comparative analysis of 31 provinces in China to analyse the characteristics of spatial heterogeneity in the coordinated development of industrialization and resource environmental bearing capacity. First, a comprehensive evaluation index system for resource environmental bearing capacity was established based on the differences in resource environmental bearing capacities in various regions of China. Combined with the coordination degree for evaluation model, the coordination between the resource environmental bearing capacity and the industrialization of the 31 provinces in 2018 was evaluated and compared based on their comprehensive evaluation index. Finally, a cluster comparison analysis was performed in the 31 provinces using the three-level comprehensive evaluation matrix of coupling development of regional economy and resource environmental bearing capacity. Moreover, the accuracy of the coordination degree model was verified according to the clustering results. Results show that the regions with good ordination between industrialization and resource environmental bearing capacity include East and North China. Meanwhile, the provinces with poor coordination mainly include Southwest and Northwest China. Resource environment still restricts the coordination between resource environmental bearing capacity and industrialization development. This study provides reference for developing differentiated resource environment management measures and countermeasures in various regions in China.

INTRODUCTION

Industrialization, as an important approach for realizing social and economic development, has certainly brought severe challenges in the current resource environmental bearing capacity. This study aims to realize the coupling and harmonious development between industrialization and population, resources, and environment. Resources not only refer to scarce natural resources but also to rare assets with high significance in social development; scholars have become increasingly concerned with these matters. The contradiction between supply and demand of resource environment has become increasingly severe because of population expansion and the rapid development of industrial economy. The continuous social and economic development has brought challenges to resource environmental bearing capacity, and their relationship has become increasingly complex. The thorough summarization of the coordination relationship between industrial economy and resource environmental bearing capacity is difficult. New-type urbanization and industrialization have continuously developed, and its coordination and coupled development with regional resource environmental bearing capacity should be explored from an innovative perspective. Industrial economy and resource environment are two subsystems of the entire socioeconomic system. These subsystems interact, cooperate, collaborate, and form a virtuous development cycle, which is a strong driving force for the sustainable and healthy development of the regional economy. Therefore, the spatial quantitative evaluation of coupling strength and mutual promotion between industrialization and resource environmental bearing capacity based on panel data is of great significance to facilitate industrialization and promote the sustainable and healthy development of regional economy objectively, scientifically, and rationally.

Scholars have conducted numerous studies regarding the coordination between industrialization and resource environmental bearing capacity. However, some challenges have been encountered in selecting the appropriate coordination degree models for measuring coordination relationship. The accurate evaluation, measurement, and clustering of the coordinated coupling relationship between industrialization and resource environmental bearing capacity in China are urgent problems (Wang et al. 2015). To this end, the present study first evaluated the two subsystems of industrial economy and resource environment comprehensively. Second, the coordinated coupling relationship was analysed according to the comprehensive evaluation index, which is expected to measure the coordinated relationship accurately and comprehensively and provide a reference for evaluating the dissimilarities among different regions in China.

STATE OF THE ART

At present, researchers have conducted numerous studies on the relationship of industrialization and resource environmental bearing capacity. The study on the bearing capacity of individual resources has achieved abundant results. For example, Joardar et al. studied the bearing capacity of urban water resources from the perspective of water supply and integrated it into urban development planning, which was not coupled with economic development (Joardar et al. 1998). Rijsberman et al. also used bearing capacity as a standard for measuring the security of water resources in urban water resource evaluation and management system; however, they did not evaluate the whole resource environment system comprehensively (Rijsberman et al. 2000). Varis et al. focused on the development and utilization of water resources and analysed the pressures on water resource system caused by rapid industrialization, growth of food demand, and deterioration of ecological environment in the Yangtze River region in China. Moreover, the status of the socioeconomic development of the Yangtze River Basin was compared with its water environment bearing capacity according to the economic development process in different regions. Unfortunately, the coordination degree was not analysed (Varis et al. 2001). Scholars have investigated the relationship between economic development and geographical environment. For example, Selden et al. analysed the empirical data and proposed the "inverted U-shaped" curve relationship between economic development and environmental quality, that is, the environmental Kuznets curve. However, they did not perform the cluster analysis combined with the sample area (Selden et al. 1994). Hildebrand investigated the contradictions and conflicts between economic development and resource environment in coastal regions and analysed the vulnerability of the coastal zone and the impact of human activities based on the idea of man–earth relationship (Hildebrand 1992). Moreover, special attention was paid on the influence of the sustainable development of the coastal zone caused by global changes and their corresponding countermeasures. However, the coordination degree was not modelled or verified. The study of the quantitative relationship between industrial economy and resource environment mainly focused on the construction of indicator systems and model calculation. For example, Ayres et al. and Tapio investigated the decoupling relationship between economic development and resource consumption (Ayres et al. 2003). Both factors analysed the time series data and selected the sample area; however, they did not evaluate spatial heterogeneity (Tapio 2005). Dietz et al. and Bartelmus et al. used the System of Integrated Environmental and Economic Accounting (SEEA) to estimate resource consumption, environmental pollution, sustainable development capabilities, and currency (Dietz et al. 2007). They all used the idea of comprehensive evaluation; however, the coordinated development of the two systems of economy and environment was not analysed thoroughly (Bartelmus et al. 2007).

Qualitative study of the threat of industrialization to resource environment has achieved abundant results in China. However, few studies reported on the coordinated development of industrialization and resource environmental bearing capacity. Liao proposed the measures for industrial development in Dehong Autonomous Prefecture under the constraints of resource environment but failed to compare with other regions (Liao 2014). Guo et al. discussed the production efficiency of industrial land under environmental constraints considering the unexpected output of 33 typical cities in China; however, this study did not draw a cluster evaluation of development models in different regions (Guo et al. 2014). Zhu et al. analysed the main reasons and key issues that might cause current resource environment overload through industrialization and urbanization development and proposed to position economic and social development based on resource environment. However, their study lacked the support of quantitative data (Zhu et al. 2015). Liao et al. reviewed the importance, evaluation indicators, and standard of the four types of resource bearing capacity (e.g., land resources, water resources, energy resources, and biological resources) and two types of environmental bearing capacity (e.g., air environment and water environmental bearing capacity) that are closely related to regional sustainable development (Liao et al. 2016). Similarly, the indicator system and evaluation standard were not tested

empirically in combination with the sample area data. Some Chinese scholars have explored the coupled development of industry, resources, and environment, but most of them used micro regions as samples. For example, Wang et al. studied and evaluated the coupled development of industry, resources, and environment of Dongping City from the perspective of ecological civilization, which was somewhat one-sided (Wang et al. 2015). Zhen constructed a regression equation and a responsiveness model based on a comprehensive measurement of the industrialization process and ecological environmental quality of Inner Mongolia Zhen. In addition, they conducted a timing analysis of the influence and response characteristics of ecological environment in the industrialization process of Inner Mongolia from 1990 to 2010; however, spatial difference characteristics were neglected (Zhen 2015).

Many qualitative results about the coordinated development of regional and industrial economy and resource environment have been obtained based on the aforementioned study results. The quantitative results are mainly based on the study of micro regions; meanwhile, few results were reported about the comparison of the coordination between resource bearing capacity and industrial development in different regions. Particularly, the analysis and comparison of the spatial heterogeneity of the interactive development of regional industrialization and resource environmental bearing capacity in different regions are still blank. The present study first constructed a comprehensive evaluation index system of regional resource environmental bearing capacity to analyse and evaluate the change characteristics of the spatial heterogeneity of the coordination between industrialization and resource environment in different regions in China. Second, principal component analysis was conducted to evaluate resource environmental bearing capacity comprehensively based on Chinese interprovincial panel data in 2018. Third, the comprehensive scores of resource environmental bearing capacity and industrialization development were used to calculate the regional coordination score based on the coordination degree model. Fourth, the comprehensive evaluation matrix of the three-level cluster was constructed, and the three-level cluster analysis of the sample area was conducted according to the comprehensive evaluation and the regional economic growth rate. Finally, the empirical suggestions for rational and orderly development of industrialization, regional economy, and resource environment were proposed according to the analysis results.

The remainder of this study is organized as follows. Section 3 proposes a coordination model by constructing a comprehensive evaluation index system of resource environmental bearing capacity. Section 4 calculates the resource environmental bearing capacity index of different regions in China and uses the coordination model to analyse the spatial differentiation characteristics of coupled development of resource environmental bearing capacity and industrialization. Finally, Section 5 summarizes the study and draws the conclusions.

METHODOLOGY

Comprehensive Evaluation Indicator System of Resource Environmental Bearing Capacity

Resourced environment is a dynamic ecosystem, and the indicator system for the comprehensive evaluation of the bearing capacity can be classified based on the theoretical composition of the resource environment. Meanwhile, this system also considers the role and evolution that resulted from socioeconomic interaction. "Pressure–State–Response (PSR)" is an evaluation model commonly used in the discipline of environmental quality assessment to achieve sustainable and healthy development between ecosystems and socioeconomics. In this study, the evaluation index system first divides the resource environmental bearing capacity according to the three aspects of pressure, state, and response, and then reflects the resource environment as the support of water, land, and environment for population and economy at each level. The comprehensive evaluation index system for resource environmental bearing capacity is shown in Table 1. The proposed index system is composed of relative and absolute indicators. The original values of the indicators include the performance values in 2018. The data were collected from the official website of the National Bureau of Statistics. The indicators were calculated on the basis of the absolute indicators in combination with the characteristics and representative meaning.

Coordination Model

Industrial economy and resource environmental bearing capacity are two subsystems in the socioeconomic system. The evaluation score of industrialization development speed is measured using the growth rate of the industrial added value in 2018 relative to that in 2017. The resource environmental bearing capacity is a complex system with multivariate measures. Moreover, this system is evaluated comprehensively using the principal component analysis method for the public factor extraction of the multi-index evaluation system, and the public factor score is calculated by SPSS software based on the sample data. The weighted comprehensive model is used to calculate the comprehensive evaluation scores of each sample area. Finally, the spatial differences and comparison

Table 1: Comprehensive evaluation index system of resource environmental bearing capacity.

Category	Dimension	Evaluation index	Index calculation	Unit	Correlation
Pressure	Economy	GDP per capita		yuan	+
	Population	Population density		Ten thousand people/ha	-
Status	Land resource	Grain yield per unit area		Kg/ha	+
	Water resource	Water resources per capita		M³/person	+
		Water consumption per capita	Total water consumption/ population	M³/person	-
		Urban water penetration rate		%	-
		Water consumption per 10,000 yuan of industrial output value	Industrial water consumption/industrial added value	T/10,000 yuan	-
	Environment	Wastewater discharge per 10,000 yuan of industrial output value	Wastewater discharge/ industrial added value	T/10,000 yuan	-
		COD emissions per 10,000 yuan GDP	COD emissions/GDP	T/10,000 yuan	-
		Sulfur dioxide emissions per 10,000 yuan GDP	Sulfur dioxide emissions/ GDP	T/10,000 yuan	-
		Nitrogen oxide emissions per 10,000 yuan GDP	Nitrogen oxide emissions/ GDP	T/10,000 yuan	-
		Soot emissions per 10,000 yuan GDP	Soot emissions/GDP	T/10,000 yuan	-
Response	Water resource	Daily sewage treatment capacity		10,000 cubic meters	+
		Cumulative people benefited from rural water improvement		person	+
		Effective irrigation area		Ha	+
	Land resource	Soil erosion control area		Ha	+
		Arable land per capita		Ha/person	+
		Investment in fixed assets per unit area		10,000 yuan/ha	+
	Environment	Daily harmless garbage disposal capacity		10,000 tons	+
		Harmless treatment rate of domestic garbage		%	+
		Completed investment in industrial pollution control		10,000 yuan	+
		Completed investment in ecological construction and protection		10,000 yuan	+

of resource environmental bearing capacity can be realized based on the evaluation scores.

After obtaining comprehensive measurement values for industrialization and resource environmental bearing capacity, the coordination degree is evaluated and calculated using the following model:

$$D_{R_i I_j} = \frac{R_i + I_j}{\sqrt{R_i^2 + I_j^2}},$$

where R_i and I_j represent the comprehensive evaluation indexes of the resource environmental bearing capacity and

Table 2: Meaning of coordination degree between industrialization and resource environmental bearing capacity in different regions.

I_j \ R_i	$R_i \geq 0$	$R_i < 0$
$I_j \geq 0$	$D_{RiIj} \geq 0$, highly coordinated, and both have high development levels	$D_{RiIj} \geq 0$, slight imbalance, and the former has lower development level $D_{RiIj} < 0$, severe imbalance, and the former has lower development level
$I_j < 0$	$D_{RiIj} \geq 0$, the overall coordination is good, and the former has higher development level $D_{RiIj} < 0$, basically coordinated, and the former has higher development level	$D_{RiIj} < 0$, highly uncoordinated, and both have low development levels

industrialization development, respectively; and D_{RiIj} is the coordination degree. According to the research achievements of scholars before (Wang et al. 2016), D_{RiIj} is positively related to the coordination degree between the two systems, and the value range is [–1.414, 1.414]. The relationship between the symbols of the calculation results and the two system indexes and their definitions are listed in Table 2:

Comprehensive Evaluation Matrix

Regional economy, as a dynamic economic subsystem, is not solely determined by industrial development after evaluating the coordination between the industrialization and the resource environmental bearing capacity of the 31 provinces in China. Meanwhile, to combine time and space measures effectively, regional differences are combined with dynamic measures to display the spatial and temporal differentiation characteristics of regions from multiple perspectives intuitively.

This study combines regional resource, environment bearing capacity, and regional economic development speed in constructing a comprehensive evaluation matrix for a systematic and reasonable clustering.

Regional economic development speed can be reflected by dynamic measurement indicators. For example, the growth rate of the regional GDP in 2018 relative to that in 2017. The comprehensive evaluation matrix of resource carrying capacity is listed in Table 3. The evaluation scores of the resource environmental bearing capacity of all regions and the growth rate of regional GDP in 2018 relative to that in 2017 are considered the dividing criteria. Accordingly, the resource environmental bearing capacity and the regional economic growth rate are divided into three evaluation levels. Through pairwise combination of levels, the 31 regions can be divided into 9 categories (Table 3).

RESULT ANALYSIS AND DISCUSSION

Comparative Analysis of The Coordination Degree Between Industrialization and Resource Environmental Bearing Capacity of 31 Provinces, Municipalities and Autonomous Regions in China

The evaluation results of the coordination degree between industrialization and resource environmental bearing capacity in different regions of China in 2018 were calculated according to the comprehensive evaluation index matrix of resource environmental bearing capacity and the coordination model (Table 4 and Fig. 1). The coordination scores show that Zhejiang has obvious advantages and ranks first, followed by

Table 3: Evaluation matrix on resource environmental bearing capacity.

Resource environmental bearing capacity \ Growth rate of regional economy	1st–10th	11th–20th	21st–31st
1st–10th	Strong resource bearing capacity-fast economic growth	Strong resource bearing capacity-general economic growth	Strong resource bearing capacity-poor economic growth
11th–20th	General resource bearing capacity-fast economic growth	General resource bearing capacity-general economic growth	General resource bearing capacity-poor economic growth
21st–31st	Weak resource bearing capacity-fast economic growth	Weak resource bearing capacity-general economic growth	Weak resource bearing capacity-poor economic growth

Henan, Guangdong, Jiangsu, Shandong, and Ningxia ranking second to sixth, respectively. These regions have coordination scores greater than 1 and belong to highly coordinated regions. Inner Mongolia, Xinjiang, Anhui, Hebei, Shanghai, and Heilongjiang ranked 7th to 12th, respectively, and their coordination scores are greater than 0, all of which belong to moderately coordinated regions. From Liaoning at the 13th place and Shanxi at the 14th place, the coordination scores begin to decline sharply and become negative; however, the industrialization and resource environmental bearing capacity are still coordinated. Jilin Province, which also belongs to the basically coordinated area, ranked 17th. Guangxi, Hubei, Hunan, Fujian, Chongqing, Guizhou, Jiangxi, and Tibet belong to severely uncoordinated regions, which rank from 15 to 23 (except 17), and the eight remaining regions belong to highly uncoordinated regions. Combined with the geographical distribution of regions with different coordination types in Fig. 1, the highly and moderately coordinated regions are mainly distributed in East China and North China. Some regions, such as Zhejiang, Guangdong, and Jiangsu, have relative advantages in resource environment and industrial development and have high coordination scores. In the later period, they can maintain such a development momentum and continue to achieve the coordinated development of resource environment and industrial economy; some regions have moderate industrial development that matches with their source environment bearing capacity, and the coordination scores are also high. These regions can accelerate the development of industrial economy moderately on the premise of ensuring a good resource environmental bearing capacity. The majority of the basically coordinated regions is distributed in Northeast China and has general resource environmental bearing capacity and industrial economic development level. However, the coordination and matching advantages are not evident. In the later period, the development pace of industrialization can be adjusted appropriately to achieve the optimal matching with the resource environmental bearing capacity. Severely coordinated regions are mainly in Central China, South China, and Southwest China. Some of these provinces and cities (regions) have rapid industrial development but general or weak source environment bearing capacity and poor coordination degree. Therefore, these regions should slow the pace of industrialization moderately and enhance the self-repair flexibility of resource environment to achieve coupled and coordinated development. The highly uncoordinated regions are mainly in Southwest and Northwest China, and they have weak resource environmental bearing capacity. However, the development of the industrial economy is extremely fast or does not match the local resource bearing

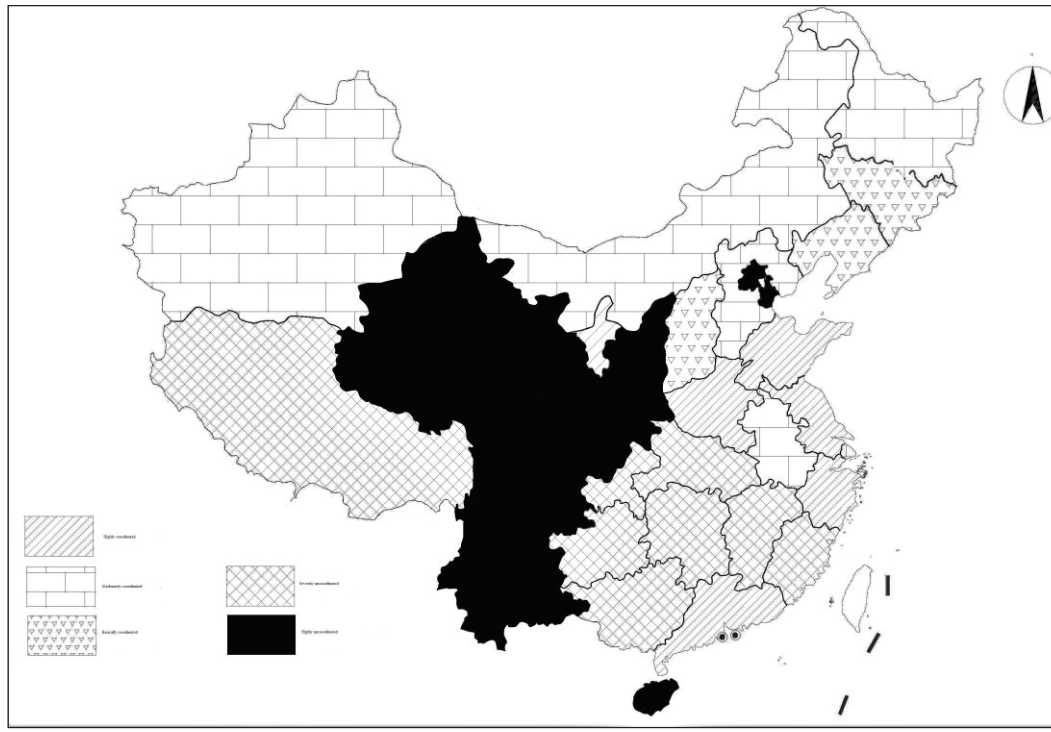

Fig. 1: Classification results based on the comprehensive evaluation matrix on coordination degree.

Table 4: Evaluation on coordination degree between industrialization and resource environmental bearing capacity in different regions in 2018.

Regions	Coordination degree	Rank	Type of coordination degree	Rank of resource and environmental bearing capacity	Rank of regional economic changes	Type of comprehensive evaluation
Zhejiang	1.413	1	Highly coordinated	14	11	General resource environmental bearing capacity-general economic growth
Henan	1.349	2	Highly coordinated	15	16	General resource environmental bearing capacity-general economic growth
Guangdong	1.326	3	Highly coordinated	8	8	Strong resource environmental bearing capacity-fast economic growth
Jiangsu	1.291	4	Highly coordinated	3	7	Strong resource environmental bearing capacity-fast economic growth
Shandong	1.189	5	Highly coordinated	5	15	Strong resource environmental bearing capacity-general economic growth
Ningxia	0.957	6	Highly coordinated	6	17	Strong resource environmental bearing capacity-general economic growth
Inner Mongolia	0.786	7	Moderately coordinated	4	27	Strong resource environmental bearing capacity-slow economic growth
Xinjiang	0.771	8	Moderately coordinated	1	26	Strong resource environmental bearing capacity-slow economic growth
Anhui	0.718	9	Moderately coordinated	11	19	General resource environmental bearing capacity-general economic growth
Hebei	0.595	10	Moderately coordinated	7	25	Strong resource environmental bearing capacity-slow economic growth
Shanghai	0.453	11	Moderately coordinated	9	12	Strong resource environmental bearing capacity-general economic growth
Heilongjiang	0.378	12	Moderately coordinated	2	28	Strong resource environmental bearing capacity-slow economic growth
Liaoning	0.172	13	Basically coordinated	12	29	General resource environmental bearing capacity-slow economic growth
Shanxi	0.149	14	Basically coordinated	10	30	Strong resource environmental bearing capacity-slow economic growth
Guangxi	–0.208	15	Severely uncoordinated	19	9	General resource environmental bearing capacity-fast economic growth
Hubei	–0.414	16	Severely uncoordinated	20	5	General resource environmental bearing capacity-fast economic growth
Jilin	–0.832	17	Basically coordinated	13	23	General resource environmental bearing capacity-slow economic growth
Hunan	–0.947	18	Severely uncoordinated	18	10	General resource environmental bearing capacity-fast economic growth
Fujian	–1.039	19	Severely uncoordinated	23	4	Weak resource environmental bearing capacity-fast economic growth
Chongqing	–1.260	20	Severely uncoordinated	29	3	Weak resource environmental bearing capacity-fast economic growth
Guizhou	–1.307	21	Severely uncoordinated	30	1	Weak resource environmental bearing capacity-fast economic growth
Jiangxi	–1.348	22	Severely uncoordinated	24	13	Weak resource environmental bearing capacity-general economic growth
Tibet	–1.358	23	Severely uncoordinated	31	2	Weak resource environmental bearing capacity-fast economic growth
Beijing	–1.390	24	Highly uncoordinated	27	6	Weak resource environmental bearing capacity-fast economic growth
Yunnan	–1.391	25	Highly uncoordinated	25	14	Weak resource environmental bearing capacity-general economic growth
Hainan	–1.395	26	Highly uncoordinated	28	18	Weak resource environmental bearing capacity-general economic growth
Gansu	–1.398	27	Highly uncoordinated	16	31	General resource environmental bearing capacity-slow economic growth
Tianjin	–1.403	28	Highly uncoordinated	17	21	General resource environmental bearing capacity-slow economic growth
Sichuan	–1.410	29	Highly uncoordinated	26	20	Weak resource environmental bearing capacity-general economic growth
Shaanxi	–1.410	30	Highly uncoordinated	22	24	Weak resource environmental bearing capacity-slow economic growth
Qinghai	–1.414	31	Highly uncoordinated	21	22	Weak resource environmental bearing capacity-slow economic growth

capacity. In the later stage, the investment in improving resource environment should be enhanced while formulating relevant policies.

Clustering Results and Cause Analysis of Spatial Heterogeneity of Coordination between Industrialization and Resource Environmental Bearing Capacity

The regional difference in the coordination between industrialization and resource environmental bearing capacity based on the coordination degree alone is not particularly significant. Therefore, the last column in Table 4 lists the comprehensive clustering results of 31 provinces (cities, districts) in China according to the comprehensive evaluation matrix in Section 2.3. Meanwhile, future improvement direction can be determined accurately by combining coordination and comprehensive evaluation types. Combined with the evaluation level of resource environmental bearing capacity in Table 4, first, the regions with high coordination degree have moderate and good resource environmental bearing capacity, which indicates the importance of resource environmental bearing capacity in coupled development. Guangdong and Jiangsu have perfectly realized the high coordination between resource environmental bearing capacity and regional economic development. As highly coordinated regions, both of regions have advantages in environment pollution control and other indicators and belong to the type of "strong resource environmental bearing capacity-fast economic growth." Other highly coordinated regions, such as Zhejiang and Henan, have general resource environmental bearing capacity, which is benefited from the balanced indicators. However, their advantages in water and land resources and environmental governance are not evident. Therefore, the resource bearing capacity has not exhibited the best performance, but it is relatively matched with the local regional economic development. The GDP growth of Shandong and Ningxia have been slowed down relatively but still matches the resource environmental bearing capacity. Second, many moderately coordinated regions, such as Inner Mongolia, Heilongjiang, and Xinjiang, have strong resource environmental bearing capacity. However, these regions fail to realize the coordinated development of resource environment and regional economy. Third, uncoordinated and even severely uncoordinated regions have weak resource environmental bearing capacity, but most regions still have rapid regional economic growth, which indicates that the regional economic development based on resource consumption and environment pollution is common.

Table 5: Factor loading of indexes regarding resource environmental bearing capacity.

Extraction dimensions	Index	Factor loading	eigenvalues	proportion
Water use	Water resources per capita	0.875	4.196	18.243
	Water consumption per 10,000 yuan of industrial output value	–0.851		
	Daily sewage treatment capacity	0.814		
	Wastewater discharge per 10,000 yuan of industrial output value	–0.753		
	Urban water penetration rate	–0.724		
	Water consumption per capita	–0.781		
Industrial pollutant emissions	nitrogen oxide emissions per 10,000 yuan GDP	–0.761		
	Sulphur dioxide emissions per 10,000 yuan GDP	–0.732		
	Soot emission per 10,000 yuan GDP	–0.661		
Pollution control and improvement of resource environment	Cumulative people benefited from rural water improvement	0.822	3.763	16.360
	Harmless treatment rate of domestic garbage	0.817		
	Harmless daily garbage disposal capacity	0.774		
	Effective irrigation area	0.726		
	Completed investment in industrial pollution control	0.680		
Land bearing	Grain production per unit area	0.927	3.434	14.930
	Arable land per capita	0.848		
	GDP per capita	–0.628		
	Investment in fixed assets per unit area	0.798	2.516	10.937
	Population density	0.784		

These regions should vigorously use green development measures to improve the current state effectively and slow down the economic growth as necessary. Meanwhile, some uncoordinated regions have no resource advantage and slow economic growth. Therefore, they should accelerate the speed of economic development while improving the resource environment in the future.

CONCLUSION

To obtain the current spatial differentiation characteristics of the resource environmental bearing capacity of 31 provinces (municipalities and autonomous regions) in China, this study established a comprehensive evaluation index system for resource bearing capacity from the three levels of PSR of resource environment theoretical system and its population and socioeconomic support and guarantee. A comprehensive evaluation matrix was constructed on the basis of the dynamic evaluation indexes of regional economic development changes, and the 31 provinces in China were divided into 9 categories according to the coordination degree clustering. Finally, the following conclusions were drawn:

1. The evaluation results of the coordination degree between industrialization and resource environmental bearing capacity in the 31 sample regions in 2018 from high to low is ranked as follows: Zhejiang, Henan, Guangdong, Jiangsu, Shandong, Ningxia, Inner Mongolia, Xinjiang, Anhui, Hebei, Shanghai, Heilongjiang, Liaoning, Shanxi, Guangxi, Hubei, Jilin, Hunan, Fujian, Chongqing, Guizhou, Jiangxi, Tibet, Beijing, Yunnan, Hainan, Gansu, Tianjin, Sichuan, Shaanxi, and Qinghai. The majority of the provinces with good coordination between industrialization and resource environmental bearing capacity are in East and North China. Meanwhile, the provinces with poor coordination are mostly in Southwest and Northwest China. Resources and environment are still the main factors that restrict coordination.
2. According to the classification results based on the three-level clustering comprehensive evaluation matrix: Guangdong and Jiangsu belong to the regions with "strong resource environmental bearing capacity-fast economic growth;" Zhejiang, Henan, and Anhui have "general resource environmental bearing capacity-general economic growth;" Shaanxi and Qinghai belong to the regions with "weak resource environmental bearing capacity-slow economic growth."
3. According to the panel data analysis of 31 provinces and autonomous regions in 2018, the main factors that influence the resource environmental bearing capacity include per capita water resources, water consumption per 10,000 Yuan of industrial output value, daily treatment capacity of urban sewage, wastewater discharge per 10,000 yuan of industrial output value, urban water penetration rate, per capita water consumption, nitrogen oxide emissions per 10,000 Yuan GDP, sulphur dioxide emissions per 10,000 Yuan GDP, soot emissions per 10,000 yuan GDP, cumulative beneficiaries of rural water conversion, harmless treatment rate of domestic waste, average daily harmless garbage disposal capacity, effective irrigated area, completed investment in industrial pollution control, grain yield per unit area, cultivated land per capita, GDP per capita, fixed asset investment per unit area, and population density.

A three-level clustering comprehensive evaluation matrix was established by combining the indicator system construction and model measurement. The evaluation matrix cannot only refine the internal differences in the types of coordination evaluation but also thoroughly present the improvement direction of resource bearing capacity, industrial development, and even regional economic growth combined with the main factor load. In addition, effective empirical suggestions are made to alleviate the contradiction between resource bearing capacity and regional economic development in China, and effective reference in policy formulation is provided to the Chinese government. However, the comprehensive evaluation index system of resource environmental bearing capacity should be continuously updated according to the development trend of resources and environment to measure the coupling relationship accurately and thoroughly because of the limited availability of the latest environmental indicator data.

ACKNOWLEDGEMENT

This study was supported by the Hubei Province Teaching and Research Projects of Colleges and Universities in 2017 (Grant No. 2017495), the Hubei Education Department Scientific Research Projects in 2018(Grant No. B2018347), and the Hebei Province Social Science Foundation in 2018 (Grant No. HB18GL053).

REFERENCES

Ayres, R.U., Ayres, L.W. and Warr, B. 2003. Energy, power and work in the US economy, 1900-1998. Energy, 28(3): 219-273.

Bartelmus, P. 2007. SEEA-2003: Accounting for sustainable development? Ecological Economics, 61(4): 613-616.

Dietz, S. and Neumayer, E. 2007. Weak and strong sustainability in the SEEA: Concepts and measurement. Ecological Economics, 61(4): 617-626.

Guo, G.C. and Wen, Q.Y. 2014. Industrial land productivity research under the environmental restriction based on unexpected outputs of 33 typical cities in China. China Population Resources and Environment, 24(6): 121-127.

Hildebrand, L.P. and Norrena, E.J. 1992. Approaches and progress toward effective integrated coastal zone management. Marine Pollution Bulletin, 25(1-4): 94-97.

Joardar, S.D. 1998. Carrying capacities and standards as bases towards urban infrastructure planning in India: A case of urban water supply and sanitation. Habitat International, 22(3): 327-337.

Liao, H.X., Ji, Y.L. and Peng, S.L. 2016. Resource and environmental carrying capacity and sustainable development. Ecology and Environmental Science, 25(7): 1253-1258.

Liao, Y.C. 2014. The Dilemma of industry in Dehongzhou under the restriction of resources and environment. Journal of the Party School of CPC Yunnan Provincial Committee, 15(2): 105-107.

Rijsberman, M.A., Van de Ven, F.H.M. 2000. Different approaches to assessment of design and management of sustainable urban water systems. Environmental Impact Assessment Review, 20(3): 333-345.

Selden, T.M. and Song, D. 1994. Environmental quality and development: Is there a Kuznets Curve for air pollution emissions? Journal of Environmental Economics and Management, 27(2): 147-162.

Tapio, P. 2005. Towards a theory of decoupling: Degrees of decoupling in the EU and the ease of road traffic in Finland between 1970 and 2001. Transport Policy, 12(2): 137-151.

Varis, O. and Vakkilainen, P. 2001. China's 8 challenges to water resources management in the first quarter of the 21st Century. Geomorphology, 41(2-3): 93-104.

Wang, R. and Yuan, Y.R. 2016. Research on the coordinated evolution law of industrialization and resource environment in China's mining economic zone. Ecological Economy, 302(2): 69-73.

Wang, X.Y., Wang, C.X. and Zhao, M.H. 2015. Research on the coupling development of regional industry, resources and environment from the perspective of ecological civilization-taking Dongying city as an example. Coal Economic Research, 35(4): 60-63.

Wang, Z. and Su, X. 2015. Dynamically hierarchical resource-allocation algorithm in cloud computing environment. The Journal of Supercomputing, 71(7): 2748-2766.

Zhen, J., Li, L., He, S. and Luo, S. 2015. Ecological environment impact and its response to the process of industrialization in Inner Mongolia. Journal of Arid Land Resources and Environment, 29(11): 86-92.

Zhu, T., Wang, T.T. and Gao, S. 2015. Orientate the development of economic society based on the environmental carrying capacity by following ecological civilization concept. environmental protection, 43(16): 12-14.

Nature Environment and Pollution Technology
An International Quarterly Scientific Journal

p-ISSN: 0972-6268
e-ISSN: 2395-3454

Vol. 19 | No. 1 | pp. 93-101 | 2020

Original Research Paper | Open Access

Real World Driving Dynamics Characterization and Identification of Emission Rate Magnifying Factors for Auto-rickshaw

Arti Choudhary*†, Pradeep Kumar, Manisha Gaur*, Vignesh Prabhu***, Anuradha Shukla* and Sharad Gokhale******

*Transport Planning and Environment Division, Central Road Research Institute, New Delhi, India
**Department of Physics, Institute of Science, Banaras Hindu University, Varanasi, India
***Centre for Study of Science, Technology & Policy, Bengaluru, India
****Department of Civil Engineering, Indian Institute of Technology, Guwahati, India
†Corresponding author: Arti Choudhary

Nat. Env. & Poll. Tech.
Website: www.neptjournal.com

Received: 07-05-2019
Accepted: 21-06-2019

Key Words:
Urban traffic flow
Traffic congestion
Vehicular emission
Speed-time factor

ABSTRACT

Most urgent transport related problems in India are traffic congestion and concomitant air pollutant emissions. During traffic flow, the common causes of congestion in urban centres are pedestrian interruption, unregulated traffic signals, unregulated bus stoppages and unauthorized roadside parking, which together, particularly during peak hours, create erratic traffic pattern causing higher emissions. In this study, we characterized auto-rickshaw driving dynamics by instantaneous measurements of speed and emission at different times of the day. Traffic speed is an important factor that is perceived by commuters. The speed variables and traffic volume are used as a base variable to examine the traffic flow patterns. The speed variables such as average speed (AS), velocity noise (VN, standard deviation of speed), and the coefficient of variation of speed (CV, the ratio of VN and AS) were examined with respect to traffic volume. The polynomial fit of CV shows three distinct zones of variations with increasing traffic volume, explaining the dynamics of traffic flow. Further, time, speed and mileage variable were investigated for the emission rate analysis in different traffic flow pattern. The analysis depicted that the combined factor of lower speed (speed ≤12 km/h) and higher time of travel in correspondence cause higher emission rate. Similarly, vehicle mileage of ≥52,000 km has significant impact on emission for pollutants CO, HC and NOx. The results provide real-time information on traffic flow characteristics and impacts of dynamic and age variables on emission rate in on-road driving condition, which may be useful for the public and transport related agencies.

INTRODUCTION

Road traffic is one of the primary sources of air quality deterioration (Gulia et al. 2015). Due to increasing urbanization and economic development, number of trips per day are increasing (Guttikunda & Mohan 2014). Urban streets are characterized as intense roadside development and intense traffic density at access point of signalized intersection, no lane discipline that cause frequent interruption and congestion (Asaithambi et al. 2016, Choudhary & Gokhale 2019a). These conditions result in higher traffic conflicts. The speed of vehicles on urban streets is influenced by three main factors, street environment, interaction a.m. Ong vehicles, and traffic control (Mohapatra 2012). As a result, these factors affect quality of service (Grote et al. 2016). Traffic flow can be interrupted due to various conditions such as road work, peak hour traffic, accidents, and weather conditions. The pedestrians also create conflicts and lane obstructions created due to stopping or standing taxis, buses, trucks and parking vehicles generates disturbance in traffic-flow. These complex characteristics of urban roadway aid to the development of congestion, like interruption of traffic flow, especially during peak hours it is very significant, causing significant rise of emission (Chen et al. 2007, Choudhary & Gokhale 2019b). Traffic interruption and congestion is a regular phenomenon on urban roads, and it becomes critical at traffic intersections and junctions. It increases commuting time, fuel consumption and cause higher pollutant emissions. Vehicular emissions depend on vehicle speed, vehicle-km, age of vehicle, and emission rate (Pandian et al. 2009). The quantity of major air pollutants, such as NO_x, HC, CO and CO_2 drastically increases with reduction in motor vehicle speeds. For example, at a speed of 75 km/h, emission of CO is 6.4 g/veh-km, which increases by five times to 33 g/veh-km at a speed of 10 km/h (Singh 2012). Problem is aggravated due to high average age and poor maintenance of vehicles.

Auto-rickshaws (the three-wheeler vehicle) are important in the Indian traffic as they are used as an intermediate public transport. They fill a vital niche in developing cities between private vehicles ownership and fixed-route and large-capacity public transit systems (i.e. bus and metro) (Reynold et al. 2009). Auto-rickshaws are the popular mode of private transportation because of the low initial and low running cost (Singh 2006, Reddy & Balachandra 2012, Iyer 2003). Because of its small size it negotiates the smaller streets and weaves through the mixed traffic (Iyer 2003). Different types of auto–rickshaws are found on Indian roads, but the auto–rickshaws of capacity less than 4 persons including the driver, occupy roads are more in number and also have the largest market share, close to 80% (Iyer et al. 2013). Considerable share of auto-rickshaws in Indian traffic fleet and lack of adherence to lane marking (no-lane discipline) are unique and important features. Auto-rickshaw generally undergoes large wear and tear of the engines due to overloading, idling, and operating at less than ideal conditions, and lack of timely engine maintenance (Reynold et al. 2011). In real-word, auto-rickshaws consume 15% more fuel and emit 49% more HC and 16% more $P.M._{2.5}$ (Grieshop et al. 2012). The present study will analyse the real-world driving dynamics of auto-rickshaw and impacts of dynamic variables on exhaust emission rate.

EXPERIMENTAL DESIGN

A highly trafficked stretch of an urban traffic corridor in Guwahati was selected for the study. This road segment represents typical urban traffic-flow with high traffic volume, mix vehicles, no-lane discipline, frequent interruption and congestion due to interaction with pedestrians and vehicles. The test-run was of 4 km long, double lane, of 16 m wide each. The road segment does not have traffic lights and both the lanes are heavily trafficked, particularly, during peak hours. Field work was carried out to collect traffic volume data, tail-pipe instantaneous emission data of the test vehicles (auto-rickshaws) along with the driving profile. The traffic volume count was done with a video camera recording. It was done for a full week, each day twelve hours from 7 a.m. to 7 p.m. The videotapes were analysed manually for a 100 m stretch on the road. Such method has also been followed by Robertson (1994). The traffic count data were analysed to determine traffic-flow patterns and traffic composition. The videotapes analysis revealed that traffic volume, commercial activity, and roadside parking on the both lanes were similar. The traffic composition was classified into four categories-two-wheelers (scooters, motorbikes and moped; 2W), three-wheelers (auto-rickshaws; 3W), four-wheelers (cars, jeeps and medium-utility vehicles; PC-MUV), and light-heavy commercial vehicles (bus, minibus and small trucks; LHCV). The speeds were estimated for each category vehicle for 5 min travel time.

The real-world measurements of instantaneous speed, acceleration, and deceleration and tail-pipe emissions of auto-rickshaws were measured with an auto-gas analyser and a V-Box. Different mileage test vehicles were selected, each test vehicle was run at three different times of the day to capture the real characteristics of the range of speed and acceleration, deceleration of urban traffic. During each time, test-run was repeated to produce at least two sets of data and each run lasting for 25 to 45 min depending upon the traffic on the road. Tests were carried out during 7:00-8:30 a.m., which is an off-peak time, during 10:30-11:30 a.m., which covers the morning peak time and 4:30-5:30 p.m., which covers the evening peak time. These time periods are described as off-peak hours (OPH), morning peak hours (MPH) and evening peak hours (EPH) respectively. Thus, collected data were analysed for the traffic composition, traffic flow pattern analysis, correlation of speed, time of travel and mileage with the emission. The detailed methodology of data analysis is described by Choudhary & Gokhale (2016).

RESULTS AND DISCUSSION

Traffic-Flow and Traffic Composition

The traffic-flow on working days exhibits a typical trend with two peaks, around noontime and in the evening. The lowest traffic was observed during 7-8 a.m. and higher traffic during 10 a.m.-12 noon and 4-7 p.m., however, the traffic composition changed every hour, especially the proportion of two-wheelers and three-wheelers. Fig. 1 shows the hourly variation of traffic-flow of different category vehicles on working days, averaged from Monday to Friday. Table 1 shows the descriptive statistics of hourly traffic volume and traffic speed for working days. The positive value of kurtosis coefficient of hourly traffic volume indicates that data distribution has heavier tails and a sharper peak than the normal distribution and the negative value of skewness of traffic volume suggest that distribution is toward left, whereas traffic speed data is slightly skewed toward right. It has been observed that about 87% of the total traffic was comprised of two and four-wheelers (2W+PC–MUV) followed by 9 to 10% of three-wheelers (3W) and mere 3 to 4% of buses (LHCV). During the OPH, PC-MUV and 2W shared 52% and 28%, respectively, while during the PH, it was observed to be 34%, and 53%, respectively (Figs. 2d, e, f).

Table 1: Descriptive statistics for hourly traffic composition and traffic fleet speed.

Descriptive Parameters	Working days	
	Hourly traffic volume (veh/h)	Hourly traffic speeds (km/h)
Mean	7676.0	33.5
Std. error	621.4	3.2
Median	8245.0	32.2
Std. deviation	2152.4	11.1
Sample variance	4632925.8	123.9
Kurtosis	2.4	0.4
Skewness	-1.8	0.9
Minimum	2591.0	19.7
Maximum	9368.0	57.5
Count	12	12

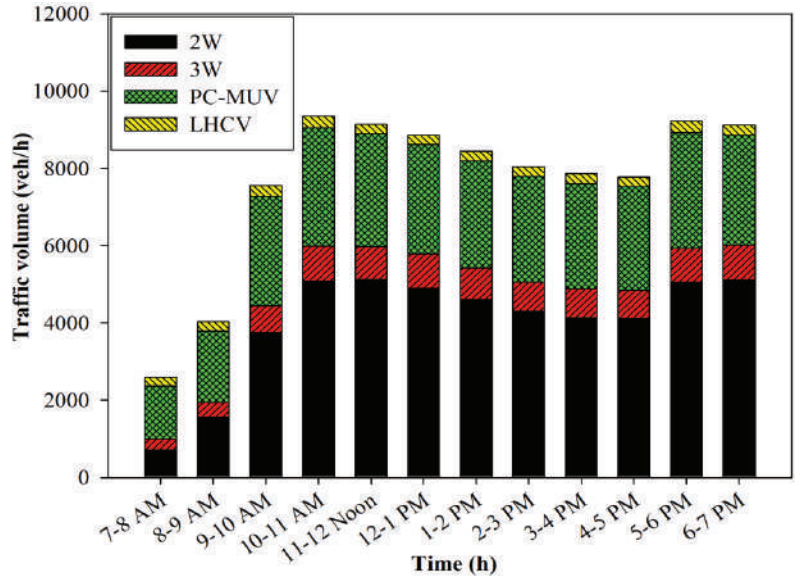

Fig. 1: The hourly variation of the proportion of traffic composition for working days (average of Monday to Friday).

Traffic-Flow vs Speed

Traffic speed and volume are two important characteristics, which directly affect the traffic-flow on roads (Anjaneyulu & Nagaraj 2009). Therefore, the time variation of speed due to traffic volume has been used to describe and define the traffic–flow patterns. The videotapes were analysed for traffic volume (veh/5 min) and traffic speed (km/h) analysis were done for defining the various traffic-flow patterns. Three descriptive statistics were used to represent the relationship, viz.-average speed (AS) in km/h; velocity noise (VN) a standard deviation of speed in km/h and the coefficient of variation of speed (CV), the ratio of VN and AS. Fig. 3-I (a, b, c) shows the relationships of-AS, VN and CV with traffic volume (veh/5 min) in which the minimum volume suggests the free-flow condition and higher volume suggests the density near roadway capacity. As the traffic volume increased, the AS decreased and VN and CV increased, which after reaching the volume of about 400, dropped continuously indicating the higher level of vehicle to vehicle interactions, which further increases.

As traffic volume increases, the interaction between the vehicles increases, i.e. the speed of a vehicle is affected by the vehicles plying together with it, which results in the increase of variation in the speed, as has been observed from the sharp rise in CV and VN. Further, increase in volume forces a vehicle to reduce its speed. In this condition, fluctuation

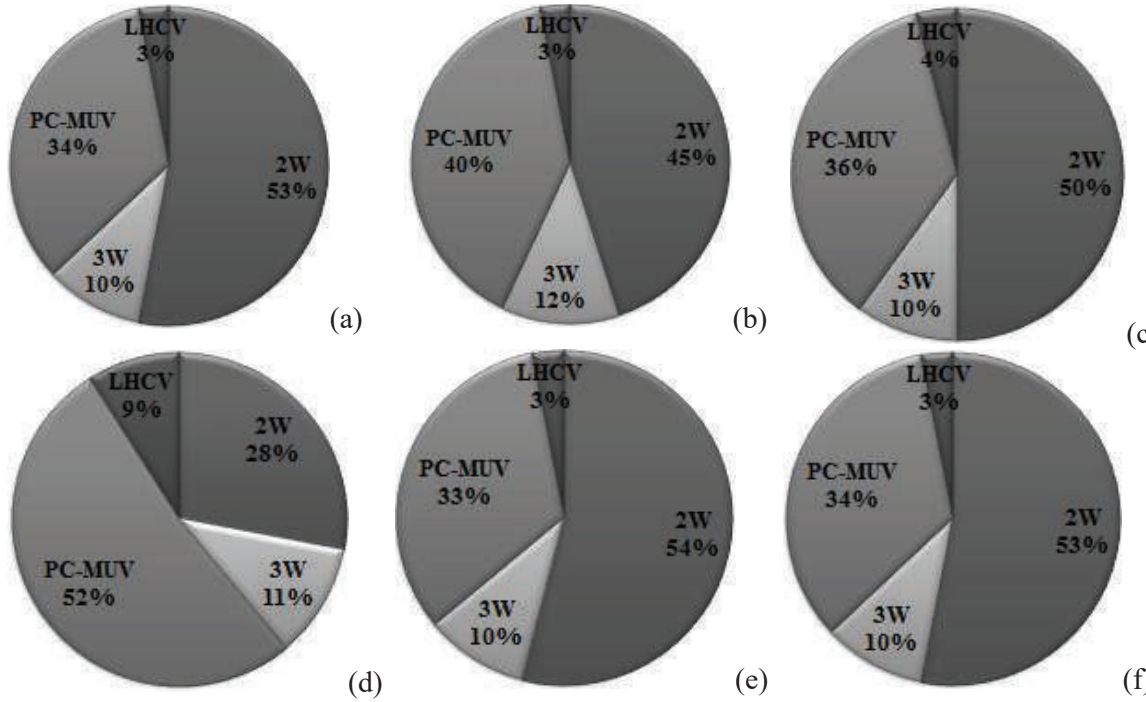

Fig. 2: The vehicle composition for (a) working days, (b) non-working days (c) a whole week, (d) morning off-peak 7-8 a.m., (e) morning peak, 10 a.m. to 12 noon, and (f) evening peak, 4-6 p.m.

in average speed is less, which decreases the standard deviation and decreases the ratio of VN/AS. Thus, these three characteristics (AS, VN and CV) together with traffic volume describe the three different traffic-flow conditions.

1. Traffic-flow condition 1: Shows slow increase in CV and VN at lower traffic volume and higher traffic speed.
2. Traffic-flow condition 2: Shows sharp increase in CV and VN with increasing traffic volume and decreasing traffic speed.
3. Traffic-flow condition 3: As traffic volume approaches to near roadway capacity CV and VN decrease sharply that forces vehicles to crawl.

The Fig. 3-II shows the best polynomial fits to the AS, VN and CV, which distinguish the traffic-flow patterns. The R^2 values were 0.95, 0.96, and 0.97 for AS vs traffic volume, AN vs traffic volume and CV vs traffic volume, respectively. The adjusted R^2 values were 0.94, 0.95 and 0.96 for AS vs traffic volume, AN vs traffic volume and CV vs traffic volume, respectively. The three distinct zones have been identified from the CV and traffic volume relationship by taking tangents at the points of inflection, which resulted into two break points classifying into three distinct levels of traffic-flow (Anjaneyulu & Nagaraj 2009). It has been observed that the speed characteristics show distinct zones with the increasing traffic volume. The best polynomial fits of AS, VN and CV with traffic volume show three distinct zones marked as Level 1, 2 and 3 based on speed gradient. The Level-1 represents the free-flow condition in which initially the traffic volume is less, the vehicular speed is more and the variation of speed (CV) is low indicating the least vehicle to vehicle interaction. As the traffic volume increases the CV sharply increases. This represents Level-2 in which a higher fluctuation in speed occurs due to phase transition from free-flow to random stop-and-go. The frequent stop-and-go causes higher deviation from mean speed and, therefore, a higher CV is observed. The Level-2 represents the interrupted traffic-flow condition. After this, vehicle to vehicle interaction increases and traffic volume approaches to roadway capacity, which forces the vehicles to crawl, leading to the decrease of CV. This represented the congested-flow condition, Level-3.

Travel Time and Speed vs Emission

The vehicular exhaust is influenced by many operating variables of which particularly important in urban driving are, speed, period and number of sharp acceleration and deceleration, number and time of the stop-and-go pattern (Faiz et al. 1996). The air to fuel ratio also changes with mode of operation, for example, whether it is cruising,

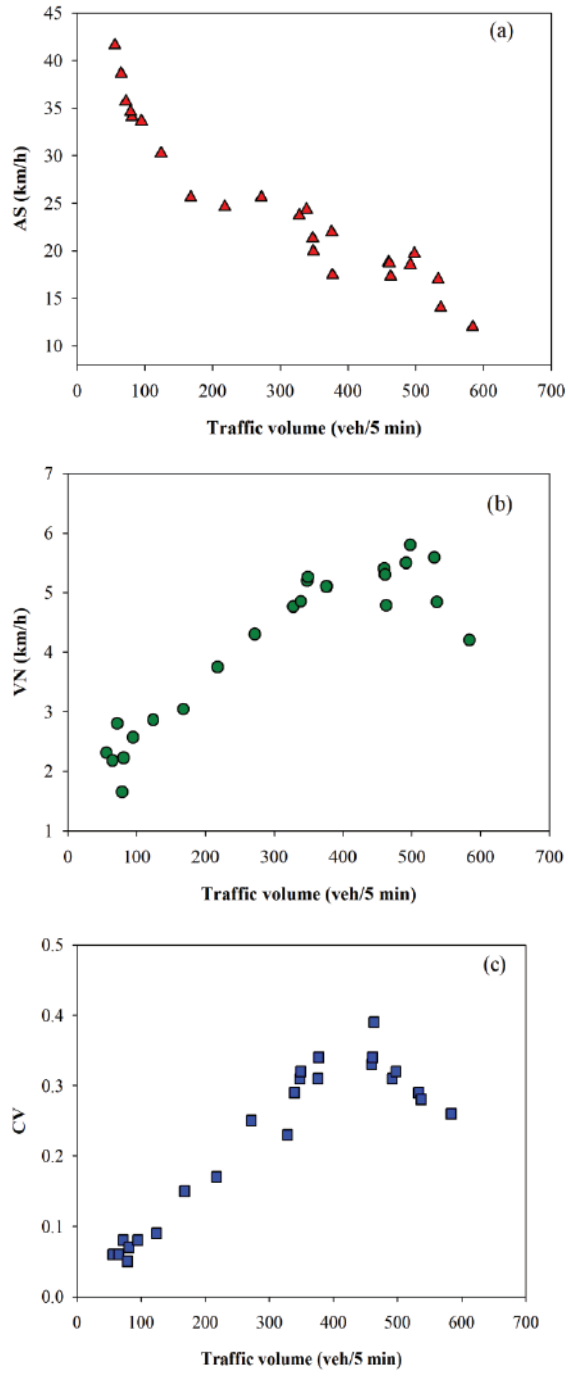

Fig. 3-I: Relationship of traffic volume and speed for the test runs.

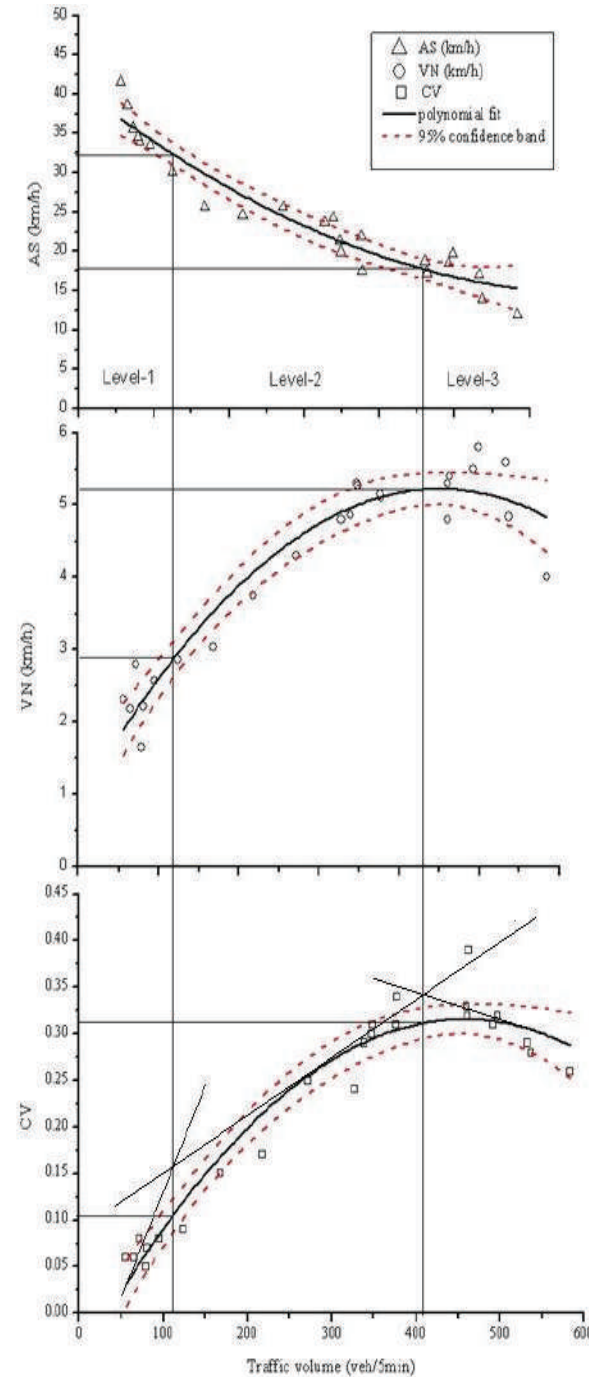

Fig. 3-II: Different levels of traffic-flow patterns observed in the test runs.

accelerating, decelerating or idling (Joumard 1999, Marsden 2001). In this study, travel time during PH was increased more than twice the travel time of OPH due to reduction in operating speed. The operating speed directly affects the vehicular exhaust emissions. Therefore, the relationship of exhaust emissions in different traffic-flow conditions corresponding to the travel time spent in those conditions for the span of 60s has been analysed for a period of 10 minutes of the test-runs. Fig. 4 shows the correlation of travel time and corresponding emission for 10 consecutive minutes of test-run for auto-rickshaw in different traffic-flow patterns respectively. The one stacked bar represents the span of 60s/

minute, so total 10 stacked bar, each representing one minute, were analysed (Fig. 4). The stacked bar colours indicating the different traffic flow patterns and the height of stacked bar depicting time spent in each traffic flow patterns. To study the correlation of operating speed and corresponding travel time, the vehicle speed categorized into 0 – 2 ± 2, 3 – 15 ± 3, 16 – 30 ± 3 and above 31 ± 3 km/h corresponding to idle–flow, congested flow (CF), interrupted flow (IF) and free-flow (FF), respectively. It was found that during the test-run auto-rickshaws travelled for over 80% of the time in the speed range 10-30 km/h.

Fig. 4 also depicting the emission rate of CO, HC, NO_x and CO_2 corresponding to different traffic-flow patterns and time spent in particular traffic-flow. It has been observed that the magnitude of emission rate in auto-rickshaw is higher due to longer time of travel and lower operating speed for the pollutants CO and HC. The emission rate of NO_x significantly increased for speed of > 30 km/h but did not show any effect for time of travel. The magnitude of CO_2 emission rate was found higher for IF condition as compared to the combination of higher travel time and lower speed.

Combined Effect of Speed-Time on Emission Rate

To determine the combined effect of travel time and associated speed on exhaust emission, a speed-time spent factor, which is a multiplication of average speed of particular speed interval and the time spent of that traffic flow, was used. Details of speed-time spent factor are tabulated in Table 2. The Fig. 5 shows the relationship of pollutants emission rate with the speed-time spent factor for auto-rickshaw. It was observed that CO, HC and CO_2 emission increase as the speed-time factor increases. It indicates that the speed at which vehicles run and the time they spend directly affects the emission rate. However, the emission of NO_x shows opposite trends; has higher emission for combination of higher speed and lesser time spent and similarly very low emission was observed for combination of lower speed and higher time spent.

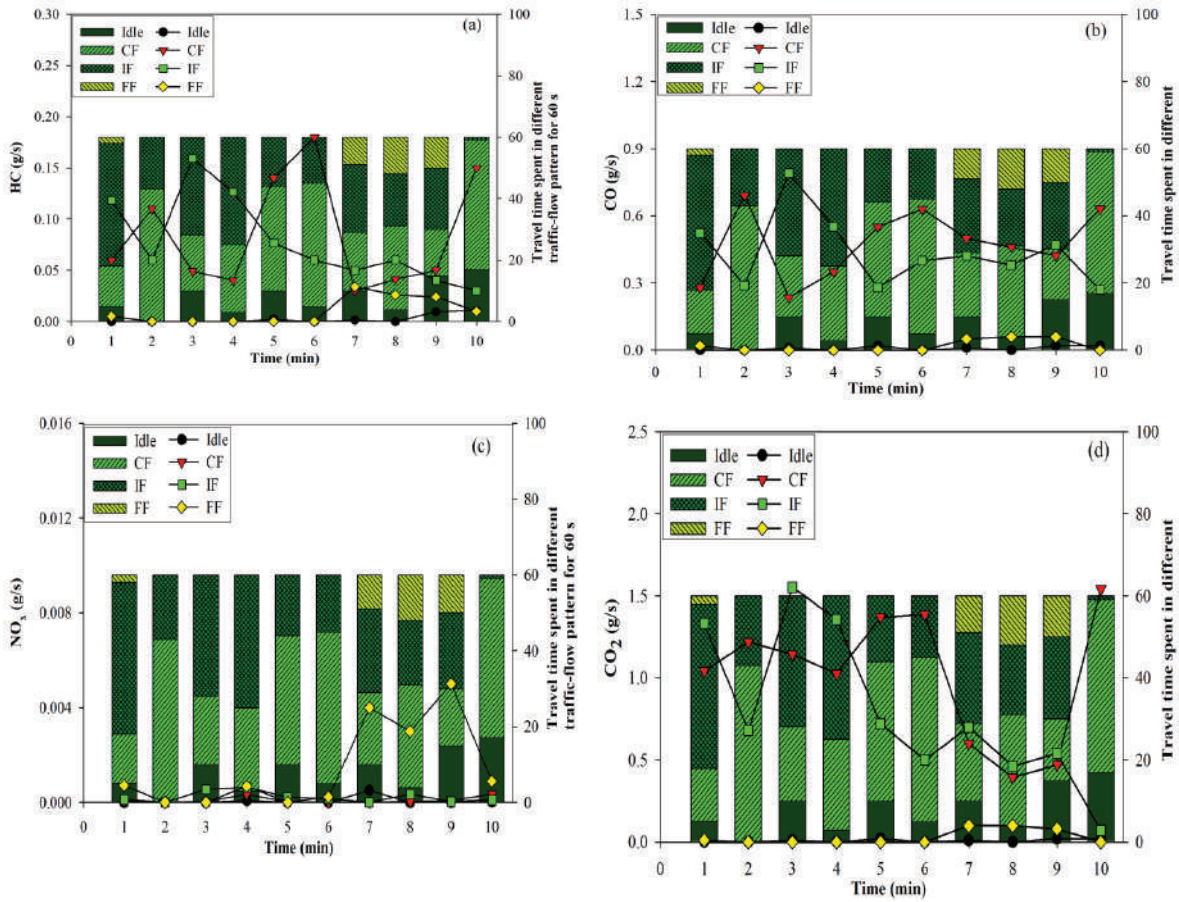

Fig. 4: The variation of pollutants emission in different traffic-flow pattern corresponding to time spent in each traffic-flow pattern during pH in auto-rickshaw.

Table 2: Speed-time factor analysis.

Speed range (km/h)	Speed (m/s)	Frequency	Factor (V*frequency)	HC (g/s)	CO (g/s)	NO_x (g/s)	CO_2 (g/s)
0-5	0.72	69	49.68	0.004	0.052	0.020	0.599
5-10	2.14	60	128.40	0.009	0.121	0.013	1.601
10-15	3.50	83	290.50	0.008	0.149	9.00e-3	1.698
15-20	4.82	81	390.42	0.010	0.192	7.20e-3	2.422
20-25	6.24	84	524.16	0.014	0.158	1.21e-3	2.256
25-30	7.51	49	367.99	0.012	0.174	9.21e-4	3.273
30-35	9.03	36	325.08	0.010	0.171	1.92e-4	3.000
35-40	10.35	27	279.45	0.012	0.147	5.00e-4	2.536

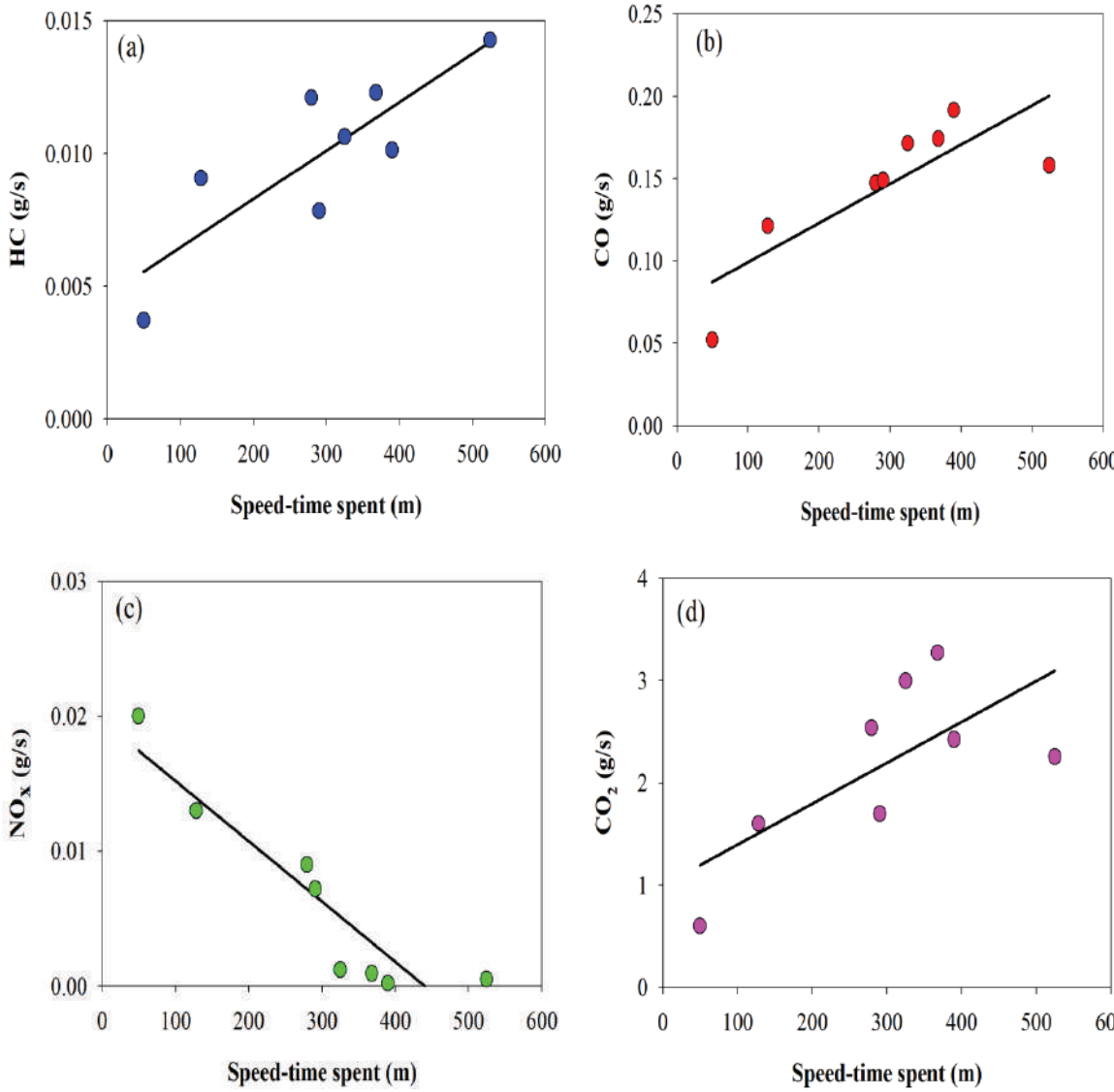

Fig. 5: The relationship of speed-time spent with the emission of pollutants (a) HC, (b) CO, (c) NO_x and (d) CO_2.

Table 3: The Tukey-Kramer emission-mileage matrix.

Test Vehicles		Test vehicle mileage		
		9,200 km	52,000 km	142,000 km
Test vehicle mileage	9,200 km	-	CO, HC	CO, HC, NO_x
	52,000 km		-	CO, HC, CO_2, NO_x
	142,000 km			-

Table 4: Summary of mean emission values ANOVA analysis.

Test vehicles	Mileage in km	CO (g/s)	HC (g/s)	NO_x (g/s)	CO_2 (g/s)
	9,200	0.12	0.0002	0.0006	9.50
	52,000	0.17	0.002	0.0005	5.18
	142,000	0.22	0.012	0.018	8.40

Mileage vs Emission

The vehicle mileage is another factor that determines the amount of emissions from a vehicle (Ntziachristos et al. 2000). The one-way ANOVA analysis was used to analyse the effect of mileage on exhaust emission. The completely randomised single-factor analysis of variance test (ANOVA) was applied to identify the statistically significant effects of vehicle mileage on emissions (Ntziachristos & Samaras 2000). Using this test, the average emission values of different mileage classes of test vehicles were compared to find any statistically significant differences between them (rejection of the null hypothesis of equal means). With the Tukey-Kramer emission mileage matrix (Barnes 1994), correlation of mileages with different mean values can be revealed. The double input matrix in Table 3 presents the results of this procedure. The cells of the matrix correspond to pair-wise comparison of different mileage classes of test vehicles found in the same row and column of the cell. This matrix has been built with 189 observations for auto-rickshaws. According to these results, it has been observed that for 52,000 km and above, mileage has significant impact on emission for pollutants CO, HC and NO_x. Summary of the mean emission values obtained from ANOVA for each mileage class is given in Table 4, which leads to the conclusion that there is a statistically significant correlation of CO, CO_2 and HC emissions with mileage.

CONCLUSIONS

Urban traffic-flow governed by many factors which mainly resulted from the poor traffic management, an unregulated roadside parking and a frequent pedestrian to vehicle interaction. These factors restrict the urban mobility and the most severe outcomes of the restricted urban mobility are increased pollutant emissions. The study identified three traffic-flow patterns classified as free-flow, interrupted-flow and congested-flow from the on-road traffic volume and traffic speed. The variable composition of vehicles on road governs the rate of exhaust emissions. The dynamic and age-related variables such as, time, speed and mileage were analysed for analytically categorized traffic-flow patterns. The analysis depicted that the combined factor of lower speed (speed $\leq$2 km/h) and higher time of travel cause higher emission rate, especially for pollutants HC and CO. NO_x emission is higher with increasing speed irrespective of time of travel. The magnitude of CO_2 emission rate mostly found higher for interrupted flow condition as compared to the combination of higher travel time and lower speed. Similarly, vehicle mileage of $\leq$2,000 km has significant impact on emission for pollutants CO, HC and NO_x.

The effective transport planning and environmental policies depends on the accurate assessment of vehicle exhaust emissions. Therefore, the finding of this study can be handy for the consideration in policy formulation and worthy for differentiation between measured and modelled results.

ACKNOWLEDGEMENTS

Arti Choudhary thankfully acknowledges the financial assistance provided by Science and Engineering Research Board (SERB), New Delhi, India, under the scheme of SERB National Post-Doctoral Fellowship (PDF/2017/001284).

REFERENCES

Anjaneyulu, M.V.L.R. and Nagaraj, B.N. 2009. Modelling congestion on urban roads using speed profile data. Journal of the Indian Roads Congress, 1: 65-74.

Asaithambi, G., Kanagaraj, V., Srinivasan, K. K. and Sivanandan, R. 2016. Study of traffic flow characteristics using different vehicle-following models under mixed traffic conditions. Transportation Letters, 1-12.

Barnes, J.W. 1994. Statistical Analysis for Engineers and Scientists: A

Computer-based Approach. McGraw-Hill, Inc.

Chen, C., Huang, C., Jing, Q., Wang, H., Pan, H., Li, L. and Schipper, L. 2007. On-road emission characteristics of heavy-duty diesel vehicles in Shanghai. Atmospheric Environment, 41(26): 5334-5344.

Choudhary, A. and Gokhale, S. 2016. Urban real-world driving traffic emissions during interruption and congestion. Transportation Research Part D: Transport and Environment, 43: 59-70.

Faiz, A., Weaver, C.S. and Walsh, M.P. 1996. Air Pollution from Motor Vehicles: Standards and Technologies for Controlling Emissions. World Bank Publications.

Choudhary, A. and Gokhale, S. 2019a. Evaluation of emission reduction benefits of traffic flow management and technology upgrade in a congested urban traffic corridor. Clean Technologies and Environmental Policy, 21(2): 257-273.

Choudhary, A. and Gokhale, S. 2019b. On-road measurements and modelling of vehicular emissions during traffic interruption and congestion events in an urban traffic corridor. Atmospheric Pollution Research, 10(2): 480-492.

Grieshop, A.P., Boland, D., Reynolds, C.C., Gouge, B., Apte, J.S., Rogak, S.N. and Kandlikar, M. 2012. Modeling air pollutant emissions from Indian auto-rickshaws: Model develop.m.ent and implications for fleet emission rate estimates. Atmospheric Environment, 50: 148-156.

Grote, M., Williams, I., Preston, J. and Kemp, S. 2016. Including congestion effects in urban road traffic CO_2 emissions modelling: do local government authorities have the right options? Transportation Research Part D: Transport and Environment, 43: 95-106.

Gulia, S., Nagendra, S.S., Khare, M. and Khanna, I. 2015. Urban air quality management-A review. Atmospheric Pollution Research, 6: 286-304.

Guttikunda, S.K. and Mohan, D. 2014. Re-fueling road transport for better air quality in India. Energy Policy, 68: 556-561.

Iyer, N.V. 2003. Three-wheelers take to South Asian streets. Smart Urban Transport, 2(2).

Iyer, N. V., Posada, F. and Bandivadekar, A. 2013. Technical assessment of emission and fuel consumption reduction potential from two and three wheelers in India (No. 2013-26-0050). SAE Technical Paper.

Joumard, R., Philippe, F. and Vidon, R. 1999. Reliability of the current models of instantaneous pollutant emissions. Science of the Total Environment, 235: 133-142.

Marsden, G., Bell, M. and Reynolds, S. 2001. Towards a real-time microscopic emissions model. Transportation Research Part D: Transport and Environment, 6(1): 37-60.

Mohapatra, S.S. 2012. Level of service criteria of urban streets in Indian context using advanced classification tools. M.Tech. Thesis.

Ntziachristos, L. and Samaras, Z. 2000. Speed-dependent representative emission factors for catalyst passenger cars and influencing parameters. Atmospheric Environment, 34(27): 4611-4619.

Ntziachristos, L., Samaras, Z., Eggleston, S., Gorissen, N., Hassel, D. and Hickman, A.J. 2000. COPERT III, Computer programme to calculate emissions from road transport, methodology and emission factors (version 2.1). European Energy Agency (EEA), Copenhagen.

Pandian, S., Gokhale, S. and Ghoshal, A.K. 2009. Evaluating effects of traffic and vehicle characteristics on vehicular emissions near traffic intersections. Transportation Research Part D: Transport and Environment, 14(3): 180-196.

Ramachandra, T. 2009. Emissions from India's transport sector: state wise synthesis. Atmospheric Environment, 43(34): 5510-5517.

Reddy, B. S. and Balachandra, P. 2012. Urban mobility: A comparative analysis of megacities of India. Transport Policy, 21: 152-164.

Reynolds, C. Grieshop, A. and Kandlikar, M. 2009. Measuring auto-rickshaw emission to inform air quality policy. University of British Columbia. Accessed on 5th March 2016, http://indiaenvironmentportal.org.in/files/EmissionTestinginInda.pdf.

Reynolds, C.C., Grieshop, A.P. and Kandlikar, M. 2011. Climate and health relevant emissions from in-use Indian three-wheelers fueled by natural gas and gasoline. Environmental Science & Technology, 45: 2406-2412.

Robertson, H.D. 1994. Queuing studies. In: Robertson, H.D., Hummer, J.E., Nelson, D.C. (Eds.), Manual of Transportation Engineering Studies, Washington, DC, pp. 347-358.

Singh, S. K. 2006. Future mobility in India: Implications for energy demand and CO_2 emission. Transport Policy, 13(5): 398-412.

Singh, S.K. 2012. Urban transport in India: Issues, challenges, and the way forward. European Transport/Trasporti Europei, Issue 52.

Nature Environment and Pollution Technology
An International Quarterly Scientific Journal

p-ISSN: 0972-6268
e-ISSN: 2395-3454

Vol. 19 | No. 1 | pp. 103-111 | 2020

Original Research Paper | Open Access

Studies on use of Cashew Nut Shell Liquid (CNSL) in Biopesticide and Biofertilizer

C. Vasanth Pandiyan*†, Gunasekaran Shylaja*, Gokul Raghavendra Srinivasan and Sujatha Saravanan***

*Department of Biotechnology, Bharath Institute of Higher Education and Research, Selaiyur, Chennai-600073, Tamil Nadu, India

**Department of Mechanical Engineering, Bharath Institute of Higher Education and Research, Selaiyur, Chennai-600073, Tamil Nadu, India

†Corresponding author: C. Vasanth Pandiyan

Nat. Env. & Poll. Tech.
Website: www.neptjournal.com

Received: 08-06-2019
Accepted: 23-07-2019

Key Words:
Cashew nut shell liquid
Biopesticide
Biofertilizer
Oil cake

ABSTRACT

Cashew is an immigrant tree from eastern Brazil and is regarded as one of the top three commercial crops of India. In general, Cashew nut shell contains 25-34% oil and was not much used earlier; however, commercial and industrial applications are being developed in the recent decade. In this present study, 100 kg of dried cashew shells yielded around 18.5 to 22.6% of cashew nut shell liquid (CNSL) while 58-63% of waste dark solid oil cake retained in extraction chamber. Eventually, these oil cakes were rich in fibre, protein and energy contents and offered as good alternative to traditional applications in the production of environmentally friendly organic fertilizer for vegetable crops. Also, this study investigated the safety of using CNSL cake as fertilizer for leaf & vegetable; and also noted improvised physico-chemical properties of soil which enhanced the soil fertility thereby leading to high crop yield and nutritional quality. Furthermore, CNSL was also proven to be a phytopesticide for eradication of serious pests, Odontopus varicornis, on cotton plant. Interestingly, toxicity study proved that the applications of CNSL was not only limited to biofertilizer but was also proven to be an effective biopesticide for the control of pest and insects.

INTRODUCTION

The developing and developed countries are seeing the rapid growth of specific wastes, such as electrical and electronics equipment waste, agricultural biomass waste, and plastic waste. These specific wastes require proper management, as most of the materials could be reduced, recycled or re-used with the help of environmentally friendly methods and technologies.

Cashew nut is one of the greatest yielded item on the planet, with production capacity more than 3.35 million tonnes per year and yet expanding in coming years. It is likewise considered as a standout amongst the most critical nuts in universal market because of its well acknowledged demand (MacLeod et al. 1982, Maia et al. 2000). Crude cashew nut contains both edible kernel with health significance; and a shell, which has been considered as waste and may bring an ecological issue if not dealt with appropriately.

The primary component of cashew plant is its cashew nuts, while the least regarded product was cashew nut shell liquid (CNSL). At a level of about 50% of cashews weight (Patel et al. 2006), a heavy liquid called cashew nut shell liquid (CNSL) is produced, which is considered an important material in view of the high centrality of unsaturated long-chain phenols, for example, cardanol, cardol and isomers (Rodriguez et al. 2006). Both anacardic and cardol corrosion were included as corrosion inhibitors (Kozubek et al. 2001, Kubo et al. 1993), antimicrobial inhibitory (Kubo et al. 1993) and lipoxygenase activities (Kubo et al. 1993). On the other hand, cardanol, because of its remarkable protection against the photolytic activity of mineral oils and the high protection of acids, alkalis, microorganisms, termites and creepers widely used in the production of caps and fabrics.

Cashew nut shell fluid or CNSL or CNSL oil is an adaptable by-product of the cashew business. CNSL is widely used in polymer-based businesses, for example, contact linings, paints and varnishes, overlaying tars, rubber aggravating saps, cashew bonds, polyurethane based polymers, surfactants, epoxy tars, foundry synthetics and intermediates for concoction industry and automobiles. In its existing form, CNSL is accounted as an effective chemical against termites and has water repellency (Lepage & Delelis l980). With the end goal of using the cashew nutshell, we have made an endeavour to change over the CNSL oils and waste cake to bio-insecticide against and bio-fertilizer. We hypothesize that if not the neat form, some particular blend may actually be

good enough for commercial use. The objective of the study was to characterize the physicochemical quality of oil from cashew nut shell and to evaluate the potential of cashew nut shell cake as natural insecticide against termites.

MATERIALS AND METHODS

Collection of Cashew Nut Shells

Cashew nut shells crude and unshelled cashew nuts were collected from the trees grown in the Panruti, Cuddalore area in Tamil Nadu (India) amid August to September 2012. Cuddalore region was chosen for the examination since this locale has the most extreme territory of cashew generation than different areas of the state. Towns from Panruti and Virudhachalam obstructs in Cuddalore locale were chosen for this examination.

Preparation of samples

The piece nuts were broken, the nuts were collected, washed, dried in a stove at 40°C. The dried, clean nuts were processed using manual blender on account of the hardness of the nut (Figs. 1 & 2). During the timeframe of August to September, 2018, four samples were gathered and CNSL oil was separated.

Extraction of Cashew Nut Shell Liquid (CNSL)

This is the most well-known technique for extraction of CNSL these days. The cashew nut shells are gathered in the chamber, where steam warming is connected at temperatures around 200-250°C for 2-3 minutes, CNSL is then discharged out of shells. Figs. 3, 4A & 4B show the small-scale extraction units at Panruti, Cuddalore area in Tamil Nadu (India).

CNSL as Biopesticide Studies

Adult insects of *Odontopus varicornis*, collected from the Annamalai University campus, were brought to the laboratory and reared in wooden cage (45 × 32 × 30 cm dimension), at laboratory temperature of 29°±1°C with 12 hours of light and dark cycle. The sides of the insect cages were fabricated with wire meshes to provide sufficient aeration and light also easy for observation. The cage surface was covered with fine sand with moderate humidity maintained by adding a little amount of water frequently. The soaked cotton seeds of *Bombax ceiba* as well as seeds of its host plant, *Stericulia foetida* and *Gossypium* sp. were fed daily to the insects. Additionally, the pieces of *Sechium edule* (Chow chow) were also fed to the insects. The cages were maintained properly by cleaning on alternative days by eliminating the excreta and other waste substances. The continuous culture was maintained by transferring the laid eggs to other cages.

The nuts *A. Occidentale* were collected from cashew plantation area of Cuddalore district, Tamil Nadu, India. Cashew nut shell liquid (CNSL) has a structure of soft honey comb with dark brownish red viscose liquid. It is a one of the by-products of the cashew production which is the pericarp fluid of the nut.

To evaluate the acute toxicity in the atmosphere, the LD_{50} values (medium tolerance limit) are positive measures to test the toxicity of the test toxicant, under definite environmental conditions. The application of LD_{50} value has significantly gained more importance among toxicologists and it is the most consistent measure to evaluate potential hazards of aquatic and terrestrial life. The LD_{50} value for the same toxicant varies due to the mode of action and animal responses. In this viewpoint, the study has been done to evaluate the LD_{50} values for the male *Odontopus varicornis* on exposure to the phytopesticide, cashew shell oil. To provide a basis for evaluating and comparing the acute toxicity with other, 24, 48, 72 and 96 hours median lethal dose (LD_{50}) values are determined for the cashew nut shell oil commercial product. The LD_{50} is a statistical estimate of the concentration of the

Fig. 1: Manually separating activity for cashew kernel and shells.

Fig. 2: Picture of cashew nut shells.

Fig. 3: Top view - Input loading cylinder with cover.

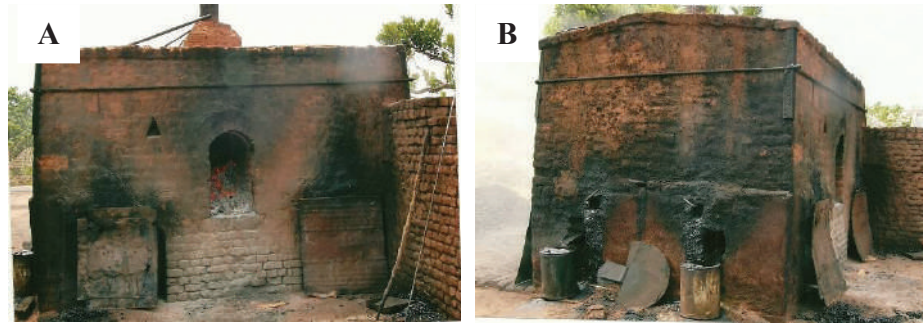

Fig. 4A: Input loading cylinder with cover. 4B: Collection container of small-scale extraction.

toxic material that kills 50 percent of the test species under experimental conditions during a specific time interval. The LD_{50} values are used because of the concentration required to affect a response in 50 percent of the test insects is more reproducible than any other values.

Range Finding Test

The solutions were made at varying range of concentrations. The tests were performed in adult insects, by injecting 0.025 mL, to each insect with a 2.6-gauge syringe needle. Ten treated insects were moved into a little insect cage (29 × 25 × 11cm) and their mortality was noted from 24 hours thereafter up to 96 hours. The results observed from the exploratory test indicated the range of the insecticide concentration.

Full Scale Test of Toxicity Evaluation

Different concentration of cashew nut shell oil was prepared. Insecticide treated and control insect were maintained for each bioassay. One hundred insects were administered with each concentration and allowed in separate insect cages. The observations on mortality are made at 25, 48, 72 and 96 hours. Insects showing no activities or response to physical stimulus were noted as dead and taken out instantly. The recorded values were used for calculating LD_{50} values.

Calculation of LD_{50}

The test was done to find the series of concentration for mortality. The mortality was recorded for *Odontopus varicornis* at 24, 48, 72 and 96 hours of exposure by injecting the insecticide of various concentrations. The LD_{50} value was determined by the profit analysis method depending on the measured percentages of test animal existing at concentrated lethal to more than half and less than half of the test subject (Huson method). This method described a quick and exact method of determining the median lethal dose (LD_{50} or ED_{50}). The method can be used to drive point and interval estimates or percentage points other than the LD_{50}. It is claimed that the method is less accurate for points other than the medium but equal to other approximate techniques. Following the probit analysis procedure, the LD_{50} values of 24, 48, 72 and 96 hours were evaluated. By using the LD_{50} values, a toxicity curve was constructed on a centimetre graph sheet (Fig. 10).

The LD_{50} values were derived by probit regression, i.e. taking test concentration and the respective mortality percentages on log values and probit scales, respectively. From the line drawn to the concentration ordinates, LD_{50} values were fixed and also calculated their 95% upper and lower

confidence limits. The method of calculation is as below:

Step 1: The doses (d_1); number of insects tested (n_1); number of insects died (r_1) were wrote down; then the natural log for the doses (x_1) were found out.

Step 2: The method of finding y_1 is as follows.

$y_1 = In\frac{r_1}{n_1 - r_1}$, if number of insects ($r_1$) died is less than number of insects tested (n_1).

$y_1 = (2n_1 - 1)$, if number of insects died is equal to number of insects tested.

$y_1 = In\frac{1}{(2n-1)}$, if number of insects died is 'zero'.

Step 3: The transformed data were divided and then set into upper lower halves.

Step 4: The total amount of transformed doses and the responses were calculated and the values were denoted as y_u, y_l, x_u, x_l where subscript U and 1 refer upper and lower halves of the data set.

Step 5: The mean of all transformed doses and the responses included in Step 3 were calculated. The means denoted as $\overline{X}$ and $\overline{Y}$ respectively.

Step 6: The slope (b) was calculated as:

$$b = \frac{(yu - y1)}{(Xu - X1)}$$

Step 7: The intercept (a) was calculated as:

$$a = \overline{y} - \overline{bx}$$

Step 8: LD_{50} was found as follows:

$$LD_{50} = e^c$$

Where, $c = \frac{(F-a)}{b}$ F is the log of LD_{50}

$$F = In\left[\frac{50}{(100-50)}\right] = 0$$

Step 9: The total number of insects tested (N) in the data included in Step 3 was calculated.

Step10: Sc was found using the formula:

$$Sc = \sqrt{\frac{5}{(b^2 \times N)}}$$

Step 11: The standard error (S) of the desired percentage was estimated as follows:

$$S\ (LD_{50}) = LD_{50} \times Sc$$

Step 12: The approximate 95% confidence interval was calculated by using the following formula:

$$LD_{50} \pm 1.96 \times S(LD_{50})$$

Bionomics

The details of its systematic position, distribution, habitat, morphology, feeding habits, cannibalism, longevity, sexual dimorphism, mating habits, oviposition, eggs, metamorphosis and adult characters are briefly presented in Table 1 and Table 2.

CNSL as Biofertilizer

Farm site: All the green leaves crops were grown in the farm house at Vallambadugai nearer to Chidambaram town. The plantation of green leaves and ornamental plants located in the region of plant research farm nearer to Annamalai University. This region is located in the central plain of Chidambaram town and characterized as clay loan soil.

De-oiled CNSL seed cake: The de-oiled CNSL cake was generously processed. The seedcake was kept back at room temperature for 90 days before using as a fertilizer.

Fig. 5: *Odontopus varicornis* in mating condition.

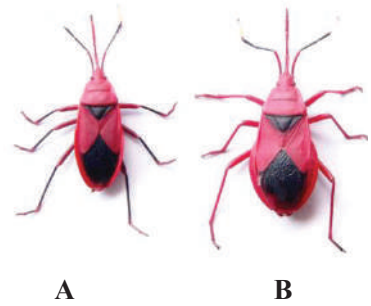

Fig. 6A: Adult male *Odontopus varicornis;* 6B: Adult female *Odontopus varicornis.*

Fig. 7: Adult male and female *Odontopus varicornis* in mating condition.

Table 1: Systematic position of *O. varicornis.*

Systematic Position	
Phylum	Arthropoda
Class	Insecta
Order	Hemiptera
Suborder	Heteroptera
Series	Geocorisae
Super family	Pyrrhocoroidea
Family	Pyrrhocoridae
Genus	*Odontopus*
Species	*varicornis*

Table 2: Details of *O. varicornis.*

Distribution	Ethiopiean and Oriental regions, *Odontopus cultellaris*, O. *nigricornis*, *O. varicornis*, and *O. sanguinolens* are found in different parts of India. *O. varicornis* and *O. sanguinolens* are found in the State of Tamil Nadu and Puducherry.
Habitat	Fallen leaves of host plants such as *Stericulia foetida* and *Gossypium* sp.
Feeding Habits	Phytophagus insect with piercing and sucking type of mouth parts. The bug exhibits minimum feeding during hot hours of the day.
Cannibalism	Cannibalism is exhibited by these insects. The eggs laid by them as well as newly moulted insects are found to be susceptible to this activity. Field observations have shown that these insects are Cannibalistic occasionally and moreover feed on snails and dead animals.
Longevity	Adult male lives for about 75 days and female for about 70 days under laboratory conditions of 282±^{o}C and 80 * 5% RH
Sexual dimorphism	Adult male is smaller in size than the female with pointed aedeagus female with broader abdomen (Figs. 6A and 6B).
Mating habits	Exactly on 7th day after last imaginable moult; it exhibits mating behaviour (Fig. 5); Male crawls over the body of the female, after gripping the male inserts its aedeagus into the gonopore and remains in end to end position in natural and laboratory condition (Fig. 7), all usual activities like roaring, feeding, etc. are carried out by the pair in copula conditions (Ranganathan 1984), it mates continuously for three days without any separation.
Oviposition	At the time of oviposition, the female separates from the male and scoops at the sand and finally lays its eggs. The first oviposition occurs at about 25 days after the last moult, depositing 80 to 120 eggs in 2 to 3 hours; second oviposition occurs a week after the first oviposition producing 50 to 70 eggs.
Meta Morphosis	Incomplete metamorphosis with five nymphal instars; to reach its final moulting, it takes about 42 to 45 days.
Adults	The fifth nymphal instar on its final moulting becomes an adult with attains sexual maturity on the 7th day of its imaginal moult.

Plant material and propagation: All the leaves and ornamental plants need different agricultural practices such as the ratio of chemical fertilizers for each plant varies based on the recommendation by the Department of Agriculture, Annamalai University, India. The development of the plant and yield is independent of each other. However, the intention of this study is to trace the growth of leaves bushiness height as well as ornamental plant height, growth etc. Different rates of CNSL cake would have the variation in influencing the growth of each plant, but propagation methods were varied between these plants. The addition of CNSL cake at land preparation would exacerbate the phorbol ester content in the soil which was reported to decompose at time of harvesting (Joshi et al. 2011).

Plant Experiments

Amaranthus seeds were planted in control medium and allowed to grow for 4 weeks (Figs. 11 & 12). seedlings were transplanted individually into different test potting media and placed in a greenhouse maintained at 28°C, 16-h day/20°C 8-h night utilizing both natural light and supplemental artificial lighting to maintain an average light intensity of approximately 600 µmol m^{-2} s^{-1}. Change in plant heights were recorded from transplanting, when further growth ceased.

RESULTS AND DISCUSSION

Extraction of CNSL

The shell is about 0.3 inches thick having a sensitive cush-

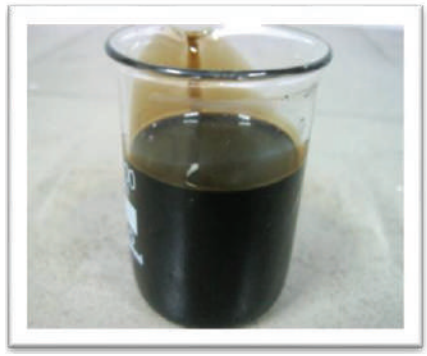

Fig. 8: Raw cashew nut shell liquid

Fig. 9: End products like oil cake

Table 3: Process and recovery rate of cashew shells.

Sample	1	2	3	4
Processing quantity of Cashew shells (kg)	100	100	100	100
Recovery of cashew nut shell oil (mL)	18.8	22.6	21	21.5
Oil cake (kg)	58.8	62.4	57.4	60.4

ioned outside skin and a pitiful hard internal skin. CNSL inside the shell is the segment wrapped by a pitiful skin known as the test. 20 to 25% partition liquid, 20 to 25% test, 2% others, rest being the shell. The raw material for the creation of CNSL is the cashew shells. Cashew nuts contain 35-45% of seeds and 55-65% of shells. The shells contain 15-30% oil. CNSL is used as oil in industries. In extraction process of 100kg of dried cashew shells, oil range between 18.5 to 22.6% was extracted (Table 3). The colour of the solution became reddish brown or dark brown as shown in Fig. 8. The end products or waste like dark solid is shown in Fig 9. It was observed that 58-63% of end product like oil cake retains in chamber.

The most generally utilized technique, the hot oil shower, removes about half of the CNSL (7-15% of nut weight) from the shell (Ohler 1966, Gedam et al.1986). A few unique medications before simmering can convey the rate up to 90-95% and with solvents 100% can be accomplished, however these strategies are costly and their utilization relies upon the CNSL value (Ohler 1966).

Toxicity Studies

The present mortality values of *Odontopus varicornis* when injected with different concentrations of cashew nut shell oil for different are presented in Table 4. Detailed probit analysis of cashew nut shell oil concentrations and present mortality of *Odontopus varicornis* for 24, 48, 72 and 96 hours of exposure were determined. The LD_{50} values were calculated for 24, 48, 72 and 96 hours as 3.3, 3.5, 3.6, and 3.8 respectively. The mortality rate showed the mode of action and toxicity of for different concentrations. Toxicity test revealed that the rates of mortality increased with the increased concentrations.

Plant Growth and Yield

To measure the growth of *Amaranthus tricolour*, five parameters were subjected to be analysed, namely leaf length, leaf width, plant height, canopy height, canopy width. The trends toward these five characters were not similar. Among all, the one with biofertilizer provided the best outcome as an appearance of the largest of the plant growth characters than control. Whereas, the control plant resulted in a medium-sized growth of the same plant. The highest yield was obtained from the treatment of biofertilizer. Therefore, it could be implied that the treatment of CNSL oil cake would be able to partly replace the usage of chemical fertilizer. The usage of CNSL oil cake as fertilizer could, therefore alleviate the problem of high price of chemical fertilizer. Among these treatments, the control without adding biofertilizer gave the poor yield of *Amaranthus* plants.

Peace lily plant planted in a pot (Fig. 13) showed comparatively more growth in height of about 6.2 cm and increased the leaf surface area of about 4.8% compared to control when the soil was mixed with CNSL cake. Further, the same trail was showed for sword fern Nephrolepis obliterate in both height and leaf area. Plant height exhibited around1.2cm increase and height surface area comparatively increased about 7.6% when compared to control.

Table 4: LD_{50} value and their 95% confidence limit (µg/insect) of cashew nut shell liquid and the difference between upper and lower confidence limits for male *Odontopus varicornis*.

Exposure time intervals (in hours)	Number of animal introduction	Number of animals died in exposure concentration (%)						LD_{50}	95% Confidence limits (upper- lower)
		0.26	0.28	0.30	0.32	0.34	0.36		
24	100	-	-	10	20	30	40	3.3	3.6-3.1
48	100	5	10	20	30	40	50	3.5	3.6-3.4
72	100	10	25	40	55	70	85	3.6	3.4-3.1
96	100	15	30	50	65	80	100	3.8	3.4-3.9

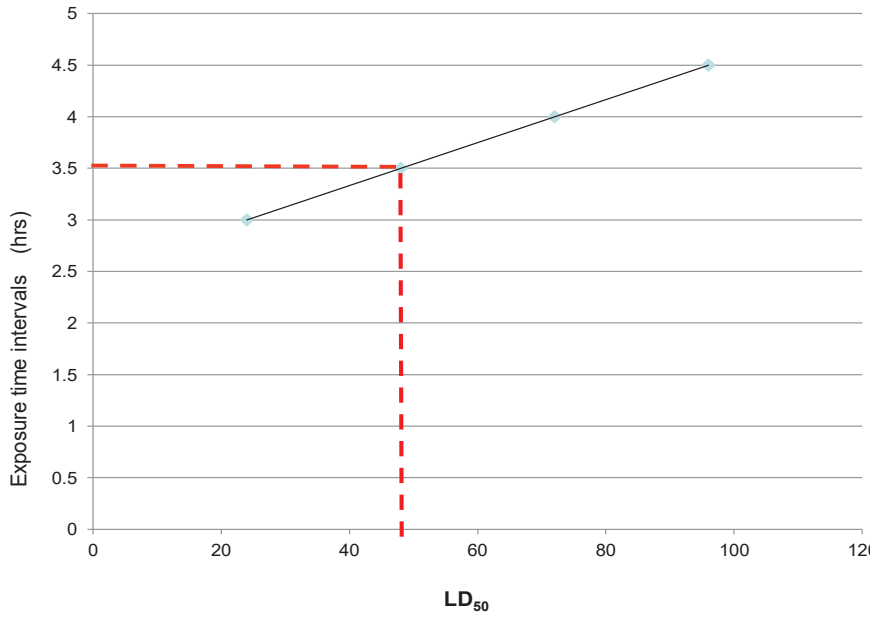

Fig. 10: LD50 values for 24h, 48h, 72h and 96h of O. varicornis (Toxicity Curve).

Nursery trial on oil extracted CNSL cake act as biofertilizer when peace lily, cobra plant, *Spathiphyllum wallisii* was planted in pot and observed that in the oil cake treated plant, the height increased by 6.2cm and leaf surface area was also increased as compared to control plant (Fig. 14).

CNSL Used as Biopesticide

The toxicity tests were ideally suited for assessing the relative impact of cashew nut shell liquid concentration on the insect for different time intervals. The toxicity level was also influenced by the size and age of the insect under study. The toxicity level also is influenced by sex; similarly, the nutrient supply to the assaying insect (Arunachalam et al. 1980) and the pH. It can be seen that the toxic action is specific for a particular insecticide in a particular insect which has been substantiated by the researchers in their studies.

The toxicity values denote the nature of cashew nut shell oil on the organism. It indicates whether the action is regular or irregular or cumulative in its effect. In the present investigation on *Odontopus varicornis* treated with cashew nut shell oil of phytopesticide, the acute toxicity level was expressed in terms of LD_{50}. The LD_{50} values of the cashew nut shell oil of *Odontopus varicornis* were 3.3, 3.5, 3.6, 3.8 at 24, 48, 72 and 96 hours, respectively.

The present experimental results were obtained with increased concentration of phytopesticide cashew nut shell liquid with decreased time of exposure, to bring about 50% mortality of insects. This trend was showing a risk in mortality rate with increasing concentration and period of administration sub-cutaneously, revealing the regular mode

Fig. 11: Control Plant *Amaranthus tricolour.*

Fig. 12: Treated plant *Amaranthus tricolour***.**

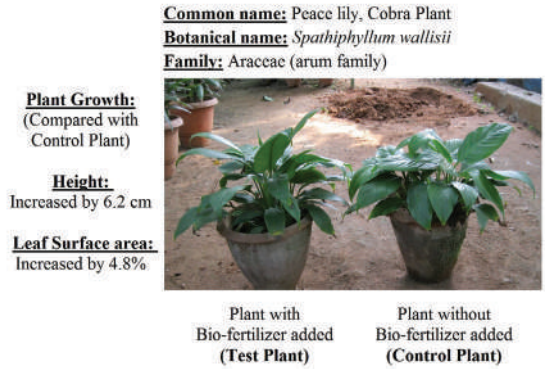

Fig. 13: Nursery trail on Spathiphyllum wallisii using oil extracted cashew nut shells (OECNS) as biofertilizers.

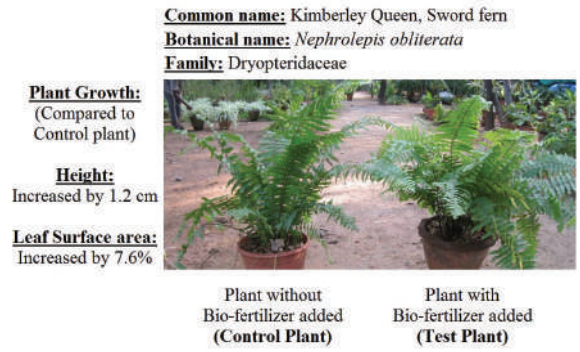

Fig.14: Nursery trail on Nephrolepis obliterata using oil extracted cashew nut shells (OECNS) as biofertilizers.

of action due to the toxicant. Cause of death may be attributed to the lethal action of cashew nut shell oil that inhibited biochemical processes and cellular metabolic pathways and other inclusions. These results are correlated with the previous reports which exposed Laccotrephes ruber, *Gryllotalpa africana*, *Spherodema ruticum*, *Odontopus varicornis* to monocrotophos, endosulfan, heavy metal mercury, pygidial secretion and nimbicidine, respectively. (Ha & Kubo 2005, Selvisabhanayakam et al. 2002, Lousia et al. 2010.

CNSL Cake Application as Biofertilizer

Organic manure, apart from supplying nutrient to the soil,

conserves soil moisture, moderates soil pH, improves bulk density, increase carbon dioxide level in plant canopy, alleviates the toxicity of A^{3+}, improves aeration and activity of beneficial soil microbes, increase cation exchange capacity and retards nitrification for longer time. The increased yield resulting from the application of fertilizer was as a result of the improved soil fertility. It has been shown that crops respond more to fertilizer application. The improved nutritional value of the crop resulting from the application of the formulations may be attributed to the increased soil fertility. Increase in yield attributes and nutritional value of crops arising from the use of combination of organic and chemical fertilizers has also been reported. It has been suggested from the present study that CNSL oil cake helps to improve the growth and canopy of both test plant. Further, the present study revealed that the use of CNSL oil cake used for both plants increased the height and leaf surface area, especially in sword fern, which absorbed the air pollutants and *Amaranthus tricolor*, which produce pure air, in addition to controlling environmental contamination.

CONCLUSIONS

Oil cakes are rich in fibre, protein and energy contents. They offer potential benefits when used as substrates in developing bioprocesses for the production of organic chemicals and bio-molecules. Also, the use of oil cakes offers good alternative to traditional applications by their exploitation in the production of environmentally friendly green biofuel. Another key point to be noted is that the bioprocess utilizing oil cakes is attractive due to relatively cheaper availability of the oil cakes throughout the year, making it even more favourable when economics is considered. The utilization of de-oiled CNSL oil cake was proven to have potential for being used as an organic fertilizer for vegetable crops. These studies implied the safety of an application of CNSL cake as fertilizer in leaf and vegetable. It has also been proved that CNSL acted as phytopesticide for the eradication of one of the serious pests on cotton plant, *Odontopus varicornis.* Toxicity study also proved the hypothesis that CNSL has an application not only as biofertilizer but also as biopesticide for the control of pest and insects.

REFERENCES

Arunachalam, S., Jeyalakshmi, K. and Aboobucker, S. 1980. Toxic and sublethal effects of carbaryl on a freshwater catfish, Mystus vittatus (Bloch). Archives of Environmental Contamination and Toxicology, 9(3): 307-316.

Gedam, P.H. and Sampathkumaran P.S. 1986. Cashew nut shell liquid: Extraction, chemistry and applications. Prog. Org. Coat., 14: 115-157.

Ha, T.J. and Kubo, I. 2005. Lipoxygenase inhibitory activity of anacardic acids. J. Agric. Food Chem., 53: 4350-4354.

Joshi, C., Mathur, P. and Khare, S.K. 2011. Degradation of phorbol esters by Pseudomonas aeruginosa PseA during solid-state fermentation of deoiled Jatropha curcas seed cake. Bioresour. Technol., 102: 4815-4819.

Kozubek, A., Zarnowski, R., Stasiuk, M. and Gubernator, J.E.R.Z.Y. 2001. Natural amphiphilic phenols as bioactive compounds. Cell. Mol. Biol. Lett., 6: 351-355.

Kubo, I., Muroi, H., Himejima, M., Yamagiwa, Y., Mera, H., Tokushima, K., Ohta, S. and Kamikawa, T. 1993. Structure-antibacterial activity relationships of anacardic acids. J. Agric. Food Chem., 41: 1016-1019.

Lepage, E.S. and De Lelis, A.T. 1980. Protecting wood against dry-wood termites with cashew nut shell oil. Forest Prod. J., 30: 35-36.

Lousia, M. and Selvisabhanayakam, V.M. 2010. Effects of pygidial secretion (zoopesticide) on histopathological changes in the male accessory reproductive glands of adult male insect Odontopus varicornis in relation to reproduction. Toxicol. Int., 17: 22.

MacLeod, A.J. and De Troconis, N.G. 1982. Volatile flavour components of cashew 'apple' (Anacardium occidentale). Phytochem., 21(10): 2527-2530.

Maia, J.G.S., Andrade, E.H.A. and Maria das Gracas, B.Z. 2000. Volatile constituents of the leaves, fruits and flowers of cashew (Anacardium occidentale L.). J. Food Compos. Anal., 13: 227-232.

Ohler, J.G. 1966. Cashew nut processing. Trop. Abs., 21: 549-554.

Patel, R.N., Bandyopadhyay, S. and Ganesh, A. 2006. Extraction of cashew (Anacardium occidentale) nut shell liquid using supercritical carbon dioxide. Bioresour. Technol., 97: 847-853.

Ranganathan, L., Sriramulu, V., Balasundaram, D. and Sridharan, G. 1984. Role of glycogen-glucose in the accessory reproductive gland and sperm transfer in Aspongopus janus (Fabr.). Curr. Sci., 53: 713-714.

Rodriguez, F.H.A., Feitosa, J., Ricardo, N.M., Franca, F.C.F.D. and Carioca, J.O.B. 2006. Antioxidant activity of cashew nut shell liquid (CNSL) derivatives on the thermal oxidation of synthetic CIS-1, 4-Polyisoprene. J. Braz. Chem. Soc., 17: 265-271.

Selvisabhanayakam, R., V. and Mathivanan, V. 2002. Toxicity studies on the impact of heavy metal mercury on Sphaerodema rusticum (Heteroptera: Belostomatidae). Indian J. Environ. and Ecoplan., 6(3): 431-434.

Nature Environment and Pollution Technology
An International Quarterly Scientific Journal

p-ISSN: 0972-6268
e-ISSN: 2395-3454

Vol. 19 | No. 1 | pp. 113-121 | 2020

Original Research Paper | Open Access

Multi-objective Ecological Operation of Reservoir in Luanhe River Based on Improved Particle Swarm Optimization

Hai-tao Chen*†, Xiao-nan Chen, Lin Qiu* and Wen-chuan Wang***

*School of Water Resources, North China University of Water Resources and Electric Power, Zhengzhou City, Henan Province, 450045, PR China

**Construction and Administration Bureau of South-to-North Water Diversion Middle Route Project, Haidian, District Beijing, 100038, PR China

†Corresponding Author: Hai-tao Chen

Nat. Env. & Poll. Tech.
Website: www.neptjournal.com

Received: 11-05-2019
Accepted: 22-07-2019

Key Words:
Luanhe river
River health
Ecological operation
Particle swarm optimization

ABSTRACT

River ecosystem is one of the most important ecosystems, and it provides many ecosystem services for human beings. However, river health has also been damaged by over-exploitation and water pollution. In the process of reservoir operation, the ecological flow demand of rivers should be fully considered and multi-objective ecological dispatch of reservoirs should be implemented. On basis of the traditional particle swarm optimization (PSO), the improved PSO with adaptive random inertia weights (ARIW) is proposed to deal with the problem of ecological optimal operation of reservoir in the paper. According to the evolutionary process, based on the probability distribution density function of triangle, the inertia weight can be adjusted randomly and adaptively to meet the global or local optimization requirements. By typical mathematical function, the improved PSO algorithm is compared with traditional PSO and genetic algorithm (GA), and is proved to be more efficient and accurate. Taking Panjiakou Reservoir on the main stream of Luanhe River in China as an example, the multi-objective ecological optimal dispatch of reservoir has been analysed and calculated with the improved PSO algorithm under different target years, considering flood control, water supply, and ecological demand. The research results can provide reference for developing rationally Luanhe River water resources, and making scientifically ecological dispatch plan of Panjiakou reservoir.

INTRODUCTION

River ecosystem is one of the most important ecosystems for human survival. A healthy river ecosystem has stability and sustainability, and has a good ability for adjusting and restoring under the external pressure and disturbance. It can provide many ecosystem services such as water, food and transportation for human production and living (Zhang et al. 2015, Hao et al. 2014). However, when the rivers contribute to the development of human society, they have also been damaged. Water resources depletion, water quality deterioration and other problems are widespread in China. It is urgent to protect river ecosystems. It is an important measure to carry out reservoir ecological dispatch to guarantee river ecosystem health.

In the past, various researchers applied a series of typical methods such as linear programming, nonlinear programming, dynamic programming, etc., to solve multipurpose reservoir operation problems (Zhao et al. 2014, Zhao et al. 2011, Liu et al. 2011). In fact, reservoir system is a complex and non-linear system, and the problems of multipurpose reservoir operation are far more complex than for single object regulation. In spite of improvement of these traditional algorithms, it is difficult to achieve satisfied performance for such a reservoir system with traditional optimization methods. Generally, the problems of multipurpose reservoir operation that have nonconvexities in domain and nonlinear relationships in objectives and constrains are complex, and the linear programming method is not fit. Dynamic programming and stochastic dynamic programming have been applied into many fields including optimal operation of reservoir, but these approaches face the problem of the dimensionality disaster. As far as traditional nonlinear programming is concerned, slow convergence rate and large amounts of calculation time are the shortage of the method. In addition, nonlinear programming easily falls into local optimal solutions (Bai et al. 2015, Huang et al. 2004).

In recent years, many heuristic algorithms have been applied into optimization. By the evolution techniques, the optimal problem can be treated better and described more realistically. Some optimal models and algorithms, which

are easy in handling the nonconvex and nonlinear relationship, are provided. In the multiple dimension optimization calculation categories, genetic algorithm (GA) (Goldberg et al. 1989) and particle swarm optimization (PSO) (Eberhart et al. 1995) are used widely, and some operation models of reservoir are established base on these algorithms. For example, Oliveira & Loucks (1997) derived multi-reservoir operation rules based on genetic algorithms. Wardlaw & Sharif (1999) made a study of alternative formulations of GA for reservoir. Chen et al. (2008) established the large scale system model based on particle swarm optimization to optimal allocation of water resources in irrigation areas. Chang et al. (2010) developed the modified adaptive PSO to deal with optimal operation of hydropower station. Yang et al. (2016) proposed the Multi-objective operating rules for Danjiangkou reservoir in China under climate change. Chang et al. (2013) employed the PSO and GA as tools to research the optimization of water resources utilization. Swarm intelligence algorithms or evolutionary algorithms (Cheng et al. 2012), such as GA and PSO, have become popular in the optimal operation and improved management of reservoir system.

According to the new mechanism, the model of PSO with adaptive random inertia weights (ARIW) is applied into solving problems for multipurpose reservoir system. To test the usefulness of PSO with ARIW, it is tested firstly by the Rastrigin function that is the one of classic nonlinear functions. To show the practical utility, operation model for reservoir based on PSO with ARIW is then applied into an existing reservoir, namely the Panjiakou reservoir in Hebei Province, China.

PARTICLE SWARM OPTIMIZATION

Traditional Particle Swarm Optimization

The swarm intelligence, which is used to describe algorithms and distributed solutions, is inspired by the collective behaviour of animals and insects. PSO is a kind of swarm intelligence technology for deal with multiple dimension optimal problems. In 1995, Eberhart and Kennedy originally put forward the particle swarm optimization algorithm, which is inspired by the social behaviour of bird flock in catching food process (Shi et al. 1998). PSO is like other evolutionary methods in some aspects, such as GA. PSO is initialized by generating randomly many feasible solutions, which are described by vectors. By a given heuristic rule, the parent population will be evolving to new generation, and search for optimum by updating generations. Different algorithm has different heuristic rule. In contrast to GA, the basic PSO has not genetic operators which are applied to generate a new generation of candidate solutions. The evolution is driven by the exchange of information between individuals and population. In evolution process, each particle adjusts its velocity to its own previous best position and towards the best position attained by all particle's trajectories. It will be easy to deal with the optimal problem of nonlinearity and nonconvexity with the standard PSO.

Suppose that the search space is n dimensional, the i^{th} feasible solution called particle is described by n dimensional vector, $X_i = (x_{i1}, x_{i2},\ldots, x_{in})$. The previous best position of the i^{th} particle is represented as $XP_i = (xp_{i1}, xp_{i2},\ldots, xp_{in})$, which corresponds to the individual optimum P. The best particle in the swarm is denoted as $XG_i = (xg_{i1}, xg_{i2},\ldots, xg_{in})$, which corresponds to the popular optimum G. The velocity that represents the change of particle is denoted as $V_i = (v_{i1}, v_{i2},\ldots,v_{in})$. The superscripts of variants represent the iteration number, and the evolution of swarm is manipulated as follows:

$$v_{id}^{k+1} = wv_{id}^{k} + c_1 r_1 (xp_{id}^{k} - x_{id}^{k}) + c_2 r_2 (xg_{d}^{k} - x_{id}^{k}) \quad \ldots(1)$$

$$x_{id}^{k+1} = x_{id}^{k} + v_{id}^{k+1} \quad \ldots(2)$$

Where $d = 1,2,\ldots,n$; $i = 1,2,\ldots,N$; N is the size of the particle swarm; w is inertial weight; c_1 and c_2 are positive constant parameters, generally let $c_1 = c_2 = 2.0$; r_1, r_2 are random numbers, which subject to uniform distribution in [0,1]; and k is iteration number.

By equation (1) and (2), each particle will oscillate in the feasible region (search space), between its own previous best position and the best solution of swarm, attempting to reach the new optimal position in its trajectory. In order to avoid escaping the constrains space in updating process because of the fast velocity, in evolution process, restricting the velocity of each particle into an interval, $|v_{id}| \le v_{\max}$, $v_{\max}$ is the maximum speed, which can be obtained by trial. The inertia weight w is to control the impact of local and global searching ability. A large inertia weight facilitates global search, while small inertia is helpful to local exploration. It is very important to select suitable value of inertia weight w for reduction of iteration times and optimal effect. The standard PSO usually uses the strategy of linear decreasing weight (LDW) for regulation weight of particle (Shi et al. 1998) as follows:

$$w^k = (w_{ini} - w_{end})(K_{\max} - k) / K_{\max} + w_{\text{end}} \quad \ldots(3)$$

Where, k is the iteration number; $K_{\max}$ is the maximal iteration number; w^k is the inertia weight after iteration of k times; w_{ini} is the initial inertia weight of particle; w_{end} is the inertia weights corresponding to the iteration number $K_{\max}$. Even though PSO is faster than other evolutionary algorithms in searching optimal solution, it faces still premature convergence and poor fine-tuning capability of the final solution. Using the LDW strategy, in the early evolutionary phases,

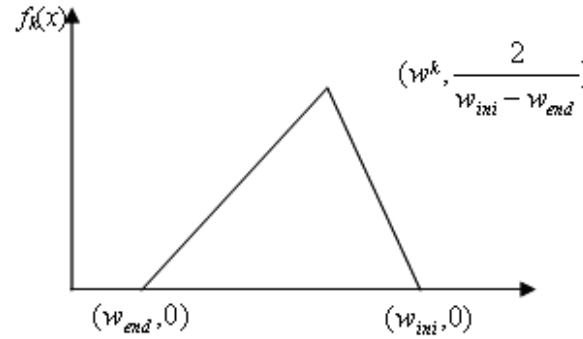

Fig. 1: Probability density of random inertial weights.

particle attends to fall into local optimum as small inertia weight, while particle may miss the optimal solution because of poor fine-tuning results from large inertia weight.

PSO Algorithm with Adaptive Random Inertia Weights

The inertia weight is randomly generated by triangle probability distribution density function. The distribution density function is updated automatically with the evolution. In the early searching phases, the possibility of achieving the larger weight values is great to facilitate global search. With the increase of the iteration number, the probability of attaining the smaller weight values will get great, tending to facilitate local exploration.

The w^k is calculated using formulation (3), $k = 0,1,2,\ldots, K_{\max}$-1, and the probability distribution density function can be established by linking the points (w_{ini}, 0), (w_{end}, 0), (w^k, $2/(w_{ini} - w_{end})$) to get a triangle, whose area equals 1 exactly. When $k = 0$, the triangle is an instructing triangle. The figure of probability distribution density function is shown as Fig. 1.

The probability distribution function can be deduced by distribution density function. Suppose that $F_X(x)$ is the distribution function of random variable X, and random variable U subjects to uniform distribution in [0,1], then

$$X = F_X^{-1}(U) \qquad \ldots(4)$$

It is easy to generate a series of random numbers by computer program, $u_1, u_2, \ldots, u_m$, which subject to uniform distribution in interval from 0 to 1. Random numbers of random variable X can be achieved as follows:

$$x_i = F_X^{-1}(u_i) \qquad i = 1,2,\cdots,m \qquad \ldots(5)$$

The step-by-step process of PSO with ARIW is demonstrated as below:

Step 1 (Initialization of particles): The initial position of all the particles is produced randomly within the limits of each component of vector that represents one particle. Velocity vector for each particle is generated randomly. Each particle of swarm is initialized with random position vectors X^0_i, and random velocity vectors V^0_i.

Step 2 (Calculation of fitness degree): The fitness degree y_i of each particle is calculated by the given objective function. According to the fitness degree, initial personal best value P_i and global best value G are picked out.

Step 3 (Updating the personal best value): Comparing y_i with the current personal best P_i, the new personal is updated. If the best fitness degree of the i^{th} particle is better than the current P_i, then P_i is to be changed to the fitness degree of the i^{th} particle and this particle is as the current personal optimal solution XP_i.

Step 4 (Updating the global best value): It is similar to calculate the personal best value. If the best fitness value of a particle in the swarm is better than the current G, then G is to be changed to the value of searching point of the corresponding particle contributing to the best fitness degree. The particle corresponding to the G is updated as the new global optimal solution XG.

Step 5 (Calculation of random inertia weight): By generating m random numbers subject to uniform in [0,1] and using above equations, inertia weight of each particle is evaluated.

Step 6 (Modification of each particle): The searching point of each particle is updated by equations (1) and (2).

Step 7 (Termination criteria): steps 2 to 6 are repeated until either the pre-set iteration maximum is reached or the calculation accuracy is satisfied.

Test of PSO with ARIW

Rastrigin function is multimodal function that has many local minima. The global minimum that equals 0 is located in the

position $X^* = (0,0,..,0)$. Rastrigin function with n dimension is described as follows:

$$f(X) = \sum_{d=1}^{n} (x_d^2 - 10\cos(2\pi x_d) + 10) \qquad -5.12 < x_d < 5.12 \qquad \ldots(6)$$

In this paper, suppose that the test functions are 10 dimensional; size of the swarm is N=30; the maximal velocity is 10; PSO other parameters c_1=c_2=2.0, w_{ini}=0.9, and w_{end}=0.4. In order to compare the performance for the PSO with ARIW, standard PSO with LDW and GA, three testing methods are suggested. Firstly, on the condition of the given calculation accuracy, compare the number of iterations. In the paper, number of iterations is K_{max}=10000, and models will be run for 100 trials. The average of iteration numbers is taken as the index to evaluate efficiency in different methods. Secondly, giving the maximal evolutionary generations, analyse the calculation accuracy in different algorithms. At last, on the condition of the same parameters and accuracy, calculate and compare the probability of achieving to the global optimum by 100 trials.

According to the given parameters, probability distribution function and corresponding density function, which are used to generate random inertia weight, are evaluated as follows:

$$F_0(x) = \begin{cases} 0 & x \le 0.4 \\ 4(x-0.4)^2 & 0.4 < x \le 0.9 \\ 1 & x > 0.9 \end{cases} \qquad \ldots(7)$$

$$F_0^{-1}(x) = 0.4 + 0.5\sqrt{x} \qquad 0 \le x \le 1 \qquad \ldots(8)$$

$$F_k(x) = \begin{cases} 0 & x \le 0.4 \\ \dfrac{2}{w^k - 0.4}x^2 - \dfrac{1.6}{w^k - 0.4}x + \dfrac{0.32}{w^k - 0.4} & 0.4 < x \le w^k \\ -\dfrac{2}{0.9 - w^k}x^2 + \dfrac{3.6}{0.9 - w^k}x - \dfrac{w^k + 0.72}{0.9 - w^k} & w^k < x \le 0.9 \\ 1 & x > 0.9 \end{cases} \qquad \ldots(9)$$

$$F_k^{-1}(x) = \begin{cases} 0.4 + \sqrt{0.5x(w^k - 0.4)} & 0 \le x \le 2(w^k - 0.4) \\ 0.9 - \sqrt{0.5(1-x)(0.9 - w^k)} & 2(w^k - 0.4) \le x \le 1 \end{cases} \qquad \ldots(10)$$

Where, k=1,2,…,K_{max}-1.

The test results by three methods are presented in Table 1 and Table 2.

The data in these tables show clearly that the PSO with ARIW can reach the best solution, with least number of function evaluations and higher precision as compared to other models. The detailed discussion is following:

(1) It is very clear to know that the PSO with ARIW in performance is better than other algorithms, by three different testing methods, according to the results of Tables 1 to 2. Particularly, when the accuracy demanded is same, the number of iterations calculated by ARIW mechanism is much less than the calculation number by LDW. Algorithm based on the ARIW mechanism can automatically regulate suitable weight for each particle, by the evolution process.

(2) The best results calculated by PSO with ARIW in 100 trials are picked out. For Rastrigin function, the best solution is X^* = 3.586×10^{-10}, 4.732×10^{-11}, -4.675×10^{-10}, -4.321×10^{-10}, -5.794×10^{-10}, 3.635×10^{-11}, 4.299×10^{-10}, 9.017×10^{-11}, 4.118×10^{-10}, 4.711×10^{-11}), and the global minimum is $f(X^*)$ = 0.0000. By comparing with theory optimum of testing functions, the calculation outcomes are satisfied.

APPLICATION OF THE IMPROVED PSO

Introduction of Panjiakou Reservoir

To calculate the practical effect of the proposed model, an existing reservoir, namely Panjiakou Reservoir, was taken up as a case study. The Panjiakou Reservoir is in the mainstream of the Luanhe River, in Hebei province, China. The reservoir has the total storage capacity of 29×10^8 m^3 and the water-spread area at full reservoir level is about 70 km^2. The Panjiakou Reservoir is multipurpose and serves for flood control, water supply, hydropower generation and ecological water demand of river. In these served objects, hydropower generation subjects to water supply. Only during the process of water supply, hydropower is generated according to the discharge and water level of the reservoir. The detailed information related to regulation of Panjiakou Reservoir is described below:

(1) The process of water demand: The primary areas of water supply from Panjiakou Reservoir are Tianjian and

Table 1: Comparison of evolution generations among different methods at certain accuracy.

Accuracy	GA	LDW	ARIW
1	6645	5794	4718

Table 2: Comparison of accuracy among different methods at certain evolution generations.

Iterations number	GA	LDW	ARIW
2000	2.8465	2.7173	2.4844

Tangshan, which are the important cities. According to the data of actual monthly water supply from 1983 to 2002, the averages of monthly water supply for many years are evaluated as given in Table 3.

(2) The ecological water demand of Luanhe River: In the paper, ecological water demand of each month was evaluated using Tennant methods, considering ecological base flow, the river evaporation and water leakage and so on. The monthly ecological water demand is calculated as given in Table 4.

(3) Rules of flood control of Panjiakou Reservoir: In major flood period (21 July~15 August), if the water level of reservoir is below 216 m, the main task is storing water, with ensuring the water demand of downstream; while the water level is between 216 to 222 m, reservoir discharges flood steadily by the 10000 m^3/s; when the water level is in the interval from 222 to 225 m, the release of reservoir is controlled by the 28000 m^3/s; and while the water level is beyond 225 m, all flood discharge facilities of reservoir are opened entirely.

In later flood season (16 August~30 September), the water level raised gradually to 222 m from 16 August to 31 August, and the highest water level of reservoir can be controlled in 225 m from 1 September to 30 September.

(4) Water leakage and evaporation of reservoir: By observation and experience of many years for Panjiakou Reservoir, the water leakage and evaporation can be estimated to be about 16.4 $\times 10^4$ m^3 every day.

Mathematical Model Formula

The two objectives considered in the model are minimization of the deficits for water supply and ecological water of river, and the regulation rules of flood control are taken as one of the constraints. Because of the limitation of water storage in reservoir, the two objectives are conflicting. To handle these multipurpose, a weighted approach is adopted in this study. By giving the weights to the objects, multipurpose problem is transferred to single objective question. The object function is following:

$$\text{ob} = \min(a \cdot f(x_1,x_2,\cdots,x_m) + b \cdot g(y_1,y_2,\cdots,y_m)) \quad \ldots(11)$$

Where, $f(x_1,x_2,\cdots,x_m)$ is object of water supply, which reflects the comprehensive extent of water deficits for water supply, and is calculated by the following equation.

$$f(x_1,x_2,\cdots,x_m) = \sqrt{\sum_{i=1}^{m}(x_i - w_i)^2} \quad \ldots(12)$$

Where, x_i is the actual water supply of each calculation period (10^8 m^3); w_i is the water demand of each period (10^8 m^3); and m=18, is the number of calculation periods. From July to September, the length of calculation period is 10 days, and the rest calculation periods are evaluated by the interval of a month. $g(y_1,y_2,\ldots,y_m)$ is the ecological water object, reflecting the integral deficits extent of ecological water, and is evaluated as follows:

$$g(y_1,y_2,\cdots,y_m) = \sqrt{\sum_{i=1}^{m}(y_i - s_i)^2} \quad \ldots(13)$$

Where, y_i is the actual water released to the river in each calculation period (10^8 m^3); s_i is the ecological water demand of river in each period (10^8 m^3); the number of calculation periods m=18. a, b are the weight coefficients, represent the importance of object s for decision maker subject to the following constrains:

(1) Water level of reservoir:

$$Z_{\min,i} \le Z_i \le Z_{\max,i} \quad \ldots(14)$$

Where, Z_i is water level of the i^{th} calculation period (m); $Z_{\min,i}$ is the allowed lowest water level (m); $Z_{\max,i}$ is the allowed highest water level (m).

(2) Discharge limits:

$$0 \le x_i \le w_i \quad 0 \le y_i \le q_{\max} \quad \ldots(15)$$

Where, $q_{\max}$ is the discharge capacity of each period (10^8 m^3).

(3) Mass balance equation:

$$V_{t+1} - V_t = (Q_t - q_t) \cdot \Delta t \quad \ldots(16)$$

Where, V_{t+1} is the reservoir storage in the end of period (10^8 m^3); V_t is the reservoir storage in the beginning

Table 3: Average of monthly water supply (108 m3) from Panjiakou Reservoir.

Month	1	2	3	4	5	6
Water	0.35	0.07	0.91	0.53	1.13	1.12
Month	7	8	9	10	11	12
Water	0.40	0.48	0.84	0.49	0.54	0.72

Table 4: Ecological water demand of Luanhe River (10^8 m^3).

Month	1	2	3	4	5	6
Water	0.178	0.19	0.312	0.337	0.208	0.38
Month	7	8	9	10	11	12
Water	1.76	2.424	0.988	0.551	0.363	0.23

of period (10^8 m^3); Q_t is the inflows average during the period (m^3/s); q_t is the release average during the period (m^3/s); Δt is the length of calculation period.

(4) Rules of flood control: In flood season, reservoir regulations obey the rules of flood control.

Regulation Results

According to historical data of the inflows of Panjiakou Reservoir, three typical years were chosen, which respectively represent the low flow year, normal flow year and high flow year, and the periods corresponding to typical years are July 1981 to June 1982, July 1993 to June 1994, and July 1994 to June 1995. The multipurpose ecological regulation model of Panjiakou Reservoir is solved using PSO with ARIW, for three typical years.

(1) Low flow year: The inflows of Panjiakou reservoir in low flow year are given in Table 5.

The initial water level that is also the allowed lowest level during regulation was 164.48 m, which was achieved by the end water level of reservoir in 30 June, 1981. Let the weight of water supply object=0.9, the weight of the object for ecological water=0.1. By PSO with ARIW, the regulation results of Panjiakou Reservoir are as given in Table 6.

Water deficits of each month are shown Figs. 2-3.

(2) Middle flow year: The inflows of Panjiakou Reservoir in middle flow year are presented in Table 7.

The initial water level that is also the allowed lowest level during regulation is 208.73 m, which is achieved by the end water level of reservoir on 30 June, 1993. Weights of the objects are same with values of low flow year, respectively. The regulation results of Panjiakou Reservoir are as given in Table 8.

Water deficits of each month in middle flow year are shown in Figs. 4-5.

(3) High flow year: The inflows of Panjiakou Reservoir in high flow year are as given in Table 9.

The initial water level that is also the allowed lowest level during regulation is 213.13 m, which is achieved by the end water level of reservoir on 30 June, 1995. Weights of tow objects are same with values of low flow year, middle flow year. Using the improved PSO to solve the regulation model of Panjiakou Reservoir, results are as given in Table 10.

According to the calculation results for three typical years, it is easy to draw the following conclusions: In high flow year, by optimal regulation for Panjiakou Reservoir, the requirement of water supply can be fulfilled, and the

Table 5: Inflows of Panjiakou Reservoir in low flow year.

No.	Period	Water (10^8 m^3)
1	Early July	0.1520
2	Middle July	0.2220
3	Late July	0.5830
4	Early August	0.1587
5	Middle August	0.2546
6	Late August	0.2805
7	Early September	0.2297
8	Middle September	0.3030
9	Late September	0.3887
10	October	0.7727
11	November	0.4821
12	December	0.3026
13	January	0.2268
14	February	0.2658
15	March	0.5704
16	April	0.6286
17	May	0.3537
18	June	0.8303

Table 6: Regulation results of Panjiakou Reservoir in low flow year.

Period	Water supply (10^8 m^3)	Ecological water (10^8 m^3)	Water level (m)
Early July	0.1290	0.0066	164.4800
Middle July	0.1290	0.0766	164.4800
Late July	0.1419	0.4230	164.4800
Early August	0.1423	0.0000	164.4800
Middle August	0.1548	0.0834	164.4800
Late August	0.1703	0.0921	164.4800
Early September	0.2133	0.0000	164.4800
Middle September	0.2800	0.0066	164.4800
Late September	0.2800	0.0923	164.4800
October	0.2727	0.0208	168.6631
November	0.3793	0.0800	168.4064
December	0.4200	0.0217	166.5753
January	0.0205	0.0113	167.9942
February	0.0335	0.0728	169.0675
March	0.6875	0.0451	167.0107
April	0.1882	0.0555	170.1893
May	0.7393	0.0057	165.9912
June	0.8899	0.0465	164.4800

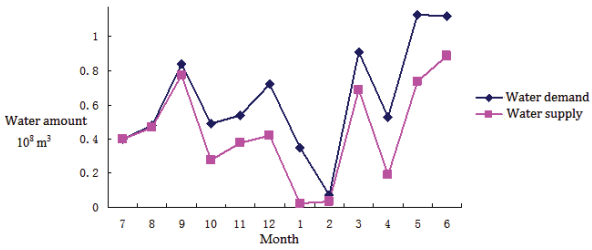

Fig. 2: Water deficit of each month in low flow year.

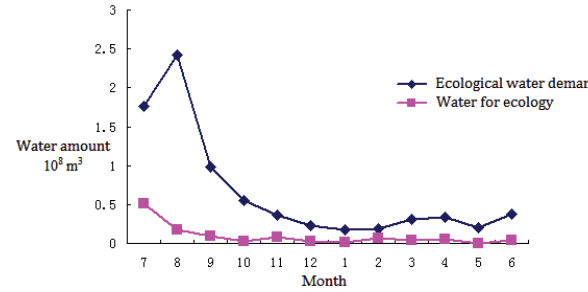

Fig. 3: Ecological water deficit of each month in low flow year.

Table 7: Inflows of Panjiakou Reservoir in middle flow year.

No.	Period	Water (10^8 m^3)
1	Early July	0.5235
2	Middle July	1.8023
3	Late July	2.2656
4	Early August	3.6091
5	Middle August	2.5993
6	Late August	1.2993
7	Early September	0.6274
8	Middle September	0.8672
9	Late September	0.5012
10	October	1.3479
11	November	0.9953
12	December	0.566
13	January	0.4085
14	February	0.4302
15	March	0.6186
16	April	1.0012
17	May	0.822
18	June	0.3161

Table 8: Regulation results of Panjiakou Reservoir in middle flow year.

Period	Water supply (10^8 m^3)	Ecological water (10^8 m^3)	Water level (m)
Early July	0.1290	0.3781	208.7300
Middle July	0.1290	1.6568	208.7300
Late July	0.1419	2.1057	208.7300
Early August	0.1548	3.4379	208.7300
Middle August	0.1548	2.4281	208.7300
Late August	0.1703	1.1109	208.7300
Early September	0.2800	0.3310	208.7300
Middle September	0.2800	0.5708	208.7300
Late September	0.2800	0.2048	208.7300
October	0.4057	0.1094	210.3341
November	0.4953	0.0953	210.9975
December	0.6104	0.0929	210.6496
January	0.2789	0.0593	210.6890
February	0.0561	0.0524	211.1973
March	0.9006	0.1893	210.2263
April	0.4742	0.0233	211.0741
May	1.0036	0.0562	210.5387
June	1.0856	0.0746	208.7300

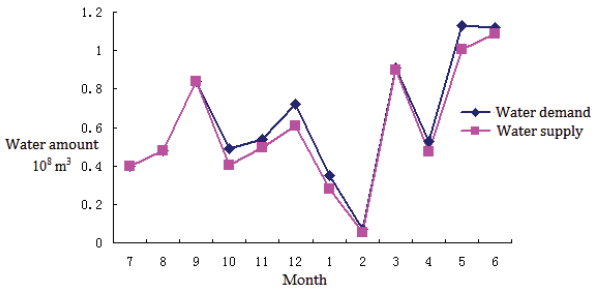

Fig. 4: Water deficit of each month in middle flow year.

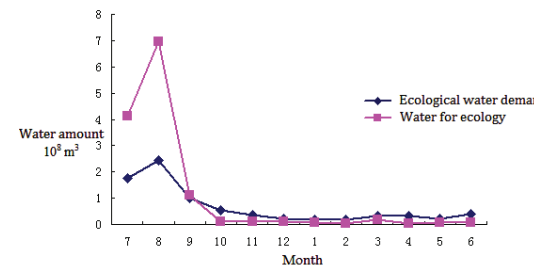

Fig. 5: Ecological water deficit of each month in middle flow year.

Table 9: Inflows of Panjiakou Reservoir in high flow year.

No.	Period	Water (10^8 m^3)
1	Early July	0.3393
2	Middle July	0.5319
3	Late July	3.0473
4	Early August	5.9128
5	Middle August	1.8991
6	Late August	1.5059
7	Early September	1.0206
8	Middle September	0.6249
9	Late September	1.0583
10	October	2.6076
11	November	1.4466
12	December	0.7827
13	January	0.5594
14	February	0.4284
15	March	0.7688
16	April	0.9787
17	May	0.5485
18	June	0.9722

Table 10: Regulation results of Panjiakou Reservoir in high flow year.

Period	Water supply (10^8 m^3)	Ecological water (10^8 m^3)	Water level (m)
Early July	0.1290	0.1938	213.1300
Middle July	0.1290	0.3864	213.1300
Late July	0.1419	2.8874	213.1300
Early August	0.1548	5.7416	213.1300
Middle August	0.1548	1.7278	213.1300
Late August	0.1703	1.3175	213.1300
Early September	0.2800	0.7242	213.1300
Middle September	0.2800	0.3285	213.1300
Late September	0.2800	0.7619	213.1300
October	0.5510	0.4900	215.8820
November	0.3630	0.5400	216.7286
December	0.230	0.7200	216.3578
January	0.1780	0.3500	216.3274
February	0.1900	0.0700	216.5315
March	0.3120	0.9100	215.6712
April	0.3370	0.5300	215.7782
May	0.2080	1.1300	214.2832
June	0.3800	1.1200	213.2067

ecological water demand can be satisfied. Ecological water deficits are happened only in few periods in flood season. In these periods of deficit, as the inflows are less than ecological water demand, release flood by the inflow amount to keep current water level; in middle flow year, by regulation, the water needs in season can be mainly met, but water supply is lacking in non-flood season; in low flow year, water demands cannot be satisfied whether water supply or ecological water. By optimal calculation using improved PSO, the extent of water deficits will be flatted to reduce the destructions deriving from water shortage.

ACKNOWLEDGEMENTS

This work was supported by the Key Scientific and Technological Research Projects in Henan Province (Grants No. 192102110199).

REFERENCES

Bai, T., Wu, L.Z., Chang, J.X. and Huang Q. 2015. Multi-objective optimal operation model of cascade reservoirs and its application on water and sediment regulation. Water Resour. Manage., 29(3): 2751-2770.

Chang, J.X., Meng X.J. and Wang Z.Z. 2014. Optimized cascade reservoir operation considering ice flood control and power generation. J. Hydrol., 519: 1042-1051.

Chang, J.X., Bai, T. and Huang Q. 2013. Optimization of water resources utilization by PSO-GA. Water Resour. Manag., 27(4): 3525-3540.

Chang, L.C. and Chang F.J. 2009. Multi-objective evolutionary algorithm for operating parallel reservoir system. Journal of Hydrology, 377: 12-20.

Chang, L.C., Chang, F.J. and Wang, K.W. 2010. Constrained genetic algorithms for optimizing multi-use reservoir operation. J. Hydrol., 390: 66-74.

Chen, X.N., Duan, C.Q., Qiu, L. and Huang, Q. 2008. Application of large scale system model based on particle swarm optimization to optimal allocation of water resources in irrigation areas. Transactions of the CSAE, 24(3): 103-106.

Cheng, C.T., Shen, J.J. and Wu, X.Y. 2012. Short-term hydroscheduling with discrepant objectives using multi-step progressive optimality algorithm. J. Am. Water Resour. Assoc., 48(3): 464-479.

Eberhart, D.E. and Kennedy, J. 1995. A new optimizer using particle swarm theory. In: Proc., 6th Symp. on Micro Machine and Human Science, IEEE Service Center, Piscataway, N.J.. 39-43.

Goldberg, D.E. 1989. Genetic Algorithms in Search, Optimization, and Machine Learning. Addison-Wiley, Reading, N.Y.

Hao, L.X., Sun, R.H. and Chen, L.X. 2014 Health assessment of river ecosystem in Haihe River Basin, China. Environmental Science, 35(10): 3692-3710.

Huang, W.C. and Yuan, L.C. 2004. A drought early warning system on real-time multi-reservoir operation. Water Resour. Res., 40(6): W06401.

Liu, P., Cai, X.M. and Guo, S.L. 2011. Deriving multiple near-optimal solutions to deterministic reservoir operation problems. Water Resour. Res., 47: W08506.

Oliveira, R. and Loucks, D.P. 1997. Operating rules for multi-reservoir systems. Water Resour. Res., 33(4): 839-852.

Shi, Y. and Eberhart, R.C. 1998. A modified particle swarm optimizer. In: Proceedings of the 1998 IEEE International Conference on Evolutionary Computation, IEEE Press. Pp. 69-73.

Wardlaw, R. and Sharif, M. 1999. Evaluation of genetic algorithms for optimal reservoir system operation. Water Resour. Planning Manage., 125(1): 25-33.

Yang, G., Guo, S.L., Li, L.P., Hong, X.J. and Wang, L. 2016. Multi-objective operating rules for Danjiangkou reservoir under climate change. Water Resour. Manage., 30: 1183-1202.

Zhao, T.T.G. and Zhao, J.S. 2014. Improved multiple-objective dynamic programming model for reservoir operation optimization. Journal of Hydroinformatics, 16(5): 1142-1157.

Zhao, J.S., Cai, X.M. and Wang, Z.J. 2011. Optimality conditions for a two-stage reservoir operation problem. Water Resour. Res., 47: W08503

Zhang, Y.Z., Huang, W.D. and Wang, Z.Y. 2015. Evaluation of aquatic ecosystem health in Aojiang Basin, Fujian Province. Journal of Lake Science, 27(6): 1079-1086.

Zheng, J., Yang, K. and Ni, F.Q. 2013. Research on overall improved genetic algorithm applied in optimal operation. J Hydra. Eng., 44(2): 205-211.

Nature Environment and Pollution Technology
An International Quarterly Scientific Journal

p-ISSN: 0972-6268
e-ISSN: 2395-3454

Vol. 19 | No. 1 | pp.123-132 | 2020

Original Research Paper | Open Access

Macroscopic Factors Decomposition of Methane Emissions from Livestock Based on the Empirical Analysis of 31 Provinces in China

Wenjie Yao*† and Huili Wang**

*Research Institute of Water Culture and Resources Economy, Zhejiang University of Water Resources and Electric Power, Hangzhou, 310018, China

**School of Economy and Management, Zhejiang University of Water Resources and Electric Power, Hangzhou, 310018, China

†Corresponding author: Wenjie Yao

Nat. Env. & Poll. Tech.
Website: www.neptjournal.com

Received: 16-05-2019
Accepted: 22-07-2019

Key Words:
Methane emissions
Livestock
Factor decomposition
Population

ABSTRACT

This paper builds a factor decomposition model of methane emissions from livestock from the three dimensions of technology, economy and population, by using the panel data covering 31 provincial regions in China during 2003-2016, and aims to reveal the macroscopic causes of methane emissions from livestock. The research shows that technical, economic and population factors of methane emissions from livestock have diminishing marginal contribution. The methane emissions from intestinal fermentation is mainly restricted by livestock's physiological structure. Following increase or decrease of livestock feeding quantity, it changes with a relatively stable parameter and has little controllability. Methane emissions from faecal management is limited little by livestock's physiological structure and it is largely controllable. The government should increase technical input to reduce methane emission factors of livestock, deal with livestock manure through resource utilization, and reduce raising scale by using a certain market mechanism in due course.

INTRODUCTION

Since the beginning of the new century, animal husbandry, as the most dynamic pillar industry in China's agricultural economy, has achieved rapid development again with increasing policy support. According to China Statistical Yearbook (2017), by 2016, the output value of animal husbandry in China (excluding Taiwan, Hong Kong and Macao) had accounted for 28.3% of the total agricultural output value and 4.2% of the total GDP. At the end of the year, the stock of cattle, goats and sheep had reached 106.679 million head, 139.769 million head and 161.351 million head respectively, and the number of pigs kept and raised had reached 435.037 million and 685.02 million respectively. However, the rapid growth of animal husbandry inevitably brought about some environmental problems, especially the emissions of carbon dioxide, methane, nitrous oxide and other greenhouse gases that cause global warming. Livestock accounts for an estimated 18 percent of global greenhouse gas emissions (Fao 2006). Methane contributes 15 percent of global warming to greenhouse gases (Dui 2003), and although it emits less overall than carbon dioxide, the greenhouse effect of the same volume is 20 to 25 times that of carbon dioxide (Shengli et al. 2010). Methane emissions from livestock mainly come from intestinal fermentation and faecal management (Chianese et al. 2009). With the substantial increase of livestock feeding quantity, methane emissions from livestock also increases year by year. According to statistics, global methane emissions were 5.5×10^8 tons, while livestock methane emissions were 8.5×10^7 tons, accounting for 15.5% (Mcginn et al. 2006), and cattle and sheep were the largest emitters. In China, methane emissions from livestock that are fermented in the gut alone account for 29.7 percent of total methane emissions, excluding those from manure management (Renhua 2010). Therefore, it is extremely urgent for China to establish low-carbon production mode of animal husbandry and promote energy conservation and emission reduction to cope up with climate change.

Carbon dioxide emissions have been paid great attention by researches on greenhouse gas emissions that cause climate change. In spite of this, still some scholars remain highly alert to persistent warming caused by methane emissions from livestock. Taking cows, sheep and other major methane emitters as research objects, many workers analysed the biological and chemical mechanism of methane emissions from intestinal fermentation and faecal management, calculated the corresponding emission factors by various methods, and finally proposed scientific methods to curb methane

emissions from livestock at the micro level (Bo et al. 2009, Min et al. 2013, Zhi et al. 2017, Yunlong et al. 2018). Some scholars, like Jing et al. (2012) after subdividing the livestock categories, found that the number of pigs, cows, sheep and other livestock had a significant impact on methane emissions through regression analysis of the number of livestock raised in China in the past 20 years, so as to determine the reasonable path for the low-carbon development of animal husbandry in China. At the macro level, however, what causes methane emissions from livestock? How to combine the micro-level scientific methods to control methane emissions from livestock for effective policy regulation? To these questions, the existing literature so far has little discussion. Therefore, we used panel data of 31 provinces in China from 2003 to 2016 to construct decomposition models from three dimensions of technology, economy and population, aiming at revealing the cause of methane emissions of livestock, to supplement the strength of macro explanation in addition to micro explanation. This is of great significance for China to improve the efficiency of livestock breeding, optimize the strategy of reducing greenhouse gas emission and promote the sustainable development of animal husbandry.

MATERIALS AND METHODS

Econometric Model

The study on the decomposition of factors influencing environmental variation began with the IPAT model proposed by Ehrlich P. R. and Holdren J. P. The basic form of this model is as follows:

$$I = P \cdot A \cdot T \quad \ldots(1)$$

Here, I, P, A and T respectively stand for environmental indicator, population indicator, economic indicator and technical indicator. The combination of population and economy will cause great environmental pressure, which must be alleviated through technical adjustment. Later, in order to facilitate empirical analysis, Yorker et al. (2002) proposed the following STIRPAT model based on IPAT model.

$$I = a \cdot P^b \cdot A^c \cdot T^d \cdot \mathrm{m} \quad \ldots(2)$$

Here, a represents constant term, b, c, d are the exponents of P, A, T, and μ represents error term.

So far, both the models have been widely used, mainly focusing on the decomposition of the influencing factors of carbon emission (Ang et al. 1998, Zhang 2000, Poumanyvong & Kaneko 2010, Qiang et al. 2012, Xiao & Yaohui 2012, Zhangqi et al. 2018) and industrial emission (Nan & Weiyang 2016, Ling et al. 2017), but empirical analysis of agricultural non-point source pollution (Yuzhuo et al. 2017, Yigen et al. 2017) is rare. Based on the existing empirical studies, we will decompose and investigate the influencing factors of methane emissions from livestock based on the two models. Firstly, according to equation (1), the decomposition form of influencing factors of methane emissions from livestock is set as below:

$$M = \frac{M}{A_n} \cdot \frac{A_n}{A_g} \cdot \frac{A_g}{Y} \cdot \frac{Y}{P} \cdot P \quad \ldots(3)$$

Here, M is methane emissions from livestock, A_n is animal husbandry output value, A_g is total agricultural output value, Y is total output value, and P is population. We set M (methane emissions from livestock) as an environmental indicator, $MPA = M/A_n$ (methane emissions from livestock per unit animal husbandry output value) as a technical indicator, $AAP = A_n/A_g$ (proportion of animal husbandry output value in total agricultural output value) and $AGP = A_g/Y$ (proportion of total agricultural output value in total output value) as economic structure indicators, $PGDP = Y/P$ (per capita total output value) as an economic scale indicator, and $POP = P$ (population) as a population indicator. Secondly, according to equation (2), the decomposition form of influencing factors of methane emissions from livestock can be further obtained as follows:

$$M = \mathrm{a}_0 \cdot MPA^{\mathrm{a}_1} \cdot AAP^{\mathrm{a}_2} \cdot AGP^{\mathrm{a}_3} \cdot PGDP^{\mathrm{a}_4} \cdot POP^{\mathrm{a}_5} \cdot \mathrm{d} \quad \ldots(4)$$

Here, a_0 is a constant term, a_1, a_2, a_3, a_4, a_5 are the indices of MPA, AAP, AGP, $PGDP$, POP, respectively, and d is a random error. After taking the logarithm form of both sides of the equal sign, equation (4) is changed into as below:

$$\ln M = \ln \mathrm{a}_0 + \mathrm{a}_1 \ln MPA + \mathrm{a}_2 \ln AAP + \mathrm{a}_3 \ln AGP + \mathrm{a}_4 \ln PGDP + \mathrm{a}_5 \ln POP + \ln \mathrm{d} \quad \ldots(5)$$

Method for Estimating Methane Emissions from Livestock

There are two main sources of methane emissions from livestock, namely, intestinal fermentation and faecal management, so a set of equations can be set as follows:

$$M = M_1 + M_2 \quad \ldots(6)$$

$$M_1 = \sum_{i=1}^{n} \left(u_i \cdot Q_i \right) \quad \ldots(7)$$

$$M_2 = \sum_{i=1}^{n} \left(v_i \cdot Q_i \right) \quad \ldots(8)$$

Here M_1 and M_2 are respectively methane emissions from intestinal fermentation and methane emissions from faecal management, u_i is the intestinal fermentation methane emission factor of category i livestock, v_i is the faecal management methane emission factor of category i livestock, and Q_i is the feeding quantity of category i livestock.

Table 1: Methane emission factors of intestinal fermentation of livestock [kg/(h.a)].

Feeding way	Cow	Bull	Water buffalo	Sheep	Goat	Pig	Horse	Donkey/Mule	Camel
Large-scale feeding	88.1	52.9	70.5	8.2	8.9	1	18	10	46
Cage-free feeding	89.3	67.9	87.7	8.7	9.4				
Grazing feeding	99.3	85.3	-	7.5	6.7				

Table 2: Methane emission factors of faecal management of livestock [kg/(h.a)].

District	Cow	Non-cow	Buffalo	Sheep	Goat	Pig	Horse	Donkey/Mule	Camel
North	7.46	2.82	-	0.15	0.17	3.12	1.09	0.60	1.28
Northeast	2.23	1.02	-	0.15	0.16	1.12	1.09	0.60	1.28
East	8.33	3.31	5.55	0.26	0.28	5.08	1.64	0.90	1.92
South-central	8.45	4.72	8.24	0.34	0.31	5.85	1.64	0.90	1.92
Southwest	6.51	3.21	1.53	0.48	0.53	4.18	1.64	0.90	1.92
Northwest	5.93	1.86	-	0.28	0.32	1.38	1.09	0.60	1.28

Methane emissions from livestock are estimated to involve cattle, horse, donkey, mule, camel, pig, goat and sheep in eight categories. The feeding cycle of 7 kinds of livestock other than pig is long, and the amount of livestock raised at the end of every year is small, so the amount of livestock kept at the end of every year is used to indicate the feeding quantity. The feeding cycle of pig is generally 180 days, and the feeding quantity is calculated by adding up the annual output and annual stock at the end of every year. The data of the amount of 8 categories of livestock kept and raised at the end of every year are all derived from *China Statistical Yearbook* from 2004 to 2017. The methane emission factors of intestinal fermentation and faecal management of all kinds of livestock were mostly taken from *IPCC Guidelines for National Greenhouse Gas Inventories* (2006) in existing researches. In order to better adapt to the actual situation of each province in China, we refer to *Provincial Greenhouse Gas Inventory Compilation Guide (Trial)* (China National Development and Reform Commission, 2011) compiled by the Climate Division of China National Development and Reform Commission, as given in Table 1 and Table 2.

It should be noted that the methane emission factors of intestinal fermentation of cattle or sheep in different feeding methods in Table 1 are not consistent. Because it is difficult to count the number of cattle or sheep in each province under various feeding methods, and the cattle and sheep in China are still mainly raised by grazing, we decide to adopt the methane emission factors of intestinal fermentation of cattle and sheep under grazing feeding. At the same time, still given that it is difficult to distinguish the number of cows, non-cows and buffaloes in a province, the mean value of methane emission factors of intestinal fermentation of cow, non-cow and buffalo under grazing feeding in Table 1 (excluding the default term) is unified as the methane emission factor of intestinal fermentation of cattle, and the mean value of methane emission factors of faecal management of cow, non-cow and buffalo in Table 2 (excluding the default term) is unified as the methane emission factor of faecal management of cattle. In addition, according to *Provincial Greenhouse Gas Inventory Compilation Guide (Trial)*, in Table 2, North District consists of five provinces (Beijing, Tianjin, Hebei, Shanxi, Inner Mongolia), Northeast District consists of three provinces (Liaoning, Jilin, Heilongjiang), East District consists of seven provinces (Shanghai, Jiangsu, Zhejiang, Anhui, Fujian, Jiangxi, Shandong), South-central District consists of six provinces (Henan, Hubei, Hunan, Guangdong, Guangxi, Hainan), Southwest District consists of five provinces (Chongqing, Sichuan, Guizhou, Yunnan, Tibet), and Northwest District consists of five provinces (Shaanxi, Gansu, Qinghai, Ningxia, Xinjiang).

Other Variables

Methane emissions from livestock per unit animal husbandry output value is calculated by dividing methane emissions of livestock by animal husbandry output value. Proportion of animal husbandry output value in total agricultural output value is calculated by dividing animal husbandry output value by total agricultural output value. The data of animal husbandry output value, total agricultural output value, proportion of total agricultural output value in total output value, per capita total output value, and population are all directly derived from *China Statistical Yearbook* from 2004 to 2017.

Table 3: Means and proportions of the methane emissions for various types of livestock in China from 2003 to 2016.

Livestock		Cattle	Horse	Donkey	Mule	Camel	Pig	Goat	Sheep
Methane emissions from intestinal fermentation	Quantity (10,000 t/a)	1,061.63	12.09	6.60	2.85	1.31	112.82	106.27	114.27
	Proportion (%)	74.88	0.85	0.47	0.20	0.09	7.96	7.49	8.06
Methane emissions from faecal management	Quantity (10,000 t/a)	54.54	0.92	0.43	0.20	0.04	509.63	5.03	3.70
	Proportion (%)	9.49	0.16	0.07	0.03	0.01	88.71	0.88	0.64

RESULTS AND ANALYSIS

Estimation of Results and Comparative Analysis of Methane Emissions from Livestock

We estimated the methane emissions from all types of livestock in China from 2003 to 2016. In order to facilitate the comparison among livestock categories, we calculated the means of methane emissions from intestinal fermentation and the means of methane emissions from faecal management of all kinds of livestock during 14 years, and the corresponding proportions, as given in Table 3.

Among the 8 types of livestock, cattle have the highest methane emissions from intestinal fermentation, about 10 times as much as pig, goat and sheep, and account for nearly 75% of all kinds of livestock. However, since the number of cattle is smaller than that of goats and sheep, and much smaller than that of pigs, obviously, high emission factor is the main reason for high emissions. Both goat and sheep are similar, and both have low emission factors, but both have a higher breeding, so their emissions are high. On the contrary, the emission factor of pig is the lowest, but the number of pigs is 9-10 times that of goats or sheep, so the emissions are almost no less than those of goat or sheep. Although the emission factors of horse, donkey, mule and camel are much higher than those of goat and sheep, the emissions of these four types of livestock are very low due to the small number of breeding, accounting for no more than 1% of all kinds of livestock.

Among the 8 types of livestock, pig has the highest methane emissions from faecal management, about 10 times as much as cattle, 100 times as much as goat, and account for nearly 90% of all kinds of livestock. Obviously, higher breeding is the main reason for high emissions, while high emission factor is the second. Cattle has the highest emission factor, and therefore has the high emissions, accounting for nearly 10% of all kinds of livestock. Both, goat and sheep are equivalent. Although both have a higher breeding, but have the lowest emission factors, so their emissions are low. On the contrary, the emission factors of horse, donkey, mule and camel are all higher than those of goat and sheep. However, due to the low breeding, the emissions of these four types of livestock are very low. Except for horse, the proportions of these four types of livestock do not exceed 0.1% of all kinds of livestock.

Given that cattle, pig, goat and sheep are the main sources of methane emissions from livestock, we calculated the proportions of methane emissions from intestinal fermentation and the proportions of methane emissions from faecal management of these four types of livestock in all districts and provinces of China in 2016, as given in Table 4 and Table 5.

The regions with the largest proportion of methane emissions from intestinal fermentation of cattle, pig, goat and sheep are southwest, south-central, southwest and north respectively and the provinces are Sichuan, Sichuan, Henan and Inner Mongolia respectively. This is determined by the breeding quantity of each major livestock under a certain animal husbandry structure. In general, southwest and south-central are the main regions for raising cattle and goat, south-central, east and southwest are the main regions for raising pig, and northwest and north are the main regions for raising sheep, each region accounting for more than 20% of the total emissions. Sichuan, Henan, Yunnan, Inner Mongolia and Tibet are the main provinces for raising cattle, Sichuan, Henan, Hunan, Shandong, Hubei, Yunnan and Guangdong are the main provinces for raising pig, Henan, Sichuan, Inner Mongolia, Shandong and Yunnan are the main provinces for raising goat, Inner Mongolia, Xinjiang, Gansu, Qinghai, Shandong, Tibet and Hebei are the main provinces for raising sheep, each province accounting for more than 5% of the total emissions.

The regions with the largest proportion of methane emissions from faecal management of cattle, pig, goat and sheep are south-central, south-central, southwest and northwest respectively, and the provinces are Henan, Henan, Sichuan and Xinjiang respectively. This is determined by the different emission factors in different regions in addition to the breeding quantity of each major livestock under a certain livestock husbandry structure. Overall, the

top three regions with the highest cattle emission factor are in turn south-central [7.14kg/(h.a)], east [5.73kg/(h.a)] and north [5.14kg/(h.a)], with the highest pig emission factor are in turn south-central, east and southwest, with the highest goat emission factor are in turn southwest, northwest and south-central, and with the highest sheep emission factor are in turn southwest, south-central and northwest. Thus, it can be seen that the large number of breeding mainly determines the high emissions of cattle breeding in southwest, goat breeding in south-central, and sheep breeding in northwest and north, the high emission factors mainly determine the high emissions of cattle and goat breeding in south-central, and both the large number of breeding and the high emission factors determine the high emissions of pig in south-central, east and southwest and those of goat in southwest, each region accounting for more than 20% of the total emissions. Further, at the provincial level, the higher breeding mainly determines the high emissions of cattle breeding in Sichuan, Yunnan and other provinces, those of pig breeding in Sichuan, Shandong and other provinces, those of goat breeding in Henan, Shandong and other provinces, those of sheep breeding in Inner Mongolia, Gansu, Qinghai,

Table 4: Proportions of the methane emissions from intestinal fermentation from major types of livestock in the regions of China in 2016 (%).

District	Province	Methane emissions from intestinal fermentation							
		Cattle		Pig		Goat		Sheep	
North	Beijing	0.15	11.28	0.39	8.04	0.13	16.95	0.26	34.34
	Tianjin	0.28		0.50		0.04		0.26	
	Hebei	3.71		4.69		3.36		5.68	
	Shanxi	1.00		1.07		2.60		3.39	
	Inner Mongolia	6.14		1.38		10.82		24.75	
Northeast	Liaoning	3.75	12.39	3.58	8.66	3.37	5.08	2.59	9.19
	Jilin	4.01		2.29		0.38		2.39	
	Heilongjiang	4.63		2.79		1.33		4.20	
East	Shanghai	0.05	10.14	0.24	22.99	0.18	17.73	0.01	6.87
	Jiangsu	0.28		4.05		2.82		0.06	
	Zhejiang	0.14		1.56		0.29		0.45	
	Anhui	1.57		3.88		4.69		0.01	
	Fujian	0.62		2.41		0.92		0.00	
	Jiangxi	2.83		4.21		0.44		0.00	
	Shandong	4.65		6.63		8.40		6.35	
South-central	Henan	8.32	22.77	9.19	34.66	12.46	21.86	0.73	0.73
	Hubei	3.33		5.94		3.37		0.00	
	Hunan	4.28		8.80		3.79		0.00	
	Guangdong	2.19		5.01		0.31		0.00	
	Guangxi	3.92		4.91		1.46		0.00	
	Hainan	0.72		0.82		0.48		0.00	
Southwest	Chongqing	1.36	28.43	3.07	21.71	1.55	25.75	0.00	7.50
	Sichuan	9.09		10.36		11.24		1.18	
	Guizhou	4.86		2.91		2.36		0.12	
	Yunnan	7.40		5.32		6.93		0.47	
	Tibet	5.72		0.05		3.67		5.73	
Northwest	Shaanxi	1.39	14.99	1.76	3.94	3.97	12.64	0.76	41.38
	Gansu	4.19		1.12		2.91		9.11	
	Qinhai	4.53		0.23		1.31		7.49	
	Ningxia	1.06		0.15		0.80		2.91	
	Xinjiang	3.83		0.69		3.64		21.11	

Table 5: Proportions of the methane emissions from faecal management from major types of livestock in the regions of China in 2016 (%).

District	Province	Methane emissions from faecal management							
		Cattle		Pig		Goat		Sheep	
North	Beijing	0.17	12.50	0.27	5.57	0.07	8.70	0.16	21.69
	Tianjin	0.31		0.35		0.02		0.16	
	Hebei	4.11		3.25		1.73		3.59	
	Shanxi	1.11		0.74		1.34		2.14	
	Inner Mongolia	6.80		0.96		5.55		15.64	
Northeast	Liaoning	1.31	4.34	0.89	2.15	1.63	2.45	1.64	5.80
	Jilin	1.40		0.57		0.18		1.51	
	Heilong-jiang	1.62		0.69		0.64		2.66	
East	Shanghai	0.06	12.53	0.27	25.92	0.15	14.98	0.01	7.52
	Jiangsu	0.35		4.57		2.39		0.06	
	Zhejiang	0.17		1.75		0.24		0.50	
	Anhui	1.94		4.37		3.96		0.01	
	Fujian	0.77		2.72		0.77		0.00	
	Jiangxi	3.49		4.75		0.37		0.00	
	Shandong	5.74		7.48		7.10		6.95	
South-central	Henan	12.80	35.04	11.93	45.01	11.66	20.45	1.04	1.04
	Hubei	5.12		7.72		3.15		0.00	
	Hunan	6.59		11.43		3.54		0.00	
	Guangdong	3.38		6.50		0.29		0.00	
	Guangxi	6.04		6.37		1.36		0.00	
	Hainan	1.10		1.06		0.45		0.00	
Southwest	Chongqing	1.10	22.99	2.85	20.14	2.48	41.20	0.00	15.16
	Sichuan	7.35		9.61		17.99		2.38	
	Guizhou	3.93		2.70		3.78		0.24	
	Yunnan	5.99		4.93		11.08		0.95	
	Tibet	4.62		0.05		5.87		11.58	
Northwest	Shaanxi	1.17	12.59	0.54	1.21	3.84	12.21	0.90	48.79
	Gansu	3.52		0.34		2.82		10.74	
	Qinhai	3.81		0.07		1.26		8.83	
	Ningxia	0.89		0.05		0.77		3.43	
	Xinjiang	3.21		0.21		3.52		24.89	

Shandong and other provinces. The high emission factors mainly determine the high emissions of cattle breeding in Henan, Inner Mongolia, Hunan, Guangxi, Shandong, Hubei and other provinces, those of pig breeding in Henan, Hunan, Hubei, Guangdong, Guangxi and other provinces, those of goat breeding in Sichuan, Yunnan, Tibet, Inner Mongolia and other provinces, those of sheep breeding in Xinjiang, Tibet and other provinces; each province accounting for more than 5% of the total emissions.

General Regression Results and Analysis

We made a general regression of the factors affecting methane emissions from livestock. Before the regression estimation, the variance inflation factor (VIF) was used to verify that the VIF values of all explanatory variables in the model were within the interval [1.00 4.50], far less than 10, and there was no multicollinearity. LSDV test showed that the individual effect of the panel data was obvious, indicating

that mixed OLS regression should not be used. According to Hausman test, compared with fixed effect regression, random effect regression was more consistent with the statistical characteristics of the panel data. Therefore, we used the random effect regression results of clustering robust standard deviation, as provided in Table 6.

The results of Regression 1 show that the model fits well. The influence coefficient of each explanatory variable on methane emissions from livestock is within the range (0.8, 1), that is, the marginal contribution of technical, economic and population factors to environmental variation is decreasing, and higher the influence coefficient is, the smaller the rate of diminishing marginal contribution is. In fact, except for proportion of total agricultural output value in total output value, the influence coefficients of other explanatory variables on methane emissions of livestock are all close to 1, with a very small rate of diminishing marginal contribution. Specifically, the impact coefficient of population on methane emissions from livestock is the highest, indicating that expansion of consumption demand for livestock caused by increase of population is the most important reason for high methane emissions from livestock. The impact coefficient of methane emissions from livestock per unit animal husbandry output value on methane emissions from livestock is second only to population, and poor technology is not conducive to controlling methane emissions from livestock. The impact coefficient of per capita total output value on methane emissions from livestock is high, meaning that greater economic size drives livestock production growth and increases methane emissions from them. Proportion of animal husbandry output value in total agricultural output value and proportion of total agricultural output value in total output value are two economic structural factors, the former undoubtedly has a higher influence coefficient on methane emissions of livestock than the latter, and the larger the proportion of livestock production value is, the larger the relative economic scale of livestock will be, and the higher the methane emissions of livestock will be.

In order to test the robustness of the regression model, we combine the two economic structure factors of proportion of animal husbandry output value in total agricultural output value (*AAP*) and proportion of total agricultural output value in total output value (*AGP*) into one, that is, proportion of animal husbandry output value in total output value (*AAGP*), and the calculation method is $AAGP = A_n/Y$. After testing, we used the random effect regression results of clustering robust standard deviation, as given in Table 6. The results of Regression 2 show that the sign and significance of the influence coefficient of each explanatory variable on methane emissions from livestock are consistent with the results of Regression 1, and the values of each coefficient are only slightly changed, indicating that the results of Regression 1 are robust.

CLASSIFICATION REGRESSION RESULTS AND ANALYSIS

Furthermore, we made two separate regressions of the factors affecting methane emissions from livestock from intestinal fermentation and faecal management. For each regression, LSDV test showed that the individual effects of the panel data were obvious, indicating that mixed OLS regression should not be used. According to Hausman test, compared with random effect regression, fixed effect regression was

Table 6: Regression results for the methane emissions from livestock.

Influencing factors	Regression 1		Regression 2	
	Coefficient	Z-value	Coefficient	Z-value
ln*MPA*	0.985 6***	45.89	0.981 1***	43.55
ln*AAP*	0.959 0***	30.02	-	-
ln*AGP*	0.870 6***	25.40	-	-
ln*AAGP*	-	-	0.893 0***	25.88
ln*PGDP*	0.966 6***	50.01	0.963 9***	42.77
ln*POP*	0.998 9***	44.47	0.992 9***	39.47
Intercept	-17.122 5***	-53.12	-12.769 1***	-38.85
Wald-Statistic	4 810.22***		2 956.27***	
Adj-R^2	0.945 5		0.944 2	
VIF	2.54		2.88	
Observations	434		434	

Note: ***, ** and * respectively indicate that the estimated results are significant at the levels of 1%, 5% and 10%, respectively; is the default.

Table 7: Regression results for the methane emissions from intestinal fermentation and faecal management.

Influencing factors	Methane emissions from intestinal fermentation		Methane emissions from faecal management	
	Coefficient	T-value	Coefficient	T-value
ln*MPA*	1.107 3***	16.95	0.600 0***	5.90
ln*AAP*	0.995 9***	11.28	0.786 6***	6.65
ln*AGP*	0.989 0***	9.05	0.615 1***	8.47
ln*PGDP*	1.032 1***	13.85	0.711 0***	7.21
ln*POP*	1.117 8***	5.40	0.526 5***	2.89
Intercept	-19.288 8***	-7.82	-11.908 2***	-4.85
F-Statistic	69.35***		33.38***	
Adj-R^2	0.875 7		0.610 2	
Observations	434		434	

Note: ***, ** and * indicate that the estimated results are significant at the levels of 1%, 5% and 10%, respectively.

more consistent with the statistical characteristics of the panel data. Therefore, we used the fixed effect regression results of clustering robust standard deviation, as provided in Table 7.

The results of each regression show that the model fits well. Each explanatory variable has a significant positive effect on methane emissions both from intestinal fermentation and from faecal management. Differently, on the one hand, the influence coefficient of each explanatory variable on methane emissions from intestinal fermentation is close to 1, which indicates that methane emissions from intestinal fermentation is mainly restricted by livestock's physiological structure. Following increase or decrease of livestock feeding quantity determined by each explanatory variable, it changes with a relatively stable parameter and has little controllability. On the other hand, the influence coefficient of each explanatory variable on methane emissions from faecal management is within the range (0.5, 0.8), lower than the influence coefficient of each explanatory variable on methane emissions from livestock in the results of Regression 1, and technical, economic and population factors all have diminishing marginal contribution, which indicates that methane emissions from faecal management is limited little by livestock's physiological structure, and it is largely controllable. In fact, whether and to what extent methane emissions, both from intestinal fermentation and from faecal management, are constrained by livestock's physiological structure can be reflected in methane emission factors of livestock. Table 1 and Table 2 show that the methane emission factors of intestinal fermentation are relatively stable, while those of faecal management have large regional differences.

DISCUSSION

Due to different degrees of constraints by livestock's physiological structure, it is necessary to distinguish methane emissions between from intestinal fermentation and from faecal management to control methane emissions from livestock at the macro level. To control methane emissions from intestinal fermentation, which is more restricted by livestock's physiological structure, the primary task is to increase technical input to reduce methane emission factors of intestinal fermentation, and then reduce methane emissions from livestock per unit animal husbandry output value. First, through breeding and improvement, the level of yield per unit can be improved, and the number of livestock breeding can be reduced under the premise of meeting the established demand for livestock products. Second, the quantity and quality of food intake should be standardized, and the specific measures include promotion of straw silage and ammonification, rational preparation of fine/coarse ration of daily food, and appropriate use of nutritional additives. Third, the production of methane in the rumen can be inhibited by inhibiting methanogenic bacilli. In addition, to adjust economic structure in order to reduce proportion of animal husbandry output value in total agricultural output value, in turn, reduce proportion of total agricultural output value in total output value, or to shrink economic scale in order to reduce per capita total output value, or to control population size to reduce population, will have a negative impact on the overall economic quality, and thus is not desirable. For the areas with a large stock of livestock, reducing scale of breeding may be the most direct and effective measure, but the policy of prohibition and restriction should be avoided, and it can be solved through a certain market mechanism, that is, taxes can be levied on the ruminant animal (cattle, goat or sheep) husbandry industry, on the one hand, to promote industrial substitution from the supply side, and on the other hand, to encourage reduction of meat consumption from the demand side.

The diminishing marginal contribution of technological level, economic structure, economic scale and population scale essentially reflects the effective role of some external forces in controlling methane emissions from faecal management. Due to small degree of restriction by livestock's physiological structure, in the exogenous factors of controlling methane emissions from manure management, it is very important to deal with livestock manure through resource utilization, and using biogas project to recover methane is particularly effective. Enterprises or farmers should be given a certain subsidy for purchase and construction of biogas facilities according to livestock type and breeding scale, at the same time, fines should be imposed for illegal discharge and release of livestock waste. Of course, methane emissions from livestock per unit animal husbandry output value could still be reduced by investing more in technology to reduce methane emission factors of faecal management. There are two specific ways: first, to reduce faecal production through scientific selection of feed, precise control of food, the use of feed additives and other methods; second, to realize updating and upgrading of the technology for cleaning up faeces by changing water flushing and blisters into dry cleaning or adopting automatic dry and wet separation to clean.

CONCLUSION

Finally, we came to five conclusions. Firstly, the methane emissions of four main types of livestock are different in categories. Large number of breeding is the main reason for high emissions of pig, goat and sheep, and high emission factor is the main reason for high emissions of cattle. Secondly, the methane emissions of four main types of livestock are different in regions. Methane emissions from intestinal fermentation is determined by breeding quantity of each major livestock under a certain animal husbandry structure, and methane emissions from faecal management is determined by different emission factors in different regions in addition to breeding quantity of each major livestock under a certain livestock husbandry structure. Thirdly, in general, technical, economic and population factors of methane emissions from livestock have diminishing marginal contribution. Fourthly, methane emissions from intestinal fermentation are mainly restricted by livestock's physiological structure. Following, increase or decrease of livestock feeding quantity, it changes with a relatively stable parameter and has little controllability. Methane emissions from faecal management is limited little by livestock's physiological structure, and it is largely controllable. Fifthly, in order to control methane emissions from intestinal fermentation, technical investment should be increased to reduce methane emission factors of intestinal fermentation and a certain market mechanism should be used in due course to reduce raising scale. In order to control methane emissions from faecal management, it is very important to deal with livestock manure through resource utilization, but technical input should still be increased to reduce methane emission factors of faecal management.

REFERENCES

Ang, B.W., Zhang, F.Q. and Choi, K.H. 1998. Factorizing changes in energy and environmental indicators through decomposition. Energy, 23(6): 489-495.

Bo, Z., Rongzhen, Z. and Zhiliang, T. 2009. Methane emission and abatement strategy in animal husbandry. Chinese Journal of Eco-Agriculture, 17(4): 811-816

Chianese, D.S., Rotz, C.A. and Richard, T.L. 2009. Whole-farm greenhouse gas emissions: A review with application to a Pennsylvania dairy farm. Applied Engineering in Agriculture, 25(3): 431-442

China National Development and Reform Commission 2011. Provincial Greenhouse Gas Inventory Compilation Guide (Trial). The Climate Division of China National Development and Reform Commission, Beijing, China

Dui, W. 2003. Greenhouse gases and greenhouse effect. China Meteorological Press, Beijing, China

Ehrlich, P.R. and Holdren, J.P. 1971. Impact of population growth. Science, 171 (3977): 1212-1217.

Fao, 2006. Livestock a major threat to the environment: Remedies urgently needed. Available at: http://www.fao.org./newsroom/en/news/2006/1000448/index.html

Jing, Z., Junna, Z. and Rongrong, D. 2012. Path selection for low-carbon development of animal husbandry in China: Based on regression analysis of emission sources of animal husbandry to methane growth. Guangxi Social Science, 9: 50-54.

Ling, B., Lei, J. and Yaobin, L. 2017. Spatio-temporal characteristics of environmental pressures of the urban agglomeration in the middle reaches of the Yangtze River: A case study based on industrial SO_2 emissions. Economic Geography, 37(3): 174-181.

McGinn, S.M., Flesch, T.K., Harper, L.A. and Beauchemin, K.A. 2006. An approach for measuring methane emissions from whole farms. Journal of Environmental Quality, 35(1): 14-20.

Min, G., Honglian, H. and Ruiping, D. 2013. Ruminant methane emission and emission reduction strategies. Chinese Journal of Animal Science, 49(18): 35-41.

Nan, H. and Weiyang, Y. 2016. Spatial characteristics and influencing factors of industrial waste gas emission in China. Scientia Geographica Sinica, 36(2): 196-203.

Poumanyvong, P. and Kaneko, S. 2010. Does urbanization lead to less energy use and lower CO_2 emissions? A cross-country analysis. Ecological Economics, 70(2): 434-444.

Qiang, D., Qiao, C. and Ning, L. 2012. Forecast of China's carbon emissions based on modified IPAT model. Acta Scientiae Circumstantiae, 32(9): 2294-2302.

Renhua, N. 2010. Effects of diet composition on methane and nitrogen emissions from lactating cattle. Chinese Academy of Agricultural Sciences, Beijing, China.

Shengli, L., Jin, X., Fan, X., Huang, W. and Cao, Z. 2010. Ruminant production and carbon emission reduction measures. Chinese Journal of Animal Nutrition, 22 (1): 2-9.

Xiao, G. and Yaohui, Z. 2012. Influence factors and environmental Kuznets curve relink effect of Chinese industry's carbon dioxide emission: Empirical research based on STIRPAT model with industrial dynamic panel data. China Industrial Economics, 1: 26-35

Yigen, W., Kaiwen, F. and Gucheng, L. 2017. Population growth, structural adjustment and agricultural non-point source pollution: An empirical study based on STIRPAT model of spatial panel. Journal of Agrotechnical Economics, 3: 75-87.

Yorker, R., Rosae, E. A. and Dietz, T. 2002. Bridging environmental science with environmental policy: Plasticity of population, affluence, and technology. Social Science Quarterly, 83(1): 18-31.

Yunlong, L., Bing, W., Qiyu, D. et al. 2018. Study on the methane emission pattern and the methane inhibition methods in sheep. Feed Industry, 39 (15):43-47.

Yuzhuo, S., Gangyi, W., Xinhui, W. et al. 2017. Analysis of water's nitrogen pollution caused by hog industry agglomeration: Based on the analytical framework of IPAT. Chinese Journal of Animal Science, 53 (11): 117-122.

Zhangqi, Z., Lei, J., Lingyun, H., Zheng, W. et al. 2018. Global carbon emissions and its environmental impact analysis based on a consumption accounting principle. Acta Geographica Sinica, 73(3): 442-459.

Zhang, Z.X. 2000. Decoupling China's carbon emissions increase from economic growth: An economic analysis and policy implications. World Development, 28(4): 739-752.

Zhi, C., Tingning, W., Yang, L. et al. 2017. Methane emission of animal husbandry and reduction measures in Ningxia. Journal of Agricultural Sciences, 38(1): 7-9.

Nature Environment and Pollution Technology
An International Quarterly Scientific Journal

p-ISSN: 0972-6268
e-ISSN: 2395-3454

Vol. 19 | No. 1 | pp. 133-140 | 2020

Original Research Paper | Open Access

Field Research on Nitrogen Removal Performance of Aerobic Denitrifiers in Source Water Reservoir by Mixing Aeration

Zhou Zi-zhen*†, Huang Ting-lin(***), Gong Wei-jin*, Li Yang*, Liu Yue*, Zhao Fu-wang*, Zhou Shi-lei**** and Dou Yan-yan***

*School of Energy and Environment, Zhongyuan University of Technology, Zhengzhou, 450007, China
**School of Environmental and Municipal Engineering, Xi'an University of Architecture and Technology, Xi'an, 710055, China
***Key Laboratory of Northwest Water Resource, Environment and Ecology, MOE, Xi'an University of Architecture and Technology, Xi'an, 710055, China
****School of Environment Science and Engineering, Hebei University of Science and Technology, Shijiazhuang, 050018, China
†Corresponding author: Zhou Zi-zhen

Nat. Env. & Poll. Tech.
Website: www.neptjournal.com

Received: 18-05-2019
Accepted: 22-07-2019

Key Words:
Water reservoir
Nitrogen
Denitrification
Microbial diversity

ABSTRACT

Changes of total nitrogen (TN), organic matter, microbial metabolic activity, aerobic denitrifying bacteria and aerobic denitrifying genes (*nir*S and *nir*K) in water and surface sediments under mixing aeration were studied in Heihe Jinpen Reservoir. Results showed that compared with the control area, the total nitrogen concentration of water and surface sediments in the enhanced area decreased by 29.7%~49.2% and 17.9%. Metabolic activity of microorganisms increased by more than 14%, the utilization rate of carbon source increased by 30% and the McIntosh diversity index of microorganisms increased by 20%. The number of aerobic denitrifiers and genes of aerobic denitrifiers were also increased by 20%. Illumina high-throughput DNA sequencing results showed that the proportion of aerobic denitrifiers such as *Acidovorax* increased from 0.01% to 0.15%, showing an increase by 15 times. The production practice showed that mixed aeration can improve the metabolic activity and denitrification characteristics of indigenous aerobic denitrifiers, providing theoretical support and technical guarantee for denitrification and carbon removal of slightly polluted source water.

INTRODUCTION

More and more lakes and reservoirs have become the sources of drinking water in cities, and most lakes and reservoirs have problems of eutrophication of different degrees (Huang et al. 2014). Higher concentrations of nitrogen and phosphorus led to excessive algae reproduction, which not only endangers the aquatic ecosystem of lakes and reservoirs, but also threatens the safety of water supply. Excess nitrogen in the water also produced certain disinfection by-products, which directly affects human health (Kang et al. 2014). Physical, chemical and biological methods have been reported for nitrogen removal. However, both physical and chemical methods have problems of high cost and incomplete removal of nitrogen. More and more attention has been paid to biological nitrogen removal (Song et al. 2014, Sun et al. 2010, Patureau et al. 1998, Chen et al. 2015).

It is generally believed that nitrogen removal mainly depends on bacterial autotrophic nitrification and heterotrophic denitrification, and nitrification was carried out under aerobic conditions; denitrification was carried out under anaerobic conditions, and finally nitrogen was formed to N_2, achieving the purpose of removal (Patureau et al. 2001). Strict anaerobic condition was required for denitrification, which made denitrification process difficult to be used in drinking water treatment. Robertson (1982) first reported aerobic denitrification at the beginning of 1980s. Aerobic denitrifying bacteria using oxygen and nitrate as electron acceptors provided a new perspective for biological denitrification of drinking water. Aerobic denitrification and nitrification existed simultaneously in a system and can provide a certain basicity to balance the acidity produced by nitrification. Robertson separated aerobic denitrifying bacteria from desulfurization and denitrification wastewater treatment systems (Robertson et al. 1982). Other studies showed that aerobic denitrifying bacteria were also isolated from marine sediment (Gao et al. 2010) and constructed wetland system (Coban et al. 2015). In recent years, more and more aerobic denitrifying bacteria

have been isolated from lake sediments: three aerobic denitrifying bacteria H-30, X-10 and C-30 with total nitrogen removal rate of more than 80% under laboratory conditions were separated by Kang et al. (2014); 14 strains with high aerobic denitrification characteristics from reservoir sediments, mainly *Acinetobacter* spp. and *Nova* spp. were isolated and enriched by Zhou et al. (2016). The removal rates of TN (total nitrogen) and TOC (total organic matter) were 80.42% and 98.30% respectively. The isolation and screening of many aerobic denitrifying bacteria not only enriched and improved the theory of aerobic denitrification, but also laid a foundation for its engineering application (Huang et al. 2015, Xu et al. 2018, Epsztein et al. 2016, Alzate et al. 2016).

In order to improve the water quality, water-lifting aerators were installed in the reservoirs to supply oxygen to the water column, which provided a good experimental platform for the study of aerobic denitrification. Nitrate nitrogen concentration in the mixed aeration area decreased from 1.71 mg/L to 0.80 mg/L, and the TN removal rate reaching 38.33% were observed in a previous study (Zhou et al. 2016). Under the conditions of production scale of mixed aeration, the mechanism of water quality improvement, especially the removal of TN, was explored at the genetic level from the perspective of microorganisms, which provided theoretical support and technical support for the application of aerobic denitrifying bacteria in engineering and the nitrogen removal of water source reservoirs.

MATERIALS AND METHODS

Sampling Sites and Sampling Methods

As shown in Fig. 1, Heihe Jinpen Reservoir (latitude: 34°13′N- 34°42′N, longitude: 107°43′E-108°24′E) was a canyon shaped reservoir located at the foot of Qinling Mountains. Heihe Jinpen Reservoir was the important drinking water source of Xi'an City (its water supply accounted for 80% of the total drinking water of Xi'an City). The total reservoir capacity of Heihe Jinpen Reservoir is 2.0×10^8 m^3 and the effective reservoir capacity is 1.8×10^8 m^3. The main function of the reservoir was water supply and auxiliary functions were flood control and irrigation. Eight water-lifting aerators were installed in the main reservoir area. Detailed introduction is given in the previous report (Zhou et al. 2017). Enhanced area was in the middle of the main reservoir area, which was affected by the operation of the water-lifting aerator, represented by E. The control area was about 2 km away from the main reservoir area, and was less affected by water-lifting aerator, represented by C, as shown in Fig. 1.

Water samples were drawn every 3 days. Water temperature, dissolved oxygen (DO) and pH were measured *in situ* by HACH DS5 multi-parameter water quality analyser. Water quality indicators such as total nitrogen (TN), nitrate nitrogen, total phosphorus (TP) and total organic carbon (TOC) were measured in the reservoir field laboratory according to the "Water and Wastewater Monitoring and Analysis Methods (4^{th} edition)". Surface sediments were sampled once a week with a columnar sampler. Surface sediments of 0.5 cm were sampled and stored at 4°C.

Methods for Determination of Chemical Indicators of Water and Sediments

TN and nitrate nitrogen were determined by AA3 continuous flowing analyser (SEAL, Germany); TOC was determined by TOC-L analyser of Shimadzu, Japan. Sediment samples were dried, ground and sifted. TN in sediments was digested

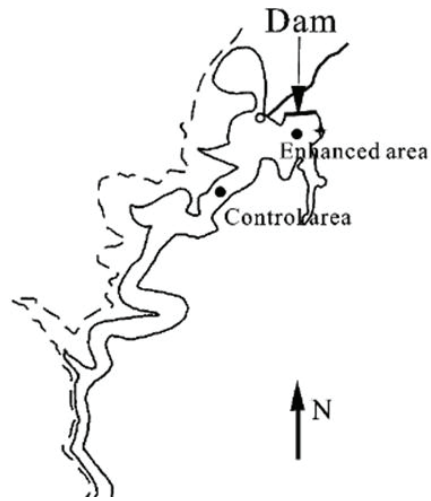

Fig. 1: Distribution map of mixing aeration area (Enhanced area) and reference area (Control area) of Heihe Jinpen Reservoir.

at 121°C for 1 hour and then determined by zinc-cadmium reduction spectrophotometry (Jiyeon et al. 2016). Organic matter in sediments was determined by potassium dichromate method (Jiyeon et al. 2016).

Methods for Determination of Microbial Metabolic Activity and Carbon Source Utilization

Microbial samples were collected at the same time as water samples for determination of chemical indicators. Microbial metabolic activity, carbon source utilization and McIntosh diversity index were measured by Biolog ECO microporous plate. Microbial metabolic activity was expressed by AWCD (average well colour development). AWCD = $\Sigma(C_{590} - C_{750})/31$. Carbon source utilization (dimensionless) was calculated by the average absorbance of microorganisms to each carbon source in each pore (Fang et al. 2016). For example, amino acid = $(C_{\text{L-arginine}} + C_{\text{L-asparagine}} + C_{\text{L-phenylalanine}} + C_{\text{L-serine}} + C_{\text{L-threonine}} + C_{\text{L-glutamic-acid}})/6$. McIntosh diversity index was also calculated by absorbance.

Aerobic Denitrifying Bacteria Count and Denitrifying Functional Gene Quantification

Through gradient dilution, the number of aerobic denitrifying bacteria in enhanced area and control area was determined by plate counting method. The preparation method of gradient dilution solution is as follows: 10^{-3}, 10^{-4}, 10^{-5}, 10^{-6} and 0.2 mL diluent was added to solid denitrification screening medium (The composition of the medium was: CH_3COONa, 0.10 $g \cdot L^{-1}$; $NaNO_3$, 0.02 $g \cdot L^{-1}$; $K_2HPO_4.3H_2O$, 0.02 $g \cdot L^{-1}$; $CaCl_2$, 0.01 $g \cdot L^{-1}$; $MgCl_2.6H_2O$, 0.01 $g \cdot L^{-1}$; agar, 20 $g \cdot L^{-1}$, and the pH was adjusted to 7.2 (Kang et al. 2018). Culturing of bacteria was carried out for 5 days at 30°C, then counted and calculated.

The copies of denitrifying functional genes *nir*S and *nir*K were determined by quantitative PCR. 2-L water samples were filtered by 0.22 μm filter membrane and extracted by a rapid DNA kit. The amplification sequence of *nir*S and *nir*K genes is given in Table 1. QPCR was tested by ABI 7500 of Life Technologies, USA, and the amplification reaction method was found in the previous study (Zhou et al. 2016).

Table 1: Primer sequences for gene amplification.

Gene	Primer sequence
*nir*S	cd3aF, 5′-GTSAACGTSAAGGARACSGG-3′
	R3cd, 5′-GASTTCGGRTGSGTCTTGA-3′
*nir*K	F1aCu, 5′-ATYGGCGGVCAYGGCGA-3′
	R3Cu, 5′-GCCTCGATCAGRTTRTGGTT-3′

Illumina High Throughput Sequencing

2-L water sample was filtered by 0.22 μm filter membrane and stored at ultra-low temperature. The determination was completed by Meiji Biology in Shanghai.

Operating Conditions of Water-Lifting Aerator

Destroying water stratification and improving water quality was the purpose of the operation of water-lifting aerator. In this stage, the algal density of surface layer of the reservoir was only about 200×10^4 cells/L, which was quite low, and there was no control of algae. The compressed air flow rate of each water-lifting aerator was 30-40 m^3/h, and the air supply of 8 water-lifting aerators was controlled in this range. During this researching period, 8 water-lifting aerators operated 24 hours a day, uninterruptedly. The power of the air compressor (Anruiko, Bengbu) was 132 kW, 2975 r/min, dual-purpose equipment.

RESULTS AND DISCUSSION

Changes of TN and Organic Compounds in Water and Surface Sediments

The basic situation of water quality in the control area and enhanced area before the operation of the water-lifting aeration system is given in Table 2. Before the operation of the system, water quality of the two areas tended to be consistent. For example, the results of October 10 water sample showed that the TN concentrations of the two areas were 1.81 $mg \cdot L^{-1}$ and 1.70 $mg \cdot L^{-1}$, respectively, and the difference between the two areas was only 0.11 $mg \cdot L^{-1}$, with a difference of about 6%. The TOC concentrations of the two regions were almost the same. The density of aerobic denitrifying bacteria (ADB) was 4.34×10^4 $cfu \cdot mL^{-1}$ and 4.03×10^4 $cfu \cdot mL^{-1}$, respectively, with a difference of 7%. According to the above analysis, there was a slight difference in the concentrations of TN, TOC and aerobic denitrifying bacteria between the two areas before the operation of the aeration system, and the difference was less than 10%.

In this study, the surface water temperature in the enhanced area decreased from 17.1°C (Oct-15) to 14.8°C (Nov-02), and the bottom water temperature increased from 10.1°C (Oct-15) to 14.3°C (Nov-02). DO increased from 0 $mg \cdot L^{-1}$ (Oct-15) to 9.8 $mg \cdot L^{-1}$ (Nov-02) in the enhanced area. While there was still a temperature difference of 6°C between the upper and lower water layers in the control area. On Nov-02, the concentration of DO in the control area was still 0 $mg \cdot L^{-1}$ (Nov-02) in the bottom water, which indicated that the operation of the water-lifting aeration system accelerated the damage of water stratification and had a significant effect on mixing aeration.

The variations of TN and organic matter concentrations in the enhanced area during operation are given in Table 3. The DO concentration in the water body, especially in the bottom water, increased gradually with the operation of the system. After 19 days of operation, TN and TOC in different water layers in the enhanced area reduced sharply. The TN concentration in the bottom water body decreased from 2.36 $mg \cdot L^{-1}$ to 1.20 $mg \cdot L^{-1}$, with a reduction rate of 49.2%, and the TOC reduction rate in vertical water body also reached more than 22.5%. Compared with enhanced area, in the control area the highest removal rate of TN was only 7.7%, and the removal rate of TOC 6.5%.

Compared with the control area, the removal rate of TN and TOC in the enhanced area was higher. In order to further explore that where nitrogen and organic matter gone, surface sediment samples were also taken under the corresponding water column of the sampling site and their TN and OC were determined. As presented in Table 3, the concentration of TN and OC in surface sediment also decreased by 17.9% and 20.5% respectively. However, the concentration of TN and OC in surface sediment of the control area was almost the same.

Based on the above results, not only in the water, but also in the surface sediment nitrogen and organic matter in the enhanced area have been greatly reduced, and the accumulation of nitrite nitrogen was not found. Previous studies showed that the activities of indigenous microorganisms and community structure have changed during this process, and the presence of aerobic denitrifying bacteria have been found. Biolog technology was used to explore metabolic activity of microorganisms in water and surface sediments and utilization of different carbon sources in this study.

Microbial Metabolic Activity and Carbon Source Utilization in Water and Surface Sediments

Biolog ECO microporous plate was used to measure microbial metabolic activity in water and surface sediments (gradient dilution 10^4 times) in enhanced area and control area, respectively, on Oct-15 at the beginning and on Nov-02 at the end of the operation of the water-lifting aeration system. Results are shown in Fig. 2, and the microbial metabolic activity of water and surface sediments in enhanced area have been greatly increased. For example, at 144-hour time, after 19 days of mixed aeration, the microbial metabolic activity in water increased by 14.3%, while that in the control area increased by only 3%. As for the surface sediments, the microbial metabolic activity in the enhanced area increased by 14.9%, while that in the control area increased by only 6%.

Thirty-one different carbon sources available to microorganisms were classified into 6 categories. The utilization rates of microorganisms in water and surface sediments were determined by using Biolog ECO microporous plate as given

Table 2: Distribution of TN, TOC and aerobic denitrifying bacteria in water and surface sediments in control area and mixing aeration area before operation of the system.

	Indicators	Sites	Oct-01	Oct-05	Oct-10
Water	TN ($mg \bullet L^{-1}$)	E	1.74	1.68	1.81
		C	1.68	1.65	1.70
	TOC ($mg \bullet L^{-1}$)	E	3.51	3.58	3.62
		C	3.60	3.58	3.56
	ADD ($\times 10^4$ cfu/$mg \bullet L^{-1}$)	E	4.32	4.35	4.34
		C	3.84	4.24	4.03

Table 3: Total nitrogen and organic matter concentrations in water and surface sediments and their reduction rates in mixing aeration area.

	Indicators	Sites	Oct-15	Oct-21	Oct-28	Nov-02	Reduction rate（%）
Water	TN (mg/L)	0.5m	1.72	1.48	1.39	1.21	29.7
		40m	1.75	1.56	1.42	1.23	29.7
		90m	2.36	2.09	1.53	1.20	49.2
	TOC (mg/L)	0.5m	3.69	3.02	2.87	2.72	26.3
		40m	3.42	3.09	2.88	2.65	22.5
		90m	4.02	3.56	3.08	2.85	29.1
Sediment	TN (mg/L)	0.5m	1532	1482	1314	1258	17.9
	OC (%)	0.5m	3.42	2.95	2.79	2.72	20.5

in Table 4. The results showed that the utilization rates of carbonyl compounds, amino acids, esters, alcohols, amines and carboxylic acids increased by 39.7%, 66.7%, 62.5%, 33.8%, 69.2% and 7.9%, respectively by the end of mixed aeration. In the control area, the utilization rate of different carbon sources increased by only 15%, and the utilization rate of some carbon sources by microorganisms decreased slightly. This may be due to the further anoxia of water body and the further decrease of water temperature. The utilization of different carbon sources by microorganisms in sediments showed the same trend as that of water body, and increased by 28.7%, 29.3%, 36.4%, 37.5%, 37.1% and 5.2% respectively. The above results were in accordance with the TOC determination, indicating that the utilization of organic matter in water and sediment was accelerated by the increase of microbial activity.

Changes of Aerobic Denitrifying Bacteria and Functional Genes

The number of aerobic denitrifying bacteria and the functional genes of aerobic denitrification (*nir*K and *nir*S) in control area and enhanced area were quantitatively determined. The results are shown in Fig. 3, the average number of aerobic denitrifying bacteria in water column of sampling site in enhanced area increased from 2.14×10^4 CFU/m.L^{-1} to 5.84×10^4 CFU/m.L^{-1}, while the number of aerobic denitrifying bacteria in control area maintained at 0.98×10^4 CFU/m.L^{-1} to 1.85×10^4 CFU/m.L^{-1} during the operation of the aeration system and showed a slight downward trend.

There were two forms of nitrite reductase with different structure but with the same function: copper-containing *nir*K and iron-containing *nir*S genes. As shown in Fig. 3, the copies of *nir*K and *nir*S genes in the mixed aeration region increase gradually from 7.18×10^3 μ.L^{-1} to 9.61×10^3 μ.L^{-1}, while the copies of *nir*K and *nir*S genes in the control region remained at 6.73×10^3 μ.L^{-1} to 7.65×10^3 μ.L^{-1}, showing no significant change in number.

Previous pilot-scale experiments showed that the number of aerobic denitrifying bacteria and the denitrifying functional genes (*nir*K and *nir*S) at the control area decreased (Zhou et al. 2016), but this phenomenon was not found in this study. This may be due to the lack of carbon source in the closed test (previous study), which led to the inhibition of microbial metabolism and reproduction. This study was conducted in the reservoir field site, and the exchange between water bodies would not lead to the lack of carbon source.

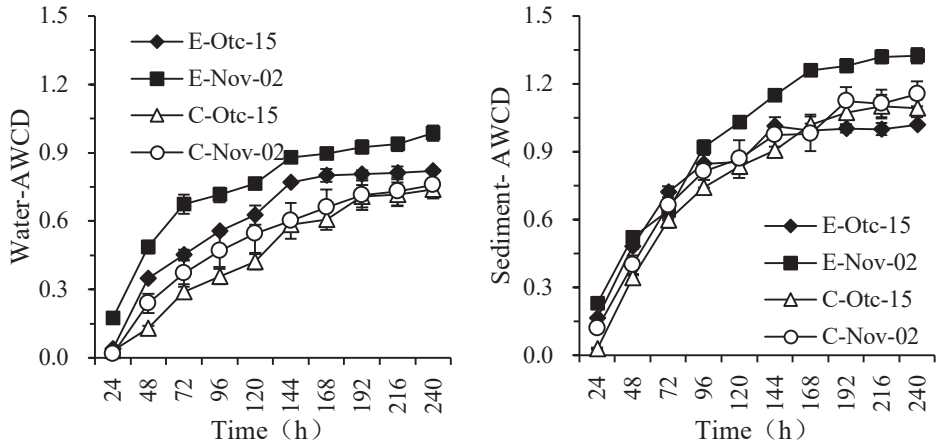

Fig. 2: Changes of AWCD in water and surface sediments in enhanced area (E) and control area (C).

Table 4: Utilization rate of carbon sources by microorganisms and U index changes in water and surface sediments in mixing aeration area.

Samples		carbonyl compounds	amino acids	esters	alcohols	amines	carboxylic acids	U index
Water	Oct-15	0.73	0.72	0.80	0.71	0.65	0.88	3.24
	Nov-02	1.02	1.20	1.30	0.95	1.10	0.95	4.28
	Increase proportion（%）	39.7	66.7	62.5	33.8	69.2	7.9	32.1
Sediment	Oct-15	0.94	0.85	0.99	0.88	0.89	1.05	5.21
	Nov-02	1.21	1.09	1.35	1.21	1.32	1.21	6.32
	Increase proportion（%）	28.7	29.3	36.4	37.5	37.1	15.2	21.3

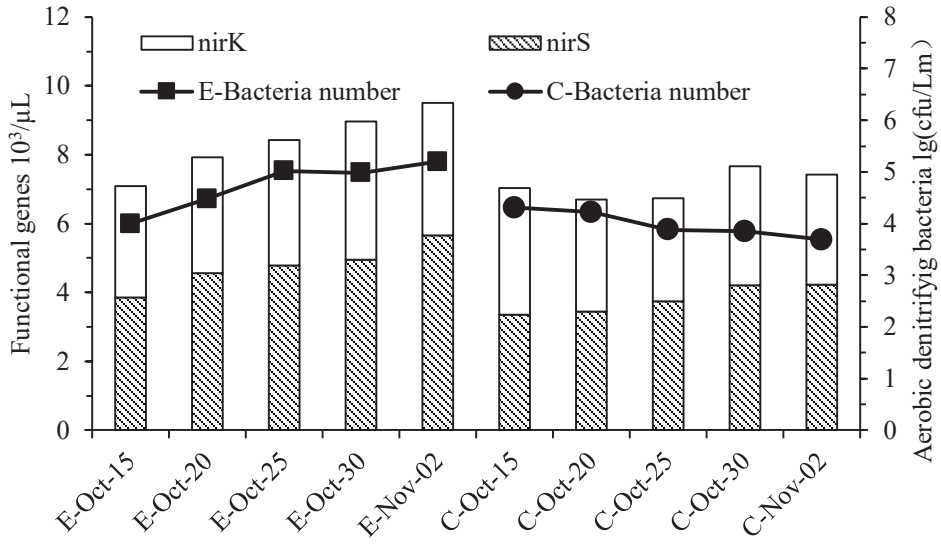

Fig. 3: Changes of aerobic denitrification genes and density of aerobic denitrifying bacteria in water in enhanced area (E) and control area (C).

High-throughput sequencing was used to analyse the proportion of aerobic denitrifying bacteria in the operation of the water-lifting aeration system. The results (Table 5) showed that after the operation of the system, the density of the main aerobic denitrifying bacteria *Acidovorax*, *Novosphingobium*, *Hydrogenophaga*, *Pseudomonas*, *Methylophaga*, *Bacteroidetes* and *Sphingomonadaceae* increased significantly. For example, the proportion of *Acidovaxor* increased from 0.01% before the operation of the system to 0.15%. The operation of water-lifting aeration system increased the proportion of aerobic denitrifying bacteria in total bacteria. This conclusion also helped to reveal the mechanism of denitrification nitrogen removal in water.

Principal Component/Redundancy Analysis of Environmental Factors and Microorganisms

Principal Component Analysis (PCA) is a powerful tool for analysing sample differences. In this paper, PCA was carried out based on environmental factors (water quality parameters) and microbial composition, respectively, to analyse the differences between enhanced and control areas in the operation of water-lifting aeration system. The results showed that the principal component analysis of the environmental factors and microbial composition can explain 95.41% and 87.19% of water quality and microbial composition respectively, which can well reflect the whole process. As shown in Fig. 4, at the beginning, there was no obvious difference in water quality and microorganisms composition between the enhanced area and the control area, and the distribution of sample sites in each depth was concentrated. However, with the operation of the aeration system, DO and T in the enhanced area changed, and the microbial population also changed. The difference between the enhanced area and the control area was more and more obvious. It was clear

Table 5: Variations of aerobic denitrifying bacteria in water in mixing aeration area (E) and control area (C).

Species/sampling sites-dates	E-Oct-15	E- Nov-02	C-Oct-15	C-Nov-02
Acidovorax	0.01%	0.15%	-	0.02%
Novosphingobium	0.01%	0.10%	0.01%	-
Hydrogenophaga	-	0.05%	0.02%	0.01%
Pseudomonas	0.01%	0.02%	0.01%	0.01%
Methylophaga	0.01%	0.06%	0.01%	-
Bacteroidetes	0.02%	0.02%	0.01%	0.03%
Sphingomonadaceae	0.01%	0.03%	0.02%	0.02%

Note: "-" means undetected

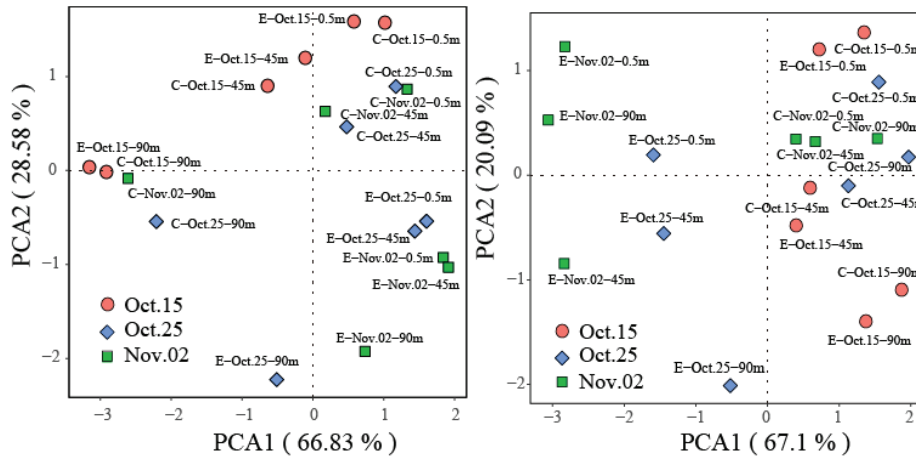

Fig. 4: Principal component analysis of environmental factors and microorganisms.

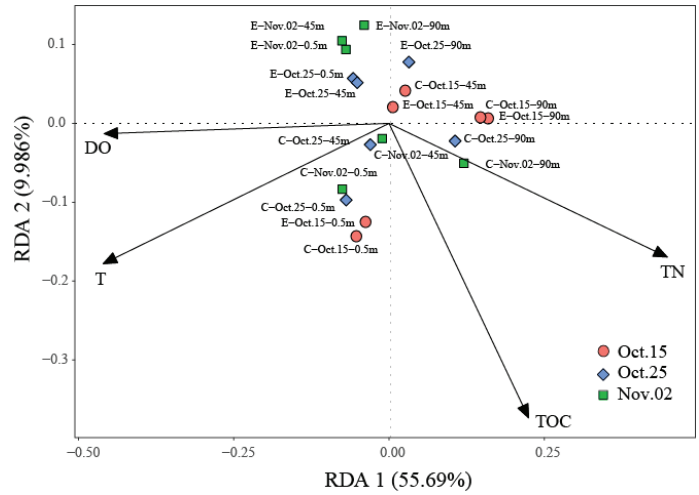

Fig. 5: Redundancy analysis of species and environmental factors during operation.

that water-lifting aeration can change water environment to regulate microbial community composition and finally improving water quality.

The relationship between microbial species and environmental factors is shown in Fig. 5. It was obvious that with the operation of the system, the differences between the enhanced area and the control area gradually increase. The correlation between environmental factors and microbial communities showed that DO, T and TN had a very significant correlation with RDA1 ($P < 0.001$), TOC and RDA1 had a significant correlation ($P < 0.05$). DO and T had a significant correlation with RDA1 ($P < 0.05$). The results of TN showed that the microorganisms in nitrogen cycle increase with the operation of water-lifting aeration. The water-lifting aeration system can control the microbial composition by changing the water environment, thus achieving nitrogen removal and improving water quality.

CONCLUSIONS

(1) *In-situ* water quality improving study was carried out in the water source reservoir at field scale. It was found that TN and TOC in the enhanced area reduced by 29.7%-49.2%, 22.5%-29.1%, and TN and OC in the surface sediment reduced by 17.9% and 20.5%, respectively, while the reduction rate in the control area was not obvious.

(2) Biolog ECO microporous plate was used to measure microbial activity and carbon utilization in water and surface sediments. It was found that mixed aeration

increased microbial metabolic activity by more than 14%, carbon utilization by more than 30% and microbial McIntosh diversity index by more than 20% in the enhanced area.

(3) The results of high-throughput sequencing and amplification of aerobic denitrifying functional genes (*nir*K and *nir*S) showed that the number of functional genes and their proportion of aerobic denitrifying bacteria in the enhanced area increased by the mixed aeration process.

(4) Mixed aeration can improve microbial metabolic activity, the number of aerobic denitrifying bacteria and the number of functional genes (*nir*K and *nir*S) and enhance their denitrification performance. Satisfying results of denitrification and carbon removal have been achieved in field experiments of reservoirs, which further enriched the mechanism and practice of denitrification and carbon removal in source water.

(5) In order to destroy the stratification of water body and the oxygen-filled the bottom in field research, the air supply can be controlled at 30-40 m^3/h from the point of view of energy saving.

ACKNOWLEDGEMENT

This research was funded by National Natural Science Foundation of China (51909056), Key Scientific Research Projects of Higher Education Institutions in Henan Province (20A560023), Science and Technology Guidance Project of China Textile Industry Federation (2018040), Research Team Development Project of Zhongyuan University of Technology (K2018TD004), Young Backbone Teachers Grant Scheme of Zhongyuan University of Technology.

REFERENCES

Alzate Marin, J.C., Caravelli, A.H. and Zaritzky, N.E. 2016. Nitrification and aerobic denitrification in anoxic-aerobic sequencing batch reactor. Bioresource Technology, 200: 380-387.

Chen, Q., Ni, J., Ma, T., Liu, T. and Zheng, M. 2015. Bioaugmentation treatment of municipal wastewater with heterotrophic-aerobic nitrogen removal bacteria in a pilot-scale SBR. Bioresource Technology, 183: 25-32.

Coban, O., Kuschk, P., Kappelmeyer, U., Spott, O., Martienssen, M., Jetten, M. S. M. and Knoeller, K. 2015. Nitrogen transforming community in a horizontal subsurface-flow constructed wetland. Water Research, 74: 203-212.

Epsztein, R., Beliavski, M., Tarre, S. and Green, M. 2016. Simplified model for hydrogenotrophic denitrification in an unsaturated-flow pressurized reactor. Chemical Engineering Journal, 306: 233-241.

Fang, J.J., Li, Q., Liu, C., Jin, Z., Liang, Y., Huang, B., Lu, Xiao. and Peng, W. 2018. Carbon metabolism characteristics of the karst soil microbial community for Pb-Zn mine tailings. Environmental Science, 39(5): 2420-2430.

Gao, H., Schreiber, F., Collins, G., Jensen, M.M., Svitlica, O., Kostka, J.E., Lavik, G., Zhou, H. and Kuypers, M. 2010. Aerobic denitrification in permeable Wadden Sea sediment. Isme Journal, 4(3): 417-426.

Huang, T. L. and Li, X., H. Rijnaarts, Grotenhuis, T., Ma, W., Sun, X. and Xu, J. 2014. Effects of storm runoff on the thermal regime and water quality of a deep, stratified reservoir in a temperate monsoon zone, in Northwest China. Science of the Total Environment, 485-486(3): 820-827.

Huang, T.L., Zhang, L.N., Zhang, H.H., Su, J.F., Guo, L., Zhao, J.Y. and Zhang K. 2015. Screening and nitrogen removal characteristics of a heterotrophic nitrification-aerobic denitrification strain. Ecology and Environmental Sciences, 24(1): 113-120.

Jiyeon, C., Maniquiz, M.C., Byungsik, L., Jeong, S. and Kim, L. 2012. Characteristics of contaminant and phosphorus existence types in sediment of a constructed wetland. Desalination & Water Treatment, 38(1-3): 285-291.

Kang, P. L., Chen, S.N., Huang, T.L., Zhang, H.H., Shang, P.L., Zhao, Z.F., Wang, Y. and Tan, X. L. 2018. Denitrification characteristics and functional genes of denitrifying bacteria under aerobic or anaerobic conditions. Environmental Science, 8: 3790-3796.

Kang, P.L., Zhang, H.H., Huang, T.L. Zhang, H.H., Shang, P.L., Zhao, Z.F., Wang, Y. and Tan, X. L. 2018. Denitrification characteristics and community structure of aerobic denitrifiers from lake and reservoir sediments. Environmental Science, 39(5): 2431-2437.

Patureau, D., Godon, J., Dabert, P., Bouchez, T., Bernet, N., Delqenses, J.P. and Moletta, R. 1998. Microvirgula aerodenitrificans gen. nov. sp. nov. a new Gram-negative bacterium exhibiting co-respiration of oxygen and nitrogen oxides up to oxygen-saturated conditions. Int. J. Syst. Bacteriol., 48 Pt 3(3): 775-782.

Patureau, D., Helloin, E., Rustrian, E., Bouchez, T., Delgenese, J.P. and Moletta, R. 2001. Combined phosphate and nitrogen removal in a sequencing batch reactor using the aerobic denitrifier, Microvirgula aerodenitrificans. Water Research, *35*(1): 189-197.

Robertson, L.A. and Kuenen, J.G. 1982. *Thiosphaera pantotropha* gen. nov. sp. nov. a facultatively anaerobic, facultatively autotrophic sulphur bacterium. Journal of General Microbiology, 129(9): 2847-2855.

Song, Z.F., An, J., Fu, G.H. and Yang, X. L. 2011. Isolation and characterization of an aerobic denitrifying Bacillus, sp. YX-6 from shrimp culture ponds. Aquaculture, 319(1): 188-193.

Sun, S.P., Pelliceri, N. C. Merkey, B., Zhou, Q., Xia, S.Q., Yang, D.H. and Sun, J.H., Barth, S. 2010. Effective biological nitrogen removal treatment processes for domestic wastewaters with low C/N ratios: A review. Environmental Engineering Science, 27(2): 111-126.

Xu, Z., Dai, X. and Chai, X. 2018. Effect of different carbon sources on denitrification performance, microbial community structure and denitrification genes. Science of the Total Environment, 634: 195-204.

Zhou, S., Huang, T., Zhang, H., Zeng, M., Liu, F., Bai, S., Shi, J., Qiu, X. and Yang, X. 2016. Nitrogen removal characteristics of enhanced *in situ* indigenous aerobic denitrification bacteria for micro-polluted reservoir source water. Bioresource Technology, 201: 195-207.

Zhou, S.L., Huang, T.L., Huu, H.N., Zhang, H., Liu, F., Zeng, M., Shi, J. and Qiu, X. 2016. Nitrogen removal characteristics of indigenous aerobic denitrifiers and changes in the microbial community of a reservoir enclosure system via in situ oxygen enhancement using water lifting and aeration technology. Bioresour. Technol., 214: 63-73.

Zhou, S.L., Huang, T.L., Bai, S.Y. and He, X. 2016. Isolation, identification, and nitrogen removal characteristics of oligotrophic aerobic denitrifiers. China Environmental Science, 36(1): 238-248.

Zhou, Z.Z., Huang, T.L., Li, Y., Long, S. and Zhou, S. 2017. Improvement of water quality and sediment control by WLAs in a source water reservoir. China Environmental Science, 37(1): 210-217.

Nature Environment and Pollution Technology
An International Quarterly Scientific Journal

p-ISSN: 0972-6268
e-ISSN: 2395-3454

Vol. 19 | No. 1 | pp. 141-147 | 2020

Original Research Paper

Open Access

Environmental Pollution and Energy Efficiency of Regional Transportation Industry: A Case Study of Jilin Province, China

Rongbo Wu
School of Railway Transportation, Jilin Railway technology college , Jilin, 132001, China
†Corresponding author: Rongbo Wu

Nat. Env. & Poll. Tech.
Website: www.neptjournal.com

Received: 12-12-2019
Accepted: 20-01-2020

Key Words:
Transportation industry
Environmental pollution
Energy efficiency
Jilin Province

ABSTRACT

The transportation industry is the fundamental and strategic industry for social and economic development. However, this industry becomes a considerable barrier against green, sound, and sustainable economic and social development due to the rapid increase in energy consumption and greenhouse gas emission. Transportation industry becomes one of weakness of energy saving and emission reduction with its increasing energy consumption and carbon emission. Environmental pollution caused by the transportation industry can be relieved effectively by increasing energy efficiency. A case study based on Jilin Province, China is carried out. First, environmental pollution types caused by regional transportation industry are analysed. Second, energy efficiency of transportation industry in eight prefecture-level cities in Jilin Province from 2011 to 2017 is determined using the DEA-Malmquist index. Finally, measures to control environmental pollution caused by the transportation industry are proposed. Results show that in Jilin Province, environmental pollution caused by the transportation industry manifests through increasing energy consumption, pollution from car exhaust, and degree of traffic jams. In its eight prefecture-level cities, the average energy efficiency change index of transportation industry is 1.054, which is higher than 1. The means of technological efficiency and progress are 0.973 and 1.084, respectively. The mean pure technological efficiency of energy use slightly increases, while the mean scale efficiency decreases significantly. Results can provide beneficial references for full understanding on energy consumption and environmental emission of transportation industry in Jilin Province. This understanding can lead to the exploration of scientific and reasonable energy-saving and emission-reduction ways and countermeasures, aiming to offer decision-making references for energy saving and emission reduction of the transportation industry in Jilin Province.

INTRODUCTION

The transportation industry is the fundamental and strategic industry for social and economic development. However, this industry becomes a considerable barrier against green, sound, and sustainable economic and social development due to the rapid increase of energy consumption and greenhouse gas emission. Moreover, the transportation industry is typically characterized by high-energy consumption, which increases with continuous economic, social, and industrial developments and proposes a huge challenge to the whole society and energy-saving development of the industry. Nevertheless, industry energy consumption show significant regional differences in China. Lack of regional energy-saving goals and policy may cause mutual restraints between development and energy saving of regional transportation industries.

Jilin Province experiences continuous economic prosperity and accelerating urbanization. As such, pressure over resources and environment intensifies due to the rapid growth of urban population and dramatically expanding urban scale, accompanied with increasing prominent negative externality of economic agglomeration. "Urban diseases," which are centred at atmospheric pollution and traffic jams, are becoming important factors that restrict the development of different cities in Jilin Province. In this province, the transportation industry is the pillar industry of national economic development, attracting wide attention and serving as a key industry with high-energy consumption and pollutant emission. Table 1 shows that this transportation industry accounts for high-energy consumption and causes heavy environmental pollution. As a response to economic development and rising population and number of vehicles in Jilin Province, transportation demands continuously increase. Moreover, problems such as traffic jams, transportation pollution, energy consumption, and public health become more prominent. Therefore, full understanding on energy consumption and pollutant emission of Jilin Province under various transportation policies is significant to the future sustainable development of the province. In addition, this understanding can provide decision-making references to

Table 1: Energy consumption of transportation industry in Jilin Province from 2010 to 2017.

Year	Raw coal (10,000 tons)	Gasoline (10,000 tons)	Coal oil (10,000 tons)	Diesel (10,000 tons)	Electricity (TWh)
2010	125.3	40.43	0.23	194.06	12.76
2011	116.97	40.27	0.23	213.42	13.94
2012	85.32	43.51	0.25	238.58	14.47
2013	76.89	37.85	0.25	256.74	17.43
2014	249.62	39.06	0.25	216.33	17.87
2015	312.73	37.58	0.26	198.68	19.22
2016	294.01	35.98	0.36	193.12	22.95
2017	214.04	45.88	5.2	213.91	24.63

realize the goal of energy saving and emission reduction and increase environmental performance of industries.

EARLIER STUDIES

Environmental pollution from and energy efficiency of the transportation industry are key concerns of the academic circle. Recently, the energy efficiency of the transportation industry has been widely discussed, but environmental constraints and the unexpected output from energy input are mostly ignored. Given that carbon emission is a by-product of transportation, studies on energy efficiency of highway traffic should consider the negative effects of and consider CO_2 emission as an unexpected output. These studies aim to accurately evaluate energy efficiency of the transportation industry under environmental constraints. With respect to environmental pollution caused by the transportation industry, Bose (1998) mainly estimated the traffic demands of residents in Delhi, Calcutta, Bombay, and Bangalore in India from 1990 to 2011. SO_2 and NOx emissions caused by the transportation industry were believed to be the main causes of environmental pollution. Poon et al. (2006) simulated influences of energy, transportation, and trade activities on local air pollutant emission (e.g., SO_2 and smoke particles) based on the environmental Kuznets model. Carbon black particle pollution in China caused by the transportation industry is more severe than SO_2 pollution. Atabani et al. (2011) pointed out that the transportation industry is the second highest in energy consumption, next to the industrial sectors. Energy consumption of the transportation industry accounts for 30% of global transmission energy. Highway traffic leads in oil consumption, accounting for 81% of total energy transportation demands. The transportation industry causes significant environmental pollution. Peng et al. (2015) believed that the increasing urban passenger transportation, as a result of the rapid growth of vehicle quantity in China, causes energy consumption, greenhouse gas emission, and atmospheric pollutants (NOx, CO, HC, and PM). In addition, the most effective regulation of vehicle quantity could reduce energy consumption, CO_2, and atmospheric pollutant emissions to the maximum extent. Bansal (2018) believed that in developing countries, such as India, urbanization hinders sustainable growth of rapid mechanization and transportation infrastructures, and emissions from highway transportation are partial causes of ozone consumption, acid deposition, and other climatic changes. With respect to energy efficiency, Wang et al. (2012) believed that transportation industry accounted for approximately 8% of total energy consumption in China. The direct rebound effect of urban passenger transportation is also investigated and validated empirically. Using the double logarithmic regression equation and error correction model, Wang et al. (2014) measured the long- and short-term direct rebound effects through panel data of 31 provinces in China from 1999 to 2011. A partial rebound effect is observed in highway freight transportation in China, and the increasing energy efficiency independently is not very satisfying. Liu et al. (2016) measured energy environmental efficiency of highway and railway departments in 30 Chinese provinces by combining non-radial data envelopment analysis (DEA) model and window analysis. The findings show U-shaped and inverted U-shaped curves of the relations between energy environmental efficiency and income level of highway and railway departments. Wu et al. (2016) measured energy and environmental performances of China's transportation system using DEA. Empirical findings demonstrate relatively low energy efficiency of transportation system in most provinces and effective control measures are proposed. Song et al. (2016) calculated environmental efficiency of highway transportation system in different regions in China. The environmental efficiency of China's highway transportation system is found generally unsatisfying, accompanied with considerable regional differences, excessive energy consumption, and motor vehicle pollution in most regions. Liu et al. (2018) studied interprovincial energy efficiency of the transportation industry in China and relevant influencing factors, finding evident gradient distribution

of energy efficiency. The highest energy efficiency among the transportation industries are found in provinces in East China, followed by those in central and West China. This interprovincial difference in energy efficiency is gradually narrowing. Liu et al. (2019) evaluated energy and environmental efficiencies of the highway transportation industry in China. Empirical proof shows that diffusion and use of optical production technology in the highway transportation industry in Western and Central China is superior to technological innovation progress. Omrani et al. (2019) evaluated energy efficiency of transportation departments in 20 Iran provinces by combining DEA and cooperative game method. Compared with large economic provinces, several small economic provinces show better energy efficiency in their transportation industry. Extant studies show that the transportation industry cause heavy environmental pollution during its development, but such pollution can be relieved effectively through technological progress and improvements in energy efficiency. Increasing energy utilization of the transportation industry is the most important way to solve the contradiction between its rapid development and the goals of energy saving and emission reduction. Therefore, scientific evaluation of energy efficiency of the transportation industry in prefecture cities of Jilin Province (China), exploring key factors to improve energy efficiency, and proposing specific suggestions present important practical significance to green sound development of the transportation industry.

TRAFFIC POLLUTION STATUS OF JILIN PROVINCE

Continuous Increase of Energy Consumption by the Transportation Industry

The automobile industry of Jilin Province is flourishing. The quantity of cars in cities is quickly increasing in recent years. Fig.1 shows that the quantity of cars for highway transportation in Jilin Province increased from 179,700 in 2006 to 351,900 in 2018. This sharp increase causes energy consumption and tail gas pollution that are difficult to avoid. The transportation industry is a major energy consumer, and the proportion of its energy consumption to total social energy consumption increases continuously.

Continuous Intensification of Tail Gas Pollution of Cars

Most cities in Jilin Province have developed highway transportations and various types of motor vehicles, resulting in highly excessive tail gas emission compared with standard figures. Dust particle density is relatively high and urban air pollution is observed. Fig. 2 shows the external diseconomies brought by rapid development of the transportation industry and inappropriate transportation development in Jilin Province. PM2.5 emission is rapidly intensifying. Vehicle emission has become a primary pollution source such as CO and hydrocarbon. Tail gas emission from cars is extremely high in most cities of Jilin Province. In addition, externality of air pollution caused by the increased tail gas emission of vehicles cannot be ignored, thus resulting in chronic intoxication of the central nervous system and functions of the human body, manifested by headaches and crossing eyes.

Gradual Intensification of Traffic Jams

With the increasing traffic demands of residents in Jilin Province, road traffic changes from smooth to disordered, and commuting takes longer to reach destinations. When traffic demands further increase and exceed the ultimate traffic efficiency in places with minimum traffic capacity, the road traffic state changes accordingly. Traffic jams not only cause invalid waiting and wasted times, but also decreases efficiency of the transportation system and causes traffic accidents.

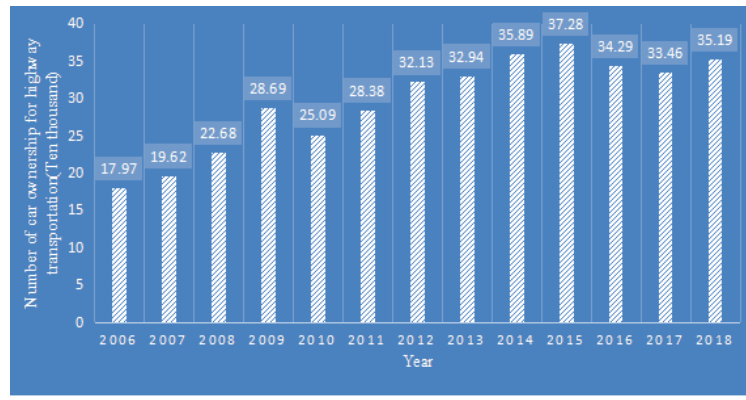

Fig.1: Number of car ownership for highway transportation in Jilin Province in 2006-2018. (Data source: Jilin Statistical Yearbook)

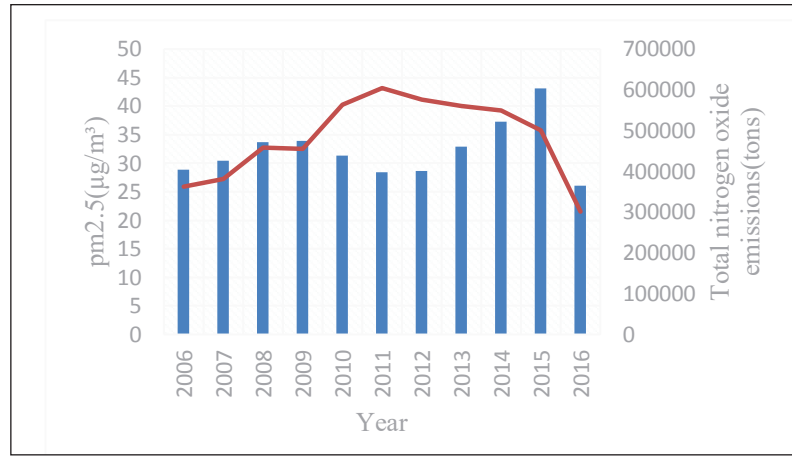

Fig. 2: PM2.5 and total Nitrogen oxide emissions in Jilin Province in 2006-2016.
(Data source: Jilin Statistical Yearbook)

More importantly, traffic jams cause negative external cost. Fuel utilization decreases whereas energy consumption and pollutant emissions increase, because pollutant emissions from incomplete combustion during traffic jams are far higher than pollutant emissions during normal driving.

Brief Introduction to The Model and Data Specification

Introduction to the model: Following Färe et al. (1992), the DEA-Malmquist Index, which is under variable returns to scale, oriented to output, and uses t and t+1 as technical references, is defined in formula (1):

$$M_{t,t+1} = \frac{D^v_{t+1}(x_{t+1},y_{t+1})}{D^v_t(x_t,y_t)} \times \left[\frac{D^v_t(x_t,y_t)}{D^c_t(x_t,y_t)} \div \frac{D^v_{t+1}(x_{t+1},y_{t+1})}{D^c_{t+1}(x_{t+1},y_{t+1})} \right] \times \left[\frac{D^c_t(x_t,y_t)}{D^c_{t+1}(x_t,y_t)} \times \frac{D^c_t(x_{t+1},y_{t+1})}{D^c_{t+1}(x_{t+1},y_{t+1})} \right]^{\frac{1}{2}} \quad \ldots(1)$$

Where $D^c(x,y)$ is the distance function under constant returns to scale and $D^v(x,y)$ is the distance function under variable returns to scale. $\frac{D^v_{t+1}(x_{t+1},y_{t+1})}{D^v_t(x_t,y_t)}$ is the change of pure technological efficiency (PTEC), $\frac{D^v_t(x_t,y_t)}{D^c_t(x_t,y_t)} \div \frac{D^v_{t+1}(x_{t+1},y_{t+1})}{D^c_{t+1}(x_{t+1},y_{t+1})}$ is the change of scale efficiency (SE), $\left[\frac{D^c_t(x_t,y_t)}{D^c_{t+1}(x_t,y_t)} \times \frac{D^c_t(x_{t+1},y_{t+1})}{D^c_{t+1}(x_{t+1},y_{t+1})} \right]^{\frac{1}{2}}$ and is technological progress (TC). In other words, the product of the previous two terms is the change of technological efficiency (EC). When $M_{t,t+1} > 1$, total factor productivity (TFP) progresses. When $M_{t,t+1} < 1$, TFP regresses. When $M_{t,t+1} = 1$, TFP is constant. In the panel data analysis of the transportation industry in Jilin Province, TFP decomposes into the product of TC and EC. EC is further decomposed into the product of PTEC and SE. On this basis, the influence of PTEC and SE on technological efficiency can be determined. Contributions of pure technological inefficiency and scale inefficiency to influences of PTEC and SE, respectively, can be recognized separately as long as nontechnological efficiency is discovered in efficiency estimation of the transportation industry. On the basis of these results, policy suggestions are proposed. Specific meanings of different indexes are introduced as follows: Malmquist Index refers to the change process of TFP. The change index of EC is to measure whether production meets the optimal resource allocation. The change index of TC reflects changes of production technologies. The change index of PTEC is part of production technological inefficiency caused by pure technological inefficiency. The change index of SE is to judge whether the decision-making units are in the optimal production scale.

Data specification: Input indexes include capital, labour, and energy input. Capital input refers to fixed-asset investments (10,000 Yuan) to transportation industry in different cities of Jilin Province. Labour input refers to the number of employees in the transportation industry at year-end (10,000 persons). Energy input refers to energy consumption of the transportation industry (10,000 tons of standard coal). Energy resources consumed by transportation industry, such as coal, oils, natural gas, heating power, and electricity, are all transformed to standard coal. Output indexes include turnover vol-

ume of passenger traffic and of freight transport. The former is mainly expressed by annual passenger person-kilometres (10,000 persons km) and the latter is mainly expressed by freight turnover (10,000 tons km) in each city. This study uses panel data of eight prefecture cities of Jilin Province from 2011 to 2017. Data of various input and output indexes are all collected from Statistics Yearbook of Jilin Province.

RESULT ANALYSIS

Energy efficiency of the transportation industry in different prefecture cities of Jilin Province was decomposed dynamically using the Malmquist Index by estimating the comprehensive efficiency of energy utilization. Regional differences and their causes were analysed. Annual variations of TFP of the transportation industry in Jilin Province from 2011 to 2017 were estimated using the DEAP2.1-XP software package from the perspective of output. Table 2 lists the results.

Table 2 shows that in eight cities of Jilin Province, the mean energy efficiency change index of transportation industry was 1.054 from 2011 to 2017, which was higher than 1. Energy utilization of transportation industry in Jilin Province increased to a certain extent during the study period. In view of the decomposition results, the mean EC and TC are 0.973 and 1.084, respectively. This finding reflects that energy utilization of the transportation industry increased by 0.54%, including 0.84% attributed to TC and 0.27% attributed to EC. Specifically, EC hindered the improvement of energy utilization. The mean PTEC of energy utilization increased slightly whereas the mean SE decreased significantly, indicating that EC reduction was mainly attributed to SE reduction. EC and SE were relatively low and could potentially increase. EC reached 1.015, and could further increase. The energy utilization of the transportation industry in Jilin Province was generally low due to low SE. EC and SE of the transportation industry in Jilin Province from 2011 to 2017 generally decreased, but PTEC was relatively stable. This finding possibly occurred because of the increased efforts in external industrial structural transfer and transportation enterprises made fundamental investments in response to the government's call of "industrial transfer". Enterprises were in the investment period and were exploring new technologies. Meanwhile, production scale was not controlled at a reasonable level. Enterprises were adapting to new policies. After 2012, Jilin Province increased investment to traffic infrastructure, released various successive policies, and encouraged investments of abundant capital and labour forces into the "Harbin-Changsha Urban Agglomeration" and "Changsha-Jilin-Tumen Development and Opening Up Pilot Region". These programs promoted the overall technological innovation transportation industry in Jilin Province, and comprise one possible cause why the EC of the transportation industry in Jilin Province was retained over 0.9 before 2012. However, SE was not as high as PTEC, because huge capital investment was mainly applied to technological innovation and expansion in the enterprise scale. Instead, enterprise problems of production efficiency were ignored, thus resulting in high PTEC and low SE.

POLICY SUGGESTIONS

Improve the Transportation Structure and Accelerate Development Transportation Mode with Low Energy Consumption

Jilin Province can accelerate energy-saving comprehensive transportation system, develop relative advantages of different transportation modes by planning the transportation system, and promote reasonable equilibrium development of different transportation modes by closely combining natural geological environment and economic development status. These improvements likewise increase the connection and informatization level of infrastructures of the comprehensive transportation system, realize fast transit of passenger and freight, and improve quality and efficiency of transportation services. Jilin Province can increase investment and support for railway, shipment, and pipeline transportation, increase proportion of transportation modes with low

Table 2: Variations of energy production efficiency indexes of the transportation industry of Jilin Province.

Year	EC	TC	PTEC	SE	TFP
2011-2012	0.755	1.021	1.087	0.695	0.771
2012-2013	0.832	0.976	1.002	0.830	0.812
2013-2014	0.925	1.286	0.982	0.942	1.190
2014-2015	0.987	1.042	0.998	0.989	1.028
2015-2016	1.123	1.153	1.008	1.114	1.295
2016-2017	1.214	1.025	1.012	1.200	1.244
Mean	0.973	1.084	1.015	0.958	1.054

single consumption, and guide transfer of bulk cargo to energy-saving environment-friendly transportation mode. Railway transportation in the market can be increased, and attention is necessary to improve service quality of railway passenger transportation. The speed and comfort advantages of railway, in relation to highway, can be improved through the development of high-speed rails. Considerable efforts can be made to develop urban public transport and railway system to increase public commuting rates.

Reduce Energy Consumption Intensity and Increase Energy Utilization of The Transportation Industry

Jilin Province can formulate more energy-saving policies to decrease energy intensity. With the improvement of transport tools and development of clean energies, the existing transportation industry still has high energy-saving potential. For highway transportation, old vehicles with high-energy consumption can be eliminated. Instead, highway transportation vehicles can be developed in larger sizes and fuelled by diesel. Moreover, Jilin Province can promote the development of new energy automobiles, improve quick charge technology of electric cars and cruising ability of batteries, increase subsidies for electric cars, and strengthen competitive advantages of new energy cars in relation to traditional vehicles. For railway transportation, Jilin Province can promote the application of electric locomotives, gradually decrease proportion of diesel locomotives, and decrease dependence on petroleum products. In addition, the province can update old ships to larger sizes and professional makes, increase proportions of ships using clear energy dynamics, decrease energy-saving construction of civil air transportation system, choose the latest energy-saving transportation vehicles, and improve organization and management technologies of civil transportation.

Strengthen Energy Saving and Emission Reduction of the Transportation Industry, and Develop Public Transport System

Jilin Province can pay much attention to energy saving and emission reduction of land transportation, such as by implementing policies of public transport priority, perfecting relevant infrastructure equipment, and decreasing energy wastes while assuring and increasing transportation capacity. In addition, Jilin Province can increase proportion of clean energy in land transportation and shipment. Pilot projects and construction of relevant infrastructures from aspects which are easy to be regulated, including public bus, taxi, and water bus, can also be implemented. Good commuting conditions can be achieved to encourage citizens to choose biking and walking and advocate slow commuting. Moreover, these conditions enrich transportation mode, optimize transportation layout, combine land transportation and shipment organically, and take advantage of both transportation modes.

Pay Attention to the Development of Energy-Saving Technologies and Increase Technological Input

As a significantly effective transition direction, energy-saving technological development for the transportation industry can effectively save energies and decrease emissions in a relatively short period, which is a strong stimulus of the market and consumers. TC not only increases traditional energy efficiency, but also accelerates transition of other transportation modes such as electrification. Attention and investment to energy-saving technologies can be increased appropriately, while diversified parties, including scientific research units and enterprises, can be encouraged to participate in R&D. As such, potentials of technological energy saving from aspects of light weight, small size, and low-resistance electronic control, car network and intelligent driving, and applications of new materials, biofuel, and liquid hydrogen can be explored. Such enhancements can quickly and effectively accomplish energy transition of the transportation industry. With respect to transportation energy technologies, Jilin Province can respond to national policies to develop energy-saving technologies and assure marketing of energy-saving vehicles. For energy structure in the transportation industry, energy updating of urban transportation requires completion as soon as possible through economic means from private sectors and relevant enterprises, mandatory requirements on public sectors, and increased promotion of new clean energy vehicles.

CONCLUSIONS

Influences of the transportation industry on environmental pollution in urban areas of a certain region are increasing gradually. Energy consumption and atmospheric pollution are intensifying gradually. The transportation industry has rapidly become the highest contributor to energy consumption in the region. Accordingly, CO_2 emission from the transportation industry is increasing gradually. Hence, its energy transition development is urgently necessary. Development modes in foreign countries prove that the main direction to realize such energy transition in urban transportation is through increased energy efficiency of the industry by adjusting energy structure and developing energy-saving technologies. In this study, a case study is carried out on Jilin Province, China. Types of environmental pollutions caused by the regional transportation industry are analysed. Additionally, energy efficiency of the transportation industry in eight prefecture cities of Jilin Province from 2011 to 2017 is estimated using DEA-Malmquist. The results demonstrate that in Jilin

Province, continuously increasing energy consumption of the transportation industry, tail gas pollution of vehicles, and degree of traffic jams are the main types of environmental pollutions caused by the transportation industry. In the eight prefecture cities of Jilin Province, the mean energy efficiency change index of the transportation industry is 1.054, indicating the improvement of energy efficiency. The mean EC and TC are 0.973 and 1.084, respectively. The mean PTEC slightly increases whereas the mean SE significantly decreases. Further exploration is suggested for the factor decomposition of energy consumption of the transportation industry, interaction mechanism among different influencing factors of energy efficiency, systematic dynamic simulation between transportation industry and ecological environment, practicability of transportation energy policies in different regions, and effects of environmental and economic policies on transportation-induced environmental pollution control in cities with different development degrees.

REFERENCES

Atabani, A. E., Badruddin, I. A., Mekhilef, S. and Silitonga, A. S. 2011. A review on global fuel economy standards, labels and technologies in the transportation sector. Renewable and Sustainable Energy Reviews, 15(9): 4586-4610.

Bansal, A. 2018. Analysis of traffic related environment pollution in Indian cities: Need of the hour. Asian Journal of Engineering and Applied Technology, 7(1): 70-73.

Bose, R. K. 1998. Automotive energy use and emissions control: A simulation model to analyse transport strategies for Indian metropolises. Energy policy, 26(13): 1001-1016.

Färe, R. and Grosskopf, S. 1992. Malmquist productivity indexes and Fisher ideal indexes. The Economic Journal, 102(410): 158-160.

Liu, H., Wu, J. and Chu, J. 2019. Environmental efficiency and technological progress of transportation industry-based on large scale data. Technological Forecasting and Social Change, 144: 475-482.

Liu, W. and Lin, B. 2018. Analysis of energy efficiency and its influencing factors in China's transport sector. Journal of cleaner production, 170: 674-682.

Liu, Z., Qin, C. X. and Zhang, Y. J. 2016. The energy-environment efficiency of road and railway sectors in China: Evidence from the provincial level. Ecological indicators, 69: 559-570.

Omrani, H., Shafaat, K. and Alizadeh, A. 2019. Integrated data envelopment analysis and cooperative game for evaluating energy efficiency of transportation sector: a case of Iran. Annals of Operations Research, 274(1-2): 471-499.

Peng, B., Du, H., Ma, S., Fan, Y. and Broadstock, D. C. 2015. Urban passenger transport energy saving and emission reduction potential: a case study for Tianjin, China. Energy Conversion and Management, 102: 4-16.

Poon, J. P., Casas, I. and He, C. 2006. The impact of energy, transport, and trade on air pollution in China. Eurasian Geography and Economics, 47(5): 568-584.

Song, M., Zheng, W. and Wang, Z. 2016. Environmental efficiency and energy consumption of highway transportation systems in China. International Journal of Production Economics, 181: 441-449.

Wang, H., Zhou, P. and Zhou, D. Q. 2012. An empirical study of direct rebound effect for passenger transport in urban China. Energy Economics, 34(2): 452-460.

Wang, Z. and Lu, M. 2014. An empirical study of direct rebound effect for road freight transport in China. Applied Energy, 133: 274-281.

Wu, J., Zhu, Q., Chu, J., Liu, H. and Liang, L. 2016. Measuring energy and environmental efficiency of transportation systems in China based on a parallel DEA approach. Transportation Research Part D: Transport and Environment, 48: 460-472.

Nature Environment and Pollution Technology
An International Quarterly Scientific Journal

p-ISSN: 0972-6268
e-ISSN: 2395-3454

Vol. 19 | No. 1 | pp. 149-157 | 2020

Original Research Paper | Open Access

Preparation of Polyvinyl Alcohol/Graphene Oxide Composites and Their Adsorption Properties

Yanyan Dong*, Manuel J. Lis Arias, Chengye Hu*, Wendan Wu*, Liping Liang*, Xinlan Mou* and Xu Meng*(***)†**
*College of Textile and Garment, College of Life Science, Shaoxing University, Shaoxing, 312000, China
**Textile Research Institute of Terrassa (INTEXTER-UPC), 08222, Terrassa, Spain
***Key Laboratory of Clean Dyeing and Finishing Technology of Zhejiang Province, Shaoxing University, Shaoxing, 312000, China
†Corresponding author: Xu Meng

Nat. Env. & Poll. Tech.
Website: www.neptjournal.com

Received: 18-06-2019
Accepted: 30-08-2019

Key Words:
PVA/GO
Polymer
Composite material
Adsorption

ABSTRACT

The polyvinyl alcohol/graphene oxide (PVA/GO) hydrogel was prepared. It was confirmed that the adsorption performance of polyvinyl alcohol/graphene oxide hydrogel composite material was improved, and it does not cause secondary pollution. According to adsorption experiments, it was found that PVA/GO adsorbent with a content of 30 % graphene oxide has the best comprehensive performance. The suitable environment of adsorption was under 25°C, 12-18 h for adsorption time and acidic conditions. The suitable adsorbent dosage was 0.3g and the suitable concentration of the dye was 10 mg/L.

INTRODUCTION

With the development of industrial activities, a large amount of industrial wastewater has resulted in a number of environmental problems. Effective separation of wastewater is regarded as a potential solution for environmental protection (Gan et al. 2015, Nevárez et al. 2011, Sehaqui et al. 2015). There are various methods being used nowadays. Among them, adsorption has been confirmed to be a promising treatment because of its low cost and simple operation (Hameed et al. 2009, Adebajo et al. 2003, Gore et al. 2016). This method is especially suitable for printing and dyeing wastewater treatment. One of the most critical factors about the treatment is the properties of adsorbent, which determines the effect of adsorption. Graphene is the most widely used adsorbent in the adsorption. It has a large specific surface area as one of the structure features, but such as poor hydrophilicity, decreased adsorption effect in the later stage, and difficulty in removing after adsorption are its disadvantages (Kumar et al. 2016, Satti et al. 2010).

Compared to graphene's single molecular layer, GO has some advantages such as large number of hydrophilic groups, good dispersibility in water and easy surface modification (Russo et al. 2013). However, GO has tiny size and low cytotoxicity to normal cell. These cause the problem of secondary pollution if GO disperses in water. Researchers tried to compound GO with other compounds to form membranes, pellets or fibres (Shen et al. 2015). But these methods rely on the other compounds to wrap GO for forming, which reduces the content of graphene oxide in the compound and hinders the advantage of specific surface area (Tiwari et al. 2013). In order to solve the above problems and ensure the adsorption effect at the same time, polyvinyl alcohol and GO will be combined into hydrogel materials in this experiment, and its adsorption properties will be explored further.

PVA is a kind of white, non-toxic and odourless solid, with a large number of hydrophilic groups on the molecular chain, which is the reason of its excellent water-solubility (Wahab et al. 2019). The intermolecular interaction force of polyvinyl alcohol molecules is large, which can form a high strength film in close contact. In the experiment, PVA/GO composite hydrogel was synthesized by using PVA as the carrier and fixing GO on the polyvinyl alcohol matrix to form a three-dimensional hydrogel adsorbent with network structure. This hydrogel can be deposited in water after adsorption and separated well without affecting the adsorption effect of GO. PVA/GO composite material is simple to prepare and easy to operate. It is also an excellent adsorption material due to which it not only guarantees the adsorption performance of adsorbent, but also overcomes the disadvantage of secondary pollution.

After the PVA/GO composites were successfully prepared, a series of batch adsorption experiments were designed to explore their adsorption properties. The influencing factors on the adsorption process were investigated, such as the content of GO in the composites, material dosage, initial concentration of dye solution, adsorption temperature, adsorption time and pH value.

MATERIALS AND METHODS

Preparation of graphene oxide: All the test specimens were prepared by adding 2 g graphene and 1 g sodium nitrate to 46 mL concentrated sulphuric acid in an ice bath, and stirring for 15 min. At the time of the specimens keeping at a temperature of 20°C, 6 g $KMnO_4$ was added slowly and stirred fully for 2 h, and then the specimens were placed at 35°C for 30min. 92 mL of deionized water was added to them for diluting it. After standing about 15 min, 20 mL of 30% H_2O_2 was added after adding 280 g of water into the test specimens for further dilution. Then the samples reacted to bright yellow. After filtrating, the final product was washed in 5% diluted hydrochloric acid firstly and then washed in deionized water to neutral. Samples were dried under vacuum at 50°C. Finally, the samples were ground to a fine powder and stored for reserve.

Preparation of PVA/GO composites: All the working solutions were prepared by adding 90 g deionized water in a beaker with 10 g PVA and stirred to dissolve PVA at 90°C. 9.2 g NaOH and 6mL epichlorohydrin were added and stirred in the beaker. Samples were reacted over 6 h in the oven at 35°C. After forming gel material, freeze dryer was used to dry the material until its weight is constant. Finally, PVA hydrogel without graphene oxide was obtained. According to the above method and on the basis of the above steps, new samples were prepared by adding 0.1 g and 0.2 g, 0.3 g and 0.4 g of graphene oxide powder into the hydrogel, and reacted over 6 h at 35°C in the oven until forming gelatinous material. With the help of the freeze dryer, the material was dried until its weight became constant. Then the gel composite was cut up and labelled for storage.

Pre-experimental treatment: The standard navy-blue dye was configured with a concentration of 1 g/L. The absorbance of the standard navy-blue dye was measured at different concentrations (10 mg/L, 20 mg/L, 30 mg/L, 40 mg/L, 50 mg/L, 60 mg/L, 70 mg/L), and the standard curve was obtained. According to the curve equation, $R^2 = 0.999$, which proved that the prepared solution could meet the standard.

Diluting part of the standard dye solution and five groups of dye solution with a concentration of 10 mg/L (200 mL in each group) were obtained. Some dye was kept before adsorption, and then adsorbed with 0.5 g composite materials with different contents of grapheme oxide. Soaking the samples over 12 h at the constant temperature of 25°C, it was observed that the colour of dye became shallow after the reaction, and the adsorbent was adhered with navy-blue, which proved that composite material has good adsorption effect and deserved the follow-up study.

Batch adsorption experiments: To explore the adsorption effect of different contents of graphene oxide, 0.3 g PVA/GO composite hydrogel was taken separately which contains 0, 10 %, 20 %, 30 %, 40 % of graphene oxide and these samples were added to 200 mL navy-blue dye solution, whose initial concentration was 10 mg/L. The samples were placed in an

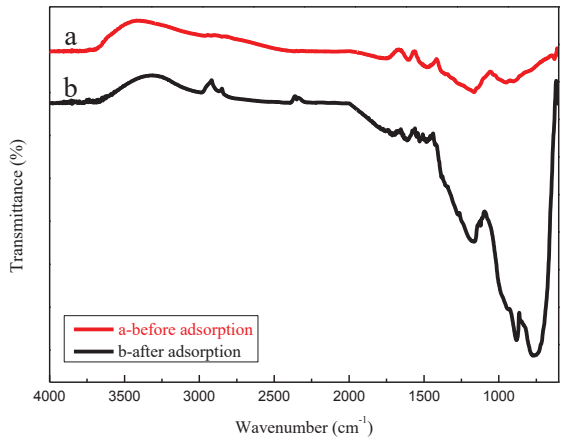

Fig. 1: Infrared spectra of PVA/GO composite before and after adsorption.

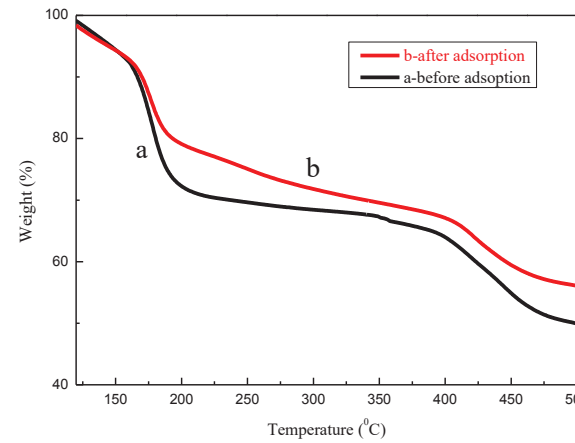

Fig. 2: Thermo gravimetric characterization of PVA/GO composite before and after adsorption.

oscillator with a constant temperature and oscillated for about 15 h until adsorption saturation. The absorbance of the dye was measured before and after adsorption.

To explore the effect of the adsorbent dosage on the adsorption, different doses (0.1 g, 0.3 g, 0.5 g, 0.7 g, 0.9 g) of the PVA/GO composite hydrogel (containing 30 % GO) respectively were taken and added to 200 mL navy-blue dye with an initial concentration of 10 mg/L. The samples were placed in an oscillator with a constant temperature and oscillated for about 15 h until the adsorption saturation. The absorbance of the dye was measured before and after adsorption.

To explore adsorption effect of adsorbent on different concentrations of the dye, 200 mL navy-blue dye with concentrations of 10 mg/L, 20 mg/L, 30 mg/L, 40 mg/L, 50 mg/L respectively was prepared. 0.3 g PVA/GO composite hydrogel (containing 30 % graphene oxide) was added into these samples. The samples were placed in an oscillator with a constant temperature and oscillated for about 15 h until adsorption saturation. The absorbance of the dye was measured by ultraviolet spectrophotometer before and after adsorption.

To explore the influence of temperature on the adsorption process, 0.3 g PVA/GO composite hydrogel (containing 30 % graphene oxide) was added to 200 mL navy-blue dye (initial concentration of 10 mg/L) at different temperatures of 25°C, 35°C, 45°C, 55°C and 65°C, respectively. The samples were placed in an oscillator with a constant temperature and oscillated for about 15 h until adsorption saturation. The absorbance of the dye was measured before and after adsorption.

To explore the influence of reaction time on adsorption, 0.3 g PVA/GO composite hydrogel (containing 30 % graphene oxide) was added to 200 mL navy-blue dye with the initial concentration of the dye at 10mg/L. The adsorption time was 6 h, 9 h, 12 h, 18 h and 24 h. The absorbance of the dye was measured by ultraviolet spectrophotometer before and after adsorption.

To explore the effect of pH on adsorption, pH of the solutions was adjusted to 1, 3, 5, 7, 9, 11, and 13 by adding HCl or NaOH. 0.3 g PVA/GO composite hydrogel (containing 30 % graphene oxide) was added to 200 mL navy-dye with initial concentration of 10 mg/L at different pH values. The samples were oscillated for about 15 h until adsorption saturation. The absorbance of the dye was measured before and after adsorption.

RESULTS AND DISCUSSION

Infrared Spectroscopy

In Fig.1, curve a is the infrared spectrum of the adsorbent before adsorption. 3420 cm^{-1} is the stretching vibration peak of the hydroxyl group, and such strong peaks also appear at

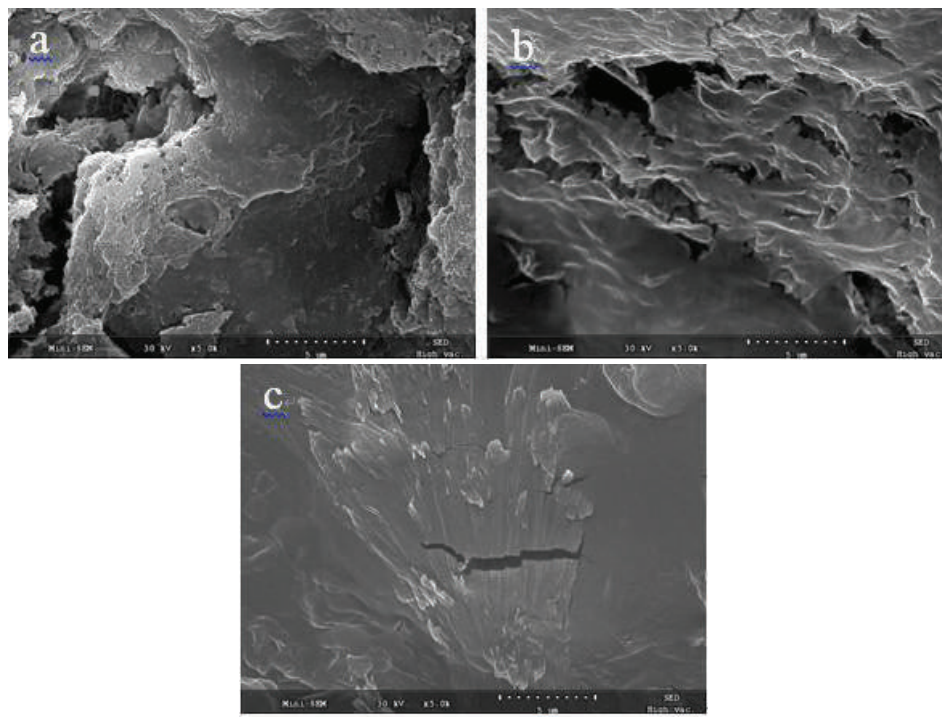

Fig. 3: a. SEM image of PVA hydrogel; b. SEM image of PVA/GO composite before adsorption; c. SEM image of PVA/GO composite after adsorption.

1400 cm^{-1} and 1630 cm^{-1}, which indicated the symmetric and asymmetric stretching vibration peaks of the carbonyl group. This indicated that GO was fixed on the substrate of PVA, the hydroxyl group of PVA, and the carboxyl group of GO were esterified. The two formed a three-dimensional network structure through covalent cross-linking. Curve b is the infrared spectra of the adsorbent after adsorption. It found that strong peak appeared in the front position obviously. The adsorption mechanism depends on hydrogen bonding, electrostatic effect, and molecular inter-atomic forces between the adsorbent and dye molecules. Contrasting with the images, the adsorbent adsorbing on dye made polymer material structure to change, and proved that adsorbent's success for the efficiency of dye adsorption.

Thermo Gravimetric Characterization

Fig. 2 shows the thermo gravimetric characterizations of PVA/GO composite material with 30 % GO before and after the adsorption. Curve b is the thermo gravimetric characterization of the composite after adsorption, and the results show that the weight loss occurs between 100°C to 200°C, and the main reason for this change is the thermal decomposition of functional groups. Compared to curve a, the thermal decomposition temperature increases after adsorption, which proved the successful adsorption of the dye by the adsorbent.

SEM Characterization

Fig. 3a is the SEM image of PVA without GO, and sparse holes are observed on the material surface. Fig. 3b is the SEM image of PVA/GO with a content of 30 % graphene oxide, showing a more regular layered porous structure. This is due to the covalent cross-linking reaction between PVA and GO, and forming a three-dimensional network structure. At the same time, during the preparation of hydrogel composites, some pores appeared by water evaporation during drying. Fig. 3c is the SEM image of the composite after adsorption. There are no empty holes and the texture is flat. This is because the dye molecules are attached to the composite during the adsorption process and the water grains appeared during the oscillation adsorption.

Langmuir, Freundlich and Temkin Adsorption Isotherm Fitting

The adsorption isotherm can be used to evaluate the adsorption capacity of the adsorbent (Qe=V×(co-ce)/m). Fig. 4 shows the adsorption performance of PVA/GO with 30 % GO with the blue dye. It was found that higher the initial concentration, higher the adsorption capacity. Because the dye molecules with high concentration distribution have greater diffusion driving force, they overcome more mass transfer resistance of solid phase and water phase, and more dye molecules combine with adsorbent molecules fully to play a role. Langmuir equation is as below:

$$\frac{C_e}{q_m} = \frac{1}{q_m b} + \frac{C_e}{q_e}$$

Where, q_e is the equilibrium adsorption capacity and q_m is the limit adsorption capacity. C_e is the equilibrium concentration, and b is the adsorption equilibrium constant.

The above adsorption isotherm data were fitted by the Langmuir isotherm equation, and the curve in Fig. 5 was obtained. The curve equation y = 0.5031x+0.0062(R^2=0.9894) indicated that the adsorption of navy blue dye by the com-

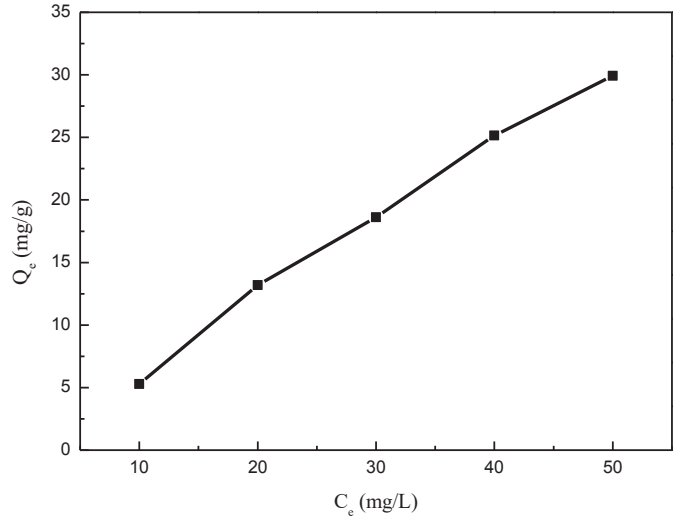

Fig. 4: Adsorption isotherm of PVA/GO composites with a content of 30% GO.

posite material was consistent with the Langmuir isotherm adsorption model, indicating that the composite material had excellent adsorption performance.

In addition, in the Langmuir isothermal model, the dimensionless equilibrium parameter RL = 1/(1+KL×Co) was used to obtain the RL values of different initial concentrations of the colourant. When RL = 0, the adsorption process is irreversible; when 0<RL<1, the adsorption process is favourable; when RL = 1, the adsorption process is linear; when RL>1, the adsorption process is unfavourable. When the RL values ranged from 0.19 to 0.32, the adsorption process was favourable.

Freundlich's isothermal equation is as follows:

$$\log q_e = \log K_F + \log C_e$$

Where, K_F and n are the adsorption empirical constants, C_e is the adsorption equilibrium concentration (mg/L), and q_e is the equilibrium adsorption quantity (mg/g). The curve in Fig. 6 was obtained, and the equation of the curve was y = 1.0749x-0.324, R^2=0.9899.

The equation of Temkin is as follows:

$$q_e = A + B \log C_e$$

The Temkin equation describes the energy relation of adsorption heat decreasing linearly with adsorption amount, and the curve in Fig. 7 is obtained. The curve equation is y = 50.266x-30.21, R^2 = 0.8986, which does not conform to the Temkin isothermal equation.

Based on the above three isothermal adsorption equations, the data in Table 1 are obtained. It can be known that the adsorption of PVA/GO composite on navy dye conforms to Langmuir and Freundlich equations, but not to Temkin equation. In addition, the isothermal adsorption model proves that PVA/GO composite has a good adsorption effect.

The Effect of PVA/GO Composites with Different GO Content

The (0) bottle in Fig. 8 is the navy blue dye with a concentration of 10 mg/L before adsorption, and the (a) - (e) bottles are 0.3 g dye which were fully adsorbed by PVA/GO composites containing 0, 10 %, 20 %, 30 % and 40 % GO respectively. It was found that the composites containing 30 % and 40 % GO have better adsorption effect. The absorbance of the solution was further measured. The concentration of the solution was calculated according to the standard curve of the dye, and then the adsorption rates were obtained, which were used to draw the graph as shown in Fig. 8. According to the data analysis, the adsorbent containing 30 % graphene oxide can be selected.

The Effect of PVA/GO Composites with Different Dosage

No. 0 bottle in Fig. 9 is navy blue dye with a concentration of 10 mg/L, while Nos. 1-5 bottles are PVA/GO composite hydrogel (containing 30 % graphene oxide) with dosages of 0.1 g, 0.3 g, 0.5 g, 0.7 g and 0.9 g, respectively, and the colour is a result of the full adsorption with the dye. It was observed that more the dosage, better the adsorption effect, but with the increase of the dosage, the adsorption effect did not change much. The absorbance of the solution was further measured, and the solution concentration was calculated according to the standard curve of the dye. According to the data analysis, the selection of 0.3 g adsorbent is fine to adsorb on 200 mL navy blue dye with a concentration of 10 mg/L.

The effect of PVA/GO Composites with Different Dye Concentrations

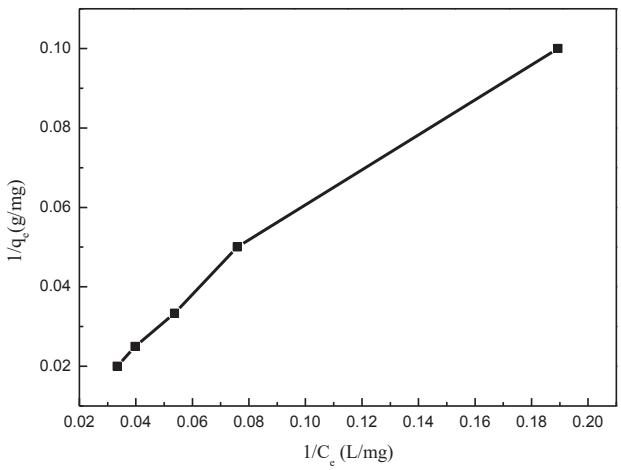

Fig. 5: Adsorption isotherm of Langmuir.

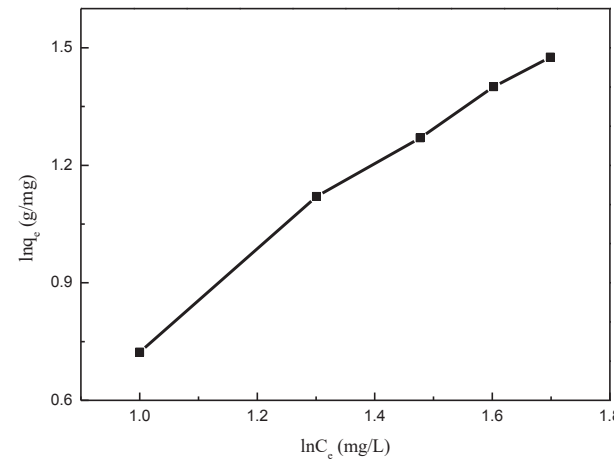

Fig. 6: Adsorption isotherm of Freundlich.

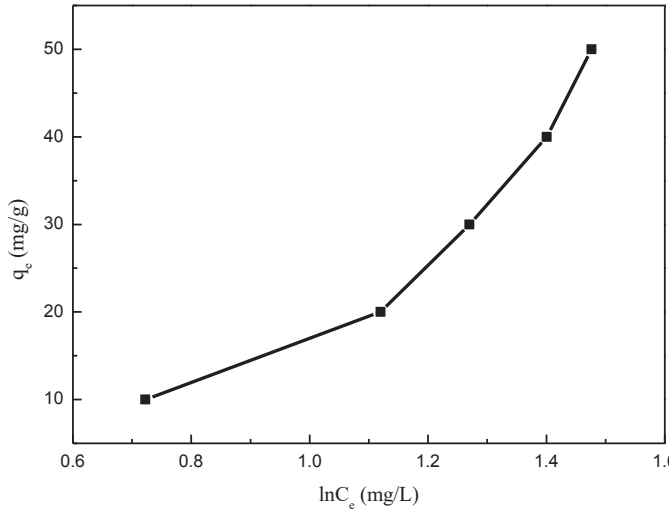

Fig. 7: Adsorption isotherm of Temkin.

Table 1: The Langmuir, Freundlich and Temkin isothermal adsorption model constants and their correlations for the adsorption of colorants by composites.

Isothermal equation of Langmuir			Isothermal equation of Freundlich			Isothermal equation of Temkin		
R^2	Qm	k	R^2	k	N	R^2	A	B
0.9894	0.5031	0.0062	0.9899	1.0749	0.324	0.8986	50.266	30.21

The above figure in Fig. 10 shows the navy blue dye before adsorption with concentrations of 10 mg/L, 20 mg/L, 30 mg/L, 40 mg/L and 50 mg/L. The below figure in Fig.10 is the effect picture which shows the full adsorption of 200 mL navy blue dye and 0.3 g PVA/GO composite hydrogel (containing 30 % graphene oxide). The absorbance of the solution was further measured. The solution concentration was calculated according to the standard curve of the dye, and then the adsorption rates were obtained. According to the data analysis, 0.3 g adsorbent (containing 30 % graphene oxide) has the best adsorption effect on 200 mL dye with a concentration of 10 mg/L.

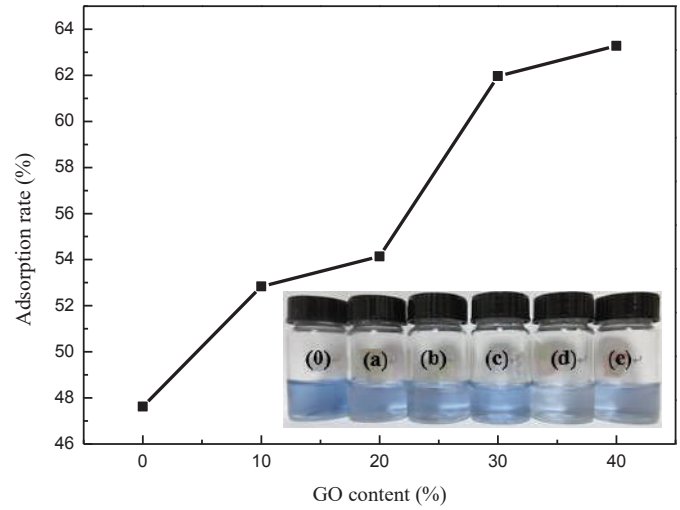

Fig. 8: Adsorption curves of composite materials with different GO contents.

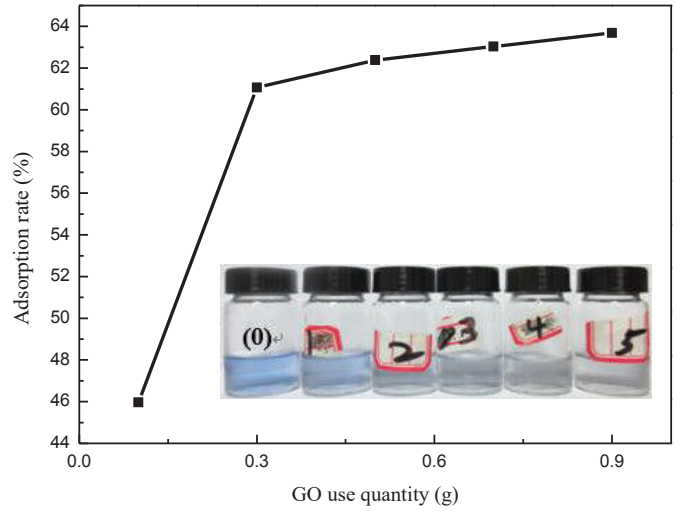

Fig. 9: Adsorption curves of composites with different dosage.

The Adsorption Rates of PVA/GO Composite at Different Temperatures

In Fig. 11, No. 0 bottle is dye with a concentration of 10 g/L before adsorption and Nos. (a)-(e) bottles are adsorbed fully by 0.3 g PVA/GO composite hydrogel (containing 30% graphene oxide) at the temperature of 25°C, 35°C, 45°C and 55°C, 65°C respectively. It was observed that the adsorption effect decreased when the temperature was too high. The absorbance of the solution was further measured. The solution concentration was calculated according to the standard curve of the dye, and then the adsorption rates were obtained, which were used to draw the graph shown in Fig. 11. According to the data analysis, the adsorption effect is suitable under 25°C.

The Adsorption of PVA/GO Composites at Different Adsorption Time

In Fig. 12, bottle (0) was the dye before adsorption, and bottle (a)-(e) were the navy blue dye, which were prepared by adding 0.3 g (graphene oxide content was 30 %) PVA/GO composite hydrogel to 200 mL dye with the initial concentration of 10 mg/L and being adsorbed for 6 h, 9 h, 12 h, 18 h and 24 h. The absorbance of the solution was further measured. The solution concentration was calculated according to the standard curve of the dye, and then the adsorption rates were calculated, which were used to draw the

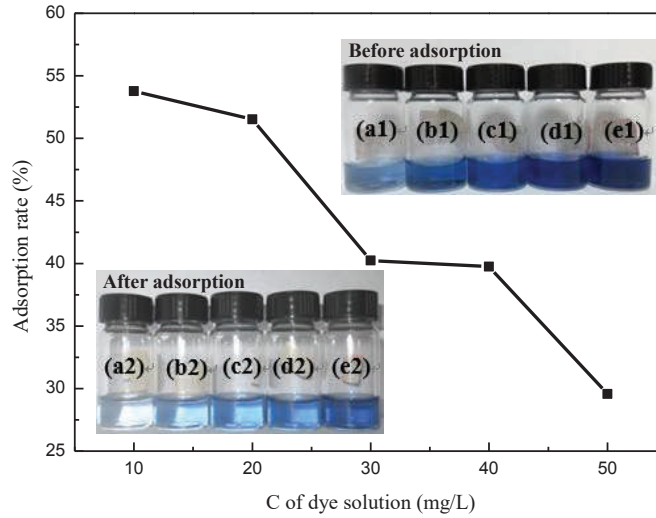

Fig. 10: The adsorption rate of PVA/GO composite for different concentrations of dye.

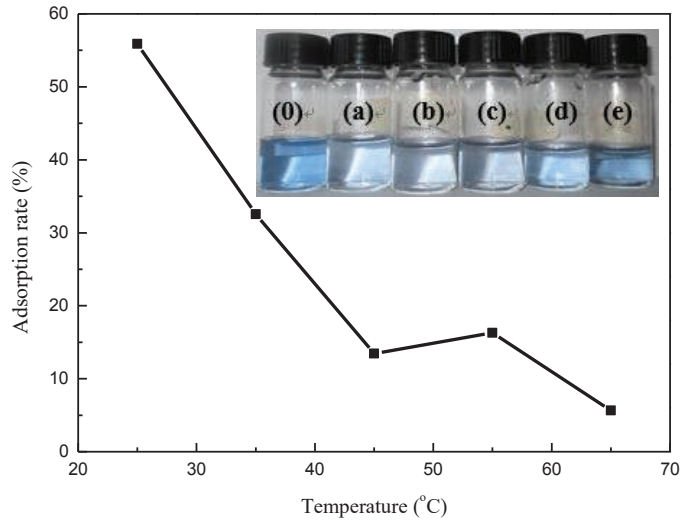

Fig. 11: Adsorption rates of PVA/GO composite at different temperatures.

following graph. According to the data analysis, the longer the adsorption time, the better the effect.

The Adsorption Rates of PVA/GO Composites at Different pH

In Fig. 13, (a1)-(g1) were the solutions before adsorption with pH values of 1, 3, 5, 7, 9, 11 and 13 respectively. In the figure, (a2)-(g2) were the navy blue dye, which was prepared by adding 0.3 g PVA/GO composite hydrogel (containing 30 % graphene oxide) and adsorbing on the 200 mL dye with initial concentration of 10 mg/L at pH values of 1, 3, 5, 7, 9, 11 and 13 respectively. The absorbance of the solution was further measured. The solution concentration was calculated according to the standard curve of the dye, and then the adsorption rates were obtained. According to the data analysis, the adsorption effect of the adsorbent is the best under acidic conditions, moderate under the neutral environment, and the worst under the alkaline environment.

CONCLUSION

The polyvinyl alcohol/graphene oxide (PVA/GO) hydrogel as adsorbent was prepared, and the adsorption performance was investigated. The results showed that the GO content, dosage, dye concentrations, temperatures, adsorption time,

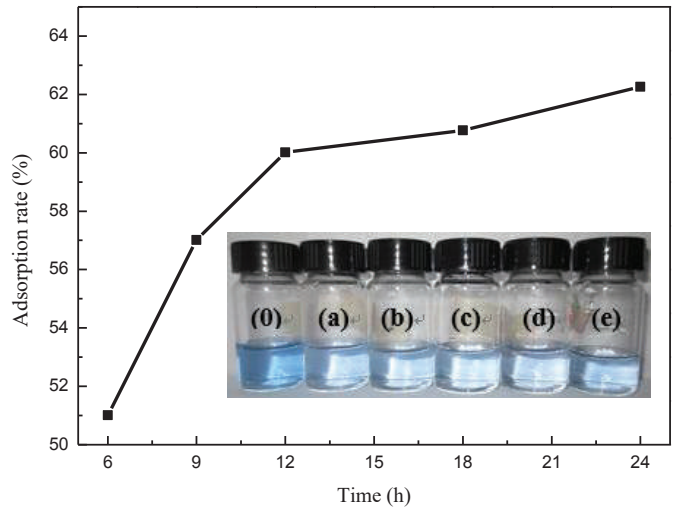

Fig. 12: The adsorption rates of PVA/GO composite for different adsorption time.

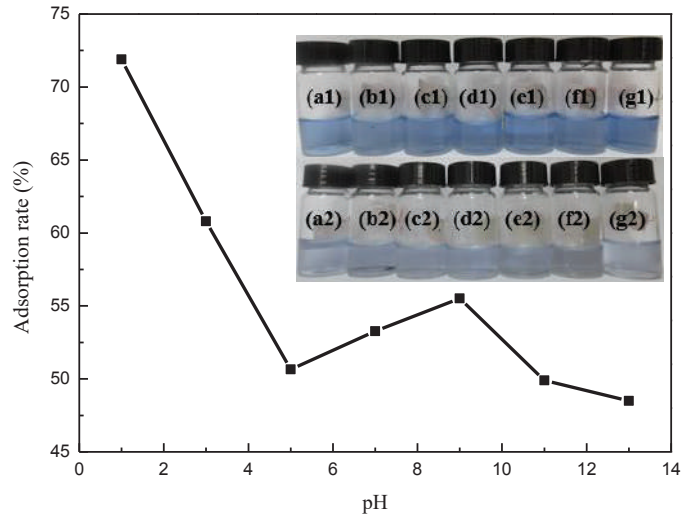

Fig. 13: Adsorption rates of PVA/GO composites in different pH environments.

and pH value have an influence on the removal rate of the dye from wastewater. It was confirmed that PVA/GO adsorbent with a content of 30 % graphene oxide had the best comprehensive performance. The suitable environment of adsorption is at 25°C, 12-18 h for adsorption time and acidic conditions. The suitable adsorbent dosage is 0.3 g and the suitable concentration of the dye is 10 mg/L.

ACKNOWLEDGEMENT

The authors gratefully acknowledge the financial support of the Shaoxing Public Welfare Project (Grant No. 2017B70042), and the International Science and Technology Cooperation Project of Shaoxing University (Grant No. 2019LGGH1004).

REFERENCES

Adebajo, M.O., Frost, R.L., Kloprogge, J.T., Carmody, O. and Kokot, S. 2003. Porous materials for oil spill cleanup: A review of synthesis and absorbing properties. Journal of Porous Materials, 10: 159-170.

Gan, L., Shang, S., Hu, E., Yuen, C.W.M. and Jiang, S.X. 2015. Konjac glucomannan/graphene oxide hydrogel with enhanced dyes adsorption capability for methyl blue and methyl orange. Applied Surface Science, 357: 866-872.

Gore, P.M., Dhanshetty, M. and Balasubramanian, K. 2016. Bionic creation of nano-engineered Janus fabric for selective oil/organic solvent absorption. Rsc Advances, 6: 111250-111260.

Hameed, B., Ahmad, A. and Aziz, N. 2009. Adsorption of reactive dye on palm-oil industry waste: Equilibrium, kinetic and thermodynamic studies. Desalination, 247: 551-560.

Kumar, A.S.K. and Jiang, S.J. 2016. Chitosan-functionalized graphene oxide: A novel adsorbent an efficient adsorption of arsenic from aqueous solution. Journal of Environmental Chemical Engineering, 4: 1698-1713.

Nevárez, L.M., Casarrubias, L.B., Canto, O.S., Celzard, A., Fierro, V., Gómez, R.I. and Sánchez, G.G. 2011. Biopolymers-based nanocomposites: Membranes from propionated lignin and cellulose for water purification. Carbohydrate Polymers, 86: 732-741.

Russo, P. and Hu, A.G. 2013. Compagnini, Synthesis, properties and potential applications of porous graphene: A review. Nano-micro Letters, 5: 260-273.

Satti, A., Larpent, P. and Gun'ko, Y. 2010. Improvement of mechanical properties of graphene oxide/poly (allylamine) composites by chemical crosslinking. Carbon, 48: 3376-3381.

Sehaqui, H., de Larraya, U.P., Tingaut, P. and Zimmermann, T. 2015. Humic acid adsorption onto cationic cellulose nanofibers for bioinspired removal of copper(II) and a positively charged dye. Soft Matter, 11: 5294-5300.

Shen, Y. and Chen, B. 2015. Sulfonated graphene nanosheets as a superb adsorbent for various environmental pollutants in water. Environmental Science & Technology, 49: 7364-7372.

Tiwari, J.N., Mahesh, K., Le, N.H., Kemp, K.C., Timilsina, R., Tiwari, R.N. and Kim, K.S. 2013. Reduced graphene oxide-based hydrogels for the efficient capture of dye pollutants from aqueous solutions. Carbon, 56: 173-182.

Wahab, A.H.A., Saad, A.P.M., Harun, M.N., Syahrom, A., Ramlee, M.H., Sulong, M.A. and Kadir, M.R.A. 2019. Developing functionally graded PVA hydrogel using simple freeze-thaw method for artificial glenoid labrum. Journal of the Mechanical Behavior of Biomedical Materials, 91: 406-415.

Nature Environment and Pollution Technology
An International Quarterly Scientific Journal

p-ISSN: 0972-6268
e-ISSN: 2395-3454

Vol. 19 | No. 1 | pp. 159-168 | 2020

Original Research Paper

Open Access

Comprehensive Assessment of Water Supply Benefits for South-to-North Water Diversion in China from the Perspective of Water Environmental Carrying Capacity

Haitao Chen*, Xiaonan Chen†, Lin Qiu* and Wenchuan Wang***

*School of Water Resources, North China University of Water Resources and Electric Power, Zhengzhou, 450045, PR China

**Construction and Administration Bureau of South-to-North Water Diversion Middle Route Project, Beijing, 100038, PR China

†Corresponding Author: Xiaonan Chen

Nat. Env. & Poll. Tech.
Website: www.neptjournal.com

Received: 11-06-2019
Accepted: 24-07-2019

Key Words:
Water environment
Variable cloud model
Water diversion
Carrying capacity

ABSTRACT

The South-to-North Water Diversion Project in China is an important measure to promote the ecological civilization construction in the receiving areas. Since the operation of the east and middle routes, the comprehensive benefits are more and more remarkable. It is very significant to quantitatively evaluate the comprehensive benefits of the South-to-North Water Diversion Project. The idea of quantitative evaluation by the improved degree of the carrying capacity of regional water environment after water diversion is put forward in this paper. On the basis, combining with variable fuzzy set and cloud theory, a new comprehensive assessment model is established. According to the evaluation index system of water environmental carrying capacity and the index values of research area, the linear difference function value is generated randomly by triangular forward cloud generator, and then the variable fuzzy comprehensive evaluation is carried out. Taking Haihe River Basin and Beijing City as typical research areas respectively, the comprehensive benefits of water supply from the diversion project in 2030 are analysed. The comprehensive evaluation method with variable cloud model considers both "good" and "bad" aspects and considers both randomness and fuzziness. Results show that the model is feasible and efficient. It is worth popularizing and applying.

INTRODUCTION

Water is the basis of ecology and the basic resource for the construction of ecological civilization. The South-to-North Water Diversion Project is an important measure to promote the construction of ecological civilization in the receiving area. The project that is planned east, middle, and west three lines is a major strategic infrastructure to relieve the severe water shortages in northern China, and promote the optimal allocation of water resources. In November 2013 and December 2014, the East Route Project and the Middle Route Project were put into operation respectively. Since the operation of the East and Middle Routes of the South-to-North Water Diversion Project, the total amount of water transported has been nearly 24 billion m^3, and the beneficiary population has exceeded 100 million. The guarantee rate of water supply of cities along the route has been improved, the regional sustainable development has been promoted, and the social, economic and ecological comprehensive benefits have become increasingly prominent. It is of great significance to scientifically evaluate the comprehensive benefits of the South-to-North Water Diversion Project. At present, many people have carried out preliminary studies on the water supply benefits of the South-to-North Water Diversion Project and obtained some achievements, but most of the researches are only statistical analysis for some aspects. The comprehensive evaluation system has not been established and the quantitative calculation of the comprehensive benefits has not been realized. Benefits assessment of South-to-North Water Diversion Project is a complex system. The following aspects should be considered.

Firstly, it is necessary to establish a scientific evaluation index system. Select indicators reflect social, economic, ecological and other aspects. Based on the principle of sustainable development and on the premise of maintaining the virtuous development of ecological environment, the critical value of evaluation grade for individual indicators is determined. Secondly, there are many factors to promote regional development, and the effect of water resources is affected by the optimal allocation of regional water resources, industrial structure, science and technology, etc. Studies on the

contribution of water diversion to the receiving area should be based on certain technical level and conditions. Thirdly, benefits evaluation involves many indexes and belongs to multiple objective comprehensive assessments, which generally involve fuzziness and randomness. A comprehensive evaluation model established should reflect these characteristics to realize quantitative analysis scientifically. At last, in order to facilitate practical application, index selection should consider achieving index data easily.

The main research results about water resources carrying capacity and water environmental carrying capacity were completed by Chinese scholars. Pan et al. (2007) studied the evaluation method for water resources carrying capacity based on GIS techniques. Cheng et al. (2015) evaluated the capacity of water resources in Heilongjiang Province based on entropy weight and cloud model. Dong et al. (2010) studied population carrying capacity of Beijing in China by dynamic simulation. Duan et al. (2010) made preliminary research on regional water resources carrying capacity conception and method. Sun et al. (2006) proposed a quantification and appraisal method for carrying capacity of water resources. Wang et al. (2017) studied on index system and judgment criterion of water resources carrying capacity. Zhao et al. (2008) analysed the evolution of water resources carrying capacity of Haihe River Basin in China. Li et al. (2017) simulated dynamically the policy implications for water resources carrying capacity of megacities. At present, there is no completely unified understanding and definition, but they all emphasize the supporting capacity of water environment to the socio-economic system and ecological system, reflect the principle of sustainable development, and take into account all aspects of society, economy and ecological environment. Over the past decades, abundant achievements have been made in the research of water environmental carrying capacity. The evaluation index system has been also established and applied to practice. Therefore, the comprehensive benefits of water diversion can be analysed from the point of view of improving the carrying capacity of water environment in the receiving area.

At present, there are many comprehensive evaluation methods, each of which has its own characteristic. Chen et al. (2007, 2008) proposed variable fuzzy set considering "good" and "bad" two aspects of things to apply optimum decision making for flood control dispatch, land suitability evaluation and so on. Li (2000) suggested cloud models by combining randomness and fuzziness. Chen et al. (2008) applied cloud model into making of the medium and long term irrigation schedule. Sun et al. (2015) established the cloud model based on entropy weight method to study the capacity evaluation of flood disaster prevention and reduction in Chaohu Basin in China. Zhang et al. (2017) suggested the cloud theory-based regional water resources carrying capacity evaluation model. In this paper, the improvement of regional water environmental carrying capacity by water diversion is taken as the standard to quantify the comprehensive benefits of water supply. A comprehensive evaluation model based on variable cloud model is established by combining the basic ideas of variable fuzzy set theory and cloud theory.

EVALUATION INDEX SYSTEM OF WATER SUPPLY BENEFITS

Evaluation of comprehensive benefits of water supply is transformed into evaluation of water environmental carrying capacity before and after regional water diversion. Water environmental carrying capacity refers to the maximum supporting capacity of water environment for social and economic development under a specific historical development condition, based on the level of technology, economic and social development, the principle of sustainable development, and the condition of maintaining the virtuous cycle of ecological system. After the development of more than several decades, the research results have gradually matured, and some representative definitions and methods have been formed. The analysis methods of water environmental carrying capacity can be divided into two categories. One is to evaluate comprehensively the water environmental carrying capacity of the study area according to the established evaluation index system, and to evaluate the saturation degree or potential of water environmental carrying capacity under given social, economic and technological conditions. The other is to calculate the population size, social and economic scale that can be carried by water environment after optimizing the allocation of water resources, under certain conditions of water resources development and utilization. Considering the simplicity of calculation and the accessibility of data, this paper uses the method of evaluation to analyse the carrying capacity of water environment.

Determine the evaluation index system of regional water environmental carrying capacity with the existing research results. The grade of comprehensive evaluation of water environmental carrying capacity is divided into five grades. The smaller the grade value is, the greater the carrying capacity of water environment is, and the larger the grade value is, the closer the carrying capacity of water environment is to saturation. Considering the economy, water resources, ecology and other factors, as well as the easy access to data, the evaluation index is selected, and the threshold of the classification of each index is determined. Among them, some indicators belong to the "bigger is better" type, while

Fig. 1: Sketch of relative position.

others are the opposite. The specific evaluation index system is given in Table 1 and Table 2.

According to the index system suggested, water environmental carrying capacity of receiving area in typical year can be evaluated respectively under water diversion and without water diversion conditions. Suppose that the grade value of water environmental carrying capacity in the area before water diversion is D_0, and after water diversion, the carrying capacity of water environment is D_1. The comprehensive benefit of water diversion can be defined by the following formula:

$$B = \frac{D_0 - D_1}{D_0} \quad \ldots(1)$$

Table 1: Evaluation index system of water environmental carrying capacity.

Category	Evaluation index	Number
Socio-economic conditions	GDP per capita (Yuan/person)	1
	Proportion of the tertiary industry (%)	2
	Population density (person/km^2)	3
	Urbanization rate (%)	4
	Water consumption of 10 thousand Yuan GDP (m^3/10^4 Yuan)	5
Water resources conditions	Annual per capita water resources (m^3)	6
	Utilization rate of water resources development (%)	7
	Water supply modulus of other sources (10^4 m^3/km^2)	8
	Annual water shortage rate (%)	9
Ecological environment conditions	Water quality standard rate of rivers and lakes (%)	10
	Sewage treatment rate (%)	11
	Forest coverage rate (%)	12
	Ecological environment water consumption rate (%)	13

Table 2: Criteria for evaluating water environmental carrying capacity.

Grade 1	Grade 2	Grade 3	Grade 4	Grade 5
50000~35000	35000~21000	21000~7000	7000~4000	4000~0
70~60	60~50	50~30	30~20	20~0
0~10	10~100	100~200	200~400	400~600
70~60	60~50	50~30	30~15	15~0
0~80	80~110	110~250	250~600	600~700
3000~2200	2200~1700	1700~1000	1000~500	500~0
0~10	10~40	40~50	50~60	60~100
30~20	20~10	10~5	5~1	1~0
0~10	10~20	20~30	30~40	40~100
100~70	70~50	50~30	30~10	10~0
100~80	80~60	60~40	40~20	20~0
40~30	30~25	25~20	20~10	10~0
50~40	40~30	30~20	20~10	10~0

Where, B is the comprehensive benefit of water diversion; D_1 is the quantitative value of water environmental carrying capacity evaluation after water diversion; D_0 is the quantitative value of regional water environmental carrying capacity evaluation without water diversion.

COMPREHENSIVE EVALUATION MODEL BASED ON VARIABLE CLOUD

Variable Fuzzy Set Theory

The theory of variable fuzzy set is a dynamic variable theory, model and method of fuzzy set about things, phenomena and concept membership. Based on relative difference function and considering advantages and disadvantages, the theory of variable fuzzy set has been widely applied into hydrology and water resources fields.

Suppose that $\tilde{A}$ and $\tilde{A}_c$ are a pair of concepts (things or phenomena) in discourse domain U, $u \in U$. As for the point on the reference continuum axis of the relative membership function, the relative membership degree of u to $\tilde{A}$ is $\mu_{\tilde{A}}(u)$, and the degree of u to $\tilde{A}_c$ is $\mu_{\tilde{A}_c}(u)$, $\mu_{\tilde{A}}(u) \in [0,1]$, $\mu_{\tilde{A}_c}(u) \in [0,1]$. Let

$$D_{\tilde{A}}(u) = \mu_{\tilde{A}}(u) - \mu_{\tilde{A}_c}(u) \quad \ldots(2)$$

$D_{\tilde{A}}(u)$ is called the relative difference degree of u to $\tilde{A}$.

Because $\mu_{\tilde{A}}(u) + \mu_{\tilde{A}_c}(u) = 1$, the relation between $\mu_{\tilde{A}}(u)$ and $\mu_{\tilde{A}_c}(u)$ can be described as follows:

$$\mu_{\tilde{A}}(u) = (1 + D_{\tilde{A}}(u))/2 \quad \ldots(3)$$

The mapping

$$\begin{cases} D_{\tilde{A}} : D \to [-1,1] \\ u \mapsto D_{\tilde{A}}(u) \in [-1,1] \end{cases} \quad \ldots(4)$$

is called the relative difference function of u to $\tilde{A}$. Let

$$\tilde{V} = \{(u,D) | u \in U, D_{\tilde{A}}(u) = \mu_{\tilde{A}}(u) - \mu_{\tilde{A}_c}(u), D \in [-1,1]\} \quad \ldots(5)$$

$$A_+ = \{u | u \in U, 0 < D_{\tilde{A}}(u) \le 1\} \quad \ldots(6)$$

$$A_- = \{u | u \in U, -1 \le D_{\tilde{A}}(u) < 0\} \quad \ldots(7)$$

$$A_0 = \{u | u \in U, D_{\tilde{A}}(u) = 0\} \quad \ldots(8)$$

$\tilde{V}$ is called variable fuzzy set. A_+, A_-, A_0 are the attraction domain, exclusion domain and gradual qualitative change boundary.

Set the attraction domain of variable fuzzy set $\tilde{v}$ is (a, b), the exclusion domain is [c, a) and (b, d]. $D_{\tilde{A}}(u) = 1$ at the point M. Let x be any point in interval [c, d], the relative difference function can be calculated by the relative position of the points on the real axis, as shown in Fig. 1.

When x is on the left side of point M, the relative difference function can be calculated by the following formula:

$$D_{\tilde{A}}(u) = \left(\frac{x-a}{M-a}\right)^{\beta}, x \in [a, M] \quad \ldots(9)$$

$$D_{\tilde{A}}(u) = -\left(\frac{x-a}{c-a}\right)^{\beta}, x \in [c, a] \quad \ldots(10)$$

When x is on the right side of point M, the relative difference function can be computed as follows:

$$D_{\tilde{A}}(u) = \left(\frac{x-b}{M-b}\right)^{\beta}, x \in [M, b] \quad \ldots(11)$$

$$D_{\tilde{A}}(u) = -\left(\frac{x-b}{d-b}\right)^{\beta}, x \in [b, d] \quad \ldots(12)$$

Where, β is non-negative exponent. Generally, let $\beta = 1$.

Cloud Theory

Cloud theory is formed on the basis of probability statistics and fuzzy mathematics to realize the uncertainty transformation between qualitative and quantitative concepts. The cloud model uses numerical characteristics of expectation, entropy and hyper entropy to describe fuzziness and randomness. The fuzziness is used to describe by membership degree based on expectation and entropy and the randomness of membership degree is described by hyper entropy.

Let U={u} be the domain of discourse described numer-

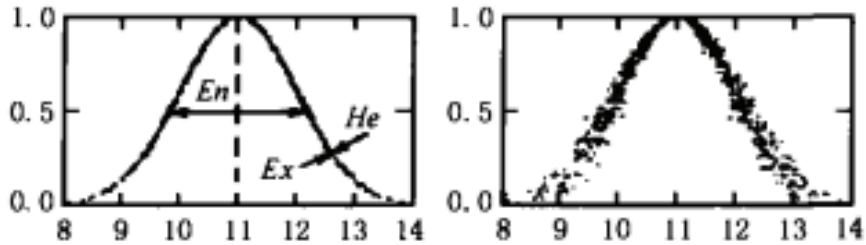

Fig. 2: Sketch of one-dimensional Normal Cloud.

ical value, and C be the qualitative conception associated with U. The membership degree of u to U for the conception C, $\mu(u)$, is a random number generated in the interval [0, 1]. That is,

$$\mu: U \to [0,1] \quad \forall u \in U \; u \to \mu(u) \qquad ...(13)$$

The mapping from the universe U to the interval [0, 1] is called a compatibility cloud, and each u is called a cloud drop.

Normal cloud described by expectation E_x, entropy E_n and hyper entropy H_e is the most widely used cloud model at present. It is based on normal distribution function. Set x submit to normal distribution, taking E_x as expectation, E_n' as standard deviation. E_n' is also a random variable that obeys normal distribution of expectation E_n and standard deviation H_e. The certainty degree of x, $\mu(u)$, is calculated by the following formula:

$$\mu(x) = \exp\left\{-\frac{(x-E_x)^2}{2E_n'^2}\right\} \qquad ...(14)$$

The distribution of x is called normal cloud (Fig. 2).

Normal distribution function is universal and widely used, but linear distribution is often used in practice. For example, membership functions of triangle style or linear style that can be taken as a side of triangle are often used in evaluation. Based on the idea of cloud theory, the cloud model with triangle distribution is deduced in this paper. The method of generating random numbers subjecting to triangle distribution density is introduced.

Let the probability density function of triangle distribution be an isosceles triangle, as shown in Fig. 3.

The probability distribution function can be calculated by distribution density function.

$$F(x) = \begin{cases} 0 & x \le E_x - E_n \\ \frac{1}{2(E_n)^2}x^2 - \frac{E_x - E_n}{(E_n)^2}x + \frac{(E_x - E_n)^2}{2(E_n)^2} & E_x - E_n < x \le E_x \\ -\frac{1}{2(E_n)^2}x^2 + \frac{E_x + E_n}{(E_n)^2}x - \frac{(E_x)^2 + 2E_xE_n - (E_n)^2}{2(E_n)^2} & E_x < x \le E_x + E_n \\ 1 & x > E_x + E_n \end{cases}$$

...(15)

The inverse function of distribution function is shown as follows:

$$F^{-1}(x) = \begin{cases} (E_x - E_n) + E_n\sqrt{2x} & 0 \le x \le 1/2 \\ (E_x + E_n) - E_n\sqrt{2(1-x)} & 1/2 < x \le 1 \end{cases} \qquad ...(16)$$

According to the inverse function, take a series of random numbers submitting to uniform distribution in interval [0, 1] into equation (16), and achieve random numbers subjecting to triangle distribution with the numerical characters E_x and E_n.

Let three numerical characters of cloud based on triangle distribution density be (E_x, E_n, H_e). The steps of triangular cloud generator are as follows:

(1) According to the method of generating random number of triangle distribution, produce random samples E_n' that are based on the numerical characters (E_n, H_e). H_e can be selected by experience.

(2) According to the parameters (E_x, E_n'), generate the random number x obeying triangle distribution density.

(3) The certainty degree of x, $\mu(x)$, can be calculated by the following equation:

$$\mu(x) = \begin{cases} \frac{x - E_x + E_n'}{E_n'} & E_x - E_n' \le x \le E_x \\ \frac{E_x + E_n' - x}{E_n'} & E_x < x \le E_x + E_n' \end{cases} \qquad ...(17)$$

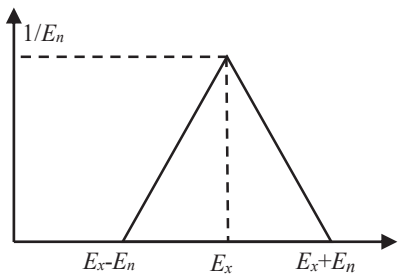

Fig. 3: Probability density function submitting to triangle distribution.

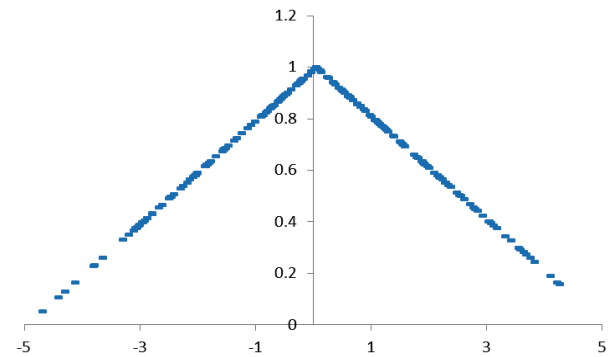

Fig. 4: One-dimensional triangular cloud map.

(4) x_i with the certainty degree μ_i is called the cloud drop. Repeat the above steps to create n cloud drops, and form the triangular cloud.

Giving a number a, the corresponding certainty degree can be calculated by forward cloud generator as follows:

(1) According to the numerical characters (E_n, H_e), generate random number $E_n^{'}$ subjecting to triangle distribution.

(2) According to the given number a, compute the corresponding certainty degree by the formula (17).

Let E_x=0, E_n=5, H_e=0.01. Generate 200 cloud drops, and form the cloud map as given in Fig. 4.

Evaluation Method Based on Variable Cloud Model

The comprehensive evaluation method with variable cloud is established by combining variable fuzzy set with cloud theory. According to the evaluation index system, the triangular cloud model is used to generate the difference degree randomly, and then the variable fuzzy comprehensive evaluation is carried out by difference degree. The specific steps are as follows:

(1) According to the above evaluation index system and classification criteria, the relative difference function of each evaluation grade is established for each index. Taking the population density index as an example, the corresponding grade 3 difference functions can be seen in Fig. 5.

(2) According to the graph of relative difference function, the expectation and entropy digital characteristics of each index for different grades are determined, and the hyper entropy value is determined according to experience. On the basis of the relative difference function corresponding to each grade, according to each index value of the evaluated object, the corresponding difference degree is randomly generated by the forward triangular cloud generator.

(3) According to the relative difference degree, the relative membership degree of each grade can be calculated.

(4) Suppose that the number of evaluation indicators is m and the number of evaluation grade is c. According to the relative membership degree generated above, the comprehensive grade of the evaluated object is calculated according to the following formula:

$$u_h^{'} = \frac{1}{\left[1+\left(\frac{d_{hg}}{d_{hb}}\right)^{\alpha}\right]} \qquad h = 1,2,\cdots,c \qquad ...(18)$$

$$d_{hg} = \{\sum_{i=1}^{m}[w_i(1-\mu_{\tilde{A}}(u_{ih}))]^p\}^{1/p} \qquad ...(19)$$

$$d_{hb} = [\sum_{i=1}^{m} w_i \mu_{\tilde{A}}(u_{ih}))^p]^{1/p} \qquad ...(20)$$

Where, $u_h^{'}$ is the membership degree corresponding grade h; p is the distance parameter. Generally, let p=2; a is the parameter of optimization criterion. Let a=1; w_i is the weight of the i^{th} evaluation index; $\mu_{\tilde{A}}(u_{ih})$ is the relative membership degree of the i^{th} evaluation index to the h^{th} grade.

Take the normalized membership degrees as weights, and calculate the comprehensive grade as follows:

$$D = \sum_{h=1}^{c} u_h \cdot h \qquad ...(21)$$

$$u_h = \frac{u_h^{'}}{\sum_{h=1}^{c} u_h^{'}} \qquad ...(22)$$

Where D is the comprehensive grade of evaluated object.

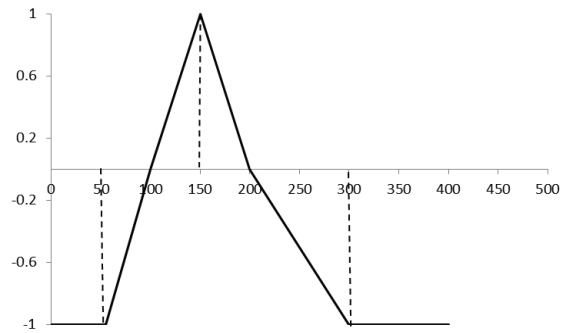

Fig. 5: Relative difference function.

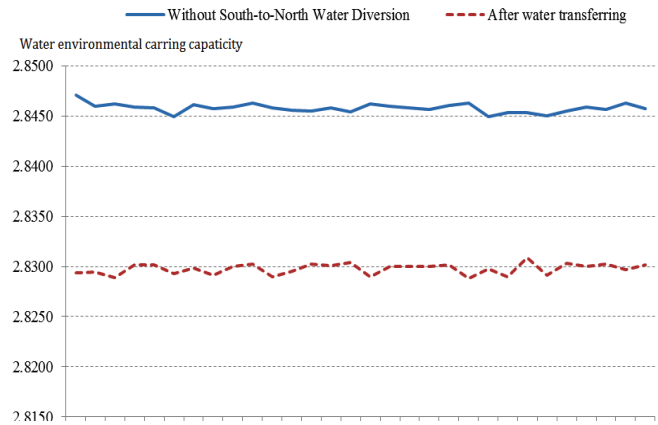

Fig. 6: Water environmental carrying capacity under different conditions in Haihe River Basin.

APPLICATION OF THE VARIABLE CLOUD MODEL

Evaluation of Comprehensive Benefits for Haihe River Basin

The Haihe River Basin is taken as a typical research area. The basin is bordered by the Mongolian Plateau in the north, the Yellow River in the south, the Bohai Sea in the east and Shanxi in the west. The total area of the basin is 318,200 km^2, accounting for about 3.3% of the total area of the country. The administrative areas of Haihe River Basin include Beijing, Tianjin, most of Hebei Province, eastern part of Shanxi Province, northern part of Shandong and Henan Province, and parts of Liaoning Province and Inner Mongolia Autonomous Region. The Haihe River Basin has a rapid economic development, and many large and medium sized cities, but the total amount of water resources is small, and the spatial and temporal distribution is uneven. The shortage of water resources is restricting the sustainable development of regional social economy. The South-to-North Water Diversion Project is a strategic project to alleviate the shortage of water resources in northern China. The East Route Project and the Middle Route Project have begun to operation since December 2013 and December 2014, respectively. By the end of March 2019, the cumulative water supply to the receiving area along the line exceeded 24 billion m^3, and the comprehensive benefits of the project are remarkable. According to relevant planning and information, by 2030, on the basis of diverting water

Table 3: Evaluation index value of Haihe River Basin in 2030.

Evaluation index	Without South-to-North Water Diversion	After water transferring
GDP per capita (Yuan/person)	81000	81000
Proportion of the tertiary industry (%)	53	53
Population density (person/km^2)	497	497
Urbanization rate (%)	60	60
Water consumption of 10 thousand Yuan GDP ($m^3/10^4$ Yuan)	95	95
Annual per capita water resources (m^3)	266	342
Utilization rate of water resources development (%)	96	96
Water supply modulus of other sources (10^4 m^3/km^2)	1.57	5.34
Annual water shortage rate (%)	30	9.5
Water quality standard rate of rivers and lakes (%)	40	40
Sewage treatment rate (%)	82	82
Forest coverage rate (%)	18	18
Ecological environment water consumption rate (%)	12.1	12.1

Table 4: Evaluation index value of Beijing City in 2030.

Evaluation index	Without South-to-North Water Diversion	After water transferring
GDP per capita (Yuan/person)	215983	215983
Proportion of the tertiary industry (%)	82.43	82.43
Population density (person/km^2)	1402	1402
Urbanization rate (%)	88.8	88.8
Water consumption of 10 thousand Yuan GDP (m^3/10^4 Yuan)	11	11
Annual per capita water resources (m^3)	149	210
Utilization rate of water resources development (%)	100	100
Water supply modulus of other sources (10^4 m^3/km^2)	0	8.53
Annual water shortage rate (%)	38.79	13.37
Water quality standard rate of rivers and lakes (%)	90	90
Sewage treatment rate (%)	99	99
Forest coverage rate (%)	45	45
Ecological environment water consumption rate (%)	14.58	14.58

about 5 billion m^3 from the Yellow River each year, about 12 billion m^3 of water will be diverted to the Haihe River Basin through the South-to-North Water Diversion Project. Taking 2030 as a typical year, by relevant research results and data, according to the above evaluation index system and variable cloud model, the impact of South-to-North Water Diversion on water environmental carrying capacity of Haihe River Basin is analysed. In 2030, without considering the South-to-North Water Diversion and after water transferring, the index values of water environmental carrying capacity under the two kinds of conditions are indicated as given in Table 3.

Using analytic hierarchy process, the weight of each index is determined as follows: (0.127, 0.089, 0.111, 0.057, 0.155, 0.073, 0.047, 0.021, 0.023, 0.036, 0.051, 0.095, 0.116).

Based on the above evaluation system and index values, the carrying capacity of water environment in Haihe River Basin is calculated and analysed by using variable cloud model. Set hyper entropy equal 0.1. Thirty calculations have been made in this paper, and the results are as shown in Fig. 6.

According to the Fig. 6, there is certain randomness in the calculation results using the variable cloud model, that is, the results are not exactly the same each time, but results have a stable tendency value. The cloud model reflects the fuzzy uncertainty and random uncertainty. Without considering the water conveyance from South-to-North Water Diversion Project, the average value of water environmental carrying capacity in Haihe River Basin in 2030 is 2.8458. After water diversion, the average grade of water environmental carrying capacity is 2.8298. It is considered that the carrying capacity of water environment in Haihe River Basin will be increased by 0.5625% by water diversion from the South-to-North Water Diversion Project. According to the calculation results, the analysis is as follows:

(1) In 2030, with the advancement of technology, the improvement of water use efficiency and the optimization of industrial structure, the carrying capacity of water environment in Haihe River Basin will be basically at the middle level. Water environment could bear the social and economic scale at that time, but still at the general level.

(2) To a certain extent, the carrying capacity of regional water environment can be improved through water diversion, but it is more important that the region itself should vigorously save water, optimize the industrial structure, improve the utilization rate of water resources, improve the ecological environment and implement green development.

(3) The benefits of water diversion are not only related to the total amount of water diversion, but also to the degree of local social and economic development, technological level and optimal allocation of water resources. Therefore, the evaluation of water diversion benefits is dynamic.

(4) This paper takes Haihe River Basin as an example, and the scope of the research object is large. If a small area is chosen for research, such as province or city, the proportion of water diversion in the total water supply is larger, and the contribution of water diversion to the improvement of water environmental carrying capacity in the local area is greater. Therefore, the evaluation results of water diversion benefits are also related to the study object.

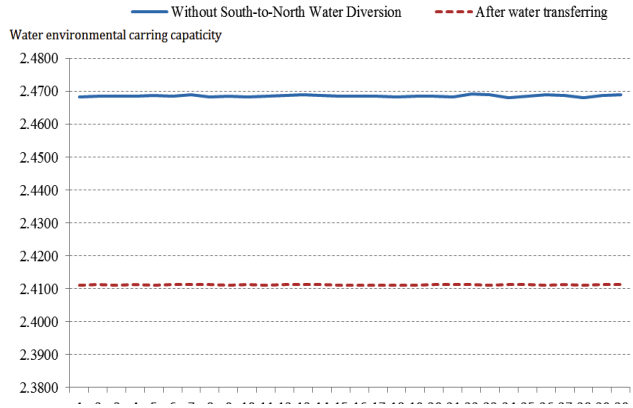

Fig. 7: Water environmental carrying capacity under different conditions in Beijing City.

Evaluation of Comprehensive Benefits for Beijing City

Taking Beijing as an example, which is the main receiving area of South-to-North Water Diversion Middle Route Project, the model can be validated. Beijing is located at the north-west end of the North China Plain, adjacent to Tianjin in the east, surrounded by Hebei Province in the west, south and north. The total area of the city is about 16410 km^2, of which the mountainous area accounts for about 60% and the plain area accounts for about 40%. The seasonal variation of precipitation in Beijing is great, and the precipitation is mostly concentrated in summer. The average annual precipitation in Beijing is about 585 mm. The shortage of water resources in Beijing is very serious. The per capita water resources are less than 9% of the national level. In order to alleviate the shortage of water resources in Beijing, from September 2008 to April 2014, the Middle Route Project diverted water from reservoirs in Hebei Province by using the pre-built Beijing-Shijiazhuan section project, and implemented four emergency water supplies to Beijing, with a total water supply of 1.6 billion m^3. Since December 2014, the Middle Route Project has been in operation, and by the end of March 2019, about 4.4 billion m^3 of water from Dajiankou reservoir has been transported to Beijing. Taking 2030 as a typical year, by relevant research results and development plan, on basis of the above evaluation index system and variable cloud model, the impact of South-to-North Water Diversion on water environmental carrying capacity of Beijing is analysed. In 2030, without considering the South-to-North Water Diversion and after water transferring, the index values of water environmental carrying capacity under the two kinds of conditions are indicated as given in Table 4.:

The weight is the same as the previous example. Let hyper entropy be 0.1. Thirty calculations have been made. The results calculated with the variable cloud model have certain randomness, and each result is not completely the same, but the calculated results have a stable tendency value. Without considering the water conveyance from South-to-North Water Diversion Project, the average value of water environmental carrying capacity of Beijing in 2030 is 2.4685. After water diversion, the average grade of water environmental carrying capacity is 2.4112. It is considered that the carrying capacity of water environment in Beijing will be increased by 2.32% by water diversion from the South-to-North Water Diversion Project. The carrying capacity of water environment in Beijing is basically in the middle level. Water environment can bear the social and economic scale at that time, but it is still at the general level. Although water transfer can improve the carrying capacity of water environment in water receiving areas, it mainly depends on local efforts to save water and improve the utilization rate of water resources. The calculated results under different conditions for Beijing are as shown in Fig. 7.

CONCLUSIONS

Considering the uncertainty and multiple criteria feature of the comprehensive benefits evaluation of the South-to-North Water Diversion Project, the idea of benefits evaluation based on the improvement of water environmental carrying capacity in the receiving area is put forward. On this basis, combined with variable fuzzy set theory and cloud theory, a new comprehensive evaluation model based on variable cloud model is established. The model not only considers the membership degree of "good" and "bad" in comprehensive evaluation, but also takes into account the fuzziness and randomness in evaluation. Examples show that the method based on variable cloud model is reasonable and easy to use. It provides a new

idea for the quantitative evaluation of the benefits produced by the South-to-North Water Diversion Project.

ACKNOWLEDGEMENT

This research was supported by the Key Scientific and Technological Research Projects in Henan Province (Grant No. 192102110199).

REFERENCES

Chen, S.Y. 2008. Theory of variable fuzzy sets and variable model sets. Mathematics in Practice and Theory, 38(18): 146-453.

Chen, S.Y., Chai, C.L. and Su, Y.N. 2007. Variable fuzzy sets methods and application on land suitability evaluation. Transactions of the Chinese Society of Agriculture Engineering, 23(3): 95-97.

Chen, X.N., Duan, C.Q., Qiu, L. and Huang, Q. 2008. Application of cloud reasoning model in making of the medium and long term irrigation schedule in irrigation area. Systems Engineering-Theory & Practice, 28(11): 115-121.

Cheng, K., Fu, Q., Ren, Y.T., Guo, J. and Lu, X.P. 2015. Evaluation of bearing capacity of water resources in Heilongjiang Province based on entropy weight and cloud model. Journal of Northeast Agricultural University, 46(8): 75-80.

Dong, Y.F. 2010. Dynamic simulation and analysis to population carrying capacity of Beijing. China Population Resources and Environment, 20(9): 42-47.

Duan, C.Q., Liu, C.M., Chen, X.N., Liu, W.H. and Zheng, H. X. 2010. Preliminary research on regional water resources carrying capacity conception and method. Acta Geographica Sinica, 65(1): 82-90.

Li, D.Y. 2000. Uncertainty in knowledge representation. Engineering Science, 2(10): 73-79.

Li, L.L. and Xu L.Y. 2017. Dynamic simulation of policy implications for the water resources carrying capacity of megacities. China Environment Science, 37(11): 4388-4393.

Pan, X.Y., Xiao, J., Li, F.H., Li, F.H., Liu, H.L., Ma, M., Liu, C.Z. and Li, R.X. 2007. Applied study of evaluation method for water resources carrying capacity based on GIS techniques in typical north district. Journal of Natural Resources, 22(4): 664-671.

Sun, F.X., Zheng, C.Y. and Wang, Z.H. 2006. Quantification and appraisal method for carrying capacity of water resources. Water Resources and Hydropower Engineering, 37(3): 1-4.

Sun, H.H., Cheng, X.F., Ni L. and Zhu, M. 2015. Capacity evaluation of flood disaster prevention and reduction in Chaohu Basin based on cloud model and entropy weight method. Journal of Catastrophology, 30(1): 222-226

Wang, J.H., Zhai, Z.L., Sang, X.F. and Li, H.H. 2017. Study on index system and judgment criterion of water resources carrying capacity. Shuili Xuebao, 48(9): 1023-1029.

Zhang, A., He, J. and Chen X.N. 2017. Study on cloud theory-based regional water resources carrying capacity evaluation model. Water Resources and Hydropower Engineering, 48(1): 18-22.

Zhao, J.X., Wang Z.J., Qin T. and Li, H. H. 2008. Analysis on evolution of water resources carrying capacity of Haihe River Basin. Shuili Xuebao, 39(6): 647-651.

Nature Environment and Pollution Technology
An International Quarterly Scientific Journal

p-ISSN: 0972-6268
e-ISSN: 2395-3454

Vol. 19 | No. 1 | pp. 169-178 | 2020

Original Research Paper | Open Access

Centrifugal Reduction Treatment Process for High-Water-Content Sludge in Oilfield

Xingwang Wang†, Xiaoxuan Xu, Wei Dang, Changchao Hu, Zhiwei Tang and Bei Wei
Petroleum Exploration and Production Research Institute, SINOPEC, Beijing 100083, China
†Corresponding author: Xingwang Wang

Nat. Env. & Poll. Tech.
Website: www.neptjournal.com

Received: 02-06-2019
Accepted: 24-07-2019

Key Words:
Oilfield sludge
Horizontal screw centrifuge
Reduction treatment
Process design

ABSTRACT

To ensure that injection water quality reaches the standard, oil field sewage stations adopt a continuous sludge dredging process to reduce the content of suspended solids and sand. A large amount of high-water-content oily sludge is produced, which results in increased costs of transportation and subsequent harmless treatment. Therefore, a sludge reduction treatment is necessary. A set of centrifugal reduction processes for oily sludge was designed in this study, with the horizontal screw centrifuge as the key piece of equipment. In the laboratory, CPAM flocculant was screened. In the field test, the effects of four factors rotational speed, differential speed, the feeding quantity of sludge, and flocculant dosage on the reduction effect were determined. The results show that when the rotational speed is higher, the differential speed is lower, and the feeding quantity of sludge remains lower, and the flocculant dosage remains higher, after treatment, the water content of the sludge is lower and the solid content of the sludge is higher. The optimal parameters of the centrifugal reduction process were determined using an orthogonal experimental design as follows: rotational speed 2,607 rpm, differential speed 8 rpm, the feeding quantity of sludge 7 m^3/h, and flocculant dosage 100 g/m^3. After treatment, the average water content of the sludge decreased from 92.75% to 56.57%, and the average solid content of the sludge increased from 2.30% to 36.72%. The split ratio of the water-outlet and sludge-outlet was in the range of 8.71:1 to 12.57:1, and the corresponding sludge reduction ratio was 89.70% to 92.63%, confirming successful sludge reduction.

INTRODUCTION

With the popularization of polymer flooding technology in oilfields, the suspended solids and sand contents in oilfields producing water have increased, placing an enormous amount of pressure on the sewage treatment system, causing substandard injection water quality and formation pollution. This has negatively influenced the oilfield development efficiency. These problems are effectively alleviated by the continuous sludge dredging process in the sewage treatment system, and shortening the dredging cycle. However, the water content of sludge dredged from the sewage treatment system can be up to 90%, which requires a significant capacity increase in the accumulation, transportation, and subsequent treatment of sludge. If this sludge is not rapidly and effectively treated, risks to safety and the environment increase. Firstly, the crude oil component in the sludge easily volatilizes, which makes the total hydrocarbon concentration exceed the standard in the production area. Secondly, many toxic and hazardous wastes are present in the sludge, such as petroleum, sulfide, benzene series, and phenols.

At present, the harmless treatment methods of oily sludge mainly include ultrasonic pretreatment, incineration, pyrolysis, and extraction (Leonardo et al. 2012, Galil et al. 2015, Wang et al. 2013). Ultrasonic treatment has a sponge and local heating effect on sludge, which can increase sludge dewatering (Hu et al. 2014, 2016, Gao et al. 2015, Zhang et al. 2013). Short-term and low-intensity ultrasonic treatment can simultaneously reduce the sludge water content to below 85% and reduce the flocculant dosage by 25%–50%. Incineration obviously reduces the volume of sludge and eliminates pathogenic bacteria, and it is the primary method of sludge harmless treatment (Braguglia et al. 2016, Heidarzadeh et al. 2010, Nima et al. 2009). The cost of incineration is high, and burning one ton of sludge uses 18.5 kg of fuel. When oxygen is sufficient, pyrolysis is used to convert the heavy components in oily sludge into light components, and then the volatile and semi-volatile organic compounds are recovered (Wu et al. 2003, Hou et al. 2012, Marcelo et al. 2016). Using the different solubilities of the solutes in the solvent, the extraction method can be used to extract the lighter oil components, and the residual heavy oil components are combined with other processes for treatment (Kumar et al. 2015, Liang et al. 2014, Zubaidy et al. 2010, Hu et al. 2015, Kumar et al. 2013). These sludge harmless treatment methods are expensive. Therefore, it is necessary to reduce the water content in sludge that is produced by

Table 1: Analysis of crude oil components in sludge.

Crude oil component	Content (%)
saturated hydrocarbons	50.76-51.97
aromatic hydrocarbon	16.03-17.36
non-hydrocarbon	7.91-8.56
asphaltene	13.68-14.27
colloid	9.09-10.15

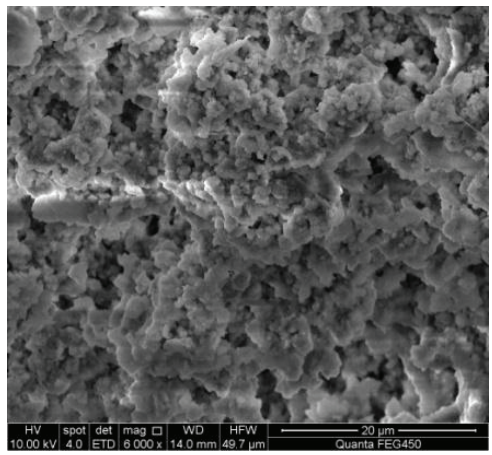

Fig. 1: Sludge micro-morphology (6,000 magnification).

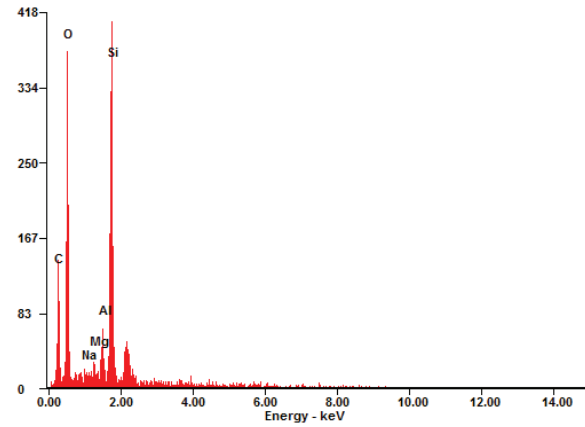

Fig. 2: Energy spectrum of spectrometer.

the continuous sludge dredging process. Such a method would help reduce transportation costs and the amount of subsequent processing, and ensure the efficient operation of harmless treatment processing and devices.

Oilfield sewage stations are common and widely distributed. Considering treatment capacity, energy consumption, and costs, the conditioning-mechanical separation method is used for sludge reduction treatment. By adjusting the characteristics and arrangement of the sludge solid particles, the method can ensure the sludge solid particles are suitable for mechanical separation, which can remarkably improve the dehydration effect. This method is often applied when the water content of sludge is 30%-70%. However, the water content of sludge dredged from the sewage treatment system can reach 90%. Therefore, a centrifugal reduction process must be designed to manage high-water-content sludge in oilfields. This process could be employed to determine the factors influencing the reduction effect and to optimize the process' parameters.

OILY SLUDGE COMPONENT ANALYSIS

In the continuous sludge dredging process, sludge samples were obtained from the sludge outlet of the gravity sedimentation tank. According to the analysis of the oil component in the sludge in Table 1, we found that the volatile organic compound content in the sludge was high. If not treated in time, the total hydrocarbon concentration of the ambient air in the production area may exceed the limit, posing a security risk. From the micro-morphology presented in Fig. 1, oily sludge is formed by the accumulation and cementation of fine particles, and the minerals within it show no regular morphology, with spherical calcium carbonate and amorphous silicon dioxide displaying a packing appearance. According to the analysis of the relative content of the elements (Fig. 2), the main elements of inorganic substances in oily sludge are Si, O, C and Al. Table 2 shows that the main inorganic substances in oily sludge were aluminosilicate (66.24%-67.64%) and carbonate (16.37%-18.29%), produced during the process of oilfield development, and iron oxide (11.21%-11.93%), due to the corrosion of pipelines and facilities in the process of transportation. These inorganic substances are characterized by high density and loose structure. Therefore, a good separation effect could be obtained by centrifugation.

CENTRIFUGAL REDUCTION PROCESS FOR OILY SLUDGE

According to the structure, working principle, and efficiency of factors influencing a horizontal screw centrifuge, the centrifugal reduction process for oily sludge was designed

Table 2: Analysis of inorganic components in sludge.

Inorganic component	Content (%)	Inorganic component	Content (%)
SiO_2	53.08-53.77	Na_2O	0.67-1.01
Al_2O_3	13.16-13.87	K_2O	0.72-0.88
Fe_2O_3	11.21-11.93	$SrSO_4$	0.34-0.46
$BaCO_3$	9.36-10.04	TiO_2	0.21-0.31
$CaCO_3$	3.89-4.42	ZnO	0.27-0.36
$MgCO_3$	3.12-3.83		

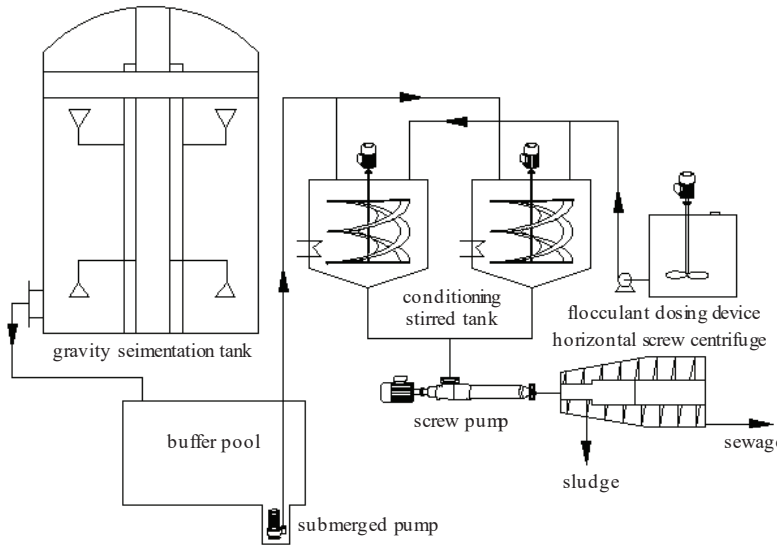

Fig. 3: Centrifugal reduction process for oily sludge.

as shown in Fig. 3. Here, pressurized-boiler hot water is applied to jet and strip oily sludge when artificial dredging is engaged, and sludge is then discharged to the buffer pool outside the gravity sedimentation tank. The submerged pump in the buffer pool delivers high-water-content sludge to the conditioning stirred tank to heat, mix, and homogenize it. Flocculant is added to the tank to create the suspended solids, and solids in the sludge flocculate reduce the fragmentation and dispersion of the solid phase during high-speed centrifugal treatment. Mixing in the tank can significantly reduce the required dosage of the flocculant. After centrifugal treatment, the water phase in the sludge is discharged into the recovery pool, and the concentrated sludge loading is outbound. Before treatment, the water content, oil content, and solid content of sludge were 92.9%, 4.43% and 2.67%, respectively.

SCREENING AND DOSAGE OF FLOCCULANT

Flocculant Screening

Adding flocculant in the centrifugal test helped with sludge dewatering, so it was necessary to screen the commonly used flocculants in the laboratory, including PAC, CPAM, and alum. The high-water-content sludge that is produced by a continuous sludge dredging process is a kind of suspension liquid, so the standard *Q/SY90-2007 Technical Requirements for Flocculant Used in Oilfield Water Treatment* was adopted to screen the flocculant (Zhao et al. 2007). The specific operation method was as follows. Take 500 mL of high-water-content sludge at a 50°C constant temperature and stir for 5 min at 11,000 rpm. Add 5 mL flocculant solution, so that the concentration is 100 mg/L, and mix the sludge and flocculant solution using inertia after the blender is closed. Then, pour the suspension liquid into the cylinder with a plug, and invert and shake the cylinder 60 times. After 15 min static settlement, use a pipetting gun to extract a sample from the central section. The absorbance was measured at the wavelength of 650 nm using a spectrophotometer, with distilled water as the reference. The following formula was applied to calculate absorbance decrease rate, and the specific results are given in Table 3.

$$R = (A_0 - A_1)/A_0 \times 100\% \quad \ldots(1)$$

Where, R is the rate of absorbance decrease after adding flocculant, A_0 is the absorbance of the blank suspension liquid, and A_1 is the absorbance of suspension liquid after adding flocculant.

The experimental results showed that compared with the other two kinds of flocculant, CPAM has a neat interface, fast settling speed, and high absorbance decrease rate. The positivey charged group of CPAM has a good electrical neutralization effect on the negatively charged organic colloids of sludge. Through its excellent polymer bridging and aggregation ability, CPAM prompts colloidal particles to gather into large pieces of flocs and obviously separates them from the suspension liquid. Therefore, CPAM was chosen for the field test.

Flocculant Dosage

A flocculant can be used to flocculate the dispersed particles in the sludge and enhance the solid-liquid separation effect with a centrifuge. The solid and water contents in sludge before and after the centrifugal treatment provides an evaluation index of the field test results. Using *the Device and Method for Measuring Oil or Water Content in Samples* that was published by the China University of Petroleum for reference, the assembled sludge testing device is shown in Fig. 4 (Zhang et al. 2012). The device, through the distributed tube, reads out the water content, and the solid content is obtained by Soxhlet extraction and dry weighing, after which the difference is obtained to determine the oil content.

As shown in Fig. 5, the change law of the flocculant dosage and the treatment effect was determined with a flocculant dosage of 100-350g/m^3, centrifuge rotational speed of 2,530 rpm, differential speed of 11 rpm, and feeding quantity of sludge of 6 m^3/h.

The sludge particles are negatively charged and repel each other. After the addition of the flocculant, the particles' potential decreases, and the particles attract each other to form flocs. Simultaneously, the adsorption and bridging action of the flocculant cause the small flocs to form larger flocs. This is beneficial to the solid phase separation under centrifugal action. Therefore, as shown in Fig. 5, with the increase in flocculant dosage, the water content of treated sludge decreases and the solid content of treated sludge increases. The dosage increases from 100 to 200 g/m^3, and the water content of sludge decreases sharply. When the dosage was within 200-350 g/m^3, the water content of sludge decreases slowly. When the dosage increases within 100-350 g/m^3, the solid content of sludge increases continuously. The sludge in the conditioning stirred tank is maintained at 60°C, which helps the flocculant play a better role in flocculation. Because the water viscosity is related to temperature, the higher temperatures reduce the water viscosity. This enhances the Brown exercise intensity of solid particles and oil-containing

Table 3: Flocculant screening.

Flocculant	Phase interface	Settling speed	Absorbance decrease rate (%)
PAC	neat	fast	45.01
CPAM	neat	fast	81.65
Alum	relatively neat	slow	25.97

Fig. 4: Oily sludge testing device.

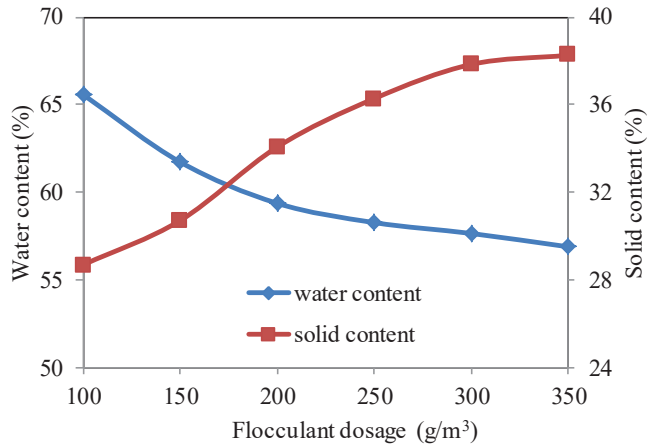

Fig. 5: Flocculant dosage on treatment effect.

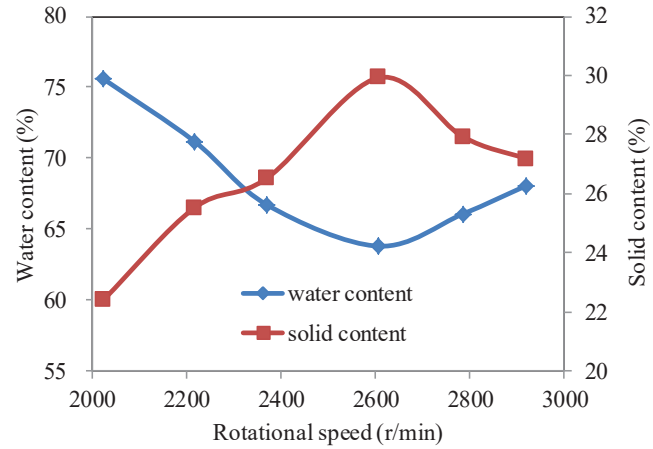

Fig. 6: Rotational speed on treatment effect.

colloidal particles, thus increasing the chance of collision and condensation.

CENTRIFUGE PARAMETERS TEST

Rotational Speed

The treatment effect of different rotational speeds on sludge in the same conditioning was studied. The samples were obtained 10 min after adjusting the speed to ensure that the sample corresponded to the rotational speed. The specific process parameters were as follows: centrifuge rotational speed 2000-3000 rpm, differential speed 10 rpm, the feeding quantity of sludge 5 m^3/h, and flocculant dosage 100 g/m^3.

Fig. 6 shows that when the rotational speed ranges from 2,000 to 2,600 rpm, with the increase in rotational speed, the sludge discharged from the sludge-outlet has a lower water content and a higher solid content. However, when the rotational speed is more than 2,600 rpm, the water content increases and the solid content decreases with the increase in rotational speed. This occurs because the flocs formed by flocculation are not stable and can be separated by an external force. The interior of the oily sludge is combined by the bridging action and Van der Waals forces, including flocculant, solid phase, and oil-contained colloidal particles. For the three as a whole, the density is slightly higher than the oil-water mixture. However, at the individual level, the density of oil-containing colloidal particles is lower than that of the flocculant. Therefore, with the increase in the centrifuge rotational speed, the centrifugal force caused by the density difference increases. When the centrifugal force is larger than the bridging action and Van der Waals forces

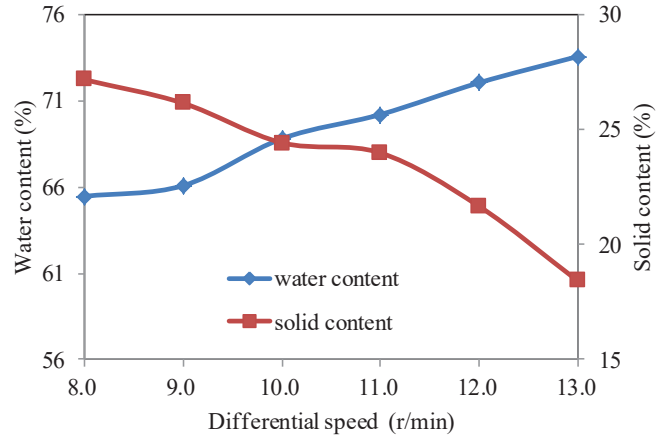

Fig. 7: Differential speed on treatment effect.

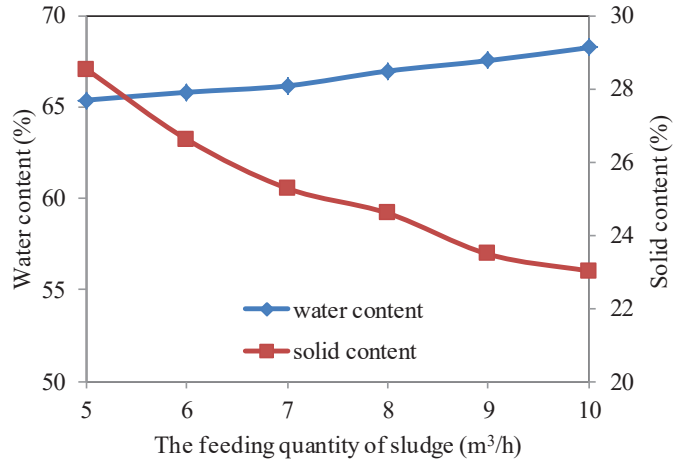

Fig. 8: The feeding quantity of sludge on the treatment effect.

that are between internal components of relatively stable flocs, the flocculation is weakened and the stable flocs are destroyed. Therefore, an excessively high rotational speed will result in a poor treatment effect.

Differential Speed

The speed difference of the rotary drum and screw conveyor push the solid phase to separate the solids and liquids. The magnitude of the differential speeds has an important influence on the treatment effect. As shown in Fig. 7, the change law of the differential speed and the treatment effect were determined under a differential speed of 8-13 rpm, rotational speed of 2,300 rpm, the feeding quantity of sludge 6 m^3/h, and flocculant dosage of 100 g/m^3.

In the test, with the increase in differential speed, the water content of the sludge increased and the solid content of sludge decreased after treatment. This occurred because the magnitude of the differential speed influences the amount of solids resulting from the centrifuge. If the differential speed is too high, the disturbance effect of the fluid in the rotary drum is strengthened. This strengthens the fluid scoured to the deposited solid phase on the inner wall of the rotary drum, thereby affecting the separation effect.

The Feeding Quantity of Sludge

The amount of sludge determines the processing load, which is the residence time of the sludge in the centrifuge, which influences the treatment effect. As shown in Fig. 8, the change law of the feeding quantity of sludge and the treatment effect were determined under the feeding quantity of sludge of 5-10 m^3/h, rotational speed of 2,370 rpm, differential speed of 11 rpm, and flocculant dosage of 150 g/m^3.

With the increase in the feeding quantity of sludge, the water content of the sludge increased and the solid content of sludge decreased after centrifugal treatment. The centrifugal force generated by the high-speed rotation of the rotary drum forces the solid phase to cling to the inner wall of the drum. Under the effect of the axial force of the spiral vane of the screw conveyor, sludge is tightly pressed to the drum cone and the solid phase is discharged from the sludge-outlet along the spiral flow path of the screw conveyor. With the increase in the feeding quantity of sludge, the residence time of the unit volume sludge in the centrifuge decreases, and the treatment effect worsens.

PROCESS OPTIMIZATION

Parameter Optimization

The combined action of the rotational speed, differential speed, the feeding quantity of sludge, and flocculant dosage determines the effect of the centrifugal treatment of oily sludge. The orthogonal experimental design method was used to optimize the process plan (Jean et al. 1999, Lin et al. 2005, Bo et al. 2004, Chang et al. 2001, Verma et al. 2010). The test scheme and results are shown in Tables 4-6.

After centrifugal treatment, the lower the water content and the higher the solid content of the sludge, the better the treatment effect. The calculation results for the ranges of water and solid contents are $R_{W\_A} > R_{W\_B} > R_{W\_D} > R_{W\_C}$ and $R_{S\_A} > R_{S\_B} > R_{S\_D} > R_{S\_C}$, respectively. Within the numerical range of the factor level, the range results show that the rotational speed is the main factor affecting the centrifugal treatment effect, and the other influential factors are the differential speed, the flocculant dosage, and the feeding quantity of sludge, in decreasing order. The factor level change of factor A influences the experimental result. The results of $k_{W\_A3} < k_{W\_A2} < k_{W\_A4} < k_{W\_A1}$ and $k_{S\_A3} > k_{S\_A2} > k_{S\_A4} > k_{S\_A1}$ show that A3 is the optimal factor level

Table 4: Factor levels table.

S. No.	A (rotational speed) (rpm)	B (differential speed) (rpm)	C (the feeding quantity of sludge) (m^3/h)	D (flocculant dosage) (g/m^3)
1	2023	8	5	100
2	2371	9	7	200
3	2607	11	10	250
4	2920	13		350

Table 5: Test scheme and results.

S. No.	A	B	C	D	Water content (%)	Solid content (%)
1	1	1	1	1	68.91	28.15
2	1	2	3	4	71.44	25.09
3	1	3	1	2	72.01	21.38
4	1	4	2	3	74.95	19.83
5	2	1	1	3	64.34	29.58
6	2	2	2	2	65.17	28.91
7	2	3	1	4	66.25	27.72
8	2	4	3	1	68.24	24.96
9	3	1	2	4	58.8	33.71
10	3	2	1	1	61.20	32.45
11	3	3	3	3	63.08	28.68
12	3	4	1	2	65.86	27.39
13	4	1	3	2	65.08	28.58
14	4	2	1	3	67.19	27.96
15	4	3	2	1	67.87	27.43
16	4	4	1	4	70.44	24.39

Table 6: The results of range calculation.

Index	Water content				Solid content			
Factors	A	B	C	D	A	B	C	D
K1	287.31	257.13	536.20	266.22	94.45	120.02	219.02	112.99
K2	264.00	265.00	266.79	268.12	111.17	114.41	109.88	106.26
K3	248.94	269.21	267.84	269.56	122.23	105.21	107.31	106.05
K4	270.58	279.49		266.93	108.36	96.57		110.91
k1	71.83	64.28	67.03	66.56	23.61	30.01	27.38	28.25
k2	66.00	66.25	66.70	67.03	27.79	28.60	27.47	26.57
k3	62.24	67.30	66.96	67.39	30.56	26.30	26.83	26.51
k4	67.65	69.87		66.73	27.09	24.14		27.73
R	9.59	5.59	0.33	0.84	6.95	5.86	0.64	1.74

of factor A (rotational speed). Similarly, B1, C2, and D1 can be identified as the optimal factor levels for factors B, C, and D, respectively. The best factor level combination of this test is $A_3B_1C_2D_1$, which means that the optimal operation scheme of this test is a rotational speed of 2,607 rpm, differential speed of 8 rpm, the feeding quantity of sludge of 7 m^3/h, and flocculant dosage of 100 g/m^3.

Process Stability Analysis

To examine the stability of the process, the optimal scheme was operated continuously for three hours. During this period, samples were taken five times each hour from the inlet, water outlet, and sludge outlet. The test results are given in Table 7. As shown in Fig. 9, the physical properties of the treated sludge were stable under these process parameters. The fluctuation in water content and solid content of the sludge discharged from the sludge outlet was small. After treatment, the average water content of sludge decreased from 92.75% to 56.57%, and the average solid content of sludge increased from 2.30% to 36.72%.

The split ratio is the ratio of the amount of fluid media flowing out from the water outlet and sludge outlet, which is a key parameter for evaluating centrifuge performance. The total mass flow of sludge that flows into the centrifuge through the inlet is defined as 1, and the mass flows of fluid medium discharged from the water outlet and sludge outlet are *a* and *b*. The mass conservation equations of oil, water, and solid phases are established:

$$\begin{aligned} 1 \times W_{win\_w} &= 1 \times a \times W_{wout\_w} + 1 \times b \times W_{sout\_w} \\ 1 \times W_{win\_o} &= 1 \times a \times W_{wout\_o} + 1 \times b \times W_{sout\_o} \\ 1 \times W_{win\_s} &= 1 \times a \times W_{wout\_s} + 1 \times b \times W_{sout\_s} \end{aligned} \quad \ldots(2)$$

Where, W_{win_w} is inlet water content, W_{win_o} is inlet oil content, W_{win_s} is inlet solid content, W_{wout_w} is water outlet water content, W_{wout_o} is water outlet oil content, W_{wout_s} is water outlet solid content, W_{sout_w} is sludge outlet water content, W_{sout_o} is sludge-outlet oil content, and W_{sout_s} is sludge-outlet solid content.

The equations are overdetermined equations that the number of equations is greater than the number of unknowns. The least square method was used to calculate the equations in Lingo software, and the results show that the split ratio of the water outlet and the sludge outlet is in the range of 8.71:1 to 12.57:1, meaning the sludge reduction ratio is 89.70% to 92.63%. The aim of sludge reduction was thus achieved.

CONCLUSIONS

In this paper, we introduced a centrifugal reduction process for oily sludge using a horizontal screw centrifuge as the key piece of equipment, which is combined with a buffer pool, submerged pump, conditioning stirred tank, flocculant dosing device, and recovery pool. The flocculant was important in the field test, and according to the standard, the CPAM flocculant was screened from PAC, CPAM, and alum in the laboratory as the ideal flocculant. Field tests were conducted to analyze the factors influencing the centrifugal reduction process for oily sludge, including the rotational speed, differential speed, the feeding quantity of sludge and flocculant dosage. The results show that if the rotational speed is higher, the differential speed is lower, the feeding quantity of sludge remains at a lower level, and the flocculant dosage remains higher, which considerably reduces the water content and improves the solid content of sludge. The optimal parameters of the centrifugal reduction process were obtained through an orthogonal experimental design as follows: rotational speed 2,607 rpm, differential speed 8 rpm, the feeding quantity of sludge 7 m^3/h, and flocculant dosage 100 g/m^3. After treatment, the average water content of sludge decreased from 92.75% to 56.57%, and the average

Table 7: Sludge test results of process stability.

	Inlet			Water outlet			Sludge outlet		
S. No.	Water content (%)	Solid content (%)	Oil content (%)	Water content (%)	Solid content (%)	Oil content (%)	Water content (%)	Solid content (%)	Oil content (%)
1	92.10	2.11	5.79	97.26	0.97	1.77	56.11	36.67	7.62
2	92.23	2.79	4.98	97.64	1.09	1.27	55.06	38.04	7.30
3	92.52	2.16	5.32	97.52	0.81	1.67	56.18	35.72	8.51
4	92.88	2.39	4.73	97.86	0.83	1.31	56.08	37.41	6.91
5	93.16	2.73	4.11	97.17	1.27	1.56	58.05	38.04	4.31
6	92.41	2.19	5.40	97.57	0.79	1.64	55.92	37.56	6.91
7	93.27	2.06	4.67	97.97	0.68	1.35	58.13	37.08	5.19
8	93.42	2.29	4.29	98.09	0.75	1.16	57.27	36.44	6.69
9	91.53	2.69	5.78	97.15	1.07	1.78	54.96	38.23	7.21
10	92.76	2.15	5.09	97.52	0.95	1.53	55.19	35.93	9.28
11	92.80	2.37	4.83	97.47	0.86	1.67	58.49	37.46	4.43
12	93.53	2.01	4.46	97.43	0.93	1.64	56.49	35.69	8.22
13	92.94	2.33	4.73	98.09	0.77	1.14	57.54	34.46	8.40
14	92.96	2.18	4.86	97.99	0.80	1.21	56.59	36.59	7.22
15	92.75	2.07	5.18	98.26	0.61	1.13	56.48	35.52	8.40

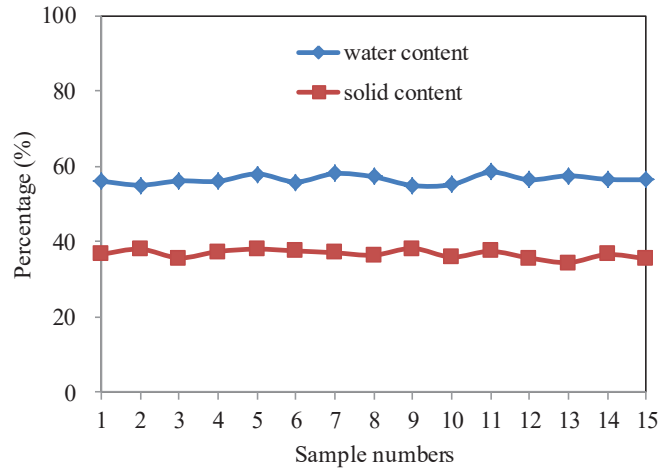

Fig. 9: Process stability test (15 samples).

solid content of sludge increased from 2.30% to 36.72%. The physical properties of the treated sludge were stable under these process parameters. The split ratio of the water outlet and the sludge outlet ranged from 8.71:1 to 12.57:1, and the corresponding sludge reduction ratio was 89.70% to 92.63%. The sludge was therefore effectively reduced.

ACKNOWLEDGEMENTS

This research was supported by the National Natural Science Foundation of China (Grant No. 51508573, 51674086).

REFERENCES

Bo, J., Wilén, B.M. and Paul, L. 2004. Impacts of morphological physical and chemical properties of sludge flocs on dewaterability of activated sludge. Chemical Engineering Journal, 98(1): 115-126.

Braguglia, C.M., Bagnuolo, G. and Gianico, A. 2016. Preliminary results of lab-scale investigations of products of incomplete combustion during incineration of primary and mixed digested sludge. Environmental Science and Pollution Research, 23(5): 4585-4593.

Chang, G.R., Lee, D.J. and Liu, J.C. 2001. Co-conditioning and dewatering of chemical sludge and waste activated sludge. Water Research, 35(3): 786-794.

Galil, N. and Rebhun, M. 2015. Waste management solutions at an integrated oil refinery based on recycling of water, oil and sludge. Water Science & Technology, 25(3): 101-106.

Gao, Y.X., Ding, R. and Wu, S. 2015. Influence of ultrasonic waves on the removal of different oil components from oily sludge. Environmental Technology, 36(14): 1771-1775.

Heidarzadeh, N., Gitipour, S. and Mohammad, A.A. 2010. Characterization of oily sludge from a tehran oil refinery. Waste Management and Research: The Journal of The International Solid Wastes and Public Cleansing Association, ISWA, 28(10): 921-927.

Hou, B., Xie, S.X. and Chen, M. 2012. Recycling oily sludge pyrolysis residues as nano-adsorbents. Journal of Residuals Science and Technology, 9(3): 95-99.

Hu, G., Li, J. and Hou, H. 2015. A combination of solvent extraction and freeze thaw for oil recovery from petroleum refinery wastewater treatment pond sludge. Journal of Hazardous Materials, 283: 832-840.

Hu, G.J., Li, J.B. and Huang, S.H. 2016. Oil recovery from petroleum sludge through ultrasonic assisted solvent extraction. Journal of Environmental Science and Health, Part A: Toxic/Hazardous Substances and Environmental Engineering, 51(11): 921-929.

Hu, G.J., Li, J.B. and Thring, R.W. 2014. Ultrasonic oil recovery and salt removal from refinery tank bottom sludge. Journal of Environmental Science and Health, Part A, 49(12): 1425-1435.

Jean, D.S. and Lee, D.J. 1999. Expression deliquoring of oily sludge from a petroleum refinery plant. Waste Management, 19(5): 349-354.

Kumar, B. and Mohan, B.R. 2013. Petroleum refinery oily sludge: the quantitative and qualitative analysis of its composition. Indian Streams Research Journal, 3(10): 1-6.

Kumar, B. and Mohan, B.R. 2015. Microwave-assisted extraction of wax from oily sludge: an experimental study and its process variables optimization using response surface methodology. Soil and Sediment Contamination: An International Journal, 24(5): 588-607.

Leonardo, J.S., Flávia, C.A. and Francisca, P.F. 2012. A review of the technological solutions for the treatment of oily sludges from petroleum refineries. Waste Management and Research, 30(10): 1016-1030.

Liang, J.L., Zhao, L.X. and Du, N. 2014. Solid effect in solvent extraction treatment of pre-treated oily sludge. Separation and Purification Technology, 130: 28-33.

Lin, Y., George, N. and Amarjeet, B. 2005. Electro-kinetic dewatering of oily sludges. Journal of Hazardous Materials, 125(1-3): 130-140.

Marcelo, M.V., Brites, F.R. and Alex, N.J. 2016. Semi-pilot scale sewage sludge pyrolysis and characterization of obtained fractions by thermal analysis. Journal of Thermal Analysis and Calorimetry, 123(2): 981-991.

Nima, H., Saeid, G. and Ali, A.M. 2009. Statistical sampling and sludge characterization at Tehran oil refinery. Research Journal of Chemistry and Environment, 13(4): 41-47.

Verma, S., Prasad, B. and Mishra, I.M. 2010. Pretreatment of petrochemical wastewater by coagulation and flocculation and the sludge characteristics. Journal of Hazardous Materials, 178(1-3): 1055-1064.

Wang, Q., Qu, C.T. and Qin, F.L. 2013. Development of resource processing technology for heavy oil sludge. Advanced Materials Research, 807: 1402-1408.

Wu, R.M., Chu, C.P. and Lee, D.J. 2003. Modeling sludge as continuous mixture during thermal pyrolysis. Journal of the Chinese Institute of Chemical Engineers, 34(5): 587-593.

Zhang, J., Li, J.B. and Ronald, T. 2013. Application of ultrasound and Fenton's reaction process for the treatment of oily sludge. Procedia Environmental Sciences, 18: 686-693.

Zhang, K. and Zhu, J.H. 2012. The device and method for measuring oil or water content in sample. Chinese patent.

Zhao, J.Y. and Su, H.M. 2007. Q/SY90-2007 technical requirements for flocculant used in oilfield water treatment. Chinese standard.

Zubaidy, E.A.H. and Abouelnasr, D.M. 2010. Fuel recovery from waste oily sludge using solvent extraction. Process Safety and Environmental Protection: Transactions of the Institution of Chemical Engineers, Part B, 88(5): 318-326.

Nature Environment and Pollution Technology
An International Quarterly Scientific Journal

p-ISSN: 0972-6268
e-ISSN: 2395-3454

Vol. 19 | No. 1 | pp.179-189 | 2020

Original Research Paper | Open Access

Nitrogen Occurrence Characteristics and Reason Analysis in Different Trophic Status Freshwater Lakes

Yu Wan*(**), Nan Shan*†, Sichen Tong*, Yao Chen and Jia He*****

*School of River and Ocean Engineering, Chongqing Jiaotong University, Chongqing, China

**College of Resources and Environment, Southwest University, Chongqing, China

***Nanjing Institute of Environmental Sciences, Ministry of Ecology and Environment of the People's Republic of China, Nanjing, China

****National Research Center for Upper Yangtze Economy, Chongqing Technology and Business University, Chongqing, China

†Corresponding author: Nan Shan

Nat. Env. & Poll. Tech.
Website: www.neptjournal.com

Received: 27-05-2019
Accepted: 22-07-2019

Key Words:
Nitrogen
Trophic state
Spatial-temporal variation
Influence factors
Lake Taihu

ABSTRACT

Based on one-year monitoring about the different trophic status freshwater regions of Lake Taihu, the temporal-spatial distribution and occurrence characteristics of nitrogen in the water, porewater, and sediments and their correlation with main aquatic environmental factors were analysed. The results showed that the concentrations of TN in overlying water and sediment ranged from 0.22 to 7.74 mg/L and 551.5 to 1542.8 mg/kg, respectively. The concentrations of NO_3^--N in overlying water, sediment, and porewater ranged from 0.04 to 3.86 mg/L, 14.3 to 42.5 mg/kg, and 0.01 to 0.72 mg/L, respectively. The concentrations of NH_4^+-N in overlying water, sediment, and porewater ranged from 0.03 to 0.25 mg/L, 17.7 to 78.2 mg/kg, and 0.41 to 7.03 mg/L, respectively. NH_4^+-N in overlying water had no significant spatial-temporal variation, and the annual mean of NH_4^+-N in sediments was highest in Meiliang Bay. The annual mean of TN and NO_3^--N in overlying water and sediments was highest in Western Taihu Lake. The spatial and temporal distribution characteristics of NH_4^+-N and NO_3^--N in porewater were roughly consistent with those in sediments. Nitrogen in the sediment occurs in the form of organic nitrogen. Nitrogen in the overlying water was principally of NO_3^--N in Meiliang Bay and Gonghu Bay, and was principally of organic nitrogen in Xukou Bay. In the Western Taihu Lake, nitrogen in the overlying water was principally of NO_3^--N in summer and fall, and organic nitrogen in spring and winter. The results suggest that the type of organic matter in sediments was an important factor affecting the nitrogen occurrence characteristics and trophic status in aquatic environment. The correlation analysis showed that TN and NO_3^--N in overlying water was positively correlated with various forms of nitrogen in sediments, indicating that there was a strong exchange of nitrogen nutrients between water and sediments.

INTRODUCTION

Lake Taihu is the third largest freshwater lake in China. Eutrophication caused by human activities was particularly serious and the trophic states of lake regions were quite different. Therefore, identifying the nitrogen occurrence characteristics, recognizing its spatial-temporal variation pattern, and analysing its causes of formation has important significance for control of lacustrine eutrophication.

In order to control the eutrophication of Lake Taihu in recent years, a considerable number of researches about the temporal and spatial distribution of nitrogen in Lake Taihu have been made. These investigations helped to establish a broad understanding concerning the physical properties of sediment and its contribution to waterbody eutrophication. For example, Wang et al. (2010), Zhao et al. (2007) and Jin et al. (2006) analysed the temporal and spatial distribution characteristics of various forms of nitrogen in the heavily polluted region of northern Lake Taihu. In addition, Deng et al. (2008) studied the spatial distribution characteristics of nitrogen in overlying water of Lake Taihu and its relationship with algae and chlorophyll, and contribute to understood the relationship between phytoplankton and nitrogen occurrence characteristics in overlying water. The above results indicate that previous studies focused on the nitrogen occurrence characteristics and its spatial-temporal variation pattern in eutrophication lake region. However, the detailed information about the spatial-temporal variation pattern of nitrogen occurrence characteristics and its genesis analysis in different trophic status regions of Lake Taihu was still insufficient. More importantly, due to the migration and transformation of various forms of nitrogen in different media of the lacustrine environment, nitrogen in the sediment was released into the porewater and overlying water by molec-

ular diffusion and bioturbation, thus the trophic status of the waterbody has changed (Wang et al. 2008). Therefore, sediment play a critical role in trophic status of waterbody and occurrence characteristics of nitrogen. Consequently, a thorough understanding of the nitrogen spatial-temporal variation characteristics in overlying water, pore water, and sediment was critical for us to understand the pattern of nitrogen migration and transformation in various media of lacustrine environments.

Lake Taihu is a typical large shallow eutrophic lake. Due to geographical features and differences in river input, there were a series of environmental gradients from Meiliang Bay in the northern to Eastern Lake Taihu in the southeast. Therefore, taking Western Lake Taihu (west), Meiliang Bay (north), Gonghu Bay (northeast), and Xukou Bay (east) as research region, one-year monitoring of lacustrine environment was carried out. The aim of this study is to dissect spatial-temporal variation of nitrogen in sediments, porewater, and overlying water of different trophic status lake regions (1) to recognized the change regularity of trophic status in lake regions, (2) to determine the relations of various nitrogen occurrence forms with aquatic environmental factors, (3) and to identify nitrogen migration and transformation pattern in various media.

MATERIALS AND METHODS

Sampling Sites and Procedure

The study area (Fig. 1) is located at the north to east side of the Lake Taihu with total nitrogen decreasing from Western Lake Taihu (region A-1, west) and Meiliang Bay (region A-2, north), to Gonghu Bay (region A-3, northeast), and finally to Xukou Bay (region A-4, east). Area A-1 and A-2 are highly enriched with nutrients and have frequent algal blooming incidents. In contrast, the low nutrient waterbody in A-4 is characterized by submersed vegetation and diverse communities of fishes and invertebrates and, in fact, is a drinking water source for local communities. The water in A-3 was similar to that in A-1 and A-2 till about 15 years ago but has since improved its quality due to the interference of local government.

Sample collection was carried out in fall of 2015, and winter, spring, and summer of 2016. For sediments, loose sediment samples in the depth of less than 5 cm was collected using a 1/16 m^2 Petersen grab sampler. Triplicate samples from three separate grabs were homogenized to generate one composite sample in each sampling site. Water samples were taken together at the same locations. All the samples were immediately stored in an icebox and transported back to the lab within 3 hours. Once in the lab, an aliquot of the sediment samples was stored in a 100 mL sterile centrifuge tube at -80°C until the analysis of physico-chemical index was completed. The remaining portion was further processed (freeze-dried to collect sediment particles, and centrifuged to collect the porewater) for physico-chemical analyses.

Physicochemical Analyses

Sixteen physicochemical parameters of the overlying water, porewater, and freeze-dried sediments were analysed (Table 1).

Details of the measurement procedures for each parameter can be found in Lu (1999), Wei (2002). Temperature (T), chlorophyll-*a* (Chla), algal density (AD), and dissolved oxygen (DO) of the overlying water were measured *in situ* using an YSI 6600 Multi-Parameter Water Quality Sonde, whereas the transparency was determined by a standard Secchi disc (SD) (diameter 20 cm) with black and white quadrants (Canfield et al. 1985).

Statistics Analysis

The Trophic Status Indices (*TSI*) (Aizaki 1981) at all the sampling sites were calculated using the measured Chl-*a*, W-TP, W-TN, COD, and SD by the following expression:

$$TSI\left(\sum\right) = \sum_{i=1}^{m} w_j \, TSI\left(j\right) \quad ...(1)$$

Where, $TSI\left(\sum\right)$ is the completed *TSI*; w_j is the relative weight of *TSI* of the *j* parameter; and *TSI(j)* is *TSI* of the *j* parameter. The mean value of all the samples in each region was used to represent the local trophic status, which based upon the value of $TSI\left(\sum\right)$, can be classified as: oligotrophication ($0 < TSI \leq 30$), mesotrophication ($30 < TSI \leq 50$), light eutrophication ($50 < TSI \leq 60$), medium eutrophication ($60 < TSI \leq 70$), and hypereutrophication ($70 < TSI \leq 100$) on a scale of 0 to 100.

Pearson's correlation analysis (SPSS, v20.0) was performed to determine the links between environmental factors (AD, Chl-*a*, DO) and various forms of nitrogen in the overlying water, sediment, and porewater (W-TN, W-NH_4, W-NO_3, S-TN, S-NH_4, S-NO_x, P-NH_4, P-NO_3). Analysis of similarity (ANOSIM) was conducted to statistically test the variation of aquatic environmental indexes across seasons and regions. ANOSIM is a nonparametric test of significant difference between 2 or more groups based on any distance measure (Clarke 1993). ANOSIM then generates a test statistic, R, the magnitude of which indicates the degree of separation between groups, with a score of 1 indicating complete separation and 0 indicating no separation.

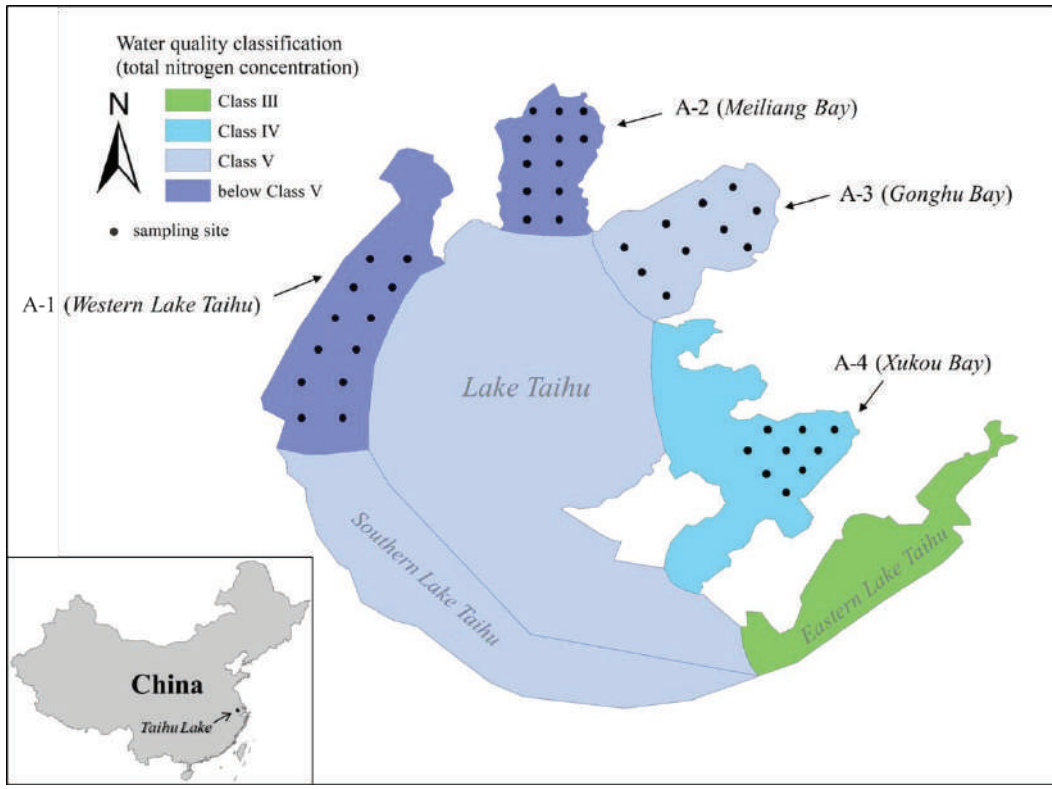

Fig. 1: The 43 sampling sites in the different trophic states regions of Lake Taihu. Water quality classification of the lake regions referred to the Standard GB3838-2002 of China. The data of total nitrogen concentration in the figure is from *the Health Status Report of Taihu Lake 2015* in Water Resources Department of Jiangsu Province.

Table 1: physico-chemical parameters of the overlying water, porewater, and freeze-dried sediments.

	Physicochemical Parameters
Sediment	total nitrogen (S-TN), ammonium nitrogen (S-NH_4), nitrate-nitrite nitrogen (S-NO_x), total organic matter (TOM)
Overlying water	total nitrogen (W-TN), ammonium nitrogen (W-NH_4), nitrate nitrogen (W-NO_3), total phosphorus (W-TP), Chemical Oxygen Demand (COD), temperature (T), chlorophyll-*a* (Chl), algal density (AD), and dissolved oxygen (DO), Secchi Disc (SD)
Porewater	ammonium (P-NH_4), nitrate nitrogen (P-NO_3)

RESULTS

Trophic Status of Four Lake Regions

Physico-chemical properties of the overlying water in four lake regions are shown in Fig. 2. The average annual value of DO and SD in A-4 is significantly higher than other regions (Fig. 2-1, 2-2). The annual average values of Chl-*a*, AD, TP and COD_{Mn} in the four lake regions were A-1 and A-2 > A-3 > A-4 (Figs. 2-3, 2-4, 2-5, 2-6). The Trophic Status Indices (*TSI*) of four lake regions in the four seasons are given in Table 2. Measured *TSI* in the study area decreased in the direction of A-1, A-2, A-3, to A-4 with average values changing from 61.3, 60.7, 56.2 to 45.4, respectively. Since region A-2 has been affected by the rivers of Zhihu Port and Wujin Port (Zhang et al. 2004), it was in a state of medium eutrophication all the year around, and the trophic status was highest in summer and lowest in winter. Region A-1 was the inflow area of Lake Taihu, affected by the upstream water, was in a state of medium eutrophication in spring, summer and autumn, and light eutrophication in winter. The water quality of region A-3 has been greatly improved after water diversion projects implementation (Hu et al. 2008), and it was in a state of light eutrophication throughout the year. The region A-4 enriched in aquatic vegetation (Qin et al. 2004), and was in a state of mesotrophication during the whole year.

Table 2: The trophic status of the five lake regions.

Lake regions	Season	*TLI* (Chl-a)	*TLI* (TP)	*TLI* (TN)	*TLI* (SD)	*TLI* (COD_{Mn})	*TLI*(Σ)	Trophic states
Western Lake Taihu (region A-1)	Spring	48.3	61.4	86.9	76.2	39.6	62.4	Medium eutrophication
	Summer	44.8	72.2	69.9	76.2	48.5	62.7	
	Autumn	43.1	70.2	69.4	80.3	46.7	61.9	
	Winter	36.8	57.9	73.1	78.7	42.5	58.3	Light eutrophication
Meiliang Bay (region A-2)	Spring	55.8	53.7	74.1	77.7	43.4	60.5	Medium eutrophication
	Summer	53.7	64.8	65.6	75.7	47.1	61.3	
	Autumn	47.9	59.9	63.8	80.5	58.7	60.6	
	Winter	48.6	57.4	70.2	80.6	50.6	60.2	
Gonghu Bay (region A-3)	Spring	51.9	56.6	73.5	69.6	34.5	57.0	Light eutrophication
	Summer	48.0	62.6	62.6	69.3	44.1	56.5	
	Autumn	45.2	55.9	62.6	68.8	63.3	58.0	
	Winter	45.0	46.2	68.6	72.3	38.4	53.2	
Xukou Bay (region A-4)	Spring	42.0	40.5	63.3	65.6	37.4	49.0	Mesotrophication
	Summer	39.0	44.9	59.0	65.1	42.9	49.1	
	Autumn	35.2	45.7	43.1	64.6	25.6	42.2	
	Winter	30.9	39.0	32.9	66.2	42.9	41.4	

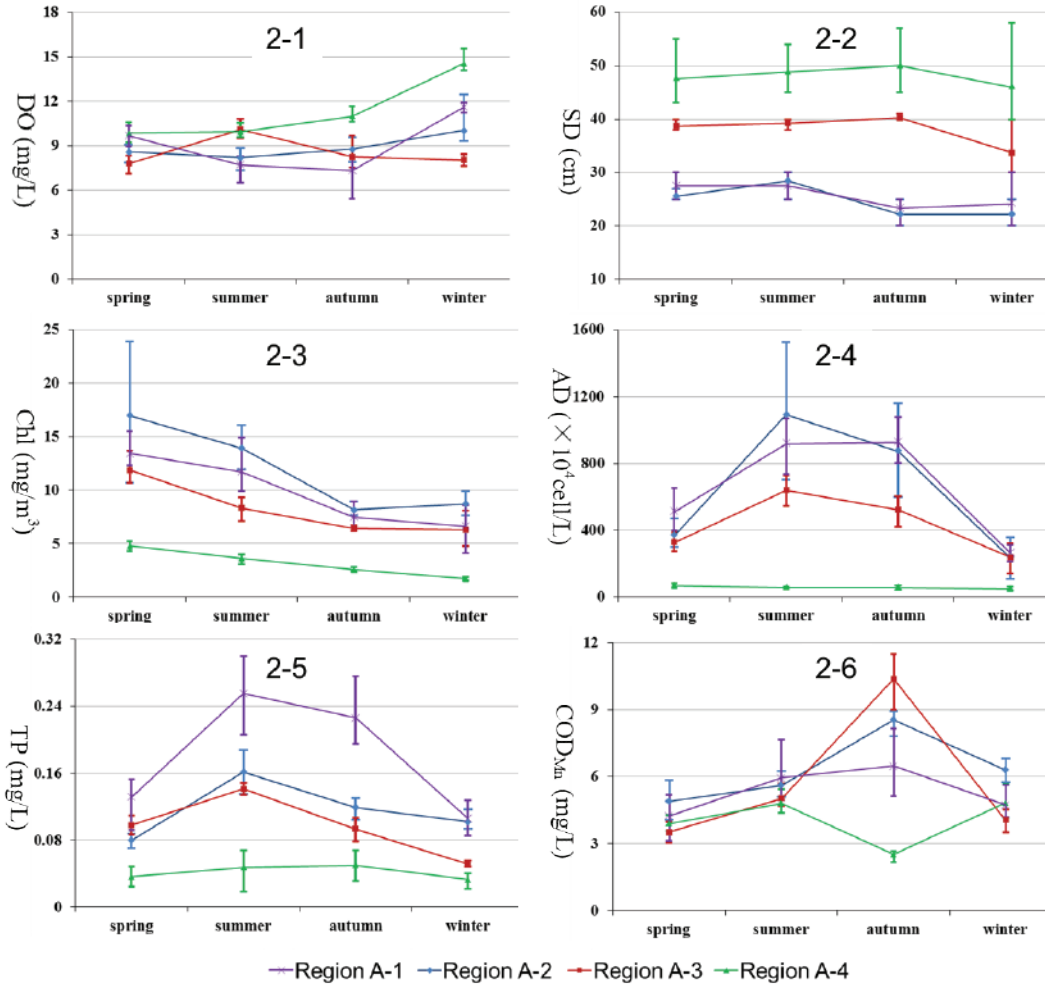

Fig. 2: The indexes of trophic status in the four lake regions in four seasons. A monitoring index concentration of each lake was calculated by taking average value of the monitoring index concentration of the all sample site in this lake.

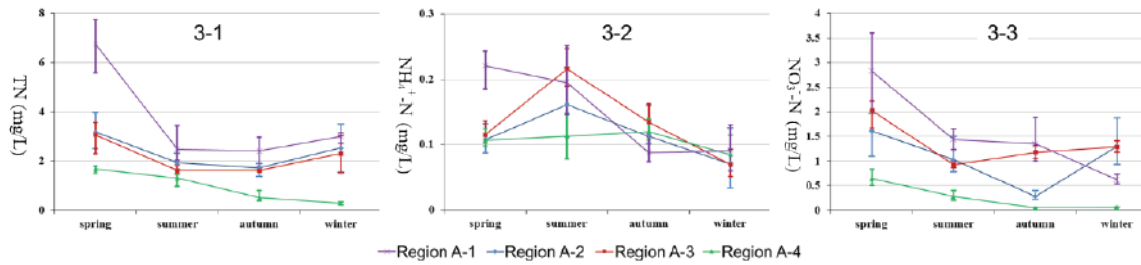

Fig. 3: Physico-chemical properties of the overlying water in different trophic states lake in four seasons. A monitoring index concentration of each lake was calculated by taking average value of the monitoring index concentration of the all sample site in this lake.

Table 3: Analysis of similarity (ANOSIM) R statistics for comparisons of spatial differences in overlying water environmental indexes.

	Meiliang Bay (A-2)	Gonghu Bay (A-3)	Western Lake Taihu (A-1)
Gonghu Bay (A-3)	0.04		
Western Lake Taihu (A-1)	0.11	0.10	
Xukou Bay (A-4)	0.43	0.45	0.64

Table 4: Analysis of similarity (ANOSIM) R statistics for comparisons of seasonal differences in overlying water environmental indexes.

	Spring	Summer	Autumn
Summer	0.28		
Autumn	0.28	0.06	
Winter	0.15	0.18	0.09

Temporal and Spatial Distribution Characteristics of Nitrogen in Overlying Water

As shown in Fig. 3 (3-1), the average annual concentration of TN decreased in the same direction as *TSI* does, and TN concentration of each lake region was highest in spring. The temporal and spatial distribution characteristics of NO_3^--N were consistent with TN (Fig. 3-3). The spatiotemporal variation of NH_4^+-N in the overlying water was not significant (Fig. 3-2).

The main form of nitrogen occurrence in overlying water of four lake regions is shown in Fig. 4. Nitrogen in the overlying water was principally of NO_3^--N in region A-2 (Fig. 4-2) and region A-3 (Fig. 4-3), and was principally of organic nitrogen (ON) in region A-4 (Fig. 4-4). In region A-1, nitrogen in the overlying water was principally of NO_3^--N in summer and fall, and organic nitrogen in spring and winter (Fig. 4-1).

The result of ANOSIM showed that there were significant spatial variations in nitrogen distribution characteristics of the overlying water between eutrophication and mesotrophication region (Table 3), and the seasonal variation was not significant (Table 4).

Temporal and Spatial Distribution Characteristics of Nitrogen in Sediment and Porewater

As shown in Fig. 5 (5-1), the TN content in sediment in region A-1, A-2, A-3, and A-4 was highest in summer, spring, autumn and spring, respectively. The sediment NH_4^+-N (Fig. 5-2) and NO_x^--N (Fig. 5-3) content in four lake regions reaching their maximal level in autumn. In addition, the contents of TN, NH_4^+-N and NO_x^--N in sediments were reduced with decreasing trophic status (Fig. 5). The main form of nitrogen occurrence in sediment of four lake regions was organic nitrogen, and the main form of inorganic nitrogen occurrence in sediment and porewater were NH_4^+-N (Fig. 7).

Spatial and temporal distribution trend of NH_4^+-N in porewater was similar to that in sediment Fig. 6 (Fig. 6-1). The concentration of NO_3^--N in porewater showed a strong seasonal variation with NO_3^--N reaching its maximal level in summer (Fig. 6-2).

Relationship Between Various Nitrogen Occurrence Forms and Aquatic Environmental Factors

Pearson's correlation analysis indicated that chlorophyll-*a* and algal density in the study area appeared to be correlated

Table 5: Relationship between environmental factors and various forms of nitrogen in the overlying water, sediment and porewater.

		Chl	W-TN	AD	DO	W-NH_4	W-NO_3	P-NH_3	P-NO_3	S-TN	S-NH_4
spring	W-TN										
	AD	0.66	0.77								
	DO										
	W-NH_4		0.91	0.66							
	W-NO_3	0.48	0.84	0.73		0.74					
	P-NH_3	0.61	0.75	0.88		0.73	0.68				
	P-NO3										
	S-TN	0.66	0.49	0.55				0.48			
	S-NH_4	0.62	0.47	0.73			0.57	0.57		0.58	
	S-NO_x	0.48	0.61	0.77		0.52	0.59	0.76			0.78
summer	W-TN	0.57									
	AD	0.83	0.60								
	DO	-0.71	-0.75	-0.68							
	W-NH_4		0.60								
	W-NO_3	0.74	0.85	0.77	-0.68	0.62					
	P-NH_3	0.50	0.78		-0.63		0.72				
	P-NO3										
	S-TN	0.63	0.68	0.60	-0.58		0.64	0.68			
	S-NH_4	0.83	0.49	0.71	-0.47	0.48	0.69	0.49		0.57	
	S-NO_x	0.52	0.47	0.67			0.64				0.74
autumn	W-TN	0.81									
	AD	0.90	0.83								
	DO	-0.72	-0.89	-0.68							
	W-NH_4										
	W-NO_3	0.45	0.72	0.47	-0.70						
	P-NH_3	0.64	0.83	0.76	-0.70		0.64				
	P-NO3	0.75	0.78	0.70	-0.79		0.64	0.58			
	S-TN	0.57	0.46		-0.59				0.54		
	S-NH_4	0.64	0.50	0.65				0.50			
	S-NO_x		0.58		-0.58		0.65	0.58			
winter	W-TN	0.74									
	AD	0.67	0.79								
	DO	-0.69	-0.65	-0.66							
	W-NH_4										
	W-NO_3	0.77	0.70	0.65	-0.86						
	P-NH_3	0.68	0.43				0.54				
	P-NO3										
	S-TN		0.79	0.57							
	S-NH_4	0.76	0.42		-0.56		0.74	0.87			
	S-NO_x	0.50	0.68	0.51			0.70				

Only $p < 0.01$ shown in the table

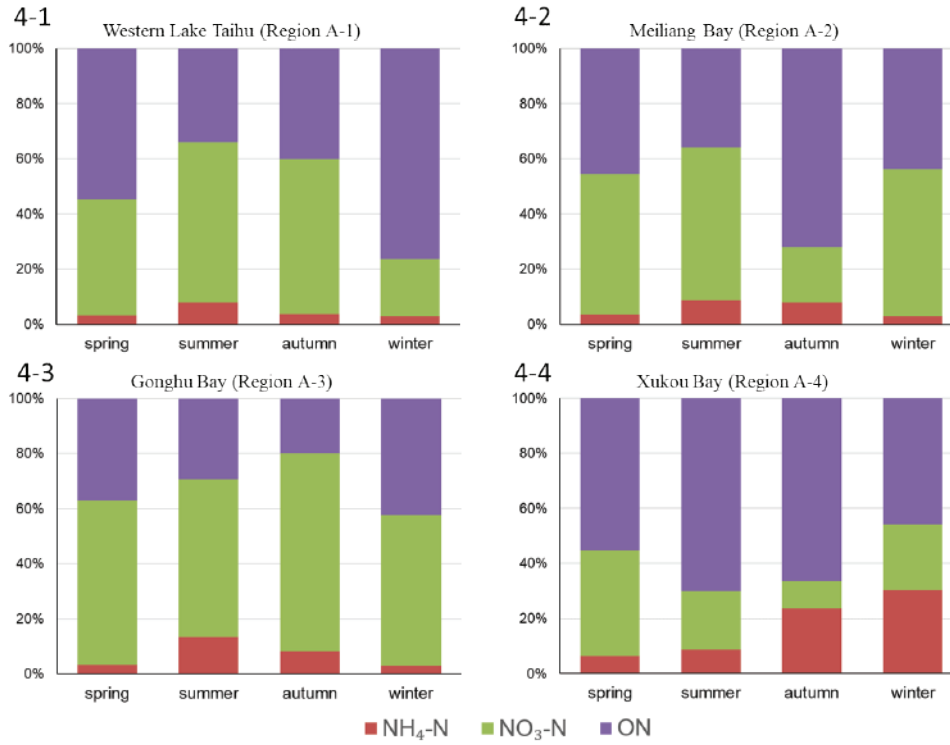

Fig. 4: various forms of nitrogen occurrence in the overlying water in different trophic states lake regions in four seasons.

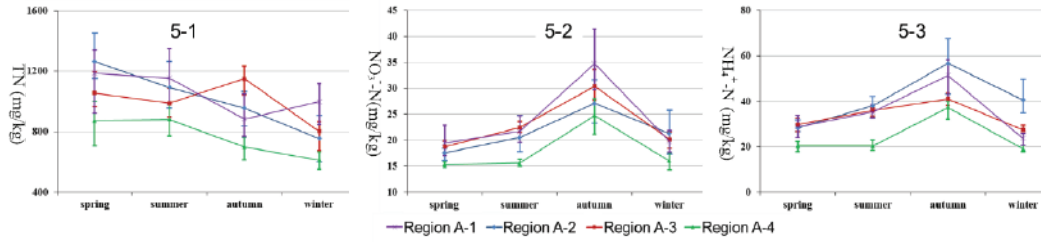

Fig. 5: Physico-chemical properties of the sediment in different trophic states lake regions in four seasons. A monitoring index concentration of each lake was calculated by taking average value of the monitoring index concentration of the all sample sites in this lake.

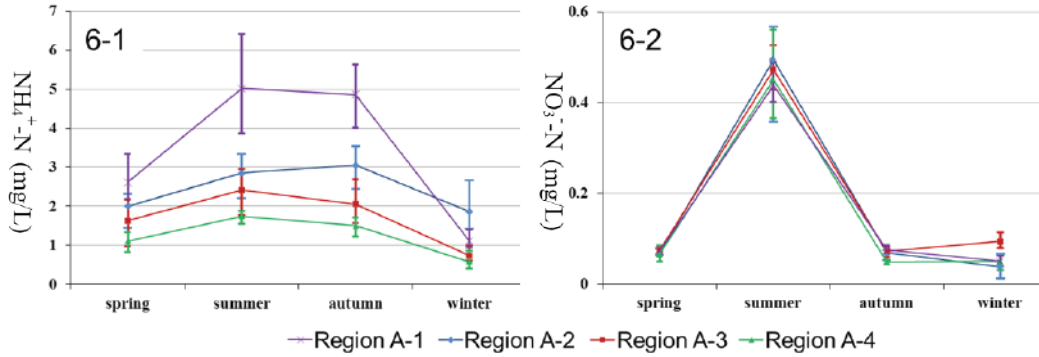

Fig. 6: Physico-chemical properties of the porewater in different trophic states lake regions in four seasons. A monitoring index concentration of each lake region was calculated by taking average value of the monitoring index concentration of the all sample sites in this lake.

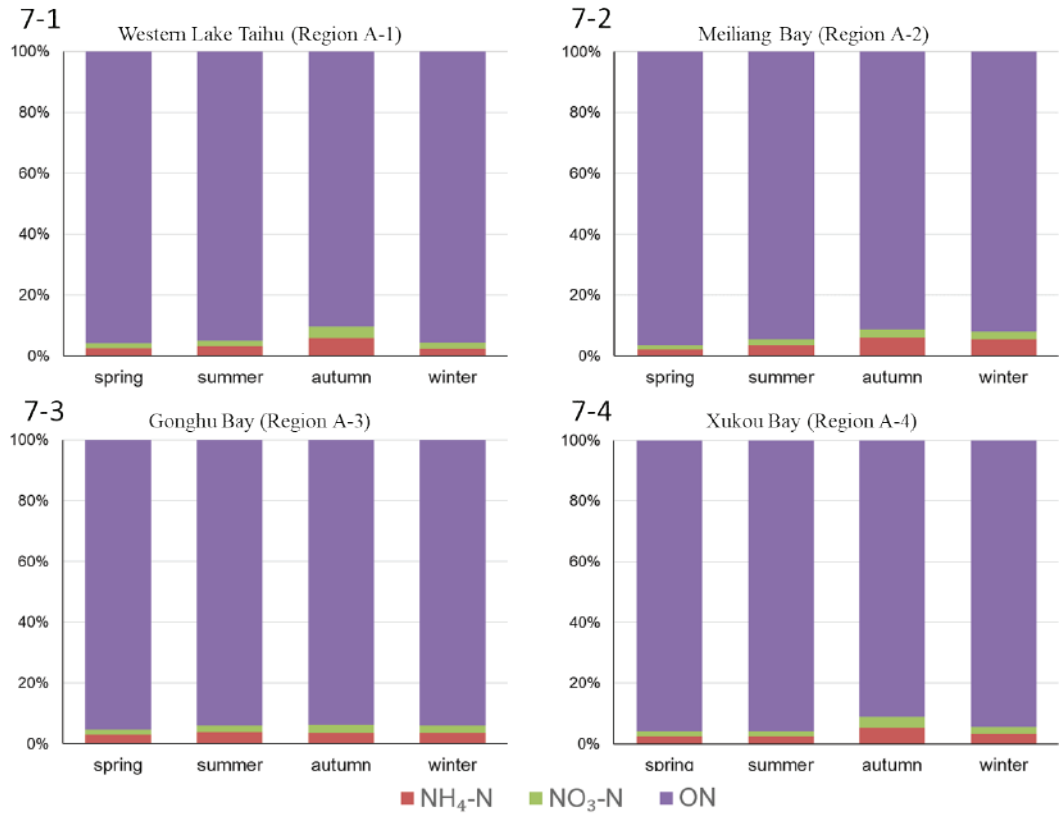

Fig. 7: various forms of nitrogen occurrence in the sediment in different trophic states lake regions of four seasons.

positively with the W-TN, W-NO_3, P-NH_3, S-TN, S-NH_4, and S-NO_x but negatively with DO (Table 5). For the different nitrogen occurrence forms in various media, a positive correlation between TN and NO_3^--N in overlying water and TN, NH_4^+-N, and NO_3^--N in sediment was observed (Table 5). Meanwhile, TN and NH_4^+-N in sediment exhibited a significant correlation with NH_4^+-N in porewater (Table 5).

DISCUSSION

Analysis of Temporal and Spatial Distribution Characteristics of Nitrogen Forms

The type of organic matter in sediment has an important influence on the migration and transformation of nitrogen (Zhu et al. 2011). Therefore, in this study, various sedimentary organic matter types will cause the difference of nitrogen occurrence forms in overlying water and trophic status of lake region. Different organic matter types have different mineralization products. On the one hand, organic compounds rich in carbon chains (cellulose, sugars, simple hydrocarbons, and lipids) produced monosaccharides in the degradation process, and eventually released CO_2 and CH_4 after mineralization (Xiao et al. 2009). On the other side, organic compounds rich in peptide ammonia bonds were degraded to amino acids, and finally NH_4^+-N was released through mineralization (Xiao et al. 2009).

In the algal bloom and eutrophic region, A-2 and A-3, the main source of organic matter was the algae which settled in the lake regions after death. While algae rich in nitrogen, sedimentary organic matter released a large amount of nitrogen such as NH_4^+-N during degradation and mineralization. The reason why nitrogen in the overlying water of regions A-2 and A-3 was principally of NO_3^--N may be two-fold. First of all, phytoplankton preferred to absorb NH_4^+-N than NO_3^--N, and NH_4^+-N was preferentially absorbed by algae. Secondly, due to the high content of DO in the lake regions (mean 8.5 mg/L), NH_4^+-N would be transformed into NO_3^--N under aerobic conditions. In the mesotrophic region A-4, the main source of organic matter was aquatic plants rich in cellulose. While cellulose was mainly composed of C, H and O, sedimentary organic matter released CO_2 and CH_4 during degradation and mineralization, therefore, organic nitrogen was the main form of nitrogen occurrence in region A-4. In the algal bloom and eutrophic region, A-1, as

the main inflow regions of Lake Taihu, the impact of inflow rivers on the main form of nitrogen occurrence in overlying water was more pronounced. Previous analysis of nitrogen sources in region A-1 show that nitrogen in the inflow river was mainly from fertilizers during dry seasons, while from sewage during wet seasons (Wu et al. 2015). Thus, it caused that nitrogen in the overlying water was principally of NO_3^--N in summer and fall (wet season), and organic nitrogen in spring and winter (dry season).

The growth cycle of algae was short (1~2 weeks), and nutrients in the algae were quickly released into the water after algal death. Therefore, algae cannot fix nitrogen in water body for a long time as plants do. After algal death, nitrogen released into water in the form of ion state or gel state and reused by algae again (Sun et al. 2007). Whereas, aquatic plants cannot be decomposed quickly, and released nitrogen slowly by mineralization after their death. The released nitrogen quickly absorbed by aquatic plants, and significantly reduce the concentration of nutrients in water (Zhang et al. 2004). In conclusion, regions A-1, A-2 and A-3 with frequent algal bloom were in a state of eutrophication, while region A-4 with rich in aquatic vegetation was in a state of mesotrophication.

In the same sampling site, NO_3^--N concentration in the porewater was much lower than that in the overlying water. This was due to a significant denitrification took place in the sedimentary environment, and NO_3^--N, as an oxidant, participated in denitrification and degradation of organic matter in sediments. Besides, in the same sampling site, NH_4^+-N concentration in the porewater was much higher than that in the overlying water. NH_4^+-N in porewater mainly came from the ammonification of organic nitrogen in sediments under the action of anaerobic microorganisms (Hou et al. 2014), and its content was determined by the decomposition rate of organic nitrogen and the diffusion rate of NH_4^+-N in the sediment-water interface. The sediment of lake Taihu was rich in organic nitrogen and low in dissolved oxygen, which was easy to form a reducing environment (Qiao et al. 2012), and denitrification and ammonification were significant under microbial action. Hu et al. (2004) reported that the particulate matter of sediment had a strong adsorption on NH_4^+-N, while it had a weak even negative adsorption on NO_x^--N. NH_4^+-N usually exist in the sediment in the form of adsorption state and free state, and NH_4^+-N adsorbed on the sediment was the main source of NH_4^+-N in porewater (Bao et al. 2006).

Difference Analysis of Nitrogen Occurrence Characteristics

Agreeing with previous studies in other similar eutrophicated freshwater lakes (Shu et al. 2012, Zhao et al. 2013), the result of ANOSIM showed that the seasonal variation of nitrogen distribution characteristics in overlying water was not significant. Besides, there were significant spatial variations in nitrogen distribution characteristics of the overlying water between eutrophication and mesotrophication region. The reason might be that the northern and western lake regions had been affected by the input of polluted upstream water for a long time, and they were the main algal bloom areas of Lake Taihu. The death and subsidence of algae caused the release of nitrogen nutrients to overlying water (Qin et al. 2004), further aggravating the eutrophication state of the lake region. The region A-4 had no input of nitrogen pollutants and was rich in aquatic vegetation. Aquatic plants not only purified water quality (Li et al. 2010), but also inhibited the release of nutrients in sediment (Barko et al. 1998), which lowers the trophic status of lake region. Therefore, due to the exogenous input and endogenous release of nitrogen, cause a significant difference of nitrogen occurrence characteristics between mesotrophication and eutrophication lake regions.

Influence Factors of Nitrogen Occurrence Characteristics

Chlorophyll-*a* was one of the important components of the algae, its content reflected the biomass and growth of phytoplankton, and was closely related to the species and quantity of algae (Agawin et al. 2000), so the algal density and chlorophyll-*a* showed significant positive correlation. The negative correlation between algal density and dissolved oxygen indicated that with the increasing of algal density, algae consumed more dissolved oxygen in water through respiration, which results in the decrease of dissolved oxygen concentration.

In this study, the concentration of TN in overlying water showed a significant positive correlation with algal density in the four seasons. Previous studies had shown that TN not only affected the growth and reproduction of algae, but also affected the algal community structure (Zhu et al. 2010). Zhu et al. (2013) discussed the relationship between algal community structure and environmental factors in Southern Lake Taihu, and found that TN had a more significant impact on the growth of algae than other environmental factors. After the death of algae, the nitrogen in the algae could be released into the water quickly, providing nutrients for the growth of more algae, and at the same time, the concentration of TN in the overlying water increased. This conclusion could explain that, in the eutrophicated algae-dominated lake regions, the algal density in summer and autumn was higher than that in winter and spring, but the TN concentration in overlying water was lower.

Consistent with the observations made in freshwater lake (Trevisan et al. 2007), algal density and chlorophyll showed

a positive correlation with NO_3^--N concentration, that might be because phytoplankton usually tend to absorb ammonia, nitrite, and nitrate nitrogen in water to synthesize amino acids and other substances needed by algal cells (Wafar et al. 2004). Chlorophyll and algal density were positively correlated to P-NH_3, S-TN, S-NH_4, and S-NO_x, which might be due to the release of nitrogen from sediment to overlying water and porewater, thus indirectly affecting the algal density and chlorophyll content in the overlying water.

Nitrogen in overlying water, porewater, and sediment was transferred and transformed under different conditions. On the one hand, nitrogen in porewater and sediment was exchanged with overlying water through molecular diffusion, which affected the occurrence form and characteristics of nitrogen in overlying water. On the other hand, sediment had adsorption effect on nitrogen in porewater and overlying water. Driven by the concentration gradient, the nitrogen in the sediment and porewater diffused to the overlying water (Zhang et al. 2013). Therefore, the forms and contents of nitrogen in various media could influence each other through migration and transformation.

W-TN and W-NO_3 in overlying water of each lake region showed a positive correlation with P-NH_3, S-TN, S-NH_4 and S-NO_x, indicating that there was a strong nitrogen exchange between water and sediment. The endogenous nutrients entered the overlying water from the sediments mainly through the resuspension process of surface sediments and the concentration diffusion of porewater. Some scholars considered that the process of nitrogen release into overlying water was a mechanism that nitrogen in the sediment supply nutrients to the overlying water (Xia et al. 2009). Therefore, while the exogenous source was effectively controlled, the endogenous release could not be ignored.

Nitrogen nutrients not only diffused between overlying water and porewater, but also migrated and transformed between sediment and porewater. There was a significant correlation between various forms of nitrogen in sediments and porewater, among them, the correlation of NH_4^+-N in the two media was the best, indicating that NH_4^+-N in porewater was mainly affected by NH_4^+-N in sediment. The effect was mainly manifested in two aspects. On the one hand, the organic matter in sediments generated NH_4^+-N through mineralization under anaerobic environment, and then releases NH_4^+-N into porewater by adsorption and desorption. For another, the concentration of NH_4^+-N in porewater also affected the adsorption capacity of sediment for NH_4^+-N. The study about NH_4^+-N adsorption characteristics of shallow lakes surface sediment in the middle and lower Yangtze River, confirmed the existence of the interaction (adsorption and desorption) in the sediment of Lake Taihu (Wang et al. 2007). A positive correlation between NH_4^+-N in porewater and TN in sediment suggest that, as the main component of TN in sediment (more than 90%), organic nitrogen transformed to NH_4^+-N by ammonification, and NH_4^+-N migrated to porewater and overlying water through diffusion. Previous studies suggest that the above process was the main way of nitrogen exchange between sediment and overlying water (Li et al. 2009).

ACKNOWLEDGEMENTS

This research was supported by Natural Science Foundation of Chongqing, China (cstc2019jcyj-bshX0007, cstc2018jcyjAX0534, cstc2017jcyjAX0292), Central Public-interest Scientific Institution Basal Research Fund (GYZX190306), National Natural Science Foundation of China (51709024), and Science and Technology Project of Chongqing Urban Administration (2019-23).

REFERENCES

Agawin, N.S., Duarte, C.M. and Agustí, S. 2000. Nutrient and temperature control of the contribution of picoplankton to phytoplankton biomass and production. Limnol. Oceanogr., 45: 591-600.

Aizaki, M. 1981. Application of modified Carlson's trophic state index to Japanese lakes and its relationships to other parameters related to trophic state. National Institute for Environmental Studies, Japan 23: 13-31.

Bao, X., Chen, K. and Fan, C. 2006. Effects on nitrogen and phosphorus distribution in interstitial water and sediment-water nitrogen and phosphorus release with growing of submerged macrophytes. Journal of Lake Sciences, 18: 515-522.

Barko, J.W. and James, W.F. 1998. Effects of submerged aquatic macrophytes on nutrient dynamics, sedimentation, and resuspension. The structuring role of submerged macrophytes in lakes. Springer, New York, NY, pp. 197-214.

Canfield, D.E., Langeland, K.A., Linda, S.B. and Haller, W.T. 1985. Relations between water transparency and maximum depth of macrophyte colonization in lakes. J. Aquat. Plant Manage., 23: 25-28.

Clarke, K.R. 1993. Non-parametric multivariate analyses of changes in community structure. Australian journal of Ecology, 18: 117-143.

Deng, J.C., Chen, Q., Zhai, S.J., Yang, X.C., Han, H.J. and Hu, W.P. 2008. Spatial distribution characteristics and environmental effect of N and P in water body of Taihu Lake. Environmental Science, 29: 3382-3386.

Hou, D., He, J., Lu, C., Dong, S., Wang, J., Xie, Z. and Zhang, F. 2014. Spatial variations and distributions of phosphorus and nitrogen in bottom sediments from a typical north-temperate lake, China. Environmental Earth Sciences, 71: 3063-3079.

Hu, W., Zhai, S., Zhu, Z. and Han, H. 2008. Impacts of the Yangtze River water transfer on the restoration of Lake Taihu. Ecological Engineering, 34: 30-49.

Hu, Z.T., Sun, H.W. and Tan, Y. 2004. Adsorptive characteristic of nutrient elements and influential factors in Taihu Lake sediment. Journal of Agro-Environment Science, 23: 1212-1216.

Jin, X.C., Jiang, X. and Xu, Y.H. 2006. Seasonal variation of dissolved nitrogen and phosphorus in sediments in northeast part of Lake Taihu. China Environmental Science, 26: 409-413.

Li, X.N., Song, H.L., Li, W., Lu, X.W. and Nishimura, O. 2010. An integrated ecological floating-bed employing plant, freshwater clam and biofilm carrier for purification of eutrophic water. Ecol. Eng., 36: 382-390.

Li, Y., Hu, X. and Nian, Y. 2009. Experimental Comparison of Nutrient Characters of Pore Water Between Macrophytic and Algal Lakes. Journal of Hydroecology, 5: 5.

Lu, R.K. 1999. Soil Argrochemistry Analysis Protocoes. China Agriculture Science Press, Beijing.

Qiao, J., Yang, L., Yan, T., Xue, F. and Zhao, D. 2012. Nitrogen fertilizer reduction in rice production for two consecutive years in the Taihu Lake area. Agr. Ecosyst. Environ. 146: 103-112.

Qin, B.Q., Hu, W.P. and Chen, W.M. 2004. Process and Mechanism of Environmental Changes of the Taihu Lake. Science Press, Beijing.

Shu, F.Y., Liu, Y.P., Zhao, Y., Wu, Y.P. and Li, A.H. 2012. Spatio-temporal distribution of TN and TP in water and evaluation of eutrophic state of Lake Nansi. Environmental Science, 33: 3748-3752.

Sun, X., Qin, B.Q. and Zhu, G.W. 2007. Release of colloidal phosphorus, nitrogen and organic carbon in the course of dying and decomposing of cyanobacteria. China Environmental Science, 27: 341-345.

Trevisan, G.V. and Forsberg, B.R. 2007. Relationships among nitrogen and total phosphorus, algal biomass and zooplankton density in the central Amazonia lakes. Hydrobiologia, 586: 357-365.

Wafar, M., L'Helguen, S., Raikar, V., Maguer, J.F. and Corre, P. L. 2004. Nitrogen uptake by size-fractionated plankton in permanently well-mixed temperate coastal waters. J. Plankton Res., 26: 1207-1218.

Wang, J., Wang, S., Jin, X. and Zhu, S. 2007. Ammonium adsorption characteristics onto the sediments from shallow lakes in the middle and lower reaches of the Yangtze River. Journal of Agro-Environment Science, 26: 1224-1229.

Wang, Q., Li, Y., Jiang, X., Wang, S. and Jin, X. 2010. The distribution of nitrogen speciation in three lake regions of North of Taihu Lake. China Environmental Science, 30: 1537-1542.

Wang, S.R., Jiao, L.X. and Jin, X.C. 2008. Distribution of total, exchangeable and fixed nitrogen in the sediments from shallow lakes in the middle and lower reaches of the Yangtze River. Acta Scientiae Circumstantiae, 28: 37-43.

Wei, F.S. 2002. Determination Methods for Examination of Water and Wastewater. China Environmental Science Press, Beijing.

Wu, Q.L., Ruan, X.H., Wu, C.M., Li, R.F., Wang, C.W. and Wan, Y. 2015. Analysis of sources and transformation of nitrogen as a contaminant in the river and lake water in the western region of the Taihu Lake basin. Acta Sci. Circum. 35: 3883-3889.

Xia, X., Yang, Z. and Zhang, X. 2009. Effect of suspended-sediment concentration on nitrification in river water: Importance of suspended sediment-water interface. Enviro. Sci. Technol., 43: 3681-3687.

Xiao, L., Yang, L., Zhang, Y., Gu, Y., Jiang, L. and Qin, B. 2009. Solid state fermentation of aquatic macrophytes for crude protein extraction. Ecol. Eng., 35: 1668-1676.

Zhang, L., Fan, C.X., Chi, Q.Q., Wang, J.J. and Qin, B.Q. 2004. Phosphorus species distribution of sediments in Lake Taihu and its main inflow rivers. Geochimica, 33: 423-432.

Zhang, L., Wang, L., Yin, K., Lu, Y., Zhang, D., Yang, Y. and Huang, X. 2013. Porewater nutrient characteristics and the fluxes across the sediment in the Pearl River estuary and adjacent waters, China. Estuar. Coast. Shelf S., 133: 182-192.

Zhao, H., Wang, S., Jiao, L., Yang, S. and Liu, W. 2013. Characteristics of temporal and spatial distribution of different forms of phosphorus in the sediments of Erhai Lake. Research of Environmental Sciences, 26: 227-234.

Zhao, X.Q., Yang, L.Y., Yu, Z.Y., Fan, Q.H., Zhan, Z., Xiao, Y. and Qin, B. 2007. Temporal and spatial distribution of physicochemical characteristics and nutrients in sediments of Lake Taihu. J. Lake Sci., 19: 698-704.

Zhu, M., Zhu, G., Zhao, L., Yao, X., Zhang, Y., Gao, G. and Qin, B. 2013. Influence of algal bloom degradation on nutrient release at the sediment-water interface in Lake Taihu, China. Environ. Sci. Pollut. R., 20: 1803-1811.

Zhu, W., Wan, L. and Zhao, L. 2010. Effect of nutrient level on phytoplankton community structure in different water bodies. J. Environ. Sci-China, 22: 32-39.

Zhu, Z.Y., Zhang, J., Wu, Y., Zhang, Y.Y., Lin, J. and Liu, S.M. 2011. Hypoxia off the Changjiang (Yangtze River) Estuary: Oxygen depletion and organic matter decomposition. Marine Chemistry, 125: 108-116.

Nature Environment and Pollution Technology
An International Quarterly Scientific Journal

p-ISSN: 0972-6268
e-ISSN: 2395-3454

Vol. 19 | No. 1 | pp. 191-199 | 2020

Original Research Paper

Open Access

Heavy Metal Accumulation of 13 Native Plant Species Around a Coal Gangue Dump and Their Potentials for Phytoremediation

Yafen Han*, Qi Li*(**)† and Na Liu*

*School of Environment and Surveying Engineering, Suzhou University, Suzhou 234000, China

**National Engineering Research Center of Coal Mine Water Hazard Controlling, Suzhou 234000, China

†Corresponding author: Qi Li

Nat. Env. & Poll. Tech.
Website: www.neptjournal.com

Received: 18-05-2019
Accepted: 22-07-2019

Key Words:
Heavy metal
Phytoremediation
Rhizosphere soil
Coal gangue dump

ABSTRACT

This study was designed to investigate the heavy metal accumulation characteristics of 13 native plant species and associated rhizosphere soils around Taoyuan coal gangue dump, and to determine their potentials for phytoremediation. The mean concentrations of Cu, Cd, Pb and Cr in rhizosphere soils were 46.70, 0.43, 16.86 and 109.67 $mg \cdot kg^{-1}$, respectively. According to the pollution load index, the soils were strongly contaminated by Cd, moderately contaminated by Cu, slightly contaminated by Cr and uncontaminated by Pb. The concentrations of Cu, Cd, Pb and Cr in shoots of the 13 plant species ranged as 1.86-33.10, 0.10-0.94, 2.04-14.72 and 0.49-9.03 $mg \cdot kg^{-1}$, respectively, while in roots ranged as 0.44-91.56, 0.31-1.82, 4.83-50.49 and 0.37-99.63$mg \cdot kg^{-1}$, respectively. No plant species satisfied the concentration criteria of hyperaccumulator, but two high Cd-enriched species of *M. falcata* and *C. japonicum*, whose BCF and TF values were all greater than one, were recorded. Based on the Individual Phytoremediation Factors (IPF), *S. viridis* showed the strongest remediating capability per a single plant for Cu, while *M. falcata*, *S. viridis*, *C. eragrostis* and *C. japonicum* had relatively strong remediating capability per a single plant for Cd. The four plant species were proposed to be preferentially taken as the candidates for phytoremediation.

INTRODUCTION

Coal gangue, produced during the coal ore mining and utilization processing, is one of the greatest industrial solid wastes in China (Xue et al. 2014). Currently, the annual discharged amount of coal gangue is up to 1.5×10^8 t in China and only about 40% of it can be comprehensively utilized. The excessive coal gangues are inevitably piled up in the open in most coal mining areas of China. Under the long-term effect of external factors (weathering, leaching and biological reaction), heavy metals in these coal gangues will be released and cause serious pollution to the surrounding soil (You et al. 2016). Jiang et al. (2014) reported that potential ecological damage degrees of heavy metals in soils around Yangcaogou coal gangue dump were moderate to strong, and it decreased with increasing distance from the coal gangue dump. He et al. (2016) found high accumulation of toxic metals, especially Mn, Fe and Cr, in the soils within 250 m away from Liejiaqiao coal gangue dump.

Heavy metals accumulated in soils can cause great damage to the stability of the ecological environment, and harm human health through the food chain (Ahmad et al. 2011). It is necessary to reduce the negative effect of heavy metals and make the land resource available for agricultural production. Traditional remediation techniques, including excavation, leaching, electro kinetics, chemical stabilization, etc., for removing heavy metals from contaminated soils or reducing their availabilities are expensive and environmentally destructive. In contrast, phytoremediation is a less expensive and environmentally non-destructive restoration method for decreasing the environmental risk from the contaminated soils (Ali et al. 2013). This technology is carried out by using plants to extract the toxic metals from soil or to render them harmless in the contaminated sites. The efficiency of phytoremediation strongly depends on the accumulation and tolerance abilities of heavy metals in soil by the selected plant species. Thus, screening appropriate plant species is a critical step for successful phytoremediation. However, the species suitable for phytoremediation are relatively rare, and even usually endemic at the metal-enriched sites, because the accumulation and tolerance abilities of plant were generally evolved from the long-term stress of high concentration of heavy metals in soils (Ghaderian et al. 2012). Moreover, compared with the introduced plant species from other environment, the native species have more excellent adaptability of survival, growth and reproduction in the contaminated area. Therefore, increasing interests have been focused on the investigation and seeking of suitable metal-accumulator

from the native plant species growing in metalliferous soils (Liu et al. 2014).

Taoyuan coal mine, located in the Huaibei coalfield in Anhui province of China, has a mining history of more than 20 years. The present study was conducted to investigate the accumulation characteristics of Cu, Cd, Pb and Cr in the 13 native plant species and associated rhizosphere soils around the coal gangue dump of Taoyuan mine, and to screen the species with phytoremediation potentials. This research is of important practical value for polluted soil treatment and ecological restoration in the coal mining area.

MATERIALS AND METHODS

Study Area and Sample Collection

Taoyuan coal mine is located in north-eastern Anhui Province, about 12 km from Suzhou urban area (Fig. 1). This region is characterized by a sub-humid monsoon climate, with an annual average rainfall of 890 mm and an annual average temperature of 14.4°C. The main soil types in Suzhou are Yellow fluvo-aquic soil and Lime concretion black soil. Taoyuan mine began production in October 1995 with an annual coal output of 1.6 million tons. During the past two decades, large amounts of coal gangue were produced going with coal exploitation, and a large coal gangue dump, covering an area of approximately 38800 m^2, was formed in eastern of the mining area. The height of the coal gangue dump is 65 m and the coal gangue stock is approximately 1.3 million tons.

Field sampling was carried out in October 2017. Fifty two plants and their corresponding rhizosphere soils were collected form the wastelands within 200 m from the coal gangue dump in Taoyuan mining area. The collected plants were consisted of thirteen species and eight families (Table 1). All the plant species were the common species in the mining area. For each species, three to five individual plants were selected randomly. Each soil sample was approximately 0.5 kg. After collection, the plant and soil samples were put into plastic self-sealing bags and labelled.

Sample Analysis and Quality Control

After the collected samples were transported to the laboratory, bulk density and moisture contents of soil were tested immediately. Then, each soil sample was air-dried at room temperature for two weeks and pulverised to pass through a 0.25-mm sieve. Soil pH was determined in a 1:2.5 soil/water (w/v) suspension using a pH meter. Organic matter of soil was measured by the Walkley-Black method. Total nitrogen (TN), total phosphate (TP) and total potassium (TK) were estimated by the standard methods of the Soil Science Society of China. Soil samples were digested with the mixed acids of aqua regia, $HClO_4$ and HF (4:1:1, v/v) in Teflon beakers, and the concentrations of Cu, Cd, Pb and Cr in soils were tested by an atomic absorption spectrophotometer (AAS, Model

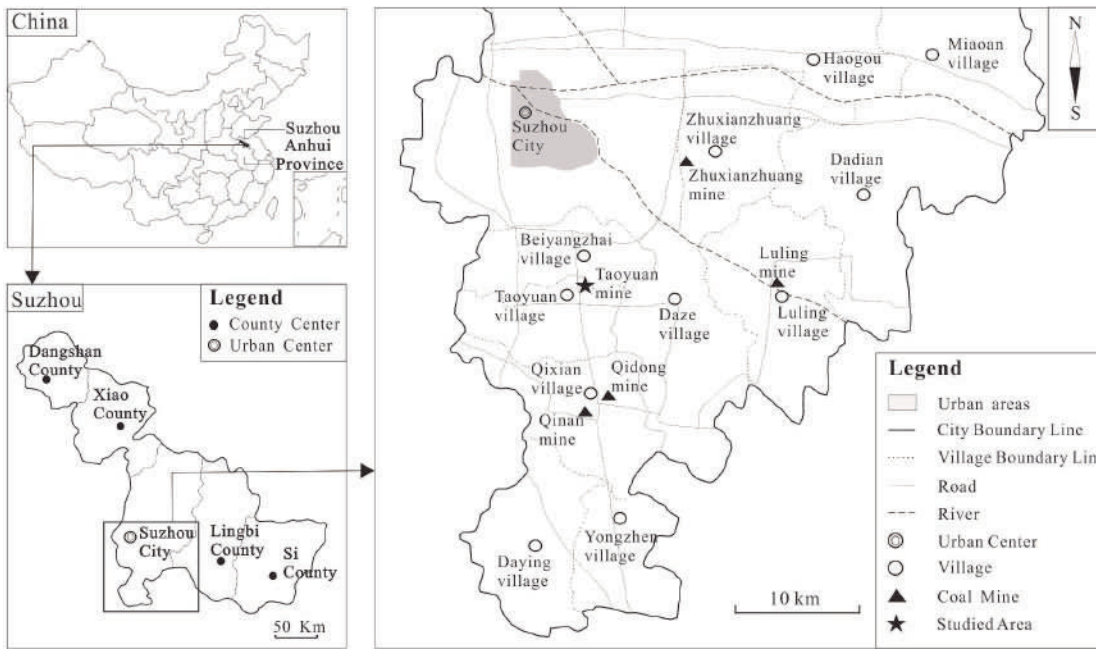

Fig. 1: Location of Taoyuan coal mine in Suzhou City, Anhui Province, China.

Table 1: Plant species collected from the investigated area and number of samples.

Family	Plant species	Species Code	Brief name	Sample number	Biomass (g·plant^{-1}, dry weight)	
					Shoot	Root
Compositeae	*Artemisia argyi* Levl. Et Vant.	1	A. argyi	4	0.82±0.16	0.19±0.05
	Conyza canadensis (Linn.) Cronq.	2	C. canadensis	5	5.02±0.63	0.21±0.04
	Cirsium japonicum Fisch. ex DC.	3	C. japonicum	3	3.83±0.47	0.33±0.02
	Xanthium sibiricum Patrin ex Widder	4	X. sibiricum	4	2.77±0.31	2.34±0.58
	Artemisia annua Linn.	5	A. annua	4	2.71±0.54	0.31±0.04
Gramineae	*Eleusine indica* (Linn.) Gaertn.	6	E. indica	3	8.76±1.98	0.16±0.04
	Setaria viridis (Linn.) Beauv.	7	S. viridis	5	12.25±2.05	0.18±0.02
Leguminoseae	*Medicago falcata* Linn.	8	M. falcata	4	5.95±1.36	0.78±0.05
Amaranthaceae	*Amaranthus spinosus* Linn.	9	A. spinosus	4	2.26±0.51	0.16±0.02
Crucifereae	*Capsella bursa-pastoris* (Linn.) Medic.	10	C. bursa-pastoris	4	1.93±0.10	0.15±0.01
Cyperaceae	*Cyperus eragrostis* Lam.	11	C. eragrostis	4	5.16±0.95	0.14±0.04
Solanaceae	*Physalis pubescens* Linn.	12	P. pubescens	4	0.59±0.11	0.13±0.03
Plantaginaceae	*Plantago asiatica* Linn.	13	P. asiatica	4	1.36±0.17	0.22±0.02

TAS-990FG, Purkinje General Instrument, Beijing, China).

Each wheat sample was carefully cut into two parts of root and shoot with a scissors. All the parts were thoroughly washed with running tap water to remove dirt and rinsed three times with deionized water. Then, the plant tissues were oven-dried at 80°C to constant weight and ground to pass through a 0.25-mm sieve. The plant powder samples were digested with the mixed acids of HNO_3, HCl and $HClO_4$ (5:1:1, v/v) in glass beakers, and the concentrations of Cu, Cd, Pb and Cr in different plant parts were also determined by AAS.

To ensure experimental accuracy, the reference materials (GBW07430 for soils and GBW007604 for plants) were performed through the digestion and determination processes. The recoveries of Cu, Cd, Pb and Cr in the soil and plant reference materials were all in the range of 100±10%. Reagent blanks were also employed in the analysis to eliminate analytical bias. All chemicals used in the experiment were of analytical grade, and all the vessels were treated with dilute nitric acid for 24 h followed by rinsing with MilliQ water for three times before use.

Data Analysis

Pollution load index (PLI) was applied in this study to evaluate the extent of the contamination by heavy metals in soil samples. It can be calculated by the following formula (Muhammad et al. 2011):

$$PLI = (CF_1 \times CF_2 \times \cdots \times CF_n)^{\frac{1}{n}} \quad \ldots(1)$$

Where, CF represents contamination factor of a single metal, and is obtained by dividing the concentration of each metal in the soil by the local background value. Based on the values of CF and PLI, the classification criterion of contamination level is listed in Table 2.

Table 2: Pollution load index and classification criterion of contamination level.

Contamination degree	CF		PLI	
	Value range	Contamination Level	Value range	Contamination Level
0	CF ≤ 0.7	No contamination	PLI ≤ 1.0	No contamination
1	0.7<CF ≤ 1.0	Light contamination	1.0<CF≤2.0	Slight contamination
2	1.0<CF ≤ 2.0	Slight contamination	2.0<CF≤3.0	Moderate contamination
3	2.0<CF ≤ 3.0	Moderate contamination	CF>3.0	Strong contamination
4	CF > 3.0	Strong contamination		

$$CF = \frac{C_{metal}}{C_{Background}} \quad \ldots(2)$$

Bioconcentration factor (BCF) and Translocation factor (TF) of the studied plant species were calculated based on the following equations.

$$BCF = \frac{C_{root}}{C_{soil}} \quad \ldots(3)$$

$$TF = \frac{C_{shoot}}{C_{root}} \quad \ldots(4)$$

In the above equations, C_{shoot} (mg·kg^{-1}), C_{root} (mg·kg^{-1}) and C_{soil} (mg·kg^{-1}) are the concentrations of a particular metal in shoot (including seed, leaf and stem aboveground), root and rhizosphere soil, respectively.

For comparing the phytoremediation potentials of different plant species, the coefficient of Individual phytoremediation factor (IPF) proposed by Li et al. was used in this study (Li et al. 2011). The formula is as follows:

$$IPF = \frac{C_{shoot} \times Biomass_{shoot}}{C_{soil}} \quad \ldots(5)$$

Where, $Biomass_{shoot}$ (g·plant^{-1}) is the dry weight of plant shoot.

Data reported in this article were analysed by Excel 2013 and SPSS 22.0 package for Windows, and all the figures were drawn by CorelDraw 2017. The mean values and the standard deviation of the metal concentrations in soil and different plant parts, and of BCF, TF and IPF were calculated.

RESULTS AND DISCUSSION

Physico-chemical Properties and Heavy Metal Contents in Rhizosphere Soil

The physico-chemical properties and heavy metal contents in rhizosphere soils around the coal gangue dump in Taoyuan mine are presented in Tables 3 and 4. As shown in Table 3, the investigated soils were found to be weakly alkalic, with the mean pH value of 7.81. The mean values of bulk density and moisture content were 1.32 g·cm^{-3} and 15.83%, respectively. Organic matter, total nitrogen, phosphate and potassium are the important indicators of soil nutrients and fertility. Compared with the classification criteria for soil nutrients in the second national census of soil in China, organic matter and total nitrogen in the studied soil samples were both in lacking level, total phosphate belonged to very lacking level, and total potassium remained at medium level.

Obvious differences between the minimum and maximum concentrations of Cu, Cd, Pb and Cr in rhizosphere soils were observed (Table 4), and indicated that metal concentrations varied widely among the soil samples collected from the studied area. It could be explained from the two respects. On one hand, heavy metals accumulated in soil around gangue dump were mostly released from the coal refuses, and their transporting process might be affected by many factors, such as landform, wind direction, the distance away from the gangue dump, etc. On the other hand, 13 plant species growing in different sampling sites had different uptake capacities for heavy metals from rhizosphere soil. The mean concentrations of Cu, Cd and Cr in rhizosphere soils were 46.70, 0.43 and 109.67 mg·kg^{-1}, respectively, which were evidently higher than the soil background values of Anhui province, while Pb concentration was lower compared to the background Pb level in Anhui. Based on Environmental Quality Standard for Agricultural Soil in China (GB15618-2018, Grade II), the levels of Cu, Pb and Cr satisfied grade II quality, and only Cd concentration significantly exceeded the standard.

According to the equation (1) and (2), contamination factor (CF) and pollution load index (PLI) of heavy metals in soils were calculated and given in Table 5. The highest mean CF value of selected metals was Cd (4.45), followed by Cu (2.29), Cr (1.62) and Pb (0.63), suggesting that soil in the investigated area was strongly contaminated by Cd, moderately contaminated by Cu, slightly contaminated by Cr and uncontaminated by Pb. Taking all metals as a whole,

Table 3: Physico-chemical properties of soils around the coal gangue dump in Taoyuan mine, Suzhou, Anhui Province, China (N=52).

Parameters	Values (Mean±Standard deviation)
pH	7.81±0.79
Bulk density (g·cm^{-3})	1.32±0.08
Moisture content (%)	15.83±1.87
Organic matter (g·kg^{-1})	13.76±2.02
Total nitrogen (g·kg^{-1})	0.95±0.18
Total phosphate (g·kg^{-1})	0.33±0.05
Total potassium (g·kg^{-1})	16.91±2.43

Table 4: Heavy metal contents (mg·kg^{-1}) in soils around the coal gangue dump in Taoyuan mine, Suzhou, Anhui Province, China (N=52).

	Cu	Cd	Pb	Cr
Min.	25.52	0.26	10.94	53.32
Max.	79.72	0.68	25.08	243.79
Mean	46.70	0.43	16.86	109.67
SD	12.90	0.09	3.19	34.41
Background[a]	20.4	0.097	26.6	67.5
EQS[b]	100	0.3	120	200

[a]Background values of Cu, Cd, Pb, Cr in soil of Anhui Province; [b]Environmental quality standard for agricultural soil in China (GB15618-2018, Grade II)

the mean PLI value was 1.76, which indicated that the soil suffered moderate compositive contamination from the investigated metals.

Heavy Metal Contents in Different Parts of the Investigated Plants

Heavy metal contents in different parts of the investigated plants growing around the coal gangue dump are presented in Table 6. As given in Table 6, heavy metal contents in the plants of different species displayed great differences. The highest Cu content in plant shoot was found in *X. sibiricum* (33.10 mg·kg^{-1}), and in root was found in *C. bursa-pastoris* (91.56 mg·kg^{-1}). Besides, compared to other plant species, *P. pubescens* accumulated considerably higher Cu content in both shoot (31.86 mg·kg^{-1}) and root (82.61 mg·kg^{-1}). The lowest Cu content in shoot and in root were found in *E. indica* (1.86 mg·kg^{-1}) and *C. japonicum* (0.44 mg·kg^{-1}), respectively. Total Cd contents in plant samples were ranged from 0.10 to 0.94 mg·kg^{-1} in shoot and from 0.31 to 1.82 mg·kg^{-1} in root, and the highest content in the shoot and root were obtained in *C. japonicum* and *P. pubescens*, respectively. Pb contents differed among plant species from 2.04 to 14.72 mg·kg^{-1} in shoot and from 4.83 to 50.49 mg·kg^{-1} in root. Among the 13 plant species, *P. asiatica* had the maximum Pb content in shoot and the minimum Pb content in root. For Cr in plants, the highest content in shoot of *P. asiatica* (9.03 mg·kg^{-1}) and in root of *A. annua* (99.63 mg·kg^{-1}) were recorded, while the lowest content in shoot was found in *E. indica* (0.49 mg·kg^{-1}) and in root was found in *C. japonicum* (0.37 mg·kg^{-1}).

Bioconcentration Factor and Translocation Factor

To evaluate the ability of different plant species for metal accumulation and translocation, BCF and TF values of 13 plant species were calculated and listed in Table 7. As given in Table 7, BCF values of Cd of most plant species were higher than those of the other three metals, indicating that Cd in soil environment was more readily absorbed by plant roots. Among the four metals, BCF values of Cr of almost all the plant species were lowest, with only one exception of *A. annua*. The highest BCF values of Cd and Pb were 4.97 and 2.77 by *P. pubescens*, of Cu was 2.08 by *C. bursa-pastoris*, and of Cr was 1.58 by *A. annua*. Conversely, the lowest BCF values of Cu (0.01), Pb (0.29) and Cr (0.003) by *C. japonicum*, and of Cd (0.77) by *X. sibiricum* were found.

Metal translocation abilities from roots to shoots can be quantitative as indicated by the TF values, which varied greatly among different plant species in this study. *C. japonicum* and *A. argyi* were found to be the excellent transporter of Cu, with the TF values of 9.09 and 8.93, respectively, which were over 100 times than the lowest TF value of Cu by *C. bursa-pastoris* (0.07). Among all the plant species, *M. falcata* and *C. japonicum* were the only two species whose TF values of Cd were greater than one, while *P. asiatica* was the only one species whose TF value of Pb was greater than one. Besides, the highest TF value of Cr was also found in *P. asiatica* (15.74), showing its exceptional ability of Cr transferring from roots to aerial parts.

Table 5: Contamination factor (CF) and pollution load index (PLI) of heavy metals in soils (n=52).

Item	CF				PLI
	Cu	Cd	Pb	Cr	
Min.	1.25	2.73	0.41	0.79	1.21
Max.	3.91	7.03	0.94	3.61	2.25
Mean	2.29	4.45	0.63	1.62	1.76
Contamination level	Moderate	Strong	No contamination	Slight	Moderate

Table 6: Heavy metal contents in different parts of plant samples from the investigated area.

Plant species	Plant part	Cu	Cd	Pb	Cr
		Content (mg·kg^{-1})	Content (mg·kg^{-1})	Content (mg·kg^{-1})	Content (mg·kg^{-1})
A. argyi	Shoot	9.95±2.14	0.35±0.05	2.96±0.77	0.75±0.28
	Root	1.12±0.05	0.48±0.14	6.98±2.32	1.98±0.55
C. canadensis	Shoot	10.65±2.17	0.53±0.15	4.49±0.49	1.54±0.60
	Root	40.25±3.96	1.26±0.09	20.03±6.95	8.44±3.17
C. japonicum	Shoot	4.00±0.27	0.94±0.02	3.50±0.37	0.77±0.10
	Root	0.44±0.01	0.88±0.48	4.83±1.87	0.37±0.06
X. sibiricum	Shoot	33.10±3.46	0.10±0.02	4.73±1.71	8.14±3.80
	Root	30.11±5.83	0.31±0.07	14.31±0.93	4.53±1.91
A. annua	Shoot	18.64±1.88	0.35±0.22	6.14±0.74	3.03±0.81
	Root	6.50±1.30	0.52±0.17	12.25±4.14	99.63±23.72
E. indica	Shoot	1.86±0.01	0.11±0.02	2.04±0.40	0.49±0.17
	Root	53.82±5.16	0.78±0.15	10.68±3.68	2.33±1.03
S. viridis	Shoot	15.83±3.57	0.30±0.14	4.77±1.29	1.31±0.67
	Root	38.28±8.60	1.04±0.24	16.81±5.64	4.38±2.10
M. falcata	Shoot	4.98±1.36	0.74±0.21	3.88±1.17	1.31±0.34
	Root	6.22±0.34	0.47±0.15	7.71±1.68	5.90±2.05
A. spinosus	Shoot	20.38±1.34	0.22±0.04	4.61±1.39	0.86±0.22
	Root	42.30±9.31	0.45±0.12	11.12±2.42	1.56±0.69
C. bursa-pastoris	Shoot	6.06±0.74	0.34±0.10	2.19±0.66	2.57±0.65
	Root	91.56±15.31	0.58±0.26	16.11±3.50	8.87±5.55
C. eragrostis	Shoot	11.52±1.26	0.77±0.13	3.83±1.16	1.12±0.46
	Root	12.83±3.15	1.50±0.46	23.43±5.09	5.34±1.41
P. pubescens	Shoot	31.86±5.90	0.31±0.08	3.21±0.97	0.56±0.18
	Root	82.61±7.92	1.82±0.21	50.49±10.98	7.44±1.83
P. asiatica	Shoot	7.66±0.86	0.52±0.17	14.72±4.44	9.03±1.03
	Root	1.97±0.50	0.85±0.27	4.83±1.05	0.63±0.19

Accumulated Amount of Heavy Metal in The Investigated Plants

Combined with plant biomass, metal amounts accumulated in different parts of 13 plant species were calculated and illustrated in Fig. 2. As shown in Fig. 2, *S. viridis* accumulated the largest amounts of Cu (202.1 μg·plant^{-1}) and Pb (60.73 μg·plant^{-1}), *M. falcate* had the largest accumulated amount of Cd (4.65 μg·plant^{-1}), while *A. annua* had the largest accumulated amount of Cr (38.63 μg·plant^{-1}). The lowest amounts of Cu (8.45 μg·plant^{-1}), Cd (0.37 μg·plant^{-1}), Pb (3.72 μg·plant^{-1}) and Cr (0.99 μg·plant^{-1}) were found in the plant species of *A. argyi*. Compared with the different parts of plant, the mean amounts of Cu, Cd, Pb and Cr in shoots of the 13 plant species were 52.25, 1.82, 18.32 and 7.73 μg·plant^{-1}, respectively, which were significantly higher than that of 10.38, 0.23, 5.43 and 4.05 μg·plant^{-1} in roots (two-tailed t test, $p<0.05$, $n=52$). In most plant species, the aerial part, occupying over 80% of the total metal amount in the whole plant, was proved to be the dominant organ involved in heavy metal accumulation.

Screening for The Plant Species with Phytoremediation Potential

The plant species naturally growing on the metal contaminated soil are precious germplasm resources for phytoremediation. For the purpose of identifying hyper accumulator and the native plant species with phytoremediation potentials, several judging standards have been given in the previous

Table 7: Bioconcentration factors (BCF) and translocation factor (TF) of the studied plant species.

Plant species	BCF				TF			
	Cu	Cd	Pb	Cr	Cu	Cd	Pb	Cr
A. argyi	0.03±0.01	1.66±0.58	0.43±0.21	0.02±0.01	8.93±2.18	0.78±0.30	0.43±0.04	0.40±0.18
C. canadensis	1.07±0.34	2.66±0.58	1.28±0.63	0.08±0.02	0.27±0.06	0.42±0.12	0.25±0.09	0.19±0.06
C. japonicum	0.01±0.00	1.81±0.82	0.29±0.14	0.00±0.00	9.09±0.44	1.26±0.71	0.77±0.22	2.10±0.09
X. sibiricum	0.46±0.06	0.77±0.15	0.86±0.07	0.05±0.03	1.11±0.09	0.33±0.08	0.33±0.11	2.20±1.64
A. annua	0.22±0.07	1.26±0.10	1.04±0.38	1.58±0.37	3.00±0.97	0.69±0.40	0.55±0.23	0.03±0.00
E. indica	1.29±0.47	1.75±0.05	0.65±0.23	0.03±0.00	0.03±0.00	0.15±0.05	0.20±0.03	0.25±0.19
S. viridis	1.04±0.37	2.22±0.30	0.79±0.21	0.04±0.02	0.43±0.13	0.31±0.21	0.33±0.19	0.36±0.27
M. falcata	0.15±0.03	1.14±0.39	0.45±0.06	0.06±0.02	0.80±0.23	1.71±0.87	0.50±0.11	0.26±0.17
A. spinosus	0.65±0.09	1.12±0.32	0.69±0.31	0.02±0.01	0.50±0.16	0.53±0.24	0.41±0.09	0.68±0.49
C. bursa-pastoris	2.08±0.39	1.35±0.54	1.02±0.32	0.08±0.05	0.07±0.01	0.65±0.27	0.14±0.03	0.36±0.20
C. eragrostis	0.24±0.10	2.85±1.22	1.38±0.12	0.05±0.02	0.92±0.12	0.54±0.19	0.16±0.04	0.22±0.11
P. pubescens	1.75±0.28	4.97±1.12	2.77±0.46	0.04±0.02	0.39±0.10	0.17±0.04	0.06±0.01	0.08±0.03
P. asiatica	0.04±0.01	2.09±0.80	0.34±0.15	0.01±0.00	4.13±1.52	0.61±0.03	3.04±0.68	15.74±7.00

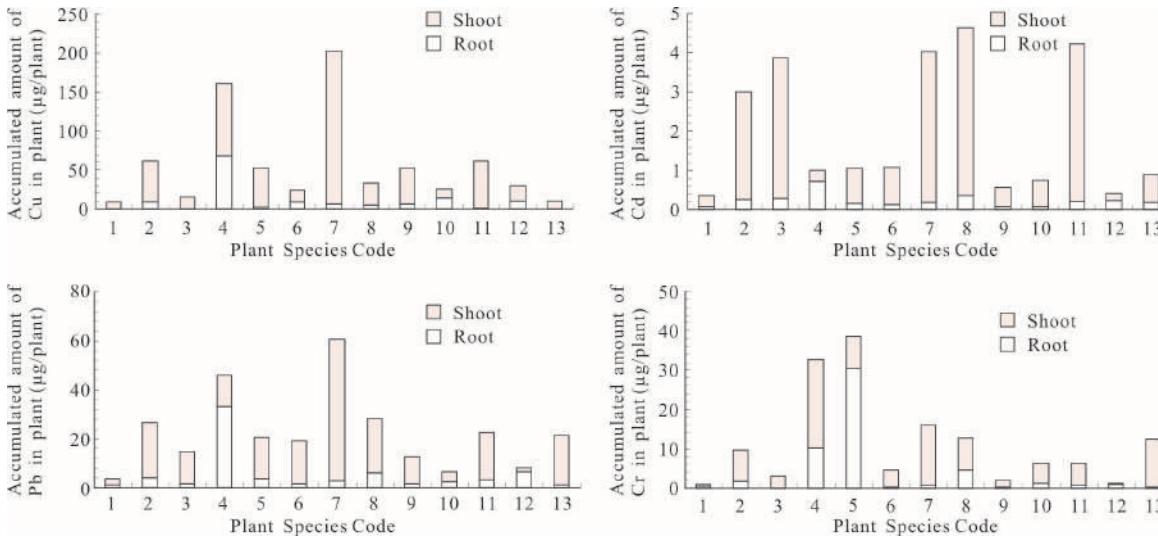

Fig. 2: Accumulated amount of heavy metals in the investigated plants.

literatures. Baker & Brooks (1989) suggested that the critical contents of different metals and metalloids in the stems or foliage of hyper accumulator were 100 mg·kg^{-1} for Cd, 1000 mg·kg^{-1} for Cu, Pb, Co, Ni and As, and 10000 mg·kg^{-1} for Zn and Mn. Subsequently, Van der Ent et al. (2013) proposed that these values should be 100 mg·kg^{-1} for Cd, 300 mg·kg^{-1} for Cu, Cr and Co, 1000 mg·kg^{-1} for Pb, Ni and As, 3000 mg·kg^{-1} for Zn, and 10000 mg·kg^{-1} for Mn. In this study, metal concentrations in all the 13 plant species were far below these criteria, thus none of them could be considered as a hyper accumulator.

Generally, metal concentration in plant is directly associated with that in the soil where it grows. In the polluted sites, bioconcentration factor (BCF) and translocation factor (TF) have been considered to be the important indicators widely used for determining metal accumulation abilities and distinguishing phytoremediation potentials of different plant species. Plant species with both BCF and TF values greater than one can potentially be used for heavy metal phytoremediation (Boechat et al. 2016, Yoon et al. 2006). Based on this view, only two species *M. falcata* and *C. japonicum* in this investigation satisfied the criteria for phytoremediation of Cd.

Table 8: Individual phytoremediation factor (IPF) of the studied plant species.

Plant species	PM			
	Cu	Cd	Pb	Cr
A. argyi	0.24±0.10	0.96±0.09	0.15±0.08	0.01±0.00
C. canadensis	1.42±0.61	5.76±2.51	1.39±0.39	0.07±0.02
C. japonicum	0.28±0.04	7.59±0.02	0.78±0.08	0.02±0.00
X. sibiricum	1.42±0.27	0.72±0.32	0.77±0.24	0.26±0.17
A. annua	1.70±0.30	2.19±0.87	1.39±0.28	0.13±0.05
E. indica	0.40±0.20	2.15±0.25	1.06±0.03	0.05±0.02
S. viridis	5.33±2.22	8.46±5.33	2.93±1.60	0.16±0.06
M. falcata	0.67±0.16	10.21±1.9	1.35±0.52	0.08±0.04
A. spinosus	0.70±0.04	1.26±0.44	0.68±0.40	0.02±0.00
C. bursa-pastoris	0.27±0.07	1.54±0.42	0.27±0.09	0.05±0.02
C. eragrostis	1.13±0.49	7.84±3.50	1.19±0.51	0.05±0.02
P. pubescens	0.40±0.10	0.50±0.20	0.11±0.04	0.00±0.00
P. asiatica	0.22±0.07	1.78±0.78	1.45±0.80	0.09±0.02

Furthermore, phytoremediation potential does not merely depend on the concentration of heavy metal in the plant. The dry biomass of plant is also considered to be a very influential factor. Large dry biomass is the indispensable requirement for an efficient phytoremediator, as a plant with low biomass production could hardly possess excellent capability for accumulating the elevated amount of heavy metal though the metal concentration in the plant would be very high. Besides, to be an efficient phytoremediator, the plant species, even though sharing a large dry biomass and high concentration of heavy metal, should also satisfy another requirement that a considerable metal amount accumulate in the easily harvestable plant organs (e.g., shoots). For screening the native plant species with phytoremediation potentials in the investigated area, the individual phytoremediation factor (IPF), reflecting the remediating capability per a single plant, was used to compare metal removing capabilities of the 13 plant species. This factor refers to the ratio of the metal amount accumulated in plant shoot to the metal concentration in soil. The IPF values of 13 plant species were calculated and listed in Table 8. As provided in Table 8, the IPF value of *S. viridis* for Cu and Pb was obviously higher than that of the other plant species. *M. falcata* showed the highest IPF value for Cd, while *S. viridis*, *C. eragrostis* and *C. japonicum* also had relatively high IPF values for Cd. Considering that the soils in the investigated area were strongly contaminated by Cd and moderately contaminated by Cu (Table 5), the above 4 screened plant species with excellent remediating capability per a single plant can be preferentially taken as the candidates for further examining, since the plant biomass per unit area and the growth cycle of different plant species are not taken into consideration in the present study.

CONCLUSION

According to the results of this study, obvious accumulation of heavy metals, especially Cd and Cu, were found in the soils around Taoyuan coal gangue dump compared to the background values. Heavy metal concentrations in the plant of different species varied greatly. For most plant species, the accumulated amounts of Cu, Cd, Pb and Cr mainly existed in the aerial part. Among the 13 native plant species, none of them satisfied the concentration criteria of hyperaccumulator, but two high Cd-enriched species of *M. falcata* and *C. japonicum* with both BCF and TF values greater than one were recorded. Finally, based on the individual phytoremediation factor (IPF), four species of *M. falcata*, *S. viridis*, *C. eragrostis* and *C. japonicum* with strong remediating capability per a single plant were screened and proposed to be further studied for restoring Cd and Cu contaminations of the soils in the mining area.

ACKNOWLEDGEMENTS

This work was financially supported by Domestic Studying Foundation for Outstanding Young Scholar of Anhui Province (Gxgnfx2018054), Key Natural Science Foundation of Suzhou University (2016yzd07, 2017yzd10) and Workstation for Promoting Application Ability for Teacher of Suzhou University (2016XJYY03).

REFERENCES

Ahmad, A., Ghufran, R. and Zularisam, A.W. 2011. Phytosequestration of metals in selected plants growing on a contaminated Okhla industrial areas, Okhla, New Delhi, India. Water, Air, & Soil Pollution, 217: 255-266.

Ali, H., Khan, E. and Sajad, M.A. 2013. Phytoremediation of heavy metals-concepts and applications. Chemosphere, 91(7): 869-881.

Baker, A.J.M. and Brooks, R.R. 1989. Terrestrial higher plants which hyperaccumulate metallic elements- A review of their distribution, ecology and phytochemistry. Biorecovery, 1: 811-826.

Boechat, C.L., Pistóia, V.C., Gianelo, C. and Camargo, F.A.O. 2016. Accumulation and translocation of heavy metal by spontaneous plants growing on multi-metal-contaminated site in the Southeast of Rio Grande do Sul state, Brazil. Environmental Science and Pollution Research, 23(3): 2371-2380.

Ghaderian, S.M. and Ravandi, A.A.G. 2012. Accumulation of copper and other heavy metals by plants growing on Sarcheshmeh copper mining area, Iran. Journal of Geochemical Exploration, 123: 25-32.

He, H., Hong, F.F., Tao, X.X., Huang, G.H., Leng, Y.W., Shao, J.F. and Zhao, Y.D. 2016. A study on soil basic characteristics, main microbial flora and typical metal fraction surrounding coal gangue dump in Xiangtan Hunan Province, south of China. Environmental Earth Sciences, 75(6): 488.

Jiang, X., Lu, W.X., Yang, Q.C. and Yang, Z.P. 2014. Potential ecological risk assessment and prediction of soil heavy metal pollution around coal gangue dump. Natural Hazards and Earth System Sciences, 2(3): 1977-2010.

Li, G.Y., Hu, N., Ding, D.X., Zheng, J.F., Liu, Y.L., Wang, Y.D. and Nie, X.Q. 2011. Screening of plant species for phytoremediation of uranium, thorium, barium, nickel, strontium and lead contaminated soils from a uranium mill tailings repository in south China. Bulletin of Environmental Contamination and Toxicology, 86(6): 646-652.

Liu, J., Zhang, X.H., Li, T.Y., Wu, Q.X. and Jin, Z.J. 2014. Soil characteristics and heavy metal accumulation by native plants in a Mn mining area of Guangxi, South China. Environmental Monitoring and Assessment, 186(4): 2269-2279.

Muhammad, S., Shah, M. T. and Khan, S. 2011. Heavy metal concentrations in soil and wild plants growing around Pb-Zn sulfide terrain in the Kohistan region, northern Pakistan. Microchemical Journal, 99(1): 67-75.

Van der Ent, A., Baker, A.J.M., Reeves, R.D., Pollard, A.J. and Schat, H. 2013. Hyperaccumulators of metal and metalloid trace elements: Facts and fiction. Plant Soil, 362: 319-334.

Xue, Q., Lu, H.J., Zhao, Y. and Liu, L. 2014. The metal ions release and microstructure of coal gangue corroded by acid-based chemical solution. Environmental Earth Sciences, 71(7): 3235-3244.

Yoon, J., Cao, X., Zhou, Q. and Ma, L.Q. 2006. Accumulation of Pb, Cu, and Zn in native plants growing on a contaminated Florida site. Science of the Total Environment, 368: 456-464.

You, M., Huang, Y.E., Lu, J. and Li, C.P. 2016. Fractionation characterizations and environmental implications of heavy metal in soil from coal mine in Huainan, China. Environmental Earth Sciences, 75(1): 78.

Nature Environment and Pollution Technology
An International Quarterly Scientific Journal

p-ISSN: 0972-6268 e-ISSN: 2395-3454	Vol. 19	No. 1	pp. 201-210	2020

Original Research Paper **Open Access**

Selecting Environmental Indicators for Sustainable Smart Cities Mission in India

Prabhat Kumar Singh, Shruti† and Anurag Ohri
Department of Civil Engineering, Indian Institute of Technology (BHU), Varanasi-221005, Uttar Pradesh, India
†Corresponding author: Shruti

Nat. Env. & Poll. Tech.
Website: www.neptjournal.com

Received: 15-06-2019
Accepted: 23-07-2019

Key Words:
Smart cities
Sustainable cities
Environment decision support system (EDSS),
Environmental indicators

ABSTRACT

Government of India (GOI) initiated Smart Cities Mission in June 2015. In order to guide the process, evaluate the performance, and finally move towards making a Sustainable Smart Cities program, the objective is to develop software based Environmental Decision Support System for Sustainable Smart Cities in India (EDSS-SSCI). Identification and finalization of indicators to be used in the framework for evaluation of Sustainable Smart Cities in Indian context is the objective of the present study. The analyses indicate that Smart Cities Mission guidelines of GOI include 14 performance parameters related with environment, out of which 11 qualify the criteria required for being considered as environmental indicator as per World Bank Environment Development (WBED) considerations and 3 of them do not meet the requirements in terms of clarity of design and quantification for development costs. Further, a set of 20 additional environmental performance indicators are identified from the available literatures on requirements of Sustainable Cities, many of which are generally used as monitoring parameters in various programs of GOI. Subjecting these 20 additional indicators for suitability as environmental indicators based on WBED criteria and City Key Indicators criteria, results in finalizing a set of 13 indicators which meet all requirements and qualify to be used in development of framework for EDSS-SSCI. 10 of these indicators are already part of monitoring programs of Ministry of Urban Development (MoUD), 2 have been suggested by Bureau of Standards (BIS 2016) and 1 considered important by Japan International Corporation Agency (JICA 2016). Thus, taking 11 environmental indicators from Smart Cities Mission Guidelines and 13 selected indicators for Sustainable Cities, a total of 24 environmental indicators are finalised to be used in the framework of EDSS-SSCI for benchmarking, performance evaluation and guiding the investment plans for most effective resource utilization under Indian conditions.

INTRODUCTION

Rapid growth of urbanisation has taken place over the years in India. As per available records, there were 5161 classified towns and 384 urban agglomerations in the country in 2001, which increased to 7935 classified towns and 475 urban agglomerations in 2011 (Khadke et al. 2018). This massive growth made India the second largest urban system in the world (Abbu et al. 2015). According to UN Report, India is estimated to add 300 million more urban residents by 2050 to its existing 377 million populations. In July 2015, Ministry of Urban Development (MoUD), Government of India (GOI) announced the program for developing 100 Smart Cities in the country with emphasis on use of technologies to convert existing cities into Smart Cities to face the challenge of accommodating the needs of growing population (MoUD 2015).

The philosophical background of Smart City may be seen in the 'hierarchy of needs' given by great psychologist Abraham Maslows in 1943. It says that human motivations move through five levels of needs as shown in the pyramid (Fig.1). The physiological needs, such as clean air, healthy food, pure water, shelter etc. are the first level of requirements as they are the basic components for human survival. The humans cannot prosper unless these physiological needs are fulfilled. Safety and security needs, which include health and employment are the next level of requirements. Family, affection, belongingness constitutes the third level of human needs. As such, Smart Cities Mission in its current form has been targeted to achieve up to the second level of human needs.

It is common to understand that the conditions of each city differ from other; hence the meaning of smartness may also change from one situation to another. In larger perspective, parameters of a Smart City depend upon its current development level, available resources and the willingness of people to change for the decided objectives.

Application of information and communication technology (ICT) in the city development program is the core feature of Smart City initiatives. As noted by Lazaroiu & Roscia (2012), "Smart City" is a city, well performing in 6 characteristics: smart people, smart governance, smart living, smart

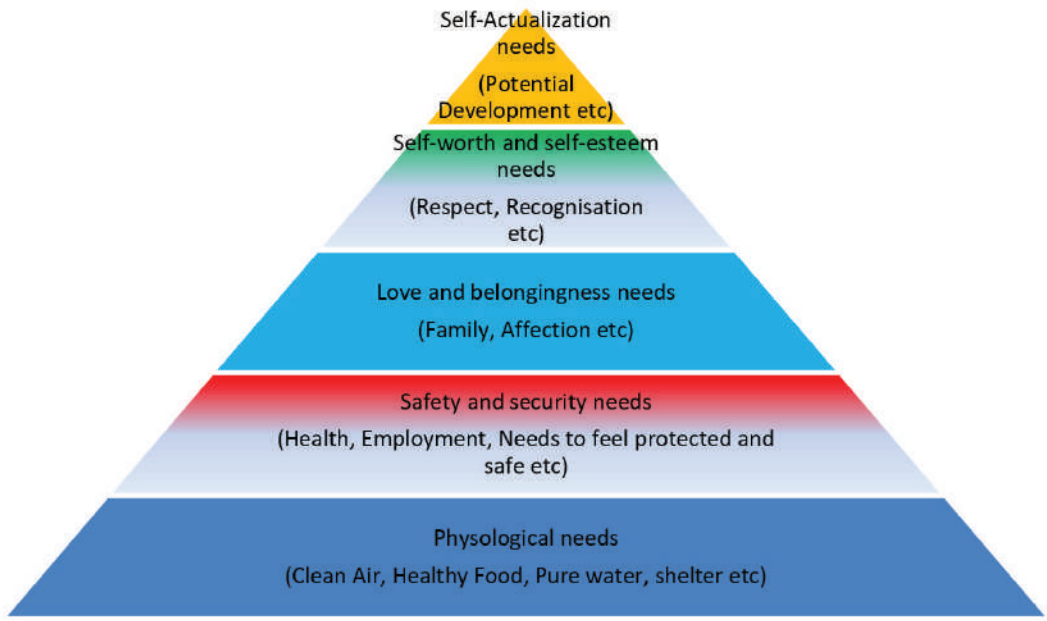

Fig. 1: Maslow's hierarchy of needs (Maslow 1943).

environment, smart economy and smart mobility. These six characteristics are the smart combination of activities and endowments of citizen awareness. As many cities of Europe and other parts of the world have been working towards 'Sustainable Cities' since past several decades, there is a renewed impetus to add smartness in the program using ICT. Thus, there are several definitions for "Smart Sustainable Cities", based on specific conditions and objectives of the program. On the other hand, there has been no specific sustainability focused City Development Plan in India. Smart Cities Mission is a major initiative by the Government to reinforce the urban life to face the growing challenges. Hence, planning towards "Sustainable Smart Cities" may be just required and appropriate for the country.

The International Telecommunication Union (ITU 2014) gave a comprehensive definition of Smart Sustainable City as 'a novel city which uses ICTs for urban services delivery and improving the quality of life, without compromising the needs of the present and future generations. Höjer & Wangel (2015) states that 'a Smart Sustainable City is a city that meets the needs of its present inhabitants without compromising the ability for other people or future generations to meet their needs, and thus, does not exceed local or planetary environmental limitations, and where this is supported by ICT.' Bibri & Krogstie (2017) summarised that a Sustainable City improves environmental quality by adopting sustainable development strategies for innovation and advancement. Sustainable cities optimize the use of its resources with reduced pollution and zero-waste system to promote liveability. But sustainable cities overlook smart solutions, i.e. the use of ICT which is the characteristic of Smart Cities. For cities to foster sustainability they should incorporate smart targets and Smart Cities should be in line with the vision of sustainability. Thus, there is emphasis towards "Smart Sustainable City" in developed parts of the world. In contrast, the focus of Indian Smart Cities Mission is on the use of ICTs and providing technology-based solutions to urban challenges, thus sustainability is not the objective part of program. Under the condition, planning and motivating for 'Sustainable Smart Cities' in India appears very much timely and desirable for long term benefits from the infrastructure developed and investment made. The objective of the present study is to select environmental indicators applicable in the framework of 'Sustainable Smart Cities', which can be used for evaluation and guidance of initiatives for long term sustainability and maximum environmental benefits.

SMART CITIES MISSION (SCM) IN INDIA

Smart Cities Mission (SCM) in India was launched in June 2015. Guidelines have been proposed by the Ministry of Urban Development (MoUD 2015) to highlight the requirements for development of a smart city. SCM is a bold initiative by the government to reduce the urban service de-

Table 1: Environmental indicators in smart cities mission of government of India.

Environmental Component	Indicators (Smart solutions+ Essential features)
A. Solid Waste Management	1. Waste to energy and fuel
	2. Waste to compost
	3. Recycling and reduction of construction and demolition waste
	4. Solid waste management programs carried in the city during last 3 years
B. Water Supply Management	5. Smart meters and Management
	6. Leakage identification
	7. Water quality monitoring
	8. Adequate water supply
	9. Extent of cost recovery in water supply services
C. Sewerage and Sanitation	10. Coverage of toilets
	11. Waste water recycling
	12. Extent of cost recovery
D. Storm Water Drainage	13. Storm water reuse
E. Pollution	14. Improvement in air quality

ficiencies and focuses towards making the cities sustainable and inclusive. The launch of SCM has brought an optimistic approach among decision-makers and had attracted financial investors. The core infrastructure development through SCM in Indian scenario comprises of 10 features: i. Adequate water supply of 24×7, ii. Assured electricity supply, iii. Sanitation, iv. Urban mobility, v. Affordable housing, vi. ICT and digitalization, vii. e-governance, viii. Sustainable environment, ix. Security, safety, and good health and, x. Compulsory education for all (MoUD 2015).

Smart City needs to create an approach towards socially inclusive communities with a low ecological imbalance (MEM 2015). Accordingly, environmental sustainability must be of greater importance along with other indicators in a Smart City. Thus, a wider model of City Development Plan including elements of environmental sustainability along with information-communication technology (ICT) appears desirable to be adopted for Smart Cities Mission in India. The environmental indicators included in the present SCM guidelines are as given in Table 1.

Need of a Framework for 'Sustainable Smart Cities' in India

European cities, which have been working in this direction since many years and have taken initiatives in various forms, such as green cities, eco- cities, sustainable cities and alike are desirous to include 'smartness' through application of ICT in urban infrastructure and services systems. However, in India, although several city development plans and programs have been implemented so far, 'environmental sustainability' has not been an included objective (Randhawa et al. 2017). Hence, the Smart Cities Mission, which is a focussed 5 years (2015-20) program, may be taken as an opportunity to plan and develop models of 'Sustainable Smart Cities' for the country which may serve as examples for smaller towns to follow and grow in the given socio-economic environment.

It is proposed to develop an Environmental Decision Support System for Sustainable Smart Cities in India (EDSS-SSCI) to be used as a decision-making tool for sustainable development and growth of Smart Cities. It may also help in strategic planning especially in the context of policy decisions for investment in city infrastructure development. The first step towards developing this tool is the selection of indicators, which are commonly monitored under various plans of the Government and may be used as parameters of sustainability and smartness with improving social infrastructure and increasing investments.

The key functional role of the indicator is to reduce the information complexity being conveyed to the decision makers. The indicators should be precise, measurable and independent. It should not be affected by other factors leading to ambiguous results. Data availability is major challenging task while selecting the indicators. The data should be easily gathered from Government reports, public sources, interviews, or from observations. Data which are expensive to obtain or needs extensive calculations (such as carbon footprint indicators) should not generally be included. Non-availability of data affects the overall result of index developed. Thus, there is a need to enlist the usable indicators

and prepare a framework for evaluating the improvements in quality of life with developing infrastructure.

Selection of Environmental Indicators for Sustainable Smart Cities

The 14 environmental indicators included in the MoUD (2015) guidelines for Smart Cities Mission of Government of India were tested for their appropriateness based on World Bank Environment Development (WBED) 2002 criteria (Segnestam 2002). Six criteria used to decide the appropriateness of indicators are: (i) Direct relevance to objectives (ii) Direct relevance to the target group (iii) Clarity in design (iv) Realistic collection or development costs (v) High quality and reliability (vi) Appropriate spatial and temporal scale (Segnestam, 2002). Table 2 summarises the appropriateness of indicators used in Smart Cities Mission of GoI based on WBED (2002) criteria. It is observed that 11 indicators fully satisfy all the six criteria of WBED (2002). However, three indicators (A.1, A.2 and D.13) do not fully meet the appropriateness criteria fully. It is observed that the indicators A.1: Waste to energy and fuel, and A.2: Waste to compost do not meet the requirements of appropriateness in terms of clarity in design and realistic collections or development costs. The Smart Cities Mission guidelines does not have a target-based plan on these areas. However, in Swachh Bharat Mission (MoUD 2017) the degree of waste treatment is measured in terms of decreasing amount of waste going to landfill. If a city manages to dispose less than 20% of its total solid waste generated to landfills, it gets the highest score of 45 and if the waste going to landfill is more than 20%, it gets zero score. From this, it is may be inferred that in Smart Cities, 80% or more of the total

Table 2: Appropriateness of environmental indicators used in smart cities mission of GOI based on WBED (2002) Criteria.

Environmental Indicators	WBED (2002) Criteria(Segnestam 2002)						
	(i) Direct relevance to objectives	(ii) Direct relevance to the target group	(iii) Clarity in design	(iv) Realistic collection or development costs.	(v) High quality and reliability	(vi) Appropriate spatial and temporal scale	% of compliance out of six criteria
A. Solid Waste Management							
1.Waste to energy and fuel	✓	✓	×	×	✓	✓	66.6%
2.Waste to compost	✓	✓	×	×	✓	✓	66.6%
3.Recycling and reduction of construction and demolition waste	✓	✓	✓	✓	✓	✓	100%
4. Solid waste management programs carried in the city during last 3 years.	✓	✓	✓	✓	✓	✓	100%
B. Water Supply Management							
5.Smart Meters	✓	✓	✓	✓	✓	✓	100%
6.Leakage identification	✓	✓	✓	✓	✓	✓	100%
7.Water quality monitoring	✓	✓	✓	✓	✓	✓	100%
8.Adequate water supply	✓	✓	✓	✓	✓	✓	100%
9.Extent of cost recovery in water supply services	✓	✓	✓	✓	✓	✓	100%
C. Sewerage and Sanitation							
10.Coverage of toilets	✓	✓	✓	✓	✓	✓	100%
11.Waste water recycling	✓	✓	✓	✓	✓	✓	100%
12.Extent of cost recovery	✓	✓	✓	✓	✓	✓	100%
D. Storm Water Drainage							
13.Storm water reuse	✓	✓	×	×	✓	✓	66.6%
E. Pollution							
14. Improvement in air quality	✓	✓	✓	✓	✓	✓	100%

organic waste generated should be targeted to be processed for energy conversion or composting. With a clear mention of proportion of waste planned to be converted to energy or fuel (A.1) and waste to fertilizer as compost (A.2), these two environmental indicators included in SCM guidelines may also qualify as appropriate as per WBED (2002) criteria. The indicator D.13: Storm water reuse does not fulfil the criteria in terms of clarity in design and realistic collection. In line with environment guidelines of Mauritius, (MEM 2015), if achievable targets with probable cost of storm water reuse such as toilet flushing, car washing, garden irrigation etc. are defined in Smart Cities Mission monitoring program, this indicator may also be considered appropriate. In cases where cities report groundwater depletion, ground water recharge through storm water reuse may be an option. Till the time these parameters are made objective and target based, in the present form they cannot be considered appropriate indicators for measuring environmental sustainability of the proposal. Hence, these three indicators are not included in the proposed framework for Sustainable Smart Cities.

Additional Indicators for Sustainable Cities and Evaluation of Their Appropriateness

From the perspectives of environmental sustainability, apart from 14 indicators included in the Smart Cities Mission Guidelines (Table 1), 20 additional indicators were screened from available literature on Sustainable Cities (Table 3). Significantly, these indicators have largely been considered important are being used as monitoring parameters in different plans of Government of India. Appropriateness of these additional 20 indicators screened from available literature for Sustainable Cities have been examined similarly based on WBED (2002) criteria, as given in Table 4. It is observed that among these 20 indicators, 4 do not fully meet the requirements of criteria for being considered appropriate. In the Smart Cities Mission, frequency of street sweeping per day has not been decided based on total amount of waste generation. Hence the indicator A.1: Street Sweeping may not be considered appropriate at this stage to be included as a measure of Sustainable Smart City framework design. A7: Availability of collection bin is considered inappropriate because for a smart city, zero bin concept is desirable objective. A.9: Availability of roadmap does not fulfil the requirements of appropriateness in terms of clarity in design. D.18: Incidence of water logging defined in the terms of number of times water logging reported per year does not give the clear picture in terms of percentage of area flooded with respect to the total area of the city. Hence, this indicator also does not provide clarity in design and hence may not be considered appropriate to be included in the framework. The remaining 16 indicators which fulfil the WBED (2002) criteria for appropriateness were further tested on criteria given by City Key Indicators (Bosch et al. 2017)indicators have been selected that can function as Key Performance Indicators for tracking the progress towards city and project objectives. The indicators for assessing smart city projects serve to assess or evaluate single projects. They indicate the difference the project has made, by comparing the situation without the project with the situation after the implementation of the project. As such they can also serve to benchmark projects against each other. The indicators for smart cities focus on monitoring the evolution of a city towards an even smarter city. The time component -\u201cdevelopment over the years\u201d- is an important feature. The city indicators may be used to show to what extent overall policy goals have been reached, or are within reach. With a starting point in the smart city definition, and taking into account the wishes of cities and citizens with regard to smart city projects and indicators, the indicators are arranged in an extended triple bottom line sustainability framework, including the themes people, planet, prosperity, governance and propagation. Under the main themes subthemes conforming with major policy ambitions have been identified. Under these subthemes in total 99 project indicators and 76 city indicators have been selected. Not all indicators are equally suited for evaluating all types of smart city projects. Although there is a considerable body of common indicators, for specific sector projects a relevant subset of these may be used (i.e. some indicators are specifically suited for transport projects, other for building related projects, etc.. The criteria include (i) Relevance (ii) Completeness (iii) Availability (iv) Measurability (v) Reliability (vi) Familiarity (vii) Non-Redundancy and (viii) Independence (Table 5). In the evaluation process of appropriateness, the redundancy of the indicators needs to be examined with due care.

In planning a sustainable smart city, 100% coverage of collection of the solid waste appears essential. Hence, household coverage in terms of percentage of houses has been taken as redundant. Instead, efficiency of collection which is reflected in the sanitary and aesthetic environment of the city has been considered relevant. For water supply management, 'coverage of the area' is expressed in terms of total number of households with direct water supply connection in reference to the total number of households in the city. 'Adequate water supply' is expressed in the terms of total quantity of water supplied into the distribution system with respect to the total population of the city. Hence the first (coverage of area) is considered redundant. In the sewerage and sanitation sector, 'coverage of sewerage network' denotes the extent to which wastewater management facilities are available to individual properties across the city whereas 'collection efficiency' denotes the actual proportion of waste water generated in

the city that is collected by the available sewerage network. Hence, former is taken as redundant for the purpose of preparation of this framework. After such scrutiny, out of the screened 16 indicators, a list of 13 indicators is finalized. With 11 environmental indicators found appropriate from the list of 14 included in the Smart Cities Mission program, and 13 selected from the requirements of environmental sustainability, all together these 24 indicators are finalised to be used in the framework of EDSS-SSCI (Table 6).

Data availability is important criteria for selection of indicators. For the indicators selected, the probable sources for data for different environmental management sectors such as Solid Waste Management, Water Supply Management and Sewerage, Sanitation and Pollution have been attempted to be compiled for Indian conditions. City Development Plan (CDP) and Swachh Sarvechhan Report (SSR) from the Swachh Bharat Mission program are found prominent sources of these data required for such indicators. Data about groundwater is normally available from reports of Central Groundwater Board (CGWB) of Government of India. Air quality and noise quality data can be obtained through Central Pollution Control Board (CPCB) and ENVIS sources respectively. Thus, the indicators selected are considered well supported with data from available sources for evaluation of a Sustainable Smart City.

CONCLUSIONS

The current guidelines for Smart Cities Mission (SCM) of Government of India include 14 environmental parameters: 4 under Solid Waste Management (A), 5 under Water Supply Management (B), 3 under Sewerage and Sanitation (C), and 1 each under Storm Water Drainage (D) and Pollution (E). When scrutinized on the criteria for appropriateness of an indicator, as suggested by World Bank Environment

Table 3: Additional environmental indicators required for sustainable cities.

Environmental Indicators	References for relevance
A. Solid Waste Management	
1) Street Sweeping	CPHEEO 2016; JICA 2016; MoUD 2017;Ministry of Urban Development (MoUD Garau et al. 2018
2) Household Coverage	CPHEEO 2016; MoUD 2012; MoUD 2017
3) Degree of Segregation	CPHEEO 2016; MoUD 2012; MOUD 2017
4) Efficiency in collection of MSW	BIS 2016; MoUD 2012; MoUD 2017
5) Extent of solid waste recovered	BIS 2016; EIU 2012; MoUD 2012
6) Degree of scientific disposal of MSW	BIS 2016; EIU 2012; MoUD 2012
7) Availability of collection bin at appropriate place at commercial and residential areas	Garau et al. 2018; MoUD 2017
8) Availability of roadmap for waste transportation of MSW as per Swachh city plan	MoUD 2017
9) Extent of cost recovery in Solid Waste Management services	MoUD 2012
B. Water Supply Management	
10) Coverage of water supply connections	MoUD 2012
11) Continuity of water supplied in terms of average number of hours per day	MoUD 2012
12)Identification of water sources and exploitation of underground water	JICA 2016 Howard et al. 2005
C. Sewerage and Sanitation	
13) Coverage of sewerage	BIS 2016; Dong et al. 2017
14) Collection efficiency of sewage network	MoUD 2012
15) Adequacy of sewage treatment capacity	EIU 2012; MoUD 2012
16)Quality of treated sewage	MoUD 2012
D. Storm Water Drainage	
17) Coverage of storm water drainage	MoUD 2012
18) Incidence of water logging	MoUD 2012
E. Pollution	
19) Noise pollution	Bosch et al. 2017 BIS2016
20)Quality of surface water bodies	BIS 2016

Table 4: Appropriateness of 20 additional environmental indicators for sustainable cities based on WBED (2002) criteria.

	Suitability of Indicator based on World Bank (2002) Criteria (Segnestam 2002)						
Environmental Indicators for Sustainable Cities	(i) Direct relevance to objectives	(ii)Direct relevance to the target group	(iii) Clarity in design	(iv) Realistic collection or development costs.	(v)High quality and reliability	(vi)Appropriate spatial and temporal scale	
A. Solid Waste Management							
1 Street Sweeping	✓	✓	×	×	×	✓	50%
2 Household Coverage	✓	✓	✓	✓	✓	✓	100%
3 Degree of Segregation	✓	✓	✓	✓	✓	✓	100%
4 Efficiency in collection of MSW	✓	✓	✓	✓	✓	✓	100%
5 Extent of solid waste recovered	✓	✓	✓	✓	✓	✓	100%
6 Degree of scientific disposal of MSW	✓	✓	✓	✓	✓	✓	100%
7 Availability of collection bin at appropriate place at commercial and residential areas	×	✓	✓	✓	×	✓	66.6%
8 Extent of cost recovery in	✓	✓	✓	✓	✓	✓	100%
9 Availability of roadmap for waste transportation of MSW as per Swachh city plan	×	×	✓	✓	✓	✓	66.6%
B. Water Supply Management							
10. Coverage of water supply connections	✓	✓	✓	✓	✓	✓	100%
11. Continuity of water supplied in terms of average number of hours per day	✓	✓	✓	✓	✓	✓	100%
12. Identification of water sources and exploitation of underground water	✓	✓	✓	✓	✓	✓	100%
C. Sewerage and Sanitation							
13. Coverage of sewerage	✓	✓	✓	✓	✓	✓	100%
14. Collection efficiency of sewage network	✓	✓	✓	✓	✓	✓	100%
15.Adequacy of sewage treatment capacity	✓	✓	✓	✓	✓	✓	100%
16.Quality of treated sewage	✓	✓	✓	✓	✓	✓	100%
D. Storm Water Drainage							
17.Coverage of storm water drainage	✓	✓	✓	✓	✓	✓	100%
18.Incidence of water logging	×	✓	×	×	×	✓	33.3%
E. Pollution							
19.Noise pollution	✓	✓	✓	✓	✓	✓	100%
20.Quality of surface water bodies	✓	✓	✓	✓	✓	✓	100%

Table 5: Appropriateness of environmental indicators for sustainable cities based on city key indicators criteria (Bosch et al. 2017)

	City Key Indicators criteria (Bosch et al. 2017)								
Sustainable City Environmental Indicators	(i) Relevance	(ii) Completeness	(iii) Availability	(iv) Measurability	(v) Reliability	(vi) Familiarity	(vii) Non-Redundancy	(viii) Independence	
A. Solid Waste Management									
1. Household Coverage	✓	✓	✓	✓	✓	✓	×	×	75%
2. Degree of Segregation	✓	✓	✓	✓	✓	✓	✓	✓	100%
3. Efficiency in collection of MSW	✓	✓	✓	✓	✓	✓	✓	✓	100%
4.Extent of solid waste recovered	✓	✓	✓	✓	✓	✓	✓	✓	100%
5.Degree of scientific disposal of MSW	✓	✓	✓	✓	✓	✓	✓	✓	100%
6.Extent of cost recovery in Solid Waste Management	✓	✓	✓	✓	✓	✓	✓	✓	100%
B. Water Supply Management									
7.Coverage of water supply connections	✓	✓	✓	✓	✓	✓	×	✓	87.5%
8.Continuity of water supplied in terms of average number of hours per day	✓	✓	✓	✓	✓	✓	✓	✓	100%
9. Identification of water sources and exploitation of underground water	✓	✓	✓	✓	✓	✓	✓	✓	100%
C. Sewerage and Sanitation									
10. Coverage of sewerage	✓	✓	✓	✓	✓	✓	×	×	75%
11.Collection efficiency of sewage network	✓	✓	✓	✓	✓	✓	✓	✓	100%
12.Adequacy of sewage treatment	✓	✓	✓	✓	✓	✓	✓	✓	100%
13.Quality of treated sewage	✓	✓	✓	✓	✓	✓	✓	✓	100%
D. Storm Water Drainage									
14.Coverage of storm water drainage	✓	✓	✓	✓	✓	✓	✓	✓	100%
E. Pollution									
15.Noise pollution	✓	✓	✓	✓	✓	✓	✓	✓	100%
16.Quality of surface water bodies	✓	✓	✓	✓	✓	✓	✓	✓	100%

Table 6: Finalized environmental indicators suggested for 'Sustainable Smart Cities' framework.

Indicators included in Smart Cities Mission (MoUD 2015)	Additional indicators desirable to be included for 'Sustainable Smart Cities' and their sources in India
A. Solid Waste Management	
1. Recycling and reduction of construction and demolition waste	1. Degree of segregation (MoUD 2012, MoUD 2017)
2. Solid waste management programs carried in the city during last 3 years.	2. Efficiency in collection of MSW (MoUD 2012, MoUD 2017)
	3. Extent of solid waste recovered (MoUD 2012)
	4. Degree of scientific disposal of MSW (MoUD 2012)
	5. Extent of cost recovery in Solid Waste Management (MoUD 2012)
B. Water Supply Management	
3. Adequate water supply	6. Continuity of water supplied in terms of average no of hrs per day (MoUD 2012)
4. Smart meters and Management	7. Identification of water sources and Exploitation of underground water (JICA 2016)
5. Leakage identification	
6. Water quality monitoring	
7. Extent of cost recovery in water supply services	
C. Sewerage and Sanitation	
8. Coverage of toilets	8. Adequacy of sewage treatment capacity (MoUD 2012)
9. Waste water recycling	9. Collection efficiency of sewage network (MoUD 2012)
10. Extent of cost recovery	10. Quality of treated sewage (MoUD 2012)
D. Storm Water Drainage	
	11. Coverage of storm water drainage (MoUD 2012)
E. Pollution	
11. Improvement in Air Quality	12. Noise Pollution (BIS 2016)
	13. Quality of surface water bodies (BIS 2016)

Development (WBED 2002), only 11 (2 under category A. 5 under B, 3 under C and 1 under E) are found suitable, while 3 are considered inadequately defined in terms of clarity or objective evaluation.

In order to propose and plan Smart Cities as 'Sustainable Smart Cities' in India, a set of 20 additional parameters are screened from available literature related with sustainable cities across the world. Out of these 20 additional parameters, only 16 could be found satisfying the requirements of appropriateness as indicator, as per WBED (2002) criteria. When these 16 indicators are further subjected to evaluation on 7 criteria, used by City Key Indicator program, only 13 (5 under category A, 2 under category B, 3 under category C, 1 under D and 2 under category E) are found fully satisfying the requirements as environmental indicators and 3 parameters are found to be inadequately defined. Accordingly, a set of 24 indicators are finalized (7 for Solid Waste Management, 7 for Water Supply Management, 6 for Sewerage and Sanitation, 1 for Storm Water Management and 3 under Pollution) which can be used in the scientific framework, named as Environmental Decision Support System for Sustainable Smart Cities in India (EDSS-SSCI) for evaluation and monitoring purposes. The sources of data under Indian administrative set up and programs have also been identified. On the lines of the indices developed for Smart Cities, the selected indicators are envisaged to be used to develop a Sustainable Smart Cities Index (SSCI) which may be used to assess the comparative performance of cities on the scale of smartness and sustainability with increasing investment and improving urban infrastructure.

ACKNOWLEDGEMENTS

All the necessary facilities for this work have been provided by the Indian Institute of Technology (Banaras Hindu University) Varanasi.

REFERENCES

Abbu, N., Kumar, E. and Saini, V. 2015. Urban green growth strategies for Indian cities. ICLEI-Local Government for Sustainability, South Asia (1).

Bibri, S. and Krogstie, J. 2017. Smart sustainable cities of the future: An extensive interdisciplinary literature review. Sustainable Cities and Society.

Bosch, P., Jongeneel, S., Rovers, V., Neumann, H.M., Airaksinen, M. and

Huovila, A. 2017. CITYkeys indicators for smart city projects and smart cities.

BIS 2016. Smart Cities-Indicators ICS 13.020.20.

CPHEEO 2016. Municipal Solid Waste Management Manual (12).

Khadke, P.A. and Waghmare, P.B. 2018. Class and size wise distribution of urban centre and their determinants in Maharashtra. Research Review. International Journal of Multidisciplinary and Current Research, 8(3): 722-730.

Dong, Y. and Hauschild, M.Z. 2017. Indicators for Environmental Sustainability. In Procedia CIRP, 61: 697-702.

EIU 2012. The Green City Index. The Economist Intelligence Unit (EIU), 25. Retrieved from http://aiph.org/wp-content/uploads/2015/04/Green City - Guidelines.pdf

Garau, C. and Pavan, V. M. 2018. Evaluating urban quality: Indicators and assessment tools for smart sustainable cities. Sustainability (Switzerland), 10(3): 575.

Howard, G. and Bartram, J. 2005. Effective water supply surveillance in urban areas of developing countries. J. Water Health, 3: 31-42.

Höjer, M. and Wangel, S. 2015. Smart sustainable cities: Definition and challenges.In: L. Hilty & B. Aebischer (Eds.), ICT Innovations for Sustainability. Berlin, Springer-verlag, pp. 333-349.

ITU 2014. Agreed definition of a smart sustainable city, Focus Group on Smart Sustainable Cities, SSC-0146 version Geneva, 5-6 March.

JICA 2016. Republic of India Data Collection Survey on Improvement of Environment in Varanasi City, Republic of India Final Report (Main Report).

Lazaroiu, G.C. and Roscia, M. 2012. Definition methodology for the smart cities model. Energy, 47(1): 326-332.

Maslow, A.H. 1943. A theory of human motivation.Psychological Review, 50: 370-396.

MEM 2015. Cleaner greener and safer Mauritius, environmental guideline for smart cities. Ministry of Environment, Sustainable Development, and Disaster and Beach Management.

MoUD 2017. Swachh Survekshan 2017, A Guidebook for Urban Local Bodies.

MoUD 2012. Service levels in urban water and sanitation sector. Retrieved from http://mohua.gov.in/upload/uploadfiles/files/SLB%20National%20Data%20Book_0.pdf

MoUD 2015. Mission statements and Guidelines. Retrieved from http://smartcities.gov.in/upload/uploadfiles/files/SmartCityGuidelines(1).pdf

Segnestam, L. 2002. Indicators of Environment and Sustainable Development. World Bank Environment Development (WBED), Paper No. 89.

Randhawa, A. and Kumar, A. 2017. Exploring sustainability of smart development initiatives in India. International Journal of Sustainable Built Environment, 6(2):.701-710.

Nature Environment and Pollution Technology
An International Quarterly Scientific Journal

p-ISSN: 0972-6268 e-ISSN: 2395-3454	Vol. 19	No. 1	pp. 211-219	2020

Original Research Paper | Open Access

Impact of Carbon Nanotubes as Additives with Cotton Seed Biodiesel Blended with Diesel in Ci Engine - An Experimental Analysis

G. Ninawe† and M. Tariq
Department of Mechanical Engineering, Sam Higginbottom University of Agriculture, Technology and Sciences, Prayagraj (Allahabad), India
†Corresponding author: G. Ninawe

Nat. Env. & Poll. Tech.
Website: www.neptjournal.com

Received: 10-06-2019
Accepted: 23-07-2019

Key Words:
Diesel engine
Additives
Diesel-biodiesel blends
Carbon nanotubes

ABSTRACT

In the present global scenario, fossil fuels are facing challenges due to escalating costs, increasing demand and impact on environmental pollution. In internal combustion engines, the emission characteristics and economy of the fuel are controlled by the chemical and physical properties of the fuel. Various additives are being used to act like catalysts with the fuels to improve quality of fuel, to obtain better combustion and to reduce exhaust emissions. At the time of combustion process, fuel instability reactions get accelerated by the catalysts which improve the performance of the engine. In this study, the B10, B15 and B20 fuel blends of cotton seed oil and diesel were mixed with the carbon nanotubes (CNTs) as an additive to analyse the performance and exhaust emissions of a CI engine. The carbon nanotubes were mixed with each fuel blend with the concentration of 50 ppm. All the tests were carried out for different engine loads. Tested characteristics were power, brake thermal efficiency (BTE), specific fuel consumption (SFC), and analysis of exhaust gases like hydrocarbons (HC), CO_2, CO and smoke. The experimental results showed that there was significant reduction of SFC and improved combustion by addition of CNTs. It was also observed that the exhaust emissions, CO, HC and smoke percentage got decreased by the influence of CNTs.

INTRODUCTION

The environmental degradation and atmospheric pollution are the two main factors which cause imminent harm to the existence of the world. There are number of reasons for the pollution, but the pollution caused by the exhaust emissions from automobiles and power generation unit takes major part in degradation of environment and global warming. The primary source of energy for vehicles and power generators are the petroleum fuels which are depleting very rapidly. In country like India, 2/3rd of the total economy was spent to acquire petroleum products despite they being responsible for environmental pollution. But the use of transportation vehicles and power generation cannot be neglected as they both are the foundation for the economic growth of the country (Perumal & Ilangkumaran 2017). Therefore, the search for renewable alternative fuels which are environment friendly has been enforced. Particularly, biofuels are the replacement for the fossil fuels and becoming a renewable source of energy. Hence, the use of biodiesel blend with diesel fuel in engines is a promising option. The reason behind using biodiesel as an alternative fuel is that, it can be used without any modification in engine and the power generated from engine using biodiesel fuels are similar to the engine using diesel fuel (Caliskan 2017). The commercialization of bio fuel and related projects enforces the employment either in direct or indirect manner. These projects are responsible to employ all the categories of people, including skilled and unskilled workers from different departments. The government has already initiated programs for urban, industrial and commercial applications. These programs aimed to evaluate energy from vegetable wastes, agriculture residue, municipal wastes, and industrial wastes (Gaurav et al. 2017).

Biodiesel is nothing but methyl or ethyl ester of fatty acids which is made from both edible and non-edible vegetable oils and animal fats. For the production of biodiesel the main resources are non-edible oils extracted from plant species such as *Calophyllum inophyllum, Pongamia pinnata, Jatropha curcas, Hevea brasiliensis* etc. Biodiesel can be used in its unadulterated form in engine or can be blended with pure diesel fuel in any proportion. Like petroleum diesel, biodiesel has similar properties and works in compression ignition engine with minor or no engine modifications. It can be stored just like pure diesel and does not require any separate storage. The use of biodiesel in compression ignition engines results in reduction of emissions like carbon monoxide, unburned hydrocarbons and particulate matters (Agarwal 2007) Presently, the first-generation biofuels are dominating

Fig. 1: TEM image of carbon nanotubes.

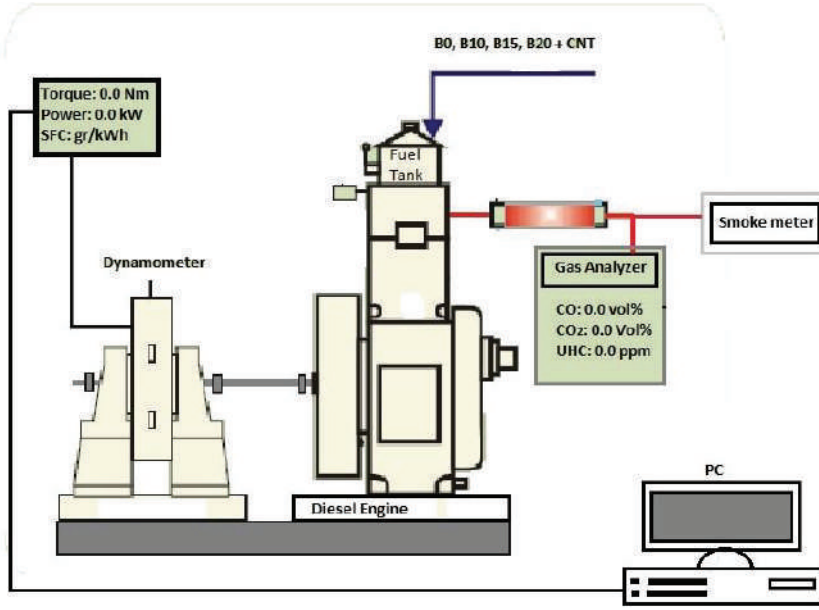

Fig. 2: Measurement setup and devices for the experiments.

the biofuel sector, such as bioethanol and biodiesel. These biofuels can be used as blends with petroleum fuels in low percentage and can be utilized with existing infrastructure. The main advantage of using vegetable oils as alternative to conventional fuels exist in their renewable nature and there is wide availability from different variety of sources. There are also some disadvantages of using these vegetable oils which has incompatibility with petroleum lubricating oils, higher viscosity and problem of foul injector nozzles. To minimize the viscosity as well as problems related to lubrication, trans-esterification method and de-gumming of vegetable oil has been used (Eevera & Pazhanichamy 2013).

MATERIALS AND METHODS

In this research, the cotton seed biodiesel was produced from the cotton seed oil, using trans-esterification process. The carbon nanotubes (CNTs) used with the dose of 50 ppm and then mixed with B10, B15 and B20 fuel blends. Each fuel blends were made of 500 mL sample to be tested in the engine.

Multi-walled carbon nanotubes (MWNTs) were supplied from Platonic Nanotech Private Limited, India with purity more than 97%. The average diameter of the carbon nanotubes varied from 10-15 nm and their length from 2-10 μm.

Carbon nanotubes acts as an useful additives for improving the quality of the fuels (Hosseini et al. 2017). Recently, several researchers have incorporated different additives to improve the fuel properties of the biofuels. Addition of CNTs with the diesel fuel increases the cetane number, burning rate and suppresses the smoke formation in the engine cylinder during combustion process (Basha 2015, Tennent et al. 2002). The carbon nanotubes contain amide group and has property of reacting with many chemicals. The TEM (transmission electron microscopy) image of carbon nanotubes which was used with diesel-biodiesel blended fuel is shown in Fig.1. The CNTs added to all fuel blends were stirred for 15 min to get the homogeneous emulsion fuel.

Experimental Set-up

The experimental system consists of one cylinder, four strokes, VCR (Variable Compression Ratio) diesel engine which was connected to eddy current type dynamometer for loading with its main parameters are given in Table 1.

In order to compute and assess the exhaust gas emissions a mobile AVL DITEST GAS analyser was also used for this experiment. A smoke opacity meter was used to calculate the amount of soot coming out from the exhaust which is attached to exhaust gas duct coming from engine. An onboard computer system is used to perform the common combustion calculations to eliminate the use of tables and complex calculations. Details of the measuring instruments used for testing are given in Table 1.

Experimental Procedure

For the experiment different fuel blends (i.e. diesel base, B10, B15, B20, B10C50, B15C50, B20C50) were prepared. The blending of diesel fuel with biodiesel was made in 500 mL flask which was directly poured in fuel tank. The kinematic viscosity, fire point, flash point, density and calorific value were calculated immediately after the biodiesel preparation. The experiments were performed under variable loads on engine to get different speeds. Various parameters such as torque, specific fuel consumption (SFC), mechanical efficiency, power, volumetric efficiency and brake thermal efficiency were recorded and the data was transferred to the computer which was connected to the engine setup. The analysis done for the performance of engine is for 500 mL quantity of fuel for each fuel blend. To establish the baseline data, first the diesel fuel was used in the engine at varied loading conditions. Similarly, the testing was executed for different biodiesel blends at different load conditions. To attain the steady state conditions and to minimize the residual from previous fuel blends each test was started by a 10 min start-up period.

RESULTS AND DISCUSSION

Table 2 gives the characteristics, which were measured based on ASTM (American Society for Testing and Materials) standards for the tested fuel blends. By adding carbon nanotubes in fuel blends the viscosity decreases and makes it easier to slip. Because of this the spraying and powdering of fuel inside combustion chamber is more proper. Duraisamy & Gowrishankar (2011) proved that the volatility and viscosity have interdependency with the dose of carbon nanotubes (20-80 ppm).

Engine Torque and Power

Table 3 gives the effect of addition of CNTs with diesel-biodiesel blends on engine torque. It is observed that maximum torque for each fuel blends is at higher loads and as the load decreases there is decrease in torque. By decreasing the engine load from 12 to 0 kg the torque decreases on an average by 4.20%. It can be observed that use of CNTs with diesel-biodiesel blends leads to improve the engine torque at certain loads compared to pure diesel and diesel-biodiesel blends. The output torque increases by raising the concen-

Table 1: Specifications of all equipment and devices used in the experiments.

Engine type	4-stroke VCR diesel engine
Number of cylinders	One
Bore × stroke	87.5 × 110 mm
Swept volume	661 cc
Compression ratio	17.5:1
Rated power	3.5 kW at 1500 rpm
Fuel injection timing	23º BTDC
Dynamometer type	Eddy current, water cooled with loading unit
Emission Analyzer	AVL DITEST GAS 1000, Emission diagnostics of HC, CO, CO_2
Smoke Opacity Meter	Model AVL DiSmoke 480 BT

Table 2: Properties of all the fuel blends.

Properties	Diesel base	B10	B15	B20
Kinematic Viscosity (mm^2/sec)	2.25	2.38	2.56	2.73
Density (kg/m^3)	790	802	810	817
Calorific value (MJ/kg)	43.25	42.89	42.16	41.35
Flash point (ºC)	56	71.60	80.25	88.5

Table 3: Torque at different loads for all the fuel blends.

Load (kg)	B0	B10	B10C50	B15	B15C50	B20	B20C 50
0 kg	0.91	0.97	0.98	0.98	0.98	0.99	0.70
3 kg	5.81	5.84	6.03	5.85	5.73	5.88	5.76
6 kg	11.24	11.29	11.27	11.27	11.28	11.28	11.21
9 kg	16.68	16.71	16.70	16.71	16.87	16.70	16.64
12 kg	21.91	22.14	22.10	22.29	22.10	22.11	22.06

Table 4: Power at different loads for all the fuel blends.

Load (kg)	B0	B10	B10C50	B15	B15C50	B20	B20C 50
0 kg	0.14	0.15	0.15	0.15	0.15	0.15	0.11
3 kg	0.89	0.91	0.91	0.90	0.88	0.90	0.90
6 kg	1.71	1.72	1.72	1.73	1.73	1.71	1.72
9 kg	2.53	2.54	2.54	2.54	2.56	2.52	2.52
12 kg	3.29	3.32	3.32	3.35	3.31	3.30	3.31

tration of CNTs in fuel blends, which improves the complete combustion inside the cylinder.

Table 4 gives the power variation at different loads for all fuel blends. As seen from the table, the power increases sharply as the load is increased. B0, B10 and B20 have lower power output as compared to B10C50, B15, B15C50, B20C50. In general, the brake power increases with the use of CNTs in fuel blends at variable loads. The reason for increased power with CNTs and fuel blends is energy produced inside the cylinder. According to the earlier research, the catalyst reduces the combustion duration and ignition delay, which leads to faster heat release rate and higher peak pressure inside the cylinder (Heydari-Maleney et al. 2017, Ma et al. 2013, Kannan et al. 2011). The addition of nanoparticles modifies the mechanism of ignition for liquid fuels, which accelerates the thermal interchangeability between the surrounding air and fuel droplets (Solero 2012).

Brake Thermal Efficiency (BTE)

The brake thermal efficiency for all the fuel blends is given in Table 5. Due to reduction in volumetric efficiency the BTE increases as the load on engine increases. The lowest values of BTE are for B20C50, B0 and B10 fuels and the maximum values of BTE are related to B10C50, B15, B15C50 and B20 fuel blends. Therefore, adding CNTs (50ppm) in fuel blends shows increase in amount of BTE due to better fuel spraying and dropped viscosity for some of the fuel blends.

Specific Fuel Consumption (SFC)

The variations of SFC of all fuel blends for the different loads are shown in Table 6. At different loads the SFC is lower for B15, B15C50, B20 and B10C50, whereas B0, B10, and B20C50 had the higher SFC. The reason for higher SFC is higher viscosity, lower heating value and oxygenated characteristic of biodiesel fuels (Singh et al. 2012, Porteiro et al. 2007). Therefore, addition of CNTs to the diesel-biodiesel fuel blends improves combustion, increases power and decreases the SFC of the engine. It has been observed from Table 6 that as the load is increased there is reduction in SFC. The reason for lower SFC values is the higher BTE of the fuels with CNTs, which is due to existence of oxygen molecules and CNTs.

Table 5: Brake thermal efficiency at different loads for all fuel blends.

Load (kg)	B0	B10	B10C50	B15	B15C50	B20	B20C 50
0 kg	3.50	3.74	3.81	4.42	4.40	3.81	2.69
3 kg	17.01	17.36	17.71	17.25	16.88	17.25	15.45
6 kg	26.72	26.85	26.80	27.10	27.07	26.74	24.67
9 kg	31.08	31.17	31.12	31.27	31.53	31.04	30.93
12 kg	35.43	33.61	33.48	33.93	33.55	33.45	31.61

Table 6: Brake specific fuel consumption at different loads for all fuel blends.

Load (kg)	B0	B10	B10C50	B15	B15C50	B20	B20C 50
0 kg	2.45	2.29	2.25	1.94	1.95	2.25	3.18
3 kg	0.50	0.49	0.48	0.50	0.51	0.50	0.55
6 kg	0.32	0.32	0.32	0.32	0.32	0.32	0.35
9 kg	0.28	0.28	0.28	0.27	0.27	0.28	0.28
12 kg	0.24	0.26	0.26	0.25	0.26	0.26	0.27

Analysis of Emissions

Carbon monoxide (% Vol)

The carbon monoxide emissions which comes from engine exhaust represents the loss of chemical energy which is not fully employed to generate engine power. Fig. 3 shows the percentage of concentration of CO emissions for all the fuel blends at variable loads. It has been noticed that at higher loads the CO emissions are less and at medium loads the CO emissions are highest in all the fuel blends. B10, B10C50, B15C50 had the lower CO content, whereas B0, B15, B20, B20C50 had the higher CO content. The average CO emissions decreased 27.27 % for the fuel blends with CNTs when compared to neat diesel and biodiesel blends. It was observed that there is significant lowering of CO emissions when CNTs, biodiesel and its blends were used as compared to pure diesel. The reason behind lowering of CO emission is existence of more oxygen content in biodiesel than pure diesel fuel, which causes to make complete combustion of the mixture present in combustion chamber and ensures less CO emissions (Taghizadeh-Alisaraei and Rezaei-Asl 2016). Decreased viscosity of the fuel plays significant role in minimizing CO emissions by improving fuel atomization. As the CNTs had larger surface area, it increases the chemical reactivity by which the ignition delay gets consecutively shortened. Due to the effect of shortened ignition delay uniform burning and fuel-air mixing had been improved which promotes complete combustion of fuels in presence of potential CNTs (Javed et al. 2016, Srinivas et al. 2016).

Carbon dioxide

Fig. 4 shows the carbon dioxide emissions at different loads for various fuel blends. After comparing CO and CO_2 emissions, it has been noted that the molecular component and balance for a given fuel have opposite behaviours. Therefore, the carbon present in exhaust gas has potential to become CO_2 or CO. As the load on the engine was increased then the CO_2 content got increased. B15, B20, B10C50, B15C50 had the higher CO_2 content while B0, B10, B20C50 had the lower CO_2 content.

As a rule, the most cost effective and efficient use of fuel takes place when the CO_2 content in the exhaust is maximized. This happens only when there is sufficient O_2 present in the supplied air to react with carbon present in the fuel. Therefore, as the amount of air gets increased in the combustion chamber the concentration of CO molecules gets decreased. Due to this, the additional atoms of oxygen present in the air reacts with this CO molecules and form CO_2. The maximum amount of CO_2 depends upon the category of fuel used (TSI 2004).

Hydrocarbons emissions

The unburned hydrocarbon present in the exhaust is the consequence of incomplete combustion of fuel. The variations of HC emissions are shown in Fig. 5 for all the fuel blends at variable loads. The minimum and maximum HC emissions are observed at lower and higher loads respectively. The larger reduction of HC emissions is for the B20C50, B20, B15C50 and B15 fuel blends. This is because of higher oxygen content present in the biodiesel which makes possible to obtain more complete combustion inside the combustion chamber (Sahoo et al. 2007). The HC emissions are found to be noticeably reduced due to addition of CNTs to the fuel blends. The reason behind this is significant fuel distribution

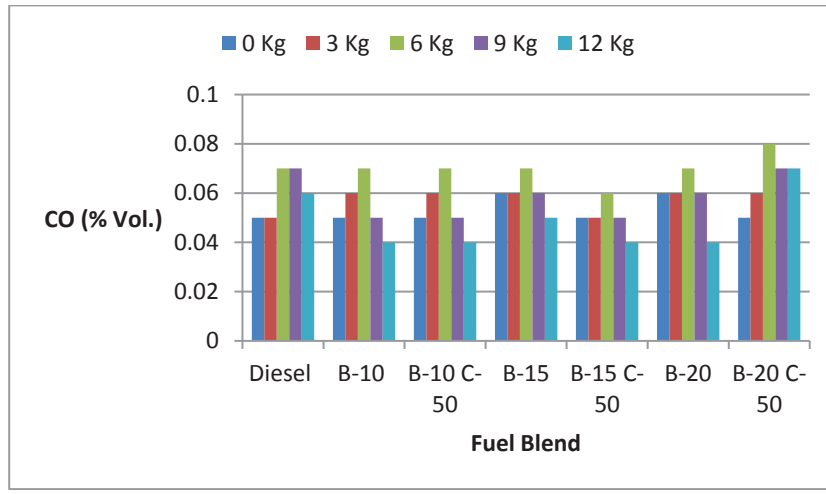

Fig. 3: CO for different fuel blends at different loads.

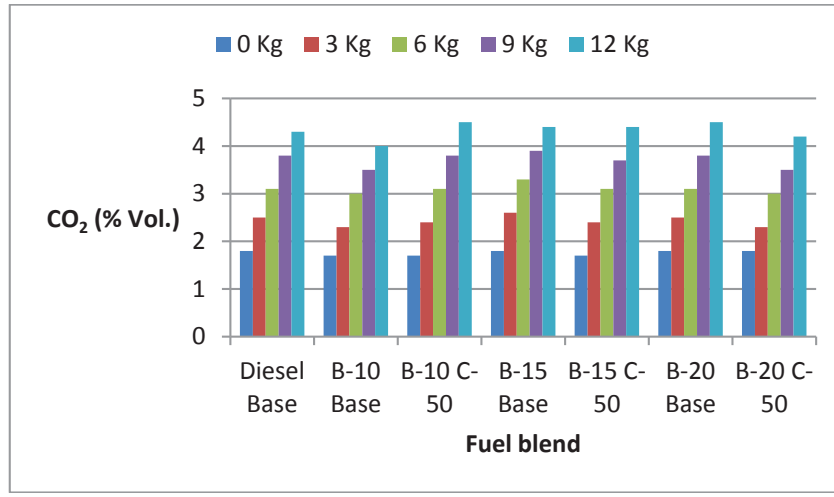

Fig. 4: CO_2 for different fuel blends at different loads.

and intensive atomization with the existence of CNTs in combustion chamber which causes CO and HC oxidation during the combustion (Sadhik Basha & Anand 2014).

Smoke

Fig. 6 shows the trend of smoke opacity at different loads for different fuel blends. The percentage of smoke opacity for pure diesel was higher while for the fuel blends with CNTs were drastically lesser. The reason for reduction of smoke for the fuel blends is probably due to intensive atomization, better fuel-air mixing and enhanced air spray momentum (Subramanian & Ramesh 2002, Armas et al. 2005, Rao & Anand 2016)50 and 100 ppm. In case of B20 and B20C50 the smoke opacity is minimum than that of other fuel blends. This is due to higher oxygen content present in the biodiesel which facilitates the complete combustion. Because of heterogeneous nature of the diesel combustion there is variation of fuel-air ratios inside the cylinder of diesel engine, which affects the smoke formation. The smoke formation primarily takes place at higher pressure and temperature in the fuel rich zone of the engine cylinder. As the fuel used in diesel engine is partially oxygenated the major smoke formation can be reduced (Puhan et al. 2005).

Optimal Fuel

In all the fuel blends, addition of CNTs proved to be a better additive which increased the amount of torque. It can be observed that larger power and BTE belongs to B15C50,

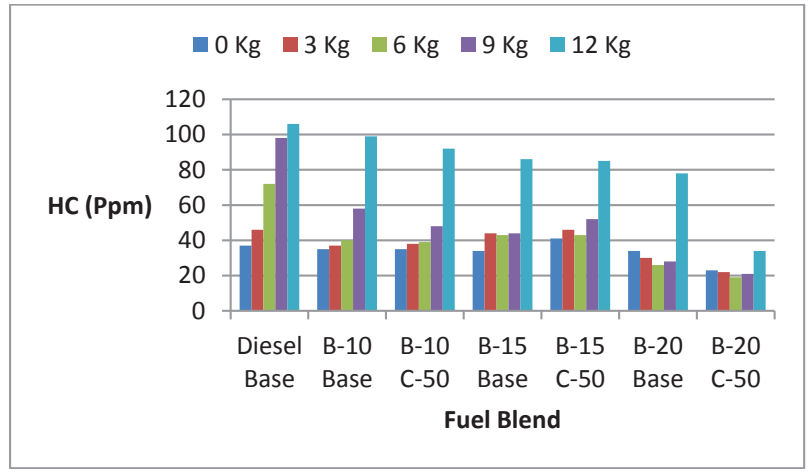

Fig. 5: HC for different fuel blends at different loads.

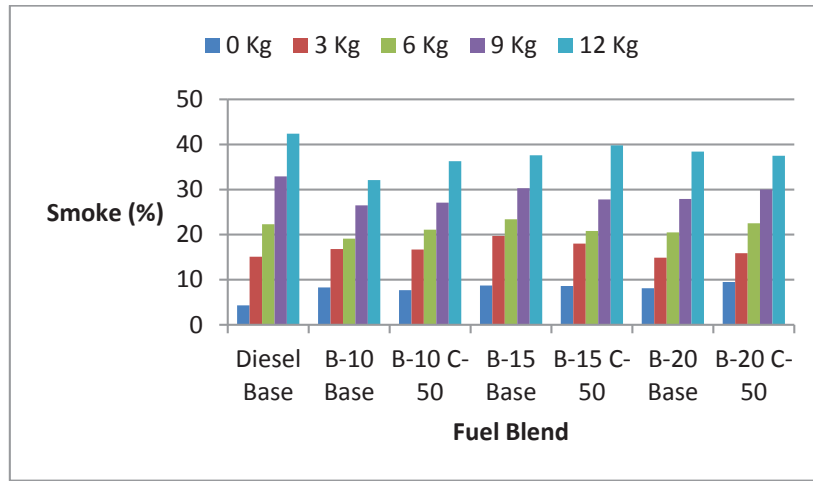

Fig. 6: Variation of smoke opacity for different fuel blends at different loads.

B20C50, B15 and B10C50 fuel blends respectively. Similarly, the torque trend follows the power table and has matching results. B15, B15C50, B20 and B10C50 have the minimum SFC.

According to the emissions results, B10C50, B15C50 had the lower CO content. B20C50, B20, B15C50 and B15 fuel blends have the lowest HC emissions. The smoke opacity is lesser for all the fuel blends with CNTs than the pure diesel. Based on these results, the optimal fuel can be selected as B15C50 fuel blend. Therefore, B15C50 is considered as the best fuel in terms of performance and emissions parameters. The greatest variations occurred for all the parameters are for higher loads.

Cost Analysis

The cost of the CNTs used in the present experiments is about 384 US$ per kg in India and the dose of 50 ppm are respectively 0.05 g per 500 mL for B10, B15 and B20 fuel blends. The specific cost for 50 ppm CNT is 0.0192 US$ for per 500 mL of B10, B15 and B20 fuel blends. In addition, the diesel fuel cost in India is about 0.92 US$. Adding CNTs with the dose of 50 ppm to B10, B15 and B20 fuel blends, the fuel price increases by 2%. In country like India the higher price of diesel fuel enforces the use of additives as it results in reduction of SFC. Hence, the use of CNTs with diesel fuel is much more economical and affordable in India. However, other advantage such as reduction in exhaust emissions can also be contemplated.

CONCLUSIONS

In this study, the B10, B15 and B20 fuel blends included with carbon nanotubes (CNTs) were used to analyse the exhaust emissions and performance characteristics of a single cylinder CI engine. The CNTs were mixed with the dosage of 50 ppm to all the fuel blends. The experiments were conducted by varying the loads on the engine. The results indicated that the performance characteristics such as power, torque, BTE, SFC of B15C50 fuel blend is optimum as compared to other fuel blends and pure diesel. The exhaust emissions of B15C50 fuel blend like CO, HC and smoke opacity were found minimum as compared to pure diesel and other fuel blends. The existence and translocation of CNTs in the fuel molecules improved the fuel atomization and decreased the viscosity. Overall, it has been found that the CNT used with fuel blends has potential advantage to improve the performance and to reduce the exhaust emissions from the diesel engine.

ACKNOWLEDGMENT

The first author would like to express his gratitude to Dhanushkar S., Naik S. N., Centre for Rural Development and Technology, IIT Delhi, India for their support.

NOMENCLATURE

B0	Pure Diesel	nm	nanometer
B10	90% Diesel + 10% Biodiesel	μm	micrometer
B15	85% Diesel + 15% Biodiesel	ppm	part per million
B20	80% Diesel + 20% Biodiesel	CI	Compression ignition
B10C50	B10 + 50 ppm CNTs	HC	Hydro carbons
B15C50	B10 + 50 ppm CNTs	CO	Carbon monoxide
B20C50	B10 + 50 ppm CNTs	CO_2	Carbon dioxide
BTE	Brake thermal efficiency (%)	rpm	Revolutions per minute
CNTs	Carbon Nanotubes	SFC	Specific fuel consumption
kW	kilo Watt	Nm	Newton meter

REFERENCES

Agarwal, Avinash Kumar. 2007. Biofuels (alcohols and biodiesel) applications as fuels for internal combustion engines. Progress in Energy and Combustion Science, 33(3): 233-71.

Armas, O., Ballesteros, R., Martos, F.J. and Agudelo, J.R. 2005. Characterization of light duty diesel engine pollutant emissions using water-emulsified fuel. Fuel, 84: 1011-18.

Basha, J.S., 2015. Applications of functionalized carbon-based nanomaterials. In: Chemical Functionalization of Carbon Nanomaterials, CRC Press, pp. 598-613.

Caliskan, Hakan 2017. Environmental and enviroeconomic researches on diesel engines with diesel and biodiesel fuels. Journal of Cleaner Production, 154: 125-29.

Duraisamy, Ganesh and Gowrishankar, G. 2011. Effect of nano-fuel additive on emission reduction in a biodiesel fuelled CI engine. In 2011 International Conference on Electrical and Control Engineering, IEEE, pp. 3453-3459.

Eevera, T. and Pazhanichamy, K. 2013. Cotton seed oil: a feasible oil source for biodiesel production. Energy Sources, Part A: Recovery, Utilization and Environmental Effects, 35(12): 1118-28.

Gaurav, N., Sivasankari, S., Kiran, G.S., Ninawe, A. and Selvin, J. 2017. Utilization of bioresources for sustainable biofuels: A review. Renewable and Sustainable Energy Reviews, 73: 205-14.

Heydari-Maleney, K., Taghizadeh-Alisaraei, A., Ghobadian, B. and Abbaszadeh-Mayvan, A. 2017. Analyzing and evaluation of carbon nanotubes additives to diesohol-B2 fuels on performance and emission of diesel engines. Fuel, 196: 110-23.

Hosseini, S.H., Taghizadeh-Alisaraei, A., Ghobadian, B. and Abbaszadeh-Mayvan, A. 2017. Performance and emission characteristics of a ci engine fuelled with carbon nanotubes and diesel-biodiesel blends. Renewable Energy, 111: 201-13.

Javed, S., Murthy, Y.S., Baig, R.U. and Rao, T.N. 2016. Vibration analysis of a diesel engine using biodiesel fuel blended with nano particles by dual fueling of hydrogen. Journal of Natural Gas Science and Engineering, 33: 217-30.

Kannan, G. R., Karvembu, R. and Anand, R. 2011. Effect of metal based additive on performance emission and combustion characteristics of diesel engine fuelled with biodiesel. Applied Energy, 88(11): 3694-3703.

Ma, Y., Zhu, M. and Zhang, D. 2013. The effect of a homogeneous combustion catalyst on exhaust emissions from a single cylinder diesel engine. Applied Energy, 102: 556-62.

Perumal, V. and Ilangkumaran, M. 2017. Experimental analysis of engine performance, combustion and emission using pongamia biodiesel as fuel in CI engine. Energy, 129: 228-36.

Porteiro, J., Granada, E. and Mora, J. C. 2007. Performance and exhaust emissions in the use of biodiesel in outboard diesel engines. Fuel, 86: 1765-71.

Puhan, S., Vedaraman, N., Ram, B.V., Sankarnarayanan, G. and Jeychandran, K., 2005. Mahua oil (Madhuca Indica seed oil) methyl ester as biodiesel-preparation and emission characterstics. Biomass and Bioenergy, 28(1): 87-93.

Rao, M. Srinivasa and Anand, R.B. 2016. Performance and emission characteristics improvement studies on a biodiesel fuelled DICI engine using water and AlO(OH) nanoparticles. Applied Thermal Engineering, 98: 636-45.

Sadhik Basha, J. and Anand, R.B. 2014. Performance, emission and combustion characteristics of a diesel engine using carbon nanotubes blended jatropha methyl ester emulsions. Alexandria Engineering Journal, 53(2): 259-73.

Sahoo, P. K., Das, L. M., Babu, M.K.G. and Naik, S. N. 2007. Biodiesel development from high acid value polanga seed oil and performance evaluation in a CI Engine. Fuel, 86(3): 448-54.

Singh, Bhupendra, Naveen Kumar and Haeng Muk, 2012. A study on the performance and emission of a diesel engine fueled with jatropha biodiesel oil and its blends. Energy, 37(1): 616-22.

Solero, Giulio 2012. Experimental analysis of the influence of inert nano-additives upon combustion of diesel sprays. Nanoscience and Nanotechnology, 2(4): 129-33.

Srinivas, Dilip, Puneesh Puri and Vigor Yang 2016. A general theory of ignition and combustion of nano- and micron-sized aluminum particles. Combustion and Flame, 169: 94-109.

Subramanian, K. A. and Ramesh, A. 2002. Use of diethyl ether along with water-diesel emulsion in a di diesel engine. In: SAE Technical Paper, SAE International.

Taghizadeh-Alisaraei, Ahmad and Abbas Rezaei-Asl. 2016. The effect of added ethanol to diesel fuel on performance, vibration, combustion and knocking of a CI engine. Fuel, 185: 718-33.

Tennent, Howard, Kennett Square and References Cited 2002. (12) United States Patent (10) Patent No.: 2(0): 4-7.

TSI 2004. Combustion analysis basics: An overview of measurements, methods and calculations used in combustion analysis. TSI Incorporated, 2004

Nature Environment and Pollution Technology
An International Quarterly Scientific Journal

p-ISSN: 0972-6268
e-ISSN: 2395-3454

Vol. 19 | No. 1 | pp.221-227 | 2020

Original Research Paper | Open Access

Factors Influencing the Environmental Performance of Prefabricated Buildings: A Case Study of Community A in Henan Province of China

Jin Zhao, Yi Wang† and Zhengwei Ma
School of Civil and Transportation Engineering, Henan University of Urban Construction, Pingdingshan 467000, China
†Corresponding author: Yi Wang

Nat. Env. & Poll. Tech.
Website: www.neptjournal.com

Received: 09-12-2019
Accepted: 16-01-2020

Key Words:
Prefabricated building
Environmental performance
Influencing factor

ABSTRACT

Various problems of traditional cast-in-place buildings, such as heavy energy consumption, severe environmental pollution, and low labour productivity, have hindered the development of the construction industry. Prefabricated buildings have a direct bearing on national economic development and transformation of people's lifestyle because of their high economic, environmental, social, and safety benefits. The technological research and development level for prefabricated buildings and system policies in China are still in the initial stage, and the environmental performance and influencing factors of prefabricated buildings limit their large-scale implementation. The literature in developed countries regarding the environmental performance and influencing factors of prefabricated buildings was first reviewed in this study. Community A in Zhengzhou City, Henan Province was used as the case study. AHP (Analytic Hierarchy Process) was applied to measure the factors influencing the environmental performance of prefabricated buildings, and policy suggestions were proposed to improve their environmental performance. Results indicate that developed countries tend to construct prefabricated buildings in large areas because of their remarkable economic, environmental, social, and safety benefits. Measurement results of Community A in Zhengzhou City, Henan Province show that the main environmental pollution factor of prefabricated buildings is waste discharge, accounting for 40%, followed by noise pollution, energy consumption, and dust pollution. The environmental performance of prefabricated buildings can be improved by promoting their development, reducing their environmental pollution, establishing a standard prefabricated concrete system, enhancing the environmental standards for buildings, expanding the application scope of prefabricated concrete, encouraging environmental technology innovation of buildings, cultivating prefabricated building bases, and strengthening environmental governance of construction sites. The findings will serve as reference in determining the main factors influencing the environmental performance of prefabricated buildings, establishing an evaluation system for the environmental benefits of prefabricated buildings, promoting their improvement and optimized development, and enriching and perfecting an evaluation research system for their comprehensive benefits.

INTRODUCTION

As a pillar industry in China, building construction has experienced remarkable development and improved production with rapid urbanization. Buildings should satisfy basic requirements, such as construction quality and use functions, and should minimize resource and energy consumption, improve labour productivity, and protect the environment during construction and use. The emergence of prefabricated buildings has provided a new direction in the development of the construction industry. The components and members of prefabricated buildings are prefabricated in a plant based on design standards and transported to the construction site for assembly, thereby accelerating the construction speed, reducing the construction period, and has remarkable advantages in terms of improved labour productivity, energy consumption reduction, and environment protection.

Henan Province in China has a large population with rapidly developing construction industry. As shown in Fig. 1, the gross output value of construction in Henan Province has increased from RMB 359.649 billion in 2009 to RMB 1,136.052 billion in 2018 with an average annual growth rate of 23.98%. The development of prefabricated buildings in Henan Province is still in the initial stage, and their prefabrication degree remains at a low level. Incomplete technical specifications, low modulus coordination degree between product materials, absence of standard modulus system that can be implemented at the national level, and the uncertainty in the comprehensive benefits of prefabricated buildings hinder their development progress. The development of prefabricated buildings should be accelerated and the innovation of building construction and high-efficiency coordination between production departments should be promoted on the

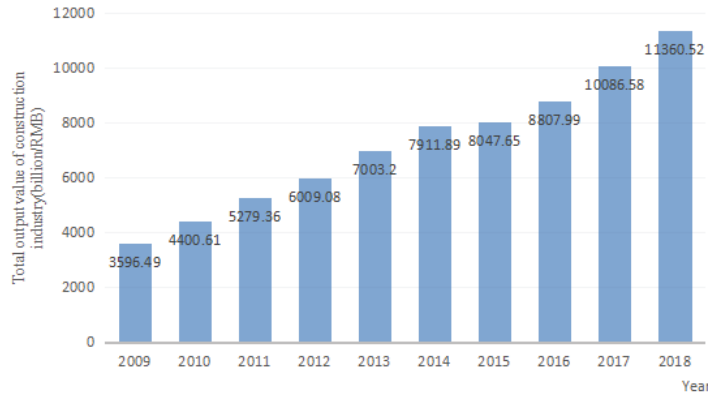

Fig. 1: Gross output values of the construction industry in Henan Province during 2009-2018. (Data derived from Henan Statistical Yearbook)

basis of the modernization requirements and development tendency of the current construction industry. An evaluation research system should be developed to identify the comprehensive benefits of prefabricated buildings for satisfying the fundamental realities existing in the development of China's construction industry. The evaluation research system should cover the entire life cycle of prefabricated buildings and analyse and evaluate their comprehensive benefits during construction, operation, use, recycling, and demolition to support the development of the construction industry.

PAST STUDIES

Foreign prefabricated buildings have originated from Western Europe. Prefabricated buildings can overcome the limitations of current buildings, such as slow construction and long construction period, and they have been implemented in developed countries, such as America and Japan, in the 1960s. Construction technologies and related theoretical studies on prefabricated buildings are the most mature in western countries among other foreign studies. Most of these studies have focused on the production system of prefabricated construction accessories, energy conservation, and emission reduction, and studies on their comprehensive benefits have mainly concentrated on single aspects, such as economic and environmental benefits. Tam et al. analysed and investigated the reduction of construction wastes from four prefabricated buildings compared with traditional cast-in-place buildings, and their results showed that prefabricated buildings have satisfactory environmental benefits in energy conservation and emission reduction, where the quantity of construction wastes and concrete use and template consumption are reduced by approximately 55% and 80% compared with those of traditional cast-in-place buildings (Tam et al. 2005). Altes conducted a statistical analysis on the factors influencing the development of prefabricated buildings and indicated that the prefabrication degree worldwide is low because of unstable industrial chain and the lack of long-term strategic cooperative relationship of enterprises between industrial (Altes 2005). Jaillon et al. believed that a standardized design of prefabricated buildings could effectively improve the production efficiency of product components and achieve remarkable environmental advantages, such as energy conservation and emission and environmental pollution reduction (Jaillon et al. 2009). Begum et al. compared the prefabrication mode with the traditional cast-in-place mode of buildings and stated that the prefabrication mode could reduce the use of building materials and improve the environmental performance of buildings in terms of reduced construction period, energy source conservation, and environment protection (Begum et al. 2010). Mohamad et al. mainly studied the ability of industrial prefabrication to solve the shortage of houses, discussed the results using a SWOT (Strength Weakness Opportunity Threat) method, and concluded that prefabricated buildings could effectively reduce environmental pollution and realize large-scale house provision (Mohamad et al. 2012). Bari et al. selected four low-rise buildings using IBS and conventional construction methods as a case study. Their results showed that prefabricated buildings could help reduce waste pollution from the environmental perspective and provide their positive economic benefits and environmental performance (Bari et al. 2012). Silva et al. analysed the module transformation scheme for exterior walls of existing prefabricated buildings, including 3D model construction and cost effectiveness analysis. Their results showed that prefabricated buildings could notably realize energy conservation and greenhouse gas emission reduction (Silva et al. 2013). Agren et al. presented the five phases of prefabricated buildings from appearance to mature development and analysed their environmental performance under different phases (Agren et al. 2014). Yashiro explained the concept of prefabricated buildings and related theories, proposed a whole-life-cycle

management method for prefabricated buildings, and indicated that the organizational form of prefabricated building construction is crucial in the environmental performance of prefabricated buildings (Yashiro 2014). Hong et al. explored the life-cycle energy utilization of prefabricated members and their influence on overall energy utilization by using actual building projects as the study objects. Their results showed that prefabricated buildings could reduce wastes and conserve energy sources, and minimize whole-life-cycle energy consumption by approximately 4%-14% (Hong et al. 2016). Chang et al. (2018) believed that the Chinese government should actively promote building prefabrication, analysed the advantages and disadvantages of building prefabrication in China in terms of productivity, resources, and environmental sustainability, and constructed a strategic concept of obtaining green benefits through prefabricated buildings (Chang et al. 2018). Li et al. conducted qualitative and quantitative analyses of the indoor thermal environment of prefabricated houses by taking Zhengzhou City in central China as an example. Their results indicated that prefabricated buildings have important advantages in terms of energy source conservation (Li et al. 2019). Navaratnam et al. reviewed the existing literature related to the structural behaviour, advantages, limitations, and challenges of prefabricated building systems by taking Australia as an example and believed that prefabricated buildings have good application prospects (Navaratnam et al. 2019). Lindblad analysed the environmental pollution caused by prefabricated concrete components during transportation (Lindblad 2019). Wang et al. utilized a performance analysis method to investigate the critical risk factors related to prefabricated buildings in China, and the results indicated that the risks of prefabricated buildings are caused by incomplete decomposition system, low plant management level, imperfect quality assurance system, and to-be-improved environmental benefits (Wang et al. 2019). Existing studies have indicated that prefabricated buildings are a kind of architectural model with high cost and scientific and technological level. Prefabricated buildings have remarkable economic, environmental, social, and safety benefits. Most studies on prefabricated buildings have analysed and evaluated their quality and cost. Some scholars have investigated the environmental benefits of prefabricated buildings, and few studies have comprehensively evaluated the angles of society and safety. Some case studies have ignored the factors influencing the environmental performance of prefabricated buildings and the specific solutions. Therefore, the environmental performance of prefabricated buildings was analysed and evaluated in this study. Community A in Zhengzhou City, Henan Province was used as the study object. Analytic hierarchy process (AHP) was used to assign weight values for various indicators of prefabricated buildings, followed by an analysis of factors influencing environmental performance of prefabricated buildings. The results of this study will serve as reference for standardizing the market of prefabricated buildings.

MODEL PROFILE AND INDEX CONSTRUCTION

AHP

AHP, which is proposed by an American operational research expert T. L. Saaty, is an analytical method combining qualitative analysis and quantitative research. AHP has systematic and hierarchical characteristics with high practicability and effectiveness for complex decision problems by modelling and quantifying the decision-making process of a decision maker of a complex system.

Construction of a hierarchical structure model: Problems are analysed with a priori knowledge and data, and the factors influencing them and their mutual relations are established. The factors are decomposed into several layers based on their property, and the factors at the same layer are subjected to the factors in a previous layer or a layer that impacts them. The factors can dominate the factors in the previous layer or be influenced by them. The top layer is the target layer, that is the general objective that must be reached by AHP. The bottom layer contains measures or schemes used to solve the problem. The middle layer is the criterion layer that includes intermediate processes, such as adopted rules to realize a preset goal.

Construction of paired comparison matrix: A comparison matrix is constructed through paired comparison and 1-9

Table 1: Comparison matrix.

	B1	***B2***	**…**	**…**	***Bn***
B1	b11	b12	…	…	b1n
B2	b21	b22	…	…	b2n
…	…	…	…	…	…
…	…	…	…	…	…
Bn	bn1	bn2	…	…	bnn

scale until the bottom layer is reached on the basis of related data, expert opinions, and analyser experience by starting from the middle layer of the hierarchical structure model to determine the relative importance of factors at the same layer that are subject to each factor at the previous layer. The paired comparison matrix is shown in Table 1.

As shown in Table 1, the corresponding relation between the b_{ij} value in the matrix and the relative importance of the compared factor is presented as follows: B_i is as important as B_j because $b_{ij} = 1$ and $b_{ji} = 1$; B_i is slightly more important than B_j because b_{ij}=3 and $b_{ji} = 1/3$; B_j is more important than B_j because $b_{ij} = 5$ and $b_{ji} = 1/5$; B_j is more important than B_j because $b_{ij} = 7$ and $b_{ji} = 1/7$; B_j is more important than B_j because B_j and $b_{ji} = 1/9$.

Weight calculation and consistency test: The maximum characteristic root and its eigenvector are calculated using the comparison matrix of factors. Consistency index (*C.I.*), random consistency (*R.I.*), and consistency ratio (*C.R.*) are used to perform the consistency test. $C.I. = \frac{\lambda \max - n}{n-1}$, where *C.I.* denotes the deviation degree of the comparison matrix through crash consistency. *R.I.* is a given constant that changes with the order number of the comparison matrix. $C.R. = \frac{C.I.}{R.I.}$. The comparison matrix has acceptable consistency, and the eigenvector (normalized) is the weight value when $C.R. < 0.10$. Otherwise, the judgment matrix should be adjusted and corrected to satisfy the consistency requirement.

Synthetic weights and ranking: The weight vectors in all layers are calculated, and the weights of factors are synthesized and ranked. The weight value of each evaluation index relative to the overall objective is expressed as $w_j = l_j \prod_{j=1}^{k} a_{ij}$, and $i = 1, 2, ..., n,$ where l_j is the weight value obtained by evaluation index v_i in hierarchical single sorting at the bottom layer, k is the number of ancestors used to evaluate index v_i in the target tree, a_{ij} is the weight value of ancestor j of index v_i in hierarchical single sorting, and $a_{i1} = 1$ is the root node.

Index Construction

Resource consumption: Material and resource consumption during building construction mainly include water, rebar, and template consumption. The material expenses in building construction account for approximately 70% of the total construction and installation costs. The generation of prefabricated buildings has provided a new idea to reduce the resource consumption in the construction industry.

Energy consumption: The total energy consumption during building construction, operation, and use refers to the total energy quantity consumed in the usage of buildings, including daily use of heating, air conditioning, and illuminating lamps. Related energy-saving designs can be combined with the standardized design of prefabricated buildings to reduce energy consumption.

Waste discharge: The total waste discharge generated during building construction, recycling, and demolition specifically includes solid building wastes, waste gases, and wastewater.

Dust pollution: Dust pollution is generated during building construction. The dust pollution in the current construction industry of China must be solved to improve air quality and protect and enhance the atmospheric environment.

Noise pollution: Harmful noise pollution is generated by large-scale mechanical equipment during building construction. During the entire building construction, the noise pollution generated by the construction of a major structure has a great impact on the surrounding environment. Therefore, the noises generated by concrete pump truck, vibrating equipment, electric generator, and electric saw, which are used in the major structure construction, are all higher than the limiting noise value in the environment.

EMPIRICAL ANALYSIS

A survey questionnaire method was adopted based on the evaluation model of environmental performance of prefabricated buildings to analyse the index weights. The questionnaires were mainly provided to the relevant technical personnel of prefabricated buildings in Community A in Zhengzhou City, Henan Province and technology R & D personnel and constructors of enterprises constructing prefabricated buildings. A total of 1,032 questionnaires were distributed. Invalid questionnaires and those with incomplete information were excluded from the study. The valid questionnaires (876) obtained an effective rate of 84.9%, indicating the validity of the survey. The judgment matrix of index systems at all levels is shown in Table 2.

1. Calculation of importance ranking

$\overline{W_{B_i}} = \sum_{1}^{n} \frac{b_{ij}}{\sum_{1}^{n} b_{ij}} (i, j = 1,2,...,n)$, where

$(\overline{W_{B_1}}, \overline{W_{B_2}}, \overline{W_{B_3}}, \overline{W_{B_4}}, \overline{W_{B_5}}) = (0.55, 0.81, 1.96, 0.82, 0.86)$.

Vector $\overline{W_A} = (\overline{W_{B_1}}, \overline{W_{B_2}}, \overline{W_{B_3}}, \overline{W_{B_4}}, \overline{W_{B_5}})$ is normalized to obtain eigenvector W_A = (0.11, 0.16, 0.40, 0.16, 0.17), which yields:

.

Table 2: Judgment matrix of environmental benefits.

Target layer A	*Resource consumption B1*	*Energy consumption B2*	*Waste discharge B3*	*Dust pollution B4*	*Noise pollution B5*
Resource consumption B1	1	1/2	1/3	1/2	1
Energy consumption B2	2	1	1/2	1	1/2
Waste discharge B3	3	2	1	3	3
Dust pollution B4	2	1	1/3	1	1
Noise pollution B5	1	2	1/3	1	1

$$BW_A = \begin{pmatrix} 1 & \frac{1}{2} & \frac{1}{3} & \frac{1}{2} & 1 \\ 2 & 1 & \frac{1}{2} & 1 & \frac{1}{2} \\ 3 & 2 & 1 & 3 & 3 \\ 2 & 1 & \frac{1}{3} & 1 & 1 \\ 1 & 2 & \frac{1}{3} & 1 & 1 \end{pmatrix} \bullet \begin{pmatrix} 0.11 \\ 0.16 \\ 0.40 \\ 0.16 \\ 0.17 \end{pmatrix} = \begin{pmatrix} 0.576 \\ 0.828 \\ 2.053 \\ 0.849 \\ 0.899 \end{pmatrix}$$

The maximum characteristic root of the matrix is $\lambda_{\max} = \sum_{1}^{n} \frac{(BW_A)_i}{nW_i}$.

2. Consistency test

$C.I. = 0.049$ is obtained using $C.I. = \frac{\lambda_{\max} - n}{n-1}$ of the matrix. Random consistency ratio is $C.R. = \frac{C.I.}{R.I.}$, where $R.I. = 1.24$ under a five-order matrix, and $C.R. = 0.044 < 0.10$, indicating that the judgment matrix has satisfactory consistency. The weights of five influencing factors are listed in Table 3.

As shown in Table 3, the main environmental pollution factor of prefabricated buildings is waste discharge, accounting for 40%. The main problem existing in the current prefabricated buildings is the connection between the prefabricated portion and cast-in-place structure node because of the lack of fundamental studies on prefabricated buildings in China. In the broad application of prefabricated concrete shear wall structures, the effective occlusal force of sleeve grouting connection remains unclear in practical engineering construction. The longitudinal bars on the wall body are mainly connected through sleeve grouting, and the connection of concrete-reinforced sandwich panels is influenced by many external factors, such as stress bearing, endurance, and expansion under heating and contraction under cold conditions. Thus, a complete construction scheme has not been formed for node connection. Therefore, a large quantity of waste discharge is generated in the construction of prefabricated buildings.

The secondary factor influencing environmental pollution of prefabricated buildings is noise pollution. The prefabricated concrete structures used in housing construction should be completed in a plant without requiring additional workers, and these prefabricated concrete structures should be spliced. Therefore, noise pollution is mainly generated in the construction site. Night-time construction is absolutely forbidden in the building field, and noisy construction is not allowed at midday break in residential areas. The punishment imposed on building enterprises violating the rules in noise pollution during building construction process is heavy, forcing them to optimize their designs and construction schemes and immediately complete the noisy construction in their plants.

In the aspects of energy consumption and dust pollution, the transportation of prefabricated parts is expensive. A large quantity of manpower, transportation, and moving workload are needed from raw materials to the completion of major structure. Prefabricated parts in the construction site are directly transported to the workbench for on-site assembly, and cooperation with cast-in-place after parts are produced on the plant production line in the plant is maintained to reach the construction intensity. Therefore, the energy consumption generated in the transportation and loading and unloading processes is the main factor causing environmental pollution of prefabricated buildings. Meanwhile, beams, plates, and columns of building structures in the construction site is directly manufactured in the plant production line and transported to the construction site, thereby generating dust pollution.

Table 3: Weights of environmental pollution factors of prefabricated buildings.

Index	***Resource consumption***	***Energy consumption***	***Waste discharge***	***Dust pollution***	***Noise pollution***
Weight	0.11	0.16	0.40	0.16	0.17

POLICY SUGGESTIONS

Promoting the Development of Prefabricated Buildings and Reducing Their Environmental Pollution

The proportion occupied by prefabricated concrete buildings in the industrial production technology should be enhanced, and technical and economic policies conforming to the construction features of prefabricated concrete buildings should be provided. National policies should be partial to links, such as approval and initiation of projects, planning, and construction, the supporting force of financial funds should be enlarged, and the research and application of crucial technologies should be supported. Local governments should reinforce their policy support and implement supporting policies, including area calculation, area reward, financial fund reward, forward sale of houses, and scientific research. Following the development trend of prefabricated buildings, governments at all levels in China should guide government investment projects, newly built public rental and settlement houses for shantytown transportation to implement prefabricated buildings. Under the support of governmental preferential policies, additional enterprises will be attracted to join the development team of prefabricated buildings.

Build A Standard System for Prefabricated Buildings and Promote Their Environmental Standard

The building goals should be understood and the solving of actual system problems of prefabricated buildings should be used as the criterion to build a standard system for prefabricated concrete buildings. A supporting system should be built, and the integrated industrialization of prefabricated buildings, including the entire set of systematic and diversified standard systems for prefabricated concrete buildings from design, R & D, and member production to on-site installation, should be realized. The standard system, node design, and standard schematic handbook of prefabricated concrete structures must be compiled and completed in designing a standard system. Appropriate prefabricated concrete buildings should be selected based on different conditions to meet the concrete requirements of some special areas, such as high seismic intensity, collapsible loess, and some western underdeveloped areas. Special prefabricated structure systems and construction technologies should be investigated for special areas. Should focus on investigating the construction precision, separation system, high-efficiency node, and technology implementation of prefabricated concrete buildings.

Expand the Application Scope of Prefabricated Concrete Buildings and Encourage Environmental Technology Innovation of Buildings

The government should encourage the use of prefabricated concrete buildings. We should actively implement prefabricated concrete buildings in public buildings, such as medical, cultural, sports, and commercial buildings. The government should invest on constructing prefabricated concrete buildings. The construction of prefabricated concrete buildings should be considered a key project plan in urban construction. The management reform should be accelerated, and the original cast-in-place construction mode should be transformed into the mechanical hoisting mode. Building members should be spliced in the plant assembly to reduce the wet construction workload. The training of constructors should be orderly implemented. Workers should be transformed from laborers to technology-based employees. The certification work of corresponding industrial workers should be strengthened to realize production efficiency improvement under the precondition of guaranteed construction quality, thereby reducing the cost and labour intensity.

Cultivate Prefabricated Building-Based Enterprises and Strengthen Environmental Governance on Construction Sites

Although supported by national policies, prefabricated concrete buildings should be encouraged to set as typical examples. We should enlarge the input of advanced construction technologies and production equipment and improve the production quality of related components of prefabricated concrete buildings through R & D of new products and new materials in this field. The construction technology and construction facilities should be correspondingly improved. Plants for the prefabrication of small members can be constructed in the construction sites, thereby realizing the member production in the production line of the construction site, followed by assembly after the intensity is reached. This process can remarkably reduce transportation cost and accelerate the transformation of construction workers, thereby cooperating with flow construction and improving construction speed. The prefabricated parts in the construction site are directly transported to the workbench for on-site assembly, and cooperation with cast-in-place after parts produced in the plant production line are maintained to reach the construction intensity, thereby reducing the transportation and loading and unloading costs to a great extent. Beams, plates, and columns of building structures in the construction site are directly manufactured in the plant production line and transported in the construction site, thereby reducing construction speed and cost. Meanwhile, corresponding standards, such as manufacturing standards of prefabricated parts, should be completed.

CONCLUSION

The rapid economic development in China cannot be separated from the support of building infrastructures, and limited urban resources should be utilized to provide a large social value. However, unreasonable occupation and utilization of land resources, destruction of ground vegetation, flowing dust caused by earth excavations, and heavy construction noise have led to severe environmental pollution. Prefabricated buildings can realize continuous construction, effectively reduce cost and energy, protect the environment, and reach the goal of green construction through design diversification, function modernization, manufacturing standardization, and construction assembly. In this study, Community A in Zhengzhou City, Henan Province was used as the study area, and AHP was utilized to measure the factor weights influencing the environmental performance of prefabricated buildings. Policy suggestions were proposed to improve their environmental performance. The study results indicate prefabricated buildings have remarkable economic, environmental, social, and safety benefits. The primary factor of prefabricated buildings causing environmental pollution is waste discharge, accounting for 40%, followed by noise pollution, energy consumption, and dust pollution based on the measurement results of Community A in Zhengzhou City. Policy suggestions to improve the environmental performance of prefabricated buildings are proposed as follows: promote the development of prefabricated buildings and reduce their environmental pollution, build a standard system for prefabricated buildings and enhance their environmental standard, expand the application scope of prefabricated concrete and encourage the environmental technology innovation of buildings, cultivate prefabricated building-based enterprises, and strengthen the environmental governance in construction sites. Continuous in-depth study should be conducted on the aspects of whole-life-cycle environmental performance evaluation of prefabricated buildings, comparative analysis of environmental benefits between prefabricated and traditional cast-in-place buildings, and environmental performance and benefit testing of prefabricated buildings.

ACKNOWLEDGEMENT

This work was supported by the Foundation of Henan Educational Committee (20A560004), Foundation of Henan Science and Technology Project (182102311086), and Foundation for University Key Teacher (990/G2019001, YCJXSJSDTR201801).

REFERENCES

Agren, R. and Wing, R.D. 2014. Five moments in the history of industrialized building. Construction Management and Economics, 32(1-2): 7-15.

Altes, W.K.K. 2005. The capacity of local government and continuing the decentralized urban regeneration policies in the Netherlands. Journal of Housing and the Built Environment, 20(3): 287.

Bari, N.A.A., Abdullah, N.A., Yusuff, R., Ismail, N. and Jaapar, A. 2012. Environmental awareness and benefits of industrialized building systems (IBS). Procedia-Social and Behavioral Sciences, 50: 392-404.

Begum, R.A., Satari, S.K. and Pereira, J.J. 2010. Waste generation and recycling: Comparison of conventional and industrialized building systems. American Journal of Environmental Sciences, 6(4): 383.

Chang, Y., Li, X., Masanet, E., Zhang, L., Huang, Z. and Ries, R. 2018. Unlocking the green opportunity for prefabricated buildings and construction in China. Resources, Conservation and Recycling, 139: 259-261.

Hong, J., Shen, G.Q., Mao, C., Li, Z. and Li, K. 2016. Life-cycle energy analysis of prefabricated building components: An input-output-based hybrid model. Journal of Cleaner Production, 112: 2198-2207.

Jaillon, L. and Poon, C.S. 2009. The evolution of prefabricated residential building systems in Hong Kong: A review of the public and the private sector. Automation in Construction, 18(3): 239-248.

Lindblad, F. 2019. A comparative study of the environmental impact from transportation of prefabricated building elements using wood or concrete. International Journal of Engineering and Technology, 11(3): 154-161.

Li, R., Wang, M. and Zhu, J. 2019. indoor thermal environment monitoring and evaluation of double-deck prefabricated house in central china-taking Zhengzhou area as an example. Energy Procedia, 158: 2812-2819.

Mohamad, M.I., Nekooie, M.A., Taherkhani, R., Saleh, A.L. and Mansur, S.A. 2012. Exploring the potential of using industrialized building system for floating urbanization by SWOT analysis. Journal of Applied Sciences (Faisalabad), 12(5): 486-491.

Navaratnam, S., Ngo, T., Gunawardena, T. and Henderson, D. 2019. Performance review of prefabricated building systems and future research in Australia. Buildings, 9(2): 38.

Silva, P.C.P., Almeida, M., Bragança, L. and Mesquita, V. 2013. Development of prefabricated retrofit module towards nearly zero energy buildings. Energy and Buildings, 56: 115-125.

Tam, C.M., Tam, V.W.Y., Chan, J.K.W. and Ng, W.C.Y. 2005. Use of prefabrication to minimize construction waste - A case study approach. International Journal of Construction Management, 5(1): 91-101.

Wang, Z.L., Shen, H.C. and Zuo, J. 2019. Risks in prefabricated buildings in China: Importance-performance analysis approach. Sustainability, 11(12): 3450.

Yashiro, T. 2014. Conceptual framework of the evolution and transformation of the idea of the industrialization of building in Japan. Construction Management and Economics, 32(1-2): 16-39.

Nature Environment and Pollution Technology
An International Quarterly Scientific Journal

p-ISSN: 0972-6268
e-ISSN: 2395-3454

Vol. 19 | No. 1 | pp. 229-236 | 2020

Original Research Paper | Open Access

LSTM-based Air Quality Predicted Model for Large Cities in China

Shuyue Zhang*, Minfeng Lin*, Xiuguo Zou*†, Steven Su, Wentian Zhang**, Xuhui Zhang* and Zijie Guo***
*College of Engineering, Nanjing Agricultural University, Nanjing, Jiangsu, 210031, China
**Faculty of Engineering and Information Technology, University of Technology Sydney, NSW 2007, Australia
†Corresponding author: Xiuguo Zou

Nat. Env. & Poll. Tech.
Website: www.neptjournal.com

Received: 29-04-2019
Accepted: 02-07-2019

Key Words:
Air Quality
LSTM model
$PM_{2.5}$

ABSTRACT

In this paper, the LSTM model is used to predict the PM2.5 concentrations in five representative Chinese cities with the GDP exceeding 1 trillion Yuan, including Beijing, Chengdu, Shanghai, Shenzhen and Wuhan. The $PM_{2.5}$ concentration data in 2015-2017 are selected for training, and the results are optimized to achieve an efficient solution by adjusting the parameters. Based on the optimized solution, a test is carried out to predict the $PM_{2.5}$ concentration in 2018, and the results are compared with the real value obtained from the monitoring centre. According to the comparison results, the correlation coefficient of Wuhan and Chengdu is 0.86724 and 0.80070, which are the highest in these five cities. While the correlation coefficient of Shenzhen and Shanghai, are 0.78225, 0.72147, Beijing, as the capital city of China achieved the lowest correlation coefficient which is 0.64118. The LSTM-based predictive model has relatively good reliability and transferability. More effective predictive results can be achieved by implementing deep learning to analyse PM2.5 concentration.

INTRODUCTION

Due to the speeding up of the industrialization, environmental pollution issues have rapidly escalated since the 20th century. Particularly, the air pollution caused by $PM_{2.5}$ becomes more and more prominent. According to the findings by research scholars, $PM_{2.5}$, compared with other pollutants, contains more substances that damage human health, especially for the respiratory system. Moreover, $PM_{2.5}$ also has a severe effect on the visibility of atmospheric, and climate change. Therefore, $PM_{2.5}$ becomes a key research topic in the field of environmental science. Based on the assessment of U.S. Environmental Protection Agency (EPA), the economic loss caused by death accounted for 89% of the total loss caused by the health losses related to $PM_{2.5}$ pollution (Evans et al. 2019). In China, considering the research methods of $PM_{2.5}$ concentration is restricted by many factors (e.g. the vast territories, complex topographic changes, variable meteorological conditions, and large populations, etc.), general research methods like projection pursuit regression are not suited to solve $PM_{2.5}$ issues (Liu et al. 2019). Therefore, the methods of multivariate statistical analysis and traditional machine learning have been chosen by most scholars. In 2016, Fu et al. (2016) proposed five factors contributing to the smog pollution in Jiangsu Province based on the data collected from 2000 to 2014. By using the multiple linear regression model, a quantitative measure of the influence degree and significance level of these factors are studied in this paper. This paper also researched the specific measures for smog management from factors with significant influence. In the same year, He et al. (2016) analysed the spatial distribution features of $PM_{2.5}$ concentration in 2014 in Jiangsu Province using Kriging interpolation method. A grey correlation model is used to calculate the degree of association between $PM_{2.5}$ concentration and influence factors and shown its superiority compared with the other methods. Therefore, the method of multivariate statistical analysis plays an important role in $PM_{2.5}$ concentration analysis. However, it is not possible to use this method to obtain a good fitting model for air pollution prediction and to cope with sudden environmental changes. As a result, it has been mostly used in the auxiliary study of atmospheric pollution in recent years.

George et al. (2000) used the traditional machine learning method Bayesian Maximum Entropy (BME) mapping to study the influence factors of $PM_{2.5}$ concentration. Wang et al. (2009) explored a new urban air pollution prediction model based on Bayesian network, which is mainly designed for the middle and small cities in China. Zhou et al. (2004) proposed a BP network model for predicting air pollution indexes and researched comparative prediction. According to the verification result, the predictive model generated based on the BP method can provide an accurate prediction of mutational trends and is better than the stepwise regression model. Bai et al. (2013) researched the ten years (2001 to 2010) surface meteorological observation data and air

pollution indexes in Beijing using the BP neural network model. In this paper, the air pollution index predictive model which trained in different seasons shows the superior performance of the BP model.

Relatively high accuracy can be obtained in using the machine learning method to predict atmospheric pollutant concentration, but how to combine the various attributes of nodes more effectively and achieve the better performance is that we need to do. The traditional machine learning methods have very poor transferability and limited application. Since 2012, the deep learning method has attracted considerable attention all over the world and stepped into a booming development stage. Deep learning has given rise to many frameworks which can be applied to various practical problems. Besides, the performance of the deep learning model is rapidly improved and its accuracy in dig data prediction is far beyond other models. The algorithms for deep learning are regenerated constantly, therefore the problems in $PM_{2.5}$ concentration analysis can be well solved with the development of the more effective models. Yin et al. (2015) used the deep learning framework DBN to establish an air pollution predictive model, through which they found out that the predictability of this model is higher than other classical predictive models under the two evaluation indexes set by them. Sun (2018) predicted the air quality indexes using the deep belief network predictive model, where the accuracy of predicted results is 91.4%, which is 32.2% and 25.7% higher than that of the integrated auto-regressive moving average model and BP neural network model. The LSTM model has been widely used by scholars considering its long-term and short-term memory function and forgetting mechanism. Li et al. (2018) designed an experiment based on the power plant load data and found out that the predicted effect of LSTM recurrent neural network algorithm based on Tensor Flow is better than that of the traditional machine learning algorithms. The model showed good robustness with the increasing number of data. An et al. (2018) established an LSTM model and analysed the degree of fitting and accuracy of the model, providing a reference for tilapia breeding and cultivation. Besides, LSTM also has good effects on practical problems such as short-term traffic flow (Qiao et al. 2017), stock price trend (Liu 2016), ship track (Quan et al. 2018) and other data trends that are difficult to determine.

In this paper, the original features of $PM_{2.5}$ concentration data can be well turned into a new feature space by using the LSTM algorithm. This method can obtain a more hierarchical feature representation through active learning, which can improve the predicted performance. Compared with the traditional methods, this method is paid more attention to the change rules of $PM_{2.5}$ concentration. In addition, according to the results obtained with other existing air pollutant predicted methods, the appropriate application range and advantages and disadvantages of models could be learned through active learning.

MATERIALS AND METHODS

Study Objects

There are 14 cities with GDP reaching 1000 billion Yuan in China, and all these cities are in the southeast of "Hu Line", which makes "Hu Line" become the dividing line of urbanization level to a certain extent. "Hu Line" is a boundary dividing the population density in China by "Aihui-Tengchong" Line (from Heihe City of Heilongjiang Province to Tengchong City of Yunnan Province) proposed by Chinese geographer Huanyong Hu in 1935 (Guo et al. 2016). Pursuant to the fifth national population census in 2000, the calculation by using ArcGIS software shows that the south-eastern region accounts for 43.8% of the total national area and the population accounts for 94.1% according to the "Hu Line". It suggests great significance in economic production, social development, and scientific research.

The spatial distribution of the 14 cities is shown in Fig. 1, where the city locations are represented by blue dots, and the straight line represents "Hu Line". The $PM_{2.5}$ concentration data at 3-9 monitoring points of each city has been recorded.

Five representative cities, including Shanghai, Shenzhen, Chengdu, Beijing, and Wuhan, are selected from these 14 cities as the study objects for air quality analysis. The selected cities are separate in the East of China, the South of China, the West of China, the North of China, and Central China respectively. All of them are in the southeast of "Hu Line, and located in East China, South China, West China, North China, and Central China respectively.

Data Acquisition

China National Environmental Monitoring Centre releases the monitoring concentration data of $PM_{2.5}$ and other standard pollutants every hour in Shanghai, Shenzhen, Chengdu, Beijing and Wuhan. The $PM_{2.5}$ concentration data at 3-9 monitoring points of each city has been recorded every one hour. We have downloaded the data of each point from January 2015 to December 2018. The statistical analysis results of $PM_{2.5}$ data are shown in Table 1.

There are some unavoidable errors in the large sample test. Improving data quality is an effective way to reduce errors. For this reason, null values in the measurement are eliminated. The table in the above shows the result after abnormal data is eliminated. From the statistical analysis of $PM_{2.5}$ concentration data combined with the urban spatial distribution map, it can be found that while Beijing has

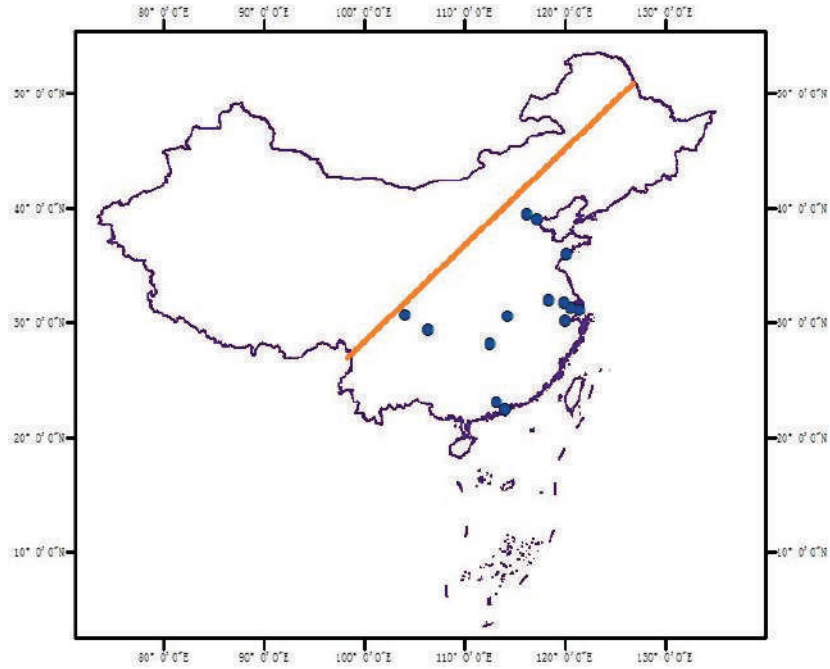

Fig. 1: The spatial distribution of the 14 cities with "Hu Line".

Table 1: The statistical analysis results of $PM_{2.5}$ data.

City	Data Volume	Mean value	Standard Deviation	Maximum value	Minimum value
Beijing	339119	63.27370	56.62778	457.97570	4.32110
Shanghai	287847	41.47401	25.61609	204.22689	5.64216
Wuhan	297741	57.22271	35.14301	280.37768	8.24057
Shenzhen	358087	27.70851	14.34911	100.72137	6.56870
Chengdu	260548	55.46151	37.24526	290.30208	7.26984

the largest $PM_{2.5}$ mean value, the smallest $PM_{2.5}$ mean value is recorded in Shenzhen. The $PM_{2.5}$ concentration in north-western China is higher than that in the southeast.

Data Processing Method

Data normalization: Data normalization is a processing method of transforming dimensional data into non-dimensional data. In order to improve the rate of convergence and the accuracy of the models, the data were normalized.

The purpose of data normalization is to concentrate all values into the interval of (0,1). The commonly-used data normalization methods are linear function normalization, and 0 mean standardization. The 0 mean standardization method is usually used when the data distribution approximates to Gaussian distribution. It is obvious that the data in the study does not meet this condition. Therefore, we adopted linear function normalization. The normalization equation is shown in Equation (1).

$$X_{norm} = \frac{X}{X_{\max} - X_{\min}} \quad \ldots(1)$$

Where, X_{norm} represents normalized data, X represents original data, X_{max} represents the maximum in original data, and X_{min} represents the minimum in original data.

LSTM model: The LSTM model, namely long short-term memory model, was adopted in the study. In LSTM, a node like the valve is added to the RNN structure. There are three kinds of valves: forgetting valve, input valve, and output valve. According to the on-off status of these valves, it can be determined that whether the network's memory state has reached the threshold in the output results of the layer and then is added to the calculation of the layer (Graves et al. 2012). RNN is still a neural network. The recurrent neural network can be sued to find the sequence correlation between samples. As a result, it is often used for modelling of

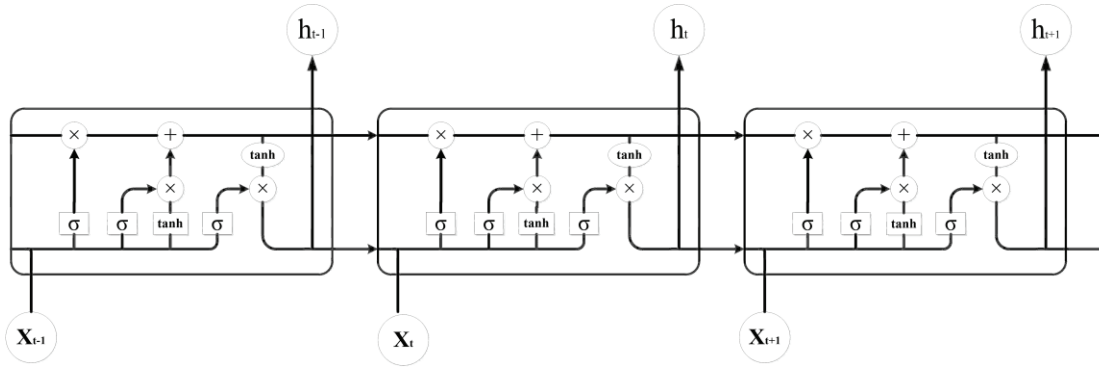

Fig. 2: LSTM network structure.

sequence data (Lipton et al. 2015).

The calculation equations of the recurrent neural network are shown in Equation (2) and Equation (3).

$$O_t = s(V \cdot S_t) \quad \ldots(2)$$

$$S_t = f(U \cdot X_t + W \cdot S_{t-1}) \quad \ldots(3)$$

Where, O represents the value of the output layer, and S represents the value of the hidden layer. The weight matrix of the hidden layer to the output layer is represented by V. The weight matrix of input layer to the hidden layer is represented by U. W is the weight matrix with the last value as this time input of the hidden layer.

$f()$ function is an activation function which can filter out unimportant information. The commonly-used activation functions are sigmoid function and tanh function, and the function expression is shown in Equation (4) and Equation (5).

$$f(z) = \frac{1}{1+\exp(-z)} \quad \ldots(4)$$

$$f(z) = \frac{e^z - e^{-z}}{e^z + e^{-z}} \quad \ldots(5)$$

This study uses tanh as the activation function, and the LSTM network structure is shown in Fig. 2.

Where, x_t and h_t represent the inputs and outputs of the current cyclic neural network, respectively.

The calculation of the input gate during forwarding propagation is according to Equation (6); Equation (7) shows the calculation of the forgetting gate, and the output gate is based on Equation (8).

$$a_l^t = \sum_{i=1}^{I} w_{il} x_i^t + \sum_{h=1}^{H} w_{hl} b_h^{t-1} + \sum_{c=1}^{C} w_{cl} s_c^{t-1} \quad \ldots(6)$$

$$a_\phi^t = \sum_{i=1}^{I} w_{i\phi} x_i^t + \sum_{h=1}^{H} w_{h\phi} b_h^{t-1} + \sum_{c=1}^{C} w_{c\phi} s_c^{t-1} \quad \ldots(7)$$

$$a_w^t = \sum_{i=1}^{I} w_{iw} x_i^t + \sum_{h=1}^{H} w_{hw} b_h^{t-1} + \sum_{c=1}^{C} w_{cw} s_c^{t-1} \quad \ldots(8)$$

Where, w_{ij} represents the connection weight from nerve cell i to nerve cell j. The input of nerve cells is represented by "a" and their output is indicated by "b". Subscripts l, ϕ and w refer to the input gate, output gate, and forgetting gate respectively. Subscript c refers to the cell. The peephole weights from cell to the input gate, forgetting gate, and output gate are w_{cl}, $w_{c\phi}$, and w_{cw} respectively. s_c refers to the status of cell c. f refers to the activation function of the control gate, and h is the output activation function of the cell.

During back propagation, suppose that:

$$\varepsilon_c^t = \frac{\partial l}{\partial b_c^t} \qquad \varepsilon_s^t = \frac{\partial l}{\partial s_c^t} \quad \ldots(9)$$

Then, the calculation of the output gate is as shown in Equation (10) and the status is shown in Equation (11).

$$\delta_w^t = f'(a_w^t) \sum_{c=1}^{C} h(s_c^t) \varepsilon_c^t \quad \ldots(10)$$

$$\varepsilon_s^t = b_w^t h'(s_c^t) \varepsilon_c^t + b_\phi^{t+1} \varepsilon_s^{t+1} + w_{cl} \delta_l^{t+1} + w_{c\phi} \delta_\phi^{t+1} + w_{cw} \delta_w^t \quad \ldots(11)$$

The Adam algorithm was used for model optimization in this study. The squared-gradient normalized learning rate was used for gradient descent in the Adam algorithm (Kingma 2015). Firstly, a first-order momentum equivalent to the gradient was maintained. Then a momentum equivalent to the squared gradient was maintained. At last, the learning rate was normalized using the squared gradient v, as shown in Equation (12). The update amplitude is gradient m which is shown in Equation (13).

$$v_t = \beta v_{t-1} + (1-\beta) \cdot \nabla Q(w)^2 \quad \ldots(12)$$

$$m_t = \alpha m_{t-1} + (1-\alpha) \cdot \nabla Q(w) \quad \ldots(13)$$

Table 2: Basic Code Framework of LSTM.

Function	Code framework
Model-based category	nn.Module
Establish RNN layers	nn.LSTM (input_size, hidden_size, num_layers)
Establish linear layers	nn.Linear (hidden_size, output_size)
Loss function	torch.nn
Optimization function	torch.optim
Back propagation	optimizer.zero_grad loss.backward optimizer.step

Table 3: Parameter Setting.

Parameter	Parameter value
Training set	The data of 2015-2017
Test set	The data of 2018
Activation function of the hidden layer	Sigmoid
Batch size	3
Input dimension	2
Hidden layer dimension	4
Number of network layers	3
Activation function of the output layer	tanh
Learning rate	0.01

LSTM Algorithm Framework and Parameter Setting

Algorithm framework: The training algorithm of LSTM is a back-propagation algorithm. According to the above LSTM model algorithm, the steps are as follows.

Step 1: Calculate the output value of each nerve cell through forwarding propagation.

Step 2: Calculate the error value of each nerve cell through back-propagation.

Step 3: Calculate the weighted gradient.

In this paper, the Pytorch was applied for all experiments. The Pytorch is a Python-first deep learning framework which can realize acceleration on GPU, with the function of a dynamic neural network. The basic code framework of LSTM algorithm is shown in Table 2.

Parameter setting: We took the 2015-2017 data as a training set for predicting the data of 2018. For details of parameters are set in Table 3.

RESULTS AND DISCUSSION

Model Prediction Results

We predicted based on the above parameters and compared the prediction results of the five cities with the real values in 2018. Besides, we provided a decreasing figure of loss functions in the iteration. The results are shown in Fig. 3-7.

According to Figs. 3-7, the prediction results are very close to the real values and the loss ratio finally outputted by the loss function after 1000 times of iteration is close to 0. It can be seen from the trend of $PM_{2.5}$ concentration in 2018, the data (recorded or something else) for these five cities are the lowest in summer and the highest in winter.

Output Analysis

Hereinbefore, we have obtained a predicted model and outputted the predicted results. Table 4 shows the test results of the predicted values and the real ones.

The coefficient of association between the $PM_{2.5}$ means, standard deviations, the correlation coefficient between real values and predicted values in 2018 of the five cities are given in Table 4. The mean values of the real values and predicted values are approximate. According to the standard deviation, the $PM_{2.5}$ concentration data of Beijing, Chengdu and Wuhan are very discrete. It indicates that there is a large fluctuation

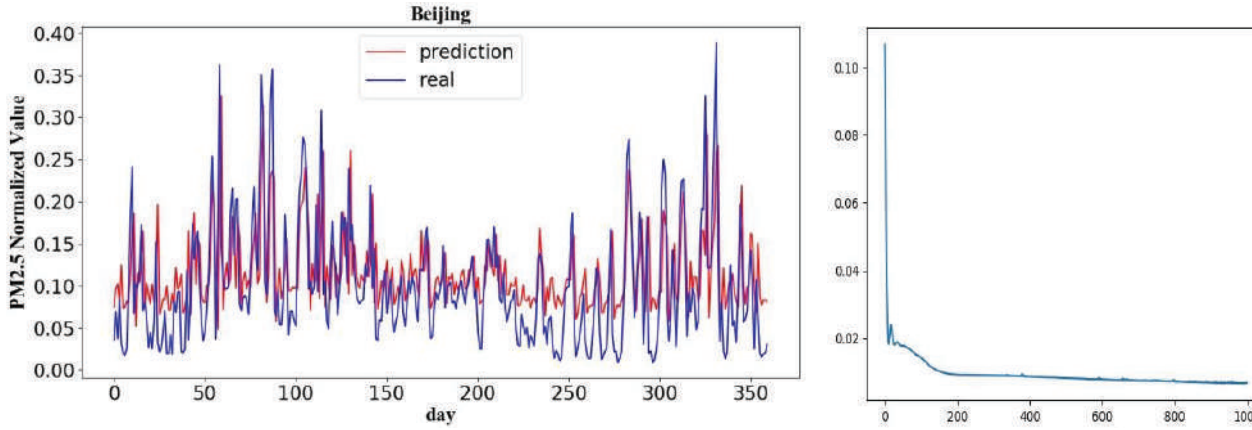

Fig. 3: Model prediction result of Beijing City. (a) Comparison between prediction values and real values (b) Loss rate during iteration.

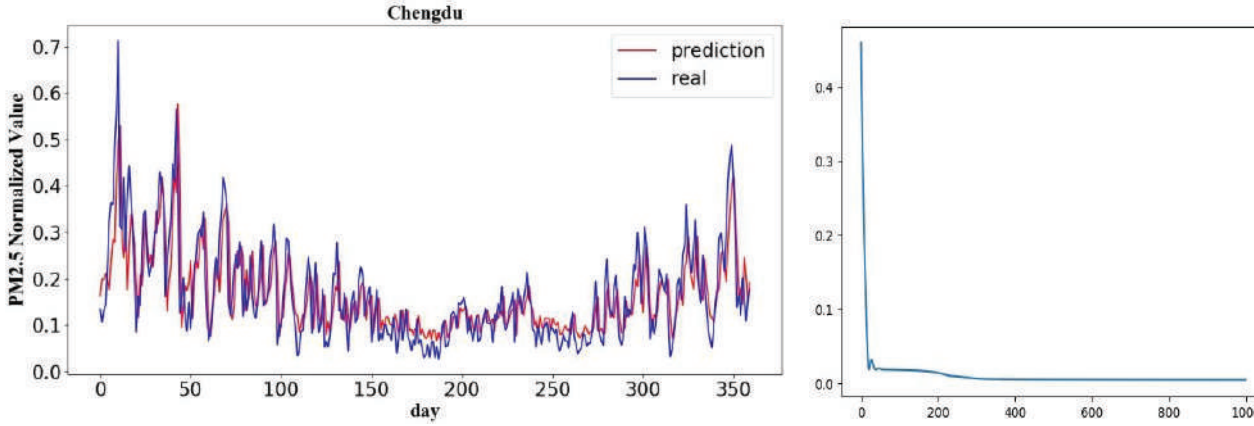

Fig. 4: Model prediction result of Chengdu City. (a) Comparison between prediction values and real values (b) Loss rate during iteration.

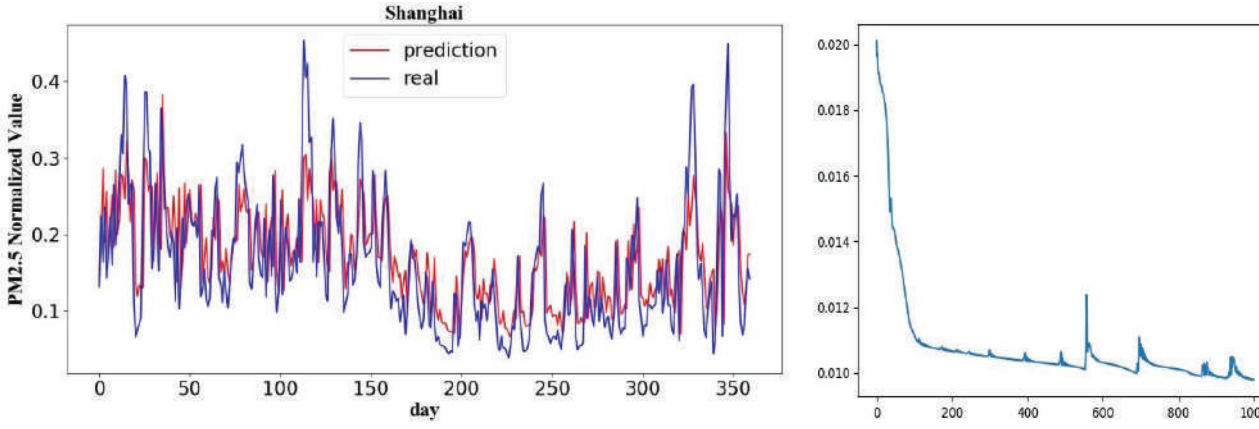

Fig. 5: Model prediction result of Shanghai City. (a) Comparison between prediction values and real values (b)Loss rate during iteration.

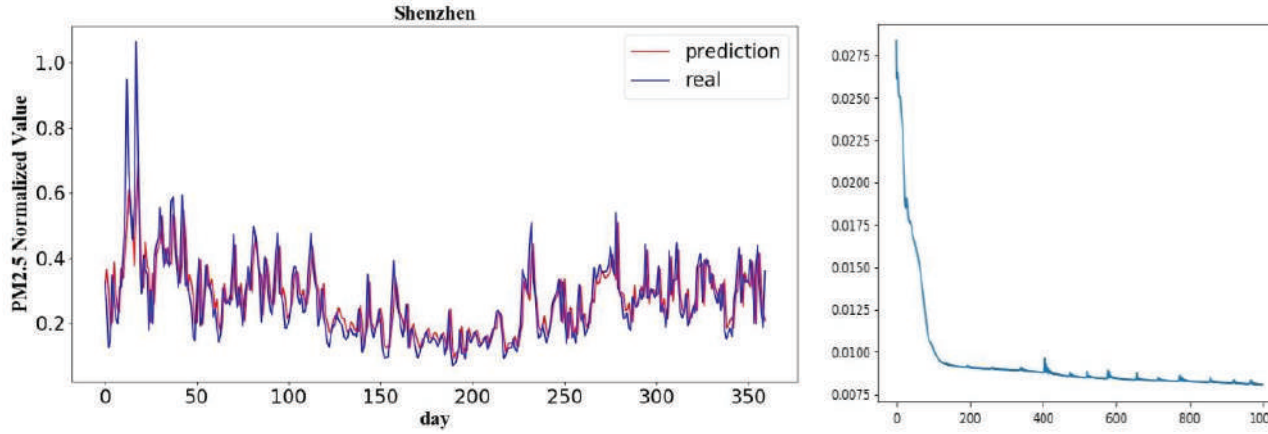

Fig. 6: Model prediction result of Shenzhen City. (a) Comparison between prediction values and real values (b) Loss rate during iteration.

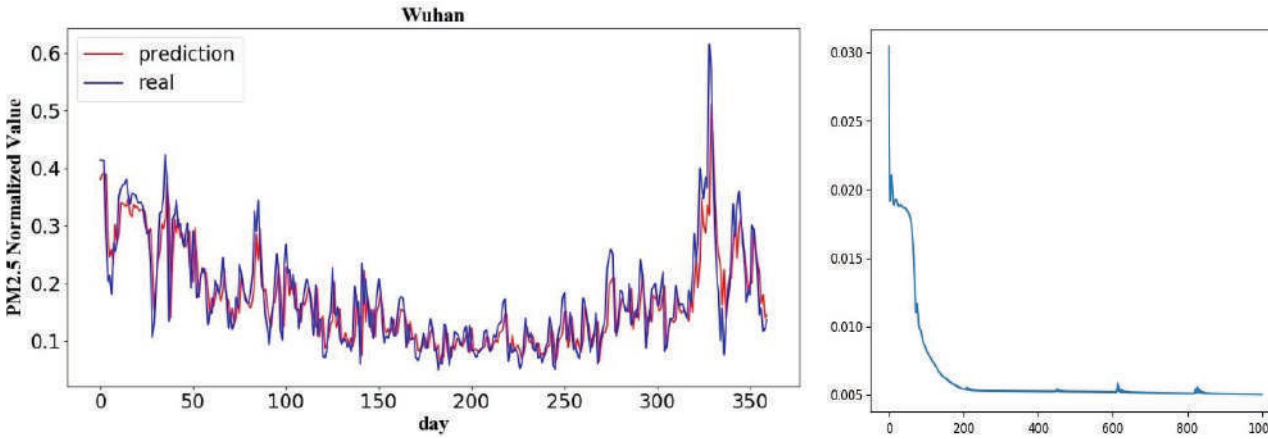

Fig. 7: Model prediction result of Wuhan City. (a) Comparison between prediction values and real values (b) Loss rate during iteration.

in the $PM_{2.5}$ concentration of these three cities. From the coefficient of association, except that the correlation coefficient of Beijing between the real values and predicted ones is 0.64118, the coefficients of the other four have exceeded 0.7, while that of Wuhan reaches 0.86724. This shows a relatively strong association. It also indicates that the trend of predicted values is the same as that of the real ones.

CONCLUSION

In this paper, by using the LSTM model, the $PM_{2.5}$ concentrations in five Chinese cities with GDP reaching 1000 billion Yuan were predicted based on the $PM_{2.5}$ data selected from 2015-2017 Based on the training results, the number of hidden neurons and neural network layers, the learning rate, and other parameters were adjusted. Then, the $PM_{2.5}$ concentration in 2018 was predicted after 1000 times of iteration and compared with the real $PM_{2.5}$ data collected in 2018. According to the comparison results, the real values and predicted values are approximately the same, and the coefficients of association between the real values and predicted ones of all cities are around 0.8. The predicted results have relatively high reliability and universality.

The LSTM model studied in this paper can be used to realize the good predicted of $PM_{2.5}$ concentration data with relatively high fluctuation. The model is applicable to cities with large air quality difference, especially the large cities with rapid industrial development. As an accurate method for predicting urban air quality, the LSTM model can help large cities to reduce the harm of $PM_{2.5}$ pollution to the human body by taking timely measures to predict and control $PM_{2.5}$ pollution.

ACKNOWLEDGEMENTS

This study was supported by the Fundamental Research Funds

Table 4: The test results of the predicted values and the real ones.

City	Real Value Predicted value	Mean value	Standard deviation	Correlation coefficient
Beijing	Real Value	45.43884	31.55345	0.64118
	Predicted value	48.81304	21.91014	
Chengdu	Real Value	47.06011	29.95005	0.80070
	Predicted value	48.50343	24.61025	
Shanghai	Real Value	31.99997	17.01369	0.72147
	Predicted value	33.00228	11.96767	
Shenzhen	Real Value	25.22512	11.71571	0.78225
	Predicted value	25.54528	9.60629	
Wuhan	Real Value	47.94295	24.91919	0.86724
	Predicted value	46.56945	21.82955	

for the Central Universities of China (No. KYTZ201661), China Postdoctoral Science Foundation (No. 2015M571782), and Jiangsu Agricultural Machinery Foundation (No. GXZ14002), Student Research Training Project of College of Engineering, Nanjing, Agricultural University (No. 1830C29). Thanks to Qingyue Open Environmental Data Centre (https://data.epmap.org) for support on Environmental data processing.

REFERENCES

An, F., Yuan, Y., Ma, X. and Shen, N. 2018. Tilapia growth prediction model based on Long Short-term Memory neural network. Journal of Southern Agriculture, 49(10): 2110-2116.

Bai, H., Shen, R., Shi, H. and Dong, Y. 2013. Forecasting model of air pollution index based on BP neural network. Environmental Science & Technology, 36(3): 186-189.

Christakos, G. and Serre, M.L. 2000. BME analysis of spatiotemporal particulate matter distributions in North Carolina. Atmospheric Environment, 34(20): 3393-3406.

Evans, J., van Donkelaar, A., Martin, R.V., Burnett, R., Rainham, D.G., Birkett, N.J. and Krewski, D. 2013. Estimates of global mortality attributable to particulate air pollution using satellite imagery. Environ. Res., 120: 33-42.

Fu, L., Yang, M. and Chen, Y. 2016. Factors influencing $PM_{2.5}$ and the governance strategies in Jiangsu, China. Nature Environment and Pollution Technology, 15(4): 1401-1408.

Graves, A. 2008. Supervised Sequence Labelling with Recurrent Neural Networks. Ph.D. Dissertation.

Guo, H., Wang, X., Wu, B. and Li, X. 2016. Cognizing population density demarcative Line (Hu Huanyong-Line) based on space technology. S&T and Society, 31(12): 1385-1394.

He, X., Lin, Z., Liu, H. and Qi, X. 2016. Analysis of the driving factors of $PM_{2.5}$ in Jiangsu province based on grey correlation model. Acta Geographica Sinica, 71(7): 1119-1129.

Kingma, D.P. and Ba, J.L. 2015. Adam: A method for stochastic optimization. International Conference on Learning Representations, 1-15.

Li, S. 2018. LSTM recurrent neural network short-term power load forecasting based on TensorFlow. Shanghai Energy Conservation, 12: 974-977.

Lipton, Z.C., Berkowitz, J. and Elkan, C. 2015. A critical review of recurrent neural networks for sequence learning. Computer Science, 1-38.

Liu, Q. 2016. Short term stock price forecasting based on fuzzy deep learning network algorithm. Harbin Institute of Technology.

Qiao, S., Sun, R. and Liu, J. 2017. Short-term traffic flow forecast based on deep learning. Journal of Qingdao University (Natural Science Edition), 30(4): 65-69.

Quan, B., Yang, B., Hu, K., Guo, C. and Li, Q. 2018. Prediction model of ship trajectory based on LSTM. Computer Science, 45(11): 126-131.

Sun, M. 2018. Prediction model of air quality index based on optimized deep belief network. China University of Geosciences (Beijing).

Wang, Q., Xia, S., Wan, Y. and Jin, L. 2009. A new idea for urban air pollution forecast. Environmental Science & Technology, 32(3): 195-198.

Yin, W., Zhang, D., Yan, J., Zhang, C., Li, Y. and Rui, X. 2015. Deep learning based air pollutant forecasting with big data. Chinese Journal of Environmental Management, 7(6): 46-52.

Zhou, X., Su, X. and Yuan, M. 2004. Forecast of air pollution index based on BP neural network. Journal of Harbin Institute of Technology, 36(5): 582-585.

Nature Environment and Pollution Technology
An International Quarterly Scientific Journal

p-ISSN: 0972-6268
e-ISSN: 2395-3454

Vol. 19 | No. 1 | pp. 237-244 | 2020

Original Research Paper | Open Access

Changes in the Microbial Succession During Sewage Sludge Composting and its Correlation with Physico-Chemical Properties

Chuang Ma*, Bin Hu*, FU-Yong Liu*, Ai-Hua Gao*, Ming-Bao Wei* and Hong-Zhong Zhang**†**

*Zhengzhou University of Light Industry, Zhengzhou 450001, PR China

**Collaborative Innovation Center of Environmental Pollution Control and Ecological Restoration, Henan Province, Zhengzhou 450001, PR China

*** Zhengzhou Sewage Purifying Co., Ltd., Zhengzhou 450000, PR China

†Corresponding author: Hong-Zhong Zhang

Nat. Env. & Poll. Tech.
Website: www.neptjournal.com

Received: 08-05-2019
Accepted: 22-07-2019

Key Words:
Sewage sludge
Composting
Microbial succession
Physico-chemical properties

ABSTRACT

Sewage sludge composting is a process entailing a continuous succession of microorganisms. To understand the microbial mechanisms involved in sewage sludge composting, we performed an aerobic static composting of sewage sludge and sawdust (ratio = 3:1 m/m) in medium-scale bioreactor systems. The associated changes in physico-chemical parameters (i.e., temperature, organic matter, pH, ammonium nitrogen) were studied parallelly to those in the microbial (i.e., bacteria, fungi, archaea) succession. Additionally, we discussed correlations between these physico-chemical parameters and the microbial communities. The results showed that the pile temperature went through mesophilic phase, thermophilic phase, and cooling phase. The pile temperature reached a maximum of 78.68°C by day 3 and remained above 55°C for more than 6 days, complying with the harmless composting requirements. The organic matter content decreased gradually, the pH increased after a first decrease, and the NH_4^+-N content showed a consistent trend. The dominant bacteria during composting were *Ureibacillus*, *Bacillus*, *Sphaerobacter* and *Thermobifida*, while the dominant fungi were unclassified_f_*Trichocomaceae*, unclassified_d_*Eukaryota*, *Hypocrea* and *Thysanophora*; finally, the dominant archaea were *Methanobrevibacter*, *Methanosaeta*, *Methanobacterium* and unclassified_k_norank. The composting stages were characterized by different microbial compositions. The mesophilic phase presented a relatively uniform proportion of bacterial genera, while the thermophilic and cooling phases were dominated by *Ureibacillus* and *Bacillus*, respectively. The fungus unclassified_f_*Trichocomaceae* played a major role during the mesophilic, thermophilic, and cooling phases, while unclassified_d_*Eukaryota* played a major role during the mesophilic and thermophilic phases. For what concerns the archaea, *Methanobrevibacter* played a major role in the mesophilic, thermophilic, and cooling phases, *Methanosaeta* during the mesophilic and thermophilic phases, and *Methanobacterium* during the thermophilic and cooling phases. Additionally, the bacterium *Ureibacillus* and the archaea *Methanospirillum* were positively correlated with temperature, while the bacteria norank_Pem15, norank_JG30-KF-CM45, and the archaea *Methanosphaera* were negatively correlated with temperature. The fungi *Thysanophora*, unclassified_d_*Eukaryota*, and unclassified_p_*Ascomycota* were negatively correlated with pH. Moreover, the bacterium norank_c_1-20, the fungi *Trichosporon*, norank_o_*Saccharomycetales*, unclassified_o_*Pleosporales,* and the archaea *Methanosaeta*, *Methanomethylovorans* were positively correlated with organic matter. On the other hand, the bacteria *Bacillus*, *Thermobifida*, the fungus unclassified_f_*Trichocomaceae*, and the archaea *Methanobrevibacter* were negatively correlated with organic matter. Finally, the bacteria *Bacillus*, *Thermobifida*, the fungus unclassified_f_*Trichocomaceae*, and the archaea *Methanobrevibac*ter were positively correlated with ammonium nitrogen, while the bacterium norank_c_1-20, the fungi *Trichosporon*, norank_o_*Saccharomycetales*, unclassified_o_*Pleosporales*, and the archaea *Methanosaeta*, *Methanomethylovorans* were negatively correlated with ammonium nitrogen. This paper provides new solid bases to understand changes in microbial composition and their correlation with physico-chemical parameters during sewage sludge composting.

INTRODUCTION

Due to the high moisture content and biodegradability of sewage sludge (SS), its treatment is considered a pressing environmental challenge, especially in developing countries (Onwosi et al. 2017). Aerobic composting is an eco-friendly and inexpensive method to convert SS into a relatively steady humus, which can be used to improve soil structure, fertility, and quality (Han et al. 2019, Yuan et al. 2016). Composting is a biological process, through which aerobic microorganisms consume organic matter (OM) as food and convert it into CO_2 and H_2O, releasing heat (Bernal et al. 2009) and generating stabilized organic compounds (e.g., humic

compounds) (Jalili et al. 2019). Microorganisms (mainly bacteria, fungi, and archaea) play a key role during the SS composting process (Zhao et al. 2019). Bacteria and fungi are both functional communities in this process, although bacteria are more influential, due to their metabolic versatility. Some researchers have tried to evaluate the influence of bacterial, but not of fungal communities, on the composting performance (López-González et al. 2015). Overall, fungi occur in relatively low abundances during composting and their role in the process is considered minor compared to that of bacteria (Bonito et al. 2010); however, fungi tend to dominate during the maturation or mesophilic phase, perhaps due to lignin degradation and to the maturity of sludge composting (Amir et al. 2008). On the other hand, archaea are important participants to the aerobic composting process and play an important role in CH_4 production, although their dynamic change is still not well understood. Hence, the monitoring of bacterial, fungal, and archaea population structure dynamics can provide comprehensive information on the microbial community succession during SS composting.

This paper focuses on several aspects of the SS composting process: 1) dynamic changes in the physico-chemical parameters; 2) dynamic changes in the bacterial, fungal, and archaeal communities; 3) correlations between the physico-chemical parameters and the bacterial, fungal, and archaeal communities. The results of our study contribute to the understanding of microbial mechanisms during SS composting.

MATERIALS AND METHODS

Compost Materials and Environmental Design

Dewatered SS was collected from the Zhengzhou Wulongkou municipal wastewater treatment plant (China). The sawdust used for our experiment consisted of pine wood particles (1-2 mm). The SS and sawdust were used as raw materials and homogenized to obtain a mixture (ratio of 3:1 m/m, fresh weight), for a total weight of 132.5 kg. The initial physico-chemical properties of the raw materials and of the mixture are shown in Table 1.

Table 1: Initial physico-chemical properties of the raw materials and of the mixture.

Parameters	SS	Sawdust	Mixture
pH	8.12	5.55	8.30
Moisture content	80.52%	8.23%	51.34%
Total carbon	28.11%	52.82%	35.79%
Total nitrogen	2.05%	0.41%	3.23%
C/N ratio	13.32	140.30	35.51

Composting System and Sampling

The SS aerobic composting was performed in a medium-scale (400 L) bioreactor, described in detail in one of our previous studies (Du et al. 2019). This study focused on the first fermentation stage of aerobic composting, which usually takes 10-12 days and indicated the microbial metabolic process. The sampling was done on days 1, 3, 5, 7, and 10 (after aerobic fermentation), so to include the composting mesophilic (sample 1d), thermophilic (samples 3d, 5d, 7d), and cooling (sample 10d) phases. Three samples of composting material were obtained from each pile at a depth of ~ 50 cm. Approximately 500 g of material was collected during each sampling and divided into two parts: one part was used for enzyme activity measurements, while the other part was homogenized and kept in a refrigerator at -80°C for subsequent DNA analysis (Du et al. 2019).

The diversity of bacterial, fungal, and archaeal communities during the composting process were calculated based on the microbial DNA extracted from each pile (on days 1, 3, 5, 7, and 10), using a FastDNA® SPIN Kit for Soil (Mpbio, USA) according to the manufacturer's protocols. The DNA was hence purified and its concentration was determined using a NanoDrop 2000 UV-vis spectrophotometer (Thermo Scientific, Wilmington, USA). The V3-V4 hyper variable regions of the bacterial 16S rRNA gene were amplified with primers 338F (ACTCCTACGGGAGGCAGCAG) and 806R (GGACTACHVGGGTWTCTAAT), while the V5-V7 regions of the fungal 18S rRNA gene were amplified with primers SSU0817F (TTAGCATGGAATAATRRAATAGGA) and 1196R (TCTGGACCTGGTGAGTTTCC); finally, the archaeal gene were amplified with primers 524F10extF (5′-TGYCAGCCGCCGCGGTAA-3′) and Arch958RmodR (5′-YCCGGCGTTGAVTCCAATT-3′).

Analysis Methods

The moisture content (MC) of the raw materials and composting mixtures were determined by drying samples at 105°C for 24 h (Tiquia & Tam 1998). The OM content was determined instead by measuring the loss of dry solid mass after ignition at 550°C in a muffle furnace for 24 h (Awasthi et al. 2015). The change in NH_4^+-N content was determined according to the method used by Fang et al. (1999). The pH value was measured at a ratio of 1:5 (wet weight of composting sample/water volume), after shaking equilibration for ~30 min, using a combination pH meter (E-201-C, Lei-ci, Shanghai, China). The total carbon and nitrogen contents were instead detected using a Vario EL elemental analyser (Elemental Vario MICRO, Germany).

RESULTS AND DISCUSSION

Dynamic Changes in Physico-Chemical Parameters During Composting

Temperature: Temperature is one of the most important parameters for the composting process (Zhou 2016), since it reflects the degradation of organic components and is used to evaluate the composting efficiency (Wu et al. 2017). As shown in Fig. 1, the pile experienced three stages: a mesophilic phase, a thermophilic phase, and a cooling phase. Due to the decomposition of degradable components during the mesophilic phase (Guo et al. 2012), the pile temperature rapidly increased to over 50°C by day 2 and reached a maximum of 78.68°C by the day 3 (heating rate = 26.43 °C/day). During the thermophilic phase (i.e., ≥ 50°C), which lasted for 8 days, the temperature remained >55°C for more than 6 days; these high temperatures destroyed the pathogens (Sadef et al. 2014), complying with the harmless composting requirements (United States Environmental Protection Agency, 1994). On day 8 the pile entered the cooling phase, during which temperatures dropped from 65.04°C (day 8) to 41.19°C (day 10), at a rate of 11.9°C/day.

Organic matter (OM): Readily biodegradable OM gets degraded by microorganisms during composting into CO_2 and H_2O, generating heat and promoting the thermophilic phase (Petric et al. 2012), which results in a stable final product. The stability of a compost is determined in relation to the rate of OM decomposition (Xiao et al. 2009). As shown in the Fig. 2a, the OM content decreased continuously during the whole composting process, consistently with the results obtained by Liu et al. (2019). Between days 1-3, due to the decomposition of easily degradable OM, its content significantly ($p < 0.05$) decreased from 84.42% (day 1) to 81.72% (day 3). Subsequently, the degradation rate of OM began to decrease, due to the almost complete decomposition of easily degradable OM and to the start of refractory OM (Lignin and Cellulose) degradation. Between days 3-10, the degradation rate of the OM decreased gradually, but its content did not decrease significantly (from 81.72% on day 3, to 77.44% on day 10).

NH_4^+-N: The change in NH_4^+-N content during composting reflects the nitrogen transformation process (Fang et al. 1999). As shown in Fig. 2b, the NH_4^+-N content increased during the whole composting process: from a minimum of 0.3 mg/g (day 1) to a maximum of 1.68 mg/g (day 10). The maximum rate of NH_4^+-N increase was between the fifth day to the seventh day of thermophilic phase, reflecting significant increases in the NH_4^+-N content of all samples ($p < 0.05$). NH_4^+-N contents increased due to the degradation of urea, uric acid, and proteins during the composting process. The results of our experiment are similar to those of Ren et al. (2010). In this study, the NH_4^+-N content increased during the composting process, reached its maximum at the end; these results were attributed to the occurrence of ammonification and to the particularly strong inhibition of nitrification at high temperatures (Thompson et al. 2004).

pH: The pH of the compost material tends to be directly related to the amount of NH_3 released as well as to the microbial activity (Spencer et al. 2013). As shown in the Fig. 2c, the pile pH first decreased and then increased during the composting process. The pH of the first day to the third day of compost showed a significant ($p < 0.05$) decreased from

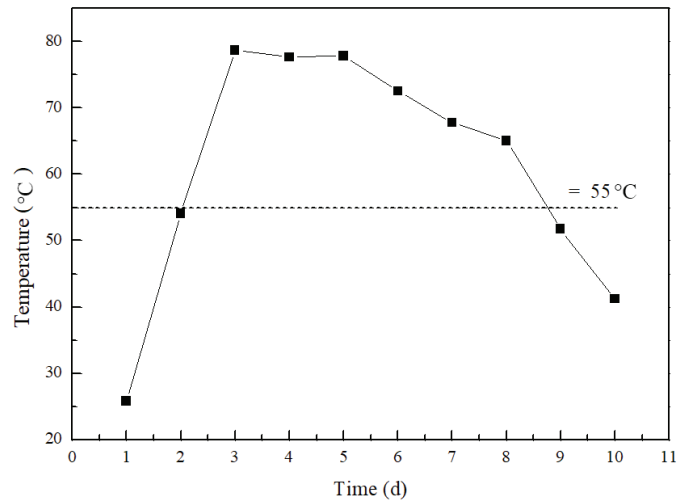

Fig. 1: Evolution of temperature during the composting process.

day 1 (8.3) to day 3 (8.13), and then fell to a minimum of 8.11 on day 5, due to the formation of volatile fatty acids (Gajalakshmi & Abbasi 2008). The release of ammonia during ammonification and the mineralization of organic nitrogen during composting caused an increase of the composting mixture pH (Wang et al. 2013). Between days 5-10 the pile pH increased significantly ($p < 0.05$), from 8.11 to 9, and then remained at alkaline levels (Hosseini et al. 2013).

Microbial Composition

The bacterial community dynamics at the genus level are shown in Fig. 3a. *Ureibacillus*, *Bacillus*, *Sphaerobacter*, and *Thermobifida* were overall the dominant genera within the bacterial community. On the first day of composting, the bacterial community was relatively homogeneous: the bacterial genera showed similar relative abundances. The thermophilic phase was dominated by *Ureibacillus* and *Bacillus*; however, while *Ureibacillus* decreased gradually, *Bacillus* increased gradually with time (Zhang et al. 2018). These two genera accounted for 46.4% and 2.2% of the bacterial community, respectively, on day 3 (early stage of the thermophilic phase). Between days 3-7 (late stage of the thermophilic phase), the proportion of *Ureibacillus* decreased to 8.8%, while that of *Bacillus* increased to 27.7%. The relative abundance of other bacteria did not change significantly during the thermophilic phase. On day 10 (cooling phase), the abundance of *Ureibacillus* and *Bacillus* decreased slightly (to 7.1% and 16.3%, respectively), while that of *Sphaerobacter* and *Thermobifida* increased significantly (from 0% and 0.7%, to 7% and 6.6%, respectively): *Ureibacillus*, *Bacillus* (Vieira et al. 2019), *Sphaerobacter*, and *Thermobifida* were the dominant bacterial general during the cooling phase.

Fungi are considered an important microbial group in composting materials, due to their superior ability in decomposing recalcitrant acid (Langarica-Fuentes et al. 2014a) and low-nitrogen substrates compared to bacteria (Langarica-Fuentes et al. 2014b). Unclassified_f_*Trichocomaceae*, unclassified_d_*Eukaryota*, *Hypocrea*, and *Thysanophora* represented the major fungal genera, whose dynamic changes are shown in Fig. 3b. Unclassified_f_*Trichocomaceae* was overall the most abundant fungus in our samples. Its relative abundance increased during the composting process (from 30.2% on day 1, to 90.8% on day 10). The relative abundances of unclassified_d_*Eukaryota* and *Thysanophora* accounted for a higher proportion during the mesophilic and thermophilic phase of composting. They reached 17.5% and 8.0% on day 5 (during the middle thermophilic phase), respectively; during the cooling phase they corresponded instead to only 0% and 1.4%, respectively. These results

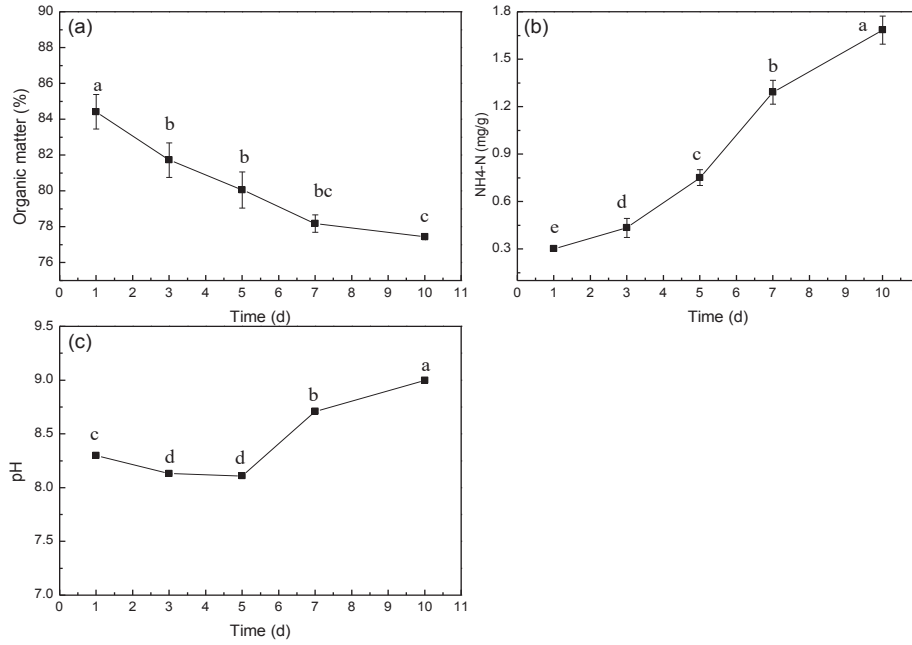

Fig. 2: Evolution of the physico-chemical parameters during the sludge composting process. Note: The letters indicate the occurrence of significant differences ($p < 0.05$) among samples. The same below.

indicate that unclassified_d_*Eukaryota* and *Thysanophora* were among the major fungal genera during the mesophilic and thermophilic phases. *Hypocrea* increased gradually from 5.2% (day 1) to 11.7% (day 7), reaching a minimum of 2.2% during the cooling phase: it also represented a major fungal genus during both the mesophilic and thermophilic phases.

The archaeal community composition is shown in Fig. 4c. Throughout the composting process, the archaeal communities were dominated by (from the most to the less abundant): *Methanobrevibacter*, *Methanosaeta*, *Methanobacterium*, and unclassified_k_norank. During the mesophilic phase, *Methanobrevibacter*, *Methanosaeta*, *Methanobacterium*, and unclassified_k_norank accounted for 30.0%, 44.7%, 7.3%, and 3.2% of the total archaeal community, respectively. Between days 2-10 the relative abundance of *Methanobrevibacter* rose gradually: from 20.3% (during the early period of the thermophilic phase) to 55.8% (during the cooling phase). The temporal evolution of *Methanosaeta* was completely opposite to that of *Methanobrevibacter*: *Methanosaeta* gradually decreased between days 2-10: from 54.4% (during the early period of the thermophilic phase) to 4.0% (during the cooling phase). *Methanobacterium* gradually increased between days 2-7: from 7.0% (during the thermophilic phase) to 21.9% (during the late thermophilic phase); then, it slightly decreased to 14.6% (during the cooling phase). Unclassified_k_norank showed an increasing and then decreasing trend: increased from 3.2% (on day 1) to 12.7% (on day 7, during the middle of the thermophilic phase); then, it gradually decreased to 8.2% (during the cooling phase). *Methanosaeta* was most active during the mesophilic phase and the early stage of the thermophilic phase, while *Methanobrevibacter*, *Methanobacterium*, and unclassified_k_norank were more active during the middle and late stages of the thermophilic and cooling phases.

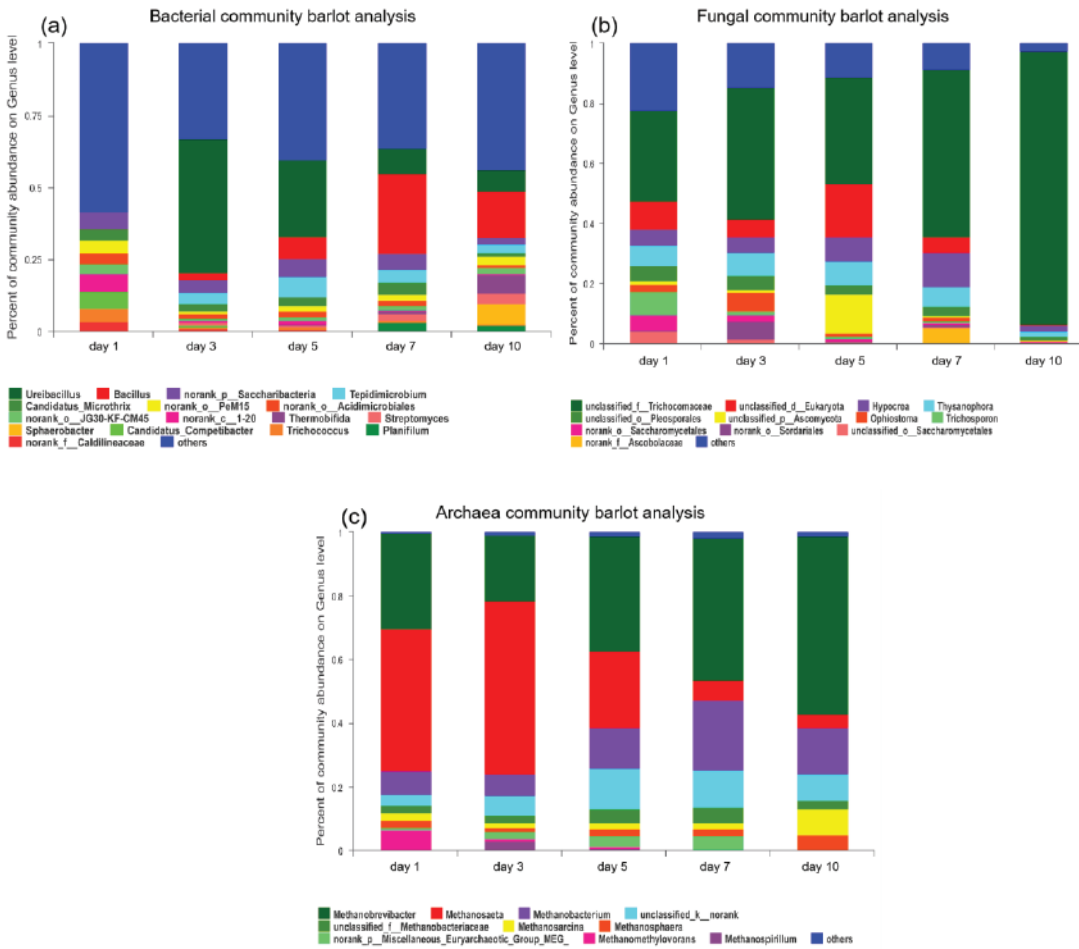

Fig. 3: Evolution of the microbial composition during sludge composting.

Correlation Between Physico-Chemical Parameters and Microorganisms

The diversity of the microbial community was closely correlated with the physico-chemical properties of the compost (Hosseini et al. 2013). A correlation heat map (Fig. 4a) showed that several physico-chemical parameters influenced the functional bacterial community. It is known that microbial activities can be enhanced by increasing temperatures (Yuan et al. 2016). In the studied bacterial communities, *Ureibacillus* (r = 1, $p = 0$) was significantly and positively correlated with temperature, while norank_Pem15 (r = -1, $p = 0$) and norank_JG30-KF-CM45 (r = -1, $p = 0$) were negatively correlated. Additionally, we observed that norank_c_1-20 (r = 0.9, $p = 0.037$) was significantly and positively correlated with OM, while *Bacillus* (r = -0.9, $p = 0.037$) and *Thermobifida* (r = -0.975, $p = 0.005$) were negatively correlated. Moreover, *Bacillus* (r = 0.9, $p = 0.037$) and *Thermobifid*a (r = 0.975, $p = 0.005$) were significantly and positively correlated with NH_4^+-N, while *norank_c_1-20* (r = -0.9, $p = 0.037$) was negatively correlated to NH_4^+-N.

Fungi have the ability to survive in extremely adverse habitats, due to their great physiological adaptability (Sarsaiya et al. 2018). Our correlation heat map (Fig. 4b) shows that several physico-chemical parameters should have influenced the functional fungal community. Firstly, *Thysanophora* (r = -1, $p = 0$), unclassified_d_*Eukaryota* (r = -0.9, $p = 0.037$), and unclassified_p_*Ascomycota* (r = -0.9, $p = 0.037$) significantly and negatively correlated with pH. Secondly, *Trichosporon* (r = -1, $p = 0$), norank_o_*Saccharomycetales* (r = -1, $p = 0$), and unclassified_o_*Pleosporales* (r = -1, $p = 0$) were significantly and negatively correlated with NH_4^+-N, while unclassified_f_*Trichocomaceae* (r = 0.9, $p = 0.037$) was positively correlated with NH_4^+-N. Thirdly, *Trichosporon* (r = 1, $p = 0$), norank_o_*Saccharomycetales* (r = 1, $p = 0$), and unclassified_o_*Pleosporales* (r = 1, $p = 0$) were significantly and positively correlated with OM,

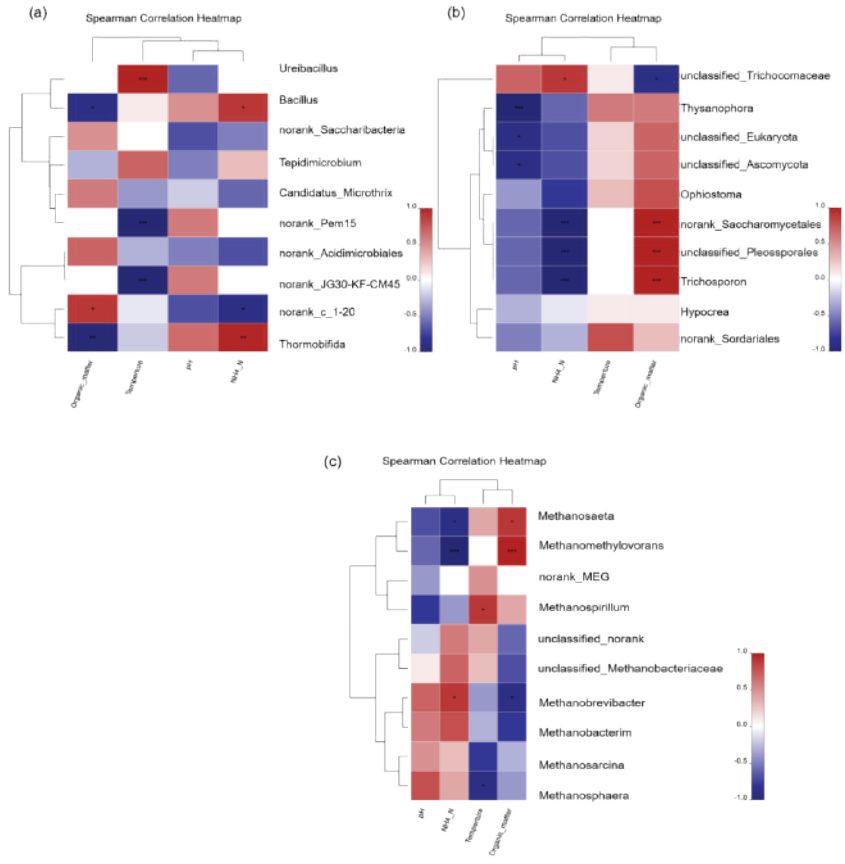

Fig. 4: Spearman correlation maps, showing the correlations between several physico-chemical parameters and the microbial community at the genus level.

while unclassified_f_*Trichocomaceae* (r = -0.9, p = 0.037) was negatively correlated with OM.

The archaeal community is known for being strongly influenced by environmental factors (e.g., temperature, pH, and various forms of nitrogen; Sun et al. 2019). Our correlation heat map (Fig. 4c) showed that several physico-chemical parameters should have influenced this functional archaeal community during the composting process. Firstly, *Methanobrevibacter* (r = 0.9, p = 0.037) was significantly and positively correlated with NH_4^+-N, while *Methanomethylovorans* (r = -1, p = 0) and *Methanosaeta* (r = -0.9, p = 0.037) were negatively correlated with NH_4^+-N. Secondly, *Methanosaeta* (r = 0.9, p = 0.037) and *Methanomethylovorans* (r = 1, p = 0) were significantly and positively correlated with OM, while *Methanobrevibacter* (r = -0.9, p = 0.037) was negatively correlated with OM. Thirdly, *Methanospirillum* (r = 0.9, p = 0.037) was significantly and positively correlated with temperature, while *Methanosphaera* (r = -0.9, p = 0.037) was negatively correlated with temperature.

CONCLUSION

The microbial succession during the SS composting process and its correlation with the analysed physico-chemical parameters are complex. The OM content of the composting material decreased gradually with time, while its pH increased after a first decrease, and the NH_4^+-N gradually increased. The composting stages were characterized by different microbial compositions; nevertheless, bacteria generally dominated the community, followed by fungi and, finally, archaea. The most abundant bacterial genera were *Ureibacillus*, *Bacillus*, *Sphaerobacter*, and *Thermobifida*. They showed different temporal evolutions; in particular, the proportion of *Ureibacillus* gradually decreased, while that of *Bacillus* gradually increased. The most abundant fungal genera were unclassified_f_*Trichocomaceae*, unclassified_d_*Eukaryota*, *Hypocrea*, and *Thysanophora*. The proportion of unclassified_f_*Trichocomaceae* showed a gradual increase with time. Finally, the most abundant archaeal genera were *Methanobrevibacter*, *Methanosaeta*, *Methanobacterium*, and unclassified_k_norank. Within this group, we noticed that the proportion of *Methanobrevibacter* gradually increased with time, while that of *Methanosaeta* gradually decreased. The bacterial communities were strongly correlated with temperature, while fungi were strongly and negatively correlated with pH; additionally, fungi and archaea were strongly correlated with OM and ammonium nitrogen. The results of this study provide new information about not only the structure and diversity of microbial communities during the SS composting process, but also about the interrelationships between microorganisms and various physico-chemical parameters. Overall, this information improves our understanding of microbial mechanisms during SS composting.

ACKNOWLEDGEMENTS

This research was financially supported by the Key Projects of National Water Pollution Control and Management of China (2017ZX07403002-06), and the Zhengzhou University of Light Industry (Grant No. 2013BSJJ022).

REFERENCES

Amir, S., Merlina, G., Pinelli, E., Winterton, P., Revel, J.C. and Hafidi, M. 2008. Microbial community dynamics during composting of sewage sludge and straw studied through phospholipid and neutral lipid analysis. Journal of Hazardous Materials, 159(2): 593-601.

Awasthi, M.K., Pandey, A.K., Bundela, P.S. and Khan, J. 2015. Co-composting of organic fraction of municipal solid waste mixed with different bulking waste: Characterization of physico-chemical parameters and microbial enzymatic dynamic. Bioresource Technology, 182: 200-207.

Bernal, M., Alburquerque, J. and Moral, R. 2009. Composting of animal manures and chemical criteria for compost maturity assessment. A review. Bioresource Technology, 100: 5444-5453.

Bonito, G., Isikhuemhen, O.S. and Vilgalys, R. 2010. Identification of fungi associated with municipal compost using DNA-based techniques. Bioresource Technology, 101(3): 1021-1027.

Du, J., Zhang, Y., Qu, M., Yin, Y., Fan, K., Hu, B., Zhang, H., Wei, M. and Ma, C. 2019. Effects of biochar on the microbial activity and community structure during sewage sludge composting. Bioresource Technology, 272: 171-179.

Fang, M. and Wong, J.W.C. 1999. Effects of lime amendment on availability of heavy metals and maturation in sewage sludge composting. Environmental Pollution, 106(1): 0-89.

Gajalakshmi, S. and Abbasi, S.A. 2008. Solid waste management by composting: State of the art. Critical Reviews in Environmental Science and Technology, 38: 311-400.

Guo, R., Li, G., Jiang, T., Schuchardt, F., Chen, T., Zhao, Y. and Shen, Y. 2012. Effect of aeration rate, C/N ratio and moisture content on the stability and maturity of compost. Bioresource Technology, 112: 171-178.

Han, Z., Qi, F., Wang, H., Li, R. and Sun, D. 2019. Odor assessment of NH3 and volatile sulfide compounds in a full-scale municipal sludge aerobic composting plant. Bioresource Technology, 282: 447-455.

Hosseini, S.M. and Aziz, H.A. 2013. Evaluation of thermochemical pretreatment and continuous thermophilic condition in rice straw composting process enhancement. Bioresource Technology, 133(133C): 240-247.

Jalili, M., Mokhtari, M., Eslami, H., Abbasi, F., Ghanbari, R. and Ebrahimi, A.A. 2019. Toxicity evaluation and management of co-composting pistachio wastes combined with cattle manure and municipal sewage sludge. Ecotoxicology and Environmental Safety, 171: 798-804.

Langarica-Fuentes, A., Handley, P.S., Houlden, A., Fox, G. and Robson, G.D. 2014a. An investigation of the biodiversity of thermophilic and thermotolerant fungal species in composts using culture-based and molecular techniques. Fungal Ecology, 11: 132-144.

Langarica-Fuentes, A., Zafar, U., Heyworth, A., Brown, T., Fox, G. and Robson, G.D. 2014b. Fungal succession in an in-vessel composting system characterized using 454 pyrosequencing. Fems Microbiology Ecology, 88(2): 296-308.

Liu, H., Wang, L. and Lei, M. 2019. Positive impact of biochar amendment on thermal balance during swine manure composting at relatively low ambient temperature. Bioresource Technology, 273: 25-33.

López-González, J.A., Suárez-Estrella, F., Vargas-García, M.C., López, M.J., Jurado, M.M. and Moreno, J. 2015. Dynamics of bacterial microbiota during lignocellulosic waste composting: studies upon its structure, functionality and biodiversity. Bioresource Technology, 175: 406-416

Onwosi, C.O., Igbokwe, V.C., Odimba, J.N., Eke, I.E., Nwankwoala, M.O., Iroh, I.N. and Ezeogu, L.I. 2017. Composting technology in waste stabilization: On the methods, challenges and future prospects. Journal of Environmental Management, 190: 140-157.

Petric, I., Helic, A. and Avdic, E.A. 2012. Evolution of process parameters and determination of kinetics for co-composting of organic fraction of municipal solid waste with poultry manure. Bioresource Technology, 117: 107-116.

Ren, L., Schuchardt, F., Shen, Y., Li, G. and Li, C. 2010. Impact of struvite crystallization on nitrogen losses during composting of pig manure and cornstalk. Waste Management, 30: 885-892.

Sadef, Y., Poulsen, T.G. and Bester, K. 2014. Impact of compost process temperature on organic micro-pollutant degradation. Science of The Total Environment, 494-495: 306-312.

Sarsaiya, S., Awasthi, S.K., Awasthi, M.K., Awasthi, A.K., Mishra, S. and Chen, J. 2018. The dynamic of cellulase activity of fungi inhabiting organic municipal solid waste. Bioresource Technology, 251: 411-415.

Spencer, J.L. and Heyst, B.J.V. 2013. Effect of different intermediate amendments on pH and ammonia emissions of composted poultry mortalities. Journal of Applied Poultry Research, 22(4): 700-714.

Sun, Y., Zhu, L., Xu, X., Meng, Q., Men, M., Xu, B. and Deng, L. 2019. Correlation between ammonia-oxidizing microorganisms and environmental factors during cattle manure composting. Revista Argentina de Microbiologia.

Thompson, A.G., Wagner-Riddle, C. and Fleming, R. 2004. Emissions of N_2O and CH_4 during the composting of liquid swine manure. Environmental Monitoring and Assessment, 91: 87-104.

Tiquia, S.M. and Tam, N.F. 1998. Composting of spent pig litter in turned and forced-aerated piles. Environmental pollution (Barking, Essex: 1987), 99: 329-37.

United States Environmental Protection Agency. 1994. Composting: yard trimmings, and municipal solid waste. Lancaster.

Vieira, F.R., Pecchia, J.A., Segato, F. and Polikarpov, I. 2019. Exploring oyster mushroom (*Pleurotus ostreatus*) substrate preparation by varying phase I composting time: changes in bacterial communities and physico-chemical composition of biomass impacting mushroom yields. Journal of Applied Microbiology, 126(3): 931-944.

Wang, Z., Gao, M., Wang, Z., She, Z., Hu, B., Wang, Y. and Zhao, C. 2013. Comparison of physico-chemical parameters during the forced-aeration composting of sewage sludge and maize straw at different initial C/N ratios. Journal of the Air & Waste Management Association, 63(10): 1130-1136.

Wu, J., He, S., Liang, Y., Li, G., Li, S., Chen, S., Nadeem, F. and Hu, J. 2017. Effect of phosphate additive on the nitrogen transformation during pig manure composting. Environmental Science and Pollution Research, 24(21): 17760-17768.

Xiao, Y., Zeng, G.M., Yang, Z.H., Shi, W.J., Huang, C., Fan, C.Z. and Xu, Z.Y. 2009. Continuous thermophilic composting (CTC) for rapid biodegradation and maturation of organic municipal solid waste. Bioresource Technology, 100(20): 4807-4813.

Yuan, J., Chadwick, D., Zhang, D., Li, G., Chen, S., Luo, W., Du, L., He, S. and Peng, S. 2016. Effects of aeration rate on maturity and gaseous emissions during sewage sludge composting. Waste Management, 56: 403-410.

Zhang, M., Luo, J., Yan, S., Chen, W., Liu, X. and Zhang, Z. 2018. Changes in bacterial communities during two agricultural solid wastes' co-composting processes. Annals of Microbiology, 68(11): 743-754.

Zhao, X., Wei, Y., Zhang, F., Tan, W., Fan, Y. and Xi, B. 2019. How do fungal communities and their interaction with bacterial communities influence dissolved organic matter on the stability and safety of sludge compost? Environmental Science and Pollution Research, 26(4): 4141-4146.

Zhou, J.M. 2017. The effect of different C/N ratios on the composting of pig manure and edible fungus residue with rice bran. Compost Science & Utilization, 25(2): 120-129.

Nature Environment and Pollution Technology
An International Quarterly Scientific Journal

p-ISSN: 0972-6268
e-ISSN: 2395-3454

Vol. 19 | No. 1 | pp. 245-251 | 2020

Original Research Paper | Open Access

Numerical Analysis of Growth of Coal-fired Particles Promoted by Condensation of Water Vapour in Oversaturated Environment

Ju Gao, Ting-fang Yu†, Lin Wang and Run-guo Chen
School of Mechanical and Electrical Engineering, Nanchang University, Jiangxi Nanchang 330031, China
†Corresponding author: Ting-fang Yu

Nat. Env. & Poll. Tech.
Website: www.neptjournal.com

Received: 16-04-2019
Accepted: 02-07-2019

Key Words:
Coal-fired particles
Condensation growth
Supersaturation
Particle size

ABSTRACT

A kinetics model was established to investigate the effects of condensation of water vapour on the growth of coal-fired particles. The effects of operating parameters on particle growth were numerically studied, including growth time, supersaturation, flue gas temperature and particle number concentration. The results showed that almost all the particles could grow rapidly more than 2.7 microns in tens of milliseconds. When initial super saturation is constant, the higher the temperature of flue gas, the larger the amount of condensable vapour and the final diameter of particles. Moreover, when the gas temperature is constant, the higher the degree of saturation, the larger the driving force for vapour condensation and the particle size distribution becomes narrower. Additionally, with the increasing of particle number concentration, the competition between particles for water vapour become more intense, and the final diameter for particles are smaller.

INTRODUCTION

In recent years, frequent occurrence of haze weather has aroused people's extensive attention to fine particle matters. The particles with an aerodynamic diameter less than 2.5 microns are defined as $PM_{2.5}$. These small particles can not only cause serious environmental problems but also pose a serious threat to people's health (Curtis et al. 2006). As those fine particles commonly carry multiple hazardous and toxic substances, such as poisonous heavy metals, bacteria, viruses, acid oxides and so on. Even more seriously, $PM_{2.5}$ could enter human respiratory tract and deposit in the lungs, and then participate in human blood circulation, which could induce a variety of diseases and causes serious harm to the functions of heart and lung (Bentayeb et al. 2012).

Analysis of the source of particulate matter in the ambient atmosphere shows that the flue gas emitted from the coal-fired power station carries a large amount of fly ash fine particles, which is one of the main sources of fine particles in the atmosphere (Hao et al. 2016a). At present, electrostatic precipitators are widely used in large coal-fired power stations to remove fly ash particles in the flue gas, and the mass removal efficiency can reach more than 99%. However, due to limited by the mechanism of charging, the removal efficiency of submicron particles is inefficient and a large number of fine particles are emitted into the atmosphere (Zhou et al. 2016). Therefore, it has become an urgent problem that how to remove fine particles more effectively. However, high removal efficiency could be achieved if the size of particle could be enlarged by means of preconditioning techniques such as heterogeneous condensation of water vapour (Tammaro et al. 2012), turbulent agglomeration (Chen et al. 2016), acoustic agglomeration (Liu et al. 2017) and chemical agglomeration (Hu et al. 2018) and so on.

According to many researchers, condensation of water vapour on the surface particles is one of the most promising preconditioning technologies to promote fine particle to be larger. Heidenreich et al. (1995) carried out the study of removing sub-micron quartz and paraffin oil particles in the tower by using the technology of multi-stage packed tower in series and alternately spraying cold and hot water. Yan et al. (2007) injected water vapour into the flue gas to achieve super saturation and coal-fired particles become larger by vapour condensation of steam in front of the scrubber, and the grown particles can be more effectively removed by wet scrubber. Fan et al. (2013) investigated the effects of different operational parameters on $PM_{2.5}$ particle size distribution based on the theory of polydisperse particle. Wen et al. (2014) studied the condensation growth characteristics of soluble ammonium sulphate particles in supersaturated steam environment by numerical analysis. Hao et al. (2016b) proposed a novel process for fine particles abatement via heterogeneous condensation of water vapour coupling two impinging steams technique. Bao et al. (2017) reported that nearly all the fine particles could be activated and grow up to be larger droplets in the desulfurized flue gas by adding

steam to form a supersaturated environment, and these droplets could be removed by the mesh wire demister. All the above studies had proved that the principle of condensation of water vapour could effectively promote the growth of fine coal-fired particles in flue gas.

At present, the large coal-fired power plants are generally equipped with wet flue gas desulfurization system, and the temperature of the outlet flue gas is between 313.15K ~ 333.15K, the flue gas is close to saturation state and it is easy to realize the construction of a supersaturated environment. Therefore, studying the condensation growth characteristics of coal-fired particles in supersaturated water vapour environment is of great significance for realizing the ultra-low emission of fine particulate matters in coal-fired power plants.

Based on the previous studies, a kinetics model was established for the growth of coal-fired particles by the condensation of water vapour. Additionally, the effects of operational parameters such as growth time, degree of saturation, gas temperature and particle number concentration, on particle growth were numerically studied. Then the results could provide theoretical support for removing of fine particles, which could be larger by using vapour condensation technology.

PHYSICAL MODEL

Simplification Assumption

The researches on the fly ash fine particles of coal-fired power plants indicate that the fine particles in the flue gas are mostly spherical and the surface is smooth (Sun et al. 2015). In addition, the compositions of fine particles are silicon-aluminous minerals insoluble in water (Li et al. 2009).

Based on the above research results, the model calculation can be simplified by the following assumptions.

1. Coal-fired particles are regarded as spherical insoluble particles and the collision between particles is ignored.
2. At the beginning of steam condensation, the particles can be completely covered by the liquid and the number concentration of particles are considered to be constant.
3. The system is an adiabatic system, and the heat transfer process between steam and droplets is a quasi-static process.
4. The temperature is uniformly distributed inside the environment and dust-containing droplets, the temperature between droplets and flue gas is defined as the temperature difference.

Model of Condensation Growth Kinetics

The water vapour condenses on the surface of coal-fired particles to form dust-containing droplets and the surface equilibrium steam pressure of droplets are:

$$P_{va} = P_{sat}(T_l)\exp\left(\frac{4\sigma_l M_l}{RT_l \rho_l d_p}\right) \quad \ldots(1)$$

Where, P_{sat} is the droplet surface saturation vapour pressure, Pa; T_l is the temperature of droplet, K; σ_l is the surface tension of droplet, $N \cdot m^{-1}$; M_l represents the molar mass of the droplet, $kg \cdot mol^{-1}$; R is the ideal gas constant, $R = 8.314\ J \cdot mol^{-1} \cdot K^{-1}$; ρ_l is the density of droplet, $kg \cdot m^{-3}$; d_p is the diameter of droplet, m.

The surface tension and saturation vapour pressure of droplet are given by (Yu et al. 2014).

$$P_{sat}(T_l) = \exp\left(77.34491296 - \frac{7235.424651}{T_l} - 8.2\ln T_l + 5.7113\cdot 10^{-3} T_l\right) \quad \ldots(2)$$

$$\sigma_l = 0.001\exp\left(4.859191 - 1.951091\cdot 10^{-3} T_l\right) \quad \ldots(3)$$

The density of droplet is a function of temperature, which is given by:

$$\rho_l = \frac{w_1}{w_2} \quad \ldots(4)$$

Where,

$$w_1 = 999.83952 + 16.945176 T_c - 7.9870401\cdot 10^{-3} T_c^{\,2} - 4.6170461\cdot 10^{-5} T_c^{\,3} + 1.0556302\cdot 10^{-7} T_c^{\,4} - 2.8054253\cdot 10^{-10} T_c^{\,5} \quad \ldots(5)$$

$$w_2 = 1 + 1.687985\cdot 10^{-2} T_c \quad \ldots(6)$$

$$T_c = T_l - 273.15 \quad \ldots(7)$$

The mass flux of the vapour diffusing to the droplet surface is written as (Heidenreich et al. 1995).

$$q_m = \frac{2\pi d_p M_v D_v (P_{v\infty} - p_{va})\left(1 + Kn_v\right)}{RT_l\left(1 + 1.71\,Kn_v + 1.33\,Kn_v^{\,2}\right)} \quad \ldots(8)$$

Where, M_v represents the molar mass of vapour, $kg \cdot mol^{-1}$; D_v is the diffusion coefficient, $m^2 \cdot s^{-1}$; $P_{v\infty}$ is the ambient vapour pressure, Pa; Kn_v is the Knusen number of vapour, $Kn_v = 2l_v/d_p$; l_v is the vapour molecular mean free path, m;

And (Fan et al. 2013):

$$D_v = 2.50\times 10^{-3}\left(P_{cg}P_{cv}\right)^{1/3}\left(T_{cg}T_{cv}\right)^{5/12}\left(\frac{1}{M_g} + \frac{1}{M_v}\right)^{1/2}\left(\frac{T_\infty}{\sqrt{T_{cg}T_{cv}}}\right)^{2.334}\frac{1}{P_\infty} \quad \ldots(9)$$

Where, P_{cg} and P_{cv} are the critical pressure of flue gas and steam, Pa; T_{cg} and T_{cv} are the critical temperature of the flue gas and steam, K; M_g represents the molar mass of flue gas, kg·mol^{-1}; T_∞ is the temperature of flue gas, K; P_∞ is the total pressure of flue gas, Pa.

The growth rate of droplet diameter is defined as:

$$\frac{dd_p}{dt} = \frac{2q_m}{\pi d_p^2 \rho_l} \quad \ldots(10)$$

When the steam condenses, the latent heat is released to the droplet, causing the rise of droplet temperature. According to the law of conservation of energy, the raised droplet temperature is (Wen et al. 2014):

$$T_l = T_\infty + \frac{q_m L\left(1+1.71\,Kn_g+1.33\,Kn_g^2\right)}{2\pi d_p \lambda\left(1+Kn_g\right)} \quad \ldots(11)$$

Where, L represents latent heat of phase change, J · kg^{-1}; Kn_g is the Knusen number of flue gas, $Kn_g = 2l_g/d_p$; l_g is the molecular mean free path of flue gas, m; λ is the thermal conductivity of flue gas, W · m^{-1} · K^{-1}.

The rate of change of the ambient vapour pressure is:

$$\frac{dp_{v\infty}}{dt} = -\frac{RT_\infty}{M_v}\sum_{i=1}^{K} n_i q_{m,i} \quad \ldots(12)$$

Where, n is the number concentration of particles, m^{-3}; the subscript i represents different intervals.

The release of latent heat of vapour will also cause the rise of flue gas temperature, and the change rate of flue gas temperature is:

$$\frac{dT_\infty}{dt} = -\frac{RT_\infty L}{\left(P_\infty - P_{v\infty}\right)M_g c_{pg} + P_{v\infty} M_v c_{pv}}\sum_{i=1}^{K} n_i q_{m,i} \quad \ldots(13)$$

Where, c_{pg} and c_{pv} are the constant pressure specific heat of flue gas and vapour, J·kg^{-1}·K^{-1}.

Initial Size Distribution

It is assumed that the initial particle size distribution of coal particle complies to log-normal distribution, in which the geometric standard deviation $\sigma_{g0} = 1.5$, average particle size $d_{g0} = 0.25$ μm. The number density function of the initial distribution for coal-fired particles is expressed as:

$$\frac{dn}{dd_p} = \frac{n_t}{\sqrt{2\pi}\, d_p \ln \sigma_{g0}} \exp\left[-\frac{\ln\left(d_p / d_{g0}\right)}{2\ln^2 \sigma_{g0}}\right] \quad \ldots(14)$$

Fig.1 shows the initial particle size distribution. Among the fine particle groups of the distribution, the particles with the diameters ranging from 0.07 μm to 0.84 μm account for 99.73% of the total particles.

RESULTS AND DISCUSSION

The Evolution of Particle Size Distribution with Growth Time

In order to investigate the evolution of particle size distribution with growth time, we set the calculation conditions as

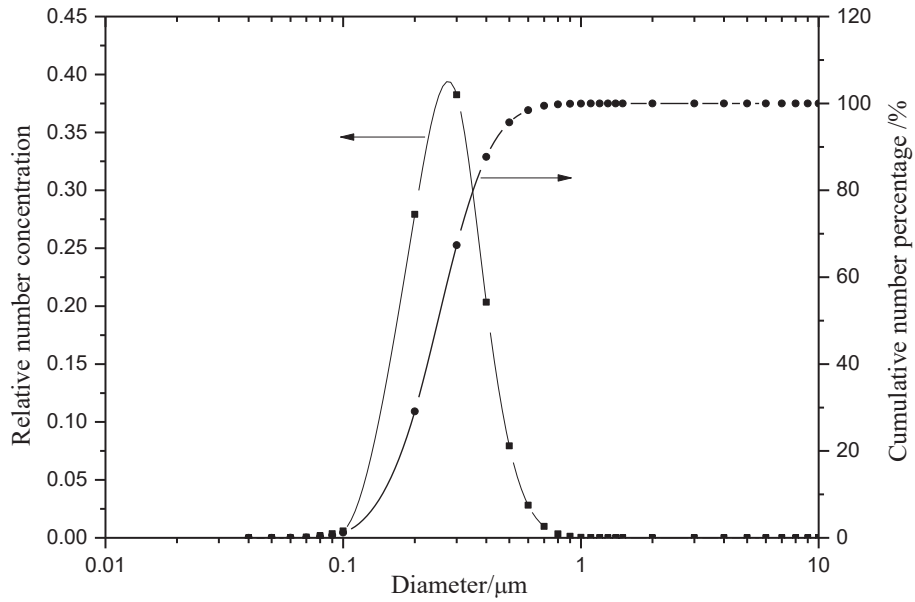

Fig. 1: Initial particle size distribution.

follows: the temperature of flue gas is 323.15 K, the number concentration of particles is $10^6/cm^3$, the initial super saturation is 1.25. Fig. 2 shows the evolution of particle size distribution with time. It can be seen from Fig. 2 that with the prolongation of growth time for coal-fired particles in the super saturation vapour environment, the final particle size becomes larger and the distribution becomes more concentrated. When the growth time is 20 ms, almost all particle sizes are concentrated at 3.33~3.87 μm.

Fig. 3. shows the evolution of typical particle size and ambient vapour pressure with time. It can be seen that the process of particle growth is basically completed in the first 20 ms, fine particles larger than 0.05 μm can grow to more than 3.33 μm and the grown particles can be effectively removed by conventional dust removal equipment. The conclusion is consistent with the result of Heidenreich et al. (1995). In addition, it is found that as the growth time increases, the growth speed becomes slower. It could be explained

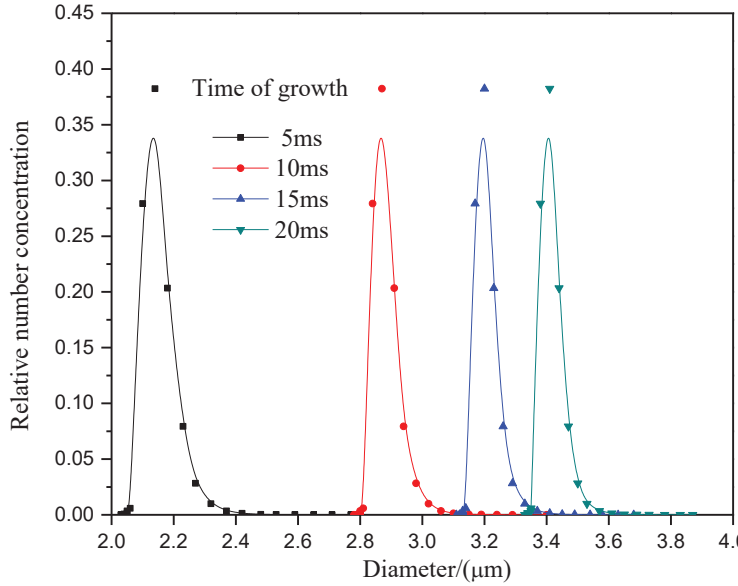

Fig. 2: Evolution of typical particle as a function of time.

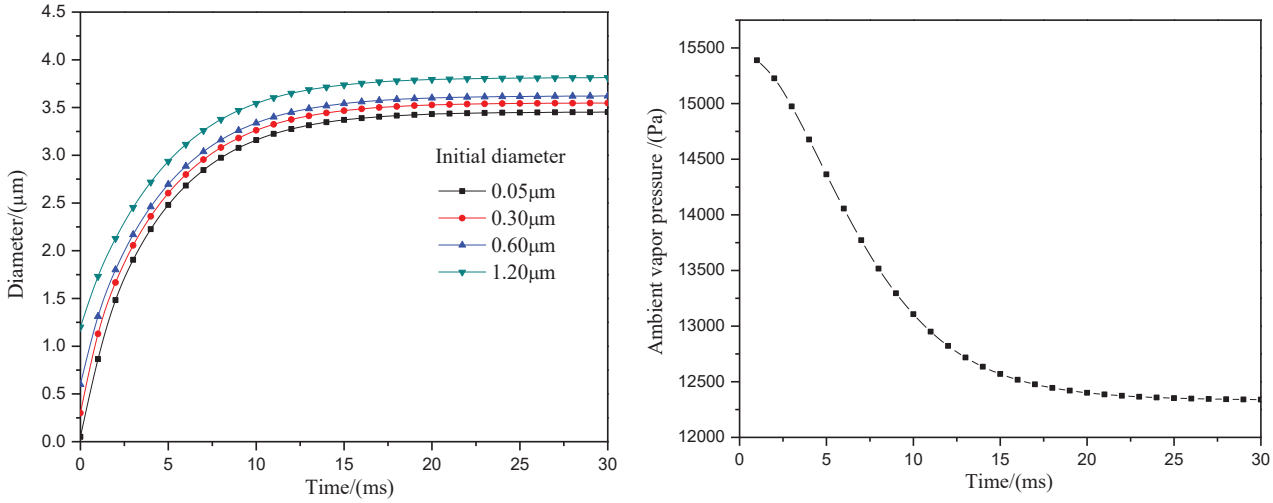

Fig. 3: Evolution of typical particle size and ambient vapour pressure with time. (a) Evolution of typical particle size with time (b) Evolution of ambient vapour pressure with time

as follow: on the one hand, as the vapour condenses on the particle surface, the ambient vapour pressure decreases and the amount of condensable vapour in the environment is reduced, resulting in the reduction of condensation power. On the other hand, water vapour condenses on the surface of coal-fired particles and releases latent heat of phase transformation resulting in the increase temperature and equilibrium steam pressure of particle, which is conducive to growth of particles.

Effects of Supersaturation on Condensation Growth of Particles

To research the effects of super saturation on condensation growth of particles, the calculation conditions are as follows: the temperature of flue gas is 323.15 K, the number concentration of particles is $10^6/cm^3$, the growth time is 30 ms and the initial degree of saturation are set as 1.15, 1.20, 1.25 and 1.30, respectively. Fig. 4 shows the effects of super saturation on condensation growth of particles. As the increase of super saturation, the final diameter of particle increases and the range of particle size becomes narrower. This is because when the gas phase temperature is constant, the greater the super saturation of vapour, the higher the ambient vapour pressure and the larger vapour condensation driving force, which is conductive to the growth of coal-fired particle. Under the condition of superstation 1.3, the final diameter for coal-fired particles is ranging from 3.56 μm to 4.08 μm, which is consistent with the results of Wen et al. (2014).

Effects of Flue Gas Temperature on Condensation Growth of Particles

In order to explore the effects of flue gas temperature on condensation growth of particles, we set the calculation conditions as follows: the number concentration of particles is $10^6/cm^3$, the growth time is 30 ms, the initial saturation is set as 1.25 and the gas temperature are set as 313.15K, 318.15K, 323.15K and 328.15K, respectively. Fig. 5 shows the effects of flue gas temperature on condensation growth of particles. It can be seen that when the flue gas temperatures are 313.15K, 318.15K, 323.15K and 328.15K, respectively, the final diameters for particles are concentrated at 2.73~3.52 μm, 3.69~3.03 μm, 3.89~3.33 μm and 4.12~3.64 μm, respectively. When the degree of super saturation is constant, the higher the gas phase temperature, the larger the final diameter of particles after condensation growth. It could be explained that when the saturation of vapour is constant, the higher the temperature of flue gas is, the larger the amount of condensable vapour in the environment. Thereby, more steam can condense on particle surface, increasing the final size of the particle.

The wet desulfurization of coal-fired power stations produce high-humidity flue gas with a temperature ranging from 313.15K to 333.15K, only a small amount of steam is added to the flue gas to build an over-saturated environment, which is meaningful for phase change condensation to promote the growth of coal-fired particles.

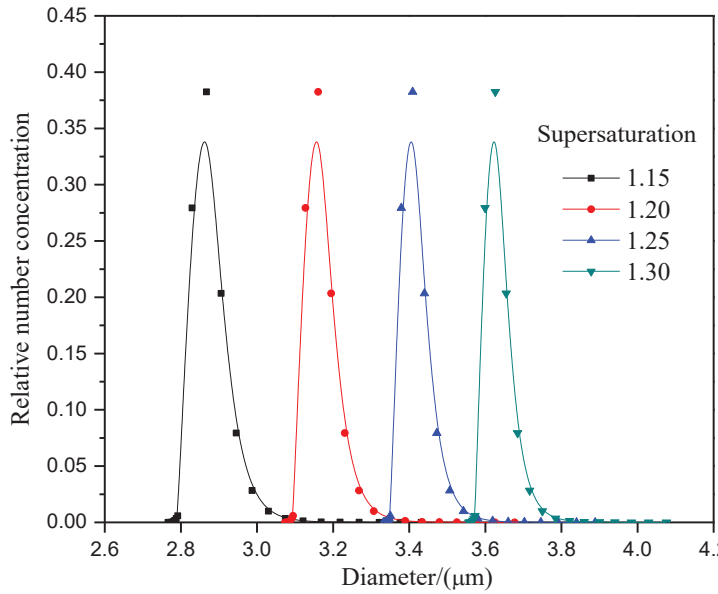

Fig. 4: Effects of super saturation on condensation growth of particles.

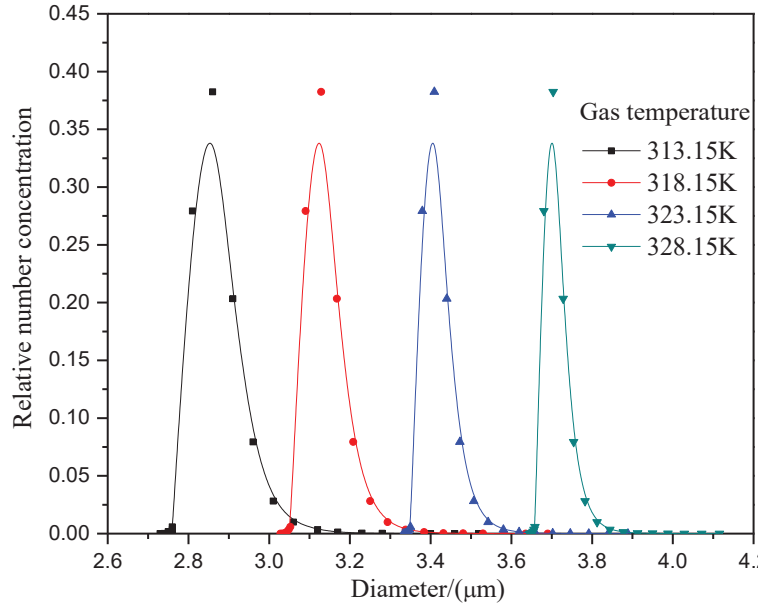

Fig. 5: Effects of gas temperature on condensation growth of particles.

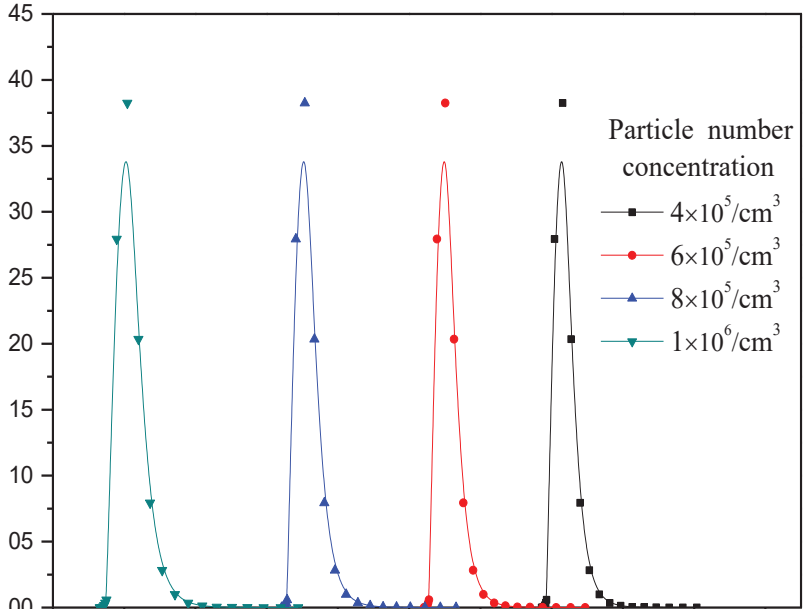

Fig. 6: Effects of particle number concentration on condensation growth of particles.

Effects of Particle Number Concentration on Condensation Growth of Particles

To study the effects of particle number concentration on condensation growth of particles, the calculation conditions are as follows: the initial super saturation is 1.25, the temperature of flue gas is 323.15K, the growth time is 30ms and the number concentration of particles are $4 \times 10^5/cm^3$, $6 \times 10^5/cm^3$, $8 \times 10^5/cm^3$ and $1 \times 10^6/cm^3$, respectively. Fig. 6 shows the effects of particle number concentration on condensation growth of particles. It can be seen from Fig. 6 that the smaller the number concentration of particles, the better growth effect of particles. When the number concentration of fine particles is $4 \times 10^5/cm^3$, the fine particles after growth are ranging from 4.58 μm to 5.01 μm. It could be explained as follow: when the flue gas temperature and initial

super saturation are constant, the amount of condensable steam in the environment is certain. Increasing the number concentration of fine particles is bound to intensify the competition for steam among particles. Therefore, the amount of steam obtained by a single particle is reduced and the final diameter of particle after condensation growth will be smaller. Therefore, an appropriate supersaturated steam field should be constructed, according to the number and concentration of fine particles.

CONCLUSION

A dynamics model was established for condensation of water vapour on the surface of coal-fired particles. The influences of operational parameters, including growth time, degree of saturation, temperature of flue gas and particle number concentration on particle growth were numerically investigated. The calculation results show that coal-fired particles can grow rapidly in the over saturated steam environment, the growth process can complete within a few tens of milliseconds, and the size distribution of fine particles becomes narrower after the growth. Increasing the initial super saturation and temperature of flue gas can increase the amount of condensable steam and enhance the driving force of condensation, which effectively promotes the condensation growth of particles. Additionally, increasing the number concentration of coal-fired particles will intensify the competition between particles for water vapour, which is not conducive to the condensation growth of particles.

ACKNOWLEDGEMENTS

This study was supported by National Natural Science Foundation of China (No. 61262048).

REFERENCES

Bao, J. J., Xu, J.L., Tang, J.G., Xie, G., Liu, H.T. Sun, L.C and Yang, H. M. 2017. Study on the nucleation and growth of fine particles in flue gas promoted by heterogeneous condensation of water vapour. Advanced Engineering Sciences, 49(5): 171-177.

Bentayeb, M., Simoni, M., Baiz, N., Norback, D., Baldacci, S., Maio, S., Viegi, G. and Annesi-Maesano, I. 2012. Adverse respiratory effects of outdoor air pollution in the elderly. International Journal of Tuberculosis & Lung Disease, 16(9): 1149-1161.

Chen, D.L., Wu, K. and Mi, J.C. 2016. Experimental investigation of aerodynamic agglomeration of fine ash particles from a 330 MW PC-fired boiler. Fuel, 165: 86-93.

Curtis, L., Rea, W., Smith-Willis, P., Fenyves, E. and Pan, Y. 2006. Adverse health effects of outdoor air pollutants. Environment International, 32(6): 815-830.

Fan, F.X. and Zhang, M.J. 2013.Influence of vapour heterogeneous condensation on the $PM_{2.5}$ particle size distribution. Journal of China Coal Society, 38(4): 694-699.

Hao, W., Pan, D.P., Xiong, G.L., Jiang, Y.Z., Yang, L.J., Yang, B., Peng, Z.M. and Hong, G.X. 2016a. The abatement of fine particles from desulfurized flue gas by heterogeneous vapour condensation coupling two impinging steams. Chemical Engineering and Processing, 108: 174-180.

Hao, W., Pan, D.P., Huang, R.T., Hong, G.X., Bing, Y., Peng, Z.M. and Yang, L.J. 2016b. Abatement of fine particle emission by heterogeneous vapour condensation during wet limestone-gypsum flue gas desulfurization. Energy & Fuels, 30(7): 6b00673b.

Heidenreich, S. and Ebert, F. 1995. Condensational droplet growth as a preconditioning technique for the separation of submicron particles from gases. Chemical Engineering & Processing, 34(3): 235-244.

Hu, B., Yang, Y., Cai, L., Yuan, Z.L., Roszak, S. and Yang, L.J. 2018. Experimental study on particles agglomeration by chemical and turbulent agglomeration before electrostatic precipitators. Powder Technology, 335: 186-194.

Li, H. L., Zhang, J. Y., Zhao, Y. C., Zhang, K., Zhang, L. L. and Zheng, C. G. 2009. Study on the physicochemical characteristic and wetting mechanism of fly ash in coal fired power plant. CIESC Journal, 30(9): 1597-1600.

Liu, D. P. and Luo, W. L. 2017.Investigation into coagulation of fine particles by combination of seed particles with acoustic wave. Journal of South China University of Technology (Natural Science Edition), 45(6): 131-138.

Sun, D.S., Zhu, T., Hu, X.J., Ji, Y. Q., Xi, H. H. and Fang, L. 2015. Physicochemical properties and wettability of fine particles of fly ash from different combustions. Environmental Science & Technology, 38(8): 6-10.

Tammaro, Marco, Natale, D. I., Francesco, Salluzzo, Antonio, Lancia and Amedeo 2012. Heterogeneous condensation of submicron particles in a growth tube. Chemical Engineering Science, 74(22): 124-134.

Wen, G.S. and Fan, F.X. 2014. Numerical analysis on growth of soluble PM2.5 by vapour heterogeneous condensation. China Environmental Science, 34(5): 1119-1124.

Yan, J.P., Yang, L.J., Zhang, X., Sun, L.J., Zhang, Y. and Shen, X.L. 2007. Experimental study on separation of inhalable particles from coal combustion by heterogeneous condensation enlargement. Proceeding of the CSEE, 27(35): 12-16.

Yu, F., Qin, F.H., L, X.S., Zhang, J.S., Jie, W., Gui, H.Q. and Liu, J.G. 2015. A modified expression for the steady-state heterogeneous nucleation rate. Journal of Aerosol Science, 87: 17-27.

Zhou, D. L., Li, S.Q., Jin, X., Xiong, G.L. and Huang, W. 2016. Experiments and numerical simulations of the removal of fine particles in the coupling field of electrostatic precipitators. Proceedings of the CSEE, 36(2): 453-458.

Nature Environment and Pollution Technology
An International Quarterly Scientific Journal

p-ISSN: 0972-6268
e-ISSN: 2395-3454

Vol. 19 | No. 1 | pp. 253-261 | 2020

Original Research Paper | Open Access

The Use of Mercury-Resistant Bacteria to Enhance Phytoremediation of Soil Contaminated with Small-scale Gold Mine Tailing

Reni Ustiatik*, Siska Nurfitriani*, Amrullah Fiqri and Eko Handayanto*†**

*Postgraduate Program, Faculty of Agriculture, Brawijaya University, Jl. Veteran No. 1, Malang 65145, East Java, Indonesia

**Gunung Rinjani University, Suralaga, East Lombok, West Nusa Tenggara 83661, Indonesia

†Corresponding author: Eko Handayanto

Nat. Env. & Poll. Tech.
Website: www.neptjournal.com

Received: 31-05-2019
Accepted: 24-07-2019

Key Words:
Mercury-resistant bacteria
Phytoremediation
Gold mine tailings
Contaminated soil

ABSTRACT

In the phytoremediation process, there is an interaction between plants and microorganisms in the soil. The objective of this study was to explore the effect of mercury-resistant bacteria on phytoremediation of soil contaminated with small-scale gold mine tailings that contain mercury. Two isolates of mercury-resistant bacteria (*Brevundimonas vesicularis* and *Nitrococcus mobilis*) were applied to *Paspalum conjugatum* as a mercury accumulator plant that was grown for 70 days on gold mine tailing-contaminated soil. Ammonium thiosulfate was used as a chelating agent to stimulate mercury extraction by the plant. After *P. conjugatum* was harvested (60 days), the remaining soil in the pot was planted with maize until the maximum vegetative period. The results showed that the application of mercury-resistant bacteria and ammonium thiosulfate increased 157-162% of *P. conjugatum* biomass compared to that without the application of mercury-resistant bacteria. The application of mercury-resistant bacteria with ammonium thiosulfate in soil phytoremediation with *P. conjugatum* reduced 18% and 20% mercury content in the soil contaminated with small-scale gold mine tailings containing mercury. The decrease in mercury content in the soil due to the application of *B. vesicularis* and *N. mobilis* in soil phytoremediation with *P. conjugatum* increased biomass production of a maize plant by 131% and 145%, respectively.

INTRODUCTION

The declining production of crops due to contamination of tailings from traditional gold processing to agricultural land is one of the negative effects of small-scale gold mining activities in Lombok, Indonesia. The tailings contain mercury and several other heavy metals that are toxic to plant growth. The results of a survey conducted by Krisnayanti et al. (2012a) at small-scale gold mining sites in West Lombok showed that tailings of the gold amalgamation process contained 3002 mg Hg/kg which caused high Hg content (25-40 mg/kg) in soil contaminated with the tailings (Krisnayanti et al. 2012b). Mercury ion (Hg^{2+}) in the soil can be taken up by plants causing toxicity (Su et al. 2009, Tangahu et al. 2011). The presence of mercury in planting media inhibits the growth and biochemical composition of maize seeds (Muddarisna et al. 2013a). Hyperaccumulator plants can be used to extract or eliminate metals polluting the soil (Tangahu et al. 2011). Muddarisna et al. (2013b) reported that *Paspalum conjugatum, Cyperus kylingia*, and *Lindernia crustacea* are three local plant species having the potential to be used as mercury accumulator plants on agricultural soils contaminated with small-scale gold mine tailings containing mercury in West Lombok, Indonesia. Phytoremediation of heavy metals can be driven through the addition of chelating agents (Wang et al. 2013). Ammonium thiosulfate has been used as a chelating agent to stimulate the accumulation of Hg in a plant grown in gold mine tailings contaminated with Hg (Moreno et al. 2004). Handayanto et al. (2016) reported that the high mercury accumulation (30.09 mg/kg) was found in the *P. conjugatum* shoot with the addition of ammonium thiosulfate. The addition of ammonium thiosulfate increased the accumulation of Hg in the shoot by 71% compared to the treatment without the addition of ammonium thiosulfate.

Although phytoremediation of heavy metals can be stimulated through the addition of chelating agents, phytoremediation is not only carried out by plants because there is always an interaction between plants and microorganisms in the soil which causes increased activity associated with remediation (Compant et al. 2010). Some bacteria can reduce enzymatically Hg^{2+} to Hg with mercuric reductase, MerA. Another enzyme, organomercurial lyase (MerB), which is present in several bacteria, catalyses the release of Hg-carbon bonds from several forms of organic mercury (Wang 2004). Therefore, efforts to find an application of heavy metal ac-

cumulator plants combined with soil microbial communities that are resistant to mercury are thought to further increase the efficiency of phytoremediation of heavy metal contaminated soils. Some bacteria can survive in an environment contaminated with mercury even though the mechanism of resistance to mercury is not known (Nascimento & Chartone-Souza 2003). Chasanah et al. (2018) who isolated and identified mercury-resistant bacteria from small-scale gold mine tailings in Central Lombok obtained four isolates of mercury-resistant bacteria that were indicated as *Brevundimonas vesicularis, Nitrococcus mobilis, Fusobacterium aquatile* and *Fusobacterium necrogenes*. Tests for mercury accumulation in the laboratory showed that these four species were able to accumulate more than 70% of mercury from small scale gold mine tailings.

The purpose of this study was, therefore, to study the effect of the combined application of mercury-resistant bacteria and mercury accumulator plant in the phytoremediation of soil contaminated by gold mine tailings containing mercury.

MATERIALS AND METHODS

Site Description

A pot experimental study was conducted in a 4 m × 5 m screen house situated at the Bonjeruk Village, Jonggat District of Central Lombok Regency, Indonesia ($8^o24'$ - $8^o57'$ S and $116^o05'$ - $116^o24'$ E). The study was carried out from November 2018 to March 2019. The location of the screen house was at the farmers' land that had been buried/contaminated with gold amalgamation tailings containing mercury since 2011. Soil contaminated with the tailings used for this study had the following characteristics: pH = 6.4, C = 0.95%, N = 0.10%, P = 0.98 mg/kg, S = 8.92 mg/kg, cation exchange capacity = 14.25 cmol/kg, K = 3.25 cmol/kg, Ca = 3.04 cmol/kg, Mg = 1.26 cmol/kg, Na = 0.89 cmol/kg, and Hg = 41.37 mg/kg. The total value of Hg exceeded the threshold of the Indonesian Government Regulation for Hg in solid waste of 0.03 mg/kg. The research materials used were two isolates of mercury-resistant bacteria (*Brevundimonas vesicularis* and *Nitrococcus mobilis*) (Chasanah et al.2018), *Paspalum conjugatum* P.J. Bergius, ammonium thiosulfate ($[NH_4]_2S_20_3$) as a chelating agent, and maize seeds.

Experiment 1: Mercury Extraction by *P. conjugatum*

The research treatments consisted of a combination of applications of mercury-resistant bacterial isolates (*B. vesicularis* and *N. mobilis*), ammonium thiosulfate with doses of 0 and 2 g/kg that were applied together with the use of *P. conjugatum* as a mercury accumulator plant. The treatment combinations were (1) B1K0 (*B. vesicularis* isolate without ammonium thiosulfate), (2) B2K0 (*N. mobilis* isolate without ammonium thiosulfate), (3) B1K1 (*B. vesicularis* isolate with ammonium thiosulfate, (4) B2K1 (*N. mobilis* isolate with ammonium thiosulfate, (5) B0K0 (without isolates of mercury-resistant bacteria, and ammonium thiosulfate), and (6) B0K1 (without isolates of mercury-resistant bacteria, and with ammonium thiosulfate).

Each bacterial isolate of 12.5 mL (10^3 cfu/mL) (Chasanah et al. 2018) was applied to each pot containing small-scale gold mine tailing-contaminated soil. The six treatments were arranged in a randomized block design with four replications. Each pot received NPK fertilizer of 100kg/ha and organic matter of 10t/ha (Handayanto et al. 2016). The NPK fertilizer is produced by PT. Petrokimia Gresik, Indonesia, as Phonska, which contains 15% N, 15% P_2O_5, 15% K_2O and 10% S. The organic matter used for this study was local cow manure containing 1.46% N, 0.98% P_2O_5 and 0.65% K_2O. Before being planted, the 2-week-old *P. conjugatum* seedling was acclimatized for one week in a polybag containing soil contaminated with small-scale gold mine tailings.

For all the treatments, each plant seedling was grown in a 30 cm diameter plastic pot filled with fifteen kilograms of soil contaminated with small-scale gold mine tailings (air-dried and sieved to pass through a 2 mm sieve) and placed in the screen house. During the experiment, well water was supplied daily to each pot in order to keep the moisture content of the soil at the approximate water holding capacity so as not to inhibit the growth of *P. conjugatum*. The ammonium thiosulfate (2 g/kg) was supplied at 8 weeks after planting (Wang et al. 2013). At harvest (70 days after planting), *P. conjugatum* shoots and roots were separated manually from the soil by sieving and rinsing with water. The shoots and roots were then oven-dried at 60^oC for 48 hours, weighed and ground to pass through a 1 mm sieve for analysis of mercury content. Measurement of Hg content in plant samples was carried out following the method of Moreno et al. (2005). A total of 0.2 g of ground plant sample was put into a 50mL borosilicate beaker, added with 10 mL of nitric acid, and then left for 10-15 hours. The next day the mixture of plant sample and nitric acid was heated for 2 hours at 120°C and then added with 20 mL of distilled water. Standard determination of 0.5, 1, 2, 4, 7.5 and 10 ppb Hg referred to the standard of tomato leaves containing 0.034 ppm Hg. Mercury concentration was measured by a Cold Vapour Atomic Absorption Spectrometer F732-S (Shanghai Huaguang Instrument Company). The ability of *P. conjugatum* for mercury translocation upwards from root to shoot was evaluated by determining the translocation factor (TF) (Yoon et al.2006). TF = concentration of mercury in shoots/ concentration of mercury in roots.

The data obtained were analysed by performing the

one-way analysis of variance, and further statistical test for significant differences among treatment means was conducted by employing the least significant difference test at the 95% level of confidence with the aid of Microsoft Excel Office 2016 software.

Experiment 2: Growth and Yield of Maize Biomass

After harvesting *P. conjugatum,* the remaining soil in the pot was used for the growing a local variety of maize. Six treatments similar to experiment 1 and one control (soil contaminated with small-scale gold mine tailings without phytoremediation treatment), were arranged in a randomized block design with four replicates. Each pot was supplied with the Phonska NPK fertilizer with a dose equivalent to 100 kg/ha. Three pre-germinated maize seeds were planted in each pot and thinned to one after one week. During the experiment, water was supplied daily to each pot to maintain soil moisture in the condition of the water holding capacity so as not to inhibit the growth of maize. Maize plant was harvested at the maximum vegetative period (60 days). Maize shoots and roots were separated, washed, weighed, and dried in an oven at 40^{o}C for 48 hours for mercury analysis. Mercury concentrations in maize shoots and roots and the planting media were analysed using the same method as in Experiment 1. The data obtained were also subjected to statistical analysis as Experiment 1.

RESULTS AND DISCUSSION

P. conjugatum Biomass

The application of mercury-resistant bacteria combined with ammonium thiosulfate significantly ($p<0.05$) improved the growth of *P. conjugatum* as a mercury accumulator plant (Fig. 1). Compared with the B0K0 treatment (without application of mercury-resistant bacteria and ammonium thiosulfate), the highest increase (162%) in total biomass (shoot + root) of *P. conjugatum* was obtained in the B1K1 treatment (application of *B. vesicularis* with ammonium thiosulfate). However, the increase in total biomass of *P. conjugatum* in the B1K1 treatment was not significantly different from that of the B2K1 treatment (application of *N. mobilis* with ammonium thiosulfate) of 157%. The lowest increase in *P. conjugatum* biomass (50%) was obtained in the B2K0 treatment (application of *N. mobilis* without ammonium thiosulfate).

Data presented in Fig. 1 show that the addition of ammonium thiosulfate increased plant biomass even without application of mercury-resistant bacteria. Muddarisna et al. (2013a) reported that addition of ammonium thiosulfate had a significant effect on the dry weight of the shoots of *P. conjugatum, Cyperus kyllingia* and *Lindernia crustacea* used for phytoremediation of mercury-polluted soil. The increase in plant biomass due to the addition of ammonium thiosulfate was probably because of the addition of plant

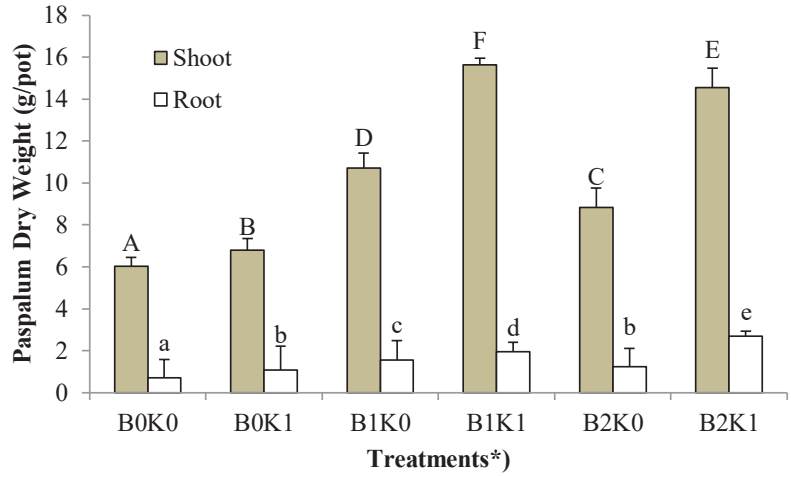

Fig. 1: Effect of application of mercury-resistant bacteria and ammonium thiosulfate on the biomass of *P. conjugatum* at 70 days. Vertical bars represent standard deviation while the same capital and small letters are not significantly different for each treatment mean at 0.05 level of probability. *) B0 = no bacterial isolate, B1 = *B. vesicularis* isolate, B2 = *N. mobilis* isolate, K0 = without ammonium thiosulfate, K1 = with ammonium thiosulfate 2 g/kg.

nutrients (nitrogen and sulphur) supplied through ammonium thiosulfate at the 8-week old plant that was able to enhance plant growth (Handayanto et al. 2016). Chelating agents, such as ammonium thiosulfate, have been used as soil extractants, a source of micronutrient fertilizers and to maintain solubility of micronutrient in hydroponic solutions (Salt et al. 1995). If the addition of ammonium thiosulfate was combined with the application of mercury-resistant bacteria, it further enhanced the improvement of accumulator plant growth, which in turn improved the absorption of mercury by the mercury accumulator plant.

Liagat & Eltem (2016) reported that *B. vesicularis* is an endophytic bacterium that can produce indole acetic acid (IAA) phytohormone to stimulate plant growth (Ying et al. 2015), and produce more nutrient uptake from the soil (Li et al. 2008). Endophytic bacteria can supply nutrients for plant growth by dissolving phosphate and fixing nitrogen (Marra et al. 2012). In addition, endophytic bacteria can also protect plants against pathogenic microorganisms (Khalifa et al.2015) and degradation of toxic compounds (Sheng et al. 2008). *N. mobilis* is known as an ammonia-oxidizing bacterium which can oxidize nitrite to nitrate (Yu et al. 2012, Koide et al.2014). This bacterium can derive energy from the oxidation of ammonia and nitrite in the degradation of organic wastes and recycling of nutrients in subterranean habitat (Koilraj et al. 2012). *N. mobilis* is also an important and dominant ammonia-oxidizing bacterium in various wastewater treatment systems (Thandar et al. 2016).

Accumulation of Mercury by *P. conjugatum*

Referring to the *P. conjugatum* biomass and mercury concentration in the *P. conjugatum* plant, mercury accumulation in *P. conjugatum* plant can be calculated. The highest mercury accumulation (8.29 mg/kg dry weight) was found in the B1K1 treatment (*B. vesicularis* with ammonium thiosulfate), and the lowest was found in the B0K0 treatment (without bacterial isolates and ammonium thiosulfate) (Fig. 2). The application of mercury-resistant bacteria with ammonium thiosulfate to *P. conjugatum* reduced the mercury content in the soil contaminated by small-scale gold mine tailings which was 41.73 mg/kg, reduced by 3% (B0K0 treatment) up to 20% (B1K1 treatment). Microbes have developed a mechanism for detoxifying mercury based on intracellular reduction of Hg^{2+} to Hg^0 which is non-toxic by mercury reductase enzymes and the loss of diffusional Hg^0 from cells (Wagner-Dobler 2003).

From the accumulation of mercury in the *P. conjugatum* plant, more than 80% of Hg accumulation was found in the shoot of the plant. In line with the dry weight of plant biomass, the use of ammonium thiosulfate stimulated Hg uptake by plants. This is thought to occur because mercury has a strong affinity with thiol groups, especially sulphide and bisulphide complexes (Moreno et al. 2004, Selin 2009). Moreno et al. (2005) reported that *Bracia juncea* could ac-

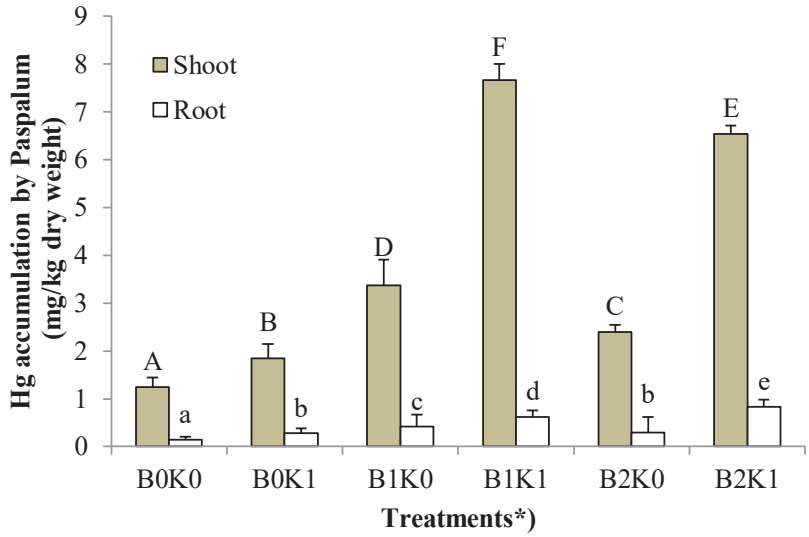

Fig. 2: Effect of application of mercury-resistant bacteria and ammonium thiosulfate on the accumulation of mercury by *P. conjugatum* at 70 days. Vertical bars represent standard deviation while the same capital and small letters are not significantly different for each treatment mean at 0.05 level of probability. *) B0 = no bacterial isolate, B1 = *B. vesicularis* isolate, B2 = *N. mobilis* isolate, K0 = without ammonium thiosulfate, K1 = with ammonium thiosulfate 2 g/kg.

cumulate Hg to 40 mg/kg in plant tissue after the application of ammonium thiosulfate to mine tailings contaminated with 2.8 mg Hg/kg. However, the use of ammonium thiosulfate can also create the risk of underground water pollution by Hg which is mobilized by the thiosulfate.

The increase in mercury accumulation by *P. conjugatum* in the B1PK1 treatment (*B. vesicularis* and ammonium thiosulfate) was probably due to the symbiotic relationship between microorganisms and plants that increased heavy metal extraction from the soil (Tangahu et al. 2011). In this study, the symbiosis of mercury-resistant bacteria and mercury accumulator plant increased mercury accumulation up to 459% (B1PK1 treatment) compared to treatments without the application of mercury-resistant bacteria. High mercury accumulation in the *P. conjugatum* plant caused mercury content in the soil to decrease up to 20% (B1PK1 treatment) from the original mercury content in the soil of 41.37 mg/kg. This technology can be used to extract mercury from agricultural soil before it is used to grow food crops. However, this technology still raises the problem of processing the biomass of extracting plants containing mercury so as not to re-pollute the environment.

Translocation Factor of Mercury

As the effect on Hg accumulation of shoot and root, the application of mercury-resistant bacteria and ammonium thiosulfate also had a significant effect on the *P. conjugatum* translocation factor (TF) values for mercury which were all greater than 1 (Fig. 3). The highest translocation factor value (1.54) was found in the B1K1 treatment (*B. vesicularis* and ammonium thiosulfate) which was not significantly different from the TF value in the B2K1 treatment (*N. mobilis* and ammonium thiosulfate) of 1.47 (Fig. 3). The lowest TF value (1.02) in the B0K0 treatment (without mercury-resistant bacteria and ammonium thiosulfate). Differences in TF values in the treatments showed differences in the effectiveness of each treatment in the transport of mercury from the root system to the shoot as a place of accumulation (Selin 2009). This difference is also thought to be related to the modification of plant growth under conditions of heavy metal stress as a result of the absence of certain amino acids in plants (Ashraf et al. 2011).

Growth and Biomass Yield of Maize

At harvest time of the maximum vegetative age (60 days), the height of maize plants varied from 45.7 cm (control) to 105.8 cm (B1K1 treatment) (Fig. 4). Compared with the control, phytoremediation of soil with *P. conjugatum* and application of mercury-resistant bacteria and ammonium thiosulfate increased plant height by 96% (B1K0), 108% (B2K0), 145% (B1K1), 131% (B2K1), 110% (B0K1), and 69% (B0K0). Application of mercury-resistant bacteria in the soil phytoremediation process further enhanced the growth of maize plants. The combination of treatment in the soil

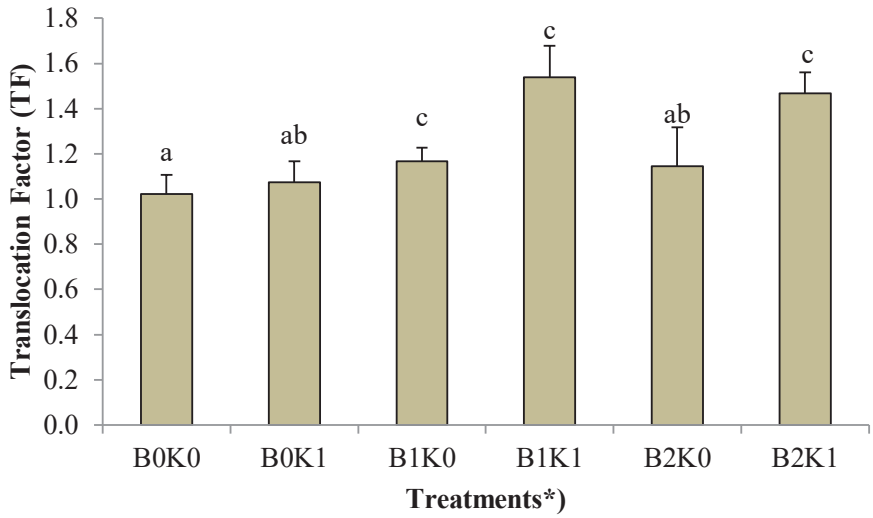

Fig. 3: Effect of application of mercury-resistant bacteria and ammonium thiosulfate on the translocation factor of mercury by *P. conjugatum* at 70 days. Vertical bars represent standard deviation while the same letters are not significantly different for each treatment mean at 0.05 level of probability. *) B0 = no bacterial isolate, B1 = *B. vesicularis* isolate, B2 = *N. mobilis* isolate, K0 = without ammonium thiosulfate, K1 = with ammonium thiosulfate 2 g/kg.

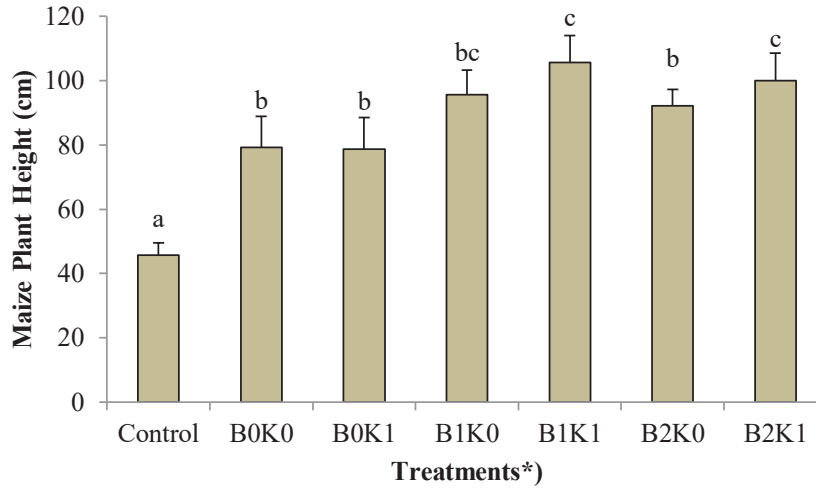

Fig. 4: Height of maize grown on post-phytoremediation soil at 60 days. Vertical bars represent standard deviation while the same letters are not significantly different for each treatment mean at 0.05 level of probability. *) B0 = no bacterial isolate, B1 = *B. vesicularis* isolate, B2 = *N. mobilis* isolate, K0 = without ammonium thiosulfate, K1 = with ammonium thiosulfate 2 g/kg, Control = soil not subjected to phytoremediation.

phytoremediation process which then resulted in the best growth of maize plant was the B1K1 treatment. This is in line with the results of the highest Hg reduction in soil by the B1K1 treatment (Fig. 2).

The dry weight of the shoots and roots of maize plants increased on the soils which had been remediated with a combination of *P. conjugatum* and mercury-resistant bacteria. Consistent with the capability of the B1K1 treatment (*B. vesicularis* with ammonium thiosulfate) in accumulating the highest Hg, the highest increase in the dry weight of

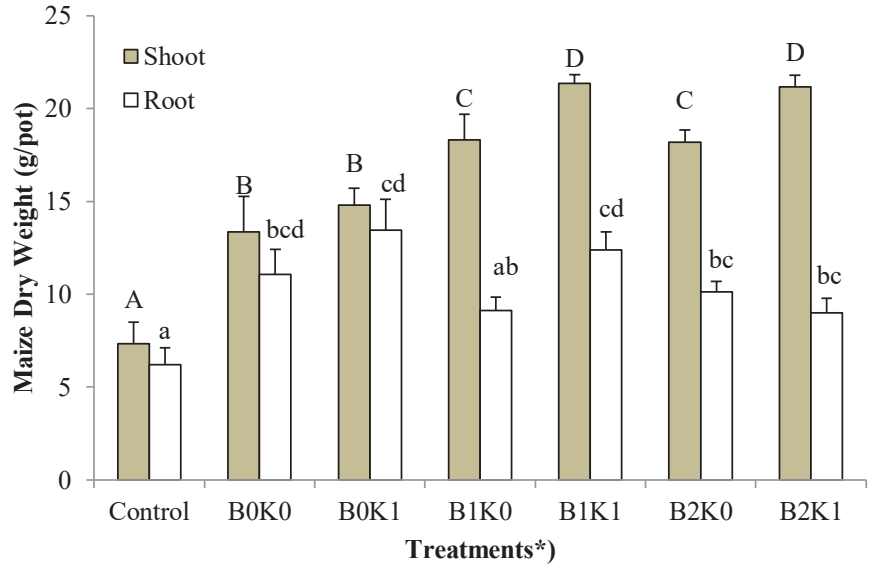

Fig. 5: Shoot and root dry weight of maize grown on post-phytoremediation soil at 60 days. Vertical bars represent standard deviation while the same capital and small letters are not significantly different for each treatment mean at 0.05 level of probability. *) B0 = no bacterial isolate, B1 = *B. vesicularis* isolate, B2 = *N. mobilis* isolate, K0 = without ammonium thiosulfate, K1 = with ammonium thiosulfate 2 g/kg, Control = soil not subjected to phytoremediation.

shoots and roots were also found in the B1K1 treatment although it was not significantly different from the B2K1 treatment (Fig. 5). Compared to the control, the increase in maize biomass (shoot and root) grown on soil previously remediated through the B1K1 and B2K1 treatments were 145% and 131%, respectively, while those grown on soil previously remediated through the B1K0 and B2K0 treatments were 96% and 108% respectively. Biomass of maize plants grown on the soil remediated with *P. conjugatum* without mercury-resistant bacteria and ammonium thiosulfate were low and not significantly different from the control. The low increase of maize plant growth and yield of maize biomass on post-phytoremediation without the addition of mercury-resistant bacteria and ammonium thiosulfate compared to those grown on post-phytoremediation with the addition of mercury-resistant bacteria and ammonium thiosulfate was associated with mercury uptake by plants (Fig. 6).

The remaining mercury in the growing media without the addition of mercury-resistant bacteria and ammonium thiosulfate was higher than in the growing media with the addition of ammonium thiosulfate, thus inhibiting plant growth. In plants, mercury causes damage to enzymes, polynucleotides, nutrient transport systems, and disrupts cell membrane integrity (Nagajyoti et al. 2010). Root extension is often used as the first indication that plants are poisoned by Hg elements (Moldovan et al. 2013). Symptoms of mercury toxicity, in general, are the inhibition of seed and root growth, and the inhibition of photosynthesis, which in turn reduces crop production. In addition, mercury accumulated in plant root can inhibit the absorption of K by plants (Hooda 2010). Mercury absorbed by plants can cause some enzymes to be inactive because of the incorporation of mercury into sulfhydryl peroxide through the formation of reactive oxygen compounds, such as superoxide, hydroxyl radicals, and hydrogen peroxide (Chen & Yang 2012).

Mercury Uptake by Maize

The results of the analysis of mercury in the maize shoots and roots showed that the accumulation of Hg in the maize plant was mostly found in the roots. From the average accumulation of Hg in the maize shoots and roots in all treatments, about 98% of the mercury was accumulated in the roots, while in the shoot was only 2% or an average of 0.008 mg/kg dry weight. This was in line with a study on the potential of maize for phytoremediation of soil contaminated with gold mine tailings conducted in Lombok by Afandi et al. (2019) that 95.7-98.6% of the Hg absorbed by the maize plant was concentrated in the maize root, and no mercury was detected in maize seeds. Therefore, it can be stated that the maize shoot is safe to be used as livestock feed because it is below the threshold of mercury content according to the threshold of the Indonesian Government Regulation of 0.03 mg Hg/kg.

Maize is capable of continuous phytoextraction of metals from contaminated soils by translocating them from roots

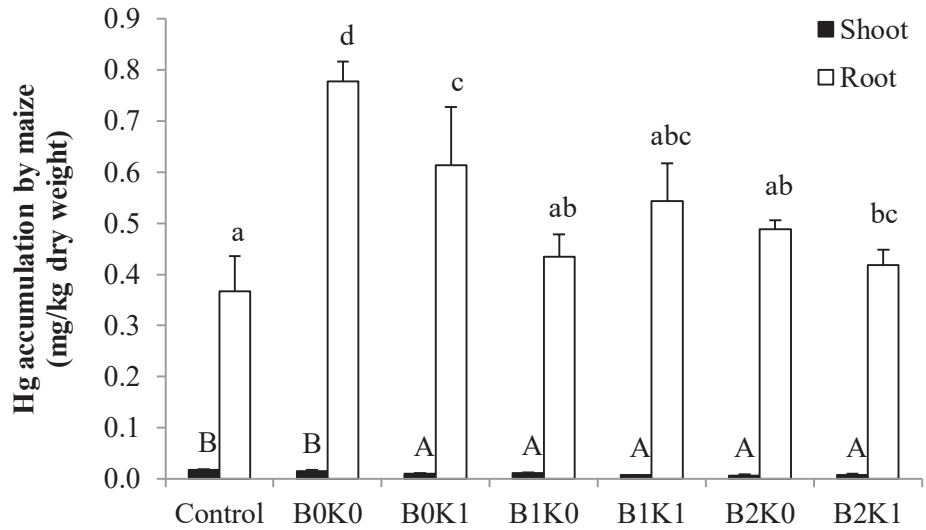

Fig. 6: Accumulation of mercury by maize grown on post-phytoremediation soil at 60 days. Vertical bars represent standard deviation while the same capital and small letters are not significantly different for each treatment mean at 0.05 level of probability. *) B0 = no bacterial isolate, B1 = *B. vesicularis* isolate, B2 = *N. mobilis* isolate, K0 = without ammonium thiosulfate, K1 = with ammonium thiosulfate 2 g/kg, Control = soil not subjected to phytoremediation.

to shoots (Nascimento & Xing 2006). The maize plant has been even shown to accumulate certain heavy metals such as Cd (Kimenyu et al. 2009) and Pb (Pereira et al. 2007) above levels that define metal hyperaccumulation. Máthé-Gáspár & Anton (2005) have grouped maize as an accumulator and a metal tolerant plant. The potential use of maize in phytoextraction technology is thus advocated, especially for developing countries with scarce funds available for environmental restoration (Wuana & Okieimen 2010).

CONCLUSION

The application of *B. vesicularis* and *N. mobilis* combined with ammonium thiosulfate as a chelating agent enhanced the growth and biomass of *P. conjugatum* in the phytoremediation process of soil contaminated with small-scale gold mine tailings. This, in turn, increased mercury accumulation in plants so that it reduced 18-20% of mercury content in the soil contaminated with gold mine tailings. The decrease of mercury content in the soil led to improved growth and yield of maize planted after soil phytoremediation through the application of *B. vesicularis* and *N. mobilis*.

ACKNOWLEDGEMENTS

The authors thank the Ministry of Research, Technology, and Higher Education of Indonesia for supporting this study through Project No. 054/SP2H/LT/DRPM/2018. Field and technical assistance of the Bonjeruk Farmers of Central Lombok is gratefully acknowledged.

REFERENCES

Afandi, Y., Tejowulan, R.S. and Krisnayanti, B.D. 2019. Mercury uptake by *Zea mays* L. grown on an inceptisol polluted by amalgamation and cyanidation tailings of small-scale gold mining. Journal of Degraded and Mining Lands Management, 6(3): 1821-1828.

Ashraf, M.A., Maah, M.J. and Yusoff, I. 2011. Heavy metals accumulation in plants growing in ex-tin mining catchment. International Journal of Environmental Science and Technology, 8: 401-416.

Chasanah, U., Nuraini, Y. and Handayanto, E. 2018. The potential of mercury-resistant bacteria isolated from small-scale gold mine tailings for accumulation of mercury. Journal of Ecological Engineering, 19(2): 236-245.

Chen, J. and Yang, Z.M. 2012. Mercury toxicity, molecular response and tolerance in higher plants. BioMetals, 25: 847-857.

Compant, S., Clément, B. and Sessitsch, A. 2010. Plant growth-promoting bacteria in the rhizo- and endosphere of plants: their role, colonization, mechanisms involved and prospects for utilization. Soil Biology and Biochemistry, 42: 669-678.

Handayanto, E., Nuraini, Y. and Muddarisna, N. 2016. Optimization of plant species and chelating agents in phytoextraction of gold from small-scale gold mine tailings. Nature Environment and Pollution Technology, 5(3): 1083-1088.

Hooda, P.S. 2010. Trace Elements in Soils. Blackwell Publishing Ltd.

Khalifa, A.Y.Z., Alsyeeh, A.M., Almalki, M.A. and Farag, A. 2015. Characterization of the plant growth promoting bacterium, *Enterobacter cloacae* MSR1, isolated from roots of non-nodulating *Medicago sativa*. Saudi Journal of Biological Science, 23(1): 79-86.

Kimenyu, P.N., Oyaro, N., Chacha, J.S. and Tsanuo, M.K. 2009. The potential of *Commelina bengalensis, Amaranthus hybridus, Zea mays* for phytoremediation of heavy metals from contaminated soils. Sains Malaysiana, 38(1): 61-68.

Koide, M., Higa, F., Tateyama, M., Cash, H.L., Hokama, A. and Fujita, J. 2014. Role of *Brevundimonas vesicularis* in supporting the growth of Legionella in nutrient-poor environments. New Microbiologica, 37: 33-39.

Koilraj, A.J., Prabhavathi, P., Rajendran, R., Kuberan, T., Gowri, R.S. and Selvi, C.P. 2012. Degradation of organic wastes and recycling of nutrients enhanced by microbes in subterranean habitat. African Journal of Microbiology Research, 6(21): 4449-4456.

Krisnayanti, B.D., Anderson, C.W.N., Utomo, W.H., Feng, X., Handayanto, E., Muddarisna, N., Ikram, H. and Khususiah. 2012a. Assessment of environmental mercury discharge at a four-year-old artisanal gold mining area on Lombok Island, Indonesia. Journal Environmental Monitoring, 14: 2598-2607.

Krisnayanti, B.D., Arifin, Z. Bustan, Sudirman, and Yani, A. 2012b. Mercury Concentration on Tailing and Water from One Year of ASGM at Lantung, Sumbawa, Indonesia. In: Environmental, Socio-economic, and Health Impacts of Artisanal and Small-Scale Minings. E. Handayanto, B.D. Krisnayanti and Suhartini (Eds). pp. 61-66, ISBN: 978-602-203-276-2, UB Press, Malang, Indonesia.

Li, J.H., Wang, E.T., Chen, W.F. and Chen W.X. 2008. Genetic diversity and potential for promotion of plant growth detected in nodule endophytic bacteria of soybean grown in Heilongjiang province of China. Soil Biology and Biochemistry, 40: 238-246.

Liagat, F. and Eltem, R. 2016. Identification and characterization of endophytic bacteria isolated from in vitro cultures of peach and pear rootstocks. 3 Biotech, 6(2): 120.

Marra, L.M., Soares, C.R.F.S., de Oliveira, S.M., Ferreira, P.A.A., Soares, B.L., de Fráguas Carvalho, R., de Lima J.M. and de Souza Moreira, F.M. 2012. Biological nitrogen fixation and phosphate solubilization by bacteria isolated from tropical soils. Plant and Soil, 57: 289-307.

Máthé-Gáspár, G. and Anton, A. 2005. Phytoremediation study: Factors influencing heavy metal uptake of plants. Acta Biologica Szegediensis, 49(1-2): 69-70.

Moldovan, O.T., Meleg, I.N., Levei, E. and Terente, M. 2013. A simple method for assessing biotic indicators and predicting biodiversity in the hyporheic zone of a river polluted with metals. Ecological Indicators, 24: 412-420.

Moreno, F.N., Anderson, C.W.N., Robinson, B.H. and Stewart R.B. 2004. Phytoremediation of mercury-contaminated mine tailings by induced plant-Hg accumulation. Environmental Practice, 6(2): 165-175.

Moreno, F.N., Anderson, C.W.N., Stewart, R.B., Robinson, B.H., Nomura, R., Ghomshei, M. and Meech, J.A. 2005. Effect of thiol ligands on plant-Hg accumulation and volatilization from mercury-contaminated mine tailings. Plant and Soil, 275: 233-246.

Muddarisna, N., Krisnayanti, B.D., Utami, S.R. and Handayanto, E. 2013a. Effects mercury on growth and biochemical constituents of maize seedlings. Plant Sciences Feed, 3(4): 50-55.

Muddarisna, N., Krisnayanti, B.D., Utami, S.R. and Handayanto, E. 2013b. The potential of wild plants for phytoremediation of soil contaminated with mercury of gold cyanidation tailings. Journal of Environmental Science, Toxicology and Food Technology, 4(1): 15-19.

Nagajyoti, P.C., Lee, K.D. and Sreekanth, T.V.M. 2010. Heavy metals, occurrence and toxicity for plants: a review. Environmental Chemistry Letters 8: 199-216.

Nascimento, A.M.A. and Chartone-Souza, E. 2003. Operon mer: Bacterial resistance to mercury and potential for bioremediation of contaminated

environments. Genetics and Molecular Research, 2(1): 92-101.

Nascimento, C.W.A. and Xing, B. 2006. Phytoextraction: A review on enhanced metal availability and plant accumulation. Scientia Agricola (Piracicaba, Brazil), 63(3): 299-311.

Pereira, B.F.F., de Abreu, C.A., Romeiro, S., Lagôa, A.M.M.A. and Paz-Gonzále, A. 2007. Pb-Phytoextraction by maize in a Pb-EDTA treated oxisol. Scientia Agricola (Piracicaba, Brazil), 64(1): 52-60.

Salt, D.E., Blaylock, M., Kumar, P.B.A.N., Dushenkov, V., Ensley, B.D., Chet, L. and Raskin, L. 1995. Phytoremediation: a novel strategy for the removal of toxicants from the environments using plants. Biotechnology, 13: 468-474.

Selin. N.E. 2009. Global biogeochemical cycling of mercury: A review. Annual Review of Environment and Resources, 34: 43-63.

Sheng, H.M., Gao, H.S., Xue, L.G., Ding, S., Song, C.L., Feng, H.Y. and An, L.Z. 2011. Analysis of the composition and characteristics of culturable endophytic bacteria within subnival plants of the Tianshan Mountains, northwestern China. Current Microbiology, 62: 923-932.

Su, Y., Han, F.X., Chen, J., Shiyab, S. and Monts, D.L. 2009. Phytotoxicity and phytoremediation of mercury in Indian mustard and two Ferns with mercury-contaminated water and Oak Ridge soil. WM2009 Conference.

Tangahu, B.V., Abdullah, S.R.S., Idris, H.B.M., Anuar, N. and Mukhlisin, M. 2011. Review on heavy metal (As, Pb and Hg) uptake by plants through phytoremediation. International Journal of Chemical Engineering, 31: 20-26,

Thandar S.M., Ushiki, N., Fujitani, H., Sekiguchi, Y. and Tsuneda, S. 2016. Ecophysiology and comparative genomics of *Nitrosomonas mobilis* Ms1 isolated from autotrophic nitrifying granules of wastewater treatment bioreactor. Frontiers in Microbiology, Volume 7, Article 1869.

Wagner-Dobler, I., von Canstein, H., Li Y., Timnis, K.N. and Deckwer, W.D. 2000. Removal of mercury from chemical wastewater by microorganisms in technical scale. Environmental Science and Technology, 34: 4628-4634.

Wang, J., Feng, X. and Anderson, C.W.N. 2013.Thiosulfate assisted phytoextraction of mercury (Hg) contaminated soils at The Wanshan Mercury Mining District, Southwest China. Journal of Degraded and Mining Lands Management, 1(1): 1-8.

Wang, Y. 2004. Phytoremediation of Mercury by Terrestrial Plants. Doctoral thesis in Botany. Department of Botany, Stockholm University.

Wuana, R.A. and Okieimen, F.E. 2010. Phytoremediation potential of maize (*Zea mays* L.). A Review. African Journal of General Agriculture, 6(4): 275-287.

Ying, W., Cheng-de, Y., Yu-ling, Y., Yu-qin, W., Zhen-fen, Z. and Li, X. 2015. The diversity and potential function of endophytic bacteria isolated from *Kobreasia capillifolia* at alpine grasslands on the Tibetan Plateau, China. Journal of Integrative Agriculture, Advance Online Publication 2015.

Yoon, J., Cao, X. and Zhou, O. 2006. Accumulation of Pb, Cu, and Zn in native plants growing on a contaminated Florida site. Science of the Total Environment, 368: 456-464.

Yu, L., Peng, D. and Pan, R. 2012. Shifts in nitrification kinetics and microbial community during bioaugmentation of activated sludge with nitrifiers enriched on sludge reject water. Journal of Biomedicine and Biotechnology, Article ID 691894.

Nature Environment and Pollution Technology
An International Quarterly Scientific Journal

p-ISSN: 0972-6268
e-ISSN: 2395-3454

Vol. 19 | No. 1 | pp. 263-268 | 2020

Original Research Paper | Open Access

Performance Study of Cellulose Acetate Blended Polyvinylchloride Membranes

Pawan Kumar and Vijay Laxmi Yadav†
Department of Chemical Engineering and Technology, IIT-BHU, Varanasi-221005, Uttar Pradesh, India
†Corresponding author: Vijay Laxmi Yadav

Nat. Env. & Poll. Tech.
Website: www.neptjournal.com

Received: 08-05-2019
Accepted: 21-06-2019

Key Words:
Polyvinyl chloride
Cellulose acetate
Antifouling membrane
Alcohol water mixture

ABSTRACT

In this paper, polymeric membranes were prepared by uniformly dispersing the cellulose acetate, polyethylene glycol and polyvinyl pyrrolidone particles in a polyvinyl chloride matrix for resolving the demand for azeotropic mixture separations. The polymeric membranes were characterized using SEM, FTIR and XRD analysis. The results show that the blending of cellulose acetate and plasticizer diethyl phthalate significantly improved the separation performance of the membranes. The selectivity was increased by adding cellulose acetate up to 2% wt and polyethylene glycol 1% wt. Pervaporation setup was used to separate azeotropic mixture using the prepared membrane. The optimum results were obtained for dehydration of alcohol where the composition plasticizer was 0.5% wt. Based on the findings of the research, it was observed that the PVC membrane can be modified with CA and PEG due to their hydrophobic nature. The results show that the synthesized membrane can be used for removal of water from alcohol.

INTRODUCTION

In the present scenario, the most established membrane separation processes are reverse osmosis, microfiltration, ultra-filtration, and electro dialysis. Except them, two new growing industrial processes are gas separation and pervaporation for separation of an azeotropic mixture (Qureshi 2016). Pervaporation is among the least studied of all membrane separation processes (Pramanik 2017). The work herein has the motive to show the effect of fabrication conditions on membrane performance. The work is mainly focused on the preparation of hydrophobic membranes for the separation of ethanol water mixture. In recent decades, membranes have occupied a major role worldwide in chemical technologies because of a vast diversity of separations can be done by membranes such as separation of gaseous mixtures, filtration of particles from solutions, even membrane are separating close boiling liquids from each other, to name a few (Yamamoto 2017). There is a large number of industries in which such separations are carried out on a large scale such as pharmaceutical, food science and chemical processes (Ayman 2012).

This paper is concerned with the advanced development of polymeric membranes for pervaporation by solution casting method (Sadri 2017). All membranes were prepared using a phase inversion process. Early research was focused on the development of viable membranes (Han 2017 and Zhao 2017).

By the start of the 20th-century, membranes became popular and by the late 1960s onwards many improvements also started in the field of dialysis in medicine and controlled drug delivery by the membranes. This led to the development of microfiltration, ultrafiltration, reverse osmosis and electrodialysis during the 1970's (Chun 2016). Last two decades of the 20th century showed the development of gas separation and pervaporation membrane technologies and current membrane industries took its shape (Imbrogno 2017 and Gu 2016).

A variety of research has been done on the preparation of membranes using polyvinylchloride (PVC) because of their flexibility in operation, durability and better performance and resistance to chemicals. PVC membranes are hydrophobic in nature (Bandi 2016, El-Gendi 2012 and El-Gendi 2014). Commonly, PVC is one of the most common and easily available polymers because of its low price which is less than 1/10 of most common commercial polymer for membrane, i.e. PVDF polymer. Hence, PVC is a major concern for researchers for membrane preparation as it is very competitive to other polymers (Mokhtari 2016).

The objective of this study was to prepare a suitable blend of PVC/CA/PEG membrane for separation of alcohol from an alcohol-water mixture by non-solvent induced phase inversion technique. The prepared membranes were characterized with SEM, X-ray diffractometer and Fourier

Table 1: Polymeric membrane composition for PVC/CA, for different samples of (S-1 to S-4) membrane (weight percentage).

	PVC %	CA %	PEG %	THF %	Plasticizer %
S-1	18	0	2	80	0
S-2	16	2	2	80	0
S-3	15	3	2	80	0
S-4	15	2.5	2	80	0.5

Table 2: Performance of different membranes for separation of ethanol-water.

Membrane	Product Flux for feed conc. 15% alcohol ($kg.m^{-2}hr^{-1}$)	Product Flux for feed conc. 30% alcohol ($kg.m^{-2}hr^{-1}$)	Product Flux for feed conc. 45% alcohol ($kg.m^{-2}hr^{-1}$)
S-1	5.93	5.8	5.88
S-2	4.88	4.99	5.02
S-3	3.773	3.01	3.134
S-4	2.5	2.62	2.53

Table 3: Thickness of prepared membrane samples.

Membrane	Thickness (mm)
S-1	0.41
S-2	0.14
S-3	0.24
S-4	0.30

transform infrared (FTIR) (Oh & Jang 2016). Performance of lab made membranes was investigated by treating a sample of an alcohol-water mixture with different concentration.

MATERIALS AND METHODS

Materials

Polyvinylchloride (PVC) the base polymer, cellulose acetate (CA), polyvinyl pyrrolidone (PVP) and polyethylene glycol (PEG) were purchased from Sigma Aldrich. Tetrahydrofuran (THF) was used as a solvent and was purchased from Spectrochem, Mumbai. Absolute alcohol was used to check the performance of the membranes.

Preparation of Membranes

Blended PVC/CA/PVP membranes were prepared by the phase inversion process (Saljoughi et al. 2009). The known amounts of polymers were dissolved in NMP and compositions of samples are shown in Table 1. After this, the solution was stirred for 12 hr. The solution of polymer was cast on a glass plate, and glass plate was subsequently dipped in a non-solvent bath of deionized water. The water was changed three times for complete exchange of solvent THF. And finally, the membrane was dried in the oven at 50^oC and then used further.

Membrane Characterization

Surface morphology of prepared membrane samples was investigated by scanning electron microscopy (SEM). Samples were pre-coated with gold to provide electrical conductivity. The instrument used for the purpose was EVO - Scanning Electron Microscope MA15/18, Carl Zeiss Microscopy Ltd., USA. The crystalline or amorphous nature of polymeric membranes was investigated using X-ray diffractometer (XRD, model - EDS System, Carl Zeiss Microscopy Ltd., USA) with a scanning rate of 5^o per minute in the range of 0^o to 70^o (2θ). The functional changes in the polymeric membranes were analysed in the transmittance mode from 4000 to 400 cm^{-1} wavelength range using Fourier Transform Infrared Spectroscopy (FTIR) Varian 1000, USA.

A lab scale dead end pervaporation setup was used to study the performance of samples using an alcohol water mixture. Performance of membrane was expressed in terms of permeate flux.

RESULTS AND DISCUSSION

Thickness of Membrane

The thickness of the different membrane samples, measured using digital Vernier callipers, is given in Table 3. The

Table 4: Wavelength for cellulose acetate group.

Wavelength cm^{-1}	Chemical bond
2918.9-3406.1	-OH
1633.3-1738.2	C=O
1370.9-1489.7	CH_3
1769.7	-CH
1044.9	C-O-C
669.3	R-COH

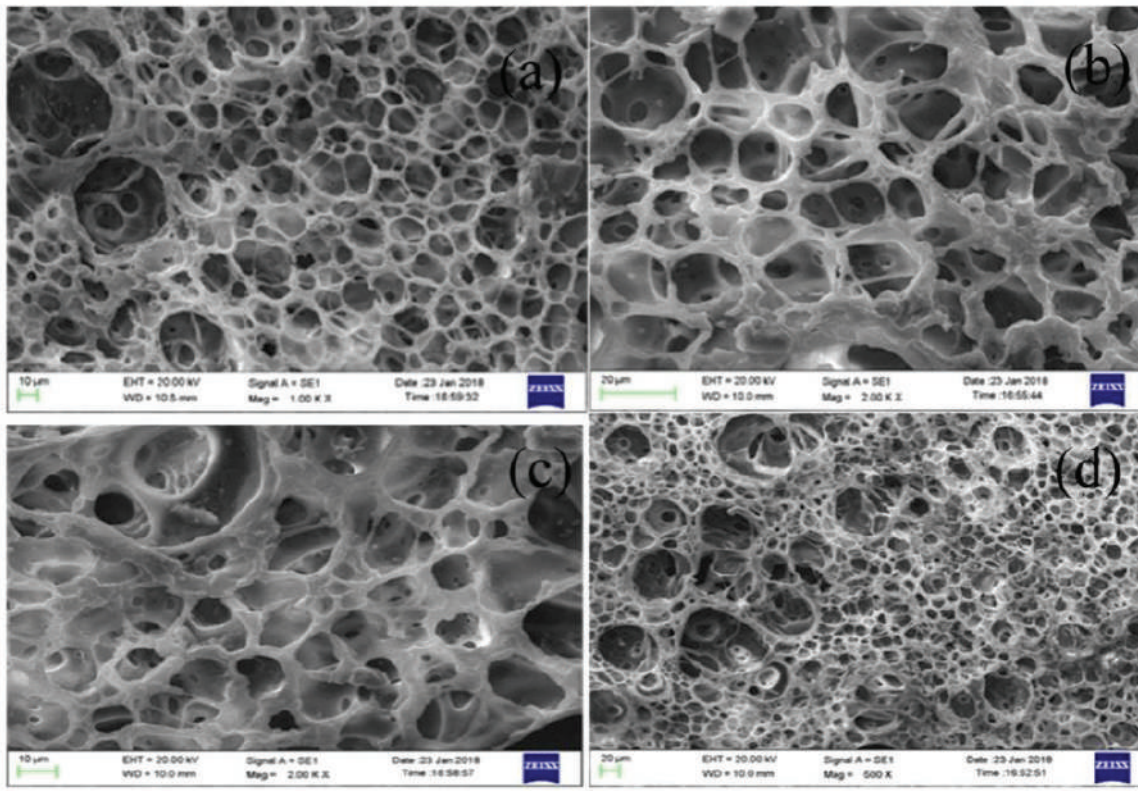

Fig. 1: SEM images of prepared PVC membranes (a)- sample S-1, (b)- sample S-2, (c)- sample S-3, (d)- sample S-4.

thickness of the membrane increased when the amount of the cross linker was increased. This occurs due to high bonding between cross linker and polymer. It is seen that as the amount of cross-linking agent is increasing, membrane thickness is also increasing due to the formation of an intermediate layer of fillers due to the polymerization of cross linker.

Membrane Morphology

SEM micrographs of different samples have been shown in Fig. 1(a-d). SEM images show a cross section of the (S-1) membrane. Expected asymmetric pores are observable in the entire surface as the CA was added to the system. At the same time S-2 shows different surface pattern. It was seen in the image of S-2 that surface become rougher and pores become denser as the result of blending. Saljoughi et al. (2009) had also shown similar changes. Similarly, by addition of more CA in S-3, number of pores decreased and it was visible in SEM image. In S-4, plasticizer was added to see its effect on the surface. It was seen that by addition of plasticizer, pores became large which in turn increased the flux through the membrane and this phenomenon was verified by performance studies where S-4 shown better flux.

FTIR Analysis

Membranes were further characterized by Fourier Transform

Infrared (FTIR) spectroscopy in the range 4000-400 cm^{-1} to know the functional groups present in the samples to verify the formation of desired composites. The membrane samples (S1 - S4) were tested for comparison and the result is shown in Fig. 2. The peaks corresponding to 2520 cm^{-1} for sample S-1, 2640 cm^{-1} for sample S-2, 2750 cm^{-1} for sample S-3, 2610 cm^{-1} for sample S-4 and at 2595 cm^{-1} for sample S-4 corresponding to C-H stretching (Saljoughi et al. 2009).

Functional groups and their peaks which are common for CA are given in Table 4. A peak at 1470 cm^{-1} was observed (except in sample-1) corresponding to -CH_2 bonding. The C-Cl stretching was indicated by the 4 peaks at 727 cm^{-1}, 685 cm^{-1}, 715 cm^{-1} and 750 cm^{-1} for the sample S-1, S-2, S-3, and S-4 respectively. The effect of adding PEG was observed in sample-1 at peak 683 $cm^{-1,}$ indicating that PEG mostly influences the membrane structure.

After blending of PVC with CA and PEG, a shift was observed for PVC and CA peaks.

X-Ray Diffraction (XRD) Analysis

The crystalline and amorphous character of the membrane was studied by X-ray diffraction measurement and has been shown in Fig. 3. We can see from Fig. 3(a) of sample-1 the XRD patterns two peaks are observed. Here peaks are seen at a 2-theta value of 17° and 26°. Broad peaks appeared at 26° and smaller peak appeared at 17°.

Further, from Fig. 3(b) of sample-2, we can also see that when we increase the amount of PVC again, we observed 2 peaks at a 2-theta value of 27° and 38°, but the peak corresponding to 27° is more intense and higher. These peaks are sharper than sample-1 that can be attributed to the involvement of cellulose acetate. Such results are also observed by Saeki et.al (2013) while preparing poly amide membrane with similar procedure.

From the Fig. 3(c) of sample-3, we observe the same XRD pattern as in the graph of sample-2. There are 2 peaks at a 2-theta value of 27° and 38°, but this time high peak appears at 27° and a smaller peak at 38°. The intensity of peaks is higher than those of sample-2. This can be due to the addition of 2% PEG as a pore creator.

From the Fig. 3(d) of sample-4 in which 0.5% plasticizer was also added to increase the elastic nature of the sample. In this case, it was observed same XRD pattern as in Fig. 3(b) of sample-2 and in Fig. 3(c) of sample-3. In this, we

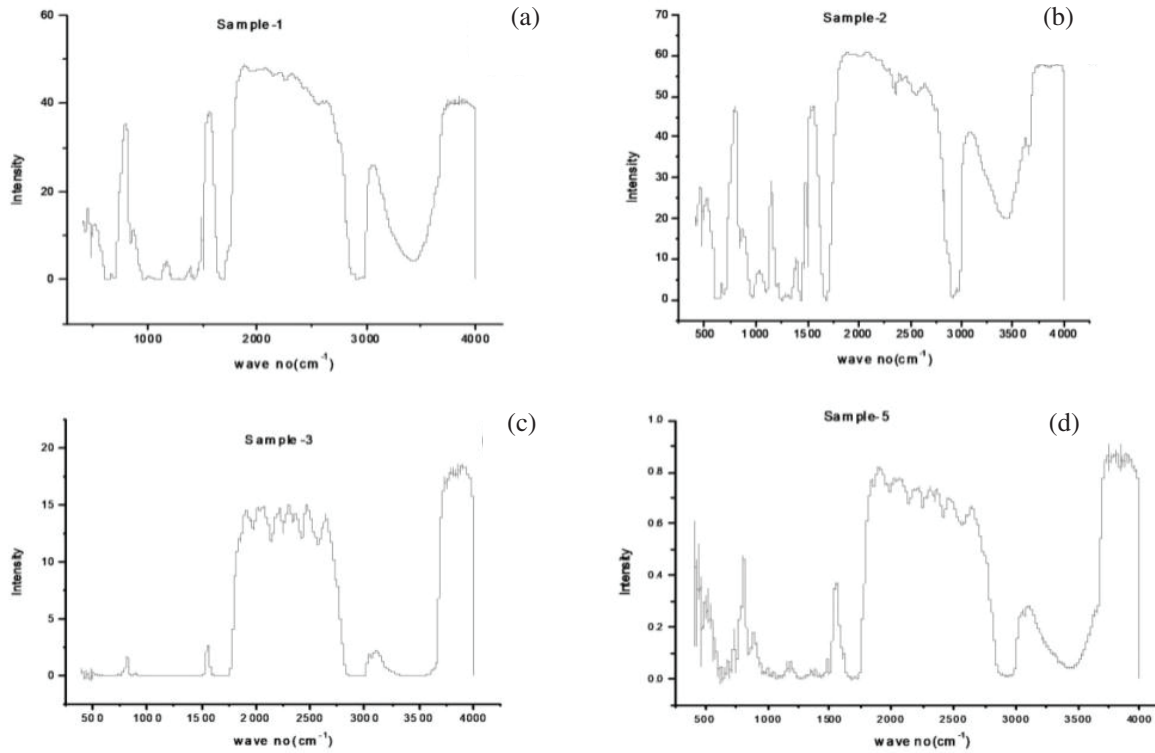

Fig. 2: FTIR spectra of prepared membranes (a) sample S-1, (b) sample S-2, (c) sample S-3, (d) sample S-4.

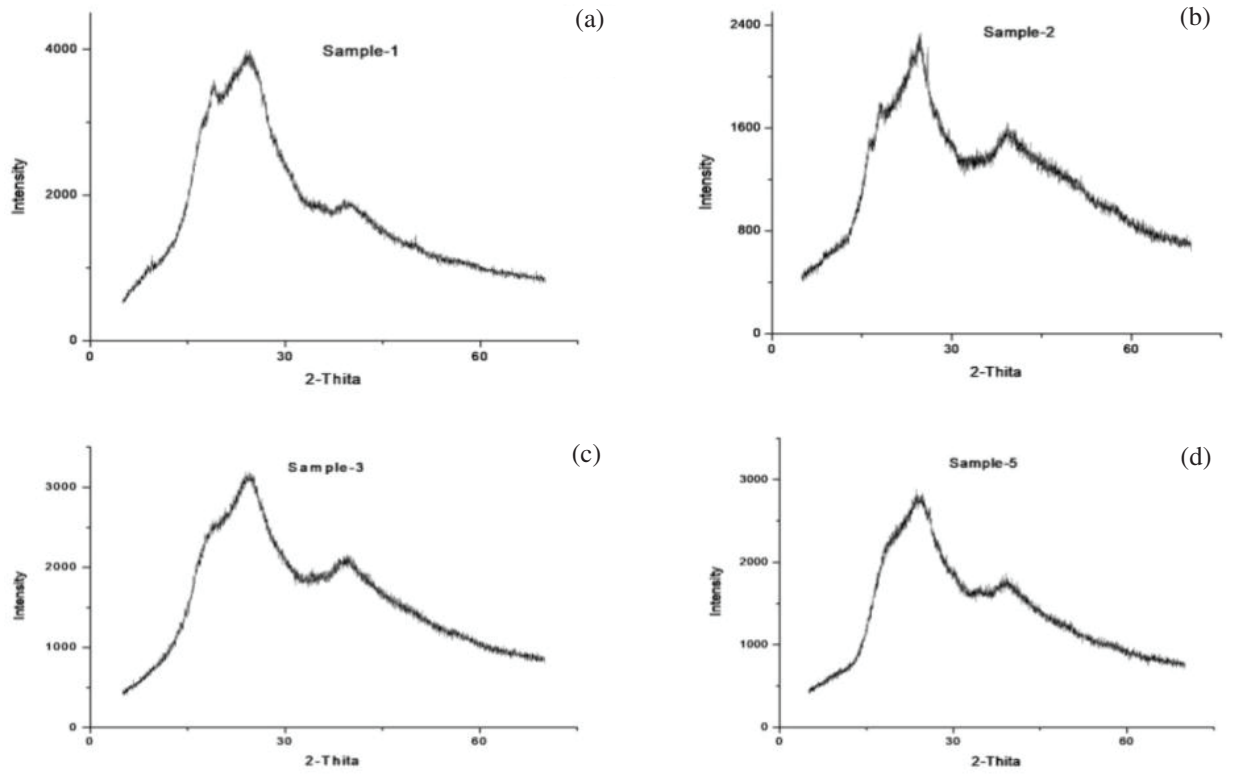

Fig. 3*:* XRD patterns for different samples.

observed 2 peaks at 26.5° and 33°, but this time high peak appears at 26.5°, and smaller one appears at 33°, but the intensity of peaks is higher than in Fig. 3(b) of sample-2 and in Fig. 3(c) of sample-3. This can be due to the addition of 0.5% plasticizer to increase elasticity.

Membrane Performance

In order to check the performance of the membrane, the ethanol-water mixture was used as the feed. Several compositions of the ethanol-water mixture were used to measure the flux of ethanol across the membrane to study the performance of the prepared membrane. Table 2 shows the observations regarding the flux of product for various samples.

From Table 2 we can say that the total flux through the membrane is in the order of S-1 > S-2 > S-3 > S-4. In S-1, equal amount of PVC and PEG were involved and porosity of this membrane is highest resulting in maximum flux compared to other membrane samples.

In S-2 (PVC blend with CA and PEG), we observed less product flux compared to S-1. This can be due to the fact that on increasing the amount of PVC and adding one more additive PEG, the porosity goes down.

In the preparation of S-3 flux of product again decreases and is less than S-2. This can be due to the fact that on adding more polymer, particles started aggregating and, pore would be denser, hence the resulting flux decreases. When we use S-4 membrane for pervaporation of given feed, we observed that the flux decreases but the change in amount was less than S-2 and S-3. In S-4 membrane we have added a plasticizer to enhance the elasticity.

CONCLUSION

PVC/CA/PEG and PVP blended membrane were successfully prepared via wet phase inversion technique using different concentrations of the component polymers. The following conclusions can be drawn from the above work: From SEM analysis membranes were found to be a dense and asymmetric membrane. Characterization results indicate that membrane S-4 is the best membrane among the prepared membranes S-1 to S-4. The durability test of membrane S-4 was conducted, and the membrane performance was approximately constant and stable over 20 days. FTIR and XRD analysis showed the proper formation of the composite by the process and by performance studies, it was observed

that membrane containing PVC, CA and plasticizer has the highest flux, so the blend of sample 4 was optimum according to our study for separation of alcohol water mixture.

REFERENCES

Ayman, E.G., Heba, A. and Sahar A. 2012. Construction of ternary phase diagram and membrane morphology evaluation for polyamide/formic acid/water system. Australian J. Basic App. Sci., 6(5): 62-68.

Bandi, C.S., Uppaluri, R. and Kumar, A. 2016. Global optimization of MSF seawater desalination processes. Desalination, 394: 30-43.

Chun, Y., Zaviska, F., Kim, S.J. and Mulcahy, D. 2016. Yang, E., Kim, I. S. and Zou, L., Fouling characteristics and their implications on cleaning of a FO-RO pilot process for treating brackish surface water. Desalination, 394: 91-100.

El-Gendi, A., Ali, S.S., Ahmed, S.A. and Talaat, H.A. 2012. Development of membrane blend using casting technique for water desalination. Membrane Water Treatment, 3(3): 201-209.

El-Gendi, A., Deratani, A., Ahmed, S.A. and Ali, S.S. 2014. Development of polyamide-6/chitosan membranes for desalination. Egyptian J. Petro., 23(2): 169-173.

Gu, H., Rahardianto, A., Gao, L.X., Christofides, P.D. and Cohen, Y. 2016. Ultrafiltration with self-generated RO concentrate pulse backwash in a novel integrated seawater desalination UF-RO system. J. Memb. Sci., 520: 111-119.

Han, S., Rhee, Y.W. and Kang, S.P. 2017. Investigation of salt removal using cyclopentane hydrate formation and washing treatment for seawater desalination. Desalination, 404: 132-137.

Ibrahim, S.M., Nagasawa, H., Kanezashi, M. and Tsuru, T. 2015. Robust organosilica membranes for high temperature reverse osmosis (RO) application: Membrane preparation, separation characteristics of solutes and membrane regeneration. J. of Memb. Sci., 493: 515-523.

Imbrogno, J., Keating IV, J.J., Kilduff, J. and Belfort, G. 2017. Critical aspects of RO desalination: A combination strategy. Desalination, 401: 68-87.

Mokhtari, H. and Sepahvand, M. 2016. Thermoeconomic and exergy analysis in using hybrid systems (GT+ MED+ RO) for desalination of brackish water in Persian Gulf. Desalination, 399: 1-15.

Oh, J.H. and Jang, A. 2016. Application of chlorine dioxide (ClO2) to reverse osmosis (RO) membrane for seawater desalination. J. Taiwan Inst. Chem. Engg., 68: 281-288.

Pramanik, B.K., Gao, Y., Fan, L., Roddick, F.A. and Liu, Z. 2017. Antiscaling effect of polyaspartic acid and its derivative for RO membranes used for saline wastewater and brackish water desalination. Desalination, 404: 224-229.

Qureshi, B.A., Zubair, S.M. 2016. Exergetic efficiency of NF, RO and EDR desalination plants. Desalination, 378: 92-99.

Sadri, S., Ameri, M. and Khoshkhoo, R.H. 2017. Multi-objective optimization of MED-TVC-RO hybrid desalination system based on the irreversibility concept. Desalination, 402: 97-108.

Saeki, D., Nagao, S., Sawada, I., Ohmukai, Y., Maruyama, T. and Matsuyama, H. 2013. Development of antibacterial polyamide reverse osmosis membrane modified with a covalently immobilized enzyme. J. Memb. Sci., 428: 403-409.

Saljoughi, E. and Mohammadi, T. 2009. Cellulose acetate (CA)/polyvinylpyrrolidone (PVP) blend asymmetric membranes: Preparation, morphology and performance. Desalination, 249(2): 850-854.

Yamamoto, K., Koge, S., Gunji, T., Kanezashi, M., Tsuru, T. and Ohshita, J. 2017. Preparation of POSS-derived robust RO membranes for water desalination. Desalination, 404: 322-327.

Zhao, Y., Zhang, Z., Dai, L., Mao, H. and Zhang, S. 2017. Enhanced both water flux and salt rejection of reverse osmosis membrane through combining isophthaloyl dichloride with biphenyl tetra acyl chloride as organic phase monomer for seawater desalination. J. Memb. Sci., 522: 175-182.

Nature Environment and Pollution Technology
An International Quarterly Scientific Journal

p-ISSN: 0972-6268
e-ISSN: 2395-3454

Vol. 19 | No. 1 | pp. 269-275 | 2020

Original Research Paper | Open Access

Extraction and Spectrophotometric Estimation of Fe^{3+}, Cd^{2+}, Pb^{2+} and Zn^{2+} From Industrial Effluents Using Synthetic Supramolecular Ligand

Sachin Patil*, Milind Kondalkar*, Umesh Fegade, Sanjay Attarde*† and Sopan Ingle***
*School of Environmental and Earth Sciences, KBC North Maharashtra University, Jalgaon, Maharashtra, India
**Department of Chemistry, Bhusawal Arts, Science and P. O. Nahata Commerce College, Bhusawal, Maharashtra, India
†Corresponding Author: Sanjay B. Attarde

Nat. Env. & Poll. Tech.
Website: www.neptjournal.com

Received: 28-06-2019
Accepted: 29-08-2019

Key Words:
Toxic metals
Extraction
Ligand
Solvent

ABSTRACT

Increased water pollution due to toxic heavy metals is becoming a serious threat which has been faced by the entire world in the last few decades. To overcome this problem a suitable complex ligand was designed for removal of Fe^{3+}, Cd^{2+}, Pb^{2+} and Zn^{2+} from the effluents. The work incorporated the synthesis of (4Z)-4-((2Z)-2-(2,5-dihydro-2,3-dimethyl-5-oxo-1-phenyl-1H-pyrazol-4-ylimino) ethylidene amino)-1,2-dihydro-1,5-dimethyl-2-phenylpyrazol-3-one (Supramolecular Ligand) by the condensation method and confirmed by FTIR and 1HNMR spectroscopic methods. The batch extraction experiments designed to examine the effect of various experimental parameters on the extraction efficiency of the heavy metals. The experimental results depicted that up to 30 min time for supramolecular ligand is enough for the significant extraction of all the metals under study. The pH level, slightly acidic to the neutral condition is favourable for maximum extraction of metals. The percent extraction at optimized conditions of time and pH were found to be 98.29, 96.63, 96.95 and 95.64% for Fe^{3+}, Cd^{2+}, Pb^{2+} and Zn^{2+} respectively. The extraction efficiency was governed by chloroform as a solvent. Simple to synthesize, faster extraction of metals, slightly acidic to neutral pH conditions for extraction are the characteristic features of the compound which governs its applicability.

INTRODUCTION

Water, being a limited resource, an increase in water pollution due to metal ions and other pollutants is of great concern throughout the world (Jethave et al. 2017). The different pollutants responsible for water pollution are organic dyes, inorganic oxyacids and heavy metals etc. Amongst these, heavy metals are considered as more dangerous because even trace quantity in water is considered as carcinogenic (Li et al. 2011, Tang et al. 2008). Though the metals play a vital role in human metabolism and photosynthesis, an excess of these metals in living organisms is responsible for genetic and metabolic diseases (Fraga 2005). Heavy metals have widespread applications in different industrial units, viz. paint, fertilizer, metal industry and electroplating industries (Hua et al. 2012). Particularly in developing countries like India, the local communities have often encountered hazardous effects of pollutants (Himadri et al. 2014).

Different methods like solid-phase extraction and liquid-liquid extraction, adsorption, co-precipitation, and ion exchange have been applied for the removal of heavy metals from water. (Oliva et al. 2002, Saracoglu et al. 2003, Okamoto et al. 2000, Jethave & Fegade 2018, Fegade et al. 2018, Kondalkar et al. 2018). Amongst these, liquid-liquid extraction is considered more effective because it is a simple, low cost, highly selective and has more removal efficiency. Till now, diverse complexing agents have been synthesized for metal extraction (Sarode et al. 2015, Costa et al. 2013). The aim of the present study is to synthesize a suitable chelating agent for liquid-liquid extraction of Fe^{3+}, Cd^{2+}, Pb^{2+} and Zn^{2+} from effluents. For this purpose, a supramolecular ligand was synthesized by a simple condensation reaction between 2 moles of 4-amino antipyrine and one mole of glyoxal in methanol. This chelating agent was characterized by NMR, FTIR and mass spectroscopy. The effect of various analytical parameters such as time, pH, concentrations, stripping agents and the presence of other ions on the extraction efficiency was examined. The experimental sets carried out to optimize the above parameters for removal of Fe^{3+}, Cd^{2+}, Pb^{2+} and Zn^{2+} from industrial wastewater. The remaining concentration of these metals in the reaction mixture was estimated by atomic absorption spectrophotometer.

MATERIALS AND METHODS

All chemicals and reagents used for the experiment and preparation of ligand were of analytical grade and procured from Sigma Aldrich and applied without further purification. Milli-Q water was used at every stage of the experiment.

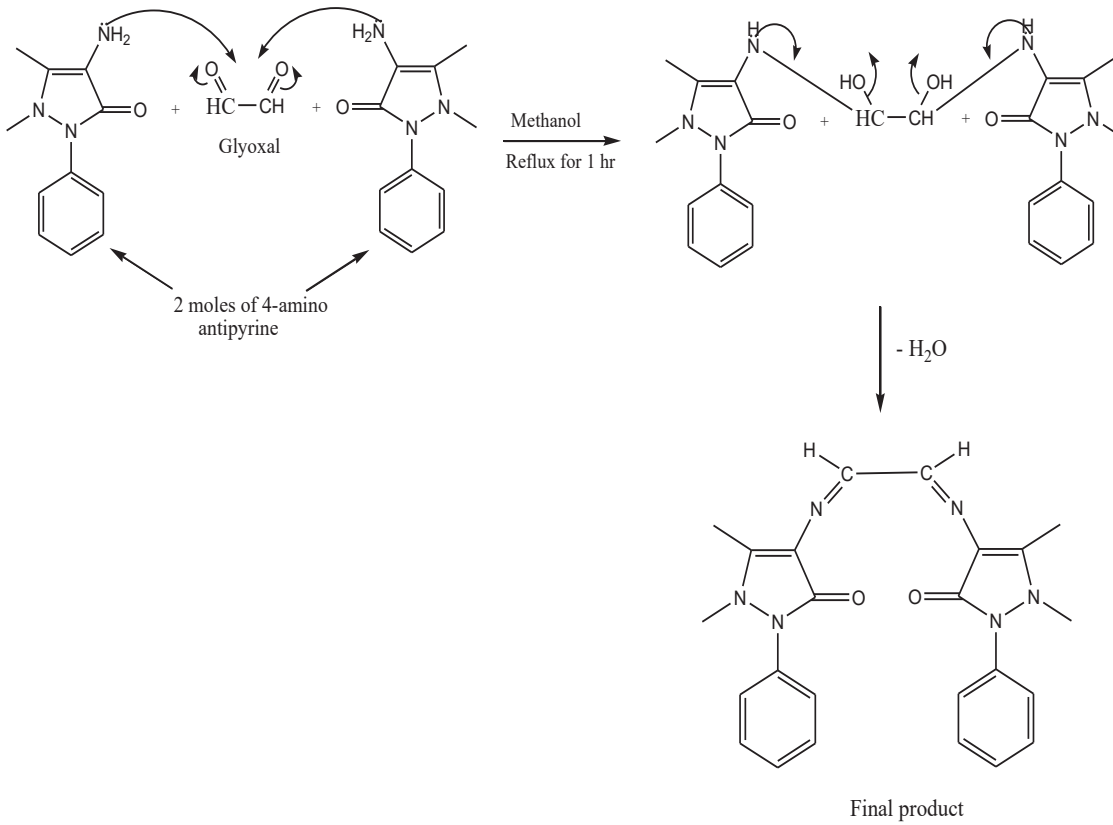

Fig. 1: Possible mechanism of the formation for supramolecular ligand compound.

Digital pH-meter (India, EQUIP-TRONICS model EQ 610) was used for pH determination. Concentration of chromium was estimated using AAS. FTIR spectrum (in the range of 500-4000 cm^{-1}) of the ligand was obtained using FTIR spectrophotometer (Germany, Model: Bruker). H^1NMR was recorded on (Germany, Model: Bruker Advance) 400MHz.

Batch Extraction Experiment for Metal Removal

Optimization of diverse analytical parameters on extraction efficiency for metals was carried out by conducting experiments at various experimental parameters. For the choice of solvent, the extraction experiments were performed on different solvents like chloroform, N-butanol, ethyl acetate, toluene and N-hexane. In these experiments, the solvent was optimized based on contact time for chromium extraction at a various time interval. Suitable pH for maximum extraction of chromium was determined by running the experiments at a particular pH range from 2 to 10, provided other optimized variables kept constant. The percent metals extracted (% E) was calculated by applying an Eq. 1.

$$\% E = (\text{concentration of metals after extraction} / \text{total concentration of metals}) \times 100 \quad \ldots(1)$$

RESULTS AND DISCUSSION

Synthesis of the Ligand Compound

The 0.2 moles of 4-amino antipyrine were poured in a 100 mL round bottom flask containing 25 mL methanol and the mixture was homogeneously mixed by a magnetic stirring. To these solutions, 0.1 moles of glyoxal was added drop-wise and the reaction solution was refluxed for 1 hr till the yellow residue was obtained and then filtered by a Whatman filter paper. The obtained yellow residue washed with distilled water several times to remove unreacted compounds and impurity forms. The obtained compound was stored in a bottle for characterization and batch extraction purpose. The possible mechanism for the ligand synthesis proposed in Fig. 1.

Characterization of the Compound

The formations of the compound were confirmed by various structural elucidation techniques like FTIR and ^{1}HNMR and presented in Fig. 2 and 3 respectively. FTIR spectrum of the compound showed stretching frequency at 1557 cm^{-1} which indicates the presence of NH_2 which in term indicates the

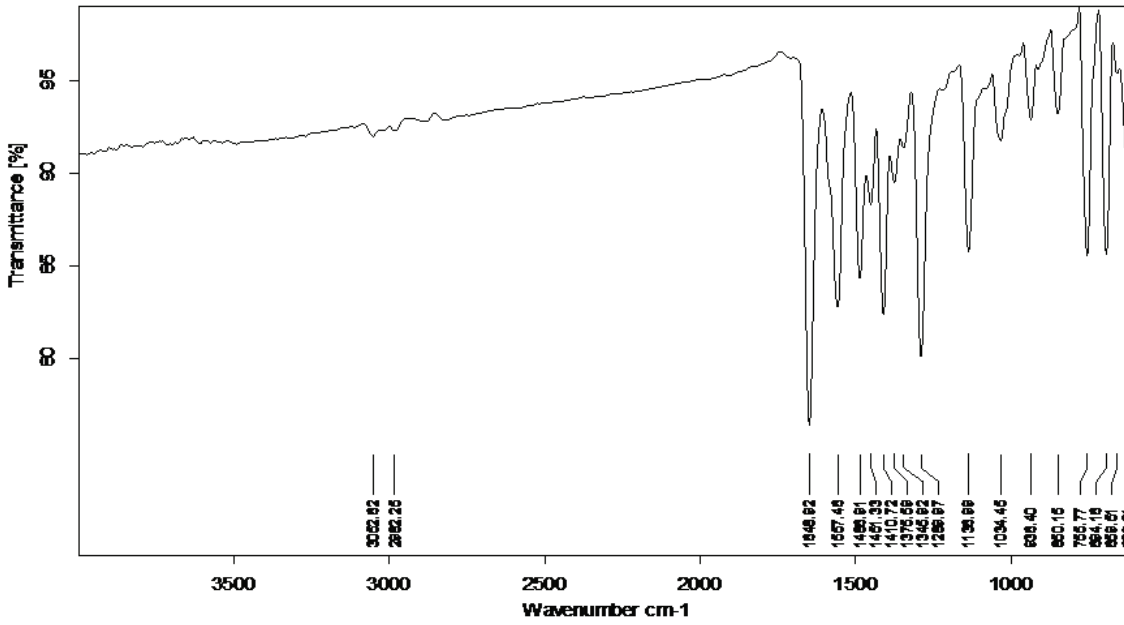

Fig. 2: FTIR spectrum of the supramolecular ligand.

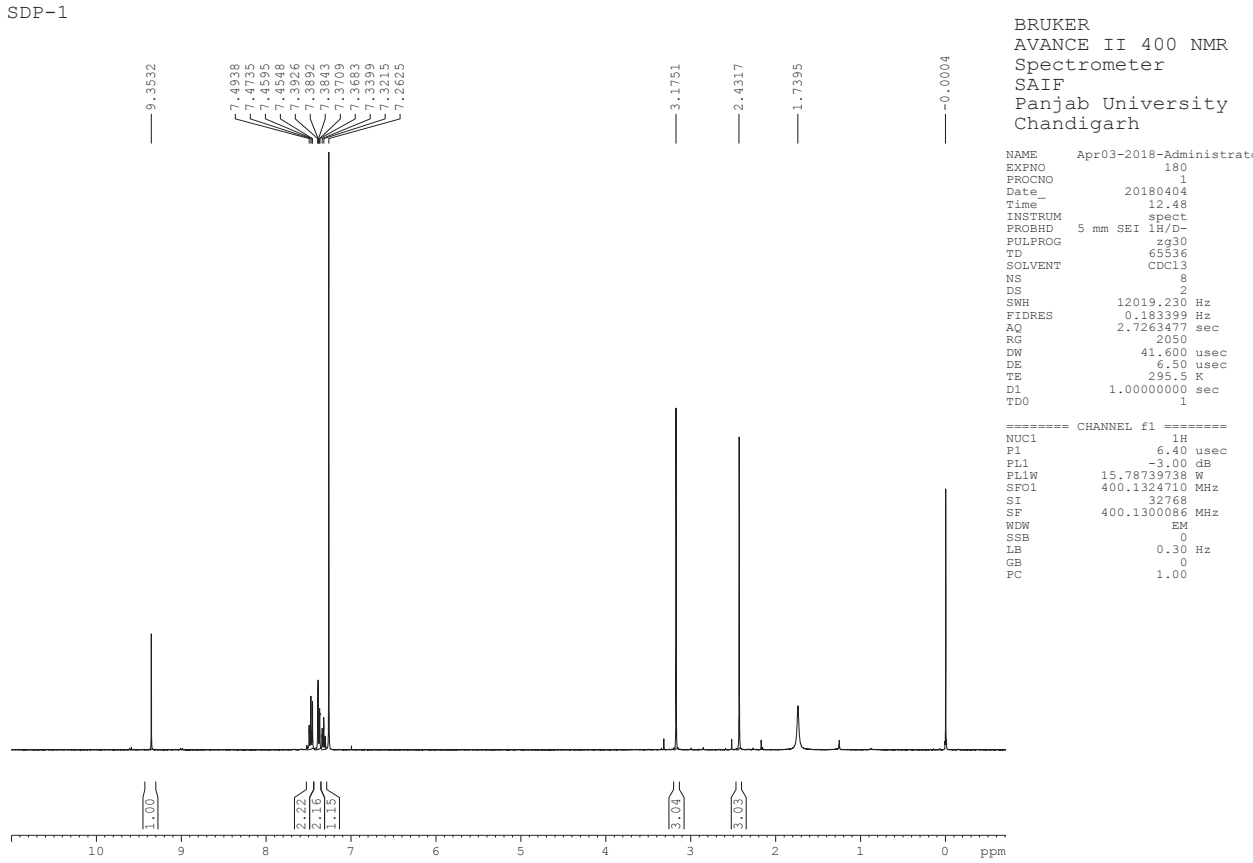

Fig. 3: H^1NMR spectrum of the supramolecular ligand.

formation of a compound. The different IR frequencies with functional groups are summarized in Table 1. The ^{1}HNMR spectrum of the compound shows a peak near 7.5 which is assigned to 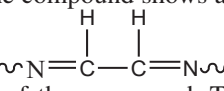 . This peak confirms the formation of the compound. The ^{1}HNMR peaks with functional groups are summarized in Table 2. Both FTIR and ^{1}HNMR characterization showed the formation of the compound.

Selection of A Suitable Solvent for Metal Extraction

Solvent selection is an important part of liquid-liquid extraction. Stability of a complex formed between ligand and metal is highly dependent on the polarity of a solvent (In et al. 2008). Five different solvents were used for extraction of metals by supramolecular ligand, viz., chloroform, N-butanol, ethyl acetate, toluene and N-hexane. The obtained results from the experiment are illustrated in Fig. 4 and showed that chloroform is a suitable solvent for the extraction of metals. The percent extraction of Fe^{3+}, Cd^{2+}, Pb^{2+} and Zn^{2+} using chloroform found to be 86%, 61%, 66% and 44% respectively. The extraction of the above metals using other solvents was less as compared to chloroform (Sarode et al. 2012). In liquid-liquid extraction, replacement of solvent molecules by either ligand or cation is highly favourable (Nezhadali et al. 2007). This condition seems to have fulfilled by chloroform. So, chloroform is selected as a solvent for further extraction experiment.

Effect of Extraction Time

The definite time required for ligand molecules and cation to dissolve into an organic phase altogether affects the overall extraction (Dadfarnia et al. 2010). The effect of contact time on percent extraction efficiency of the ligand was observed by conducting extraction experiments at a different time interval from 5 to 40 min. The obtained results are portrayed in Fig. 5 and show that the prominent extraction efficiency for metals is noted up to 25 min and after that, no significant extraction was observed. The optimized condition of contact time of 20 min was elaborated for Fe^{+3} and Pb^{+2} while in case of Cd^{+2} and Zn^{+2} it was found to be 25 and 30 min, respectively. The percent extraction at an optimized time was noted as 85.34, 60.21, 64.12 and 43.67% for metals Fe^{+3}, Pb^{+2}, Cd^{+2} and Zn^{+2} respectively.

Optimization of pH for the Extraction of Metals

As pH of the solvent controls the stability of the complex formed between ligand and cation, it is a prime variable in the liquid-liquid extraction (Ramo et al. 2000). The effect of solution pH on the extraction efficiency of metals was observed at 0.5 to 9. The results of various experiments depicted that acidic to neutral pH condition is favourable for metal extraction (Fig. 6). In complex formation, ligand behaves like Lewis base and donate its lone pair of an electron to a metal cation to form a complex. In the case of supramolecular ligand, nitrogen and oxygen are the donor atoms and at suitable pH facilitates the formation of a complex by donating a lone pair of electrons.

Table 1: FTIR frequencies assigned to the functional groups of supramolecular ligand.

Sr. No.	FTIR frequencies (cm^{-1})	Functional groups
1.	3062	=C-H
2.	2982	-C-H
3.	1648	C=O
4.	1557	C=N
5.	1486, 1410, 1375 and 1345	CH_3 bending
6.	755, 694, 659 and 629	C-H monosubstituted benzene derivative

Table 2: Assignment of H^{1}NMR chemical shifts to the functional groups of supramolecular ligand.

Sr. No.	Chemical shifts (d)	Functional groups
1.	7.49	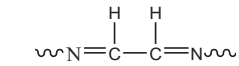
2.	7.45-7.26	Aromatic C-H
3.	2.43	N-CH_3
4.	1.73	CH_3-C=C-

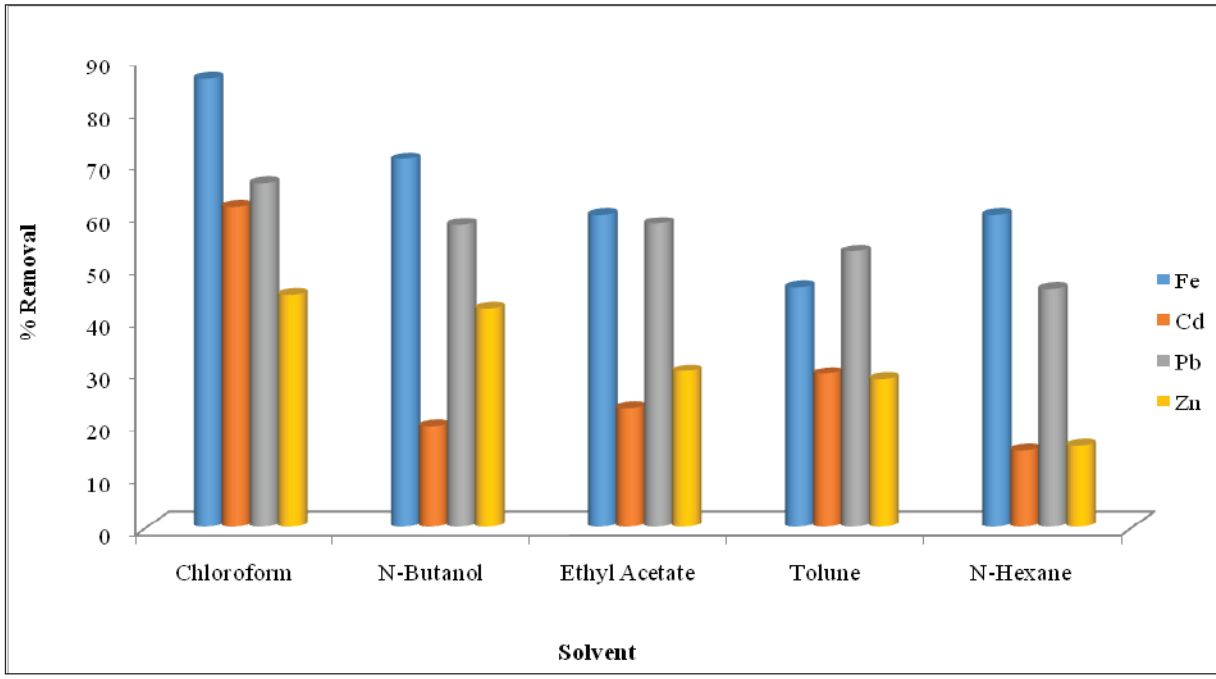

Fig. 4: Effect of different solvents on % extraction of heavy metals using supramolecular ligand.

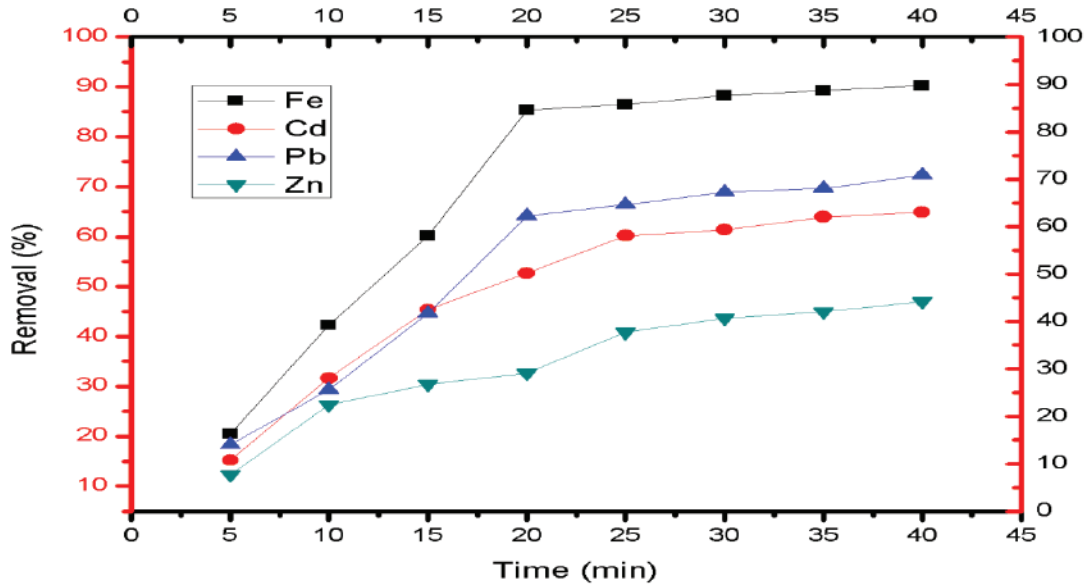

Fig. 5: Optimization of contact time for the extraction of metals using supramolecular ligand.

Effect of Stripping Agents

The recovery of metal ions from organic phase is an important step in liquid-liquid extraction. Generally, acids with different molar concentrations being used for recovery of metals are called as stripping agents. In the present study, three acids, viz. HCl, HNO_3, and H_2SO_4 with molar concentrations from 0.001 to 5 M were used for the recovery of the metals. The results of the experiment (Fig. 7) suggest that 1M HCl showed most metal recovery as compared to other acids. 81.88, 78.93, 81.73 and 80.34% of metal recovery was achieved by using 1M HCl for Fe^{3+}, Cd^{2+}, Pb^{2+} and Zn^{2+} respectively.

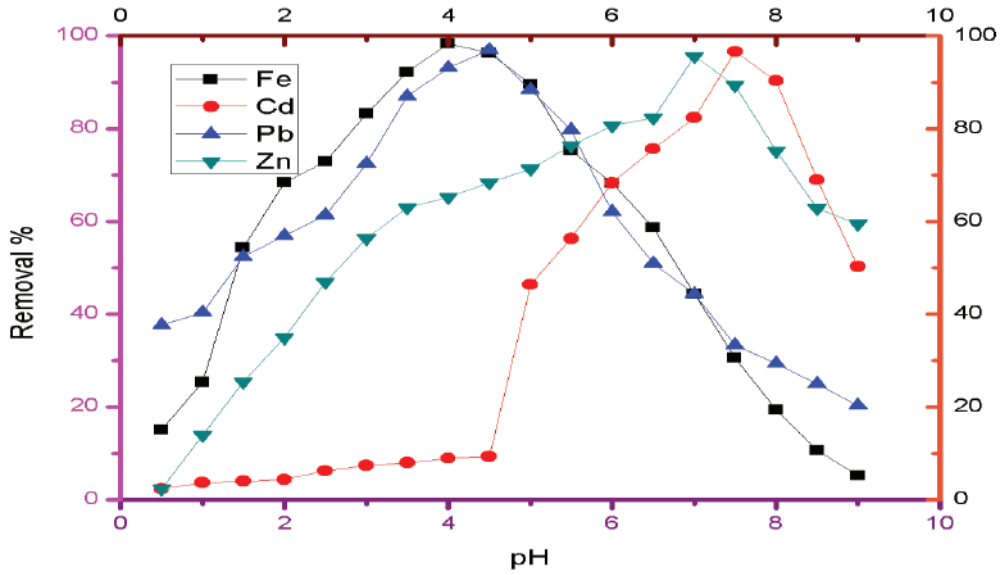

Fig. 6: Optimization of pH to achieve maximum extraction of metals using supramolecular ligand.

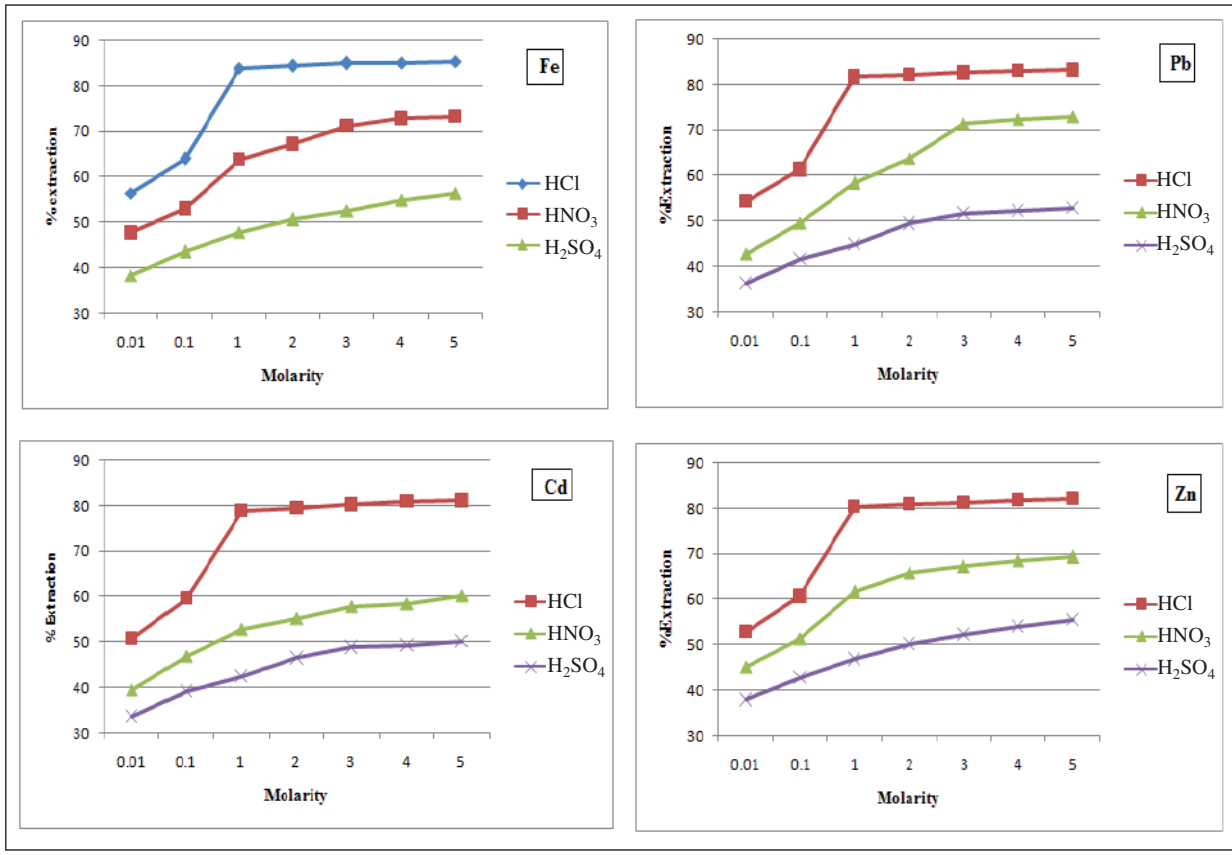

Fig. 7: Effect of the stripping agents on extraction efficiency of supramolecular ligand at different acid concentrations.

Table 3: Application of supramolecular ligand for heavy metals extraction from industrial effluent.

Metal ion	Before extraction (ppm)	After extraction (ppm)	% extraction of metal from industrial effluent
Fe^{+3}	0.3152	0.0004	99.87
Cd^{+2}	0.2398	0.0211024	91.20
Pb^{+2}	0.5856	0.00105408	99.82
Zn^{+2}	0.5043	0.04055176	91.95

Application of Supramolecular Ligand for Industrial Wastewater Samples

Real sample analysis was carried out on samples collected from local metal industry over the optimized condition of time, pH and other variables. The ligand showed impressive extraction efficiency for all four metals over optimized conditions of experimental variables. The reproducibility of the results confirmed by conducting the above experiments five times and mean of the results obtained did not show deviation above 5% from individual results. This shows the reliability and reproducibility of the results. The results of the real sample analysis are summarized in Table 3.

CONCLUSION

In this work, synthesis of a suitable complexing ligand was performed and characterized by FTIR and H^1NMR. The extraction efficiency of the compound was tested at various experimental variables such as solvent, time, pH, etc. In addition, the effect of stripping agent on extraction efficiency over industrial samples was observed. The results obtained from batch extraction experiments revealed that chloroform could efficiently remove the metals more than other solvents. 30 min is the time in which the synthesized ligand can significantly extract metals from solvents. It was noted that slightly acidic to neutral pH conditions are favourable for extraction. The significant recovery of the metals can be achieved using 1M HCl. Application of the compound for extraction of metals from real samples at optimized conditions has shown impressive results which signify the applicability of the compound for industrial purpose.

REFERENCES

Costa, M. C., Assunção, A., Ana M. Rosa da Costa, Nogueira, C. and Paiva, Ana P. 2013. Liquid-liquid extraction of platinum from chloride media by N, N′-Dimethyl, N, N′-Di cyclohexyltetradecylmalonamide. Solvent Extraction and Ion Exchange, 31: 12-23.

Dadfarnia, S., Shabani, A.M.H., Bidabadi, M.S. and Jafari, A.A. 2010. A novel ionic liquid/micro-volume back extraction procedure combined with flame atomic absorption spectrometry for determination of trace nickel in samples of nutritional interest. J. Hazard. Mater., 173: 534-538.

Fegadea, U., Jethavea, G., Su, K., Huang, W. and Wu, R. 2018. A multifunction Zn0.3Mn0.4O4 nanospheres for carbon dioxide reduction to methane via photocatalysis and reused after fifth cycles for phosphate adsorption. J. Environ. Chem. Eng., 6: 1918-1925.

Fraga, C.G. 2000. Relevance, essentiality and toxicity of trace elements in human health. Mol. Aspects Med., 26: 235-244.

Himadri, B. S., Tripathy, S., Equeenuddin, Sk. Md. and Sahoo, P. K. 2014. Utilization of ochre as an adsorbent to remove Pb(II) and Cu(II) from contaminated aqueous media. Environ. Earth Sci., 72: 243-250.

Hua, M., Zhang, S., Pan, B., Zhang, W., Lv, L. and Zhang, Q. 2012. Heavy metal removal from water/wastewater by nanosized metal oxides A review. J. Hazard. Mater., 317-331.

In, G., Kim, Y. and Choi, J. 2008. Study on solvent extraction using salen (NEt2)2 as a chelating agent for determination of trace Cu(II), Mn(II) and Zn(II) in water samples. Bull. Korean Chem. Soc., 29: 969-973.

Jethave, G., Fegade, U., Attarde, S. and Ingle, S. 2017. Facile synthesis of lead doped zinc- aluminum oxide nanoparticles (LD-ZAO-NPs) for efficient adsorption of anionic dye: kinetic, isotherm and thermodynamic behaviors. J. Ind. Eng. Chem., 53: 294-306.

Jethaveb, G. and Fegadeb, U. 2018. Design and synthesis of $Zn_{0.3}Fe_{0.45}O_3$ nanoparticle for efficient removal of Congo red dye and its kinetic and isotherm investigation. International Journal of Industrial Chemistry, 9: 85-97.

Kondalkar, M., Fegadec, U., Attarde, S. and Ingle, S. 2018. Experimental investigation on phosphate adsorption, mechanism and desorption properties of Mn-Zn-Ti oxide trimetal alloy nanocomposite. Journal of Dispersion Science and Technology, 39: 1-9.

Li, Z., Huang, P., Xi, L., Xie, G., Shi, Y., Liu, H., Xu, M., Chen, F. and Zeng, Z. 2011. A highly selective fluorescent chemo sensor for Cd (II) based on 8-hydroxyquinoline platform. Inorg. Chem. Commun., 14: 1241-1244.

Nezhadali, A., Hosseini, H. A. and Langara, P. 2007. Study of complex formation between iodoquinol (IQ) and Co^{2+}, Mn^{2+}, Cd^2+, Pb^2+ and Zn^{2+} cations in binary aqueous/non-aqueous solvent using spectrophotometry. E-J Chem., 4: 581-586.

Okamoto, Y., Nomura, Y., Nakamura, H., Iwamaru, K., Fujiwara, T. and Kumamaru, T. 2000. High pre concentration of ultra-trace metal ions by liquid-liquid extraction using water/oil/water emulsions as liquid surfactant membranes. Microchem. J., 65: 341-346.

Oliva, A., Molinari, A, Zuniga, F. and Ponce, P. 2002. Studies on the liquid-liquid extraction of nickel(II), zinc(II), cadmium(II), mercury(II) and lead(II) with 1-phenyl-3hydroxy-4-dodecyldithiocarboxylate-5-pyrazolone. Microchim. Acta., 140: 201-203.

Ramo, J., Sillanpää, M., Vickackaite, V., Orama, M. and Niinistö, L. 2000. Chelating ability and solubility of DTPA, EDTA, and ′-ADA in alkaline hydrogen peroxide environment. J. Pulp Pap. Sci., 26: 125-131.

Saracoglu, S., Soylak, M. and Elci, L. 2003. Separation/preconcentration of trace heavy metals in urine, sediment and dialysis concentrates by co-precipitation with samarium hydroxide for atomic absorption spectrometry. Talanta., 59: 287-293.

Sarode, D., Ingle, S. and Attarde, S. 2012. Formula establishment of colorless Pb(II) complex with N-Benzoyl-N-Phenyl hydroxylamine (BPA) using atomic absorption spectroscopy. Indo. J. Chem., 12: 12-19.

Sarode, D.B., Attarde, S.B., Ingle, S.T., Srivastava, V. and Sillanpää M.E. 2015. Separation and removal of $Cu^{2+,}$ Fe^{2+}& Fe^{3+} from environmental waste samples by N-benzoyl-n-phenylhydroxylamine. Environmental Technology, 36: 521-528.

Tang, X. L., Peng, X. H., Dou, W., Mao, J., Zheng, J. R., Qin, W. W., Liu, W.S., Chang, J. and Yao, X.J. 2008. Design of a semirigid molecule as a selective fluorescent chemosensor for recognition of Cd (II). Org. Lett., 10: 3653-3656.

Nature Environment and Pollution Technology
An International Quarterly Scientific Journal

p-ISSN: 0972-6268
e-ISSN: 2395-3454

Vol. 19 | No. 1 | pp. 277-285 | 2020

Original Research Paper | Open Access

2-D Unsteady Flow Modelling and Inundation Mapping for Lower Region of Purna Basin Using HEC-RAS

Azaz Khan I. Pathan† and P. G Agnihotri
Department of Civil Engineering, Sardar Vallabhbhai National Institute of Technology, Surat, Gujarat, India
†Corresponding author: Azaz Khan I. Pathan

Nat. Env. & Poll. Tech.
Website: www.neptjournal.com

Received: 27-06-2019
Accepted: 29-08-2019

Key Words:
Flood inundation mapping
2-D unsteady flow
HEC-RAS
Purna basin

ABSTRACT

Present investigations utilize two-dimensional flow modelling abilities of (HEC-RAS) Hydrologic Engineering Centres River Analysis System for flood inundation mapping in the downstream area of Purna basin, exposed to recurrent flooding. Floods are natural disasters, which cause loss of life and damages to properties and nature. 2-D Hydrodynamic model is utilized to assess geomorphic viability of floods in downstream side of Purna basin. In this research study, downstream region geometry of Purna river basin, the flood plain of the study area and historical observed flood data of unsteady flow have been used to develop the 2-D hydrodynamic model. For analysis of flooding, a reach of 20 km of river situated downstream of Purna River basin has been considered. Point-by-point fundamental terrain data is taken from a Digital Elevation Model (DEM) of 30-meter resolution image and is utilized to produce the (2D) two-dimensional flow area and stream geometries. River flow information like daily discharge during rainy months, slope available along the river reach from Mahuva gauging station close to Navsari city is utilized for the unsteady flow modeling. Depth of water, velocity distribution and water surface height obtained after 2D flow simulation are utilized to decide the degree of flooding. RAS-mapper is an effective tool in HEC-RAS, which can be utilized for inundation of research area. For unsteady flow analysis, each time step was done based on inflow hydrograph using RAS mapper tool in HEC-RAS, which gives the spatial distribution of the river flow. The outcomes from this research examination can be utilized for disaster management, flood management, early warning system by authorities in addition to infrastructure growth decisions.

INTRODUCTION

The issues of expanding environmental carbon dioxide fixations in the Earth's atmosphere is analysed and the conceivable future climatic changes which may result considering such issues. As the amount of CO_2 prone to be discharged into the environment because of fossil fuel combustion, the normal increments of other greenhouse gases that impact the world's radiation spending plan, how and when climatic changes can be distinguished, and the anticipated changes in ocean level coming about because of global warming (Bolin et al. 1989). Environmental change is required to quicken water cycles and, in this way, boost the accessible renewable freshwater resources (RFWR) that as it may, fluctuations in occasional forms and the expanding likelihood of extreme events may balance this impact. Diminishing current vulnerability will be the initial step to get ready for such foreseen changes (Oki et al. 2006). The research depicts an appraisal of the ramifications of climate change for worldwide hydrological administrations and water assets. By 2025, it is assessed that around 5 billion individuals, out of an all-out populace of around 8 billion, will live in nations suffering from water pressure (Arnell 1999). The Inter-governmental Panel on Climate Change (IPCC) ventures that more prominent fluctuation and precipitation force will build flooding risk in numerous territories on account of environmental change (Ishiwatari 2010). The ascent in worldwide temperature expands the risk of the flood disaster. Radiative impacts of anthropogenic fluctuations in atmospheric structure are relied upon to cause atmosphere fluctuations, specifically an escalation of the worldwide water rotation with a subsequent increment in flood hazard (Milly et al. 2002). Each year, flooding causes a catastrophic effect on the population, environment, economy, and everywhere throughout the world. Federal Emergency Management Agency (FEMA) has of late refreshed their flood-plain standard according to the high-level official request in 2015 on the Federal Flood Risk Management Standard. This examination joins the recently refreshed floodplain mapping standard in the flood hazard appraisal of roughly 11.3 km stretch of the Patapsco River close Ellicott City, U.S (Thakali et al. 2017). Hazard can be built up as a well-characterized strategy for taking care of flood risk because of man-made, ecological and natural risks, of which

floods are a delegate. Flood risk management plans, described at three level say project planning, project design, and the real expense of a structure, are assessed and contrasted and the advantages from the strategic scheme (Plate 2002). Of late, the tsunami in South East Asia triggered approximate 220,000 passing which makes it likely a standout amongst the most appalling floods. Amid the International Decade of Natural Disaster Reduction (IDNDR) from 1990 to 1999, it was valued that the past worldview of "flood assurance" was wrong (Schanze 2006).

Additionally, as of now ecological and local arrangements in numerous nations are beginning to move from flood assurance to flood hazard management (Dworak & Görlach 2005). Geospatial techniques are very useful to detect the flooding events through combine approach of Arc GIS and HEC-RAS.(Pathan & Agnihotri 2019a)

Decision support system (DSS) is a significant tool for decision makers throughout various period of flood organization to mitigate the major flood and develop different models like economic, forecasting and hydrodynamic to connect with each other and share information which play a crucial role for decision makers (Ahmad & Simonovic 2006). The vision of FEMA's is to fill in as an impetus that drives expanded understanding and proactive activity to help individuals in networks to reduce their losses from natural risks. To fulfil this vision, FEMA subsidizes three Hazard Mitigation Assistance (HMA) programs. Flood risk relief estimates are any manageable moves made to decrease or dispose of long-term hazard to individuals and property from future fiascos. With the continuous event of an outrageous event in urban zones, floodplain maps and flood models have become necessary for disaster authorities to mitigate flood (Knebl et al. 2002). One dimensional modelling approach has given an accurate outcome for determining flooding at different cross sections of the Purna River basin (Pathan & Agnihotri 2019b).

Now a day's different water resources models are utilized to simulate the flooding phenomena, to quantify risk and damage estimation and to help the decision-making procedure with respect to the forecast and counteractive action of floods (Todini 1999). Different examinations have exposed the ability of globally accessible adaptation of 2-Dimensional numerical simulation methods (Johns et al. 1971, Vojinovic 2013). Comparison between 1-Dimensional model over a 2-Dimensional model shows more difference in HEC-RAS when unsteady flow has been carried out; results show almost 200m horizontal difference in inundated area at high discharge (Alho et al. 2008). Generally, the results obtained from 1-D models are not accurate for the flat or flatter flood plain areas, in this way, numerous 1-Dimensional hydrodynamic models are supplanted by 2-Dimensional hydrodynamic models (Merwade et al. 2008). In spite of the fact that there is enormous vulnerability of the qualities of flood events, 2-Dimensional numerical investigation suggests an approach to all the more likely describe the flood. Hydrologic Engineering Centre- River Analysis System (HEC-RAS) hydrodynamic model has been generally utilized related to Environmental System Research Institute (ESRI), HEC-GeoRAS and Arc-GIS programming for 1-Dimensional investigation and mapping of a flood extent. The most recent adaptation, HEC-RAS 5.0.1 offers the independent ability to accomplish 2-Dimensioanal directing and capacities to fully examine and mapping of flood inside the RAS mapper in HEC-RAS model itself. Research examination investigates the 2-D presenting limit of HEC-RAS to show the Purna River around Navsari region, which is exposed to flooding during high discharge. The most recent capacities of RASmapper in HEC-RAS are used for the improved mapping of the floodplain periphery by using past flood information of the Purna River. The objective of the research study is to accomplish unsteady flow analysis, set up a flood inundation map of the study area and to plot the flood inclined territories by utilizing the 2-dimensional hydrodynamic modelling and inundation mapping capacities of most recent variant of HEC-RAS 5.0.1. Computational techniques are very effective in flood management to identify flooding scenarios at different reaches of the study area (Pathan & Agnihotri 2019c).

MATERIALS AND METHODS

Research Study Area

Navsari region lies on floodplain in the periphery of Purna. The length of Purna river considered is about 20 km for research. The river basin starts from Saputara near Maharashtra. Purna river floodplain has centroidal facilitate of 200º41' to 210º05' North latitude and 720º45' to 740º00' East longitudes. The purpose behind choosing this study area is the regular occurrence of flood events, affecting densely the populated urban area around it. The absolute catchment locale of the Purna basin is 2433 km^2. Location map and google map of the research area are as shown in Fig 1. and Fig 2 respectively. Catchment area distribution of Purna River is given in Table 1.

Digital Elevation Model (DEM) of 30-meter resolution is utilized for building the terrain of the research area in RAS-mapper tools (HEC-RAS), acquired from Indian Space Research Organization Bhuvan (ISRO BHUVAN). High resolution images are downloaded from Google earth, the water level and river discharge information of yearly and daily scales are gathered from Central Water Commission

Table 1: Catchment area distribution of Purna River.

Sr. No.	State	Catchment area (km^2)	% of the total catchment area
1	Gujarat	2373	97.61
2	Maharashtra	58	2.39
3	Total	2431	100.00

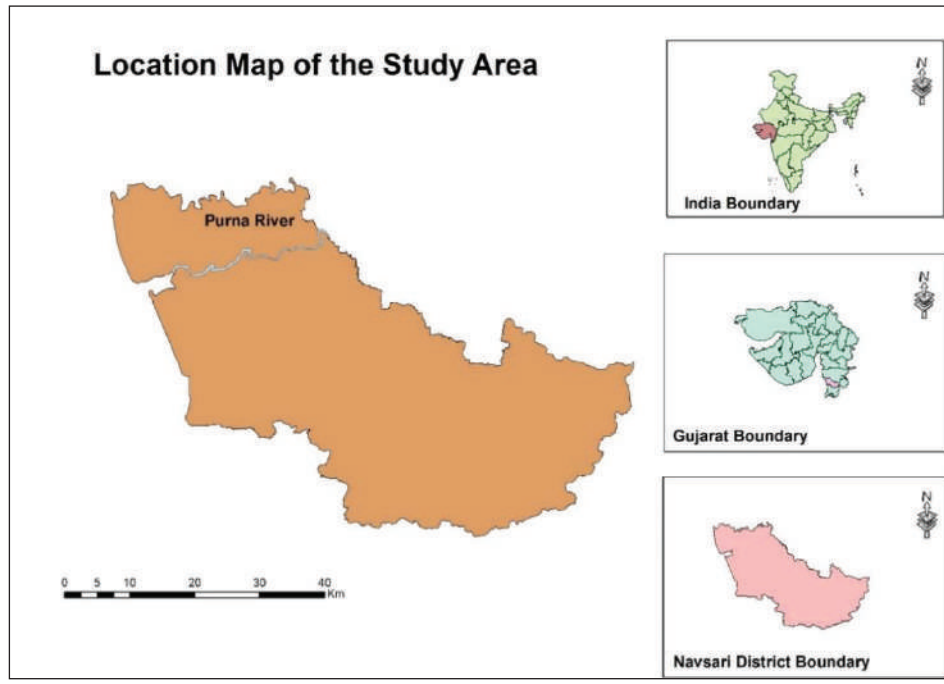

Fig. 1: Location map of study area.

(C.W.C), State Water Data Center (SWDC), Gandhinagar and Irrigation Department.

Methodology

Digital Elevation Model (DEM) of 30-meter resolution taken from ISRO Bhuvan is imported to HEC-RAS software. Now, from Tools menu in RAS-Mapper, create terrain from selected Digital Elevation Model (DEM) which is then used in RAS-Mapper to work on the hydrodynamic properties and building up the geometry of 2-D flow region of study area. Moreover, cell size of 200 m × 200 m was provided, which are created along the selected 2-D flow area of the River of the study area. Now, we utilize the geometric pre-processing tools in Ras-Mapper for creation of hydraulic properties of each cell of the reach.

Manning's roughness coefficient is allocated for the 2D area, considered for the research area in RAS-mapper. The allocated land cover value and corresponding Manning's n value are shown in Table 2.

For unsteady flow simulation in RAS-mapper, provide upstream and downstream boundary conditions of the area of the river. For upstream, Mahuva gauge station hydrograph is used for simulation, and in the downstream normal depth of channel slope (0.000425) is used as boundary condition. The created geometric layer for 2D area of river with the used boundary conditions are mentioned in Table 2 and Fig. 3.

In this research study, daily discharge data is used for two flooding events of time intervals 29th June 1976 to 26th September 1976 and from 21st July 2004 to 26th September 2004. As per past flood data, most severe flooding events occurred in Purna basin on 31st July 1976 with a peak discharge of 4380.2 m^3/s and on 04th August 2004 with a peak discharge of 8836 m^3/s. Upstream hydrographs used in check for the two flooding events are shown in Fig. 4. and Fig. 5.

Flood inundation mappings for years 1976 and 2004 events are plotted in RAS-mapper for peak discharge. For better visualization in mapping, google earth layers can be

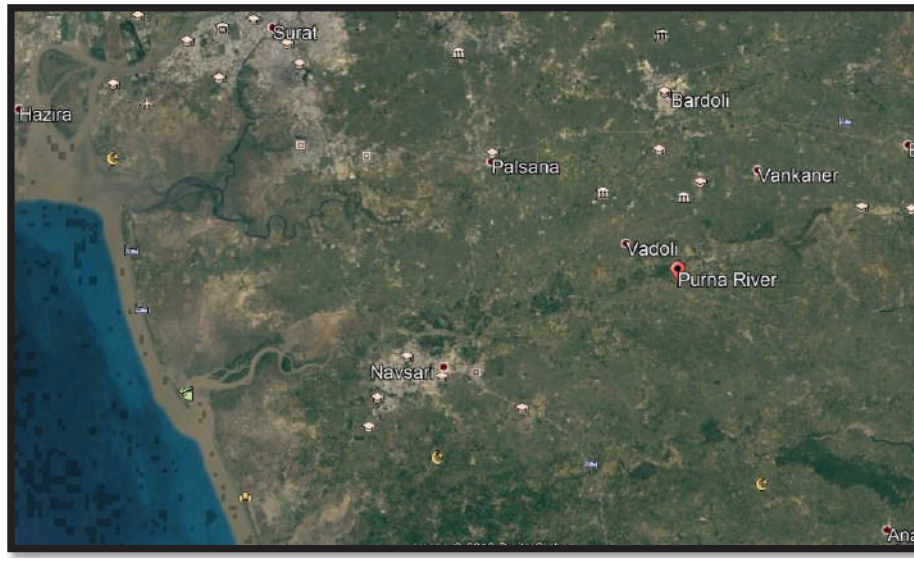

Fig. 2: Google map of study area.

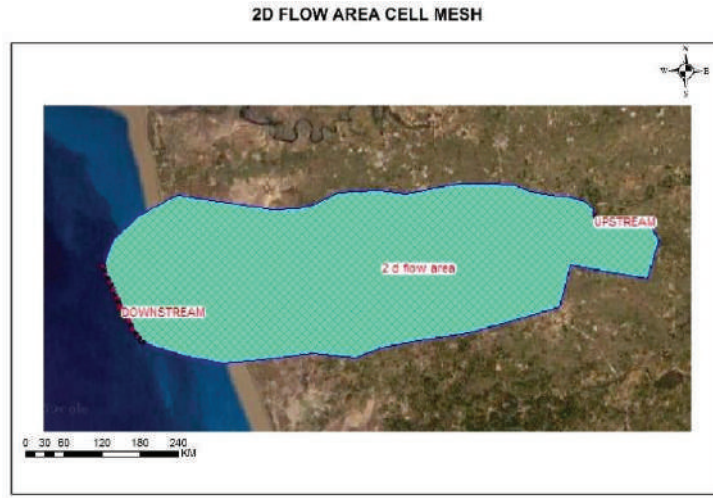

Fig. 3: Generated geometric layer with 2D flow area cell mesh.

Table 2: Manning's n for the channel (Chow 1959).

Type of Channel and Description	Minimum	Normal	Maximum
Main Channels			
a. clean, straight, full stage, no rifts or deep pools	0.025	0.030	0.033
b. same as above, but more stones and weeds	0.030	0.035	0.040
c. clean, winding, some pools and shoals	0.033	0.040	0.045
d. same as above, but some weeds and stones	0.035	0.045	0.050
e. same as above, lower stages, more ineffective slopes and sections	0.040	0.048	0.055
f. same as "d" with more stones	0.045	0.050	0.060
g. sluggish reaches, weedy, deep pools	0.050	0.070	0.080
h. very weedy reaches, deep pools, or floodways with heavy stand of timber and underbrush	0.075	0.100	0.150

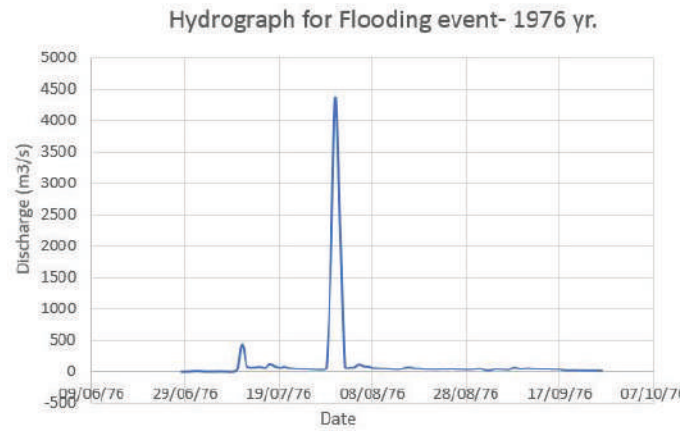

Fig. 4: Hydrograph for flooding event-1976 yr.

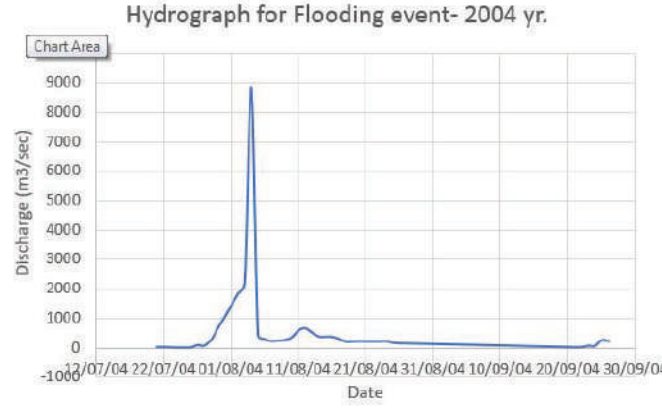

Fig. 5: Hydrograph for flooding event-2004 yr.

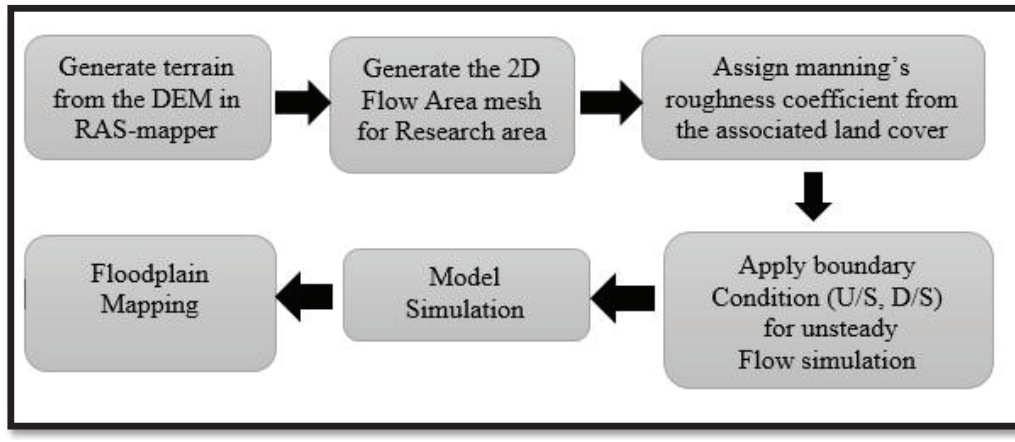

Fig. 6: Conceptual 2D model diagrams for floodplain mapping in HEC-RAS.

imported into RAS-mapper. The outline of methodology is shown in the Fig. 6.

RESULTS AND DISCUSSION

Over the 2D flow area considered in this study, a total of 15,221 cells are generated for the year 1976 flooding event and 9207 cells are generated for the year 2004 flooding event, for the 20 km river reach. Terrain information used for 2D flow area of research zone is from the geometry editor tools in HEC-RAS.

In this research work, for the study area considered, the computational time interval for the model is taken as 6 hours and output interval of the model is taken as 1 day for both flooding events with cell sizes of 200 m × 200 m used for analysis. Using a lesser value of time intervals and smaller cell sizes can produce better results, but the simulation would take more effort to complete. Initial condition of river reach for the study area was supposed to be wet for unsteady flow analysis in HEC-RAS. After considering all conditions, the entire mesh is filled up till warm-up period and when simulation is finished, fill up all cells of the river reach as open channel flow implementing diffusion wave equation in which finite volume approximation is considered.

Hydraulic properties of every cell must be assigned before doing the analysis in RAS-mapper. RAS-mapper has good capability for making hydrodynamic properties of every mesh generated in each cell, which in turn depends on the terrain data considered in the study area and their Manning's "n" values.

The 2D output results can be observed in the form of inundation area, velocity and water surface elevation profile within RAS Mapper tools in HEC-RAS.

Comparison of 1976 and 2004-Year Flood Depth Map

It is observed that in the 1976-year flood, the depth of flooded water at Purna River Bridge, Navsari is 20.550 m and in 2004-year flood, depth of flood water is 23.490 m (Fig. 7 & 8). We have simulated both flood year data in RAS-mapper

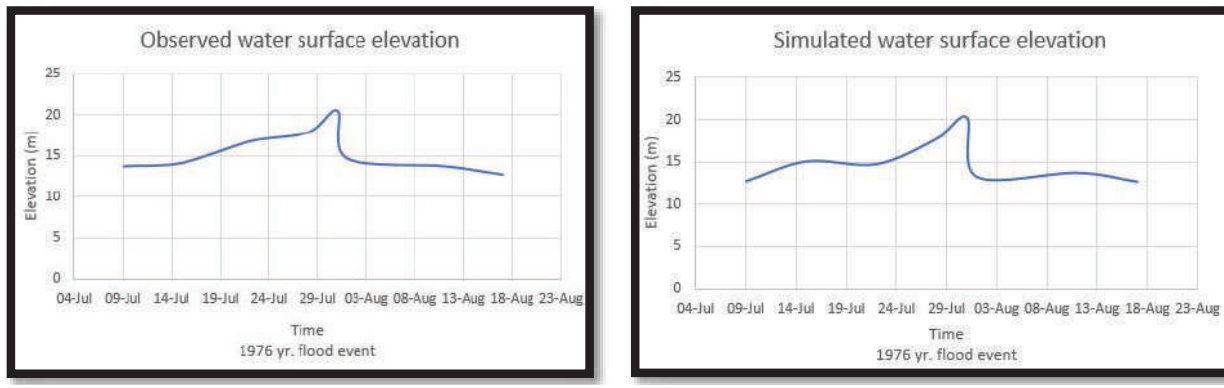

Fig. 7: Observed vs simulated water surface elevation for 1976 yr flood event.

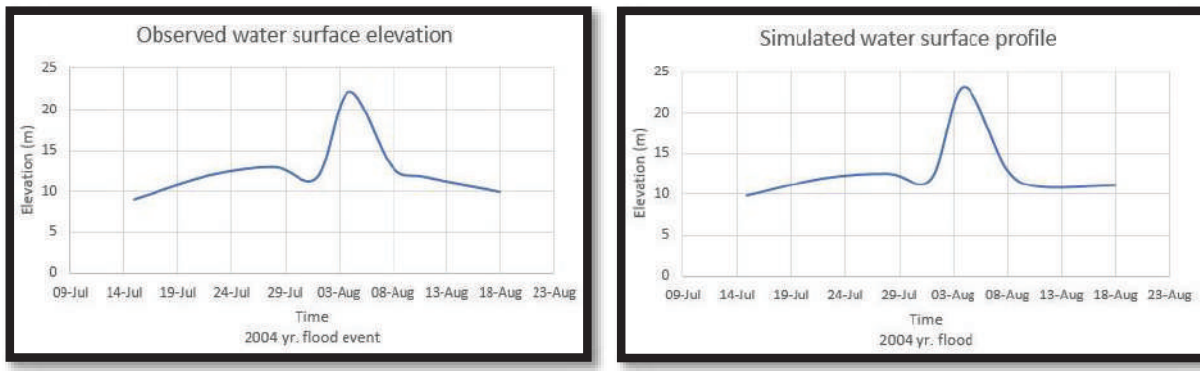

Fig. 8: Observed vs simulated water surface elevation for 2004 yr flood event.

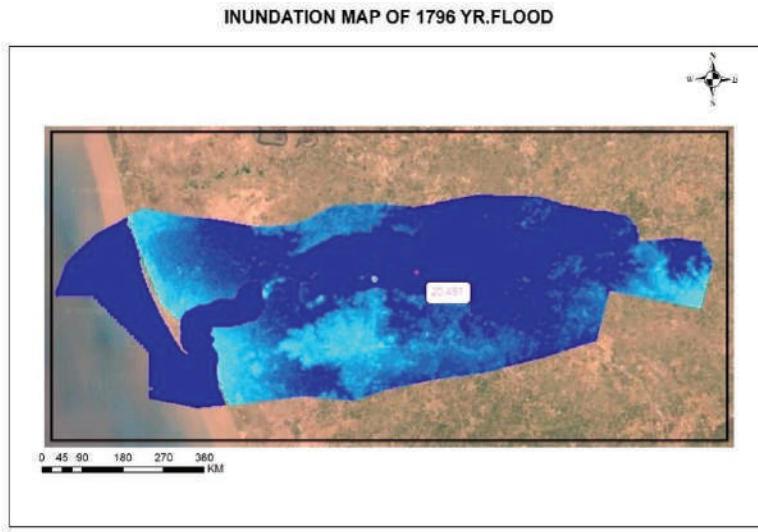

Fig. 9: Inundation map of 1976 year flood

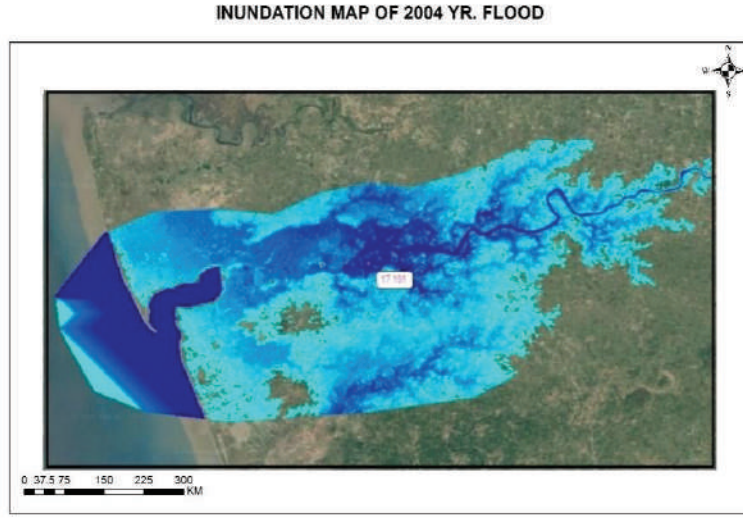

Fig. 10: Inundation map of 2004 year flood.

and developed the inundation map for both 1976-year flood depth and 2004-year flood depth and are shown as in Fig. 9 and Fig.10.

Comparison of 1976 and 2004-Year Flood Velocity Map

It is observed that in 1976-year flood, velocity of flood water was 3.13 m/sec at Purna River Bridge, Navsari and for 2004-year flood, velocity of flood water was 2.57 m/sec. We have simulated both flood year data in RAS mapper and developed velocity maps of both 1976-year flood and 2004-year flood as shown in Fig. 11 and Fig.12.

CONCLUSION

This analysis is meant to lead 2D unsteady flow simulation using HEC-RAS 5.03 in downstream of Purna River, Navsari city. For the stream of 20 km reach, stream hydrograph of 1976-year flood event, occurred between 29th June 1976 and 1st December 1976 and for 2004-year flood event, occurred between 22th June 2004 and 29th September 2004 are routed. Assessment of unsteady flow conditions for the stormy month just as flooding event is completed. From the analysis, following conclusions can be drawn.

- During the study period, the maximum depth of water found was 19.976 m and maximum velocity of water

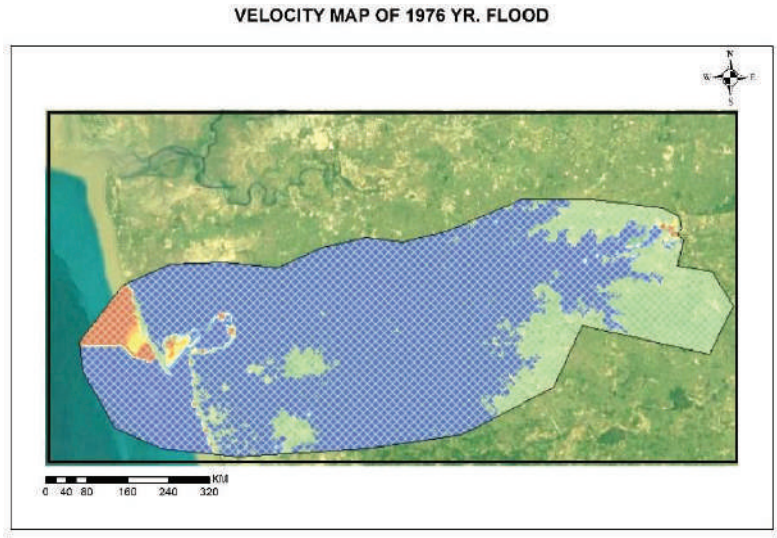

Fig. 11: Velocity map of 1976 year flood.

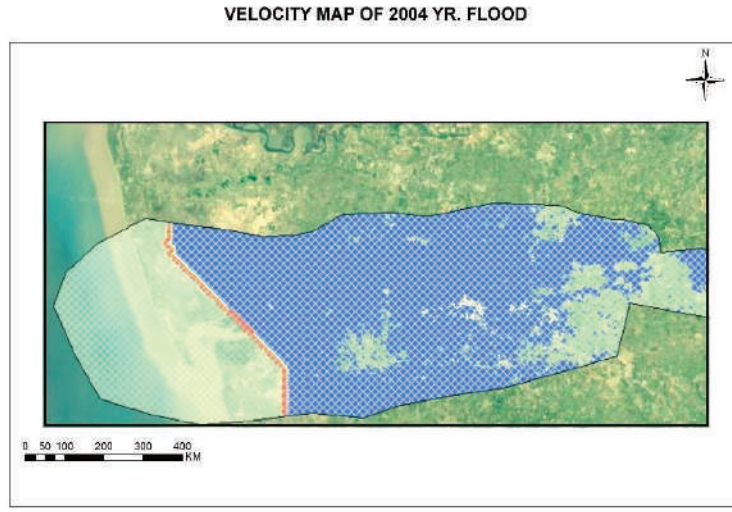

Fig. 12: Velocity map of 2004 year flood.

found was 0.4 m/s for 1976 year flood event with a peak discharge of 4380.20 m^3/sec, the maximum depth of water found was 21.325 m and maximum velocity of water was 0.038 m/s for 2004 year flood event with a peak discharge of 8836 m^3/sec at the Purna River Bridge, Navsari.

- When maximum discharge of 8836 m^3/s is routed, areas near Purna River Bridge like Viraval, Jalalpur are found to be inundated. The highest flood level reached was 24.8 m.
- To develop flood warning and using this information for protecting areas of Navsari district from inundation.

The outcome proposed correlates the parameter's maximum depth and velocity distribution with the past flood events. Smaller cell size and smaller computational intervals give better results but take more time to complete the unsteady flow simulation.

The process described in this study can be upgraded to facilitate analysis and better visualisation capacities. Some additional research recommended for this study are as mentioned below.

- Analysis of the Purna River may help the areas for demarcating safe and vulnerable zones based on the extent of the flood. Such analysis can also be used for

the prediction of flood hazard as well as its extent.

- The peak urban runoff might also be the cause behind such unpredicted flooding, which would require additional research to validate.
- The future work can be useful for applying the methodology to produce the flood risk map of entire Navsari district.

REFERENCES

Ahmad, S. and Simonovic, S.P. 2006. An intelligent decision support system for management of floods. Water Resources Management, 20(3): 391-410.

Alho, P. and Aaltonen, J. 2008. Comparing a 1D hydraulic model with a 2D hydraulic model for the simulation of extreme glacial outburst floods. Hydrological Processes: An International Journal, 22(10): 1537-1547.

Arnell, N.W. 1999. Climate change and global water resources. Global Environmental Change, 9: S31-S49.

Bolin, B. and Doos, B. R. 1989. Greenhouse Effect. John Wiley & Sons.

Chow, V.T. 1959. Open-channel Hydraulics. MacGraw-Hill Book Co., NY

Dworak, T. and Görlach, B. 2005. Flood risk management in Europe@ the development of a common EU policy. International Journal of River Basin Management, 3(2): 97-103.

Ishiwatari, M. 2010. Climate Change Adaptation in Flood Risk Management Through Utilizing Datasets Produced by Supercomputer.

Johns, P. B. and Beurle, R. L. 1971. Numerical solution of 2-dimensional scattering problems using a transmission-line matrix. In: Proceedings of the Institution of Electrical Engineers, 118(9): 1203-1208).

Knebl, M. R., Yang, Z. L., Hutchison, K. and Maidment, D. R. 2005. Regional scale flood modeling using NEXRAD rainfall, GIS, and HEC-HMS/RAS: a case study for the San Antonio River Basin Summer 2002 storm event. Journal of Environmental Management, 75(4): 325-336.

Merwade, V., Cook, A. and Coonrod, J. 2008. GIS techniques for creating river terrain models for hydrodynamic modeling and flood inundation mapping. Environmental Modelling & Software, 23(10-11): 1300-1311.

Milly, P. C. D., Wetherald, R. T., Dunne, K. A. and Delworth, T. L. 2002. Increasing risk of great floods in a changing climate. Nature, 415(6871): 514.

Oki, T. and Kanae, S. 2006. Global hydrological cycles and world water resources. Science, 313(5790): 1068-1072.

Pathan, A. I. and Agnihotri, P. G. 2019a. A combined approach for 1-D hydrodynamic flood modeling by using Arc-GIS, Hec-Georas, Hec-Ras Interface - A case study on Purna River of Navsari City, Gujarat. IJRTE, 8(1): 1410-1417.

Pathan, A. I. and Agnihotri, P. G. 2019b. One dimensional floodplain modelling using soft computational techniques in HEC-RAS - A case study on Purna basin, Navsari District. In: International Conference on Intelligent Computing & Optimization, Springer, Cham., pp. 541-548).

Pathan, A. I. and Agnihotri, P. G. 2019c. Use of Computing Techniques for Flood Management in a Coastal Region of South Gujarat – A Case Study of Navsari District. In International Conference on Intelligent Computing & Optimization. Springer, Cham., pp. 108-117.

Plate, E. J. 2002. Flood risk and flood management. Journal of Hydrology, 267(1-2): 2-11.

Schanze, J. 2006. Flood risk management–a basic framework. In: Flood Risk Management: Hazards, Vulnerability and Mitigation Measures (pp. 1-20). Springer, Dordrecht.

Thakali, R., Bhandari, R., Kandissounon, G. A. A. D., Kalra, A. and Ahmad, S. 2017. Flood risk assessment using the updated FEMA floodplain standard in the Ellicott City, Maryland, United States. World Environmental and Water Resources Congress 2017.

Todini, E. 1999. An operational decision support system for flood risk mapping, forecasting and management. Urban Water, 1(2): 131-143.

Vojinovic, Z., Seyoum, S., Salum, M. H., Price, R. K., Fikri, A. K. and Abebe, Y. 2013. Modelling floods in urban areas and representation of buildings with a method based on adjusted conveyance and storage characteristics. Journal of Hydroinformatics, 15(4): 1150-1168.

Nature Environment and Pollution Technology
An International Quarterly Scientific Journal

p-ISSN: 0972-6268
e-ISSN: 2395-3454

Vol. 19 | No. 1 | pp. 287-293 | 2020

Original Research Paper | Open Access

Removal of Nickel and Iron from Metal Injection Moulding Industry Effluent by Adsorbent Method: A Comparative Study

Akshatha K. U. and Hina Kousar†
Department of P.G Studies & Research in Environmental Science, Kuvempu University, Jnana Sahyadri, Shankaraghatta, Shivamogga, Karnataka, India
†Corresponding author: Hina Kousar

Nat. Env. & Poll. Tech.
Website: www.neptjournal.com

Received: 21-03-2019
Accepted: 31-05-2019

Key Words:
Nickel
Iron
Industry effluent
Rice husk
Adsorption

ABSTRACT

In the present investigation, the efficiency of rice husk in removal of nickel and iron from metal injection moulding industry effluent has been investigated. Adsorption was carried out in a batch experiment to investigate the parameters such as initial metal ion concentration, adsorbent dose, pH and contact time, under constant shaking of 100 mL sample in a heavy rotatory shaking apparatus for 2 hours. Analysis of physico-chemical characteristics of effluent was also carried out. The results revealed that maximum adsorption capacity of rice husk was about 92.84% for nickel using 8 g and about 90.12% for iron using 9 g at pH 9. Due to its good uptake capacity, rice husk has proved to be an excellent low-cost adsorbent for removing nickel and iron from effluent. The result showed that the percentage removal of nickel was high compared to iron.

INTRODUCTION

Toxic industrial waste, runoff from agricultural waste and discharge of untreated domestic waste are the main sources of water pollution (Adegoke et al. 2014). Heavy metal pollution is a major issue due to its toxic effect even at low concentration. Nickel and iron are the heavy metals used in the manufacturing process in metal injection moulding industry. Nickel is a non-biodegradable toxic metal which causes chronic bronchitis, reduced lung function, cancer, nasal sinus, etc. Iron is the 2nd most important metal for the survival and growth of the living organisms on the earth. But it is very toxic to the cells when given endogenous. Therefore, it becomes imperative to remove toxic metals like nickel and iron before discharging industrial effluent into water bodies.

Adsorption process is one of the best water treatment technique among various available methods. Adsorbent removes different pollutants in an easy way and economical and eco-friendly in nature. Rice husk is used as an adsorbent to remove nickel and iron from metal injection moulding industry effluent. The composition of main organic compounds like cellulose, hemicellulose and lignin renders rice husk as a possible adsorbent. In the present study, the applicability of rice husk for the removal of nickel and iron from industry waste water and effects of various parameters such as initial concentration of effluent, adsorbent dosage and pH has been investigated.

Rice Husk

Rice is a strategic crop all over the world and every year large amount of rice husk is produced. Structurally, it consists of crude protein (3%), ash (including silica 17%), lignin (20%), hemicellulose (25%) and cellulose (35%) which renders it suitable for metallic cations fixation. It has been used in the removal of some of the metal ions (Ajmal et al. 2003, Bishnoi et al. 2004, Dadhlich et al. 2004).

MATERIALS AND METHODS

Rice husk was collected from a rice mill at Ripponpete, Shivamogga Dist., Karnataka State and used as adsorbent for the removal of nickel and iron from effluent. It was washed with distilled water and dried in an oven at about 60°C for 4h and again washed with acetone and NaOH (0.3M) to remove dirt and other contaminants, dried in an oven at about 60°C for 4h and crushed until powdered fine particles were obtained. The powdered sample was examined by XRD (X-Ray Diffraction), SEM and BET analysis to assess the purity of the expected phases and the degree of crystallization, i.e. size, composition and crystal structure. The effect of

different parameters, adsorbent and pH on the adsorption was carried out. pH was adjusted by HCL and NaOH (Thakur et al. 2013).

Instrumentation

Characterization of rice husk powder was performed by X-Ray diffraction (Rigaku Diffractometer) using Cu-Kα radiation (105406A°) in a θ - 2θ configuration and the average size of powder was calculated using Debye Scherrer's formula. Scanning Electron Micrograph determines the morphology of rice husk. Specific Surface Area (SSA) of rice husk was measured at 77 K by Brunauer-Emmett-Teller (BET) nitrogen adsorption-desorption (NOVA-1000 version 3.70 Instrument) (Morlu & Bareki 2017).

RESULTS AND DISCUSSION

Physico-chemical Properties of the Effluent

The physico-chemical properties of the metal injection moulding industry effluent are mentioned in Table 1.

Characterization of Rice Husk

X- Ray diffraction (XRD)

Using Cu-Ka radiation (105406A°) in a θ - 2θ configuration characterization of rice husk was performed by powder X- Ray diffraction (Rigaku Diffractometer). The average crystalline size of examined powdered rice husk was found to be around 28 nm and it was calculated using Debye Scherrer's formula (Fig. 1).

$$D = (K\lambda/(b \cos q)) \quad \ldots(1)$$

Table 1: Characterization of metal injection moulding industry effluent.

S.NO	Parameter	Before treatment	After treatment Nickel/Iron
1	pH	1	7/7
2	Temperature (°C)	28.9	24.4/25.1
3	Biological Oxygen Demand (mg.L-1)	30	25/26
4	Chemical Oxygen Demand (mg.L-1)	1250	956/980

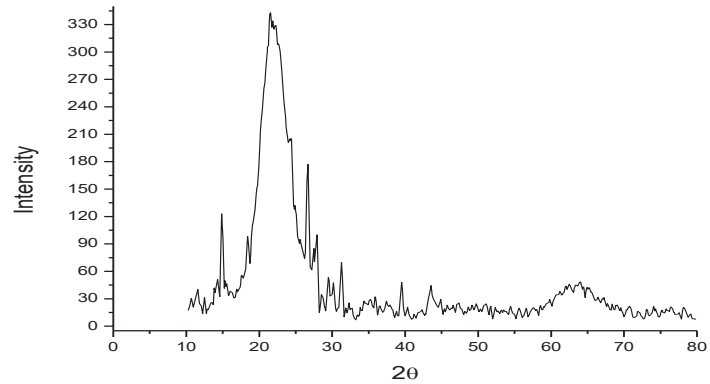

Fig. 1: XRD of the powdered rice husk.

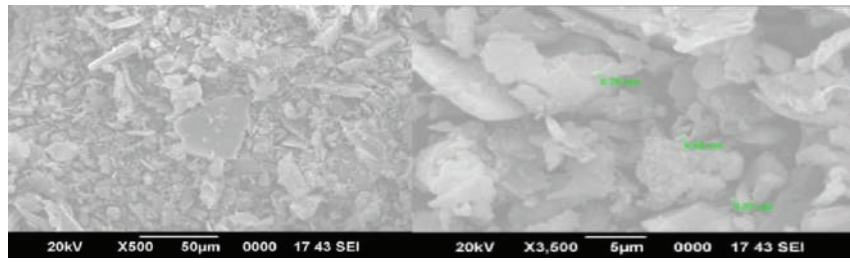

Fig. 2: Scanning Electron Micrograph of powdered rice husk.

Table 2: Surface properties of powdered rice husk.

	Surface area	Pore volume	Average pore diameter
Rice husk	13.386 m^2/g	0.022 cc/g	1.557 nm

Table 3: Concentration of nickel and iron before and after treatment with rice husk.

Concentration of Effluent	Nickel (mg/L)		Iron (mg/L)	
	Before	After	Before	After
25%	15.01 ± 0.005	6.93 ± 0.005	21.82 ± 0.005	12.02 ± 0.005
50%	18.02 ± 0.01	5.65 ± 0.01	24.31 ± 0.005	9.64 ± 0.01
75%	20.22 ± 0.005	10.97 ± 0.01	27.63 ± 0.005	16.59 ± 0.01
100%	23.14 ± 0.005	13.94 ± 0.01	30.47 ± 0.005	19.64 ± 0.01

Scanning Electron Microscope (SEM)

The SEM image of powdered rice husk is shown in Fig. 2 indicating the aggregation particles and cluster shape with sharp edge. The properties of the powdered rice husk are mentioned in Table 2

Bet Surface Analysis

To determine the adsorption efficiency of nickel and iron, batch experiments were conducted and the effect of parameters such as adsorbent dose, pH and contact time was studied.

A known weight of rice husk with 100 mL effluent of different dilutions was kept for treatment in heavy rotatory shaking apparatus for 2 hours. Initial concentration of nickel and iron was determined and found to be as follows. Nickel, 15.01 mg/L in 25% concentration, 18.02 mg/L in 50% concentration, 20.22 mg/L in 75% concentration and 23.14 mg/L in raw effluent (100% concentration). After treatment samples were filtered using Whatman No. 41 filter paper and measured by AAS. The concentration of nickel reduced to 6.93 mg/L (25% concentration), 5.65 mg/L (50% concentration), 10.97 mg/L (75% concentration) and 13.94 mg/L (raw effluent) (Table 3). Maximum reduction of 18.02 mg/L (68.64%) was observed in 50% concentration (Fig. 3) i.e. from 18.02 ± 0.01 to 5.65 ± 0.01 (Table 3).

Initial concentration of iron was 21.82 mg/L in 25% effluent concentration, 24.31 mg/L in 50% concentration, 27.63 mg/L in 75% concentration and 30.47 mg/L in raw effluent. After treatment the concentration of iron reduced to 12.02 mg/L (25% concentration), 9.64 mg/L (50% concentration), 16.59 mg/L (75% concentration) and 19.64 mg/L in raw effluent (Table 3). Maximum reduction of iron was found to be 24.31 mg/L (60.34%) in 50% concentration (Fig. 4) i.e. 24.31 ± 0.005 to 9.64 ± 0.01 (Table 3) because of availability of more adsorption activated sites. Metal ions are easily adsorbed on vacant sites at low concentration. The percent removal of nickel and iron was calculated by the formula:

$$\text{Percent removal} = \frac{C_o - C_i}{C_o} \times 100 \quad \ldots(2)$$

Where, C_o is initial concentration and C_i is final concentration of nickel/iron metal. Further experiment was carried out based on the results obtained.

To know the effect of adsorbent, experiment was carried out with different dosage of rice husk from 1-10g/100 mL at pH 7 in conical flasks in a heavy rotatory shaking apparatus for 2 hours. Maximum percentage removal of nickel was 92.84% at 8g/100 mL (Fig. 5) and iron was 90.12% at 9g/100 mL in 50% concentration (Fig. 6).

Nickel reduced from 18.02 ± 0.01 to 1.29 ± 0.01 andiron decreased from 24.31 ± 0.005 to 2.40 ± 0.005 in 50% concentration (Table 4). It was observed that the percentage removal of nickel and iron increased with increased adsorbent dose which means that when the concentration of adsorbent increases, the availability of high active sites will increase the adsorption capacity which helps to remove the metal ion.

In the adsorption process, pH is considered as the speciation and surface charge of the adsorbent because of its great impact in the metal ion removal. Experiment was carried out with a pH range of 1, 3, 5, 7, 9 and 11. The results show that nickel removal increased from 30.24% to 92.23% (Fig. 3) i.e. 18.02 ± 0.01 to 1.40 ± 0.005 (Table 5) and iron increased from 16.7% to 90.25% (Fig. 4) i.e. 24.31 ± 0.005 to 1.93 ± 0.01 in 50% effluent concentration. Maximum removal of nickel was at pH 9 with 8 g of rice husk and it slightly decreased at pH 11 (Fig. 7). Maximum removal of iron was at pH 9 with 9 g of rice husk and it gradually decreased at pH 11 (Fig. 8). The results easily show that the removal of nickel and iron by rice husk increases with increasing pH and culminates at pH 9.

Similar work has been reported by Abbas et al. (2013) on utilization of Iraqi rice husk in the removal of heavy metals from wastewater. The results showed that maximum removal of Ni by Iraqi rice husk was 95.82% and the percentage removal decreased with increasing pH respectively. Hegazi (2013) worked on removal of heavy metals from wastewater using agricultural and industrial wastes as adsorbents. The result indicated that the maximum removal of iron was 99.25%.

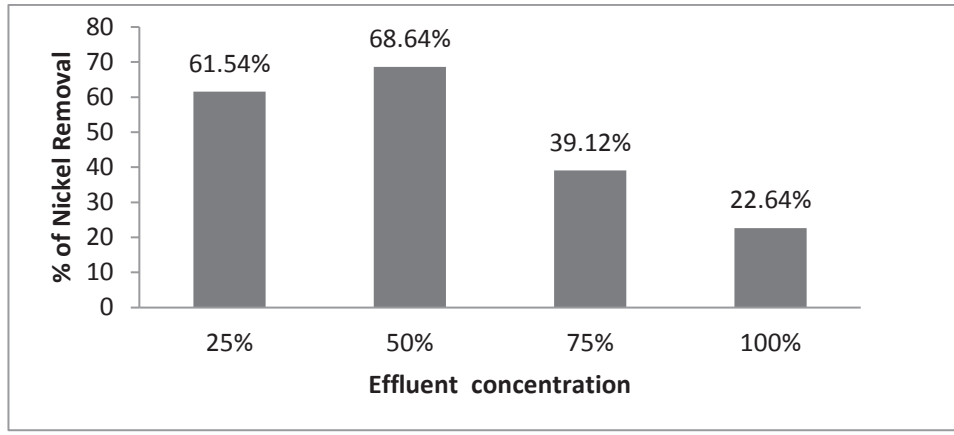

Fig. 3: Removal of nickel with rice husk at different effluent concentration.

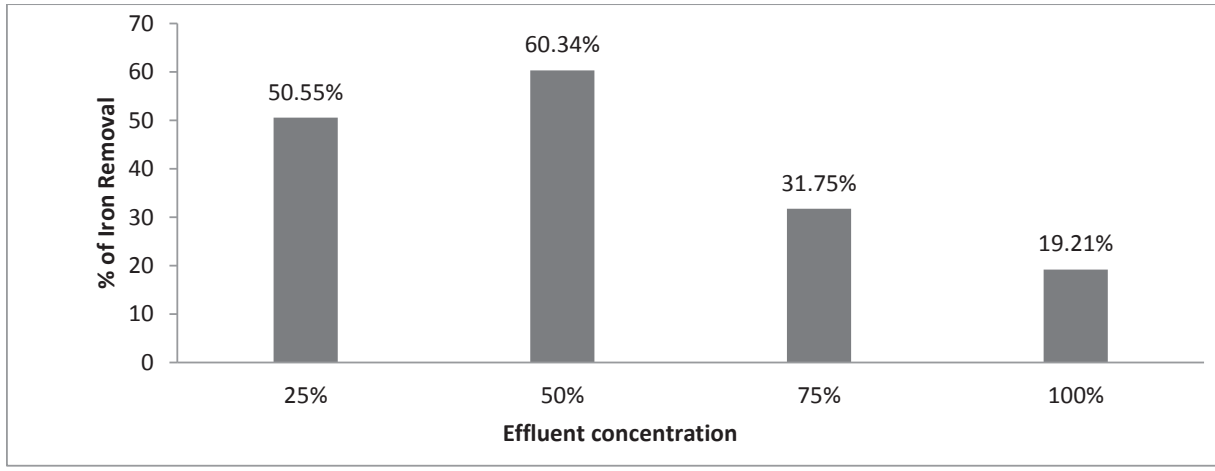

Fig. 4: Removal of iron with rice husk at different effluent concentration.

Table 4: Effect of adsorbent on nickel and iron before and after treatment (1-10g/100 mL at pH 7).

Adsorbent dosage (g)	Nickel (mg/L)		Iron (mg/L)	
	Before	After	Before	After
1	18.02 ± 0.01	9.91 ± 0.02	24.31 ± 0.005	18.73 ± 0.005
2	18.02 ± 0.01	8.97 ± 0.005	24.31 ± 0.005	16.93 ± 0.005
3	18.02 ± 0.01	7.80 ± 0.005	24.31 ± 0.005	13.44 ± 0.01
4	18.02 ± 0.01	6.97 ± 0.01	24.31 ± 0.005	11.65 ± 0.005
5	18.02 ± 0.01	5.65 ± 0.005	24.31 ± 0.005	9.62 ± 0.05
6	18.02 ± 0.01	4.41 ± 0.01	24.31 ± 0.005	7.88 ± 0.005
7	18.02 ± 0.01	2.97 ± 0.01	24.31 ± 0.005	5.94 ± 0.01
8	18.02 ± 0.01	1.29 ± 0.01	24.31 ± 0.005	4.12 ± 0.005
9	18.02 ± 0.01	1.52 ± 0.10	24.31 ± 0.005	2.40 ± 0.005
10	18.02 ± 0.01	1.56 ± 0.005	24.31 ± 0.005	2.50 ± 0.005

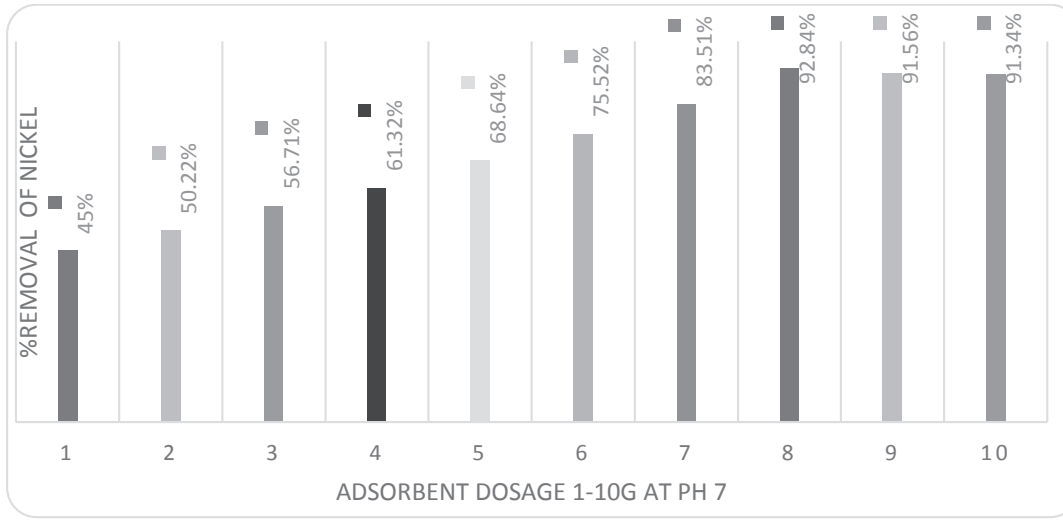

Fig. 5: Removal of nickel for different adsorbent dosage (1-10g/100 mL at pH 7).

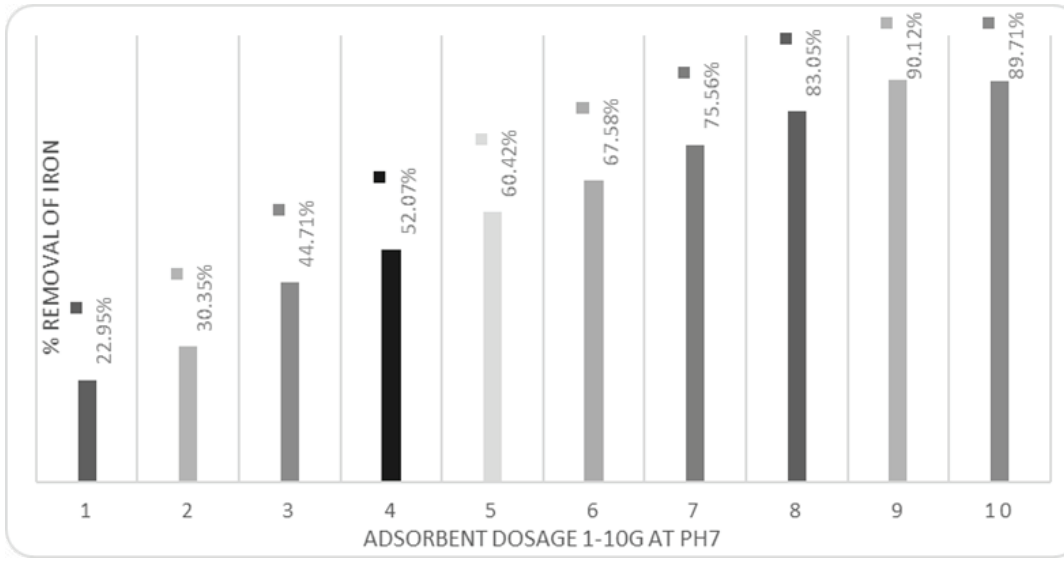

Fig. 6: Removal of iron for different adsorbent dosage (1-10g/100 mL at pH 7).

Table 5: Effect of pH on the adsorption of nickel and iron before and after treatment with rice husk.

pH range	Nickel (mg/L)		Iron (mg/L)	
	Before	After	Before	After
1	18.02 ± 0.01	12.57 ± 0.01	24.31 ± 0.005	20.25 ± 0.01
3	18.02 ± 0.01	8.20 ± 0.005	24.31 ± 0.005	12.63 ± 0.005
5	18.02 ± 0.01	5.07 ± 0.005	24.31 ± 0.005	9.12 ± 0.005
7	18.02 ± 0.01	2.93 ± 0.005	24.31 ± 0.005	2.37 ± 0.01
9	18.02 ± 0.01	1.40 ± 0.005	24.31 ± 0.005	1.93 ± 0.01
11	18.02 ± 0.01	1.97 ± 0.005	24.31 ±0.005	2.02 ± 0.01

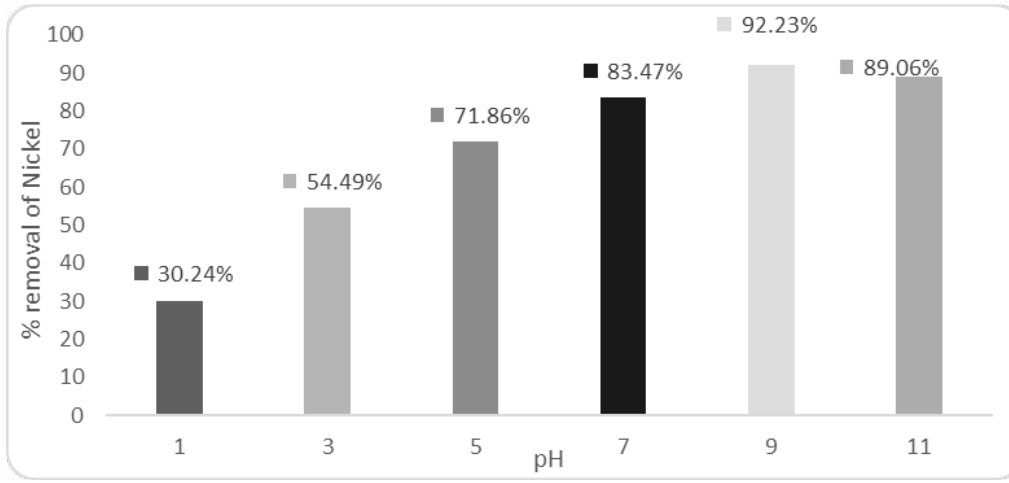

Fig. 7: Effect of pH on the adsorption of nickel.

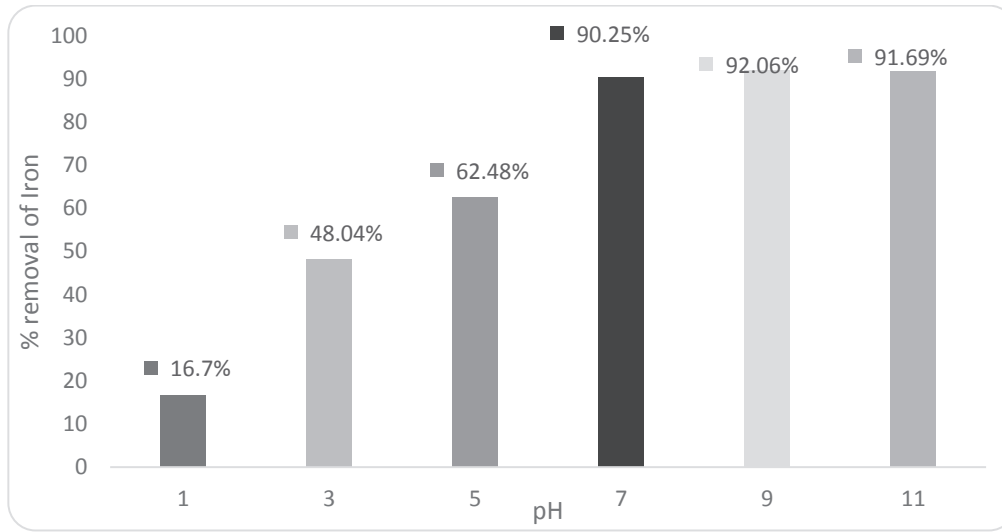

Fig. 8: Effect of pH on the adsorption of iron.

CONCLUSION

The adsorption efficiency of rice husk and comparative study of nickel and iron removal has been studied. XRD and SEM analysis showed that the average crystalline size of powdered rice husk was around 28 nm and morphologically was cluster shape with sharp edge. BET analysis explained the surface properties like pore diameter, pore volume and surface area of powdered rice husk. It was observed that 92.84% nickel was removed by 8 g of rice husk and 90.12% iron was removed with 9 g of rice husk in 50% concentration with 2-hour treatment at 25°C. The maximum removal of nickel and iron was obtained at pH 9. Comparatively rice husk was found to be efficient in removal of nickel than iron.

REFERENCES

Abbas, M.N. and Abbas, F.S. 2013. Utilization of Iraqi rice husk in the removal of heavy metals from wastewater. Research Journal of Environmental and Earth Sciences, 5(7): 370-380.

Adegoke, K.A., Bello, O.S., Bello, O.U. and Lateef, I.O. 2014. Sequestering nickel (II) ions from aqueous solutions using various adsorbents: A review. Pakistan Journal of Analytical & Environmental Chemistry, 15(1): 17.

Ajmal, M. Rao R.A.K., Anwar, S., Ahmad, J. and Ahmad R. 2003. Adsorption studies on rice husk: Removal and recovery of Cd(II) from waste

water. Bioresource Technology, 86: 147-149.

Bishnoi, N.R., Baja, J. M., Sharma, N. and Gupta, A. 2004. Adsorption of Cr(VI) on activated rice husk carbon and activated alumina. Bioresource Technology, 91: 305-307.

Dadhlich, A.S., Beebi, S.K. and Kavitha, G.V. 2004. Adsorption of Ni (II) using agro waste, rice husk. J. Environ. Sci. Eng., 46: 179-185.

Hegazi, H.A. 2013. Removal of heavy metals from wastewater using agricultural and industrial wastes as adsorbents. Housing, Building and Research Center Journal, 9: 276-282.

Morlu, Stevens and Bareki, Batlokw 2017. Removal of nickel (II) and cobalt (II) from wastewater using vinegar-treated eggshell waste biomass. Journal of Water Resource and Protection, 9: 931-944.

Thakur, L.S. and Parmar, M. 2013. Adsorption of heavy metal (Cu2+, Ni2+ and Zn2+) from synthetic waste water by tea waste adsorbent. International Journal of Chemical and Physical Sciences, 2(6): 6-19.

Nature Environment and Pollution Technology
An International Quarterly Scientific Journal

p-ISSN: 0972-6268
e-ISSN: 2395-3454

Vol. 19 | No. 1 | pp. 295-302 | 2020

Original Research Paper | Open Access

Numerical Investigation of Heterogeneous Nucleation of Supersaturated Water Vapour on Coal-fired PM_{10}

Ju Gao, Ting-fang Yu†, Run-guo Chen, Hao-jie Zhang and Lin Wang

†School of Mechanical and Electrical Engineering, Nanchang University, Jiangxi, Nanchang 330031, China

†Corresponding author: Ting-fang Yu

Nat. Env. & Poll. Tech.
Website: www.neptjournal.com

Received: 16-06-2019
Accepted: 24-07-2019

Key Words:
Heterogeneous nucleation
Coal-fired PM_{10}
Critical supersaturation
Nucleation rate

ABSTRACT

The kinetic model is adopted to describe heterogeneous nucleation of supersaturated water vapour on coal-fired PM_{10}. To verify the accuracy of the kinetic model, it is compared with the Fletcher model and experimental data. Additionally, the comparison for condensation and evaporation coefficients and the relative importance of two diffusion condensation mechanisms are systematically analysed during embryo growth process. Furthermore, the influence of vapour temperature on nucleation rate and critical supersaturation for coal-fired PM_{10} are researched. The results show that the predicted critical supersaturation for Kinetic model is far closer to the experimental data compared with the Fletcher model. What is more, once the embryo radius rn reaches to the critical embryo radius r*, it can grow spontaneously, and the indirect surface diffusion mechanism is more important than the direct addition mechanism to embryo growth, the value of RTO is always above 100. It is also found that increase in the vapour temperature is conductive to nucleation process, which can increase the nucleation rate and decrease the barrier of nucleation free energy.

INTRODUCTION

The frequent haze weather has attracted people's extensive attention to the particulate matters in recent years (Siddharth et al. 2008). Coal-fired power plants are one of the main sources for particulate matter in the atmosphere environment (Liu et al. 2016). These particles can not only cause serious environmental problems but also pose a serious threat to people's health. Particles with the diameter less than 10 microns can enter the respiratory system of the human body, causing damage to the heart and lung functions, resulting in arrhythmia, myocardial infarction, heart failure, atherosclerosis and other diseases (Bentayeb et al. 2012).

However, conventional particle abatement devices such as cyclone separator, water scrubber, fabric filters, electrostatic precipitator and so on have less effective in collecting submicron particles (Hu et al. 2018, Zhou et al. 2016). Therefore, to find a valid preconditioning method to improve the removal efficiency for fine particles has become an urgent problem. Heterogeneous condensation as a promising preconditioning technique has been widely used in the traditional particle separation processes (Heidenreich et al. 1995, Hao et al. 2016). At present, a large number of experimental and theoretical researches focus on the removal efficiency for fine particles by means of vapor heterogeneous condensation technology, while ignoring the heterogeneous nucleation process at the initial stage of heterogeneous condensation of water vapor (Hao et al. 2016, Zhou et al. 2016, Wen et al. 2014). Fan et al. (2013) pointed out that the whole process for heterogeneous condensation include three stages: nucleation, transition and growth stage. The heterogeneous nucleation stage plays an important role in the process of steam heterogeneous condensation, so it is of great significance to study the heterogeneous nucleation characteristics for supersaturated steam on particle surface.

Studies on heterogeneous nucleation have a long history. Fletcher (1958) was the first to study heterogeneous nucleation of vapor on insoluble spherical particles, which contained the effect of particle size. Fan et al. (2007) numerically investigated the water vapor (with or without wetting agents) on $PM_{2.5}$ heterogeneous nucleation behaviour according to Fletcher's classical nucleation theory. However, Chen et al. (2000) revealed that the prediction of critical supersaturation for Fletcher classical nucleation theory was flawed, which was too high compared with experimental data. In recent years, the kinetic model has been widely used to investigate heterogeneous nucleation of supersaturated vapor on particles. Luo et al. (2014) derived the growth rate for the cap shaped embryo formed on the particle surface based on the kinetic nucleation model. Fan et al. (2015) put forward to a modified expression for the steady-state heterogeneous nucleation rate based on the kinetic model and validated the advantage of the expression. All these

researches indicate that the kinetic model is a valid tool to investigate the phenomenon for heterogeneous nucleation of supersaturated water vapor on particle.

In this paper, we apply the kinetic model (Luo et al. 2014), in which three factors are taken in account, including the effect of line tension, two mechanisms of embryo growth and coal-fired PM_{10} surface wettability, to research the heterogeneous nucleation characteristics of supersaturated vapor on spherical coal-fired PM_{10}. In addition, the effects of operational parameters including temperature and supersaturation of vapor on heterogeneous nucleation parameters are also investigated.

Physical Model

Fig.1 shows the growth process of embryo formed on coal-fired PM_{10} surface. The embryo can grow via the condensation of water vapor molecules direct diffusion from the vapor phase and the indirect diffusion for particle surface absorbed water at the rate of $C_n(\alpha)$ and $C_n(\beta)$, respectively. Meanwhile, condensation and evaporation occur simultaneously, the embryo droplet could also shrink by evaporation of water molecules to both the vapor phase and particle surface at the rate of E_n (α) and E_n (β), respectively.

Fig. 2. shows the process of the number changes for embryo. The number of embryos formed on particle surface per unit area is defined as f_n and the change rate of f_n is written as:

$$\frac{df_n}{dt} = C_{n-1}f_{n-1} - \left(C_n + E_n\right)f_n + E_{n+1}f_{n+1} \qquad \ldots(1)$$

Where, C_n and E_n denote the coefficients of condensation and evaporation for embryo droplet, respectively.

When we take into account the effect of line tension in kinetic nucleation model, the free energy for forming an embryo on coal-fired PM_{10} is given by (Luo et al. 2014).

$$\Delta G = \Delta G_v V + \sigma_{lv} S_{lv} + \left(\sigma_{sl} - \sigma_{sv}\right) S_{sl} + \tau L_{scv} \qquad \ldots(2)$$

Where, V is the volume of embryo droplet (m^3), ΔG_v represents the free energy difference between vapor phase and liquid phase unit volume ($J \cdot m^{-3}$), σ_{ij} ($N \cdot m^{-1}$) is the surface free energy between phase i and j, and S_{ij} is the surface area of the interface (m^2). τ (N) is the line tension at the triple phase boundary between embryo, substrate, and vapor phase and L_{scv} is the total length for the three-phase contact line (m).

From Fig. 1, the geometric parameters are written as:

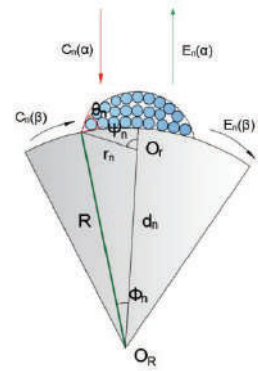

Fig. 1: Schematic diagram for the growth process of embryo.

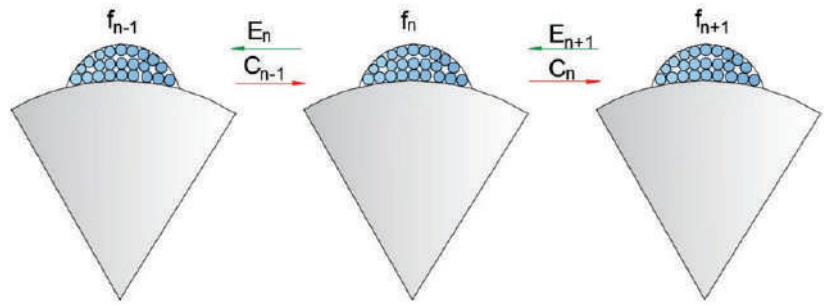

Fig. 2: Kinetic process for the change rate of the embryo number.

$$V = \frac{1}{3}\pi r_n^3\left(2-3\cos\theta_n+\cos^3\theta_n\right) - \frac{1}{3}\pi R^3\left(2-3\cos\Phi_n-\cos^3\Phi_n\right) \quad \ldots(3)$$

$$S_{lv} = 2\pi r_n^2\left(1-\cos\theta_n\right) \quad \ldots(4)$$

$$S_{sl} = 2\pi R^2\left(1-\cos\Phi_n\right) \quad \ldots(5)$$

$$L_{scv} = 2\pi r_n \sin\theta_n \quad \ldots(6)$$

$$d = \sqrt{r_n^2+R^2-2mr_nR} \quad \ldots(7)$$

$$\cos\theta_n = \frac{mR-r_n}{d} \quad \ldots(8)$$

$$\cos\Phi_n = \frac{R-r_n m}{d} \quad \ldots(9)$$

Where, r_n represents embryo radius (m), R is the radius of coal-fired particle (m), d is the distance between the centre of embryo droplet and that of particle (m), m is the cosine of microscopic contact angle θ_n.

The microscopic contact angle θ_n is a function of line tension τ and macroscopic contact θ_∞ (Hienola et al. 2007).

$$\cos\theta_\infty = \cos\theta_n + \frac{\tau\left(R-r\cos\theta_n\right)}{\sigma_{lv} r_n R\sin\theta_n} \quad \ldots(10)$$

The radius of the critical embryo is:

$$r_n^* = \frac{2\sigma_{lv}V_{wm}}{k_B T\ln S} \quad \ldots(11)$$

Where, k_B is the Boltzmann constant (1.38×10^{-23} J·K^{-1}), T (K) is the temperature of water vapour, V_{wm} is the volume of a water molecule (m^3), S is water vapour supersaturation, which is the ratio of the ambient vapour pressure to saturation vapour pressure.

The heterogeneous nucleation free energy barrier corresponds to the maximum value of ΔG, which is the formation energy for the critical embryo (Hienola et al. 2007).

$$\Delta G^* = \frac{2\pi r^{*2}\sigma_{lv}}{3} f(m,x) + 2\pi R\tau\left(\frac{1-\cos\Phi_n}{\sin\Phi_n}\right) \quad \ldots(12)$$

Where, $f(m,x)$ is the geometrical factor (Fan et al. 2007).

The expression of condensation coefficient in the kinetic model for embryo is (Xu et al. 2017):

$$C_n = C_n(\alpha)+C_n(\beta) \quad \ldots(13)$$

$$C_n(\alpha) = \alpha_n \frac{p_v}{\sqrt{2\pi m_{wm}k_B T}} S_{cv}(r_n) \quad \ldots(14)$$

$$C_n(\beta) = N_1 \upsilon\delta \exp\left(-\frac{\Delta G_{diff}}{k_B T}\right) L_{cvs}(r_n) \quad \ldots(15)$$

$$N_1 = \frac{p_v}{\upsilon\sqrt{2\pi m_{wm}k_B T}} \exp\left(\frac{\Delta G_{des}}{k_B T}\right) \quad \ldots(16)$$

Where, P_v is the ambient pressure of water vapor (Pa), υ denotes the vibration frequency of one molecule on the surface (s^{-1}), δ is the mean jump distance for one water molecule (m), ΔG_{diff} is the surface diffusion energy for one water molecule (J), α_g denotes the sticking coefficient of embryo droplet. N_1 is the surface concentration of water molecules. ΔG_{des} is the desorption energy for individual water molecule (J).

The explicit expression of evaporation coefficient is written as (Fan et al. 2015):

$$E_n = E_n(\alpha)+E_n(\beta) \quad \ldots(17)$$

$$E_n(\alpha) = \exp\left(\frac{2\sigma V_{wm}}{k_B T r_n}\right)\frac{P_v^{sat}}{\sqrt{2\pi m_{wm}k_B T}} S_{cv}(r_n) \quad \ldots(18)$$

$$E_n(\beta) = \exp\left(\frac{2\sigma V_{wm}}{k_B T r_n}\right)\delta N_1^{sat}\upsilon\exp\left(\frac{\Delta G_{diff}}{k_B T}\right) L_{cvs}(r_n) \quad \ldots(19)$$

The heterogeneous nucleation rate is one of crucial parameters to research heterogeneous nucleation process and the expression of nucleation rate is (Fan et al. 2015):

$$J = Z\cdot\left[C_n^*(\alpha)+C_n^*(\beta)\right]\cdot\exp\left(-\frac{\Delta G^*}{k_B T}\right) \quad \ldots(20)$$

and

$$Z = \sqrt{\frac{\sigma}{k_B T\left(2+\cos\theta_{n^*}\right)}}\cdot\frac{V_{wm}}{\pi r_{n^*}^2\left(1-\cos\theta_{n^*}\right)} \quad \ldots(21)$$

Table 1: Parameters for the coefficients of condensation and evaporation in heterogeneous nucleation on coal-fired particle.

Parameter	Symbol	Value
Mean jump distance	δ (nm)	0.32
Line tension	τ (N·m^{-1})	-1×10^{-11}
Macroscopic contact angle	θ_∞ (°)	40
Surface diffusion energy	ΔG_{diff} (J·molecule^{-1})	2.9×10^{-21}
Desorption energy	ΔG_{des} (J·molecule^{-1})	2.9×10^{-20}

Where, Z is the Zeldovich non-equilibrium factor, the superscript '*' denotes the parameters for critical embryo.

The parameters that we used in the kinetic model is listed in Table 1 (Fan et al. 2019 & Xu et al. 2017).

RESULTS AND DISCUSSION

Comparison with the Experimental Data

When the heterogeneous nucleation rate J = 1 s^{-1}, the supersaturation is defined as critical supersaturation, which is the minimum barrier to form a new phase from vapor phase. Fig. 3 shows the comparison of predicted critical supersaturation for Fletcher model (Fletcher 1956) and kinetic model (Luo et al. 2014) with the experimental data (Chen et al. 2000) in heterogeneous nucleation of water vapor on SiO_2 particles. It is found that compared with Fletcher model, the predicted critical supersaturation for kinetic model is much closer to the experimental data. Our prediction results are more consistent with the experimental data for small particles. With the increase of particle size, the prediction data for kinetic model are a little larger than the experimental data, which may be accounted by the roughness of particles.

Contribution of Two Diffusion Mechanisms to Embryo Growth

To investigate the relative importance of the two mechanisms to embryo growth, we define a dimensionless number *RTO* as:

$$RTO = C_n(a)/C_n(b) \quad \ldots(22)$$

Fig. 4 shows the variations of *RTO* with particle diameter and embryo radius. The temperature for supersaturated water vapour is 40°C (313.15K), the supersaturation is 1.2, and under this condensation the critical embryo radius r^* is about 5.31nm. It is found from Fig. 4 that when $r_n < r^*$, the particle surface diffusion mechanism plays a dominant action in embryo growth and the value of *RTO* is always above 100. Additionally, for a given particle diameter, the value of *RTO* decreases remarkably with the increasing of embryo radius, which indicates that the mechanism of direct diffusion condensation begins to make more contributions to embryo growth. All these results indicate that the surface diffusion mechanism is more important than the direct addition mechanism when the embryo radius is less than critical embryo radius, and the direct diffusion mechanism plays a significant contribution to the growth of embryo with the increase of embryo size, which is consistent with the conclusion of Fan et al. (2019).

Coefficients of Evaporation and Condensation

Fig. 5 shows the variation of the coefficients of evaporation and condensation with the radius of embryo under different temperatures. It is found that the coefficients of evaporation and condensation increase nearly linearly with the increase of embryo radius r_n. When the embryo radius is less than the

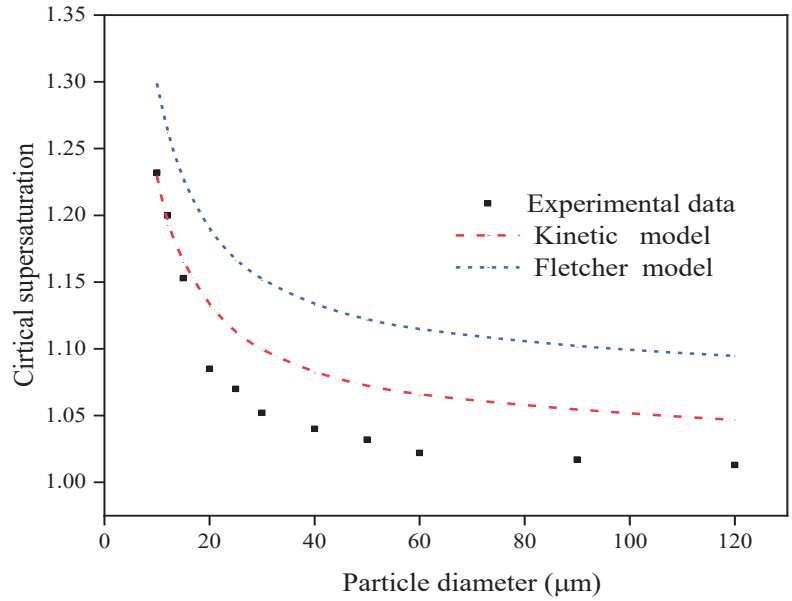

Fig. 3: Comparison with the experimental data.

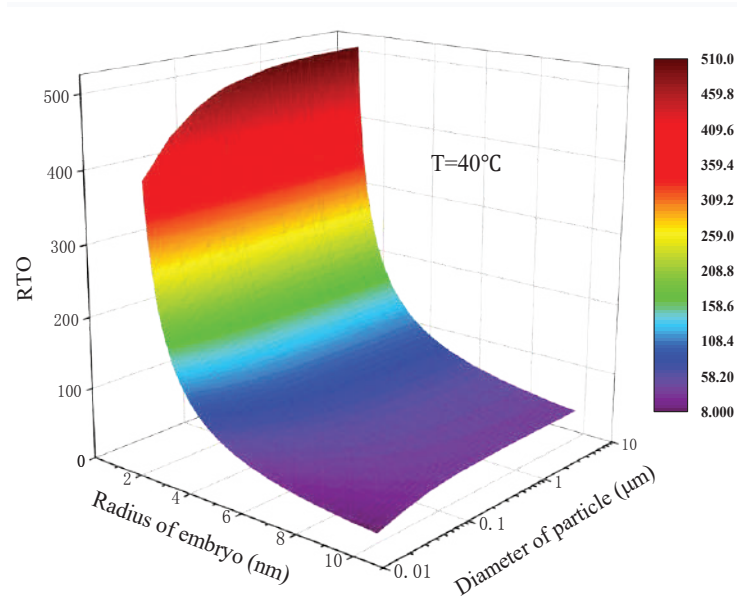

Fig. 4: Variations of *RTO* with particle diameter and embryo size.

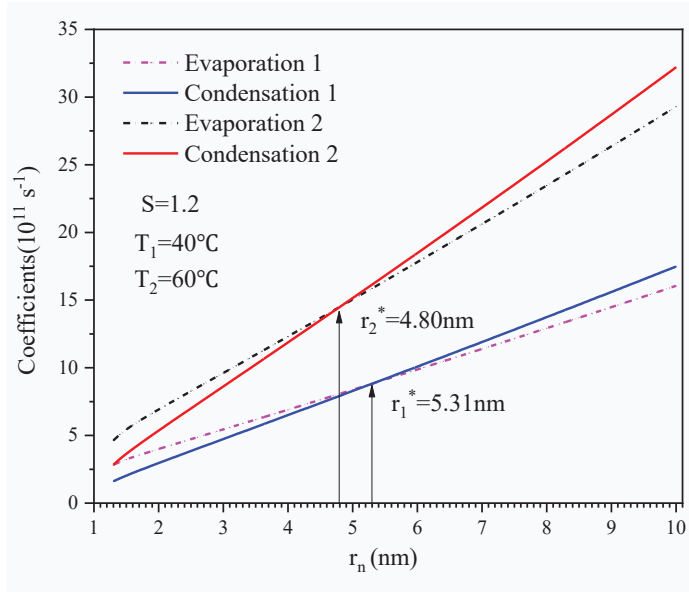

Fig. 5: Variations of evaporation and condensation coefficients with embryo radius.

critical embryo radius $r_n < r^*$, the evaporation coefficient is larger than condensation coefficient and the formed embryo tends to disappear. When $r_n > r^*$, the evaporation coefficient is less than condensation coefficient and the formed embryo tends to be larger. When $r_n = r^*$, the value of evaporation coefficient is equal to condensation coefficient, which means that the embryo is in metastable state and the size of the embryo keeps constant.

Moreover, with the increase of temperature, the value of evaporation and condensation coefficients are enlarged and the laws between them remain the same at different temperatures, which manifests that the improvement of vapour temperature can accelerate the growth of embryo and benefit the heterogeneous nucleation process.

Nucleation Rate

Nucleation rate refers to the number of critical embryos formed on coal-fired PM_{10} surface unit time. Fig. 6 shows

that the nucleation rate varies with supersaturation at different particle surface. It can be seen from Fig. 6(a) that the nucleation rates increase exponentially with the increase of supersaturation for a given particle diameter. In the case of particles with the diameter of 2.5 microns, the nucleation rate increases from 6.5×10^5 to 6.9×10^{18}, when the supersaturation increases from 1.2 to 1.3. This is because the increase of supersaturation can reduce the free energy barrier of nucleation and decrease the size of critical embryo radius. Additionally, with the increase of supersaturation, the number of water vapor molecules around the particles is further increased, and there will be more water vapor molecules condensed on particle unit time, all these reasons can account for the changes of nucleation rate.

Fig. 6(b) shows the variations of nucleation rate with vapor supersaturation under different temperatures. It is found that nucleation rate is increased with temperature when the supersaturation is constant. With the temperature increased from 313.15K to 333.15K, the nucleation rate is increased from 1.39×10^{25} to 3.45×10^{26} under the condition S = 1.5. This is because the improvement of temperature can dramatically increase the diffusion condensation rates for water vapor molecules and decrease the surface tension of embryo droplet. Furthermore, as the supersaturation to be larger, temperature is not the dominant factor to affect the condensation rate and the increase of temperature is not obvious to accelerate the improvement of nucleation rate.

Critical Supersaturation

Fig. 7 shows the variation of critical supersaturation with particle diameter and temperature. It can be seen from Fig. 7; the critical supersaturation decreases remarkably with the increase of particle diameter when the particle diameter is less than 0.1μm at different temperatures. As the particle diameter becomes larger, the trend of decrease for critical supersaturation tends to level off. Additionally, the critical supersaturation decreases with vapour temperature for a given particle, when the temperature rises from 313.15K (40°C) to 333.15K (60°C), and the critical supersaturation for coal-fired particles with a diameter of 2.5μm is reduced from 1.180 to 1.152. This is because the increase of temperature can not only decrease the critical embryo size, but also reduce the barrier of free energy for heterogeneous nucleation, which can also account for the increase of nucleation rate with the increase of temperature. Therefore, the improvement of temperature is conducive to the occurrence of heterogeneous nucleation of supersaturated vapour on coal-fired PM_{10} surface.

CONCLUSIONS

1. The kinetic model, in which three factors are considered including the effect of line tension, two mechanisms of embryo growth and the wettability of coal-fired PM_{10} can be used to accurately predict the heterogeneous nucleation process.
2. When the embryo radius is less than critical embryo radius $r_n < r^*$, the mechanism of particle surface diffusion plays a dominant action in embryo growth and the value of *RTO* is always above 100.
3. The heterogeneous nucleation rate is very sensitive to

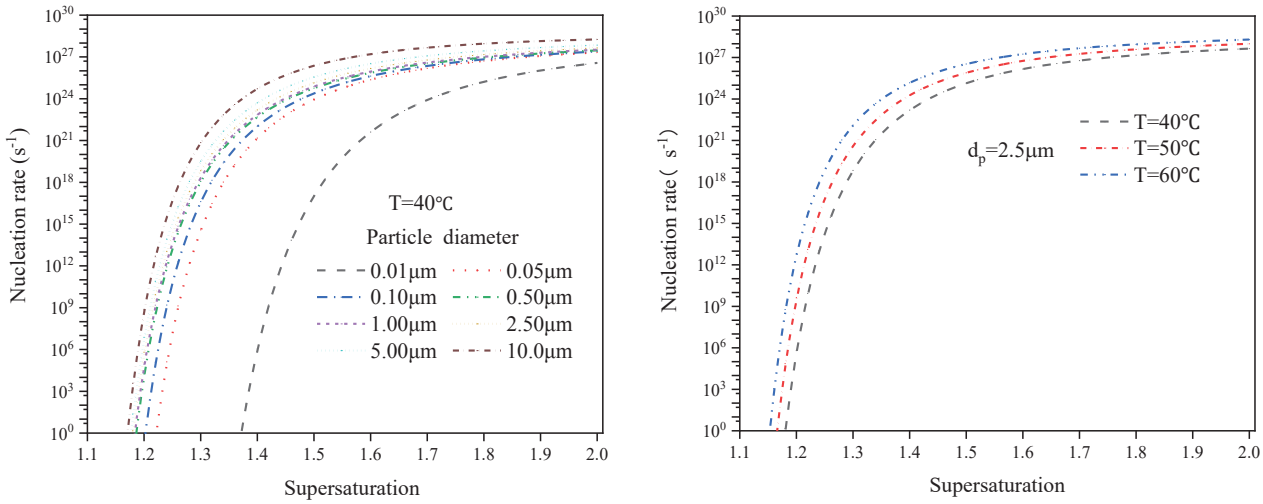

Fig. 6: Variations of nucleation rate with the supersaturation.

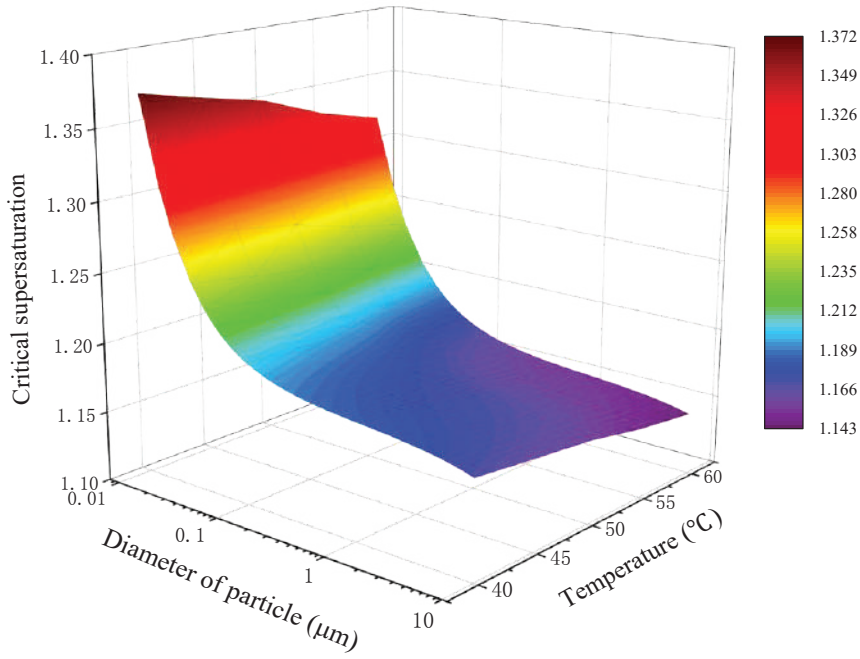

Fig. 7: Variations of critical supersaturation with particle diameter and temperature.

supersaturation, and it increases exponentially with the increase of supersaturation.

4. The critical supersaturation decreases remarkably with the increase of particle diameter when the particle diameter is less than 0.1μm at different temperatures. With the increase of particle diameter, the trend of the decrease of critical supersaturation tends to level off.
5. The improvement of supersaturated vapour temperature can decrease critical embryo size, increase diffusion condensation rates, thereby increasing the nucleation rate then decreasing the critical supersaturation, which is beneficial to heterogeneous nucleation on coal-fired particles.

ACKNOWLEDGEMENT

This study was supported by the National Natural Science Foundation of China (No. 61262048), the Key Research and Development Project of Jiangxi Province (No. 2017ACG70012).

REFERENCES

Bentayeb, M., Simoni, M., Baiz, N., Norback, D., Baldacci, S., Maio, S., Viegi, G. and Annesi-Maesano, I. 2012. Adverse respiratory effects of outdoor air pollution in the elderly. International Journal of Tuberculosis & Lung Disease, 16(9): 1149-1161.

Chen, C.C. and Tao, C. J. 2000. Condensation of supersaturated water vapour on submicrometer particles of SiO_2 and TiO_2. Journal of Chemical physics, 112(22): 9967-9977.

Fan, F. X., Yang, L. J., Yuan, Z. L. and Yan, J. P. 2007. Numerical prediction of water vapour nucleation behaviour on $PM_{2.5}$ from coal combustion. Journal of Chemical Industry and Engineering (China), 58(10): 2561-2566.

Fan, F.X., Zhang, S.H., Peng, Z. B., Chen, J., Su, M. X., Moghtaderi, B. and Doroodchi E. 2019. Numerical investigation of heterogeneous nucleation of water vapour on PM_{10} for particulate abatement. The Canadian Journal of Chemical engineering, 97: 930-939.

Fan, Y., Qin, F. H., Luo, X. S., Zhang, J. S., Wang, J., Gui, H. Q. and Liu, J. G. 2015. A modified expression for the steady-state heterogeneous nucleation rate. Journal of Aerosol Science, 87: 17-27.

Fan, Y., Qin, F.H., Luo, X.S., Lin, LY., Gui, H.Q., and Liu, J.G. 2013. Heterogeneous condensation on insoluble spherical particles: Modeling and parametric study. Chemical Engineering Science, 102: 387-396.

Fletcher, H. N. 1958. Size effect in heterogeneous nucleation. The Journal of Chemical Physics, 29: 572-576.

Hao, W., Pan, D.P., Huang, R.T., Hong, G.X., Bing, Y., Peng, Z.M. and Yang, L.J. 2016. Abatement of fine particle emission by heterogeneous vapour condensation during wet limestone-gypsum flue gas desulfurization. Energy & Fuels, 30(7): 6103-6109.

Heidenreich, S. and Ebert, F.1995. Condensational droplet growth as a preconditioning technique for the separation of submicron particles from gases. Chemical Engineering & Processing, 34(3): 235-244.

Hienola, A. I., Winkler, P. M., Wagner, P. E., Vehkamäki, H., Lauri, A., Napari I. and Kulmala, M. 2007. Estimation of line tension and contact angle from heterogeneous nucleation experimental data. The Journal of Chemical Physics, 126: 094705.

Hu, B., Yang, Y., Cai, L., Yuan, Z.L., Roszak, S. and Yang, L.J. 2018. Experimental study on particles agglomeration by chemical and turbulent agglomeration before electrostatic precipitators. Powder Technology, 335: 186-194.

Liu, Q.Z., Shen, Z.G. and Tao, L.X. 2016. Research on the application of a wet electrostatic precipitator in coal-fired power plant for "Gypsum

Rain" prevention and treatment. Nature Environment and Pollution Technology, 15(3): 867-872.

Luo, X. S., Fan, Y., Qin, F. H., Gui, H.Q. and Liu, J.G. 2014. A kinetic model for heterogeneous condensation of vapour on an insoluble spherical particle. The Journal of Chemical Physics, 024708.

Siddharth, K. Sharma and Gupta, A.B. 2008. Ambient air interactions between particulate matter and gases of combustion. Nature Environment and Pollution Technology, 7(2): 257-260.

Wen, G.S. and Fan, F.X. 2014. Numerical analysis on growth of soluble PM2.5 by vapour heterogeneous condensation. China Environmental Science, 34(5): 1119-1124.

Xu, J. C., Yu, Y., Zhang, J. and Zhong, H. 2017. Kinetics study of droplet growth on surface of coal-fired fine particles. Journal of Southeast University (Natural Science Edition), 47(3): 506-512.

Zhou, D.L., Li, S.Q., Jin, X., Xiong, G.L. and Huang, W. 2016. Experiments and numerical simulations of the removal of fine particles in the coupling field of electrostatic precipitators. Proceedings of the CSEE, 36(2): 453-458.

Nature Environment and Pollution Technology
An International Quarterly Scientific Journal

p-ISSN: 0972-6268 e-ISSN: 2395-3454	Vol. 19	No. 1	pp. 303-309	2020

Original Research Paper **Open Access**

Estimation of Evaporation Trends in Six Major River Basins of China Using a New Nonlinear Formula of the Complementary Principle of Bouchet

Jing Guo*, Guodong Zhang, Fahong Zhang*, Jiali Guo***†, Xiaozhong Sun* and Biyun Sheng***
*PowerChina Huadong Engineering Corporation Limited, Hangzhou 311122, China
**Henan Yellow River Hydrological Survey and Design Institute, Zhengzhou 450004, China
***College of Hydraulic and Environmental Engineering, China Three Gorges University, Yichang 443002, China
†Correspondence: Jiali Guo

Nat. Env. & Poll. Tech.
Website: www.neptjournal.com

Received: 19-06-2019
Accepted: 30-08-2019

Key Words:
Evaporation trend
Meteorological data
Principle of Bouchet
River basins
Evaporation trend

ABSTRACT

Evaporation (*Ea*) is a key component of the hydrological cycle. Under the impact of global change, *Ea* has changed significantly, both globally and regionally. A number of methods have been developed to estimate *Ea* and its trends. Among them, methods based on the complementary principle of Bouchet estimate *Ea* using only routine meteorological data as inputs and greatly simplify the *Ea* estimation. In this study, a new nonlinear formulation of this principle was tested for estimating *Ea* trends in 6 major river basins of China. The results indicate that the estimated annual *Ea* trends were in good agreement with that obtained from the water balance approach with the relative errors ranging from -12.0 to 11.2%. In addition, in two humid basins of this study, decreasing *Ea* trends were estimated from decreasing potential evaporation, although the nonlinear formulation is based on the complementary principle between *Ea* and potential evaporation. One advantage of the method is that only routine meteorological data are required as inputs and that it can be used to estimate *Ea* trends, wherever such data are available.

INTRODUCTION

Evaporation (*Ea*) is the crucial link between surface water and energy balances. In the context of global warming, *Ea* has changed significantly both globally and regionally (Zhang et al. 2007, Zhang et al. 2016, Jung et al. 2010, Brutsaert 2015, Yang et al. 2017). Accurate estimation of *Ea* trends is a fundamental task for hydrologic research. A number of methods such as land surface models, global climate models and hydrologic models have been developed to estimate regional and global *Ea* trends (Mueller et al. 2011, Wang & Dickinson 2012, Liu et al. 2016). These models need land, soil and vegetation information as inputs, and using these methods in practice sometimes remains a challenge due to lack of input data. Over the years among various methods for estimating *Ea*, methods based on the complementary principle (Bouchet 1963) estimate *Ea* using only routine meteorological data as inputs and greatly simplify the *Ea* estimation (Hobbins et al. 2001, Han et al. 2014, Ma et al. 2015).

The original complementary principle involved only one boundary condition and resulted in a series of linear formulations (Brutsaert & Sticker 1979, Morton 1983, Granger 1989, Brutsaert 2005). Using a linear formulation, Brutsaert (2006) obtained the increasing trend of land surface *Ea* as 0.44 mm a-2 during the second half of the 20th century, which is close to the value (i.e., 0.42 mm a-2) estimated based on the global FLUXNET network in Jung et al. (2010). Using the same linear formulation, Brutsaert (2013) estimated that the *Ea* trend on the Tibetan Plateau was 0.69 mm a-2 during 1966 to 2000, which is in agreement with the value (0.70 mm a-2) estimated based on the water balance approach in Zhang et al. (2017).

By imposing three additional but necessary boundary conditions based on strictly physical considerations, a nonlinear formulation of the complementary principle was proposed in Brutsaert et al. (2017). The nonlinear formulation has a better physical meaning than former linear formulations and has been evaluated in flux stations of China and Australia (Brutsaert 2015, Zhang et al. 2017). While the nonlinear formulation had good performance for estimating *Ea* in flux stations, its capability of simulating basin *Ea* trends has not yet been evaluated. It is the objective of the present study to test the nonlinear formulation for estimating *Ea* trends in 6 major river basins of China. The result will advance the application of the nonlinear formulation to estimate *Ea* trends under global warming.

METHODS, STUDY AREA AND DATA USED

The nonlinear formulation of the complementary principle

is written as follows:

$$E_a = \left(\frac{E_{po}}{E_{pa}}\right)^2 \left(2E_{pa} - E_{po}\right) \quad \ldots(1)$$

Here, *Epa* is the evaporation that would take place from a small saturated surface inside the large (normally) drier surface, from which *Ea* is taking place. It can be obtained from measurements by different types of pans. The variable *Epo* is the true potential evaporation, i.e., the evaporation that would take place from the same large surface as *Ea*, when it is well supplied with water. *Epo* can be calculated by Priestley and Taylor equation (Priestley & Taylor 1972):

$$E_{po} = \mathtt{a}_e \frac{\Delta}{\Delta + \mathtt{g}}\left(R_n - G\right) \quad \ldots(2)$$

Where, R_n - G is the available energy flux, in which R_n is the net radiation and G the heat flux into the ground. When the variables were daily means, the ground heat flux G could be neglected. Δ is the slope of saturated vapour pressure at the given air temperature (Ta), $\Delta = 4098(0.6108 \exp(17.27T_a/(T_a + 237.3))/(T_a + 237.3)^2$; $\mathtt{g}$ is the psychrometric constant. Combining (1) and (2), the nonlinear formulation is written as follows:

$$E_a = f\left(R_n, E_{pa}, T_a\right) = \left(\frac{\mathtt{a}_e \frac{\Delta}{\Delta+\mathtt{g}} R_n}{E_{pa}}\right)^2 \left(2E_{pa} - \mathtt{a}_e \frac{\Delta}{\Delta+\mathtt{g}} R_n\right) \quad \ldots(3)$$

Where, $\mathtt{a}_e$ is the only adjustable parameter. We note that $\mathtt{a}_e$ is not quite the Priestley-Taylor parameter, but merely a weak analog of it. When R_n, E_{pa} and T_a are time-dependent, one obtains for the E_a trend as follows:

$$\frac{dE_a}{dt} = \frac{\partial E_a}{\partial E_{pa}}\frac{dE_{pa}}{dt} + \frac{\partial E_a}{\partial T_a}\frac{dT_a}{dt} + \frac{\partial E_a}{\partial R_n}\frac{dR_n}{dt} \quad \ldots(4)$$

Based on (3), $\frac{\partial E_a}{\partial E_{pa}}$, $\frac{\partial E_a}{\partial T_a}$ and $\frac{\partial E_a}{\partial R_n}$ can be calculated as follows:

$$\begin{cases} \dfrac{\partial E_a}{\partial E_{pa}} = \dfrac{2{E_{po}}^2(E_{po} - E_{pa})}{{E_{pa}}^3} \\ \dfrac{\partial E_a}{\partial T_a} = \mathtt{a}_e R_n \left[4\dfrac{E_{po}}{E_{pa}} - 3\left(\dfrac{E_{po}}{E_{pa}}\right)^2\right] \dfrac{\mathtt{U}}{(\mathtt{D}+\mathtt{U})^2} \\ \qquad \dfrac{(3623.571 - 2T_a)\mathtt{D}}{(T_a + 237.3)^2} \\ \dfrac{\partial E_a}{\partial R_n} = 4\mathtt{a}_e \dfrac{\mathtt{D}}{\mathtt{D}+\mathtt{U}}\dfrac{E_{po}}{E_{pa}} - 3\mathtt{a}_e \dfrac{\mathtt{D}}{\mathtt{D}+\mathtt{U}}\left(\dfrac{E_{po}}{E_{pa}}\right)^2 \end{cases} \quad \ldots(5)$$

The water balance approach is typically used to estimate the reference value of E_a for a basin:

$$E_a = \mathrm{P} - \mathrm{R} - \mathtt{D}S/\mathtt{D}t \quad \ldots(6)$$

Where, P is the total precipitation (mm a^{-1}), R is the river discharge (mm a^{-1}), and $\Delta S/\Delta T$ is the change in

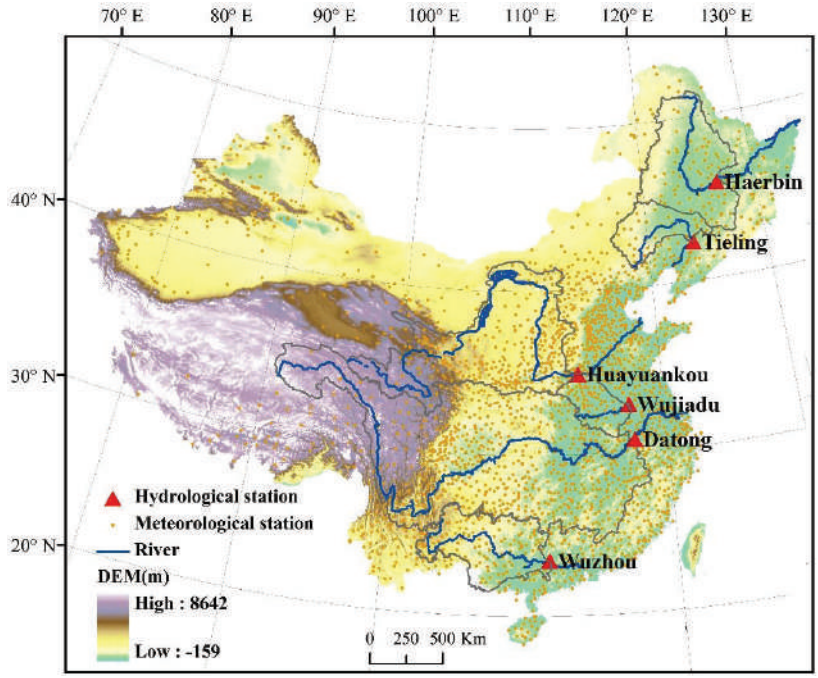

Fig. 1: The location of the 6 major river basins and corresponding hydrological stations.

Table 1: The hydro-meteorological information of the 6 basins.

Basin	Control Station	Control Area (km^2)	Ta (°C)	P (mm)
Songhua	Haerbin	389, 769	2.4	492.9
Liao	Tieling	120, 764	6.1	410.4
Yellow	Huayuankou	730, 036	6. 6	430.0
Huai	Wujiadu	121, 330	14.9	906.3
Yangtze	Datong	1,705, 383	12.5	1020.3
Pearl	Wuzhou	327, 006	18.8	1352.9

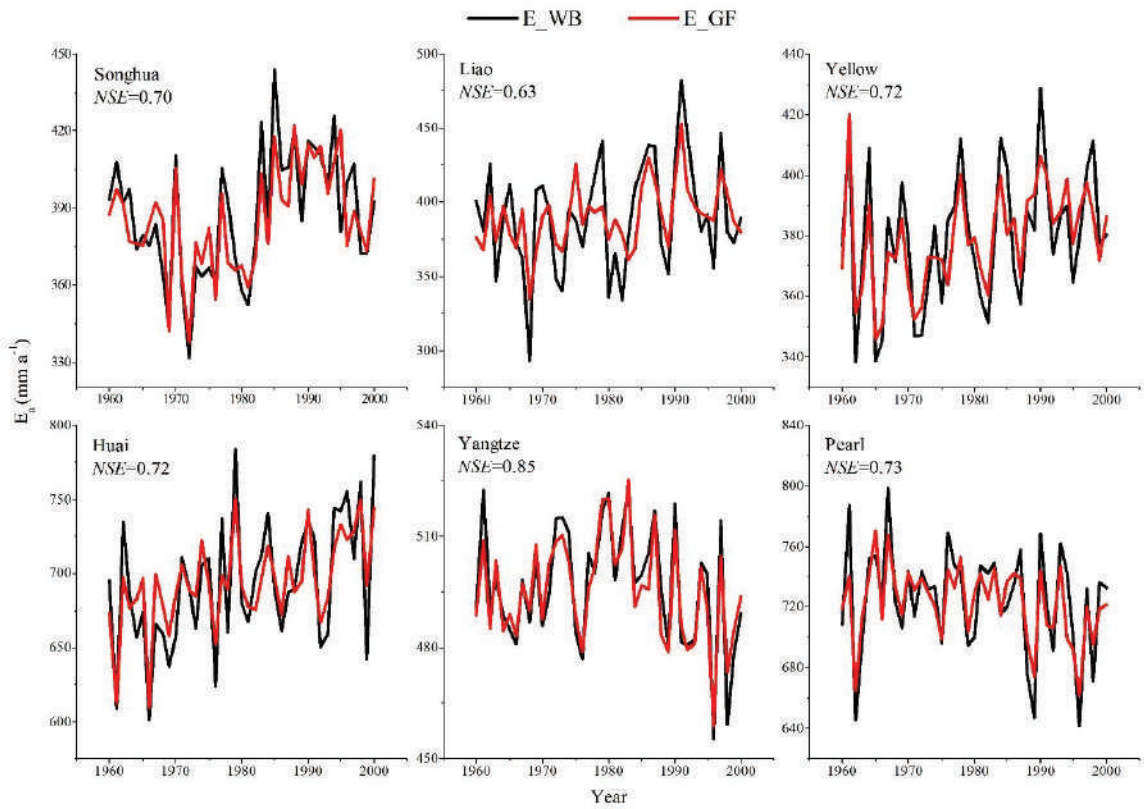

Fig. 2: Comparisons of estimated annual evaporation values using the nonlinear formulation (E_GF) against water budget approach (E_WB) for the 6 basins.

terrestrial water storage (mm a^{-1}).

Six major river basins in China, namely the Songhua River, Liao River, Yellow River, Huai River, Yangtze River and Pearl River basin, were chosen to estimate *Ea* trends in this study (Fig. 1). The 6 basins are located from northern China to southern China, with areas ranging from 120,764 to 1,705,383 km^2 (Table 1). Mean annual air temperatures of the 6 basins range from 2.4 to 18.8°C, and mean annual precipitations range from 410.4 to 1352.9 mm. The monthly streamflow data for the 6 basins from 1960 to 2000 were provided by the China Hydrological Bureau (http://www.hydroinfo.gov.cn/).

Monthly meteorological data from 1960 to 2000 at 2407 national meteorological stations, which include precipitation (*P*), air temperature (*Ta*), China D20 pan evaporation (*Epa*) and sunshine hours, were acquired from the National Meteorological Information Center of the China Meteorological Administration (http://data.cma.cn/en). The net radiation (*Rn*) at the national meteorological stations was estimated from sunshine hours following the method recommended by Allen et al. (1998). All the meteorological data were spatially averaged across each

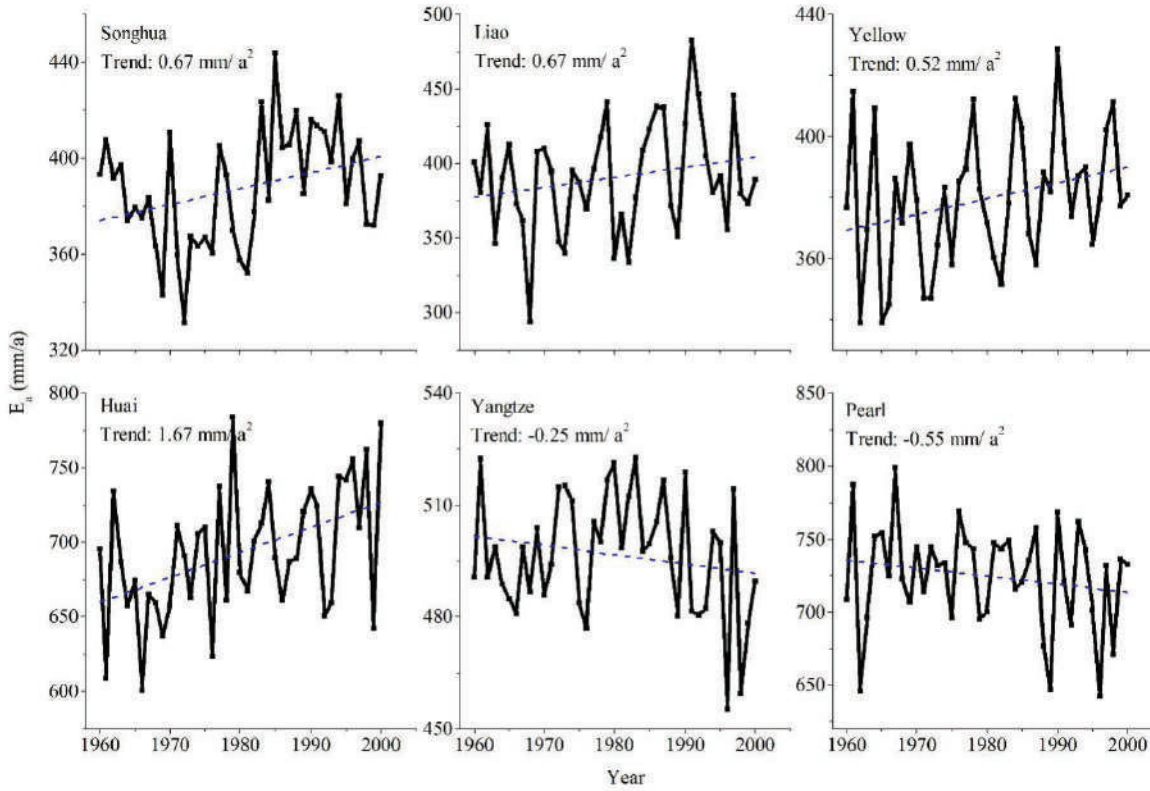

Fig. 3: Trends in annual evaporation obtained from the water balance approach for the 6 basins.

Table 2: Calculation of evaporation trends using (Eq. 4) for the 6 basins.

Basin	*Ea* trend estimation equation	$\frac{dE_{pa}}{dt}$	$\frac{dT_a}{dt}$	$\frac{dR_n}{dt}$	Sum	$\frac{dE_a}{dt}$	Error
Songhua	$-0.20dE_{pa}/dt + 24.10dT_a/dt + 0.70dR_n/dt$	–2.29	0.041	–1.16	0.63	0.67	–4.9
Liao	$-0.17dE_{pa}/dt + 21.49dT_a/dt + 0.66dR_n/dt$	–2.44	0.032	–0.61	0.69	0.67	2.6
Yellow	$-0.17dE_{pa}/dt + 20.45dT_a/dt + 0.56dR_n/dt$	–4.65	0.027	–1.39	0.57	0.52	10.1
Huai	$-0.27dE_{pa}/dt + 24.20dT_a/dt + 0.98dR_n/dt$	–9.23	0.012	–1.35	1.47	1.67	-12.0
Yangtze	$-0.24dE_{pa}/dt + 20.10dT_a/dt + 0.73dR_n/dt$	–3.69	0.007	–1.72	–0.23	–0.25	-9.1
Pearl	$-0.28dE_{pa}/dt + 20.93dT_a/dt + 0.99dR_n/dt$	–3.68	0.006	–1.78	–0.61	–0.55	11.2

of the 6 basins by the CoKriging interpolation algorithm using ArcGIS software, which takes a digital elevation model as an additional input. Annual $\Delta S/\Delta T$ were derived from the Global Land Data Assimilation System (GLDAS) Noah land surface model (Rodell et al. 2004) (http://daac.gsfc.nasa.gov/services/grads-gds/gldas). These values have a spatial resolution of 0.25° × 0.25° from 1960 to 2000.

RESULTS

The only parameter of the nonlinear formulation, namely a_e, was calibrated based on the minimal error between the average annual *Ea* calculated from the multiyear average water budget equation (6) and that from the nonlinear formulation (3) for each basin. The optimized α_e for the 6

basins is 1.08, 1.03, 1.04, 1.13, 1.18 and 1.22, respectively. Fig. 2 shows the comparisons of estimated annual E_a values using the nonlinear formulation (*E_GF*) against water budget approach (*E_WB*) for the 6 basins. The Nash-Sutcliffe efficiency coefficient (*NSE*) between *E_GF* and *E_WB* was 0.70, 0.63, 0.72, 0.72, 0.85 and 0.73 for the 6 basins, respectively. Generally, the nonlinear formulation had good performance for annual E_a estimation in the 6 basins.

Annual *Ea* trends of the 6 basins were estimated using (Eq. 4), and the detailed estimation equations for each basin are listed in Table 2. The trends of annual *Rn*, *Epa* and Ta used to estimate *Ea* trend for each basin are also listed in Table 2. With these trends together, (Eq. 4) yielded the trends of *Ea* as 0.63, 0.69, 0.57, 1.47, -0.23 and -0.61 mm a-2 for the 6 basins, respectively. Fig. 3 shows that *Ea* trends obtained from the water balance approach were 0.67, 0.67, 0.52, 1.67, -0.25 and -0.55 mm a-2 for the 6 basins, respectively. The relative errors between *Ea* trends from the nonlinear formulation and that from the water balance approach were -4.9, 2.6, 10.1, -12.0, -9.1 and 11.2%, respectively. The nonlinear formulation produced good agreement with annual *Ea* trends obtained from the water balance approach in the 6 basins.

$\frac{dE_{pa}}{dt}$, $\frac{dT_a}{dt}$ and $\frac{dR_n}{dt}$ denote annual trend in *Epa*, *Ta* and *Rn* respectively. Sum denotes the sum of the right-side hand of (Eq. 4); $\frac{dE_a}{dt}$ annual *Ea* trend obtained from the water balance approach. Error denotes the relative errors between *Ea* trends estimated from (Eq. 4) and that obtained from the water balance approach.

DISCUSSION

Table 2 shows that *Ta* has increasing trends for all the 6 basins, while *Rn* and *Epa* had decreasing trends. According to the detailed estimation equation of *Ea* trend in Table 2, the increasing *Ta* trends and decreasing *Epa* trends will lead to an increase in *Ea*, while decreasing *Rn* will result in a decrease in *Ea*. *Ea* trends for a basin were the combined effects of *Rn*, *Epa* and *Ta*. The increasing *Ea* trends in the Songhua River, Liao River, Yellow River and Huai River basin indicate that the negative *Rn* trend term was not strong enough to overcome the positive *Epa* and *Ta* trend terms. In the Yangtze River and Pearl River basin, the negative *Rn* trend term overcame the positive *Epa* and *Ta* trend terms and resulted in decreasing *Ea* trends.

The Songhua River, Liao River, Yellow River and Huai River basins are located in northern China and belong to water-limited basins, where annual precipitation is less than atmospheric evaporative demand. The Yangtze River and Pearl River basins are located in southern China and belong to energy-limited basins, where annual precipitation is larger than atmospheric evaporative demand (Mcvicar et al. 2012). In this study, decreasing *Epa* was accompanied by increasing *Ea* in the 4 water-limited basins, while decreasing *Epa* was accompanied by decreasing *Ea* in the 2 energy-limited basins. This result is consistent with the findings that *Ea* and *Epa* could be generally complementary in water-limited basins and proportional in energy-limited basins (Yang et al. 2006, Yang et al. 2007, Cong et al. 2010, Zhang et al. 2017). Interestingly, although the nonlinear formulation is based on the complementary principle between *Ea* and *Epa*, decreasing trends in *Ea* were still estimated from decreasing *Epa* in the two energy-limited basins. This provides additional support for the plausibility of the nonlinear formulation for estimating *Ea* trends.

While the agreement is excellent, admittedly *Ea* trends here and also the equation (4) used to estimate *Ea* trends are subject to some uncertainty. Firstly, the reference *Ea* trends were obtained from the water balance approach with $\Delta S/\Delta T$ simulated by the GLDAS Noah land surface model. Errors existed between the simulated and the true values of $\Delta S/\Delta T$ (Long et al. 2017). Such errors can then lead in turn to inconsistencies between Ea trends from the water balance approach and that from the nonlinear formulation. We note that these errors had limited effect on the calibration of a_e for each basin, because a_e was calibrated by the multiyear average water balance equation during 1960 to 2000, and D $\Delta S/\Delta T$ can be assumed to equal zero (Miao et al. 2015, Sun et al. 2018). Secondly, on the right-side hand of (Eq. 4), *Rn*, *Epa* and *Ta* could impact each other, and were not totally independent (Liu et al. 2011). However, the differential equations assumed that they were independent. This could lead to errors of *Ea* trends estimated from (Eq. 4). This issue will require further research.

Different methods have been developed to estimate *Ea* trends. One of the difficulties is that *Ea* trends could be significantly impacted by human activities, such as irrigation (Kong et al. 2015, Miao et al. 2016, Yang et al. 2017) and reservoir construction (Yang et al. 2017). Mao et al. (2016) indicates that with or without considering the water storage change due to reservoir construction can even obtain opposite *Ea* trends in the major river basins of China. However, the human influences on hydrologic cycle are typically difficult to quantify due to lack of data. The nonlinear formulation of the complementary principle can avoid directly estimating human influences on *Ea*, while it can indirectly reflect human influences on *Ea* (Liu et al. 2017). Theoretically, the observed

trends in *Rn*, *Epa* and *Ta* were already influenced by human influences such as irrigation and reservoir construction, and thus the corresponding *Ea* trends estimated using the nonlinear formulation reflected these human influences.

CONCLUSIONS

A nonlinear formulation of complementary principle was tested for estimating *Ea* trends in 6 major river basins of China. The resulting method is shown to be fairly accurate in estimating annual *Ea* trends from routine meteorological data. In the two energy-limited basins, namely the Yangtze River Basin and Pearl River Basin, both *Ea* and *Epo* had decreasing trends during 1960 to 2000. Although the nonlinear formulation is based on the complementary principle between *Ea* and *Epo*, it accurately simulated the decreasing *Ea* trends in the two basins. In the context of global warming, accurate prediction of *Ea* trends is of great importance for estimating the changes in hydrologic cycle. The results from this study are promising as they indicate the potential of this method for predicting *Ea* trends from projections of changes in routine meteorological variables.

ACKNOWLEDGEMENTS

We thank China Meteorological Administration for providing the routine meteorological data (http://data.cma.cn/en) and China Hydrological Bureau for providing the streamflow data of the six basins (http://www.hydroinfo.gov.cn/).

REFERENCES

Allen, R. G., Pereira, L. S., Raes, D. and Smith, M. 1998. Crop evapotranspiration: Guidelines for computing crop requirements. Irrigation Drainage Pap. 56, Food and Agric. Organ., Rome.

Bouchet, R. J. 1963. Evapotranspiration réelle, évapotranspirationpotentielle, et production agricole. Ann. Agron., 14: 743-824.

Brutsaert, W. and Stricker, H. 1979. An advection-aridity approach to estimate actual regional evapotranspiration. Water Resour. Res., 15: 443-450.

Brutsaert, W. 2005. Hydrology: An Introduction. 605 pp., Cambridge Univ. Press, New York.

Brutsaert, W. 2006. Indications of increasing land surface evaporation during the second half of the 20th century. Geophys. Res. Lett., 33: 4.

Brutsaert, W. 2013. Use of pan evaporation to estimate terrestrial evaporation trends: The case of the Tibetan Plateau. Water Resour. Res., 49: 3054-3058.

Brutsaert, W. 2015. A generalized complementary principle with physical constraints for land-surface evaporation. Water Resour. Res., 51: 8087-8093.

Brutsaert, W., Li, W., Takahashi, A., Hiyama, T., Zhang, L. and Liu, W. 2017. Nonlinear advection-aridity method for landscape evaporation and its application during the growing season in the southern Loess Plateau of the Yellow River basin. Water Resour. Res, 53(1): 270-282.

Cong, Z., Zhao, J., Yang, D. and Ni, G. 2010. Understanding the hydrological trends of river basins in China. J. Hydrol., 388(3): 350-356.

Granger, R. J. 1989. A complementary relationship approach for evaporation from non-saturated surfaces. J. Hydrol., 111: 31-38.

Han, S., Tian, F. and Hu, H. 2014. Positive or negative correlation between actual and potential evaporation? Evaluating using a nonlinear complementary relationship model. Water Resour. Res., 50(2): 1322-1336.

Hobbins, M.T., Ramírez, J. A. and Brown, T. C. 2001. The complementary relationship in estimation of regional evapotranspiration: An enhanced advection-aridity model. Water Resour. Res., 37(5): 1389-1403.

Jung, M., Reichstein, M., Ciais, P., Seneviratne, S.I., Sheffield, J., Goulden, M.L., Bonan, G., Cescatti, A., Chen, J., De Jeu, R. and Dolman, A.J. 2010. Recent decline in the global land evapotranspiration trend due to limited moisture supply. Nature, 467(7318): 951-954.

Kong, D.X., Miao, C.Y., Borthwick, A.G.L., Duan, Q.Y., Liu, H., Sun, Q.H., Ye, A.Z., Di, Z.H. and Gong, W. 2015. Evolution of the Yellow River Delta and its relationship with runoff and sediment load from 1983 to 2011. J. Hydrol., 520: 157-167.

Liu, X., Liu, C. and Brutsaert, W. 2016. Regional evaporation estimates in the eastern monsoon region of China: Assessment of a nonlinear formulation of the complementary principle. Water Resour. Res., 52: 9511-9521.

Liu, X., Luo, Y., Zhang, D., Zhang, M. and Liu, C. 2011. Recent changes in pan-evaporation dynamics in China. Geophys. Res. Lett., 38(13): 1-4.

Liu, X., Yang, T., Hsu, K., Liu, C. and Sorooshian, S. 2017. Evaluating the streamflow simulation capability of PERSIANN-CDR daily rainfall products in two river basins on the Tibetan Plateau. Hydrol. Earth Syst. Sci., 21(1): 169-181.

Long, D., Pan, Y., Zhou, J., Chen, Y., Hou, X., Hong, Y., Scanlon, B. R. and Longuevergne, L. 2017. Global analysis of spatiotemporal variability in merged total water storage changes using multiple GRACE products and global hydrological models. Remote Sens. Environ., 192: 198-216.

Ma, N., Zhang, Y., Szilagyi, J., Guo, Y., Zhai, J. and Gao, H. 2015. Evaluating the complementary relationship of evapotranspiration in the alpine steppe of the Tibetan Plateau. Water Resour. Res, 51(2): 1069-1083.

Mao, Y., Wang, K., Liu, X. and Liu, C. 2016. Water storage in reservoirs built from 1997 to 2014 significantly altered the calculated evapotranspiration trends over China. J. Geophys. Res., 121: 10,097-10,112.

McVicar, T.R., Roderick, M.L., Donohue, R.J., Li, L.T., Van Niel, T.G., Thomas, A., Grieser, J., Jhajharia, D., Himri, Y., Mahowald, N.M. and Mescherskaya, A.V. 2012. Global review and synthesis of trends in observed terrestrial near-surface wind speeds: Implications for evaporation. J. Hydrol., 416-417: 182-205.

Miao, C.Y., Ashouri, H., Hsu, K., Sorooshian, S. and Duan, Q.Y. 2015. Evaluation of the PERSIANN-CDR daily rainfall estimates in capturing the behavior of extreme precipitation events over China. Journal of Hydrometeorology, 16: 1387-1396.

Miao, C.Y., Kong, D.X., Wu, J.W. and Duan, Q.Y. 2016. Functional degradation of the water-sediment regulation scheme in the lower Yellow River: Spatial and temporal analyses. Science of the Total Environment, 551-552: 16-22.

Morton, F. I. 1983. Operational estimates of areal evapotranspiration and their significance to the science and practice of hydrology. J. Hydrol., 66(1-4): 1-76.

Mueller, B., Seneviratne, S.I., Jimenez, C., Corti, T., Hirschi, M., Balsamo, G., Ciais, P., Dirmeyer, P., Fisher, J.B., Guo, Z. and Jung, M. 2011. Evaluation of global observations-based evapotranspiration datasets and IPCC AR4 simulations. Geophys. Res. Lett., 38: 1-7.

Priestley, C. H. B. and Taylor, R. J. 1972. On the assessment of surface heat flux and evaporation using large-scale parameters, Mon. Weather Rev., 100: 81-92.

Rodell, M., Houser, P.R., Jambor, U.E.A., Gottschalck, J., Mitchell, K., Meng, C.J., Arsenault, K., Cosgrove, B., Radakovich, J., Bosilovich, M. and Entin, J.K. 2004. The global land data assimilation system. Bull. Am. Meteorol. Soc., 85(3): 381-394.

Sun, Q.H., Miao,C.Y., Duan, Q.Y., Ashouri, H., Sorooshian, S. and Hsu, K. 2018. A review of global precipitation datasets: data sources, estimation, and intercomparisons. Reviews of Geophysics, 56(1): 79-107.

Wang, K. and Dickinson, R. 2012. A review of global terrestrial evapotranspiration: Observation, modeling, climatology, and climatic variability. Rev. Geophys.,50: RG2005

Yang, D., Sun, F., Liu, Z., Cong, Z. and Lei, Z. 2006. Interpreting the complementary relationship in non-humid environments based on the Budyko and Penman hypotheses. Geophys. Res. Lett., 33(18): 1-5.

Yang, D., Sun, F., Liu, Z., Cong, Z., Ni, G. and Lei, Z. 2007. Analyzing spatial and temporal variability of annual water-energy balance in nonhumid regions of China using the Budyko hypothesis. Water Resour. Res., 43: W04426.

Yang, T., Akbari Asanjan, A., Welles, E., Gao, X., Sorooshian, S., and Liu, X. 2017. Developing reservoir monthly inflow forecasts using artificial intelligence and climate phenomenon information. Water Resour. Res, 53(4): 2786-2812.

Yang, T., Asanjan, A.A., Faridzad, M., Hayatbini, N., Gao, X. and Sorooshian, S. 2017. An Enhanced Artificial Neural Network with A Shuffled Complex Evolutionary Global Optimization with Principal Component Analysis. Information Sciences.

Yang, T., Tao, Y., Li, J., Zhu, Q., Su, L., He, X. and Zhang, X. 2017. Multi-criterion model ensemble of CMIP5 surface air temperature over China. Theoretical and Applied Climatology, 132(3-4): 1057-1072.

Zhang, L., Cheng, L. and Brutsaert, W. 2017. Estimation of land surface evaporation using a generalized nonlinear complementary relationship. J. Geophys. Res., 122(3): 1475-1487.

Zhang, Y., Chiew, F., Peña-Arancibia, J., Sun, F., Li, H. and Leuning, R. 2017. Global variation of transpiration and soil evaporation and the role of their major climate drivers. J. Geophys. Res., 122: 6868–6881.

Zhang, Y., Liu, C., Tang, Y. and Yang, Y. 2007. Trends in pan evaporation and reference and actual evapotranspiration across the Tibetan Plateau. J. Geophys. Res., 112: D 12.

Zhang, Y., Peña-Arancibia, J. L., McVicar, T. R., Chiew, F. H., Vaze, J., Liu, C., Lu, X., Zheng, H., Wang, Y. and Liu, Y.Y. 2016. Multi-decadal trends in global terrestrial evapotranspiration and its components, Sci. Rep., 6 (19124): 1-12.

Nature Environment and Pollution Technology
An International Quarterly Scientific Journal

p-ISSN: 0972-6268
e-ISSN: 2395-3454

Vol. 19 | No. 1 | pp. 311-318 | 2020

Original Research Paper | Open Access

Pb(II) Adsorption onto Urea Treated *Leucaena leucocephala* Leaf Powder: Characterization, Kinetics and Isotherm Studies

Noor Fhadzilah Mansur*, Megat Ahmad Kamal Megat Hanafiah*(**)† and Mardhiah Ismail*
*Faculty of Applied Sciences, Universiti Teknologi MARA, 26400, Jengka, Pahang, Malaysia
**Institute of Science (IOS), Universiti Teknologi MARA, 40450, Shah Alam, Selangor, Malaysia
†Corresponding author: Megat Ahmad Kamal Megat Hanafiah

Nat. Env. & Poll. Tech.
Website: www.neptjournal.com
Received: 27-06-2019
Accepted: 30-08-2019

Key Words:
Adsorption
Isotherms
Kinetics
Lead
Leucaena leucocephala

ABSTRACT

The use of *Leucaena leucocephala* leaf powder treated with urea (treated-ULLP) as an alternative adsorbent for the adsorption of Pb(II) ions has been investigated. The adsorption studies were performed under batch mode and focused on the effects of pH, adsorbent dosage and initial Pb(II) concentrations. The pseudo-second order kinetics model fitted well the adsorption data with the values of correlation coefficient (R^2) > 0.97. Large amounts of hydroxyl, carboxyl and amine as detected by the Fourier transform infrared (FTIR) spectrophotometer suggested that these functional groups were responsible for the adsorption of Pb(II) ions. Treated-ULLP demonstrated a good potential for Pb(II) ions removal with the maximum adsorption capacity of 90.09 mg/g, calculated from the Langmuir isotherm model.

INTRODUCTION

A lot of heavy metals are released into the environment, which include copper (Cu), chromium (Cr), lead (Pb), zinc (Zn), cadmium (Cd), nickel (Ni), manganese (Mn), and mercury (Hg) (Babarinde et al., 2006). Volesky (2001) stated that lead [Pb(II)] is one of the most toxic metals that has gained major attention due to its health impact on humans. Pb(II) could be stored in human tissues such as kidney and liver and can pose health hazards even in small concentrations (Puranik & Pakniker 1997). Pb(II) may originate from different types of industrial activities such as electronic, fossil fuel, painting, mining, automobile, sewage wastewater and fertilizer (Singh et al. 2008). A few decades ago, various conventional methods such as ion exchange, filtration, chemical precipitation, reverse osmosis, and electro deposition have been applied to remove Pb(II) from industrial wastewaters (Zheng et al. 2008). However, these treatments suffered some limitation such as production of sludge at the end of the treatment process (Papandreou et al. 2007), and less effective at trace levels of Pb(II). So, adsorption is an alternative process which has several advantages such as low cost, simple, more effective and records a high adsorption capacity value (q_{max}). A variety of adsorbent materials have been applied to remove Pb(II) from aqueous solutions, which include activated carbon, zeolites, resins and plant wastes. *Leucaena leucocephala* leaves was used in this study because it contains various organic compounds such as lignin, cellulose, hemicellulose, polyphenols, protein, lipids, flavonoids, mimosine and tannins (Zarin et al. 2016), which can act as the active sites for Pb(II) adsorption. The main objectives of this work were to evaluate the parameters that could influence the uptake of Pb(II) on urea treated *L. leucocephala* leaves, to determine the rate of Pb(II) adsorption based on kinetics models, and to determine the maximum adsorption capacity based on the Langmuir isotherm model.

MATERIALS AND METHODS

Materials

Leucaena leucocephala leaves were collected in Jengka, Malaysia. The leaves were brought to the lab and washed several times with deionized water. The leaves were dried in an oven overnight at 353 K. Then, the leaves were ground and sieved to obtain the particle size of 180-355 µm. Working solutions of Pb(II) were prepared from a 1000 mg/L Pb(II) stock solution and diluted to desired concentrations using deionized water. The chemical treatment of *L. leucocephala* leaf powder was performed according to the method proposed by Kong et al. (2014). In brief, 3 g of *L. leucocephala* leaf

powder was mixed with 50% (w/v) of urea [$CO(NH_2)_2$] solution and underwent steamed process at 398 K for 30 min by using a steam bath. The urea solution was placed in a round bottom flask with steam below it and this process was carried out for 30 min. During the treatment, the mixture was stirred by using a glass rod, cooled and washed several times with deionized water until the solution reached near neutral. The sample was dried in an oven at the temperature of 378 K for 24 h. The adsorbent sample was designated as Treated-ULLP.

Characterization of Treated-ULLP

The pH_{slurry} was determined by mixing 0.10 g of Treated-ULLP with 100 mL deionized water in a stoppered flask. The mixture was shaken at 100 strokes/min for 24 h at room temperature (298 K) in a water bath shaker. The mixture was filtered, and the final pH of this solution was determined by a pH meter. The zero-point charge of Treated-ULLP at a particular pH or pH_{zpc} was also determined. Firstly, 25 mL of 0.01 M KNO_3 was placed in a series of 100 mL conical flasks. The initial pH of the solution (pH_i) was adjusted from 2 to 9 by adding drops of 0.05 M HCl or NaOH solution. Then, 0.10 g of Treated-ULLP was added to each flask and shaken in a water bath shaker for 24 h at 100 strokes/min. Finally, the mixture was filtered and the final pH (pH_f) of each solution in the flasks was measured by using a pH meter. The pH_{zpc} value was determined from the curve that intercepts the x-axis of the plot ΔpH ($pH_i - pH_f$) versus pH_i. The functional groups responsible for uptake of Pb(II) were analysed by a Fourier transform infrared spectrophotometer (PerkinElmer, Spectrum 100, USA). The total content of carbon, hydrogen, nitrogen, oxygen and sulphur in Treated-ULLP was determined by a CHNS analyser (vario MACRO cube CHNS, Germany). The scanning electron microscope (SEM, Carl Zeiss SMT, Germany) coupled with energy dispersive x-ray (EDX, Oxford Instrument, UK) spectrometer was used to analyse the surface morphology and the elemental composition of Treated-ULLP. Prior to this analysis, Treated-ULLP was coated with a thin layer of gold to improve conductivity, signal to noise ratio, and to reduce charging of the adsorbent material. The SEM image was scanned at 500 X magnification.

Adsorption Experiments

The pH ranging from 2 to 5 was selected and the adsorbent dosage was varied from 0.02 to 0.10 g for the effects of pH and adsorbent dosage, respectively. Drops of 0.05 M NaOH or HCl solution were added to adjust the pH. Three different concentrations of Pb(II) (50, 100, 150 mg/L) were used in the kinetics study and the concentrations were varied from 50 to 250 mg/L in the isotherm study. The dosage of Treated-ULLP was maintained at 0.02 g while the volume of Pb(II) solution was fixed at 50 mL. All Pb(II) solutions were shaken in a water bath shaker at 100 strokes/min. After adsorption, the adsorbent was filtered and the filtrates were analysed for unadsorbed Pb(II) by an Atomic Absorption Spectrometer (AAS, Perkin Elmer, PinAAcle 900T, USA). The linear range for Pb(II) in the calibration curve was from 0

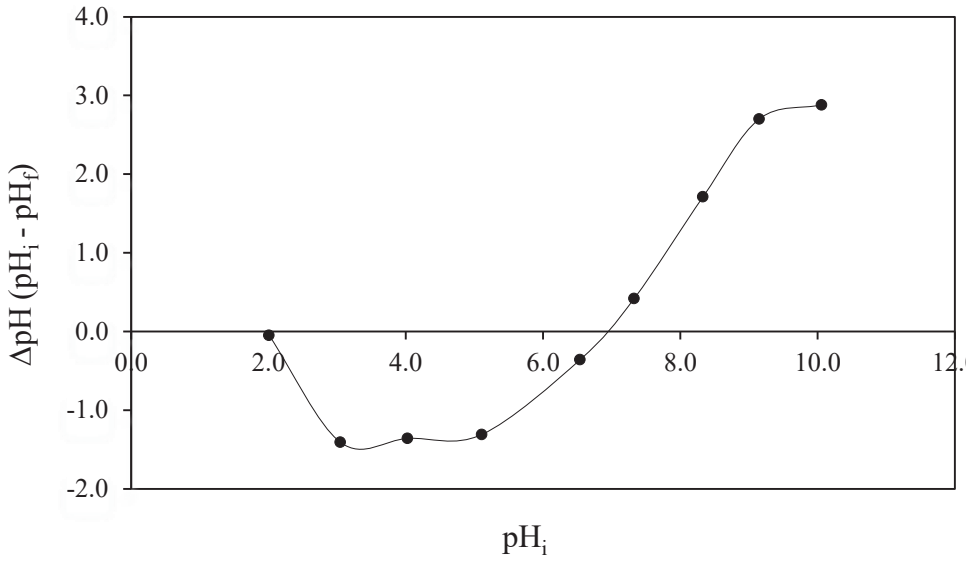

Fig. 1: The pH_{zpc} plot of Treated-ULLP.

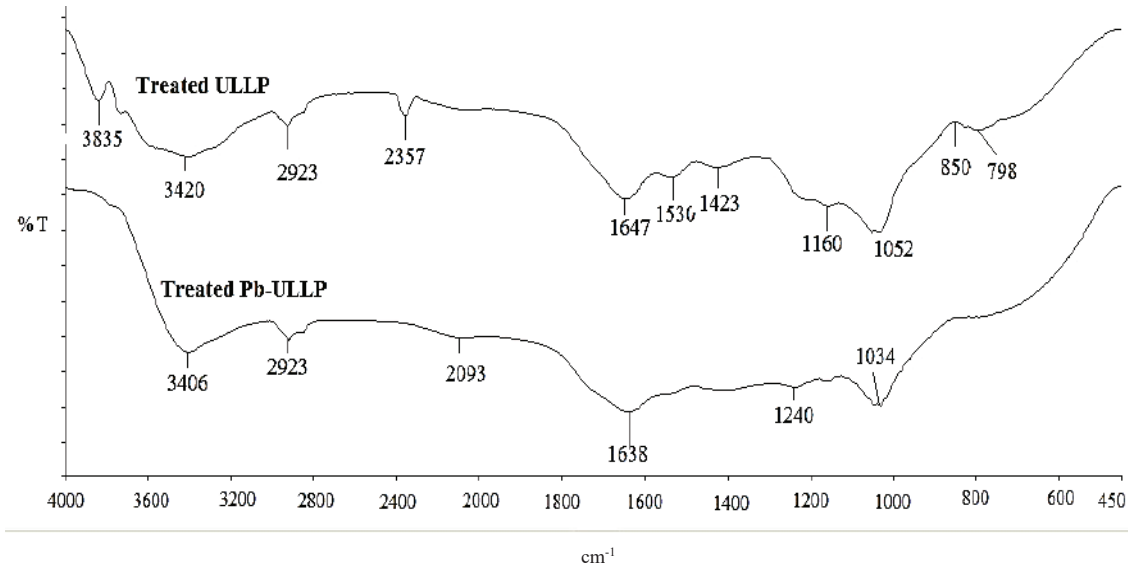

Fig. 2: FTIR spectra of Treated-ULLP before and after adsorption of Pb(II) ions.

Table 1: CHNOS content of treated-ULLP.

Elemental composition (%)				
C	H	N	S	O*
47.67	7.19	7.58	0.29	37.27

*by difference

to 20 mg/L. All the experiments were conducted in duplicate and the results were presented as the average. The relative standard deviation was < 3%. The amount of Pb(II) adsorbed at equilibrium (q_e) and the percentage removal (%) were calculated by using the following equations:

$$q_e = \frac{V(C_0 - C_e)}{m} \quad \ldots(1)$$

$$\text{Removal}(\%) = \frac{C_0 - C_e}{C_0} \times 100 \quad \ldots(2)$$

Where, C_0 and C_e represent the Pb(II) concentration before and after adsorption (mg/L), respectively. V is the volume of adsorbate (L), q_e is the amount of Pb(II) adsorbed (mg/g) at equilibrium and *m* is the weight of Treated-ULLP (g).

RESULTS AND DISCUSSION

Characterization of Treated-ULLP

The pH_{slurry} of Treated-ULLP was found to be 6.74, which is slightly acidic, possibly due to the presence of carboxylic acid group (Zayed & Samling 2016). The pH_{zpc} plot is shown in Fig. 1 and the value was found to be 6.90. At $pH < pH_{zpc}$, the surface of Treated-ULLP would carry more positive charge than the negative charge. More negative charge, however, would appear at $pH > pH_{zpc}$.

Fig. 2 shows the FTIR spectra for Treated-ULLP before and after Pb(II) adsorption. The strong and broad peak from 2600 to 3600 cm^{-1} confirmed the presence of carboxylic acid group (-COOH) (Kong et al. 2013), which overlapped with -OH and -NH groups. The peak observed at 2923 cm^{-1} was assigned to the stretching C-H of alkyl group. The peak at 1647 cm^{-1} was attributed to the stretching of C=O or C=C groups. The peaks appeared at 1160 and 1052 cm^{-1} indicated the stretching of C-N and C-O-C groups, respectively (Chen et al. 2010, Saygideger et al. 2005). The presence of -CH group of aromatics was represented by the peak at 850 cm^{-1}.

The wave number at 3420 cm^{-1} had shifted to 3406 cm^{-1}, indicating that Pb(II) was adsorbed to the hydroxyl, -COOH and amine groups. The wave number at 1647 cm^{-1} shifted to 1638 cm^{-1}, suggesting the involvement of C=O and C=C groups in the removal of Pb(II). Other functional groups possible for attracting Pb(II) ions would be the C-N and

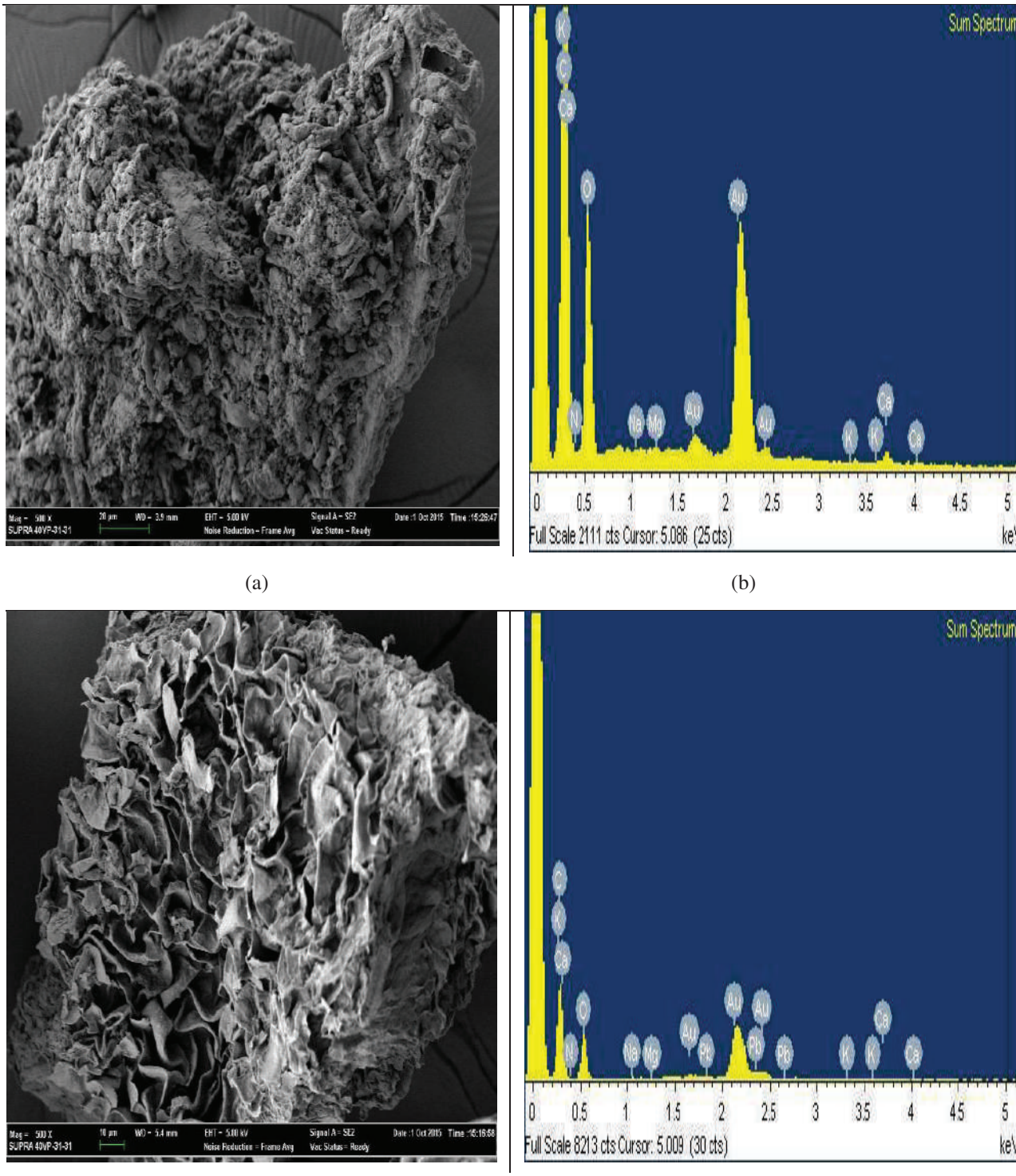

(a) (b)

(c) (d)

Fig. 3: SEM (500 X magnification) and EDX images of treated-ULLP before (a and b) and after Pb(II) adsorption (c and d).

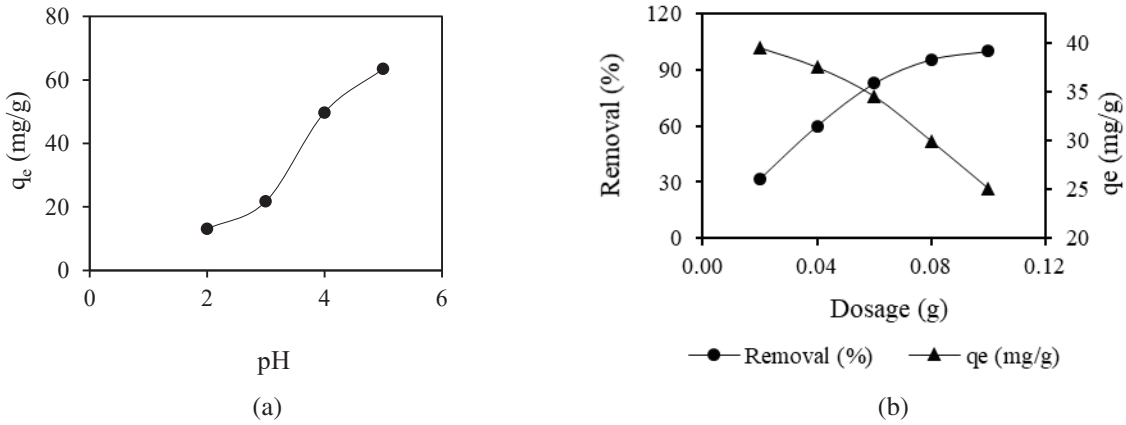

Fig. 4: Effects of pH (a) and dosage (b) on the Pb(II) adsorption on treated-ULLP.

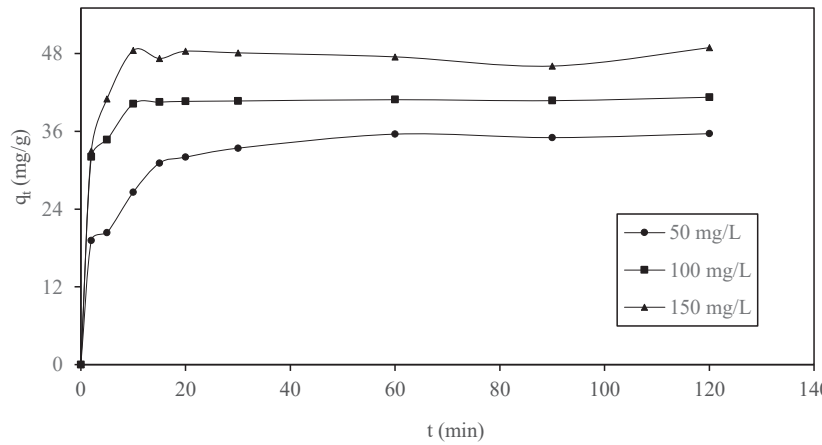

Fig. 5: Effects of concentration and contact time on the Pb(II) adsorption.

C-O-C as there was a decrease in the intensity of the peak at 1160 cm^{-1} and the shift in wave number from 1052 to 1034 cm^{-1}, respectively. The presence of hydroxyl, amino, ether, aromatics and carbonyl functional groups acted as the active sites for adsorption process to occur. Meanwhile, the elemental composition of the Treated-ULLP is given in Table 1. The percentage of N contained in the Treated-ULLP was much higher than pristine *L. leucocephala* leaf (4.2 %), reported by Meena Devi et al. (2013). This finding concludes that after chemical modification, the urea was successfully introduced in the Treated-ULLP.

The SEM and EDX images of Treated-ULLP before and after Pb(II) adsorption are shown in Fig. 3. Treated-ULLP (Fig. 3a) possesses rough, irregular and nonporous surface morphology. Important minerals for plants such as Na, Mg, K and Ca were clearly detected EDX as shown in Fig. 3b. Pb(II) however, was not present. After adsorption (Figs. 3c and 3d), Pb(II) was clearly detected on the surface of Treated-ULLP at 1.8, 2.3 and 2.7 keV (Fig. 3d). This finding concludes the success of removal of Pb(II) from the aqueous solution onto the adsorbent surface.

Effects of pH and Dosage

The effects of pH and adsorbent dosage on Pb(II) adsorption are shown in Fig. 4. Pb(II) adsorption increased with increasing pH of the solution, started from pH 2 to 5 for initial Pb(II) concentration of 50 mg/L [Fig. 4(a)]. The amount of Pb(II) adsorbed was very low at pH 2 due to the stiff competition between protons (H^+) in the solutions and the Pb(II) for the adsorption sites. Furthermore, it was also due to the stronger electrostatic repulsion between Pb(II) and the positively charged adsorbent surface. At pH 3, the amount of Pb(II) adsorbed started to increase because the -COOH started to dissociate to liberate more $-COO^-$ groups, which could easily adsorb the positively charged Pb(II) (Lalhruaitluanga et al. 2010). The amount of Pb(II) adsorbed

Table 2: Adsorption kinetics parameters at different Pb(II) concentrations.

Kinetics models		Pb(II) concentrations		
	Parameters	50 mg/L	100 mg/L	150 mg/L
Pseudo-first-order	$q_{e,cal}$ (mg/g)	46.71	91.41	276.24
	$q_{e,exp}$ (mg/g)	35.63	41.27	48.90
	k_1 (1/min)	0.049	0.025	0.008
	R^2	0.673	0.413	0.050
Pseudo-second-order	$q_{e,cal}$ (mg/g)	36.54	41.28	48.12
	$q_{e,exp}$ (mg/g)	35.63	41.27	48.90
	k_2 (g/mg.min))	0.008	0.046	0.039
	R^2	0.999	1.000	0.999

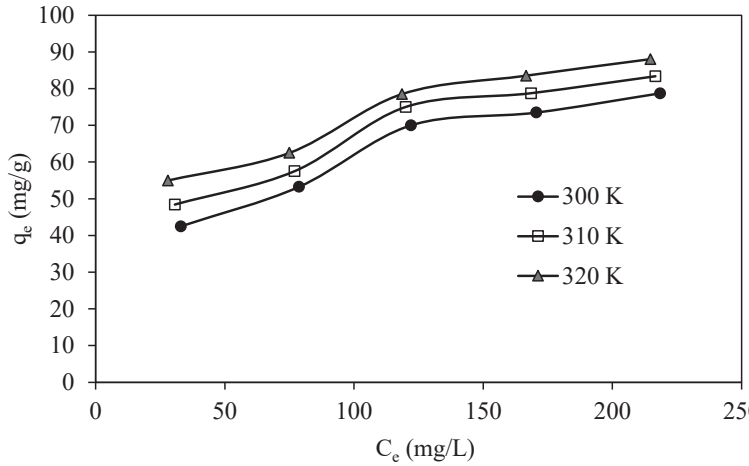

Fig. 6: Pb(II) adsorption isotherm plots at different temperatures.

continued to increase at pH 4 and 5 due to a much lower concentration of H^+ in the solution, hence less competition between H^+ and the metal ions (Wu et al. 2011). Therefore, more Pb(II) could easily be adsorbed to the adsorption sites. The subsequent adsorption experiments were conducted at pH 4 only to avoid the formation of precipitate ($Pb(OH)_2$) or $Pb(OH)^-$ due to the high number of OH^- ions present in the solution at pH > 5 (Sheng et al. 2004). Adsorbent dosage experiment was conducted to give an idea on the effectiveness of the amount of adsorbent used. The percentage removal of Pb(II) increased as the adsorbent dosage increased from 0.02 to 0.10 g [Fig. 4(b)].

This phenomenon confirmed that more active sites as well as surface area were available for the binding of Pb(II) with increasing the adsorbent dosage. However, the amount of Pb(II) adsorbed showed the opposite trend and it was associated to the increased number of unadsorbed sites when the dosage was increased (Yu et al. 2002). Aggregation also occurred due to the particles interaction that led to the surface area reduction of Treated-ULLP.

Effects of Initial Pb(II) Concentrations and Contact Time

The effect of initial concentration and contact time of Pb(II) on Treated-ULLP is shown in Fig. 5. The plots showed that three main phases were involved during the adsorption process. The first phase was called the initial rapid adsorption process followed by slow adsorption process and the last phase was dynamic equilibrium time. The initial rapid adsorption process occurred in the first 3 min. It was possibly due to high number of available adsorption sites (Kousha et al. 2012), causing the rapid transfer of Pb(II) to the external surface of Treated-ULLP. The slow adsorption rate was observed in the range of 5 to 10 min due to the less availability

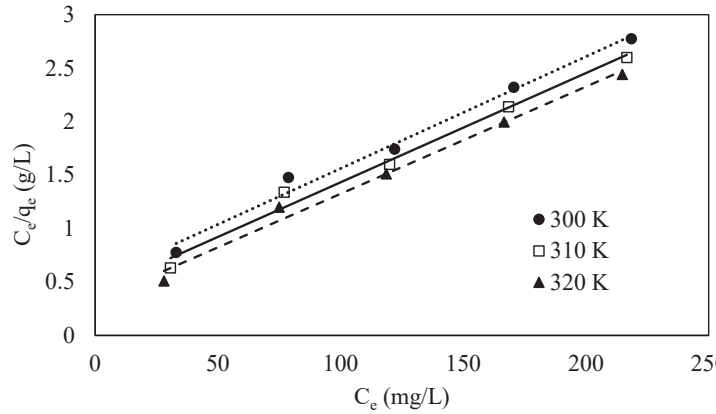

Fig. 7: Langmuir isotherm plots at different temperatures.

Table 3: Langmuir adsorption isotherm parameters at different temperatures.

Isotherm model	Parameters	Temperatures (K)		
		300	310	320
Langmuir	q_{max} (mg/g)	82.65	86.21	90.09
	$q_{e,exp}$ (mg/g)	78.00	83.65	87.90
	K_L (L/mol)	0.046	0.050	0.063
	R^2	0.965	0.966	0.978

of active sites or stiff competition among the Pb(II) ions for the active sites. After 30 min, there was only a small change in the amount of Pb(II) adsorbed, which the process was considered to have achieved the equilibrium time.

Adsorption Kinetics Models

Adsorption kinetics models were applied to further investigate the rate of Pb(II) adsorption process. The pseudo-first-order (Ho & McKay 1999) and pseudo-second-order models (Ho & McKay 2000) were expressed in Equations 3 and 4, respectively.

$$\log\left(q_e - q_t\right) = \log q_e - \frac{k_1}{2.303}t \qquad \ldots(3)$$

$$\frac{t}{q_t} = \frac{1}{h} + \frac{1}{q_e}t \qquad \ldots(4)$$

Where the symbols q_e and q_t indicate the amount of Pb(II) adsorbed (mg/g) at equilibrium and at time t (min), respectively. k_1 (1/min) is the rate constant of adsorption process for the pseudo-first-order model. The initial adsorption rate (mg/g.min) is represented by the symbol of *h* while the k_2 [g/(mg.min)] is the rate constant for the pseudo-second-order model. The values of k_2 and h were obtained by using an equation of $h = k_2 q_e^{\,2}$.

Both the plots have not shown, but the values of correlation coefficient (R^2) were close to unity (0.999-1.000) as in the case of the pseudo-second-order kinetics model. In addition, the values of calculated adsorption capacities ($q_{e,cal}$) were almost match to the values of experimental ($q_{e,exp}$). Based on these two observations, it can be concluded that the adsorption kinetics fitted well the pseudo-second-order kinetics model (Table 2).

Adsorption Isotherms

The adsorption isotherm plots at three different temperatures are presented in Fig. 6. In general, the adsorption capacities were found to increase with increasing temperatures, an indication of an endothermic reaction. The plots were further analyzed using the most widely used isotherm model, which is the Langmuir model (Langmuir 1918), developed based on the assumption that all the adsorption sites have the same energy and is given by Equation 5:

$$\frac{C_e}{q_e} = \frac{C_e}{q_{max}} + \frac{1}{q_{max}K_L} \qquad \ldots(5)$$

Where, q_{max} is the maximum adsorption capacity and K_L represents the Langmuir constant. The Langmuir plots showed good linearity ($R^2 > 0.96$) and the predicted

maximum adsorption capacity values were close to the experimental values (Table 3 & Fig. 7). The increase in the maximum adsorption capacity values with increasing temperatures suggested the endothermic type of adsorption. The adsorption mechanism of Pb(II) onto Treated-ULLP could be understood in terms of hard-soft acid base principle (HSAB). Table 3 shows that Treated-ULLP contains N (a borderline ligand), S (a soft-base ligand) and O (a hard-base ligand). These three types of atoms could act as metal-binding donor atoms for Pb(II). As Pb(II) is classified as a borderline metal ion (Nieboer & Richardson 1980), it would be attracted to all categories of ligands to form stable complexes.

CONCLUSION

Treated-ULLP showed a satisfactory removal of Pb(II) from aqueous solutions under batch mode sorption techniques. Based on the FTIR spectrum of Treated-ULLP, the detected functional groups such as carbonyl (C=O), hydroxyl (-OH) carboxylic acid (-COOH), amino (-NH_2) and ether (C-O-C) acted as the active sites for Pb(II). The attachment of Pb(II) on Treated-ULLP was confirmed by the EDX images. The rate of Pb(II) removal was considered quite rapid as the time to reach equilibrium was less than 30 min. Pb(II) adsorption was more favoured at a higher temperature, an indication of endothermic adsorption process.

ACKNOWLEDGEMENT

Special thanks are due to the Malaysian Ministry of Education for the financial support of this work (Grant no. 600 – RMI/RAGS 5/3 (3/2013).

REFERENCES

Babarinde, N.A.A., Babalola, J.O. and Sanni, R. A. 2006. Biosorption of lead ions from aqueous solution by maize leaf. International Journal of Physical Sciences, 1: 23-26.

Chen, W., Yan, L. and Bangal, P. R. 2010. Preparation of graphene by the rapid and mild thermal reduction of grapheme oxide induced by microwaves. Carbon, 48: 1146-1152.

Ho, Y. S. and McKay, G. 1999. The sorption of lead (II) ions on peat. Water Research, 33: 578-584.

Ho, Y.S. and McKay, G. 2000. The kinetics of sorption of divalent metal ions onto Sphagnum moss peat. Water Research, 34: 735-742.

Kong, J., Yue, Q., Sun, S., Gao, B., Kan, Y., Li, Q. and Wang, Y. 2014. Adsorption of Pb(II) from aqueous solutions using keratin waste-hide waste. Equilibrium, kinetic and thermodynamic modeling studies. Chemical Engineering Journal, 241: 393-400.

Kong, J., Yue, Q., Huang, L., Gao, Y., Sun, Y., Gao, B., Li, Q. and Wang, Y. 2013. Preparation, characterization, and evaluation of leather waste base activated carbon via physical and chemical activation. Chemical Engineering Journal, 221: 62-71.

Kousha, M., Daneshvar, E., Sohrabi, M. S., Jokar, M. and Bhatnagar, A. 2012. Adsorption of acid orange II dye by raw and chemically modified brown macroalga *Stoechospermum marginatum*. Chemical Engineering Journal, 192: 67-76.

Lalhruaitluanga, H., Jayaram, K., Prasad, M. N. V. and Kumar, K. K. 2010. Lead(II) adsorption from aqueous solutions by raw and activated charcoals of *Melocanna baccifera* Roxburgh (bamboo). A comparative study. Journal of Hazardous Materials, 175: 311-318.

Langmuir, I. 1918. The adsorption of gases on plane surfaces of glass, mica and platinum. Journal of the American Chemical society, 40(9): 1361-1403.

Meena Devi, V.N., Ariharan, V. N. and Nagendra Prasad, P. 2013. Nutritive value and potential uses of *Leucaena leucocephala* as biofuel-A mini review. Research Journal of Pharmaceutical, Biological and Chemical Sciences, 4(1): 515-521.

Nieboer, E. and Richardson, D.H.S. 1980. The replacement of the nondescript term 'heavy metals' by a biologically and chemically significant classification of metal ions. Environmental Pollution (Series B): 1, 3-26.

Papandreou, A., Stournars, C. J. and Panias, D. 2007. Copper and cadmium adsorption on pellets made from fired coal fly ash. Journal of Hazardous Materials, 148: 538-547.

Puranik, P.R. and Pakniker, K.M. 1997. Biosorption of lead and zinc from solutions using *Streptoverticillium cinnamoneum* waste biomass. Journal of Biotechnology, 55: 113-124.

Saygideger, S., Gulnaz, O., Istifli, E.S. and Yucel, N. 2005. Adsorption of Cd(II), Cu(II), and Ni(II) ions *Lemna minor L* : Effect of physicochemical environment. Journal of Hazardous Materials, 126: 96-104.

Sheng, P. X., Ting, Y. P. and Hong, L. 2004. Sorption of lead, copper, cadmium, zinc and nickel by marine algal biomass: characterization of biosorptive capacity and investigation of mechanisms. Journal of Colloid and Interface Science, 275: 131-141.

Singh, C. K., Sahu, J. N., Mahalik, K. K., Mohanty, C. R., Mohan, B. R. and Meikap, B. C. 2008. Studies on the removal of Pb(II) from wastewater by activated carbon developed from tamarind wood activated with sulphuric acid. Journal of Hazardous Materials, 153: 221-228.

Volesky, B. 2001. Detoxification of metal-bearing effluents: Biosorption for the next century. Hydrometallurgy, 59: 203-216.

Wu, J. L., Fan, X. Z., Hong, J. and Xue, S. Z. 2011. Adsorption of lead (Pb) from aqueous solution with *Typha angustifolia* biomass modified by $SOCl_2$ activated EDTA. Chemical Engineering Journal, 170: 21-28.

Yu, L.J., Shukla, S.S., Dorris, K.L., Shukla, A. and Margrave, J.L. 2002. Adsorption of chromium from aqueous solutions by maple sawdust. Journal of Hazardous Materials, 100: 53-63.

Zarin, M.A., Wan, H.Y., Isha, A. and Armania, N. 2016. Antioxidant, antimicrobial and cytotoxic potential of condensed tannins from *Leucaena leucocephala* hybrid-rendang. Food Science and Human Wellness, 75-65 :(2)5.

Zayed, M.Z. and Samling, B. 2016. Phytochemical constituents of the leaves of *Leucaena leucocephala* from Malaysia. International Journal of Pharmacy and Pharmaceutical Sciences, 12(8): 174-179.

Zheng, W., Li, X. M., Wang, F., Yang, Q., Deng, P. and Zheng, G. M. 2008. Adsorption removal of cadmium and copper from aqueous solution by areca- a food waste. Journal of Hazardous Materials, 157: 490-495.

Nature Environment and Pollution Technology
An International Quarterly Scientific Journal

p-ISSN: 0972-6268
e-ISSN: 2395-3454

Vol. 19 | No. 1 | pp. 319-324 | 2020

Original Research Paper | Open Access

Degradation of Methylene Blue Wastewater by Fe^{2+} Coupling Persulphate Using Online UV-Vis Spectrophotometry

Wanchao Duan, Hang Xu†, Hongna Ren, Qihui Men and Hangfei Fan

Chemical Engineering and Pharmaceutics School, Henan University of Science and Technology, Luoyang 471023, China

†Corresponding author: Hang Xu

Nat. Env. & Poll. Tech.
Website: www.neptjournal.com

Received: 29-06-2019
Accepted: 30-08-2019

Key Words:
Ferrous ion
Persulphate
Methylene blue
Wastewater

ABSTRACT

Online UV-Vis spectrophotometer technology as accurate, convenient and fast monitoring method was used to detect instantaneous dye concentration in aqueous medium. Ferrous ion coupling with Persulphate to degrade methylene blue (MB) exhibited a very high degradation rate, and therefore online UV-Vis spectrophotometer showed great advantage in this study. The effects of ferrous ion concentration, sodium Persulphate concentration, pH value and initial MB concentration on MB degradation were investigated. The online spectrophotometer could minimize the systematic error caused by the termination of adding chemicals and manual operation. At room temperature, the optimal condition was acquired with 73.6% MB removal after 100s at neutral medium when initial ferrous dosage and sodium Persulphate were 1.25 mmol/L and 0.2 mmol/L, respectively. $Fe^{2+}/S_2O_8^{2-}$ system exhibited a great degradation efficiency in acidic or neutral environment.

INTRODUCTION

Dyes are widely used in textile industry, leather industry, printing industry and food industry. According to statistics, one million tons of dyes were produced in the world every year, of which about 15% dyes entered the natural environment in the process of production and usage (Yang et al. 2011). The dye entering the natural environment not only influenced the natural water colour, but also had a negative impact on the ecological environment (Zhu et al. 2013). Conventional wastewater treatment such as adsorption, filtration and flocculation mainly transferred pollutants to other phases which were easy to cause secondary pollution (Zhang et al. 2015).

Advanced oxidation technology (AOP) has been proved to be a very effective method to remove organic pollutants from water because of fast degradation speed, high treatment efficiency and little secondary pollution (Jia et al. 2017, Feng et al. 2015). The reason was that high active hydroxyl radical could be produced during AOP and hydroxyl radical could non-selectively destroy the structure of organic matter in water. Because hydroxyl radical only stably existed in acidic medium, this problem restricted its application in wastewater treatment. Sulphate radical was another high active radical to use pollutant degradation especially in neutral and acidic medium (Deng et al. 2015) which was more beneficial for wastewater treatment.

Fenton reagent (ferrous ions/hydrogen peroxide) was one of the AOPs which could produce hydroxyl radical and display a high degradation performance in acidic medium (2-4 pH value). Ferrous ion also could catalyse Persulphate to produce sulphate radical for the degradation of organic pollutants. In this study, methylene blue (MB) was used as the target pollutant which was degraded by ferrous ion coupling sodium Persulphate. Because of very high reactive speed, the online UV-Vis spectrophotometry was used to monitor instantaneous concentration of MB in dyeing wastewater (Xu et al. 2018, Xu et al. 2016). The effects of ferrous ion concentration, sodium Persulphate (SP) concentration, pH value and initial MB concentration on MB degradation were investigated.

MATERIALS AND METHODS

Experimental Reagents

The methylene blue (MB), ferrous sulphate ($FeSO_4$), sodium Persulphate ($Na_2S_2O_8$, SP), sodium hydroxide (NaOH), hydrochloric acid (HCl) were of analytical grade and purchased from Tianjin Chemical Reagent Technology Company (China).

Experimental Apparatus

The online reaction and spectrophotometric analysis system are shown in Fig. 1. This system consisted of a reaction

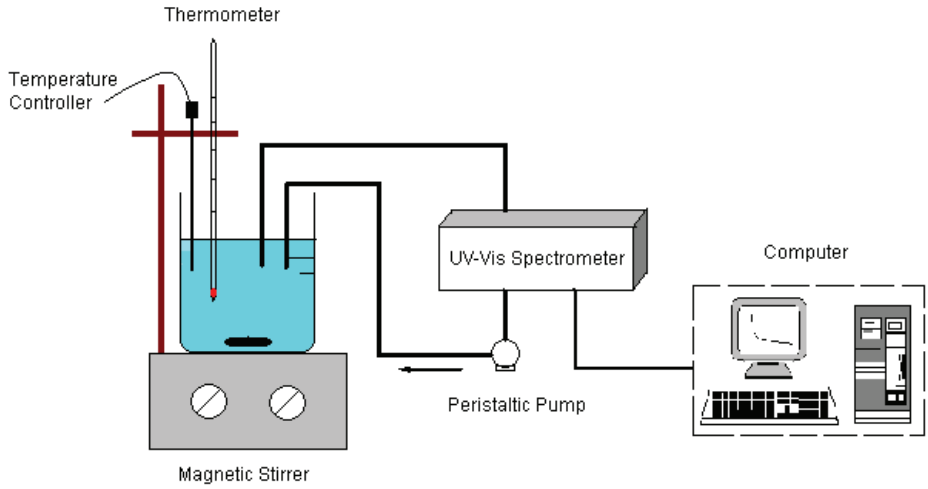

Fig. 1: Online spectrophotometric system.

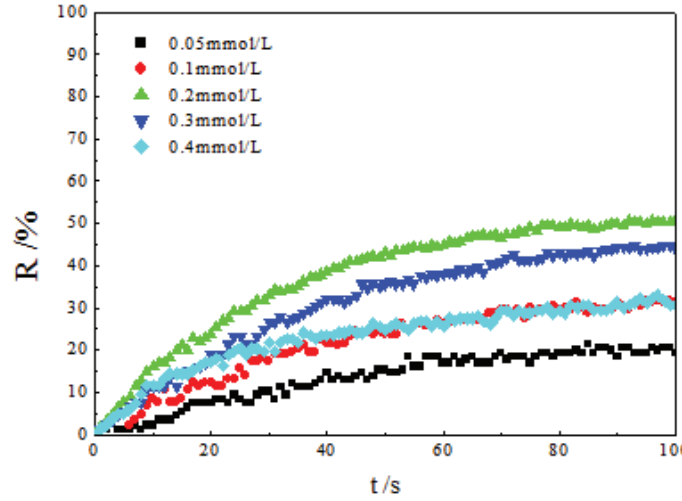

Fig. 2: Effect of initial Fe^{2+} concentration on MB degradation (MB = 7.5mg/L, SP = 0.5mmol/L, pH = 6.99, room temperature).

container, a digital display thermostat magnetic stirrer (85-2 Shanghai instrument manufactory), a digital pH meter (PHS-3C-01 experimental pH meter Hangzhou instrument limited corporation), a UV-Vis spectrophotometer (SP-756PC Shanghai spectrometric instrument manufactory), a peristaltic pump (HL-1D Beijing instrument manufactory) and a computer. A plastic hose with an inner diameter of 2 mm linked the reactive solution with the flowing cell cuvette within the spectrophotometer with the solution pumped by the peristaltic pump. The return liquid was sent back to beaker to form the cycle. UV-Vis spectrophotometry was used to monitor the colour change in the flowing cell cuvette at $1s^{-1}$.

Experimental Method

200 mL MB wastewater was added in 250 mL beaker. Next, the ferrous sulphate and hydrochloric acid were added in MB wastewater. The detected wavelength was adjusted to 664 nm. When the sodium Persulphate was added, the computer began to record the absorbance at different times. The degradation rate (R) of methylene blue is shown in Eq. 1.

$$R = \frac{A_0 - A_t}{A_0} \times 100\% \quad \ldots(1)$$

Where, A_t is the absorbance of wastewater solution when t = t s and A_0 is the absorbance of wastewater solution when t = 0 s.

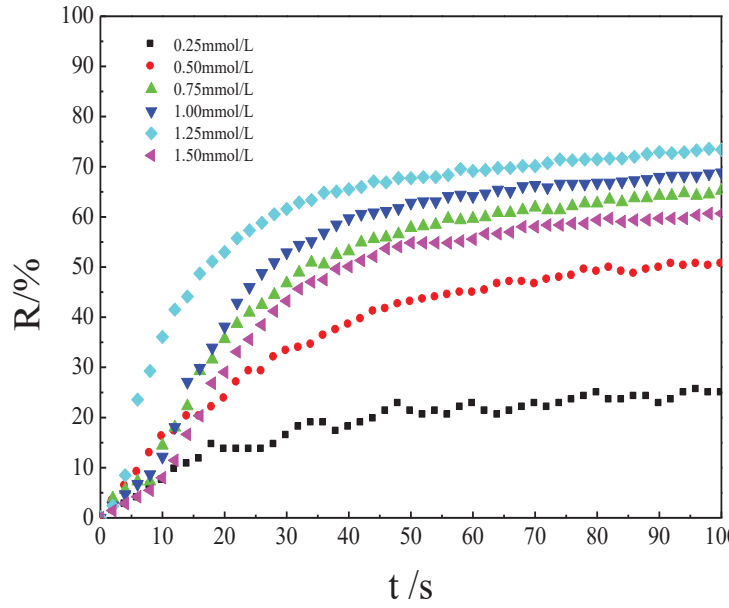

Fig. 3: Effect of sodium persulfate concentration on MB degradation system (MB = 7.5mg/L, Fe^{2+} = 0.2mmol/L, pH = 6.99, room temperature).

RESULTS AND DISCUSSION

Effect of Ferrous Ion Concentration

Sodium Persulphate is difficult to decompose by itself to produce sulphate radicals because of its stable ionic compound structure. Ferrous ion can catalyse Persulphate to produce sulphate radicals. The initial concentrations of methylene blue and sodium Persulphate were 7.5 mg/L and 2.0 mmol·L^{-1}, respectively. Fig. 2 showed the effect of the change of initial Fe^{2+} concentration in the range of 0.05 to 0.4 mmol/L for the MB removal at 100s at neutral medium. From Fig. 2, it could also be seen that the MB removal increased rapidly in the first 60s and increased slowly after 60s to 100s. With the addition of Fe^{2+}, the sulphate radicals were produced with Persulphate (Shang et al. 2017). It is shown in Eq. 2. The MB in aqueous solution was decomposed by sulphate radicals because of its strong oxidizability. With the reaction proceeding, the Fe^{2+} in system was continuously consumed, resulting in the reduction of sulphate radicals, so the degradation efficiency of MB showed a gentle upward tendency (Wang et al. 2010).

$$S_2O_8^{2-} + Fe^{2+} \rightarrow SO_4^{\cdot -} + SO_4^{2-} + Fe^{3+} \quad \ldots(2)$$

$$SO_4^{\cdot -} + Fe^{2+} \rightarrow SO_4^{2-} + Fe^{3+} \quad \ldots(3)$$

The MB removal increased from 19.2% to 50.5% with the rise of initial Fe^{2+} dosage from 0.05 to 0.2 mmol/L after 100s. When Fe^{2+} dosage continuously added to 0.3 mmol/L, the MB removal was decreased to 43.8% at 100s. The MB removal was only 31.1% with 0.4 mmol/L Fe^{2+} dosage. The optimal initial Fe^{2+} dosage was 0.2 mmol/L with 50.5% MB removal after 100s. This phenomenon suggested that appropriate concentration of ferrous ions could promote the degradation of MB, and when the concentration of ferrous ions was excessive, it would inhibit the degradation. This was because when the system contained excessive ferrous ions, it would react with sulphuric acid radical and result in consuming SO_4^{2-} in the system, thus inhibiting the degradation of methylene blue (Shao et al. 2017). The mechanism of SO_4^{2-} consumption is shown in Eq. 3. Taking ferrous ion dosage and degradation efficiency into consideration, ferrous ion concentration of 0.2 mmol·L^{-1} was selected for the next experiment.

Effect of Sodium Persulphate Concentration

Sodium Persulphate is a strong oxidizing agent, which was the source of sulphate radical in this system. The initial Persulphate dosage was an important factor for affecting the MB removal. The effects of initial sodium Persulphate dosage from 0.25 to 1.5 mmol/L on MB removal was investigated at neutral medium and the results are shown in Fig. 3, when the initial concentration of methylene blue was 7.5 mg·L^{-1}, and the concentration of ferrous ions 0.2 mmol·L^{-1}. As could be seen from Fig. 3, when the concentration of sodium Persulphate increased from 0.25 to 1.25 mmol/L, the

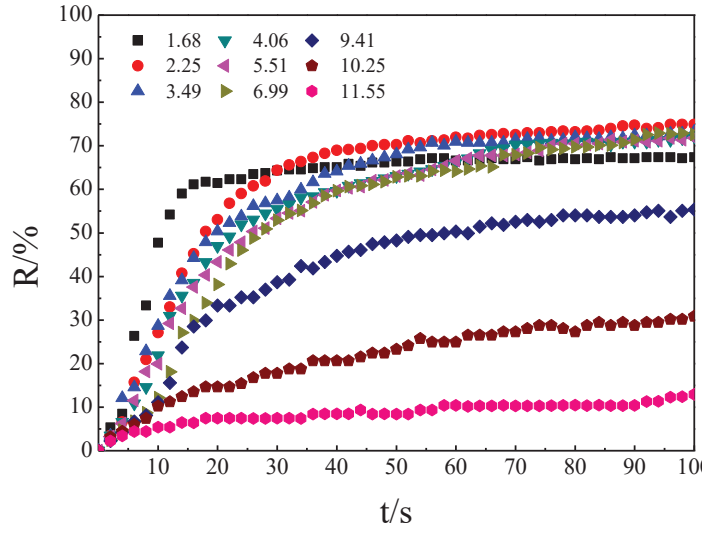

Fig. 4: Effect of pH value on MB degradation system (MB = 7.5mg/L, Fe^{2+} = 0.2mmol/L, SP = 1.25mmol/L, room temperature).

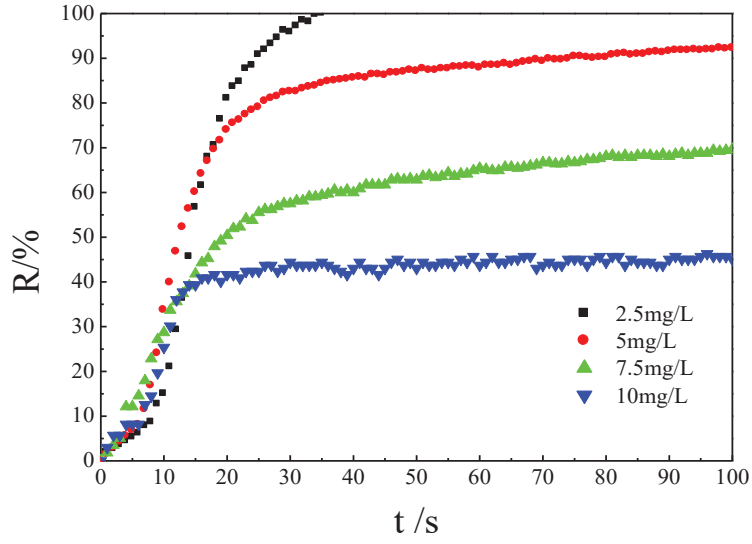

Fig. 5: Effect of different initial concentrations of MB on degradation system (Fe^{2+} = 0.2mmol/L, SP = 1.25mmol/L, pH = 6.99, room temperature).

MB removal increased from 24.8% to 73.6% at 100s. When sodium Persulphate continued to increase to 1.5 mmol/L, the MB removal decreased to 60.7%. The best sodium Persulphate dosage was 1.25 mmol/L with the 73.6% MB removal.

$$SO_4 \cdot^- + S_2O_8^{2-} \rightarrow SO_4^{2-} + S_2O_8 \cdot^- \quad \ldots(4)$$

$$SO_4 \cdot^- + SO_4 \cdot^- \rightarrow S_2O_8^{2-} \quad \ldots(5)$$

This was because the ferrous ion acted as an electron donor to catalyse the decomposition of Persulphate to produce sulphate radicals which could result in stability in the system removing MB (Liang et al. 2009). With the increase of sodium Persulphate concentration, more sulphate radicals were generated to improve degradation efficiency of MB. When the sodium Persulphate concentration was excessive, $S_2O_8^{2-}$ would interact with sulphate radical in the system and consume sulphate radical in the system, thus inhibiting MB degradation (Xu et al. 2011). The reaction equation was shown in Eq.4. In addition, because there was a large number of sulphate radicals in the system, there would be a certain disproportionate reaction between them, and sulphate radical was also consumed. The reaction equation is shown as Eq. 5, thus reducing the concentration of sulphate radicals

in the system and affecting the degradation efficiency of MB. Considering the dosage and cost of the oxidant, sodium Persulphate concentration of 1.25 mmol·L^{-1} was selected for the next experiment.

Effect of pH Value

$$Fe^{2+} + H_2O \rightarrow H^+ + FeOH^+ \quad \ldots(6)$$

$$Fe^{2+} + OH^- \rightarrow Fe(OH)_2 \quad \ldots(7)$$

The pH value in solution is one of the important factors to influence the reaction process in advanced oxidation technology (Ye et al. 2016). In this study, the effect of pH value on the MB degradation system was investigated in Fig. 4 when the initial concentrations of sodium Persulphate and ferrous ions were 1.25 mmol/L and 0.2 mmol/L, respectively at room temperature. It could be seen from Fig. 4 that the initial pH value significantly affected the MB degradation efficiency. When the pH values of the oxidizing environment ranged from 2.25 to 6.99, there were similar MB removal efficiencies which were over 70% after 100s. When the pH value of solution was 1.68, the MB removal was 67.7%, which exhibited a slight decline. When the pH value increased from 9.49 to 11.25, the MB removal significantly decreased from 55.7% to 9.3%. $Fe^{2+}/S_2O_8^{2-}$ system revealed an excellent oxidizing ability in weak acidic and neutral medium. The alkaline or strong acidic medium were disadvantage for degradation process. The reason for the decrease of MB removal in alkaline environment is that ferric divalent ions in solution changed to the ferric composite [$Fe(OH)_2$ or $FeOH^+$] and mechanism is shown in Eq. 6 and Eq. 7. As the result, the amount of ferric divalent ions, which reacted with Persulphate in the system were reduced, thereby reducing the degradation efficiency of MB (Yuan et al. 2014). And $Fe(OH)_2$ and $FeOH^+$ had no catalytic activity resulting in reduced number of sulphuric acid radical in the system, thus reducing the degradation efficiency of MB (Miao et al. 2018). The greatest advantage of $Fe^{2+}/S_2O_8^{2-}$ system was that it had a great degradation effect in acidic or neutral environment.

Effect of the Initial Concentration of Methylene Blue

The initial concentration of pollutant in printing and dyeing wastewater is an important factor influencing the reaction process. In this study, the effect of different initial methylene blue concentrations on MB degradation system were investigated when the sodium Persulphate and ferrous ion concentration were 1.25 mmol.L^{-1} and 0.2 mmol.L^{-1} at neutral environment. The experimental results are shown in Fig. 5. It could be seen that when the initial concentration of MB increased from 2.5 mg·L^{-1} to 10.0 mg·L^{-1}, the degradation efficiency was 100%, 92.2%, 73.6% and 45.1%, respectively after 100s. As the initial concentration of MB increased, the degradation efficiency of MB decreased. This was because the ferrous ion and concentration of sodium Persulphate were constant. Therefore, the number of sulphate radicals were constant. When the initial concentration of MB in the system increased, the molar ratio of sulphate radical to MB was lower, and the amount of degraded methylene blue was limited. Therefore, when the concentration of the ferrous ions and sodium Persulphate was constant, the degradation efficiency of low MB concentration was higher.

CONCLUSION

The oxidizing efficiency of ferrous/Persulphate system to degrade methylene blue in aqueous solution was investigated in this study using online monitoring technology. The ferrous ion coupling Persulphate exhibited a very fast MB degradation process. The online spectrophotometer showed a great advantage to measure the change of MB concentration in a quick, accurate and convenient way. It could minimize the systematic error caused by the termination of adding chemicals and manual operation. At room temperature, the optimal condition was acquired with 73.6% MB removal after 100s at neutral medium when initial ferrous dosage and sodium Persulphate were 1.25 mmol.L^{-1} and 0.2 mmol.L^{-1}, respectively. $Fe^{2+}/S_2O_8^{2-}$ system exhibited a great degradation efficiency in acidic or neutral environment.

REFERENCES

Deng, J., Yuan, L.U. and Xiao, Y.M. 2015. Degradation of carbamazepine by Persulphate activated with Fe_3O_4/GO nanocomposites. Journal of China University of Mining & Technology, 67: 120-123.

Feng, M., Qu, R. and Zhang, X. 2015. Degradation of flumequine in aqueous solution by Persulphate activated with common methods and polyhydroquinone-coated magnetite/multi-walled carbon nanotubes catalysts. Water Research, 85: 1-10.

Jia, Z., Liang, S.X. and Zhang, W.C. 2017. Heterogeneous photo Fenton-like degradation of cibacron brilliant red 3B-A dye using amorphous Fe 78 Si 9 B 13, and Fe 73.5 Si 13.5 B 9 Cu 1 Nb 3, alloys: The influence of adsorption. Journal of the Taiwan Institute of Chemical Engineers, 452: 71.

Liang, C. and Su, H.W. 2009. Identification of sulphate and hydroxyl radicals in thermally activated Persulphate. Industrial & Engineering Chemistry Research, 48: 472-475.

Miao, J., Zhang, R. and Zhang, L. 2018. Photocatalytic degradations of three dyes with different chemical structures using ball-milled TiO_2. Materials Research Bulletin, 97: 47-48.

Shang, K., Wang, X. and Li, J. 2017. Effect of Persulphate on the degradation of acid orange 7 (AO7) by dielectric barrier discharge plasma. Topics in Catalysis, 60: 1-7.

Shao, Y., Xiao, L. and Yun, X.W. 2017. Research progress of sodium Persulphate degradation of dyeing wastewater. Applied Chemical Industry, 89: 34-37.

Wang, P., Yang, S. and Shan, L. 2010. Waste heat-activated Persulphate degradation of dye wastewater. International Conference on Bioinformatics and Biomedical Engineering. IEEE, 57: 1-4.

Xu H., Yu T.L., Guo X.X. and Wang J.X. 2016. Fe^{3+}/H_2O_2 Fenton degradation of wastewater containing dye under UV irradiation. Desalination

and Water Treatment, 57: 18028-18037.

Xu, H. and Tang, Q. 2011. Degradation kinetics and mechanics of methylene blue by complex ultraviolet and hydrogen peroxide process. Advanced Materials Research, 360: 1066-1069.

Xu, H., Liu, BB., Yu T.L. Wu F.M. and Lin, K. 2018. Online spectrometric decolorization of Rhodamine B and Acid Yellow G by homogeneous cobalt-activated peroxymonosulphate reaction. Nature Environment and Pollution Technology, 17: 93-98.

Yang, S., Yang, X. and Shao, X. 2011. Activated carbon catalyzed Persulphate oxidation of azo dye acid orange 7 at ambient temperature. Journal of Hazardous Materials, 186: 659.

Ye, W., Zhao, B. and Gao, H. 2016. Preparation of highly efficient and stable Fe, Zn, Al-pillared montmorillonite as heterogeneous catalyst for catalytic wet peroxide oxidation of Orange II. Journal of Porous Materials, 23: 301-310.

Yuan, R., Wang, Z. and Hu, Y. 2014. Probing the radical chemistry in UV/persulfate-based saline wastewater treatment: Kinetics modeling and byproducts identification. Chemosphere, 109: 106-112.

Zhang, B.T., Zhang, Y. and Teng, Y. 2015. Sulfate radical and its application in decontamination technologies. Critical Reviews in Environmental Science and Technology, 45: 1756.

Zhu, L., Ai, Z. and Ho, W. 2013. Core-shell Fe-Fe_2O_3 nanostructures as effective Persulphate activator for degradation of methyl orange. Separation and Purification Technology, 108: 159.

Nature Environment and Pollution Technology
An International Quarterly Scientific Journal

p-ISSN: 0972-6268
e-ISSN: 2395-3454

Vol. 19 | No. 1 | pp. 325-331 | 2020

Original Research Paper | Open Access

Analysis and Quantification of Airborne Heavy Metals and RSPMs in Dehradun City

Abhinav Srivastava*†, Arnab Mondal, N.A. Siddiqui* and S.M. Tauseef***

*University of Petroleum and Energy Studies, Bidholi campus, Energy Acres, Dehradun-248007, Uttarakhand, India

**Banaras Hindu University, Varanasi, U.P., India

†Corresponding author: Abhinav Srivastava

Nat. Env. & Poll. Tech.
Website: www.neptjournal.com

Received: 24-07-2019
Accepted: 26-08-2019

Key Words:
Heavy metals
Air pollution
RSPMs
Dehradun city

ABSTRACT

Air pollution is becoming a major environmental and public health problem worldwide. Exposure to different air pollutant have several adverse effects on human health. In the present study, we attempt to determine the concentration of respirable suspended particulate matters (RSPMs) and levels of the heavy metals in ambient air of Dehradun city. The RSPM concentration of all the areas under study were well under the NAAQ standard limit. The Ghantaghar area reported the maximum RSPMs of 87.5507 µg.m-3. The samples collected from four different locations of Dehradun were primarily analysed for heavy metals like Pb, Fe, Cr and Cd using atomic absorption spectrophotometer. The measured concentrations were compared with the standard safe limits provided by United States Environmental Protection Agency (USEPA). It is seen that all the heavy metals as well as the RSPM are well under permissible safe limits set by USEPA, OSHA and CPCB. It can therefore be concluded that the ambient air quality of Dehradun, in terms of heavy metal contamination as well as RSPM concentration in air is safe. Strict monitoring of heavy metal emissions in air should be done regularly to maintain the ambient air of Dehradun area as healthy.

INTRODUCTION

The immense growth of the human population lead to extensive utilization of natural resources and the technological advances have significantly affected the atmospheric air. The contamination of air occurs from both natural sources as well as anthropogenic sources. Usually, any substance that gets introduced to the atmosphere due to the above activities can become the cause of air pollution and they may have a detrimental effect on human health. The air pollutant generally includes particulate matter (smoke, dust, fumes and aerosols), gases (sulphur dioxides, nitrogen dioxides, hydrocarbons, etc.), radioactive materials, hazardous air pollutants (HAPs), heavy metals and many others (Godish 2004, Rana 2006). The presence of heavy metals in the environmental air above safe limits as approved by international and national agencies like U.S. Environmental Protection Agency (USEPA), Occupational Safety and Health Administration (OSHA), and Central Pollution Control Board (CPCB) are of important concern as they cause many health problems when they get absorbed, ingested/inhaled inside the human body (Duruibe et al. 2007).

It has been found that the natural emission of heavy metal pollutants are minimal and their concentration in the air is rising due to anthropogenic activities such as mining and smelting operations, industrial production and use, and domestic and agricultural use of metals and metal-containing compounds (Goyer 2001, He et al. 2005, Herawati et al. 2000, Shallari et al. 1998). Some studies have reported that the anthropogenic activity generates about 2000 tons of lead and 6000 tons of cadmium which contributed the most i.e. 333 times more than natural (lead) activities in the environment (Nriagu & Pacyna 1988, Chen & Graedel 2012).

Heavy metals are the metallic elements that have a relatively high density compared to water. With the assumption that heaviness and toxicity are inter-related, heavy metals also include metalloids, such as arsenic, that are able to induce toxicity at a low level of exposure. It has been described that metals such as cobalt (Co), copper (Cu), chromium (Cr), iron (Fe), magnesium (Mg), manganese (Mn), molybdenum (Mo), nickel (Ni), selenium (Se) and zinc (Zn) are essential nutrients that are required for various biochemical and physiological functions but these metals become toxic when present in larger quantities. Other heavy metals like Cr, Cd, Hg, Pb, etc. are extremely fatal for human health (Yu et al. 2011). Their presence is also associated with severe diseases in human bodies like metal plume fever, itai-itai (Tohyama et al. 1982), mina-mata, Hunter-Russel syndrome, etc. They promote insomnia, sleep disorder, blurred vision, speech and hearing impairment, etc. Due to the above concerns,

Table 1: Maximum permissible limit for heavy metals as per USEPA[1] and OSHA[2]

S. No.	Heavy Metal	Prescribed Conc. Limit[1] Living Standards (in $\mu g.m^{-3}$)	Max Permissible Limit[2] Industrial Standards (in $\mu g.m^{-3}$)
1	Lead (Pb)	0.5000 [1]	1.0000 [2]
2	Iron (Fe)	5.0000 [1]	10.000 [2]
3	Chromium (Cr)	0.5000 [1]	1.0000 [2]
4	Cadmium (Cd)	0.1000 [1]	0.5000 [2]

Table 2. Maximum permissible limit for SPMs and RSPMs as per NAAQ standards.

S. No.	Type	Prescribed Limit
1.	Suspended Particulate Matters (SPMs)	200 $\mu g.m^{-3}$
2.	Respirable Suspended Particulate Matters (RSPMs)	100 $\mu g.m^{-3}$

extensive study has been carried out to find out the heavy metal presence in water, air, and soil all around the world to inform the local and Government agencies for taking suitable measures for controlling toxic elements in the environment.

The prescribed concentration limits of the heavy metals set by the USPEA and OSHA are summarised in Table 1. Table 2 provides information about the permissible limit of respirable suspended particulate matter (RSPM) and suspended particulate matter (SPM) as per the National Ambient Air Quality Standards (NAAQ).

Different research work has been reported in various parts of India for determining the number of heavy metals in the air as well as their impacts on human beings (Kulshrestha et al. 2009, Mohanraj et al. 2004, Sharma et al. 2008, Sharma & Maloo 2005, Shridhar et al. 2010, Thakur et al. 2004). But till date, no such study has been performed to quantify the heavy metals particles in the ecologically sensitive region i.e. Dehradun city. The present study is extremely important as Dehradun is a valley and the dispersion of contaminated air entirely depends on the rain. Herein the present study, we have chosen four different locations of Dehradun city (Sahaspur, Ballupur, Dalanwala, and Ghantaghar) to determine the concentration of RSPM and levels of the heavy metals in the air of Dehradun. The RSPM levels were compared with the NAAQ standard limits. The samples collected from four different locations of Dehradun were further analysed for heavy metals like Pb, Fe, Cr and Cd using atomic absorption spectrophotometer (AAS). The measured concentrations were then compared with the standard safe limits provided by USEPA.

MATERIAL AND METHODS

Sites for sample collection: The air samples for the study were collected from four different localities of Dehradun city. The different locations were:

- Location I- Sahaspur: Sahaspur is an industrialised area with many manufacturing units of various MNCs and other small-scale industries.
- Location II- Ballupur: Ballupur is a residential cum market area with heavy population and witness a large no of vehicular movement throughout the day.
- Location III- Dalanwala: Dalanwala is an extensively populated area consisting of many slum areas and situated nearby the railway station.
- Location IV- Ghantaghar: Ghantaghar area is the prime location and main market place of Dehradun area, consisting of many residential complexes and shopping malls and other markets drawing huge population towards it. Different locations have been depicted in the Fig. 1.

Estimation of RSPM: The air samples were collected using Ecotech AAS127 Air Sampler for PM_{10} on a glass-fibre filter paper (GFF) cut-out of radius 2 cm. The initial weight of filter-paper cut-out were recorded after conditioning them in hot air oven at 105°C for 2 hrs and the kept in desiccator for 2 hrs. Each filter papers were weighed five times and the mean weight was recorded. The filter-papers were carried in a filter-paper holder to avoid any kind of contamination.

The instrument was operated for around 23 hrs approximately at a height of around 5 ft above the ground and the flow rates before and after each experiment run were recorded. After 24 hrs, the filter paper was removed from the instrument and was kept again in filter paper holder carefully to retain the actual deposition of particulate matters on filter paper. The filter papers were kept in desiccator for 2 hrs. Then the filter papers were first weighed and then digested to extract out the particulate matters.

Estimation of heavy metals: The extraction and analysis of heavy metals from the filter paper were conducted as per

USEPA method of hot-acid digestion (USEPA 1999). The filter papers were digested using 15 mL HCl and HNO_3 acid mixture (3:1). The concentration of the heavy metals was analysed using AAS (ThermoScientificiCE 3000 Series). For quality control, standard stock solutions were prepared for each metal. The standard Reference Materials (SRMS) were prepared using Certipur® standard solution (1000 ppm).

Detection range: The calibration plot method was used for the analysis. The air-acetylene gas was used for the analysis of Pb, Cd and Hg while nitrous-oxide gas along with air-acetylene gas was used for the analysis of Cr. The wavelengths for the determination of the elements were 217.0 nm, 228.8 nm, 248.3 nm and 357.9 nm for Pb, Cd, Fe and Cr respectively.

Quality control: For precision and accuracy, all the glass-ware's and filter assemblies were acid-washed and dried in hot-air oven. Only the calibrated glassware's were used. HPLC Grade de-ionised water was used for calibration of the device.

RESULTS AND DISCUSSION

Presence of respirable suspended particulate matters: The concentration of PM_{10} in the air at different locations of Dehradun city were taken under study and the RSPMs data collected from the study locations is presented in Table 3. All the data at study stations are under 100 $\mu g.m^{-3}$ that is under considered safe by NAAQ standards (for 24-hour duration; annual avg. of 60 $\mu g.m^{-3}$) as shown in Fig. 2. The results show that high content and concentration of RSPMs are responsible for some difficulties for some age groups like toddlers and old-age groups, lung diseases causing difficulty in breathing and may trigger respiratory as well as cardiovascular diseases (Kim et al. 2015, Li et al. 2018). Hence, the results prove that the particulate matter present in the air can be very fatal and is severe for human health as they reach deep into the respiratory system. Particulate matter pollution in ambient air has been labelled as Group-1

Table 3: Respirable suspended particulate matters in air and their probable causes.

Sr. No.	Location Name	Initial Wt (Filter Paper)	Final Wt (Filter Paper)	Difference	Initial Flow Rate (L/min)	Final Flow Rate (L/min)	Avg. Flow Rate (L/min)	Total Sampling Time (min)	RSPM ($\mu g.m^{-3}$)	Activities around the sampling sites
1.	Sahaspur	1.14317	1.24695	0.10378	1.6	1.4	1.5	1380	50.2810	Industrial area
2.	Ballupur	1.25693	1.33635	0.07942	1.3	1.2	1.25	1380	46.0405	Vehicular emissions
3	Dalanwala	1.12291	1.22973	0.10682	1.2	1.1	1.15	1380	67.8006	Vehicular emission, construction sites, roadside piles of garbage
4	Ghantaghar	1.14133	1.32256	0.18123	1.6	1.4	1.5	1380	87.5507	Heavy pollution due to vehicles, generator, roadside dust piles, construction sites

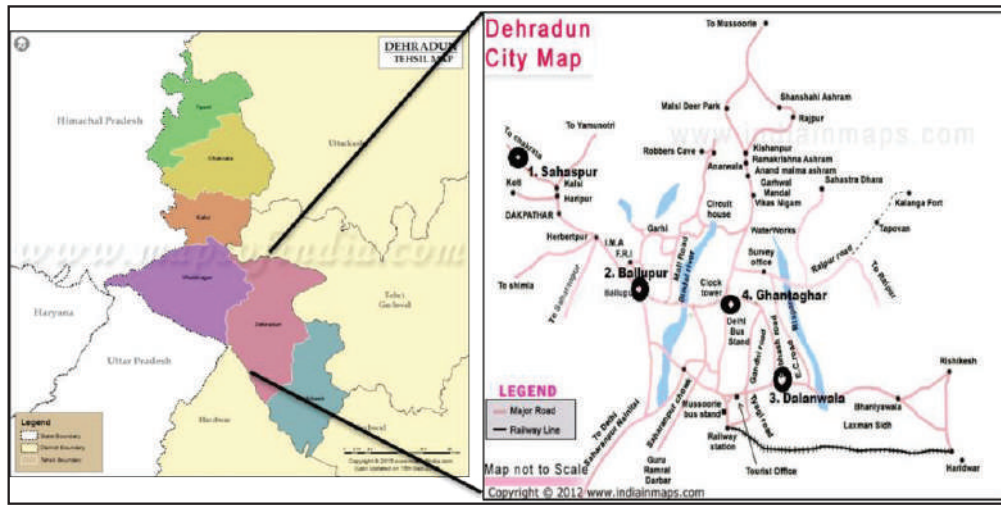

Fig.1 (a): Dehradun district map (b) Dehradun City map.

(Image Courtesy: http://www.indiainmaps.com)

Carcinogen by the International Agency for Research on Cancer (IARC) (Loomis et al. 2013).

Presence of heavy metals in the air: The heavy metals concentration in the particulates were found by digesting the filter paper and analysing the presence of the metals in the sample using the atomic absorption spectrophotometer. Table 4 depicts the concentration of Pb, Cr, Cd, and Fe at different locations of Dehradun. From the acquired data it was found that Pb and Fe concentration is higher in Sahaspur and Ghantaghar area respectively, however the Cr and Cd concentrations found negligible in these areas. The concentrations of all the heavy metals taken into consideration are considered toxic if the concentrations in air are found beyond permissible safe limits.

The concentration of Pb in ambient air is demonstrated in the Fig. 3. The data confirmed that the concentration of Pb at different locations of study was slightly higher in the Sahaspur area (0.1288 $\mu g.m^{-3}$) but in other areas it is below the permissible safe limit set by USEPA.

The trend of Cr concentration in the environment can be seen steady and almost negligible as shown in Fig. 4. The concentration is way below than the standards set by USEPA for safe living.

The Cd concentration was also studied at different areas of Dehradun (Fig. 5) which depicts that Cd is present at prescribed safe limits and are almost negligible as compared to other pollutants.

As shown in Fig. 6 the concentrations of Fe were found slightly higher in the Ghantaghar location (0.70068 $\mu g.m^{-3}$) and at Sahaspur area (0.56594 $\mu g.m^{-3}$). The level of Fe was not much higher in other two areas.

The data obtained for heavy metals from the four different locations was compared with the prescribed concentration limits set by USEPA considered safe for living for the inhabitants of the areas. The data predicts that the heavy metal presence is inconsequential as their concentrations in ambient air are negligible and are documented under the safe limits as shown in Table 5 which suggest that the peak concentration of Pb was recorded to be 74.24% less than the prescribed safe concentration by USEPA, which is the highest among the percentages of other heavy metals in air. On the other hand, the concentration of iron being maximum still is 99.86% less than that of the prescribed safe limits set by USEPA. It also confirms that the maximum concentrations of heavy metals taken for the under study were found in Ghantaghar area.

Fig. 7 depicts the bar graph showing the comparison of

Table 4: The actual concentrations of heavy metals in ambient air of Dehradun.

S. No.	Location I.D.	Location Name	Pb ($\mu g.m^{-3}$)	Cr ($\mu g.m^{-3}$)	Cd ($\mu g.m^{-3}$)	Fe ($\mu g.m^{-3}$)
1.	I	Sahaspur	0.12882	0.01661	0.00664	0.56594
2.	II	Ballupur	0.01434	0.01232	0.00115	0.14085
3.	III	Dalanwala	0.04607	0.01161	0.00280	0.22782
4.	IV	Ghantaghar	0.02185	0.02319	0.01220	0.70068

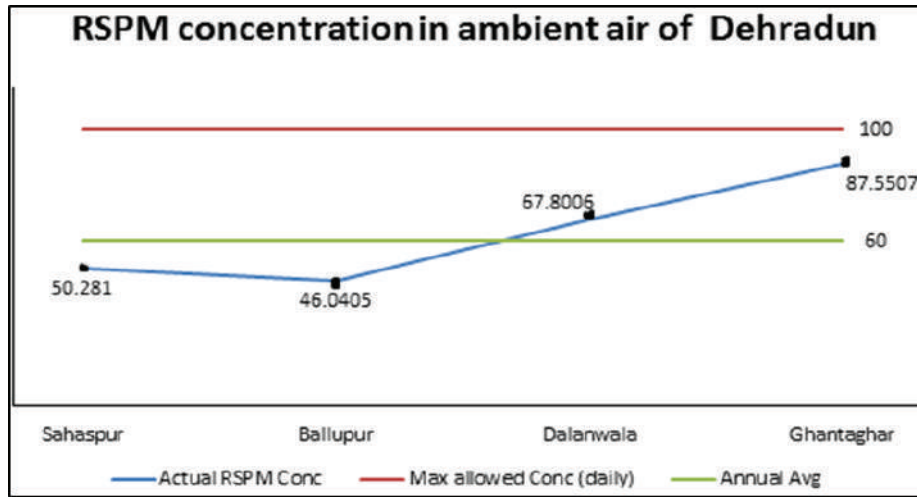

Fig. 2: Presence of RSPMs at different locations of the Dehradun city.

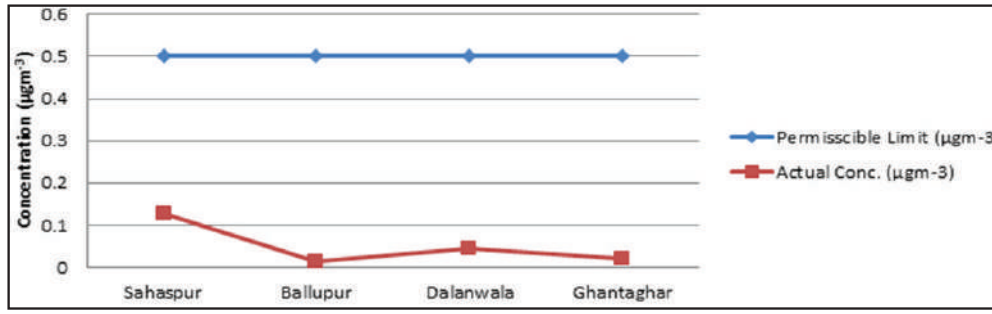

Fig. 3: Presence of lead at different locations of Dehradun.

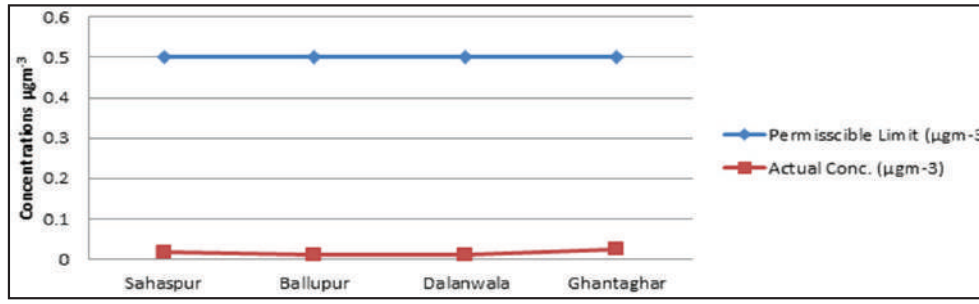

Fig. 4: The occurrence of chromium at different locations of Dehradun.

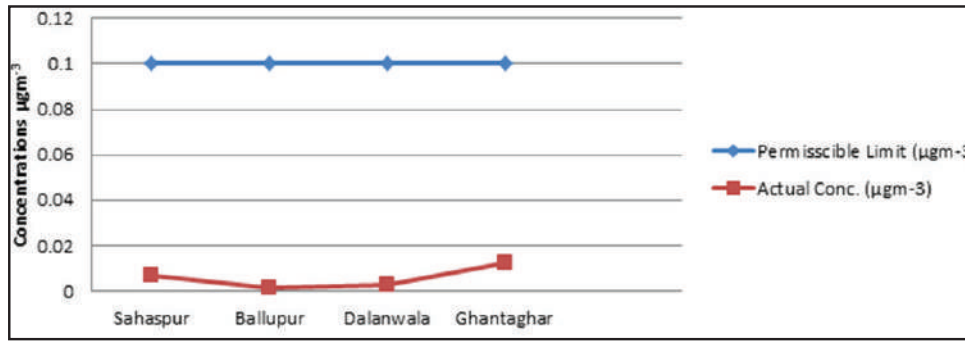

Fig. 5: The graph demonstrates the presence of cadmium as a pollutant in different locations of Dehradun.

the presence of different heavy metals (Pb, Cr, Cd, Fe) in the environment. The iron concentration has been found higher in almost all the study locations. Although its concentration is way more than the other heavy metals concentration, its impact on human health is negligible since it is about 99.86% less than the prescribed safe limits. The other significant heavy metal present in air is Pb whose concentration is maximum in Sahaspur area is comparatively higher with respect to the safe concentration limits. Other heavy metals are negligible and can be ignored safely.

Finally, we have compared our results with different study performed in various other locations as summarised in the Table 6. Here, we have also taken up the study of the three other major cities (Delhi, Kanpur, Mumbai) of India into account. From all the comparative study we found the conclusion that the air quality of Dehradun is comparatively safe than other Indian cities.

CONCLUSION

The pollutants get added up in the environment through both the natural sources as well as anthropogenic sources. The air pollutant generally includes particulate matter, harmful gases, and heavy metals. In the study, we have obtained the data from different locations of Dehradun which firmly illustrates

Table 5: Percentage of peak concentration of heavy metals in air less than that of the prescribed safe limits.

Peak Conc. of Heavy Metals (and their Study Area)	Peak Concentration Recorded	Safe limit set by USEPA	%age of Peak Conc. less than that of Prescribed Safe Limits
Lead (Sahaspur)	0.12882	0.50000	74.24%
Chromium (Ghantaghar)	0.02319	0.50000	99.95%
Cadmium (Ghantaghar)	0.01220	0.10000	99.88%
Iron (Ghantaghar)	0.70068	5.00000	99.86%

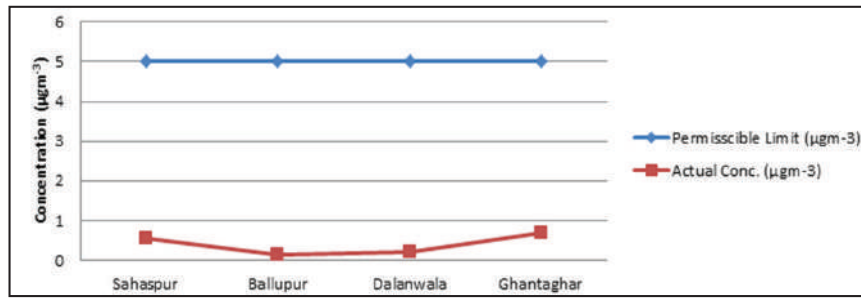

Fig. 6: The graph illustrates the occurrence of Iron in the environment at different locations of Dehradun.

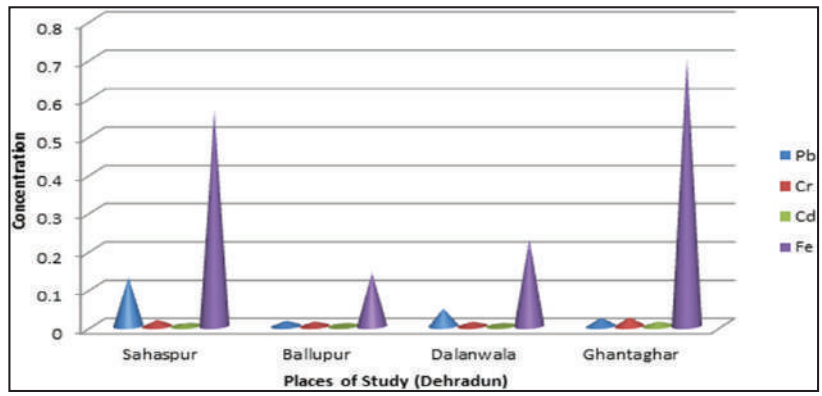

Fig. 7: Comparisons of the heavy metals in the air of different sites of study in Dehradun.

that all the parameters have not crossed the permissible safe limits set by the OSHA and USEPA which are considered safe for human inhabitation. While the respirable suspended particulate matters (RSPMs) are on rise at Ghantaghar and Dalanwala areas and nearing the prescribed limits of NAAQ standards set by CPCB. Ghantaghar area is the oldest inhabited market place of Dehradun and the centre point, making it the most crowded place in Dehradun which clarifies the significant RSPM concentration and slight increasing trend of the concentrations of heavy metals in the ambient air quality. Dalanwala and Ballupur are primarily residential areas where a sudden fall in concentration of heavy metals can be observed. Since Dalanwala is located near railway station of Dehradun and also a home of several slum areas, the RSPM concentration is little on the higher side. Almost all the major inhabited areas of Dehradun are located near the surroundings of these four locations. Hence, it can be concluded that the Dehradun city is free of any kind of heavy metals contamination in air but the RSPMs may pose threat to health conditions of certain special groups of the society like infants, children and aged people.

ACKNOWLEDGEMENTS

The authors gratefully acknowledge the University of Petroleum and Energy Studies, Dehradun for providing funding and resources for the study.

REFERENCES

Balachandran, S., Meena, B.R. and Khillare, P.S. 2000. Particle size dis-

Table 6: Comparison of concentration of heavy metals in air at different parts of the world.

Location	Pb	Cd	Cr	Fe	References
Spain	0.008 - 0.698	0.0001 - 0.004	0.0001 - 0.022	0.2 - 10.0	(Querol et. al. 2002)
Taiwan	0.133	--	0.656	6.99	(Fung & Wong 1995).
Norway	0.00036 -0.01036	0.00001 -0.00028	0.00021 - 0.00156	--	(NILU 2002b).
Delhi	0.6 - 1.9	0.020 - 0.150	0.3 - 0.7	5.0 - 20.0	(Balachandran et. al. 2000).
Mumbai	1.06	--	0.15	--	(Kumar et. al. 2001).
Kanpur	0.07 - 1.03	0.002 - 0.043	0.032 - 0.4	0.3 - 6.17	(Sharma & Maloo 2005).
Dehradun (Present Study)	0.0205	0.01178	0.0056975	0.4088	--

tribution and its elemental composition in the ambient air of Delhi. Environ. Int., 26: 49-54.

Chen, W.Q. and Graedel, T.E. 2012. Anthropogenic cycles of the elements: A critical review. Environ. Sci. Technol., 46: 8574-8586.

Duruibe, J.O., Ogwuegbu, M.O.C. and Egwurugwu, J.N. 2007. Heavy metal pollution and human biotoxic effects. Int. J. Phys. Sci., 2(5): 112-118.

Fung, Y.S. and Wong, L.W.Y. 1995. Apportionment of air pollution sources by receptor models in Hong Kong. Atmos. Environ., 29: 2041-2048.

Godish, T. 2004. Air quality, Chapter 2. In: Atmospheric Pollution and Pollutants, 4th Edition, Lewis Publishers.

Goyer, R.A. 2001. Toxic effects of metals. In: Klaassen C.D., (ed.) Cassarett and Doull's Toxicology: The Basic Science of Poisons. New York: McGraw-Hill Publisher, pp. 811-867.

He, Z.L., Yang, X.E. and Stoffella, P.J. 2005. Trace elements in agroecosystems and impacts on the environment. J. Trace Elem. Med. Biol., 19: 125-140.

Herawati, N., Suzuki, S., Hayashi, K., Rivai, I.F. and Koyama, H. 2000. Cadmium, copper, and zinc levels in rice and soil of Japan, Indonesia, and China by soil type. Bull. Environ. Contam. Toxicol., 64: 33-39.

Kim, K.H., Kabir, E. and Kabir, S. 2015. A review on the human health impact of airborne particulate matter. Environ. Int., 74: 136-143.

Kulshrestha, A., Satsangi, P.G., Masih, J. and Taneja, A. 2009. Metal concentration of $PM_{2.5}$ and PM_{10} particles and seasonal variations in urban and rural environment of Agra, India. Sci. Total Environ., 407: 6196-6204.

Kumar, A.V., Patil, R.S. and Nambi, K.S.V. 2001. Source apportionment of suspended particulate matter at two traffic junctions in Mumbai, India. Atmos. Environ., 35: 4245-4251.

Li, T., Hu, R., Chen, Z., Li, Q., Huang, S., Zhu, Z. and Zhou, L.F. 2018. Fine particulate matter (PM2. 5): The culprit for chronic lung diseases in China. Chronic. Dis. Transl. Med., 4: 176-186.

Loomis, D., Grosse, Y., Lauby-Secretan, B., El Ghissassi, F., Bouvard, V., Benbrahim-Tallaa, L., Guha, N., Baan, R., Mattock, H. and Straif, K. 2013. The carcinogenicity of outdoor air pollution. Lancet Oncol., 14: 1262-1263.

Mohanraj, R., Azeez, P.A. and Priscilla, T. 2004. Heavy metals in airborne particulate matter of urban Coimbatore. Arch. Environ. Con. Tox., 47: 162-167.

NILU, 2002b. Heavy metals and POPS within the EMEP region 2000. EMEP/CCC-Report 9/2002, Norwegian Institute of Air Research, Kjeller, Norway.

Nriagu, J.O. and Pacyna, J.M. 1988. Quantitative assessment of worldwide contamination of air, water and soils by trace metals. Nature, 333: 134.

Querol, X., Alastuey, A., de la Rosa, J., Sánchez-de-la-Campa, A., Plana, F. and Ruiz, C.R. 2002. Source apportionment analysis of atmospheric particulates in an industrialised urban site in southwestern Spain. Atmos. Environ., 36: 3113-3125.

Rana, S. V. S. 2006. Environmental Pollution, Health and Toxicology. Alpha Science International Ltd., pp. 10-40.

Shallari, S., Schwartz, C., Hasko, A. and Morel, J.L. 1998. Heavy metals in soils and plants of serpentine and industrial sites of Albania. Sci. Total Environ., 209: 133-142.

Sharma, M. and Maloo, S. 2005. Assessment of ambient air PM_{10} and $PM_{2.5}$ and characterization of PM_{10} in the city of Kanpur, India. Atmos. Environ., 39: 6015-6026.

Sharma, R.K., Agrawal, M. and Marshall, F.M. 2008. Atmospheric deposition of heavy metals (Cu, Zn, Cd and Pb) in Varanasi city, India. Environ. Monit. Assess., 142: 269-278.

Shridhar, V., Khillare, P.S., Agarwal, T. and Ray, S. 2010. Metallic species in ambient particulate matter at rural and urban location of Delhi. J. Hazard. Mater., 175: 600-607.

Thakur, M., Deb, M.K., Imai, S., Suzuki, Y., Ueki, K. and Hasegawa, A. 2004. Load of heavy metals in the airborne dust particulates of an urban city of central India. Environ. Monit. Assess., 95: 257-268.

Tohyama, C., Shaikh, Z.A., Nogawa, K., Kobayashi, E. and Honda, R. 1982. Urinary metallothionein as a new index of renal dysfunction in "Itai-itai" disease patients and other Japanese women environmentally exposed to cadmium. Arch. Toxicol., 50: 159-66.

USEPA 1999. Compendium of methods for the determination of inorganic compounds in ambient air. Compendium of Method IO-3.2, EPA/625/R-96/010a.

Yu, M., Tsunoda, H. and Tsunoda, M. 2011. Environmental Toxicology: Biological and Health Effects of Pollutants. CRC Press.

Nature Environment and Pollution Technology
An International Quarterly Scientific Journal

p-ISSN: 0972-6268
e-ISSN: 2395-3454

Vol. 19 | No. 1 | pp. 333-338 | 2020

Original Research Paper | Open Access

Adsorption Process of Ammonia Nitrogen in Solution by the Modified Biochar from Corn Straw

Ruolin Xu*, Li Han*, Chengcai Huang*, Hao Zhang, Rui Qin*, Linli Zhang* and Muqing Qiu*†**

*College of Life Science, Shaoxing University, Shaoxing, 312000, P.R. China

**Key Laboratory of Agro-Ecological Processes in Subtropical Region, Institute of Subtropical Agriculture, Chinese Academy of Sciences, Changsha, 410125, China

†Corresponding Author: Muqing Qiu

Nat. Env. & Poll. Tech.
Website: www.neptjournal.com

Received: 03-04-2019
Accepted: 02-07-2019

Key Words:
Adsorption
Ammonia nitrogen
Modified biochar
Corn straw

ABSTRACT

The biochar was prepared by pyrolyzing corn straw at 773 K temperature under an oxygen-limited condition. Then, the gained biochar samples were further modified with $MgCl_2$ solution through mixing method for 3 h at the speed of 120 rpm. The physicochemical properties of the modified biochar from corn straw were investigated by surface area analysis, elemental analysis, scanning electron microscope, X-ray diffraction and Fourier transform infrared spectroscopy spectra. The adsorption experiments of ammonia nitrogen in aqueous solution by modified biochar were carried out. The results showed that the modified biochar contains high surface area, rough surface and a lot of oxygen-containing functional groups. The adsorption process fits well with the pseudo-second-order kinetics equation and Langmuir isotherm equation. The adsorption mechanism of modified biochar to NH_4^+ ion in aqueous solution includes ion exchange and physical adsorption. The ion exchange is primary in the process of adsorption.

INTRODUCTION

With the rapid development of industry and agriculture, the emission of eutrophic substances, such as nitrogen element and phosphorus element, has also increased in China (Liu et al. 2010). The eutrophication of water bodies is harmful to environment. Therefore, research on an efficient method to treatment the eutrophication of water bodies has become a hot studying area for many scholars (Duan et al. 2012, Haseena et al. 2016).

For a long time, in order to control the eutrophication of water bodies, many scholars have begun to study on the removal methods of nitrogen and phosphorus in water bodies, such as adsorption, chemical oxygen, ions exchange and so on (Christoph & Thomas 2009, García-Martínez et al. 2018). Among these methods, the adsorption method is widely applied because of its simple operation process, high efficiency and nontoxic by-products (Qiu et al. 2018, Seabra et al. 2019). The development and utilization of adsorbents is an important research content of the adsorption method (Tokay et al. 2010). Biochar is a rich carbon solid prepared by pyrolyzing biomass under anoxic or anaerobic and low temperature conditions. It is an excellent adsorption material with well-developed pore structure, large specific surface area, rich oxygen-containing functional groups and excellent adsorption properties (Rahmati & Modarress 2009, Paz-Ferreiro et al. 2018). Therefore, in order to obtain biochar with superior adsorption performance, many scholars began to explore the effects of biochar raw materials, pyrolysis temperature and modification conditions on the physical and chemical properties of biochar (Herrera et al. 2008, Hu et al. 2017). Raw materials for the production of biochar include agricultural and forestry waste, such as straw, weeds, wood chips, manure and so on. Among them, the agricultural straw waste is the main biochar raw material. It consists mainly of cellulose, hemicellulose and lignin (Ryu et al. 2000, Moghaddam et al. 2010, Vinitnantharat et al. 2010, Siswoyo et al. 2014). In China, every year, a large amount of agricultural straw is produced, but the utilization rate of agricultural straw is very low. The new method of seeking the resource utilization of agricultural straw has been concerned by many researchers (Sprynskyy et al. 2005, Gendel & Lahav 2013).

In this paper, the biochar was prepared by pyrolyzing corn straw under an oxygen-limited condition. Then, the biochar samples were modified with $MgCl_2$ solution. The adsorption experiments of ammonia nitrogen in solution were carried out. The main object of this study is, (1) the characteristic of the modified biochar from corn straw. The obtained modified biochar from corn straw was determined by surface area analysis, elemental analysis, scanning electron microscope, X-ray diffraction and Fourier transform infrared spectroscopy spectra respectively. (2) The

adsorption kinetic and adsorption isotherm of ammonia nitrogen in solution by the modified biochar were studied. (3) The adsorption mechanism of ammonia nitrogen in solution by the modified biochar is discussed in details.

MATERIALS AND METHODS

The Preparation of The Modified Biochar

The corn straws are collected from farmland in the suburbs of Dongyang City, Zhejiang Province. They were washed several times with water, and dried to a constant weight at 378 K, pulverized and passed through a 40 meshes sieve. 20 g of sample was pyrolyzed for 3 h under a nitrogen atmosphere at a temperature of 773 K. After cooling to room temperature, it was pulverized to 80 meshes. Then, the biochar from corn straw was obtained.

10 g biochar was added to the 1000 mL beaker containing 500 mL 0.01 mol/L $MgCl_2$. Then the mixture was stirred for 3 h at the speed of 120 rpm. The sample is filtered, washed with distilled water and dried to constant weight at 378 K. Then, the modified biochar by $MgCl_2$ solution was obtained.

Adsorption Experiments

Adsorption experiments were conducted in a set of 250 mL Erlenmeyer flasks containing modified biochar and 100 mL of NH_4^+ with initial concentrations in aqueous solution. The flasks were placed in a shaker at a constant temperature of 298 K and 120 rpm. The samples were then filtered and the residual concentration of NH_4^+ was analysed using Nessler reagent spectrophotometry.

Analytical Method

The concentration of NH_4^+ ion in solution was measured with a UV-1600 spectrophotometer. The adsorption capacity of NH_4^+ was calculated as following:

$$q_e = \frac{(C_0 - C_e) \times V}{m} \quad \ldots(1)$$

Where, C_0 and C_e (mg/L) are the initial and equilibrium concentrations of NH_4^+ in solution respectively. q_e (mg/g) is adsorption amount per unit mass of the modified biochar at adsorption equilibrium. V (mL) is volume of solution, m (g) is the mass of the modified biochar.

The physicochemical properties of the modified biochar from corn straw were investigated by surface area analysis (ASAP 2460), elemental analysis (EURO EA 3000), scanning electron microscope (Ultra 55), X-ray diffraction (Ulitma IV) and Fourier transform infrared spectroscopy spectra (Nicolet 5700).

RESULTS AND DISCUSSION

The Structural Characteristics and Properties of the Modified Biochar

The elements of C, H, O and N of the modified biochar are determined. They are 69.24%, 3.64%, 15.21% and 0.51% respectively. BET specific surface area of the modified biochar is 98.86 m^2/g, and the total of pore volume is 0.1236 cm^3/g.

The scanning electron micrograph of the modified biochar is shown in Fig. 1. From Fig.1, it can be shown that the microporous edge on the surface of the modified biochar is ablated by high temperature, and the distribution of the pores becomes disordered. It increases the surface roughness of the modified biochar, and it will benefit to improve the adsorption capacity.

The XRD spectrum is shown in Fig. 2. From Fig. 2, it can be thought that it is assigned to be broad and diffuse peak when 2θ is ranged from 15° to 22°. It is assigned to be quartz diffraction peak at 26.5°. It is assigned to be three potassium salt diffraction peaks at 28.5°, 40.6° and 50.5°. It

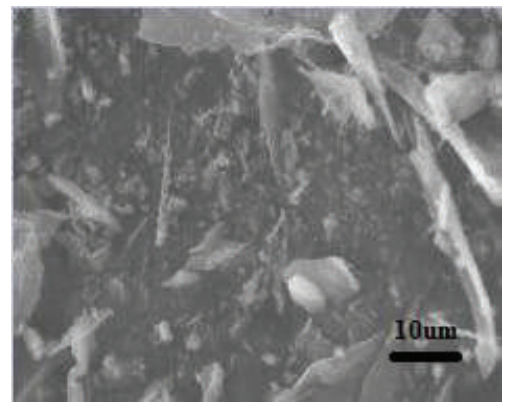

Fig. 1: SEM image of the modified biochar.

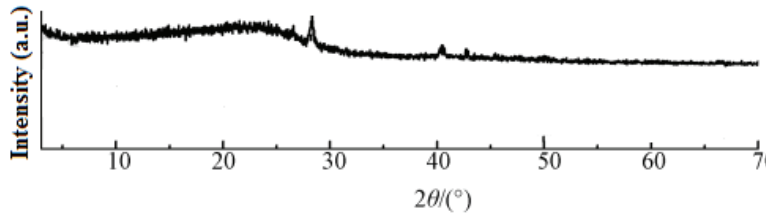

Fig. 2: X-ray diffraction spectrum of the modified biochar from corn straw.

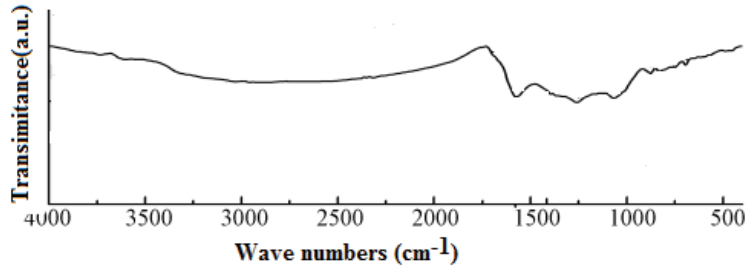

Fig. 3: Infrared spectrum of the modified biochar from corn straw.

is assigned to be diffraction peaks at 42.7°. This peak should be the characteristic peak of MgO. It indicates that Mg^{2+} ions have been loaded on the biochar.

From Fig. 3, there is a C = O absorption peak at 1702 cm^{-1}. They were assigned to be acyclic ring C = C stretching vibration peak, C = O stretching vibration peak and phenolic hydroxyl stretching vibration peak respectively, at 1609 cm^{-1}, 1442 cm^{-1} and 1259 cm^{-1}. It was assigned to be C – O stretching vibration peak at 1068 cm^{-1}. They were assigned to be C - H stretching vibration peak between 649 cm^{-1} and 878 cm^{-1}. The modified biochar contains an increased number of oxygen-containing functional groups and an increased polarity.

Adsorption Kinetic

In order to investigate the adsorption kinetics, the adsorption test was carried out. Adsorption experiments were conducted in a set of 250 mL Erlenmeyer flasks containing 0.05 g modified biochar and 50 mL 25 mg/L of NH_4Cl in aqueous solution. The flasks were placed in a shaker at a constant temperature of 298 K and 120 rpm. The reaction time is 5, 10, 15, 20, 30, 40, 60, 80, 120, 180, 240, 360 and 420 min respectively. The samples were then filtered and the residual concentration of NH_4^+ was analysed using Nessler reagent spectrophotometry.

The experimental results were shown in Fig. 4. In the initial stage, the adsorption amount of NH_4^+ ion by the modified biochar increases rapidly. Then, it tends to balance slowly.

In order to describe the adsorption kinetic of NH_4^+ ion by the modified biochar, pseudo-first-order kinetic equation and pseudo-second-order kinetic equation were adopted in this study. Their equations are as follows (Eugene 2016):

$$q_t = q_e\left(1 - e^{-K_1 t}\right) \quad \ldots(2)$$

$$\frac{t}{q_t} = \frac{1}{K_2 q_e^2} + \frac{t}{q_e} \quad \ldots(3)$$

Where q_t (mg/g) and q_e (mg/g) are adsorption capacity of NH_4^+ ion solution by modified biochar at adsorption time t and adsorption equilibrium respectively. K_1 (min^{-1}) and K_2 (min^{-1}) are the adsorption rate constant.

According to Eq. (2) and Eq. (3), the results are shown in Table 1.

From Table 1, it can be shown that the adsorption process fits well with the pseudo-second-order kinetics equation according to the value of R^2 (0.9984). It implies that the predominant process is chemisorption, which involves a sharing of electrons between the adsorbate and the surface of the adsorbent.

Adsorption Isotherm

In order to investigate the adsorption isotherm, the adsorption test was carried out. Adsorption experiments were conducted in a set of 250 mL Erlenmeyer flasks containing 0.05 g modified biochar and 50 mL of NH_4^+ ion with initial concentrations (5, 10, 25, 40, 50 mg/L) in aqueous solution. The flasks were placed in a shaker at a constant

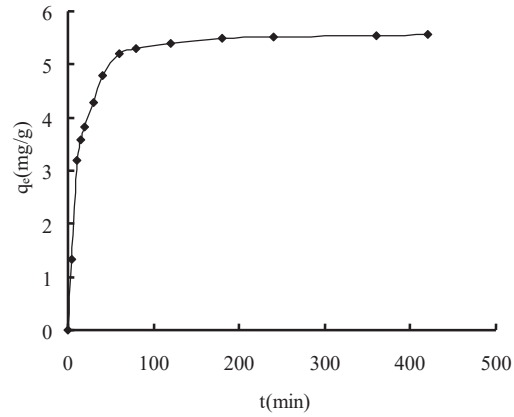

Fig. 4: The effect of reaction time on the adsorption capacity of NH_4^+ ion by the modified biochar.

Table 1: Parameters of the pseudo-first-order kinetic equation and the pseudo-second-order kinetic equation for the description of NH_4^+ ion adsorption onto modified biochar.

Pseudo-first-order kinetic equation			Pseudo-second-order kinetic equation		
K_1(min^{-1})	q_e (mg/g)	R^2	K_2 (min^{-1})	q_e (mg/g)	R^2
0.21	4.81	0.8258	0.0086	5.54	0.9984

temperature of 298 K and 120 rpm. The reaction time is 360 min. The samples were then filtered and the residual concentration of NH_4^+ was analysed using Nessler reagent spectrophotometry.

The experimental results are shown in Fig. 5. The sorption of NH_4^+ ion in aqueous solution by modified biochar increased with the initial concentration of NH_4^+ ions in aqueous solution increased.

In order to describe the adsorption isotherm of NH_4^+ ion by the modified biochar, Langmuir isotherm equation and Freundlich isotherm equation were applied in this study. Their equations are follows (Tu et al. 2019):

$$\frac{c_e}{q_e} = \frac{c_e}{q_{\max}} + \frac{1}{K_L q_{\max}} \quad \ldots(4)$$

$$\lg q_e = \lg K_F + \frac{1}{n} \lg c_e \quad \ldots(5)$$

Where q_e (mg/g) are adsorption capacity of NH_4^+ ion solution by modified biochar at adsorption equilibrium. $q_{\max}$ (mg/g) is the maximum adsorption capacity of the adsorbent under specific adsorption conditions. K_L (L/mg) and K_F (L/mg) are the adsorption rate constant. c_e (mg/L) is equilibrium concentrations of NH_4^+ ion in solution.

According to Eq. (4) and Eq. (5), the results are shown in Table 2. As shown from Table 2, the value of is 0.9326 according to the Langmuir isotherm equation. The value of R^2 is 0.8943 according to the Freundlich isotherm model. Therefore, the adsorption process of NH_4^+ ion in aqueous solution by the modified biochar fitted well with the Langmuir isotherm equation. This indicated that the surface of the adsorbent is a uniform surface. The adsorption process is a monolayer adsorption process.

Adsorption Mechanism

The adsorption mechanism of biochar on NH_4^+ ion in solution has been discussed by many researchers (Huo et al. 2012). At present, it is generally thought that the adsorption mechanism of biochar on NH_4^+ ion includes ion exchange, physical adsorption and electrostatic adsorption. In this study, biochar was modified by $MgCl_2$ solution. The surface of biochar contains a large number of functional groups, and they have a certain adsorption effect on NH_4^+ ion in aqueous solution. The reaction of biochar to NH_4^+ ion in aqueous solution is as follows:

$$Biochar - Mg^{2+} + 2NH_4^+ + 6H_2O \rightarrow Biochar - Mg\left(NH_4^+\right)_2 \cdot 6H_2O \quad \ldots(6)$$

$$Biochar - Mg^{2+} + 2NH_4^+ \rightarrow Biochar - \left(NH_4^+\right)_2 + Mg^{2+} \quad \ldots(7)$$

In a word, the adsorption mechanism of modified biochar to NH_4^+ ion in aqueous solution includes ion exchange and physical adsorption. The ion exchange is primary in the process of adsorption.

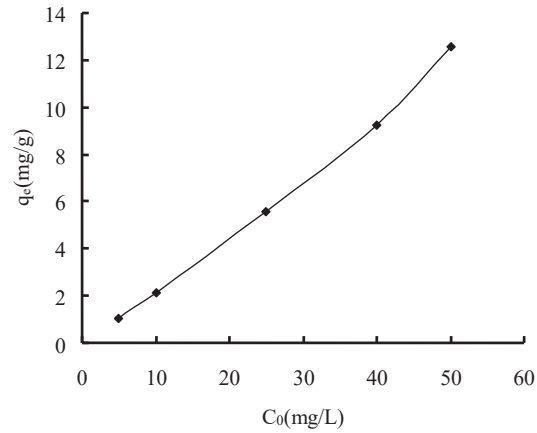

Fig. 5: The effect of initial concentration of NH_4^+ ion on the adsorption capacity of NH_4^+ ion by the modified biochar.

Table 2: Parameters of Langmuir isotherm equation and Freundlich isotherm equation for the description of NH_4^+ ion adsorption onto the modified biochar.

Langmuir			Freundlich		
q_{max} (mg/g)	K_L	R^2	K_F	n	R^2
5.12	0.26	0.9326	1.74	4.09	0.8943

CONCLUSIONS

Through the above experiments and discussions, the following results can be obtained.

1. The elements of C, H, O and N of the modified biochar were determined. They are 69.24%, 3.64%, 15.21% and 0.51% respectively. BET specific surface area of the modified biochar is 98.86 m^2/g, and the total of pore volume is 0.1236 cm^3/g. The distribution of the pores on the surface of modified biochar becomes disordered. The modified biochar contains a lot of oxygen-containing functional groups.
2. The adsorption process fits well with the pseudo-second-order kinetics equation. The predominant process is chemisorption, which involves a sharing of electrons between the adsorbate and the surface of the adsorbent. The adsorption process of NH_4^+ ion in aqueous solution by the modified biochar fitted well with the Langmuir isotherm equation. The adsorption process is a monolayer adsorption process.
3. The adsorption mechanism of modified biochar to NH_4^+ ion in aqueous solution includes ion exchange and physical adsorption. The ion exchange is primary in the process of adsorption.

ACKNOWLEDGEMENTS

This study was financially supported by the project of science and technology plan in Zhejiang Province (LGF19C030001), Guangxi Key Research and Development Program (AB17129002 and AB18050018) and the project of science and technology plan in Shaoxing City (2017B70058).

REFERENCES

Christoph, R. and Thomas, B. 2009. Adsorption of nitrogen and ammonia at zirconia surfaces. J. Mol. Struc., Theochem., 903: 89-99.

Duan, X.H., Srinivasakannan, C., Qu, W.W., Wang, X., Peng, J.H. and Zhang, L.B. 2012. Regeneration of microwave assisted spent activated carbon: process optimization, adsorption isotherms and kinetics. Chem. Eng. Process., 53: 53-62.

Eugene, A.U. 2016. Effect of crystallization and surface potential on the nitrogen adsorption isotherm on graphite: A refined Monte Carlo simulation. Carbon, 100: 52-63.

García-Martínez, J.C., González, H.A., Uribe, M.M., González-Brambila, J.A., Colín-Luna, Y.E., Escobedo-García, A., López-Gaona, L. and Alvarado, P. 2018. Selective adsorption of nitrogen compounds using silica-based mesoporous materials as a pretreatment for deep hydrodesulfurization. Catal. Today, 305: 40-48.

Haseena, P.V., Padmavathy, K.S., Krishnan, P.R. and Madhu, G. 2016. Adsorption of ammonium nitrogen from aqueous systems using chitosan-bentonite film composite. Procedia Tech., 24: 733-740.

Herrera, L.F., Do, D.D. and Birkett, G.R. 2008. Comparative simulation study of nitrogen and ammonia adsorption on graphitized and non graphitized carbon blacks. J. Colloid Interf. Sci., 320: 415-422.

Hu, B.W., Qiu, M.Q., Hu, Q.Y., Sun, Y.B., Sheng, G.D., Hu, J. and Ma, J.Y. 2017. Decontamination of Sr(II) on magnetic polyaniline/graphene oxide composites: evidence from experimental, spectroscopic, and modeling investigation. ACS Sustain. Chem. Eng., 5: 6924-6931.

Huo, H.X., Lin, H., Dong, Y.B., Cheng, H., Wang, H. and Cao, L.X. 2012. Ammonia-nitrogen and phosphates sorption from simulated reclaimed waters by modified clinoptilolite. J. Hazard. Mater., 229-230: 292-297.

Gendel, Y. and Lahav, D. 2013. A novel approach for ammonia removal

from fresh-water recirculated aquaculture systems, comprising ion exchange and electrochemical regeneration. Aquacult. Eng., 52: 27-38.

Liu, H.E., Dong, Y.H., Liu, Y. and Wang, H.Y. 2010. Screening of novel low-cost adsorbents from agricultural residues to remove ammonia nitrogen from aqueous solution. J. Hazard. Mater., 178: 1132-1136.

Moghaddam, S.S., Moghaddam, M.R.A. and Arami, M. 2010. Coagulation/flocculation process for dye removal using sludge from water treatment plant: Optimization through response surface methodology. J. Hazard. Mater., 175: 651-657.

Paz-Ferreiro, J., Marinho, M.A., Abreu, C.A. and Vidal-Vázquez, E. 2018. Soil texture effects on multifractal behaviour of nitrogen adsorption and desorption isotherms. Biosystems Eng., 168: 121-132.

Qiu, M.Q., Wang, M., Zhao, Q.Z., Hu B.W. and Zhu, Y.L. 2018. XANES and EXAFS investigation of uranium incorporation on nZVI in the presence of phosphate. Chemosphere, 201: 764-771.

Rahmati, M. and Modarress, H. 2009. Nitrogen adsorption on nanoporous zeolites studied by Grand Canonical Monte Carlo simulation. J. Mol. Struc. Theochem., 901: 110-116,

Ryu, Z.Y., Zheng, J.T., Wang, M.Z. and Zhang, B.J. 2000. Nitrogen adsorption studies of PAN-based activated carbon fibers prepared by different activation methods. J. Colloid Interf. Sci., 230: 312-319.

Seabra, R., Ribeiro, A.M., Gleichmann, K., Ferreira, A.F.P. and Rodrigues, A.E. 2019. Adsorption equilibrium and kinetics of carbon dioxide, methane and nitrogen on binderless zeolite 4A adsorbents. Micropor. Mesopor. Mat., 277: 105-114.

Siswoyo, E., Mihara, Y. and Tanaka, S. 2014. Determination of key components and adsorption capacity of a low cost adsorbent based on sludge of drinking water treatment plant to adsorb cadmium ion in water. Appl. Clay Sci., 97-98: 146-152.

Sprynskyy, M., Lebedynets, M., Zbytniewski, R., Namiesnik, J. and Buszewski, B. 2005. Ammonium removal from aqueous solution by natural zeolite, transcarpathian mordenite, kinetics, equilibrium and column tests. Sep. Purif. Technol., 46: 155-160.

Tokay, B., Karvan, O. and Erdem-Şenatalar, A. 2010. Nanoparticle silicalite-1 crystallization as monitored by nitrogen adsorption. Micropor. Mesopor. Mater., 131: 230-237.

Tu, Y.N., Feng, P., Ren, Y.G., Cao, Z.H., Wang, R. and Xu, Z.Q. 2019. Adsorption of ammonia nitrogen on lignite and its influence on coal water slurry preparation. Fuel, 238: 34-43.

Vinitnantharat, S., Kositchaiyong, S. and Chiarakorn, S. 2010. Removal of fluoride in aqueous solution by adsorption on acid activated water treatment sludge. Appl. Surf. Sci., 256: 5458-5462.

Nature Environment and Pollution Technology
An International Quarterly Scientific Journal

p-ISSN: 0972-6268
e-ISSN: 2395-3454

Vol. 19 | No. 1 | pp.339-348 | 2020

Original Research Paper | Open Access

Imperious Approach Towards Justifiable Strategic Lake Sediment Regulation

Shekhar Salunke* and Balbhim Chavan**
*Dept. of Environmental Science, Solapur University, Solapur, Maharashtra, India
** Dept of Environmental Science, Dr. B.A.M. University, Aurangabad, Maharashtra, India

Nat. Env. & Poll. Tech.
Website: www.neptjournal.com

Received: 03-07-2019
Accepted: 29-08-2019

Key Words:
Erosion
Sedimentation
Control strategies
Restoration actions

ABSTRACT

Lakes are extremely appreciated for the ecological, aesthetic and recreational values supporting rich biodiversity. As such, their preservation is of supreme importance. A global common problem of sedimentation that eventually seems to be responsible for eutrophication should be immediately attended to, before the degradation begins, since the restoration measures are expensive and may go beyond control. Erosion causes detachment, transportation and deposition of sediments and is the prime source of contamination where it accumulates in lakes and interrupts the ecological processes and functioning in the lake ecosystem, hence it is important to determine the risk to design management strategies for control. For the present investigation, thematic layers slope identification, NDVI, LULC, lineament density and RUSLE were employed to compute spatially distributed erosion and contaminant sources for the lake Ekrukh of Solapur district of Maharashtra State, India. The research identifies five hazardous erosion zones as; low, moderate, high, very high and severe, through the applied model and dictates formulation and implementation of innovative control strategies preventing soil and water (surface) pollution. The Soil Erosion in Maharashtra, Technical Bulletin, 2001 (Challa et al. 2001) was also referred for the studies.

INTRODUCTION

Exploration and delineation of erosion zones is important to design control strategies to prevent erosion at lakes, since the main problem faced by the lakes across the globe is siltation. Massive quantities of sediments add to the lake waters resulting in decreased water retaining capacity and increased nutrients that deteriorates the ecological health of the lakes. The eutrophic conditions of the lake indicate the presence of abundant aquatic weeds along the shoreline. As a lake or reservoir becomes rich in nutrients, it develops dense populations of planktonic algae that usually dominate. Such intense populations create unacceptable taste and odour problems, along with an increase in organic loading of the lower layers as the algae complete their life cycle and fall to the bottom. This reduces the aesthetic value of the lakes. Aside from the aesthetic deterioration of water quality, eutrophication presents many other difficulties for the aquatic life. Such water is less palatable, algae-laden water has high chlorine and coagulant demands. It often reduces filter runs, necessitating excessive backwash; it may also require certain specific forms of taste and odour control such as activated carbon, chlorine, dioxide, or permanganate. This increases the cost of lake management programmes. Certainly, a preventive measure calls an immediate attention rather than to cure later. As such the siltation through soil erosion should be controlled as an action with respect to the phrase 'prevention is better than cure'. For the reason, it is necessary to ascertain the erosion possibilities at the lakes and to define the control measures to avoid siltation. The aim can be better achieved by operating various methodological processes through Remote Sensing and Geographic Information System (GIS) techniques. As such, to define restoration strategies, a study was undertaken to understand the erosion sources and status of the lake Ekrukh. Previously our studies indicated two models to prevent or avoid siltation at the lake and were assessed to be effective in reducing the silt loads at the lake waters. However, to determine the sites of installations for the designed models to reduce silt loading, Lake Ekrukh was assessed for the significant sites of silt loading.

MATERIALS AND METHODS

Digital Data

The conduct of the investigative approach included the use of LANDSAT-7. Enhanced Thematic Mapper (ETM+) digital data was used, during fieldwork 200 Ground Control Points (GCPs) were collected with attributes using a handheld Global Positioning System (GPS) receiver with an expected error of 3-4 m. This data was used for georeferencing and ground truthing, as well as for accuracy assessment of the imageries and DEMs. Soil samples were also collected for the Revised Universal Soil Loss Equation (RUSLE).

NDVI Classification

NDVI (Normalized Difference Vegetation Index) at red wavelengths and lower reflectance at near-infrared wavelengths was used to differentiate between healthy, stressed vegetation

and sparse or non-vegetated surface. High NDVI was classified as healthy and growing vegetation and low NDVI was considered to locate areas that absorb red and near-infrared radiations, like water. The analysis of the topography was done by constructing. NDVI was used for identification of bare and sparse vegetation surface, where infiltration of contaminated water is more. Using the reflectance images of band 3 (red) and band 4 (Near InfraRed – NIR) NDVI map of the study areas were generated as followed by Joshi et. al (2004).

LULC Classification

Land Use/Land Cover (LULC) classification map was generated for analysis using ERDAS Imagine 9. Ground truth and topographic sheets were used for accuracy assessment. Digital Terrain Model (DTM) was created with the help of DEM data by creating terrain surface and adding attributes and colour code to each pixel. A classified slope map was prepared with the spatial analyst module in ArcGIS environment. Soil erosion zones were identified along with the accumulation points.

DTM

DTM was carried out for the basins of study areas for the interpretation of geomorphology of the area, to delineate lineaments and to generate digital drainage from DEM, represented in the respective figures for the DTM of the basins under the study areas.

Ground Data

Regarding the ground data, during fieldwork 200 ground control points (GCPs) were collected with attributes using a handheld global positioning system (GPS) receiver with an expected error of 3-4 m. This data was used for georeferencing and ground truthing, as well as for accuracy assessment of the imageries and DEMs. Soil samples were also collected for the Revised Universal Soil Loss Equation (RUSLE). Filled and finished Shuttle Radar Topographic Mission (SRTM) data of 3arc second WRS-2 of 90 m resolution was downloaded from the GLCF website. Two tiles of height data (SRTM_ff03_p145r048.tifand SRTM_ff03_p146r047.tif) of WRS-2 have been used for the pre-processing and generation of the DEM followed by mosaic and image subset of the study area clipped from the whole scene. This work analyses LANDSAT 7 ETM+ and SRTM DEM data for the generation of erosional and contamination zones in the study areas. The flow chart has been applied for the lake studies.

RUSLE Parameters

All the RUSLE parameters determined for the study area were either in spatial format and/or in numerical format. The results of R, K, and C factors are assigned to each pixel of DEMs of the basin, as there is no variation in the results. The variables in the results of LS and P factors assigned to DEMs of the basin is presented in, for LS-factor 7 and 8 for P factor. The spatial maps were integrated using RUSLE

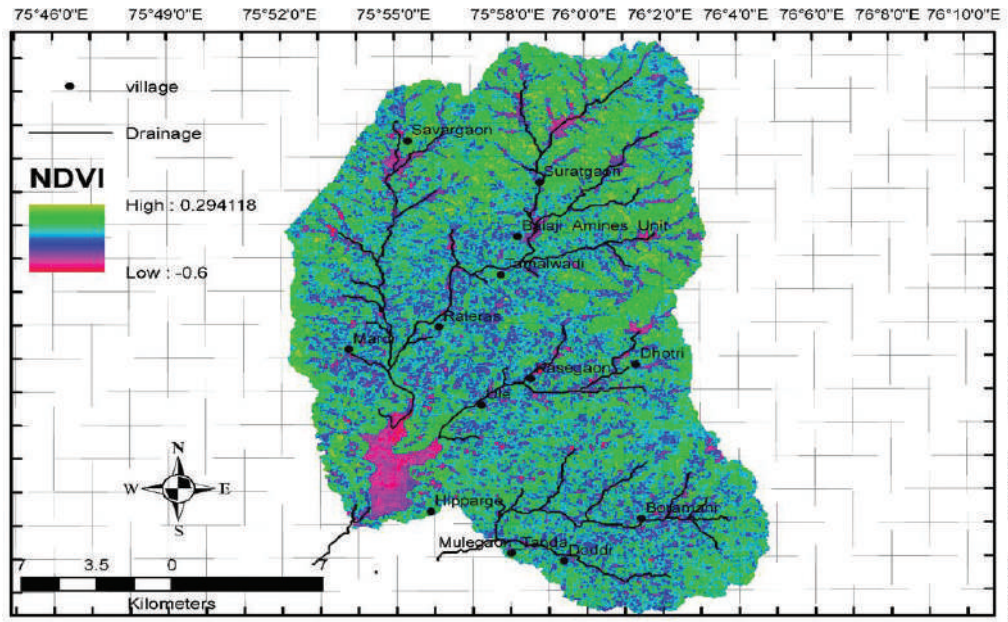

Fig. 1: NDVI classification of Ekrukh Lake basin.

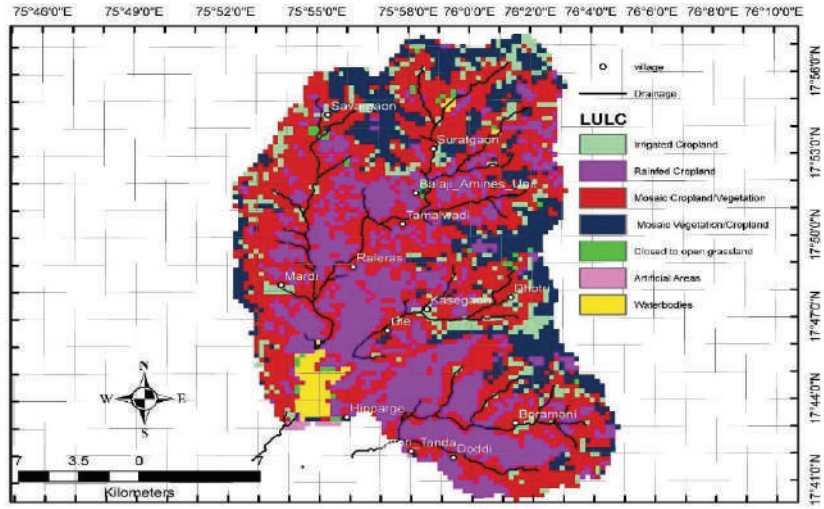

Fig. 2: LULC classification of Ekrukh.

empirical formula for the lake, basin. In the present study, LANDSAT-7 Enhanced Thematic Mapper (ETM+) digital data was used. Landsat-7 ETM+ as it is a multispectral scanner that provides a multispectral image data set in eight spectral bands. Pre-processing of images was carried out by ortho-rectification and geometrical correction. A Landsat 7 ETM+ image (path 146/ row 047 and path 145/ row 048) of Solapur and surroundings was acquired, for the study. The digital data was radiometrically corrected to remove atmospheric effects. Further the digital numbers of the pixels were converted to reflectance to understand reflectance of the objects on the earth. The soil credibility factor K of the USLE is evaluated according to soil texture classification using the values from Stewart et al. (1975) considering that the organic matter content is less than 4%.

RESULTS AND DISCUSSION

NDVI

Low NDVI values (Fig. 1) in all three lakes indicate water bodies while higher values dictate healthy vegetation. The NDVI of Ekrukh Lake Basin shows healthy vegetation (green colour), either cultivated or non-cultivated, are located along its periphery. The blue coloured area, even near to lake, indicates presence of non-healthy vegetation around Tamalwadi, Mardi, Raleras, Kasegaon and Ule may be because of contaminated sediments transported from upper reaches of the streams.

LULC

Fig. 2 represents LULC classification of Ekrukh. The area denoted as artificial area is settlement zone. The area is considered as a source of contamination and assigned a highest number in statistical and weighted overlay analysis.

DTM

DTM was carried out for the Ekrukh lake basin for the interpretation of geomorphology of the area, to delineate lineaments and to generate digital drainage from DEM. Fig. 3 represents the DTM of the basin in the study area.

Geomorphology of The Area

The study area falls in the sub-basin of Seena River, which is a tributary of Bhima River. The Bhima River itself is a tributary of Krishna River. The Krishna River has developed its basin in regional scale. Krishna River generated its plain by depositing transported load of sediments. The study area is a small part of the Krishan River basin. Geomorphologically three basins of the area are lying in the almost plain to rolling topography. Variations in the elevation are very less. This topography represents peneplain stage of erosion cycle. The streams in the area have reached their graded stage and they are flowing over the sediments deposited by their own.

Two small hillocks are located in the NE direction of Ekrukh basin at an elevation of 589 m above mean sea level (Fig. 3). The elevation difference is about 139 m spatially distributed in the 378.6309 sq. km. area of the Ekrukh basin. Geomorphologically these small isolated hillocks are inselbergs, ruminants of hills after erosion. The slopes on these hills are sources of sediments for erosion and transportation.

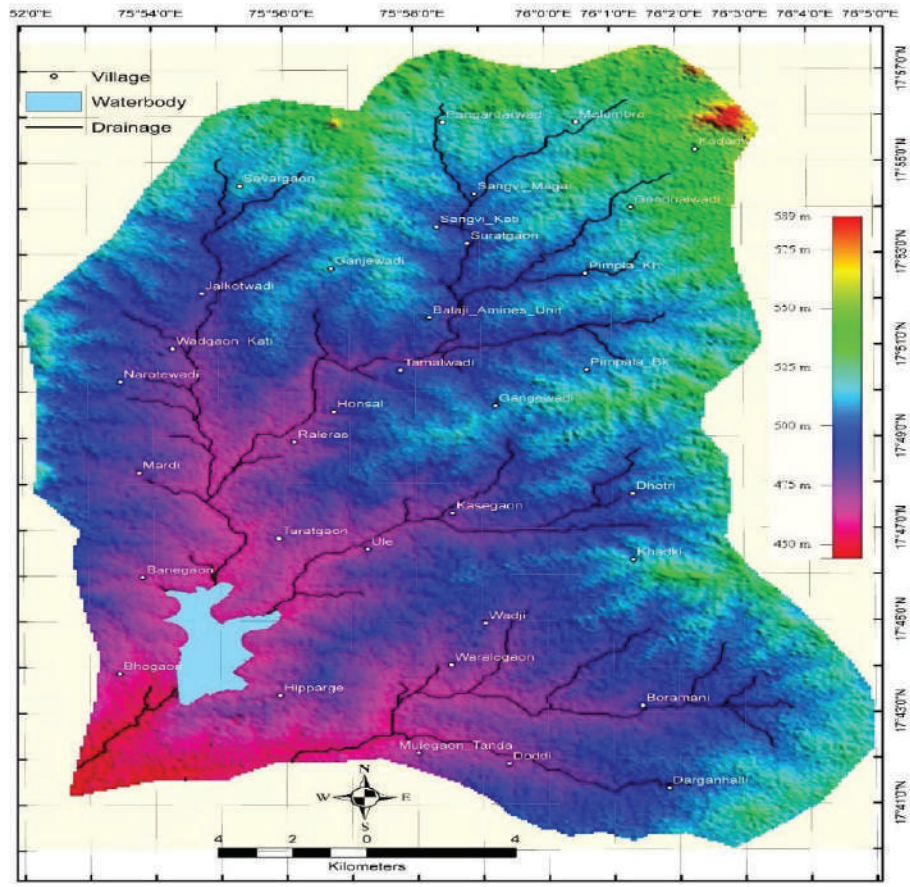

Fig. 3: Digital Terrain Map of the Ekrukh Lake basin.

Drainages and Lineaments

Digital drainage network extraction and analysis has been carried out using DEM. Digital data (SRTM DEM) and non-digital data (1:50,000 scale topographic maps) were used to extract channel networks. An extraction of the channel network from digital data was carried out in the ArcGIS 9.3 environment using D8 algorithm of ArcHydromodule. Both river 'basins' and 'watersheds' are areas of land that drain to a water body, such as a lake, stream, river or estuary. In a river basin, all the water drains to a large river. The term 'watershed' is used to describe a smaller area of land that drains to a smaller stream, lake or wetland. Figs. 4 and 5 exhibit digital drainages of Ekrukh basin. Stream order calculated using Strahler Stream Order (Strahler 1952) in hydrography deals with the hierarchy of streams from the source (or headwaters) downstream.

Ekrukh basin shows dendritic pattern of the stream, indicating plain, uniform and homogeneous surface on which these streams are flowing. The general slope of the area is towards south. The accumulation points (marked by 'x') are the sites of accumulation of water and sediments transported by headwaters. These accumulated water and sediments are further driven away when the kinetic energy of the stream increases. The increase in kinetic energy of the stream depend on the factors like increase in velocity, amount of water due to heavy rainfall, steepness of slopes, amount of vegetation, amount of load to be carried etc.

The lineaments are the surface expressions of weaknesses in the underlying rock. These are mainly fracturing, faults, dykes, jointed zones etc. The lengths of lineaments vary from 1.833303 km to 9.529145 km in Ekrukh basin, while it varies from 1.760651 km to 7.959094 km. These lineaments are deeply incised in the ground and are connected to underground fractures or joints, which are yet not reached on the surface. Therefore, water from rainfall or surface runoff infiltrate into subsurface and travel through this underground network of fractures and settled below the water table. Water table is a level, at subsurface, below which all the fractures, cracks, voids, fissures, crevices and joints are filled with

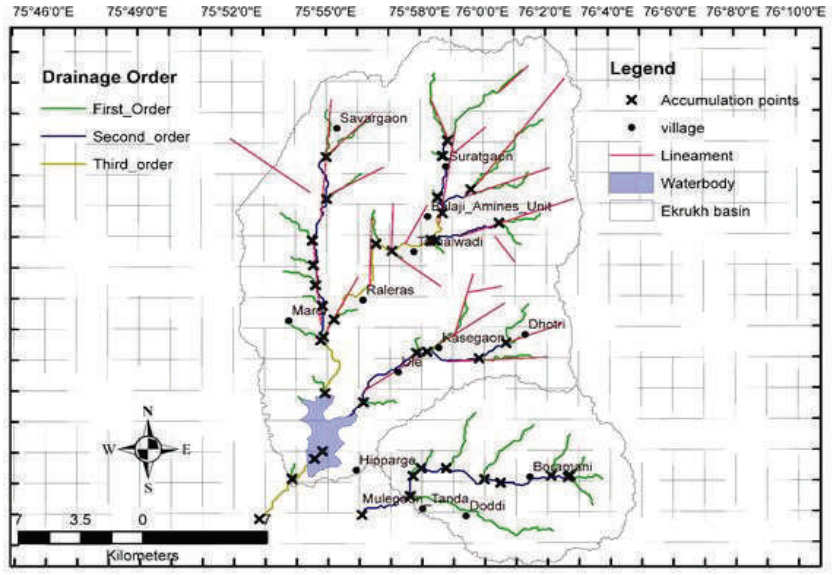

Fig. 4: Watershed boundary, drainages and lineaments of Ekrukh basin.

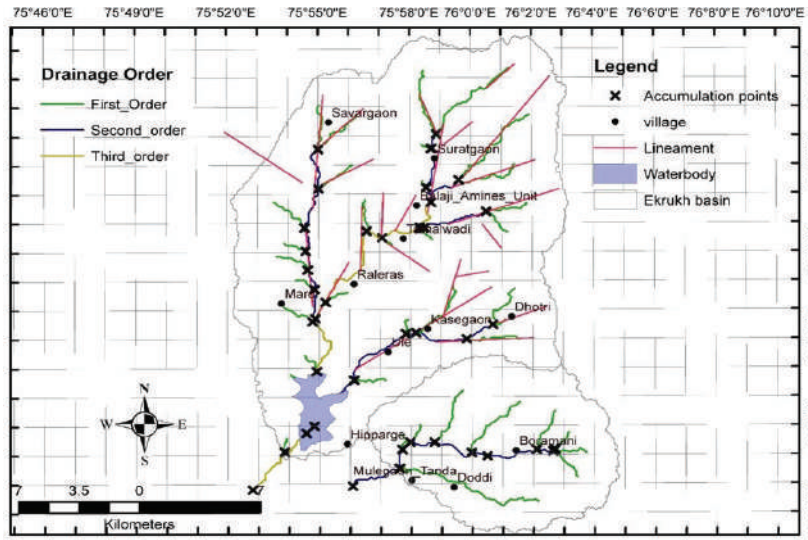

Fig. 5: Watershed boundary, drainages and lineaments of Ekrukh basin.

water. At downstream direction, when water table intersects with ground surface, the groundwater sips out in the form of spring, seepage or lake. Hence, the contamination can occur on the surface during transportation, at the accumulation points and during the infiltration through fractures and joints. This contaminated water can come up in the lakes or in the major river where these tributaries joins. Fig. 5 shows both the lineaments and accumulation points. The most possible contamination sites are intersection of lineaments and accumulation points. The density of such intersections occurs at Tamalwadi, industry of Balaji Amine units and Mardi in the Ekrukh basin. Streams flowing from Shanti Nagar and combination of stream and lineament trending NE-SW are the sources of contamination of groundwater.

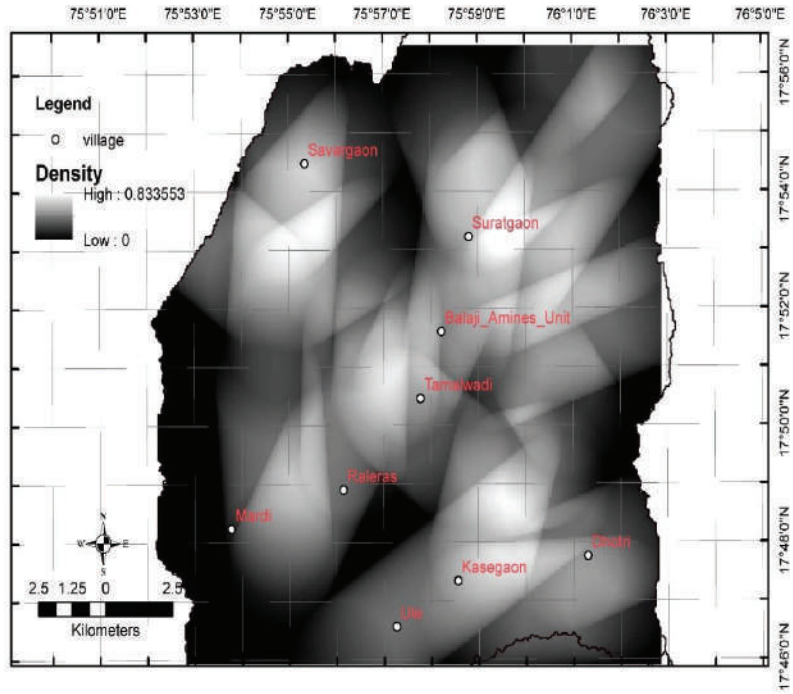

Fig. 6: The integration of data of lineaments density and buffer of accumulation points of Ekrukh basin.

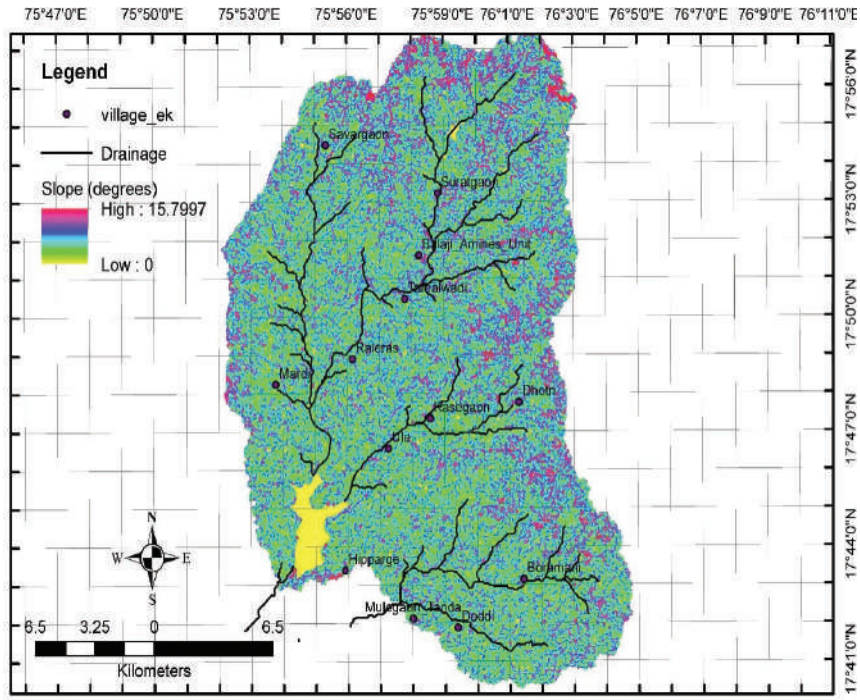

Fig. 7: Slope map of the Ekrukh Lake basin.

To understand and delineate erosion hazard zones of such intersection of accumulation points and lineaments, integrated maps lineament density (2 km periphery) and buffer zone (2 km) around accumulation points have been prepared for Ekrukh Lake basin. Fig. 6 shows the integration of data of lineaments density and buffer of accumulation points of the Ekrukh basin.

The bright coloured zones reveal high values that indicate higher possibilities of contamination hazards, while dark pixels indicate lower ordered contamination hazard zones. The accumulation points are processed for the buffer analysis in ArcGIS. The buffer was set for 100 m periphery around each accumulation points. There are more possibilities of accumulation of contaminants in these points from their area around 100 m radius. The overlapping buffers are more hazardous for contamination.

Slope

Slope is one of the controlling factors of erosion. The slope (also called grade, incline, gradient, pitch or rise) of a physical feature or landform refers to the tangent of the angle of that surface to the horizontal. It is a special case of the slope, where zero indicates horizontality. The slope angle is maximum as 90 degrees. The slope accelerates erosion as it increases the velocity of the flowing water. Table 1 gives the classes.

A slope of 9° is ideal for the soil erosion, greater than 9° causes increase in rate of erosion of soil (Challa et. al 1995 and 2001). The Ekrukh Lake basin exhibit highest slope angle of 15.7997° of moderately steep slope. Slopes of moderately steep category are situated at the northern border and eastern border of the basin at Dhotri and Kasegaon villages. Strongly sloping grounds are bordering the whole basin. These slopes are prone to weathering and erosion and can be classified as hazardous for erosion. The slope angle in this basin has very little effect on erosion, but these may take a vital part in contamination of surface flow of water.

Table 1: Slope classes.

Class	Slope range (in %)	Slope Class
1	0 - 1	Nearly level
2	1 - 3	Very gently sloping
3	3 - 5	Gently sloping
4	5 - 10	Moderately Sloping
5	10 - 15	Strongly Sloping
6	15 - 25	Moderately steep to steep Sloping
7	25 - 33	Steep Sloping
8	33 - 50	Very steep
9	>50	Extremely steep slope

Source: Soil Survey Manual (Anonymous 1971)

Soil Erosion Zones by RUSLE Analysis

The goal of this study was to test the RUSLE model in the study area for prediction of erosion risk. All the RUSLE parameters determined for the study area were either in spatial format and/or in numerical format (Table 2). The results of R, K, and C factors are assigned to each pixel of DEMs of all basins, as there is no variation in the results. The variables in the results of LS and P factors assigned to DEMs of all basins are presented in Fig. 7 for LS-factor and Fig. 8 for P factor. The spatial maps were integrated using RUSLE empirical formula Equation (1) and presented in Fig. 9 for Ekrukh basin.

Topographic influence on LS factor can be noted in LS-factor map of three basin. The slope mainly controls this factor. Light coloured pixels indicate areas of high LS factor and these pixels are spatially distributed in the basin. Clusters of high LS factor occur at eastern border of the basin as well as at the highest elevation in the basin. General slope direction of the basin is east to west; hence, LS factors are clustered near eastern side of the basin. This eastern region can be considered as high erosion zone. The high LS factor is well conglomerated around the drainage lines. The spatial distribution of P-factor presented in maps 8, where P-factors are found to be aligned well with the LS-factors of Ekrukh basin.

The annual average soil loss estimated using RUSLE for the study area are 25.8593 tonnes/ha/year for Ekrukh Lake basin. The zones of higher soil erosion are linearly accumulated around the drainage line in Ekrukh basin. It indicates that the major drainage lines are eroding more than its tributaries. The soil loss for Ekrukh basin is 25.8593 tonnes/ha/year. The K factor for soils for various organic carbon contents (%) was studied and calculated using guidelines provided by Stewart et al., (1975) (Table 3),

Referring the Table 3a., the rate of soil erosion for Ekrukh lake basin (25.8593 tonnes/ha/year) is severe.

Weighted Overlay Analysis

Table 2: Results of RUSLE parameters.

RUSLE factors	Ekrukh Lake values
R-Factor	412.809
K-Factor	0.25
LS-Factor	0.0 - 2.15
C-Factor	0.43
P-Factor	0.270 - 0.50

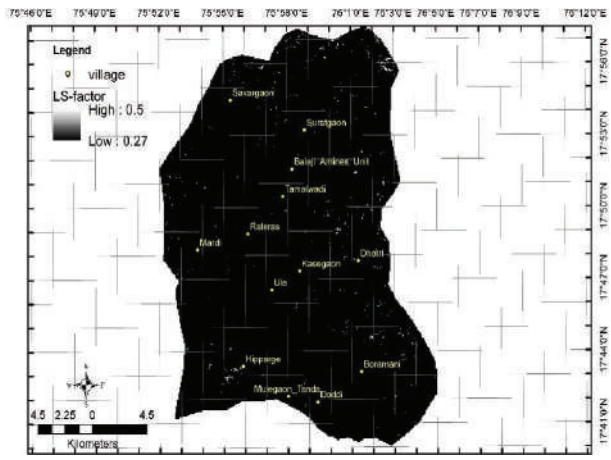

Fig. 7: LS factor map of Ekrukh basin.

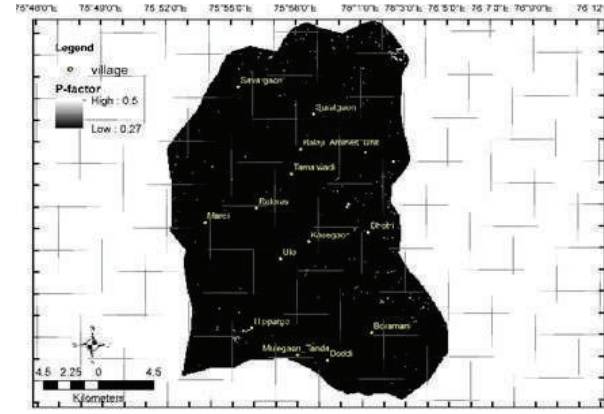

Fig. 8: P factor map of Ekrukh basin.

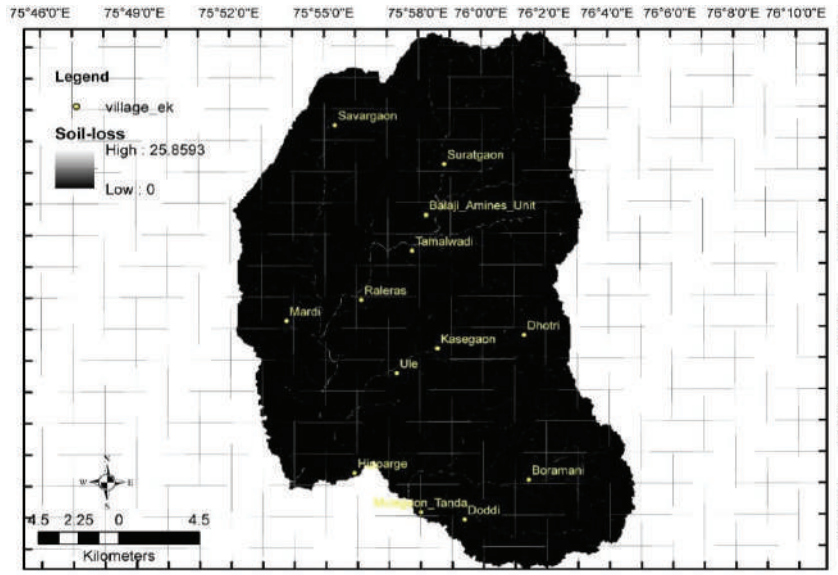

Fig. 9: Average annual soil loss map and zones of erosion of Ekrukh basin.

Weighted overlay is a type of suitability analysis that helps in analysing site conditions based on multiple criteria. Weighted overlay analysis allows to combine, weight and rank several different types of information and visualize it so one can evaluate multiple factors at once.

As with all overlay analysis, in weighted overlay analysis, to define the problem, breaking of the major model in to sub-model is essential. Hence, layers of the sub-models are created and weights are assigned to their attributes. The raster layers for each sub-models (basins) generated are: 1. Slope, 2. NDVI, 3. LULC, 4. lineament and accumulation point's density and 5. soil erosion model by RUSLE. Since the input criteria layers will be in different numbering systems with different ranges, to combine them in a single analysis, each cell for each criterion is reclassified into a common preference scale such as 1 to 5, with 5 being the most affinity for erosion. An assigned preference on the common scale implies the phenomenon's preference for the criterion. The preference values not only should be assigned relative to each other within the layer but should have the same meaning between the layers. For example, if a location for one criterion is assigned a preference of 5, it will have

Table 3. Soil Erodibility Factor K-factor (after Stewart et al. 1975)

	K for Organic Matter Content (%)						
Textural Class	<0.5	2	4	Textural Class	<0.5	2	4
Sand	0.05	0.03	0.02	Loam	0.38	0.34	0.29
Fine sand	0.16	0.14	0.10	Silt loam	0.48	0.42	0.33
Very fine sand	0.42	0.36	0.28	Silt	0.60	0.52	0.42
Loamy sand	0.12	0.10	0.08	Sandy clay-loam	0.27	0.25	0.21
Loamy fine sand	0.24	0.20	0.16	Clay loam	0.28	**0.25**	0.21
Loamy very fine sand	0.44	0.38	0.30	Silty clay-loam	0.37	**0.32**	0.26
Sandy loam	0.27	0.24	0.19	Sandy clay	0.14	0.13	0.12
Fine sand yloam	0.35	0.30	0.24	Silty clay	0.25	0.23	0.19
Very fine sandy loam	0.47	0.41	0.33	Clay		0.13-0.2	

Table 3a.: Classification of Soil loss annual erosion.

Sr. No.	Class	Amount (tonnes/ha/year)
1	Very slight	<5 tonnes/ha/year
2	Slight	5 – 10 tonnes/ha/year
3	Moderate	10 – 15 tonnes/ha/year
4	Moderately severe	15 – 20 tonnes/ha/year
5	Severe	20 – 40 tonnes/ha/year
6	Very severe	40 – 80 tonnes/ha/year
7	Extremely severe	>80 tonnes/ha/year

the same influence on the phenomenon as a 5 in a second criterion. For example, in a slope model of the study area, steeper slopes are prone to erosion and hence they are assigned to 5 preference. As the slopes become levelled, they are prone to deposition, they are assigned decreasing value of preference as 1. Hence, each pixel of every model is assigned numbers from 1 to 5 according their properties of affinity to erosion. In the process of reclassification, raster models of slope, higher slopes (>10), in NDVI, lower values, in LULC, settlement and open bare spaces, in density models, higher values and in RUSLE model, higher values were assigned to preference level 5.

For the processing of weighted overlay, five raster images of reclassification generated for each basin (1) slope, 2) NDVI, 3) LULC, 4) lineament and accumulation point's density and 5) soil erosion model by RUSLE) were further processed and presented in the Fig. 10, for Ekrukh, basin. The results of hazard zonation mapping are classified as 1. low, 2. moderate, 3. high, 4. very high, and 5. severe. The results of RUSLE analysis are corroborating the results of hazard zonation mapping. Fig. 10 explains hazard zonation map of possible zones of erosion and zones of infiltration of contaminants in Ekrukh basin. The severe erosion rate occurs at Suratgaon village and very high rate of erosion occurs around Savargaon, Suratgaon, Balaji Amines Unit, Kasegaon and Dhotri.

CONCLUSIONS

The indication of non-healthy vegetation beyond the peripheral region towards associated villages is a result of contaminated sediments transported through the streams, directs to consider development of vegetation as protective shield against soil erosion to prevent sedimentation. The slopes of two small hillocks located in the NE direction of Ekrukh basin at elevation of 589 m above mean sea level are sources of sediments for erosion and transportation call for the attention to install slope protection methods. The density of such intersections occurs at Tamalwadi, industry of Balaji Amine units and Mardi in the Ekrukh basin. Streams flowing from Shanti Nagar and combination of stream and lineament trending NE-SW are the sources of contamination of groundwater. The high possibilities of contaminations identified need to be addressed to prevent sedimentation at the lake. The basin exhibits highest slope angle of 15.7997° which is a moderate steep slope. Slopes of moderately steep category are identified at the northern border and eastern periphery of the basin and strongly sloping grounds are identified to surround the whole basin and are found prone to weathering and erosion and hazardous for erosion.

At Ekrukh, the areas with high LS factor is spatially distributed across the basin. Clusters of high LS factor are identified at eastern border of the basin. General slope direction of the basin is from east to west. Hence, LS factors are clustered near eastern side of the basin indicating high erosion zone the rate of soil erosion for Ekrukh lake basin (25.8593 tonnes/ha/year) which is severe. The zones of higher soil erosion are linearly accumulated around the

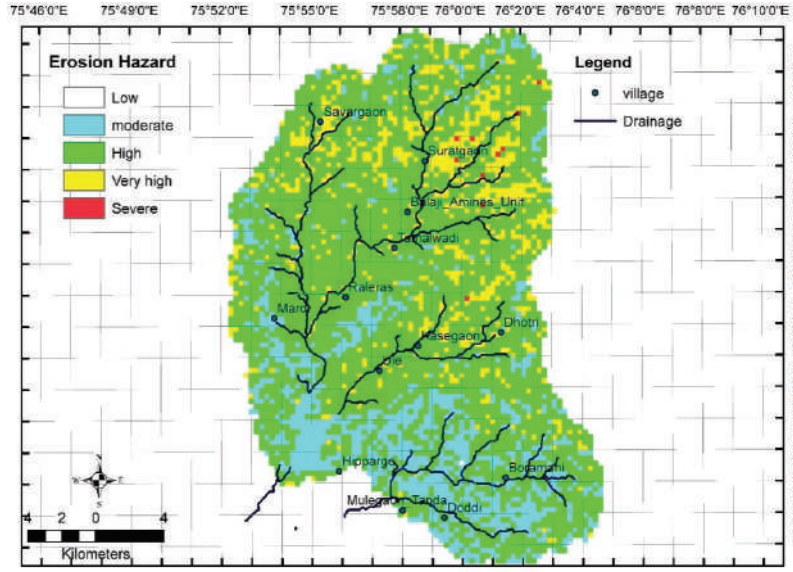

Fig. 10: Hazard zonation map of Ekrukh lake basin.

drainage line in Ekrukh basin, indicating major drainage lines eroding more than its tributaries. Ekrukh basins shows dendritic pattern of the stream, indicating plain, uniform and homogeneous surface on which these streams are flowing. The general slope of the area is towards south. The accumulation points (marked by 'x') are the sites of accumulation of water and sediments transported by headwaters and are the reasons for sedimentation. The lineament lengths vary from 1.833303 km to 9.529145 km in Ekrukh basin are the indicators of contamination on the surface during transportation, at the accumulation points and during the infiltration through fractures and joints, at downstream direction. The intersection of lineaments and accumulation points are identified as the most possible contamination sites at the lake.

The study calls immediate attention to implement integrated approaches for implementation of control measures towards prevention of soil erosion and pollution measures. In the subsequent phase, the research embarks upon designing innovative approaches to address the same.

ACKNOWLEDGEMENT

The author expresses gratitude to Dr. Vinay Dixit, Department of Geology, Dayanand College, Solapur, M.S., for his proficient and crucial directions and inputs towards the course of action and pivotal analytical assistance for the entire venture, devoid of which, it was unattainable to disembark. Sum of all the efforts has generated the organized scientific evidence supporting the investigative conclusions directing action plan for sustainable development.

REFERENCES

Anonymous 1971. Soil Survey Manual. All India Soil, Landuse Survey Organisation, IARI, New Delhi.

Challa, O., R.S. Kurothe and K.S. Gajbhiye, 2001. Soil Erosion in Maharashtra. NBSS Publ. No. 82, NBSS and LUP, Nagpur, 51 p + 1 sheet of map (1:1 M scale).

Challa, O., Vadivelu, S. and Sehgal, I. 1995. Soils of Maharashtra for optimising land use. NBSS Publ. 54b (Soils of India Series), National Bureau of Soil Survey and Land Use Planning, Nagpur, India, 112p + 6 sheets of Map (1:500,000 scale).

Joshi, P.K. Kumar, Roy, P.S., Singh Sarnam, Agrawal, Shefali and Yadav, Deepshikha 2004. Vegetation cover mapping in India using multi-temporal IRS Wide Field Sensor (WiFS) data.

Stewart, B.A. (Bobby Alton) 1932 Woolhiser, D. A., Wischmeier, W. H. and Caro, J. H. 1975. Control of Pollution from Cropland. U.S. EPA Report No. 600/2-75-026 or U.S.D.A. Rep No. ARS-H-5-1. Washington, DC.

Strahler, A.N. 1952. Hypsometric (area-altitude) analysis of erosion topology, Geol. Soc. of America Bulletin 63(11): 1117-1142.

Nature Environment and Pollution Technology
An International Quarterly Scientific Journal

p-ISSN: 0972-6268
e-ISSN: 2395-3454

Vol. 19 | No. 1 | pp. 349-353 | 2020

Original Research Paper | Open Access

Bacteriological Quality Assessment of Groundwater and Surface Water in Chennai

SK. Jasmine Shahina†, D. Sandhiya and Summera Rafiq
Department of Microbiology, Justice Basheer Ahmed Sayeed College for Women, Chennai, Tamil Nadu, India
†Corresponding author: SK. Jasmine Shahina

Nat. Env. & Poll. Tech.
Website: www.neptjournal.com

Received: 18-06-2019
Accepted: 23-07-2019

Key Words:
Groundwater
Surface water
Bacteria
Antibiotic resistant
MPN

ABSTRACT

Water bodies have played a vital role throughout civilizations in the growth and continue to be a factor of importance in the modern economic growth of all the contemporary societies. Contamination of water sources with microbes can occur through rainfall overflow and agricultural inputs, mixing with sewage effluents. Water acts as a medium for the proliferation and dissemination of bacteria which cause human disease. Therefore, consumption of safe water is one of the most important requirements in public health. A total of 20 water samples were collected from both surface and groundwater from in and around Chennai. The MPN index of the surface water was found to be high when compared with groundwaters. Total coliform count of as many as 1100 MPN/100 mL and greater were obtained. A total of 11 different bacterial species were identified from both ground and surface water samples. The prevalence of bacterial isolates was of *Staphylococcus aureus, CoNS, Enterococcus faecalis, Escherichia coli, Klebsiella pneumoniae, Enterobacter aerogenes, Pseudomonas aeruginosa, Vibrio cholera, Salmonella typhi, Aeromonas hydrophila* and *Citrobacter freundii*. These organisms were resistant to many classes of antibiotics. The facts on multiple antibiotic resistance profiles of bacteria isolated from water and the resistance patterns suggested that there has been an indiscriminate use of the antibiotics tested. High occurrence of these multiple antibiotic resistant organisms in the drinking water distribution system could potentially pose a threat to humans consuming this water.

INTRODUCTION

About 75% of the earth's surface is covered by water which is vital for all forms of life. Groundwater refers to water that occurs below the water-table in the zone of saturation. Groundwater is the only source of fresh water which is utilized in many parts of the world, whereas most of the times surface waters are either absent or polluted (Haniffa et al. 1993). Surface water is water that gets collected in a stream, river, lake, wetland etc. Many industries and municipalities use treated surface water due to high cost of drinking water. In the recent past there has been a steady increase in the pollution of river waters with deleterious microbes, including bacteria, viruses, parasites, as well as fungi (Niyogi 2005, Abraham et al. 2007). Majority of microbes in water are from faeces from human and other mammals. Pathogens can enter waters either from a point source, non-point sources or both. Rainwater surface run-offs, storm sewer spillages or overflow cause non-point microbial pollution of waters, while point-source pollution comes from discharge of untreated or partially treated effluents from wastewater treatment plants (Donovan et al. 2008, Musyoki et al. 2013).

When the water is contaminated with faecal material a wide range of pathogenic microorganisms can be transmitted to humans. Some of them include enteropathogenic agents such as Salmonella, Shigella, Enteroviruses, and multi cellular parasites as well as opportunistic pathogens, like *Pseudomonas aeruginosa*, *Klebsiella* sp., *Vibrio parahaemolyticus* and *Aeromonas hydrophila* (Hodgkiss 1988). The occurrence and spread of antibiotic-resistant bacteria (ARB) are grave public health problems worldwide. Now aquatic ecosystems are a recognized reservoir for ARB and antibiotic resistance genes. An emerging issue for the general public and the drinking water industry is the presence of trace levels of antibiotics and ARB in source water and finished drinking water which affects public health (Scott et al. 2000). The aim of the present study was to characterize the presence of coliforms from surface and groundwater bodies in and around Chennai and to determine the resistance pattern of the isolates towards commonly used antibiotics. This study was done keeping in view the recent Chennai floods and Vardah cyclones that caused devastations to both human lives and the environment.

MATERIALS AND METHODS

Study Area

A total of 20 water samples were collected, of which 10 were

from surface waters (Lakes) and 10 from groundwater (Well) in and around Chennai. Water samples were collected from North Jaganadhan Nagar, Thathan Kuppam, Villivakkam, Teynampet, Chrompet, Chitlapakkam, Pallavaram, Hasthinapuram, Velachery, Chembarabakkam, Chitlapakkam, Namangalam, Pallikaranai, Puzhal, Ambattur and Porur.

Collection of Samples

Water samples were aseptically collected in 1 litre sterile bottles. Prior to sampling, the bottles were rinsed thoroughly with the water of the same source from which the sample was to be collected and rinsed water was discarded. The bottle cap was aseptically removed, and the bottle was immersed into the lake to collect the water. The bottle was brought up to the surface and covered with the bottle cap.

In open wells, water is available from 1 meter below from the ground. A sterile sampler was introduced into the well with the help of a rope and the water was taken out. The sampling bottle was kept unopened until the moment at which it was required for filling. During sampling the stopper and neck of the bottle were protected from contamination. Samples were labelled and transported in ice packs to the laboratory. They were examined for precipitate, colour, pH and odour. They were further processed for microbiological examination of coliforms and other pathogens.

Processing of the Water Samples

The water samples were subjected to MPN (Most Probable Number) technique to detect the quality of water. MPN is most commonly applied for quality testing of water, i.e. to ensure whether the water is safe or not in terms of bacteria present in it. A group of bacteria commonly referred as faecal coliforms act as an indicator for faecal contamination of water. It was done by multiple tube fermentation test to determine the total coliform count as per the standard methods. (Bartram & Pedley 1996)

Detection of Selected Pathogenic Bacteria from Water Samples

One mL of each water sample was inoculated into 5 mL of nutrient broth, selenite F enrichment broth and alkaline peptone water and was incubated at 37°C for 6-8 hrs. They were further inoculated on to MSA (Mannitol salt agar) media, Cetrimide agar, DCA (Deoxycholate citrate agar) media and TCBS (Thiosulfate citrate bile salt agar) and the plates were incubated for about 24-48 hrs at 37°C, respectively.

Antibiotic Sensitivity Testing

Once the organism was identified, the antibiotic sensitivity testing was carried out as per the standard protocol by Kirby Bauer disc diffusion method (Bauer et al. 1966) towards the following antibiotics - Erythromycin (15 mcg), Nalidixic acid (30mcg), Rifampicin (30 mcg), Teicoplanin (30 mcg), Vancomycin (30 mcg), Amoxyclav (30 mcg), Amikacin (30 mcg), ceftazidime/clavulanic acid (30/10 mcg), ceftriaxone (30 mcg), ciprofloxacin (5 mcg), ceftazidime (30 mcg) and gentamicin (10 mcg).

RESULTS

Physical Properties of Water Samples

Water samples were tested for their physical properties like pH, colour, odour and precipitate. The pH of all the ground as well as the surface water was found to be neutral. The colour of the water samples ranged from being colourless to slight yellowish. Strong odour and precipitates were observed predominantly in surface waters when compared to groundwaters.

MPN Technique

The water samples were subjected to MPN technique to detect the quality of water. MPN is the most commonly applied method for quality testing of water to ensure whether the water is potable or not. The MPN index of the surface water was found to be high when compared with groundwater. Total coliforms of as many as 1100 MPN/100 mL and greater were enumerated in surface water. With respect to groundwater, MPN index of >1100 MPN/100 mL was observed at North Jaganadhan Nagar and the least MPN index of 28 MPN/100 mL was observed at Teynampet. All the sampling places of both ground and surface waters showed the presence of coliform bacteria. Hence, it can be concluded that the water samples were heavily contaminated with coliform bacteria and were found to be unsatisfactory for drinking purpose (Tables 1 & 2).

Prevalence of Bacterial Isolates from Water Samples

A total of 11 different bacterial species were identified from both ground and surface water samples. The prevalence of bacterial isolates was *Staphylococcus aureus, CoNS, Enterococcus faecalis, E. coli, Klebsiella pneumoniae, Enterobacter aerogenes, Pseudomonas aeruginosa, Vibrio cholerae, Salmonella typhi, Aeromonas hydrophila* and *Citrobacter freundii* (Table 3).

Determination of MPN Index for Boiled Water

As a control study, one surface and one groundwater sample was boiled to check the efficiency of boiling in killing the coliforms present in them. MPN technique was done and it was found to be negative for the presence of coliforms.

Table 1: MPN Index of groundwater.

Sample Number	Area	MPN Index per 100 mL
1A	North Jaganadhan Nagar (3rd street)	>1100
2A	Thathan Kuppam	460
3A	Villivakkam	75
4A	North Jaganadhan Nagar	210
5A	Teynampet	28
6A	Chrompet	150
7A	Villivakkam	150
8A	Chitlapakkam	460
9A	Pallavaram	460
10A	Hasthinapuram	210

Table 2: MPN Index of surface water.

Sample Number	Area	MPN Index per 100 mL
1B	Velachery (100 feet road)	1100
2B	Chembarabakkam	1100
3B	Chitlapakkam	>1100
4B	Namangalam	460
5B	Pallikaranai	1100
6B	Puzhal	460
7B	Ambattur	1100
8B	Porur	>1100
9B	Pallavaram	>1100
10B	Hasthinapuram	>1100

Table 3: Prevalence of bacterial isolates from water samples. Groundwater (n = 74), Surface water (n = 52)

S. No	Name of the organisms	Percentage (Groundwater)	Percentage (Surface water)
1	*Staphylococcus aureus*	5(6%)	3(6%)
2	*CoNS*	3(4%)	1(2%)
3	*Enterococcus faecalis*	8(11%)	5(10%)
4	*E. coli*	10 (13%)	10(19%)
5	*Klebsiella pneumoniae*	10(13%)	10(19%)
6	*Enterobacter aerogenes*	10(13%)	10(19%)
7	*Pseudomonas aeruginosa*	6(8%)	2(4%)
8	*Vibrio cholerae*	7(9%)	3(5%)
9	*Salmonella typhi*	6(8%)	5(10%)
10	*Aeromonas hydrophila*	5(6%)	2(4%)
11	*Citrobacter freundii*	4(5%)	1(2%)

Antibiotic Sensitivity Testing

Antibiotic sensitivity testing of the bacterial isolates was done as per Kirby Bauer's disc diffusion method. Gram positive organisms showed 100% resistance towards vancomycin, nalidixic acid, erythromycin, ciprofloxacin and teicoplanin. They were 100% sensitive towards rifampicin. Gram negative organisms exhibited 100% resistance towards ceftazidime/clavulanic acid, amoxyclav followed by gentamicin, ceftriaxone and ceftazidime. These isolates were sensitive towards amikacin and ciprofloxacin.

DISCUSSION

Potable water must be free from pathogenic microorganisms and chemical substances that are hazardous to health (Lamikanra 1999). Bacteria indicative of faecal pollution or pathogens should not be found in drinking water. A sensitive method of quality assessment of drinking water is the detection of faecal indicator bacteria as it is not possible to examine water for every possible pathogen that might be present (WHO 2004). There has been an imbalance between supply and demand and it is the main reason which has led to competition and thereby resulted in pollution and environmental degradation. Failure of disinfection methods of raw water at the treatment area or mixing of sewage through cross-connections, leakages could cause bacteriological pollution of drinking water supplies.

Main cause of water pollution is due to human impact (Palit 2012). By studying the physico-chemical and microbial characteristics, the significance of water as a potent ecological factor can be appreciated. In the present study, water samples were tested for their physical properties like pH, colour, odour and precipitate found. The pH of all the ground as well as the surface water was found to be neutral. The colour of the water samples ranged from being colourless to slight yellowish. Strong odour and precipitates were observed predominantly in surface waters when compared to groundwaters. The negative logarithm of hydrogen ion concentration is known as pH. It expresses the intensity of acidic or alkaline condition of a solution. pH is an extremely important variable because most microorganisms can survive within a narrow range of pH and it also helps in the solubility of most metals. pH is also an important factor with respect to chemical treatment of water including disinfection process.

Microbial contamination of drinking water is the most common and wide spread health risk and therefore its control must always be of supreme importance. Monitoring microbial presence, especially faecal coliform bacteria (FC) determines the quality of water. In this study, the MPN index was high for surface waters when compared to groundwater. The water analysed in this study has clearly shown that they are loaded with indicator organisms which are the indication of faecal pollution and thus the human interference.

In our study, a total of 11 different bacterial species were identified from both ground and surface water samples. The prevalence of bacterial isolates was *Staphylococcus aureus, CoNS, Enterococcus faecalis, E. coli, Klebsiella pneumoniae, Enterobacter aerogenes, Pseudomonas aeruginosa, Vibrio cholerae, Salmonella typhi, Aeromonas hydrophila* and *Citrobacter freundii*. According to EPA, the presence of *E. coli* indicates recent sewage or animal waste contamination (EPA 2001). The temperature and the presence of nutrients in the tank favours the survival of enteric bacteria, like *Salmonella* spp. and *E. coli* (Leclerc et al. 2002). Enteric pathogens such as *Salmonella, Shigella* and *Vibrio* are principally transmitted through contaminated drinking water, as reported by Edberg et al. (2000).

P. aeruginosa is ubiquitous, free-living bacterium in the environment. It is often found in natural waters such as lakes and rivers in concentrations of 10/100 mL to >1,000/100 mL. Nevertheless, it is not often found in drinking water. *Pseudomonas* is usually found in 2% of samples, or less, and at concentrations up to 2,300 mL or more often at 3-4 CFU/mL. The occurrence of *Pseudomonas* in drinking water is due to its ability to form biofilms and colonize the plumbing fixtures (i.e., faucets, showerheads, taps, pipelines, etc.) than its presence in the water system or treated drinking water (Mena & Gerba 2009).

The occurrence and spread of antibiotic-resistant bacteria (ARB) globally are serious public health problems. Aquatic ecosystems are a designated reservoir for ARB and antibiotic resistance genes. The existence of trace levels of antibiotics and ARB in source water and finished drinking water may also greatly affect public health and is an emerging issue for the general public and the drinking water industry (Scott et al. 2000). In our study, antibiotic sensitivity testing of the bacterial isolates was done as per Kirby Bauer's disc diffusion method. Gram positive organisms showed 100% resistance towards vancomycin, nalidixic acid, erythromycin, ciprofloxacin and teicoplanin. They were 100% sensitive towards rifampicin. Gram negative organisms exhibited 100% resistance towards cefotaxime/clavulanic acid, and amoxyclav followed by gentamicin, ceftriaxone and ceftazidime. These isolates were sensitive to amikacin and ciprofloxacin.

CONCLUSION

An assessment of the bacteriological quality of drinking water in the present study confirmed the presence of various bacterial species including opportunistic pathogens such as

Aeromonas and Pseudomonas spp. This drastic effect in the increase of microorganisms may be because of the recent Chennai floods followed by Vardah cyclone. This has caused the mix up of sewage with the water bodies resulting in water pollution. This could have been the reason for all the water samples showing the presence of coliforms and other organisms. The isolated bacteria were found to be resistant to several classes of antibiotics. The data on multiple antibiotic resistance (MAR) profiles of bacterial isolates from water and the resistance patterns of organisms in drinking water suggested that there has been an indiscriminate use of the antibiotics tested. The high occurrence of multi-drug resistant organisms in the drinking water system may possibly pose a risk to humans consuming this water.

ACKNOWLEDGEMENT

The authors would like to thank the Management and Principal of Justice Basheer Ahmed Sayeed College for Women, for the financial support given under the Post Graduate student project scheme sanctioned through the Multi-Disciplinary Research and Consultancy Centre (MRCC) of the College for the promotion of research.

REFERENCES

Abraham, W. R. 2010. Megacities as sources for pathogenic bacteria in rivers and their fate downstream. International Journal of Microbiology, 2011.

Bartram, J. and Pedley, S. 1996. Water quality monitoring - a practical guide to the design and implementation of freshwater quality studies and monitoring programmes. Chapter 10 - Microbiological Analyses. Published on behalf of United Nations Environment Programme and the World Health Organization © 1996 UNEP/WHO.

Bauer, A.W., Kirby, W.M., Sherris, J.C. and Turck, M. 1966. Antibiotic susceptibility testing by a standardized single disk method. Am. J. Clin. Pathol. 45(4): 493-496.

Donovan, E., Unice, K., Roberts, J. D., Harris, M. and Finley, B. 2008. Risk of gastrointestinal disease associated with exposure to pathogens in the water of the Lower Passaic River. Applied and Environmental Microbiology, 74(4): 994-1003.

Edberg, S.C., Rice, E.W., Karlin, R.J. and Allen, M.J. 2000. *Escherichia coli*: The best biological drinking water indicator for public health protection. Symp. Ser. Soc. Appl. Microbiol., 29: 106S-116S.

EPA 2001. Environment Public Authority Decision No. 210/2001 Pertaining to the Executive By-Law of the Law of Environment Public Authority.

Haniffa, M.A., Arockiasamy, S. and Martin, P. 1993. Physico-chemical and microbiological studies in the Perenial River Thabaraparani for the assessment of water quality. Indian J. of Env. Protec., 13(7): 533-538.

Hodgkiss, I.J. 1988. Bacteriological monitoring of Hong Kong marine water quality. Environment International, 14(6): 495-499.

Lamikanra, A. 1999. Essential Microbiology for Students and Practitioner of Pharmacy, Medicine and Microbiology. Amkra Books, pp. 406.

Leclerc, H., Schwartzbrod, L. and Dei-Cas, E. 2002. Microbial agents associated with waterborne diseases. Critical Reviews in Microbiology, 28(4): 371-409.

Mena, K.D. and Gerba, C.P. 2009. Risk assessment of *Pseudomonas aeruginosa* in water. In: Reviews of Environmental Contamination and Toxicology, 201: 71-115.

Musyoki, A.M., Abednego, M., Suleiman, M.A., Mbithi, J.N. and Maingi, J.M. 2013. Water-borne bacterial pathogens in surface waters of Nairobi river and health implication to communities downstream Athi river. International Journal of Life Science and Pharma Research, 3(1): 4-10.

Niyogi, S.K. 2005. Shigellosis. Journal of Microbiology (Seoul, Korea), 43(2): 133-143.

Palit, A., Batabyal, P., Kanungo, S. and Sur, D. 2012. In-house contamination of potable water in urban slum of Kolkata, India: a possible transmission route of diarrhea. Water Science and Technology, 66(2): 299-303.

Scott, K.P., Melville, C.M., Barbosa, T.M. and Flint, H.J. 2000. Occurrence of the new tetracycline resistance gene test (W) in bacteria from the human gut. Antimicrobial Agents and Chemotherapy, 44(3): 775-777.

WHO 2004. Guidelines for Drinking Water Quality: Recommendations, (Vol. 1). World Health Organization, Geneva.

Nature Environment and Pollution Technology
An International Quarterly Scientific Journal

p-ISSN: 0972-6268
e-ISSN: 2395-3454

Vol. 19 | No. 1 | pp. 355-359 | 2020

Original Research Paper | Open Access

Use of Pyrophyllite as Soil Conditioner in Lettuce Production

Senad Murtić*†, Ćerima Zahirović, Lutvija Karić**, Josip Jurković***, Hamdija Čivić*** and Emina Sijahović*****

*Department of Plant Physiology, Faculty of Agriculture and Food Science University of Sarajevo, 71 000 Sarajevo, Bosnia and Herzegovina

**Department of Vegetable, Faculty of Agriculture and Food Science, University of Sarajevo, 71 000 Sarajevo, Bosnia and Herzegovina

***Department of Plant Nutrition, Faculty of Agriculture and Food Science, University of Sarajevo, 71 000 Sarajevo, Bosnia and Herzegovina

†Corresponding author: Senad Murtić

Nat. Env. & Poll. Tech.
Website: www.neptjournal.com

Received: 19-05-2019
Accepted: 22-07-2019

Key Words:
Agriculture
Environment
Fertilizer
Pyrophyllite
Soil conditioner

ABSTRACT

In recent years, there has been an increasing interest in the possibility of the use of aluminosilicate minerals in order to maintain and improve soil productivity. The unique ion-exchange and adsorption properties of pyrophyllite minerals indicate the possibility of its application in agriculture as soil conditioner. The aim of this study was to evaluate whether the application of pyrophyllite could reduce the use of mineral fertilizers in lettuce production without adverse effects on its yield and quality. The experiment was carried out from November 2018 to April 2019 inside a polyethylene covered greenhouse in Gornji Moranjci, Bosnia and Herzegovina. The following quality parameters were analysed using standard methods: ascorbic acid content, total phenolic content, total antioxidant capacity and content of potentially toxic heavy metals (Cr, Pb, Ni, Cu, Zn and Mn) in lettuce. The results of this study showed that the substitution of fertilizers with pyrophyllite in amount of 25% and 50% of recommended fertilizer rate under experimental conditions increase lettuce yield and total antioxidant capacity compared to the control treatment, i.e. 100% recommended fertilizer rate. The results of this study also support the hypothesis that pyrophyllite could be used as remediation material in polluted soils by heavy metals. However, further investigation is necessary to confirm these hypotheses across different soil ecosystems.

INTRODUCTION

Applying fertilizer in agricultural production has shown a steady increase in recent decades, resulting in the gradual soil degradation. The numerous other processes, such as nutrient depletion, leaching and pollution of soils by hazardous substances from industry have also contributed to the soil degradation (Lal 2015). Although the soil degradation is a worldwide phenomenon, it is fact that is in most developing countries the phenomenon is being hastened by land use mismanagement. Better use of soil resources through optimizing fertilization, increasing biodiversity and improving soil quality has therefore been considered as a priority for achieving sustainable agriculture (Gomiero 2016).

In recent years, there is an increasing interest for using of natural aluminosilicates in order to maintain and improve soil productivity. Clay minerals, e.g. zeolite and bentonite are known to have ability to increase soil capacity to hold available forms of nutrients (Ghazavi 2015, Jakkula & Wani 2018). Contrary to zeolite and bentonite, pyrophyllite application in agriculture is not substantially present due to its lower availability and insufficient knowledge of its potential use in agriculture.

Pyrophyllite is a dioctahedral 2:1 clay mineral with the chemical formula $Al_2Si_4O_{10}(OH)_2$. It resembles closely with talc and the only difference between them is that talc contains Mg^{2+} instead Al^{3+} in octahedral positions. The elementary sheet of pyrophyllite is composed by aluminium-oxygen/hydroxyl octahedra between two layers of silicon-oxygen tetrahedra. The basal surfaces of this elementary sheet do not contain hydroxyl groups, which explains the hydrophobicity of pyrophyllite (Drits et al. 2012).

Resemblance to the structure with talc and some other clay minerals indicate that pyrophyllite application in soil could also be effective in increasing soil's ability to hold nutrients and thus reducing leaching. The fact that pyrophyllite is used in the agriculture industry as a carrier for fertilizers and pesticides supports this hypothesis.

The present study was conducted to evaluate whether the application of pyrophyllite can reduce the use of mineral fertilizers in lettuce production without adverse effects on its

yield and quality. If that is possible, the additional aim of this study was to determine the optimal ratio between fertilizer and pyrophyllite in order to achieve this purpose. Lettuce was selected as the subject of this study, primarily because the production of this vegetable is consistently increasing in this country and therefore any effort to improve lettuce production is of great interest for both the producer and the consumer.

MATERIALS AND METHODS

Aluminosilicate minerals (pyrophyllite): The pyrophyllite materials used in this study were obtained by grinding and sieving pyrophyllite ore from deposits in Parsovići-Konjic, Bosnia and Herzegovina and characterized by following properties: alkaline, hydrophobic material, very soft and white to grey in colour. The hardness on the Mohs' scale is 1.5 and cation exchange capacity (CEC) ranges between 50 and 70 meq/100g. Median total SiO_2, Al_2O_3, K, Ca, Mg, Cu, Ni, Zn, Co, Mn, Pb and Cr contents were 67.55%, 19.10%, 0.3%, 6.65%, 0.14%, 1.40 mg/kg, 2.74 mg/kg, 25.68 mg/kg, 0.4 mg/kg, 93.14 mg/kg, 7.97 mg/kg and 0.76 mg/kg, respectively. The above-mentioned results of pyrophyllite chemical analysis were obtained at Faculty of Agriculture and Food Sciences University of Sarajevo.

Lettuce (*Lactuca sativa* L. var. *shangore*): This lettuce is one of the favourite butterhead lettuce varieties in Bosnia for producers as well as consumers. It is cultivated from late autumn to spring in greenhouses and its vegetation period ranges from 45 to 50 days after planting in a heated greenhouse. This lettuce is adaptable to most soil types, it has green leaves and form tight and heavy heads, more than 0.3 kg. It grows fast and keeps the leaves out upright.

Study area: The experiment was carried out from November 2018 to April 2019 inside a polyethylene covered greenhouse in Gornji Moranjci, Srebrenik Municipality, Bosnia and Herzegovina (44°41′N, 18°26′E and altitude 275 m). The length, width, eaves height and ridge height of the experimental greenhouse were 50 m, 8 m, 2.2 m and 3.7 m, respectively. Humidity regulation in greenhouse was achieved by opening of two side roll-up vents while the row cover was used to protect the lettuce against frosts. The climate in studied area is classified as Cfb by Köppen and Geiger climate classification (Rubel & Kottek 2010). The annual mean air temperature is 11.1°C and precipitation 856 mm with significant rainfall even in the dry months. The soil of the experimental site is classified as Dystric Cambisol, according to FAO Soil Classification (FAO 2014). This type of soil is characterized by an ochric (Aoh horizon) or umbric (Aum horizon), which lies directly above the cambic horizon (B)v horizon, acidic reaction, base saturation less than 50%, low to moderate water storage capacity and a medium nutrient storage capacity.

Soil pH in KCl, organic matter, available phosphorus (P_2O_5) and potassium (K_2O) contents in the 0-30 cm studied soil layer before lettuce planting were 5.1, 3.83%, 15.1 mg/100g and 31.3 mg/100g, respectively. Median total Cr, Pb, Ni, Cu and Zn contents were 128.48 mg/kg, 17.68 mg/kg, 104.55 mg/kg, 15.76 mg/kg and 36.95 mg/kg, respectively. In accordance with results of soil chemical analysis and nutrient needs of lettuce, the following fertilization recommendation was given: 300 kg/ha NPK 7:20:30 (nitrogen-phosphorus-potassium) as part of the basic fertilization and if necessary 100 kg/ha KAN (calcium ammonium nitrate) as part of fertilization during vegetation (recommended fertilizer rate was recalculated based on plot area).

Experimental design and treatments: The experimental area in greenhouse was divided into twenty-one equal plots. Each plot had an area of 5 m^2. The experiment was laid out in randomized complete block design with seven treatments in three replications. Experiment treatments (T) were as follows:

T1 - recommended fertilizer rate (RFR) without pyrophyllite (PP), i.e. control treatment (150 g NPK 7:20:30 at each plot)

T2 - 25% of RFR was replaced with PP particle size 3 mm (112.5 g NPK 7:20:30 + 37.5 g PP)

T3 - 25% of RFR was replaced with PP particle size 0.1 mm (112.5 g NPK 7:20:30 + 37.5 g PP)

T4 - 50% of RFR was replaced with PP particle size 3 mm (75 g NPK 7:20:30 + 75 g PP)

T5 - 50% of RFR was replaced with PP particle size 0.1 mm (75 g NPK 7:20:30 + 75 g PP)

T6 - 75% of RFR was replaced with PP particle size 3 mm (37.5 g NPK 7:20:30 + 112.5 g PP)

T7 - 75% of RFR was replaced with PP particle size 0.1 mm (37.5 g NPK 7:20:30 + 112.5 g PP)

Fertilizers and pyrophyllite material in the all experimental plots were applied two weeks before planting lettuce (7 December 2019). No other fertilizers were added during the lettuce vegetation. All other agrotechnical measures needed for optimum lettuce growth (pest control measures, irrigation) were performed identically on all experimental plots until the time of lettuce technological maturity.

Analysis of lettuce yield and quality: All lettuce plants in the experiment area were harvested at the same time (31 March 2019). Average yield was determined as the average fresh harvest weight per m^2.

Lettuce nutritional quality was analysed by detecting the following parameters: ascorbic acid content, total phenolic content, total antioxidant capacity and content of potentially toxic heavy metals (Cr, Pb, Ni, Cu, Zn and Mn). Ascorbic acid (AA) was estimated by 2,6-dichlorophenolindophenol titration method (AOAC 2006). Lettuce extract for estimation of total phenolics, total flavonoids and total antioxidant capacity was prepared by macerating of lettuce powder (1 g) in 30% ethanol for 6 hours. Thereafter, the extract was filtered. Total phenolic content (TPC) was estimated by the Folin-Ciocalteu method (Ough & Amerine 1988) and total antioxidant capacity (TAC) by ferric reducing antioxidant power (FRAP) assay (Benzie & Strain 1996).

Extraction of heavy metals from lettuce powder was performed using HNO_3-H_2SO_4 solution (Lisjak et al. 2009) as follows: 1 g of lettuce powder was placed into 100 mL round bottom flask and then 10 mL 65% HNO_3 and 4 mL 95-98% H_2SO_4 were added. The reaction mixture in flask was covered with a watch glass, allowed to stand for few hours and then heated gently on a hot plate for 30 min. Thereafter, the flask with reaction mixture was allowed to cool to room temperature, filtered through quantitative filter paper into 50 mL flask and diluted to the mark with distilled water. The content of Cr, Pb, Ni, Cu, Zn and Mn in obtained extract was determined by atomic absorption spectrophotometry on AA-7000 Shimadzu, according to method ISO 11047 (ISO 1998). Standard solutions of the examined heavy metals were prepared by appropriate dilution of stock standards (Merck) with deionized water.

Statistic data processing: All the experimental measurements were made in triplicate and the results were expressed as mean ± standard deviation. Analysis of variance (ANOVA) was performed using Microsoft Excel 2013 software program, and the significant differences between the variants were determined using Least Significant Differences test at 0.05 level of probability ($P \leq 0.05$).

RESULTS

The results of the analysis of yield and some quality parameters of lettuce depending on the experimental treatment are given in Table 1.

As presented in Table 1, the partial replacement of fertilizer by pyrophyllite did not negatively affect the yield and quality compared to the control treatment. Moreover, the yield and examined lettuce quality parameters were mainly higher in the treatment where the pyrophyllite was applied as a replacement for a part of the fertilizer. The highest yield was obtained in treatment 2 and 3 where pyrophyllite was applied as a replacement for 25% of recommended fertilizer rate. The data in Table 1 also indicate that all treatments with pyrophyllite increase the antioxidant capacity of lettuce, especially where pyrophyllite (particle size 0.1 mm) was applied as a replacement for 75% of recommended fertilizer rate.

Heavy metal contents (Zn, Cu, Mn, Ni, Cr, Pb) in the plant samples depending on the experimental treatment are presented in Table 2. Presented data have shown that the content of Zn, Cu, Ni, Cr and Pb in lettuce was below the maximum permissible value of heavy metals in food crops reported by FAO/WHO (2001). Accordingly, the maximum permissible value for Zn, Cu, Ni and Cr is 100 mg/kg, 40 mg/kg, 4 mg/kg and 2.3 mg/kg on dry weight basis, respectively. Upper limits of Pb in edible products is regulated by EU Legislation (2011). Accordingly, Pb threshold limit for lettuce is 3.6 mg/g on dry mass basis.

DISCUSSION

The results of this study showed that the substitution of fertilizers with pyrophyllite in amount of 25% and 50% of recommended fertilizer rate increase lettuce yield compared to the yield achieved in the control treatment, i.e. 100% NPK recommended rate. Only the treatments where the pyrophyllite was applied as a replacement for 75% of recommended fertilizer rate did not show a positive effect on lettuce yield. The above-mentioned results indicate that pyrophyllite may increase soil's ability to hold and slow release of nutrients, thus preventing fertilizer leaching. Consistently, the inclusion of the pyrophyllite in fertilizer management can play a significant role in food crops production as a soil conditioner for improving fertilizer efficiency.

Mukherjee (2013) noted that the increase in crop yield due to the pyrophyllite addition in soil is result of its ability to release the tightly bound phosphates already existing in the soil making them available for plants. At the same time, pyrophyllite contains certain amounts of potassium, calcium, magnesium and iron, contributing significantly to the plant growth and development.

The results of this study also showed that treatments with pyrophyllite, to a greater or lesser extent, increase the content of phenolics and antioxidant capacity of lettuce, especially where pyrophyllite (particle size 0.1 mm) was applied as a replacement for 75% of recommended fertilizer rate. We assume that the lettuce in treatments where pyrophyllite was applied as a partial replacement for fertilizer had a lower amount of available nutrients in the soil resulting in its temporary stress, and consequently in higher synthesis of phenolics and other antioxidants. Relationship between treatment with pyrophyllite and ascorbic acid content in lettuce in the present study was not observed.

Table 1: Yield, ascorbic acid content (AA), total phenolic content (TPC) and total antioxidant capacity (TAC) in lettuce.

Treatment[1]	Yield (kg/m^2)	AA (mg/100 g)	TPC (mg/100 g)	TAC μmol Fe^{2+}/100 g
T_1	7.00 ± 1.47^{d}	12.88 ± 8.31	6.13 ± 13.61^{d}	109.47 ± 76.93^{c}
T_2	9.57 ± 1.28^{ab}	15.97 ± 8.31	18.46 ± 29.13^{bc}	188.84 ± 195.69^{bc}
T_3	9.74 ± 0.50^{a}	12.28 ± 4.75	30.56 ± 8.84^{ab}	263.78 ± 241.65^{ab}
T_4	9.08 ± 1.31^{abc}	15.89 ± 8.31	8.05 ± 5.85^{d}	157.77 ± 103.25^{bc}
T_5	7.46 ± 1.65^{d}	14.58 ± 4.26	9.93 ± 3.63^{d}	182.50 ± 50.35^{bc}
T_6	6.82 ± 2.62^{d}	12.20 ± 7.32	8.24 ± 4.49^{d}	145.07 ± 154.71^{bc}
T_7	6.86 ± 0.14^{d}	13.88 ± 8.31	39.00 ± 17.77^{a}	365.80 ± 166.83^{a}
$LSD_{0.05}$	1.34	-	13.52	125.57

* Means denoted by the same letter indicate no significant difference ($P \leq 0.05$)

[1] Experimental treatment: T_1 - recommended fertilizer rate (RFR) without pyrophyllite (PP), i.e. control treatment; T_2 - 25% of RFR was replaced with PP (3 mm); T_3 - 25% of RFR was replaced with PP (0.1 mm); T_4 - 50% of RFR was replaced with PP (3 mm); T_5 - 50% of RFR was replaced with PP (0.1 mm); T_6 - 75% of RFR was replaced with PP (3 mm); T_7 - 75% of RFR was replaced with PP (0.1 mm)

Table 2: Heavy metal contents in lettuce (mg/kg dry mass).

Treatment[1]	Zn	Cu	Ni	Cr	Pb
T_1	74.2 ± 14.2^{abcd}	3.71 ± 0.7^{a}	1.88 ± 0.6	2.0 ± 1.2	3.28 ± 1.4^{a}
T_2	78.4 ± 9.1^{a}	3.39 ± 0.9^{abc}	1.39 ± 0.8	1.9 ± 1.1	3.23 ± 2.8^{ab}
T_3	58.0 ± 13.2^{e}	3.69 ± 0.9^{ab}	1.22 ± 0.4	2.5 ± 1.5	2.55 ± 0.2^{abc}
T_4	76.6 ± 11.4^{abc}	3.32 ± 1.2^{abcd}	1.51 ± 0.2	1.9 ± 0.4	2.0 ± 0.9^{abcd}
T_5	77.8 ± 11.5^{ab}	3.3 ± 0.5^{abcde}	1.69 ± 0.6	1.2 ± 0.4	2.0 ± 1.9^{abcde}
T_6	51.3 ± 12.1^{ef}	2.7 ± 0.7^{cdef}	1.12 ± 0.2	2.2 ± 0.8	0.77 ± 1.2^{def}
T_7	42.4 ± 15.2^{f}	2.2 ± 1.3^{f}	1.41 ± 1.3	1.6 ± 0.3	0.46 ± 0.1^{f}
$LSD_{0.05}$	11.81	0.91	-	-	1.34

* Means denoted by the same letter indicate no significant difference ($P \leq 0.05$)

[1] Experimental treatment: T_1 - recommended fertilizer rate (RFR) without pyrophyllite (PP), i.e. control treatment; T_2 - 25% of RFR was replaced with PP (3 mm); T_3 - 25% of RFR was replaced with PP (0.1 mm); T_4 - 50% of RFR was replaced with PP (3 mm); T_5 - 50% of RFR was replaced with PP (0.1 mm); T_6 - 75% of RFR was replaced with PP (3 mm); T_7 - 75% of RFR was replaced with PP (0.1 mm)

Another important effect of pyrophyllite is related to the removal of toxic heavy metals from soil (Prasad & Saxena 2008) and results of the present study support this hypothesis. Namely, the content of all examined heavy metals in lettuce in treatments with pyrophyllite was lower compared to the content of heavy metals in lettuce obtained in the control treatment. These differences between treatments were not only significant for the content of Cr and Ni in lettuce. We assume that the reason for that was the high content of Cr and Ni in the studied soil and therefore the amount of applied pyrophyllite was not adequate to significantly reduce mobility of Cr and Ni in the soil and thus their availability to plants. Namely, the average content of Ni and Cr in studied soil was 104.55 mg/kg and 128.48 mg/kg, respectively. These values greatly exceeded the limit value prescribed by legislation in Bosnia and Herzegovina (Official Gazette of FBIH 2009) or by legislation in some European countries (Pérez et al. 2002). Accordingly, the maximum permissible value for Ni and Cr in soil is 40 mg/kg and 100 mg/kg, respectively.

Many scientists agree that the ability of clay minerals to decrease the mobility of heavy metals in soils is the result of adsorption of heavy metals in their interlayers or on its surface areas (Ijagbemi et al. 2009, Khan & Singh 2010, Ararem et al. 2011, Demirkiran et al. 2016) but this adsorption mechanism is still not fully understood. Some clay minerals that have high cation exchange capacity, i.e. montmorillonite and bentonite in principle achieve this effect through ion exchange reaction (Önal 2007, Wigger & Loon 2017). The cation exchange capacity for pyrophyllite is lower, but not its efficiency in removing heavy metals from the soil, and results of many studies confirm this hypothesis (Scheidegger et al. 1996, Caporale & Vioalante 2016, Uddin 2017). Bergaya et al. (2006) reported that pyrophyllite has ability to easily disperse in water due to weak van der Waals bounds, resulting in less clumping. This dispersing property allows higher exposure area for pyrophyllite in soil

and therefore more heavy metals or other pollutants could potentially be absorbed and thus neutralized. Furthermore, pyrophyllite contributes to the increase of soil pH, resulting in lower mobility and thus the availability of heavy metals for plant.

In general, the results of this study indicate that the application of pyrophyllite under experimental conditions can reduce the use of mineral fertilizers in lettuce production without adverse effects on its yield and quality, especially where the pyrophyllite is applied in the amount of 25% of recommended fertilizer rate. The results of this study also support the hypothesis that pyrophyllite could be used as the resort to help clean up the soils from the damage caused by heavy metal pollution.

REFERENCES

AOAC 2006. Vitamin C in juices and vitamin preparations, method 967.21. In: AOAC Intl. (ed.) Official Methods of Analysis (ed.) Arlington, USA.

Ararem, A., Bouras, O. and Arbaoui, F. 2011. Adsorption of caesium from aqueous solution on binary mixture of iron pillared layered montmorillonite and goethite. Chem. Eng. J., 172(1): 230-236.

Benzie, I.F. and Strain J.J. 1996. Ferric reducing ability of plasma (FRAP) as a measure of antioxidant power: The FRAP assay. Anal. Biochem., 239(1): 70-76.

Bergaya, F., Theng, B.K.G. and Lagaly, G. 2006. Handbook of Clay Science. Elsevier, Amsterdam, London, pp. 231-296.

Caporale A.G. and Vioalante, A. 2016. Chemical processes affecting the mobility of heavy metals and metalloids in soil environments. Current Pollution Reports, 2(1): 15-27.

Demirkiran, A.R., Acemioglu, B. and Gonen, T. 2016. Sorption of copper and nickel ions from solution by clay minerals. Oxid. Commun., 39(1): 817-829.

Drits, V.A., Guggenheim, S., Zviagina, B.B. and Kogure, T. 2012. Structures of the 2:1 layers of pyrophyllite and talc. Clays Clay Miner., 60(6): 574-587.

EU 2011. Commission Regulation (EU) No 420/2011 of 29 April 2011 amending Regulation (EC) No. 1881/2006 setting maximum levels for certain contaminants in foodstuffs. Available online: https://www.fsai.ie/uploadedFiles/Reg420_2011.pdf

FAO 2014. World Reference Base for Soil Resources. Available online: http://www.fao.org/3/i3794en/I3794en.pdf

FAO/WHO 2001. Report on the 32nd Session of the Codex Committee on Food Additives and Contaminants, Codex Alimentarius Commission, Geneva, Switzerland.

Ghazavi, R. 2015. The application effects of natural zeolite on soil runoff, soil drainage and some chemical soil properties in arid land area. International Journal of Innovation and Scientific Research, 13(1): 172-177.

Gomiero, T. 2016. Soil degradation, land scarcity and food security: reviewing a complex challenge. Sustainability, 8(3): 1-41.

Ijagbemi, C.O., Baek, M.H. and Kim D.S. 2009. Montmorillonite surface properties and sorption characteristics for heavy metal removal from aqueous solutions. J. Hazard. Mater., 166(1): 538-546.

ISO 1998. International Standard ISO 11047: Soil quality determination of cadmium, chromium, cobalt, copper, lead, manganese, nickel and zinc- Flame and electrothermal atomic absorption spectrometric methods. International Organization for Standardization, Geneva, Switzerland.

Jakkula, V.S. and Wani, S.P. 2018. Zeolites: Potential soil amendments for improving nutrient and water use efficiency and agriculture productivity. Sci. Revs. Chem. Commun., 8(1): 119.

Khan, T.A. and Singh, V.V. 2010. Removal of cadmium (II), lead (II), and chromium (VI) ions from aqueous solution using clay. Toxicol. Environ. Chem., 92(8): 1435-1446.

Lal, R. 2015. Restoring soil quality to mitigate soil degradation. Sustainability, 7(5): 5875-5895.

Lisjak, M., Spoljarevic, M., Agic, D. and Andric, L. 2009. Practicum-Plant Physiology. Joseph George Strossmayer University of Osijek, pp. 24-25.

Mukherjee, S. 2013. The Science of Clays: Applications in Industry, Engineering, and Environment. Springer, New York, USA, pp. 54-68.

Official Gazette of FBiH 2009. Rulebook on determination of allowable quantities of harmful and hazardous substances in soils of Federation of Bosnia and Herzegovina and methods for their testing, No. 72/09. Edit. Official Gazette of FBiH, Sarajevo, Bosnia and Herzegovina. Available online: http://www.fzofbih.org.ba/userfiles/file/izmj_zakon_otpad.pdf

Önal, M. 2007. Swelling and cation exchange capacity relationship for the samples obtained from a bentonite by acid activations and heat treatments. Appl. Clay Sci., 37(1-2): 74-80.

Ough, C.S. and Amerine, M.A. 1988. Phenolic compounds. In: Wiley (ed.) Methods for Analysis of Must and Wines. New York, USA.

Pérez, C., Martínez, M.J., Vidal, J. and Navarro, C. 2002. Proposed reference values for heavy metals in calcaric fluvisols of the Huerta de Murcia (SE Spain). In: Quaderna Editorial (ed.) Sustainable Use and Management of Soils in Arid and Semiarid Regions. Cartagena, Murcia, Spain, pp. 495-496.

Prasad, M. and Saxena, S. 2008. Attenuation of divalent toxic metal ions using natural sericitic pyrophyllite. J. Environ. Manage., 88(4): 1273-1279.

Rubel, F. and Kottek, M. 2010. Observed and projected climate shifts 1901-2100 depicted by world maps of the Köppen-Geiger climate classification. Meteorol. Z., 19(2): 135-141.

Scheidegger, A.M., Sparks, D.L. and Fendorf, M. 1996. Mechanisms of nickel sorption on pyrophyllite: macroscopic and microscopic approaches. Soil Sci. Soc. Am. J., 60(6): 1763-1772.

Uddin, M.K. 2017. A review on the adsorption of heavy metals by clay minerals, with special focus on the past decade. Chem. Eng. J., 308: 438-462.

Wigger, C. and Loon, L.R.V. 2017. Importance of interlayer equivalent pores for anion diffusion in clay-rich sedimentary rocks. Environ. Sci. Technol., 51(4): 1998-2006.

Nature Environment and Pollution Technology
An International Quarterly Scientific Journal

p-ISSN: 0972-6268
e-ISSN: 2395-3454

Vol. 19 | No. 1 | pp. 361-365 | 2020

Original Research Paper | Open Access

Nutrient Limit Estimation for Eutrophication Modelling at Sengguruh Reservoir, Malang, Indonesia

Evellin Dewi Lusiana*(**)†, Nanik Retno Buwono*(**), Mohammad Mahmudi*(**) and Pramunita Putri Noviasari*
*Department of Water Resources Management, Faculty of Fisheries and Marine Science, Universitas Brawijaya, Malang 65138, Indonesia
**AquaRES Research Group, Universitas Brawijaya, Malang 65138, Indonesia
†Corresponding author: Evellin Dewi Lusiana

Nat. Env. & Poll. Tech.
Website: www.neptjournal.com

Received: 30-04-2019
Accepted: 22-07-2019

Key Words:
Trophic status
TSI method
Nutrient limit
Quantile regression

ABSTRACT

Sengguruh Reservoir located in Malang Regency has important function as sediment barriers for Sutami Reservoir. The water contains many organic matters that will cause eutrophication. The effect of eutrophication can reduce the biodiversity in the reservoir. The purpose of this study is to identify the trophic status of Sengguruh Reservoir using TSI method and to estimate the nutrient limit (nitrate and phosphate) to predict the eutrophication using quantile regression approach. The results show that Sengguruh Reservoir is in heavy eutrophic state. On the other hand, the nutrient limit estimation to predict heavy eutrophication is at 0.853 mg/L for nitrate and 0.862 mg/L for phosphate.

INTRODUCTION

Aquatic ecosystems can be divided into natural and artificial waters. The artificial waters were usually built for many purposes such as irrigation, power generation, navigation, flood control, water supply, and recreation. Reservoir is one example of artificial waters which is made by damming rivers, and has distinguished characteristics where it receives waters continuously from the rivers that are embodied with organic and inorganic matters. Moreover, they also contain fertilizer residues from agricultural activities and lead to nutrient (nitrogen and phosphorus) enrichment that is affecting phytoplankton community (Sugiura et al. 2004, Suryanto 2011).

Sengguruh reservoir is located in Malang regency, in the lower reaches of the Brantas River and Lesti River; also, at the end of the Sutami Reservoir inundation area. It is categorized as a multipurpose reservoir which aims to meet the availability of irrigation water, power plant, and the most important function as a sediment barrier that enters the Sutami Reservoir. Sedimentation in Sengguruh Reservoir increases every year. Since 2000, there is significant rise in population and industry around the reservoir area which result into the increasing of water use and pollution, especially by organic pollutants from domestic and industry wastes (Yetti 2007).

As an aquatic ecosystem, Sengguruh Reservoir contains high biodiversity because it is the habitation for aquatic organisms. The addition of organic matters in aquatic ecosystem can boost the nutrient (nitrogen and phosphorus) enrichment, and at any level results into eutrophication. The phenomenon of eutrophication brings negative effects for aquatic ecosystems such as mass mortalities of aquatic organisms and creating a dead zone where no organisms can survive. Thus, the biodiversity will reduce (Isnaini et al. 2014, Paiki & Kalor 2017, Putri et al. 2014, Rashidy et al. 2013, Widyastuti et al. 2015). Therefore, in order to prevent the eutrophication, it can be sought through making an observation to nutrient concentration in the waters. The estimation of nutrient limit that may cause eutrophication can be performed by use of quantile regression. The method has advantages to model the relationship between nutrient concentrations thoroughly, not only at mean level of response variable as in linear regression (Lusiana et al. 2019, Xu et al. 2015, Yu & Moyeed 2001).

The purpose of this study is to identify the eutrophication state of Sengguruh Reservoir by using Trophic State Index (TSI) and estimating the nutrient limit as the indicators to predict the eutrophication. Since this study concerns to the high abundance of phytoplankton which indicates eutrophication, then the relationship between nutrient and phytoplankton abundance will be modelled at upper quantile. The index was introduced by Carlson (1977) and has been widely used to assess the trophic status of many lakes and reservoirs (Bekteshi & Cupi 2014).

MATERIALS AND METHODS

The research was conducted in Sengguruh Reservoir located in Kepanjen District, Malang. The sampling locations consist of four sites, they are (1) inlet from Brantas River; (2) inlet from Lesti River; (3) inner part of reservoir; (4) outlet or water exit which nears to residential area, power generating plant, and aquacultures. The study area can be seen in Fig. 1. The data were collected in January-February 2018.

The observed variables in this study are chlorophyll-*a* (mg/m^3), total phosphate (mg/L), visibility (m), phytoplankton abundance (ind/mL), orthophosphate (mg/L), and nitrate (mg/L). The first three variables were used to determine the trophic status of Sengguruh Reservoir using TSI method. Meanwhile, orthophosphate and nitrate, known as nutrients, in aquatic ecosystem become the predictors for phytoplankton abundance in order to estimate the nutrient limit for predicting eutrophication by modelling using quantile regression approach.

TSI Method

Trophic State Index (TSI) is the indicator of aquatic ecosystem fertility through algae biomass. The algae biomass estimates through chlorophyll-*a*, Secchi disc depth or visibility, and total phosphate. TSI ranged from 0 to 100. Trophic status classification using TSI is presented in Table 1 (Carlson 1977).

TSI score can be calculated using formula in equation (1)

$$TSI(SD) = 60 - 14.41 \ln (SD)$$

$$TSI(CHL) = 30.6 + 9.81 \ln (CHL)$$

$$TSI(TP) = 4.15 + 14.42 \ln (TP)$$

$$TSI = \frac{TSI(SD) + TSI(CHL) + TSI(TP)}{3} \quad \ldots(1)$$

Where,

SD = Secchi disc depth (m)

CHL = Chlorophyll-*a* (µg/L)

TP = Total phosphate (µg/L)

Quantile Regression

Quantile regression is a method to analyse relationship between variables at various quantile of the response variable (Koenker & Hallock 2001). Equation (2) shows the general

Fig. 1: Sampling location in Sengguruh reservoir.

Table 1: TSI score classification.

Score	Trophic State
<30	Ultraoligotrophic
30 – 40	Oligotrophic
40 – 50	Meso-trophic
50 – 60	Light Eutrophic
60 – 70	Medium Eutrophic
70 – 80	Heavy Eutrophic
>80	Hyper-eutrophic

form of quantile regression model (Buhai 2005).

$$y_i = \mathbf{x}_i^t \beta(\theta) + e(\theta)_i \quad 0 < \theta < 1 \qquad \ldots(2)$$

Where,

y_i = response variable of the ith observation

$\mathbf{x}_i^t = \left(1, x_{1i}, x_{2i}, ..., x_{pi}\right)$

$\beta(\theta)$ = parameter regression at the θ^{th} quantile

$e(\theta)_i$ = error/residual model of the θ^{th} quantile

i = 1, 2, ..., n

According to Koenker & Basset (1978), parameter estimation of equation (3) and (4) is the solution of minimization.

$$\min_{\beta \in \mathbb{R}^p} \left[\sum_{i \in \{i: y_i \geq \mathbf{x}_i' \beta\}} \theta \left| y_i - f(\mathbf{x}_i) \right| + \sum_{i \in \{i: y_i < \mathbf{x}_i' \beta\}} (1-\theta) \left| y_i - f(\mathbf{x}_i) \right| \right] \qquad \ldots(3)$$

$$\min_{\beta \in \mathbb{R}^p} \left[\sum_{i \in \{i: y_i \geq \mathbf{x}_i' \beta\}} r_\theta \left(y_i - f(\mathbf{x}_i) \right) \right] \qquad \ldots(4)$$

$r_\theta(u) = (\theta - 1_{\{u<0\}})u$, is called as *check function* which is illustrated in Fig. 2.

According to Chen (2005), equation (4) does not have fixed derivative form, so that a common numerical iteration cannot be performed to obtain the parameter estimation. Thus, an alternative method of linear programming was considered namely simplex method.

RESULTS AND DISCUSSION

Trophic Status of Sengguruh Reservoir

The TSI scores of each sampling site in Sengguruh Reservoir are given in Table 2.

According to Table 2, it can be seen that the TSI scores of the four sampling sites in Sengguruh Reservoir are between 68.64 and 74.35. It means that the trophic status is categorized as medium eutrophic and heavy eutrophic, but mostly the status is heavy eutrophic. These results show that the TSI score for medium eutrophic almost reach the upper limit for this category. So, on the whole, the eutrophication status in Sengguruh Reservoir is heavy eutrophic.

The status indicates that Sengguruh Reservoir has high fertility and this condition can reduce fishery production and biodiversity. The increase of fertility in aquatic ecosystem due to nutrient enrichment by the addition of organic matters into waters. According to Firdaus (2015), there is a tendency of land use changes and use of natural resources that do not consider aspects of soil and water conservation around the upstream Brantas River (Site 1) and Lesti River (Site 2) which cause the decline in watershed function, specifically

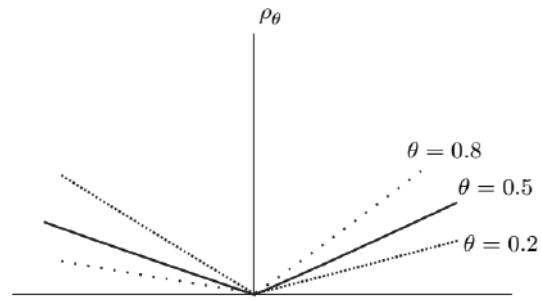

Fig. 2: Check function.

Table 2: Result of TSI Scores in Sengguruh Reservoir.

Site	Week	TSI Scores	Remarks
1	1	71.1025	Heavy eutrophic
	2	73.2234	Heavy eutrophic
	3	72.269	Heavy eutrophic
2	1	69.805	Medium eutrophic
	2	74.0642	Heavy eutrophic
	3	72.0439	Heavy eutrophic
3	1	68.6458	Medium eutrophic
	2	74.2981	Heavy eutrophic
	3	73.8333	Heavy eutrophic
4	1	70.5054	Heavy eutrophic
	2	74.3593	Heavy eutrophic
	3	73.864	Heavy eutrophic

to hold sediment materials.

As the consequence, the water entry of Brantas River and Lesti River into Sengguruh Reservoir embodied by a lot of sediments and organic matters as the result of domestic and agricultural wastes. Moreover, the residential areas and aquaculture activities (Site 4) around the Sengguruh Reservoir also contribute to the accumulation of sediment and organic matter in the waters. Especially, the use of fertilizer in agricultural activities and fish feed residues in aquaculture activities that contain nitrogen and phosphate may result in nutrient enrichment in the reservoir ecosystem.

Eutrophication Model

Eutrophication predictive model through nitrate and phosphate concentration in Sengguruh Reservoir as the predictors conducted using quantile regression. The scatterplot to describe the relationship between nutrients and phytoplankton abundance is shown in Fig. 3.

Fig. 3(a) reveals that the relationship between nitrate and phytoplankton abundance is not uniform of each quantile. Negative relationship was found in quantile 0.25 and 0.75, and the rest quantiles showed positive relationship. Meanwhile in Fig. 3b, the positive relationship carried out on quantile 0.25 and 0.75, but the remaining quantiles have negative relationship. The positive relationships of the variables explain that the increasing of nutrient content will result in the higher abundance of phytoplankton. This finding is relevant to the eutrophication theory due to nutrient enrichment. However, in some quantiles, the relationship is negative or in other words the increase of nutrient will cause the phytoplankton abundance to decrease instead.

According to Table 2, current Sengguruh Reservoir is in heavy eutrophic state. It means that the eutrophication modelling at high quantile ($\theta = 0.95$) level will be used to predict heavy eutrophication. The parameter estimates of quantile regression are presented in Table 3.

Based on Table 3, nitrate and phosphate concentration of 0.853 mg/L and 0.862 mg/L respectively will cause medium eutrophication in Sengguruh Reservoir. If the results compared are to Wetzel (2001), then such concentration of nitrate and phosphate indicate the that the water is oligotrophic. These findings indicate that the classification cannot be used to identify the eutrophication in Sengguruh Reservoir since the sedimentation has been too high, and moreover a bit increase of nutrients will boost the abundance of phytoplankton.

CONCLUSION

Trophic status of Sengguruh Reservoir is classified as heavily eutrophic. The level of nitrate concentration to predict the heavy eutrophication is 0.853 mg/L, and phosphate is 0.862 mg/L. This result indicates that when the measurement of

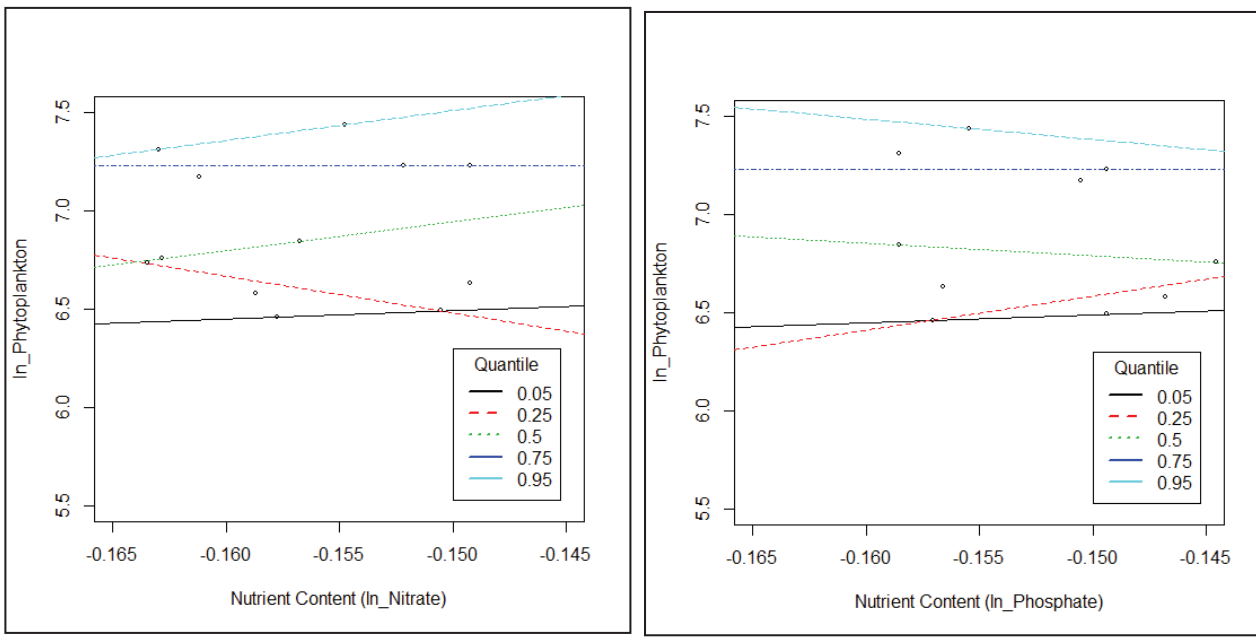

(a) (b)

Fig. 3: Scatterplot of phytoplankton abundance with quantile lines (a) nitrate; (b) phosphate.

Table 3: Parameter estimates of quantile regression.

Quantile	Phytoplankton-abundance (ind/mL)	Parameter estimates			
		Nitrate		Phosphate	
		Intercept	Slope	Intercept	Slope
0.05	650.92	7.137	4.282	7.092	4.012
0.25	749.80	3.687	-18.637	9.199	17.428
0.50	899.11	9.140	14.636	5.839	-6.349
0.75	1380.00	7.230	0.000	7.230	0.000
0.95	1586.91	9.799	15.254	5.849	-10.224

nitrate and phosphate almost reach such concentrations, then handling action must be carried out in order to prevent heavy eutrophication.

ACKNOWLEDGEMENTS

This research was funded through Hibah Peneliti Pemula (HPP) of Brawijaya University in 2019. The authors would like to thank all those who helped to complete the research.

REFERENCES

Bekteshi, A. and Cupi, A. 2014. Use of Trophic State Index (Carlson, 1977) for assessment of trophic status of the Shkodra Lake. Journal of Environmental Protection and Ecology, 15(1): 359-365.

Buhai, I.S. 2005. Quantile regression: Overview and selected applications. Ad Astra, 4: 1-17.

Carlson, R.E. 1977. A trophic state index for lakes. Limnology and Oceanography, 22(2): 361-369.

Chen, C. 2005. An Introduction to Quantile Regression and The QUANTREG Procedure. Retrieved October 20th, 2014, from http://www2.sas.com/proceedingd/sugi30/213-30.pdf

Firdaus, M.R. 2015. Analisis Sedimentasi DAS Lesti dengan Perubahan Tata Guna Lahan di Kabupaten Malang. Rekayasa Sipil, 3(1): 19-28.

Isnaini, Surbakti, H. and Aryawati, R. 2014. Komposisi dan Kelimpahan Fitoplankton di Perairan Sekitar Pulau Maspari, Ogan Komering Ilir. Maspari Journal, 6(1): 39-45.

Koenker, R. and Basset, G. 1978. Regression Quantiles. Econometrica, 46: 33-50.

Koenker, R. and Hallock, K. 2001. Quantile regressions. Journal of Economic Perspectives, 15: 143-156.

Lusiana, E.D., Arsad, S., Kusriani, Buwono, N.R. and Putri, I.R. 2019. The application of Bayesian quantile regression to analyse the relationship between nutrients content and phytoplankton abundance in Sutami reservoir. IOP Conference Series: Earth and Environmental Science, 230: 1-5.

Paiki, K. and Kalor, J.D. 2017. Distribusi Nitrat dan Fosfat Terhadap Kelimpahan Fitoplankton di Perairan Pesisir Yapen Timur. Journal of Fisheries and Marine Science, 1: 65-71.

Putri, F.D.M., Widyastuti, E. and Christiani 2014. Hubungan Perbandingan Total Nitrogen dan Total Fosfor dengan Kelimpahan Fitoplankton di Perairan Waduk Panglima Besar Soedirman, Banjarnegara. Scripta Biologica, 1: 96-101.

Rashidy, E.A., Litaay, M., Salam, M.A. and Umar, M.R. 2013. Komposisi dan Kelimpahan Fitoplankton Di Perairan Pantai Kelurahan Tekolabbua, Kecamatan Pangkajene, Kabupaten Pangkep, Provinsi Sulawesi Selatan. Jurnal Alam dan Lingkungan, 4(7): 1-6.

Sugiura, N., Utsumi, M., Wei, B., Iwami, N., Okano, K., Kawauchi, Y. and Maekawa, T. 2004. Assessment for the complicated occurence of nuisance odours from phytoplankton and environmental factors in a eutrophic lake. Lake & Reservoirs: Res. and Man, 9: 195-201.

Suryanto, A.M. 2011. Abundance and phytoplankton composition in Selorejo Reservoir, Ngantang District, Malang Regency. Jurnal Kelautan, 4(2): 34-39.

Wetzel, R.G. 2001. Limnology: Lake and River Ecosystems. Elsevier Academic Press, New York.

Widyastuti, E., Sukanto and Setyaningrum, N. 2015. Pengaruh Limbah Organik terhadap Status Tropik, Rasio N/P serta Kelimpahan Fitoplankton di Waduk Panglima Besar Soedirman Kabupaten Banjarnegara. Biosfera, 32(1): 36-40.

Xu, Y., Schroth, A., Isles, P. and Rizzo, D. 2015. Quantile regression improves models of lake eutrophication with implications for ecosystems-specific management. Freshwater Biology, 60: 1841-1853.

Yetti, E. 2007. Evaluasi Kualitas Air Sungai-sungai di Kawasan DAS Brantas Hulu Malang dalam Kaitannya dengan Tata Guna Lahan dan Aktivitas di Sekitarnya. (Post Graduate), Institut Pertanian Bogor, Bogor.

Yu, K. and Moyeed, R.A. 2001. Bayesian quantile regression. Statistics and Probability Letters, 54: 437-447.

Nature Environment and Pollution Technology
An International Quarterly Scientific Journal

p-ISSN: 0972-6268
e-ISSN: 2395-3454

Vol. 19 | No. 1 | pp. 367-372 | 2020

Original Research Paper | Open Access

Concrete Construction Waste Pollution and Relevant Prefabricated Recycling Measures

Zhang Jie† and Chen Nan
Department of Architectural Engineering, Jiyuan Vocational and Technical College, Jiyuan 459000, China
†Corresponding author: Zhang Jie

Nat. Env. & Poll. Tech.
Website: www.neptjournal.com

Received: 10-12-2019
Accepted: 16-01-2020

Key Words:
Concrete architecture
Construction waste
Waste pollution
Recycling measures

ABSTRACT

Architectural construction has expanded continuously in recent years as a response to China's accelerating urbanization, thus further leading to the dramatic increase of concrete usage. This expansion may cause serious threats to the ecological environment because the production and construction of traditional concrete materials may consume abundant resources, such as coals and limestone, and thus emit air pollutants. Prefabricated concrete building can significantly reduce the use of water, timber, thermal insulation materials, and cement mortar, thereby decreasing construction waste and carbon emissions greatly. Based on the review of the measures for concrete construction waste recycling in developed countries, this study summarized the types of hazards of concrete construction waste pollution, analysed the advantages of prefabricated concrete constructions, and proposed prefabricated recycling measures of concrete construction wastes. Results demonstrate that developed countries have relatively perfect concrete construction waste recycling systems. The hazards of concrete construction wastes are mainly manifested by the embezzlement of lands, water pollution, atmosphere pollution, soil pollution, and damage to physical health. The advantages of prefabricated concrete construction are manifested by high production efficiency, energy conservation, environmental protection, and overall high quality. Finally, several recycling measures were proposed, including strengthened policy support to prefabricated concrete construction; appropriate relevant laws, regulations, and standard systems; improved prefabricated construction enterprises; and enhanced environmental protection in prefabricated construction sites. Research conclusions can serve as reference for understanding the hazards of concrete construction-induced environmental pollution, recognizing the advantages of prefabricated concrete construction mode, increasing prefabricated concrete market shares comprehensively, and alleviating environmental pollutions.

INTRODUCTION

China's construction industry improves residents' quality of life and drives the growth of GDP (Gross Domestic Product). The sustainable, sound development of construction industry is vital to the development of China. Construction waste refers to the waste soil and other materials produced by construction companies and units during new construction, reconstruction, expansion, and demolishment of various buildings, structures, and pipe networks and by residents during home decoration. Currently, the construction wastes in urban areas in China are a major proportion of the total urban waste. If these construction wastes cannot be recycled reasonably, then they would increase continuously, and their proportion in the total urban waste may further increase with the China's continuous urbanization. Muck, waste concrete blocks, waste mortar, brick fragments, cullets, tile fragments, waste asphalt blocks, waste plastics, waste metals, and waste bamboo and timber materials are the major components of construction wastes. Most construction wastes, especially concrete construction wastes from demolishing buildings, can be recycled after screening, deletion, or smashing. Currently, the majority of concrete construction wastes in China are not reused. Instead, concrete construction wastes are transported to suburbs or rural areas and disposed in dump sites or landfills in open spaces, thus causing serious hazards to the ecological environment.

China's construction industry has recently achieved rapid development. Fig. 1 shows that the total output of China's construction industry rose from 6,203.681 billion Yuan in 2008 to 23,508.553 billion Yuan in 2018, showing an annual average growth of 28%. The building area of China's construction industry increased from 5,305,186,300 m^2 in 2008 to 14,089,204,000 m^2 in 2018, showing an annual average growth rate of 17%. These numbers fully reflect the considerable consumption of basic materials, such as concrete, in China's construction industry, resulting in massive amounts of construction wastes. However, the traditional dump sites or landfills of concrete construction wastes may occupy

large areas of cultivated land. Moreover, long-term piling or landfills of concrete construction wastes may cause soil, underwater, and atmosphere pollution. In addition, concrete construction wastes are generally transported by open vehicles. Waste leakage, dusts, and lime sands may influence urban appearance and environmental health seriously and bring serious threats to the production and life of residents during transport. To sum up, the existing disposal means of concrete construction wastes cannot satisfy the needs of sustainable urban development, and the recycling of concrete construction wastes is essential in realizing the sustainable development of China's construction industry and a harmonious ecological environment.

PAST STUDIES

With the strengthening of environmental protection and resource saving consciousness, countries worldwide are enhancing the recycling of urban construction wastes. Many studies and applications on recycling technologies for construction wastes have been undertaken. Developed countries, such as US, Germany, and Japan, have achieved high construction waste recycling rates, whereas the recycling rate of construction wastes in China remains low. Hsiao et al. believed that the concrete logistics amount produced by new construction and demolishment projects was increasing dramatically in Taiwan. They simulated concrete wastes in the material flow based on a dynamic model and found that the concrete construction wastes were expected to increase continuously. Concrete construction waste recycling must be increased comprehensively to decrease the environmental pollution in Taiwan (Hsiao et al. 2002). Gotoh et al. analysed the total suspended particulates concentration in regions damaged seriously during the Hanshin Earthquake and found that the elements in the concrete dusts (Ca and S) in construction wastes are similar to those in mortar dust, which is one of the major sources of air pollution (Gotoh et al. 2002). Andersson M. et al. studied polychlorinated biphenyl (PCB) pollution in gypsum on the external building walls in Bergen, Norway and reported that the PCB concentration in soil and plaster of residential buildings and schools was higher than those in office buildings, warehouses, or industrial buildings (Andersson et al. 2004). Lindgren investigated a concrete contamination indoor ammonia event in an office of one airline in Beijing and found that the ammonium hydroxide pollution in the Beijing Office might come from the additives in concretes (Lindgren 2010). Taylor-Lange et al. predicted the specific activity of radium and the probability of radon precipitation through Monte Carlo simulation and estimated the indoor radon concentration and the effective annual dose under two different concrete floors (one has fly ash, whereas the other has no fly ash) in a typical single-family house in the US. Their results show that exposure to radon in concrete buildings could influence human health significantly (Taylor-Lange et al. 2012). Arunvivek et al. believed that commercial concrete industries worldwide are producing abundant wastewater and fresh concrete waste aggregate, which may cause serious environmental pollution upon improper disposal (Arunvivek et al. 2015). Wu et al. believed that the accelerating modern industrialization and urbanization in China might cause construction dust emission. He investigated the current dust control situations in China's construction industry, determined the main sources of construction dust, and proposed a case study to interpret the major dust control measures in construction sites (Wu et al. 2016). With respect to the recycling measures of concrete construction wastes, Eguchi et al. proposed a concrete recycling method that was different from that of

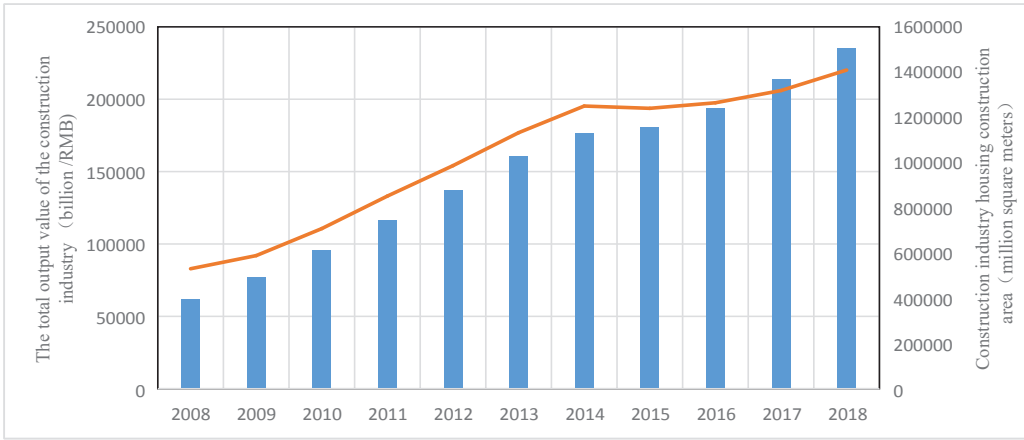

Fig. 1: Total output and building areas of China's construction industry during 2008-2018. (Data source: China Statistical Yearbook 2009-2019).

ordinary concrete, thus obtaining data needed to determine the mixing ratio design and the quality control method. The economic efficiency and environmental loads of this method were assessed, and the validity of this method was verified (Eguchi et al. 2007). Rao et al. reviewed the international production of C&D wastes and the utilization of recycled aggregates (RAs) and summarized influences of RA use on fresh and hardened concretes' performance (Rao et al. 2007). Tam believed that construction materials were poured to landfills, and abundant wastes might be produced from construction sites. As a method of reducing concrete wastes, using recycled concrete wastes as RA can be an economical and effective method for China's construction industry; this method is also conducive to environmental protection (Tam 2008). Naik believed that Portland cement is an important component of concrete, and abundant greenhouse gas, that is, CO_2, is released during the production of Portland cement. He suggested the construction of a sustainable concrete structure to ensure minimum influence on the environment within its service life (Naik 2008). Khatib et al. suggested the reduction of urban pollution through the innovative use of building materials, the reduction of the dependence on traditional concrete construction, and the effective recycling of concrete construction wastes (Khatib et al. 2018). Xing et al. pointed out that dust pollution is a key problem in the construction process that must be addressed, and the government should assume partial responsibility and reduce dust emission at construction sites for the public. According to data analysis, the preferred technologies and organization measures of the Chinese government, institutional guarantees, and technological innovation are prerequisites of dust-free construction (Xing et al. 2018). Akhtar et al. pointed out that the production of concretes and construction wastes are among the major causes of continuous CO_2 emission in the atmosphere. According to the sorting and critical analysis of information from 40 countries in six continents, he suggested the use of 30%-50% RA-assisted concrete with binding materials to achieve the strength of natural aggregate concrete (Akhtar et al. 2018). Colangelo et al. suggested the use of "green" RA in concrete production to mitigate the potential adverse effects on environment and energy (Colangelo et al. 2018). Based on existing studies, developed countries have relatively perfect recycling systems of concrete construction wastes and carried out abundant studies on waste concrete RA and prepared RA concretes. On the basis of the comprehensive analysis of the pollution hazards of concrete construction wastes, this study analysed the advantages of prefabricated concrete construction and proposed prefabricate construction waste recycling measures to provide references for solving construction waste pollution control problems, standardizing construction waste management, and reducing abundant construction resource wastes.

HAZARDS OF CONCRETE CONSTRUCTION WASTES

Embezzlement of Lands

In China, construction waste results in considerable annual embezzlement of land areas. Moreover, the output of construction wastes will increase continuously as a result of China's economic development, the continuous expansion of the urban construction scale, and the increasing demand for living conditions. The embezzlement of lands will intensify continuously because of the delayed processing and utilization of concrete buildings. Concrete is essential to construction and transportation infrastructure construction. In particular, the demands for concrete will increase greatly with China's continuous urbanization, thus resulting in increased demands for sands and stones, which are used as concrete aggregates. Such huge demands for sands and stones will surely lead to large-scale mountain quarrying and the exploitation of river sands, which will in turn cause serious damages to the ecological environment.

Water Pollution

Concrete in construction waste is rich in water soluble calcium silicate and calcium hydroxide. Waste plaster contains many sulphate ions. Waste metals involves the dissolution of heavy metal ions. Through anaerobic degradation, waste paper plates and timbers may generate lignins and tannin, which are further decomposed into organic acids. Thus, the percolating water of concrete construction waste after immersion in rainwater in landfill is generally strong in alkali and contains heavy metal ions, hydrogen sulphide, and certain amounts of organic matters. If this percolating water is not controlled and flows into rivers and lakes or penetrated underground, then the surface and underground water pollution is intensified accordingly, thus damaging the survival of aquatic organisms and affecting the secondary use of water resources. This phenomenon will cause irreversible damage to the water environment.

Atmospheric Pollution

Waste plaster in concrete construction waste contains abundant sulphate ions, which are transformed to hydrogen sulphide and volatile organic acids under anaerobic conditions. These harmful gases cause atmospheric pollution once emitted to the air. Resource reserves and output, such as natural sands and stones, are decreasing annually due to exploitation. Particularly, natural river sands cannot satisfy

the demands, a shortcoming that is worsened by the increasing supply–demand contradictions. Resource shortage is particularly serious in certain big cities. Thus, finding alternative resources is an urgent concern. Many artificial sands have been put into use. In coastal regions with relatively high economic development, sea sands are applied to prepare concretes by taking advantage of geology. However, sea sands have a relatively high Cl-content. The illegal or unreasonable use of sea sands can easily cause the corrosion of reinforcement in concrete, eventually bringing potential safety risks in architectural structures.

Soil Pollution

Harmful substances in construction wastes and their percolating water cause soil pollution, which is manifested in changes in physical structures and in the chemical properties of soil. Soil pollution influences the nutrient adsorption and growth of plants and the activity of microorganisms in soils, breaks the ecological balance in soils, and promotes the accumulation of harmful substances in soils. Consequently, the harmful substances in soils exceed the standards, thus inhibiting plant growth and even causing plant death. In addition, harmful substances may be transferred to fruits through plant adsorption and further influence the physical health of humans and animals through the food chain.

Threats to Physical Health

Concrete construction wastes, which are piled up randomly without processing, produce harmful substances that may enter the atmosphere, water, and soil. Subsequently, these harmful substances may enter the human body through various ways, thus resulting in poisoning. Many toxic and harmful components in concrete construction wastes enter the food chain through animals and plants, which further lead to lesions and affect the physical health of humans. During respiration, harmful dusts from concrete construction wastes may enter the human body through the respiratory tract and diffuse in the circulatory system, thus causing substantial damage to the human body.

ADVANTAGES OF PREFABRICATED CONCRETE CONSTRUCTION

High Production Efficiency

The prefabricated parts of prefabricated concrete construction are manufactured through assembly lines in factories and then transported to construction sites for mechanical hoisting assembly. This path not only saves in labour force and materials significantly but also increases concrete construction efficiency. Furthermore, the convenience and efficiency of construction work is increased. Thus, planned tasks can be accomplished in a short period, which is desirable. The construction of prefabricated buildings is affected slightly by severe weather conditions. Therefore, prefabricated concrete construction significantly increases production efficiency and shortens construction period in comparison with traditional construction means.

Coexistence of Energy Saving and Environmental Protection

Traditional architectural construction requires the frequent casting-in-situ of concretes, which may cause serious dust and wastewater pollution as well as noise pollution in construction sites. On the contrary, prefabricated concrete construction can decrease casting-in-situ significantly. The direct assembly and installation of prefabricated components not only save in field wetting operation to a large extent but also decrease dust and wastewater pollution and the production of construction wastes. They result in a green construction environment. During the production of prefabricated components, reusing moulds and assembly line-based production can maximize resources. Mechanical hoisting assembly is basically applied in installing parts, which decreases the use of many scaffolds and templates and promotes resource saving and environmental protection.

Guarantee of Overall High Quality

Prefabricated components are manufactured through standard production line. Improving production technologies and the standardized production procedure can guarantee the satisfactory quality of prefabricated components. Components, such as prefabricated external wall panels, can maintain the stability of walls, while water-proofing, heat insulation, and thermal insulation are considered. This strategy decreases field construction and promotes quality components. The manufacturing of prefabricated components in factories plays an important role in effectively controlling architectural quality.

PREFABRICATED RECYCLING OF CONCRETE CONSTRUCTION WASTES

Strengthen Policy Supports to Prefabricated Concrete Construction

The guidance and support of governments provide a development direction for prefabrication construction and guarantee benefits for prefabricated construction enterprises. The reasonable management by the government determines the development of prefabricated construction. The development of prefabricated construction realizes the

philosophy of China's green energy-saving push. China should increase its investment on prefabricated construction development; formulate various supporting policies that provide capital subsidies, preference policies for land bidding, loans with discounted interests, and preferences to economic technological indexes (like plot ratio and building area); set up a special promotion department for the large-scale propaganda of the advantages of prefabricated construction; formulate an excitation mechanism; and develop the guidance of government. To provide reliable guarantees to real estate developers and construction units, the government of China can apply special funds for prefabricated construction, formulate preference policies to attract foreign investment, and increase marketing efforts. Moreover, the Chinese government should set up a series of special key subjects of prefabricated construction in colleges and universities, offer financial assistance to relevant experiments and practices in universities, train talented individuals with technological and management skills, and establish key technology R&D funds to promote R&D and the innovation of structure and technological systems for prefabricated construction.

Perfect Laws and Regulations of Prefabricated Concrete Construction

Currently, the prefabricated component manufacturing market in China is chaotic. Owing to the lack of production standards and norms, the component cost remains high, thereby restricting the expansion of prefabricated component manufacturing. Provinces and cities have released relevant laws and regulations, and some standards have been formed in local regions. However, these laws, regulations, and standards are independent from one another and are lacking in authority and universality, thus resulting in diversity and chaotic national industrial standards. China has published the industrial standards of Technical Regulations on Prefabricated Concrete Structure several years ago. The standards propose explicit technical regulations in different links of the entire process, and they restrict construction chaos to a certain extent. Thus, relevant departments of China should concentrate their industrial powers to formulate China's standards or norms, implement specific rules, realize standardized production, expand the manufacturing scale of prefabricated components, and decrease the production cost of single components, thereby lowering the engineering cost and facilitating the industrialized development of construction. In addition, the formulation and further perfection of universal standard atlas or technical design scheme must be accelerated; unique, standardized, systematic, and supporting technical standard systems must be formed; the requirements of different provinces and cities for building functions and performances should be met; laws for reference throughout the prefabricated construction process must be offered; and technical foundations for expanding the prefabricated construction scale must be laid out.

Improve Levels of Prefabricated Construction Enterprises

The prefabricated construction industry is developing slowly in China and remains in the initial stage. China has successively released many supporting policies and incentive measures to guide the sound development of prefabricated construction. Owing to hindering factors, such as excessively high investment, prefabricated component manufacturers are few and are lacking enthusiasm to scale up. Thus, prefabricated component manufacturers are costly, which further restricts scale expansion. Therefore, different provinces and cities of China should perfect supporting policies, implement specific rules, provide certain guarantee, stimulate the enthusiasm of manufacturers, introduce benefits to manufacturers, expand market demands, improve the productivity, and form scale benefits. Additionally, local governments should improve the professional quality of workers in prefabricated component manufacturers and train professional technicians and managers through regular professional trainings to improve the production efficiency and professional degree of enterprises and bring them additional benefits. To encourage prefabricated construction industrial development, the provinces and cities of China launched many pilot projects. Through these pilot projects, China should integrate resources effectively, increase the R&D of key technologies and talent training, and accelerate the training of professional production and construction and leading enterprises that integrate the design, production, and construction of prefabricated components.

Strengthen Environment Protection at Prefabricated Construction Site

Enterprises should pay attention to the environmental management of construction sites. Enterprise protection is an important factor in modern construction industry. The management level of enterprises determines the construction schedule and level. Therefore, managers with rich management experiences and strong coordination ability should be selected for construction site management. Additionally, several management measures should be adopted to increase the management level and decrease unnecessary expenditures. The construction schedule should be planned reasonably to control the construction period, and the use of expensive heavy hoisting equipment should be minimized. Moreover, construction sites should be managed through an environmental protection method that includes material wastes reduction, reasonable arrangement of construction order, and slowdown phenomenon prevention.

The assembly efficiency should be improved to increase the components produced in factories, decrease the field management of components, increase the construction efficiency, and save cost.

CONCLUSIONS

The output of construction wastes in China is increasing annually, resulting in the increasingly prominent problem of construction waste pollution control. Construction wastes not only occupy large-scale land resources but also cause substantial damage to soil, air, and water environments. Moreover, China has failed in recycling construction wastes. With continuous urbanization, the volume of construction waste may increase, and its proportion in total urban wastes may increase further. This study reviewed the recycling measures of concrete construction wastes in developed countries, summarized the types of hazards of concrete construction waste pollutions, and analysed the advantages of prefabricated concrete construction. Results demonstrate that developed countries have relatively perfect recycling systems for concrete construction wastes. The embezzlement of lands, water pollution, atmospheric pollution, soil pollution, and threats to physical health are the five types of concrete construction waste hazards. Prefabricated concrete construction has several major advantages, such as high production efficiency, energy saving and environmental protection, and overall high quality. Certain measures can be adopted to decrease the environmental pollutions from concrete construction wastes, including the strengthening of policy supports for prefabricated concrete construction, appropriate relevant laws, regulations and standard systems, improving the levels of prefabricated construction enterprises, and enhancing the environmental protection of prefabricated construction sites. Intensive studies on concrete construction waste recycling systems, information disclosure systems that connect different stages of concrete waste disposal, comprehensive evaluation of prefabricated concrete construction quality, and environmental pollution control at prefabricated concrete construction sites must be continued.

REFERENCES

Akhtar, A. and Sarmah, A. K. 2018. Construction and demolition waste generation and properties of recycled aggregate concrete: A global perspective. Journal of Cleaner Production, 186: 262-281.

Arunvivek, G. K., Maheswaran, G. and Senthil Kumar, S. 2015. Eco-friendly solution to mitigate the toxic effects of hazardous construction industry waste by reusing in concrete for pollution control. Nature Environment & Pollution Technology, 14(4): 963-966.

Andersson, M., Ottesen, R. T. and Volden, T. 2004. Building materials as a source of PCB pollution in Bergen, Norway. Science of the Total Environment, 325(1-3): 139-144.

Colangelo, F., Forcina, A., Farina, I. and Petrillo, A. 2018. Life cycle assessment (LCA) of different kinds of concrete containing waste for sustainable construction. Buildings, 8(5): 70.

Eguchi, K., Teranishi, K., Nakagome, A., Kishimoto, H., Shinozaki, K. and Narikawa, M. 2007. Application of recycled coarse aggregate by mixture to concrete construction. Construction and Building Materials, 21(7): 1542-1551.

Gotoh, T., Nishimura, T., Nakata, M. and Nakaguchi, Y. 2002. Air pollution by concrete dust from the great hanshin earthquake. Journal of Environmental Quality, 31(3): 718-723.

Hsiao, T. Y., Huang, Y. T., Yu, Y. H. and Wernick, I. K. 2002. Modeling materials flow of waste concrete from construction and demolition wastes in Taiwan. Resources Policy, 28(1-2): 39-47.

Khatib, J. M., Elkordi, A. A. and Saleh, Z. A. 2018. Mitigating Urban Pollution through Innovative use of construction materials. Urban Pollution: Science and Management, pp. 235-247.

Lindgren, T. 2010. A case of indoor air pollution of ammonia emitted from concrete in a newly built office in Beijing. Building and Environment, 45(3): 596-600.

Naik, T.R. 2008. Sustainability of concrete construction. Practice Periodical on Structural Design and Construction, 13(2): 98-103.

Rao, A., Jha, K. N. and Misra, S. 2007. Use of aggregates from recycled construction and demolition waste in concrete. Resources, conservation and Recycling, 50(1): 71-81.

Taylor-Lange, S. C., Stewart, J. G., Juenger, M. C. G. and Siegel, J. A. 2012. The contribution of fly ash toward indoor radon pollution from concrete. Building and Environment, 56: 276-282.

Tam, V. W. Y. 2008. Economic comparison of concrete recycling: A case study approach. Resources, conservation and recycling, Resources, Conservation and Recycling, 52(5): 821-828.

Wu, Z., Zhang, X. and Wu, M. 2016. Mitigating construction dust pollution: State of the art and the way forward. Journal of Cleaner Production, 112: 1658-1666.

Xing, J., Ye, K., Zuo, J. and Jiang, W. 2018. Control dust pollution on construction sites: What governments do in China? Sustainability, 10(8): 2945.

Nature Environment and Pollution Technology
An International Quarterly Scientific Journal

p-ISSN: 0972-6268
e-ISSN: 2395-3454

Vol. 19 | No. 1 | pp. 373-377 | 2020

Original Research Paper | Open Access

Evaluation of Iron and Manganese Levels from Ramgarh Lake, Gorakhpur, U.P., India

Mahima Chaurasia*† and Sanjeev Kumar Srivastava**
*Institute of Engineering & Technology, Dr. R. M. L. Avadh University, Ayodhya, U.P., India
**Department of Basic Science, SRMS College of Engineering & Technology, Bareilly, U.P., India
†Corresponding author: Mahima Chaurasia

Nat. Env. & Poll. Tech.
Website: www.neptjournal.com

Received: 27-04-2019
Accepted: 21-06-2019

Key Words:
Iron
Manganese
Ramgarh lake
Water analysis

ABSTRACT

Natural waters vary in chemical composition and the factors controlling the composition include physical, chemical and biological processes. Water is one of the most important natural resources for all the living organisms because it is required for various metabolic activities. In addition, water is required for various domestic purposes, irrigation and power generation and the industries. Amongst various organic components, the iron and manganese are an important trace metal required for all the biological systems. The occurrence of iron and manganese, in the present study, was reported from Ramgarh Lake in Gorakhpur, India. Two sampling stations were selected for the present study. The iron and manganese have several effects due to their high concentration. The study was carried out for one year (January 2017 to December 2017). The significance of iron and manganese is discussed in the present investigation.

INTRODUCTION

The environment is a system of physical, chemical and biological factors and dynamic equilibrium. The indiscriminate industrial, domestic water discharged into natural water system has created the hazards to the aquatic life. Water is the most versatile, vital and essential component for all life forms. It is abundant on our planet occurring as a universal solvent, an indispensable component of nature holding both biotic and abiotic entities in a complex, dynamic and delicate ecological balance by virtue of its unique capacity existing in solid, liquid and gaseous states. Energy and water are indeed two essential components for the propagation of life. Quality of water, therefore, bears profound significance for conditioning the quality of life and environment in both aquatic and terrestrial.

The increasing industrialization, urbanization and development activities to cope with the population explosion have brought inevitable water crisis (Rao & Rameshwari 1998). The discharge of industrial effluent into the natural water bodies causing severe water pollution. Alteration in the chemical composition of a natural aquatic environment by industrial effluents usually induces changes in the aquatic ecosystem particularly aquatic organisms. Pollution is befouling the environment by man's activities particularly by the disposal of solid, gaseous and liquid waste products. Most of our water bodies, rivers and streams have become polluted and unfit for human use. Ramgarh Lake in Gorakhpur district is no exception. Gorakhpur city and several villages and residential colonies are settled around the Ramgarh Lake. The load of pollutants is increasing day by day in Ramgarh Lake and this poses a formidable challenge to water quality. (Srivastava et al. 2006, 2007).

Food and water are the main sources of our daily requirements of essential metals. These (with the addition of air) are also the media through which we are constantly exposed to the various toxic metals. The body, through urine and faeces, exerts metals, which are in excess, otherwise, there may be a chance of their accumulation in various body tissues. Metals are indestructible poison. Their dispersion into streams, rivers and oceans for a long duration may be highly dangerous, because they may affect the production of atmospheric oxygen, contaminate the water and affect the life of freshwater ecosystem influenced by air-heavy metals and addition from anthropogenic sources. At present, several metals are believed to be essential for life; some of them are iron, copper, zinc, manganese, cobalt, molybdenum, selenium, chromium, nickel, tin and vanadium, etc. Metals usually considered to be toxic at 'physiological dose' may be stimulatory or essential in very minute doses depending upon the environment and state of the organism.

The indispensability, deficiency or toxicity of metal is manifestations of dose response effect. However, environmental conditions, natural and biological factors, such as age, sex, species differences, stress, and relationship of one metal with the other metal and metal ion imbalance in biological system, in turn influences the toxicity of metal. Uptake of heavy metals through food chain in human beings may cause various physiological disorders, like hypertension, sporadic fever, renal damage, cramps, etc. The bioaccumulation of metal toxicants in plants and fish depends on availability and persistence of the contaminants in water and the physic-chemical properties of the toxicants. Iron is the second most abundant metal after aluminium in the earth's crust. Iron is an essential trace metal, required as a constituent of oxygen-carrying and oxidative-reductive micro molecules, such as haemoglobin, myoglobin and cytochrome. Manganese is a greyish similar to the appearance of cast-iron. Manganese, an essential element for animals and man, occurs in the cells of all living organisms. It is the twelfth most abundant element and the fifth most abundant metal. Manganese is also an essential trace element required by the plants. In some waters, it may limit either directly or indirectly the growth of algae. The present study has been carried out to find the levels of iron and manganese in Ramgarh lake in Gorakhpur.

MATERIALS AND METHODS

The Ramgarh lake is spread over 669.73 ha near Gorakhpur city on Gorakhpur-Deoria highway, which lies between Lat. 26°13'N-27°29'N and Long. 83°05'E-83°56' E. The height above sea level ranges from 107 meters in northwest to 93 meters in the southeast. The lake receives urban sewage through a wide network of the drain during the past few years. The water of this lake is widely used for agricultural, irrigation, domestic and industrial purposes. The lake is useful for fish culture and, nearly 20 to 25 villages water supply is carried out from the lake. Metals transported from the nearby silts, rocks, etc., can play a vital role in supplying micro-metals for the human consumption. It is very important to investigate a few metals, which are very essential for our life. Hence, we selected the useful two metals present in the lake. For the present analytical study, we divided the lake into two parts. A good population of submerged aquatic plants is found in this area.

The study of iron and manganese content from the Ramgarh Lake was undertaken and it was estimated by spectrophotometer method. The water samples from both sampling stations were brought to the laboratory regularly in clean containers at early hours. Standard methods prescribed by APHA (2012) were applied for the collection and analysis of the water samples. The concentration of iron and manganese was measured on a spectrophotometer at a specific filter. Results were expressed as mg/L and compared with permissible levels.

RESULTS AND DISCUSSION

Several heavy metals are essential for the growth and survival of plants and animals. These are originated from both natural and anthropogenic sources (Wintz et al. 2002). The results obtained in the present work are illustrated in Tables 1 and 2. The iron concentration of the water sample-1 varied from 0.65 mg/L to 1.69 mg/L. Sample-2 showed iron content ranging between 1.32 to 1.98 mg/L (Fig. 1). The mean values for the sample-1 and 2 were 1.17 mg/L and 1.67 mg/L, respectively. Overall results showed the minimum iron content in monsoon and maximum in summer season. Iron is an essential heavy metal for higher plants and algae, particularly for photosynthesis. Higher concentration of iron in water imparts a bitter taste and inky flavour (Khurshid et al. 1997, Rana et al. 2016). Iron in surface water is generally present in the ferric (Fe^{+3}) state. The maximum allowable concentration of iron in drinking water is 1.0 mg/L, according to WHO (2004) report. Indian Standard Institute (ISI) and Indian Council of Medical Research (ICMR), the permissible concentration of iron and manganese in drinking water is 1.0 and 0.3 mg/L, respectively. In the present investigation, the mean iron concentration was observed more than the permissible limit. Increased concentration of iron has earlier been reported in river Kali and Hindon waters (Ajmal & Razi-Uddin 1988) and in river Ganga (Ray 1989).

Sharma et al. (2000), monitored the iron content in the 13 drinking water sources from a predominantly rural area of Goalpara district (Assam). They reported 0.02 to 1.50 mg/L iron concentration, which is quite low from the present investigation. Mohapatra & Singh (1999), reported iron content in Mahanadi river water fluctuates between 0.468 and 2.18 mg/L with a mean value of 1.35 mg/L. Nag & Das (1995) analysed surface drinking water in the Purulia district of West Bengal and reported iron content from 0.1 to 13.22 mg/L. However, the mean value was found to be 0.2 mg/L. Manganese is an essential element which does not occur naturally as a metal but is found in various salts and minerals frequently in association with iron compounds (Dwivedi & Tiwari 1997, Srivastava & Pandey 2008, Priyadarshinee & Verma 2016). In the present investigation, sample-1 showed the minimum manganese ion content (0.24 mg/L) in the month of June and maximum value (0.47 mg/L) in the month of December. Sample-2 showed lowest manganese concentration (0.37 mg/L) in the month of June and highest (0.58 mg/L) in the month of December (Fig. 2). The average

concentration was 0.36 mg/L and 0.47 mg/L for Sample-1 and 2, respectively. The permissible limit for manganese set by WHO is 0.05 mg/L. Both water samples have higher mean values than the permissible limit.

Some workers previously reported manganese levels of river water. Sinha (2004), monitored the Mn^{+2} content in water of Sai river at Rai Bareilly, and reported that it varied from 0.08 to 2.2 mg/L. They further reported that manganese in high concentration becomes toxic to plants also. Manganese is found as a cofactor in several enzyme systems. It plays a role in the proper functioning of flavour-proteins and in the synthesis of cholesterol, haemoglobin and in many other important metabolic processes (Tale & Bhosle 2010, Ingole et al. 2016). The water samples having more than 0.1 mg/L of manganese for long exposure is harmful for all animals (WHO 1988). Israili (1991), analysed water of Ganga river from eight different sampling stations and reported that Mn^{+2} content varies from 35.0 to 211.0 µg/L. Furthermore, Israili & Khurshid (1991) studied the distribution of heavy metals in Yamuna river water, which they observed within the permissible limit. Dwivedi & Tiwari (1997) studied Mn^{+2} content of Ganga river and reported the mean Mn^{+2} values ranged from 19.1 to 15.2 µg/L.

From the present investigation, both iron and manganese ion values were observed higher than the permissible limit due to the discharge of sewage, municipal and small-scale industrial waste. Thus, the toxic impact of sewage rendering the lake water unsuitable for sustenance and propagation of aquatic life and unfit for animal and human consumption. Authorities should make concrete efforts, particularly effective and feasible plans for the treatment of waste released into lake.

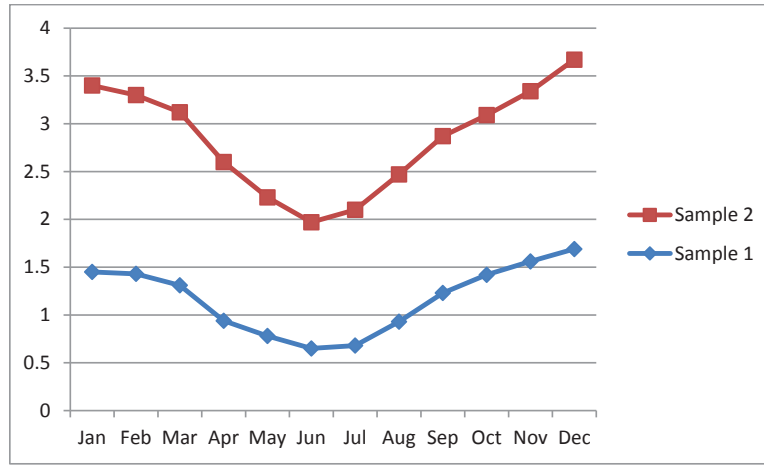

Fig. 1: The iron levels (mg/L) from Ramgarh Lake during January to December 2017.

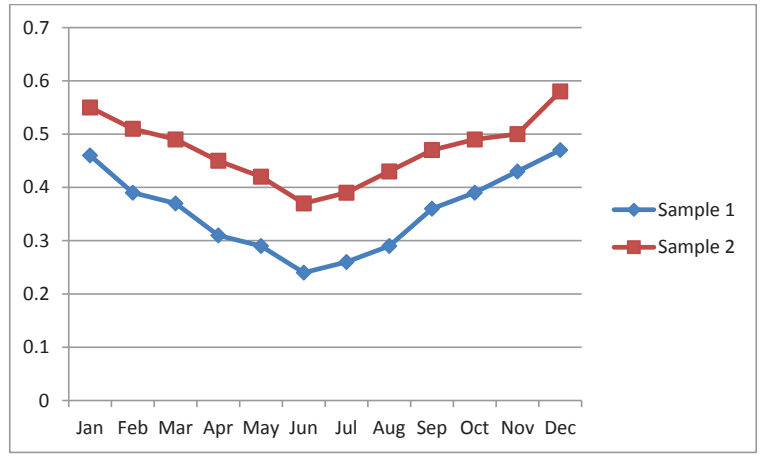

Fig. 2: The manganese levels (mg/L) from Ramgarh Lake during January to December 2017.

Table 1: The iron levels from Ramgarh Lake during January to December 2017 in mg/L.

Month	Sample-1	Sample-2
January	1.45 ± 0.12	1.95 ± 0.16
February	1.43 ± 0.13	1.87 ± 0.17
March	1.31 ± 0.12	1.81 ± 0.16
April	0.94 ± 0.10	1.66 ± 0.15
May	0.78 ± 0.09	1.45 ± 0.13
June	0.65 ± 0.05	1.32 ± 0.14
July	0.68 ± 0.06	1.42 ± 0.13
August	0.93 ± 0.07	1.54 ± 0.14
September	1.23 ± 0.11	1.64 ± 0.15
October	1.42 ± 0.10	1.67 ± 0.14
November	1.56 ± 0.12	1.78 ± 0.18
December	1.69 ± 0.11	1.98 ± 0.16

All the values have been represented as mean ± SEM of three replicates

Table 2: The manganese levels from Ramgarh Lake during January to December 2017 in mg/L.

Month	Sample-1	Sample-2
January	0.46 ± 0.02	0.55 ± 0.06
February	0.39 ± 0.02	0.51 ± 0.05
March	0.37 ± 0.02	0.49 ± 0.05
April	0.31 ± 0.03	0.45 ± 0.04
May	0.29 ± 0.03	0.42 ± 0.04
June	0.24 ± 0.02	0.37 ± 0.04
July	0.26 ± 0.01	0.39 ± 0.03
August	0.29 ± 0.02	0.43 ± 0.03
September	0.36 ± 0.02	0.47 ± 0.04
October	0.39 ± 0.03	0.49 ± 0.05
November	0.43 ± 0.03	0.50 ± 0.04
December	0.47 ± 0.04	0.58 ± 0.04

All the values have been represented as mean ± SEM of three replicates

ACKNOWLEDGMENT

The authors are grateful to the authorities of Dr. R. M. L. Avadh University, Ayodhya and Sri Ram Murti Smarak College of Engineering and Technology, Bareilly, for rendering their support and help for completion of this work.

REFERENCES

Ajmal, M. and Razi-Uddin 1988. Studies on the pollution of Hindon river and Kali Nadi. In: R. K. Trivedy (ed.) Ecology and Pollution of Indian Rivers. Ashish Publishing House, New Delhi. 87-112.

APHA 2012. Standard Methods for the Examination of Water and Wastewater, 22nd edn., American Public Health Association, Washington DC.

Dwivedi, S. and Tiwari, I. C. 1997. A study on heavy metals in the Ganga water at Varanasi. Poll. Res., 16(4): 265-270.

Ingole, Nandkishor A., Ram, R. N. and Nain, A. S. 2016. Study of present status of fish fauna and water level at Tumaria wetland from U. S. Nagar of Uttarakhand. J. Env. Bio-Sci., 30(1): 123-126.

Israili, A. W. 1991. Occurrence of heavy metals in Ganga river water and sediments of western Uttar Pradesh. Poll. Res., 10(2): 103-109.

Israili, A. W. and Khursid, S. 1991. Distribution of heavy metals in Yamuna river water and sediments from Delhi to Allahabad. Poll. Res., 10(4): 215-222.

Khurshid, S., Mohd, Z. and Shabeer, U. 1997. Degradation of water quality to heavy metal pollution in Faridabad district, Haryana. Poll. Res., 16(1): 41-43.

Mohapatra, U. K. and Singh, B. C. 1999. Trace metals in drinking water from different sources in the old capital city of Cuttack. Indian J. Env. Health, 41(2): 115-120.

Nag, J. K. and Das, A. K. 1995. Status of drinking water in the Purulia district of West Bengal. Poll. Res., 14(1): 113-121.

Priyadarshinee, Amrita and Verma, P. K. 2016. Limnological investigation of Sunderdam reservoir of Godda district (Santal Pargana) Jharkhand. J. Env. Bio-Sci., 30(1): 39-46.

Rao, L. M. and Rameshwari, K. 1998. Incidence of heavy metal pollution in Mehadrigedda stream of Vishakhapatanam. Poll. Res., 17(2): 153-155.

Rana N., Verma, M. and Jain, S. 2016. Assessment of different water quality parameters of water sources of Meerut region (Uttar Pradesh, India) for suitability of fish production. J. Env. Bio-Sci., 30(2): 381-382.

Ray, P. K. 1989. Measurement of Ganga River Water Quality - Heavy Metals and Pesticides. Final Report. Industrial Toxicological Research Centre, Lucknow.

Sharma, B. C., Mishra, A. K. and Bhattacharyya, K. G. 2000. Metal in drinking water in a predominantly rural area. Indian J. Env. Protec., 21(4): 315-322.

Sinha, D. K. 2004. Level of some heavy metals in waters from Sai river at Rae Bareli for the pre-monsoon period and after the onset of monsoon. Poll. Res., 23(1): 113-116.

Srivastava, Sanjeev K., Pandey, G. C., Mahanta, P. C., Patiyal, R. S. and Lakra, W. L. 2006. Seasonal variations in hydrological parameters of Ramgarh Lake, Gorakhpur, U.P. J. Adv. Zool., 27(1): 46-51.

Srivastava, Sanjeev K., Pandey, G. C., Mahanta, P. C. and Gopal, K. 2007. Assessment of water quality of a freshwater body, Ramgarh Lake, Gorakhpur, U. P. Asian Jr. of Microbiol. Biotech. Env. Sci. 9(3): 683-686.

Srivastava, Sanjeev K. and Pandey, G. C. 2008. Study of hydrological characteristics and level of metals present in four sites of sewage released into holy river Saryu of Ayodhya-Faizabad. The ICFAI Jr. of Env. Science., 2(2): 54-62.

Tale, S. S. and Bhosle, A. B. 2010. Evaluation of iron and manganese ion levels from Manar Dam of Barul, Maharashtra. Indian J. Env. Protec., 30(2): 110-114.

WHO 1988. Guidelines for Drinking Water Quality, Vol. II. World Health Organization, Geneva.

WHO 2000. Guidelines for Drinking Water Quality, Vol. I. Recommendations (3rd edn). World Health Organization, Geneva. pp 210-438.

Wintz, H., Fox, T. and Vulpe, C. 2002. Functional genomics and gene regulation in biometals research. Biochem. Soc. Transactions., 30(1): 166-168.

Nature Environment and Pollution Technology
An International Quarterly Scientific Journal

p-ISSN: 0972-6268
e-ISSN: 2395-3454

Vol. 19 | No. 1 | pp. 379-383 | 2020

Original Research Paper | Open Access

Biological Remediation of the Municipal Solid Waste Leachate - A Case Study of Hyderabad Integrated MSW Limited

Konda Durga Sindhu Sree*, Surya Narayan Dash* and Anagani Leelavathi†**
*Department of Chemical Engineering, GMR Institute of Technology, Rajam-532 127, India
**Environment Protection Training and Research Institute, Gachibowli, Hyderabad-500 032, India
†Corresponding author: Anagani Leelavathi

Nat. Env. & Poll. Tech.
Website: www.neptjournal.com

Received: 21-06-2019
Accepted: 23-07-2019

Key Words:
Biological treatment
Municipal solid waste
BOD
COD
Leachate
Odour
TDS

ABSTRACT

A prominent issue associated with the handling of municipal solid waste is the generation of a highly toxic semi-solid matter namely, leachate. The consequences of mishandling the aforementioned are widespread. Hence, the present study tried to take an initiative to remediate the same in an eco-friendly way. The research included a detailed investigation of the existing conditions in terms of quality, quantity, climatic condition, etc. The entire study primarily focused on the biodegradability of the toxic pollutants with the help of EM.1 solution procured from Pragati Enterprises and bringing down the pollution level during the treatment tenure. The major three parameters of interest include chemical oxygen demand (COD), biochemical oxygen demand (BOD), and total dissolved solids (TDS). A pilot pond of 7.5 kL capacity was prepared at the east corner of Hyderabad Integrated MSW facility to facilitate the practical studies. Four major remediates, i.e. coir pith powder, Bokashi balls, EM culture, and Bokashi powder were added weighing 34 MT, 560 kg, 10.5 kL, and 75 kg respectively, over the due course of 4 months and successive reduction in pollution levels were noted. Depletion in the level of all the prior-mentioned parameters was observed ranging 42.6%, 45.4%, and 37.8% respectively for COD, BOD and TDS. Furthermore, a notable reduction in obnoxious odour was observed around the pilot plant after the 15th day of the initiation of the operation. It signifies the feasibility of the experimented technology towards the treatment of municipal solid waste leachate (MSWL), and hence the study recommends the usage of the same as a potential pre-treatment before the tertiary purification units.

INTRODUCTION

Despite a considerable amount of effort has been made to extend realistic solutions for the MSWL treatment, an ultimate wholesome treatment is still unachieved. Treating leachate and bringing down the pollution level to the disposal limits or reuse is not an easy task. It requires a series of operations. Otherwise, it may cause serious environmental concern such as groundwater contamination, odour formation etc. Furthermore, an ancillary headache associated with advanced treatment is the disposal of secondary pollutants (Heng et al. 2012). In most of the cases the process reject goes for the forced evaporation and finally, the salts land up in the secured land filling. In the majority of the cases due to the absence of any pertinent pre-treatment method, direct pollution load gets subjected to the tertiary unit, resulting in fouling of the membrane and other complicated and expensive issues. Thus, a simple, scalable, and inexpensive pre-treatment technology is the need of the hour. A diverse range of secondary treatment techniques have been already investigated and demonstrated by several researchers (Choudhury et al. 2019, Er et al. 2018, Jeyapriya & Saseetharan 2007), but most of it lags in terms of up-scalability and affordability. Moreover, utilizing the external researches and products in Indian conditions is again questionable due to the contradictory climatic and native conditions (Gupta et al. 1998, Jampala et al. 2016, Jeyapriya & Saseetharan 2007, Krishna et al. 2015, Ramesh et al. 2009). Therefore, it's highly recommended to check the adaptability of certain products and its functionality. Based on the aforementioned, it's advisable to go for the mixed consortium of organisms instead of indigenous culture, moreover the usage of native species is utterly recommended (Choudhury et al. 2018a, Choudhury et al. 2018b, Tighiri & Erkurt 2019, Snehlata et al. 2015). Zhang et al. (2016) have also investigated on the effectiveness of native species of organisms towards the removal of substances such as volatile fatty acids, micro-scale xenobiotic organic chemicals, and refractory aquatic humic substances and stated that the native organisms remove the pollution load more proficiently when compared to externally introduced indigenous species. Ultimately, the superiority of biological process towards the stabilization of organic pollutants is a well-established fact and Kurniawan et al. (2010) have reviewed a wide range of biological applications based on the target pollutants.

Finally, it was concluded by them that the bio-aerobic treatment units are most useful in terms of pollution removal if energy recovery is not possible.

The objective of the present research was to understand the behavioural characteristics and the functionality of certain organisms towards the bioremediation of the RO reject of MSWL and also to demonstrate a realistic secondary treatment mechanism to be utilized as the pre-treatment technique prior to advanced treatment units.

MATERIALS AND METHODS

The present study was conducted within the premises of Hyderabad Integrated MSW processing and disposal facility (HIMSW), which handles approx. 5000-6000 tons of MSW on a regular basis. The facility is located at Jawahar Nagar Gram Panchayat area, at the outskirts of Hyderabad city and operating in Public-Private Partnership (PPP) mode. The work has been carried out as a joint venture between HIMSW and Environment Protection Training and Research Institute (EPTRI). Further details are delineated below.

Preparation of Pilot Pond

The study involved the formation of an open circular pond of 7.5 kL capacity. The same was prepared with the help of JCB by digging up the soil at the east corner of the facility at a coordinate value of approx 78°35'39.51" E and 17°31'32.94" N. The dimensions of the pond include 2 m of radius and 0.6 m of depth. The depth was kept minimal to maximise the surface area and thus the evaporation. The pond was protected with the help of high-density polyethylene liner to arrest the downward leachate movement, garland drains to avoid the risk of any sort of spillage, and protective barriers to mitigate human and animal interference.

Leachate Source Selection

Due to the intrusion of leachate into the rainwater ponds (i.e. Malkaram Pond) located at the North-East side of the facility, approx. 6.5 lakh m^3 of fresh surface water was previously transformed into diluted leachate, locally termed as legacy leachate. At present, the same is getting treated with the help of reverse osmosis (RO) technique by Rochem Separation Systems India Pvt Ltd. The present research work incorporated remediation for the RO reject generated by the aforementioned and used the same as influent.

Characterization

The leachate sample was collected following the BIS standard method and analysed during the different periods of the research tenure. The primary parameters taken into consideration include pH, Electrical conductivity (EC), TDS, BOD, COD, and NH_3-N. Additionally, monitoring parameters included temperature and precipitation. The onsite parameters such as pH, TDS, temperature etc. were analysed using the portable mobile probes of EZDO PH5011A and TDS5031 and MEXTECH multi-thermometer, respectively. Whereas, the gas generation in and around the area was strictly monitored with multi-gas analyser of INSTRUKART (i.e., CO, CO_2, H_2S, CH_4, NH_3). The frequency of analysis was optimized as once a day.

Factors of Interest

As the study aimed to constitute a comparison between the pre and post-monsoon data, therefore, it was necessary to undertake two parameters for the primary comparisons namely, temperature and precipitation. The total research tenure so far is 4 months (Feb' 19-May'19) and the rain has been observed on 12th of April. Based on that, the entire period was divided into two parts, pre and post-monsoon period. The pre-monsoon study was carried out over a period of February to March 2019 whereas, post-monsoon studies were undertaken after 20th April to 31st of May 2019.

Introduction of the Conversion Agents

The study inculcated inclusion of four major conversion cum stabilization agents, which are EM.1 solution, Bokashi balls, Bokashi powder, and coir pith powder. Blower with suitable piping & diffusers were utilized to spray the EM culture after the successive intervals. While other solid products were manually mixed and stirred with the help of Noble NPEAG281450 MI High-Speed Stirrer. The set of operation performed alongside the sequence are showcased in Table 1.

Therefore, a total amount of 34MT of coir pith powder, 560 kg of Bokashi balls, 10.5 kL of EM culture, and 75 kg of Bokashi powder were added during the treatment tenure.

RESULTS

The remediation system was prepared and operated under the open atmospheric condition and hence atmospheric agents and seasonal variation found to play a significant role in the performance of it. The culture utilized for the study was majorly mesospheric to minimise the impact of temperature and can be easily found in the open environment. The natural habitats for all the three primary organisms include lactose substrate for lactobacillus, bread and such similar products for yeast, and roots of the plants/trees for certain essential prototroph. Other crucial information is depicted below.

Reduction of Pollution Load

Generally, RO reject constitutes elevated TDS concentration thus safe handling of the same possesses a major challenge.

Table 1: Set of operations.

Days	Date	Particulars	
		Product	Quantity added
DAY -1	20/02/2019	Bokashi balls	60.0 kg
		EM culture (Raw)	3.0 L
		Bokashi powder	15 kg
DAY -4	23/02/2019	Bokashi balls	60 kg
		EM culture (Raw)	3.0 L
		Bokashi powder	15.0 kg
DAY -11	01/03/2019	Bokashi balls	60.0 kg
		EM culture (Raw)	3.0 L
		Bokashi powder	15.0 kg
DAY -13	03/03/2019	Coir pith powder	14.0 MT*
DAY -19	09/03/2019	Bokashi powder	25.0 kg
		Bokashi balls	200.0 kg
DAY -29	19/03/2019	Coir pith powder	10.0 MT
DAY -56	17/04/2019	Maida	100.0 kg
		Bokashi balls	200.0 kg
		Coir pith powder	10.0 MT

*MT stands for Metric ton

Table 2: Reduction in leachate quantity.

Days	Date	Height Reduction (inch)	Volume Reduction* (m^3)
DAY -1	20/02/2019	N.A.	N.A.
DAY -4	23/02/2019	3.0	0.96
DAY -11	01/03/2019	6.0	1.91
DAY -13	03/03/2019	6.5	2.07
DAY -19	09/03/2019	8.0	2.55
DAY -29	19/03/2019	10.2	3.25
DAY-56	17/04/2019	22.0	7.02

*Values are subjected to local conditions

Initially, up to the first 30 days, the treatment rate was moderately lower. Possibly due to the activation and the acclimatization to the local conditions, but a steep growth in performance was observed after the initiation period. The observation on the reduction of leachate volume over the treatment tenure is portrayed in Table 2.

Reduction in Concentration

The target liquid was the reject of the RO process and hence it is obvious that the same should be highly concentrated and toxic in nature. Therefore regular monitoring was performed for the operating parameters. Onsite parameters were tested on a regular basis, which includes pH, temperature and precipitation. The range of pH found to be varying between 8.77 and 6.54. Though high pH value such as 8.70 or above was observed during the initial phase, the same got lowered to up to 6.50 during the treatment process. Probably, due to the inhibition of the anoxic activities during the later stage of the study. Whereas, the day and night temperature also increased between February to April 2019. The max and min temperature of Feb was recorded as 19°C and 39°C respectively. On the other hand, a much high min temperature of 25°C was observed during April'19, which facilitated higher rates of evaporation. Precipitation was only observed during the middle half of April, ranging approx. 62 mm with a maximum value of 37 mm on 12th of the month, which had

Table 3: Variation in treatment efficiency during pre and post monsoon period.

Sl. No.	Name of the Parameter	Units	Method	Raw*	Pre-monsoon	Post-monsoon
1	pH	---	APHA 4500 H^+ B	8.73@25°C	7.78@25°C	6.77@25°C
2	Electrical Conductivity	μSm^{-1}	APHA 2150 B	85800	64521 ± 1000	53890 ± 1000
3	COD	mg/L	APHA 5220 B	10524	7240 ± 00	6041 ± 200
4	Chlorides	mg/L	APHA 4500 Cl B	18802	14516 ± 200	11845 ± 200
5	Total Solids	mg/L	APHA 2540 B	44350	32473 ± 1000	29710 ± 1000
6	Total Dissolved Solids	mg/L	APHA 2540 C	43960	33985 ± 1000	27695 ± 1000
7	BOD (3days @27°C)	mg/L	IS: 3025	1020	740 ± 50	557 ± 25
8	Ammoniacal Nitrogen (NH_3-N)	mg/L	APHA 4500 NH_3-C	68	47 ± 5	32 ± 5

*All the heavy metal values were below detection limit

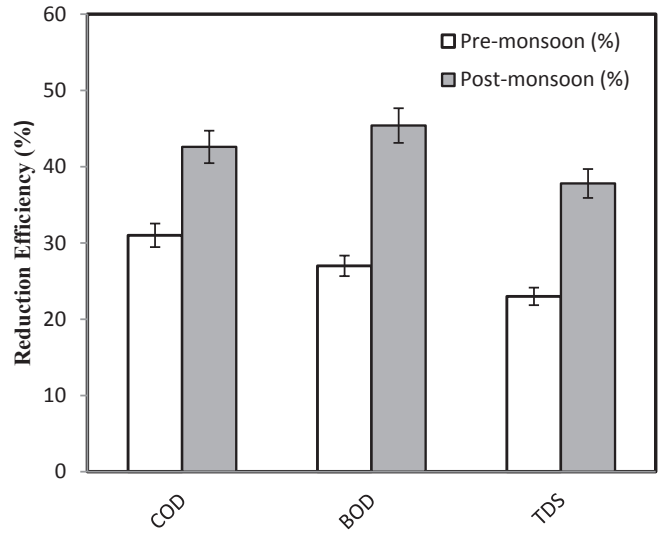

Fig. 1: Pre and post monsoon performance evaluation.

little to no effect on the study. The characteristics of the raw influent and treated effluent over the different time frame are depicted in Table 3.

Further the DO content of the influent was tested with the help of the Winkler method (APHA 2005) and found to be nil. Due to the prior mentioned condition, the influent liquid can be considered as septic and caused a possible delay in the activation of the externally introduced organisms. Later the same was elevated up to 5 mg/L, because of the mixing of atmospheric oxygen as a natural phenomenon, though the re-oxygenation process was considerably slow due to the lack of turbulence of static body. Therefore, it is recommended to install air diffusers if budget is available. It can optimise the treatment period by minimising the activation period. The overall efficiency during the pre and post monsoon period in term of percentage is shown in Fig. 1.

Both COD and TDS showed a clear pattern of reduced concentration and better treatment efficiency from post to pre-monsoon session, ranging approx. 42 and 38% respectively over the values of 31 and 23%. But though the concentration of BOD got reduced between both the sessions, a higher depletion rate was noted during the post-monsoon from 27% to 45.4%, recording an elevation of 68% enhancement in the treatment efficiency. The value is significantly almost two times the efficiency increment value of COD, which is 37.42% and the possible reason behind the same is the activation of the dormant organisms. Certainly, the boom in the ultimate removal efficiency was also dependant on a few more factors worked positively towards the treatment, includes a mesophilic range of temperature, minimal precipitation etc.

DISCUSSION

The ultimate treatment efficacy is a local phenomenon and its dependant on the various factors such as the effectivity of the organism, climatic condition, influent characteristics etc. (Choudhury & Dandapani 2018, Reddy & Reddy 2018a, Reddy & Reddy 2018b). Reddy & Nandini (2011) have reported a much lower concentration of the MSWL which clearly strengthen the factor of local influence. Moreover, Er et al. (2018) have reported much superior efficacy of micro-organic treatment towards the purification of leachate, raging approx. 75-80%. The higher rate of efficiency is probably due to the introduction of additional air diffusers and a combination of the variety of organisms utilized. Contrarily, Raghab et al. (2013) explicitly claimed the superiority of the chemical treatment over the biological mechanism and reported a much-depleted efficacy of approx. 15-20% on the overall reduction. Based on the characteristics showcased for the influent leachate for the prior mentioned study, the particular sample carried mostly inorganic pollutants and therefore biological treatment found to be quite ineffective (Sarala & Babu 2012).

CONCLUSION

The treatment depicted an explicit fact that through biological treatment units are significantly slower and moderately vulnerable to the external factors, it can yield good results if properly maintained. The present system produced a considerably acceptable treatment efficacy of 42.6%, 45.4%, and 37.8% respectively for COD, BOD, and TDS over a period of approx. 55 days. Furthermore, a notable reduction in obnoxious odour was also observed around the pilot plant after the 15th day of the beginning of the operation. It signifies the feasibility of the experimented technology towards the treatment of MSWL and thus the study recommends the usage of the same as a potential pre-treatment before the tertiary purification units.

REFERENCES

Choudhury, A.R. and Dandapani, G. 2018. Proposed waste management strategies for small pockets of greater Hyderabad city: A technical review. International Journal of Creative Research Thoughts, 6(2): 608-617.

Choudhury, A.R., Veeraraghavan, A., Kesavarapu, S. and Reddy, G.M. 2019. Bio-treatment of organic leachate and domestic wastewater, using upflow anaerobic sludge blanket reactor. International Journal of Biology, Pharmacy and Allied Sciences, 8(1): 104-18.

Choudhury, A.R., Natarajan, A.K., Kesavarapu, S., Veeraraghavan, A., Reddy, G.M. 2018a. Integrated waste management through symbiotic culture, a holistic approach. Int. J. Sci. Res. Environ. Sci. Toxicol., 3(3): 1-7.

Choudhury, A.R., Natarajan, A.K., Kesavarapu, S., Veeraraghavan, A., Dugyala, S.K., Rao, K. and Thota, K.R. 2018b. Technical feasibility of *Hermetia illucens* in integrated waste management, renovated with sewage water, an overview. Open Access Library Journal, 5: e4421.

Er X.Y., Seow, T.W., Lim, C.K., Ibrahim, Z. and Sarip, S.H.M. 2018. Biological treatment of closed landfill leachate treatment by using *Brevibacillus panacihumi* strain ZB1. IOP Conf. Ser.: Earth Environ. Sci., 140: 012012.

Gupta, S., Mohan, K., Prasad, R. and Kansal, A. 1998. Solid waste management in India: Options and opportunities. Resource, Conservation and Recycling, 24: 137-154.

Heng, G.C., Elmolla, E.S. and Chaudhuri, M. 2012. Optimization of photo-Fenton treatment of mature landfill leachate. Nat. Env. & Poll. Tech., 11(1): 65-72.

Jampala, S., Gellu, A. and Kala, D.S. 2016. Current scenario on urban solid waste with respect to Hyderabad city. International Journal of Research Studies in Science, Engineering and Technology, 3: 10-13.

Jeyapriya, S.P. and Saseetharan, M.K. 2007. Study on municipal solid waste refuse characteristics and leachate samples of Coimbatore city. Nat. Env. & Poll. Tech., 6(1): 149-52.

Krishna, V.K., Reddy, V. and Rao, P.R. 2015. Municipal solid waste management using landfills in Hyderabad city. International Journal of Engineering Research & Technology, 4: 1047-1054.

Kurniawan, T.A., Lo, W., Chan, G. and Sillanpaa, M.E.T. 2010. Biological processes for treatment of landfill leachate. Journal of Environmental Monitoring, 12: 2032-2047.

Raghab, S.M., Meguid, A.M.A.E. and Hegazi, H.A. 2013. Treatment of leachate from municipal solid waste landfill. HBRC Journal, 9(2): 187-192.

Ramesh, N., Meenambal, T. and Murugan, K. 2009. Quantification, characterization and leachate analysis of the municipal solid waste from erode municipality, Tamilnadu, India. Nat. Env. & Poll. Tech., 8(1): 21-28.

Reddy, M.R. and Reddy, U.V.B. 2018a. Smart solid waste management practice and scientific disposal for the greater Hyderabad city: a sustainable approach. International Journal of Advanced Research Trends in Engineering and Technology, 5(5): 39-43.

Reddy, M.R. and Reddy, U.V.B. 2018b. Assessment of the environmental quality in and around the municipal solid waste processing and disposal facility, HiMSW. International Journal of Research and Analytical Reviews, 5(3): 1832-36.

Reddy, P.S. and Nandini, N. 2011. Leachate characterization and assessment of groundwater pollution near municipal solid waste landfill site. Nat. Env. & Poll. Tech., 10(3): 415-18.

Sarala, C. and Babu, P.R. 2012. Assessment of groundwater quality parameters in and around Jawaharnagar, Hyderabad. International Journal of Scientific and Research Publications, 2(10): 1-6.

Snehlata, Lohchab R. and Nain, A. 2015. Anaerobic treatment of MSW using leachate recirculation bioreactor: A case study of Rohtak City. Nat. Env. & Poll. Tech., 14(4): 919-922

Tighiri, H.O. and Erkurt, E.A. 2019. Biotreatment of landfill leachate by microalgae-bacteria consortium in sequencing batch mode and product utilization. Bioresource Technology, 286: 121396.

Zhang, D., Vahala, R., Wang, Y. and Smets, B.F. 2016. Microbes in biological processes for municipal landfill leachate treatment: Community, function and interaction. International Biodeterioration & Biodegradation, 113: 88-96.

Nature Environment and Pollution Technology
An International Quarterly Scientific Journal

p-ISSN: 0972-6268
e-ISSN: 2395-3454

Vol. 19 | No. 1 | pp. 385-388 | 2020

Original Research Paper | Open Access

Detoxification of Glucose, Ammonium and Formaldehyde Using Nitrification and Plant Processes

Denesya Natalia Paris and Sarwoko Mangkoedihardjo†
Department of Environmental Engineering, Faculty of Civil, Environmental and Geo Engineering, Institut Teknologi Sepuluh Nopember (ITS), Surabaya, Indonesia
†Corresponding author: Sarwoko Mangkoedihardjo

Nat. Env. & Poll. Tech.
Website: www.neptjournal.com

Received: 18-05-2019
Accepted: 22-07-2019

Key Words:
Detoxification
Toxicity units
Nitrification
Plant processes

ABSTRACT

The purpose of this study was to obtain the removal efficiency values from glucose, ammonium and formaldehyde based on toxicity units. The nitrification process is applied using nitrifying bacteria and the process of plants using water hyacinth. The toxicity tests used were bacterial respiration test and test with batch reactor system for plants. The results show that the EC50 value of formaldehyde was smaller than ammonium and glucose. Formaldehyde was the most toxic substance among these substances, but its detoxification efficiency was high; this may be due to an antagonistic effect (from toxic to less toxic) mixture of substances.

INTRODUCTION

Toxic substances can be either organic or inorganic. These toxic substances have target selectivity, which can affect many tissues and many cells, or biological processes, and the second is that they can affect certain tissues or cells (Hayes 2003). A substance can be tested for its toxicity using exposure to the test biota. In reality, biota is exposed not only to one type of substances, but to be exposed to toxic substances that contain many substances. Negative effects are toxic for living things based on the interaction of many substances in the environment (Di Poi et al. 2018).

In this study 3 types of substances namely ammonium, glucose and formaldehyde were used. Ammonium is a source of nutrition for the growth of plants and bacteria. Glucose is also the main energy source in metabolism, the process of respiration, the growth of new cells, and in high concentrations can stimulate the growth of biota, especially acting as a carbon source for bacteria to grow (Ebel et al. 2007). Formaldehyde, when released into water, will be toxic. Formaldehyde does not last long in the environment, but its continuous release and formation can result in chronic exposure to biota near sources that produce formaldehyde (Mendez et al. 2015).

The existence of water hyacinth and nitrifying bacteria as biota can be used as indicators of certain types of pollution in water bodies and adverse effects on the surrounding ecosystem. With this toxicity test, it is intended to find out the effects of ammonium, glucose and formaldehyde on aquatic biota which can be in the form of effects on growth that results in ecosystem changes. This can show the level of certain pollutions in the environment and their adverse effects on the surrounding ecosystem.

MATERIALS AND METHODS

Initial Data Collection

The preliminary data needed in the study were the characterization of leachate in the solid waste disposal site of Surabaya city, which was located in Benowo. These data are used as the basis for making the concentration of ammonium and organic substances as BOD and COD and specifically, formaldehyde.

Preparation of Test Biota

All water hyacinth (*Eichhornia crassipes*) plants used in toxicity tests must be acclimatized in clean water for 7-14 days. After the propagules revealed that the new shoots have emerged, the latter were used for the test biota. The plants used from the propagation stage are second generation with criteria: number of leaves 3 strands, leaves that are still fresh and not yellowing, plant age is about 20 days and plant height 24-25 cm (Ebel et al. 2007, Hartanti et al. 2014).

Acclimatization was carried out for at least 7-14 days. During this process the plants must get enough sunlight for photosynthesis, the space to grow is large, the water is calm, and the temperature is between 20-30°C. The reactor is placed in greenhouse and the pH for the growth of water hyacinth ranges from 4.5 to 7.5. The microorganism, which was used in this study was *Nitrosomonas europaea*. This bacterium is in the form of liquid culture that is ready to use.

Range Finding Test

In each container 4 plants were placed with a height of about 24-25 cm. The total volume of the solution in the reactor was 4 litres. Variations in toxic concentrations are distinguished in the percentage of toxicity, which are equal to 0% (control); 20%; 40%; 60%; 80% and 100%. For control, it only contains water hyacinth and diluent water without toxicity. Range finding test (RFT) is carried out for 4 days.

In the range finding stage the toxicity test for *Nitrosomonas europaea* was carried out to determine the maximum levels of substances that could be tolerated by the test bacteria. Toxicity tests were carried out using liquid media, namely Nutrient Broth (NB) media commonly used for bacterial culture. Toxicity testing with liquid media was carried out by growing bacteria on NB media, each of which was contaminated with toxins namely ammonium, glucose and formaldehyde. The toxicity concentration used is 0, 20%, 40%, 60%, 80% and 100%. Bacteria inoculated into NB media contaminated with toxicants were then seen to decrease CO_2 gas in the test reactor. The initial number of inoculated bacteria is 10% v/v (William & Dilosi 2018).

Acute Toxicity Test

The acute toxicity test aims to determine the toxic concentration that can cause a 50% effect of the test biota in a relatively short time. For each different concentration, the test was repeated 3 times. In each reactor in the plant test, 10 water hyacinth plants were kept in 10 litres of water. Toxicants like ammonium, glucose and formaldehyde were mixed and put into the reactor according to the concentration obtained from the RFT results. Negative effect data that occur in plants obtained at 96 hours were used to determine the EC50 value. Variations in toxic concentration were determined in the narrowed range finding test. For control, it only contains water hyacinth and diluent water without toxicity.

Nitrosomonas europaea bacteria was put into a reactor containing NB media contaminated with ammonium, glucose, formaldehyde mixed. Variations in toxic concentration were determined in the narrowed range finding test. For the control, it only contained NB media without toxicity and it was incubated with *Nitrosomonas europaea* as much as 10% v/v. For the bacterial test using respiration test to determine the concentration of toxicity, which caused the inhibition of the function of respiration activity from the bacteria *Nitrosomonas europaea*, can be seen from the volume of air (CO_2 gas), which decreased 50% of the gas volume in the control at the respiration test reactor. Negative effect data on bacteria obtained at 24-hour observation were used to determine the EC50 value. The reactor used is the same as the RFT.

Detoxification Efficiency

The detoxification efficiency of toxicants was determined using toxicity units with the following equation:

$$TU = 1/EC_{50}$$

$$\text{Detoxification efficiency } (\%) = \frac{TU_{in} - TU_{eff}}{TU_{in}} \times 100\%$$

TU_{in} = toxicity unit influent (in this experiment in the reactor of nitrification process using *N. europaea*)

TU_{eff}= toxicity unit effluent (in this experiment in the reactor of plant process using *E. crassipes*)

RESULTS AND DISCUSSION

Characteristics of Leachate

Leachate used came from the Benowo landfill collection pool. Samples were analysed to determine the initial characteristics of leachate. The parameters used were BOD, COD, pH, temperature, turbidity and NH_4. Table 1 shows the characteristics of Benowo landfill leachate.

Table 1 was used as the basis for making artificial waste concentrations. Artificial waste used comes from chemicals that are made from pro analyst or pure. This study did not use original leachate in the study. This is intended because using artificial waste, desired concentration is obtained and the achievement can be close to what we want rather than original waste.

Test Against *N. europaea*

Ammonium solution used was 147 mg/L, 294 mg/L, 441 mg/L, 588 mg/L and 735 mg/L and control solution (without ammonium). The results of the range finding test revealed that the highest ammonium concentration which showed a decrease in the volume of water in the measuring cup was 294 mg/L, which was as much as 25 mL.

The glucose concentration used in the RFT stage was 203.44 mg/L; 406.88 mg/L; 610.32 mg/L, 813.76 mg/L, 1,017.2 mg/L and control solution (without glucose). The results of the range finding test showed that the highest glucose concentration which showed a decrease in the volume

Table 1: Characteristics of Benowo landfill leachate.

No.	Parameter	Unit	Results
1	Temperature	°C	28°C
2	pH	-	8.21
3	Turbidity	NTU	478
4	DO	mg/L	0.8
5	BOD	mg/L	1085
6	COD	mg/L	2560
7	NH_4	mg/L	735

of water in the measuring cup was 1,017.2 mg/L, which was 27 mL.

Formaldehyde concentration used was 0 mg/L as control, 0.24 mg/L, 1.2 mg/L, 2.4 mg/L, 12 mg/L, 24 mg/L, 120 mg/L, 240 mg/L, 480 mg/L, 960 mg/L, 1,440 mg/L, 1,920 mg/L and 2,400 mg/L. The results of the range finding test showed that glucose concentration which showed a decrease in the volume of water in the measuring cup was 0.24 mg/L which is 10 mL.

After obtaining the concentration range in each test solution, namely the concentration where *Nitrosomonas europaea* is able to produce CO_2 gas reduction seen from the decrease in water volume in the reverse measuring cup, the three test solutions, namely NH_4Cl, glucose and formaldehyde were mixed to determine the effect that occurs when these substances interact. In this main test, NB media was mixed with toxic substances, NH_4Cl, glucose and formaldehyde, then the bacterium was added to the reactor by 10% of the volume of the test media.

Test Against *E. crassipes*

At this stage it will be known that what maximum toxic concentration that can be received by *E. crassipes*. Definition of toxic effects of exposure to NH_4 solution on water hyacinth is that which does not appear to produce new shoots in plant tissues due to pollution (Mangkoedihardjo & Samudro 2014).

The results of the range finding test that will be selected are ammonium concentrations that do not have a negative effect on plants, namely the concentration that makes water hyacinth show new shoots and remain fresh. In this case NH_4 inhibits the growth of shoots, but not the leaves and stems so they remain green. In the first stage, namely with NH_4 until the fourth day, so the concentration of NH_4 used is at 40%, namely the concentration of NH_4 294 mg/L in plants of *E. crassipes*, because at concentrations of 60%, 80% and 100% all do not show new shoots. The highest concentration of ammonium which is toxic or inhibits growth is unknown, but water hyacinth begins to experience stunted growth at concentrations of NH_4 in water at 370 mg/L (Qin et al. 2016).

In glucose solutions, water hyacinth is able to show new shoots in all the toxic concentrations within 2 days. In RFT glucose solution using a concentration of 100%, which is 1.017 mg/L for the main test. This is because each plant produces glucose in the photosynthesis process which is used as an energy source by these plants. Therefore, organic matter, namely glucose, is a carbon source that is non-toxic, so it does not have a toxic effect on all the concentrations above (Lastdrager et al. 2014). The temperature and pH during the study were 29-30°C and 6.9-7 respectively, which allowed water hyacinth to grow.

In formaldehyde, water hyacinth is able to show new shoots at a concentration of 1% which is 24 mg/L within 3 days, while concentrations above 1% some do not show new shoots. Formaldehyde includes non-biodegradable organic substances which are toxic. Formaldehyde is a toxic organic matter, and with the increasing level of toxicity it can cause the biota to die.

Concentration where water hyacinth is able to live 100% or show new shoots, the three test solutions, namely NH_4Cl, glucose and formaldehyde were mixed to determine the effects that occur when these substances interact. In the main test 10 hyacinth plants were put into each reactor containing toxicant and diluted water with a total volume of 10 L. The mixture of ammonium, glucose and formaldehyde has a 50% toxic effect on biota at the concentration of each substance when mixed, i.e. 360 mg/L, 1300 mg/L and 40 mg/L, respectively.

EC_{50} and Detoxification Efficiency

The EC_{50} value of non-biodegradable organic substance, namely formaldehyde, is smaller than ammonium solution and biodegradable organic substances, namely glucose (Table 2). This shows that formaldehyde is more toxic than glucose and ammonium. In addition, plant processes can reduce the level of substance toxicity.

Table 2: EC_{50}-96h (mg/L) for the test toxicants.

Toxicants	*N. europaea*	*E. crassipes*
Glucose	1066.2	1307.12
Ammonium	329.07	361.31
Formaldehyde	0.34	0.4033

Based on Table 2 data, the detoxification efficiency can be calculated with the following results: glucose (16%) > formaldehyde (15%) > ammonium (7%). Formaldehyde is the most toxic substance among these substances, but its efficiency is high, this may be due to an antagonistic effect (from toxic to less toxic) mixture of substances.

CONCLUSION

The results of the study of the effects of glucose, ammonium and formaldehyde concentration on *N. europaea* bacterium and plant *E. crassipes* showed that the most toxic substance was formaldehyde. However, the efficiency of detoxifying mixed substances indicates the possibility of an antagonistic effect of the mixture of substances. And, that possibility requires further research.

REFERENCES

Di Poi, C., Costil, K., Bouchart, V., Lemeille, H. and Pierre, M. 2018. Toxicity assessment of five emerging pollutants, alone and in binary or ternary mixtures, towards three aquatic organisms. Journal of Environment Science & Pollution Resources, 25: 6122-6134.

Ebel, M., Evangelou, M.W.H and Schaeffer, A. 2007. Cyanide phytoremediation by water hyacinths (*Eichhornia crassipes*). Chemosphere, 66: 816-823.

Hartanti, P.I., Haji, A.T.S. and Wirosoedarmo, R. 2014. Pengaruh Kerapatan Tanaman Eceng Gondok Terhadap Penurunan Logam Kromium Pada Limbah Cair Penyamakan Kulit. Jurnal Sumberdaya Alam dan Lingkungan, 1(2): 31-37.

Hayes, A.W. (eds). 2003. Principles and Methods of Toxicology. CRC Press.

Lastdrager, J., Hanson, J. and Smeekens, S. 2014. Sugar signal and the control of plant growth and development. Journal of Experimental Botany, 65(3): 799-807.

Mangkoedihardjo, S. and Samudro, G. 2014. Research strategy on kenaf for phytoremediation of organic matter and metals polluted soil. Advances in Environmental Biology, 8(17): 64-67.

Mendez, J.A.O., Melian, J.A.H., Arana, J., Rodriguez, J.M.D and Diaz, O.G. 2015. Detoxification of waters contaminated with phenol, formaldehyde and phenol–formaldehyde mixtures using a combination of biological treatments and advanced oxidation techniques. Journal Catalysis Environmental, 163: 63-73.

Qin H., Zhang Z., Liu M., Liu H., Wang Y., Wen X., Zhang Y. and Yan S. 2016. Site test of phytoremediation of an open pond contaminated with domestic sewage using water hyacinth and water lettuce. Ecological Engineering, 95(1): 753-762.

William, J.O. and Dilosi, L.B. 2018. Response of chemolithotrophic Nitrobacter, Nitrosomonas to toxicity of organophoshphate and pyrethroid pesticides. Asian Journal of Biology, 7(1): 1-8.

Nature Environment and Pollution Technology
An International Quarterly Scientific Journal

p-ISSN: 0972-6268
e-ISSN: 2395-3454

Vol. 19 | No. 1 | pp. 389-393 | 2020

Original Research Paper | Open Access

The Removal of Phosphorus in Solution by the Magnesium Modified Biochar from Bamboo

Jing Dai*, Xitong Zheng*, Hong Wang, Hao Zhang**, Linli Zhang, Tianbiao Lin, Rui Qin* and Muqing Qiu*†**
*College of Life Science, Shaoxing University, Shaoxing, 312000, P.R. China
**Key Laboratory of Agro-Ecological Processes in Subtropical Region, Institute of Subtropical Agriculture, Chinese Academy of Sciences, Changsha 410125, China
†Corresponding author: Muqing Qiu

Nat. Env. & Poll. Tech.
Website: www.neptjournal.com

Received: 14-06-2019
Accepted: 24-07-2019

Key Words:
Phosphorus
Magnesium modified biochar
Bamboo

ABSTRACT

The eutrophication of water would cause the quality of the water to deteriorate and the algae to grow in large quantities. The recovery of phosphorus from sewage can not only purify the water quality, but also achieve the recycling of phosphorus. Its environmental and economic benefits are considerable. In this study, bamboo was used as raw material and modified with MgCl2 solution to prepare Mg-loaded biochar from bamboo (Mg@B). The adsorption experiments of phosphorus in solution by Mg@B were carried out. The adsorption kinetics of phosphorus by Mg@B was depicted by pseudo-first order kinetic and pseudo-second order kinetic models. The results showed that the surface of Mg@B is covered with the compound of Mg(OH)2. The adsorption process fits well with the pseudo-second order kinetics equation. The predominant process is chemisorption, which involves a sharing of electrons between the adsorbate and the surface of the adsorbent. The factor limiting the rate of reaction is primarily the number of surface-active sites of the adsorbent. The mechanism of Mg@B adsorbing phosphate ions in solution has physical adsorption, electrostatic adsorption and chemical precipitation.

INTRODUCTION

With the rapid development of industry and agriculture, the emissions of eutrophic substances, such as N, P, and so on, have also increased dramatically. The eutrophication of water would cause the water quality of the water to deteriorate and the algae to grow in large quantities (Jiang et al. 2019, Pinto et al. 2019). For a long time, in order to control the eutrophication of water bodies, many scholars have carried out related scientific research work, such as A/O, A/A/O, UASB and so on (Shamim & Joann 2016, Elsa et al. 2018, Khouloud et al. 2018, Zhang et al. 2018). These wastewater treatment methods are effective in treatment of phosphorus in solution, and the effect is better. As a non-renewable resource, phosphorus is a kind of the indispensable resource in agricultural development. The recovery of phosphorus from sewage can not only purify the water quality, but also achieve the recycling of phosphorus. Its environmental and economic benefits are considerable (Sarah et al. 2018, Sun et al. 2018). At present, the development direction of phosphorus treatment technology has shifted from removal of phosphorus in solution to recovery of phosphorus in wastewater (Fang et al. 2015). The treatment methods used for phosphorus recovery mainly include chemical precipitation, crystallization, ion exchange, adsorption, and so on (He et al. 2014, Huang et al. 2018, Qiu et al. 2018, Sanna et al. 2018). The adsorption method is applied widely because of its simple operation, no secondary pollution, and low price. The most commonly used adsorbents are activated carbon, modified cellulose, etc., but these adsorbents are limited in their application due to their high cost (Jessica et al. 2017). Therefore, some researchers have begun to use low-cost agricultural waste to prepare biochar, such as bamboo, peanut shell, tangerine skin, corn straw, rice straw, sawdust, reeds, and so on (Gottipati & Mishra 2013, Xu et al. 2014, Hu et al. 2017, Sarah et al. 2018). However, the surface of the prepared biochar contains a large amount of negative charge (Yigit & Mazlum 2007). These negative charges are very easy to generate electrostatic repulsion with anions, so it is difficult to adsorb PO_4^{3-} ions in solution. In order to improve their adsorption capacity of anions, many scholars apply acid, alkali, iron oxide, magnesium ion, rare earth and so on to modify the surface of these biochars (Stratful et al. 2001, Tansel et al. 2018).

In this study, bamboo was used as raw material and modified with $MgCl_2$ solution to prepare Mg-loaded biochar from bamboo (Mg@B). The adsorption experiments of phosphorus in solution by Mg@B were carried out. The adsorption kinetics of phosphorus by Mg@B was depicted by pseudo-first order kinetic and pseudo-second order kinetic models. The adsorption characteristics of phosphorus in

solution were studied by scanning electron microscope (SEM), Fourier infrared spectroscopy (FTIR) and X-ray diffraction spectrum (XRD) techniques. The adsorption mechanisms have also been discussed.

MATERIALS AND METHODS

Preparation of Mg@B

The biochar from bamboo is ground and passed through a 100 meshes sieve. Its specific surface area is 60.125 m^2/g, and average pore size is 10. 2.109 nm. The 10 g biochar from bamboo was added to the 500 mL Erlenmeyer flasks containing 100 mL 2 mol/L $MgCl_2$ solution. Then, 100 mL 4.5 mg/L NaOH was added slowly. They were shaken in an ultrasonic shaker for 60 minutes. The mixture solution was filtered through a qualitative filter paper. The precipitate was washed three times with the deionized water. The precipitate was dried at 60°C for 48 hours in an oven and calcined at 450°C for 2 hours in a muffle furnace to obtain the Mg-loaded biochar from bamboo (Mg@B).

Characterization of Mg@B

The morphology of Mg@B was observed with SEM (JEOL 6500F, Japan). The XRD analysis was conducted in a D/Max-IIIA powder X-ray diffraction spectrum (Rigaku Corp., Japan). FTIR spectra of the samples were recorded on a Nexus 670 FTIR spectrometer (Thermo Nicolet, Madison) in the wave number range of 500-4000 cm^{-1}.

Adsorption Experiment

Adsorption experiments were conducted in a set of 250 mL Erlenmeyer flasks containing 0.02 g Mg@B and 100 mL of 50 mg/L PO_4^{3-} ion solutions. The initial pH was adjusted to 4.0 with 1 mol/L HCl. The flasks were placed in a shaker at a constant temperature of 298 K and 200 rpm. The samples were filtered and analysed.

Analytical Methods

The concentration of PO_4^{3-} ion was analysed by UV-722 UV-visible spectrophotometry. The removal rate of PO_4^{3-} ion was calculated as follows:

$$Q = \frac{C_0 - C_t}{C_0} \times 100\% \quad \ldots(1)$$

Where, C_0 and C_t (mg/L) are the initial and equilibrium concentrations of PO_4^{3-} ion in solution respectively. Q is the removal rate of PO_4^{3-} ion.

Statistical Analyses of Data

All the experiments were repeated in duplicate and the data of results were the mean and the standard deviation (SD). The value of the SD was calculated by Excel software. All the error estimates given in the text and error bars in figures are standard deviation of means (mean ± SD). All the statistical significance was noted at $\alpha = 0.05$ unless otherwise noted.

RESULTS AND DISCUSSION

Characterization of Mg@B

The morphology of biochar and Mg@B were observed with SEM. The results are shown in Fig. 1.

From Fig. 1, it can be seen that biochar from bamboo is a porous material. After modification of magnesium, the surface of biochar is covered with a thick layer of flocculent material. This flocculent substance should be a compound of magnesium. The magnesium compound is uniformly

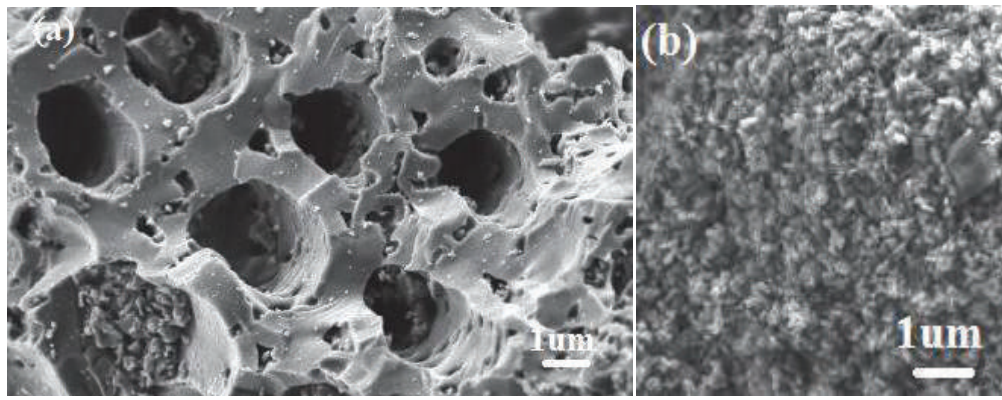

Fig. 1: The SEM images of biochar and Mg@B (a, biochar; b, Mg@B).

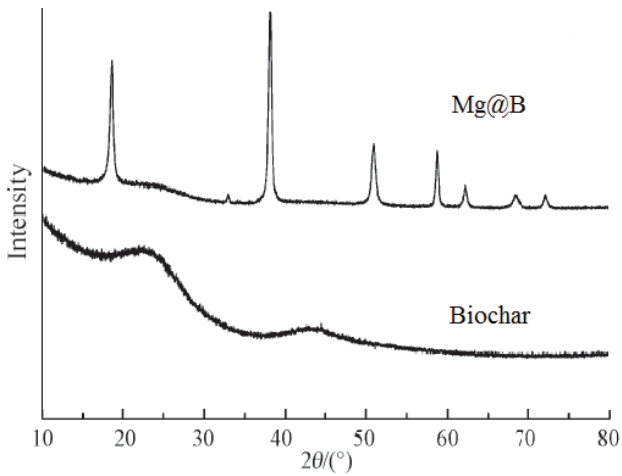

Fig. 2: The XRD spectra of biochar and Mg@B.

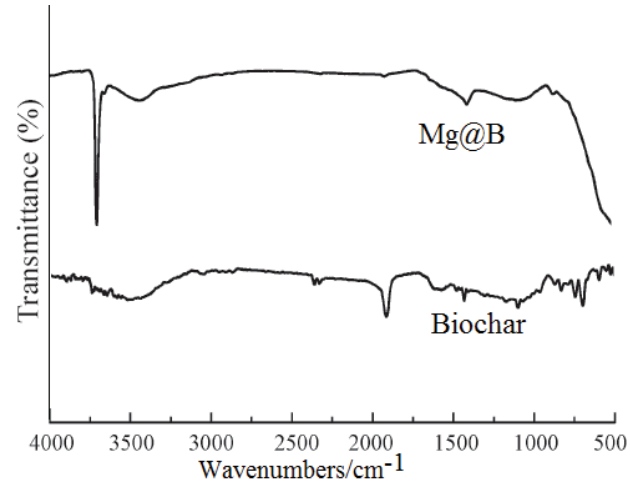

Fig. 3: FTIR spectra of biochar and Mg@B.

supported on the surface of the biochar and inside the pore diameter.

The XRD analysis of biochar and Mg@B were conducted in a D/Max-IIIA Powder X-ray diffraction spectrum. The results are shown in Fig. 2.

As shown in Fig. 2, it can be concluded that after modification of magnesium, many high-intensity diffraction peaks of $Mg(OH)_2$ appeared. It also indicates that the modified magnesium has been successfully loaded on the biochar from bamboo. It can also be shown in FTIR spectra of Mg@B (Fig. 3). There is a distinct characteristic absorption peak of $Mg(OH)_2$ at a wavelength of 3694.2 cm^{-1}.

Adsorption Experiment

The effect of adsorption time on the PO_4^{3-} ion removal rate by Mg@B is shown in Fig. 4.

As shown in Fig. 4, it can be seen that the removal rate of PO_4^{3-} ion in solution by Mg@B increased rapidly within 30 minutes. At 60 minutes, the amount of PO_4^{3-} ion adsorbed is near saturation. After 240 minutes, the adsorption process reached equilibrium. The removal rate of PO_4^{3-} ion by Mg@B was reached 64.12%.

Adsorption Kinetics

In this study, the pseudo-first order and pseudo-second order were chosen to depict the adsorption kinetics. The pseudo-first order (Choudhary & Paul 2018) and pseudo-second order (Reguyal et al. 2017) reactions were described as Eqs. (1) and (2):

$$\frac{dq_t}{dt} = k_1(q_e - q_t) \quad \ldots(1)$$

$$\frac{dq_t}{dt} = k_2\left(q_e - q_t\right)^2 \quad \ldots(2)$$

Where, q_e (mg/g) is the amount of adsorbed solute at equilibrium conditions, q_t (mg/g) is the amount of adsorbed solute at any time t (min), k_2 (min^{-1}) and k_1 (min^{-1}) are the constants of pseudo-second order and pseudo-first order kinetic models respectively.

According to the experimental data from Fig. 4 and Equations (1) and (2), the corresponding calculated parameters are listed in Table 1.

From Table 1, it can be shown that the adsorption process fits well with the pseudo-second order kinetics equation according to the value of R^2 (0.9917). It implies that the predominant process is chemisorption, which involves a sharing of electrons between the adsorbate and the surface of the adsorbent. The factor limiting the rate of reaction is primarily the number of surface active sites of the adsorbent.

Adsorption Mechanism

The mechanism of biochar adsorbing phosphate ions is that phosphate ions can be bonded to certain metal cations in biochar by electrostatic adsorption or ligand bonding (Mukherjee & Zimmerman 2013). After the biochar is modified with magnesium, the following reaction would occur between the biochar and the phosphate ions in solution.

$$Biochar - Mg(OH)_2 + PO_4^{3-} + 6H_2O \rightarrow Biochar - Mg_3(PO_4)_2 \cdot 6H_2O \downarrow \quad \ldots(3)$$

In brief, the mechanism of Mg@B adsorbing phosphate ions in solution has physical adsorption, electrostatic adsorption and chemical precipitation.

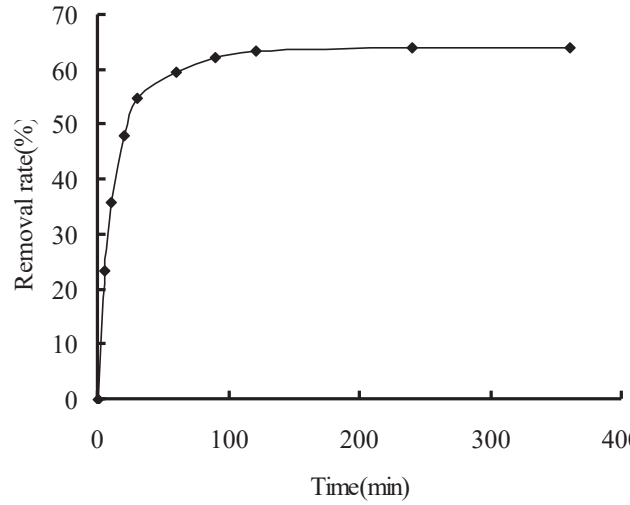

Fig. 4: Effect of adsorption time on the PO_4^{3-} ion removal rate by Mg@B.

Table 1: Pseudo-first order kinetic and pseudo-second order kinetic parameters of PO_4^{3-} ions removal by Mg@B.

Pseudo-first order			Pseudo-second order		
q_e (mg/g)	k_α (min^{-1})	R^2	q_e (mg/g)	k_β ($g/mg^{-1}/min^{-1}$)	R^2
125.17	0.0853	0.9241	130.25	0.001	0.9917

CONCLUSIONS

1. The surface of Mg@B is covered with a thick layer of flocculent material. This flocculent substance should be a compound of magnesium. According to the results of XRD spectrum and FTIR spectrum, the compound of magnesium on the surface of Mg@B is $Mg(OH)_2$.
2. The adsorption process fits well with the pseudo-second order kinetics equation. The predominant process is chemisorption, which involves sharing of electrons between the adsorbate and the surface of the adsorbent. The factor limiting the rate of reaction is primarily the number of surface active sites of the adsorbent.
3. The mechanism of Mg@B adsorbing phosphate ions in solution has physical adsorption, electrostatic adsorption and chemical precipitation.

ACKNOWLEDGEMENTS

This study was financially supported by the project of science and technology plan in Zhejiang Province (LGF19C030001), Guangxi Key Research and Development Program (AB17129002 and AB18050018)) and the project of science and technology plan in Shaoxing City (2017B70058).

REFERENCES

Choudhary, B. and Paul, D. 2018. Isotherms, kinetics and thermodynamics of hexavalent chromium removal using biochar. J. Environ. Chem. Eng., 6: 2335-2343.

Elsa, A., Mohan, V.J., Graham, B. and Philip, A.S. 2018. Isotherms, kinetics and mechanism analysis of phosphorus recovery from aqueous solution by calcium-rich biochar produced from biosolids via microwave pyrolysis. J. Environ. Chem. Eng., 6: 395-403.

Fang, C., Zhang, T., Li, P., Jiang, R.F., Wu, S.B., Nie, H.Y. and Wang, Y.C. 2015. Phosphorus recovery from biogas fermentation liquid by Ca-Mg loaded biochar. J. Environ. Sci., 29: 106-114.

Gottipati, R. and Mishra, S. 2013. Preparation of microporous activated carbon from Aegle marmelos fruit shell by KOH activation. Canadian J. Chem. Eng., 91: 1215-1222.

He, H., Qian, T.T., Liu, W.J., Jiang, H. and Yu, H.Q. 2014. Biological and chemical phosphorus solubilization from pyrolytical biochar in aqueous solution. Chemosphere, 113: 175-181.

Hu, B.W., Qiu, M.Q., Hu, Q.Y., Sun Y.B., Sheng, G.D., Hu, J. and Ma, J.Y. 2017. Decontamination of Sr(II) on magnetic polyaniline/graphene oxide composites: Evidence from experimental, spectroscopic, and modeling investigation. ACS Sustain. Chem. & Eng., 5: 6924-6931.

Huang, D.L., Deng, R., Wan, J., Zeng, G.M., Xue, W.J., Wen, X.F., Zhou, C.Y., Hu, L., Liu, X.G., Xu, P., Guo, X.Y. and Ren X.Y. 2018. Remediation of lead-contaminated sediment by biochar-supported nano-chlorapatite: Accompanied with the change of available phosphorus and organic matters. J. Hazard. Mater., 348: 109-116.

Jessica, G.S., Wolfram, B., Saran, P.S. and Kate, V.H. 2017. Bioavailability of phosphorus, other nutrients and potentially toxic elements from marginal biomass-derived biochar assessed in barley (*Hordeum vulgare*)

growth experiments. Sci. Total Environ., 584-585: 448-457.

Jiang, Y.H., Li, A.Y., Deng, H., Ye, C.H., Wu, Y.Q., Linmu, Y.D. and Hang, H.L. 2019. Characteristics of nitrogen and phosphorus adsorption by Mg-loaded biochar from different feedstocks. Bioresource Technol., 276: 183-189.

Khouloud, H., Salah, J., Mejdi, J., Aida, B.H.T. and Lionel, L. 2018. Investigations on phosphorus recovery from aqueous solutions by biochars derived from magnesium-pretreated cypress sawdust. J. Environ. Manag., 216: 305-314.

Mukherjee, A. and Zimmerman, A.R. 2013. Organic carbon and nutrient release from a range of laboratory-produced biochars and biochar-soil mixtures. Geoderma, 193: 122-130.

Pinto, M.C.E., Silva, D.D., Gomes, A.L.A., Santos, R.M.M., Couto, R.A.A., Novais, R.F., Constantino, V.R.L., Tronto, J. and Pinto, F.G. 2019. Biochar from carrot residues chemically modified with magnesium for removing phosphorus from aqueous solution. J. Clean. Prod., 222: 36-46.

Qiu, M.Q., Wang, M., Zhao, Q.Z., Hu, B.W. and Zhu, Y.L. 2018. XANES and EXAFS investigation of uranium incorporation on nZVI in the presence of phosphate. Chemosphere, 201: 764-771.

Reguyal, F., Sarmah, A.K. and Gao, W. 2017. Synthesis of magnetic biochar from pine sawdust via oxidative hydrolysis of $FeCl_2$ for the removal off sulfamethoxazole from aqueous solution. J. Hazard Mater., 321: 868-878.

Sanna, S., Mari, R., Maarit, H. and Perttu, V. 2018. Biochar addition changed the nutrient content and runoff water quality from the top layer of a grass field during simulated snowmelt. Agr. Ecosyst. Environ., 265: 156-165.

Sarah, V.N., Mariana, D.O.Z., Jairo, T., Rafaela, F.C. and Carlos, E.P.C. 2018. Poultry manure and sugarcane straw biochars modified with $MgCl_2$ for phosphorus adsorption. J. Environ. Manag., 214: 36-44.

Sarah, V.N., Mariana, D.O.Z., Matheus, S.C.B., Célia, R.M. and Carlos, E.P.C. 2018. Phosphorus removal from eutrophic water using modified biochar. Sci. Total Environ., 633: 825-835.

Shamim, G. and Joann, K.W. 2016. Biochemical cycling of nitrogen and phosphorus in biochar-amended soils. Soil Biol. Biochem., 103: 1-15.

Stratful, I., Scrimshaw, M.D. and Lester, J.N. 2001. Conditions influencing the precipitation of magnesium ammonium phosphate. Water Res., 35: 4191-4199.

Sun, D.Q., Hale, L., Kar, G., Soolanayakanahally, R. and Adl, S. 2018. Phosphorus recovery and reuse by pyrolysis: Applications for agriculture and environment. Chemosphere, 194: 682-691.

Tansel, B., Lunn, G. and Monje, O. 2018. Struvite formation and decomposition characteristics for ammonia and phosphorous recovery: A review of magnesium-ammonia-phosphate interaction. Chemosphere, 194: 504-512.

Xu, G., Sun, J.N., Shao, H.B. and Chang, S.X. 2014. Biochar had effects on phosphorus sorption and desorption in three soils with differing acidity. Ecol. Eng., 62: 54-60.

Yigit, N.O. and Mazlum, S. 2007. Phosphate recovery potential from wastewater by chemical precipitation at batch conditions. Environ. Technol. Lett., 28: 83-93.

Zhang, T., Xu, H.Y., Li, H.H., He, X.Y., Shi, Y.J. and Kruse, A. 2018. Microwave digestion-assisted HFO/biochar adsorption to recover phosphorus from swine manure. Sci. Total Environ., 621: 1512-1526.

Nature Environment and Pollution Technology
An International Quarterly Scientific Journal

p-ISSN: 0972-6268
e-ISSN: 2395-3454

Vol. 19 | No. 1 | pp. 395-402 | 2020

Original Research Paper | Open Access

Real-time Detection of Cyanide in Surface Water and its Automated Data Acquisition and Dissemination System

Alexander T. Demetillo*†, Rey Y. Capangpangan, Melbert C. Bonotan***, Jeanne Phyre B. Lagare** and Evelyn B. Taboada*****

*College of Engineering and Geosciences, Caraga State University, Butuan City 8600, Philippines
**College of Arts and Sciences, Caraga State University, Butuan City 8600, Philippines
***College of Computing and Information Systems, Caraga State University, Butuan City 8600, Philippines
****School of Engineering, University of San Carlos, Talamban, Cebu City 6000, Philippines
†Corresponding author: Alexander T. Demetillo

Nat. Env. & Poll. Tech.
Website: www.neptjournal.com

Received: 06-06-2019
Accepted: 24-07-2019

Key Words:
Real-time cyanide detection
Water quality monitoring
Electrochemical analysis

ABSTRACT

Use of cyanide in developing countries is rampant, especially in gold mining areas. Though it could cause serious environmental problems, cyanide contamination is of less priority for government monitoring because of the limited resources. The current detection and monitoring schemes of cyanide are the conventional and expensive laboratory-based methods, which need technical capabilities to conduct the actual testing and preparing manual data recording, making it tedious and too laborious. More efforts were directed towards digitizing the data recording from manual laboratory analyses as the manual data recording usually cause problems like delayed information, lost data, and erroneous data entry. Hence, the goal of this study is to provide a cost-effective and zero manual-recording measurement method for cyanide in water samples. This work focuses on the design of electrochemical measuring device with the same capability with the portable or benchtop-type of cyanide meter but with an automated and real-time data recording using global system for mobile communications (GSM) technology. Results of this study showed that with the existing GSM technology and infrastructure of the new monitoring system, the measurements are comparable to that of a commercial bench-type cyanide meter with an R-squared (R^2) of 0.9907. It was also noted that data being recorded were intact during wireless transmission testing using the GSM Network. The results obtained suggest that wireless communication using GSM Technology could be applied to environmental monitoring. Importantly, the new developed online system for cyanide monitoring offers significant advantages over the conventional techniques such as low-cost, easy deployment, and ease of use. It can increase spatiotemporal data for better analysis of the data. The automated data acquisition and display through cellular phones are also made readily-available.

INTRODUCTION

Human beings are aware of cyanide toxicity since early civilization. Cases of cyanide exposures in the Philippines, a developing country, have been reported (Stark et al. 2006). In developed countries, the cyanide disaster is well documented especially in the mining industry in which tons of cyanide were accidentally released to rivers, lakes, and oceans (Mudder et al. 2004). The need for more programs related to cyanide detection, monitoring, and fast information dissemination should be done to curtail more cyanide-related incidents.

Cyanide detection and monitoring are essential because of its toxicity to human beings and other living organisms (Ramzy 2014). Although nature produces cyanide through cyanogenic glucoside through plants, it is mostly man-made and intended for industries ranging from metal mining to medicine (Barnes et al. 2000). Cyanide toxicity is associated with various accidents, human diseases, and deaths (Guimaraes et al. 2011, Holden 2015).

Because of cyanide's toxicity and the possible damage, it could bring to humanity, several methods were developed to detect and monitor its presence. Some research deals on how to mitigate the effect of cyanide released to the environment (Gacsi et al. 2005). Despite these previous efforts, some researchers continue to pursue and explore the improvement of cyanide detection methods, protocols, and implementation. Most of these researches focus on increasing the frequency of data sensing by using mobile vehicle (Demetillo & Taboada 2019), lowering the cost to encourage implementation of monitoring and detection especially in developing countries (Nemiroski et al. 2014), improving information dissemination, effective methods of continuous monitoring, and other enhancement opportunities. Some

conventional methods involve atomic absorption spectroscopy (AAS), voltammeter (Safavi et al. 2004), titrations, high-performance liquid chromatography (HPLC) (Gamoh 2002), ion chromatography (IC), amperometry, polarograph, ion-selective electrodes (potentiometry), and fluorimetry. There are also new methods developed for cyanide detection which include electrochemical detection (ECD) (Abbaspour et al. 2005), optical sensors, gas chromatography (GC) (Gambaro et al. 2007, Murphy et al. 2006), quartz-crystal microbalance (QCM) (Sun et al. 2005), and mass spectrometry (MS). These traditional and new methods which mostly involve tedious laboratory analysis are also only capable of detecting low-level cyanide content. While these methods are accurate, they however, still have many limitations ranging from large sample size requirements, long detection period, limited frequency (limited information), and few sampling places (more sampling places increase cost). Analytical methods are also in need of expensive laboratory with high-end instruments, labor-intensive, and require highly skilled and specialized personnel, where scarcity of numbers exist in developing countries.

Cyanide concentration profile and distribution varies because of some environmental factors; thus, a need for real-time analysis is highly desirable. With much of the affected areas being far from the laboratory and considering the time of travel, it is difficult to get the real-time scenario of cyanide level especially rural and far-flung areas. Besides, the information provided by conventional off-line techniques cannot give managers and authorities, the lead time needed for mitigation measures in case of some accidents. Moreover, dynamic information through real-time data as updates and input to decision making and planning is vital for researchers, environmental managers, and other stakeholders (Bokingkito & Llantos 2017). With these, there is a need for fast and accurate acquisition of data, and it is reasonable to design alternative solutions, which could monitor the dynamic changes of cyanide concentrations in real-time. The automated detection system replaces the conventional laboratory-based cyanide detection methods because of several drawbacks like complexity, high-cost and slow information dissemination (Reddy et al. 2017, Gillooly et al. 2019).

Nowadays, the electrochemical technique has been the driving force for the continuous development and enhancement of cyanide monitoring (Jackson & Logue 2017). Advances in electronics, mobile communication technology, smartphone technology, and open source software served as enabling tools in the development of enhanced-sensing instruments. Improvement in electronics, in both size and capability, makes the new electrodes more low-cost, with the capacity for faster *in-situ* analysis, easy to prototype and deploy (Mross et al. 2015, Qin et al. 2018, Xu et al. 2016, Zhou et al. 2017). However, much of the improvement focused on the enhancement of the electrode (Ma & Dasgupta 2010) and very few for a complete system or set-up for automated cyanide monitoring (Randviir & Banks 2015).

This study aims to design, develop and implement real-time detection of cyanide in surface water and its automated data acquisition. This enables for faster information dissemination of the cyanide level of an area and automation of data recording which eliminates error caused by the manual methods.

MATERIALS AND METHODS

Chemical Reagents

All the chemical reagents used in this work were obtained from Hannah Instrument (USA). Deionized water, ionic strength (pH) adjuster (HI 4001-00) and dried KCN salt were mixed for the preparation of the standard solution. The cyanide electrode was filled with a reference fill solution (HI 7072) before starting new measurements based on the standard procedures in using ISE.

Apparatus, Electronics Components and Software

One of the most common methods in cyanide detection is using the commercial benchtop cyanide ion-selective electrode (ISE). The utilization of the customized electronics circuit and its ability to perform automation, especially in data acquisition, makes this research unique compared with the existing methods.

A commercial benchtop cyanide meter (Hannah Instrument-USA) serves as a reference method to validate the accuracy of the newly designed system. Both the methods, reference and the new system, employed a combination type of ion-selective electrode (ISE) from Hannah Instrument. This type of electrode is known for its easy usability and cost-efficiency compared to using two or three electrode systems.

The primary purpose of the interface circuit is to link the microcontroller and the ISE and condition the signal generated from the ISE as an input signal to the microcontroller. It is a customized circuit which consists of instrumentation (Philips, Japan) and an operational amplifier (Motorola, USA).

The microcontroller is an Arduino Mega 2560 (Arduino, Italy). Wireless communication transmitter and receiver (transceiver) is a GSM/GPRS module from Arduino (Italy). The system relies on battery as a power source with a lithium-ion battery (Panasonic, Japan) as the preferred battery type

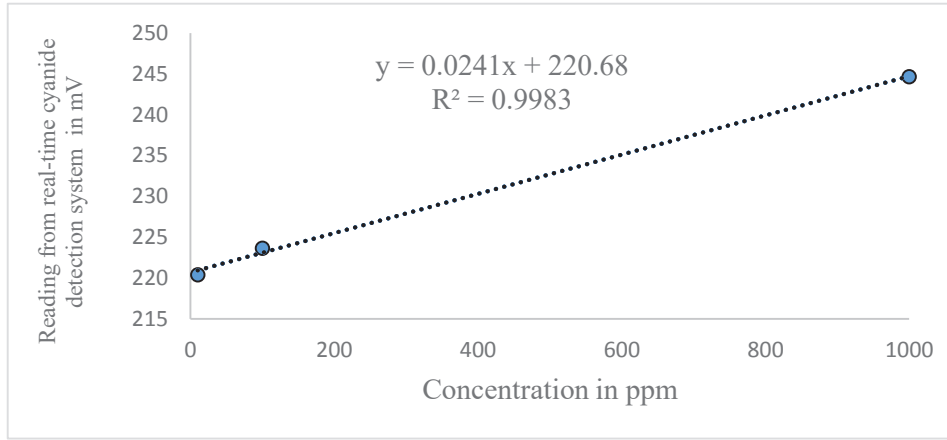

Fig. 1: Calibration curve of the cyanide sample.

for its high-energy capacity. It also has a timer circuit for its energy management, battery booster circuit and data backup circuitry (SD Card). Results generated from the new system are sent to a pre-defined cellphone (any cellphone type) using any GSM technology like 2G, 3G and 4G.

Arduino integrated development environment (IDE) is the software used for the development of the system's programs like pre-processing and conversion of signals from analog-to-digital and vice versa. Microsoft Excel VBA programming was employed to develop a tool to facilitate downloading of data from cellphone and SD card to a computer system for data banking and additional processing purposes.

Electrochemical Experiments

ISE calibration: The direct calibration method was adopted for the preparation and calibration of the cyanide ISE. A series of CN^- standard solutions with a concentration range from 0.1 ppm to 100 ppm were prepared, and the actual cyanide concentration reading (ppm) was measured using the cyanide ISE. Automatic offsetting by dipping the electrode to the prepared cyanide solutions with concentrations ranging from 0.01 to 100 ppm CN^- was conducted. Benchtop meter was calibrated using the cyanide ISE in a concentration range of 0.1 to 100 ppm. Fig. 1 is the calibration curve of cyanide sample. This graph is linear and highly reproducible which indicates good correlation with the standard samples.

Quality control: To confirm the validity and the performance of the newly-designed system, several electrochemical tests were conducted using the commercial bench-top cyanide meter and the new system under the same condition. Real water samples from the creek taken in a 15-minute interval were tested alternatively using the cyanide ISE and the newly-designed system utilizing the same electrode. Several samples were tested for its accuracy like combining water samples taken from a different location with the addition of the ionic strength adjuster (ISA) at 1000, 100 and 10 ppm.

Sampling Site

The sampling site is the creek running within the Caraga State University campus. The samples were taken at the various locations of the creek.

RESULTS AND DISCUSSION

Introduction to the Design of the System

Systems overview and design: Fig. 2 shows the block diagram of the overall system. It includes a commercial ISE as an electrochemical sensor to detect and monitor cyanide, a customized interface circuit, a controller, energy source, and the wireless transmission system. It also included other necessary electronics peripherals like a timer circuit, battery energy booster and back-up memory (SD card). The ISE through the interface circuit connected to the microcontroller using the I2C protocol. The electrode is a commercial ISE subjected to an international standard calibration and testing. Availability and easy acquisition for future implementation was also a reason for selecting the ISE based on the study (Hu et al. 2016). A customized interface circuit was designed and implemented to facilitate detection even with a small concentration of cyanide and to condition it for microcontroller input. The microcontroller preprocesses the signal into information (value of cyanide level in terms of mV). Before sending the newly processed information to the transceiver, the microprocessor converts the information into a suitable format ready for transmission using the GSM transceiver module. The receiver sent the information to the pre-identified cellphone users or computer systems. Backup information saved in the SD Card (attached

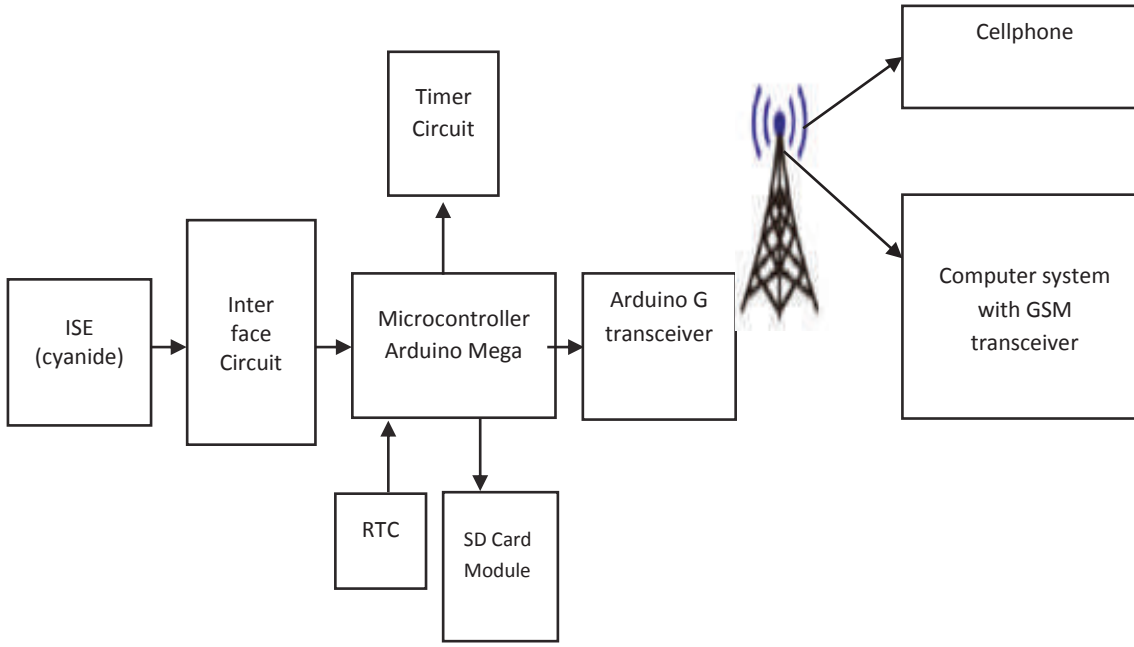

Fig. 2: Block diagram of the overall system.

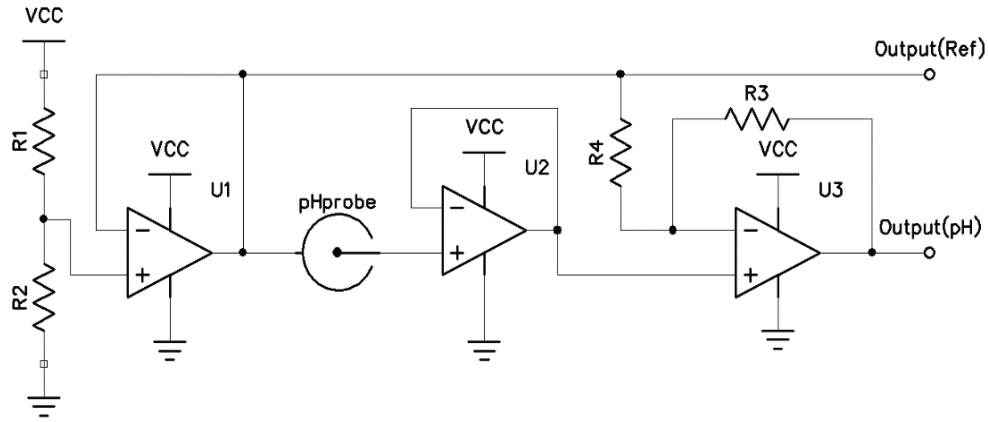

Fig. 3: Schematic diagram of the interface circuit.

to the microcontroller) can be retrieved anytime if the need arises.

Circuit system: The primary circuits of the system are the interface circuit, a microcontroller, the energy source, and management system, the wireless communication systems and other peripheral components like the SD card and real-time clock.

The customized interface circuit is based on the requirement of detecting ionic concentration which is a high input impedance. A schematic diagram of the interface circuit is shown in Fig. 3. ISE produces a small signal based on the cyanide level of the samples which the microcontroller cannot read directly. The primary function of the interface circuit is to boost and condition the detected cyanide level to be compatible with the microcontroller.

The microprocessor coordinates all the operations of the system. It preprocesses the gathered data into a usable format. Another function of the microcontroller is to prepare the signal for long-distance transmission using the wireless transceiver. The microcontroller is an Arduino Mega 2560. It

is one of the latest among Arduino development board. One of its features is the presence of an ample number of analog and digital (18) input pins for future expansion.

The timer circuit is an essential circuitry for power management. It allows the system to go to a sleep mode or wake-up mode on a prescribed time, and signal the ISE to gather data again thus, saving the much-needed battery energy and in effect extending the lifespan of the system. Another circuitry is the SD card module which hosted the micro-type of an SD memory card and served as the primary backup of the whole system. It is a backup mechanism that triggered every time the sensor-transmitted data or information. The format of the backup data is customized to fit the base station database format for easy transfer and retrieval of backup data if needed.

To energize the sensor, a lithium-ion battery with a capacity of 4350 mAh/3.7V was used. Within the sensor unit, some electronic components need up to 5 volts for their operation like the GSM module, which is an energy booster installed as part of the sensor component.

The GSM transceiver is a commercial GSM/GPRS module used to send data to a base station or directly to a pre-identified cellphone number. It can also receive SMS from the remote station for utilization during unscheduled data gathering, maintenance purposes, and others. The wireless transmission also used GSM/GPRS module which utilizes the commercial telecommunications infrastructure for the transmission.

Calibration: Before using the electrochemical probe (ISE), standard calibration sample with cyanide solutions was maintained at room temperature and stirred continuously. Calibration measurements were made with 100 mL of test solution in a suitable Pyrex beaker. All glassware was always decontaminated and washed several times with double-distilled water (DDW). Cyanide standard solutions were prepared using DDW and ionic strength (pH) adjuster (10-mL of HI 4001-00).

ISE characteristics and features: This work utilizes the ISE (HI4109) from Hannah Instrument (Rhode Island, USA), which is a solid state combination ion-selective electrode (ISE) for the determination of cyanide (CN-). The output of the ISE is a potential difference due to changes in the sample's ionic activity. Typically, ISE parts comprise of the following (i) connector to readout circuit or meter, (ii) cap, (iii) sensor body, and (iv) the sensing membrane. Protection was provided to the sensing element of the electrode by the polyetherimide (PEI) body, being the most sensitive part of the electrode and where accuracy and sensitivity set within its small and sensitive circuitry. It has a detection limit from 0.026 to 260 mg/L CN-.

Evaluation of the efficiency of the electrodes was conducted by comparing the specifications from the manufacturer (Hannah Instrument) to the actual output during the actual determination of cyanide in the laboratory or field. Also, this company specification serves as the reference in terms of the limits of detection, slope, response time and long-term stability as essential parameters to measure electrode performance. Calibrations are conducted using the manufacturer's manual of operation.

The potential response from the two testing additions of ionic strength adjuster (ISA) was linear. Tests with only freshwater samples (no mixing of ISA) show an erratic reading except for the 1st reading which shows an accurate measurement. The potential drift was approximately 20 mVh^{-1}. The response time of the ISE is approximately 10-20 seconds.

Repeatability and Accuracy of Cyanide Detection and Monitoring

In establishing the validity of the research methods, a standard sampling solution was tested by both the systems (new and a commercial benchtop meter) using the same electrodes resulting in a high R-squared value which constitute to a good accuracy of the new systems. To check the validity of the proposed method, measurement of the prepared cyanide standards solutions was made using the cyanide ISE (as the reference method) and the newly-designed system. The results of the analysis suggest that there is a higher correlation (high R^2 value) of the obtained results between the cyanide ISE method and the proposed method resulting to high R^2 value which constitutes to a good accuracy of the new systems. The results of the analysis suggest that there is a higher correlation (high R^2 value) of the obtained results between the cyanide ISE method and the proposed method.

Fig. 4 depicts the results obtained from the measurements of a mixed standard solution and the real samples. The results show that the recorded potential (200 mV) in a solution with a known cyanide concentration is in good agreement for both the applied methods. This further suggests that indeed, the newly-designed system is able to detect an accurate measurement in the manner as the cyanide ISE technique. However, it was observed that for water samples the potential reading was slightly higher using the cyanide ISE as compared to the newly-designed system. The reason for the observed nonconformity of results may be due to the effect of the ionic nature of the real water sample. For water samples, the values obtained through the commercial bench top tester was observed to be higher than those measurement readings from the new system.

Fig. 4 shows the results of twelve different setups consisting of 7 sampling sites. Data show that results from the

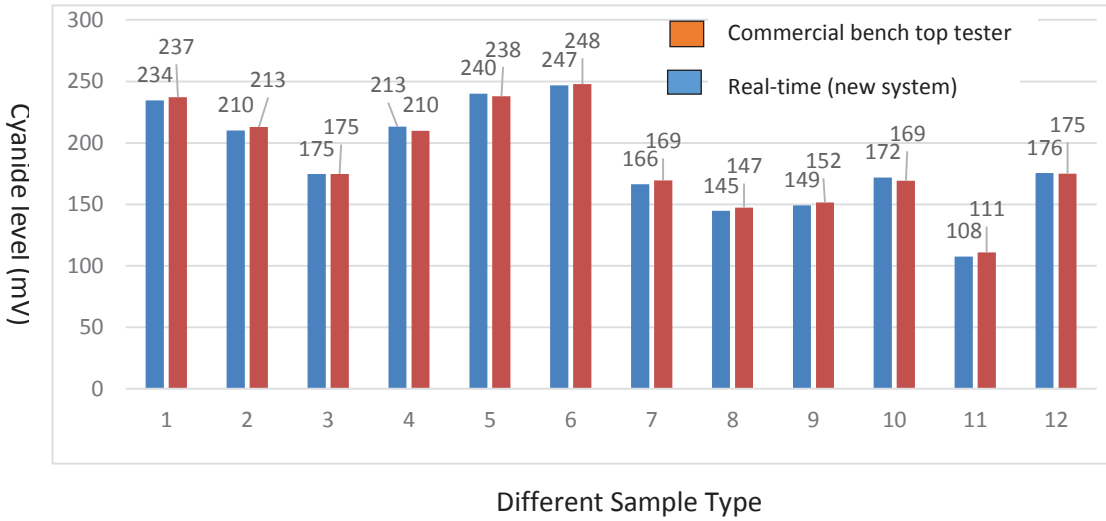

Fig. 4: Results obtained from the measurements of a mixed standard solution and the real samples.

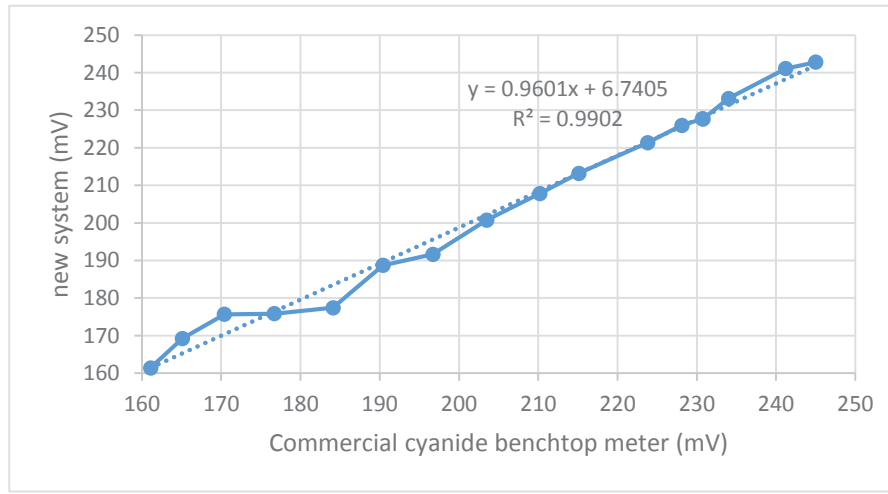

Fig. 5: Results generated from the new system with an R^2 of 0.99.

commercial benchtop meter are almost the same with the results generated from the new system with an R-squared of 0.99 as shown in Fig. 5. The average of the difference between the results of the ten samples is approximately 2mV. The lowest of these differences is 0.07 mV, and the highest is 3.35 mV. It shows that the newly developed system is capable of detecting cyanide at par with the commercial techniques available with an additional capability of automated data acquisition and reporting using GSM technology.

Fig. 6 shows the results of testing wherein the samples are tested without ISA. As expected, sample has erratic and unstable results. Fig. 7 shows the results of the testing wherein the required water samples and ISA are mixed (standard method) and resulted in stable readings.

In this work, the demonstration of the accuracy and suitability of an automated detection with real-time data acquisition and reporting prototype using ISE and wireless communication technology performed using a prototype is reported. A good correlation ($R^2 = 0.99$) between the levels determined by the accepted reference method (benchtop meter) and those measured by the new system were obtained and with no observed systematic errors.

CONCLUSIONS

Cyanide concentration can be monitored in real-time from

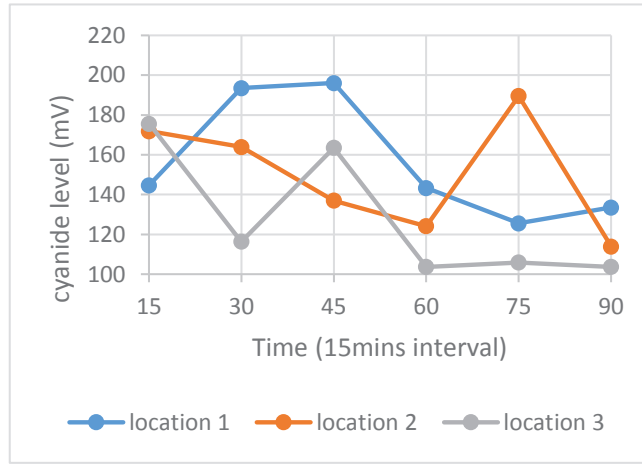

Fig. 6: Results of testing wherein the samples are tested without ISA.

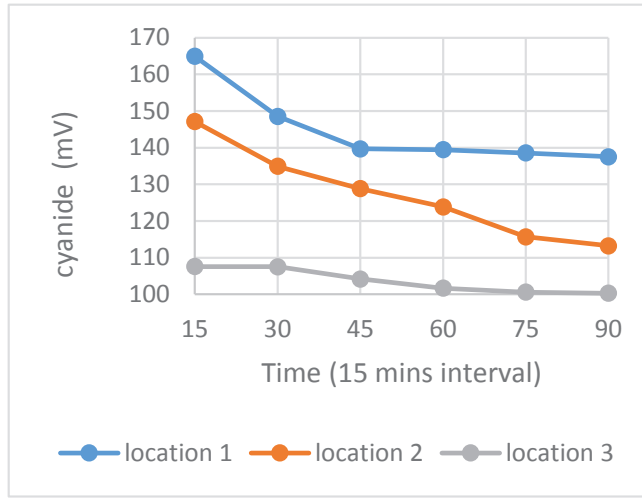

Fig. 7: Results of the testing wherein the required water samples and ISA are mixed (standard method).

the actual site and data can be transmitted immediately to the intended user's cellphones display or a centralized database system. The new system offered advantages like reduction of cost in doing multiple sampling and lesser resources both technical personnel and equipment, fewer chances of human error during the manual recording, and fast information dissemination using cellular phone technology.

Finally, the study provides proof of concept in automating the cyanide detection, analysis, and dissemination using customized circuit, electrochemical analysis, and open source software. The new system can perform the task of the commercial portable cyanide meter at a much-reduced price. It also addresses the issue of erroneous manual data recording through automated wireless transmission of data to an intended user-cellphone or computer systems. These advantages could encourage individuals, government agencies, researchers and other stakeholders from developing countries to perform cyanide monitoring in water bodies of their respective areas.

ACKNOWLEDGMENT

The authors are grateful for the funding and support given by the Philippines' Department of Science and Technology through the Engineering Research and Development for Technology (DOST-ERDT). The technical assistance was given by Engr. Freddie Homecillo, during the design and construction of the whole system. Our sincere thanks also to Engr. Ronnieto Mendoza for the technical advice. To

CRAFT, Fablab Caraga and Caraga Center for Nanotech for the laboratory and equipment use.

REFERENCES

Abbaspour, A., Asadi, M., Ghaffarinejad, A. and Safaei, E. 2005. A selective modified carbon paste electrode for determination of cyanide using tetra-3,4 pyridinoporphyrazinatocobalt(II). Talanta, 66(4): 931-936.

Barnes, D.E., Wright, P.J., Graham, S.M. and Jones-Watson, E.A. 2000. Techniques for the determination of cyanide in a process environment: a review. Geostandards Newsletter, 24(2): 183-195.

Bokingkito, P. B. and Llantos, O. E. 2017. Design and implementation of real-time mobile-based water temperature monitoring system. Procedia Computer Science, 124: 698-705.

Demetillo, A. T. and Taboada, E. B. 2019. Real-time water quality monitoring for small aquatic area using unmanned surface vehicle. Engineering, Technology & Applied Science Research, 9(2): 3959-3964.

Gacsi, M., Czegeny, I., Nagy, G. and Banfalvi, G. 2005. Survival of fish upon removal of cyanide from water. Environmental Research, 97(3): 293-299.

Gambaro, V., Arnoldi, S., Casagni, E., Dell'Acqua, L., Pecoraro, C. and Froldi, R. 2007. Blood cyanide determination in two cases of fatal intoxication: Comparison between headspace gas chromatography and a spectrophotometric method. Journal of Forensic Sciences, 52(6): 1401-1404.

Gamoh, K. 2002. Postcolumn liquid chromatographic method for the determination of cyanide with flourimetric detection. Analytica Chimica Acta, 250(2): 255-259.

Gillooly, S. E., Zhou, Y., Vallarino, J., Chu, M. D. T., Michanowicz, D. R., Levy, J. I. and Adamkiewicz, G. 2019. Development of an in-home, real-time air pollutant sensor platform and implications for community use. Environmental Pollution, 244: 440-450.

Guimaraes, J. R. D., Betancourt, O., Miranda, M. R., Barriga, R., Cueva, E. and Betancourt, S. 2011. Long-range effect of cyanide on mercury methylation in a gold mining area in southern Ecuador. Science of the Total Environment, 409(23): 5026-5033.

Holden, W. N. 2015. Mining amid typhoons: Large-scale mining and typhoon vulnerability in the Philippines. Extractive Industries and Society, 2(3): 445-461.

Hu, J., Stein, A. and Bühlmann, P. 2016. Rational design of all-solid-state ion-selective electrodes and reference electrodes. TrAC - Trends in Analytical Chemistry.

Jackson, R. and Logue, B. A. 2017. A review of rapid and field-portable analytical techniques for the diagnosis of cyanide exposure. Analytica Chimica Acta, 960: 18-39.

Ma, J. and Dasgupta, P. K. 2010. Recent developments in cyanide detection: A review. Analytica Chimica Acta, 673(2): 117-125.

Mross, S., Zimmermann, T., Winkin, N., Kraft, M. and Vogt, H. 2015. Integrated multi-sensor system for parallel *in-situ* monitoring of cell nutrients, metabolites and cell mass in biotechnological processes. Procedia Engineering, 120: 372-375.

Mudder, T. I., Botz, M. M., Engineering, E. C. and Lane, G. 2004. Cyanide and society : A critical review. The European Journal of Mineral Processing and Environmental Protection, 4(1): 62-74.

Murphy, K. E., Schantz, M. M., Butler, T. A., Benner, B. A., Wood, L. J. and Turk, G. C. 2006. Determination of cyanide in blood by isotope-dilution gas chromatography-mass spectrometry. Clinical Chemistry, 52(3): 458-467.

Nemiroski, A., Hennek, J. W., Christodouleas, D. C., Fernandez-Abedul, M. T., Maxwell, E. J., Whitesides, G. M. and Kumar, A. A. 2014. Universal mobile electrochemical detector designed for use in resource-limited applications. Proceedings of the National Academy of Sciences, 111(33): 11984-11989.

Qin, Y., Alam, A. U., Pan, S., Howlader, M. M. R., Ghosh, R., Hu, N. X. and Deen, M. J. 2018. Integrated water quality monitoring system with pH, free chlorine, and temperature sensors. Sensors and Actuators, B: Chemical, 255: 781-790.

Ramzy, E. M. 2014. Toxicity and stability of sodium cyanide in fresh water fish Nile tilapia. Water Science, 28(1): 42-50.

Randviir, E. P. and Banks, C. E. 2015. The latest developments in quantifying cyanide and hydrogen cyanide. TrAC - Trends in Analytical Chemistry, 64: 75-85.

Reddy, P. M., Hsieh, S. R., Chang, C. J. and Kang, J. Y. 2017. Detection of cyanide ions in aqueous solutions using cost effective colorimetric sensor. Journal of Hazardous Materials, 334: 93-103.

Safavi, A., Maleki, N. and Shahbaazi, H. R. 2004. Indirect determination of cyanide ion and hydrogen cyanide by adsorptive stripping voltammetry at a mercury electrode. Analytica Chimica Acta, 503(2): 213-221.

Stark, J., Li, J. and Terasawa, K. 2006. Environmental Safeguards and Community Benefits in Mining: Recent Lessons from the Philippines. Foundation for Envi Sec & Sust/USAID, (1).

Sun, H., Zhang, Y. Y., Si, S. H., Zhu, D. R. and Fung, Y. S. 2005. Piezoelectric quartz crystal (PQC) with photochemically deposited nano-sized Ag particles for determining cyanide at trace levels in water. Sensors and Actuators, B: Chemical, 108(1-2 SPEC. ISS.), 925-932.

Xu, Z., Dong, Q., Otieno, B., Liu, Y., Williams, I., Cai, D. and Li, B. 2016. Real-time *in situ* sensing of multiple water quality related parameters using micro-electrode array (MEA) fabricated by inkjet-printing technology (IPT). Sensors and Actuators, B: Chemical, 237: 1108-1119.

Zhou, B., Bian, C., Tong, J. and Xia, S. 2017. Fabrication of a miniature multi-parameter sensor chip for water quality assessment. Sensors (Switzerland), 17(1): 1-14.

Nature Environment and Pollution Technology
An International Quarterly Scientific Journal

p-ISSN: 0972-6268
e-ISSN: 2395-3454

Vol. 19 | No. 1 | pp. 403-407 | 2020

Original Research Paper | Open Access

Assessment of Agricultural Environmental Pollution Based on Fuzzy Comprehensive Evaluation: Case Study of the Yangtze River Economic Belt in China

Honglei Huang
School of Economics and Management, Hubei Engineering University, Xiaogan, Hubei, 43200, China

Nat. Env. & Poll. Tech.
Website: www.neptjournal.com

Received: 09-12-2019
Accepted: 16-01-2020

Key Words:
Yangtze river economic belt
Agricultural environment
Fuzzy comprehensive evaluation

ABSTRACT

The Yangtze River Economic Belt is an important production area of grains, oil, livestock, and aquatic products across three regions in China; thus, its agricultural environment is of particular importance. However, the agricultural environment of the Yangtze River Economic Belt has been polluted for a long time by three industrial wastes, agricultural fertilizers, pesticides, and livestock wastes. Although effort to prevent and control pollution has been increased in recent years, the situation remains severe. The assessment of agricultural environmental pollution was explored by using fuzzy comprehensive evaluation and the data from the 11 provinces and cities in the Yangtze River Economic Belt in the period of 2008-2016. The results show that agricultural environmental pollution in the Yangtze River Economic Belt is at a serious level on the basis of research on the current situation of such pollution, the use of relevant environmental pollution index data of the provinces and cities in the region from 2007 to 2016, and the performance of fuzzy comprehensive evaluation. Countermeasures to improve agricultural environmental pollution in the Yangtze River Economic Belt are proposed. They include strengthening the control of pollution caused by the three industrial wastes, pesticides, chemical fertilizers, and livestock) and the environmental education of farmers through various forms.

INTRODUCTION

The Yangtze River Economic Belt encompasses 11 provinces and cities, namely, Shanghai, Jiangsu, Zhejiang, Anhui, Jiangxi, Hubei, Hunan, Chongqing, Sichuan, Yunnan, and Guizhou. It covers an area of approximately 2.05 million km^2, with a population and gross domestic product (GDP) of more than 40% of the entire country. It is the economic and activity centres of China; it also supports the sustainable development of the nation. After years of development and construction, the traditional mode of economic development has still not fundamentally changed, and the situation of the ecological environment remains serious. In July 2017, the Ministry of Environmental Protection, in cooperation with the National Development and Reform Commission and the Ministry of Water Resources, formulated a plan for the protection of the ecological environment of the Yangtze River Economic Belt. This plan mandated that all economic activities involving the Yangtze River should be conducted on the premise of not damaging the ecological environment. Protection must be extensively implemented and large-scale developments should be avoided. In October 2018, the National Development and Reform Commission, the Ministry of Ecological Environment, the Ministry of Agriculture and Rural Areas, the Ministry of Housing and Urban Rural Development, and the Ministry of Water Resources jointly issued a notice presenting the guidelines for accelerating the treatment of agricultural non-point source pollution in the Yangtze River Economic Belt. The guidelines clearly proposed specific objectives in treating farmland, livestock breeding, and rural residential environment pollution. In recent years, the 11 provinces and cities in the Yangtze River Economic Belt have considered the restoration of the ecological environment of the Yangtze River an overwhelming task. They have made progress and achievements in pollution control and ecological restoration, exerting coordinated effort in the upper, middle, and lower reaches of the river, to implement major conservation projects. However, the state of pollution prevention and control in the Yangtze River Economic Belt remains discouraging. Hundreds of thousands of chemical enterprises are found along the Yangtze River. The total discharge of major pollutants exceeds the environmental capacity, and the environmental protection measures of some enterprises are insufficient. In addition, agricultural pollution and rural non-point source pollution remain serious due to the intensity of resource development, unreasonable production and management mode, and huge historical debts. The Yangtze River Economic Belt is a major production area of grains, oil, livestock, and aquatic products in China. It plays an important role in agricultural production safety. To further

implement precise measures, the government must strive to achieve detailed pollution prevention and control strategies, quantitatively evaluate the agricultural environmental pollution situation in the Yangtze River Economic Belt, and implement targeted pollution prevention and control. Improving the agricultural environment in the Yangtze River Economic Belt and promoting the sustainable development of the region are highly significant.

PAST STUDIES

Many scholars have studied the agricultural environment from different perspectives. Lu et al. identified the total amount of ecological resources, pollution damage, economic development, and environmental protection as major factors that affect the agricultural ecological environment (Lu et al. 2012). Han demonstrated that the overall efficiency of agricultural environmental technology is low in China, and environmental pollution causes a large degree of efficiency loss (Han 2013). On the basis of data from China's comprehensive social survey, the research of Chang showed that residents' cognition of agricultural environmental pollution is high (Chang 2015). Liang et al. reported that ecological environment problems caused by the agricultural production of farmers primarily include ecological environment damage caused by the direct development and utilization of agricultural resources, pollution caused by agricultural production (e.g., large-scale use of chemical fertilizers, pesticides, and plastic films), land pollution caused by sewage irrigation, crop straw burning, or waste pollution. However, for countries in different stages of development, agricultural ecological environment problems caused by farmers' agricultural production behaviour also vary (Liang et al. 2016). The major problem in developing countries is that the environmental cost of farmers in agricultural production is excessively high, causing a series of ecological environmental problems, such as the degradation of natural resources, food pollution, soil pollution, and rural water pollution. In developed countries, environmental problems caused by agricultural production are also serious. The primary reason is the excessive use of pollution causes, such as pesticides and fertilizers (Meijl et al. 2006). Zhang et al. indicated that factors that affect agricultural environmental pollution mostly include the large-scale discharge of three industrial wastes, dry and wet deposition, large-scale use of pesticides and chemical fertilizers, unreasonable use of agricultural films, and pollution from aquaculture waste (Zhang et al. 2017). Wang W. et al. showed that the relationship and interaction among society, economy, resources, and environment in the Yangtze River Economic Belt are continuously being strengthened, and the degree of development consistency and coordination is constantly being improved. In the coordinated development of society, economy, resources, and environment in the Yangtze River Economic Belt, we should focus on the contradiction among economic development, resource consumption, and environmental pollution (Wang et al. 2019). Shi demonstrated that the use of pesticides and other agricultural chemicals has a negative impact on soil fertility and quality (Shi 2011). In addition, the influences of the family structure, cultural level and ability, economic behaviour, and characteristics of farmers, along with the endowment of cultivated land resources in the agricultural environment, have been the focus of scholars (Hao et al. 2011, Tambo et al. 2012, Gorman et al. 2001, Li et al. 2016).

In summary, the major influencing factors of the agricultural environment include the three wastes discharged from industrial production, chemical fertilizer and pesticide pollution from agricultural production, livestock and poultry pollution from the breeding industry, and the environmental awareness of farmers.

RESEARCH METHODS

Data Collection

Based on the current research situation, this study uses the major influencing factors of the agricultural environment as the database: the three wastes discharged from industrial production, chemical fertilizer and pesticide pollution from agricultural production, and related indexes in the discharge of livestock sewage from the breeding industry. The key indicators are industrial wastewater discharge, industrial SO_2 discharge, industrial smoke (powder) dust discharge, agricultural fertilizer application, pesticide use, agricultural film use, and animal husbandry wastes (no such statistical data are available, replaced with animal husbandry output value). The data are mostly obtained from the 11 provinces and cities in the Yangtze River Economic Belt in the period of 2008-2016 from the China Urban Statistical Yearbook and the China Rural Statistical Yearbook.

Construction of Fuzzy Comprehensive Evaluation Model

The evaluation factor set of agricultural environmental pollution in the Yangtze River Economic Belt is $U = (u_1, u_2, u_n)$; u_i indicates the i-th evaluation factor, i = 1, 2, …, n. This study can be defined as $U = (u_1, u_2, u_3, u_4, u_5, u_6, u_7)$, i.e., U = [industrial wastewater discharge, industrial SO_2 discharge, industrial smoke (powder) dust discharge, agricultural fertilizer application, pesticide use, agricultural film use, animal husbandry output value].

The evaluation of agricultural environmental pollution in the Yangtze River Economic Belt is set as $V = (v_1, v_2, …,$

v_m); v_j indicates the evaluation standard, j = 1, 2, …, m. This study considers five grades: v = (very serious, more serious, general, light, very light).

The weight distribution set of the model is set as A = (a_1, a_2, …, a_n), where $a_i > 0$, and $\sum_{i=1}^{n} a_i = 1$; a_i represents the weight of the i-th factor, which reflects a trade-off of each factor. In accordance with the characteristics of the agricultural environmental pollution assessment in the Yangtze River Economic Belt, the weight distribution set of each assessment factor in this study is determined using the Delphi method, i.e., A = (0.2, 0.1, 0.1, 0.2, 0.2, 0.1, 0.1).

The relationship between the evaluation factors and the evaluation grades can be described by a fuzzy relation matrix R from U to V.

$$R = \left(r_{ij}\right)_{m\times n} \begin{pmatrix} r_{11} & r_{12} & & r_{1m} \\ r_{21} & r_{22} & & r_{2m} \\ & & & \\ r_{n1} & r_{n2} & & r_{nm} \end{pmatrix} \quad \ldots(1)$$

The element r_{ij} (i = 1, 2, …, n; j = 1, 2, …, m) indicates the possibility of making the j-th evaluation from the perspective of the i-th factor. Fixed I, (r_{i1}, r_{i2}, r_{im}) is the fuzzy subset of the single-factor evaluation for the evaluation object from the i-th factor.

A fuzzy comprehensive evaluation problem is to transform a fuzzy set A in the evaluation factor set U into a fuzzy set B in the evaluation set V through the fuzzy relation R, i.e., to establish a fuzzy comprehensive evaluation model: B = A × R = (b_1, b_2, …, b_m). By using this fuzzy evaluation model, an M-dimensional fuzzy row vector can be obtained. After normalization, the values of each vector in the vector indicate the corresponding evaluation grades (v_1, v_2, ..., v_m).

Given that B is still an M-dimensional vector; thus, if we provide another evaluation score column vector C = (c_1, c_2, c_m)^T, then the agricultural environmental pollution in the Yangtze River Economic Belt will become a clear algebraic value Q by calculating Q = B × C. Accordingly, evaluators can obtain the evaluation results intuitively and quickly.

Fuzzy Comprehensive Evaluation Model Evaluation

This study evaluates the agricultural environmental pollution in the Yangtze River Economic Belt by using the fuzzy comprehensive evaluation model. Nine experts are recruited to form a group that will evaluate each factor in the evaluation factor set U. On the basis of their assessment, a single-factor evaluation table is established (Table 1).

From Table 1, the fuzzy relation matrix R is established as follows:

$$R = \begin{pmatrix} 2/9 & 4/9 & 3/9 & 0 & 0 \\ 1/9 & 3/9 & 3/9 & 1/9 & 1/9 \\ 2/9 & 2/9 & 2/9 & 2/9 & 1/9 \\ 3/9 & 3/9 & 2/9 & 1/9 & 0 \\ 2/9 & 3/9 & 3/9 & 1/9 & 0 \\ 1/9 & 4/9 & 2/9 & 1/9 & 1/9 \\ 1/9 & 3/9 & 2/9 & 2/9 & 1/9 \end{pmatrix} \quad \ldots(2)$$

By using the established fuzzy comprehensive evaluation model, we can obtain

$$B = A \times R = (0.2, 0.1, 0.1, 0.2, 0.2, 0.1, 0.1) \begin{pmatrix} 0.22 & 0.45 & 0.33 & 0 & 0 \\ 0.11 & 0.34 & 0.33 & 0.11 & 0.11 \\ 0.22 & 0.22 & 0.22 & 0.23 & 0.11 \\ 0.33 & 0.34 & 0.22 & 0.11 & 0 \\ 0.22 & 0.34 & 0.33 & 0.11 & 0 \\ 0.11 & 0.45 & 0.22 & 0.11 & 0.11 \\ 0.11 & 0.34 & 0.22 & 0.22 & 0.11 \end{pmatrix}$$
$$= (0.231, 0.361, 0.275, 0.111, 0.044) \quad \ldots(3)$$

The calculation result B=(0.231, 0.361, 0.275, 0.111, 0.044) shows that 23.1% of the respondents believe that agricultural environmental pollution in the Yangtze River Economic Belt is "very serious," 36.1% consider it "serious," 27.5% think it is "general," 11.1% regard it as "light," and 4.4% believe it is "very light."

Given the evaluation score column vector C, let C = (100, 80, 60, 40, 20)^T. Then, the final score value of agricultural environmental pollution in the Yangtze River Economic Belt is Q = B×C = (0.231, 0.361, 0.275, 0.111, 0.044) (100, 80, 60, 40, 20)^T = 73.8.

From the preceding calculation, agricultural environmental pollution in the Yangtze River Economic Belt is at a serious level. Further measures should be taken to improve the agricultural environment in the region.

RESULT ANALYSIS AND DISCUSSION

In accordance with the research results, the state of agricultural environmental pollution in the Yangtze River Economic Belt is serious, requiring strict implementation of relevant policies issued by the state, joint management, and coordinated governance.

First, the treatment of pollution from the three industrial wastes should be strengthened. To ensure a clean environment for agricultural production, all provinces and cities

in the Yangtze River Economic Belt should strengthen law enforcement and eliminate industrial projects and machinery/equipment that cause serious pollution during operation and production in accordance with relevant national environmental protection system standards, prohibiting the spread of heavy industrial pollution to rural areas. Simultaneously, supervision should be strengthened, particularly the emission reduction of industrial enterprises in the rural economic industry along the Yangtze River. Strict regulations on pollutant emission supervision should be formulated in accordance with relevant laws and regulations and the actual local situation. The total amount of pollutants discharged by industrial enterprises must be strictly controlled.

Second, the prevention and control of pesticide and chemical fertilizer pollution should be strengthened. The key to controlling pesticide pollution is to reduce the use of pesticides as much as possible and to actively explore the use of comprehensive treatment measures. In the prevention and control of diseases and insect pests, physical, agricultural, biological, and chemical pesticide control methods should be effectively combined to minimize the use of pesticides and reduce the degree of environmental pollution. Simultaneously, new pesticides with low toxicity, low residue, and high efficiency should be actively developed, and their usage guidance must be strengthened. In addition, the supervision of the pesticide market should be reinforced, the use of drugs should be standardized, and farmers should strictly abide by the scope and standards of pesticide use. While strengthening the prevention and control of chemical fertilizer and pesticide pollution, the government must also reinforce propaganda and technical training for standardized and rational use of chemical fertilizers, guiding farmers to apply chemical fertilizers scientifically, reasonably, and effectively.

Third, the prevention and control of livestock waste pollution should be strengthened. In the process of prevention and control, the pollution-free, resource-based, and reduction principles should be adhered to. The excrement in breeding houses should be cleaned immediately, washed after cleaning, and disinfected after washing. The collected excrement should be treated in a centralized manner. Anaerobic fermentation can be applied. On the one hand, this process can save energy; on the other hand, it can lead to the development of biogas industry projects in rural areas. The collected excrement can also be fermented into an organic fertilizer, which can be used in combination with chemical fertilizers to improve agricultural production efficiency.

Fourth, the environmental education of farmers should be strengthened through various forms. Through basic education, mass media, street publicity, and the explanation and guidance of technical personnel, publicity and education regarding the agricultural environment and its protection are implemented in a simple and convenient manner. Farmers are actively guided to participate in daily environmental protection activities. In combination with activities, such as poverty alleviation through science and technology, bringing literature and art to the countryside, and organizing an environmental protection day and other important activities, and in cooperation with social organizations and associations, such as trade unions and science and technology associations, we will vigorously conduct activities that will bring environmental protection knowledge to the countryside and educate the rural population. Through text circulation, organization personnel can prepare environmental protection brochures and posters that are related to rural life and easy to understand. Accordingly, the majority of farmers can understand environmental pollution and its serious consequences in rural areas. Farmers will be educated to pay attention to environmental protection in their daily life.

CONCLUSION

This study evaluated the current situation of agricultural environmental pollution in the Yangtze River Economic Belt in accordance with the major factors of such pollution, namely, industrial wastewater discharge, industrial SO_2 discharge, industrial smoke (dust) discharge, agricultural chemical fertilizer application, pesticide use, agricultural film use, and animal husbandry and breeding wastes. Agricultural environmental pollution in the Yangtze River Economic Belt was quantitatively evaluated based on the relevant data from the region and the fuzzy comprehensive evaluation method. We attempted to quantify qualitative analysis problems as much as possible. We drew the conclusion that agricultural environmental pollution in the Yangtze River Economic Belt is at a serious level. The countermeasures were proposed to improve the state of agricultural environmental pollution in the region.

REFERENCES

Chang, Y. Q. 2015. An empirical study on the cognition of agricultural environmental pollution and its influencing factors. Environmental Science and Management, 40(10): 80-84.

Gorman, M. and Mannion, J. 2001. Connecting environmental management and farm household livelihoods: The rural environment protection scheme in Ireland. Journal of Environmental Policy and Planning, 3(2): 137-147.

Han, H. B. 2013. Analysis of technical efficiency of agricultural environment and its influencing factors in China. Research on Economy and Management, 10(9): 61-68.

Hao, H. G. and Li, X. B. 2011. Agricultural land use intensity and its determinants in ecologically-vulnerable areas in North China: A case study of Taipusi County, Inner Mongolia Autonomous Region. Journal of Resources and Ecology, 2(2): 117 -125.

Li, Q., Liu, Z., Zander, P., Hermanns, T. and Wang, J. 2016. Does farmland conversion improve or impair household livelihood in smallholder agriculture system? A case study of Grain for Green project impacts in China's Loess Plateau. World Development Perspectives, 2: 43-54.

Liang, L.T. and Zhai, B. 2016. Research progress and review of ecological environment problems at the behavioral level of farmers. China Agricultural Resources and Regionalization, 37(11): 72-80.

Lu, L. and Hu, S.D. 2012. Analysis of factors affecting agricultural ecological environment and construction of evaluation index system. Journal of Northeast Agricultural University (Social Science Edition), 10(3): 12-14.

Meijl, V. H., Van Rheenen, T., Tabeau, A. and Eickhout, B. 2006. The impact of different policy environments on agricultural land use in Europe. Agricultural Ecosystem and Environment, 114: 21-38.

Shi, X., Heerink, N. and Futian, Q.U. 2011. Does off-farm employment contribute to agriculture-based environmental pollution? New insights from a village-level analysis in Jiangxi Province, China. China Economic Review, 2(2): 524-533.

Tambo, J.A. and Abdoulaye, T. 2012. Climate change and agricultural technology adoption: the case of drought tolerant maize in rural Nigeria. Mitigation and Adaptation Strategies for Global Change, 17(3): 277-292.

Wang, J.J., Li, H., Su, X. and Du, N. 2010. Study on the coupling relationship of agricultural eco economic system in loess hilly area of Northern Shaanxi Based on the level of farmers. Journal of Natural Resources, 25(11): 1888-1897.

Wang, W. and Yu, J. 2019. Coordination mechanism and space-time pattern of society economy resource environment in Yangtze River economic belt. Journal of Capital Normal University (Natural Science Edition), 40(5): 73-82.

Zhang, G. Y. and L, Li. 2017. The current situation of agricultural environmental non-point source pollution in Hebei Province and its influencing factors and countermeasures. Hebei Agricultural Science, 21(3): 93-95.

Nature Environment and Pollution Technology
An International Quarterly Scientific Journal

p-ISSN: 0972-6268
e-ISSN: 2395-3454

Vol. 19 | No. 1 | pp. 409-412 | 2020

Original Research Paper | Open Access

First Identification of the Chlorophyte Algae *Pseudokirchneriella subcapitata* (Korshikov) Hindák in Lake Waters of India

Vidya Padmakumar and N. C. Tharavathy
Department of Studies and Research in Biosciences, Mangalore University, Mangalagangotri, Mangaluru-574199, Dakshina Kannada, Karnataka, India

Nat. Env. & Poll. Tech.
Website: www.neptjournal.com

Received: 13-06-2019
Accepted: 23-07-2019

Key Words:
Bioindicator
Ecotoxicology
Lakes of India
Pseudokirchneriella subcapitata

ABSTRACT

The species *Pseudokirchneriella subcapitata* is a freshwater microalga belonging to Chlorophyceae. It is one of the best-known bio indicators in eco-toxicological research. It has been increasingly prevalent in many fresh water bodies worldwide. They have been since times used in many landmark toxicological analyses due to their ubiquitous nature and acute sensitivity to substances. During a survey of chlorophytes in effluent impacted lakes of Attibele region of Southern Bangalore, *Pseudokirchneriella subcapitata* was identified from the samples collected from the Giddenahalli Lake as well as Zuzuvadi Lake. This is the first identification of this species in India. Analysis based on micromorphology confirmed the status of the organism to be *Pseudokirchneriella subcapitata*.

INTRODUCTION

Pseudokirchneriella subcapitata was previously called as *Selenastrum capricornatum* (NIVA-CHL 1 strain). But according to Nygaard & Komarek et al. (1986, 1987), this alga does not belong to the genus *Selenastrum* instead to *Raphidocelis* (Hindak 1977) and was renamed *Raphidocelis subcapitata* (Korshikov 1953). Hindak in 1988 made the name *Kirchneriella subcapitata* Korshikov, and it was his type species of his new Genus *Kirchneria*. But by the year 1990, Hindak realized that the name *Kirchneria* had already been in use for two other botanicals and hence further modified the name to *Pseudokirchneriella subcapitata.* Therefore, the species hence was correctly renamed as *Pseudokirchneriella subcapitata* (Korshikov) Hindak.

Though ubiquitous, this species has been recorded only in recent national and state lists which employed extensive analyses and hence a general indication of the distribution as *Pseudokirchneriella subcapitata* states its presence in Europe: Netherlands (Veen et al. 2015), Scandinavia, Slovakia, Spain and Korea (Cambra Sanchez et al. 1998).

Pseudokirchneriella subcapitata is a crescent shaped/ sickle shaped unicellular alga with an approximate 40-60 μm^3 in dimension. It belongs to the class Chlorophyceae (green algae).

Classification:

Empire:	Eukaryota
Kingdom:	Plantae
Subkingdom:	Viridiplantae
Infrakingdom:	Chlorophyta
Phylum:	Chlorophyta
Subphylum:	Chlorophytina
Class:	Chlorophyceae
Order:	Sphaeropleales
Family:	Selenastraceae
Genus:	*Pseudokirchneriella*

It has a uniform morphology and does not form chains. Colonies formed are non-mucilaginous with 4-16 cells forming matrix attaching their dorsal sides to each cell. Each cell has a single chloroplast. It is an extremely sensitive species which acts as a bio indicator detecting toxins and nutrient levels in extensively minute quantities. Hence it is considered one of the most important organisms in bioassays of water quality, algecides and environmental assessments. It has an exponentially high growth rate allowing large quantities to be grown in limited period of time (Guiry & Guiry 2017).

In March 2018, a water sample was collected from the

Lake Giddenahalli, and Lake Zuzuvadi, as part of algal diversity studies and water quality assessment in fresh water lakes of Tamil Nadu-Karnataka border zones of the south end of Bangalore region. The dominant species in both the samples collected were identified and confirmed as *Pseudokirchneriella subcapitata* by micro morphological analyses. The discovery of this species in fresh water samples in India is the first reported occurrence.

MATERIALS AND METHODS

Lake Giddenahalli (Fig. 1) is a shallow (4 ft max depth) oligotrophic lake in the Attibele region of Karnataka (12.7825°N, 77.7593°E). It is surrounded by industries that produce bulk drugs and plastics. It is a lake with a circumference of approximately 900 meters facing the Hosur-Bangalore National Highway No. 7 on one side.

Lake Zuzuvadi (Fig. 2) is a eutrophic lake located in the Hosur district of Tamil Nadu (12.7706°N, 77.7817°E). It is also located amidst a set of industries at the Sipcot Industrial area (Phase 2). It has a circumference of 1.9 kms with one side of the lake facing the residential villa colony 'Upkar Royal Gardens'.

A two-litre sample of water from both the lakes collected during March 2018, using a 100 µ plankton net as part of algal diversity studies and water quality assessment of the freshwater lakes in the area. The samples collected were allowed to settle and the 200 mL of concentrated settled subsample was separated and preserved in Lugol's Iodine solution for identification of algae.

Enumeration of the algae along with the morphological studies were done using an Olympus microscope at 40x and 100x and Utermohl's settling chamber at 200x magnification for abundance was used.

Pseudokirchneriella subcapitata was noted to be found in abundance compared to other algae and hence came into immediate notice due to its unique morphological characteristics.

Further isolation of the algal species was done using Agar plating technique for studies on micromorphology and to establish correct identity documentation of the discovered species.

RESULTS

The concentration of the algae *Pseudokirchneriella subcapitata* in the samples collected in March 2018 from the lake Giddenahalli and Zuzuvadi was 6.3×10^5 cells/mL and 5.4×10^5 cells/mL respectively. The strain obtained from both the lakes confirmed to species descriptions suggested from natural populations as explained by Hindak (1990).

The observed micro morphological characteristics that pertained for confirmation of the species type included the following: Unicellular and solitary species-forming non-mucilaginous colonies (few-celled clusters) during cell

Fig. 1: Lake Giddenahalli - An overview.

Fig. 2: Lake Zuzuvadi - An overview.

Fig. 3: The alga *Pseudokirchneriella subcapitata.*

division occasionally. Cells are helical shaped with semi circularly curved during the vegetative phase twisting one and half turns. The diameter of the 154-360° arc ranges from 4.8-10.8µm, width from 1.6-4.4µm and depth/width ratio being 1.7-4.1 (Fig. 3). The chloroplast is parietal, devoid of pyrenoid. Reproduction is generally by division of the mother cell into 2, 4 and 8 autospores (Nygaard & Komarek 1986). It is often described as a common species in planktonic environments representing both oligotrophic and eutrophic fresh water ecosystems (Vigneault & Campbell 2005).

DISCUSSION

This study has been successful in providing micro morphological clarifications for the presence of *Pseudokirchneriella subcapitata* in the freshwater lakes of the Indian Subcontinent. It is seen to be a ubiquitous species but still has received only recent mentions in National as well as State lists of few countries. It has been recorded in the Netherlands by Veen et al. (2015) and Slovakia, Scandinavia, Spain and Korea by Cambra Sanchez et al. (1998), which are a few to mention. Studies on different lakes in many other countries have led to

the mention of the species in national and state level lists that are issued in public interest in many countries.

This species has been of wide use in eco toxicological studies and algal toxicity tests. Records of the Karnataka Biodiversity Board and the authorities were referred for clarification and establishment of this work being the first identification of occurrence of the algae in Indian fresh water ecosystems.

Over the last decade, large number of works has been done on aquatic eco toxicity using the species and has been discovered in many lakes across countries growing especially in oligotrophic and eutrophic lakes and hence being bio indicators.

Micro morphological data observed in this study clearly suggest that it is *Pseudokirchneriella subcapitata*. This is the first report of the organism in India. Since the species is not been mentioned in the standard checklists published by the state as well as central Biodiversity board, it is plausible that the species was either left unidentified or misidentified.

Increased taxon sampling from other parts of India is necessarily needed to elucidate the presence and distribution of the species in the country. Further research and investigations on the genetic and phylogenetic diversity needs to be conducted in future.

REFERENCES

Cambra Sanchez, J., Alvarez Cobelas, M. and Aboal Sanjurjo, M. 1998. Floristic and bibliographic list of chlorophytes (Chlorophyta) of the Iberian Peninsula, Balearic Islands and Canary Islands. Spanish Association of Limnology, Burgos.

Guiry, M.D. and Guiry, G.M. 2017. Algaebase, world-wide electronic publication. Galway: National University of Ireland, Retrieved from https://www.algaebase.org

Hindak, F. 1977. Studies on the Clorococcal algae (Chlorophyceae) I Biologicke Prace 6. XXIV, Bratislava.

Hindak, F. 1988. Contribution to the taxonomy of some Cyanophyte genera. Preslia, 60: 289-308.

Hindak, F. 1990. Studies on the Chlorococcal algae (Chlorophyceae). V Biologicke Prace, 36: 1-227.

Korshikov, O.A. 1953. Viznachnik prisnovodnihk vodorostey Ukrainsykoi RSR [Vyp] V. Pidklas Protokokovi (Protococcineae) Bakuol 'ni (Vacuolales) ta Protokokovi (Protococcales). The Freshwater Algae of the Ukrainian. (English translation by Lund, J.W.G. and Tylka, W. 1987).

Korshikov, O.A. 1987. The Freshwater Algae of the Ukranian SSR. V. Subclass Protococcineae Vacuolales and Protococcales. Bishen Singh Mahendra Pal Singh, Dehradun and Koeltz Scientific Books, pp. 412.)

Nygaard, G. and Komarek, J. 1986. Opera Botanica, pp. 90.

Nygaard, G. and Komarek, J. 1987 Opera Botanica, pp. 46.

Veen, A., Hof, C.H.J., Kouwets, F.A.C. and Berkhout, T. 2015. Rijkswaterstaat Waterdienst, Informatihuis Water [Taxa water management the Netherlands (TWN)].

Vigneault, B. and Campbell, P.G.C. 2005. Uptake of cadmium by freshwater green algae: Effects of pH and aquatic humic substances. Journal of Phycology, 61-55: 41.

Nature Environment and Pollution Technology
An International Quarterly Scientific Journal

p-ISSN: 0972-6268
e-ISSN: 2395-3454

Vol. 19 | No. 1 | pp. 413-419 | 2020

Original Research Paper | Open Access

Reducing the Dust Generation of Haul Road by Improving Water Holding Capacity with the Application of Synthesised Polyacrylamide at Laboratory Condition

Vivek Kumar Kashi*†, N. C. Karmakar*, S. Krishnamoorthi, Ekta Sonker**, Pubali Adhikary** and Rudramani Tiwari****

*Department of Mining Engineering, IIT (BHU), Varanasi-221005, U.P., India
**Department of Chemistry, Institute of Science, BHU, Varanasi-221005, U.P., India
†Corresponding author: Vivek Kumar Kashi

Nat. Env. & Poll. Tech.
Website: www.neptjournal.com

Received: 14-06-2019
Accepted: 23-07-2019

Key Words:
Fugitive dust
Haul road
Polyacrylamide
Dust emission
Moisture holding capacity

ABSTRACT

Surface mining method enormously affects the environment in terms of fugitive dust emission than underground mining method. All the several sources of dust emission from opencast mining, haul road transportation system are the main source of fugitive dust. In this research article, a biodegradable polyacrylamide (PAM) was used to suppress dust generation from haul road of mine. It improves the moisture carrying capacity of haul road than the water. PAM has been synthesized by free radical polymerization process using ceric ammonium nitrate initiator. It was characterized by 1H NMR, IR & intrinsic viscosity measurements, whereas size distribution of haul road dust was measured by sieve analysis. Laboratory work has been carried out to investigate the water holding capacity of haul road dust particles using PAM solution and compared with only water for 8 hours duration. The temperature of the chamber was kept constant at 35°C while relative humidities (RH) varied from 40% to 70%. It was observed that moisture retention of dust with the application of PAM solution and only water were 25.65% and 20.4% at 70% RH and 7.14% and 1.65% at 40% RH, respectively after 8 hours.

INTRODUCTION

In India, coal production from opencast mining (OCM) has risen to 250 million tons (MT), which represented about 70 percent of total coal production in 2000 (Ghose 2007). After 17 years, 618.445 MT (93.31%) coal production was through OCM in 2016-17, whereas only 44.347 MT was through underground mining (UGM) (Coal India Report 2017). Excavation of minerals, done both through UGM or OCM, is extremely risky and affects the environment adversely. OCM has a high rate of production and is less risky than UGM, but at the same time, it affects the atmosphere more than UGM due to more exposure to the outside environment. Dust emission of opencast mine is high due to multiple operations take place simultaneously like drilling, blasting, coal extraction, coal handling and stockpile, screening plant, topsoil handling, overburden removal, haul road transportation system and other miscellaneous activities (Shao & Lu 2000).

Out of these, haul road transportation system produces a huge amount of dust which polluted the environment as shown in Fig. 1 (Chaulya et al., 2011). Transportation of overburden, reaching to ore and then carrying of useful material i.e. ore to mineral processing plants is done over the road with a specific direction that is known as the haul road. Movement of haul trucks and other heavy machines over the haul road system has been identified as the immense source of fugitive dust generation. It contributes approximately 78% to 97% of total dust emission (Addo et al. 2004, Reed & Organiscak 2007).

Dust generation from haul road shows that if the dust emissions are uncontrolled, there is a high risk of the safety hazard by weakening the operator's visibility and damaging his efficiency. The SIMRAC report (Simpson et al. 1996) found that 74% of the accidents were associated with ore or overburden transfer by haul tracks and service vehicle operation on haul road surface mines in South Africa (Thompson & Visser 2001). Therefore, the probability of haul road accidents will increase, and that makes a high fatality rate. Various other adverse effects can also occur by emission of dust including human health, annoyance, biological and ecological impacts. (McHattie 2015).

Spraying of water is the most common mode for handling the dust generation in the different types of mining activities (Reed & Organiscak 2008). Earlier, either due to abundance of water source or easy availability or lack of proper innovative techniques, dust suppression on haul roads mostly depended on water. But in the present scenario, water is scarce around the mining area as well as the need of people

Fig. 1: Emission of dust from haul road.

around the mining site is also increasing especially during the summer season. Several published research reports have shown that different dust suppressants, when applied after mixing with water or without water, provide more effective dust control results (Cecala et al. 2012). Recently many chemical dust suppressants are applied for controlling the haul road dust generation like calcium chloride, magnesium chloride, petroleum emulsions, lignosulphonates and polymers (Bolander 1999, Zhang et al. 2018). These may be hazardous to the environment and damaging to haul tracks to varying degree (Foley et al. 1996, Cecala et al. 2012). This has led the mining industry to look forward to reducing the application of water as well as such hazardous chemicals and introducing a suitable alternative which has the capability to reduce dust emission and is also eco-friendly in its nature.

The objective of this study is to examine the effects of PAM as a chemical dust suppressant on fugitive dust emission from haul roads at the most viable temperature of 35°C under Indian context and low as well as high relative humidity (RH) condition of 40% & 70% respectively. These experiments show the role of temperature and humidity on the performance of PAM. This paper gives a behavioural idea of controlling the dust generated by the haul road system and assist in minimising the threat of fugitive dust to workers' health and safety.

MATERIALS AND METHODS

Description of the Case Study Mine Area

Dust sample was collected from haul road of a mine which comes under Block-II of Bharat Coking Coal Limited in Dhanbad district of Jharkhand state.

Block-II area is situated about 40 km west of Dhanbad town with Latitude-23º 47'30' to 23º 46'30' and Longitude-86º 13'30' to 86º 10'30'.

Materials

Acrylamide, ceric ammonium nitrate, hydroquinone and acetone were supplied by S.D. Fine Chemicals, Mumbai, India. All the chemicals were used as they were procured without further purification.

Size Distribution

In the design of a haul road, a mining company takes into consideration the wheel load of the haul truck and the particle size distribution of the soil before deciding what type of soil will be added to the wearing course materials (Thompson & Visser 2007, Mandal et al. 2012). According to the typical design standard for the mine haul road, the particle size distribution of the used soil sample, as shown in Table 1, falls within the design limit.

The sample was screened by sieve analysis of the size of 10, 12, 20, 35, 50, 100 and 200 mesh size of ASTM standard. Screening opening size was 10 mess, particles above this size have not played any crucial role in the dust generation due to high weight.

Polyacrylamide (PAM) as a Dust Suppressant

PAM is a water soluble polymeric organic substance formed from acrylamide units ($CH_2CHCONH_2$) that dissolve, disperse or swell in water. The polymer is hydrophilic (displays an affinity for water) and can form aqueous solutions of very high concentration (Abdollahi & Gomes 2006). Usually, it has repeating units containing hydrophilic groups of the amide as in Fig. 2. PAM is most often used as a viscosifying agent (creating a thicker solution) (Woodrow et al. 2008). The main advantage of the application of PAM as a dust suppressant is because of its non-toxic nature as well as its biodegradability. Therefore, they find an extensive usage in industrial applications such as in drinking and industrial wastewater treatment, oil sand tailings treatment, improvements of soil stability, and enhanced oil recovery.

Table 1: Illustration of the particle size distribution of the dust sample used for the experiment.

Sieve size (mess)	Sieve size (mm)	Weight (g)	Weight (%)
b/t 10 to 12	2.04 to 1.68	125	25%
20	0.84	47	9.4%
35	0.5	22	4.4%
50	0.297	100	20%
100	0.14	73	14.6%
200	0.074	31	6.2%
Below 200	0.074	102	20.4%

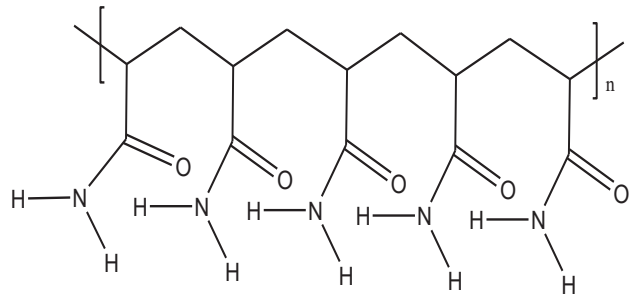

Fig. 2: **Chemical structure of polyacrylamide.**

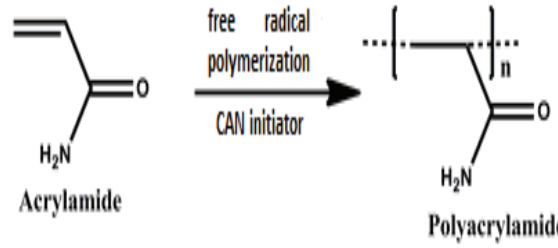

Fig. 3: Polymerization process of polyacrylamide.

Synthesis of PAM

PAM was synthesized by a free radical polymerization reaction mechanism in the laboratory. Free radical polymerization is a type of chain growth polymerization. It is a process of polymer synthesis in which polymer grows by sequential addition of the monomer units. Free radical propagates at double bond of monomer units by successive braking of monomer double bond (Fig. 3). Five g of the monomer was dissolved in 20 mL of distilled water in a conical flask. This solution was stirred for 20 min in the nitrogen atmosphere. 20 mg of ceric ammonium nitrate (CAN) was mixed with a solution as initiator and N_2 purging was done for the next 30 min at 50°C. It got viscous and left for cooling at room temperature. The reaction was terminated by adding 2 mL of a saturated solution of hydroquinone. The product was precipitated by using acetone as a non-solvent. The resultant polymer was broken into small pieces and then pulverized. It was dried into oven for 24 h at 70°C and preserved in a desiccator.

Characterization

Polyacrylamide was characterized by ^{1}H NMR spectroscopy, IR Spectroscopy and intrinsic viscosity measurements.

^{1}H NMR spectroscopy: ^{1}H NMR spectra of the polymers were recorded by FT-NMR spectrometer (Model JEOL AL 500) with sample solution in D_2O. Tetramethylsilane (TMS) was used as an internal reference.

IR Spectroscopy: Thermo Nicolet FT-IR spectrophotometer (Model JASCO FT-IR-5300) was used to record the IR

spectra within the range of 4000-400 cm^{-1} by using solid state KBr pellet method.

Intrinsic viscosity measurements: Viscosity measurements of the aqueous solutions of polyacrylamide were carried out with the help of Ubbelohde viscometer (P/2741) at 25 ± 0.1°C. Intrinsic viscosity was determined from the point of intersection of two extrapolated (to zero concentration) plots i.e., inherent viscosity (η_{inh}) versus concentration (C) and reduced viscosity (η_{red}) versus concentration (C).

Methodology of the Experiment

A general experimental procedure was followed for testing the tested chemical dust suppressant at each considered dosages under fixed temperature and humidity. 20 g dried dust sample of below 2.04 mm (sieve mess size 10, ASTM standard) was taken for an experiment (ASTM-D6913/ D6913M, 2017). The dust sample was weighed on the Petri dish before the dosage of a chemical suppressant was applied. After several trials, a depth of one cm was selected as the thickness of the dust sample on the Petri dish so that solution was equally distributed. The measured solution was applied through a plastic spray bottle. The sample was weighed along with the Petri dish after the application of 10 mL dosage before putting Petri dish into a temperature and humidity controller. 10 mL of solution was applied in a way to avoid under or over usage of the solution. The sample was then put in the temperature and humidity controller chamber. Efficiency of the chemical to retain water was studied up to 8 h. For this, at an interval of 1 h, the sample was weighed and again put in the temperature and humidity control chamber.

The experiment has been done with application of only water to compare the effectiveness of dust suppressant PAM in haul road. The same procedure was applied for knowing the % of moisture retention of water as a dust suppressant for every 1 h of duration up to 8 h. Each test was repeated 3 times to get average results.

RESULTS AND DISCUSSION

Size Distribution

A research has been done by Sinha & Banerjee (1997), on the haul road of Noamundi opencast iron ore mine, located at West Singhbhum, Jharkhand, where 60% of total suspended particulate matter was within the size range of 0 – 10 µm, remaining other 40% of SPM were size of 10 to 100 µm range. For the present experiment, haul road dust sample was screened by sieve size range of 2.04 mm to 74 µm. Particle size below 75 µm is known as silt. In this haul road dust sample, 20.4% of silt was present in total weight percentage. Emission of dust depends on the size of the road surface materials. The probability of dust emission from haul road increases as the percentage of silt increases (Kavouras et al. 2009).

^{1}H NMR spectroscopy: PAM was characterized by ^{1}H NMR spectroscopic study and the respective spectra are shown in Fig. 4. A broad peak observed at 2.07 ppm was attributed to the -CH protons present in acrylamide units and the peak observed at 1.51 ppm was because of the methylene protons present in polyacrylamide. The characteristic signals of N-H protons of amide groups present in polyacrylamide units were exchanged by deuterium present in D_2O and thus no corresponding peak was observed. Thus, the ^{1}H NMR spectroscopic data confirm the formation of polyacrylamide.

IR spectroscopy: Synthesized polyacrylamide was characterized by IR spectroscopy and its spectra are shown in Fig. 5. A broad band at 1660 cm^{-1} and 1613 cm^{-1} were due to the stretching vibrations of the >C=O group and

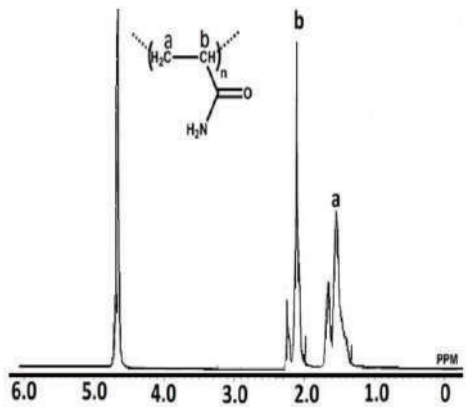

Fig. 4: ^{1}H NMR spectrum for PAM.

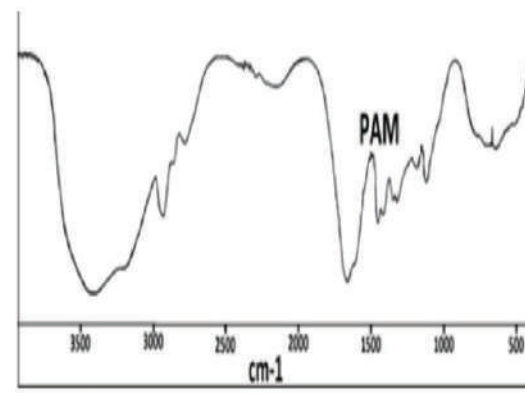

Fig. 5: IR spectrum of PAM.

bending vibration of NH_2 group respectively. Absorption bands at 1451 and 1419 cm^{-1} were due to the scissor and bending vibrations of CH_2 and CH-CO groups, respectively. Furthermore, the absorption band at 2930 cm^{-1} corresponded to the stretching vibrations of CH_2 groups. A broad absorption band at 3419 cm^{-1} was due to the absorption band of N-H group. Finally, the absorption bands at 1350 cm^{-1} region were due to the stretching vibrations of C-N group, while the broad absorption bands in the 600 to 700 cm^{-1} regions were due to out of plane bending vibration of NH_2 group.

Intrinsic viscosity measurement: Flow time of water (t_0) was measured 18 sec with the help of Ubbelohde viscometer. Flow time of PAM solution (t) at various concentrations were measured. Relative, specific, reduced and inherent viscosities were calculated and tabulated in Table 2. From Fig. 6, intrinsic viscosity was calculated and its value was 3.33 dL/g.

The Performance of Water as Dust Suppressant

Performance of water as a dust suppressant was studied at 35°C by varying the humidity level for evaporation of moisture. Low humidity of 40% RH and high humidity of 70% RH have been considered for this study.

Fig. 7 showed the percentage retention of moisture when 10 mL tap water was applied to the haul road sample at 35°C temperature, and 40% and 70% of RH at every 1 h duration respectively. After 1 h, the moisture retention capacity was 90.37 % and 88.30 % for 70% and 40% of RH respectively. However, moisture retention capacity was started to decrease with time continuously in both cases. The retention of moisture was 20.40% and 1.65% after 8 h. The rate of moisture retention was decreasing faster in case of 40% RH compared to 70% of it. As the relative humidity increases, because of the availability of more moisture in the air at the same temperature, the rate of evaporation of water from the surface of the dust sample will be slow. The vapour pressure of moisture is more when RH is 70% as compared to 40%. This helps to reduce evaporation of water from the surface of the haul road.

The Performance of PAM as Dust Suppressant

The % of moisture retention associated with each time interval was plotted corresponding to 40% and 70% of RH of PAM solution of 1000 ppm concentration applied to dust sample at 35°C temperature in Fig. 8. After 1 h inside chamber, the percentage of moisture retention was 92.27%

Table 2: Calculation of reduced and inherent viscosity of PAM.

Concentration (g/dL)	Flow time *t* (sec)	Relative viscosity ($\eta_r = t/t_0$)	Specific viscosity ($\eta_{sp} = \eta_r - 1$)	Reduced viscosity η_{sp}/C (dL/g)	Inherent viscosity [ln (ηr)/C] (dL/g)
1	271	15.06	14.06	14.06	2.71
0.5	87.2	4.84	3.84	7.69	3.16
0.25	44.5	2.47	1.47	5.89	3.62
0.125	27.3	1.52	0.52	4.13	3.33
0.0625	22.2	1.23	0.23	3.73	3.36

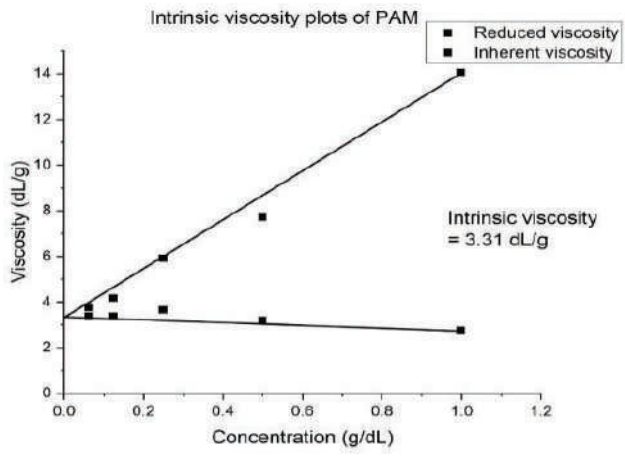

Fig. 6: Intrinsic viscosity plots of PAM.

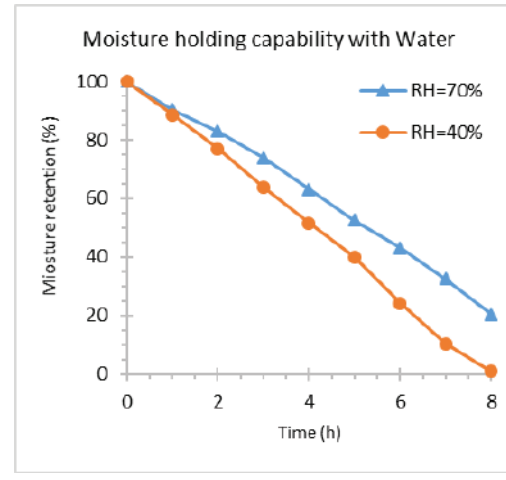

Fig. 7: Trend of moisture loss with duration of time by application of water in haul road dust.

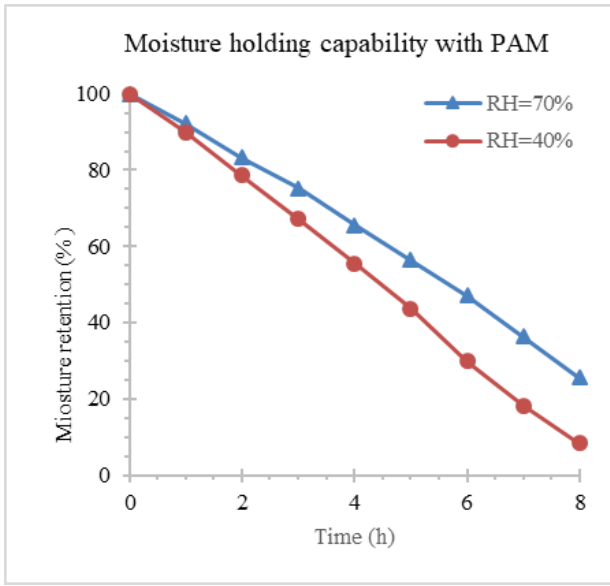

Fig. 8: Trend of moisture retention with duration of time by application of PAM in haul road dust.

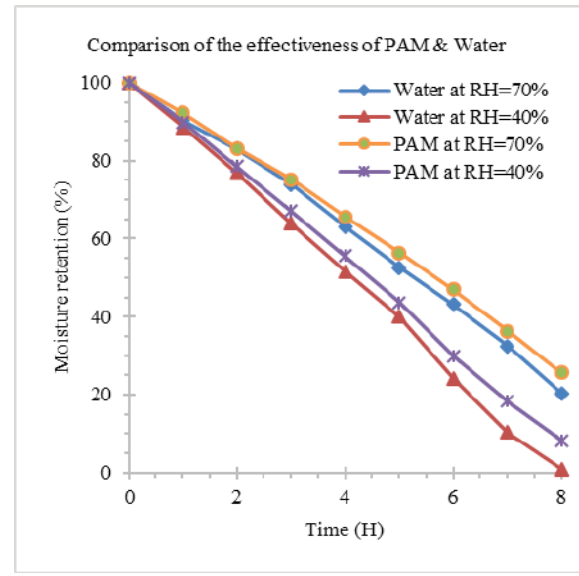

Fig. 9. Comparison of moisture retention with duration of time by application of water and PAM in haul road dust.

and 89.51% at 70% and 40% RH respectively. Fall of moisture present in the dust sample in 40% was at a higher rate than of 70% RH. After 8 h interval, moisture retention in the case of 70% RH was 25.65% which was higher than 7.14% at 40% RH. When RH was 70%, this shows that capacity of moisture holding in the haul road dust was high.

Comparing between the Effectiveness of Water and PAM

A comparative study of the effectiveness of water and PAM can easily be done by analysing Fig. 9. Initially, there is very less variation in moisture evaporation in both the cases. It has happened because a saturated amount of water molecules are present in each of the haul road dust sample. Gradually with an increase of time, the rate of evaporation in case of water spray sample is found to be higher as compared to the PAM spray sample. The deviation of moisture loss in case of 70% RH is lower than 40% RH due to the more amount of moisture present in the surrounding. The moisture retention in case of PAM treated sample is more compared to water treated sample. Every acrylamide group attach in the polyacrylamide chain have one amide group. Each amide molecules have the tendency to hold four molecules of water by hydrogen bond. Thus, water retention capability of PAM increases which facilitates better bonding between dust particles.

CONCLUSIONS

PAM has been synthesized by free radical polymerization process and confirmed through characterization by ^{1}H NMR, IR and intrinsic viscosity measurements. From sieve analysis, 20.4% silt was contented in the haul road. From results, the deviation of moisture loss in case of 70% RH is lower than of 40% RH due to the more amount of moisture present in the nearby surrounding. Also, amide group of PAM has abilities to hold the water molecules. Water molecules release slowly from PAM chain that helps to bind small particles with larger particles for a long period. Thus, PAM solution shows better efficiency than water to reduce dust emission by enhancing moisture carrying capacity of haul road of opencast coal mining. This led to the enhanced mine's productivity through improvement in visibility and health safety of miners.

REFERENCES

Addo, J. Q., Sanders, T. G. and Chenard, M. 2004. Road dust suppression: Effect on maintenance stability, safety and the environment phases 1-3. Department of Roads and Bridges, Colorado State University, 1-64.

ASTM-D6913/D6913M. 2017. Standard test methods for particle-size distribution (gradation) of soils using sieve analysis. ASTM International, 04(9): 1-34.

Bolander, P. 1999. Dust palliative selection and application guide application guide. San Dimas Technology and Development Center, San Dimas, California, 1-20.

Cecala, A.B., O'brien, A.D., Schall, J., Colinet, J.F., Fox, W.R., Franta, R.J. and Schultz, M. J. 2012. Dust Control Handbook for Industrial Minerals Mining and Processing. Retrieved from https://www.spray.com/pdf/Dust_Control_Hanbook_RI9689.

Chaulya, S.K., Kumar, A., Mandal, K., Tripathi, N., Singh, R.S., Mishra, P. K. and Bandyopadhyay, L.K. 2011. Assessment of coal mine road

dust properties for controlling air pollution. International Journal of Environmental Protection, 1(2): 1-7.

Foley, G., Cropley, S. and Giummarra, G. 1996. Evaluation of chemical dust suppressants performance. AROB Transport Research, Special Report 54: 1-143.

Ghose, M. K. 2007. Opencast coal mining in India: Analyzing and addressing the air environmental impacts opencast. Environmental Quality Management, 49(4): 71-87.

Government of India, Coal India Report, Ministry of Coal 2017. 16-17, https://www.coal.nic.in/content/annual-report-2016-17.

Kavouras, I.G., Etyemezian, V., Nikolich, G., Gillies, J., Sweeney, M., Young, M. and Shafer, D. 2009. A new technique for characterizing the efficacy of fugitive dust suppressants. Journal of the Air and Waste Management Association, 59(5): 603-612.

Mandal, K., Kumar, A., Tripathi, N., Singh, R. S., Chaulya, S. K., Mishra, P. K. and Bandyopadhyay, L. K. 2012. Characterization of different road dusts in opencast coal mining areas of India. Environmental Monitoring and Assessment, 184: 3427-3441.

McHattie, R.L. 2015. Dust Control Field Guide for Gravel Driving Surfaces. Dust Control Field Guide for Alaska Department of Transportation, 1-35.

Reed, W.R. and Organiscak, J.A. 2007. Haul road dust control fugitive dust characteristics from surface mine haul roads and methods of control. NIOSH-PRI, pp. 1-4.

Shao, Y. and Lu, H.A. 2000. Simple expression for wind erosion threshold friction velocity. J. Geophys. Res., 105(22): 437-443.

Simpson, G.C., Rushworth, A.M., Von Glehn, F.H. and Lomas, R.H. 1996. Investigation into the causes of transport and tramming accidents on mines other than coal, gold and platinum. SIMRAC project report: OTH, 202, Pretoria, South Africa.

Sinha, S. and Banerjee, S.P. 1997. Characterization of haul road dust in an Indian opencast iron ore mine. Atmospheric Environment, 31(17): 2809-2814.

Thompson, R.J. and Visser, A.T. 2001. Mine haul road fugitive dust emission and exposure characterisation. Journal of the Mine Ventilation Society of South Africa, 1-20.

Thompson, R. J. and Visser, A.T. 2007. Selection, performance and economic evaluation of dust palliatives on surface mine haul roads. The Journal of The Southern African Institute of Mining and Metallurgy, 107: 435-450.

Wen, Q., Chen, Z., Zhao, Y., Zhang, H. and Feng, Y. 2010. Biodegradation of polyacrylamide by bacteria isolated from activated sludge and oil-contaminated soil. Journal of Hazardous Materials, 175(1-3): 955-959.

Woodrow, J.E., Seiber, J.N. and Miller, G.C. 2008. Acrylamide release resulting from sunlight irradiation of aqueous polyacrylamide/iron mixtures. Journal of Agricultural and Food Chemistry, 56(8): 2773-2779.

Zhang, H., Nie, W., Wang, H., Bao, Q., Jin, H. and Liu, Y. 2018. Preparation and experimental dust suppression performance characterization of a novel guar gum-modi fi cation-based environmentally-friendly degradable dust suppressant. Powder Technology, 339: 314-325. https://doi.org/10.1016/j.powtec.2018.08.011.

Zohreh Abdollahi and Vincent G. Gomes 2006. Synthesis and Characterization of Polyacrylamide with Comtrolled Molar Weight. Chemeca Conference, 1-8.

... Continued from inner front cover

- The text of the manuscript should run into **Abstract, Introduction, Materials & Methods, Results, Discussion, Acknowledgement** (if any) and **References** or other suitable headings in case of reviews and theoretically oriented papers. However, short communication can be submitted in running with **Abstract and References.** The references should be in full with the title of the paper.
- The figures should preferably be made on a computer with high resolution and should be capable of withstanding a reasonable reduction with the legends provided separately outside the figures. Photographs may be black and white or colour.
- Tables should be typed separately bearing a short title, preferably in vertical form. They should be of a size, which could easily be accommodated in the page of the Journal.
- References in the text should be cited by the authors' surname and year. In case of more than one reference of the same author in the same year, add suffix a,b,c,.... to the year. For example: (Thomas 1969, Mass 1973a, 1973b, Madony et al. 1990, Abasi & Soni 1991).

List of References

The references cited in the text should be arranged alphabetically by authors' surname in the following manner: (Note: The titles of the papers should be in running 'sentence case', while the titles of the books, reports, theses, journals, etc. should be in 'title case' with all words starting with CAPITAL letter.)

Dutta, A. and Chaudhury, M. 1991. Removal of arsenic from groundwater by lime softening with powdered coal additive. J. Water Supply Res. Techno. Aqua., 40(1) : 25-29.

Hammer, D.A. (ed.) 1989. Constructed Wetlands for Wastewater Treatment-Municipal, Industrial and Agricultural. Lewis Publishers Inc., pp. 831.

Haynes, R. J. 1986. Surface mining and wetland reclamation. In: Harper, J. and Plass, B. (eds.) New Horizons for Mined Land Reclamation. Proceedings of a National Meeting of the American Society for Surface Reclamation, Princeton, W.V.

Submission of Papers

- The paper can be submitted by e-mail as an attachment in a single WORD file at **contact@neptjournal.com**
- The paper can also be submitted online in a single WORD file through the journal's website: **www.neptjournal.com**

Attention

1. Any change in the authors' affiliation may please be notified at the earliest.
2. Please make all the correspondence by e-mail, and authors should always quote the manuscript number.

Note: In order to speed up the publication, authors are requested to send the publication charges as soon as they get the 'initial acceptance' letter, and also correct the galley proof immediately after

Nature Environment and Pollution Technology

(Abbreviation: Nat. Env. Poll. Tech.)

(An International Quarterly Scientific Journal)

Published by

Technoscience Publications

A-504, Bliss Avenue, Opp. SKP Campus

Balewadi, Pune-411 045, Maharashtra, India

In association with

Technoscience Knowledge Communications

Mira Road, Mumbai, India

For further details of the Journal please visit the website. All the papers published on a particular subject/topic or by any particular author in the journal can be searched and accessed by typing a keyword or name of the author in the 'Search' option on the Home page of the website. All the papers containing that keyword or author will be shown on the home page from where they can be directly downloaded.

www.neptjournal.com

Published for Proprietor, Printer and Publisher: Mrs. T. P. Goel, B-34, Dev Nagar, Tonk Road, Jaipur, Rajasthan, India; Editors: Dr. P. K. Goel and Prof. K. P. Sharma